

Technical Report

TR-09-01

**Site description of Laxemar
at completion of the site
investigation phase**

SDM-Site Laxemar

Svensk Kärnbränslehantering AB

December 2009

Svensk Kärnbränslehantering AB

Swedish Nuclear Fuel
and Waste Management Co

Box 250, SE-101 24 Stockholm
Phone +46 8 459 84 00



Site description of Laxemar at completion of the site investigation phase

SDM-Site Laxemar

Svensk Kärnbränslehantering AB

December 2009

Preface

The Swedish Nuclear Fuel and Waste Management Company (SKB) is undertaking site characterisation at two different locations, the Forsmark and Laxemar-Simpevarp areas, with the objective of siting a deep geological repository for spent nuclear fuel. An integrated component in the characterisation work is the development of a site descriptive model (SDM) that constitutes a description of the site and its regional setting. The model addresses the current state of the geosphere and the biosphere as well as the ongoing natural processes that affect their long-term evolution.

The site descriptive model concluding the surface-based investigations at Laxemar, SDM-Site Laxemar, is compiled in the present report. Prior to the SDM-Site report, three full versions of a site descriptive model have been completed for the Laxemar-Simpevarp area. A preceding Version 0 established the state of knowledge prior to the start of the site investigation programme in 2002. Version Simpevarp 1.1, which was essentially a training exercise, was completed during 2004, version Simpevarp 1.2 and version Laxemar 1.2 completed in April 2005 and April 2006, respectively. Version Laxemar 1.2 of the SDM, a preliminary site description, concluded the initial site investigation work.

Two analytical and modelling stages have been carried out during the complete site investigation work in Laxemar. An important component of each of these stages has been to address and continuously try to resolve uncertainties of importance for repository engineering and safety assessment. Stage 2.1 aimed to provide feedback from the modelling group to the site investigation team to enable completion of the site investigation work. Model version SDM-Site Laxemar, based on data freeze Laxemar 2.3, has established the different discipline-specific models, which are combined into the framework of the integrated site descriptive model, SDM-Site. A synthesis of the SDM-Site report that focuses on model integration and the current understanding of the site is presented in Chapter 11. In essence, this chapter serves as an executive summary.

The overall objective of the site descriptive modelling work at Laxemar is to develop and document an integrated description of the site, based on data from the complete site investigation work, as a basis for a site-adapted design of the final repository (Layout D2) and for assessment of the repository's long-term radiological safety (SR-Site).

The site descriptive modelling work performed within the Swedish site characterisation programme is conducted by multi-disciplinary project groups and associated discipline-specific working groups (Net groups). All individuals and expert groups contributing to the projects are gratefully acknowledged, and especially the Laxemar multi-disciplinary project group, for making this report possible. Specifically, the following individuals and expert groups contributed to this final report:

- Anders Winberg – project leader, editor, primary data compilation and site synthesis.
- Björn Söderbäck – site evolutionary aspects.
- Björn Söderbäck and other members of the SurfaceNet group – abiotic and biotic properties of the surface system, interfacing between surface and deep bedrock systems.
- Carl-Henric Wahlgren (rock domain modelling), Philip Curtis (deformation zone modelling) and Aaron Fox (discrete fracture network modelling) – geology (deterministic modelling and integrated model), site synthesis and contributions to Appendix 6.
- Jan Sundberg and John Wrafter – thermal properties.
- Eva Hakami – rock mechanics.
- Ingvar Rhén and Lee Hartley – hydrogeology, interfacing between surface and deep bedrock systems, site synthesis and contributions to Appendix 6.
- Marcus Laaksoharju, John Smellie, Eva-Lena Tullborg and Bill Wallin – hydrogeochemistry.
- James Crawford – transport properties.
- Fredrik Hartz and Anders Lindblom – production of maps and figures.

The members of the multi-disciplinary project group completed Appendices 2 and 3.

Johan Andersson is specifically acknowledged for his ambitious and devoted efforts as a driving force for the confidence assessment work and as editor of the report documenting its outcome (SKB R-08-101).

The report has been formally reviewed by the following members of SKB's international site investigation expert review group (Sierg): Per-Eric Ahlström (Chairman), Jordi Bruno (Amphos), John Hudson (Rock Engineering Consultants), Ivars Neretnieks (Royal Institute of Technology), Lars Söderberg (SKB), Michael C Thorne (Mike Thorne and Associates Ltd), Roland Pusch (GeoDevelopment AB), Thomas W Doe (Golder Associates Inc.), John Cosgrove (Imperial College) and Alan Hooper (Alan Hooper Consulting Ltd). The Sierg group provided many valuable comments and suggestions for this work. However, the group is not to be held responsible for any remaining shortcomings of the work or its presentation.

Please observe that the work presented in this report was completed April 2009, i.e. well in advance of the site selection made by SKB in June 2009 and as such constituted one of the important components that enabled this selection. The issuing date of the presented report is, however, December 2009 reflecting that fact that minor adjustments have been made to the report, mainly structural and lingual. It is emphasised that no changes to the principal content of the April 2009 version of report has been made as part of this processing.

Anders Ström
Site Investigations – Site Modelling

Summary

The Swedish Nuclear Fuel and Waste Management Company (SKB) has undertaken site characterisation in two different areas, Forsmark and Laxemar-Simpevarp, in order to identify a suitable location for a geological repository of spent nuclear fuel according to the KBS-3 method. The site investigations have been conducted in campaigns, punctuated by data freezes. After each data freeze, the site data have been analysed and modelling has been carried out with the overall purpose to develop a site descriptive model (SDM). The site descriptive model is used by repository engineering to design the underground facility and to develop a repository layout adapted to the site. It is also essential for safety assessment, since the SDM is the only source for site-specific input. Another important use of the site descriptive model is in the environmental impact assessment. An SDM is an integrated model of geology, thermal properties, rock mechanics, hydrogeology, hydrogeochemistry, bedrock transport properties and a description of the surface system. The site descriptive model compiled in the current report, SDM-Site Laxemar, presents an integrated understanding of the Laxemar-Simpevarp area (with special emphasis on the Laxemar subarea) at the completion of the surface-based investigations, which were conducted during the period 2002 to 2007. A summary is also provided of the abundant underlying data and the discipline-specific models that support the site understanding. The description relies heavily on background reports that address, in particular, details of the data analyses and modelling of the different disciplines.

The Laxemar-Simpevarp area is located in the province of Småland within the municipality of Oskarshamn, about 230 km south of Stockholm. The candidate area for site investigation is located along the shoreline of the strait of Kalmarsund, within a 1.8 billion year old suite of well preserved bedrock belonging to the Transscandinavian Igneous Belt formed during the waning stages of the Svecokarelian orogeny. The candidate area is circular-shaped with an area of 54 km², and hosts the Laxemar subarea in its eastern part. The south-western part of the Laxemar subarea was selected as the focused area for the complete site investigation work, following the initial investigations at the site.

Prior to the presentation of the SDM-Site report, three versions of a site descriptive model have been completed for the Laxemar-Simpevarp area and subjected to peer review. The last version, referred to as version Laxemar 1.2, constituted a preliminary site description that concluded the initial site investigation work and was presented in 2006. This preliminary site description formed the basis for a preliminary safety evaluation (PSE) of the Laxemar subarea, a preliminary repository layout (step D1), and the first evaluation of the long-term safety of this layout for a KBS-3 repository in the context of the SR-Can project.

The final site descriptive model, SDM-Site Laxemar, builds on a coordinated geological model in 3D, into which other discipline-specific models have been integrated without any major conflicting interpretations. In particular, the bedrock thermal and strength properties of the bedrock at the site have been coupled to lithology and identified rock domains in the geological model and an integrated description has been devised that links the hydrogeology and the chemistry of the groundwater to hydraulic conductor domains (deformation zones) and hydraulic rock domains (and underlying fracture domains) and their division in depth zones. These mutually consistent results demonstrate that a fundamental understanding of the current state, properties and processes in Laxemar, from the surface down to potential repository depth, has been achieved. In addition, the properties of the area can be explained in the context of an understanding of its past evolution, throughout a long period of geological history. This integrated understanding of the area is presented in Chapter 11 of this report and this chapter effectively serves as an executive summary of the modelling work.

A systematic assessment of the confidence in the developed models, including treatment of uncertainties and evaluation of alternative interpretations, has been carried out. This assessment has taken into account the feedback obtained from the work on the preliminary repository layout step D1 and from the safety assessment SR-Can, as well as the feedback obtained on earlier versions of the site description. The overall outcome of this assessment is that most properties of importance for both repository constructability and long-term safety are bounded sufficiently, and that data collected underground now bears the prime potential to further reduce uncertainties in the focused volume. However, complementary studies to reduce some of these uncertainties are also currently in progress. Uncertainties outside the focused volume are higher, but are judged to be of less importance for the constructability and long-term safety of a repository.

Contents

1	Introduction	13
1.1	Background	13
1.2	Scope and role of the site description in the application process	15
1.3	Objectives and strategy	17
1.4	Feedback from reviews and assessments of previous model versions	17
1.5	Setting	18
1.6	Methodology and organisation of work	22
1.6.1	Methodology	22
1.6.2	Interfaces between disciplines	23
1.6.3	Organisation of work	24
1.6.4	Quality assurance aspects	25
1.6.5	Nomenclature	26
1.7	This report and supporting documents	26
2	Investigations, available data and other prerequisites for the modelling	29
2.1	Overview of investigations	29
2.1.1	Investigations and primary data acquired up to data freeze Laxemar 1.2	29
2.1.2	Data freezes 2.1, 2.2 and 2.3 – investigations performed and data acquired	30
2.2	Surface Investigations	31
2.2.1	Bedrock geology and ground geophysics	31
2.2.2	Quaternary geology	32
2.2.3	Meteorology, hydrology and hydrogeology	33
2.2.4	Hydrogeochemistry	34
2.2.5	Surface ecology	36
2.3	Borehole investigations	37
2.3.1	Drilling activities	39
2.3.2	Measurements performed during and after drilling of boreholes	40
2.3.3	Sampling and analysis of intact rock material in several types of laboratory investigations	42
2.4	Monitoring	43
2.4.1	Background	43
2.4.2	Monitoring programme	43
2.5	Geographical data	44
2.6	Other data sources	45
2.7	Databases	45
2.8	Model versions prior to SDM-Site Laxemar	46
2.9	Model volumes and model areas	46
2.9.1	Regional model area and volume	47
2.9.2	Local model volume	47
3	Evolutionary aspects of the Laxemar-Simpevarp area	49
3.1	Bedrock evolution during Proterozoic and Phanerozoic	49
3.1.1	Bedrock geological evolution in south-eastern Sweden	49
3.1.2	Bedrock geological evolution in the Laxemar-Simpevarp area	52
3.2	Palaeoclimate and geological development during the Quaternary period	54
3.3	Seismicity during the Quaternary period	57
3.4	Groundwater evolution during the Quaternary period	59
3.5	Development of ecosystems during the late Quaternary period	61
3.6	Human population and land use	62
4	The surface system and surface-bedrock interactions	63
4.1	State of knowledge at the previous model version	63
4.2	Data evaluation and modelling	64
4.2.1	Overburden and Quaternary geology	64

4.2.2	Hydrology and near-surface hydrogeology	69
4.2.3	Chemistry	72
4.2.4	Transport properties	73
4.2.5	Ecosystems	75
4.2.6	Human population and land use	78
4.3	Surface system models	79
4.3.1	Digital Elevation Model (DEM)	79
4.3.2	Depth and stratigraphy of Quaternary deposits	80
4.3.3	Hydrological-hydrogeological models	82
4.3.4	Ecosystem models	85
4.4	Integration of surface and bedrock systems	89
4.4.1	Geology	90
4.4.2	Hydrology and hydrogeology	95
4.4.3	Hydrogeochemistry	98
4.5	Overall description of the surface system	100
4.6	Evaluation of uncertainties	101
5	Bedrock geology	103
5.1	State of knowledge at previous model version	103
5.2	Evaluation of primary data	104
5.2.1	Bedrock geological map at the surface	104
5.2.2	Rock units and possible deformation zones in the sub-surface	107
5.2.3	Rock types – properties, alteration, volumetric proportions, thickness and orientation of subordinate rock types	109
5.2.4	Ductile deformation	113
5.2.5	Comparison of the orientation of ductile structures and subordinate rock types	115
5.2.6	Brittle deformation and fracture statistics	115
5.2.7	Character and kinematics of brittle deformation zones	123
5.2.8	Identification and geological significance of lineaments	125
5.2.9	Identification and geological significance of seismic reflection data	129
5.2.10	Character and geological significance of seismic refraction data	130
5.2.11	Identification and geological significance of minor deformation zones	131
5.3	Overview of geological models in relation to data resolution	132
5.4	Deterministic model for rock domains	133
5.4.1	Data input	133
5.4.2	Conceptual model	133
5.4.3	Methodology, assumptions and feedback from other disciplines	134
5.4.4	Identification of rock domains, geometric models and property assignment	135
5.5	Deterministic deformation zone modelling	139
5.5.1	Geodynamic evolution – conceptual understanding	139
5.5.2	Influence of anisotropy in the ductile regime on deformation in the brittle regime	139
5.5.3	Concepts for the deterministic modelling	141
5.5.4	Characteristics of different sets of deformation zones and property assignment	144
5.5.5	Geometric model	158
5.6	Statistical model for fractures and minor deformation zones	160
5.6.1	Division into fracture domains	160
5.6.2	Modelling assumptions and data treatment	164
5.6.3	Derivation of statistical fracture model	164
5.7	Integrated geological model	173
5.8	Verification and validation of models	177
5.8.1	Verification of lithology and alteration in KLX27A	177
5.8.2	Verification of geological DFN models and the results of a validation test	178
5.9	Remaining uncertainties	179

6	Bedrock thermal properties	183
6.1	State of knowledge at the previous model version	183
6.2	Evaluation of primary data	183
6.2.1	Thermal conductivity from measurements	184
6.2.2	Relationship between thermal conductivity and density	185
6.2.3	Measurement of anisotropy of thermal conductivity associated with foliation	186
6.2.4	Heat capacity	187
6.2.5	Thermal conductivity vs heat capacity	187
6.2.6	Temperature dependence of thermal properties	187
6.2.7	Pressure dependence of thermal conductivity	188
6.2.8	Coefficient of thermal expansion	188
6.2.9	<i>In situ</i> temperature	189
6.3	Strategy for thermal modelling	190
6.3.1	Conceptual model	190
6.3.2	Modelling approach	191
6.3.3	Modelling assumptions	193
6.3.4	Feedback from other disciplines	193
6.4	Geostatistical analyses and stochastic simulations	194
6.4.1	Thermal Rock Classes (TRC) – Definition, properties and proportions	194
6.4.2	Geological heterogeneity and division into thermal subdomains	196
6.4.3	Spatial statistical models of lithology	196
6.4.4	Stochastic simulations of lithology	197
6.4.5	Spatial statistical models of thermal conductivity	199
6.4.6	Stochastic simulations of thermal conductivity	203
6.5	Thermal domain model	205
6.5.1	Domain modelling results	205
6.5.2	Evaluation of results of domain modelling	211
6.5.3	Summary of rock domain properties	211
6.6	Evaluation of uncertainties	213
6.6.1	Data uncertainty	213
6.6.2	Model uncertainty	213
6.6.3	Summary of uncertainties	215
7	Rock mechanics	217
7.1	State of knowledge at previous model version	217
7.2	Evaluation of primary data	217
7.2.1	Laboratory tests of intact rock	217
7.2.2	Laboratory tests of fractures	223
7.2.3	Rock mass quality indices RMR and Q	224
7.2.4	Stress data	226
7.3	Rock mechanics model	230
7.3.1	Intact rock properties	230
7.3.2	Fracture properties	231
7.3.3	Rock mass properties – Fracture domains	232
7.3.4	Rock mass properties – Deformation zones	235
7.3.5	Modelling of <i>in situ</i> state of stress	235
7.4	Evaluation of uncertainties	240
7.4.1	Uncertainty in mechanical properties of intact rock	240
7.4.2	Uncertainty in mechanical properties of fractures	241
7.4.3	Uncertainty in mechanical properties for rock mass	241
7.4.4	Uncertainty in the stress model	242
8	Bedrock hydrogeology	243
8.1	Context	243
8.1.1	Hydrogeological modelling in the SDM	243
8.1.2	Model development	243
8.1.3	Main characteristics of relevance to the model	245
8.2	State of knowledge at the previous model version	247

8.3	Evaluation of primary data	249
8.3.1	Basic characteristics measured by the various hydraulic tests	249
8.3.2	Basic characteristics of the single-hole tests	251
8.3.3	Evaluation of single-hole hydraulic tests	252
8.3.4	Comparison between Laxemar and Äspö	258
8.3.5	Evaluation of hydraulic interference tests	258
8.4	Conceptual modelling	259
8.4.1	Deformation zones and associated hydraulic data	259
8.4.2	Hydraulic rock domains and associated hydraulic data	263
8.4.3	The bedrock bordering the focused volume	268
8.4.4	The hydraulic soil domains (overburden)	270
8.4.5	Palaeohydrogeological conceptual model	270
8.5	Parameterisation of hydraulic conductor domains, and hydraulic rock domains	272
8.5.1	Hydraulic conductor domains (HCD)	272
8.5.2	Hydraulic Rock Domains (HRD)	274
8.5.3	Hydraulic soil domains	288
8.5.4	Summary comparison of HRD hydraulic properties	288
8.5.5	Comparison between model and KLX27A data	289
8.6	Regional scale flow model calibration	289
8.6.1	Numerical modelling approach	289
8.6.2	Palaeohydrogeological modelling	290
8.6.3	Matching natural groundwater levels	292
8.6.4	Matching the interference tests in HLX33 (and HLX28)	294
8.6.5	Matching the drawdown due to inflow to Äspö hard rock laboratory (HRL)	294
8.6.6	Matching hydrochemical data in cored boreholes	295
8.6.7	Comment in relation to outcome of LPT (HLX28)	303
8.7	Resulting bedrock hydrogeological model	304
8.7.1	Visualisations in support of hydrochemistry interpretation	307
8.7.2	Visualisations for interpretation of flow and solute transport	311
8.7.3	Average vertical flux rates versus depth	313
8.8	Parameter sensitivity analysis	314
8.9	Confidence and remaining uncertainties	318
8.9.1	Groundwater levels in the bedrock aquifer	318
8.9.2	Structural model (HCD)	318
8.9.3	Hydraulic rock domain (HRD) model	319
8.9.4	Compartmentalised fracture networks at repository depth	319
9	Bedrock hydrogeochemistry	321
9.1	Introduction	321
9.2	State of knowledge at the previous model version	322
9.3	Conceptual model	322
9.3.1	Major concepts	322
9.3.2	Model input	324
9.3.3	Working hypothesis on the past groundwater evolution	326
9.4	Hydrogeochemical data	328
9.4.1	Borehole groundwater chemistry data	328
9.4.2	Quality assured data	328
9.5	Explorative analysis and modelling	330
9.5.1	Initial data evaluation and visualisation	330
9.5.2	Supplementary data from borehole KLX27A	338
9.5.3	Mixing calculations	339
9.5.4	The redox system	340
9.5.5	Characterisation of microorganisms, colloids and gases	344
9.5.6	Studies of fracture fillings	346
9.5.7	Porewater composition in bedrock	350
9.5.8	Groundwater residence time	355
9.5.9	Evaluation of uncertainties in field data and interpretation methods	357

9.6	Hydrogeochemical site description	359
9.6.1	Background	359
9.6.2	Hydrogeochemical visualisation	359
9.6.3	Summary of hydrogeochemical characteristics	363
9.7	Consistency with the hydrogeological model	363
9.8	Confidence and uncertainty in the integrated hydrogeochemical model	365
9.8.1	Current groundwater evolution and composition	365
9.8.2	Overall confidence	366
10	Bedrock transport properties	367
10.1	State of knowledge at previous model version	367
10.2	Evaluation of primary data	367
10.2.1	Data and models from other disciplines	368
10.2.2	Transport data	368
10.3	Conceptual model	369
10.4	Transport properties of the bedrock	372
10.4.1	Overview of rock domains and fracture domains	372
10.4.2	Representative transport property data	375
10.4.3	Application of the retardation model	389
10.5	Flow-related transport properties	390
10.5.1	Conceptualisation of flow paths	390
10.5.2	F-factor estimation	392
10.5.3	Particle tracking results from paleohydrogeological simulations	394
10.5.4	Flow channelling	401
10.6	Transport of radionuclides	403
10.7	Field-scale confirmatory testing of transport properties	406
10.7.1	Multiple well tracer tests	406
10.7.2	Single well injection-withdrawal (SWIW) tests	407
10.7.3	Evaluation of tracer test data, interpretation and consequences for safety assessment	408
10.8	Evaluation of uncertainties	410
11	Current understanding of the site	413
11.1	The surface system	414
11.1.1	Evolution during the Quaternary	414
11.1.2	Description of the surface system	415
11.1.3	Human population and land use	418
11.2	Rock domains and their associated thermal and rock mechanical properties	418
11.2.1	Rock crystallisation and cooling history	418
11.2.2	Rock composition and ductile deformation	419
11.2.3	Rock domain model	421
11.2.4	Mineral resources	423
11.2.5	Thermal properties	423
11.2.6	Strength and other mechanical properties of intact rock	425
11.3	Deformation zones, fracture domains and fractures	426
11.3.1	Origin and reactivation throughout geological time	426
11.3.2	Deterministic deformation zones	427
11.3.3	Minor deformation zones	430
11.3.4	Fracture domains, fractures and geological DFN model	431
11.3.5	Fracture mineralogy	434
11.3.6	Mechanical properties of deformation zones and fractures	434
11.4	Rock stress	435
11.4.1	Stress evolution	435
11.4.2	Stress model	436
11.5	Bedrock hydraulic properties	438
11.5.1	Evolution	438
11.5.2	Hydraulic properties of deformation zones and hydraulic rock domains	438
11.6	Groundwater	442

11.6.1	Evolution during the Quaternary	442
11.6.2	Groundwater composition and water rock interactions	443
11.6.3	Groundwater flow and consistency with groundwater signatures	446
11.7	Surface – bedrock interactions	448
11.7.1	Rock types and fracturing	448
11.7.2	Hydraulic properties and surface-bedrock interactions	448
11.7.3	Hydrogeochemistry and redox buffering	449
11.8	Transport properties	450
11.8.1	Properties of the rock matrix	450
11.8.2	Flow-related properties	452
11.9	Overall confidence	454
11.9.1	Data usage	454
11.9.2	Key remaining issues and their handling	454
11.9.3	Handling of alternatives	455
11.9.4	Consistency between disciplines	455
11.9.5	Confidence statement	455
12	Conclusions	457
12.1	Fulfilment of objectives	457
12.2	Key remaining issues	457
12.3	Implications for the underground construction phase	457
13	References	459
Appendix 1	Topography and geographical names in the Laxemar-Simpevarp area	475
Appendix 2	Nomenclature	477
Appendix 3	Tables with references to primary data	483
Appendix 4	Borehole geometric data	525
Appendix 5	WellCAD composites for cored boreholes in the focused volume	531
Appendix 6	Properties of deformation zones modelled to intersect the focused volume between –400 and –600 masl	541

1 Introduction

1.1 Background

Radioactive waste from the Swedish nuclear power plants is managed by the Swedish Nuclear Fuel and Waste Management Co (SKB). The Swedish programme for geological disposal of spent nuclear fuel is approaching major milestones in the form of permit applications for an encapsulation plant and a deep geologic repository. For siting of the geological repository, SKB has undertaken site characterisation at two different locations, Laxemar-Simpevarp and Forsmark (Figure 1-1). The site investigations have been conducted in campaigns, with well-defined data freezes distributed in time. After each data freeze, the site data have been analysed and modelling has been carried out with the overall purpose to develop a site descriptive model (SDM). A SDM is an integrated model for geology, thermal properties, rock mechanics, hydrogeology, hydrogeochemistry, bedrock transport properties and a description of the surface system.

Airborne investigations in the Laxemar-Simpevarp area commenced in 2002, followed by the start of surface-based investigations in the Simpevarp subarea the same year. Site investigations in the Laxemar subarea in started in 2004, cf. Figure 1-2. The site descriptive model concluding the surface-based investigations in Laxemar, SDM-Site Laxemar, is compiled in the present report. Prior to this SDM-Site site descriptive model, three versions of site descriptive models have been completed preceded by version 0 /SKB 2002/ which established the state of knowledge prior to the start of the site investigation programme. Version Simpevarp 1.1 /SKB 2004a/, which was essentially a training exercise, was completed during 2004, followed by versions Simpevarp 1.2 in 2005 /SKB 2005a/ and Laxemar 1.2 in 2006 /SKB 2006a/. Version Laxemar 1.2 of the SDM, a preliminary site description, concluded the initial site investigation work (ISI). The model version accounted for in this report is denoted SDM-Site Laxemar. Each of these model versions are based on a well defined database of site characterisation data (data freeze) defined at a specified point in time, cf. Table 1-1.

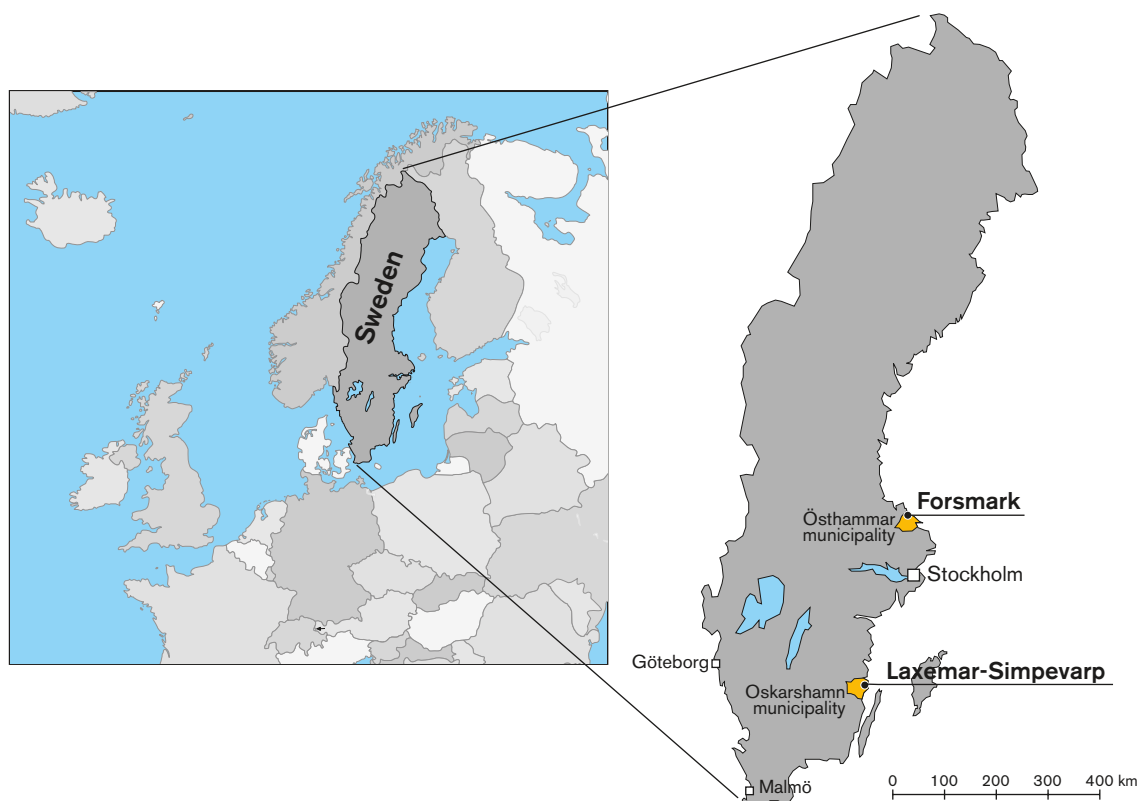
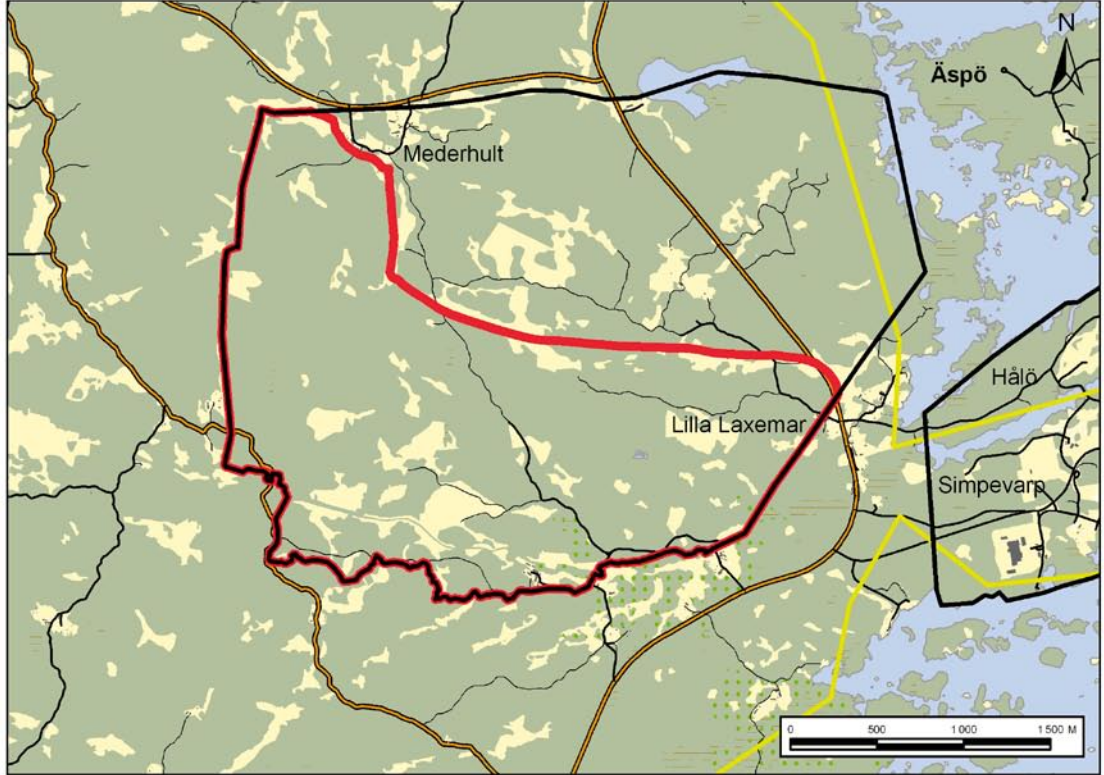
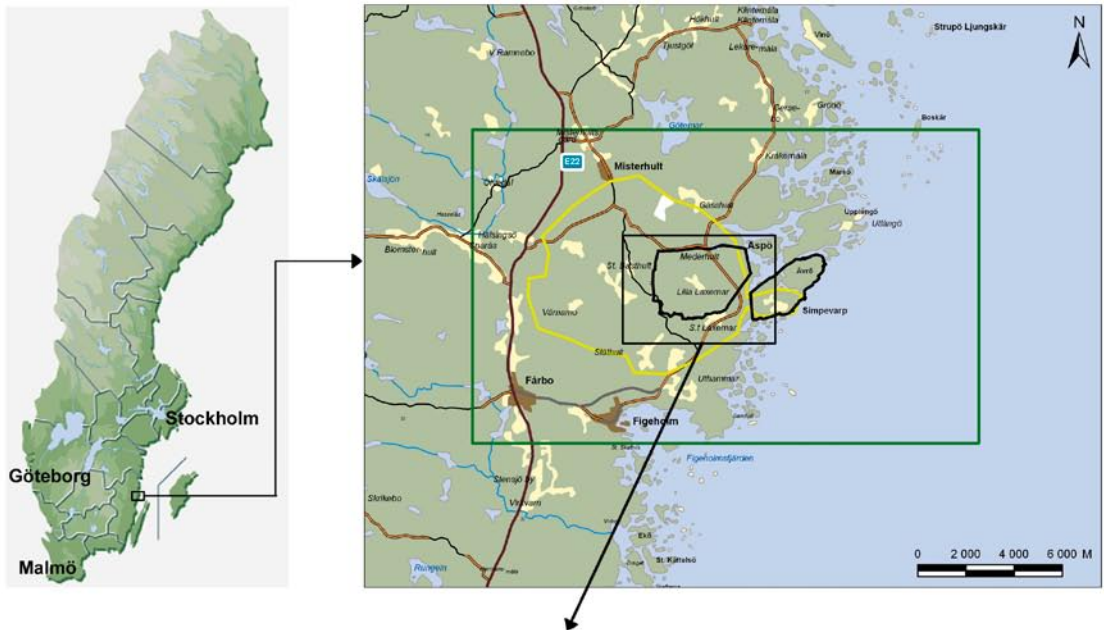



Figure 1-1. Map of Sweden showing the location of the Forsmark and Laxemar-Simpevarp sites.



-  Candidate area
-  Laxemar-Simpevarp regional model area
-  Laxemar and Simpevarp subareas
-  Focused area

Swedish Nuclear Fuel & Waste Management Co
 © Lantmäteriet
 2008-11-25, 10:25, htth

Figure 1-2. Overview of the Laxemar-Simpevarp regional model area and identification of the Simpevarp and Laxemar subareas.

Table 1-1. Summary of model versions and model steps employed in the site-descriptive modelling performed in the Laxemar-Simpevarp area and associated data freezes.

Model	Data freeze	Reference
Version Simpevarp 1.1	July 1, 2003	/SKB 2004a/
Version Simpevarp 1.2	April 1, 2004	/SKB 2005a/
Version Laxemar 1.2	November 1, 2004	/SKB 2006a/
Stage Laxemar 2.1	June 30, 2005	/SKB 2006c/
Version SDM-Site Laxemar	August 31, 2007(Laxemar 2.3) December 31, 2006 (Laxemar 2.2)	This report

In conjunction with finalisation of model version Laxemar 1.2 /SKB 2006a/ and the associated preliminary safety evaluation (PSE) /SKB 2006b/, SKB decided to proceed and complete the complete site investigation (CSI) in the Laxemar subarea /SKB 2007a/, thereby discontinuing any further detailed investigations in the Simpevarp subarea, cf. Figure 1-2. During the work on model version Laxemar 1.2, a need to further decrease the size of the investigated volume in the Laxemar subarea to cover the area considered suitable for a repository was identified. This resulted in the definition in December 2005 of a “focused area/volume” in the central, southern and southwestern parts of Laxemar /SKB 2005b/, cf. Figure 1-2. The boundaries of the focused area are to be regarded as indicative, and are not strictly geological.

Two descriptive modelling stages have been carried out at Laxemar during the complete CSI work, Laxemar 2.1 and SDM-Site Laxemar, cf. Table 1-1. An important component of each of these two stages was to address and continuously try to resolve uncertainties in the modelling of importance for repository engineering and safety assessment. Model stage 2.1 /SKB 2006c/ included important updates in the geological and hydrogeological models of Laxemar and also provided a feedback from the modelling team to the site investigation team to enable an optimised completion of the site investigation work. Only one model stage, encompassing the two data freezes Laxemar 2.2 and Laxemar 2.3, has established the different discipline-specific models which are synthesised into the current integrated site descriptive model SDM-Site Laxemar. The current SDM concludes the assessment of Laxemar based on surface-based site investigations and also constitutes the basic delivery to repository engineering (Design D2) and safety assessment (SR-Site).

1.2 Scope and role of the site description in the application process

Site characterisation should provide all data required for an integrated evaluation of the suitability of the investigated site for the construction of a deep geological repository. An important component in the characterisation work is the development of a site descriptive model.

Quality-assured data from site investigations, stored in the SKB database Sicada and the SKB geographic information system (GIS), are the input to site descriptive modelling that produces the site descriptive model. The site descriptive model is used by repository engineering to design the underground facility and to develop a repository layout adapted to the site. The site descriptive model also provides input to the safety assessment. Another important use of the site descriptive model is in the environmental impact assessment.

In order to ensure that all data and information needed for repository design and safety assessment are captured in the site characterisation work, there has been a mutual exchange of information between the various technical activities (Figure 1-3). Based on the preliminary site description (SDM Laxemar version 1.2), compiled from data collected during the initial site investigation phase (ISI), a preliminary repository layout (Laxemar step D1) /Jansson et al. 2006/ was established and a preliminary safety evaluation (PSE) /SKB 2006b/ as well as a safety assessment (SR-Can)

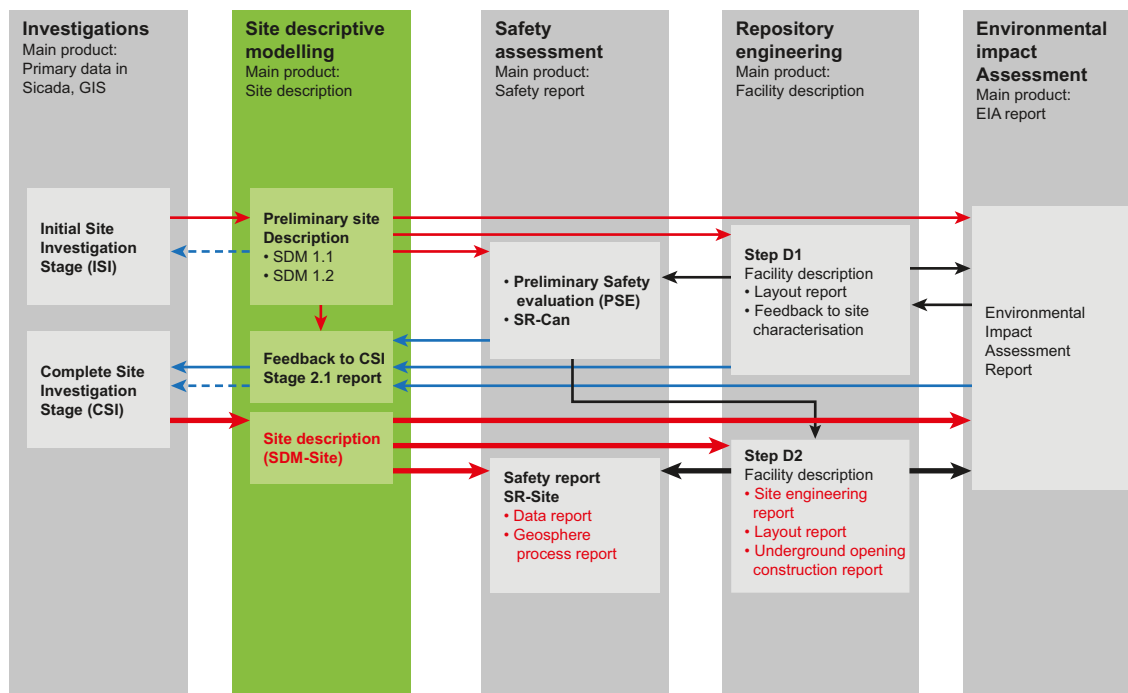


Figure 1-3. Mutual exchange of information between technical activities that provide data to site modelling or make use of the site description. Deliveries from (red arrows) and feedback to (blue arrows) site modelling are highlighted together with the final product from site modelling and the products of other technical activities that rely on this input.

/SKB 2006d/ were conducted (thin red arrows in Figure 1-3). In the course of the work on the repository engineering and the safety assessment, requests for new data and/or data with greater precision were made. This feedback (blue arrows in Figure 1-3) was included in the final programme for the completion of the site investigation phase. In addition to this formal feedback via the site modelling report from Laxemar stage 2.1 /SKB 2006c/, there has been another, less formalised feedback process continuously ongoing from site modelling to the site investigation programme (dashed blue arrows in Figure 1-3). Repository engineering and safety assessment will now update their work based on the final site description, SDM-Site Laxemar, which concludes the surface-based characterisation work (thick red arrows in Figure 1-3). The products within repository engineering that rely on an input from the site description are: the site engineering report (SER), the layout report and the rock production report. The corresponding reports in the safety assessment work are: the data report and the geosphere process report.

In the SKB programme, a site description is a description of the site covering the current state of the geosphere and the biosphere as well as descriptions of on-going natural processes that can affect their long-term evolution. However, it is not the task of the site description to present any predictions of the future evolution of site conditions. This is completed within the safety assessment based on the understanding of the current conditions and of the past evolution as compiled in the site description. Furthermore, it is not the task of the site descriptive modelling to evaluate the impact on current site conditions on the excavation or the operation of a repository at the site. This is carried out within the framework of repository engineering and as part of the environmental impact assessment, but again based on input from the site description.

1.3 Objectives and strategy

The overall objective of the Laxemar site descriptive modelling work is to develop and document an integrated description of the site, based on data from the complete site investigation work, to form a basis for a site-adapted layout of the final repository (Layout D2) and for assessment of the repository's long-term radiological safety (SR-Site). The description has to be based on a fundamental understanding of the bedrock and surface systems, which is achieved by analysing the reliability and assessing the reasonableness of the assumptions made with respect to the current state of Laxemar and naturally ongoing processes there. Furthermore, the work is required to make use of all knowledge and understanding embedded in previous model versions and also of the feedback obtained from the safety assessment SR-Can as well as of other types of feedback received on earlier versions of the site description.

The specific objectives of the work are to:

- analyse the primary data available from all surface and borehole investigations, including data from data freezes Laxemar 1.2, Laxemar 2.2 and Laxemar 2.3,
- describe evolutionary aspects at the site from the time the bedrock formed to the present day,
- develop a full three-dimensional integrated site descriptive model covering all disciplines,
- perform an overall confidence assessment including systematic treatment of uncertainties and evaluation of alternative interpretations, and
- perform modelling activities in close interaction with safety analysis and repository engineering.

The site modelling for SDM-Site Laxemar is based on data freeze Laxemar 2.3 (August 31, 2007) in its entirety. This decision was taken to safeguard inclusion of important information from south-western Laxemar, primarily detailed ground geophysical measurements from an enlarged area, and information from cored boreholes KLX15A and KLX16A. An additional cored borehole, KLX27A, was commissioned during the fall of 2007. Geometrical and tentative geological information from this borehole, although available subsequent to data freeze Laxemar 2.3, has been used in the geological modelling. Other additional data have also emerged from this borehole after data freeze Laxemar 2.3. As far as possible, these "late data" have been included in the modelling.

The strategy outlined above, see also Section 1.6, implies that all discipline-specific and interdisciplinary modelling was completed on the basis of data available at data freeze Laxemar 2.3, with select added data from borehole KLX27A. This also implies that each discipline has produced one individual background report. For further details on reporting structure and reports produced in support of SDM-Site, see Section 1.7.

1.4 Feedback from reviews and assessments of previous model versions

Feedback on previous model versions has been received by downstream users of the models and from reviews of the previous model reports by SKB's own international expert group Sierg, and also by expert groups set up by the authorities (the Insite and Oversight groups). In addition, the authorities' expert groups have continuously followed the progress of the work and the Insite group has regularly provided lists of issues of their concern to be handled in the modelling work. The handling of the issues raised has been documented by SKB as formal responses to Insite and SKI.

All feedback issues related to the Laxemar site descriptive modelling have been compiled and remaining issues have been addressed in the modelling work. A main task of the Laxemar stage 2.1 work /SKB 2006c/ was to identify and compile remaining important issues and uncertainties and suggest how these should be handled in the concluding site investigation and modelling work. The input to the compilation of issues was uncertainties in the preliminary site description of Laxemar /SKB 2006a/, the results of analyses conducted during Laxemar stage 2.1 /SKB 2006c/, the experiences from the work with repository layout D1 /Jansson et al. 2006/ and the preliminary safety evaluation (PSE) for Laxemar /SKB 2006b/. In the SR-Can safety assessment /SKB 2006d/, which is based on the preliminary site description of Laxemar /SKB 2006a/, remaining site characterisation issues of importance for assessing repository safety were identified and provided as feedback to the site investigation and site modelling teams. These issues have been addressed in the final stages of site descriptive modelling and the results were evaluated as part of the assessment of confidence and uncertainties in the site descriptive model at the conclusion of the surface-based site investigation work /SKB 2009/ and a summary is provided in Section 11.9.

1.5 Setting

Laxemar, which is part of the Laxemar-Simpevarp area, is located in the province of Småland, some 230 km south of Stockholm, within the municipality of Oskarshamn (County of Kalmar), and immediately west of the Oskarshamn nuclear power plant and the Central interim storage facility for spent fuel (Clab), cf. Figure 1-2 and Appendix 1. The Laxemar-Simpevarp area (including the Simpevarp and Laxemar subareas) is located close to the shoreline of the Baltic Sea, cf. Figure 1-4. The easternmost part (Simpevarp subarea) includes the Simpevarp peninsula which hosts the power plants and the Clab facility (cf. Figure 1-2) and the islands Hålö and Ävrö. The island of Äspö, below which the Äspö Hard Rock Laboratory (Äspö HRL) is located, is found some three kilometres northeast of the central parts of Laxemar. The Laxemar subarea covers some 12.5 km², compared with the Simpevarp subarea which is approximately 6.6 km². In the following, the term Laxemar local model area/volume (cf. Section 2.9) is used as the geographical reference in most instances while it covers the Laxemar subarea in its entirety.

The Laxemar-Simpevarp area is dominated by a 1.80 Ga suite of well preserved granitic, granodioritic, monzodioritic and gabbroic rocks belonging to the 1.86–1.65 Ga Transscandinavian Igneous Belt /SKB 2006a/. Dolerite dykes are also present but constitute a very subordinate lithological component in the bedrock /Wahlgren et al. 2008/. A non-uniformly distributed faint to weak foliation occurs, but the most prominent ductile structures are some low-grade, ductile high-strain zones of mesoscopic to regional character. Brittle deformation has given rise to small-scale fracturing as well as large-scale deformation zones, cf. Figure 1-5. The bedrock of interest for a planned repository is geologically relatively homogeneous and dominated by a rock with low quartz content, associated with fairly low thermal conductivity and moderate uniaxial compressive strength (UCS). The area of interest for a planned repository is bounded by subvertical deformation zones. No major gently dipping deformation zones are found. The intensity of conductive fractures in the rock between the interpreted deformation zones shows a clear decrease with depth, and is in the order of 0.06–0.22 m⁻¹ at approximate repository depth in the focused volume. However, below c. 650 m depth a significant additional decrease in the intensity of water conductive fractures occurs. Rock stresses are compatible with the situation at Äspö HRL with the greatest horizontal stress in a northwest-southeast direction (coinciding with the most transmissive vertical fracture set) with a magnitude of some 20–30 MPa at about 500 metre depth.



Figure 1-4. Air photographs showing the flat topography, low gradient near shore situation in the Laxemar-Simpevarp area with shallow bays, a) view from the southeast, Clab facility in the foreground, b) view from the west, drill site KLX05/KLX12A in the centre of the photograph. Both photographs show the outline of the focused area in Laxemar in red, cf. Figure 1-2.

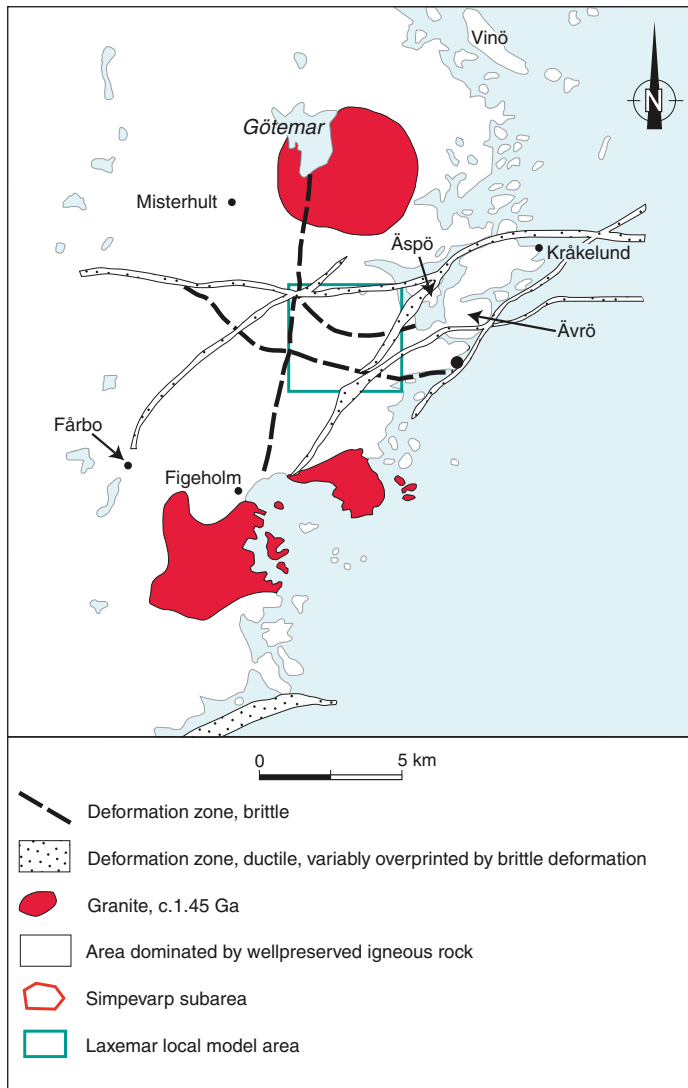


Figure 1-5. Schematic illustration of the geological situation at Laxemar (excerpt from Figure 1-4 in /Wahlgren et al. 2008/).

The Laxemar-Simpevarp area is part of the sub-Cambrian unconformity (peneplain) and is relatively flat with a gentle dip towards the east. The Laxemar-Simpevarp area is characterised by a mildly uneven topography at a relatively low altitude, but with marked both short and longer valleys/topographical depressions (Figure 1-6). The most elevated areas are located at c. 50 metres above the current sea level. The whole area is located below the highest coastline associated with the latest glaciation, and the area has emerged from the Baltic Sea during the last 11,000 years. The still ongoing shoreline displacement of c. 1 mm per year does not influence Laxemar, but will influence today's landscape closer to the shoreline of the Baltic Sea (Figure 1-7). Sea bottoms are continuously transformed to new terrestrial areas or freshwater lakes, and lakes and wetlands will successively be covered by peat.



Figure 1-6. Typical valley with steep sides. The valleys are partly filled with gyttja and peat (valley of River Laxemarån, southeastern Laxemar, 1549660 E, 6365710 N.).



Figure 1-7. An inlet with gyttja deposition in progress in the eastern part of the Laxemar-Simpevarp area (northeastern part of the island of Äspö, view to the west, 1551800E, 6368300N).

1.6 Methodology and organisation of work

1.6.1 Methodology

The site descriptive modelling project is multi-disciplinary, in that it covers all potential properties of the site that are of importance for the overall understanding of the site, for the design of the deep repository, for safety assessment and for the environmental impact assessment. The overall strategy applied in the work (Figure 1-8) has been to develop discipline-specific models by interpretation and analyses of the quality-assured primary data stored in the SKB databases Sicada and GIS, and to integrate these discipline-specific models into a unified site description. The quantitative, discipline-specific models are stored in the SKB model database Simon, from which quality-assured versions of the models can be accessed by the downstream users of the site description. Quality assurance aspects of the modelling procedure are further described in Section 1.6.4.

The site descriptive modelling comprises the iterative steps of evaluation of primary data, conceptual descriptive and quantitative modelling in 3D, and subsequent evaluation of the confidence in the resulting models. Data are first evaluated within each discipline and then the evaluations are cross-referenced/cross-checked between the disciplines. Three-dimensional modelling, with the purpose of estimating the distribution of parameter values in space, as well as their uncertainties, follows. In this context, the geological models provide the geometrical framework for all discipline-specific modelling. The three-dimensional description presents the parameters with their spatial variability over a relevant and specified scale, with the uncertainty included in this description. If required, different alternative descriptions should be provided.

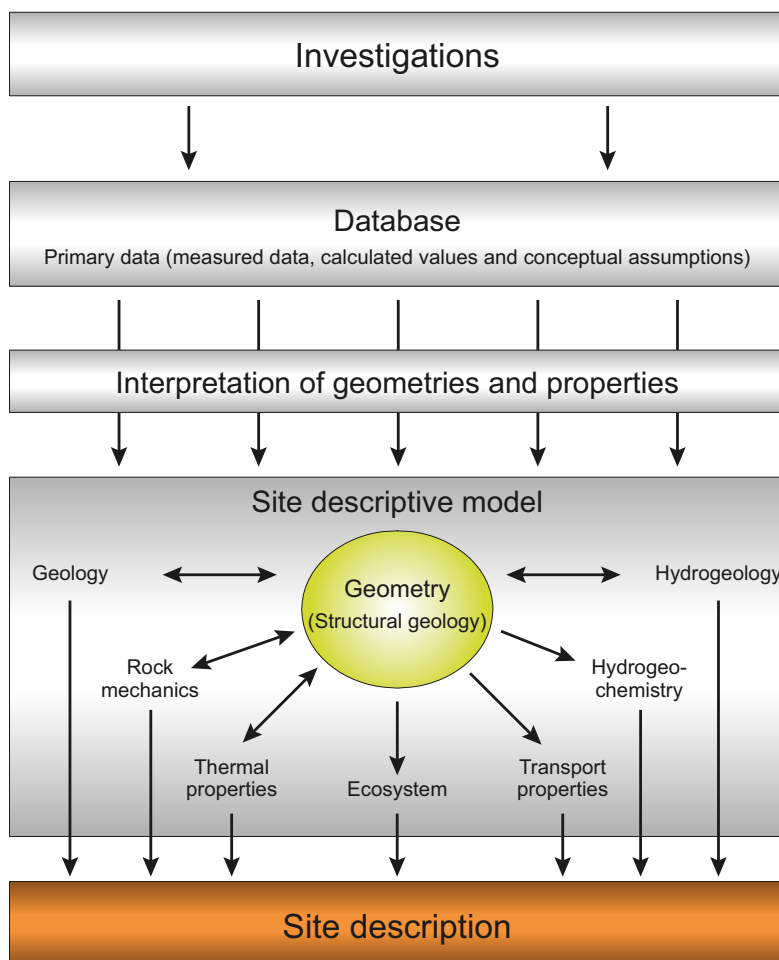


Figure 1-8. From site investigations to site description. Primary data from site investigations are collected in databases. Data are interpreted and presented in a site descriptive model, which consists of a description of the geometry of different features in the model and the corresponding properties of those features and of the site as a whole (modified after Figure 1-1 in /SKB 2002/).

Based on experience from earlier SKB projects, e.g. the Äspö HRL /Rhén et al. 1997abc, Stanfors et al. 1997/ and the Laxemar /Andersson et al. 2002c/ modelling projects, methodologies for constructing site descriptive models were developed and documented in discipline-specific strategy reports. The work conducted during the development of the preliminary site description /SKB 2006a/ followed the guide lines in these reports, which are:

- Geological site descriptive modelling /Munier et al. 2003/.
- Thermal site descriptive modelling /Sundberg 2003a/.
- Rock mechanics site descriptive modelling /Andersson et al. 2002a/.
- Hydrogeological site descriptive modelling /Rhén et al. 2003/.
- Hydrogeochemical site descriptive modelling /Smellie et al. 2002/.
- Transport properties site descriptive modelling /Berglund and Selroos 2004/.
- Ecosystem site descriptive modelling /Löfgren and Lindborg 2003/.

In addition, a strategy for achieving sufficient integration between disciplines in producing site descriptive models is documented in a separate strategy report for integrated evaluation /Andersson 2003/.

During the course of the iterative process of site descriptive modelling, considerable new experience on methodology issues has been gained. This has been worked into the methodologies applied and also, in some cases, resulted in updates or amendments to the strategy reports. The products expected from the geological discrete fracture network (DFN) modelling have been clarified and presented in detail in an updated version /Munier 2004/ of an appendix to the strategy document for geological site descriptive modelling /Munier et al. 2003/. The methodology applied for modelling of thermal properties has been considerably revised as compared with the methodology initially used. The updated strategy is based on stochastic simulations of lithologies and thermal conductivity as described in /Back and Sundberg 2007/. Finally, the strategy for hydrogeological modelling during the CSI stage has been updated to provide more focus on assessing and demonstrating the understanding of the hydrogeology and on describing the hydrogeological properties of potential repository volumes.

According to the strategy report for integrated evaluation /Andersson 2003/, the overall confidence evaluation should be based on the results from the individual discipline modelling and, thus, involve the different modelling teams. The confidence is assessed by carrying out checks concerning, for example, the status of primary data and their use, uncertainties in derived models, and various consistency checks. Procedures for this assessment have been progressively refined during the course of the site descriptive modelling at the two investigated sites, and applied to all previous versions of site-descriptive models of the Laxemar-Simpevarp area. Since the surface-based site investigations are now concluded and the current site descriptive model (SDM-Site Laxemar) is compiled with the purpose of supporting a license application to start construction of a repository for spent nuclear fuel, the approach has been further developed in order to address more specifically the confidence in the site description.

1.6.2 Interfaces between disciplines

For several of the disciplines involved in the SDM work, e.g. geology, hydrogeology and hydrogeochemistry, a distinction is made between the surface system and the bedrock system. The reasons for this distinction are both practical (large amounts of data, different objectives and different users of results) and historical, as the SKB work traditionally has been focused on the (deep) bedrock system. The delimitation between the surface and bedrock systems is, of course, artificial and somewhat arbitrary, but roughly speaking the surface system starts where the uppermost part of the bedrock ends.

Central to the description of the bedrock is the geological model which provides the geometrical context and the characteristics of deformation zones and the rock mass between the zones (see Section 1.6.5 for definitions). Using the geometric components of the bedrock geological models as a basis, descriptive models for other geoscientific disciplines (thermal properties, rock mechanics, hydrogeology, hydrogeochemistry and transport properties) are developed for the bedrock system.

Development of these models has in turn highlighted issues of potential importance for the bedrock geological model. Hydrogeology, geometry of deformation zones, hydraulic properties of the rock mass and applicable initial and boundary conditions over time largely govern the distribution of hydrogeochemical elements. The interface between hydrogeology and hydrogeochemistry has been handled, for example, by regional palaeohydrogeological simulations of variable-density groundwater flow from 8000 BC to present time.

The interface between the surface and bedrock systems has been considered in the evaluation of shallow and deep groundwater movement, as well as in the groundwater chemistry description. The present conceptualisation of the hydraulic properties of the Quaternary deposits is implemented into the near-surface hydrogeological modelling in the bedrock and also into modelling and evaluation of the impact of infiltration on the present groundwater composition. The shallow groundwater system is modelled so as to include the uppermost part of the bedrock with flow conditions that are consistent with the bedrock hydrogeological model (see Figure 1-9).

The handling of the interfaces between disciplines is described in more detail in Chapter 4 (surface system) and Chapters 5 through 10 (bedrock system).

1.6.3 Organisation of work

The work has been conducted by a project group with representatives of the disciplines geology, thermal properties, rock mechanics, hydrogeology, hydrogeochemistry, transport properties and surface systems. In addition, some group members (or affiliated experts to the group) have specific qualifications of importance in this type of project, e.g. expertise in RVS (Rock Visualisation System) modelling, GIS modelling and in statistical data analysis.

Each discipline representative in the project group has the responsibility for assessment and evaluation of primary data and for the modelling work concerning his/her specific discipline. This task was then carried out either by the representatives themselves, or together with other experts or groups of experts outside the project group. In this context, discipline-specific groups, set up by SKB, play an important role. These groups are the same for both the Forsmark and Laxemar site-modelling projects and they are essentially run by the discipline responsible, as assigned by SKB. The purpose of these groups is to carry out site modelling tasks and to provide technical links between the site organisations, the site modelling teams and the principal clients (repository engineering, safety assessment and environmental impact assessment). The discipline-specific, so-called Net-groups actively involved in the site modelling work are identified in Table 1-2.

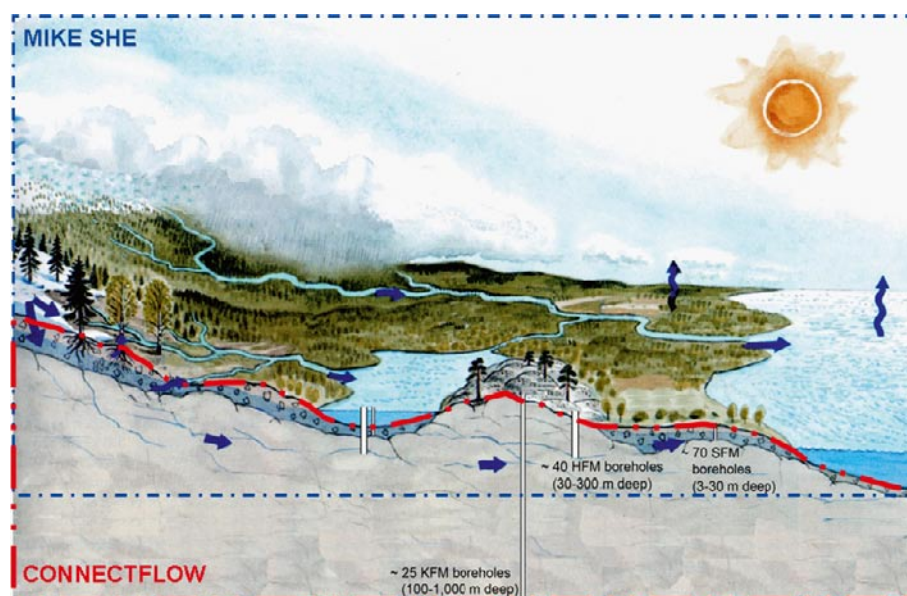


Figure 1-9. Generic cartoon showing how the modelling of the hydrologic cycle is divided into a surface-based system and a bedrock-based system. The former is modelled with the MIKE SHE code and the latter with the ConnectFlow code. Reproduced from /Follin et al. 2007c/.

Table 1-2. Discipline-specific analysis groups involved in site descriptive modelling and their mandate/objective.

Discipline	Net-group	Mandate
Geology	GeoNet	Provides a forum for the coordination of geological modelling tasks in both the Forsmark and Laxemar-Simpevarp site-modelling projects.
Rock mechanics and thermal properties	MekNet	Coordination of modelling tasks for rock mechanics and thermal properties at both sites. Resource for development and maintenance of method descriptions.
Hydrogeology	HydroNet	Execution of the hydrogeological modelling; constitutes a forum for all modellers within hydrogeology (needs of site modelling and safety assessment and repository engineering).
Hydrogeochemistry	ChemNet	Models the groundwater data from the sites and produces site descriptive hydrogeochemical models. Integrates the description with other disciplines and makes recommendations for further site investigations.
Bedrock transport properties	RetNet	Execution of the transport properties modelling; constitutes a forum for all transport related modellers within site modelling and safety assessment.
Surface system	SurfaceNet	Models and describes the surface system by description of subdisciplines (biotic and abiotic), models the properties in a distributed way (maps and 3D), models the interdisciplinary processes (over space and time), describes the different ecosystems (conceptually and in site-specific terms), describes and models the flow of matter in the landscape, defines and connects the biosphere objects, and produces site descriptions to support environmental impact assessment (EIA).

In addition to traditional project work, the project group has had several workshops together with representatives of the Laxemar site investigation team addressing uncertainties and overall confidence in the data collected and in the models produced. The objectives and scope of the uncertainty and confidence assessment have been modified during the course of the site descriptive modelling, reflecting the state of progress in the modelling work. During the initial site investigation stage, focus was on identifying important uncertainties in model versions Simpevarp 1.2 /SKB 2005a/ and Laxemar 1.2 /SKB 2006a/, and in data supporting these models, in order to guide further data collection and modelling activities. Similarly, the primary objective of the work conducted during Laxemar stage 2.1 /SKB 2006c/ was to provide feedback to the site investigations, in order to ensure that sufficient and relevant information was obtained during the remainder of the complete site investigation stage. The focus of the assessment of the final models included in SDM-Site Laxemar has been on addressing confidence in the models and on providing arguments for the confidence statements.

1.6.4 Quality assurance aspects

In order to ensure that the site descriptive model builds on qualified data and that the model and sub-models derived on these qualified data are correct and are actually the very models that are delivered to, and used by, the downstream users, a number of quality assurance procedures and instructions in the SKB quality assurance system have been followed. The process to progress from collection of primary data to models available to downstream users, as defined by the quality assurance procedures and routines and applied in the site modelling, is summarised briefly below.

All primary data collected in the field, from drill cores and from laboratory measurements are stored in the SKB databases Sicada and GIS. Before delivery to the database operator, the data are reviewed and approved by the person responsible for the field activity providing the data (activity leader). The database operator transfers the data to the database and then makes an internal order of the same data from the database. The data export from the database is then checked by the database operator and the activity leader to ensure that no mistakes have been made in the transfer of the data to the database. When everything is correct, the data are approved by the activity leader by signing the data. The execution of this process is specified in a SKB internal quality assurance document.

Only primary data collected at the site and stored in the databases Sicadea and GIS are used in the site descriptive modelling. Information regarding the procedures for data collection and circumstances of importance for the interpretation of data are given in the documentation (P-reports) of the data collection activity, but the hard data have to be ordered from the databases. Only data that are

approved (signed) are allowed for delivery to users. All orders and deliveries of data from the databases are registered, which means that it is possible to trace back all data deliveries. The execution of the process of order and delivery of data from the databases is specified in a SKB internal quality assurance document.

Errors in data identified during the subsequent analytical and modelling work are reported by the modeller who discovered the error. The errors are compiled in a list that is published on SKB's internal web site. It is also possible to subscribe to these error lists. It is the responsibility of the users of the data to report all errors found and to be updated on the data errors reported. For all errors reported, the type of error is identified and corrective actions are taken. The actions taken are documented in the data error list and corrected data are transferred to the databases according to the procedure described above. The procedures for handling non-conformance and errors in primary data are specified in internal SKB quality assurance documents.

The discipline-specific models developed within site modelling, using quality-assured data according to the procedures listed above, are stored in the SKB model database Simon. In this context, the term "models" refers to, for example, 3D models of the geometry of deformation zones, 2D models of surface objects, parameters for discrete fracture network models. Before the models are officially released to downstream users, they are approved by the person who is responsible for a specific discipline at SKB. The only models that are allowed for further use by e.g. repository engineering and safety assessment are the approved versions downloaded from the model database. The model database is also used for internal deliveries within the site modelling project. All downloads of models in the database are registered, which means that it is possible to trace when and by whom, any particular model was downloaded. Instructions for the use of the model database are compiled in a SKB internal quality assurance document.

1.6.5 Nomenclature

Some definitions are provided in Table 1-3 of terms that are of basic importance for the Laxemar site descriptive modelling and description. Most of these are geological terms that are related to the geometrical framework of the modelling and are, as a consequence, common to all disciplines. The definitions of geological terms are based on Section 2.4 in /Wahlgren et al. 2008/. Definitions of additional terms are provided in Appendix 2. Definitions of employed modelling areas/volumes are provided in Section 2.9 of the current report.

1.7 This report and supporting documents

This report presents the integrated understanding of Laxemar at the completion of the surface-based investigations and provides a summary of the models and the underlying data supporting the site understanding. The report is intended to describe the properties and conditions at the site and to give the necessary information essential for demonstrating understanding, but relies heavily on background reports concerning details of data analyses and disciplinary modelling. These background reports and their hierarchy in the SDM-Site reporting are illustrated in Figure 1-10 and are further described below.

Chapter 2 in this description summarises available primary data from Laxemar and provides an overview of previous model versions and other prerequisites for the modelling. In Chapter 3, the current understanding of the historical development of the geosphere and the surface system is described. Chapter 4 summarises the modelling of the surface system, with focus on aspects of importance for the bedrock system. The integrated description of the surface system is provided in one of the background reports (see Figure 1-10 and text below). Chapters 5 through 10 provide summaries of the modelling of the geology, thermal properties, mechanical properties, hydrogeology, hydrogeochemistry and transport properties of the bedrock, respectively. In Chapter 11, the integrated current understanding of Laxemar is provided, and Chapter 12 provides the overall conclusions from the work.

Table 1-3. Basic definitions applicable to the Laxemar site descriptive modelling and description, cf. Appendix 2 for additional definitions.

Laxemar-Simpevarp area	A general term for the Laxemar/Simpevarp region without a specified outer boundary. Essentially equating to the regional model area (see below) but also allowing for diffuse boundaries applied by the ecosystems modelling by SurfaceNET (partially adapting to groundwater divides). Note that for e.g. hydrogeochemistry purposes the entities "Oskarshamn" and KOV01 may be incorporated in the realm of this definition. The term "Laxemar-Simpevarp area" substitutes the previously used "Simpevarp area", with the same meaning/definition.
Candidate area	The candidate area refers to the area at the ground surface that was recognised as suitable for a site investigation, following the feasibility study work /SKB 2000/. Its extension at depth is referred to as the candidate volume.
Focused area/volume	The focused area in Laxemar refers to a part of the Laxemar subarea, primarily located in the southern part of the subarea, that was selected during the site investigation process as most suitable for hosting a final repository for spent nuclear fuel. Its extension at depth is referred to as the focused volume
Rock unit	A rock unit is defined in the single-hole geological interpenetration on the basis of the composition, grain size and inferred relative age of the dominant rock type. Other geological features including the degree of bedrock homogeneity, and the degree and style of ductile deformation also help to define and distinguish some rock units. N.B. Defined rock units differ between boreholes.
Rock domain	A rock domain refers to a rock volume in which rock units that show specifically similar composition, grain size, degree of bedrock homogeneity, and degree and style of ductile deformation have been combined and distinguished from each other. The term rock domain is used in the 3D geometric modelling work and different rock domains in Laxemar are referred to as RSMxxx.
Deformation zone	Employed as a general notation of an essentially 2D structure characterised by ductile or brittle deformation, or a combination of the two. Those deformation zones which are possible to correlate between the surface (lineament with a length > 1,000 m) and an interpreted borehole intercept, or alternatively between one or more borehole intercepts, or exhibit an interpreted true thickness >10 m are modelled deterministically, and are thus explicitly accounted for in the 3D RVS model. Deformation zones in Laxemar are denoted ZSM followed by two to eight letters or digits. An indication of the orientation of the zone is included in the identification code.
Fracture domain	A fracture domain is a rock volume outside deformation zones in which rock units show similar fracture intensity characteristics. Fracture domains in Laxemar are denoted FSMxx.
Repository depth	Normative depth and depth interval employed to sort and subvide data in the analysis and modelling. Repository depth at Laxemar is tentatively set to -500 m, with an interval of -400 to -700 m. The designated repository depth for Laxemar is subsequently set by Repository Engineering as part of their design D2.

The primary downstream user of bedrock geology, bedrock thermal properties, bedrock mechanical properties and hydrogeological properties, outside the site descriptive modelling team, is repository engineering for developing the underground repository design.

In addition to the discipline-specific background reports, there are two main background reports (level II) that provide important input to the site description. The procedure for, and results of, the confidence assessment of the site descriptive model are compiled in one of these reports. The other report is compiled jointly with the Forsmark site modelling project and describes the long-term geological evolution, the palaeoclimate, and the post-glacial development of ecosystems and the human population at the two sites.

Bedrock hydrogeology, in terms of hydraulic properties of fractures and deformation zones, is also essential input to the design of the underground parts of a repository. Therefore, the results of analyses and modelling to conceptualise the site, hydraulically parameterise deformation zones and the rock in between have been reported in a separate Level III report /Rhén et al. 2008/. Furthermore, the development of a conceptual flow model and the results of numerical implementation and testing of the developed hydraulic parameterisation of the bedrock using the developed regional scale flow model is reported in a Level III report by /Rhén et al. 2008a/ A summary and synthesis of the hydrogeological work are compiled in the main hydrogeology background report (level II), see below.

As a complement to Figure 1-10, the background reports (level II reports) providing direct information to the site description SDM-Site Laxemar are:

- Geology Laxemar, /Wahlgren et al. 2008/.
- Thermal properties Laxemar, /Sundberg et al. 2008a/.
- Rock mechanics Laxemar, /Hakami et al. 2008/.
- Bedrock hydrogeology Laxemar, /Rhén and Hartley 2009/.
- Bedrock hydrogeochemistry Laxemar, /Laaksoharju et al. 2009/.
- Bedrock transport properties Laxemar, /Crawford and Sidborn 2009/.
- Surface systems Laxemar, /Söderbäck and Lindborg 2009/.
- Confidence assessment Laxemar, /SKB 2009/.
- Geological evolution, palaeoclimate and historical development of the Forsmark and Laxemar-Simpevarp areas, Site descriptive modelling, SDM-Site /Söderbäck 2008/.

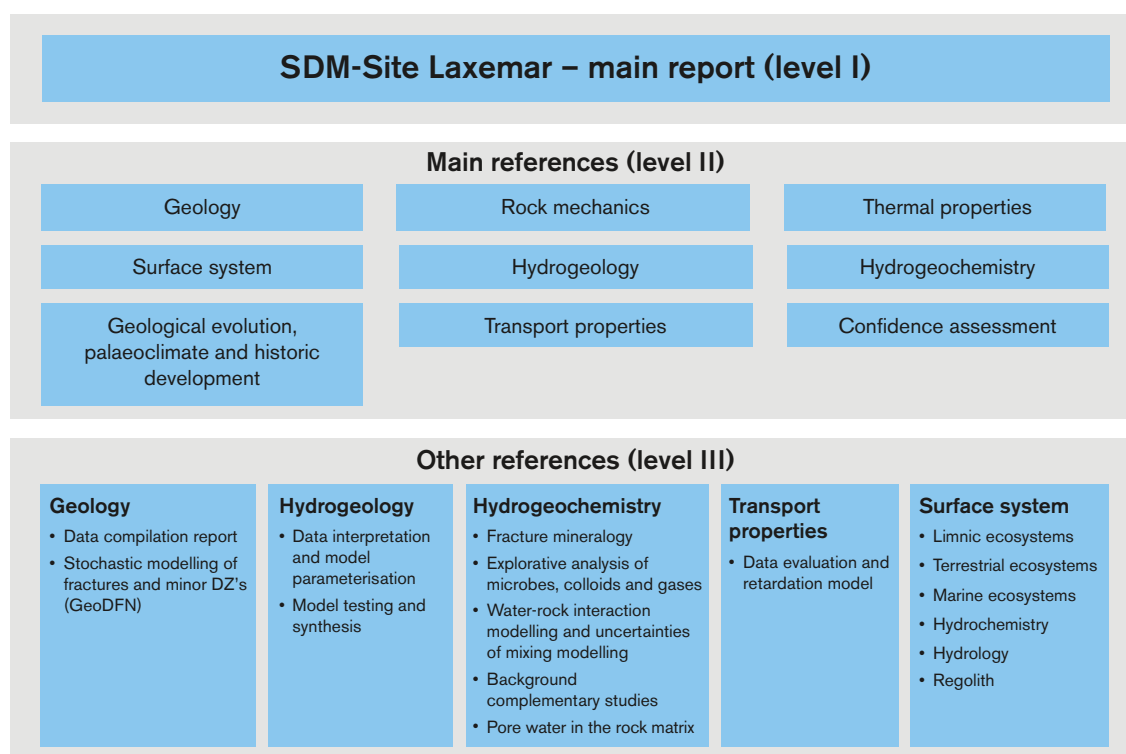


Figure 1-10. SDM-Site Laxemar main report and background reports on different levels produced during modelling version SDM-Site Laxemar.

2 Investigations, available data and other prerequisites for the modelling

Since the start of the site investigations in the Laxemar-Simpevarp area in mid 2002, successively more data have been added to the databases used in the site descriptive modelling. The modelling has now reached the final integrated model version – SDM-Site Laxemar. This chapter provides an overview of the investigations behind the databases used for modelling.

A short overview of all investigations carried out in Laxemar is presented in Section 2.1. The detailed comments on the different investigations in Sections 2.2 through 2.4 are limited to the investigations performed after the first comprehensive modelling, which was undertaken during 2005–2006 based on the investigation stage completed at data freeze Laxemar 1.2, i.e. this chapter primarily addresses the investigations carried out during the period November 1st 2004 to August 31st 2007, cf. Table 1-1. Some investigations occurred at a late stage and results could not be delivered in time for data freeze Laxemar 2.3. As a consequence, special efforts were made to include all relevant and indispensable data in the final models or, if excluded, to assess their implications for the final model version. This point is further commented on in Sections 2.2 and 2.3. Geographical data and other data sources for the modelling work are presented in Sections 2.5 and 2.6, respectively. Earlier site investigations in the Laxemar-Simpevarp area are described in more detail in /SKB 2006a/.

All reports presenting site characterisation activities and primary data (the P-reports) are listed in Appendix 3. The P-reports display data or references to data in the SKB Sicada and GIS databases and also present descriptions of the execution of these investigations and other relevant features. In this chapter, references are given to actual data sources (see Section 2.7 and Appendix 3), but data *per se* are provided in only a few instances and the reader is referred to Chapters 4 to 10 and /Söderbäck 2008/ for more details. Finally, a short summary of the model versions elaborated prior to model version SDM-Site Laxemar is presented in Section 2.8 and the locations of the areas and volumes employed in the modelling work are defined in Section 2.9. Where minor nonconformities in relation to the programme for drilling and borehole investigations are concerned, the reader is referred to the respective P-reports listed in Appendix 3.

2.1 Overview of investigations

This section presents a summary of the investigations forming the base for model version Laxemar 1.2, the preliminary site description, and also details the added contents of the last data freeze for the current SDM-Site Laxemar, cf. Table 1-1. As explained in Section 1.1 this last stage of modelling has also been preceded by a definite shift in focus and interest towards the southwestern parts of Laxemar. This has, for instance, involved expansion of the detailed ground surface geophysical grid to cover the quartz monzodiorite in the south, as well as the completion of boreholes KLX15A and KLX16A, and the further addition of borehole KLX27A, cf. Figure 2-5. The latter borehole, drilled with the aim of resolving very specific important objectives, was in fact started up at the time of data freeze Laxemar 2.3. This circumstance placed the last phase of modelling into some degree of disadvantage, and special efforts have been made to include all relevant and indispensable data in a timely fashion for the final model version or, if excluded, assess their implications for the final model version. The Laxemar 2.3 data freeze has therefore, to some extent, been adjusted in time discipline-wise, to ensure that no important data were left out of the modelling. “Late data”, that could not be used in the final model for a particular activity, but which have only been used, as appropriate, for verification or complementary analyse, are identified and presented separately below.

2.1.1 Investigations and primary data acquired up to data freeze Laxemar 1.2

Besides “older” data already included in model version 0, the data from Laxemar used in model version Laxemar 1.2 /SKB 2006a/ were acquired from the start of the site investigations in Laxemar from the beginning of 2004 until November 1 2004, but also included data related to modelling of the Simpevarp subarea /SKB 2004a, 2005a/, at the associated data freezes, cf. Table 1-1.

The data acquisition comprised three main categories of investigations, and this investigation structure was also applied for the succeeding data freezes. The three investigation categories were:

- 1) Geoscientific and ecological investigations of the surface. These included the compilation of bedrock and Quaternary geological maps.
- 2) Borehole investigations comprising:
 - a. Drilling of long, so-called telescopic boreholes (the upper c. 100 metres are percussion drilled whereas the remainder is core drilled), conventionally drilled cored boreholes, percussion boreholes and shallow boreholes through the Quaternary deposits.
 - b. Measurements carried out during drilling, investigations of drill cores and drill cuttings, and various types of down-hole borehole investigations. One example of these investigations is the geological mapping of drill cores using the Boremap system.
 - c. Sampling of intact rock material for several types of laboratory investigations.
- 3) Monitoring of geoscientific parameters and ecological objects. Monitoring has expanded successively during the entire site investigation period. The previous monitoring activities as well as the planned future monitoring after completion of the site investigations are presented in /SKB 2008b/.

The extent and character of data acquisition up to data freeze Laxemar 1.2 are described in detail in /SKB 2006a/ and associated P-reports.

2.1.2 Data freezes 2.1, 2.2 and 2.3 – investigations performed and data acquired

The investigations associated with data collection during the period between data freezes Laxemar 1.2 and Laxemar 2.3 comprised the three main categories of investigations mentioned in the previous section. Summaries of investigations made are presented in Sections 2.2 through 2.4. These summaries also include data that became available after data freeze Laxemar 2.3, here referred to as “late data”. In accordance with the earlier investigations, the data acquired during CSI were logistically and administratively subdivided into data freezes, cf. Table 1-1. Following each of these data freezes, analytical and modelling work was completed. Although the final round of SDM-Site Laxemar modelling commenced based on data freeze Laxemar 2.2, in particular the geological modelling, the major modelling activities were based on data freeze Laxemar 2.3, also incorporating “late data” for model verification, and for complementary analysis work.

Several of the field investigations (chemical monitoring) and associated laboratory analytical programmes (chemistry, retention properties of geological materials) had rather long execution periods, sometimes overlapping the indicated data freeze dates, and for some field investigations the time spent for data analyses and evaluations and delivery of P-reports exceeded the data freeze time limit. For this reason, and since all data have been used in one single step in the final modelling work for Laxemar, no subdivision into the three respective data freezes is made in the presentation below, with the exception of “late data”.

The major part of the site investigations performed after data freeze Laxemar 1.2 has been performed in compliance with the programme report for completion of the site investigations at Laxemar /SKB 2006b/. However, that report only provides a general framework for the activities. The detailed strategy regarding, for example, localisation of new boreholes, prediction of lithology, deformation zones and fracturing characteristics, selection of borehole sections for groundwater sampling, layout design for ground geophysical measurements etc was, to a large extent, designed through an iterative process, where previous results guided subsequent decisions concerning continued investigations. Important decisions regarding investigation strategy, primarily regarding new boreholes, have always been substantiated in so-called decision documents, which are registered in SKB’s internal documentation database “SKBdoc”. For late deep boreholes (KLX11 and onwards), the decision document has also been accompanied by a prediction of lithology, fracturing and the existence and geometry of deformation zones.

In conclusion, data from 46 cored boreholes in Laxemar (of which 19 reach depths below –500 m) and 43 percussion boreholes have been used in the modelling, cf. Appendix 4. Data from the cored borehole KLX27A (with the exception of basic geological data required for the modelling of rock domains and deformation zones) constitute “late data” used for verification purposes (in some cases preceded by prediction).

In order to maximise the available data for the SDM-Site modelling, select decisions were made to extend the data freeze in relation to the stipulated one. These were:

- Extended data freeze for bedrock hydrogeochemistry – November 30, 2007.
- Extended data freeze for monitoring of meteorology, surface water levels and -discharges, groundwater levels in the Quaternary deposits, and point-water heads in superficial rock – December 31, 2007.

2.2 Surface Investigations

The surface investigations performed in the Laxemar-Simpevarp local model area (and its surroundings) carried out between data freezes Laxemar 1.2 and Laxemar 2.3, cf. Table 1-1, involved the following disciplines:

1. Bedrock geology and ground geophysics.
2. Quaternary geology.
3. Meteorology, hydrology and hydrogeology.
4. Hydrogeochemistry (including surface waters and shallow boreholes in overburden).
5. Surface ecology (including marine and lacustrine investigations).

In the following sections, the investigations that have generated the new data sets are presented in greater detail according to discipline. Because of their close interrelation, bedrock geology and geophysical information are treated as one group.

2.2.1 Bedrock geology and ground geophysics

Investigations performed between data freezes L1.2 and L2.3

Following the bedrock mapping campaign performed during the site investigations up to data freeze Laxemar 1.2, the investigations at Laxemar have focused on providing improved insight in brittle structures through *geophysical measurements, lineament interpretation, characterisation of the bedrock in dug trenches* and *studies of the character and kinematics of deformation zones*, the latter both at the surface and in boreholes. Furthermore, a dedicated effort has been made to identify and characterise local minor deformation zones, both on the surface and in boreholes. Other investigations, including complementary geochronological studies, have also been completed.

No further *bedrock mapping* at Laxemar has been performed beyond that presented by /Wahlgren et al. 2005/. Minor complementary bedrock mapping campaigns have been conducted in conjunction with e.g. mapping of excavations, trenches and cleared outcrops in conjunction with drill sites, see below.

Detailed fracture mapping has been conducted at two surface excavations (drill sites for KLX09 and KLX11A/KLX20A) and along a total of 600 m dug/cleared trenches (divided into 10 segments) located in two different rock domains (cf. Section 5.4) and with variable orientations. The mapping of fractures along these trenches has been made in a 1 m wide corridor with a truncation length of 1 m. The trenches have also been subject to *high resolution photography* at 3 m altitude enabling *rectified photo mosaics* to be made along the studied trenches. The structural data from these trenches serve as complements to the information collected from the otherwise essentially vertical/subvertical boreholes.

A number of investigations have been conducted to serve as a basis for lineament characterisation and targeted investigations of minor local deformation zones (MDZ). These include *high resolution ground magnetic measurements* and *resistivity profiling and soundings*. These measurements originally only covered the northern and central parts of Laxemar, excluding areas south of the valley hosting the Laxemarån river and the interpreted deformation zone ZSMNW042A (cf. Figure 5-25). However, following the decision to enlarge the area of interest to include the quartz monzodiorite in its entirety, the detailed magnetic measurements were extended to the south. In addition, a number of magnetic profiles were extended further to the south, to cover a potential near east-west trending deformation zone south of the southern contact between quartz monzodiorite and Ävrö granite. To this information, low altitude aerial photographs and measurements by *airborne laser scanning technique* (Lidar) used to obtain a detailed high-resolution digital elevation model (DEM) of Laxemar, should also be added. *Refraction seismic measurements* have also been carried out along profiles that cover a large part of the Laxemar subarea, targeting primarily lineaments related to potential deformation zones. The geological and geophysical investigations were crowned by investigating selected lineaments by drilling (cf. Section 2.3).

A major study of predominantly brittle structures has been performed in three stages with the purpose of documenting the detailed character and kinematics of brittle deformation zones identified in the geological single-hole interpretation. Structural data were obtained from 19 cored boreholes covering some 65 deformation zones. In addition, structural data have also been obtained from outcrops in the Laxemar-Simpevarp area.

Geochronological studies comprising isotopic dating of minerals separated from whole-rock samples and specific minerals separated from fracture fillings have also been conducted.

The investigations described above, together with the previously performed surface mapping and other investigations (including reflection seismic surveys) have resulted in a bedrock geological data set of high quality and with a good density in data coverage.

Data available after data freeze L2.3

No additional data were used.

2.2.2 Quaternary geology

Investigations performed between data freeze 1.2 and 2.3

Investigations of Quaternary deposits were initiated in 2003 and continued during 2004. After data freeze Laxemar 1.2 most efforts have been directed towards stratigraphical studies, including determinations of physical and chemical properties. Most of these investigations were aimed at determining the depth and stratigraphy of the overburden in the valleys. These studies include results from both drillings and studies in machine-excavated trenches. A large number of observation points associated with geophysical activities have provided data on overburden depths in the terrestrial parts of the model area. All data concerning overburden depths and stratigraphy are presented in /Nyman et al. 2008/.

The most common Quaternary deposits in the regional model area were analysed for chemical, mineralogical and physical properties, and these data are compiled in /Sohlenius and Hedenström 2008/. Some of the data available at data freeze Laxemar 1.2 have been reinterpreted. The former soil type map was reinterpreted to be in accordance with the map of the Quaternary deposits. In the marine area, the map showing the distribution of Quaternary deposits was partly reinterpreted. A new map was constructed, which shows the interpreted distribution of Quaternary deposits in lakes and marine areas not included during the mapping programmes /Sohlenius and Hedenström 2008/. Physical properties of Quaternary deposits have been determined, in some cases with support from the literature.

Data available after data freeze L2.3

No additional data were used.

2.2.3 Meteorology, hydrology and hydrogeology

Investigations performed between data freezes L1.2 and L2.3

The time period of 34 months between the Laxemar 1.2 /Werner et al. 2006/ and Laxemar 2.3 data freezes implies that a substantially larger monitoring time series data set were made available for the SDM-Site Laxemar modelling, including meteorological data from the Äspö and Plittorp stations, lake- and sea-water levels and discharges in streams (Figure 2-1). Groundwater level data are also available from additional groundwater monitoring wells, including wells installed below Lake Frisksjön and in wetlands and bays of the Baltic Sea (Figure 2-2). In all 92 groundwater monitoring wells have been completed in the Laxemar-Simpevarp area, of which 50 have been completed during the period between the two data freezes. At the time of the Laxemar 2.3 data freeze, there were groundwater level monitoring data from a total of 76 wells, instrumented with automatic pressure transducers/loggers. Monitoring data from 58 wells were added during the period between the two data freezes. It should be noted that wells included in the monitoring programme and the associated monitoring periods have varied.

The Laxemar 2.3 data set also includes further hydrogeological property data, primarily for till in the Laxemar local model area. Whereas the Laxemar 1.2 data set contained data from slug tests in a total of 27 groundwater monitoring wells, by the Laxemar 2.3 data freeze, a total of 71 slug tests were performed. Further PSD (particle-size distribution) curves and data from so-called permeameter tests are also available for estimation of the hydraulic conductivity (including anisotropy) of the Quaternary deposits.

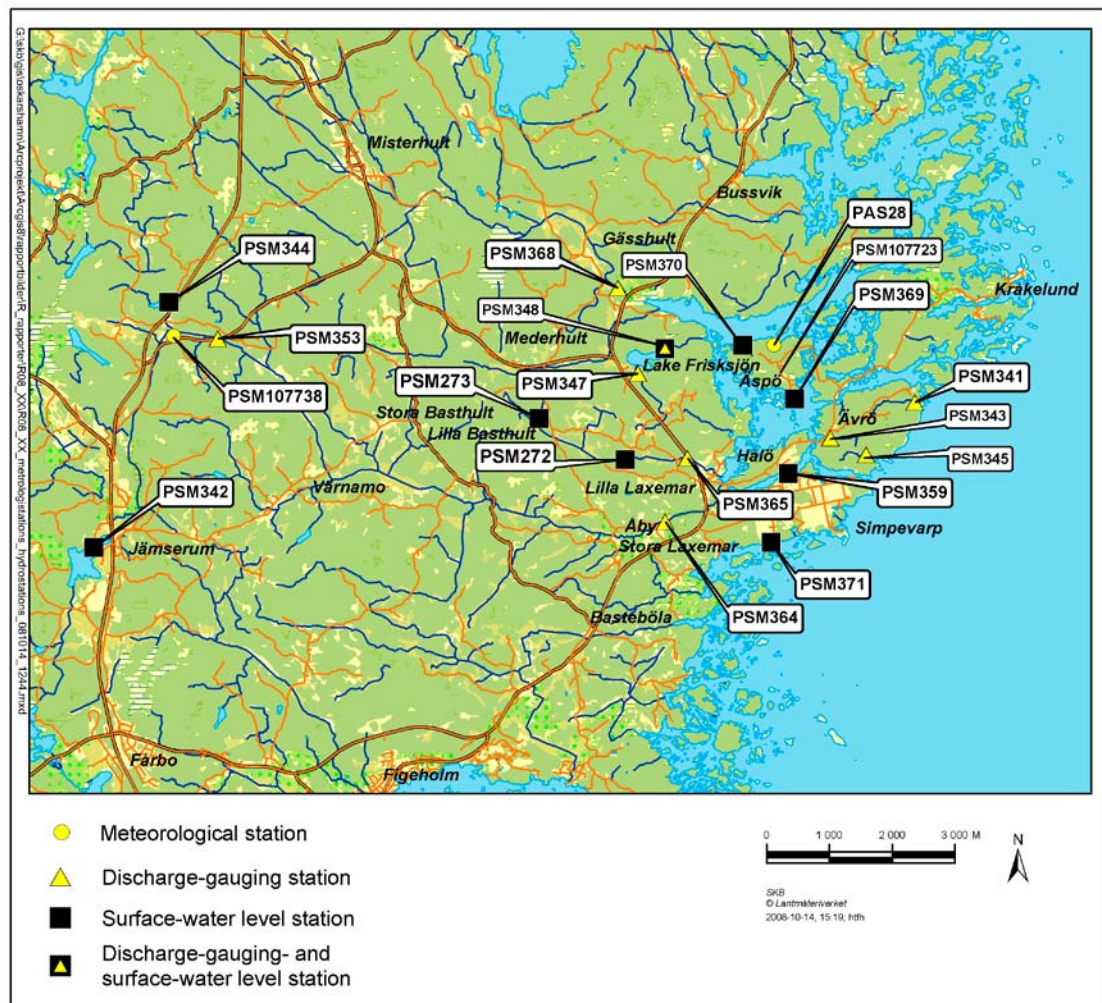


Figure 2-1. Overview map showing the locations of the Äspö and Plittorp meteorological stations and stations for monitoring of surface-water levels and -discharges.

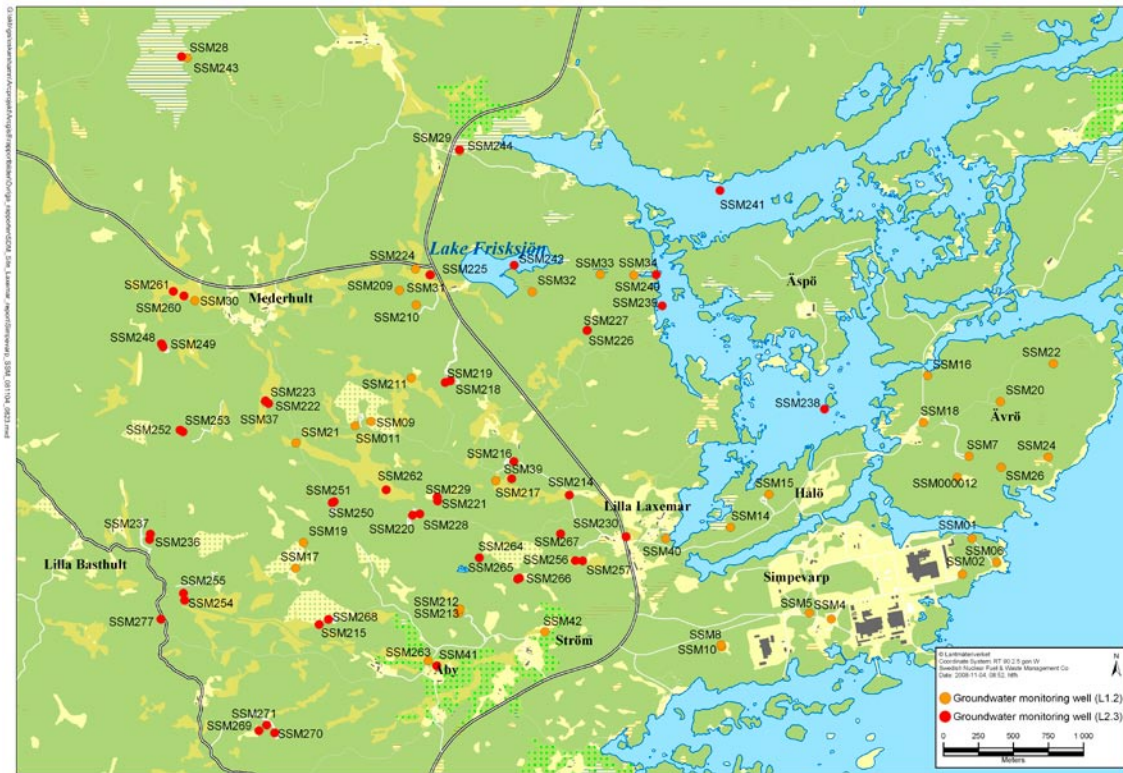


Figure 2-2. Overview maps showing the locations of groundwater monitoring wells installed up to the L2.3 data freeze. Groundwater monitoring well SSM000035 (not shown) is installed at the shore of Lake Jämsen, west of the area, cf. Appendix 1.

Between the two data freezes, single-hole and interference tests have also been performed in groundwater monitoring wells as a complement to the slug tests, including interference tests between percussion boreholes and groundwater monitoring wells. The latter type of test provides important information on Quaternary deposits and bedrock hydraulic interactions, in particular when combined with joint interpretations of undisturbed groundwater levels in the Quaternary deposits and point-water heads in the bedrock.

Data available after data freeze L2.3

Monitoring of meteorology, surface water levels and discharges, groundwater levels in the Quaternary deposits, and point-water head in the bedrock, continued after the Laxemar 2.3 data freeze. In the SDM-Site Laxemar modelling of hydrology and near-surface hydrogeology, an “extended” data freeze is adopted by using monitoring data available in the Sicada database for the period up to Dec. 31, 2007. By doing so, the conceptual and quantitative water flow modelling is based on data including the whole calendar year 2007.

2.2.4 Hydrogeochemistry

Investigations performed between data freezes L1.2 and L2.3

Hydrochemical samples from three different object types in the surface system in Laxemar-Simpevarp have been collected and analysed for a large number of hydrochemical parameters. The object types are:

- Surface waters – precipitation, lake, stream and sea water (Figure 2-3).
- Private wells and springs – drilled or dug wells and natural springs either representing shallow groundwater in the overburden or groundwater in the bedrock (Figure 2-4).
- Soil tubes – groundwater monitoring wells drilled in the overburden, usually not extending to more than 10 metres depth. The representative sampling depth corresponds to the location of the intake screen, usually the last metre of the soil tube (Figure 2-4).



Figure 2-3. Sampling sites for hydrochemical samples of surface water in the Laxemar-Simpevarp area.

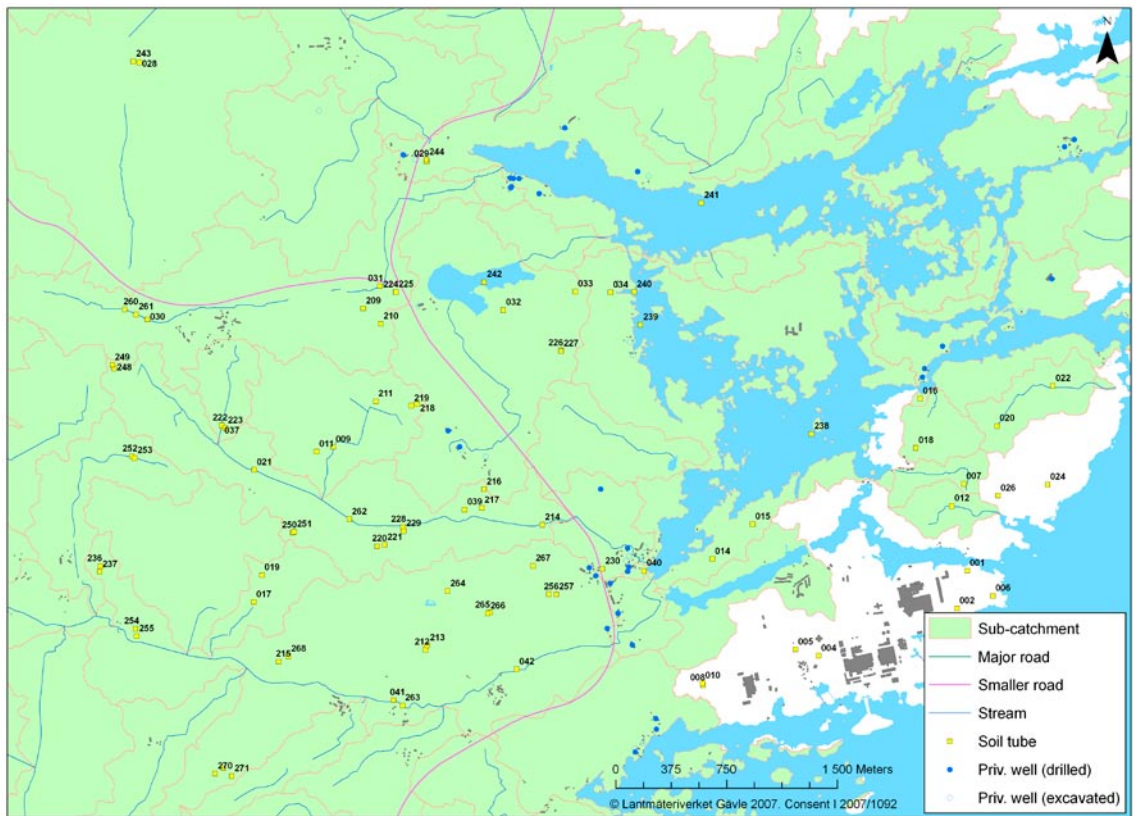


Figure 2-4. Sampling sites for hydrochemical samples of shallow groundwater in the Laxemar-Simpevarp area (soil tubes and private wells).

A detailed account of sampling frequencies and analysed parameters in the different sampling campaigns is given in /Tröjbom and Söderbäck 2006/ and /Tröjbom et al. 2008/.

Data available after data freeze L2.3

Monitoring of the hydrogeochemistry in the area continues after the Laxemar 2.3 data freeze. In SDM-Site Laxemar, some of the recent monitoring data from the soil tubes in Lake Frisksjön (PSM002065) and the sea basin Granholmsfjärden (PSM002064) have been used to verify conclusions drawn concerning discharge of deep groundwater.

Soil samples taken after data freeze Laxemar 2.3 from three different valleys in the Laxemar-Simpevarp area have been characterised for a number of parameters important for geochemical sorption. The analyses included chemical soil analysis, element analysis, mineralogical analysis and BET-surface analysis (BET is a method for measuring the specific surface area of a solid material by use of gas adsorption, see /Lundin et al. 2007/ for details). Analyses and resulting data are presented in /Lundin et al. 2007/.

2.2.5 Surface ecology

Investigations performed between data freezes L1.2 and L2.3

A variety of surface ecological investigations completed during the period from autumn 2004 to autumn 2007 are briefly described below. A more comprehensive description of the investigations and the resulting data is given in /Söderbäck and Lindborg 2009/.

Characterisation of the aquatic systems has been an essential part of the ecological investigations and included e.g. extensive inventories of phytoplankton, benthic vegetation, bacterioplankton and benthic bacteria, zooplankton, benthic macrofauna, and fish in the coastal area as well as in lakes. Furthermore, measurements of biomass and primary production, respiration and distribution of submerged vegetation have been conducted in both the marine and the limnic systems. These investigations are described in /Nordén et al. 2008/ for lakes and in /Wijnbladh et al. 2008/ for the marine system.

Investigations were carried out to estimate *soil respiration and primary production of the field layer* for four terrestrial vegetation types situated within the Laxemar-Simpevarp area. These investigations are described in /Löfgren 2008/.

Chemical characterisation of deposits and biota (213 samples) was carried out /Engdahl et al. 2006/. The samples from deposits consisted of sediment, peat and soil, and the biota samples were collected from terrestrial and aquatic environments. Besides the contents of the macro-nutrients carbon, nitrogen and phosphate, all samples were analysed for 51 chemical elements. The non-deposit samples were furthermore analysed for 10 additional elements (eight metals, P and Si), whereas for the deposit samples except peat the contents of the corresponding 10 oxides (i.e. of the same eight metals, P and Si) were determined.

In three machine-cut trenches /Sohlenius and Hedenström 2008, cf. Figure 2-6 therein/, determinations of ground *vegetation, surface organic layer and stoniness conditions* were made over the trenches. Further studies involved determining of *rooting depth, soil-profile development, soil physical conditions of the overburden including chemical properties* including soil acidity through pH measurements, as well as C, N and P contents and concentrations of alkaline earth cations. Data from these investigations are presented in /Lundin et al. 2005, 2006, 2007, Sohlenius et al. 2006/.

The *distributions of live and dead fine roots and live/dead root ratios* were analysed for trees and field layer species at three forest stands representing three different vegetation types within the Laxemar-Simpevarp regional model area. Data and results from the investigation are presented in /Persson and Stadenberg 2007/.

An investigation was made that provided *estimates of annual inputs of above-ground litter* from trees (dry mass and amounts of C and N), *litter decomposition and changes in organic and inorganic components in litter during decomposition*. Data were collected from three different sampling sites within the regional model area. The data and results from the investigation are presented in /Mjöfors et al. 2007/

The *process of material displacement, so called bioturbation*, by earthworms and ants was investigated in five sampling sites in the eastern part of the regional model area. Data and results from the investigation are presented in /Persson et al. 2006/.

Environmental samples (N=19) were collected within the regional model area and were analysed for several *artificial and naturally occurring radioisotopes*. The samples included soil and sediment, as well as plant and animal species, from terrestrial, limnic and marine environments. The data are presented in /Roos et al. 2007/.

Finally, *a selection of terrestrial mammals was surveyed* with snow tracking along line transects, aerial survey and faecal counts within and close to the Laxemar-Simpevarp investigation area and in the control area Blankaholm, north-west of Laxemar-Simpevarp. Rodents were surveyed through trapping. The investigations provided density data for fourteen wild species within the investigated areas. A compilation of all data relating to terrestrial mammals is given in /Löfgren 2008/.

Data available after data freeze L2.3

No additional data were used.

2.3 Borehole investigations

The performance and technical design of different types of boreholes drilled during the site investigation at Laxemar, telescopic boreholes, core drilled boreholes of standard type (non-telescopic), percussion-drilled boreholes in bedrock and shallow boreholes investigating Quaternary deposits (also designated soil boreholes, the majority of which are supplied with groundwater stand-pipes enabling groundwater level monitoring and groundwater sampling), are briefly described in /SKB 2006a/. Furthermore, detailed descriptions of each individual borehole are provided in associated P-reports.

The locations of all telescopic, conventionally core drilled and percussion drilled boreholes produced during the site investigation, i.e. up to data freeze Laxemar 2.3, are presented in Figure 2-5. The localisation of all soil boreholes supplied with groundwater stand-pipes is shown in Figure 2-2, where the drilling progress from data freeze Laxemar 1.2 to data freeze Laxemar 2.3 is also illustrated. Selected geometrical borehole characteristics of the telescopic and conventionally core-drilled boreholes and percussion-drilled holes in the Laxemar-Simpevarp area are presented in Appendix 4.

A major quality revision was undertaken between autumn 2006 and autumn 2007 regarding the orientation of geological structures (e.g. fractures, rock contacts, foliations) in boreholes for both Laxemar and Forsmark /Döse et al. 2008, Munier and Stigsson 2007/. These structures are identified during borehole logging with the so called Borehole Imaging Processing System (BIPS), a down-hole imaging system which, together with inspection of the drill core or, for percussion boreholes, drill cuttings, is used to support the so-called Boremap mapping. During the processing of the borehole imagery, the orientation of identified geological structures is calculated on the basis of borehole geometry and measured geometry relative to the borehole axis. The revision made was initiated due to a technical problem identified in conjunction with performance of the BIPS logging procedure. This problem caused the uncertainty of the orientation determinations of geological structures in some borehole sections to be unacceptably high. The quality revision comprised a re-check of all previously performed BIPS loggings and the correction of errors revealed.

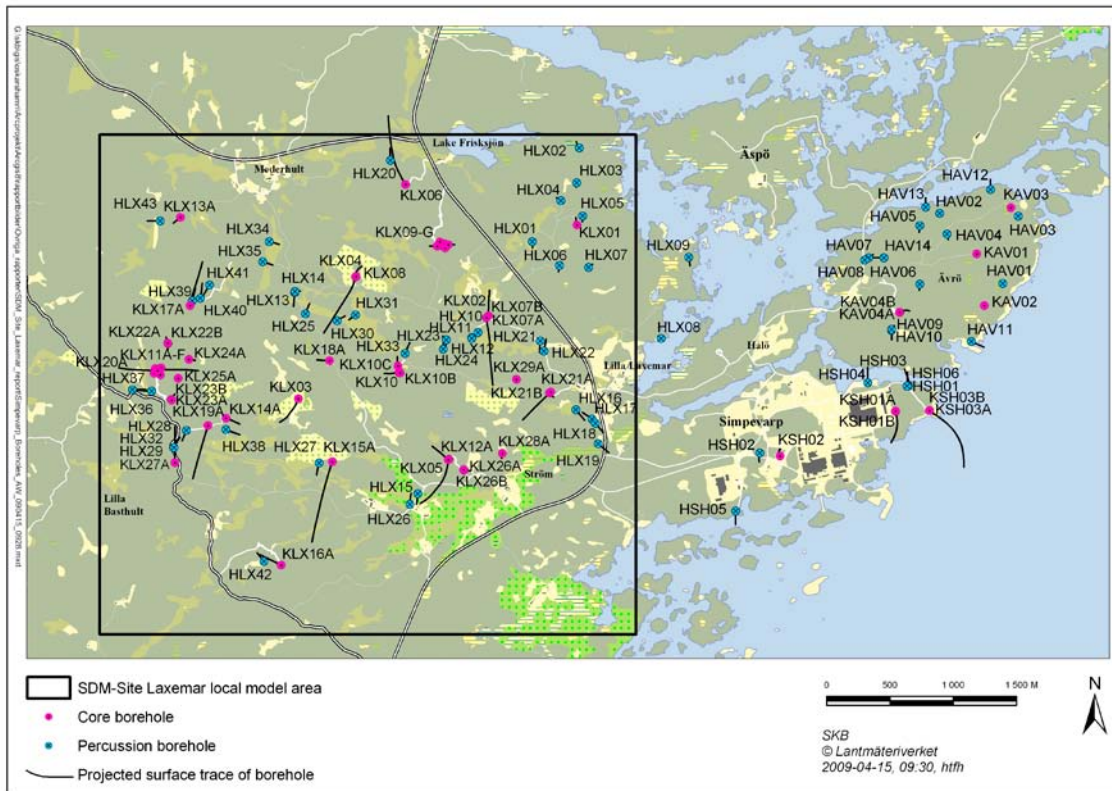


Figure 2-5. All telescopic, conventionally core-drilled and percussion-drilled boreholes produced during the site investigation at Laxemar and Simpevarp at data freeze Laxemar 2.3. The projected surface trace of inclined boreholes is also illustrated.

The accuracy in the orientation determinations is also dependent on the accuracy of the measurement of borehole geometry (or deviation) along its extent. Furthermore, precise borehole deviation measurements are crucial for reconciling data from different surveys of borehole logging into consistent interpretations based on correct positions in space. High quality borehole orientation data are also imperative for the modelling of rock domains (geometry of defined contacts) and, in particular, for deformation zones and fracture orientations used in the geological DFN modelling (see Section 5.6).

All cored and percussion drilled boreholes deviate more or less from the initial inclination and bearing at the top of the casing (the borehole collar). For this reason, the borehole location can not be described only by extrapolation of inclination and bearing at the borehole collar, but down-hole deviation measurements have to be conducted. Since full-scale *in situ* calibration of the deviation logging equipment is seldom possible (basically an intercept of a borehole by an underground opening is required), the only available quality measure is repeatability in performance, i.e. comparison of several deviation loggings conducted in the same borehole. A new strategy for deviation measurements was introduced which permits a combination and joint assessment of several deviation measurements. A quality revision of borehole deviation data was subsequently conducted for all boreholes, and new deviation data based on the new strategy were determined /Stenberg and Håkansson 2007/.

In combination, the quality revision of the BIPS loggings and deviation measurements resulted in a significant improvement, both regarding orientation data for geological structures and for borehole deviation data. Another important result of the revision was the introduction of uncertainty estimates for all relevant parameters. Two measures of the uncertainty of borehole geometry – elevation uncertainty and radius uncertainty – are tabulated in Appendix 4 for one or two levels in each borehole. For reasons of completeness, all cored and percussion boreholes in the Laxemar-Simpevarp area are included. Figure 2-6 illustrates the principles of computation of borehole deviation, i.e. the borehole geometry, from several measurements, and also displays the concept of radius uncertainty. The complete results of the revision of borehole geometry and orientation of rock structures were not available until late in the site investigation, i.e. after data freeze Laxemar 2.3. However, all relevant

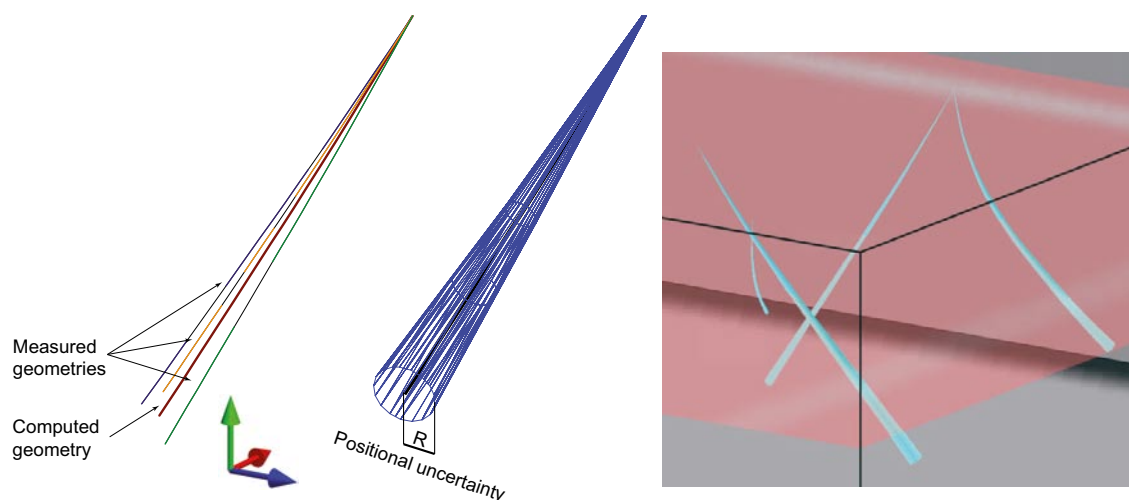


Figure 2-6. The figure to the left is an illustration of the principles for calculating the borehole geometry from several deviation measurements. The two other figures illustrate one of the uncertainty measurements introduced in connection with the SKB revision of borehole orientations. In the middle figure, “R” denotes “Radial uncertainty” given in Table 2-2 and Table 2-3. The figure to the right is a block diagram imaging four boreholes deviating in different ways and with radius uncertainty illustrated as blue cones (modified after /Munier and Stigsson 2007/).

analyses where orientation of geological structures plays an important role; discrete fracture modelling (DFN), rock domain modelling and deformation zone modelling, were able to include the corrected data and associated uncertainty measures.

2.3.1 Drilling activities

Investigations performed between data freezes Laxemar 1.2 and 2.3

Investigation data from cored boreholes for model version Laxemar 1.2 was largely provided from four cored boreholes (KLX01–KLX04, with KLX01 and KLX02 pre-existing in the area prior to the site investigations). A brief summary of all the data collection carried out from data freeze Laxemar 1.2 until data freeze Laxemar 2.3 is presented below for each type of borehole, and in approximate chronological order.

Additional information from the following boreholes in Laxemar has been collected during this period:

- 17 long (of which 15 extend below –500 m) telescopic cored boreholes for investigating conditions at depth and for verification of major local deformation zones : KLX05–KLX06, KLX07A–13A, KLX15A–KLX20A, KLX21B and KLX27A.
- 25 short to intermediate depth, conventionally cored boreholes (generally <150 m long, non-telescopic) primarily used to assess superficial fracture sets and to investigate local fracture zones: KLX07B, KLX09B–KLX09G, KLX10B–KLX10C, KLX11B–KLX11F, KLX14A, KLX22A, KLX22B, KLX23A, KLX23B, KLX24A–KLX26A, KLX26B and KLX28A–KLX29A.
- 14 percussion drilled boreholes: HLX30–HLX43.

Consequently, information for model version SDM-Site Laxemar is available from a total of 46 cored boreholes in Laxemar, including KLX01–KLX06 that were drilled at the time of the data freeze for Laxemar 1.2, of which 19 reach depths below –500 m. It should be noted that only 27 of these boreholes have a drill core and only 25 have detailed hydraulic test results from the upper 100 m of bedrock. Furthermore, a total of 43 percussion drilled boreholes exist in Laxemar. A total of 189 geotechnical drillings through the overburden are available, of which 85 were conducted during the period between the Laxemar 1.2 and Laxemar 2.3 data freezes.

Data available after data freeze Laxemar 2.3

All boreholes, with the exception of KLX27A, were drilled before data freeze Laxemar 2.3. P-reports from the following activities were not available until after data freeze Laxemar 2.3:

- Single-hole interpretation of cored borehole KLX27A.

2.3.2 Measurements performed during and after drilling of boreholes

Investigations performed between data freezes Laxemar 1.2 and 2.3

During and after drilling, the different categories of boreholes completed were subjected to standardised investigation programmes using geological, geophysical, hydrogeological and hydrogeochemical methods. In addition to different SKB method descriptions, these programmes are described in detail in /SKB 2006a/, and are not repeated here.

In the following, a summary is provided of the investigations performed from data freeze Laxemar 1.2 and onwards. The investigations are presented and grouped according to geoscientific discipline and, within each discipline, roughly in chronological order, although investigations to some extent have been conducted simultaneously. Data not available until after data freeze Laxemar 2.3 are presented separately. Comments on nonconformities in relation to original programmes and plans are given in the last part of this section.

The results from *standard geological and geophysical investigations and single-hole interpretations* became successively available from the new cored and percussion drilled boreholes as they were completed; cf. the account of the drilling succession in the previous section. However, the only investigations carried out in the shallow cored boreholes KLX09B–F and KLX11B–F were BIPS logging, Boremap mapping, PFL-f flow logging, deviation measurements and single-hole interpretation. *N.B. Fracturing data from KLX27A have not been used in the geological DFN modelling. Instead the data from this borehole have been used for comparing the developed geological DFN model with measured data.*

Results of density logs from KLX01–KLX10C, KLX12A–KLX13A, KLX17A–KLX18A, KLX21B and KLX28A–KLX29A were used to subdivide the Ävrö granite in its two varieties Ävrö granodiorite and Ävrö quartz monzodiorite. Subsequently, results from KLX05, KLX07, KLX08, KLX10–KLX13A, KLX15A–KLX19A and KLX21B were used for modelling the spatial correlation structure of thermal conductivity by variogram analysis.

Overcoring rock stress measurements were conducted successively during the drilling of KLX12A. Furthermore, *hydraulic fracturing (HF) and hydraulic tests on pre-existing fractures (HTPF)* were carried out in this borehole.

A study of borehole breakouts based on acoustical televiwer data from KAV04A (on Ävrö), KLX03, KLX04, KLX10, KLX11A, KLX12A, KLX15A, KLX17A, KLX18A and KLX21B was carried out in support of the stress modelling.

The new *single-hole hydraulic tests* comprised both flow logging (PFL-f, PFL-s) in KLX05A–KLX29A and double-packer injection tests (PSS) in KLX05–10B, 11A–13A, 15A–24A, 26A–28A. All new percussion drilled boreholes were tested with the HTHB-equipment and some of the boreholes were flow logged. *NB. Hydraulic test data from KLX27A have not been used in the hydrogeological DFN modelling.*

A number of *multiple-hole interference tests* were performed with different purposes. The two principal tests were pumping tests in HLX28A and HLX33A. The aim was to further increase the understanding of the hydraulic conditions in the area and to enable a large-scale, multiple-hole tracer test to be carried out.

Hydrogeochemical characterisation (Complete Chemical Characterisation, CCC) as well as microbial investigations were conducted in the telescopic boreholes KLX08A, KLX13A, KLX15A and KLX17A. Furthermore, groundwater chemical monitoring in packed-off borehole sections was carried out in boreholes KLX02, 04–06, 7A, 10, 11A–13A, 15A, 17A–19A. Also, chemical data were collected in conjunction with hydraulic tests (PSS) and single-hole tracer tests (SWIW) in KLX06, KLX11A and KLX19A.

In *percussion drilled holes*, *chemical characterisation* is carried out mainly by monitoring, i.e. recurrent sampling and analysis, in those boreholes which are supplied with monitoring equipment, see Section 2.4. However, groundwater sampling has also been carried out on other occasions, mainly during HTHB-logging, interference tests (in the pumping borehole) or sampling from boreholes serving as flushing water wells.

In situ formation factor logging was performed in boreholes KLX05, KLX06, KLX07A, KLX08, KLX10 and KLX12A and the results were compared with formation factors obtained in the laboratory by electrical methods.

In situ groundwater flow measurements using a dilution technique were carried out in KLX03, KLX11A, KLX18A and KLX21B. The objectives of these activities were to obtain information about groundwater flow under *in situ* (i.e. undisturbed) hydraulic gradients. Results from *SWIW-tests* were obtained from KLX03, KLX11A and KLX18A. In the case of the SWIW tests, the objective was to determine transport properties of groundwater flow paths in fractures/fracture zones.

Data available after data freeze Laxemar 2.3

Results from *standard geological and geophysical investigations and single-hole interpretations* from KLX27A were not available until after data freeze Laxemar 2.3.

The final results from *the major revision of borehole orientation measurements and orientation measurements of geological structures*, undertaken by SKB 2006–2007, became available during the later part of 2007 and during the spring 2008. In addition to inclusion of data in Sicada, the revision resulted in three P-reports and one R-report /Munier and Stigsson 2008/.

Hydrogeological investigations

Borehole KLX27A was PFL-logged and tested with the PSS method /Pöllänen et al. 2008, Enachescu et al. 2008/. The data were not used for the SDM modelling but have been used for comparison with the SDM-Site Laxemar hydrogeological DFN model results.

Groundwater flow measurements were performed in 2007 and 2008, cf. /Thur 2008, Harrström and Thur 2009/, as part of the monitoring programme and is planned to be made repeatedly once every year. The natural groundwater flow has also been measured in monitored sections as part of the sorbing tracer experiments, see below. Groundwater flow measurements with the dilution probe, have been made in eight borehole sections during late 2007 and are reported in /Thur and Gustafsson 2007/.

A sorbing tracer test was performed in the southern part of the focused area in late April 2008 and was finalised at the beginning of August 2008. The pumping well was HLX27, with nearby KLX15A as the tracer injection borehole. Pressure observations were made in several other boreholes in addition to KLX15A. The purpose of the test was to verify transport parameters previously obtained using other methods and to, at least partly, verify the hydrogeological model of the Laxemar local model area /Lindquist et al. 2009 (in prep)/.

A long-term pumping and tracer test (LPT) was started in late January 2009 with borehole HLX28 as the pumping borehole, 6 boreholes sections in the southwestern part of the focused area were used as tracer injection boreholes and a large number of borehole sections were used for pressure response observations. The purpose of the test is to verify and shed light on the connectivity between a number of deformation zones close to HLX28 and the transport properties of these zones.

Hydrogeochemical investigations

The data freeze for bedrock hydrogeochemistry was extended to November 30, 2007 in order to enable inclusion of analysis data from KLX15A, and analysis data from the monitoring performed in select packed-off sections of cored boreholes KLX02–05, KLX07A, KLX08, KLX10, KLX12A, KLX18A and KLX19A, performed during the summer of 2007. NB. Hydrogeochemical data from the new borehole KLX27A are not part of the site-descriptive modelling. However, the results have been used in a verification capacity in the site description and associated discussion where appropriate.

2.3.3 Sampling and analysis of intact rock material in several types of laboratory investigations

Drill core samples have been collected for different kinds of laboratory analyses throughout the duration of the site investigation in the Laxemar-Simpevarp area. The number of samples for rock mechanics and thermal analyses is especially abundant, but also sampling of drill cores has been made for modal and geochemical analyses, matrix pore water chemistry, analyses of fracture minerals, geochronological analyses and analyses of transport material properties (diffusivity and sorption). The most important events related to sampling/analyses of intact rock (including fracture surfaces) are presented below. These activities have provided large amounts of data and several P-reports.

Investigations performed between data freeze 1.2 and 2.3

Sampling of drill cores for the determination of the modal and geochemical composition of unaltered rock types has been carried from the following boreholes: KLX03, KLX04, KLX06, KLX07A, KLX07B, KLX08, KLX10, KLX11A, KLX12A, KLX15A, KLX16A, KLX18A, KLX19A, KLX20A and KLX21B.

Geochronological studies of rock forming and fracture minerals were carried out on drill core samples from KLX01, KLX02, KLX03, KLX06, KLX08 and KLX20A in Laxemar, KSH01, KSH03A and KSH03B in Simpevarp and KA1755A in the Äspö HRL as well as on samples from the access tunnel to the Äspö HRL. The objective of the study was to provide reliable geochronological constraints on the exhumation of the bedrock in the Laxemar-Simpevarp area and the identified fracture generations at Laxemar, cf. Section 9.5.6.

Sampling for testing of rock mechanical and thermal properties of both intact rock and fracture samples was to a variable degree performed on drill core samples from KLX05–KLX07A, KLX08–KLX09, KLX10–KLX13A, KLX15A–KLX20A and KLX21B. The microcrack volume was determined and triaxial compression tests were performed on drill core samples from KLX17A.

Results from the investigations of fracture minerals in boreholes KLX06, KLX07A+B, KLX08, KLX09B–G, KLX10, KLX11B–F, KLX13A, KLX14A, KLX15A, KLX17A, KLX19A, KLX20A, KLX26A were made available and a detailed study was also made of alteration of rock adjacent to fractures – red staining and saussuritisation – on material from KLX18A and KLX19A. The study involved mineralogy, geochemistry, porosity and redox properties of the altered rock and a comparison with fresh rock.

Special analyses to establish the redox front close to the ground surface included SEM + thin section, XRD+ICP (chemical analyses) + Uranium series analyses as well as analyses of stable O and C isotopes carried out on calcite samples. These investigations were carried out on fracture coatings from the shallow cored boreholes in the KLX09x and KLX11x arrays.

Results from rock matrix permeability measurements on core samples from borehole KLX03 became available.

Interconnected pore water was successfully extracted by laboratory out-diffusion methods from 60 samples from KLX03, KLX08 and KLX17A. The objective was to characterise these waters chemically and isotopically. Furthermore, the method of extraction, together with measurements of interconnected porosity, provided an opportunity to derive values of the *in situ* diffusion coefficient for the data collected from KLX17A, to be compared with the corresponding values derived from measurements on drill core samples in the laboratory.

Sampling of the drill cores from KLX06, KLX07A, KLX08, KLX10, KLX12A and KLX13A for investigations of transport properties was also carried out.

Data and/or P-reports available after data freeze Laxemar 2.3

- Batch sorption results related to complete drill core specimens and batch sorption data employing an additional water composition were used in the modelling.

2.4 Monitoring

2.4.1 Background

With a successively increasing number of instrumented surface and borehole installations, monitoring of geoscientific parameters and ecological objects has successively intensified during the course of the site investigation work. Monitoring is here defined as recurrent measurements of the same parameters/objects over time, such that time series are generated. The measured parameters and defined objects are characterised by a certain degree of time-dependent and site-dependent variability. The objectives of the monitoring are 1) to establish “undisturbed” conditions, the “baseline”, prior to a possible future siting of a deep repository, and 2) to enhance the knowledge about underlying, often complex processes that govern the time-dependent variations of the monitored parameters/objects.

The current monitoring programme in the Laxemar-Simpevarp area is briefly outlined in this section. The programme will, with a few modifications, continue after completion of the site investigations. The full extent of the programme from August 2007 onwards is described in detail /SKB 2008b/.

2.4.2 Monitoring programme

Monitoring of rock movements employing GPS techniques was initiated as a methodology study in 2000, i.e. before the site investigation started. The study was completed in 2004. The monitoring of seismic events is conducted within the framework of the Swedish National Seismic Network /Böðvarsson 2008/. One station is located within the Laxemar subarea and monitoring at this station continues after data freeze Laxemar 2.3.

Meteorological data have been acquired continuously from two weather stations, one in the western part of Laxemar and one located on the Äspö island in the east, where data have been recorded (with some interruptions) from October 2003 and July 2004, respectively. In addition, data have been collected from a number of SMHI-stations in a larger region around the Laxemar-Simpevarp area. Also snow depth and depth of frost in the ground, as well as ice coverage and ice break-up has been monitored every winter since the start of the site investigations in December 2002. The monitoring of these parameters continues after data freeze Laxemar 2.3.

During the site investigation work, water levels have been monitored at three locations in the Baltic Sea, in three lakes and in one water reservoir. Monitoring continues after data freeze Laxemar 2.3. Surface-water discharge is continuously measured, together with water temperature and electric conductivity, at 9 gauging stations in streams in the central parts of the regional model area (of which three are located on Ävrö). Also the monitoring of hydrological data continues after data freeze Laxemar 2.3.

The extent of monitoring of groundwater levels in boreholes in Laxemar has successively increased during the site investigations. At the end of 2007, groundwater levels were monitored in a total of 45 boreholes (i.e. all core drilled boreholes except KLX27A), all 43 percussion drilled boreholes and 70 groundwater observation wells in Quaternary deposits (variable in number over the duration of site investigations, the number given is applicable to the situation at the time of the data freeze Laxemar 2.3). The monitoring of groundwater levels continues after data freeze Laxemar 2.3, including borehole KLX27A instrumented with a multi-packer system.

Hydrogeochemical monitoring at Laxemar-Simpevarp includes precipitation, surface water, near surface groundwater (i.e. groundwater in Quaternary deposits), and deep groundwater (groundwater in bedrock). After the baseline chemical characterisation programme, which started in 2002, the sampling of precipitation, surface and near surface groundwater was changed to monitoring programmes in 2005–2006. The precipitation monitoring programme involves weekly sampling at one station. The hydrogeochemical monitoring programme of surface waters in 2007 involved monthly sampling in one lake, two sea bays and five stream sampling sites. The monitoring programme of near surface groundwater in overburden comprises 8 soil tubes sampled 4 times per year. The monitoring programme of precipitation, surface water and near surface groundwater continues after the data freeze Laxemar 2.3, with additional sampling sites in two streams.

Deeper groundwater (bedrock groundwater) baseline sampling was performed during and after drilling of percussion boreholes and cored boreholes, however, focused on a number of the cored boreholes (see Section 2.3.2). Boreholes were installed with multipacker systems to enable groundwater pressure monitoring and hydrogeochemical monitoring in selected sections. In order to enable sampling, these sections (typically one or two in the selected telescopic cored boreholes and one section in the selected percussion boreholes) were connected to the surface by means of a special tubing system. The monitoring programme in these respective cored and percussion boreholes was started upon completion of multipacker installation, i.e. at different times for individual holes. The hydrogeochemical monitoring involves sampling on two occasions every year. In 2007, the hydrogeochemical monitoring programme of deep groundwater comprised some 30 isolated borehole sections in 15 cored and 8 percussion boreholes. The monitoring/sampling activities during 2007 (and spring 2008) were modified in order to assist a complementary hydrogeochemical sampling campaign with focused objectives in the southern part of Laxemar.

There is also a programme for groundwater flow monitoring in boreholes. The flow is measured by means of the tracer dilution technique, cf. Section 10.7. This programme is closely linked to the programme for hydrogeochemical monitoring in cored and percussion boreholes. The two monitoring programmes make use of the same instrumented borehole sections, and in part also the same sampling equipment. Since 2005, one measurement campaign has been performed every year. The number of boreholes (mostly cored) and sections included in the programme has increased each year. From 2008, and onwards, the groundwater flow monitoring programme involves c. 11 packed off sections, distributed amongst c. 4 percussion boreholes and c. 5 cored boreholes.

Finally, the bird life and physiological status of the moose population (average age, weight and fecundity of the harvested moose in the area) have been monitored from the start of the site investigation programme, and will be continued.

2.5 Geographical data

The geographical data used for version Laxemar 1.2 coordinate system is the national 2.5 gon W 0:-15 RT90 system with X (easting) and Y (northing), the so-called RAK system. The elevation system used is the Swedish national system RH70/RHB70. The added notation RHB70 implies an increased local accuracy achieved through a local denser gridding. Identity should be assumed to exist between the RH70 and RHB70 systems if larger surfaces are considered. For individual reference points the difference may be in the order of a millimetre or two.

The Z coordinate in the RH70/RHB70 system is here expressed as an elevation in “metres above sea level” (m.a.s.l.) or (m). The latter implies that all data (whether surface or subsurface) are normalised to one common datum (the mean sea level). This facilitates comparison and discussion of variability in properties with depth irrespective of how the data points (boreholes) are distributed over the studied area. In consequence, the majority of subsurface data are associated with a negative number; either indicated as “- XXX *masl*” or “- XXX *m*”.

In the text the more casual “*at a depth of XXX m*” or “*vertical depth*” are used, implying that the given depth (or depth interval) is to be interpreted as being the corresponding elevation, omitting the minus sign. In this context a clear distinction is made between borehole length (m), i.e. a coordinate along the borehole axis, and elevation as defined above.

Various surveyed objects are related to different requirements on accuracy in the geodetic measurements. For example, boreholes (collar coordinates) have X,Y, Z coordinates measured within ± 0.010 m. Other objects, either hard to define or with less demand on precision, e.g. dug pits and rock specimens collected in outcrop, have X,Y, Z coordinates measured with GPS with an accuracy of within $\pm 1-2$ m. Quality assurance aspects related to borehole orientation data are discussed in Section 2.3.

In order to represent terrain relief, a digital elevation model (DEM) is an efficient tool. Such a model is a representation of a continuous variable over a two-dimensional surface by a regular array of Z-values referenced to a common datum. A DEM is required as input data for many types of surface models such as hydrological models, geomorphological models *etc.*

Two alternative DEMs were produced for the Laxemar-Simpevarp area; one version describes land surface, sediment level at lake bottoms, and the sea bottom, the other version describes land surface, lake water surface, and sea bottom. Ordinary Kriging in ArcGis 9 Geostatistical Analysis extension was chosen as the interpolation method /Davis 1986, Isaaks and Srivastava 1989/ for the DEMs. In the version that displays lake and surface water levels, the cells representing lake beds were replaced by cells representing lake water surface elevation using the Spatial Analyst extension in ArcGis 9.

Input data for the interpolation have many different sources, such as existing DEMs, high resolution Lidar imagery, elevation lines from digital topographical maps, paper nautical charts, digital nautical charts, and depth soundings in both lakes and the sea. All data were converted to point values using different techniques. The Kriging interpolation was performed in the ArcGis 8 Geostatistical Analysis extension. Both DEMs were produced on a 20×20 m grid. For more detailed descriptions of the data from which the DEMs have been derived, see /Strömngren and Brydsten 2008, Söderbäck and Lindborg 2009/.

The Lidar imagery data, which produced a high-resolution DEM on a 0.25 m grid, was also used in the geological lineament interpretation, cf. Section 2.2.1.

2.6 Other data sources

One obvious near proximity source of data is the database associated with the already performed investigations in the Simpevarp subarea, cf. Figure 1-3. This also includes old surface and borehole information from investigations performed on the islands of Ävrö and Hälö before the onset of site investigations. These databases have been used for establishing the current geological models and associated descriptions (rock domains and deformation zones) outside the local model area for SDM-Site Laxemar, cf. Figure 2-4. The associated databases are detailed in /SKB 2004a/ and /SKB 2005a/.

Another extensive source of information is associated with the characterisation and associated descriptive models available from the Äspö HRL. The position taken by the site descriptive modelling project is to make use of selective information important for filling voids in the data needs of the current modelling process. The aim is not to integrate the vast Äspö HRL database in its entirety. Examples of data of interest are various generations of geological data, models and descriptions of deformation zones and compilations of hydraulic test data, used when developing the geological and hydrogeological site-descriptive models. In the context of calibrating the parameterisation of large-scale site descriptive flow models, the drawdown caused by the successive development of the Äspö HRL is of importance. /Hartley et al. 2007/ showed that the effects of development of Äspö HRL on conditions in south/central Laxemar are minor, see also Section 8.6. Furthermore, compilations of transport properties (and associated data on geology/mineralogy) and conceptual microstructural models of rock fractures relevant to Äspö conditions have been used in the development the bedrock transport models, cf. Section 10.3.

Old data are also available from the construction of the three nuclear power reactors on the Simpevarp peninsula (and associated tunnels and storage caverns). Yet another source of old data originates from the site characterisation and construction of the central storage facility for spent nuclear fuel (Clab I and Clab II). The latter data were mainly used for reference.

2.7 Databases

The basis for the modelling work is quality-assured data acquired during the site investigations that are extracted from the two SKB databases Sicada and GIS. All available data are listed in tables provided in Appendix 3. The purpose of these tables is to give reference to and accounts of all the data that were available for consideration in the modelling work. Data *per se* are not given, but a specification and a reference to the associated P-report where the data and data collecting activity are described is provided. The use of these data in the modelling work, discipline by discipline, is also addressed in the tables in Appendix 3.

Quality assurance aspects related to the handling of data in the modelling work are described in Section 1.6.4.

2.8 Model versions prior to SDM-Site Laxemar

Prior to the current site descriptive model SDM-Site Laxemar, one complete and integrated site descriptive model for Laxemar has been produced (Laxemar 1.2), preceded by two complete integrated site descriptive models for Simpevarp (Simpevarp 1.1 and 1.2), cf. Table 1-1. The preceding Version 0 /SKB 2002/ was developed on the basis of the information available at the start of the surface-based site investigation programme. This information was mainly 2D in nature and general and regional, rather than site-specific in content.

Model versions 1.1 and 1.2 focused on the Simpevarp subarea, were developed based on data from the initial site investigation stage (ISI). Version Simpevarp 1.1 /SKB 2004a/, which was a training exercise, was built on a rather extensive set of data from the surface, whereas the data sets from boreholes were limited to two new c. 1,000 m deep cored boreholes and three new c. 150–200 m deep percussion drilled boreholes. Version Simpevarp 1.2 /SKB 2005a/ was based on data from 4 new deep cored boreholes and six new percussion drilled boreholes.

Model version Laxemar 1.2 /SKB 2006a/ constituted a transition in focus from Simpevarp to Laxemar, but retained a local model area which also included the Simpevarp subarea. A very modest amount of borehole data from Laxemar existed at the time, only some 10 months after SKB acquired access to the Laxemar subarea, largely providing information related to the northern part of the subarea. Still, and despite the lack of confirmatory drilling, the rock domains and major deformation zones were outlined with reasonable accuracy. Also, the investigations established the basic understanding of the importance of the mineralogical composition of the rock for the distribution of thermal properties and the mechanical strength. However, and in strong contrast, the information for assessing the distribution of hydraulic material properties and the distribution of hydrogeochemistry was limited. In the description of the surface system, some first steps were taken towards a unified description of the carbon cycle of the terrestrial, limnic and marine ecosystems.

Model stage Laxemar 2.1 did not constitute a complete model version. The objective of this step was to help define how to finalise the complete site investigations. At the time of the formal data freeze (June 30, 2005) new borehole data were available from KLX05–KLX07 and partly from KLX08 and KLX09, cf. Figure 2-5. To elevate the description and feedback to the site investigations further, and in particular regarding the hydraulic conditions in the southern parts of Laxemar, hydraulic data from KLX08, KLX10, KLX11A and KLX12A (obtained after the formal data freeze) were also analysed. A noted bimodal distribution of thermal properties in the Ävrö granite pointed to a need to subdivide the Ävrö granite based on mineralogical content. The results of the modelling were found to confirm the overall results of the Laxemar 1.2 modelling, the exception being the hydraulic analysis, which indicated more favourable hydraulic conditions in the southern parts of Laxemar as established on the basis of 100 m WLP hydraulic tests /SKB 2006c/. Furthermore, the identified list of site-specific critical issues was found to be largely covered by the complete site investigation programme to be launched /SKB 2006b/. The investigations proposed discipline-wise were expected to answer the remaining issues and uncertainties.

2.9 Model volumes and model areas

The site descriptive modelling is developed using two different model volumes of different scales, the *regional* and the *local* scale model volumes. Generally, the local model is required to cover the volume within which the repository is expected to be positioned, including accesses and their immediate environments. In addition to the description on the local scale, a description is also devised for a much larger volume, the regional model volume, in order to place the local model in a larger context and to allow for sensitivity analyses of, in particular, hydrogeological boundary conditions. The difference between the regional and local model volumes is the resolution of the modelled objects, which has been chosen to balance modelling efforts relative to the needs of the downstream user of the model. This comes as a natural consequence of ensuring a homogeneous resolution throughout all parts of the model volumes.

2.9.1 Regional model area and volume

The regional model area employed for model version SDM-Site Laxemar is shown in Figure 2-7. This model area, and associated volume, is the same as the one used in model version Laxemar 1.2 /SKB 2006a/, as well in model version 0 /SKB 2002/. The arguments for selecting this area/volume remain the same:

- It includes the prioritised area for site investigations in the Simpevarp area /SKB 2001/ with an approximate surface area of 273 (21×13) km²;
- It captures the extensive regional deformation zones that strike in northeasterly and near east-west directions, and surround the prioritised area for site investigations. Any expansion of the regional model area to the east or west would not provide any significant changes in the incorporated regional geological picture;
- It adequately covers the variations in rock type in the candidate area and its immediate surroundings;
- It captures the main features in the region interpreted to be of hydrogeological importance as the east-west boundaries are judged to be sufficiently well separated in space not to influence the groundwater flow in the region. Furthermore, the western boundary lies on the western side of a local topographic divide, while the boundary to the east lies in the strait of Kalmar Sund (between the mainland and the island of Öland). The area includes potential discharge areas for groundwater resulting from future shoreline displacement. The proper locations of the boundaries in the regional hydrogeological model – as well as the proper boundary conditions – are assessed through a series of sensitivity analyses in the hydrogeological modelling for Simpevarp 1.2 /SKB 2005a/. The latter modelling is supported by pre-modelling results presented by /Holmén 2008/;
- A vertical model thickness of 2.2 km (of which 100 m is above sea level) is considered to provide a reasonable context for the local description. Furthermore, this depth is considered the maximum down to which any meaningful extrapolations of deformation zones can be made.

The coordinates outlining the surface area of the regional model for Laxemar 1.2, cf. Figure 2-7, are (in metres):

RT90 (RAK) system; (Easting, Northing) :
(1539000, 6373000), (1560000, 6373000), (1539000, 6360000), (1560000, 6360000).

RHB 70; elevation: +100 m.a.s.l. –2,100 m.a.s.l.

2.9.2 Local model volume

The local model volume employed for model versions Simpevarp 1.2 and Laxemar 1.2 included both the Simpevarp subarea and the Laxemar subarea, cf. Figure 2-7. By including the two subareas in one local model volume, satisfactory coverage was also provided for alternative access tunnel and/or tunnel connection from a shaft access to either of the two subareas.

Following the decision to select Laxemar as a designated area for the conclusion of the site investigations, cf. Section 1.1, the local model area for model stage Laxemar 2.1 was reduced to focus entirely on the Laxemar subarea. For the current model version SDM-Site Laxemar, this area was somewhat extended to the south to include the quartz monzodiorite in its entirety, cf. Chapter 5.

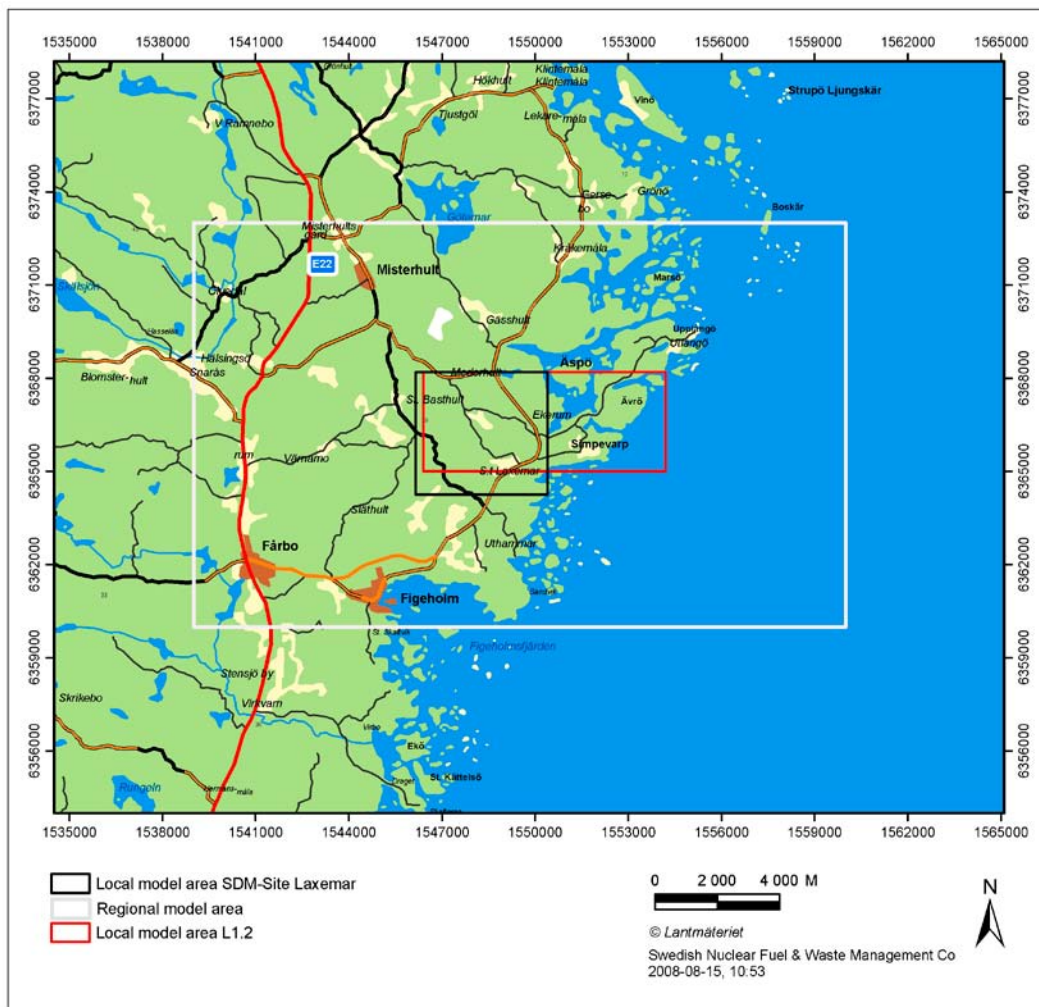


Figure 2-7. Regional and local model areas used for model version SDM-Site Laxemar. The area coverage of the regional model is the same as that employed in previous model versions, whereas the local model area is significantly reduced compared to model version Laxemar 1.2.

Basic arguments for the local model volume are given in /SKB 2006a/. The modified argumentation, given the expressed focus on Laxemar, is presented below:

- It provides a volume that includes the Laxemar subarea and the area for potential surface facilities, including current layouts for access ramps and tunnels;
- The north boundary is positioned along an interpreted deformation zone (ZSMEW002A, the Mederhult zone), cf. Figure 5-30. The south boundary is positioned such that the designated local model area encompasses the quartz monzodiorite in its entirety. The north-south boundaries of the model are not associated with any particular geographical feature;
- A depth of the model volume of 1,100 m below sea level allows inclusion of all information from the deep boreholes that have been completed at the site;
- The local scale model area covers approximately 16 (4×4) km² (see Figure 2-7).

The coordinates defining the local scale model volume for model version SDM-Site Laxemar are (in metres):

RT90 (RAK system: (Easting, Northing) : (1546150, 6368200), (1550390, 6368200), (1550390, 6364250), (1546150, 6364250).

RHB 70: elevation: +100 m.a.s.l. –1,100 m.a.s.l.

3 Evolutionary aspects of the Laxemar-Simpevarp area

This chapter constitutes a summary of the background report /Söderbäck 2008/, which provides a comprehensive account of the geological evolution, palaeoclimate and historical development of both the Forsmark and Laxemar-Simpevarp areas. A detailed reference list is given in the background report and here only a few, key references are included in the text.

3.1 Bedrock evolution during Proterozoic and Phanerozoic

The Laxemar-Simpevarp area is situated in the south-western part of one of the Earth's ancient continental nuclei, referred to as the Fennoscandian Shield /Koistinen et al. 2001/. This part of the shield belongs predominantly to the geological unit referred to as the Svecokarelian (or Svecofennian) orogen (Figure 3-1). The bedrock inside an orogen was affected by major tectonic activity at a particular time interval during the Earth's long geological evolution and the actual geological process is referred to as orogeny. Tectonic activity refers to regional deformation and metamorphism of the crust in combination with active volcanism and the intrusion of magmas at depth, i.e. major igneous activity. In essence, the branch of geology referred to as "tectonics" addresses the broad architecture of the outer part of the Earth. The bedrock in the Svecokarelian orogen is dominated by Proterozoic igneous rocks that were affected by complex ductile strain and metamorphism at predominantly mid-crustal levels, prior to later exhumation to the present level of erosion.

In order to provide the necessary boundary conditions for understanding the bedrock geological evolution of both the Forsmark and Laxemar-Simpevarp areas /Söderbäck 2008/, these areas were viewed in a broader geological perspective. For this purpose, attention has been focused on an area in the southern and eastern part of Sweden, referred to as the geological reference area (Figure 3-1).

3.1.1 Bedrock geological evolution in south-eastern Sweden

The bedrock geology at the current level of erosion in the geological reference area in south-eastern Sweden (Figure 3-1), can be divided into several major tectonic domains. These domains trend WNW more or less parallel to an older, Archaean continental nucleus to the north-east (Figure 3-1). The predominantly igneous bedrock in all these domains had largely been formed between 1.91 and 1.75 billion years ago (1.91–1.75 Ga). This bedrock was also affected by a variable degree of deformation in a hot, ductile regime and the various domains amalgamated, more or less into their current geometric configuration, during the same time interval. A remarkably thick continental crust throughout most of the Fennoscandian Shield (up to c. 60 km) is a heritage from the dramatic tectonic evolution, predominantly during the later part of the Palaeoproterozoic era. The geological time scale that has been used for assessing the bedrock evolution is shown in Figure 3-2.

Although the bedrock in south-eastern Sweden had already started to stabilise by 1.75 Ga, tectonic activity that involved continued crustal growth and crustal reworking continued during the remainder of the Proterozoic to the west and south (Gothian, Hallandian and Sveconorwegian orogenies). By c. 900 Ma, the bedrock in the northern part of Europe had collided with other continental segments to form the supercontinent Rodinia. Break-up of Rodinia, drift of the newly-formed continent Baltica from cold latitudes in the southern hemisphere over the equator to northerly latitudes, and amalgamation of the new supercontinent Pangaea occurred between c. 600 and 300 Ma. Rifting of the continental crust, and opening and spreading of the North Atlantic Ocean dominated the subsequent geological evolution to the south and west of the geological reference area. This long period of extensional tectonic activity was interrupted during the Late Cretaceous and early Palaeogene by a more compressive tectonic regime, which can be related to the collision of Eurasia and Africa.

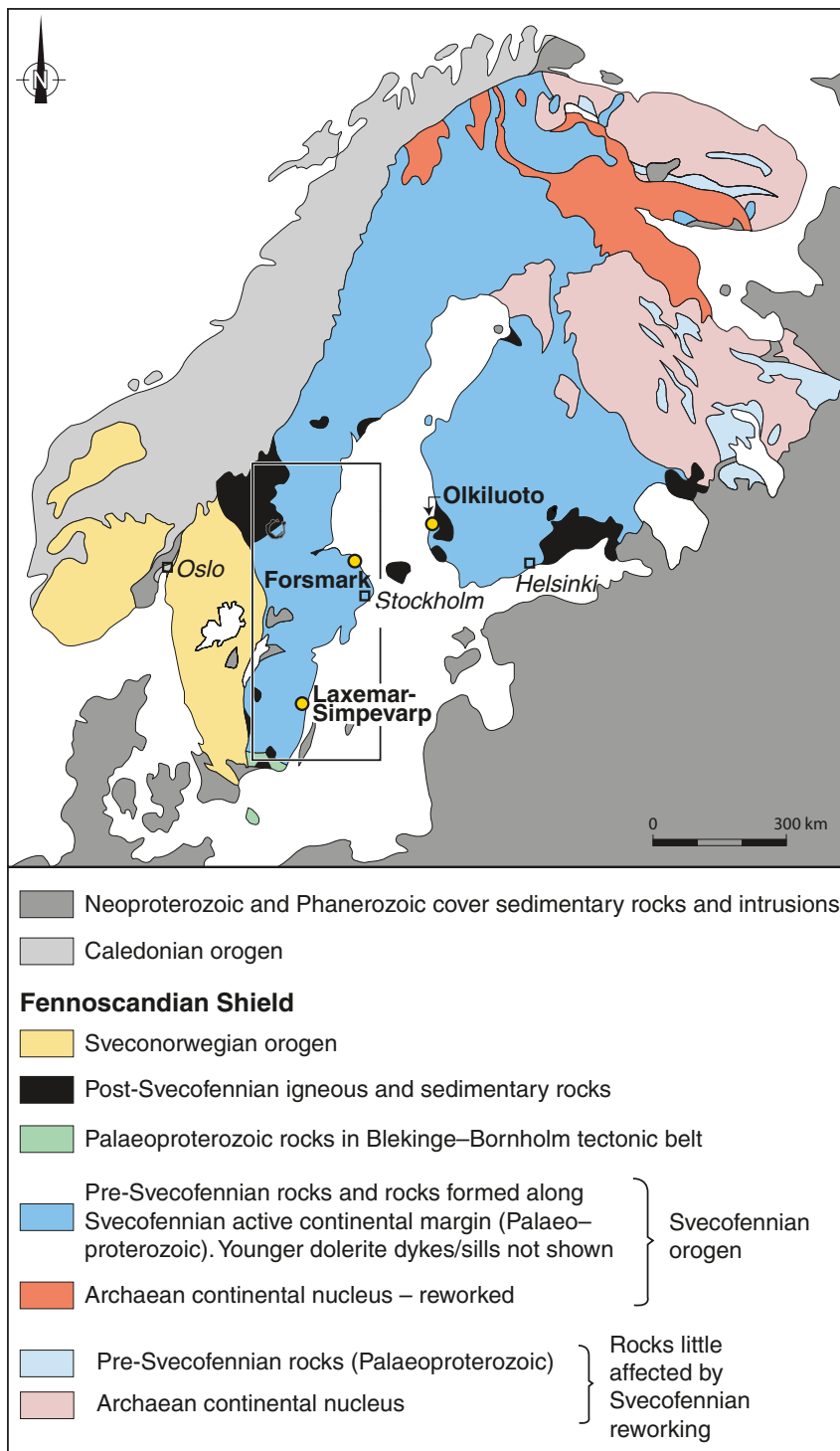


Figure 3-1. Map showing the major tectonic units in the northern part of Europe at the current level of erosion (modified after /Koistinen et al. 2001/). The area referred to in Section 3.1.1 and used to provide a regional geological perspective for both the Forsmark and Laxemar-Simpevarp areas is outlined by the rectangle. This area is referred to as the geological reference area /Söderbäck 2008/.

Geological time units						
MILLION YEARS	EON	ERA	PERIOD	AGE		
2	PHANEROZOIC	CENO-ZOIC	PLEISTOCENE / HOLOCENE IN QUATERNARY	1.635 or older		
				PALAEOGENE / NEOGENE IN TERTIARY	65	
100		MESOZOIC		CRETACEOUS	144	
200				JURASSIC	206	
				TRIASSIC	248	
300		PALAEOZOIC		PERMIAN	290	
400				CARBONIFEROUS	360	
				DEVONIAN	417	
				SILURIAN	443	
500				ORDOVICIAN	490	
				CAMBRIAN	543	
543	PRECAMBRIAN	NEO	VENDIAN	650		
				LATE	1000	
1000		MESO	RIPHEAN	MIDDLE	1400	
					EARLY	1600
1600						2500
2500			PALAEO		2500	
3000		ARCHAEAN				
3500						
4000						

Figure 3-2. Geological time scale based on the compilation used in /Koistinen et al. 2001/. Age is given in million years (Ma). 1 Ga = 1,000 Ma.

An overview of the effects of these different, far-field tectonic events in the near-field realm represented in south-eastern Sweden is described in /Söderbäck 2008/. These effects gave rise to local igneous activity during the Proterozoic, burial and denudation of sedimentary cover rocks during the Proterozoic and Phanerozoic, and predominantly brittle deformation in the bedrock at different times throughout this long time interval. At least two episodes of pre-Quaternary exhumation of the ancient crystalline bedrock can be inferred, one prior to the Cambrian and the other after the Cretaceous, probably during the Neogene. The current ground surface corresponds to the sub-Cambrian unconformity that morphologically is referred to as the sub-Cambrian peneplain.

In conclusion, it appears that two fundamental types of geological processes have made a profound impact on the geological evolution of the geological reference area in south-eastern Sweden (Figure 3-3):

- Igneous activity and crustal deformation along an active continental margin at different time intervals, mostly during Proterozoic time.
- Loading and unloading cycles in conjunction with the burial and denudation, respectively, of sedimentary rocks, around and after c. 1.45 Ga.

As the effects of regional tectonic activity mostly waned in south-eastern Sweden and became prominent solely in the far-field realm, the effects of loading and unloading related to the burial and denudation of sedimentary rocks, respectively, increased in significance (Figure 3-3).

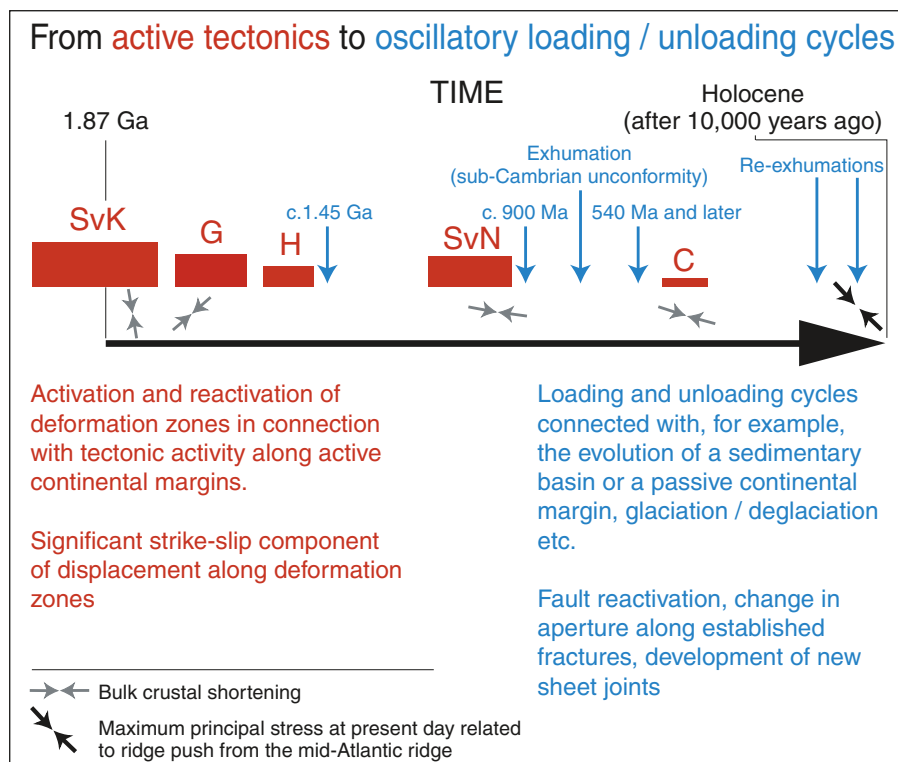


Figure 3-3. Active tectonics (red) and oscillatory loading and unloading cycles (blue) during geological time in the geological reference area (modified after /Stephens et al. 2007/). The detailed evolution during the Quaternary period with several glaciations (loading) and deglaciations (unloading) is not shown. SvK = Svecokarelian orogeny, G = Gothian orogeny, H = Hallandian orogeny, SvN = Sveconorwegian orogeny, C = Caledonian orogeny.

3.1.2 Bedrock geological evolution in the Laxemar-Simpevarp area

The bedrock geological evolution in the Laxemar-Simpevarp areas has been evaluated with the help of surface and borehole observational data as well as geochronological data /Söderbäck 2008/. The geochronological data are summarised in Figure 3-4, and the corresponding data from Forsmark are shown for comparison. The bedrock in Laxemar-Simpevarp formed after the complex geological evolution to the north in the Svecokarelian orogen, and a c. 1.80 Ga suite of more or less well-preserved intrusive rocks, which belongs to the Transscandinavian Igneous Belt, dominates the area. The rocks in this suite show variable composition (granite to quartz monzodiorite to diorite-gabbro), grain size and texture. They formed during the waning stages of the Svecokarelian orogeny, and have been affected by magma-mingling and magma-mixing processes, which confirm a close temporal and genetic relationship between the different rocks.

Although there is faint to weak, non-uniformly distributed and gently to moderately dipping foliation in the rocks, steeply dipping ductile to brittle-ductile shear zones form the most prominent structures in the area. This deformation affected the area during the time interval 1.81 to 1.76 Ga, i.e. during the waning stages of the Svecokarelian orogeny. Based on documented sinistral displacement along the NE-SW oriented most prominent ductile shear zones in the area, the development of the ductile fabric is inferred to be related to a regional north-south directed crustal shortening during oblique subduction of oceanic lithosphere. A northeast-southwest directed bulk crustal shortening has been suggested by /Viola 2008/, based on the assumption that the NE-SW oriented steep shear zones constitute second order structures to inclined E-W oriented master zones. However, in the lack of reliable ductile, kinematic data along the E-W oriented deformation zones, the northward shortening direction is the favoured interpretation. The latter is in accordance with palaeostress data reported by /Lundberg and Sjöström 2006/ for the Laxemar-Simpevarp area, and also with the direction of bulk shortening suggested for corresponding ductile deformation in Forsmark /Stephens et al. 2007, Söderbäck 2008/ and elsewhere in south-eastern and eastern Sweden /e.g. Beunk and Page 2001, Persson and Sjöström 2003/.

In sharp contrast to Forsmark, the Laxemar-Simpevarp area was affected by significant igneous activity later in the Proterozoic. Granitic magmatism at 1.45 Ga, manifested by the Götemar and Uthammar granites, is inferred to be a far-field effect of Hallandian orogenic activity further to the west and south, and dolerites with an age of c 900 Ma formed as a result of E-W crustal extension during the later part of the Sveconorwegian orogeny. As indicated by especially disturbances of the $^{40}\text{Ar}/^{39}\text{Ar}$ isotope system in different minerals (Figure 3-4), both these younger episodes of igneous activity had effects on the thermal evolution of the site. Furthermore, it is inferred that the intrusion of the 1.45 Ga granites might have caused reactivation of structures in the near-by country rocks, but only relatively minor structural effects in the Laxemar model area /Cruden 2008/.

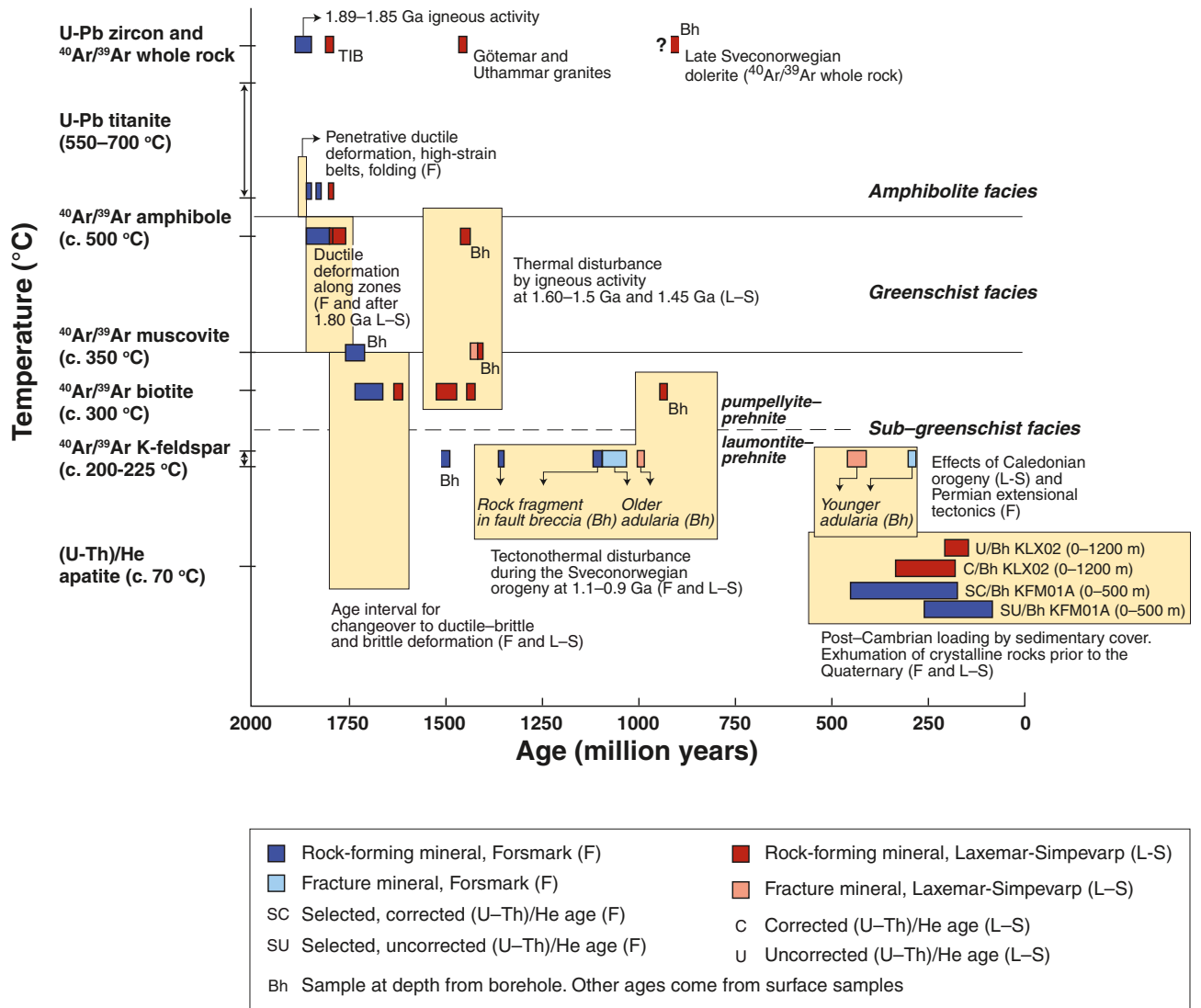


Figure 3-4. Summary of the geochronological data that constrain the bedrock geological evolution in the Laxemar-Simpevarp area. Note that corresponding data from Forsmark are shown for comparison. Some $^{40}\text{Ar}/^{39}\text{Ar}$ and (U-Th)/He data from depth in boreholes are not shown here. As expected, these data are somewhat younger than the equivalent surface and near-surface data.

The brittle deformational history in the Laxemar-Simpevarp area, which initiated some time between 1.76 and 1.62 Ga, has been evaluated with the help of three lines of approach:

- The use of low-temperature geochronological data that shed light on the exhumation and cooling history (Figure 3-4).
- The relative time relationships and absolute ages of fracture minerals (Figure 3-4).
- A comparison of kinematic data from brittle structures along deformation zones, which were evaluated during the geological modelling work at the site, with the tectonic evolution in a regional perspective (Section 3.1.1).

Different generations of fracture minerals have been recognised in the Laxemar-Simpevarp area. An early period of precipitation of a high-temperature mineral assemblage, which includes epidote, was followed by a period of hydrothermal precipitation of different, lower temperature minerals, including adularia (older generation), hematite, prehnite, and calcite. Epidote-bearing structures formed prior to 1.45 Ga, and fracture-controlled greisen (quartz, muscovite, fluorite, pyrite and topaz) and intense wall rock alteration developed in conjunction with the important thermal event at 1.45 Ga. However, thermal disturbance around 1.5 Ga, i.e. prior to the intrusion of the Götömar and Uthammar granites, is apparent (Figure 3-4). The effects of Sveconorwegian tectonothermal activity on the evolution of fracture mineral assemblages are also evident in the Laxemar-Simpevarp area (Figure 3-4). The integrated evaluation that makes use of the different lines of approach outlined above suggests that the different sets and sub-sets of deformation zones in the Laxemar-Simpevarp area had formed and were already reactivated during Proterozoic time, in connection with the late Svecokarelian, and Sveconorwegian tectonic events, and possibly also in connection with the intrusion of the 1.45 Ga granites, at least partly as conduits for hydrothermal solutions.

Several lines of evidence indicate faulting after the establishment of the sub-Cambrian unconformity in the Laxemar-Simpevarp area. Furthermore, precipitation of younger low-temperature minerals, including sulphides, clay minerals and calcite, occurred during and probably after Palaeozoic time. Adularia (younger generation) formed during the Silurian or Early Devonian has been documented (Figure 3-4), possibly as a far-field effect of the Caledonian orogenic event. Furthermore, migration of fluids downwards from the sedimentary cover into the crystalline bedrock is manifested by the occurrence of fractures filled with Cambrian sandstone. Brecciation of the sandstone in one of these fractures and documentation of a fragment of Cambrian sandstone in a deformation zone along the coast to the Baltic Sea is further evidence of Palaeozoic brittle faulting. In addition, (U-Th)/He apatite data indicate that the deformation zone along the coast has also been reactivated during or after the Mesozoic. The youngest generation of calcite occurs in hydraulically conductive fractures and zones and may have precipitated during a long period including the present.

On the basis of the (U-Th)/He apatite data from boreholes, some constraints on when different segments of the bedrock at different crustal levels passed through the c. 70°C geotherm have been obtained (Figure 3-4). These data indicate that a sedimentary cover was situated on top of the crystalline basement rocks throughout much of the Phanerozoic. At Laxemar-Simpevarp, a change to slower exhumation rate occurred during the Early Jurassic or the Late Jurassic to Cretaceous. It is assumed that renewed exhumation of the sub-Cambrian unconformity, with complete denudation of the sedimentary overburden, did not take place until some time during the Cenozoic.

3.2 Palaeoclimate and geological development during the Quaternary period

The Quaternary climate is characterised by large and sometimes rapid changes in global temperature. The present period has been preceded and will be followed by colder periods in which ice sheets cover larger areas than at present. The Laxemar-Simpevarp area has consequently been covered by glacier ice at least three times during the Quaternary period. However, the total number of glaciations covering the model areas is not known. The cold glacial periods have been much longer than the warmer interglacial periods, which are characterised by a climate similar to the present. However, long ice-free periods have also occurred during the glacials. During these ice-free periods the climate was colder than today and tundra conditions probably prevailed in large parts of Sweden.

It can consequently be assumed that permafrost has prevailed in the model areas for long periods. The latest glaciation (Weichselian) started c. 115,000 years ago, and there is geological evidence of at least two periods within it when a large part of Sweden was free of ice. However, the exact timing and duration of these ice-free periods are unknown. The onset of the latest glacial coverage in the area is not known, whereas the timing of the latest deglaciation is rather well established along the coast of the Baltic Sea.

The present interglacial, the Holocene, started with the deglaciation of Mid-Sweden when the ice margin had not yet reached Forsmark. The climate during the deglaciation became successively warmer, although some periods with colder climate did occur. In southern Sweden, the warmer climate caused a gradual change from tundra vegetation to forest dominated by deciduous trees. The Mid-Holocene climate was characterised by average temperatures a few degrees higher than today. The forests in southern Sweden have subsequently been dominated by coniferous forest. The areas covered by forest began to decrease c. 3 000 BC due to the introduction of agriculture.

The development of the Baltic Sea after the latest deglaciation has been characterised by ongoing shoreline displacement. The interaction between isostatic rebound related to the removal of ice and associated unloading, and eustatic sea level variations has caused variable depth in the straits connecting the Baltic Sea with the Atlantic Ocean in the west. In turn, this has caused variable salinity in the Baltic Sea throughout the Holocene. The development of the Baltic Sea since the latest deglaciation can be divided into four main stages (Figure 3-5). Three of these stages; Yoldia, Ancylus and Littorina, are named after molluscs which reflect the ambient salinity of the stages. The estimated salinity variations in the open Baltic Sea during the last c. 9,000 years are shown in Figure 3-6. During the period 4500–3000 BC, the salinity was almost twice as high as it is today.

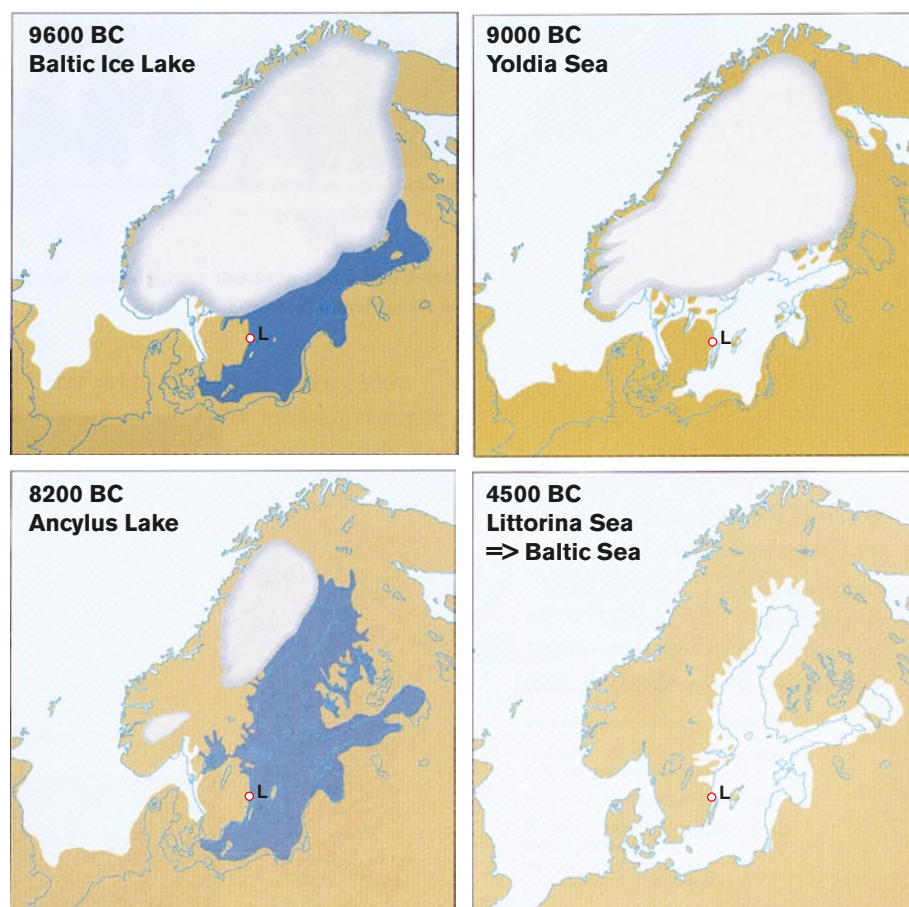


Figure 3-5. Four main stages characterise the development of the Baltic Sea since the latest deglaciation: A) the Baltic Ice Lake (13,000–9500 BC), B) the Yoldia Sea (9500–8800 BC), C) the Ancylus Lake (8800–7500 BC) and D) the Littorina Sea (7500 BC–present). Fresh water is symbolised by dark blue and marine/brackish water by light blue, from /Fredén 2002/. “L” indicates the location of Laxemar-Simpevarp.

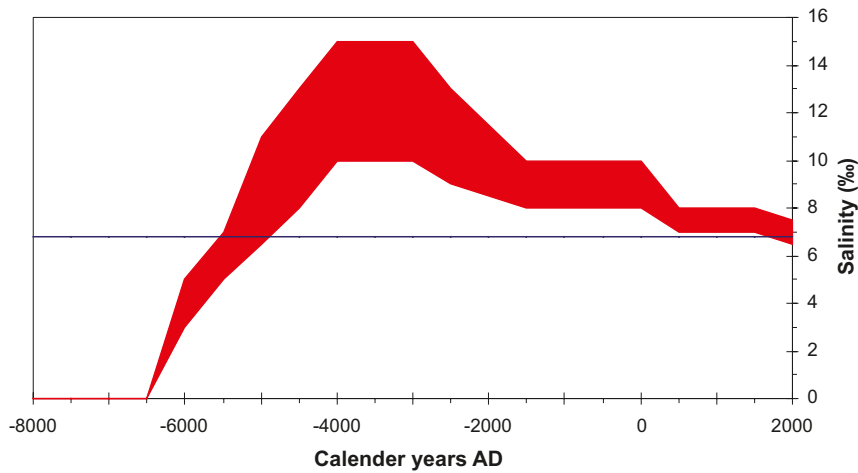


Figure 3-6. Estimated range for the salinity of sea water in the open Baltic proper off Oskarshamn during the past 10,000 years. Maximum and minimum estimates are derived from /Westman et al. 1999/ and /Gustafsson 2004ab/. The present salinity in the area is shown by the horizontal reference line.

The Laxemar-Simpevarp regional model area is situated below the highest shoreline. During the deglaciation at c. 12,000 BC, the area was, depending on the local topography, situated 50–100 m below the sea level, and the first parts of the regional model area emerged from the sea around 9400 BC (Figure 3-7).

It is suggested that all known unconsolidated deposits in the Laxemar-Simpevarp area were deposited during the last phase of the latest glaciation and after the subsequent deglaciation /Söderbäck 2008, cf. Chapter 4 therein/. However, the possibility of the occurrence of older deposits cannot be excluded and there are indications of older deposits in adjacent areas outside the regional model area.

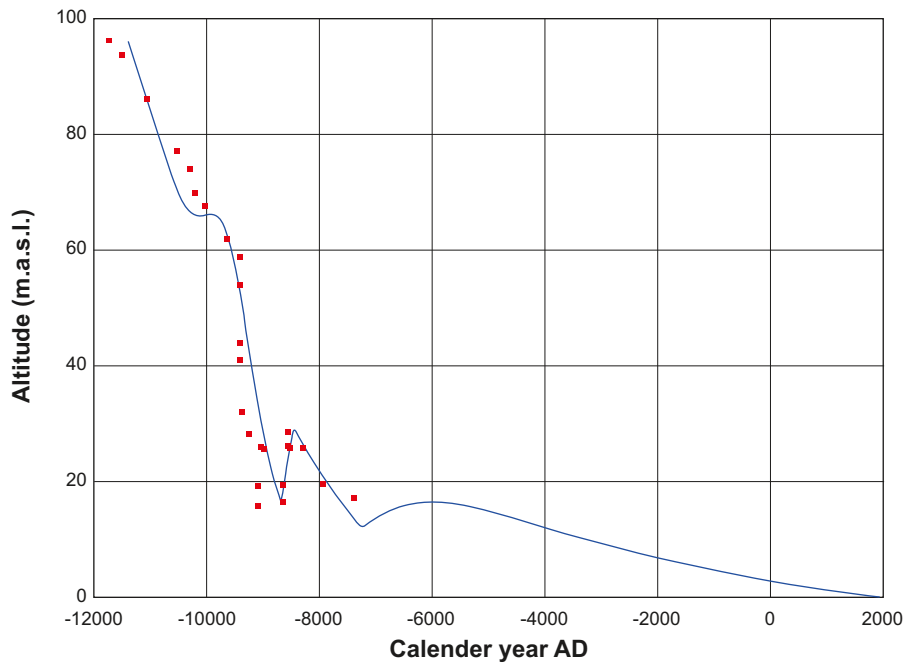


Figure 3-7. Shoreline displacement in the Laxemar-Simpevarp area after the latest deglaciation. The red symbols show the results from dating of lake sediments in the region /Svensson 1989/. The blue curve was calculated using a mathematical model /Påsse 2001/.

Till and glaciofluvial material were deposited directly by the ice sheet and by glacial meltwater, respectively. During the deglaciation, glacial clay was deposited in the lowest topographical areas. In the terrestrial valleys gyttja clay occurs, which was deposited when these areas were narrow bays. The subsequent shoreline displacement had a major impact on the distribution and relocation of fine-grained Quaternary deposits. The most exposed areas were affected by wave washing and bottom currents. Sand and gravel were consequently eroded from older deposits, transported and deposited at more sheltered locations. Periods of erosion also occurred at sheltered locations, which caused erosion of fine-grained deposits such as glacial clay. Shoreline displacement is an ongoing process and new areas are currently exposed to erosion, whereas sheltered bays, with conditions favourable for deposition of clay gyttja, have formed elsewhere.

3.3 Seismicity during the Quaternary period

An earthquake is the result of a sudden release of energy through movement (faulting) along a deformation zone, resulting in the emission of seismic waves. This movement is normally the result of stresses that have accumulated over a certain time interval in a particular volume. Overviews of palaeoseismic activity in Sweden during the latest part of and after the Weichselian glaciation, with special focus on the Forsmark and Laxemar-Simpevarp areas, as well as of seismic activity in historical time from 1375 up to 2005 AD, over the northern part of Europe, are presented in /Söderbäck 2008/.

Palaeoseismic activity has been inferred directly by, for example, distinct displacements of the surface that separates the crystalline bedrock from the Quaternary cover or indirectly by seismically derived deformation on Quaternary sediments. The interpretation of aerial photographs provides a tool for identifying morphologically conspicuous lineaments that are candidates for late- or post-glacial faults. A significant number of late- or post-glacial, reverse fault scarps have been identified in the northern part of Sweden and it has been inferred that the accompanying earthquakes reached magnitudes of up to M8, or even larger, on the Richter magnitude scale. As yet, conclusive evidence for such fault movements is lacking in the southern part of Sweden.

Detailed investigations have been carried out to evaluate the occurrence of palaeoseismic activity in and around the Laxemar-Simpevarp area within the context of the site investigation work, employing a similar methodology to that used in the northern part of the country. None of the morphological lineaments that have been recognised have been inferred to represent late- or post-glacial faults. Furthermore, no deformational features in Quaternary sediments can be unambiguously related to seismic activity. On the basis of these results, evidence for major (magnitude >M7 on the Richter scale) earthquakes in the Laxemar-Simpevarp area is lacking in the geological record.

Compared with other parts of the world, especially close to plate boundaries, there is generally a low frequency of registered earthquakes throughout historical time in the northern part of Europe, and an absence of earthquakes with a magnitude \geq M6 on the Richter scale (Figure 3-8). However, seismic activity in Sweden throughout historical time is not evenly distributed across the country (Figure 3-8). Areas of relatively high activity are conspicuously linearly aligned in the northern part of the country, in a broader region in south-western Sweden and, less conspicuously, in the southernmost part of the country (Skåne). By contrast, much of the geological reference area in south-eastern Sweden, including the Laxemar-Simpevarp area, shows relatively little evidence of past seismic activity (Figure 3-8).

The relatively high level of seismicity along the coast of the Baltic Sea is not an artefact of seismic station distribution or some other factor. The linear alignments of earthquakes, at least in the northernmost part of the country and in adjacent areas in Finland and Norway, have been attributed to the late- or post-glacial faults that have been identified as a result of palaeoseismic studies. The linear alignment along the Baltic Sea coast in the province of Norrland occurs where both land uplift related to post-glacial isostatic rebound is greatest and where there is also a tendency to a decrease in crustal thickness. A correlation between an increased frequency of seismic events and crustal thinning is apparent in south-western and southernmost Sweden. The crustal thinning occurs in areas where Late Palaeozoic and younger extensional tectonics has taken place. The crust in Sweden below c. 35 km is seismically quiet and this changeover is most probably related to the more ductile character of the crust beneath this depth. If this interpretation is correct, an average geothermal gradient of approximately 8 to 12° C/km is inferred at the current time.

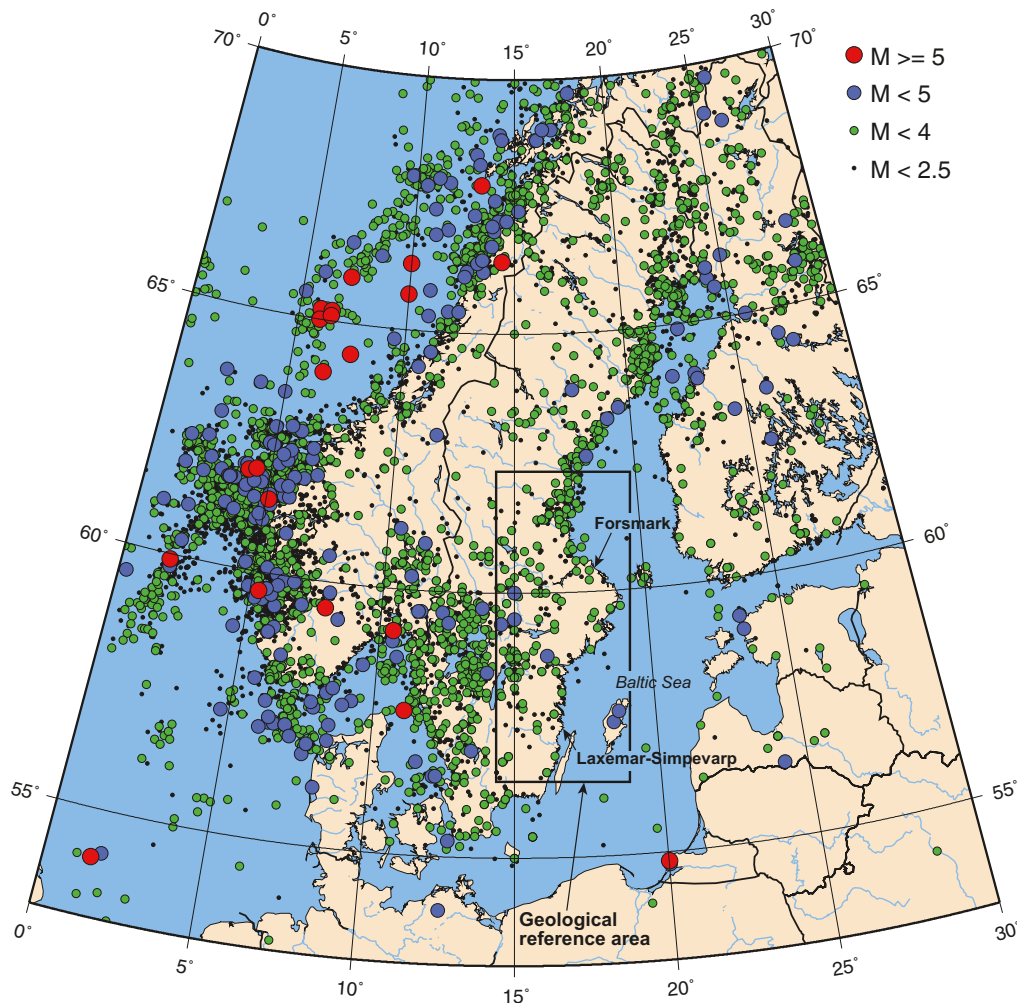


Figure 3-8. Epicentre and magnitude of earthquakes on the Richter scale (M) in the northern part of Europe between 1375 and 2005 AD. There is no lower limit on the magnitude of the earthquakes shown in the figure. However, since the ability to detect smaller events has gradually improved over time, no precise level of completeness for such data can be provided. Note that earthquake data for the neighbouring countries to the south of the Baltic Sea are also not complete. Modified after /Bödvarsson et al. 2006/.

Although strike-slip movement is the dominant focal mechanism, irrespective of where in Sweden the seismic event occurred, reverse dip-slip or oblique-slip fault plane solutions are also present. Since seismic events predominantly occur along geologically ancient fractures or planes of weakness in the bedrock, the orientation of these structures also has an influence on the focal mechanism. It is also important to keep in mind the fact that the fault plane solutions discussed above pertain to crustal stress at depths affected by seismic activity. Considerable evidence points to a reverse sense of movement in the uppermost part of the crust (c. 1,000 m) in large parts of Sweden, with a vertical or subvertical minimum principal stress.

The maximum principal stress as inferred from the seismic data is oriented WNW-ESE. This direction is in accordance with that expected from plate tectonics with ridge push forces from the mid-Atlantic ridge. These considerations lend support for the hypothesis that ongoing plate tectonic processes are important for understanding recent seismic activity. Palaeoseismic activity has been explained by release of stress accumulated during preceding glacial loading in association with long-term tectonic plate motions. An alternative mechanism that involves release of high horizontal stresses induced by flexure during loading, in combination with ambient plate tectonic stresses, has also been discussed. The release of stress and fault instability occurred during unloading and the rapid removal of the ice.

3.4 Groundwater evolution during the Quaternary period

The groundwater evolution in the Laxemar-Simpevarp area has been strongly affected by climate changes in the past. Investigations have shown that the groundwaters observed today have different origins and ages, including glacial meltwater, meteoric water, and marine water, depending on the prevailing conditions at the time of infiltration in the bedrock. Shoreline displacement plays an important role in understanding the infiltration mechanism for these waters. It is specifically emphasised for the intrusion of the saline Littorina Sea water into the bedrock, as well as for the subsequent flushing processes in the upper, more permeable bedrock horizons. It seems that the most recently recharged water tends to flush older water types, especially in the upper permeable part of the bedrock. However, hydraulic conditions vary over time, and remnants of earlier climatic fluctuations can be preserved in localised areas of low hydraulic conductivity. Palaeohydrogeochemistry thus provides an important framework for understanding the bedrock hydrogeochemical evolution which is crucial for the hydrogeochemical and hydrogeological understanding of the site.

Changes in hydrogeological development deduced from the geological and hydrogeochemical records may be repeated during the lifespan of a repository (thousands to hundreds of thousands of years). As a result, water types such as brine, glacial water, marine and meteoric waters will intrude and be mixed in a complex manner at various levels in the bedrock.

The post-glacial development reveals that when the continental ice melted and retreated from the Laxemar-Simpevarp area around 12,000 BC, glacial meltwater was hydraulically forced under considerable pressure into the bedrock. This took place before the development of the Ancylus Lake in the area. The exact penetration depth is unknown, but, according to hydrodynamic modelling, e.g. /Jaquet and Siegel 2003, 2006/ depths exceeding several hundred metres are possible, see further discussion in Chapters 9 and 8.

As described in Section 3.2, the post-glacial development of the area close to the Baltic Sea can be divided into a number of non-saline and brackish lake/sea stages (see Figure 3-5). Two stages with brackish water can be recognised; the Yoldia Sea (9500 to 8800 BC) and the Littorina Sea (7500 BC to the present). Since the saline conditions during the Yoldia Sea stage prevailed for only c. 200 years /Söderbäck 2008, cf. Section 3.3.5 therein/ and was later followed by the more saline Littorina Sea stage, there are no discernable signs of water related to the Yoldia Sea in the bedrock today. During the early part of the Littorina Sea stage, the salinity was considerably higher than at the present day, reaching a maximum of about 15‰ between 4500 and 3000 BC. Dense brackish seawater from the Littorina Sea was able to penetrate the bedrock, resulting in a density-driven intrusion that affected the groundwater in the more conductive parts of the bedrock (see Chapter 9). The density of the intruding seawater in relation to the density of the existing groundwater determined, together with the hydraulic properties of the bedrock, the final penetration depth. As the Littorina Sea stage provided the most saline groundwater, it is assumed to have had the deepest penetration depth, eventually mixing with the groundwater mixtures already present in the bedrock, e.g. deep saline water, old meteoric-glacial waters and Holocene glacial melt water, and later, during the process of regressive shoreline displacement, also with more recent meteoric water.

As a result of the late- and post-glacial development, five different water types can be identified in the bedrock today. On the basis of the hydrogeochemical data, these water types are, in relative chronological order: Deep saline water (oldest) > Mix of old meteoric-glacial waters (hypothetical) > Glacial melt water from the last deglaciation > Littorina Sea water > Present-day meteoric water (most recent). The mix of old meteoric-glacial waters is not observed as a dominant component of the present-day groundwater, and the previous occurrences of this water type can only be hypothesised. A detailed description of the different water types is given in Chapter 9 in this report.

In order to help understand the step-by-step evolution of groundwater in the Laxemar-Simpevarp area during post-glacial time, i.e. during the Holocene, a conceptual model is presented in Figure 3-9. The palaeohydrological conditions in the area have changed continuously over time and, as can be seen, the major driving mechanism behind the flow lines is the shoreline displacement due to land uplift. There remain some uncertainties with this conceptual model, and the uncertainties are greater further back in time. Hence, the largest uncertainties are associated with the stage showing the flushing by glacial melt water.

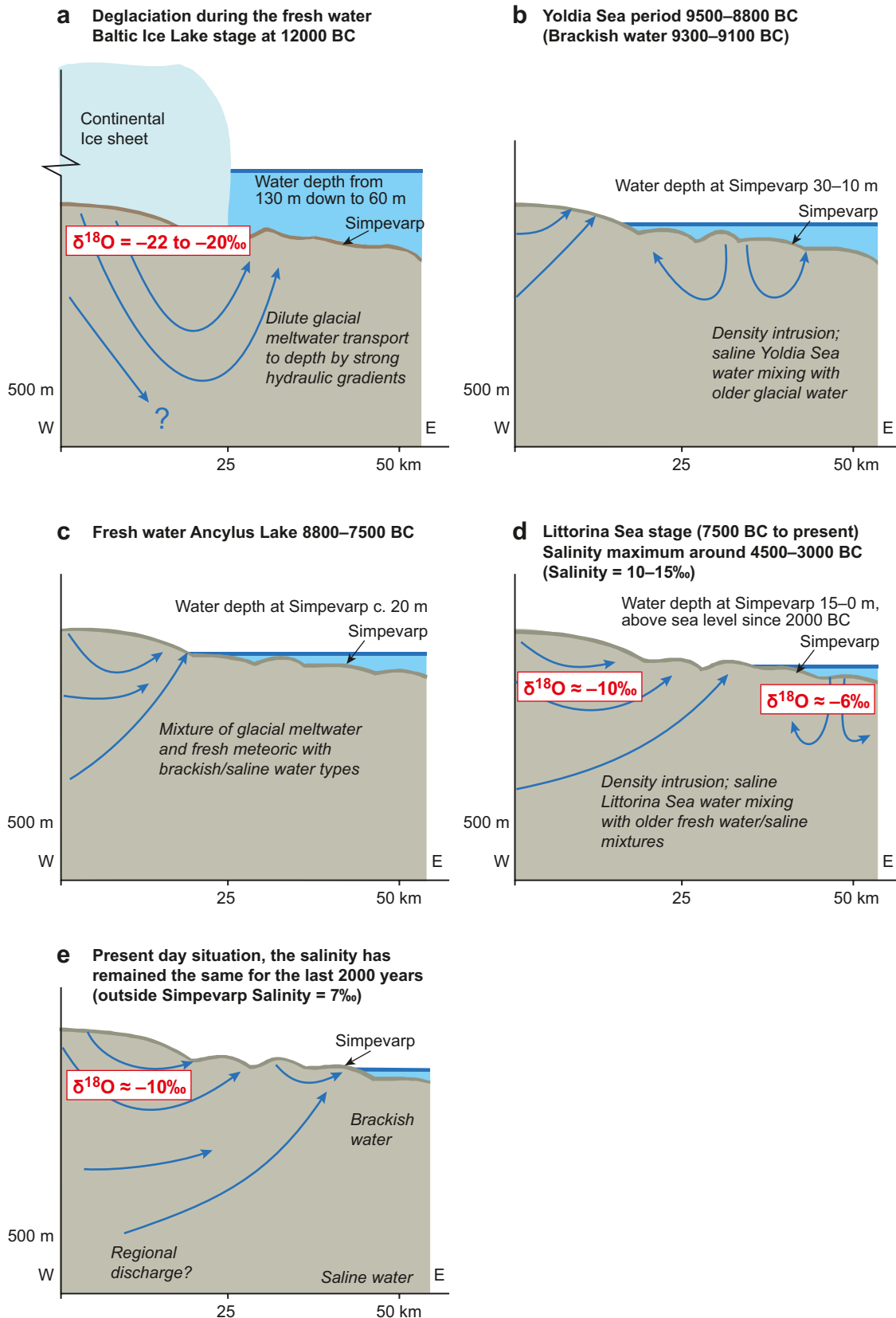


Figure 3-9. Conceptual model for groundwater evolution in the Laxemar-Simpevarp area. The sequence of pictures illustrate the post-glacial development of the area a) the deglaciation during the Baltic Ice Lake stage at about 12 000 BC, b) the Yoldia Sea period (9 500 – 8 800 BC), c) the freshwater Ancylus Lake between 8800–7500 BC, d) showing the penetration due to density driven intrusion of Littorina sea water between 7 500 BC to 0 AD, and e) the present-day situation. Blue arrows indicate flow pattern of the groundwater.

3.5 Development of ecosystems during the late Quaternary period

Long-term ecosystem development in near-coastal areas of Fennoscandia is driven mainly by two different factors; climate change and shoreline displacement. In addition, human activities have also strongly influenced the development of both terrestrial and aquatic ecosystems, especially during the last millennia.

Shortly after the latest ice retreat, which started in southernmost Sweden c. 15,000 BC, the landscape was free of vegetation and can be characterised as polar desert. Relatively soon after the deglaciation, the ice-free areas were colonised and in southern Sweden the landscape was covered by a sparse Birch forest. Thereafter, the climate has oscillated between colder and warmer periods. During the cold period called the Younger Dryas (c. 11,000–9500 BC), large areas of the deglaciated parts of Sweden were again affected by permafrost and much of the previously established flora and fauna disappeared. From the onset of the Holocene (c. 9500 BC) and thereafter, southern Sweden has been more or less covered by forests, although the species composition has varied due to climatic changes. Most of the present mammal fauna was established in southern Sweden during the early Holocene. During the last few thousand years, the composition of the vegetation has changed not only due to climatic changes, but also due to human activities which have decreased the areas covered by forest. In southern Sweden, the introduction of agriculture and the subsequent opening of the landscape started c. 3000 BC.

In coastal areas like Laxemar-Simpevarp, shoreline displacement has strongly affected ecosystem development and still causes a continuing change in the abiotic environment. As a result of sea floor uplift the sea (shoreline) is regressing and old sea floor is being transformed into new terrestrial areas, or to freshwater lakes. The initial conditions for ecosystem succession from the original near-shore sea floor are strongly dependent on the topographical conditions. In sheltered bays organic and fine-grained inorganic material accumulate, whereas along more wave exposed shorelines with a large fetch, the finer fractions are washed out. During the process of shoreline displacement, a sea bay may either become isolated from the sea at an early stage and thereafter gradually transforms into a lake as the water becomes fresh, or it may remain a bay until shoreline displacement turns it into a wetland.

After isolation from the sea, the lake ecosystem gradually matures in an ontogenetic process which includes subsequent sedimentation and deposition of substances originating from the surrounding catchment, or produced within the lake. Hence, the long-term ultimate fate for all lakes is an inevitable fill-up and conversion to either a wetland or a more dry land area, the final result depending on local hydrological and climatic conditions. A usual pattern for the lake ontogeny is the sequential development of more and more eutrophic (nutrient-rich) conditions as the lake depth and volume decreases. There are, however, examples of lake ontogeny that include a transition to more oligotrophic (nutrient-poor), as well as to more dystrophic (low pH, brown-water) conditions. All lakes in the Laxemar-Simpevarp regional model area are characterised by more or less dystrophic conditions (cf. Chapter 4), and this is typical for small forest lakes in large areas of Sweden. Dystrophic lakes are characterised by high input of allochthonous carbon (i.e. transported from the surrounding catchment area) and often by short water turnover time /Brunberg and Blomqvist 2000/.

Mires are formed basically through three different processes; terrestrialisation, paludification and primary mire formation. Terrestrialisation is the filling-in of shallow lakes by sedimentation and establishment of vegetation. Paludification, which is the dominant process of mire formation in Sweden, is an ongoing water logging of more or less water-permeable soils, mainly by expanding mires. Primary mire formation is when peat is developed directly on fresh soils after emergence from water or ice. All three processes are likely to occur in the Laxemar-Simpevarp area, but peat land filling in lakes (terrestrialisation) is probably the most common type of peat land development in the investigation area. Historically, mires have often been drained for forestry or to gain new agricultural areas, and in Sweden such activities peaked in the 1930s. In the Laxemar-Simpevarp area, a large part of today's agricultural land is characterised by a peat layer which was built up during a previous wetland phase.

3.6 Human population and land use

The coast of Småland became ice-free around 12,000 BC. At the time of the deglaciation, the whole Laxemar-Simpevarp region (an area which in this section refers to three parishes in the surroundings of Oskarshamn that together constitute approximately 1,000 km² /cf. Söderbäck 2008/) was situated beneath sea level. The oldest human remains in the region are found in the highest situated terrain, which is located in the western parts of the region 25–40 metres above sea level (which corresponds to emergence from the sea around 9400–8300 BC). There is a rich occurrence of prehistoric remains in the region, some of them indicating that the area was already exploited during the Older Stone Age (9000–4000 BC). Following the arrival of the first humans to the region, it has been characterised by its forest- and archipelago settlements. The main occupation since the colonisation of the area has been a combination of agriculture, forestry and fishing activities /Lundqvist 2006/.

The settlement structure in the region during the medieval period (1100–1550 AD) was characterised by single farms, in contrast to for example Forsmark, where settlements were organised in small villages. The farms were subdivided into several smaller farms when the population increased. An unusually large share of farms in the Laxemar-Simpevarp region belonged to the crown, and the share of freeholders was correspondingly very small. The number of freehold farmers in the region increased during the 18th century, both due to the partitioning of farms and to the fact that farmers purchased farms previously belonging to the nobility.

Following a nationwide decline in the population during the middle of the medieval period, there was a strong population expansion. The population in the region doubled or increased at an even faster rate between the 1570s and the 1750s, and the strong population growth continued until the late 19th century. At the turn of the century the increase ceased and during the latter part of the 20th century the rural population decreased. The number of people involved in agriculture has decreased during the 20th century, and instead, the number of people employed in industry and crafts has increased.

Woodland was and is dominant in the Laxemar-Simpevarp region. The forests in the region have been used for many different purposes; pastures, firewood, fencing material, subsistence needs, burn-beating, as well as production of charcoal, tar and potash. In addition to sawmill activities, the production of charcoal, tar and potash, were in many cases an important part of the economy of the individual household. Trading in timber was advantageous since the timber was easily transported in the coastal areas. In the Laxemar-Simpevarp region there was also a boat-building tradition, which grew during the 19th century to a minor shipbuilding industry /Lundqvist 2006/. The areal extent of arable land, and even more so of meadows, increased throughout the 18th and 19th centuries. Much of the new agricultural land was gained from ditching of wetlands. Some of these areas are still cultivated, whereas others are now deserted and, in some cases, have been turned into woodlands.

4 The surface system and surface-bedrock interactions

This chapter presents results from the work concerning the surface system, i.e. the geology of the overburden including Quaternary deposits, hydrology, chemistry and biota, as well as ecosystem models for the terrestrial-, limnic- and marine ecosystems.

The surface system starts where the upper part of the bedrock ends, except where the bedrock reaches the surface in the form of outcrops and thereby becomes a part of the surface system. This means that a number of different disciplines are represented in the descriptions of patterns and processes in the surface system at various spatial and temporal scales, and these descriptions are presented in a large number of background reports. A summarising, integrated description of the surface system in Laxemar-Simpevarp, based on these background reports, is presented in /Söderbäck and Lindborg 2009/. This chapter constitutes a condensation of that description, and by necessity many details are omitted or only described briefly. Hence, this chapter functions partly as a pointer to detailed descriptions in the supporting background reports.

The integrated description of the surface systems at Laxemar /Söderbäck and Lindborg 2009/ includes two main components:

- a written synthesis of information related to the site, summarising the state of knowledge, as well as describing ongoing natural processes which affect the long-term development of the site, and
- a site descriptive model in which the collected information is interpreted and presented in a form that can be used, or further synthesised, in numerical models for engineering, environmental impact- and long-term safety assessments.

The overall objective of the site descriptive modelling work concerning the surface system has been to develop and document an integrated description as a basis for a site-adapted layout of the final repository, for assessment of the repository's long-term radiological safety, and to support the environmental impact assessment of the repository with site understanding and descriptions.

An important part of the work is the ecosystem modelling, which aims at describing mass balances for different chemical elements in the terrestrial, limnic and marine environments. In this work, much focus has been put on the calculation of ecosystem carbon budgets as a tool for estimating and predicting flow and accumulation of organic matter and associated elements at a landscape scale, in preparation for the safety assessment.

4.1 State of knowledge at the previous model version

Since the previous model version, Laxemar 1.2, the volume and variety of surface system data have increased considerably. This has refined the surface descriptions and the models of the site. Furthermore, the integration of the bedrock and the surface system has been considered and the interface between the two systems has been characterised and described. This will facilitate the description and handling of potential flow paths and radionuclide retention processes between the bedrock- and surface systems in the radionuclide transport modelling.

The site description of the surface system has developed since the start of the modelling in 2002 to a general understanding of how the site functions in terms of properties in different volumes, the main functional units, processes and system descriptions from different scientific disciplines. The conceptual model that was developed at the beginning of the work has been adjusted to observed site-specific features, and site data have been used to describe stocks, flows and accumulations of matter within and between different parts of the surface system in the Laxemar-Simpevarp area.

4.2 Data evaluation and modelling

The investigations performed in the Laxemar-Simpevarp area are summarised in Section 2.2, and the data supporting this model version are summarised in Tables A3-7 and A3-8 in Appendix 3. The evaluation of these data is presented below.

4.2.1 Overburden and Quaternary geology

The overburden (or regolith) refers to the unconsolidated materials overlying the bedrock. Here the term Quaternary deposits is often used since all known components of the overburden in the Laxemar-Simpevarp area were formed during the Quaternary period. In the terrestrial area the upper c. 0.5 metre of the overburden is referred to as the soil. For a detailed description of the spatial distribution and properties of the overburden in the Laxemar-Simpevarp area including evaluations of the input data and methods used, the reader is referred to /Sohlenius and Hedenström 2008/, and to a geometrical stratigraphic model /Nyman et al. 2008/, presented in Section 4.3.2. For the geological and historical development of the site, see Chapter 3.

The description of the Quaternary deposits is focused on the spatial distribution of the different units, together with a description of their physical and chemical properties. The physical properties of the Quaternary deposits are used as input data for the hydrogeological modelling /Werner et al. 2008/, whereas the information on the chemical properties contribute to the biological models of the upper geosphere /Löfgren 2008, Nordén et al. 2008, Wijnbladh et al. 2008/ and to the hydrogeochemical modelling /Tröjbom et al. 2008/.

Spatial distribution of Quaternary deposits

The distribution of Quaternary deposits is mainly related to the local bedrock morphology. The highest situated areas have been exposed to erosion from waves and currents, and the overburden is thin. Fine-grained water-laid sediments are mostly restricted to the long and narrow valleys where the overburden is considerably thicker. The geographical distribution of Quaternary deposits and the modelled depths of the overburden in the model area are shown in Figure 4-1 and Figure 4-8, respectively. Table 4-1 shows the proportional distribution of the overburden in the central part of the Laxemar-Simpevarp area. In total, some 58% of the regional model area is covered by Quaternary deposits and the remainder consists of bedrock outcrops. Till is the most common Quaternary deposit and covers c. 34% of the regional model area.

The bedrock surface in the regional model area is often rough, indicating a low degree of glacial erosion. After the deglaciation c. 12,000 BC, the water level in the Laxemar-Simpevarp area was c. 100 m higher than at present and the area was consequently completely covered by water (see Chapter 3). The stratigraphical investigations indicate that the overburden has been formed during the end of, and after, the latest ice age. However, the existence of older parts of the overburden cannot be excluded and /Lagerbäck et al. 2006/ have suggested that some parts of the overburden in this part of the County of Småland may be older than the latest glacial phase.

The stratigraphical distribution of Quaternary deposits in the investigated area is rather uniform (Table 4-2). Till is the oldest Quaternary deposit in the area and rest directly upon the bedrock surface. The till in the valleys is often overlain by glacial clay, which, in turn, is often covered by a layer of sand followed by clay gyttja and peat (Table 4-2). The main stratigraphical units are shown in the depth and stratigraphy model of the overburden /Nyman et al. 2008/. The glaciofluvial deposits commonly rest directly upon the bedrock surface. Based on the stratigraphical and geographical distribution of the Quaternary deposits, the area has been divided in three type areas which are discussed below.

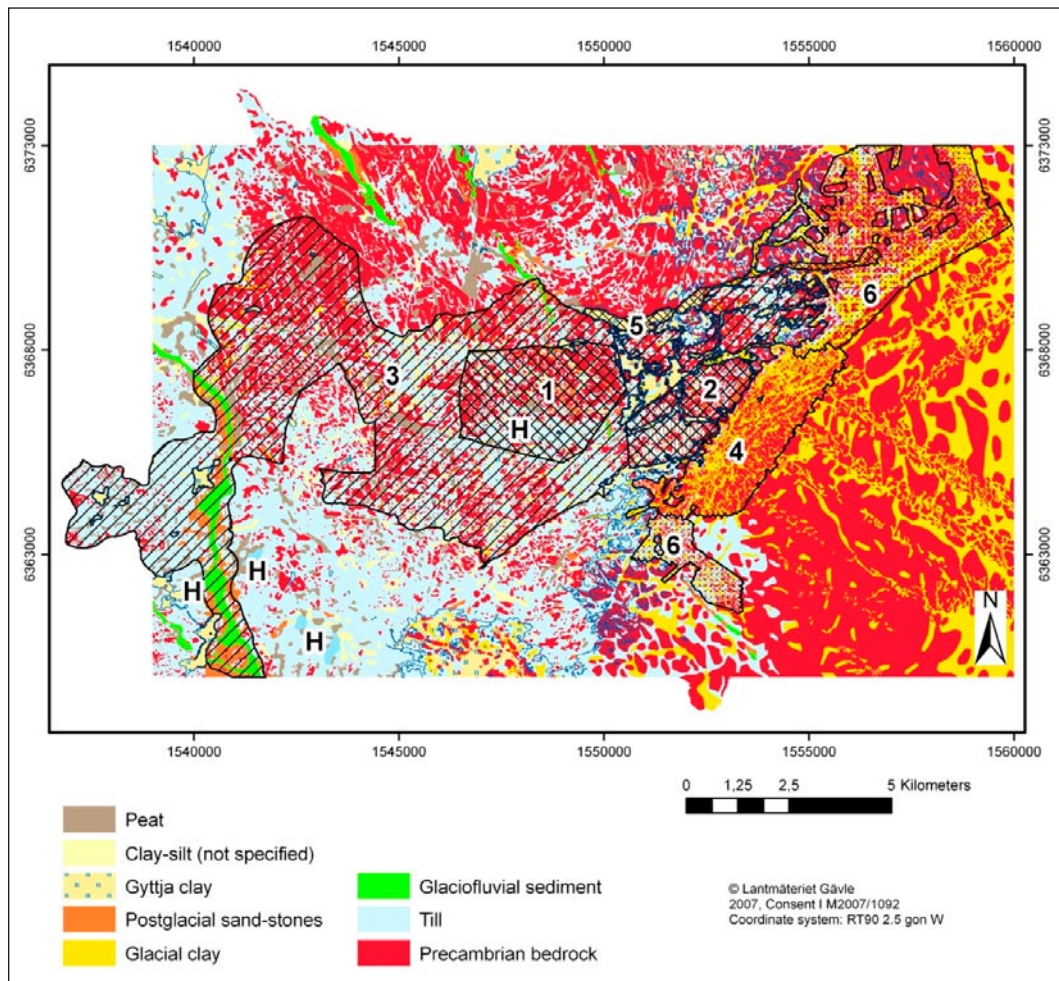


Figure 4-1. The geographical distribution of Quaternary deposits in the Laxemar-Simpevarp area. The map has been produced using data from several activities /see Sohlenius and Hedenström 2008/. The numbers refers to the different type areas (extensions indicated by different patterns) shown in Table 4-1. The topographically high areas with hummocky moraine are marked with H.

Table 4-1. The proportional distribution of Quaternary deposits in the central parts of the Laxemar-Simpevarp regional model area. The extensions of the different type areas referred to in the table are shown in Figure 4-1. Area 1 = Laxemar subarea, Area 2 = Simpevarp subarea, Area 3 = the drainage area of the Laxemarån river. Area 3 also includes areas 1 and 2. The terrestrial area was mapped by /Rudmark et al. 2005/. Areas 4, 5 and 6 refer to different parts of the marine area mapped by /Ingvarson et al. 2004/ and /Elhammer and Sandkvist 2005/.

Quaternary deposit	Area 1	Area 2	Area 3	Area 4	Area 5	Area 6	The whole area
Coverage (%)							
Peat	5.3	1.9	8.0	–	–	–	4.5
Clay gyttja (postglacial clay)	5.8	0.1	3.4	0	44.0	0.7	–
Glacial clay	0.7	1.1	1.4	41.6	13.4	33.1	16.0**
Glaciofluvial sediments	0.1	0.0	3.0	0	0	0	1.2
Postglacial sand and gravel	4.8	5.8	4.3	3.3	2.1	0.3	1.8
Till	45.2	35.0	43.3	3.4	5.1	22.5	34.3
Precambrian bedrock*	38.2	38.2	34.5	51.6	35.4	43.4	41.9
Artificial fill	0	17.9	1.3	0.1	0	0	0.4

* Areas with bedrock outcrops. ** Glacial and postglacial clays.

Table 4-2. The stratigraphical distribution of Quaternary deposits in the Laxemar-Simpevarp area. Glaciofluvial sediments are not included in the table, but commonly rest directly upon the bedrock surface.

Quaternary deposit	Relative age
Bog peat	Youngest
Fen peat	↑
Gyttja clay/clay gyttja	
Postglacial sand/gravel	↑
Glacial clay	
Till	↑
Bedrock	Oldest

The topographically high areas

The highest topographic areas are dominated by till and bedrock outcrops. In the terrestrial area this environment is completely dominated by forest. The overburden in the topographical high areas is generally less than one or a few metres thick. On land, there are numerous small peat-covered wetlands incorporated in the till and bedrock dominated areas. The Quaternary deposits in these wetlands are generally thinner than in the larger wetlands situated in the valleys. It is, however, possible that small pockets of thicker Quaternary deposits occur also in these small wetlands. The groundwater table in the small wetlands has most often not been artificially lowered.

The frequency of bedrock outcrops is high in the central and northern parts of the terrestrial areas. Also the topographically elevated areas on most of the seafloor outside the archipelago are totally dominated by till and bedrock outcrops. On land, lichen and mosses cover a large proportion of the outcrop bedrock while some bedrock areas have somewhat richer vegetation and may partly be covered by thin layers of Quaternary deposits. Till covers a larger proportion of the terrestrial areas compared with the marine areas. It is possible that the till coverage in the terrestrial areas is slightly overestimated. Observation at the sea floor shows that a thin boulder layer often covers the bedrock. Such boulder-covered bedrock areas may have been erroneously interpreted as till in the terrestrial areas where the bedrock is often covered by vegetation.

Areas with hummocky moraine (marked with H in Figure 4-1) and also with a low frequency of bedrock exposures occur in the south-western part of the model area, but also in the central part of the Laxemar subarea. The till in that environment is thicker than the till in other topographically high areas.

The valleys

In the terrestrial areas, clay gyttja, peat and postglacial sand/gravel dominate the floor of the valleys. Glacial clay and till underlie these deposits, cf. Table 4-2. A large proportion of the peat and water-laid deposits is used as arable land.

The peat areas consist both of wetlands where peat presently is accumulating, and of former wetlands where the groundwater table has been artificially lowered for agricultural purposes, or to improve the rate of forest growth. The lowered groundwater table causes the peat to be more compact and to oxidise, and following the groundwater lowering the layer of peat is successively becoming thinner. Some of the wetlands are former lakes, which have been covered by peat. Many of the present and former wetlands have, however, not experienced a lake stage, and were instead formed directly after the area rose above the sea level.

The valleys on the sea floor off the archipelago are at present exposed to the erosive forces of waves and streams (e.g. Area 4 in Figure 4-1 and Table 4-1). Consequently, there is almost no accumulation of fine-grained deposits in this area, and the valley floors are instead characterised by erosion and transportation of sediment. The glacial clay, which is often found in the bottom layer of the valleys, is therefore often covered by a layer of sand or gravel.

The lakes and bays are sheltered from strong influence of waves and currents. Consequently, clay gyttja and gyttja are accumulating in large parts of the floor of lakes and sheltered bays (e.g. Area 5 in Figure 4-1 and Table 4-1). The rate of sediment accumulation is similar in lakes and bays, and several metres of gyttja sediments have been recorded in the deepest parts of the lakes and bays. Peat is accumulating along the shores of the lakes, and the size of the lakes will successively decrease.

The total thickness of Quaternary deposits in the valleys is often several metres /Sohlenius et al. 2006, Morosini et al. 2007/. Results from drillings show a maximum overburden depth of more than 30 metres, and results from geophysical measurements indicate overburden depths of up to 50 metres. Results from geophysical measurements and drillings indicate that the different stratigraphical units are generally thicker in valleys located in the marine area compared with valleys in the terrestrial area.

The valleys reflect lineaments in the bedrock which are rich in fractures and which in some cases are associated with interpreted deformation zones, cf. Section 5.5. The bedrock underlying the Quaternary deposits in the valleys is consequently of poor quality and it may sometimes be difficult to define the interface between the bedrock and the deposits.

The glaciofluvial eskers

There are three small and one large (the Tuna esker) glaciofluvial deposits in the regional model area (Figure 4-1). These deposits are well sorted with respect to grain size, and consist mainly of sand and gravel. The glaciofluvial deposits are well drained and the vegetation is therefore adapted to dry conditions. The few available data from glaciofluvial deposits in the model area indicate that these rest directly upon the bedrock. During the latest deglaciation, the glaciofluvial sediments were deposited in tunnels formed beneath the ice by melt water running from the north. It should be noted that some of the eskers might have been formed during an older deglaciation than the latest /cf. Lagerbäck et al. 2006/.

Chemical and physical properties of Quaternary deposits

The most common Quaternary deposits and soils have been analysed with respect to chemical and physical properties and the results are compiled in /Sohlenius and Hedenström 2008/. All Quaternary deposits except peat, the latter which is almost entirely built up by organic material, were analysed with respect to grain size (Table 4-3). The quotient d_{60}/d_{10} (based on diameter of sieved material, cf. Table 4-3) has been calculated to demonstrate the degree of sorting. The deposit is considered poorly sorted with respect to grain size if d_{60}/d_{10} is above 15. Most of the till samples have a d_{60}/d_{10} well above 15.

Porosity and density has been calculated for some of the Quaternary deposits (Table 4-4). Some data in Table 4-4 were taken from the literature since site-specific data are lacking. The till in the area is characterised by a low content of fine material and high content of sand and gravel. In some of the investigated valleys, the material underlying the clay was classified as till, but has a grain size composition more similar to water-laid deposits. The latter, relatively well-sorted material is therefore referred to as sand and gravel in Table 4-3. It is assumed that the postglacial and glaciofluvial sediments have similar properties. The properties of these deposits are therefore shown jointly in Table 4-3. These deposits were both deposited in water and the material originates from till or bedrock.

The chemical composition of the deposits is close to the Swedish average /e.g. Andersson and Nilsson 1992/. The petrographic and mineralogical composition of the till reflects that of the local bedrock /Bergman and Sohlenius 2007/, even though the till has been transported from the north. However, since the till has been subjected to chemical weathering, the chemical composition of the till differs slightly from that of the bedrock. The mineralogy of the clay is different from that of the bedrock since the clay has a high content of clay minerals, which were formed after chemical alteration of some of the primary bedrock minerals. Furthermore, the chemical composition of clay is also affected by the environmental conditions prevailing during deposition.

In all investigated lakes, total contents of organic carbon (C), nitrogen (N) and sulphur (S) in the glacial clay are relatively low, but show an increasing trend from the glacial clay to the overlying younger gyttja sediments (Table 4-5). High production of organic matter in the sheltered bays and lakes probably caused the relatively high N and organic C contents preserved in the clay gyttja deposited in these environments. The high S content in the clay gyttja is interpreted to be an effect of iron sulphides present in the sediments.

There are no data describing the physical and chemical properties of the artificial fill. Most artificial fill is material which originated from the construction of the nuclear power plants. That material has probably a coarse-grained size composition, and a chemical and mineralogical composition similar to that of the local bedrock.

Table 4-3. The average grain size distribution of material <20 mm in Quaternary deposits. The ratio d60/d10 (where d60 is the particle diameter corresponding to 60% finer on the grain-size curve, and d10 is the particle diameter corresponding to 10% finer on the grain-size curve) is also called coefficient of uniformity. The smaller the coefficient of uniformity, the more uniform the material. The values are presented as the percentage by dry weight values.

Quaternary deposit	N	Gravel (%)	Sand (%)	Silt content (%)	Clay content (%)	d60/d10
Average gravelly till	31	47.7±10.5	40.1±10.4	9.4±3.6	2.8±1.2	102±134
Average sandy till	16	27.7±9.20	46.5±11.8	21.5±14.3	4.3±2.5	69.7±59.7
Average till	48	40.1±14.7	41.9±11.3	14.3±11.6	3.7±3.1	133±170
Average clay gyttja	61	0.0±0.1	20.9±11.6	46.4±11.6	32.7±12.5	–
Average glacial clay	18	0.5±1.2	9.0±7.6	31.1±9.0	59.4±12.3	–
*Average sand	9	17.4±22.1	79.5±22.0	2.3±1.5	0.8±1.1	–
**Sand and gravel	9	55.6±15.4	41.9±14.2	2.6±2.0	0	16.7±5.4

* The sand samples are both of glacial and postglacial origin.

** Sand and gravel, which were classified as till in the field but have a grain size distribution equal to water-laid sediments. These well sorted "till" samples were obtained from drillings in the valleys.

Table 4-4. The average physical properties of the Quaternary deposits. The properties of till and sand/gravel are taken from the literature and are not obtained from the site investigation. The bulk density refers to the density of water-saturated material.

	N	Water content (% by weight)	Porosity (% by volume)	Bulk density (kg/m ³)	Reference
Till			10–25	2,100–2,400	/Pusch 1974/
Glacial clay	11	51.9±8.3	73.5±6.6	1,430±105	/Nilsson 2004, Sohlenius et al. 2006/
Clay gyttja	42	83.4±5.4	90.0±3.4	1,081±33	/Nilsson 2004/
Peat	18		92.6±3.0	100±57*	/Lundin et al. 2005/
Peat	2	91.5	92.0	1,005	/Nilsson 2004/
Top sediment (clay gyttja)	58	90.8±1.6	94.7±0.9	1,043±9	/Fredriksson 2004/
Sand/gravel			15–50	1,800–2,300	/Pusch 1974/
Top sediment (sand and gravel)	22	24.8±14.7	43.4±17.3	1,914±293	/Fredriksson 2004/

* Dry bulk density.

Table 4-5. The average contents of organic carbon (C), nitrogen (N) and sulphur (S) in clay gyttja, peat and glacial clay /from Nilsson 2004, Sternbeck et al. 2006/. The N content of the glacial clay was below the detection limit. The S content was not measured by /Sternbeck et al. 2006/.

	N (C,N)	N (S)	Org. C (%)	Tot. S (%)	Tot N (%)
Peat	5	2	52.4±4.5	0.16	1.4±0.6
Clay gyttja in fens	13	13	15.3±8.1	1.5±1.1	1.3±0.6
Clay gyttja in lakes	35	31	17.4±8.1	1.4±1.2	1.6±0.6
Clay gyttja in bays	26	14	13.4±1.1	2.2±0.5	1.7±0.2
Clay gyttja (total)	74	58	15.6±6.7	1.7±1.1	1.6±0.5
Glacial clay	8	8	0.5±0.3	0.5±0.5	–

4.2.2 Hydrology and near-surface hydrogeology

Site investigations and hydrological characteristics

The site investigations in Laxemar-Simpevarp included comprehensive investigations of hydrology and near-surface hydrogeology. These investigations comprised monitoring of meteorology (including “winter parameters” such as snow depth and ice freeze/breakup), surface-water levels in lakes and bays of the Baltic Sea, stream discharges, and groundwater levels in Quaternary deposits. Moreover, different types of field and laboratory tests were conducted for hydrogeological characterisation of Quaternary deposits and the interactions between groundwater in the Quaternary deposits and groundwater in the rock. Descriptions of methods, evaluations of input data, and conceptual and quantitative water flow modelling are presented in /Werner 2008, Werner et al. 2008, Bosson et al. 2008/.

As described above, the topography of the Laxemar-Simpevarp area is characterised by relatively distinct valleys, surrounded by higher-altitude areas dominated by exposed or shallow rock. The south-western and central parts of the Laxemar-Simpevarp regional model area are characterised by hummocky moraine and thereby a smaller-scaled topography. Almost the whole area is located below 50 metres above sea level (m.a.s.l.), and the entire area is located below the highest coastline.

The site-average annual precipitation and specific discharge are estimated to be on the order of 600 mm and 160–170 mm, respectively. The precipitation demonstrates a near-coastal gradient, with less precipitation at the coast compared with areas further inland; the difference in annual average precipitation at the coastal Äspö station and the inland Plittorp station is c. 7% for the site investigation period.

The main lakes at the area are Lake Jämsen (0.24 km²), Lake Frisksjön (0.13 km²), Lake Söråmagasinet (0.10 km²), Lake Plittorpsgöl (0.03 km²), Lake Fjällgöl (0.03 km²) and Lake Grangöl (no size data), cf. Appendix 1. These relatively small lakes are shallow, with average depths in the range 1–4 m and maximum depths in the range 2–11 m. All lakes are located well above the sea level, which implies that no sea-water intrusions into the lakes take place. Wetlands in total cover c. 3% of the delineated catchment areas /Brunberg et al. 2004/.

Most streams are affected by land improvement and drainage operations. Of the monitored streams, there is flow throughout the year in the streams Laxemarån, Kåreviksån downstream from Lake Frisksjön and Kärrviksån, cf. Appendix 1. The stream Ekerumsån is dry during dry summers, whereas the other monitored small streams are dry during approximately half of the year. Except for some minor wetlands, the surface waters (lakes, streams and wetlands) are associated with low-altitude areas. These surface waters are mainly underlain by glacial and post-glacial sediments. Specifically, the general bottom-up stratigraphy of Quaternary deposits below surface waters is till and glacial clay, overlain by postglacial sediments (sand/gravel, gyttja clay/clay gyttja, overlain by fen peat and bog peat in the wetlands).

Groundwater levels in the Quaternary deposits are shallow; according to monitoring data, the average depth to the groundwater table is less than 1 m during 50% of the time. Generally, the depth to the groundwater table is larger in high-elevation areas than in low-elevation areas, but this variation is much smaller than the variation in absolute groundwater levels in the area. Accordingly, there is a

close correlation between the ground-surface topography and groundwater levels in the Quaternary deposits, which in turn implies that topography has a strong influence on near-surface patterns of groundwater recharge and discharge.

Conceptual modelling

As part of the conceptual modelling of hydrology at Laxemar, four main hydrogeological type areas have been defined, which conform to the subdivision of the Quaternary deposits (cf. Section 4.2.1). These type areas are high-altitude areas, large and small valleys, glaciofluvial deposits, and hummocky moraine areas. The type areas are mainly used as a framework for description of the overall patterns of groundwater recharge and discharge in the Laxemar-Simpevarp area. Moreover, the conceptual modelling includes parameterisations of the overall hydrogeological flow domains (Quaternary deposits and rock). Further detailed parameterisation of different types of Quaternary deposits has been done as part of the SurfaceNet work /Werner 2008, Werner et al. 2008/, whereas detailed descriptions and parameterisation of the rock (including near-surface rock) were performed within HydroNet /Rhén et al. 2008/.

The descriptions of Quaternary geology /Sohlenius and Hedenström 2008/ and the 3D model of depth and stratigraphy of the Quaternary deposits /Nyman et al. 2008/ (here denoted RDM; see Section 4.3.2) have been used as a basis for the development of a hydrogeological model of the Quaternary deposits. Specifically, the various layers of the RDM are assigned hydrogeological properties based on site investigation and generic data /Werner et al. 2008/, and the RDM is also used for the development and testing of conceptual and quantitative water flow models /Werner 2008, Bosson et al. 2008/.

Figure 4-2 shows a conceptual N-S section across a typical large valley in the Laxemar-Simpevarp area. According to the conceptual description of the Quaternary deposits, sandy-gravelly till overlies the rock in the area, also in most areas with exposed/shallow rock (which may have a thickness of up to c. 0.5 m). The exceptions are some of the exposed/shallow bedrock areas, in which organic soil and a relatively thin vegetation layer directly overlies the rock. The sandy-till is characterised by a relatively high hydraulic conductivity (c. $4 \cdot 10^{-5}$ m/s).

There are indications that the hydraulic conductivity of the Quaternary deposits overlying the rock in the deepest parts of the large valleys is about one order of magnitude higher than that of till in other parts of the area; this more permeable material is indicated as “Bottom QD” in Figure 4-2. Moreover, permeameter tests on till indicate an anisotropic hydraulic conductivity, with an anisotropy ratio (K_h/K_v) that may be in the order of 15–30. However, it should be noted that permeameter tests are associated with a smaller tested volume compared with e.g. slug tests providing *in situ* hydraulic conductivity data. Generic data are used to support the estimates of the hydrogeological properties for types of Quaternary deposits other than till.

Figure 4-3 shows a generalised section illustrating the overall conceptual model of hydrology and hydrogeology in Laxemar. The hydraulic conductivity of the rock generally decreases with depth, both in the deterministically defined deformation zones and in the rock between these zones /Rhén et al. 2008/. Hydraulic test data indicate that most of this decrease occurs in the upper 100-200 m of the rock. The horizontal conductive fractures are significant or dominant in the near-surface rock, but at deeper levels the sets of horizontal fractures generally become less significant compared with the vertical sets. As indicated in Figure 4-3, the deformation zones have a variable thickness, and are generally wider closer to the interface between the bedrock and the Quaternary deposits.

As illustrated in the conceptual section across a lake in Figure 4-4, groundwater level measurements below lakes indicate that interactions between surface water in the lakes and the underlying Quaternary deposits are limited to near-shore areas. Some parts of the streams pass through areas where there are no layers of glacial clay and postglacial sediments, which is also the case for some near-shore areas of the lakes. The local conditions for surface water-groundwater interactions are also influenced by land improvement and drainage operations, which for instance imply that water flows in subsurface “pipes” along some parts of the streams.

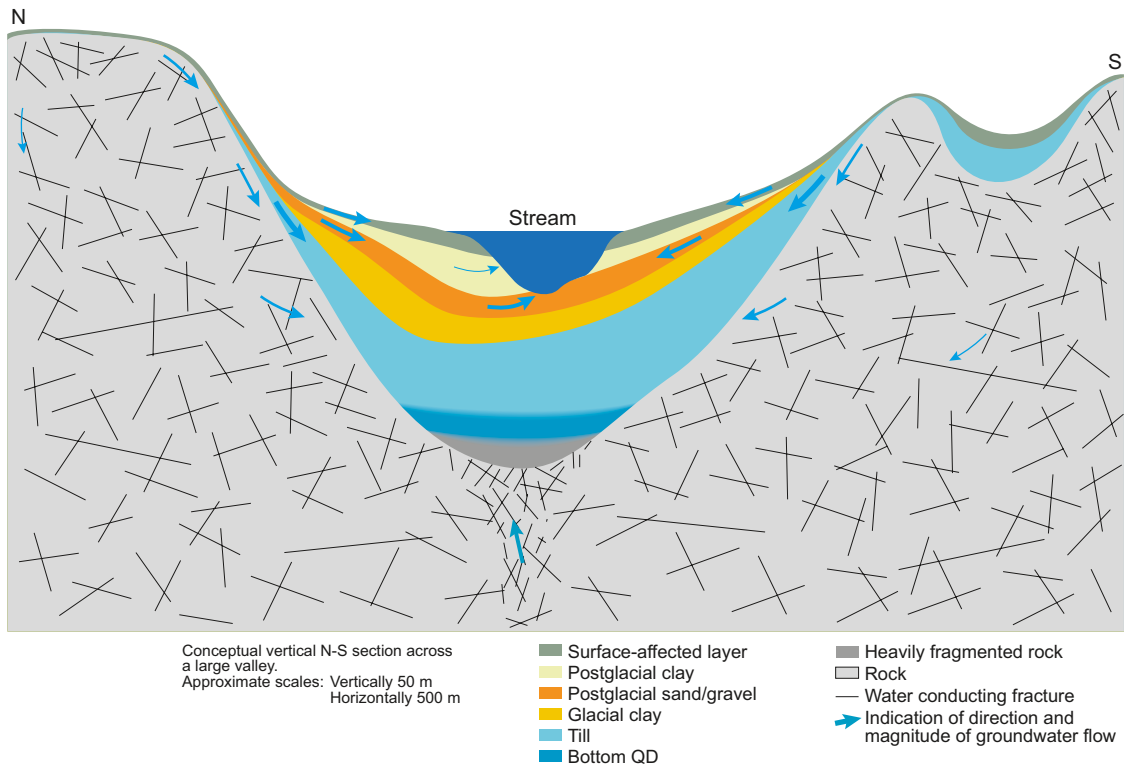


Figure 4-2. Conceptual vertical N-S section across a large valley in Laxemar. Note the different horizontal (500 m) and vertical (50 m) scales, and that the size of the stream is exaggerated in the figure. “Bottom QD” represents relatively conductive Quaternary deposits that locally overlay the rock in the deepest parts of the large valleys.

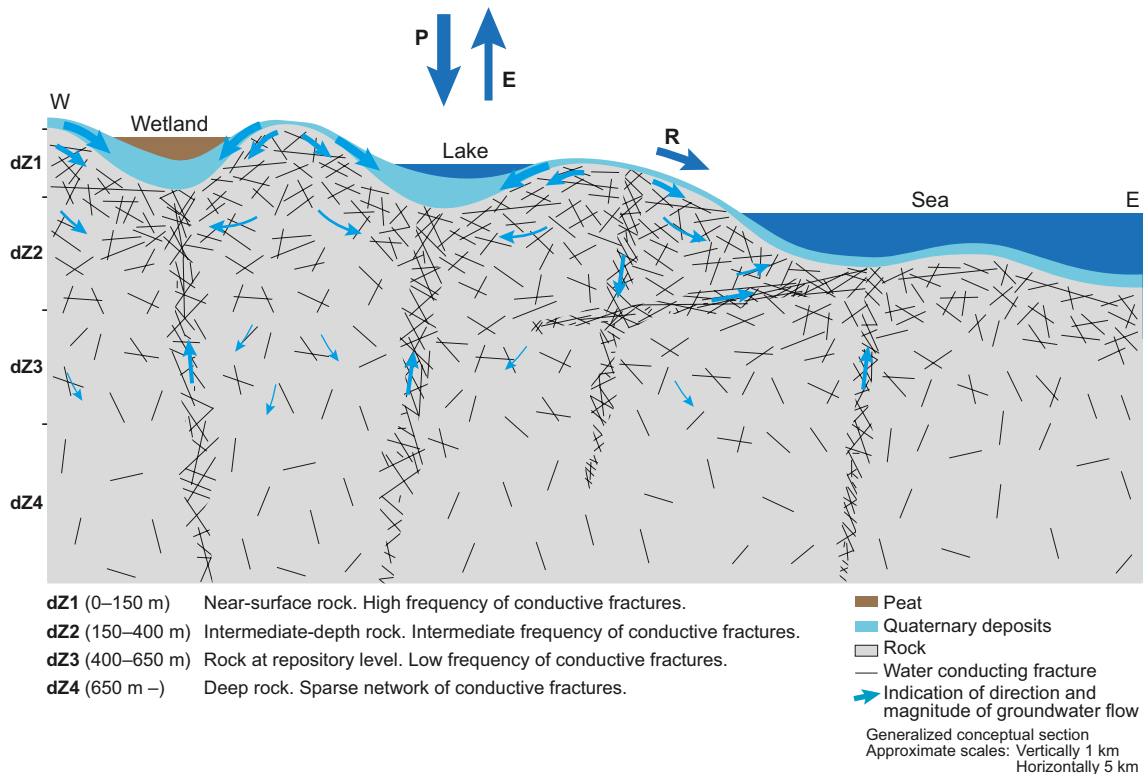


Figure 4-3. Generalised section illustrating the conceptual model of hydrology and hydrogeology in Laxemar. Note the different horizontal (5 km) and vertical (1 km) scales, and that the thickness of the Quaternary deposits is exaggerated in the figure.

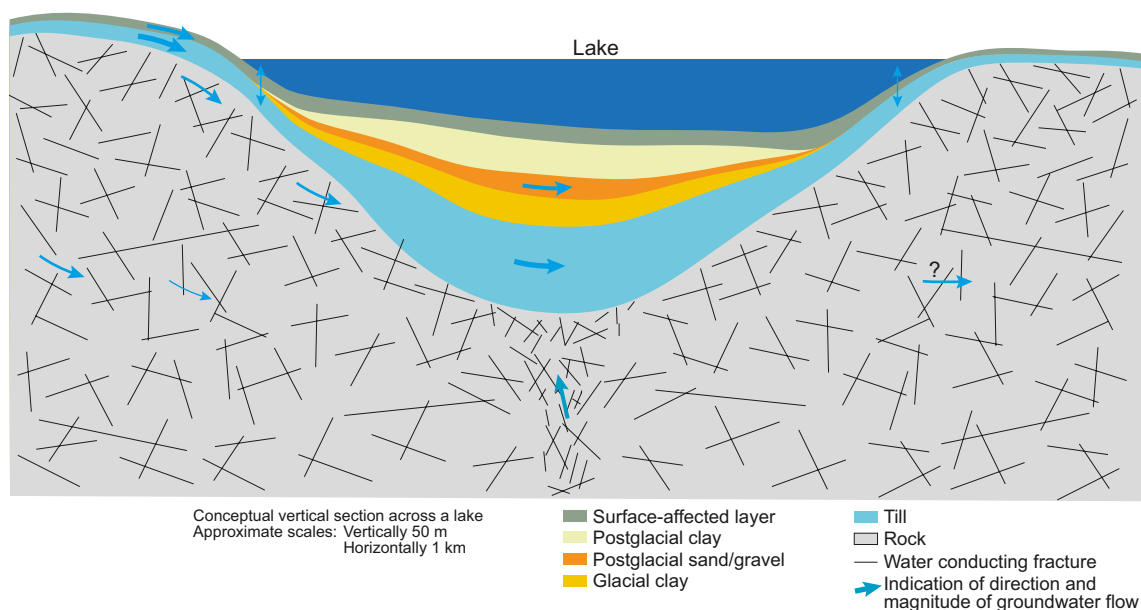


Figure 4-4. Conceptual vertical section across a lake in Laxemar, illustrating that interaction between surface water in the lakes and the underlying Quaternary deposits likely is limited to near-shore areas. Note the different horizontal (1 km) and vertical (50 m) scales in the figure.

4.2.3 Chemistry

This section describes the overall chemical characteristics of surface water and groundwater at shallow to intermediate depths (down to c. -250 m elevation), including distribution of type waters and mixing processes amongst these waters. These findings result in a conceptual profile/section as described below, and the interactions between the surface water and the groundwater are schematically presented. The detailed hydrochemistry of the deep bedrock system below this zone is described in Chapter 9.

Compilations and evaluations of hydrochemical data from surface water and shallow groundwater are presented in /Tröjbom and Söderbäck 2006/ and /Tröjbom et al. 2008/, and data on the chemical composition of the overburden are evaluated in /Tröjbom and Söderbäck 2006/.

The freshwater systems in the Laxemar-Simpevarp area are generally classified as mesotrophic brown-water (dystrophic) types. Most waters are markedly coloured due to the high content of humic substances and show, accordingly, high levels of dissolved organic carbon. Streams and lakes are also relatively rich in nitrogen and phosphorus. Fresh surface water and shallow groundwater in the area are neutral to slightly acid, and concentrations of most major ions are normal in a Swedish perspective /Tröjbom and Söderbäck 2006/.

The topography of the Laxemar-Simpevarp area is characterised by elevated areas covered by thin or no Quaternary deposits, intersected by deep fissure valleys filled with thick sediments. These topographical characteristics, in combination with the post-glacial shoreline displacement, are two important factors determining the hydrochemistry of the surface system in the area. A detailed evaluation of the hydrochemistry of surface waters and shallow groundwater in the Laxemar-Simpevarp area can be found in /Tröjbom et al. 2008/. Below follows a summary of the most important findings from that study.

In areas of low elevation close to the coast, marine remnants in the Quaternary deposits (manifested e.g. as elevated chloride concentrations) have a significant influence on the hydrochemistry, whereas areas situated at higher elevation are mostly influenced by atmospheric deposition and weathering processes. The vegetation cover has also a great impact on the hydrochemistry of the surface system. Degradation of biogenic carbon generates large amounts of H⁺ ions, which drive weathering and ion exchange processes in the Quaternary deposits, as well as in the upper parts of the bedrock.

Most of the degradation occurs in aerobic environments on or near the ground surface, but also microbial sulphate reduction in anaerobic, organic sediments is important, and this process also takes place in deeper parts of the groundwater system. This situation, together with inorganic processes and groundwater flow pattern in the upper part of the bedrock, govern the development of the redox front as illustrated in Section 4.4.

The following conceptual model, applicable to a depth of –250 m, may explain the hydrogeochemistry in the Laxemar-Simpevarp area on a regional scale:

- In low altitude areas close to the coast, relict marine water prevails in the deeper parts of the deposits and in the upper parts of the bedrock. The high salinity compared with present Baltic Sea water, in combination with negative values of deuterium excess, indicates that this relict sea water is probably a remnant of the Littorina Sea stage when sea water with a Cl concentration of approximately $6,500 \text{ mg}\cdot\text{L}^{-1}$ infiltrated the Quaternary deposits and the bedrock.
- In the Quaternary deposits of low altitude areas close to the coast, intermediate Cl concentrations, in combination with meteoric $\delta^{18}\text{O}$ isotope signatures, indicate ongoing flushing of relict marine remnants (e.g. Littorina).
- In areas at slightly higher altitudes, which have been covered by sea water after the latest glaciation, meteoric isotope signatures and low Cl concentrations indicate that marine influences (and any other older water types) have been washed out due to the meteoric recharge.
- In areas located above the highest coastline of the Littorina Sea, there are no indications on relict marine remnants, which is to be expected. Cl concentrations in surface water and shallow groundwater in these areas can be fully explained by deposition and anthropogenic point sources such as road salt.
- Deep saline signatures observed in two soil tubes located in till below thick lake and sea sediments (in Lake Frisksjön and the coastal bay Borholmsfjärden) may possibly be explained by the influence of deep groundwater discharge. Both these sites are located in the vicinity of major deformation zones, which have been proposed as potential locations for deep groundwater discharge. The differing water isotope signatures seen at these two sites indicate, however, that the soil tube located below the coastal bay is affected by regional or local meteoric discharge originating from the higher elevated areas in the north, whereas the soil tube located below Lake Frisksjön probably reflects a more stagnant relict marine groundwater, less influenced by ongoing meteoric recharge.

An important question in the hydrochemical evaluation is whether there are any indications of deep groundwater discharge into the surface system. It can be concluded from observations of major elements and environmental isotopes in shallow groundwater that deep groundwater signatures are present in the Quaternary deposits in some areas with potential deep discharge near the coast. In more inland areas, no deep signatures have been detected, neither in surface water nor in groundwater. This indicates that shallow meteoric recharge/discharge patterns dominate, and it is therefore highly unlikely that any regional deep discharge occur in the terrestrial parts of the regional model area.

4.2.4 Transport properties

Many radionuclides and other solutes transported by groundwater in bedrock and Quaternary deposits are subject to processes acting to immobilise (for shorter or longer time periods) or chemically transform the solutes along the flow paths in the subsurface. Sorption and precipitation/dissolution processes are two categories of processes that associate solutes with different types of immobile phases (primarily surfaces of geological materials). In line with common nomenclature in radionuclide transport modelling, they are here referred to as retention processes.

The handling of solute retention in transport models could range in complexity from relatively simple K_d -based modelling concepts to so-called process-based or mechanistic modelling. In K_d -based models, retention is modelled as a linear equilibrium process, which means that sorbed and aqueous concentrations are related by a constant coefficient, the K_d value. This is the modelling approach taken in the SKB safety assessment modelling, although solutes also may be subject to other retention processes (primarily diffusion). This means that site-specific data on K_d values and/or other parameters that may help in relating generic K_d databases to the conditions at Laxemar-

Simpevarp are needed. In the safety assessment modelling, also other, conceptually similar distribution coefficients are used for describing, for instance, the solute distribution between water and biota; these are referred to as transfer factors.

In the SDM-Site Laxemar work, data collection and evaluations intended to provide a basis for both K_d -based and mechanistic retention models have been performed. However, these activities, which are summarised in the remainder of the present section are to be considered as parts of a work in progress. Further studies will be performed in the subsequent SR-Site stage and the final results will be presented in the SR-Site reporting.

Transport conditions in the Quaternary deposits

The effect of radionuclide retention in the Quaternary deposits depends on a variety of physical and chemical properties of the solid materials, the groundwater and the radionuclides. The properties of the various Quaternary deposits and the near-surface groundwater are also central to the assessment of other transport scenarios, primarily those associated with downward transport through the surface system where the groundwater composition could be altered before it enters the bedrock.

Many of the site investigations providing data relevant for describing retention conditions were performed within the framework of the geological investigations, i.e. the investigations of soils and Quaternary deposits, and the hydrochemical monitoring. The physical and chemical properties of Quaternary deposits and the groundwater hydrogeochemistry of those deposits are described in /Sohlenius and Hedenström 2008/ (see Section 4.2.1 of the present report for a summary), and in /Tröjbom et al. 2008/.

In particular, data on the following properties and parameters of importance for the assessment of solute retention data are available from the Laxemar-Simpevarp area:

- Chemical compositions, i.e. elemental compositions (major and minor constituents and trace elements), of Quaternary deposits and groundwater.
- Organic content, pH values and redox conditions in the groundwater.
- Contents of clay, organic material, and calcium carbonate in the Quaternary deposits.
- Mineralogical compositions: primary minerals and clay mineralogy.
- Chemical and physical properties of solid surfaces: individual exchangeable cations, total cation exchange capacity (CEC), and BET surface areas.
- Physical properties of Quaternary deposits: grain size distribution, porosity, density and water content.

Instead of providing detailed references to where all these different data types can be found, the reader is here referred to the summary reports on Quaternary deposits /Sohlenius and Hedenström 2008/ and surface system chemistry /Tröjbom et al. 2008/. Concerning specific investigations of particular importance for the assessment of transport conditions, the following two investigation campaigns are of relevance:

- Excavation of trenches down to the rock surface across three valleys in Laxemar. In the same campaign drillings and installations of groundwater monitoring wells were performed in the vicinity of each trench and also at one valley location where the excavation was not possible due to the large depth of the Quaternary deposits. Groundwater and soil samples were taken and analysed for a variety of physical and chemical parameters including mineralogy and solid surface chemistry. These investigations are reported in /Sohlenius et al. 2006/.
- Drillings, soil sampling and installations of groundwater monitoring wells in the three deepest valleys in Laxemar, i.e. the Laxemarån, Ekerumbäcken and Mederhult valleys, cf. Appendix 1 for geographical reference. The objectives of this campaign were to investigate the depth to the rock and the material in the deepest parts of the valleys, and to take samples to be used in laboratory sorption experiments (cf. below). As part of the investigations, the soil samples were analysed for a number of parameters related to sorption; this supporting characterisation of the sorption samples included all the parameter types listed above. The drillings, sampling and characterisation of soil samples are reported in /Morosini et al. 2007, Lundin et al. 2007/.

Site-specific K_d values

In an on-going project, site-specific data on K_d values are being obtained by measuring the aqueous (pore water) and sorbed concentrations in soil samples. Sampling for these measurements has been performed in both Forsmark and Laxemar-Simpevarp; samples were taken at three locations in Forsmark and four locations in Laxemar-Simpevarp. In Laxemar-Simpevarp, the sampling included sandy till, clay gyttja (two samples), and peat. At each sampling location, ten sub-samples were taken at a depth of c. 30 cm.

The soil solids and the pore water in the general samples have been analysed for elemental composition; the methods used are described in /Sheppard et al. 2007/. This procedure will result in K_d values for approximately 50 elements. As a part of the evaluation of the resulting dataset, the site-specific K_d values will be compared with literature data from other sites. Site-specific K_d values of suspended material and sediments in lakes and sea bays obtained with similar methods are also currently under evaluation. The sampling and chemical analyses performed to obtain these K_d data are described in /Engdahl et al. 2008/.

As mentioned above, sorption experiments, in the form of so-called batch sorption experiments, have been performed on samples from the valleys in Laxemar. Eight samples representing materials ranging from till to peat were included in this programme. The sorption experiments have been finalised and the results are currently (April, 2009) being evaluated. An important part of this evaluation is to investigate relations between the K_d values and the parameters included in the sample characterisation programme.

4.2.5 Ecosystems

The description of the terrestrial, limnic and marine ecosystems in the area contains both qualitative data, such as lists of dominant species, and quantitative descriptions of a number of ecosystem properties. Information about the site-specific data from the terrestrial ecosystem, and the methods used for estimation/calculation, are presented in /Löfgren 2008/ and references therein. A number of investigations of the limnic ecosystem in the Laxemar-Simpevarp area, mainly in Lake Frisksjön, and of the marine ecosystem have been performed. Comprehensive descriptions and evaluations of the input data (site-specific and generic) and of the methods used are presented in /Nordén et al. 2008/ for the limnic ecosystem and in /Wijnbladh et al. 2008/ for the marine ecosystem.

Terrestrial ecosystems

Vegetation

The location of the investigated area close to the sea makes the seashore a prominent feature in the east along with conifer forests and some agricultural land. The terrestrial vegetation is strongly influenced by the characteristics of the Quaternary deposits and by the human land use. Below follows a brief description of three major vegetation types within the investigation area, see /Löfgren 2008, cf. Chapter 4 therein/ for more details.

Forests cover approximately 73% of the land area of the main catchments in the Laxemar-Simpevarp regional model area and the forests are dominated by Scots pine (Sw: *tall*) and Norway spruce (Sw: *gran*). Scots pine dominates on bedrock or in areas with a shallow soil layer, whereas Norway spruce becomes more abundant in areas with a deeper soil cover in combination with mesic-moist conditions. Deciduous tree species, mainly pedunculate oak (Sw: *ek*), but also hazel (Sw: *hassel*), rowan (Sw: *rönn*), Swedish whitebeam (Sw: *oxel*) and Norway maple (Sw: *lönn*), are more common near the coast, making the mixed forest the second most common forest type.

The predominant humus form in the Scots pine and Norway spruce forests is moder-humus, i.e. the intermediate form between mor and mull extremes. In these forests, the soil type regosol dominates, but podzols become more common where there is a deeper soil cover. The mull-like humus form becomes more dominant with increasing occurrence of deciduous trees /Lundin et al. 2005/ and in this type of forest, the soil types regosol and umbrisol are found. The Laxemar-Simpevarp area has a long history of forestry, currently indicated by a fairly high percentage of younger and older clear-cuts in different successional stages in the landscape. Birch (Sw: *björk*) is the dominant species in many of the earlier successional stages until it is replaced by young Norway spruce or Scots pine, depending on soil type and/or management.

Wetlands are less frequent and cover only 1% of the area in the main catchments. The wetlands consist of both coniferous/deciduous forest swamps and open mires. Although not so numerous, bogs are also present in the inland, and are continuously created due to the shoreline displacement and mineral and nutrient leaching processes. In the northern part of the area where bedrock outcrops are common, small peat-accumulating nutrient-poor wetlands are found in the depressions. Other important, but less common wetland types are the freshwater shores (wet meadows or marshes) and riparian wetlands along streams. The latter are inundated by water at least once a year and affected by overbank sedimentation. Such areas may be of importance for the retention of different substances that otherwise are transported by the water directly to the sea.

The agricultural land covers 8.5% of the land area of the main catchments and is mainly located along the valleys. The agricultural land consists of arable land and grasslands. It provides food for humans, either directly as crop production or as production of fodder for animals. The average production of barley, including threshing loss and straw yield (calculated from standard yield in the survey district in which Laxemar-Simpevarp is situated) was $190 \text{ gC m}^{-2}\text{y}^{-1}$ during the period 2000–2007.

Fauna

The fauna has been investigated in a number of different surveys /Löfgren 2008, cf. Section 4.2 therein/. The aims of the surveys were to 1) describe which species or functional groups that are present in the area, 2) establish reliable density estimates of larger animals and birds and quantify important pools/fluxes of elements, which will be used for the ecosystem models and, 3) establish a baseline for an ongoing monitoring programme that can be used to relate different kinds of disturbances to wildlife population changes.

The fauna is more difficult to associate to specific habitats than the vegetation, but for some species or functional groups an attempt has been made to distribute their consumption in the landscape, either by using their habitat preferences or their feeding preferences, or both. Density and biomass estimates for all mammals, birds, amphibians and reptiles are presented in Section 4-2 in /Löfgren 2008/, together with calculations of their production, consumption, egestion and respiration. The calculations are based on the field metabolic rate for each species.

Limnic ecosystems

The Laxemar-Simpevarp regional model area contains 26 catchments, 5 lakes and a number of streams. Only one of the lakes, Lake Frisksjön, is situated within the Laxemar local model area (cf. Figure 2-8). There are also some minor, but permanent natural pools within the regional model area.

The lakes are small with relatively shallow depths. They are characterised as mesotrophic brown-water lakes, i.e. with moderate nutrient concentrations and with brown water colour. The water colour is caused by high input of organic matter from the surrounding catchments, and the concentration of organic carbon is very high in comparison with the majority of Swedish lakes. Because of the brownish water, light penetration is poor and the depth of the photic zone is generally small. In accord with this, macrophyte coverage is small in the lakes and the biota is dominated by heterotrophic organisms, particularly bacteria. Perch is the dominant fish species in lakes in the area, in numbers as well as in weight.

Most lakes in the area are affected by human activities. The naming of some wetlands and minor fields indicate that a number of previous lakes have disappeared during the last centuries due to human activities, probably with the intention to increase farming areas. There are also indications that the water level of several of the remaining lakes has been lowered by man.

Most of the streams in the Laxemar-Simpevarp area are small with mostly calm or slowly flowing water. Similarly to the lakes, the streams are characterised as mesotrophic brown-water systems. The largest stream in the area is Laxemarån which, together with Kåreviksån and Kärreviksån, show permanent water flow throughout the year. The other small streams in the area are dry during summer (however, the stream Ekerumsån is dry only during dry summers). Five fish species have been noted in Laxemarån; ide (Sw: *id*), roach (Sw: *mört*), burbot (Sw: *lake*), pike (Sw: *gädda*) and ruffe (Sw: *gers*), and there are indications that the stream is an important spawning site for both ide and roach. The streams are to a great extent influenced by human activities, which have altered the channel by various technical encroachments.

An extensive compilation of all data from the limnic ecosystems in the Laxemar-Simpevarp area is presented in /Nordén et al. 2008/. The delimitations between different habitats in the five lakes in the area were determined in a study which also included identifications of catchment areas /Brunberg et al. 2004/. An extensive amount of biological data, including data on biomass of phytoplankton, bacterioplankton, zooplankton, benthic bacteria, benthic fauna, macrophytes and fish, have been collected from Frisksjön /Nordén et al. 2008, cf. Section 4.9 therein/. Data on the biomass of benthic fauna and fish are available also from the other four lakes in the Laxemar-Simpevarp area.

Biological data from streams include chlorophyll *a* (which can be used to estimate phytoplankton biomass), macrophyte abundance, biomass of benthic fauna, and occurrence of fish. Respiration has been measured on one occasion in Lake Frisksjön. Data on water chemistry are available for four lakes as well as for a number of streams in the area /Nordén et al. 2008, cf. Section 4.8 therein/. Data on the chemical composition of biota in Frisksjön are available for a number of functional groups from /Nordén et al. 2008, cf. Section 4.10 therein/.

Marine ecosystems

The Laxemar-Simpevarp area is situated at the coast of the Baltic Proper. The marine area in Laxemar-Simpevarp is separated from the open sea in the east by the island of Öland, forming a funnel-like strait with its wide end to the north and the narrow end southwards. The sea bottom along the Laxemar-Simpevarp coast slopes gradually in the offshore direction. The maximum depth recorded in the regional model area is c. 45 m.

The sea floor in the Laxemar-Simpevarp area can be divided into three marine subareas with more or less distinct characteristics with regard to ecosystem structuring factors, such as wave exposure, light penetration and substrate type. These subareas are; secluded bays (e.g. Borholmsfjärden and Granholmsfjärden), shallow exposed archipelago (in the southeast), and deep, exposed areas (the coast and the open sea in the eastern parts of the regional model area).

Most marine investigations have been performed in the coastal area off and around the Oskarshamn power plants. Seawater has been sampled and analysed for chemical and physical parameters biweekly to monthly during the site investigations. The sampling started in 2002 and is still continuing in a monitoring phase with reduced sampling frequency. Sediment characteristics with regard to chemical and physical composition, as well as benthic fauna and fish, have been surveyed on several occasions. Primary producers were surveyed in 2002 by dive transects and also by a general survey from boat, using hydroscope and rake, complemented by a video survey.

The coastal water in the Laxemar-Simpevarp area has an average light penetration depth (Secchi depth) of 5.5 m, which is low compared with the value at the national monitoring station located further out in the Baltic Proper (8.7 m). However, the light penetration varies within the area, and the sheltered inner bays have Secchi depths of only 2–3 m.

The local freshwater discharge to the Laxemar-Simpevarp coastal area comes mainly from small streams to the bays, and there is no larger river. The salinity in the outer, exposed parts of the regional model area is 6.8‰, which is similar to that in the Baltic Proper, whereas the salinity at sampling stations in the inner bays is lower (mean values between 5.5 and 6.3‰) and varies strongly over time due to the influence of freshwater from land.

The off-shore study area was divided into 19 sub-basins based on the current bathymetry and projected future drainage areas (Figure 4-5). For modelling purposes, the water exchange was estimated for each of the individual basins and presented as Average age of a water parcel (AvA). The AvA values show large variations between basins, from less than one day in the outer basins to 7–29 days in the secluded inner bays.

Large parts of the coastal area are shallow enough for light to reach the bottoms. Accordingly, the marine primary producers in the regional model area are dominated by benthic primary producers. On soft bottoms situated within the photic zone, green algae, stonewort (*Chara sp*) and yellow-green algae dominate. On hard substrates, i.e. till or bedrock, bladderwrack (Sw: *blåstång*) dominates in the shallow areas, whereas red algae dominate in the deeper areas. Three species dominate the benthic fauna, the blue mussel (Sw: *blåmussla*), Baltic mussle (Sw: *Östersjömussla*) and a small amphipod (Sw: *vitmärta*).

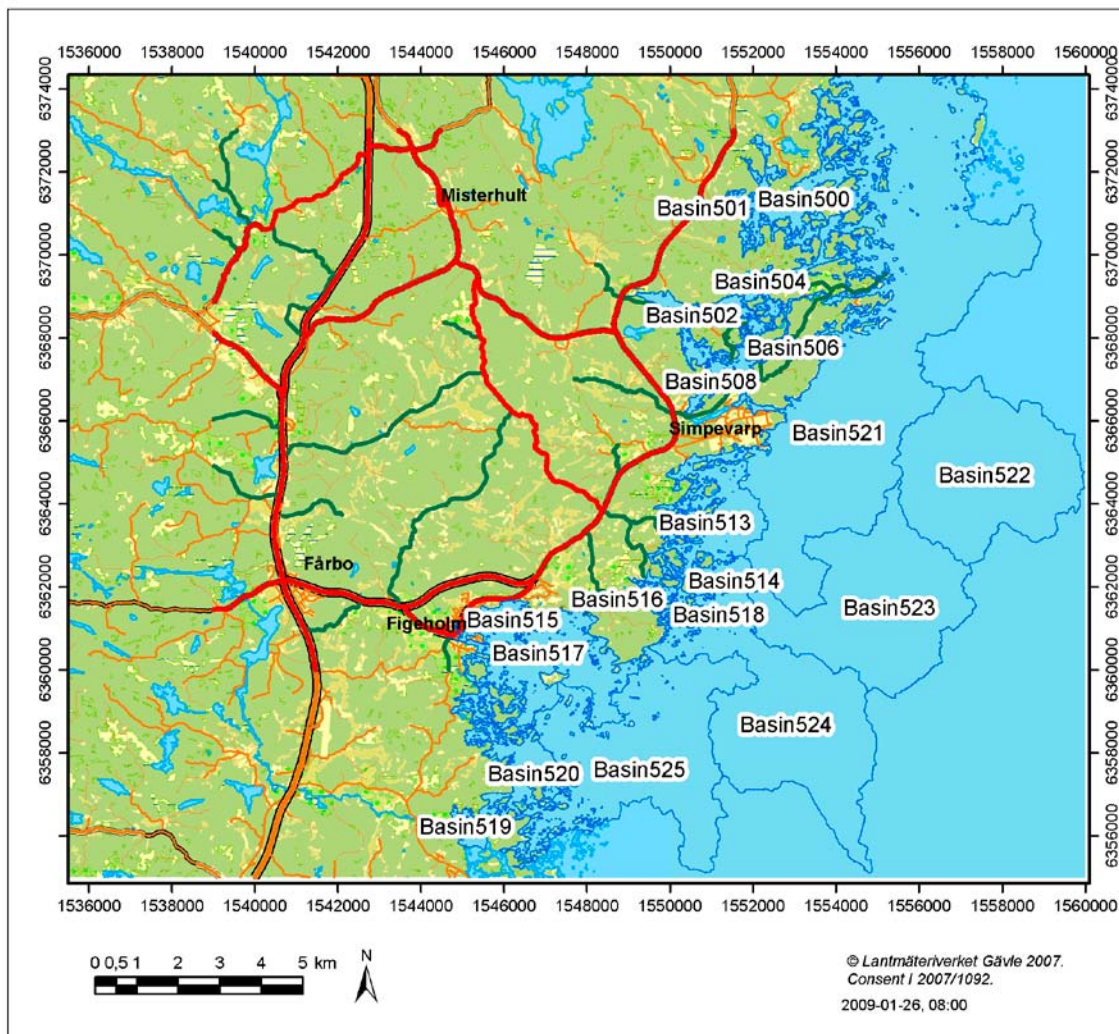


Figure 4-5. The marine area in Laxemar-Simpevarp, divided into 19 sub-basins.

Perch (Sw: *abborre*), roach (Sw: *mört*) and white bream (Sw: *björkna*) have consistently dominated the catches in the monitoring of warm-water species in the area /Andersson et al. 2005/, representative for the inner bays in the area. In the more offshore areas, the marine cold-water species herring (Sw: *strömming*) dominates the fish community. In open sea, the zooplankton community is dominated by meso-zooplankton, especially copepods. However, in the summer a more diverse zooplankton community with cladocerans, rotifers and larvae of some benthic macroinvertebrates occurs.

The mean total biomass of producers and consumers (on an annual basis) varies between the different basins, from just below 35 gC m⁻² to over 150 gC m⁻² with an average for the whole marine area of 91 gC m⁻². An extensive compilation of all the data from the marine ecosystem in the Laxemar-Simpevarp area is presented by /Wijnbladh et al. 2008, cf. Chapter 3 therein/. That report also presents details about the ecosystem models and mass balances set up for the marine ecosystem basins in the Laxemar-Simpevarp area.

4.2.6 Human population and land use

Input data, as well as a number of calculated variables used to describe humans and human land use in the Laxemar-Simpevarp area and its surroundings, are presented in detail in /Miliander et al. 2004/. The description of the human population and land use in the Laxemar-Simpevarp area (area definition is given in /Miliander et al. 2004/) can be summarised as follows:

- The Laxemar-Simpevarp area has a low population density (7.4 individuals·km⁻² in 2002) and the number of inhabitants has diminished slowly during the 1990s. The population density is one third of the mean density in the County of Kalmar.
- The main employment sector is within electricity production. There is a clear net ingoing commuting to the Laxemar-Simpevarp area during day-time due the dominant employer, the OKG Power Company that operates the Oskarshamn nuclear power plant.
- Manufacturing industry is the main employment sector among the inhabitants of the Laxemar-Simpevarp area.
- Holiday-houses make up 21% of the properties, which is similar to the amount in the County of Kalmar as a whole.
- The land use is dominated by forestry and the extraction of wood is the only significant human related outflow of biomass from the area.
- Agriculture in the area is limited. The agricultural area (arable land and grazing land) comprises only 8.1% of the total land area, compared with 16.1% in County of Kalmar. The far most dominating crop is barley, and its significance has grown during the 1990s. Only 21% of the arable area is used for seed production and the rest is used for fodder and silage production /Löfgren 2008/.
- Moose hunting is more intensive in Misterhult parish, and most likely in the Laxemar-Simpevarp area, than in Oskarshamn municipality and in the County of Kalmar. Besides hunting, the area is as well used for leisure activities such as hiking, canoeing, fishing and boating. There are primarily three areas that are used for recreation in Laxemar-Simpevarp /Ottosson 2006/. These are Ostkustleden, Kråkelund and Hamnefjärden, areas that are frequently used by both tourists and local inhabitants.

The carbon flow to humans from selected drainage areas in Laxemar-Simpevarp has been calculated according to the methodology described in /Löfgren 2008, cf. Chapter 8 therein/, where also the results from the calculations are presented.

4.3 Surface system models

4.3.1 Digital Elevation Model (DEM)

A Digital Elevation Model (DEM) is a digital representation of a continuous variable over a two-dimensional surface. Typically, digital elevation models describe the terrain relief. To construct a DEM for the Laxemar-Simpevarp area, input data from a number of different sources were used. The collection and evaluation of data used in the DEM is described in detail in /Strömgren and Brydsten 2008/.

The resulting DEM (see Figure 4-6) has a size of approximately 35 × 20 kilometres and a cell size of 20 metres. The area is undulating with narrow valleys commonly associated with bedrock deformation zones. The variability in elevation in the area is approximately 151 metres, with the highest point at 106 metres above sea level in the south-western part of the regional model area, and the deepest sea point at -45 metres in the south-eastern offshore part of the area. The mean elevation in the model is 24 metres.

The model area is covered by 73% land and 27% sea. The flat landscape is reflected in the statistics of the cell-based slope, where the mean slope is 2.52 degrees. The slope is lower than 5 degrees in 87.0% of the cells whereas 11.7% of the cells have a slope between 5 and 10 degrees. As expected, almost all of the cells with a slope steeper than 10 degrees (2.5% of all cells) are situated along the earlier mentioned narrow valleys or along lake shores.

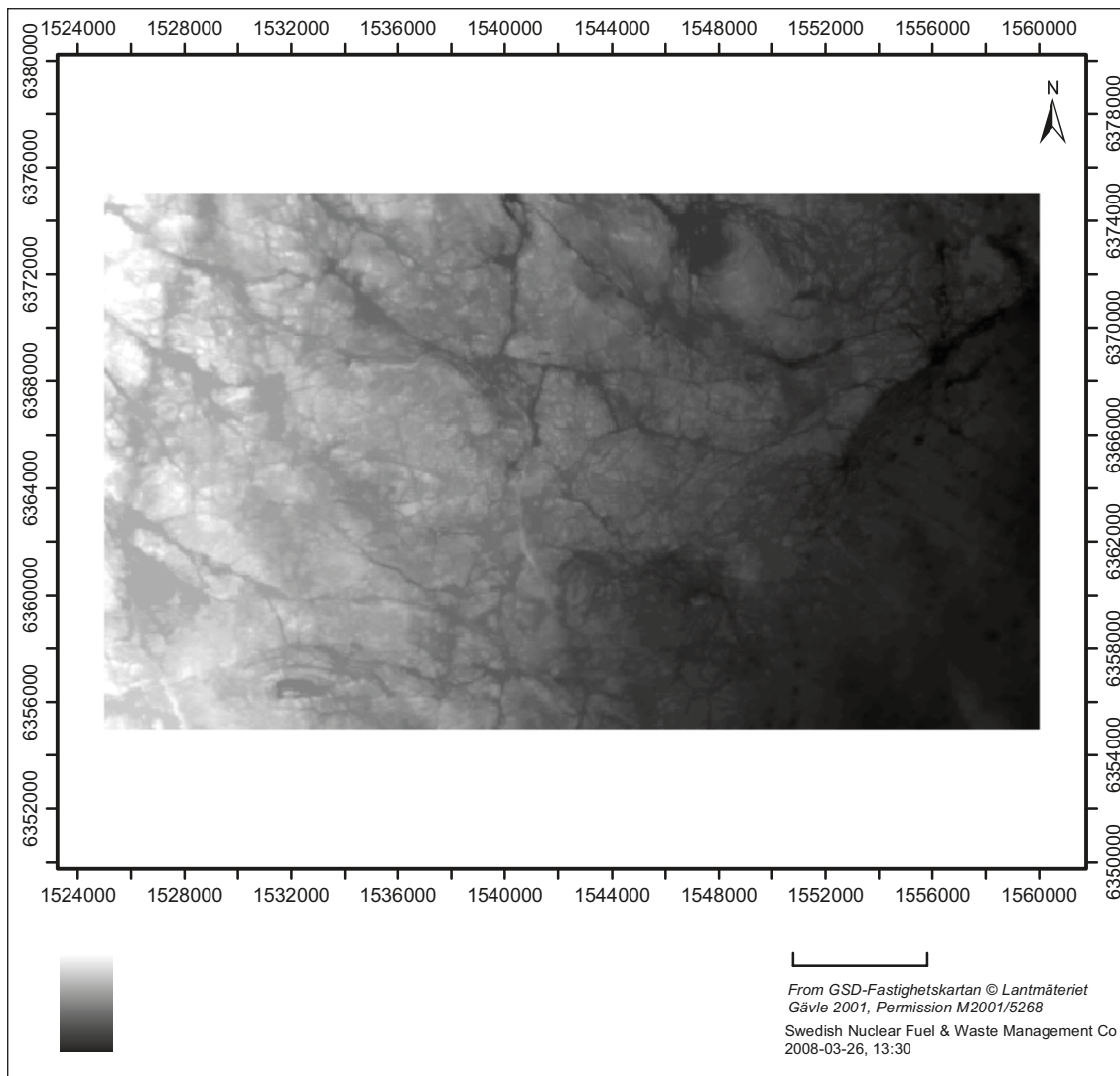


Figure 4-6. The 20-metre digital elevation model (DEM) for the Laxemar-Simpevarp area, describing the land surface, lake bottoms, and sea bottom /Strömgren and Brydsten 2008/.

4.3.2 Depth and stratigraphy of Quaternary deposits

A geometrical model of the overburden in Laxemar-Simpevarp, based on data obtained from drillings and corings, excavations and geophysical investigations, has been constructed /Nyman et al. 2008/. The model (denoted RDM) describes the total depth of Quaternary deposits from the ground surface down to the bedrock surface, subdivided into six layers (Z1–Z6), which are schematically illustrated in Figure 4-7. The layers in the model are purely geometrical, but are constructed according to the conceptual understanding of the geographical distribution of Quaternary deposits at the site. Properties of the layers are subsequently assigned by the user of the model. For example, the upper layer Z1 can be given different properties in different areas by association to, e.g. maps of Quaternary deposits or soil types.

Figure 4-8 shows the modelled distribution of total depths of Quaternary deposits in the Laxemar-Simpevarp regional model area. The model includes the stratigraphical distribution of till, glaciofluvial sediments, glacial clay, postglacial sand/gravel, clay gyttja, peat and artificial fill. A large proportion of the modelled area has a low data density and the area was therefore divided into nine domains, see /Nyman et al. 2008/. These domains were defined based on the geographical distribution of Quaternary deposits. The average depth in each domain was calculated by the use of available data, and these average depths were used together with measured depths to interpolate the depths of Quaternary deposits in the model area.

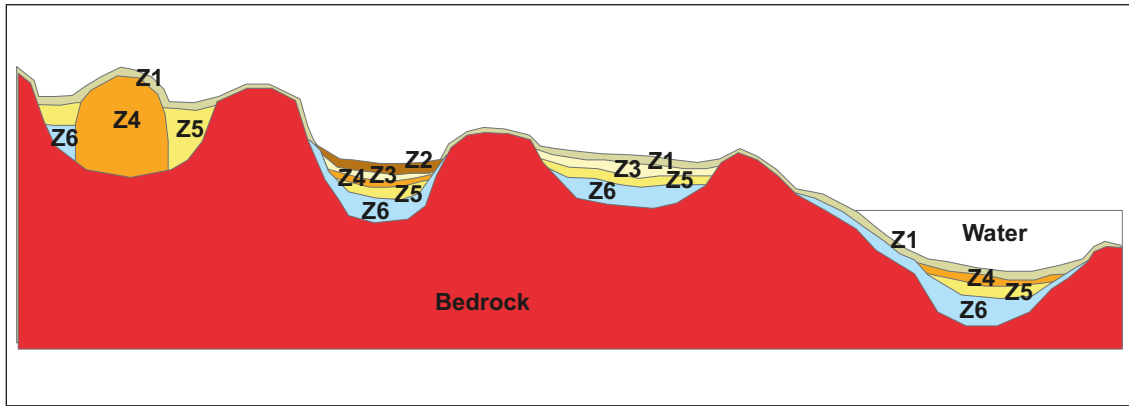


Figure 4-7. Conceptual model used for the depth and stratigraphy model of Quaternary deposits (RDM), showing the spatial distribution of the six layers /Nyman et al. 2008/.

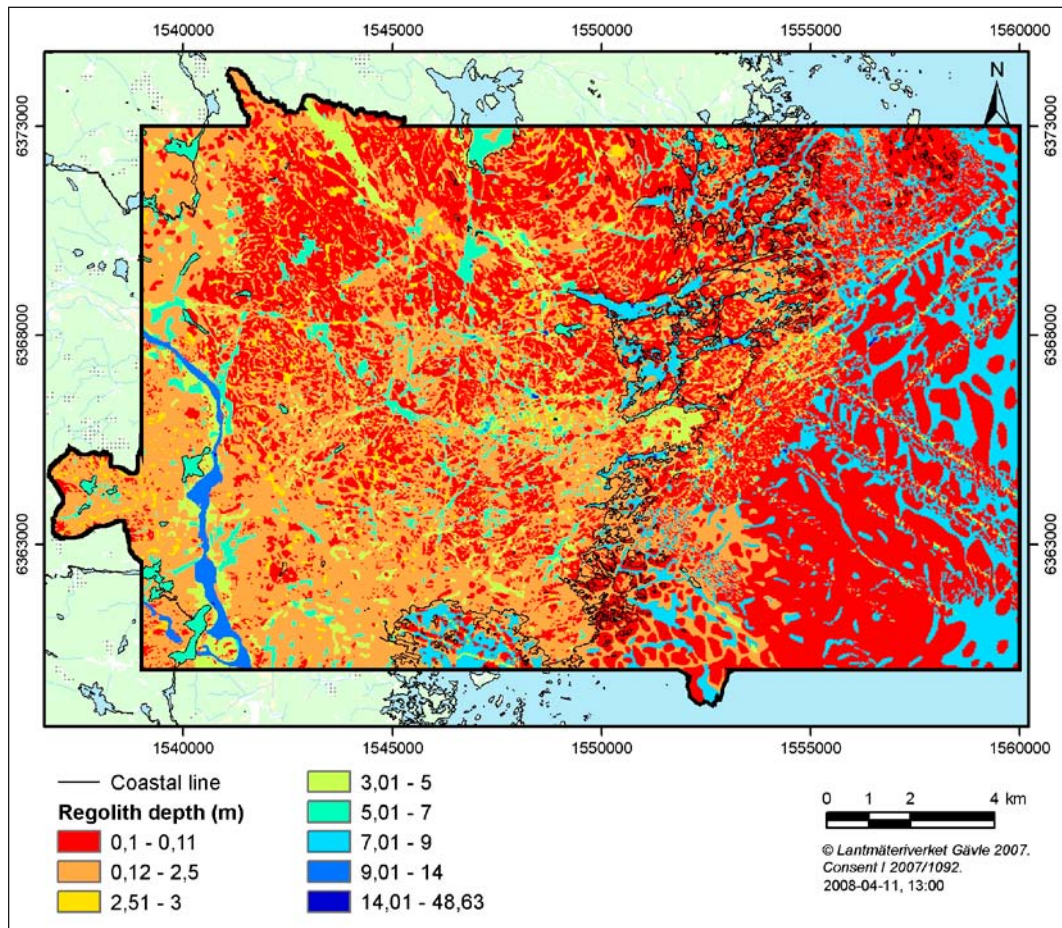


Figure 4-8. The total modelled depth of overburden /Nyman et al. 2008/.

The developed depth model clearly reflects the overall character of the area, with thin layers of Quaternary deposits in the topographically high areas and thicker layers in the valleys. The large and pervasive Tuna esker is clearly recognisable as a north-south band with thick overburden in the western part of the model area (Figure 4-8). The largest depth in the model (almost 50 metres) has been interpreted from refraction seismic data in a bay north of the island of Ävrö. The average depth of Quaternary deposits in the area is 2.2 m when bedrock outcrops are included, and 3.7 m when outcrops are excluded.

The quality of the RDM model varies within the modelled area, since the geographical density of data varies. This is particularly obvious in the marine areas, where transects with high density of data contrast with surrounding areas of low density (Figure 4-8). There are relatively few data showing the total depth in the large valleys. In the RDM model, most of the depths in the valleys are estimated from the average thickness of Quaternary deposits in these areas, based on relatively few measurements. Results from drillings indicate, however, that the depth in the large valleys generally is greater than the average values used in the model. It is therefore possible that the total depth of Quaternary deposits in the large valleys is generally greater than shown in the model. The uncertainties in the RDM model are further discussed in /Nyman et al. 2008/ and /Sohlenius and Hedenström 2008/.

4.3.3 Hydrological-hydrogeological models

Numerical modelling with the MIKE SHE tool has been performed as a part of the modelling of surface hydrology and near-surface hydrogeology at Laxemar-Simpevarp. This modelling includes evapotranspiration processes, surface-water flow and groundwater flow. However, in contrast to the bedrock hydrogeological modelling described in Chapter 8, the MIKE SHE modelling is performed for present-day conditions only. Furthermore, density-driven flow is not modelled in MIKE SHE. Some examples of the MIKE SHE modelling of hydrology and near-surface hydrogeology in Laxemar-Simpevarp are given below. For a detailed presentation of this modelling, see /Bosson et al. 2008/.

Water balance

Figure 4-9 presents the MIKE SHE-calculated annual average water balance for the time period October 1, 2004 – October 1, 2007, corresponding to three so called hydrological years /Bosson et al. 2008/. Note that the water balance in the figure is calculated for the terrestrial part of the model area only. On average per year for the considered time period, the area-averaged precipitation was 608 mm, whereas the model-calculated annual average of the actual evapotranspiration was 425 mm.

The actual evapotranspiration is the sum of several different evaporation components and the transpiration from vegetation. The largest single component is transpiration from vegetation (on average 202 mm), whereas the average calculated evaporation from soil is 88 mm and evaporation from flooded areas 5 mm. On average, interception by leaves, which evaporates directly from the

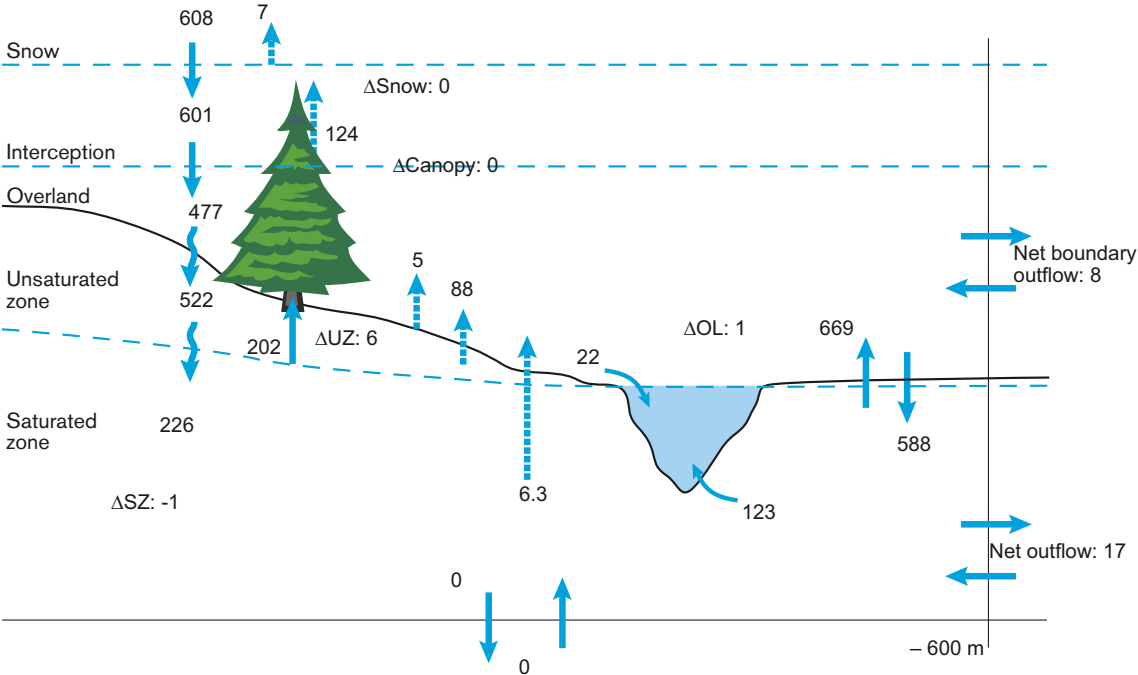


Figure 4-9. MIKE SHE-calculated average annual water balance (mm·y⁻¹) for the period Oct. 1, 2003 – Oct. 1, 2007 /Bosson et al. 2008/. Storage changes are also given in mm·y⁻¹.

surfaces of the leaves, is quantified at 124 mm and evaporation from the saturated zone 6 mm. The model-calculated annual average specific discharge is about 170 mm, which includes the two net boundary outflows shown in the figure. It should be noted that there are relatively large inter-annual differences in water balance. For instance, considering another 3-year period (October 15, 2003 – October 15, 2006), the MIKE SHE-calculated annual average specific discharge in streams is 199 mm (all values given as annual averages).

According to Figure 4-9, the net annual area-averaged groundwater recharge from the unsaturated zone to the uppermost calculation layer representing the Quaternary deposits is 226 mm. Detailed results for the different calculation layers in the MIKE SHE model (not displayed here) show that the annual area-averaged groundwater recharge to the rock is 35 mm. However, there is also upward flow (discharge) in parts of the model area corresponding to an annual area-averaged flow of 28 mm. This means that the net annual average groundwater recharge from the Quaternary deposits to the rock is 7 mm (i.e. 35 minus 28 mm). It can also be noted that the vertical groundwater flow at the level –150 m in the bedrock is 10 mm downwards and 9 mm upwards, implying a small downward net flow at that level.

Groundwater recharge and discharge

Figure 4-10 illustrates the MIKE SHE-calculated distribution of groundwater recharge and discharge areas in the Quaternary deposits /Bosson et al. 2008/. In this context, time-averaged groundwater-head differences between the two uppermost calculation layers of the MIKE SHE model are used to identify these areas. In the recharge areas (red in Figure 4-10), the hydraulic head is higher in the top calculation layer than in the underlying layer, and the opposite for the discharge areas (blue). According to the results illustrated in Figure 4-10, the near-surface groundwater flow system is dominated by recharge areas, occupying c. 70% of the MIKE SHE model area.

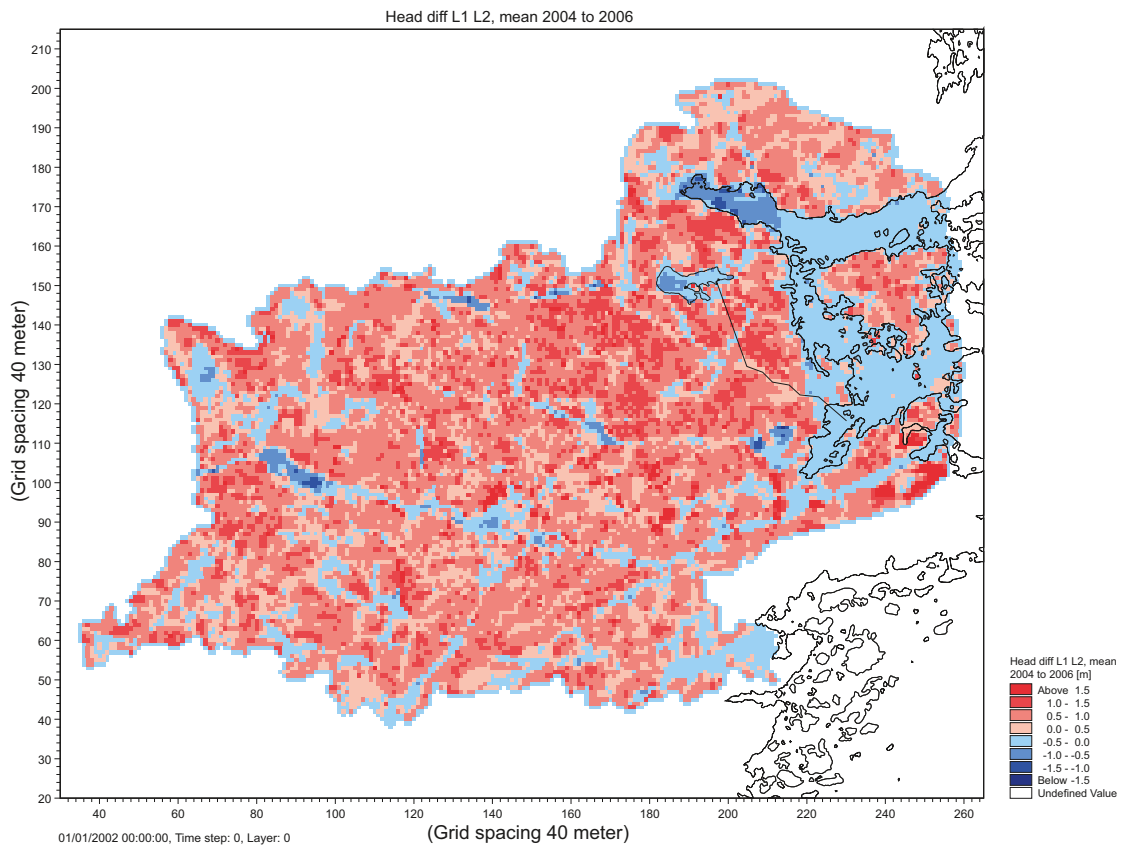


Figure 4-10. MIKE SHE-calculated distribution of near-surface groundwater recharge (red) and discharge areas (blue) /Bosson et al. 2008/. These areas are in this context identified based on time-averaged hydraulic-head differences between the two uppermost calculation layers of the model. The simulated time period is 2004–2006.

The groundwater discharge areas, hence occupying c. 30% of the model area, are associated with low-lying areas such as stream valleys, Lake Frisksjön and the sea bays near the coast. MIKE SHE-analyses of seasonal variations /Bosson et al. 2008/ show that the overall near-surface groundwater recharge/discharge pattern is relatively stable during the year; for typical wet- and dry periods, the relative change of the sizes of recharge and discharge areas is on the order of 1–7%.

The concepts of sub-flow systems and discharge are illustrated in Figure 4-11 and Figure 4-12, showing MIKE SHE-calculated hydraulic heads and groundwater flow directions in vertical cross sections (for specific locations, cf. /Bosson et al. 2008/). Specifically, Figure 4-11 shows model-calculated heads and flow directions in a c. 400 m long N-S section across the Laxemarån stream valley, whereas Figure 4-12 shows the same model outputs for a section across Lake Frisksjön indicated by the yellow line along the lake in the NE part of the model area.

In the across-valley section (Figure 4-11), groundwater flow is mainly directed from the higher-altitude areas towards the valley bottom, acting as a “drain” for groundwater flow in the rock. The local topography has a larger influence on groundwater-flow patterns closer to the ground surface. This can be seen in Figure 4-11 in the form of near-surface groundwater flow systems with more local-scale recharge/discharge patterns. The figure shows results for a point in time (July 13, 2006) representing dry conditions. The corresponding results for wet conditions presented in /Bosson et al. 2008/ show some differences, but the overall flow pattern is the same.

The hydrological interactions between lake water and groundwater in the underlying Quaternary deposits and rock are illustrated in Figure 4-12, showing MIKE SHE-calculated hydraulic heads and groundwater flow directions in a c. 1.4 km long W-E section across Lake Frisksjön. Also this plot shows results for a point in time representing dry conditions. The across-lake hydraulic heads and groundwater flow directions resemble the across-valley case (Figure 4-11); groundwater flow is mainly directed from the higher-altitude areas towards the lake, which acts as a “drain” for groundwater flow in the rock.

However, it should be noted that the flow directions and, in some areas, relatively large gradients indicated by the calculated heads are not necessarily associated with large groundwater flows, even if we assume that the model is correct. The water flow rates also depend on the hydraulic properties of the Quaternary deposits where flow takes place, which in the valleys where streams and lakes are situated are characterised by low hydraulic conductivities.

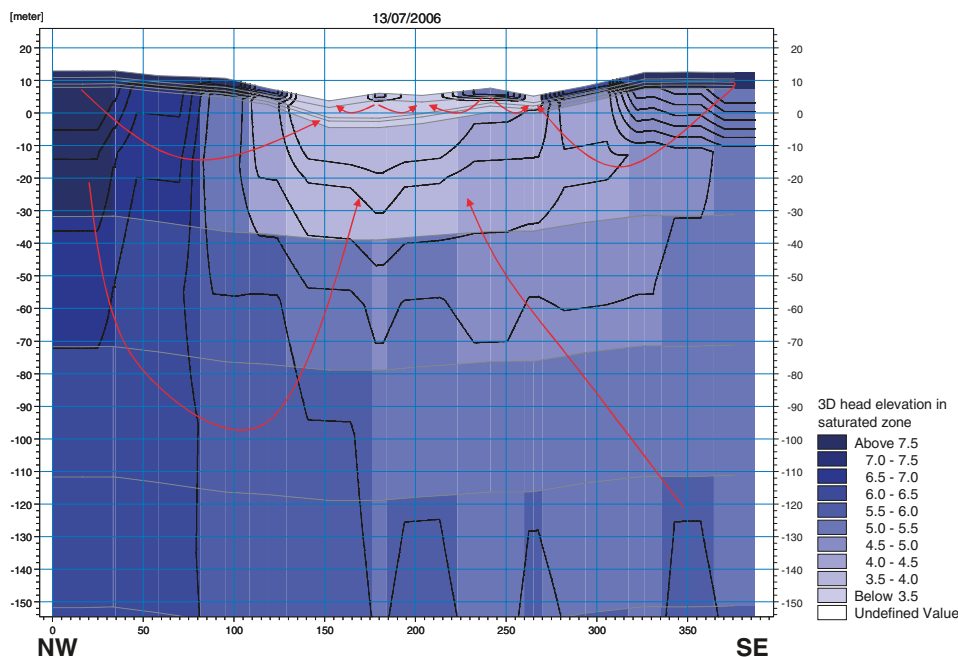


Figure 4-11. MIKE SHE-calculated hydraulic heads (m.a.s.l.) and groundwater flow directions (red arrows) in a c. 400 m long N-S section across the Laxemarån stream valley /Bosson et al. 2008/. The plot shows hydraulic heads down to –160 m representing dry conditions (July, 2006). Note that different scales are used on the vertical and horizontal axes.

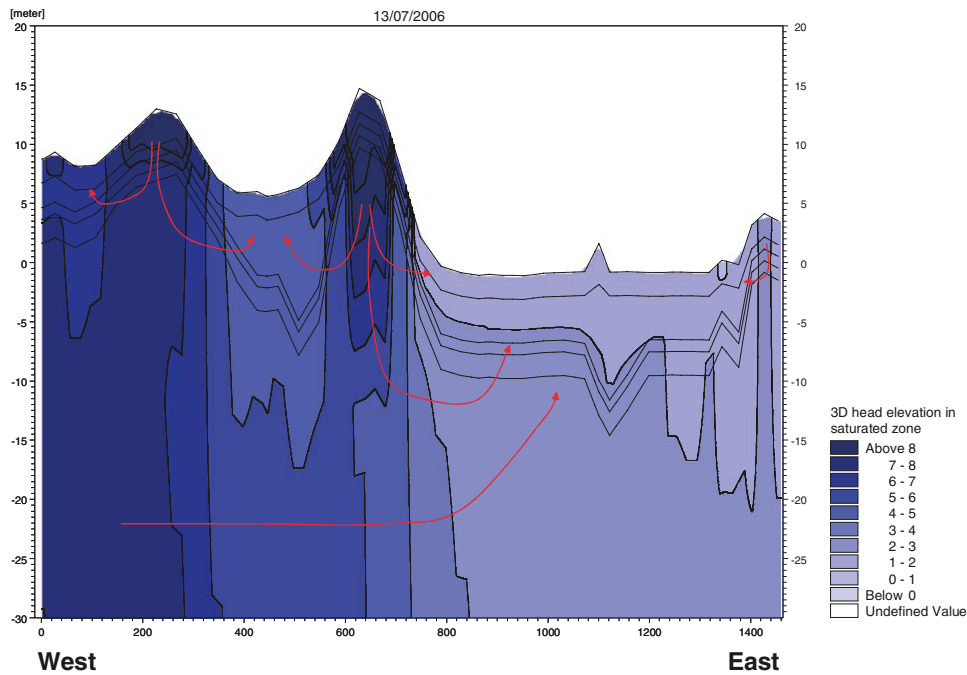


Figure 4-12. MIKE SHE-calculated hydraulic heads (m.a.s.l.) and groundwater flow directions (red arrows) in a c. 1.4 km long W-E section across Lake Frisksjön /Bosson et al. 2008/. The plots show hydraulic heads down to c. -30 m representing dry conditions (July, 2006). Note that different scales are used on the vertical and horizontal axes.

4.3.4 Ecosystem models

Elemental transport models have been set up for the terrestrial, limnic and marine ecosystems in the Laxemar-Simpevarp area, in order to describe transport of elements within and between ecosystems. To describe the transport of elements within the food web we have used *ecosystem models*, describing major pathways for the flow of matter within the trophic web in each ecosystem and revealing the major abiotic and biotic pools within the ecosystem.

In order to describe the flows of elements to and from ecosystems, as well as the permanent burial of elements in sediments and soils, the *mass balance* concept is used. The mass balance focuses on fluxes of matter, assuming that the difference between inflow and outflow represents the result of biotic and abiotic processes within the ecosystem. This is a more robust approach than the ecosystem models as less data are needed, but it reveals much less detail. The mass balance identifies the major fluxes in and out of an ecosystem. Similarly to the ecosystem model, the mass balance indicates, for example, whether a lake functions as a source or a sink for different elements. As a complement to the mass balance analysis, the amount of matter in different “pools” within the ecosystems can be estimated.

The chemical behaviour of many bioavailable (i.e. available for uptake by organisms) contaminants and radionuclides may be similar to that of other bioavailable compounds or elements, such as macronutrients or trace elements /Whicker and Schultz 1982, Sterner and Elser 2002/, and these so called analogues may thus be utilised for modelling purposes. Similarly, there are elements that are subjected to passive uptake by plants and the transport of these elements may therefore be better described by water flow through the plant, e.g. transpiration /Greger 2004/.

However, in general, a multitude of bioavailable radionuclides with various behaviours, assimilated in living tissue, will ultimately follow the fluxes of organic matter in the surface system. Consequently, the production of organic material, the Net Primary Production (NPP), may define an upper limit of the incorporation of different elements in primary producers /Kumblad et al. 2006/. Fluxes to organisms in other trophic levels than the dominant vegetation, such as large herbivores, predators and humans, may be used to evaluate their potential exposure from food intake.

Models for element transport in the terrestrial ecosystem

Pools and fluxes of organic matter and water were investigated and compiled for three localities (see example in Figure 4-13), representing vegetation types that can be regarded to be important both in respect to area coverage and as potential sinks for organic matter /Löfgren 2008, cf. Chapter 6 therein/. One coniferous forest, one oak forest and one forested wetland dominated by Alder were studied. Net Primary Production (NPP) was between 360 and 736 $\text{gC m}^{-2}\text{y}^{-1}$. The highest NPP was found in a Norway spruce forest that is situated on partially drained peat land, which might explain the rapid growth. Both the oak forest and the alder swamp forest had a net emission of carbon from the soil organic carbon pool.

Altogether, two of the investigated localities were close to zero in regard to the net ecosystem emission of carbon, whereas the Norway spruce forest had a net accumulation of carbon mainly confined to the tree layer. This model described three ecosystems using site-specific field measurements of pools and fluxes, and served as a baseline for comparison with the results of dynamic modelling /Löfgren 2008, cf. Section 4.1.3 and Chapter 7 therein/ and with more general literature data that may be used to describe pools and fluxes in long term perspectives in the safety analysis.

The dynamic vegetation model LPJ-GUESS /Sitch et al. 2003/ was used to make a regional description of carbon balances for a number of different vegetation types dominating the investigation area. Some areas (sea shore, wetlands and forested wetlands) were not covered due to the extensive work required to adapt the model for these vegetation types. For these cases, results from ground-based measurements, as well as literature data, are presented in /Löfgren 2008, cf. Chapter 7 therein/.

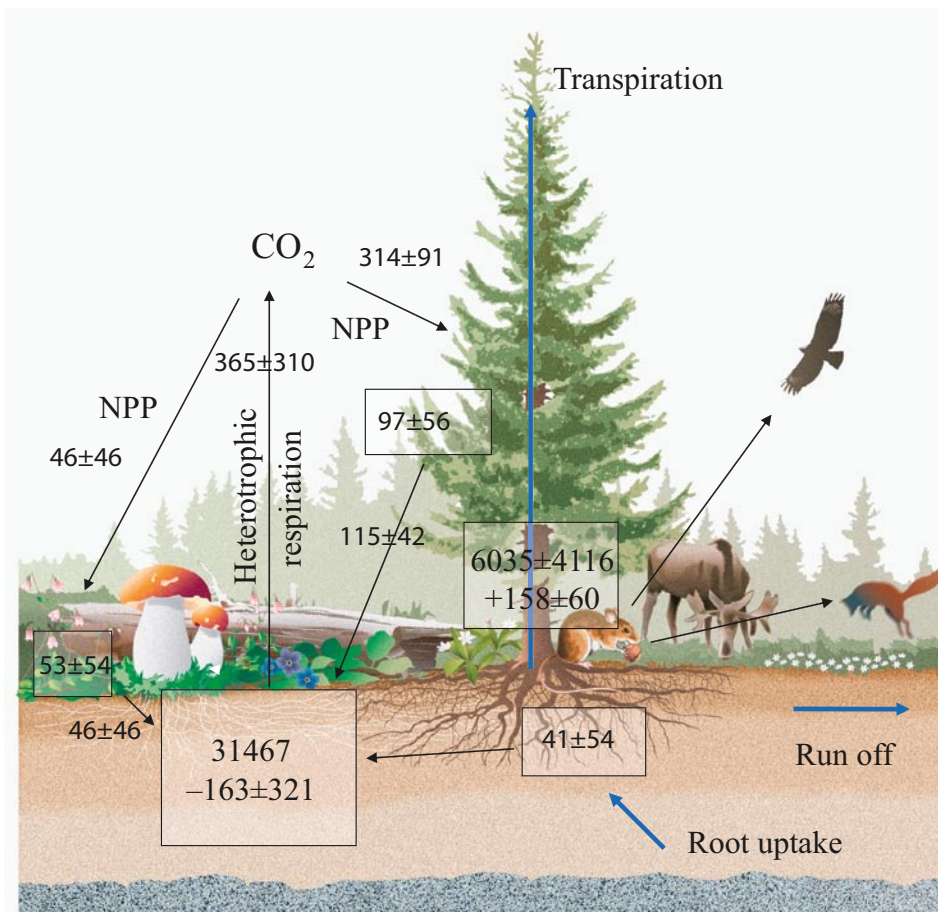


Figure 4-13. The major pools and fluxes of carbon (black boxes and arrows) and water (blue arrows) in an alder swamp forest. Figures within boxes describe pools, whereas figures outside are fluxes. Annual change in a pool is expressed with a figure preceded by a – or + (decrease/increase). Pools are in gC m^{-2} and fluxes are $\text{gC m}^{-2} \text{y}^{-1}$. The size of the water fluxes is illustrated by the length of the arrow (data from Table 6-10 in /Löfgren 2008/).

The model results include the following vegetation types; young (25 yrs) and old (80 yrs) stands of Norway spruce, Scots pine, deciduous trees (pedunculate oak and silver birch), mixed forests, dry pine on acid rocks, meadows and arable land. Model results were validated against ground-based estimates, which confirmed that estimated carbon balances are realistic in relation to measurements. Estimates of carbon balances for the year 2005 for the different vegetation types were made using the model /Löfgren 2008, cf. Table 7-5 therein/.

The modelled vegetation types all acted as net sinks, except for the clear-cut that was a carbon source, mainly due to decomposition of the large litter pool originating from the residues after the clear-cut. NPP was between 371 and 591 gC m⁻²y⁻¹ for the forested vegetation types. All vegetation types were either accumulating carbon in the SOC pool (Soluble Organic Carbon), or accumulation was close to zero, except for the old Norway spruce forest and the clear-cut being large sources of carbon during this specific year. The spatial variation of NPP was studied in the regional model area by combining remote sensing and dynamic vegetation modelling /Löfgren 2008, cf. Table 7-6 therein/. Finally, the temporal variation of a number of ecosystem properties was investigated by modelling 400 years of forest succession using a set of 100 years of site-specific climate data repeated four times.

The regional ecosystem description was complemented with estimate of site-specific element concentrations for different pools and fluxes in order to make mass balances for a number of different elements using the discharge areas as delimitations /Löfgren 2008, cf. Chapter 9 therein/.

Models for element transport in the limnic ecosystem

An ecosystem *carbon model* has been developed for Lake Frisksjön (see Figure 4-14). The model shows that biomass is clearly focused to the littoral habitat and is dominated by benthic bacteria (bacteria make up 73% of the total biomass in the lake). Primary production on the other hand, is clearly focused to the pelagic habitat where more than 99% of primary production occurs. This can be expected, considering the poor light penetration in brown-water lakes which inhibits benthic primary production.

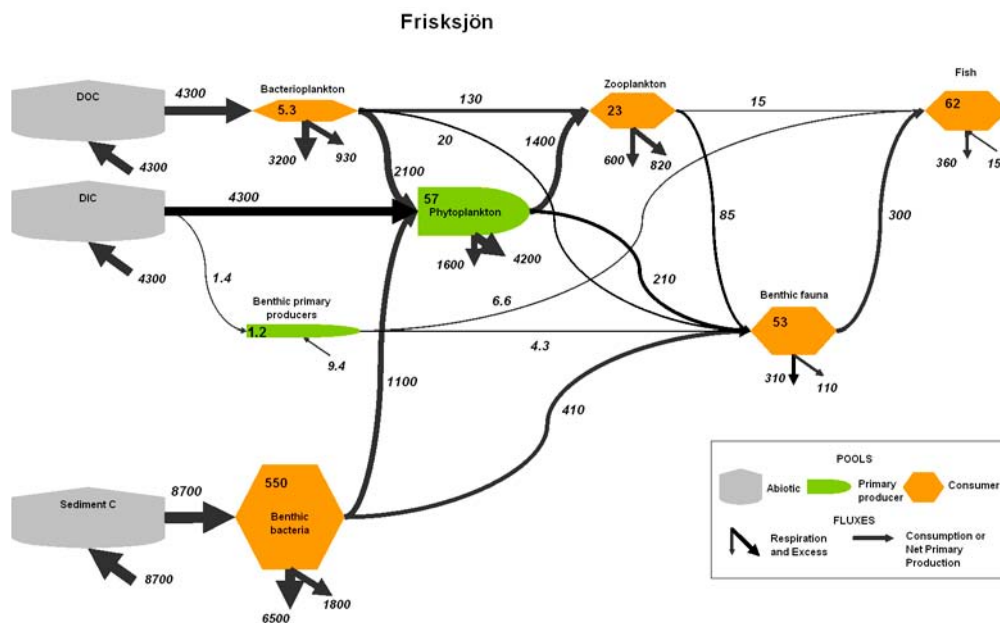


Figure 4-14. Ecosystem carbon model for the brownwater lake Frisksjön /Nordén et al. 2008, cf. Chapter 5 therein/. Sizes of boxes and arrows are relative to the sizes of pools and fluxes in the model. Values are in kgC or kgC y⁻¹. DOC = Dissolved Organic Carbon, DIC = Dissolved Inorganic Carbon, POC = Particulate Organic Carbon.

A relatively large part (34%) of the carbon produced during primary production is consumed by higher organisms and thus any pollutant incorporated during primary production would to a large degree be transported up in the food web. Respiration is much larger than primary production, indicating a net heterotrophic ecosystem. Moreover, the model indicates that respiration is relatively evenly distributed between the pelagic and littoral habitats, and is dominated by benthic bacteria, followed by bacterioplankton and mixotrophic phytoplankton.

A carbon mass balance for Lake Frisksjön /Nordén et al. 2008, cf. Chapter 5 therein/ shows concordant results with those of the carbon ecosystem model; the lake constitutes a net heterotrophic ecosystem. Thus, Lake Frisksjön is dependent on carbon entering the lake from the surrounding catchment. Much of the carbon entering the system will be consumed by bacteria and is hence incorporated into the limnic food web, but a substantial part of carbon entering the system is buried in the sediments. Accordingly, the lake may be an important site for the processing organic matter produced in the landscape of the catchment.

Element mass balances have, in addition to that for carbon, been calculated for a number of other elements, together with an assessment of the major pools of the elements /Nordén et al. 2008, cf. Chapters 5 and 7 therein/. As an example, the mass balance for phosphorus in Lake Frisksjön is presented in Figure 4-15. The dominant flows of phosphorus are the same as for most elements, i.e. the dominating inflow is via water and the dominating outflow is via sediment accumulation.

The sediment contains by far the largest phosphorus pool in Lake Frisksjön, followed by the biotic pool. The dissolved and particulate pools are small in comparison. The phosphorus pool contained in biota is about twice as large as the yearly phosphorus input (inflow via water and atmospheric deposition). Thus, concerning phosphorus, the lakes are probably more influenced by internal circulation than by external input.

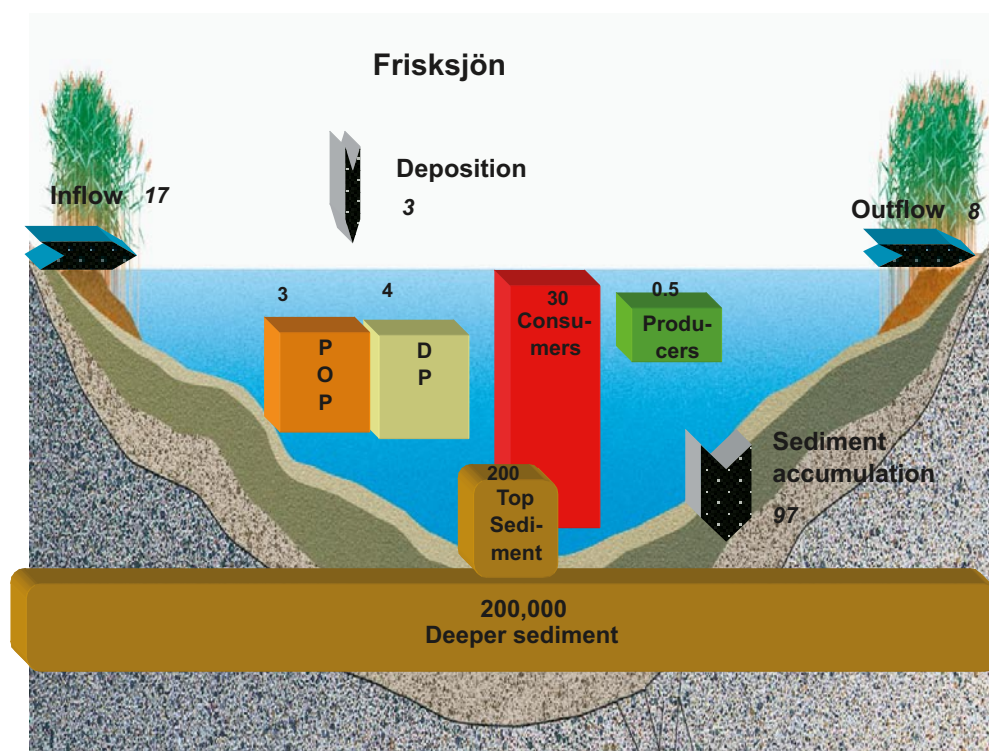


Figure 4-15. Phosphorus mass balance for Frisksjön /Nordén et al. 2008, cf. Chapter 7 therein/. Sizes of boxes and arrows are relative to the sizes of pools and fluxes in the model, although the sediment box is down-scaled to fit in the figure. Values are in kg P or kg P y⁻¹. POP = Particulate Organic Phosphorus, DP = Dissolved Phosphorus.

Models for element transport in the marine ecosystem

The marine ecosystem and its characteristics were conceptualised in an ecosystem model in order to describe the fluxes of matter between functional groups in the ecosystem, and between the basins and the surrounding environment, i.e. land ecosystem and adjacent sea. The model was calculated for each of the delimited basins on a 1,500×1,500 grid with a spatial resolution of 20×20 m. The system is assumed to be in a steady, non-seasonal, state and all input data are based on annual averages.

Model output for the whole area and for each of the 19 individual basins (Figure 4-5) is presented in /Wijnbladh et al. 2008/. The pools and fluxes of matter are summarised per basin using carbon as a proxy, and the results are presented per unit area and per basin. Coarse mass balances, identifying the major pools and fluxes have been calculated per basin for a large number of other elements.

Five out of the 19 basins were studied in more detail. These basins were chosen based on the amount of site specific data available and on the location of exit points for radionuclides determined in the preliminary safety assessment SR-Can /SKB 2006d/. In all basins, the sediment pool is the dominant pool for carbon. Among the biotic pools, macrophytes contain the largest carbon pool, and benthic detritivores and meiofauna the second largest. The dominant flux of carbon within the food-web is consumption of particulate organic carbon (POC) by benthic filter-feeders.

The marine area as a whole is heterotrophic, i.e. more carbon is released than what is fixed in biomass. Bays in the area tend to be autotrophic, whereas the more offshore basins are heterotrophic. The dominant carbon pool per unit area in the whole marine area in Laxemar-Simpevarp is that dissolved in sea water (DIC and DOC), containing 54% of the total carbon, followed by the sediment (21%), consumers (16%, dominated by filter feeders) and producers (8.5%). Macrophytes constitute the main carbon pool among the producers; other producers contribute less than 1% to the producer pool.

Considering all fluxes in the mass balance calculations, i.e. advective flux, deposition, diffusion, runoff, primary production, respiration and burial, there is a net influx of carbon to the whole marine area in Laxemar-Simpevarp. However, not all basins show this net influx and some have a net out-flux of carbon instead. The major flux of carbon is the advective flux; all other fluxes including burial are very small in comparison with the advective flux.

4.4 Integration of surface and bedrock systems

The integration and linking of the bedrock and surface systems is a multidisciplinary task. The aim of the integrated system descriptions is to describe the conceptual understanding and properties of the deep rock volumes and the upper parts of the rock, the transition between the rock and the overburden, and finally the overburden itself. However, it should be kept in mind that the ultimate goal of this integration is to provide a context for descriptions of solute transport in bedrock and Quaternary deposits. Solute transport scenarios of interest include transport from the deep rock to the surface system, primarily radionuclide transport from the potential repository, but also from surface to rock (mainly of substances with potential influence on the conditions in the repository).

The present section is mainly a summary of Chapter 5 in /Söderbäck and Lindborg 2009/. One objective of the section is to describe some of the various aspects of the surface system that are of importance for the bedrock modelling. Specifically, these aspects include the following parameters, models and observations:

- Parameters describing the properties of the upper part of the integrated domains formed by the bedrock and Quaternary deposits. Integrated model domains are considered primarily within the hydrogeological (Chapter 8) and hydrogeochemical (Chapter 9) modelling, but also in the Mike-SHE modelling (Section 4.3.3).
- Models produced and presented within the surface system modelling that are used as direct inputs to hydrogeological and hydrogeochemical models. In particular, these inputs include geometric descriptions such as the topographic and shoreline displacement models.

- Other inputs used as a basis for setting (top) boundary conditions, i.e. groundwater pressure and flux data for use in hydrogeological models and chemical compositions of infiltrating groundwater in hydrogeochemical models.
- Measured and modelled data in surface system descriptions that are used for data interpretation and/or otherwise as supporting evidence in the development of bedrock models. For example, hydrogeological and chemical data providing information on discharge of deep groundwater are important for the bedrock modelling.

The other main objective of this section is to contribute to the integration of bedrock and surface models by providing descriptions of the uppermost part of the bedrock. Geological, hydrogeochemical and hydrogeological descriptions of the upper rock have been produced and are presented in the following.

4.4.1 Geology

General character of the uppermost the bedrock

The general lithological variation in the near-surface part of the rock domains in Laxemar does not differ from that experienced at repository depth. The weathering of the bedrock surface is commonly insignificant, i.e. existing rock types are fresh, except in places where the bedrock surface has been intersected by deformation zones, in particular those of brittle character, and characterised by water-bearing fractures.

A schematic cross-section of the uppermost part of the bedrock and the typical stratigraphical distribution of Quaternary deposits in a valley is shown in Figure 4-16. The distribution and properties of Quaternary deposits in the Laxemar area is described in Section 4.2.1. The photographs in Figure 4-16 show three varieties of the uppermost bedrock. In the core of the deformation zone in Figure 4-16c, the bedrock is so strongly deformed and altered that the contact to the glacial overburden is difficult to define. The most important differences between the uppermost part of the bedrock in Laxemar and the bedrock at deeper levels are described below.

Location of the redox front

An important issue in the uppermost part of the bedrock is the location of the redox front /Drake and Tullborg 2009a/. The redox front has been evaluated by analyses of fracture minerals, chemistry and U-series isotopes. The distribution of the redox sensitive minerals pyrite and goethite in open fractures shows that the redox front, i.e. switch from mainly goethite in the fractures above the front to mainly pyrite below, generally occurs at a depth of approximately 15–20 m (Figure 4-17). Furthermore, calcite distribution shows leaching of calcite in fractures in the upper 20–30 m of the bedrock and positive Ce-anomalies suggest oxidation of Ce down to 20 m depth.

The U-series isotopes show disequilibrium in near surface fracture fillings indicating mobility of U during the last 1 Ma. In the upper 20 m, U is mainly removed due to oxidation. Both deposition and removal of U is indicated in the depth interval 35–55 m which indicates a transition to reducing conditions. Below 55 m depth, signs of recent U deposition as well as secular equilibrium indicate reducing conditions. Scattered goethite occurrences below the redox front (down to 90 m) and signs of U removal at 35–55 m generally correlate with sections of high transmissivity (and/or high fracture frequencies). For a more comprehensive evaluation and description of the location of the redox front in the bedrock at Laxemar, see /Drake and Tullborg 2009a/.

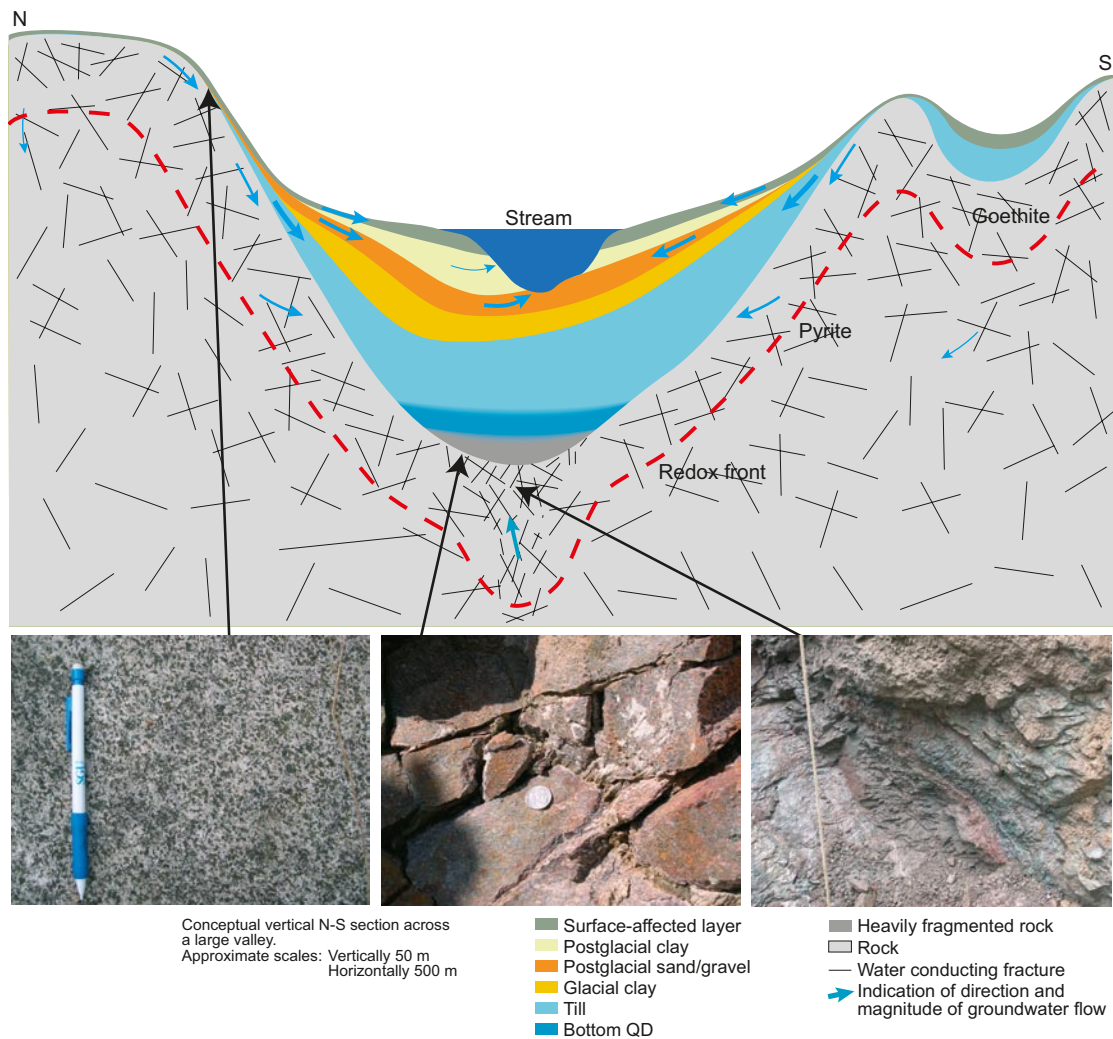


Figure 4-16. Schematic cross-section of the uppermost part of the bedrock. a) Fresh bedrock surface in areas outside deformation zones, exemplified by quartz monzodiorite in southern Laxemar. b) Strongly fractured bedrock in a trench across deformation zone ZSMNS059A (cf. Section 5.5). Several of the fractures are filled with glacial sediments /Sohlenius et al. 2006/. c) Contact between glacial overburden and the strongly deformed core of a brittle deformation zone which is associated with ZSMEW007A (cf. Section 5.5) in central Laxemar /Sohlenius et al. 2006/.

Variation in fracture frequency

An analysis of the variation in fracture frequency in the upper 100 m of the bedrock, outside deformation zones as defined in the extended single-hole interpretation, indicates a slight gradual increase in the frequency of open fractures from an elevation of -100 m and upwards towards the ground surface (Figure 4-18). In this context it must be noted that the amount of data is restricted in the uppermost part of existing drill cores since mapping is generally only carried out in sections with corresponding BIPS images. However, fractures have also been mapped in some sections that lack BIPS images.

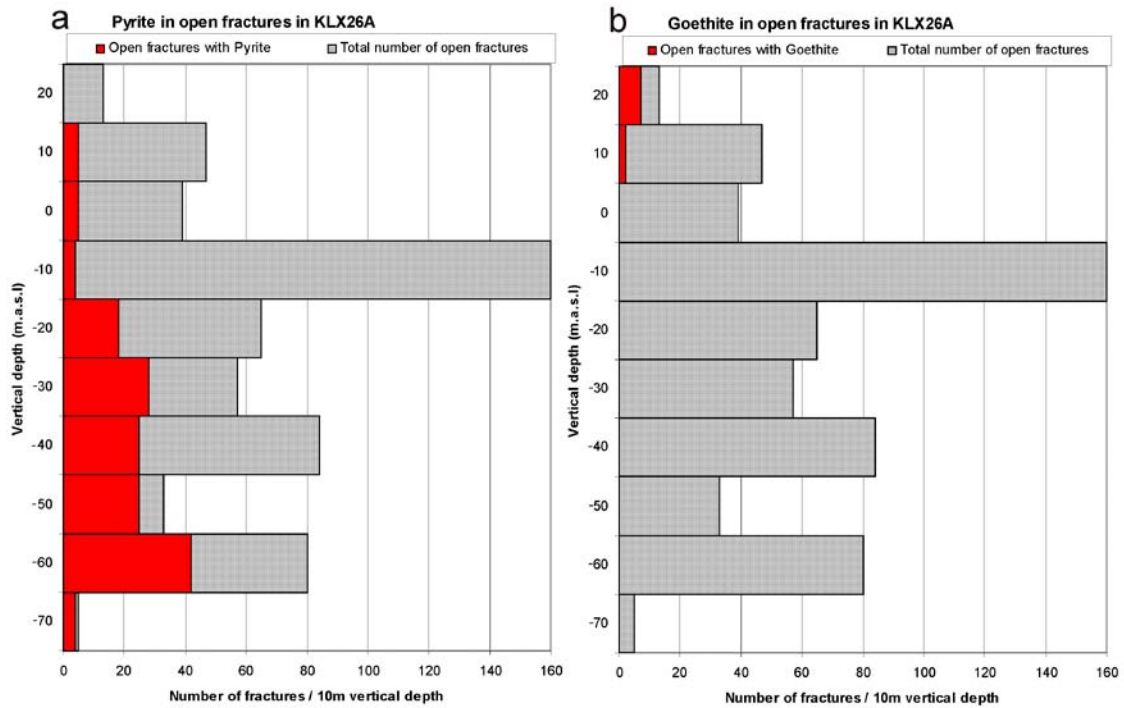


Figure 4-17. Variation with depth of pyrite (a) and goethite (b) along open fractures in KLX26A. The total number of open fractures/10 m borehole interval is also shown (figure from /Drake and Tullborg 2009a/).

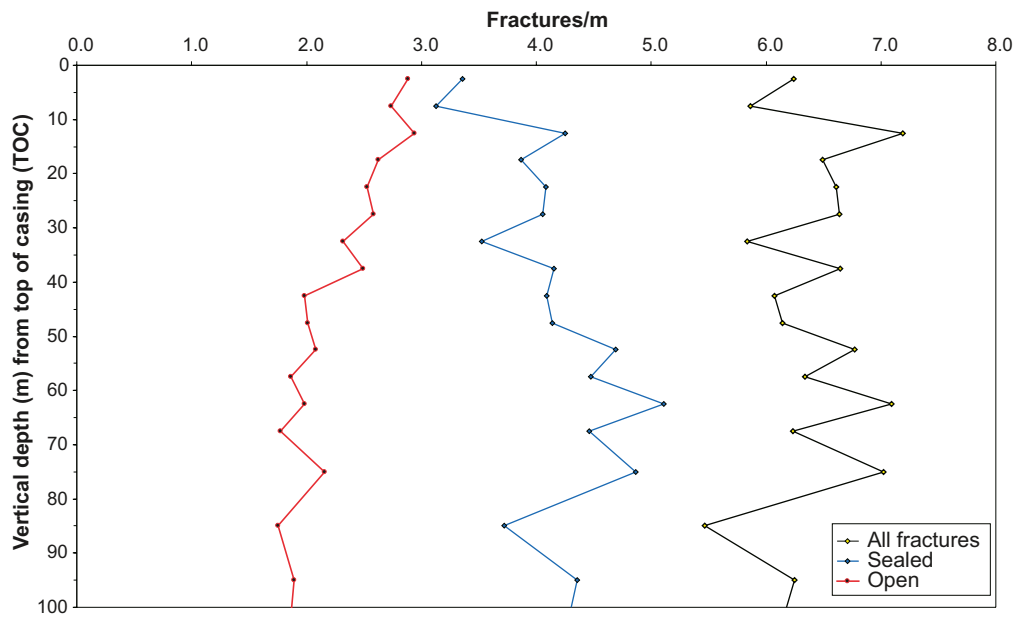


Figure 4-18. Intensity of open fractures, sealed fractures and total number of fractures (m^{-1}) for 5 metre intervals in the uppermost 100 m of the bedrock. No Terzaghi correction.

The increase in open fracture frequency appears to be coupled to a decrease in frequency of sealed fractures (Figure 4-18). This might indicate that at least some of the open fractures constitute reactivated sealed fractures. Furthermore, there is a tendency for an increase in the proportion of subhorizontally to gently dipping open fractures towards the ground surface (Figure 4-19). This may indicate that their origin, at least partly, is caused by stress release, and that they represent sheet joints (Figure 4-20).

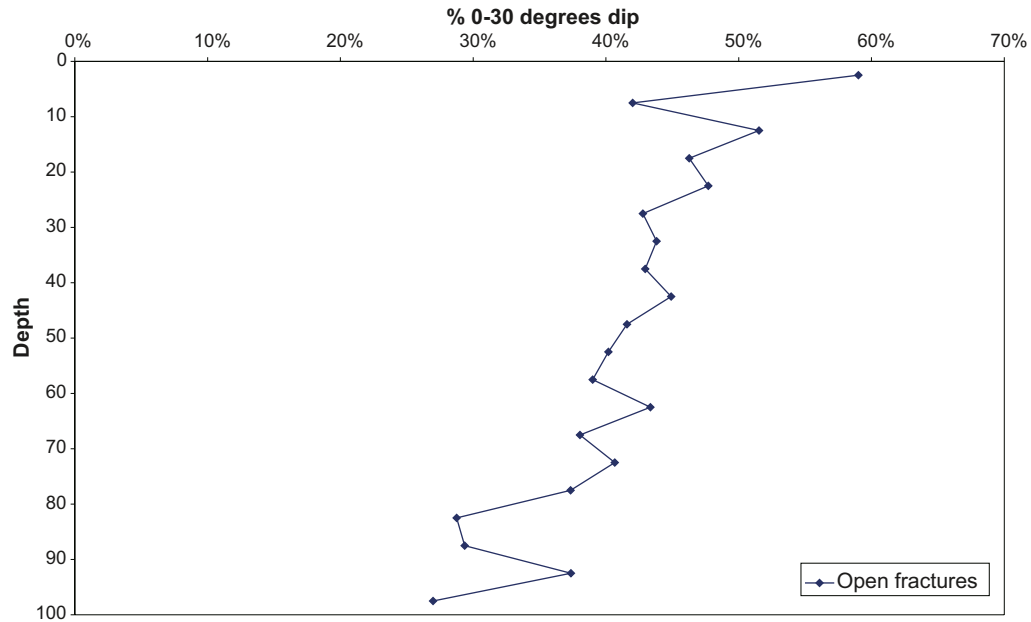


Figure 4-19. Proportion of subhorizontally to gently dipping open fractures in the uppermost 100 m of the bedrock, expressed as the percentage of fractures with dips between 0° and 30° relative to the total fracture population.



Figure 4-20. Subhorizontal, presumed sheet joint in Ävrö granite.

The calculated fracture frequency is mainly based on borehole data from fracture domain FSM_W (KLX11B-F, KLX14A, KLX22A-B, KLX23A-B, KLX24A, KLX25A) and fracture domain FSM_N (KLX07B, KLX09B-G), since available data are concentrated to these domains. For definition of fracture domains, see Section 5.6.1. As is evident from Figure 4-21 and Figure 4-22, the frequency of open and sealed fractures differs between FSM_N and FSM_W in the upper 100 m of the bedrock. FSM_W displays a higher frequency of open fractures and lower frequency of sealed fractures compared with FSM_N (Figure 4-21 and Figure 4-22). In addition, there is a tendency for a decreasing frequency of open fractures and increasing frequency of sealed fractures towards the ground surface in FSM_W, whereas FSM_N shows the opposite relation, though only for the upper 60 m for sealed fractures.

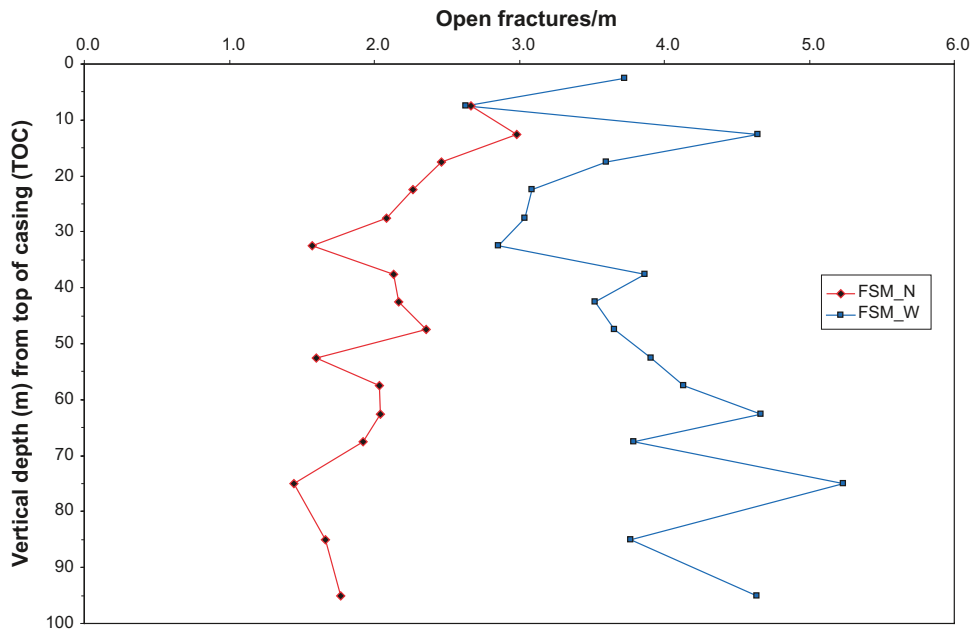


Figure 4-21. Intensity of open fractures (m^{-1}) for 5 metre intervals in the uppermost 100 m of fracture domains FSM_N and FSM_W. No Terzaghi correction.

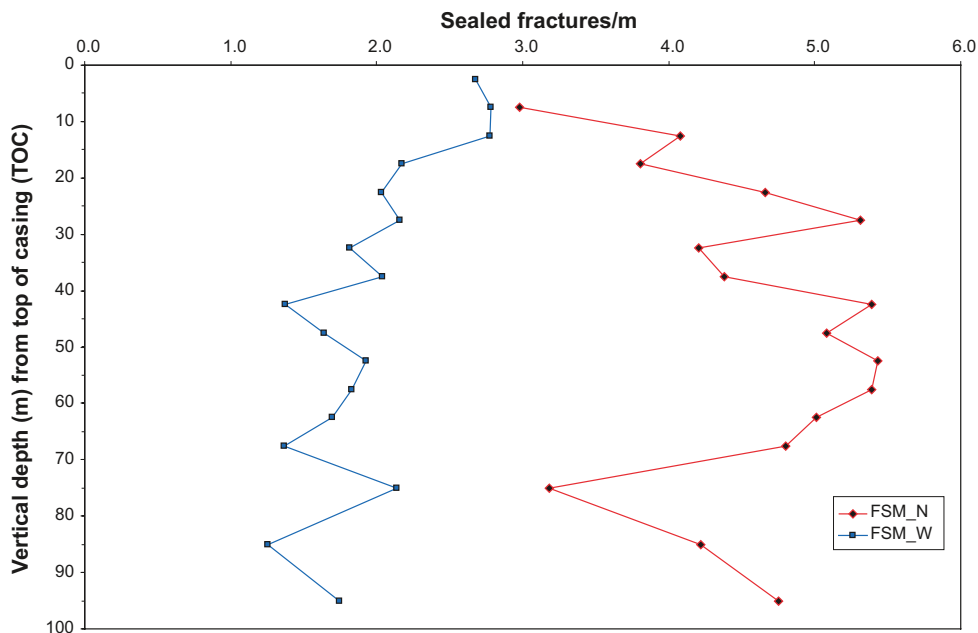


Figure 4-22. Intensity of sealed fractures (m^{-1}) for 5 metre intervals for the uppermost 100 m of fracture domains FSM_N and FSM_W. No Terzaghi correction.

4.4.2 Hydrology and hydrogeology

The conceptualisation of the hydrological-hydrogeological system in Laxemar-Simpevarp for selected local-scale type environments is summarised in Section 4.2.2. More detailed descriptions are given in the background reports for hydrology and near-surface hydrogeology /Werner 2008, Werner et al. 2008, Bosson et al. 2008/ and bedrock hydrogeology /Rhén et al. 2008, 2009/. The present section summarises results from surface and near-surface system modelling activities and joint data evaluations, focussing on those aspects that are considered important for the bedrock modelling. An account of the regional scale conceptual modelling and associated results is provided in Chapter 8. Aspects of integration and consistency are discussed in Chapter 11.

Hydrogeological properties of the near-surface bedrock

The upper part of the bedrock has been tested in various types of cored boreholes and percussion boreholes with test scales from 100 m to 5 m, see /Rhén et al. 2008/. There are no test results available that specifically quantify the properties of the uppermost c. 5–10 m of the bedrock, as the borehole casing generally makes it impossible to test the rock and also due to the fact that extraction of water was used in most cases (implying a drawdown in the borehole).

Several hydraulic tests using the different methods indicate that the hydraulic conductivity decreases with increasing depth and that most of this decrease is in the upper 100–200 m of the bedrock. Tests with a 100 m test scale indicate that the rock above elevations of about –150 m has a geometric mean hydraulic conductivity (K) of about $2 \cdot 10^{-7}$ m/s for the entire data set (deformation zones and the rock between them), this mean value is also applicable to the rock between the deformation zones. For the elevation interval –150 to –400 m the geometric mean K is about $3.5 \cdot 10^{-8}$ m/s for the entire data set and about $1.7 \cdot 10^{-8}$ m/s for the rock between the deformation zones.

The so-called PFL-s tests with a 5-metre test scale indicate that the rock between deformation zones, and above the elevation –150 m, has a geometric mean hydraulic conductivity of about $5 \cdot 10^{-9}$ m/s. For the elevation interval from –150 to –400 m the geometric mean K is about $9 \cdot 10^{-11}$ m/s for the rock mass between deformation zones. Similar trends can be seen in the data from the tests identifying flowing features only, the PFL-f tests. In particular, the results show that the frequency of open fractures decreases slightly with depth, whereas the frequency of flowing fractures with transmissivities higher than $1 \cdot 10^{-9}$ m²/s decreases significantly below –50 to –150 m.a.s.l. (the variation is rather large between different parts of the investigated rock volume).

Based on the available data, the hydraulic conceptual model of the near-surface bedrock can be summarised as follows /Rhén et al. 2008/:

- The hydraulic conductivity of the rock generally decreases with depth, both in the deterministically defined deformation zones and in the rock between these zones. Hydraulic test data indicate that most of this decrease occurs in the upper 100–200 m of the rock.
- The deformation zones are mostly subvertical and typically one order of magnitude more conductive compared with the surrounding rock. As indicated in Figure 4-3, the deformation zones have a variable thickness, and are generally wider closer to the interface between bedrock and Quaternary deposits. Many deformation zones coincide with and outcrop in valleys, which at many locations also are associated with more conductive Quaternary deposits above the rock compared with other parts of the area.
- In the rock between the deformation zones and above –150 m there is a slightly higher intensity of sets of horizontal flowing fractures compared with vertical sets. This circumstance, in combination with relatively low stress levels close to the surface (smaller rock load), probably results in that the anisotropy changes with depth observed: The horizontal conductive fractures are significant or dominant in the near-surface rock, but at deeper levels the sets of horizontal fractures generally become less significant compared with the vertical sets.
- It can be speculated that the uppermost part of the rock (say, the uppermost 5–10 m) is more fractured and more conductive compared with deeper parts of the rock. This can be explained by the influence of the latest glaciation. In particular, the glacial influence may be more pronounced on south-eastern slopes of the rock surface, due to the ice movement from NW towards SE, i.e. plucking on the lee side of the ice advancement. Data that can confirm such a hypothesis are

difficult to collect and are presently not available. However, trenches have been excavated and on top of some deformation zones there is a part of the near surface rock that is heavily weathered and fractured /Sohlenius et al. 2006/; this part of the rock is probably more conductive than the more intact rock beneath.

Boundary conditions

Groundwater levels in the Quaternary deposits are of potential interest as a basis for setting upper boundary conditions in hydrogeological models. Average groundwater elevations (head) in Quaternary deposits in the Laxemar-Simpevarp area range from c. -0.8 to 26 m, whereas there is only about a 4.5 m range in terms of groundwater levels below the ground surface.

Figure 4-23 illustrates the observed strong correlation between average groundwater levels in groundwater-monitoring wells in the Quaternary deposits and ground-surface elevations. With a few exceptions, it can be seen that the average groundwater level in the Quaternary deposits is determined by the local ground-surface elevation; the 3D “groundwater surface” in the Quaternary deposits generally follows that of the ground surface. The most pronounced outlier (SSM230) is located in glaciofluvial material.

Concerning the sea as a hydraulic boundary, the average maximum and minimum sea levels during the site-investigation period (May 2004–Dec. 2007) were -0.52 and 0.71 m, respectively, whereas the average sea level was 0.03 m (RHB 70). The largest daily sea-level changes occurred on Nov. 1, 2006 (c. +0.26 m) and Dec. 22, 2004 (c. -0.23 m). It can be noted that all lakes are located above sea level, and hence no intrusion of sea water to lakes takes place.

Quantitative modelling (ConnectFlow) of regional-scale groundwater flow in the bedrock (Chapter 8) has mainly been performed using flux boundary conditions on the top boundary. Water balances provide a basic input when assigning flux boundary conditions. For Laxemar, water-balance estimates are available both based on discharge-gauging data and model calculations (MIKE SHE). In particular, the water balance of the saturated zone is needed as an input to the modelling of groundwater flow in the rock, based on which groundwater recharge can be estimated.

According to Section 4.2.2, the site-average annual precipitation and specific discharge are estimated to be on the order of 600 mm and 160–170 mm, respectively. However, it should be emphasised that the specific discharge above is a spatial average for the whole regional model area, including both groundwater recharge and discharge areas. In some cases, spatial distributions or values representing recharge areas only are more relevant when assigning boundary conditions. This type of more detailed information can be extracted from the available model results (cf. Section 4.3.3).

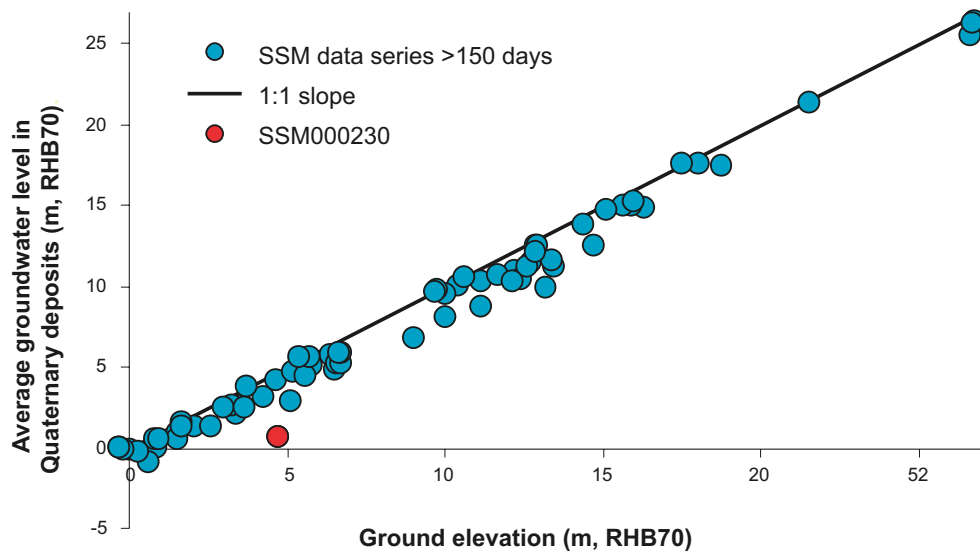


Figure 4-23. Cross plot of average groundwater levels in the Quaternary deposits versus ground-surface elevations. Data are from groundwater monitoring wells installed in the Quaternary deposits.

Infiltration and groundwater recharge

According to the conceptual hydrogeological model, groundwater recharge primarily takes place in high-altitude areas, dominated by outcrop rock or thin layers of Quaternary deposits. Groundwater recharge also takes place within the “hummocky moraine” and “glaciofluvial deposits” type areas, characterised by smaller-scale topography and eskers, respectively. Precipitation and snowmelt are thought to be the dominant sources of groundwater recharge. The infiltration capacity of the Quaternary deposits in Laxemar generally exceeds the rainfall and snowmelt intensity.

Groundwater level monitoring in the Quaternary deposits near the shore of Lake Jämsen and in the Quaternary deposits below Lake Frisksjön indicates that interaction between lake water and groundwater in the underlying Quaternary deposits is restricted to near-shore areas. In particular, the monitoring data indicate that near-shore areas of Lake Jämsen act as groundwater recharge areas during dry summer periods, whereas there is almost no vertical hydraulic gradient between Lake Frisksjön and the underlying Quaternary deposits.

The high-altitude areas containing shallow/exposed rock are difficult to parameterise in conceptual models and also to represent properly in quantitative water flow models. Conceptually, unsaturated (Hortonian) overland flow may appear on outcropping rock, but likely only over short distances (say, less than 10 m) before precipitation or snowmelt reaches open fractures or other cavities in the surface rock or a contact between the rock and the Quaternary deposits.

In the MIKE SHE modelling, cf. Section 4.3.3, near-surface drains are activated in the high-altitude areas. Results of the MIKE SHE modelling indicate that on the order of 10% of the annual precipitation enters the rock in areas with shallow/exposed rock. Hence, these results indicate that on an annual basis, the largest part of the precipitation that falls in areas with shallow/exposed rock flows towards low-altitude areas in the form of surface/near-surface water flow.

Sub-flow systems and discharge

Groundwater discharge is conceptually interpreted to take place in the low-altitude areas, corresponding to “valley” type areas as defined in the conceptual hydrogeological model. The characteristics of the hydrogeological flow domains Quaternary deposits and bedrock (see Section 4.2.2) imply that two main local-scale groundwater flow systems in the discharge areas can be identified: One near-surface system in the upper rock and the Quaternary deposits, and one deeper, larger-scale flow system primarily associated with deformation zones (of different orientation) in the rock.

According to the conceptual model of the bedrock and the Quaternary deposits, most groundwater flow towards the discharge areas in the valleys takes place in the Quaternary deposits and in the upper c. 10 m of the rock. Groundwater flow in the deeper parts of the rock occurs in a connected system of conductive fractures and deformation zones, cf. Sections 8.4 and 8.5, and the associated groundwater discharge takes place at locations where this system connects to zones that outcrop in the valleys; groundwater discharge from the deep rock is less likely in areas where there are no outcropping deformation zones. At least in a qualitative sense, interference tests have indicated the existence of such hydraulic connections between outcropping deformation zones and Quaternary deposits; see e.g. /Werner et al. 2008/.

The above concepts are illustrated in Figure 4-24, which exemplifies joint evaluations of groundwater levels in the Quaternary deposits and point-water heads in percussion and cored boreholes. These interpretations indicate that upward hydraulic gradients from bedrock to the Quaternary deposits primarily prevail in connection with deformation zones in the rock. Hence, topography in combination with the geometry and the hydrogeological properties of deformation zones and their contact with the Quaternary deposits are important factors that control groundwater discharge from the bedrock to the Quaternary deposits.

Figure 4-25 shows a conceptual vertical W-E section along a large valley in Laxemar. As visualised in this figure, groundwater discharge from the upper bedrock/Quaternary deposits part of the system to the surface (surface waters) is strongly influenced by the geometry and the hydrogeological properties of the Quaternary deposits overlying the till. Moreover, there is also an influence on this process by the horizontal extent and hydrogeological properties of the upper rock (including the deformation zones) and the high-conductive Quaternary deposits overlying the rock in the valleys.

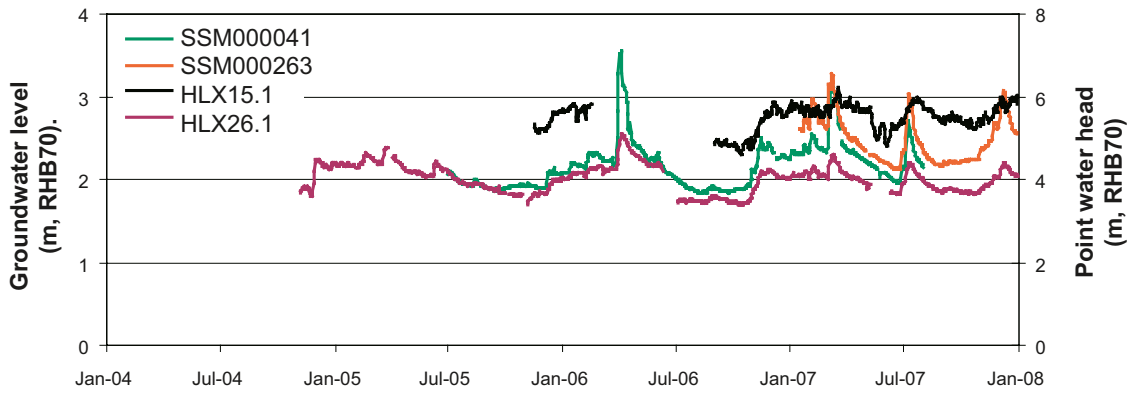


Figure 4-24. Time-series plots of groundwater levels in groundwater monitoring wells SSM000041 and -263 and point-water heads in percussion boreholes HLX15 and HLX26 in the Laxemarån stream valley; HLX15 is artesian, whereas HLX26 is not.

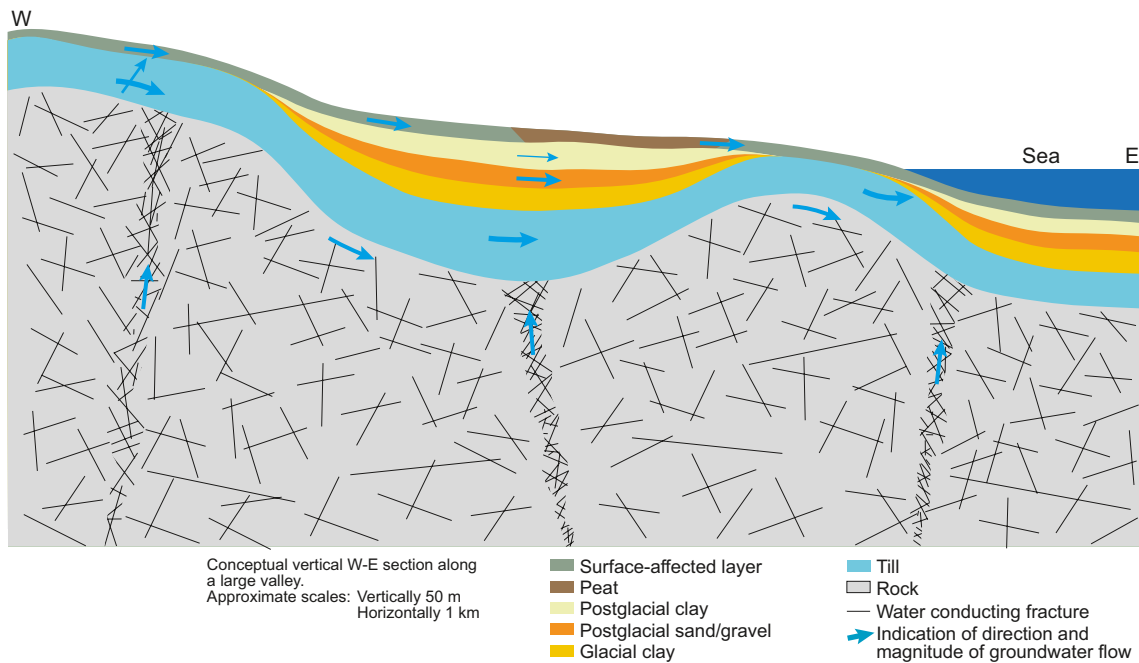


Figure 4-25. Conceptual vertical W-E section along a large valley in Laxemar. Note the different horizontal (1 km) and vertical (50 m) scales in the figure.

The large valleys in Laxemar are hence characterised by groundwater discharge to the surface, as well as more horizontal groundwater flow along the valley in the upper rock/Quaternary deposits system. Groundwater discharge to the surface is facilitated in areas where there are no layers of glacial clay and postglacial sediments acting as caps above the till.

4.4.3 Hydrogeochemistry

The hydrochemistry observed today in the surficial parts of the groundwater system (i.e. extending down to c. -250 m) is partly a consequence of the palaeohydrological development. In higher elevated areas, meteoric recharge has had a great influence on the observed hydrochemistry, which is usually characterised by dilute fresh water of low ionic strength. The meteoric recharge in the western parts of the area gives rise to two different groundwater flow movements or (sub-)systems; a) a shallow young groundwater system which partly discharges towards the east, and b) a deeper/older groundwater pathway which merges with an overall regional flow at greater depth (below -250 m) discharging further to the east.

Recharge to the deeper parts of the bedrock is probably augmented in the close vicinity of deformation zones in the more inland parts of the Laxemar-Simpevarp area. The low-elevated eastern part constitutes discharge areas for the regional flow, and groundwater discharge from deeper levels is associated with deformation zones located below lakes and brackish coastal basins and bays.

The depth variation of the current redox front, cf. Sections 4.4.1 and 9.5.6, is caused by the varying recharge/discharge conditions, as well as by the varying redox capacity of the Quaternary deposits, the bedrock and its fracture minerals. Typically, the depth is about 20 m below ground surface. As indicated in Figure 4-26 oxygenated water tends to invade deeper in deformation zones characterised by downward flow, locally resulting in a lowering of the redox front to about 60 m below ground surface. This condition is reversed at deformation zones subjected to regional discharge.

In areas of low elevation, close to the coast, elevated levels of marine ions (e.g. Na, Cl, Mg) in shallow groundwater indicate ongoing out-flushing of marine relicts that have remained in the groundwater since the area was covered by saline sea water during the Littorina stage or later. However, at most locations in the Laxemar-Simpevarp area, this flushing is more or less completed and observed concentrations of ions of marine origin can be explained mainly by deposition and anthropogenic sources. As much as 2/3 of the chloride transported by the freshwater surface system in the area is estimated to originate from an anthropogenic source, namely road salt. The influence of road salt is limited to fresh groundwater, cf. definition in Section 9.5, and is not expected to affect the composition of deep groundwaters /Laaksoharju et al. 2009/. Marine relicts, in combination with regional groundwater flow patterns, may explain the observed anomalous composition of water in shallow groundwater sampling points in till beneath lake and sea sediments. These sites are predominantly located close to major deformation zones, and may potentially indicate discharge points for deep groundwater.

On a regional scale, meteoric recharge and the subsequent flushing of ions results in the conceptual model described in /Tröjbom et al. 2008/ and illustrated in Figure 4-26. The interaction between the shallow and deeper groundwater results in complex mixtures of different water types. At greater depths, recharged meteoric water is mixed with portions of old glacial/old meteoric water. In the successive movement of these waters, processes associated with water/rock interactions take place, which can be seen in the groundwater chemistry. A groundwater chemical transition zone between -200 and

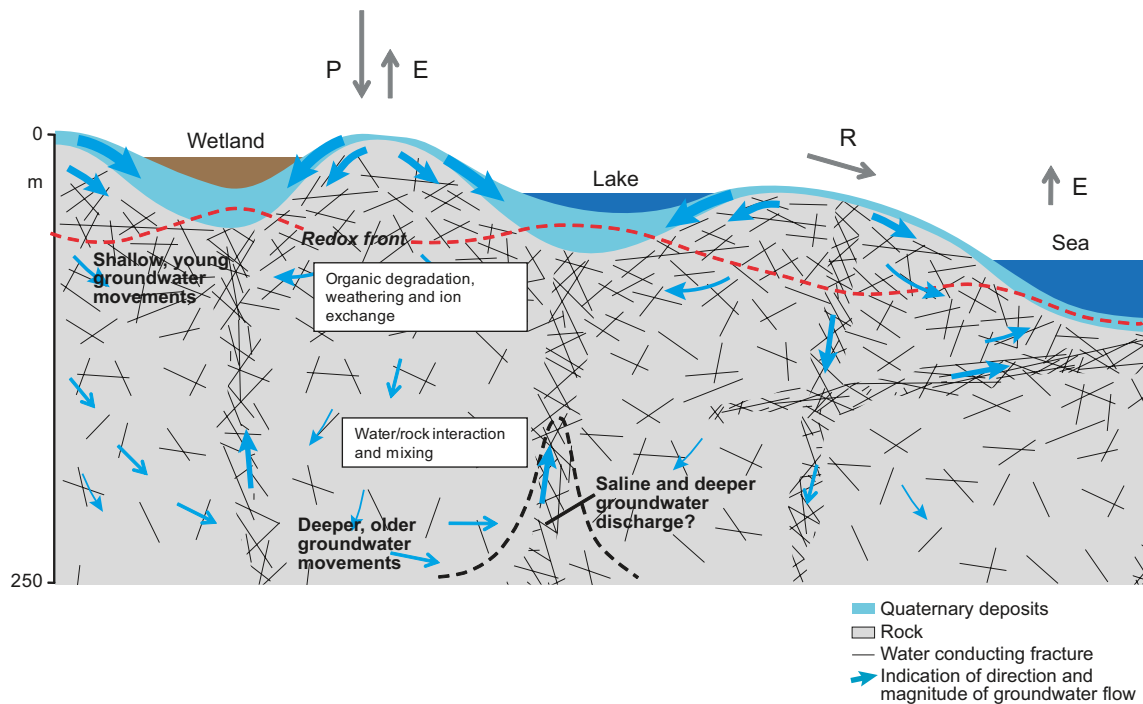


Figure 4-26. Simplified W-E cross-section of the Laxemar-Simpevarp area illustrating the major groundwater flow patterns and some important hydrochemical processes and properties in the Quaternary deposits and in the upper 250 m of the bedrock; P = precipitation, E = evapotranspiration, R = runoff. The vertical and horizontal scales in the figure are distorted, mainly by exaggerating the more surficial parts.

–500 m is developed over the greater part of the Laxemar-Simpevarp area, indicated by the occurrence of brackish glacial water types. These waters are then mixed with more saline, relict marine waters in the discharge areas in the east. Local recharge/discharge and development of smaller circulation cells in the eastern area is indicated by the occurrence of tritium-free shallow groundwater.

4.5 Overall description of the surface system

The Laxemar-Simpevarp area is located along the coastline of the Baltic Sea in south-eastern Sweden. The area, which is typical for this part of eastern Sweden, is characterised by a relatively flat topography in a fissure valley landscape, dominated by coniferous forests. The predominantly thin Quaternary deposits are mainly located in the valleys, whereas the high-altitude areas are dominated by exposed bedrock or thin layers of till and peat. Glacial till is the most common Quaternary deposit and covers half of the terrestrial part of the regional model area.

The latest deglaciation in Laxemar-Simpevarp took place during the Preboreal climatic stage, c. 12 000 years ago (cf. Chapter 3). The whole regional model area is situated below the highest shoreline. At the deglaciation, the shoreline was situated c. 20 km west of the regional model area, which, depending on the local topography, was covered by 50–100 m of sea water. The first parts of the regional model area emerged from the sea around 9 400 BC. Accordingly, the shoreline displacement has strongly affected the landscape development, especially during the first millennia after the deglaciation. Shoreline regression has prevailed, although at a lower rate, and the rate of land uplift during the past 100 years has been c. 1 mm per year.

According to the conceptual description of the Quaternary deposits, sandy-gravelly till overlies the bedrock in the whole area, also in most areas with exposed/shallow rock (which may have an overburden depth of up to c. 0.5 m). The exceptions are some of the exposed/shallow rock areas, in which organic soil and a thin vegetation layer is directly overlies the rock. The sandy-till is characterised by a relatively high hydraulic conductivity (c. $4 \cdot 10^{-5}$ m/s). Furthermore, there are indications that the hydraulic conductivity of the Quaternary deposits overlying the bedrock in the deepest parts of the large valleys is about one order of magnitude higher compared with that in other parts of the area.

The annual average precipitation in the area is c. 600 mm and the annual specific discharge is c. 170 mm. The precipitation demonstrates a near-coastal gradient, with less precipitation at the coast compared with areas further inland. Groundwater levels in the Quaternary deposits are shallow; according to monitoring data, the average depth to the groundwater table is less than 1 m during more than half of the year. Generally, the depth to the groundwater table is larger in high-elevation areas than in low-elevation areas, but this variation is much smaller than the variation in absolute groundwater levels in the area. Accordingly, there is a close correlation between the ground-surface topography and groundwater levels in the Quaternary deposits, which in turn implies that topography has a strong influence on near-surface patterns of groundwater recharge and discharge.

Most of the regional model area (73%) is covered by forests, dominated by Scots pine (Sw: *tall*) and Norway spruce (Sw: *gran*). Deciduous trees are more common near the coast, making the mixed forest the second most common forest type. Wetlands are less frequent and cover only 1% of the area, whereas agricultural land covers c. 8%. The agricultural land consists of arable land and grasslands. Many pastures were earlier intensively used but are today a part of the abandoned farmland following the nation-wide general regression of agricultural activities /Löfgren 2008/.

There are 5 lakes and a number of small streams in the regional model area. Only one of the lakes, Lake Frisksjön, is situated within the Laxemar local model area, cf. Appendix 1. Typically, the lakes are small with relatively shallow depths. They are characterised as mesotrophic brown-water lakes, i.e. with moderate nutrient concentrations and with brown water colour. The water colour is caused by high input of organic matter from the surrounding catchments. Because of the brownish water, light penetration is poor and the depth of the photic zone is generally small. As a result, macrophyte coverage is small in the lakes and the biota is dominated by heterotrophic organisms, particularly bacteria. Perch is the dominant fish species in lakes in the area, in numbers, as well as in weight. Most of the streams in the area are small with mostly calm or slowly flowing water. Many streams are dry in the summer, but a few, such as Laxemarån, have a permanent water flow. Both lakes and

streams in the area are to a large extent influenced by human activities, e.g. lowering of the lake water levels and altering the stream channels by various technical encroachments.

The marine area in Laxemar-Simpevarp is separated from the open sea in the east by the island of Öland, forming a funnel-like strait with its wide end to the north and the narrow end southwards. The bottom along the coast slopes gradually in the offshore direction. The maximum depth recorded in the regional model area is c. 45 m. The marine area can be divided into three subareas with more or less distinct characteristics concerning ecosystem structuring factors such as wave exposure, light penetration and substrate type. These subareas are; secluded bays, shallow exposed archipelago, and deep, exposed areas.

The average light penetration depth (Secchi depth) at the marine sampling sites is 5.5 m, which is low compared with that at the national monitoring station located further out in the Baltic Proper (8.7 m). However, the light penetration varies within the area, and the sheltered inner bays have Secchi depths of only 2–3 m. The salinity in the outer, exposed parts of the regional model area is 6.8‰, which is similar to that in the Baltic Proper, whereas the salinity at sampling stations in the inner bays is lower (mean values between 5.5 and 6.3‰) and varies strongly over time due to the influence of freshwater from land.

In conclusion, the surface system site description has increased the general understanding of how the site functions in terms of properties of different volumes, the main functional units, processes and system descriptions from different scientific disciplines. The initial conceptual model, developed at the beginning of the work in 2002, has been adjusted to site-specific features, and site data have been used to describe flows and accumulation of matter in and between different parts of the surface system at Laxemar-Simpevarp.

The present site description covers all available information on the natural system at Laxemar-Simpevarp. Nowhere else in Sweden, except for the corresponding description of the Forsmark, are so many background data and models available for environmental impact assessments (EIA). Main SDM references for the EIA are the ecosystem reports covering the biotic and abiotic descriptions of the Laxemar-Simpevarp surface system. Data on the hydrology and the properties of the Quaternary deposits are also available, together with the chemical descriptions of waters, soils and biota. No description of nature values, as defined by the general society, is made in the SDM itself, but all the information needed is stored in the SKB databases and is readily available.

4.6 Evaluation of uncertainties

As described in the previous section, the site descriptive model for the surface system consists of a large number of sub-models, covering a wide range of disciplines. In many cases, sub-models are combined and used as input for new models. For example, in the modelling of surface hydrology the digital elevation model (DEM), the horizontal distribution and stratigraphy of the Quaternary deposits, the hydraulic properties of till, and the distribution of different vegetation types, are used as important input data. Each sub-model contains its own uncertainties. These uncertainties are accumulated in the aggregated models, together with uncertainties associated with the assumptions and simplifications made in the development of the aggregated model.

The approach to evaluate uncertainties in the aggregated models is firstly to assess uncertainties in the underlying sub-models upon which the aggregated model is built, and secondly, to evaluate the assumptions made within the aggregated model. No quantification of uncertainties associated with the site descriptive model for the surface system is made here since this is done separately in each of the discipline-specific background reports (see Section 4.5). Instead, a brief summary of the confidence in some of the most important sub-models and aggregated models is provided.

Generally, the site descriptive model for the surface system is based on a wealth of site data. Uncertainties associated with the sub-models have been thoroughly evaluated, and descriptions and model results are in most cases consistent with regional/generic data and/or with the results from alternative models (see discipline specific background reports cited in text).

Some aspects of the site descriptive model for the surface system have low uncertainty and high confidence, whereas other aspects have a higher degree of uncertainty and, accordingly, lower confidence (see Table 4-6). However, none of these are judged to be of critical importance for the long-term safety assessment or for engineering.

Table 4-6. Degree of uncertainty for some of the most important sub-models and input data in the site descriptive model.

Aspects	Degree of uncertainty
The past development of the site, including climate changes, description of shoreline displacement, and salinity changes in the Baltic basin.	Low
Geometries, e.g. the digital elevation model, delimitation of catchment areas, horizontal distribution and stratigraphy of the overburden, distribution of vegetation types.	Low
Overall water balance, surface- and groundwater levels, general groundwater flow pattern.	Low
Hydrochemistry of surface waters with regard to nutrients, macro elements, temporal variation and mass transport in drainage areas.	Low
Hydraulic properties of till.	Low
General groundwater flow pattern.	Low
Chemistry in biota and Quaternary deposits – the data amounts are limited and spatial extrapolation of the available data is required.	High
Depth distribution of Quaternary deposits outside the local model area and Laxemarån catchment area – low spatial resolution of data.	High
Biological process estimates (e.g. plant uptake and respiration) – there are generally few measurements and short time series.	High
Influence of chemical processes on the transport of elements.	High

5 Bedrock geology

It is of primary importance for assessing the potential for disposal of highly radioactive nuclear waste that the understanding of the bedrock geology of the investigated site is as reliable and well-founded as possible prior to modelling work in other geoscientific disciplines. This also applies to the subsequent design of a potential repository, and the assessment of long-term safety and environmental impact. The deterministic geological modelling work comprises three aspects that serve the needs of different users, the modelling of rock domains, deformation zones and fracture domains. The identification and description of fracture domains also provides a basis for the stochastic modelling of fractures and minor deformation zones, the so-called geological discrete fracture network modelling (DFN). In addition, the evaluation of primary data that relates to subordinate rock types has provided an input for the development of stochastic models for the spatial distribution of these rock types inside the rock domains in the focused part of the local model volume. The result of this stochastic modelling is presented in connection with the thermal modelling work (see Section 6.4.4).

Following the establishment of the state of knowledge in model version 0 /SKB 2002/, prior to the site investigation work, deterministic modelling work in SDM versions Simpevarp 1.1 and 1.2 focused on the Simpevarp subarea and the regional model area /SKB 2004a, 2005a/. In the SDM version Laxemar 1.2, focus shifted to the Laxemar subarea /SKB 2006a/. In accordance with the decision to focus the complete site investigation to the central, western and southern part of Laxemar /SKB 2007a/, the geological work in model version SDM-Site Laxemar /Wahlgren et al. 2008/ has focused solely on Laxemar, and in particular on its southern and southwestern part. The geological DFN modelling work in stage SDM-Site Laxemar /La Pointe et al. 2008/ introduced the fracture domain concept inside the local model volume.

This chapter summarises the evaluation of primary geological data completed throughout the geological modelling work in Laxemar and presents the various geological models for the site. The deterministic geological models and the geological DFN model presented in this chapter are the same and correspond in full to those presented in the geology report /Wahlgren et al. 2008/ and the report on stochastic modelling of fractures and minor deformation zones /La Pointe et al. 2008/ produced as part of the model version SDM-Site Laxemar.

5.1 State of knowledge at previous model version

Previous geological modelling work comprises Simpevarp model versions 1.1 and 1.2 and Laxemar model version 1.2 as well as site characterisation work and modelling performed during stage 2.1. However, no complete 3D geological model versions were constructed in conjunction with modelling stage Laxemar 2.1 /SKB 2006c/. Although the Laxemar subarea was included in the Simpevarp 1.2 model version, all available information for Laxemar was based on the SDM version 0.

A great step forward in the geological modelling work was achieved in model version Laxemar 1.2. The rock domain model presented in the Laxemar 1.2 model version was considered as stabilising, and only minor modifications have been carried out in the current SDM-Site model version. Due to the generally well-preserved magmatic character of the bedrock, and in contrast to the rock domain modelling in Forsmark, no tectonic concept acting as structural guidance for the 3D geometrical modelling at depth has been established in the Laxemar-Simpevarp area. Instead, the modelling of rock domains is mainly steered by combining the 2D rock domain boundaries modelled at the surface with the defined rock domain boundaries at depth in the boreholes, supported by gravity modelling /SKB 2006a, Wahlgren et al. 2006a, 2008/. However, a structural concept has steered the definition of two rock domains in the eastern to south-eastern part of the Laxemar local model area.

The deterministic model of deformation zones was considered as stabilising in the SDM model version Laxemar 1.2 compared with the preceding Simpevarp 1.2 model version. In particular, new surface reflection seismic, refraction seismic, magnetic, electrical resistivity and electromagnetic measurements generated important data for the deformation zone model. Considerable uncertainties

still existed due to limited sub-surface data. However, targeted drilling campaigns in combination with geophysical measurements confirmed most of the modelled deformation zones in the Simpevarp 1.2 model. In particular, the lack of borehole intersections for most of the deformation zones in Laxemar made the characterisation and property assignment uncertain.

The geological DFN model created during SDM version Laxemar 1.2 was based on the concept of a global (i.e. applicable to the entire model domain) orientation model, a global fracture size model defined using data from rock domain RSMA01, and a rock domain dependent fracture intensity model. The amount of fracture data available from cored boreholes was extremely limited in Laxemar 1.2, both in quantity and spatial coverage; the subsurface DFN parameterisation was based on data from four cored boreholes (KLX01 through KLX04) and a single percussion-drilled borehole (HLX15). Fracture intensity was hypothesised to be a function of lithology, rock domain, presence or absence of ductile or brittle/ductile zones, and degree of rock alteration. However, there were insufficient data available to model spatial variability of fracture properties at the local model scale. At the end of SDM version Laxemar 1.2, considerable uncertainty remained in the understanding of fracturing within the local model volume. The spatial variability of fracture size and intensity, particularly of the global subhorizontally dipping fracture set, dominated the list of model uncertainties.

5.2 Evaluation of primary data

This section briefly describes the evaluation and interpretation of the primary data used in the SDM-Site Laxemar geological modelling work. For a comprehensive description, see /Wahlgren et al. 2008 and Chapter 3 therein, with accompanying appendices/.

For a description and characterisation of the uppermost part of the bedrock, see Section 4.4.1.

5.2.1 Bedrock geological map at the surface

Map compilation and assessment of quality

A bedrock geological map, which presents a 2D model for the distribution of rock units at the ground surface, was compiled for the Laxemar-Simpevarp area at the scale 1:10,000 and constituted an important input to the Laxemar 1.2 model version. The bedrock geological map is based on the documentation of the bedrock made during the bedrock mapping campaign 2004 /Persson Nilsson et al. 2004/. An interpretation of the magnetic anomaly map, compiled predominantly from helicopter airborne data, was also an important input in the compilation work. A description of the bedrock geological map of the Laxemar-Simpevarp area, including the rock type distribution and ductile structures, is presented in /Wahlgren et al. 2005, 2006a, SKB 2006a/.

The bedrock geological map in the regional model area, outside the Laxemar and Simpevarp sub-areas, is only of reconnaissance character as presented in the SDM Simpevarp version 0 /SKB 2002/.

An updated version of the bedrock geological map of the Laxemar area /Wahlgren et al. 2006b/ is displayed in Figure 5-1, and is also available on the DVD attached to the printed report. The main modification compared with the preceding Laxemar 1.2 version, is the definition of an area dominated by Ävrö quartz monzodiorite, i.e. a quartz poor variety of the Ävrö granite. However, in the remaining part of the area, the term Ävrö granite has been retained, since it is generally not possible to divide the Ävrö granite into quartz monzodioritic (Ävrö quartz monzodiorite) and granodioritic to granitic (Ävrö granodiorite) varieties in the bedrock map due to insufficient analytical data coverage. Note that the term Ävrö granodiorite also includes granitic varieties /cf. Wahlgren et al. 2008 and Appendix 2 therein/. Furthermore, a N-S oriented dolerite dyke is marked in the westernmost part of Laxemar along deformation zone ZSMNS001C (cf. Section 5.5).

The absolute ages and relative age relationships between the different rock types, deformation, uplift and cooling history at the site have been evaluated and used in the establishment of the geological evolution of the area, see /Söderbäck 2008, cf. Section 3.1 therein/. The character of the rock types and ductile structures are addressed in more detail in Sections 5.2.3 and 5.2.4.

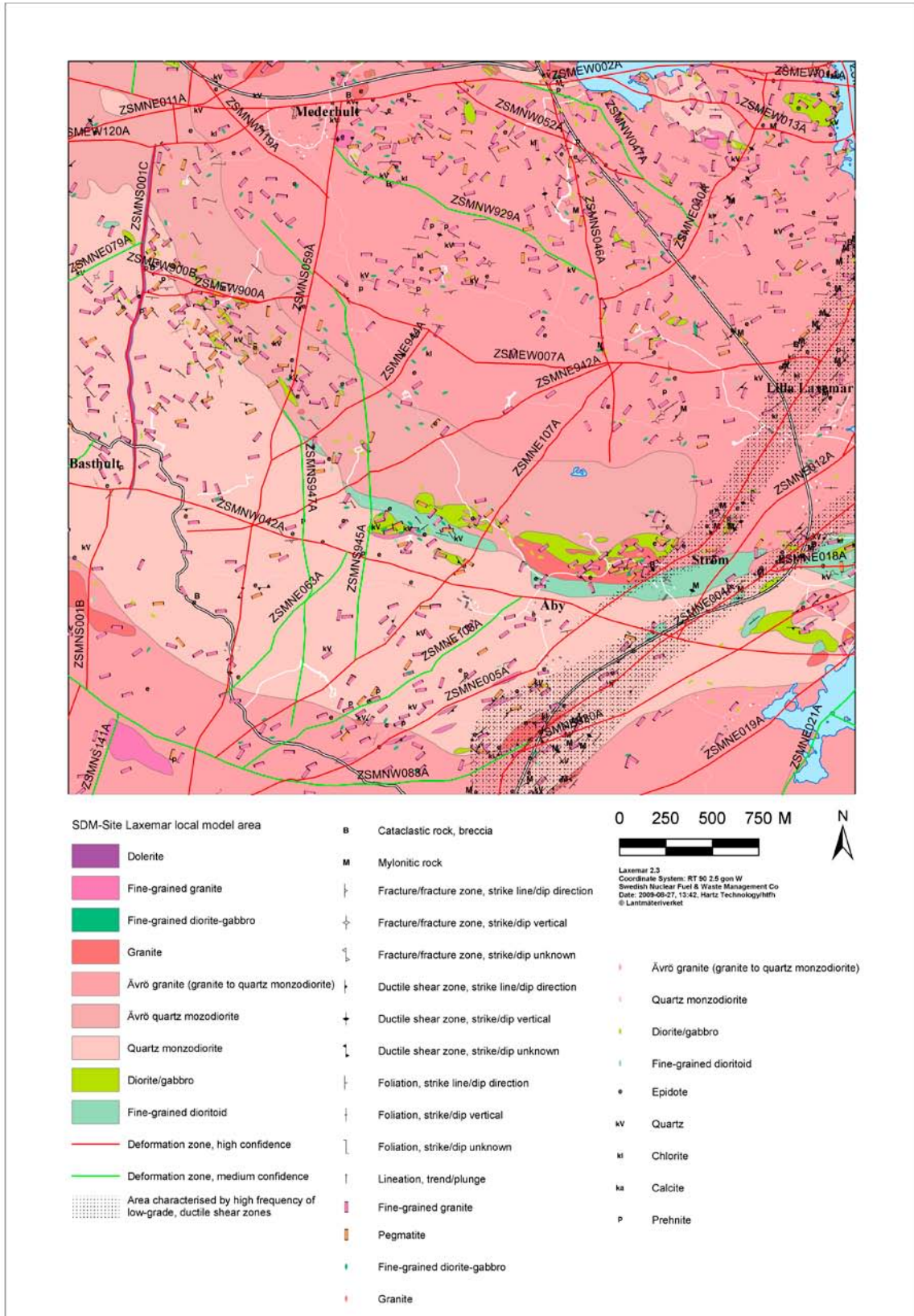


Figure 5-1. Bedrock geological map of the Laxemar local model area. The orientation of the symbols for fine-grained granite and pegmatite indicates the strike. The naming rule applicable to deformation zones is explained in Section 1.6.5.

Rock units

The major groups of rocks in Laxemar are mainly distinguished on the basis of their composition, grain size, texture and relative age. Rock units shown on the bedrock geological map (Figure 5-1) are distinguished on the basis of the character of the dominant rock type. For example, the rock unit with light pink colour on the bedrock geological map (Figure 5-1) is dominated by quartz monzodiorite but it contains different subordinate rock types as well. Apart from the dolerite dykes and the Götemar and Uthammar granites, the remaining rock types in Laxemar and its surroundings were formed more or less synchronously c. 1.8 Ga ago, though field relationships reveal their relative age. The bedrock geological map also distinguishes rock units which are characterised by a high frequency of low-grade ductile shear zones (dotted pattern in Figure 5-1), i.e. rock units that are more strongly affected by ductile strain than the country rock in general. The principal characteristics and encoding of the dominant rock types in the rock units are presented in Table 5-1.

The dominant rock types in southern and south-western Laxemar, the area of focus, are from the south (south-west) towards the north (north-east), equigranular quartz monzodiorite, porphyritic Ävrö quartz monzodiorite with inhomogeneously distributed bodies of diorite/gabbro and porphyritic Ävrö granite. Important subordinate rock types throughout Laxemar comprise fine-grained granite, fine-grained diorite-gabbro and pegmatite. The subordinate rock types occur as dyke-like bodies, patches and small irregular intrusions.

Dolerite dykes

In addition to the dolerite dyke marked on the bedrock geological map (Figure 5-1), which is based on the near-surface documentation in KLX20A and three percussion boreholes, dolerite is encountered in a number of additional cored and percussion boreholes in western Laxemar. It should be noted that dolerite has not been observed in any outcrop in Laxemar in conjunction with the bedrock mapping campaign. However, the possible hydraulic significance of such dykes emphasised the need for an assessment of the possible existence of additional dolerite dykes in the remaining part of Laxemar. Based on an interpretation of the detailed ground magnetic data and digital elevation models, /Triumpf 2007/ identified 21 linear anomalies (lineaments) that possibly could be related to dolerite dykes, two of which are confirmed to contain dolerite. However, it must be noted that the uncertainty in the prediction of the possible existence of additional dolerite dykes in Laxemar is high, since brittle and ductile to brittle-ductile shear zones have the same anomaly characteristics in the magnetic data and digital terrain models. Other than the dolerite in KLX20A, which is c. 30 m thick, the documented dolerites have a thicknesses varying between 1 decimetre and a couple of metres and it is therefore inferred that any additional dolerites can be considered as thin and, therefore, constitute a very subordinate rock component in Laxemar. For a more detailed description of the assessment of additional dolerites in Laxemar, see /Triumpf 2007/.

Table 5-1. Principal characteristics and encoding of the dominant rock types in the rock units. Note that Ävrö granodiorite (501056) is included in the Ävrö granite (501044) since it has not been possible to distinguish Ävrö granodiorite at the ground surface.

Rock units – composition, grain size and texture of dominant rock type			
Code (SKB)	Composition	Grain size	Texture
501044	Granite to quartz monzodiorite (Ävrö granite)	Medium-grained	Porphyritic
501046	Quartz monzonite to quartz monzodiorite (Ävrö quartz monzodiorite)	Medium-grained	Porphyritic
501036	Quartz monzodiorite	Medium-grained	Equigranular
501030	Dioritoid	Fine-grained	Unequigranular
501058	Granite	Medium-to coarse-grained	Equigranular to slightly porphyritic
511058	Granite	Fine- to medium-grained	Equigranular
501033	Diorite to gabbro	Medium-grained	Equigranular
521058	Granite (“Götemar type”)	Coarse-grained and fine- to medium-grained	Equigranular to slightly porphyritic
Independent	Independent	Protomylonitic to mylonitic foliation	

Mineral resources

An assessment of the potential of the Laxemar-Simpevarp area for exploitation of metallic and industrial mineral deposits is presented in /Lindroos 2004/. It was concluded that the Laxemar-Simpevarp area is sterile with regards to metallic mineralisations and there is no potential for industrial minerals.

5.2.2 Rock units and possible deformation zones in the sub-surface

Geological, geophysical and radar logs

45 cored boreholes, i.e. not including KLX01, and 28 out of 43 percussion boreholes in Laxemar have been mapped geologically using the Boremap methodology adopted by SKB, which comprises an integrated interpretation of the drill core and the oriented images of the borehole walls provided by the Borehole Image Processing System (BIPS). The mapping of the percussion boreholes is mainly based on the BIPS image complemented by analysis of drill cuttings. The uncertainties in borehole orientation data have been evaluated by /Munier and Stigsson 2007/ and are addressed briefly in Section 2.5. Note that photographs of the drill cores from all cored boreholes in Laxemar are available on the DVD attached to the report.

Standard geophysical and radar logs complement the BIPS log in the boreholes. A summary of the data that have been generated in the geophysical logging work can be found in /SKB 2006a and Section 5.2.8 therein, Wahlgren et al. 2006a and Section 2.4.4 therein/. Some of the geophysical data, e.g. density and natural gamma radiation, provide support for distinguishing between different rock types in the boreholes, especially in the percussion boreholes since no drill core exists.

It is considered that directional borehole radar reflectors most often provide orientation estimates for discrete features, even within or near a deformation zone. Thus, radar orientations are interpreted to be secondary supporting indicators of the overall geometry of a given deformation zone.

The result of the geological mapping of the boreholes together with geophysical and radar logs have been reported in 148 data reports (cf. Appendix 3), which constitute the prime input used in the geological single-hole interpretation.

Single-hole interpretation – rock units and possible deformation zones

The geological single-hole interpretation (SHI) provides an integrated synthesis of all geological and geophysical data from a borehole. SHI forms an important link between all the detailed borehole data that are generated and the subsequent geological modelling work. It therefore has a similar role to the bedrock geological map that forms an important intermediate step between the detailed outcrop data generated at the surface and the site descriptive modelling work. A description of the various stages in the SHI work is provided by /Wahlgren et al. 2008, cf. Section 3.3 therein/.

In Stage 1 of the single-hole interpretation work, rock units and possible deformation zones in each borehole are identified and described, and the result for all cored boreholes is presented in the form of WellCad diagrams /cf. Wahlgren et al. 2008 and Appendix 3 therein/. One example is displayed in Figure 5-2. Stage 2 of the single-hole interpretation work comprises a more detailed description of the characteristics of possible deformation zones that have been recognised with high confidence.

Rock units (RU) have been defined primarily on the basis of the composition, grain size and texture of the dominant rock type. However, identification of rock units can also be based on a more or less complex mixture of rock types (RU2 in Figure 5-2). These characteristics are identical to those used in the definition of rock types and rock units at the surface, in conjunction with the compilation of the bedrock geological map (see Figure 5-1). Apart from the cored boreholes KLX05, KLX06 and KLX09, rock units are characterised by either dominant Ävrö granite, quartz monzodiorite or a high frequency of diorite-gabbro in a dominant Ävrö granite (Ävrö quartz monzodiorite), as exemplified in KLX08 (Figure 5-2). These conspicuous rock units in the boreholes have had great impact and form the basis for the recognition of sub-surface rock domains in the modelling work (see Section 5.4).

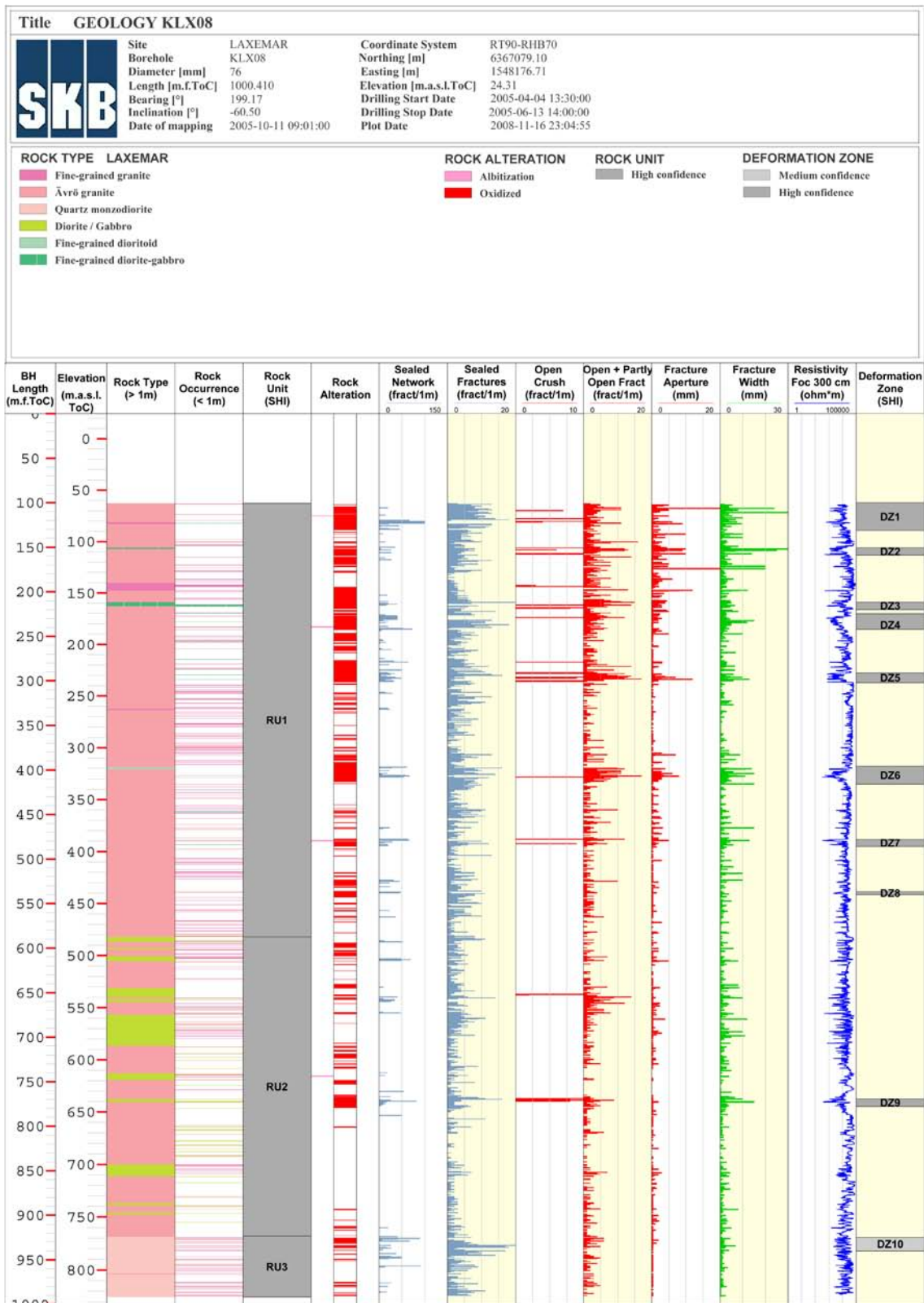


Figure 5-2. WellCad diagram for the cored borehole KLX08, showing a selected suite of base geological and geophysical data that have been used to identify rock units and possible deformation zones in the single-hole interpretation of this borehole (see also /Wahlgren et al. 2008/).

The possible deformation zones (DZ) in Laxemar are dominantly brittle in character and have been identified by integration of the geological and geophysical data sets fracture frequency, rock alteration, occurrence of fault rocks (such as cataclasites and breccia), and resistivity, single point resistivity, p-wave velocity, caliper and magnetic susceptibility from the borehole geophysical logs, in combination with an inspection of the drill core. Many of the more prominent deformation zones that are dominantly brittle in character display evidence for having been originally formed during ductile conditions. However, deformation zones that are primarily ductile in character, as evidenced by occurrence of mylonitic and protomylonite foliation, occur as well.

The identification of possible deformation zones along the boreholes provides fixed points in the sub-surface for the modelling of deformation zones in 3D space (see Section 5.5).

Extended single-hole interpretation

During SDM-Site Laxemar modelling work, a programme to update the single-hole interpretation (SHI) process for cored boreholes was undertaken. The extended single-hole interpretation (ESHI), which is a replacement for the older SHI, consisted of two activities.

- Subdivision of the Ävrö granite in the two subvarieties quartz-poor Ävrö quartz monzodiorite and quartz-rich Ävrö granodiorite. This activity included all borehole intervals where Ävrö granite constituted a dominant rock type.
- Identification of additional possible deformation zones in cored boreholes KLX02 (200–1,000 m), KLX03, KLX04, KLX05, KLX06, KLX07A, KLX07B and KLX08.

A subdivision of the Ävrö granite, similar to that presented in the bedrock map (cf. Section 5.2.1), has been carried out in all cored and percussion boreholes (including the Simpevarp subarea) in which Ävrö granite constitutes an important rock type. The subdivision was carried out by use of the density logs from the boreholes. A density of 2,710 kg/m³ was used as a threshold value for separating Ävrö quartz monzodiorite from the more quartz-rich Ävrö granodiorite. This subdivision is fundamentally important to the refinement of the rock domain model in the Laxemar local model volume (Section 5.4).

During the original single-hole interpretation process (KLX01 to KLX08), geological structures were not flagged as potential deformation zones unless their measured thickness in core was greater than c. 5 decimetres. Beginning with borehole KLX09, a new mapping procedure was implemented to map all possible deformation zones, regardless of apparent thickness. As a result, it was necessary to return to boreholes mapped previous to KLX09 and re-map them, so that all cored boreholes would be mapped at the same resolution. The identified deformation zones from the ESHI in the cored coreholes in the focused volume in Laxemar are presented in the WellCad composites in Appendix 5.

ESHI has subsequently replaced SHI in all boreholes in the Laxemar-Simpevarp area. All analyses and evaluations that have been carried out in conjunction with the SDM-Site Laxemar modelling work have utilised the ESHI. The ESHI results are also used to identify minor deformation zones in Laxemar; any possible deformation zones recorded during ESHI that are interpreted as having a true thickness of less than 10 m and not correlated to a deterministic deformation zone in the DZ model are considered to be minor deformation zones.

5.2.3 Rock types – properties, alteration, volumetric proportions, thickness and orientation of subordinate rock types

Properties

According to the strategy for model development, the geological and petrophysical character of rock types are important for the property assignment of the rock domains /Munier et al. 2003, p. 62/. In order to characterise the dominant rock types in the Laxemar local model volume, modal and geochemical analyses of fresh samples have been carried out on samples from the surface and from several drill cores /Wahlgren et al. 2005, 2006b, 2006c, 2007/. Both surface and drill core samples show the typical alkali-calcic trend of the intrusive rocks in the Transscandinavian Igneous Belt (TIB), with variations in composition from diorite-gabbro to quartz monzodiorite to granite (Figure 5-3).

The composition of the rock types, exemplified by the quartz content in the dominant rock types in Figure 5-4, has been demonstrated to correlate strongly to the thermal and mechanical properties (cf. Chapters 6 and 7). Note that the true quartz content is presented in Figure 5-4, not the recalculated Q-value in the QAP classification diagram in Figure 5-3.

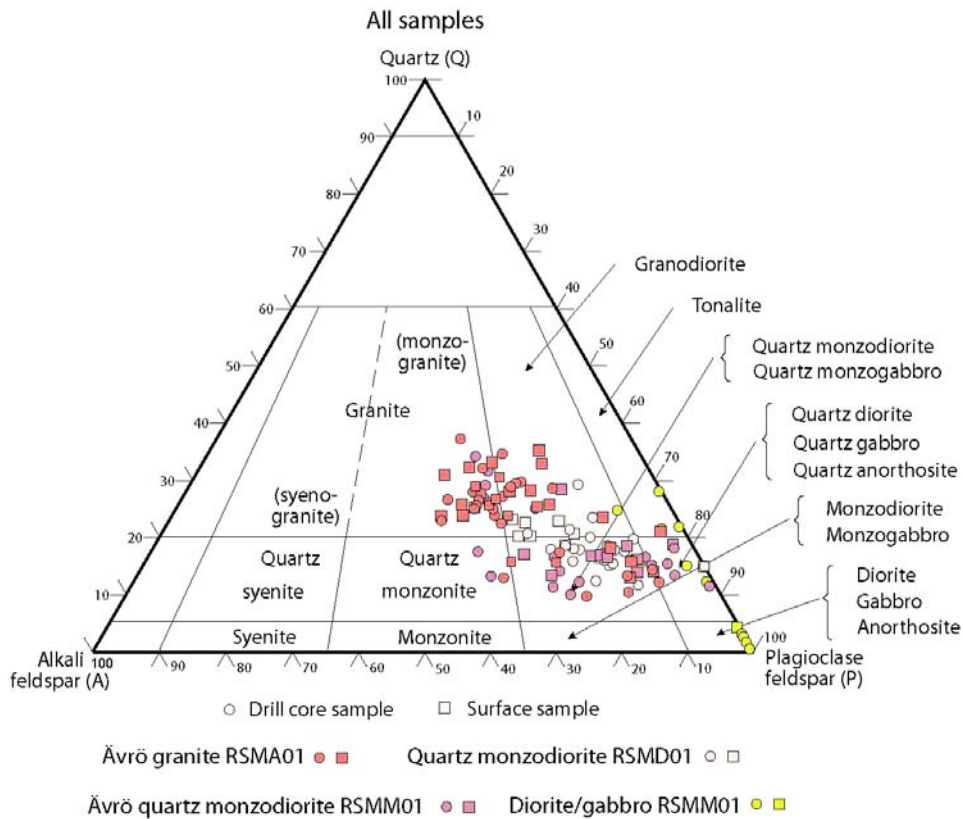


Figure 5-3. QAP modal composition of the dominant rock types in the Laxemar local model volume according to /Streckeisen 1976/.

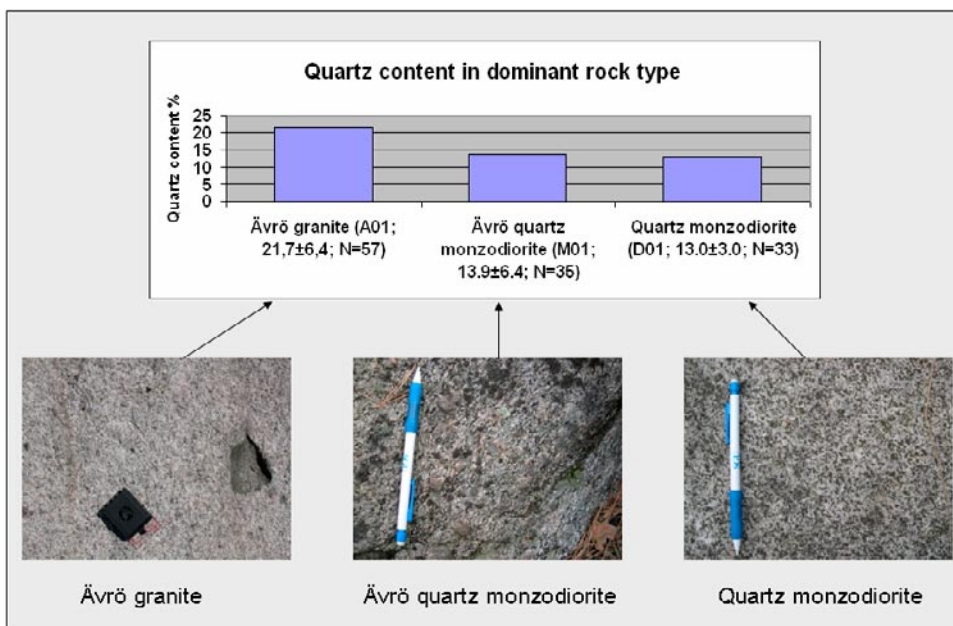


Figure 5-4. Quartz content in the dominant rock types in Laxemar.

Petrophysical properties of the dominant rock types that have been determined include density, porosity, magnetic susceptibility, electrical resistivity in fresh water, uranium content and natural exposure rate. The correlation between density and mineralogical composition formed the basis for the subdivision of the Ävrö granite in the two subvarieties Ävrö quartz monzodiorite and Ävrö granodiorite (see ESHI in Section 5.2.2).

A compilation of all properties that characterise the dominant rock types in Laxemar is presented in the SDM-Site Laxemar geology report /Wahlgren et al. 2008, cf. Appendix 11 therein/.

Alteration

An estimate of the degree of alteration is an important factor to consider for the thermal and rock mechanics modelling, since the degree and type of alteration affects the thermal and rock mechanical properties of the bedrock, see Sections 6.2.1 and 7.3.1, respectively. To meet this and other needs, an analysis of the degree of alteration in the rock in between interpreted deformation zones in the ESHI of the cored boreholes has been carried out. The degree, classified as faint, weak, medium and strong in the Boremap mapping, and type of alteration is presented in /Wahlgren et al. 2008, cf. Appendix 7 therein/ on a borehole by borehole basis, rock domain basis in each borehole and on an overall rock domain basis.

The degree of alteration in the bedrock in between the deformation zones in Laxemar is in general classified as faint to weak and, although heterogeneously distributed, approximately 20–25% of the bedrock is affected by alteration. Red staining (referred to as oxidation in the Boremap mapping) is by far the most abundant type of alteration in the Ävrö granite and Ävrö quartz monzodiorite (Figure 5-5), whereas the quartz monzodiorite displays a much higher degree of saussuritisation and epidotisation than the Ävrö granite and Ävrö quartz monzodiorite /cf. Wahlgren et al. 2008 and Appendix 7 therein/. The red staining is secondary in character and the extension is fracture-controlled, while the saussuritisation is more primary in character and interpreted to be a late-stage magmatic alteration.



Figure 5-5. Red staining (oxidation) along fractures in the Ävrö granite.

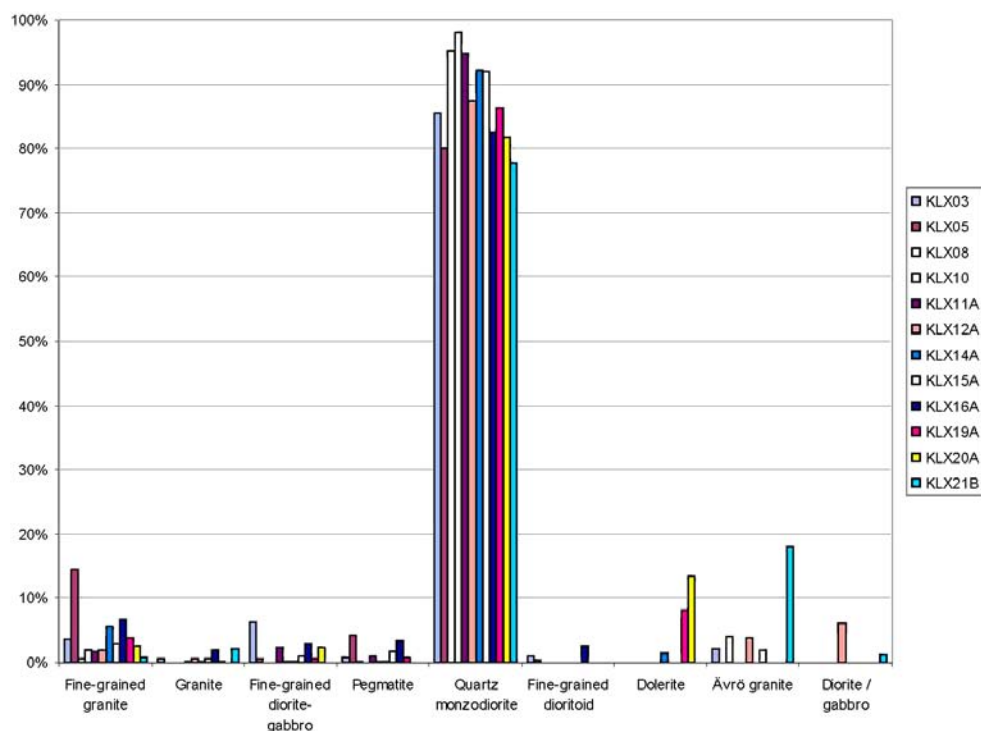


Figure 5-6. Histogram showing the quantitative estimate (volume %) of the proportions of different rock types in cored boreholes or parts of cored boreholes that are dominated by quartz monzodiorite in southern Laxemar, i.e. the RSMD01 domain (see Section 5.4).

Volumetric proportions

The proportions of different rock types, in particular the proportions of subordinate rock types in the dominant rock types is an estimate of the degree of homogeneity in the bedrock. Quantitative estimates of the proportions of different rock types in Laxemar have been made by use of data from the cored boreholes. The results of the estimates are presented on a borehole by borehole basis, on a rock domain basis in each borehole and on an overall rock domain basis in /Wahlgren et al. 2008, cf. Appendix 4 therein/. Figure 5-6 exemplifies the volumetric proportions of different rock types in the focused part of the Laxemar local model volume that is dominated by the quartz monzodiorite. For the corresponding estimates in cored boreholes that are dominated by Ävrö quartz monzodiorite and Ävrö granite northwards and northeastwards in Laxemar, see /Wahlgren et al. 2008/.

As can be seen in Figure 5-6, the boreholes that are drilled in the quartz monzodiorite in southern and southwestern Laxemar display very similar proportions of rock types. It should be noted that the dolerites in KLX14A, KLX19A and KLX20A are restricted isolated occurrences, unlike the other subordinate rock types, which are more or less evenly distributed along the boreholes.

Thickness of subordinate rock types

Knowledge of the thickness of the dyke-like subordinate rock types is of importance for the thermal modelling work because dyke-like subordinate rock types with a mineralogical composition different from the surrounding rock, and displaying a preferred orientation, have the potential to cause anisotropy in thermal properties. The borehole length and orientation of contacts of fine-grained granite, fine-grained diorite-gabbro and pegmatite in all cored boreholes (excluding the short boreholes defined for DFN-analysis) have been documented and the true thicknesses have been estimated. In the thickness calculation /Wahlgren et al. 2008, and Appendix 5 therein/, the value of the orientation of the upper contact in the Sicada database has been used.

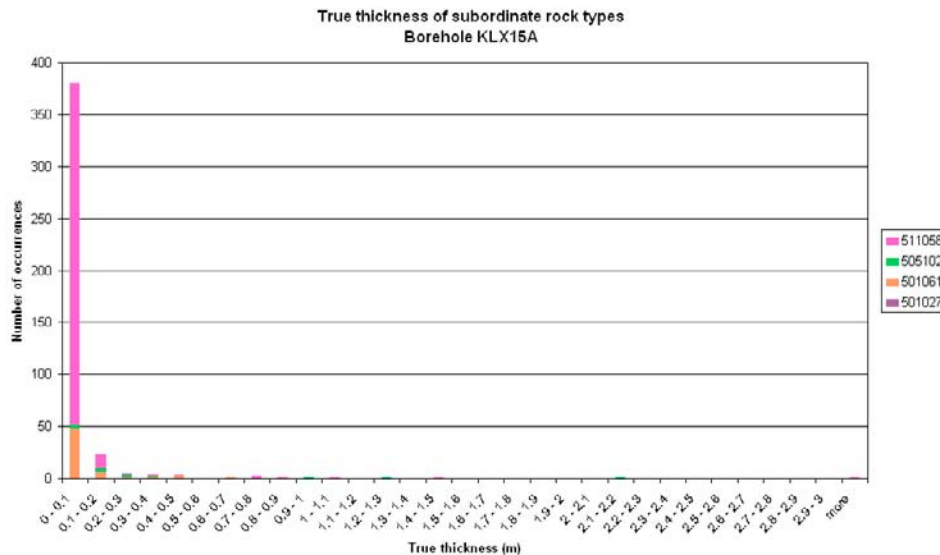


Figure 5-7. True thickness of fine-grained granite (511058), fine-grained diorite-gabbro (505102), pegmatite (501061) and dolerite (501027) in the quartz monzodiorite in southern Laxemar, i.e. the RSMD01 domain (see Section 5.4).

The number of occurrences of different thickness classes of fine-grained granite, fine-grained diorite-gabbro and pegmatite, with a truncation threshold of 0.1 m, are presented in /Wahlgren et al. 2008, cf. Appendix 5 therein/. Dolerite is also included in the estimation of true thickness for the boreholes KLX14A, KLX19A and KLX20A. Although there are a number of thicker occurrences, it is evident that the majority of the subordinate rock types have a thickness less than 0.1 m, /Wahlgren et al. 2008, and Appendix 5 therein/. This is exemplified by the thickness distribution of the subordinate rock types in the quartz monzodiorite in southern Laxemar (Figure 5-7), i.e. within the RSMD01 domain (see Section 5.4).

Orientation of subordinate rock types

In addition to thickness, the orientation of the subordinate rock types has to be considered in the thermal modelling work. Therefore, an analysis of the orientation of fine-grained granite, fine-grained diorite-gabbro and pegmatite, and, where it occurs, also dolerite, has been carried out for all cored boreholes (excluding the short boreholes defined for DFN-analysis, see Section 5.6). The orientation of the upper contact is used in the analysis. The orientation analysis is based on the assumption that the subordinate rock types can be treated as planar structures, although it is known by experience that, in particular, fine-grained granite in many cases constitutes irregular bodies.

The results of the orientation analysis are presented in /Wahlgren et al. 2008, cf. Appendix 6 therein/ on a borehole by borehole basis, on a rock domain basis in each borehole and on an overall rock domain basis. As is evident from the stereographic projections on the overall rock domain basis in /Wahlgren et al. 2008, cf. Appendix 6 therein/, the majority of the occurrences of fine-grained granite and fine-grained diorite-gabbro are subhorizontally to moderately dipping and have a dominant NE-SW strike, although a spread between N-S and E-W occur. Southerly dips are dominant in southern and central Laxemar, whereas dips both to the north and south prevail in northern Laxemar. The pegmatites display similar orientations, but are dominated by steep to subvertical dips, although a subhorizontal population exists, in particular in northern Laxemar.

5.2.4 Ductile deformation

From a structural point of view, the bedrock in Laxemar is dominated by well-preserved intrusive rocks. However, a faint to weak foliation, which is non-uniformly distributed in the bedrock in the local model volume, is present. Based on the mapping of the boreholes, c. 80% of the bedrock in Laxemar has been documented as massive, i.e. it does not contain any ductile anisotropy /Wahlgren et al. 2008, and Section 3.5.2 therein/.

It is inferred that the development of the foliation initially started at a late stage in the magmatic evolution but continued in the solid state after the crystallisation and solidification of the magmas. All rock types are affected by the foliation, in particular the dyke-like bodies of fine-grained granite and fine-grained diorite-gabbro. In many cases there is a concentration of ductile strain in the youngest dyke-like intrusions.

The orientation of non-uniformly distributed ductile foliation in the Laxemar local model volume is displayed in Figure 5-8. Although not strictly qualifying as a girdle according to the Vollmer fabric index /Vollmer 1995/, there is a girdle-like distribution when all data from Laxemar are considered. Furthermore, it is indicated that the dip of the foliation changes from being gentle to moderate, approximately to the north in northern Laxemar to gentle approximately to the south in southern Laxemar. In the intervening area in central Laxemar, the foliation displays variable dips to the north and south. Consequently, it is inferred that the non-uniformly distributed, faint to weak foliation in Laxemar defines an irregular antiformal configuration with a subhorizontal to gently west plunging fold axis. This interpretation is supported by results of measurements of the anisotropy of the magnetic susceptibility /see Wahlgren et al. 2008, cf. Section 3.5.4 therein/.

An evaluation of ductile structures from surface data was carried out in conjunction with the reporting of the Laxemar 1.2 model version /SKB 2006a, Wahlgren et al. 2006a/. The most spectacular and characteristic ductile, structural features in Laxemar are low-grade ductile to brittle-ductile shear zones that vary in thickness from decimetres up to tens of metres. A special study has been performed in order to unravel the kinematics in the ductile shear zones /Lundberg and Sjöström 2006/. The regional scale, most prominent, ductile shear zones strike NNE-SSW and NE-SW and are subvertical, whereas E-W oriented zones, though overprinted by brittle deformation display moderate to steep dips to the south. The study of the kinematics in the ductile shear zones /Lundberg and Sjöström 2006/ has revealed that the NNE-SSW and NE-SW oriented zones are characterised by sinistral strike-slip movement /cf. Viola and Venvik Ganerød 2007a/, whereas the ENE-WSW to E-W shear zones in the Simpevarp subarea show complex kinematics. This includes both reverse and normal dip-slip as well as sinistral and dextral strike-slip displacements. It has been inferred that the ductile deformation along the various sets of zones formed in response to an approximately northward-directed shortening /Lundberg and Sjöström 2006/.

/Wahlgren et al. 2008, cf. Section 3.5.2/ present the orientation of what has been classified in the Boremap mapping as mylonite, ductile and brittle-ductile shear zones. Although there is a spread in orientation, the occurrence of subhorizontal to gently dipping zones/mylonites as well as NE-SW striking and steeply to subvertically dipping zones is evident. The latter two orientations are interpreted to be small-scale equivalents to the larger sinistral zones described above.

A close temporal relationship between the emplacement of the fine-grained granite and the ductile shear deformation is supported by the variable field relationships between the fine-grained granite dykes/veins and the shear deformation. Some of these dykes/veins are affected and cut by ductile shear zones, whereas others are unfoliated and truncate the shear zones /Lundberg and Sjöström 2006/.

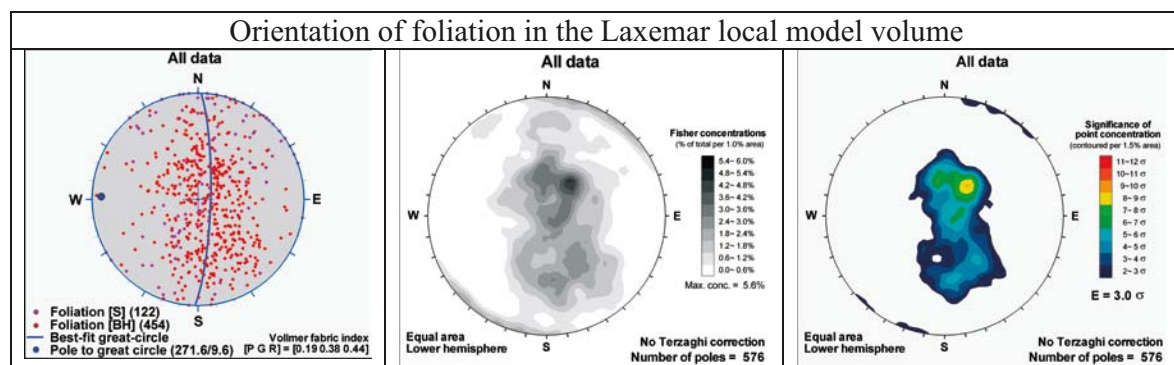


Figure 5-8. Orientation of foliation in the Laxemar local scale model volume, based on borehole data (BH) and surface data (S).

5.2.5 Comparison of the orientation of ductile structures and subordinate rock types

An evaluation of the correlation between the orientation of ductile structures, i.e. foliation and ductile and brittle-ductile shear zones, and subordinate rock types is presented in /Wahlgren et al. 2008, cf. Section 3.5.3 and Appendix 9 therein/. When assessing this comparison, it has to be remembered that only c. 20% of the bedrock in Laxemar has been documented as being faintly to weakly foliated, i.e. c. 80% of the bedrock does not display any mappable ductile structural anisotropy whatsoever. Consequently, a large amount of the subordinate rock types occur in an undeformed and well preserved host rock.

The best correlation between the orientation of the ductile structures and the subordinate rock types exists in the quartz monzodiorite in southern Laxemar. The foliation, ductile to brittle-ductile shear zones, fine-grained granite and fine-grained diorite-gabbro all display dominant subhorizontal to moderate dips to the south. However, the pegmatites are dominated by vertical to steep dips and NE-SW to ENE-WSW strike, and a set of NE-SW to ENE-WSW striking, vertical to steeply dipping fine-grained granites also occur.

Although similarities exist in the orientation of the ductile structures and the subordinate rock types in the central and northern part of Laxemar as well, there are also obvious differences. For example, in northern Laxemar, the foliation is predominantly dipping moderately to the north, while the subordinate rock types display both subhorizontal dips, as well as dips to the north and south.

In summary, the orientation of the ductile structures and the orientation of subordinate rock types display a similar pattern in southern Laxemar. However, this similarity decreases northwards. While the foliation displays dominant dips to the north, there is a larger spread in the orientation of the subordinate rock types. Despite this, the overall similarities in orientation indicate that the formation/orientation of the subordinate rock types is structurally controlled.

5.2.6 Brittle deformation and fracture statistics

The description of rock fractures and the brittle deformation history in Laxemar is based primarily on data collected from detailed mapping of surface outcrops, from scanlines along surface trenches, and from data collected during Boremap logging of drill cores. Detailed descriptions of the types and limits of fracture data from Laxemar are described in /Hermanson et al. 2008/ and /Wahlgren et al. 2008/.

Detailed mapping of fractures at the ground surface

The detailed mapping of fractures in outcrops and along surface trenches has been presented in several SKB P-reports; a complete listing of references is presented in Appendix 3. The four outcrops mapped in detail represent either natural rock exposures or areas from which the overburden has been removed. They are generally rectilinear in shape, and range from 200–600 m² in area. Three of these bedrock surfaces were used as drill sites for percussion and cored boreholes during site investigation activities and are no longer exposed.

In 2006 and 2007, additional surface mapping was done along narrow strips of cleared land in the Laxemar local model area. The goal was to investigate the surface extent of potential minor deformation zones identified in data from regional airborne geophysics, high-resolution ground magnetic surveys, and airborne laser topographic surveys (Lidar), as well as to provide additional data coverage for rock domain and DFN modelling efforts.

In general, four major fracture orientations were noted in the surface outcrop data; north-south striking, east-northeast striking, west-northwest striking, and, to a lesser extent, a group of fractures that strikes east-west and north-northwest which have moderate to subhorizontal dips (Figure 5-9). Considerable variability was observed in the strike orientation of moderately- to subhorizontally dipping fractures; this is not surprising, however, since it is difficult to accurately measure the strike of fractures that intersect flat outcrops at very small angles. Note that the relative intensities of each fracture pole cluster change from outcrop to outcrop. This observation is the basis for the fracture domain model in Laxemar (Section 5.6.1). Observed outcrop trace intensities are expressed in terms of fracture P_{2l} (Table 5-2). P_{2l} represents the sum of all surface trace lengths divided by the mapped outcrop area. Outcrop P_{2l} range from approximate 3.3 to 4 m/m².

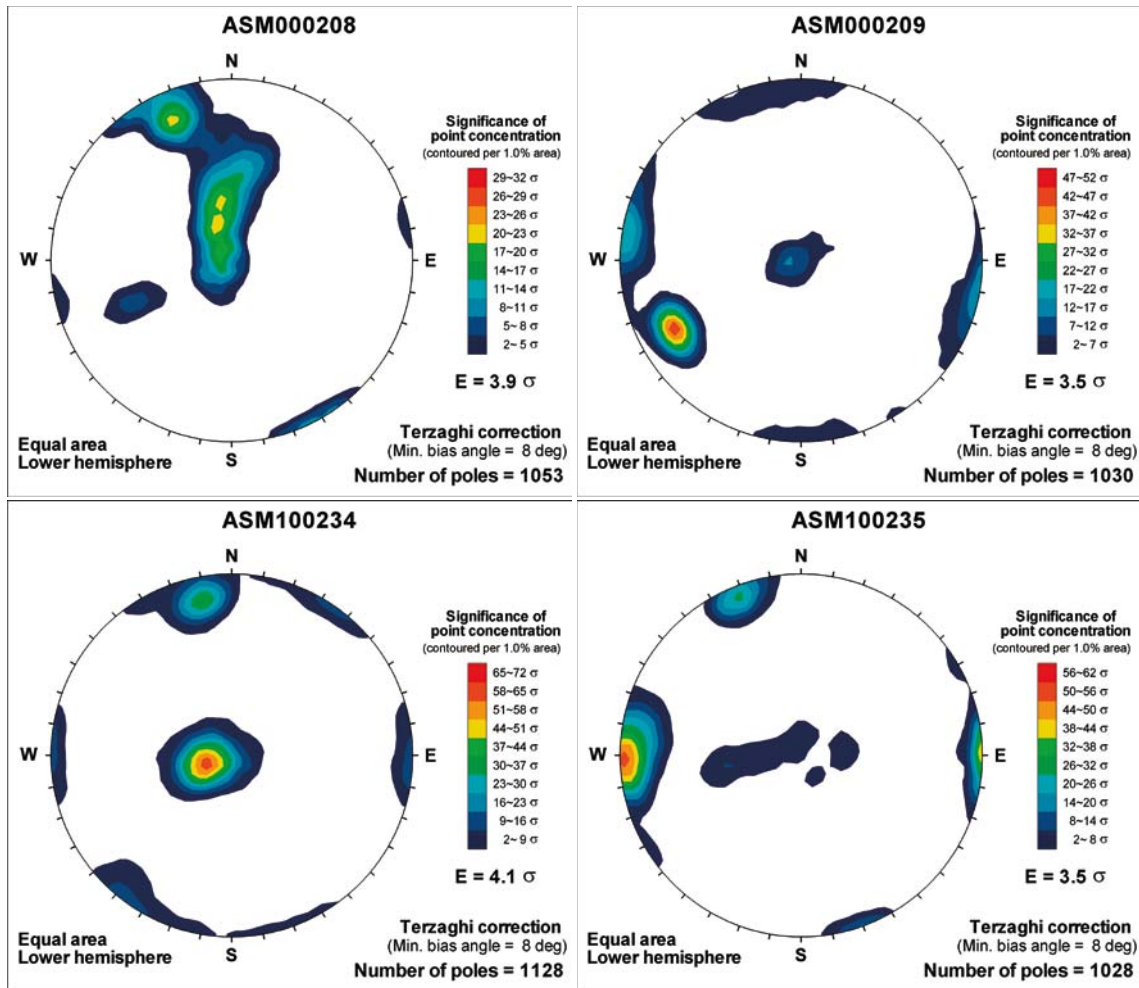


Figure 5-9. Orientations of fracture exposed as surface traces on detail-mapped fracture outcrops in the Laxemar local model area. This figure illustrates Terzaghi-compensated lower-hemisphere Kamb-contoured stereoplots of fracture poles.

Table 5-2. Statistics of fracture traces from detail-mapped fracture outcrops.

Outcrop IDCODE	# of Traces	Trace length of fractures				Outcrop area (m ²)	P ₂₁ (m/m ²)
		Total	Mean	Median	Std. dev.		
ASM000208	1,034	1,327.42	1.26	1.01	0.85	330.70	4.01
ASM000209	1,030	1,484.41	1.44	1.04	1.19	442.10	3.36
ASM100234	1,128	1,789.68	1.59	1.15	1.37	478.60	3.74
ASM100235	1,028	1,337.34	1.30	1.04	0.83	332.60	4.02

Fracture orientation from cored borehole data

Before any analyses of orientations are made, fracture data from cored boreholes are divided into two subsets: fractures inside and fractures outside cored borehole sections identified as possible deformation zones in the ESHI. This implies that fractures inside both deterministic deformation zones (Section 5.5) and stochastic minor deformation zones (Section 5.2.11) are excluded from the parameterisation of fracture size, intensity, and spatial location in the geological DFN model (Section 5.6). However, the orientations of fractures inside deterministic deformation zones are used to build confidence in the modelled limits of the deformation zones and their structural character. In addition, the orientations of fractures inside minor deformation zones were used to estimate the strike and dip of these structures when other sources of information were not available.

In general, four fracture pole clusters are visible in the Laxemar cored borehole data, with a fifth cluster visible in some, but not all, boreholes (Figure 5-10 and Figure 5-11). The relative intensities of each fracture set vary spatially; this observation is the key to the fracture domain model in Laxemar (Section 5.7).

The strongest pole cluster in the cored borehole fracture record tends to be composed of moderately- to subhorizontally dipping fractures; fracture strikes are highly variable from borehole to borehole, but on average strike north-south and dip to the east. Subvertically dipping pole clusters representing fractures with strikes north-south, east-northeast, west-northwest are also common to most boreholes. In some boreholes, a fourth subvertical cluster, representing fractures striking north-northwest is also visible.

Fracture frequency from cored borehole data

Fracture intensity in boreholes is mapped as a number of fractures intersecting the centreline of the drill core over a unit-length interval (P_{10} , units of 1/m). Fracture frequency, and, in particular, the relative intensity of certain orientations of fractures, is a key input to the geological DFN. The frequency of both open and hydraulically conductive fractures is important for the hydrogeological DFN.

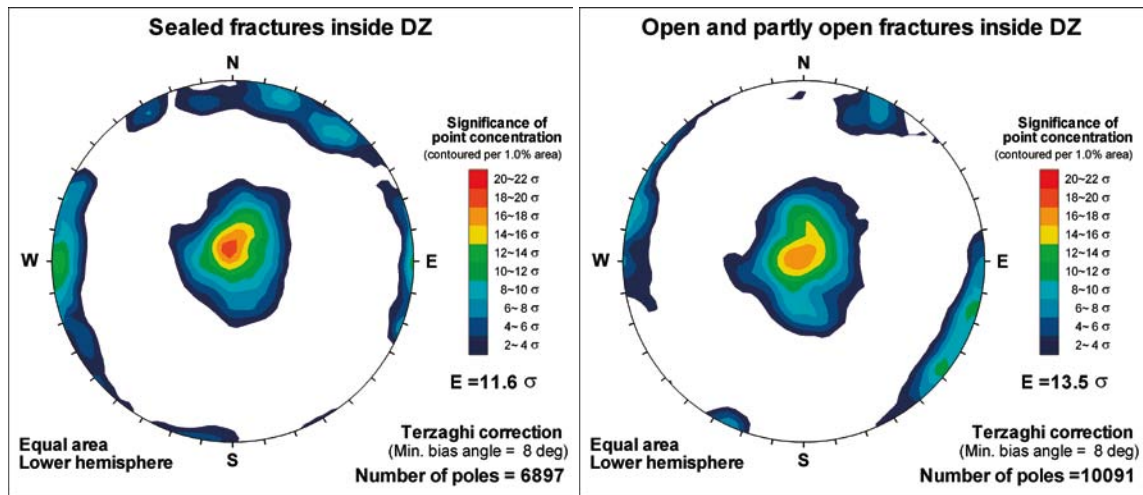


Figure 5-10. Orientations of sealed (left) and open (right) fracture poles inside identified deformation zones and minor deformation zones. Figures created using fractures marked as ‘Visible in BIPS’.

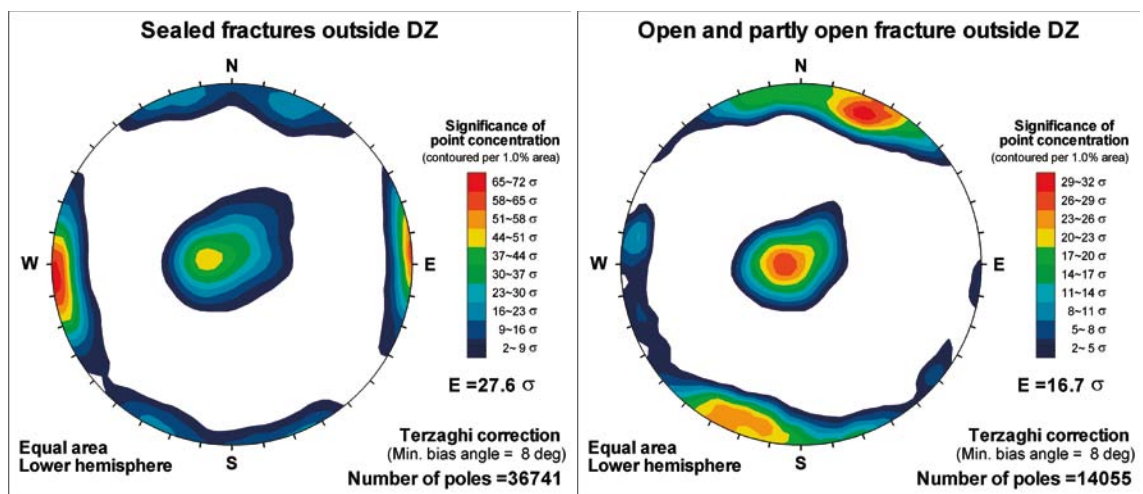


Figure 5-11. Orientations of sealed (left) and open (right) fracture poles outside of identified deformation zones and minor deformation zones. Figures created using fractures marked as ‘Visible in BIPS’.

Fracture intensity is computed from fractures mapped during the Boremap logging. The point at which the fracture intersects the borehole centreline is recorded in a table in the SICADA database (table *p_fract_core_eshi*), as well as other information describing the orientation, mineralogy, and morphology of the mapped fracture. Fracture frequencies are summarised in Table 5-3. It is important to note that Table 5-3 excludes sections of the borehole that have been mapped as ‘crushed rock’, and also omits the fractures that are contained in sealed fracture networks. Table 5-3 does not distinguish between fractures inside or outside of deterministic deformation zones and stochastic minor deformation zones; all fractures are included. In general, sealed fracture networks have such a high frequency (on the order of 30 to 100 fractures per metre) of sealed fractures in a relatively small length of drill core that it is not practical to map each individual fracture.

Table 5-3. Fracture frequency in cored boreholes in Laxemar.

Borehole IDCODE	Length outside DZ (m)	Total number of fractures	Number of open fractures	Number of partly open fractures	Number of sealed fractures	Percent open fractures	P ₁₀ open (1/m)	P ₁₀ all (1/m)
KLX02	804.56	3,070	2,103	105	862	71.90%	2.61	3.82
KLX03	896.63	4,388	679	4	3,705	15.60%	0.76	4.89
KLX04	890.85	5,498	2,009	13	3,476	36.80%	2.26	6.17
KLX05	886.55	3,539	319	1	3,219	9.00%	0.36	3.99
KLX06	893.41	5,367	1,071	11	4,285	20.20%	1.2	6.01
KLX07A	733.78	6,565	2,410	16	4,139	37.00%	3.28	8.95
KLX07B	190.49	1,374	590	6	778	43.40%	3.1	7.21
KLX08	891.01	5,296	1,959	19	3,318	37.30%	2.2	5.94
KLX09	771.76	4,662	1,954	6	2,702	42.00%	2.53	6.04
KLX09B	97.43	609	206	1	402	34.00%	2.11	6.25
KLX09C	118.3	771	279	3	489	36.60%	2.36	6.52
KLX09D	120.42	915	374	6	535	41.50%	3.11	7.6
KLX09E	119.4	1,021	331	2	688	32.60%	2.77	8.55
KLX09F	151.89	1,042	338	4	700	32.80%	2.23	6.86
KLX09G	90.32	828	299	2	527	36.40%	3.31	9.17
KLX10	895.62	5,601	2,340	11	3,250	42.00%	2.61	6.25
KLX10B	49.94	632	346	10	276	56.30%	6.93	12.66
KLX10C	145.33	1,565	421	1	1,143	27.00%	2.9	10.77
KLX11A	889.29	5,358	1,077	2	4,278	20.10%	1.21	6.03
KLX11B	95.5	444	160	0	284	36.00%	1.68	4.65
KLX11C	115.43	446	130	0	316	29.10%	1.13	3.86
KLX11D	115.2	679	204	0	475	30.00%	1.77	5.89
KLX11E	116.98	655	202	0	453	30.80%	1.73	5.6
KLX11F	114.83	413	120	0	293	29.10%	1.05	3.6
KLX12A	499.83	3,001	1,181	3	1,817	39.50%	2.36	6
KLX13A	490.73	3,736	2,082	3	1,651	55.80%	4.24	7.61
KLX14A	171.25	1,506	730	5	771	48.80%	4.26	8.79
KLX15A	922.84	5,518	1,828	9	3,681	33.30%	1.98	5.98
KLX16A	432.62	3,957	1,283	5	2,669	32.50%	2.97	9.15
KLX17A	634.75	4,468	1,067	6	3,394	24.00%	1.68	7.04
KLX18A	510.04	3,058	1,097	7	1,954	36.10%	2.15	6
KLX19A	695.54	2,722	1,200	2	1,520	44.20%	1.73	3.91
KLX20A	356.02	2,298	920	0	1,378	40.00%	2.58	6.45
KLX21B	757.95	5,900	1,663	6	4,231	28.30%	2.19	7.78
KLX22A	96.37	694	266	0	428	38.30%	2.76	7.2
KLX22B	95.87	669	252	0	417	37.70%	2.63	6.98
KLX23A	95.93	207	72	0	135	34.80%	0.75	2.16
KLX23B	45.95	115	53	0	62	46.10%	1.15	2.5
KLX24A	96.13	884	361	2	521	41.10%	3.76	9.2
KLX25A	46.1	347	98	0	249	28.20%	2.13	7.53
KLX26A	95.94	812	433	1	378	53.40%	4.51	8.46
KLX26B	46.3	346	239	1	106	69.40%	5.16	7.47
KLX28A	77.15	563	215	0	348	38.20%	2.79	7.3
KLX29A	58.88	463	201	1	261	43.60%	3.41	7.86

Fracture mineralogy from cored borehole data

The fracture mineralogy and related wall rock alteration in Laxemar has been presented in thirteen primary data reports and in four peer-reviewed publications /Drake and Tullborg 2007a, Drake et al. 2008, Tullborg et al. 2008, Drake and Tullborg 2009b/. The results from these investigations are outlined in a summarising report on the fracture mineralogy in Laxemar /Drake and Tullborg 2009a/. Documentation of quantitative amounts of different minerals along fractures is presented in a separate, complementary document /Eklund and Mattsson 2008/. The importance and character of fracture minerals for the hydrogeochemical properties is treated in Section 9.5.6.

Relative and absolute ages of fracture minerals

Different generations of fracture minerals have been recognised in Laxemar (Figure 5-12). Their relative age relationships have been distinguished using microscopy (e.g. SEM-EDS on cross-cutting fractures), stable isotopes, trace elements, fluid inclusions and geochemistry. Absolute ages of some of these generations have been obtained using $^{40}\text{Ar}/^{39}\text{Ar}$ geochronology /Drake et al. 2007/. These relative and absolute age determinations have been used in the establishment of the geological evolution of the site /Söderbäck 2008, Wahlgren et al. 2008/.

The oldest fracture mineralisations in the area, mainly fine-grained epidote, quartz, chlorite, K-feldspar and albite, are associated with mylonite (Generation 1, Figure 5-12a) and subsequently formed cataclasites (Generation 2, Figure 5-12b), which have reactivated the mylonites. The mylonites and probably most of the cataclasites are older than the Mesoproterozoic Göttemar and Uthammar granites nearby. Generation 3 fracture minerals are epidote, quartz, chlorite, pyrite, muscovite and fluorite, followed by prehnite dominated fillings and subsequently laumontite, calcite, adularia and hematite (Figure 5-12c). The majority of these fillings are interpreted to have been formed during a prolonged event with gradually lower formation temperatures in relation to the Göttemar and Uthammar intrusions. These fillings are associated with intense wall rock alteration, such as red-staining, sericitisation, saussuritisation and greisen (close to the Göttemar granite). However, some of the epidote fillings may be older. It is suggested that a younger mineral assemblage of calcite, illite, adularia, K-feldspar and hematite (Generation 4, Figure 5-12d) is related to far-field effects of the Sveconorwegian orogeny, as indicated by $^{40}\text{Ar}/^{39}\text{Ar}$ dating, although this event has not been very significant in the area.

The occurrence of Lower Cambrian sandstone in a few subvertical, near-surface fractures in Laxemar indicates that the bedrock surface is close to the sub-Cambrian peneplain. Fracture fillings dominated by calcite, adularia, chlorite, fluorite, hematite, quartz, pyrite, barite, gypsum, clay minerals, apophyllite, harmotome and REE-carbonate (Generation 5, Figure 5-12e) formed at ~ 448–400 Ma at low-temperature conditions related to far-field effects of the Caledonian orogeny. They were formed at 80–145°C from highly saline (brine type) fluids with organic influence, indicating influence from overlying, organic-rich, Cambrian-Silurian sediments. The dominant orientation of these fractures corresponds to the NW-SE maximum compressive stress during the Caledonian orogeny.

Fracture fillings of similar mineralogy to the Caledonian fracture fillings were precipitated intermittently in open bedrock fractures from the late Palaeozoic during gradually lower temperatures ranging into ambient temperatures similar to the present conditions (Generation 6, Figure 5-12f). Late Palaeozoic minerals are difficult to separate from potential recent precipitates. Calcite and pyrite show organic influence and sometimes closed system microbial influence. $\delta^{18}\text{O}$ and $^{87}\text{Sr}/^{86}\text{Sr}$ values show that some of the calcites may have formed from fluids in equilibrium with waters similar to present groundwaters at ambient temperatures. A combination of calcite $\delta^{18}\text{O}$ values and crystal morphologies indicate formation from waters with different $\delta^{18}\text{O}$ values and salinities, such as fresh and brackish water. Fracture coatings in presently water conducting fractures often consist of clay minerals, calcite, chlorite, and wall rock fragments. The amount of potentially very young (Quaternary) fracture minerals is very small compared with older fracture minerals (Generation 1 to Generation 5).

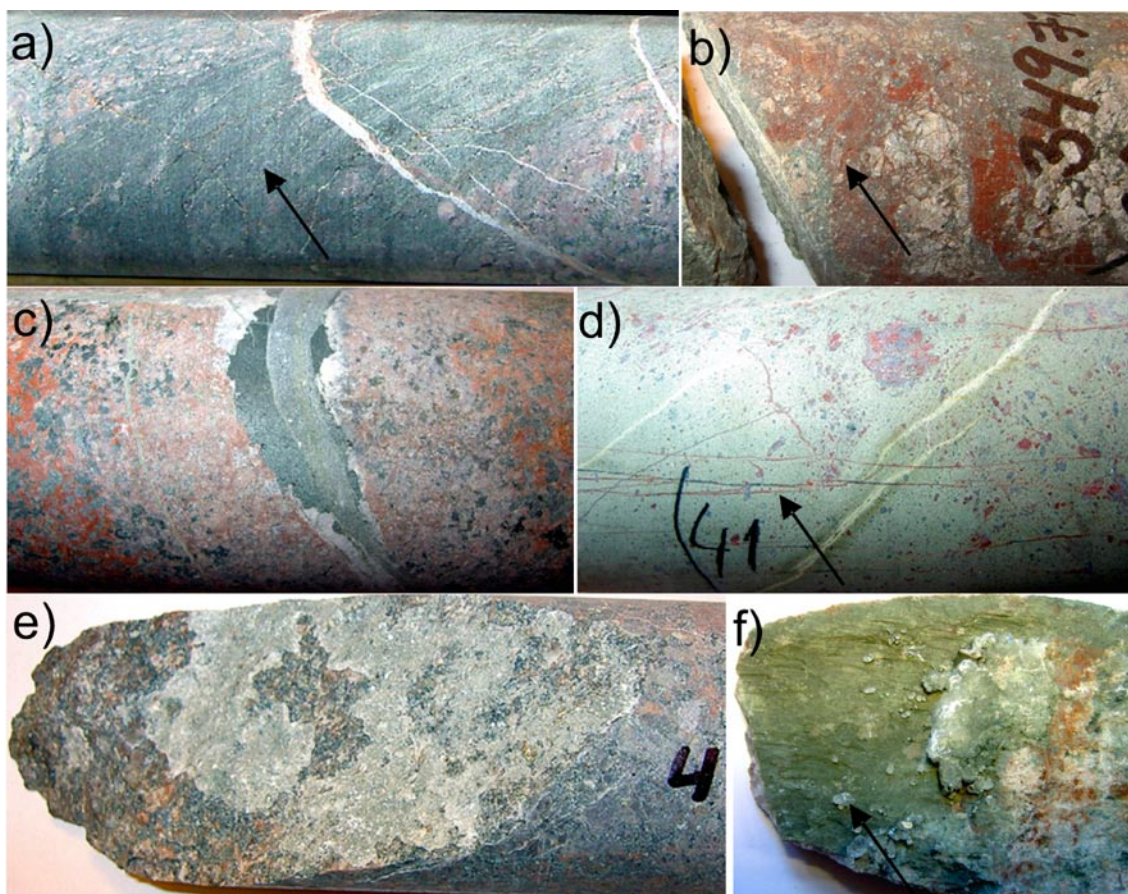


Figure 5-12. Drill core photographs showing fracture minerals in the six generations recognised in Laxemar. (a) Generation 1. Mylonite (arrow) cut by a younger calcite vein (KLX06, borehole length, c. 373 m, /Drake and Tullborg 2007b/). (b) Generation 2. Brick-red cataclasite rich in hematite-stained adularia, chlorite and wall rock fragments (KLX04, borehole length c. 349 m, /Drake and Tullborg 2007b/). (c) Generation 3. Fracture sealed with calcite, quartz, chlorite, epidote and prehnite. The wall rock is red-stained with increased sericitisation towards the fracture (KLX03, borehole length ~ 722 m. /Drake and Tullborg 2007b/). (d) Generation 4. Brick-red, hematite-stained adularia in fractures (arrow) cutting through epidote-dominated mylonite/cataclasite, (KSH03A, borehole length ~ 863 m, /Drake and Tullborg 2006c/). (e) Generation 5. Open fracture coated by barite and scalenohedral calcite (KLX03: borehole length ~ 457 m /Drake and Tullborg 2007b/). (f) Generation 6. Equant calcite crystals (arrow) on a striated fracture surface of an open fracture coated by chlorite and clay minerals (KLX07A 697 m, borehole length ~ 697 m /Drake and Tullborg 2007b/).

Distribution of fracture minerals

The frequency of occurrence of the most common fracture minerals in each interpreted deterministic deformation zone is presented in /Wahlgren et al. 2008, cf. Appendix 14 therein/ and the orientations of fractures carrying specific fracture minerals in each of the fracture domains are presented in /Drake and Tullborg 2009a/. The relative fracture mineral frequency in all deformation zones identified in the ESHI made in boreholes KLX02-KLX29A combined and in all sections of crushed rock is presented in /Drake and Tullborg 2009a, cf. Section 7.1 therein/. The distributions of different fracture minerals in different rock domains and in different fracture domains are presented in /Drake and Tullborg 2009a, cf. Sections 7.2 and 7.3 therein/.

The variation in the occurrence of different fracture minerals with depth is addressed by /Wahlgren et al. 2008, cf. Section 3.6.5 therein/ and in more detail by /Drake and Tullborg 2009a, cf. Sections 7.4 and 7.5 therein/. The variation in the occurrence of different fracture minerals with depth in water conducting fractures (Posiva flow log anomalies) is presented in /Drake and Tullborg 2009a, cf. Section 7.6 therein/. The frequency of a particular mineral in open or sealed fractures, as well as the overall fracture frequency of open or sealed fractures, has been documented for each

10 m vertical depth interval along each borehole and collectively for all boreholes in Laxemar /Drake and Tullborg 2009a/. More than 2,200 frequency plots for individual minerals have been generated and a few examples are presented in Figure 5-13, Figure 5-14 and Figure 5-15.

The most common fracture minerals, chlorite and calcite, show no distinctive variation with depth (exemplified in Figure 5-13a and Figure 5-13b, for KLX03 and KLX08, respectively). The frequency of occurrence of these minerals generally follows the variation in the total fracture frequency. Notable exceptions include slightly lower amounts of calcite in the uppermost 10–20 metres below ground surface (exemplified by KLX09D in Figure 5-13c) due to near surface dissolution.

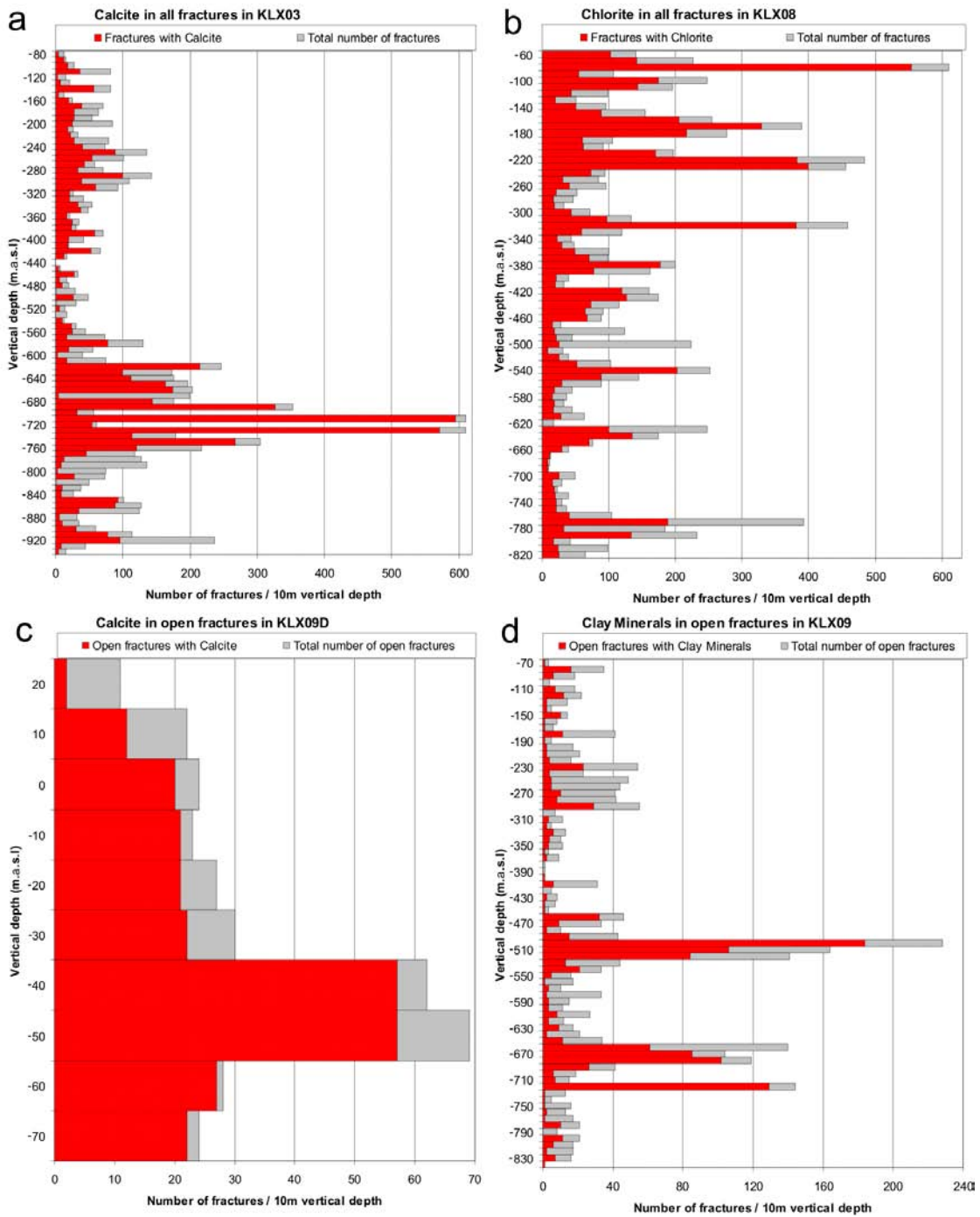


Figure 5-13. Variation in mineralogy with depth. (a) Calcite along all fractures in KLX03. (b) Chlorite along all fractures in KLX08. (c) Calcite along open fractures versus depth in KLX09D. (d) Clay minerals along open fractures in KLX09. The total number of fractures of the specific fracture type per 10 m borehole interval is also shown, from /Drake and Tullborg 2009a/.

Clay minerals are the third most frequent minerals in open fractures. Their frequency of occurrence in open fractures generally follows the variation in frequency of occurrence of open fractures with depth, although the relative frequency is commonly higher in deformation zones (see example from KLX09 in Figure 5-13d).

Most other minerals, e.g. hydrothermal minerals epidote, prehnite, adularia, quartz and hematite, show no significant variation with depth /Drake and Tullborg 2009a, cf. Section 7.4 therein/. Notable exceptions are pyrite, goethite, gypsum and fractures without visible minerals.

- Pyrite is a common mineral in open fractures at most depths, although there is a clear decrease in pyrite occurrences near the surface, and this decrease is correlated with an increase of goethite-bearing fractures (exemplified by KLX26A in Figure 5-14). This mineral distribution trend is due to oxidising conditions near the surface /Drake and Tullborg 2009a/.
- Gypsum, indicated in a few boreholes, is restricted to open fractures in isolated sections with low fracture frequencies and low transmissivity below an elevation of –350 m. This is not interpreted to represent the original gypsum distribution pattern, but instead is the result of dissolution above 350 m depth and in highly transmissive zones.
- Open fractures without any visible mineral coating and with fresh wall rock are commonly low in numbers. However, there is an increase of this fracture type towards the ground surface as shown in Figure 5-15 (showing data from all cored boreholes in Laxemar). Scattered larger occurrences at greater depths are generally related to deformation zones, e.g. in KLX04 at c. –320 to –350 m (in DZ6B in the ESHI) and at c. –880 to –950 m (in ZSMEW007A). The fractures without visible fracture minerals may potentially be recently formed. However, a number of uncertainties related to these fractures need to be addressed, e.g. the potential occurrence of microscopic minerals and potentially drilling induced fractures.

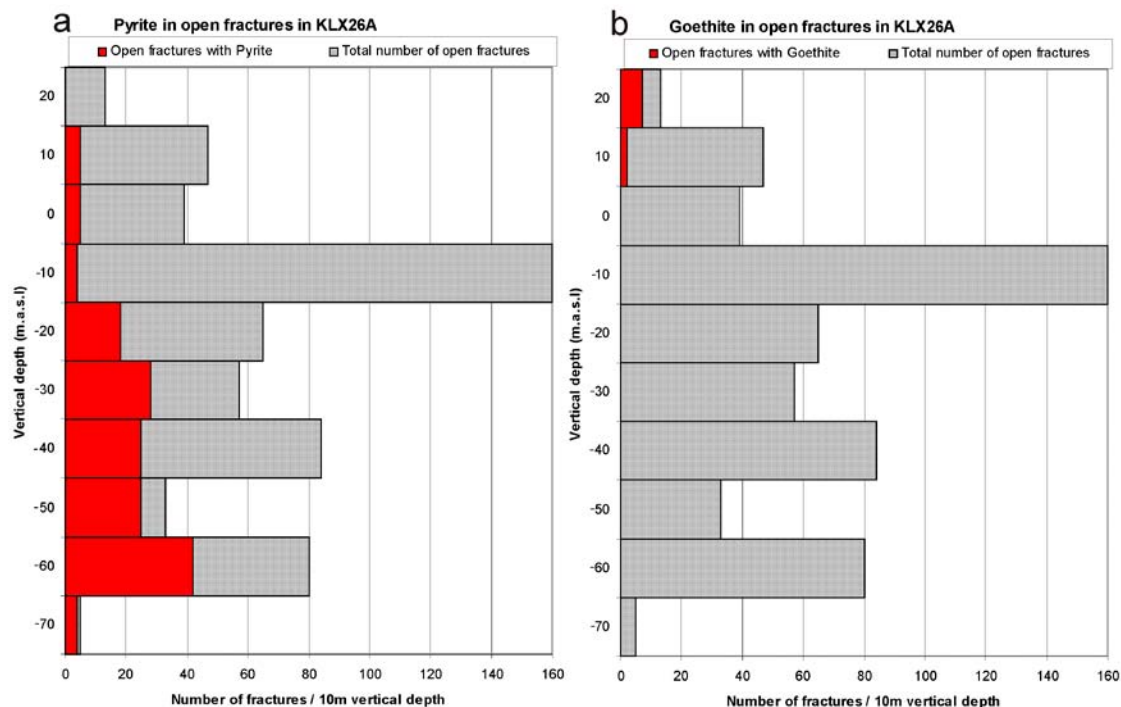


Figure 5-14. Variation with depth of pyrite (a) and goethite (b) along open fractures in KLX26A. The total number of open fractures per 10 m borehole interval is also shown, from /Drake and Tullborg 2009a/.

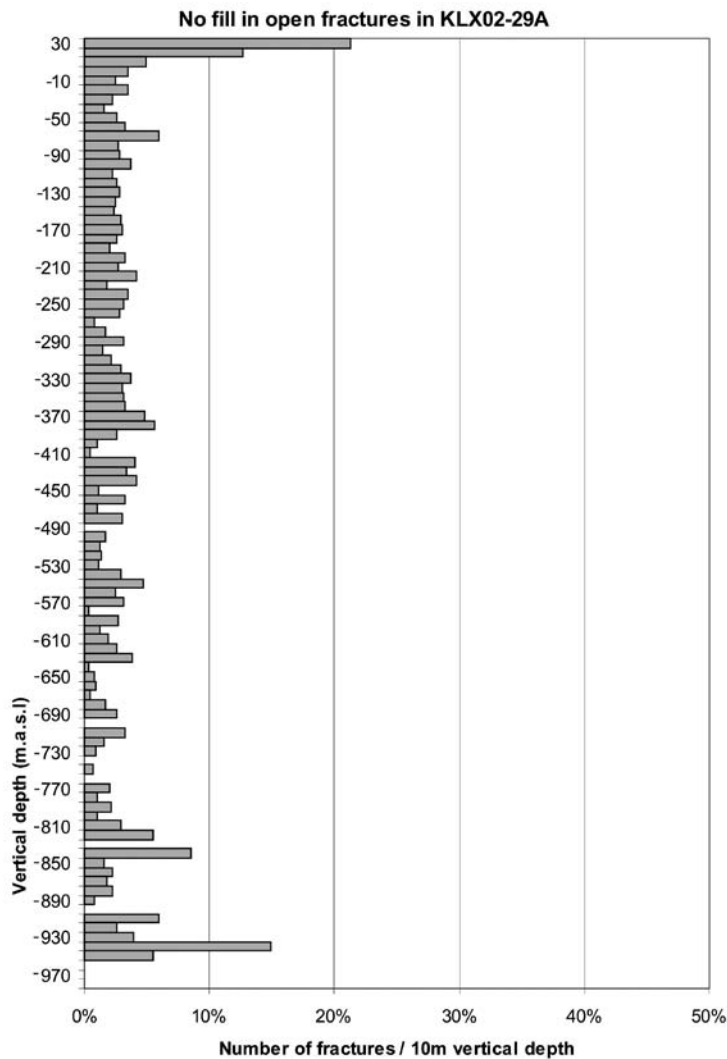


Figure 5-15. Relative frequency of open fractures without visible fracture minerals, for each 10 vertical depth interval from the cored boreholes KLX03–KLX29A. Fractures from KLX02 are excluded because this borehole was drilled with conventional drilling technique which infers potentially higher amounts of drilling induced fractures, grinding of drill core pieces and flushing away of loose fracture minerals, from /Drake and Tullborg 2009a/.

5.2.7 Character and kinematics of brittle deformation zones

Data acquisition

In order to describe the character of the brittle deformation zones and if possible to also constrain their kinematics, selected deformation zones, initially identified with high confidence of existence in the drill cores during geological single-hole interpretations, were studied in detail in a number of drill cores in three separate stages by /Viola and Venvik Ganerød 2007a, 2007b and 2008/. In addition, studies of selected outcrops and cleaned trenches were also carried out by the same authors. The results presented by /Viola and Venvik Ganerød 2007a, 2007b, 2008/ have been interpreted with the goal of producing a coherent scheme for the brittle evolution across Laxemar and Simpevarp, including an attempt at the reconstruction of the local palaeo-stress evolution over time /Viola 2008/. Furthermore, the study presents a synthesis of the brittle structural evolution of the site investigation area and its relation to far-field orogenic events that might have affected the bedrock in the Laxemar-Simpevarp area during the geological evolution /Viola 2008, Viola et al. 2009/. The results of the study confirm that the brittle history of the Laxemar-Simpevarp area is complex and involves series of reactivation events. A summary of the kinematics is presented below.

Character of brittle deformation zones

The deformation zones vary from brittle-ductile shear zones to purely brittle faults characterised by increased frequency of both open and sealed fractures as well as sealed fracture networks and alteration, most commonly oxidation (red staining). Furthermore, associated fault rocks are common, such as different types of cataclasites, breccias, gouge etc. as well as late fractures, joints, hydrofractures and hydrobreccias decorated by very low temperature minerals. All available evidence indicates that multiple episodes of deformation took place within a broadly-defined brittle regime under different environmental and physical conditions.

Kinematics

Brittle kinematic data from outcrops and drill cores were treated separately and subsequently compared and merged into a large, single dataset, considered representative of the evolution of brittle deformation in the Laxemar-Simpevarp area. Inferences on individual, discrete compressive and extensional events were made by sorting the total fault-slip dataset on the basis of geometric and kinematic compatibility criteria and on well-constrained structural relationships. Based on this sorting procedure, individual conjugate subsets were extracted from both outcrop and drill core data. The fracture sets identified in the drill core data are very similar to those identified from outcrop data.

The most striking brittle features observed on outcrops in the Laxemar-Simpevarp area are systematic sets of conjugate, steep, sinistral and dextral, brittle-ductile and brittle, strike-slip faults and fractures. These are dispersed at small angle around a north-trending axis and the systematic approach mentioned above allowed their sorting into two distinct conjugate sets, conjugate set I and II, respectively. Conjugate set I contains N-S-trending steep sinistral and NNW-SSE, steep dextral fractures/faults, that were likely formed together with low-angle, top-to-the-N/NW reverse fractures/faults. Conjugate set II is only slightly misaligned with respect to set I. It is defined by N-S-trending, steep, dextral and NE-SW, steep sinistral fractures/faults. The common spatial overlap between sinistral and dextral fractures belonging to the two different sets, together with the fact that the angles between the conjugate structures are generally small, generate significant structural complexities. A third conjugate fracture set spreads about the E-W direction. Figure 5-16 and Figure 5-17 display examples of sinistral and dextral fractures in Laxemar, respectively.



Figure 5-16. Sinistral N-S trending fractures belonging to set I at the cleaned outcrop for drill site KLX11A and KLX20A. Note the releasing bends and the associated dilation (shown by large white arrows). Inserted stereonet also displays E/ENE-W/WSW dextral fractures at the same outcrop. View to the north. Figure from /Viola and Venvik Ganerød 2007a/.

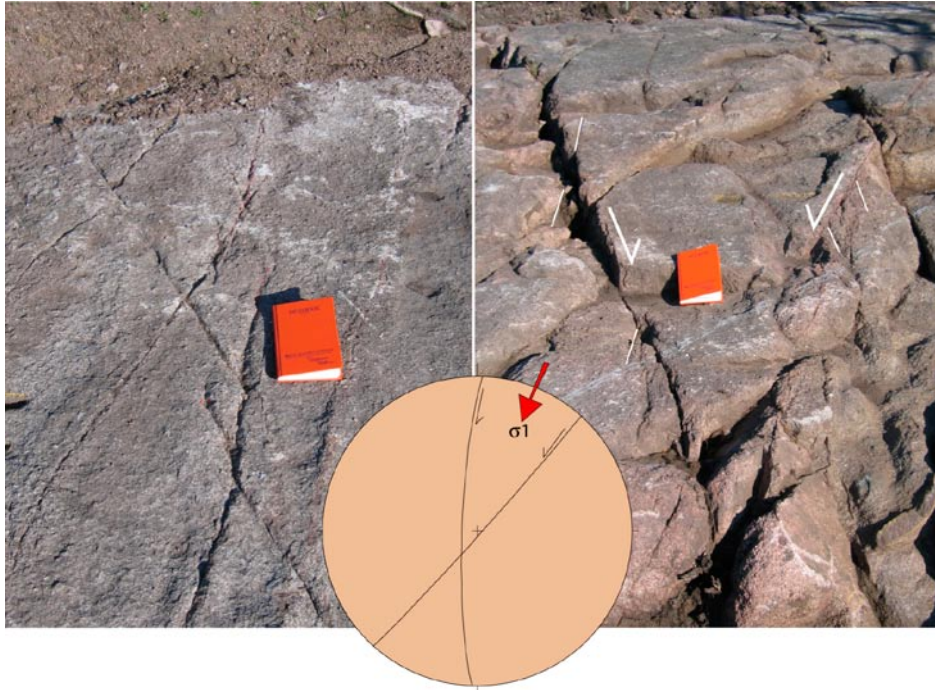


Figure 5-17. Sinistral and dextral fractures of conjugate set II. The acute angle defined by the intersection of the conjugate pairs is bisected by σ_1 . View to the northeast. Figure from /Viola and Venvik Ganerød 2007b/.

Low-angle to moderately dipping striated fracture planes were also identified in the drill cores studied and on several outcrops /Viola 2008/. These were sorted and assigned to two distinct subsets with antithetic top-to-the NE and SW and top-to-the NW and SE normal movements, respectively. Steep fracture planes/faults that bear steep striations and are characterised by transtensional movements were also recorded and are generally interpreted as being due to the extensional reactivation of pre-existing steep shear fractures.

5.2.8 Identification and geological significance of lineaments

Data acquisition, identification of lineaments and uncertainties

The work of identifying lineaments during the SDM-Site Laxemar modelling work has followed the principal methodology adapted during earlier modelling stages. The lineament map has successively developed from a coarse version through a regional overview to a detailed lineament map covering the Laxemar local model area. This development started with identification of lineaments from data of lesser resolution, followed by the use of high-resolution data to adjust or reject former lineaments and to identify new lineaments in the local model area. For this, the most important data sets have been the high resolution digital elevation model and high resolution ground magnetic total field data, primarily due to their superior coverage as compared with other data. During this evolutionary process, which has finally led to the current lineament map for the local model area, the influence from the digital elevation model has successively weakened in parallel with an increased impact from the magnetic total field data. The reason for this is found in the geological setting of Laxemar, where the magnetic total field data are reflecting deformation of the bedrock, both brittle and ductile, due to a reduction in the magnetic susceptibility in the deformation zones. Furthermore, magnetic total field data are quite insensitive to variations in the overburden thickness. This means that bedrock deformation is manifested in the magnetic total field data as lineaments of magnetic lows and that the clarity of these anomalies is relatively insensitive to variations in overburden thickness and composition typical for the area. The characteristics of magnetic surveys and data on digital elevation models are presented in Table 5-4 and Table 5-5, respectively.

Table 5-4. Characteristics of magnetic surveys in the Laxemar local model area.

Type of survey	Contractor	Line spacing	Station spacing	Survey direction	Survey elevation	Grid resolution
Airborne, fixed-wing	SGU	200 m	17 or 40 m	EW	30 m	40×40 m
Helicopter borne	NGU	50 m	3 m	NS (tie lines EW)	Approx 40 m	5×5 m
Ground	GeoVista AB	10 m	5 m	NS	ca. 1.5–2 m	5×5 m

Table 5-5. Data on digital elevation models (DEM) in the Laxemar local model area.

Type of survey	Contractor	Grid resolution
Airphoto 2,300 m	Metria	10×10 m
Lidar	Swedpower AB and Blominfo AB	1×1 m

The evaluation of the longer lineaments of regional character, started early in the site investigations and has gradually moved its focus towards shorter lineaments within the local model area with lengths less than 1,000 m. At the current stage of the modelling, extensive studies including field control of outcrops, geophysical profile measurements, excavation work, drilling activities and extended single hole interpretations indicate that less than c. 50% of these shorter lineaments are expected to coincide with minor deformation zones or dykes of any practical importance /Olsson et al. 2007/. The more significant minor deformation zones are characterised by brittle-ductile deformation and significant transmissivity which makes their geometry in terms of dip and continuity of importance. Forward and inverse modelling of geophysical data have revealed the near-surface geometry of some of these prominent minor deformation zones, but also of the deformation zone ZSMNW042A, in the southern part of Laxemar /Mattsson and Triumf 2007/.

The identification of lineaments has been carried out in several steps: they include interpretations of single data sets of varying type and resolution /Triumf 2003, Triumf et al. 2003, Thunehed and Triumf 2005, 2006, Mattsson and Triumf 2007/; co-ordination /Triumf 2004ab, Triumf and Thunehed 2007, Mattsson and Triumf 2007/ and linking that has resulted in the final product called “linked lineaments” covering the local model area /Mattsson and Triumf 2007/. Furthermore, an alternative lineament interpretation study was performed by the Geological Survey of Finland (GTK) /Korhonen et al. 2005/, with the aim of investigating consistency and repeatability in the interpretation work. A comparison of the two independent lineament interpretation studies was carried out by /Johansson 2006/.

The resulting lineament interpretation covers the regional and local model areas as seen in Figure 5-18 and Figure 5-19, respectively.

The final lineament map over the local model area contains 1,434 linked lineaments in the length interval of 100–1,000 m, and 18 longer than 1,000 m (Figure 5-19). From the attributes of each individual lineament it is e.g. possible to observe in what data sets the lineament is detected. A majority of the linked lineaments identified in the local model area are visible in both magnetic and digital elevation models for more than half of their length, however, not necessarily along the same segment of the lineaments. In areas where detailed ground magnetic total field data are missing, the density of lineaments is less due to lower resolution in the data reflecting the bedrock magnetisation; an inherent bias associated with the radically better quality and spatial resolution of the ground magnetic total field data. When studying the character of the linked lineaments it is thus important to consider the data coverage.

Some prominent low-magnetic features coupled to depressions in the terrain are observed in Laxemar. Deformation zones ZSMEW007A and ZSMNW042A (Figure 5-30) are two of the most pronounced examples of the latter type. They are also visible in the helicopter-borne electro-magnetics as electrically conductive features /Triumf et al. 2003/. On a regional scale these anomaly complexes may be represented by single lines drawn along the centre of the features.

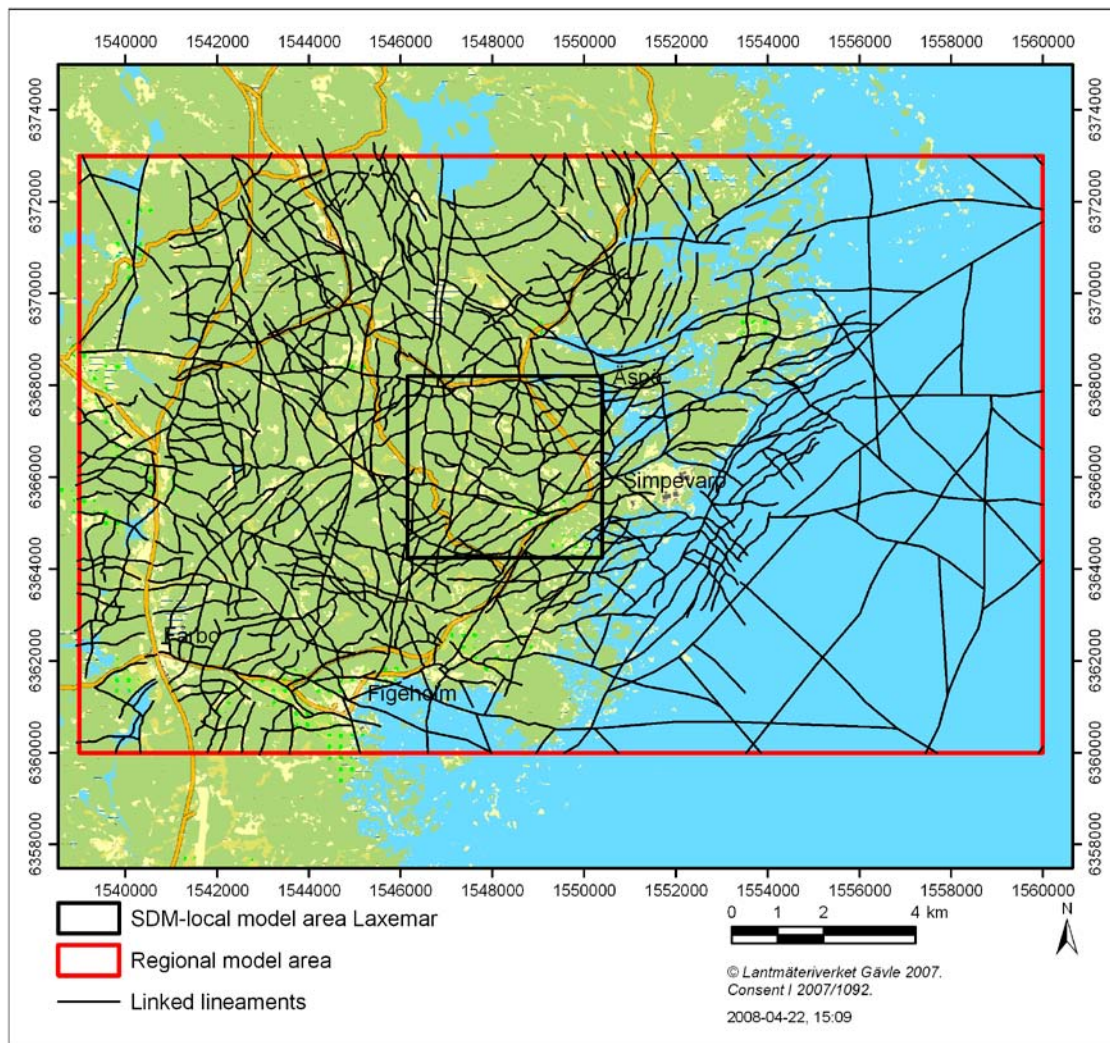


Figure 5-18. Linked lineaments in the regional model area identified by integration of airborne magnetic data and a digital terrain model /Triumpf 2004b/.

However, on a local scale their geometrical complexity becomes readily evident, and the single line representation is considered less meaningful. During the process of lineament identification these low-magnetic features were outlined and called “low magnetic belts”, the geometrical coverage of the belt reflects the extent of low magnetisation (Figure 5-19). Although the host rock within the belts appears less magnetised it is at some locations possible to follow lineaments that pass through the belt.

Lineaments and their geological significance

Investigations of the geological significance of identified lineaments and low magnetic belts have been included in the site investigation programme at Oskarshamn. Field control of outcrops, geophysical profile measurements, excavation work, drilling activities and single-hole interpretations constitute the major contributions. Lineaments verified by refraction seismics appear to be more brittle in character with a higher degree of open fractures and a greater transmissivity /Olsson et al. 2007/.

Two lineaments in the local scale model area of Laxemar are known to host dolerite as part of their anomaly source. By applying developed search criteria to all lineaments in the local model area, based on studies of the character of known dolerites in Laxemar and in the region of Oskarshamn, nineteen more lineaments have been identified that potentially could contain dolerite /Triumpf 2007/.

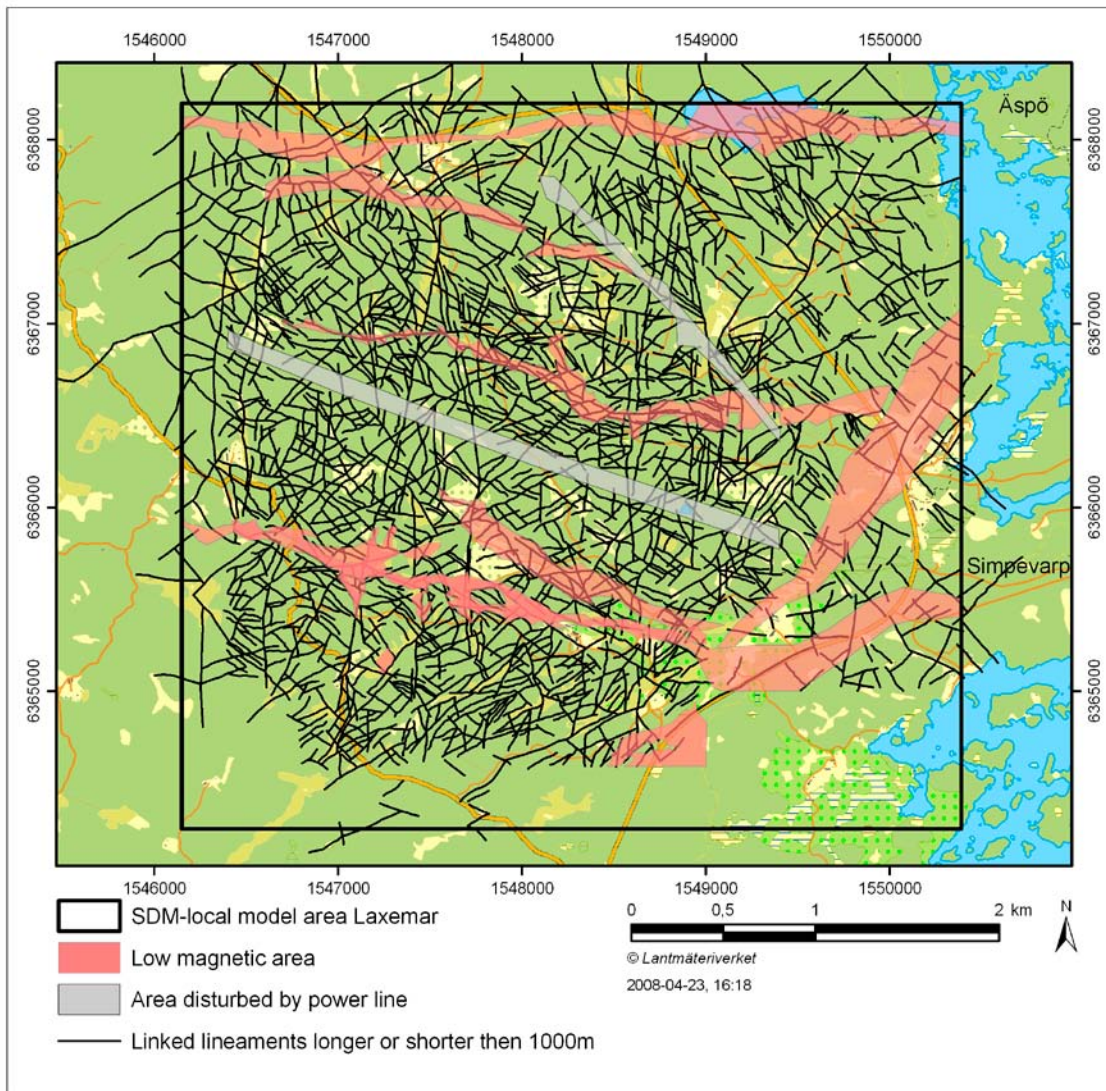


Figure 5-19. Linked lineaments in the Laxemar local model area primarily identified by integration of high resolution ground magnetic data and a digital terrain model based on Lidar data /Mattsson and Triumpf 2007/.

Forward modelling of the magnetic total field response has been carried out to reflect the simplified but realistic minimum dimensions of a low-magnetic zone to be detected in a survey using the survey parameters of the Laxemar measurements. The typical thin soil cover of a few metres and the typical magnetic susceptibilities of the bedrock in Laxemar have been used. The results show that in areas with a relatively low noise level in magnetisation due to rather a homogeneous distribution of magnetite in the bedrock, magnetic measurements on the ground are capable of detecting vertical low-magnetic zones of thicknesses down to 1–2 m. In areas with more heterogeneous lithological magnetisation, the noisy background inhibits the detection of such thin zones. Instead it is more realistic to use a cut-off thickness of around five metres in such areas. Noisy areas are easily recognised on the magnetic total field map and are most pronounced between deformation zones ZSMEW007A and ZSMNW042A (cf. Section 5.5) where mafic rocks are commonly observed.

Modelling of galvanic electric resistivity measurements has been performed to evaluate the lower resolution limit for deformation zones. Typical values of resistivity known from ground, borehole and laboratory measurements have been used. The identification of a deformation zone as a resistivity lineament is to some extent dependent upon the resistivity contrast with respect to undeformed country rock. A zone of primarily ductile character and/or with sealed fractures may be difficult to detect. Of even greater importance is the thickness of the zone. It will be difficult to detect a zone with a smaller thickness than the depth of burial. The soil cover thickness in the southern parts of

Laxemar is in general 5 to 8 metres. This means that zones with a thickness of less than 5 to 8 metres may remain undetected in a resistivity survey. A thick zone will consequently be much easier to detect, even if the resistivity contrast to undeformed country bedrock is rather subtle. The presence of a low-resistivity clayey overburden of significant thickness will also mask the appearance of minor zones.

5.2.9 Identification and geological significance of seismic reflection data

Reflection seismic data were acquired in 1999 /Bergman et al. 2001/ and the spring of 2004 /Juhlin et al. 2004/. In 2004, approximately 9.9 km of high resolution seismic data were acquired along three separate profiles, 3.9 km along the NNE-SSW profile 3, 1.8 km along the WNW-ESE running profile 4, and 4.2 km along the NNW-SSE running profile 5 (Figure 5-20).

The results from the seismic surveys were available at the beginning of the drilling campaign in Laxemar and were used in the positioning of boreholes and other investigations as well as being used as a valuable input to the overall modelling process. A number of the interpreted reflectors were found to correlate well with later drilling results and form the basis of the interpreted geometry of some of the major deformation zones such as ZSMEW002A and ZSMEW007A. After 2004 no further field reflection seismic survey work was performed. However, data from profiles 3 and 5 were reprocessed in an attempt to better image the uppermost 1,000 m of the bedrock in the vicinity of selected cored boreholes /Wahlgren et al. 2008/. Based on this reprocessing, the geometries of the main reflections observed on the profiles were updated. A number of the earlier 2004 geometries were modified and new reflections identified.

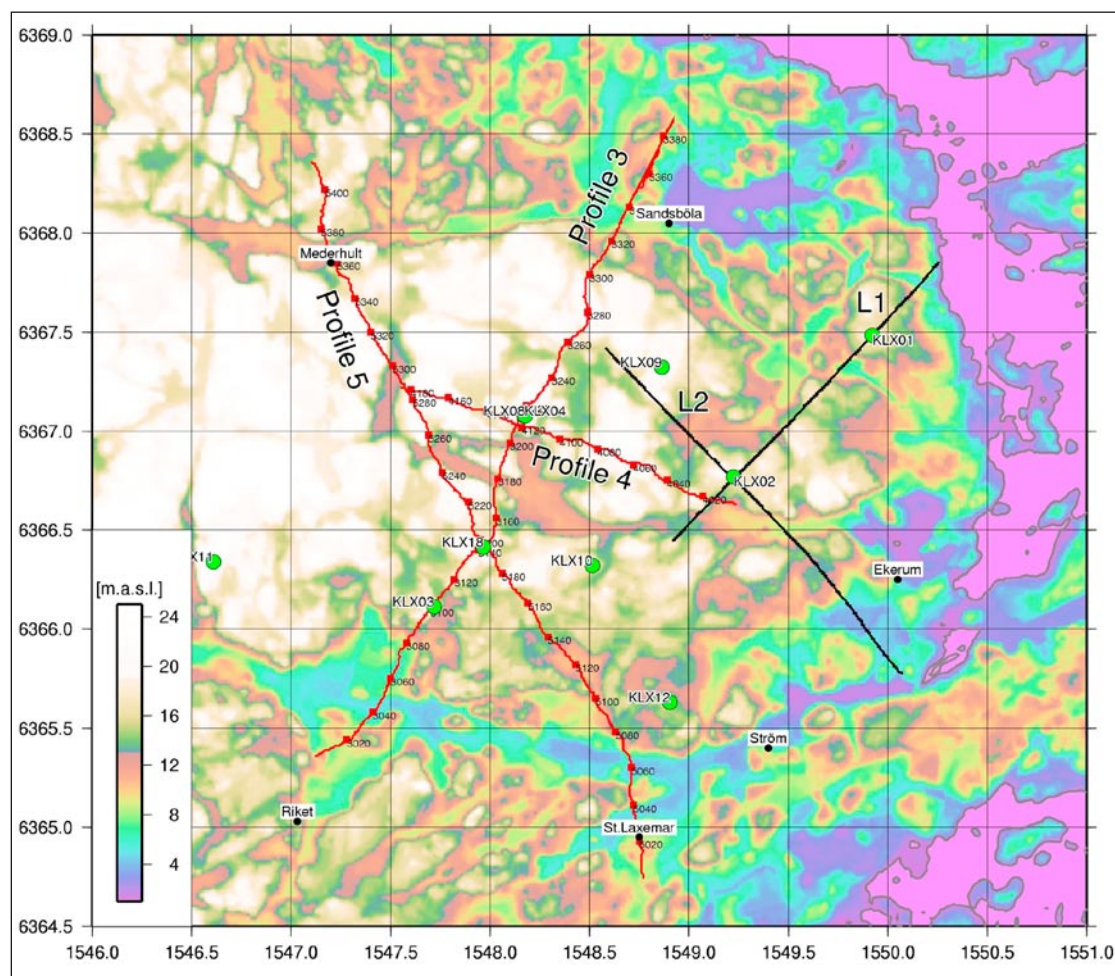


Figure 5-20. Location of the seismic reflection profiles, profile 3, LSM000704, profile 4, LSM000705 and profile 5, LSM000706 (red lines). Reflection seismic profiles acquired in 1999 (black lines) were reported on in /Bergman et al. 2001/.

Focus was on the set of so-called M reflections, which dip gently to the south in the upper 1.5 km of crust in the area. These reflections are generally discontinuous in nature, but are part of the general pattern of south dipping reflectivity seen in the profiles. In general, the interpreted reflections should not be viewed as discrete deformation zones, but rather as a group of reflections that line up along a relatively straight line. The uppermost reflector of this series, M1, intersects the likely repository depth at -500 m and was the focus of the review. Due to its perceived importance this reflector has been included in the deterministic deformation zone model as the discrete deformation zone ZSMEW946A. However, it can be more generally interpreted to represent the upper boundary of a thicker laterally discontinuous series of gently dipping minor deformation zones and mafic intrusions. Further description of M1 and ZSMEW946A can be found in /Wahlgren et al. 2008/.

5.2.10 Character and geological significance of seismic refraction data

Laxemar and Simpevarp have been investigated in a number of seismic refraction surveys between 2004 and 2007 /Lindqvist 2004abc, 2005, 2006, 2007/. The objective has been the focused investigation of possible deformation zones and to investigate the depth of the Quaternary overburden. The local major (length >1,000 m) interpreted lineaments were generally confirmed as deformation zones with lower seismic velocity, 2,500 m/s up to 4,000 m/s, whereas the velocity of the sound country rock was in the range from 5,000 m/s up to 5,900 m/s. An overview of the profile positions is presented in Figure 5-21.

Forty-four profiles with a total length of 25,015 m were measured. The interpreted zone apparent thickness varied between 2.5 m and 20 m, with a majority found in the 5 to 10 m range. The low velocity anomalies have been interpreted to provide indications of likely thicknesses and rock quality characteristics associated with brittle deformation zones.

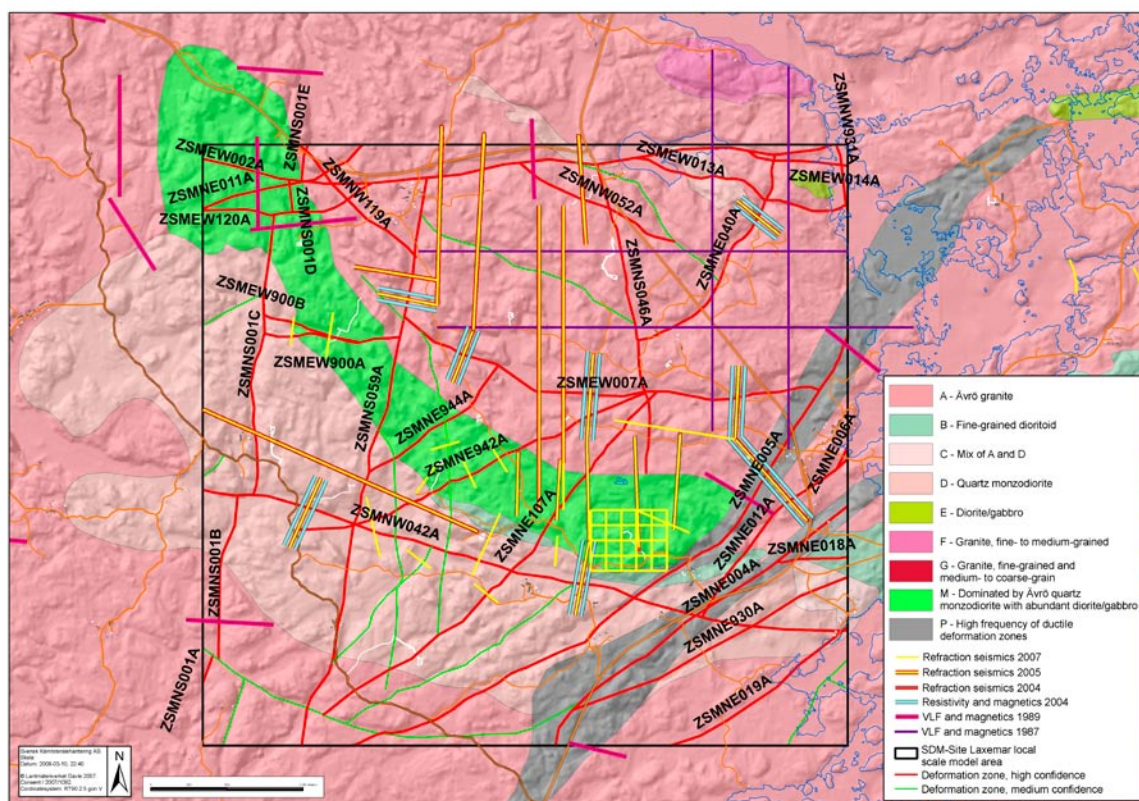


Figure 5-21. Geophysical profiling work carried out in the Laxemar local model area. For reasons of simplicity, the prefix RSM has been excluded in the denomination of the rock domains.

5.2.11 Identification and geological significance of minor deformation zones

Large deterministic deformation zones, which were defined during site descriptive modelling as regional and local major zones, are assumed to affect the overall volumes available for deposition holes and repository infrastructure. However, smaller structures, such as minor deformation zones (MDZ), are important for the location and orientation of deposition tunnels and placement of individual deposition holes. The division between minor deformation zones and local major deformation zones is set at an associated surface lineament trace length of 1,000 m, corresponding to the area of a disk-shaped fracture with a radius of 564.2 m /Wahlgren et al. 2008/. Minor deformation zones are assumed to be of limited spatial extent, and are not modelled deterministically in RVS but are instead handled stochastically in the geological DFN modelling (Section 5.6). However, the derivation of more detailed structural models, involving the deterministic modelling of MDZ will be made in conjunction with the start of the construction work.

MDZ were identified at the ground surface using a combination of high-resolution ground magnetic surveying and airborne laser scanning (Lidar) of topography. The topographic and geophysical data were used to develop a local scale linked lineament map inside the Laxemar local model area. Lineaments can potentially represent minor deformation zones in the bedrock; however, they can also potentially represent other geological structures such as long fractures, dolerite or granitic dykes, areas of pervasive ductile deformation not extensively re-activated in the brittle regime, networks of sealed fractures, elongated zones of bedrock alteration, or topographic features not associated with bedrock deformation. It is possible that a mapped lineament, when investigated, may not exhibit the structural characteristics associated with minor deformation zones as mapped in cored borehole data, but still represents a structure of geologic interest.

The connection between lineaments and minor deformation zones was explored through a coordinated surface mapping and core drilling program in 2006 at three sites inside the Laxemar local model area /Olsson et al. 2007/. Detailed surface mapping was performed with a focus on lineaments, over exposed rock or rock with shallow soil cover, with lengths in the range of 100 m to 1,000 m. Some of the more interesting lineaments were selected for excavation in order to expose their character at the bedrock surface. The focused MDZ study suggests that the most significant MDZ, indicated by lineaments < 1,000 m, are characterised by brittle-ductile deformation, increased fracturing (open and sealed fractures) and at some locations by minor volumes of crushed rock and mylonites. The study also indicates that the most significant MDZ are characterised by a significant transmissivity ($> 5 \cdot 10^{-7} \text{ m}^2/\text{s}$). Lineaments generating a seismic refraction low-velocity anomaly appear to be more brittle in character, with a higher degree of open fracturing and increased transmissivity. Some of the lineaments are connected to dykes of fine-grained granite striking north-east. They appear to be important water conduits with transmissivities greater than $1 \cdot 10^{-6} \text{ m}^2/\text{s}$. The focused surface study also suggested, that, within the limited scope of the investigation, not all investigated lineaments could be conclusively identified as MDZ 'of practical importance'. The determination of 'practical importance' was largely defined by whether the MDZ were hydraulically conductive.

In cored boreholes, MDZ were identified as part of the extended single-hole interpretation (ESHI) mapping process (Sections 2.5 and 5.2.2). Deformation zones identified in the ESHI that were not matched to geologic structures defined in the deterministic DZ model were then reclassified as MDZ. The ESHI mapping recorded a total of 281 deformation zones in Laxemar, of which 38 represent borehole intersections with structures included in the DZ model, while the remaining 243 structures represent minor deformation zones /Wahlgren et al. 2008/. More detailed discussions on the intensity of MDZ in Laxemar in the context of geological DFN modelling are presented in /Wahlgren et al. 2008, cf. Section 3.12.2 therein/ and /La Pointe et al. 2008, cf. Chapter 5 therein/.

Four groups of MDZ orientation sets were identified from the borehole review work; a subhorizontal set (SH) and three subvertically dipping sets striking approximately WSW, ESE and NS respectively. The subhorizontal set represents c. 70% of the total amount of MDZ. A high proportion (65%) of MDZ is associated with intrusions and more specifically c. 45% occurs associated with fine-grained granite. The orientation of these intrusions in southern Laxemar as shown in Figure 5-22c and Figure 5-22d shows a similar pattern to the MDZ orientation groups seen in Figure 5-22a and Figure 5-22b.

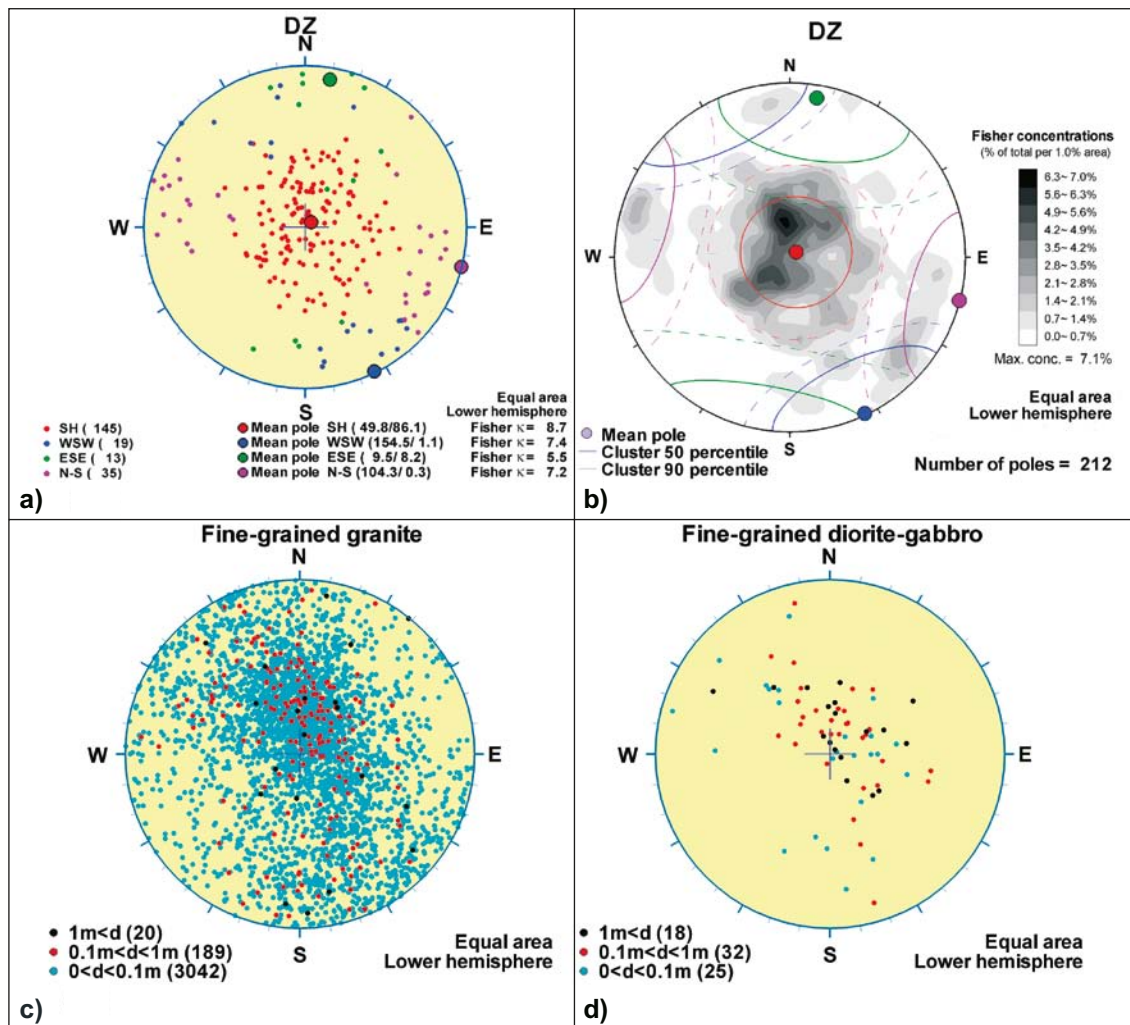


Figure 5-22. a) and b). Orientation analysis of minor deformation zones encountered in boreholes; c) and d). Orientation of fine-grained granite (c) and fine-grained diorite-gabbro (d) in the quartz monzodiorite in southern Laxemar. Based on data from all cored borehole sections that have intersected the quartz monzodiorite. Borehole KLX27A and the DFN boreholes KLX11B through KLX11F are not included in these analyses.

No particular pattern as regards to deformation type, character or orientation could be identified in the MDZ data set that showed any depth dependency. In a similar way no pattern of changing properties could be seen in the horizontal distribution of MDZ. Some 50% of the MDZ in the boreholes were interpreted as brittle, 16% as ductile and 34% as brittle-ductile in character. The MDZ identified in the boreholes have a median true thickness of 1 m.

5.3 Overview of geological models in relation to data resolution

According to the strategy for the development of geological site descriptive models /Munier et al. 2003/, it is important to note that the resolution of geological objects is a direct function of the desired modelling scale, and is the same throughout the model volume. Thus, it is essential to define the size of the smallest object that will be modelled deterministically. This is steered by the density of available data, properties and the intended use of the model.

In model version SDM-Site Laxemar, one rock domain model is presented. However, inside the local scale model volume the resolution is higher than in the surrounding regional model volume due to much higher data density.

For the deterministic deformation zone model and the geological discrete fracture network (DFN) model, the size limit of structures was set at a trace length at the ground surface of 1,000 m. Structures with a trace length that exceeds 1,000 m are included in the deterministic deformation zone model, while structures shorter than 1,000 m are described in statistical terms and modelled stochastically in the geological DFN model. Some zones identified in the ESHI, but that cannot be associated with a lineament at the ground surface, are also included at depth in the deterministic deformation zone model since they have an interpreted length that exceeds 1,000 m based on their thickness /Wahlgren et al. 2008, cf. Section 5.3.2 therein/.

Deformation zones that are 3,000 m or longer are included in the regional deformation zone model, although parts of them may intersect the local model volume. The length of gently dipping to sub-horizontal deformation zones is very difficult to estimate since they commonly cannot be connected to a lineament at the ground surface.

5.4 Deterministic model for rock domains

5.4.1 Data input

The deterministic rock domain modelling has used the following data and interpretations:

- The distribution of rock units at the ground surface as presented in the updated bedrock geological map of the Laxemar-Simpevarp area.
- The rock units identified in the ESHI of all 46 cored boreholes in Laxemar, i.e. c. 18 km of cored boreholes. ESHI from percussion boreholes with a total borehole length of c. 6.5 km have been used as complementary data.
- The character of the dominant rock types as documented both at ground surface and at depth in the boreholes and associated drill cores.

5.4.2 Conceptual model

Laxemar is dominated by well preserved rocks although a faint to weak, non-uniformly distributed foliation is developed in the bedrock. The most prominent structural features are the sinistral, north-east trending, subvertically dipping, low-grade, ductile shear zones. As can be seen in Figure 5-23, Laxemar is bounded both to the west and east by the most prominent ductile shear zones in the area. Furthermore, the Simpevarp subarea to the east is much more affected by north-east trending, ductile shear zones, which is clearly indicated by the much more banded magnetic anomaly pattern compared with that seen in Laxemar, cf. insert to Figure 5-23. Even though Laxemar is not devoid of ductile shear zones and does not have a lens-like shape, it can conceptually be regarded as a “tectonic lens”, i.e. as a low temperature analogue to the tectonic lens interpreted in the Forsmark area /Stephens et al. 2007/.

The orientation of the non-uniformly distributed faint to weak foliation in Laxemar is evaluated in Section 5.2.4. The non-pervasive foliation in Laxemar constitutes an antiformal configuration, with slightly steeper dips in the northern part compared with the southern part /Wahlgren et al. 2008/. The pole to the best-fit great circle to the girdle-like configuration of all foliation data from Laxemar indicates that the fold axis to the antiformal structure is east-west oriented and near horizontal. This interpretation is supported by AMS data /cf. Wahlgren et al. 2008/.

As pointed out in Section 5.2.5, fine-grained granite and fine-grained diorite-gabbro display a similar orientation to the foliation in southern Laxemar, whereas the similarity in orientation is less clear in central and especially in northern Laxemar. The anisotropy that the foliation gives rise to is judged to be weak, which is supported by the evaluation of the anisotropy of the magnetic susceptibility /cf. Wahlgren et al. 2008, and Section 3.5.4 therein/. Furthermore, it is important to note that the foliation is discordant to the boundaries between the dominant rock types. This discordance and generally weak structural anisotropy in Laxemar is in strong contrast with the bedrock at Forsmark /Stephens et al. 2007/, where the penetrative, yet variable, ductile deformation has developed a strong anisotropy, which has guided the geometric modelling of rock domains at that site. Consequently, a similar structural concept for the geometrical modelling of rock domains in Laxemar cannot be applied due to the weak anisotropy in the generally well preserved rocks.

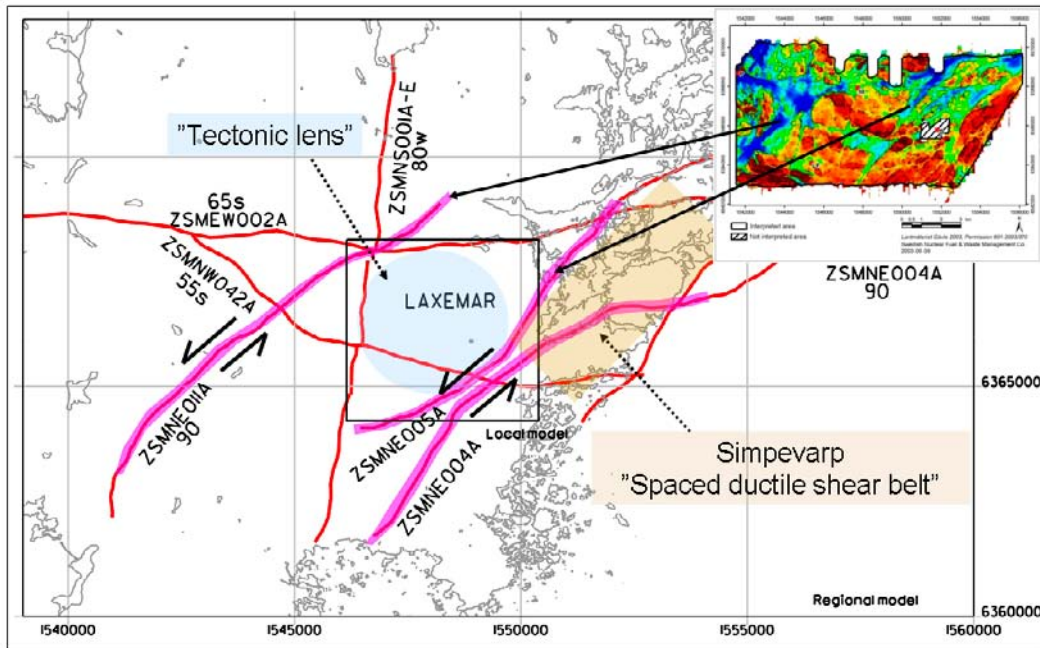


Figure 5-23. Tectonic overview of the Laxemar-Simpevarp area showing the location of Laxemar in between the prominent north-east oriented ductile shear zones (lilac colour). From /Wahlgren et al. 2008/.

From the above reasoning, it is concluded that, with one exception, that no specific concept, e.g. structural guidance, can be applied to the sub-surface geometrical modelling of the rock domains as defined at the surface in Laxemar. The exception comprises two domains that are defined on the basis of a high frequency of ductile shear zones, i.e. the NE-trending shear zones that constitute the boundary between Laxemar and Simpevarp (see Figure 5-23). For these domains, the orientation of the strong foliation and the ductile shear zones that has been documented during the bedrock mapping at the surface have conceptually been applied in defining the geometrical projection to greater depth.

5.4.3 Methodology, assumptions and feedback from other disciplines

Since no specific concept is applied to the sub-surface geometrical modelling of the rock domains, with one exception, the geometrical shapes of the rock domains at depth are determined by the defined rock domain boundaries as interpreted in the cored boreholes, further supported by geophysical modelling based on gravimetric and magnetic data /Triumf 2004c/. The orientations of the contacts between rock units that correspond to rock domain boundaries in the boreholes have not been employed as a geometrical guidance. Consequently, the geometrical modelling of rock domains is insensitive to the uncertainty in orientation of individual geological objects. However, the uncertainty in the actual orientation of the boreholes, i.e. the borehole deviation measurements /Munier and Stigsson 2007/, may affect the position of the rock domain boundary.

The following assumptions have been adopted in the modelling procedure:

- If no conflicting information exists, the major rock domains are presumed to extend at depth to the base of regional model volume (-2,100 m).
- One rock domain, with a large extent at the surface (RSMM01), is interpreted, based on sub-surface data to become successively thinner at depth and not to reach the base of the local model volume (-1,100 m) along its entire extent.
- In the absence of sufficient sub-surface data, rock domains with a limited extent at the surface are not presumed to extend to the base of the local model volume (-1,100 m), but have been extended to a depth that corresponds to the width at the surface.
- Given the lack of borehole data, the orientation of ductile shear zones and mylonitic foliation, as documented at the surface, are applied as guidance for the geometrical interpretation of two specific rock domains at depth.

As for previous model versions, judgements have been provided regarding the confidence level regarding the existence and the uncertainty relating to the geometry of the rock domains, both at surface and at depth. The confidence regarding existence at the surface and at depth is coupled to the confidence in the bedrock geological map and the mapping of the drill cores. The uncertainty in geometry of the rock domains is coupled to the amount of surface data available for the compilation of the bedrock geological map, and the number of available fixed points (intersections with boreholes at depth) for a particular rock domain boundary.

The documented properties of each rock domain comprise the character of the dominant and subordinate rock types, the degree of inhomogeneity, character and degree of alteration/metamorphism, and the character and orientation of the ductile structures. The properties of the dominant rock type comprise, for example, mineralogical composition (dominant minerals), grain size, texture, density and uranium content. Quantitative estimates of the uncertainty for some of the properties, what source the property assignment is based on and the level of confidence in the assignment (high, medium or low) are presented.

Feedback and input from the thermal and rock mechanics modelling teams have highlighted that the wide compositional range for the Ävrö granite is reflected in its thermal and rock mechanical properties. The compositional variation within the Ävrö granite prompted, on pure geological grounds, the definition of the area dominated by Ävrö quartz monzodiorite on the surface, and the subdivision of Ävrö granite into Ävrö quartz monzodiorite and Ävrö granodiorite in the boreholes, by an evaluation of available data. However, the input and feedback from the thermal and rock mechanics modelling teams further strengthened the need for this work and the subsequent refinement of the rock domain model. Furthermore, integration work with the thermal modelling team pointed to the need for better understanding the thicknesses and orientations of the subordinate rock types, in particular fine-grained granite and fine-grained diorite-gabbro, in the principal rock domains. This analysis has been completed (see Section 5.2.3) and has been utilised in the stochastic simulation of the distribution of subordinate rock types in the rock domains, which is carried out by the thermal modelling team (cf. Section 6.4.4).

No feedback was given to the Laxemar rock domain modelling from the SR-Can project /SKB 2006d/.

5.4.4 Identification of rock domains, geometric models and property assignment

The division into rock domains comprised two working stages, namely:

- Definition of rock domains at the surface.
- Definition of rock domains in the cored boreholes.

A primary step in the modelling procedure is the recognition and definition of rock domains at the surface by use of the bedrock geological map. This map includes rock units that are defined on the basis of:

- Composition, grain size and texture of the dominant rock type.
- Degree of bedrock homogeneity.
- Strong ductile structural overprinting (high frequency of ductile shear zones).

The simplification and integration procedures relating to the surface data have yielded a rock domain map at the surface in the local model area (Figure 5-24).

The rock units in the ESHI are mostly defined on the basis of rock composition, grain size and texture, as well as degree of mixing of different rock types, i.e. lithological inhomogeneity. Thus, the principles for defining rock units in the boreholes follow those applied at the surface when constructing the bedrock geological map. The definition of rock domains in cored boreholes in the focused volume in the Laxemar local model area is presented in Appendix 5. For the definition of rock domains in all cored boreholes in Laxemar, the reader is referred to /Wahlgren et al. 2008, cf. Table 4-3 and Appendix 10 therein/.

In total thirteen rock domains are defined in the local model volume. The RSMBA03 domain only occurs at depth in the lower part of the model volume. It is based on a mixture of Ävrö granite and fine-grained dioritoid between 540 and 960 m borehole length in KLX02. The geometry of the

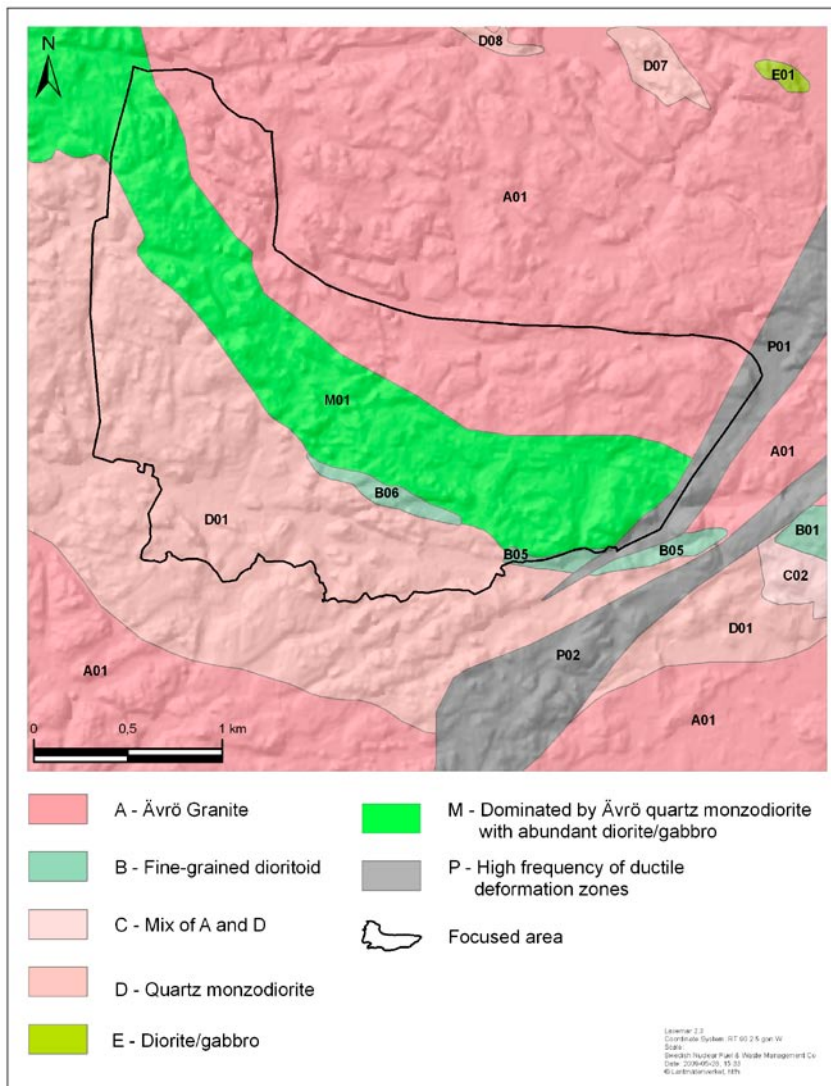


Figure 5-24. Two-dimensional model at the surface for rock domains in the Laxemar local model area /Wahlgren et al. 2008/. For reasons of simplicity, the prefix RSM has been excluded in the denomination of the rock domains. The noted discrepancy between the eastern boundary of the focused area and the delineation of the P01 rock domain is due to the indicative nature of the boundaries of the focused area, cf. Section 1.1, where its eastern boundary coincides with the centre line of the elongated P01 domain.

RSMM01 domain combined with RSMD01, RSMP01, RSMP02, RSMB05 and RSMB06 domains in the focused volume is displayed in Figure 5-25. The RSMD01 domain in combination with the RSMP01 and RSMP02 domains are shown in Figure 5-26. As is evident from the two figures, all the borehole intersections strongly indicate that the boundary surfaces between RSMD01, RSMM01 and RSMA01 (transparent in the figures) are fairly well constrained.

The properties of the rock domains in the local model volume are presented in /Wahlgren et al. 2008, cf. Appendix 11 therein/. A description of the dominant rock domains RSMD01, RSMM01 and RSMA01 is given in the sections below.

Rock domain RSMD01

The RSMD01 domain is the dominant rock domain in the southern part of the focused volume in southern Laxemar. It is strongly dominated by equigranular, medium-grained quartz monzodiorite, which is estimated to constitute c. 89% of the domain volume. The quartz monzodiorite is compositionally relatively homogeneous with a calculated quartz content of $13.0 \pm 3.0\%$ (mean \pm stdv; true quartz content). The RSMD01 domain is structurally well-preserved, although c. 22% of the domain is affected by a non-uniformly distributed faint to weak foliation with a dominant gentle dip to the south.

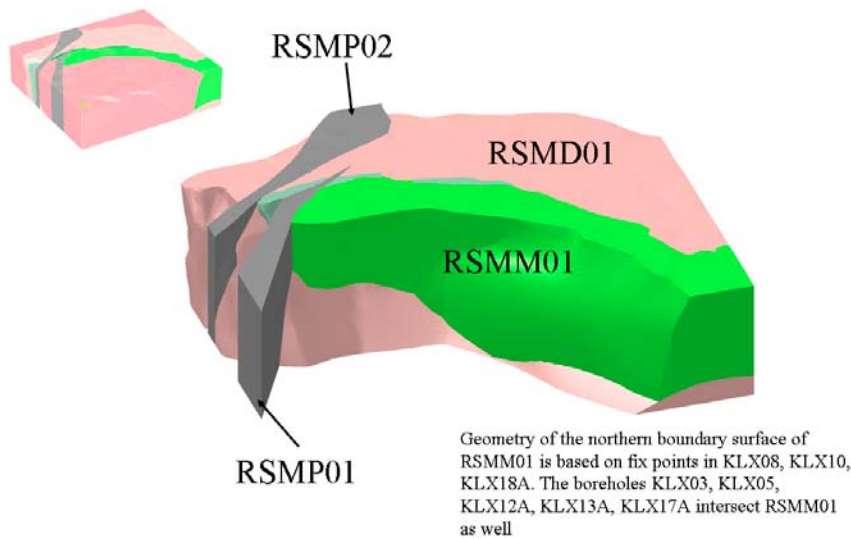


Figure 5-25. View of the RSMM01 domain combined with RSMD01, RSMP01, RSMP02, RSMB05 and RSMB06 /Wahlgren et al. 2008/. For location of the minor rock domains RSMB05 and RSMB06, see Figure 5-24. View to the south.

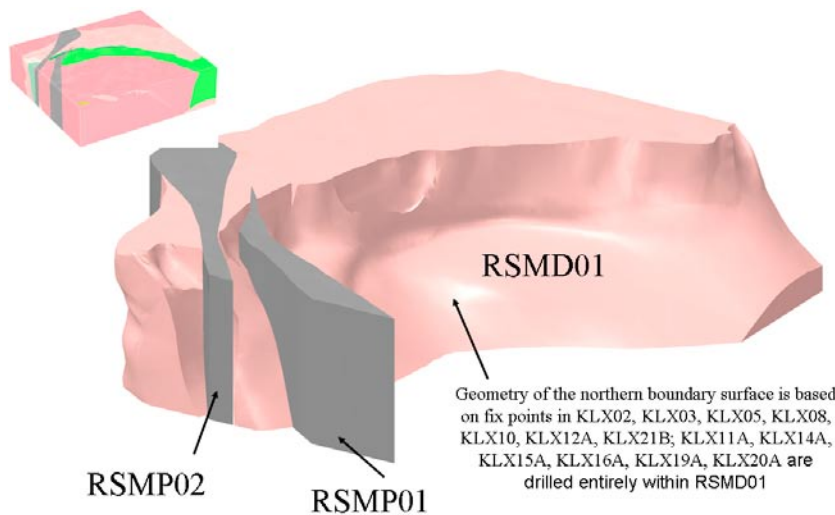


Figure 5-26. View of the RSMD01 and intersecting RSMP01 and RSMP02 domains /Wahlgren et al. 2008/. View to the south-southwest.

The most important subordinate rock types are fine-grained granite estimated to comprise 5% of this domain, fine-grained diorite-gabbro 2% and pegmatite 1.5%. Furthermore, the occurrence of dolerite is estimated to comprise 2% of the RSMD01 domain. However, dolerite is only documented in the cored boreholes KLX14A, KLX19A and KLX20A, and is considered to constitute a very subordinate rock type and not to be evenly distributed throughout the RSMD01 domain. The occurrence of dolerite dykes seems to be connected to deformation zones. As mentioned in Section 5.2.5, the subordinate rock types, except pegmatite, display dips similar to the foliation, i.e. gentle and dominantly to the south. The spatial distribution of the subordinate rock types is treated by stochastic modelling (see Section 6.4.4).

The estimated alteration of the RSMD01 domain /Wahlgren et al. 2008, cf. Appendix 7 therein/, outside the identified possible deformation zones from the ESHI, comprises equal proportions of faint to weak oxidation (red staining) and saussuritisation, i.e. c. 10% of each. Furthermore, epidotisation is observed and constitutes c. 2%. Consequently, the major part of the RSMD01 domain is judged to be composed of fresh rocks.

Rock domain RSMM01

The RSMM01 domain is dominated by the commonly medium-grained and finely porphyritic Ävrö quartz monzodiorite, including granodioritic to granitic compositions (Ävrö granodiorite). Together, these two compositional varieties constitute c. 75% of the domain, out of which Ävrö quartz monzodiorite constitutes c. 50% and Ävrö granodiorite c. 25% (cf. Section 6.4.1 and Table 6-9). Furthermore, the RSMM01 domain is characterised by a much higher proportion of diorite/gabbro (mean value c. 16%) than the other rock domains. However, the diorite/gabbro is variably distributed both at the surface and in corresponding domain sections in boreholes /Wahlgren et al. 2008, cf. Appendix 4 therein/. The Ävrö quartz monzodiorite has by definition a low content of quartz. The calculated modal quartz content of $13.9 \pm 6.4\%$ (mean \pm stdv; true quartz content) includes the Ävrö granodiorite as well. The latter gives rise to increased thermal conductivity compared with the otherwise low thermal conductivity of the Ävrö quartz monzodiorite (see Section 6.2). It should be noted that the quartz content is chosen to exemplify the difference in composition, and that thermal properties are affected by the overall mineralogical composition. Furthermore, the compositional varieties also give rise to different rock mechanics properties (see Section 7.2).

The most important subordinate rock types are the same as in the RSMD01 domain. Fine-grained granite is estimated to comprise 5%, fine-grained diorite-gabbro 2% and pegmatite 0.5%. Furthermore, medium- to coarse-grained granite (501058) comprises 2%, and fine-grained dioritoid and quartz monzodiorite occur in minor amounts. As with the RSMD01 domain, the spatial distribution of the rock types is treated by stochastic modelling (see Section 6.4.4). The RSMM01 domain is structurally well-preserved but c. 17% of the volume has been affected by a faint to weak foliation. In contrast to the RSMD01 domain, the orientation of the subordinate rock types and the foliation do not display the same similarities in the RSMM01 domain. More specifically, there is no corresponding orientation of the subordinate rock types to the north-dipping foliation, /cf. Wahlgren et al. 2008, cf. Sections 3.5.3 and 4.2 therein/.

The alteration in the RSMM01 domain /Wahlgren et al. 2008, cf. Appendix 7 therein/ outside the identified deformation zones in the ESHI is dominated by oxidation (red staining). It is mostly of faint to weak character and affects c. 14% of the domain. Other types of alteration present are saussuritisation (c. 2%), epidotisation (< 1%), as well as very minor amounts of chloritisation and silicification.

Rock domain RSMA01

The Ävrö granite, i.e. in its use as the collective term for a commonly medium-grained and finely porphyritic rock that varies in composition between quartz monzodiorite, granodiorite and granite *sensu stricto*, is the dominant rock type in the RSMA01 domain. Although quartz rich varieties, i.e. granodiorite and granite, dominate in the RSMA01 domain, parts of the domain are composed of Ävrö quartz monzodiorite. If all boreholes are considered, the Ävrö granite constitutes c. 82% of the volume of the rock domain. However, if the estimate is based only on KLX02, KLX04, KLX07A and B, KLX08, KLX10, KLX18A and KLX21B, since these boreholes are considered to be more representative for the bedrock in the central and southern part of the RSMA01 domain, the Ävrö granite constitutes c. 88%. Estimates carried out in connection with the thermal modelling, indicates that the Ävrö granodiorite constitute c.65% and the Ävrö quartz monzodiorite c. 25% of the Ävrö granite in the RSMA01 domain. The calculated modal quartz content for the Ävrö granite, comprising the granitic to quartz monzodioritic varieties, in RSMA01 is $21.7 \pm 6.4\%$ (mean \pm stdv; true quartz content).

Typical subordinate rock types are fine-grained granite which is estimated to comprise 3%, fine-grained diorite-gabbro 2%, fine-grained dioritoid 3%, quartz monzodiorite 2.5%. Furthermore, granite, pegmatite and diorite/gabbro occur in minor amounts, i.e. each rock type constitutes less than 1%. The similarities in orientation of the faint to weak foliation, which is estimated to affect c. 26% of the domain, and orientation of the fine-grained granite, fine-grained diorite-gabbro and pegmatite, are less obvious than in the RSMD01 and RSMM01 domains. This is mainly due to a larger spread in orientation of the subordinate rock types /Wahlgren et al. 2008, cf. Sections 3.5.3 and 4.2 and Figure 3-27 therein/. The difference is in particular valid for the fine-grained granite and the pegmatite, whereas the fine-grained diorite-gabbro displays an orientation pattern that is more similar to the orientation of the foliation.

The alteration in the RSMA01 domain /Wahlgren et al. 2008, cf. Appendix 7 therein/ outside the deformation zones identified by the ESHI is dominated by oxidation (red staining). It is mostly of faint to weak character and affects c. 25% of the domain. Alteration of subordinate character is saussuritisation (c. 3%) and very sparse epidotisation (< 1%). Alteration that occurs in very minor amounts comprises sericitisation, silification and chloritisation.

Rock domains RSMP01 and RSMP02

The RSMP01 and RSMP02 domains are characterised by a high frequency of ductile shear zones, i.e. the bedrock in these domains is more strongly affected by ductile strain than the country rock in general. The RSMP01 and RSMP02 domains are not intersected by any cored boreholes, apart from RSMP01 at Äspö, but are primarily based on documentation during the bedrock mapping at the surface supported by distinct low-magnetic anomalies. The documented orientation of the ductile shear zones and the mylonitic fabric at the surface is the basis for the modelled vertical geometry of these domains. The RSMP01 and RSMP02 domains constitute the eastern boundary of the focused volume for a potential repository in Laxemar, and correspond to the deformation zones ZSMNE005A and ZSMNE004A, respectively (cf. Section 5.5).

5.5 Deterministic deformation zone modelling

5.5.1 Geodynamic evolution – conceptual understanding

The following types of geological processes have been important for the conceptual understanding of the geodynamic evolution of the bedrock in south-eastern Sweden, including the Laxemar-Simpevarp area (cf. Section 3.1 and Figure 3-3):

- Igneous activity at c. 1.8 Ga along an active continental margin and subsequent ductile deformation during the waning stages of the Svecokarelian orogeny.
- Igneous activity at c. 1.45 Ga, manifested by the intrusion of granites in a stabilised brittle crust, and formation or reactivation of structures in the near-by bedrock, as a far-field effect of the Hallandian orogeny.
- Igneous activity at c. 900 Ma, manifested by the intrusion of dolerite dykes, and reactivation of deformation zones as a far-field effect of the Sveconorwegian orogeny.
- Reactivation of deformation zones as a far-field effect of the Caledonian orogeny.
- Loading and unloading cycles after c. 1.5 Ga that are related to the deposition of sediments, and subsequent formation of sedimentary rocks, or glaciation. The sedimentary rocks formed as a response to far-field orogenic activity and glaciations are caused by change in climate.

As the effect of the ductile deformation ceased, the subsequent tectonic overprinting, as a consequence of release of built-up stress in the bedrock, occurred under brittle conditions. The absolute majority of the regional and local major deformation zones that have been deterministically modelled in Laxemar, although dominated by brittle deformation, show signs of having been originally formed during ductile conditions. Consequently, it is indicated that the gross structural framework was established already during the waning stages of the Svecokarelian orogeny. In Figure 5-27, the expected kinematics during formation and brittle reactivation of deformation zones with different orientation is shown, based on the inferred bulk shortening direction during the different orogenic events that are indicated to have affected Laxemar-Simpevarp. The model is based on low-temperature geochronological data, relative time relationships and absolute ages of fracture minerals. For a more detailed overview and evaluation of these data, the reader is referred to /Söderbäck 2008/.

5.5.2 Influence of anisotropy in the ductile regime on deformation in the brittle regime

As mentioned in Section 5.5.1 above, it is strongly indicated that the overall structural framework was formed when the bedrock still responded to tectonic stresses by ductile deformation. Since the majority of these deformation zones show signs of polyphase brittle reactivation, it is apparent that

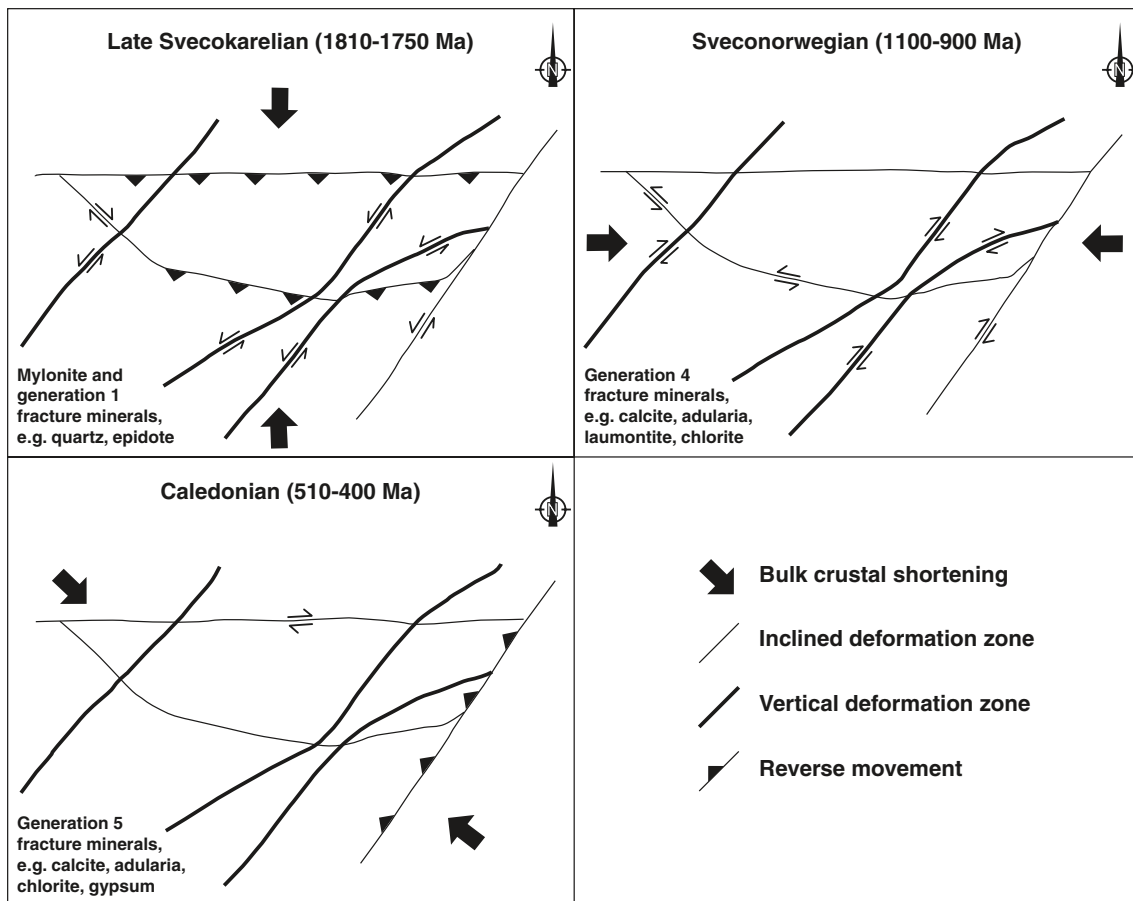


Figure 5-27. Two-dimensional conceptual illustrations of the inferred regional scale geodynamics during the formation and reactivation of deformation zones in different orientations. This includes late Svecokarelian ductile and subsequent brittle deformation and brittle reactivation during the Sveconorwegian and Caledonian orogenic events. Note that apart from the inferred E-W compression during the Sveconorwegian orogeny, the area was also subjected to E-W extension which is indicated by the occurrence of N-S trending, c. 900 Ma old dolerite dykes. See Sections 5.2.6 and 9.5.6 for description and discussion of the different generations of fracture fillings.

the framework of ductile deformation zones has localised the stress release during the subsequent geological evolution in the brittle régime. As shown in /Wahlgren et al. 2008, cf. Section 3.5.2 therein/, the non-uniformly distributed faint to weak foliation, the small-scale low-grade ductile shear zones and mylonites as recorded in the Boremap mapping, as well as the MDZ /Wahlgren et al. 2008, cf. Section 3.12.3 therein/ are dominated by subhorizontal to moderate dips. By far the strongest cluster of fractures outside deformation zones from the ESHI displays moderate to subhorizontal dip /Wahlgren et al. 2008, cf. Section 3.6.2 therein/. The orientations of fractures inside deformation zones are quite similar to those outside deformation zones /Wahlgren et al. 2008, cf. Section 3.6.3 therein/.

This similarity between the orientation of both the large- and small-scale ductile and brittle structures strongly suggests that the ductile anisotropy that developed during the waning stages of the Svecokarelian orogeny has strongly influenced the orientation of brittle structures during the geological evolution of the site. Furthermore, the similarity between the orientation of the fractures outside and inside deformation zones suggests that movements in the deformation zones have controlled the fracturing in the bedrock in the Laxemar local model volume.

The gently south-dipping deformation zone ZSMEW946A (Section 5.5), which is based on reflector M1 /Juhlin et al. 2004/, marks the upper limit of what is judged to be a thicker discontinuous series of minor deformation zones and mafic intrusions rather than an individual structure.

The orientation of the fine-grained diorite-gabbro in the RSMD01 domain /Wahlgren et al. 2008, cf. Figure 5-22 therein/ as well as the foliation is similar to the orientation of the M1 reflector. Consequently, it is inferred that the anisotropy caused by the fine-grained diorite-gabbro has steered the development of the gently dipping deformation zone (M1 reflector) ZSMEW946A.

5.5.3 Concepts for the deterministic modelling

The interpretations made in earlier modelling steps have been reassessed and where necessary revised in the light of new observations and insights. However, the set of fundamental assumptions underlying the methodology of the interpretation and development of the deformation zone model (see /Wahlgren et al. 2008/ for details) remain unchanged from earlier modelling steps.

The current deformation zone model addresses deformation zones in the regional and local model volumes on the same basis as previously employed for the Laxemar version 1.2 model /SKB 2006a/. The local scale model contains deformation zones that are interpreted to be of length 1 km or longer, i.e. local major and regional deformation zones according to the terminology of /Andersson et al. 2000/. In addition there are deformation zones interpreted from the borehole investigations that have not been correlated with any surface lineament or neighbouring boreholes. Where such deformation zones have an interpreted true thickness of 10 m or more they have also been modelled deterministically. Such deformation zones have been assigned a circular disk geometry with a surface area equivalent to a 1,000 m x 1,000 m square. In this way the resolution of the local model remains unchanged from earlier versions. The selection of a 10 m thickness as a cut off for the deterministic modelling is based on a conservative interpretation of the deformation zone thickness vs. deformation zone length relationship presented in Figure 5-28. The relationship is clearly weak and the selection of 10 m is conservative in that the site specific relationships between zone thickness and zone length, at both Laxemar and Forsmark, indicate that a zone length of 1,000 m corresponds to a thickness of around 15 m. The application of a circular disc geometry with a fixed 564 m radius may render the associated area being generally underestimated. However, further extrapolation of zone geometries beyond the defined size of the disks is considered too speculative given that the interpreted orientations are of low confidence.

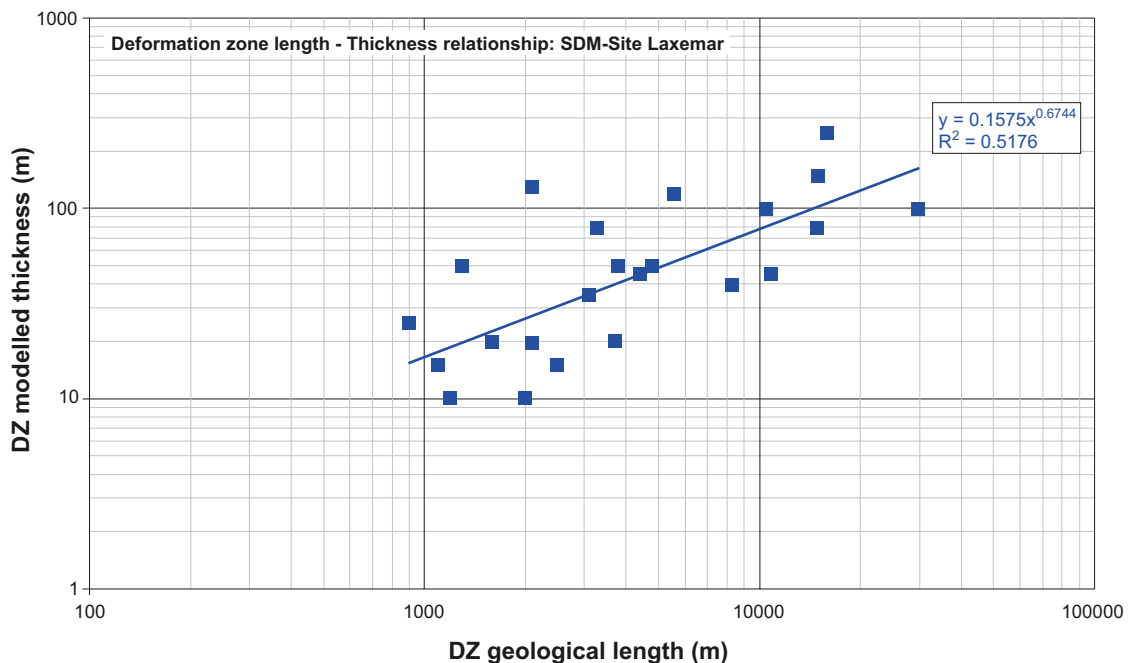


Figure 5-28. Correlation between interpreted true thickness and length for deformation zones in the Laxemar local model.

In the cases where a deformation zone can be correlated with both a lineament and a borehole, the strike of the deformation zone is assumed to be the same as the trend of the matching lineament. A dip inferred from one single borehole intercept is interpreted as being a representative average dip angle of the deformation zone, along its entire extent. Deformation zones observed only at the surface, which lack information on their subsurface extents and geometry, have been assigned a vertical dip.

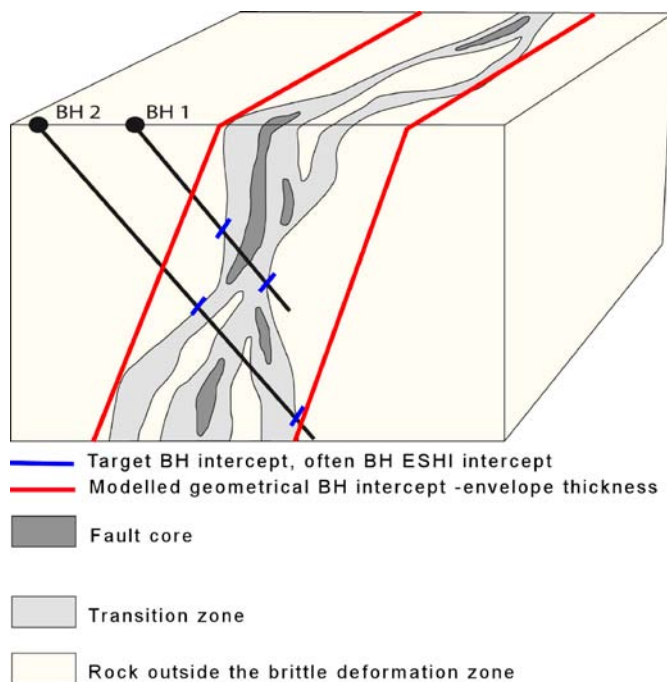
The estimates of deformation zone thickness presented in /Wahlgren et al. 2008/ refer to true thickness. More specifically, the single thickness values given in the property tables in /Wahlgren et al. 2008/ refer to modelled true thickness. This means that a value has been assigned that is assumed to provide a representative overall thickness applicable over the entire length of the zone in the deterministic deformation zone model. This modelled deformation zone thickness generates the geometrical intercepts listed in the property tables. It is based on all available data, both from surface and at depth. The presented range of deformation zone thicknesses is generally based on an inspection of surface related data since borehole data are often limited to a single, or at best, a very small number of borehole intercepts for a specific deformation zone. It is judged that the surface geophysical surveys, namely magnetics and resistivity, along with the detailed topographic elevation models (DEM) give the best indications as to how the thickness of a deformation zone varies laterally and – by inference – with depth. It is appreciated that this type of surface expression is in fact linked to an apparent rather than a true thickness but it is still considered to provide the best estimate with consideration taken of likely lateral variations in deformation zone dip. These thickness estimates encompass both deformation zone cores, transition zones and, to a certain extent, local splays. The widths of the low velocity anomalies from seismic refraction surveys are taken as giving an indication of the presence and thickness of more highly fractured rock associated with brittle deformation zone cores, whereas the magnetic anomalies are interpreted as giving an indication of the thickness of both the highly fractured core and the transition zones. The modelled thickness encompasses both ductile and brittle features, although by reactivation the brittle component generally gives the greater thickness value. Exceptions to this are the major complex ductile (deformation zone) belts, ZSMNE011A, ZSMNE004A and ZSMNE005A (Figure 5-33) where the complex ductile thickness is inferred to greatly exceed that of the brittle component.

The steeply dipping deformation zones are assumed to truncate, along their strike direction, against deformation zones as indicated by the lineament map (Figure 5-18 and Figure 5-19). Gently dipping deformation zones have been detected by an integration of data from boreholes with the interpretation of seismic reflectors. In the model the gently dipping deformation zones are truncated, both along their strike and in their down-dip directions, against regional or local major, vertical and steeply dipping deformation zones. The lateral modelled extent of the gently dipping zones has been constrained based on the lateral extent of the supporting investigation evidence and with a subsequent termination against the nearest steeply dipping zone beyond the last evidence for its occurrence. Deformation zone thickness, like deformation zone length, is often used as a general term without clear definition since it is related to the scale of interpretation. The following discussion outlines how this term and other supporting terminology have been applied in this work. The concept of a deformation zone core and transition zones for brittle deformation zones is well established /Munier et al. 2003/. In contrast to the initial concept, the use of fracture frequency to define a transition zone or zone core boundary position is not applied. Elevated fracture frequencies, in a relative sense, are implied in the definition of such brittle deformation zones but the strict application of fixed threshold values of fracture frequency is considered unwarranted. Q or RMR estimates, which include fracture frequencies, could possibly be made to better describe and quantify rock quality variations across a deformation zone. It should also be noted that deformation zone geometries are often complex, discontinuous and asymmetrical.

Various types of information, including borehole intercepts, topographic expressions, outcrop indications, borehole and surface geophysical surveys, will all generate their respective estimates of true thickness and how this may vary along strike and dip for the same deformation zone. Generally, the associated values differ to a smaller or larger degree. The current modelling process aims to take all of these indications into account and make a judgement of an overall representative measure of deformation zone thickness, along with a likely span.

Two specific borehole related terms are quoted in the deformation zone descriptions and accompanying property tables found in /Wahlgren et al. 2008/, namely ‘Target borehole intercepts’ and ‘Geometrical borehole intercepts’ (cf. Figure 5-29). These two measures underlie much of the resulting modelled 3D deformation zone geometries. Possible deformation zones, both brittle and ductile, are identified in the drill core during the ESHI process. Any interpreted deformation zone is defined by an upper and lower borehole length which defines its apparent thickness. These deformation zone boundary estimates are made by a specialist team of geophysicists and geologists and are essentially ‘best judgement’ estimates based on all of the information available from the borehole and on a hands-on joint examination of the drill-core. No reference is made to other sources of data from other studies away from the borehole. These deformation zone boundary intercepts in a borehole are referred to as ‘Target intercepts’ and are shown schematically in Figure 5-29. In general, target intercepts conform to the ESHI possible deformation zone intercepts but in certain cases adjustments have been made on the basis of other information or interpretation, related to information collected away from the specific borehole. The intercepts of the deterministically modelled deformation zones in the cored boreholes in the focused volume in Laxemar are presented in Appendix 5.

The physical location and inferred orientation of deformation zone specific target intercepts, deformation indicators from outcrop evidence, geophysical seismic reflection, refraction, magnetic and resistivity survey indications are all taken into account and an overall ‘envelope thickness’ for a deformation zone is defined in 3D. This envelope thickness aims to contain at least the majority of a deformation zone’s core(-s), transition zones and splays. It is this envelope thickness that defines the deformation zone in the 3D RVS deterministic DZ model along with a, generally centrally located, zero thickness middle plane. The ‘geometrical borehole intercepts’ listed in the deformation zone descriptions and property tables relate to where the deformation zone envelope surfaces intercept the various boreholes.



(redrawn after Caine et al. 1996)

Figure 5-29. Three-dimensional schematic conceptual geometric model for a brittle deformation zone in Laxemar along which shear displacement has occurred (redrawn after /Caine et al. 1996/). Note the variable character of the deformation zone along the two borehole intersections.

Any estimate of deformation zone length, as in the case of thickness, is also closely related to the scale of interpretation. For the purposes of the deterministic modelling, within the local model volume, 'deformation zone length' generally corresponds to the length of the associated linked lineament. However, all of the associated lineaments in the local model area have been reviewed during the modelling work and adjustments have been made. This has generally resulted in the further linking of additional segments for the definition of a deformation zone. In a very few cases a linked lineament, with a length of over 1,000 m, has not been included in the model as a deformation zone. Whilst any associated interpreted deformation zone is expected to be discontinuous to some extent, in these few cases the associated interpreted deformation zone has been 'broken up' on the basis that the lineament transects a number of extensive outcrops which have been visited in the field and at which no evidence of deformation has been identified. The review of lineaments referred to is a process performed with reference to the original background data and by the lineament interpreters but no absolute 'break up' criteria were applied.

Structures that are considered to be shorter than the deterministically modelled deformation zones in the local area ($L < 1,000$ m) are handled statistically and are presented as part of the fracture statistical description in Section 5.6 and /La Pointe et al. 2008/. Hence, all lineaments shorter than 1 km are treated as part of the geological DFN model.

5.5.4 Characteristics of different sets of deformation zones and property assignment

An overview of the location of the deterministically modelled deformation zones, along with the interpreted rock domains, in the local and regional model volumes is presented in Figure 5-30 and Figure 5-31, respectively.

Detailed descriptions of individual deterministically modelled deformation zones, geographically most relevant to design, are presented in Appendix 6, whilst a complete set of descriptions covering the entire local model area is presented in /Wahlgren et al. 2008, cf. Appendix 14 therein/. In this section of the report the main deformation zones are described in a series of groups that are based on their overall orientation, origin and character. The aim of this section is to provide an overview of the modelled deformation zones and a better understanding of structural geological model. The groups are as follows (see Figure 5-32):

- Northeast-southwest striking, moderate to steeply dipping.
- North-south striking, moderate to steeply dipping.
- East-west to northwest-southeast striking, steep to moderate dip to the south.
- East-west to northwest-southeast striking moderate dip to the north.
- Gently dipping.

Deformation zone geometries presented in red represent deformation zones that are judged to be of high confidence as to their existence and are supported by both indirect evidence such as topographic and geophysical data as well as direct evidence from surface outcrop mapping or boreholes.

Deformation zones presented in green are judged to be of medium confidence in existence and unlike high confidence deformation zones they lack direct evidence from outcrops or boreholes.

NE–SW striking deformation zones, moderate to steeply dipping

Three regional deformation zones, ZSMNE011A, ZSMNE005A and ZSMNE004A, volumetrically dominate this set of structures and roughly mark the outer NW and SE boundaries for the rock volume for a potential repository. All three deformation zones have a ductile origin and complex internal geometry as evidenced by the numerous mylonite fabrics identified during the outcrop mapping campaign. It is this distribution of mylonites and the results from the aerial magnetic survey in combination that define the surface expression of these deformation zones. All three deformation zones should be considered as deformation 'shear belts' composed of a large number of anastomosing sub-structures with an overall irregular thickness rather than three single structures. Field mapping results for all three deformation zones provide evidence of a dominant sinistral shear.

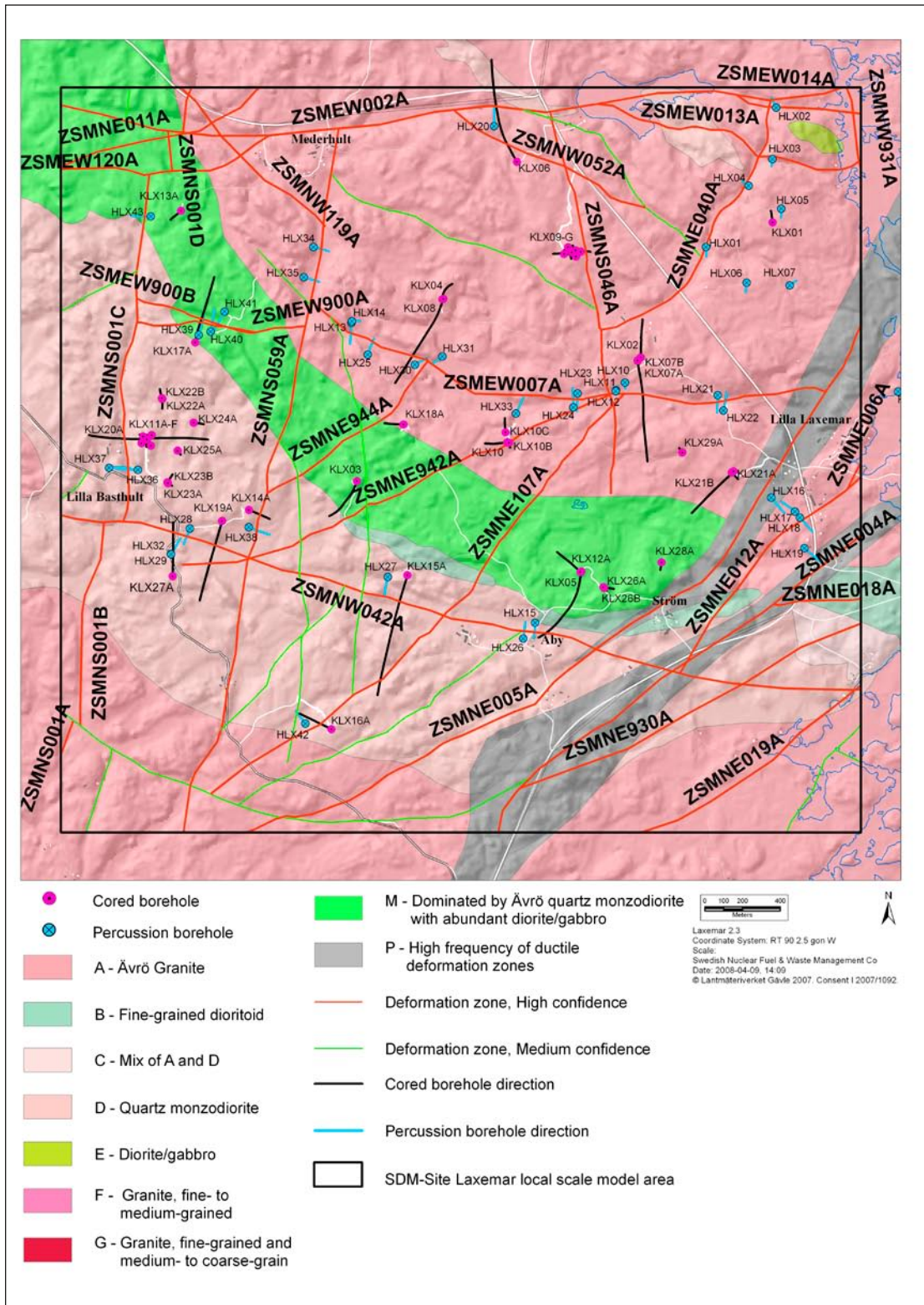


Figure 5-30. An overview of the deformation zones and rock domains modelled deterministically in the Laxemar local model area /Wahlgren et al. 2008/.

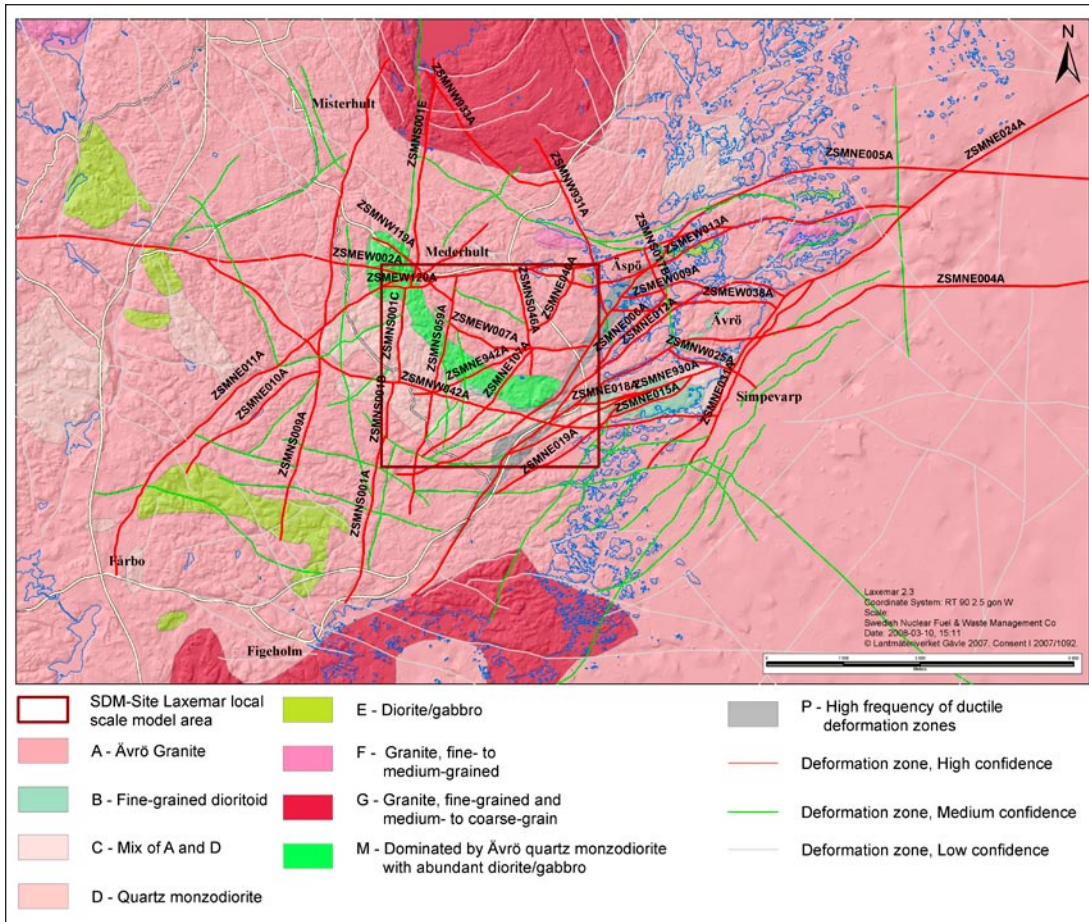


Figure 5-31. An overview of the deformation zones and rock domains modelled deterministically in the Laxemar regional model area /Wahlgren et al. 2008/.

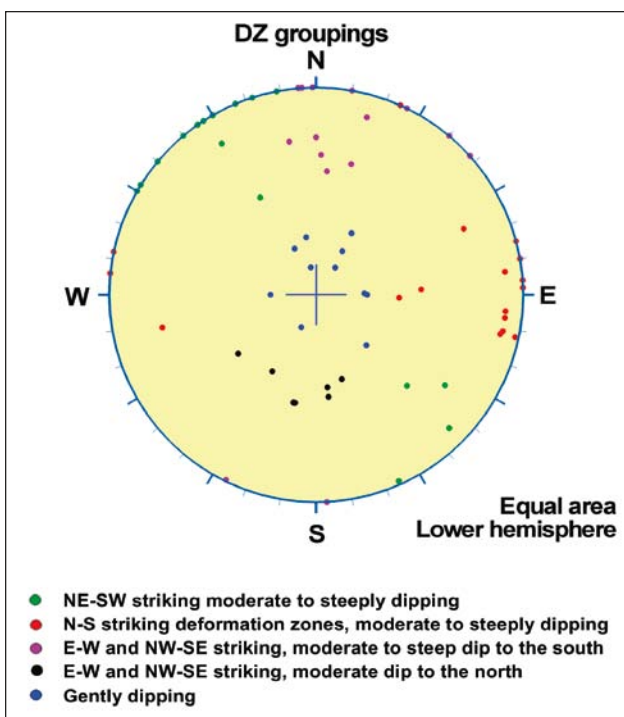


Figure 5-32. Orientation of deterministically modelled deformation zones in the Laxemar model area.

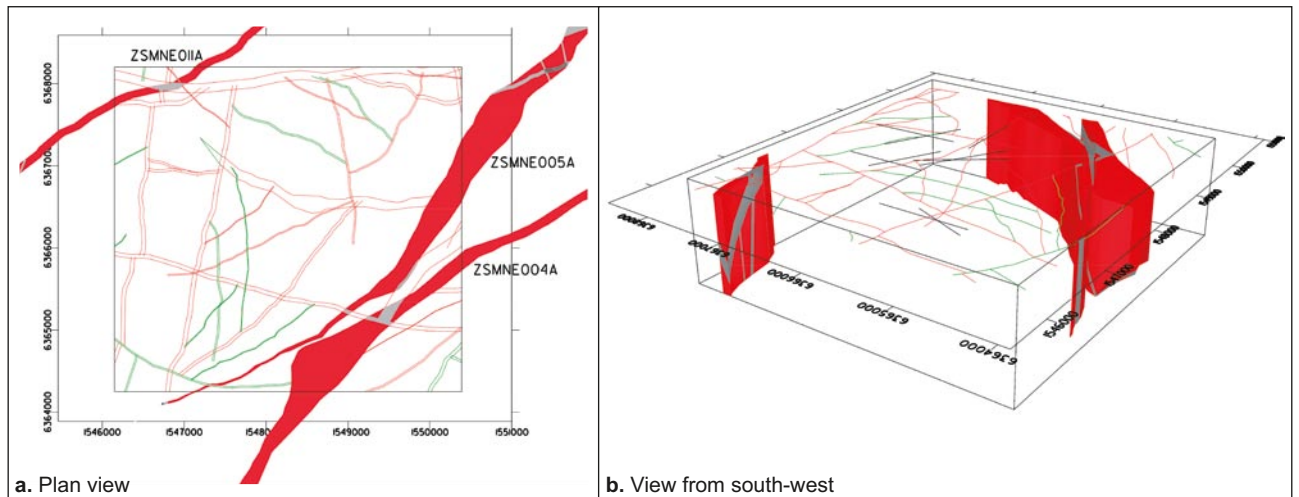


Figure 5-33. Regional NE-SW striking deformation zones which dominate in the local model area /Wahlgren et al. 2008/.

Whilst it is possible to find small deformation zones intercepted in the drill core that show exclusively ductile deformation, on the larger scale of the local model volume, all local major and regional deformation zones that have a ductile origin can also be considered to have been subjected to multiple phases of subsequent brittle reactivation. In practice, evidence of this brittle reactivation may be seen as open fractures, crush and fault gouge and/or as sealed fractures and sealed networks depending on the timing of any mineralisation. This situation is true not only for the NE-SW striking set of structures but for all Local Major and Regional deformation zones. It has become clear that the evidence from a single or couple of drill cores considered in isolation cannot be taken as providing definitive evidence of any zone's character. Ductile deformation and sealed networks found in one core intercept may vary in thickness and have an open fracture network as one moves laterally or up and down along and through a deformation zone. The best indication of whether a deformation zone has an overall open brittle fabric component is considered to be from hydrogeological investigations, cf. Chapter 8.

The three shear belts (ZSMNE004A, ZSMNE005A and ZSMNE011A) have not been the focus of detailed borehole investigations. However, ZSMNE005A has been investigated by a limited number of percussion drilled holes, indirect methods such as geophysical magnetic and resistivity profiling, a very limited seismic refraction survey and marginal drilling activities associated with investigations in conjunction with development of the Äspö HRL. Details of the investigations and interpreted results can be found in /Wahlgren et al. 2008/. A detailed characterisation of the three deformation zones is not possible. However, the available information suggests that the three belts are made up of a large number of anastomosing mylonite zones and similarly the later brittle failure is distributed across the belt in a number of sub-parallel sub-structures rather than along one single major complex zone core.

As described in /SKB 2005a/ the Simpevarp peninsula, the Ävrö and Hälö islands, together with the eastern part of Äspö island are intersected by the regional NE striking shear belts. The western boundary of these belts is formed by the Äspö shear zone (ZSMNE005A). This NE striking belt of regional deformation zones affects the whole of the peninsula. The NE-SW set of structures is also present across Laxemar, although their frequency and thickness are markedly reduced. The western limit of Laxemar is again defined by another broad shear belt, ZSMNE011A (Figure 5-33).

The NE-SW striking deformation zones located within Laxemar are dominated by three structures ZSMNE107A, ZSMNE942A and ZSMNE944A (Figure 5-34). Details concerning these deformation zones are presented in Appendix 6 and more comprehensively in /Wahlgren et al. 2008/. Generally it can be stated that these structures have a ductile origin, often associated with fine-grained granite or composite dykes and have been subjected to multiple phases of brittle reactivation. These deformation zones are relatively thin compared with the bounding major belts with thicknesses in the range of 10 to 35 m, zone core thicknesses of 1 to 5 m and steep dips $>75^\circ$ to the NW or SE.

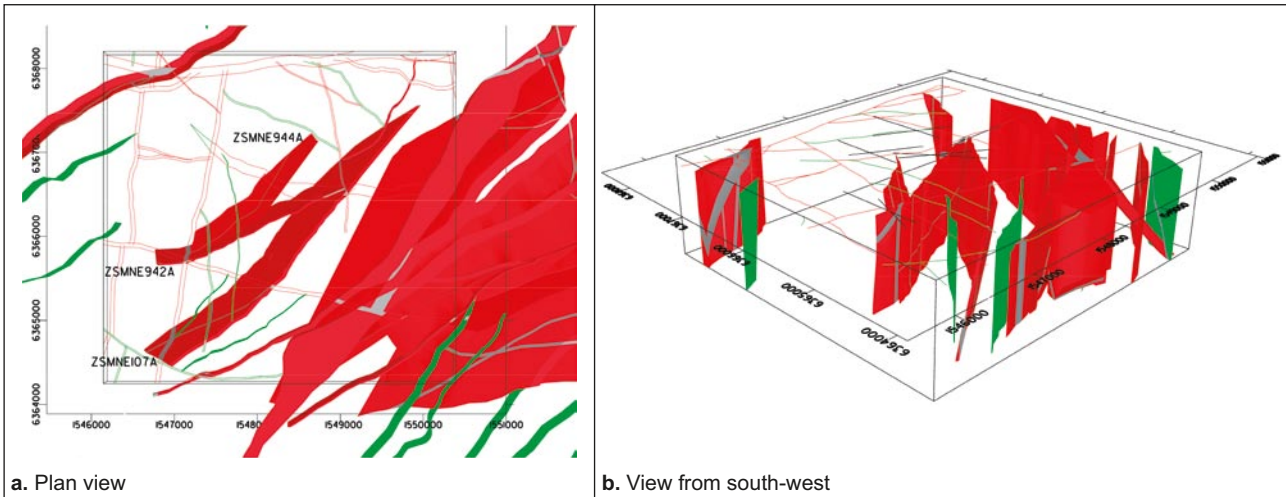


Figure 5-34. All NE-SW striking local major and regional deformation zones that are associated with surface lineaments in the local model area /Wahlgren et al. 2008/.

A summary of all the available fracture orientation data from the three central NE-SW striking deformation zones in Laxemar is presented in Figure 5-35. For comparison the orientation data from fracture domain FSM_NE005 (see Figure 5-57) is shown in Figure 5-36.

Figure 5-35 indicates that the poles are dominated by two sets, one corresponding to a set of vertical fractures parallel to the deformation zones (i.e. striking NE-SW) and a second subhorizontal set. The dominant fracture orientation in the FSM_NE005 fracture domain is more N-S and may reflect the Reidel fracture orientation associated with the main shear belt as well as the selected domain geometry (cf. Section 5.6).

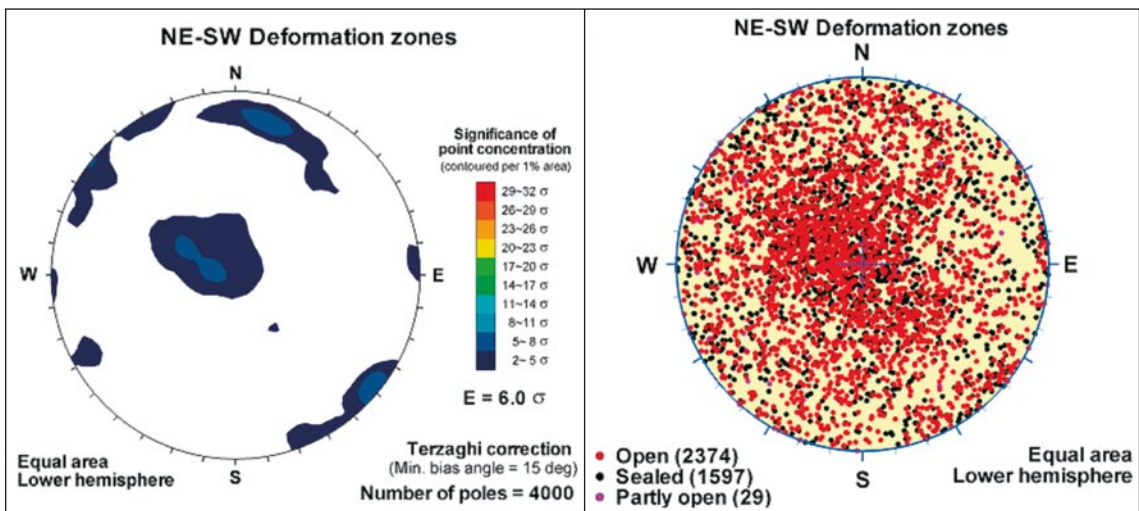


Figure 5-35. Summary of all available fracture orientation data (visible in BIPS) from the three central NE-SW striking deformation zones ZSMNE107A, ZSMNE942A and ZSMNE944A.

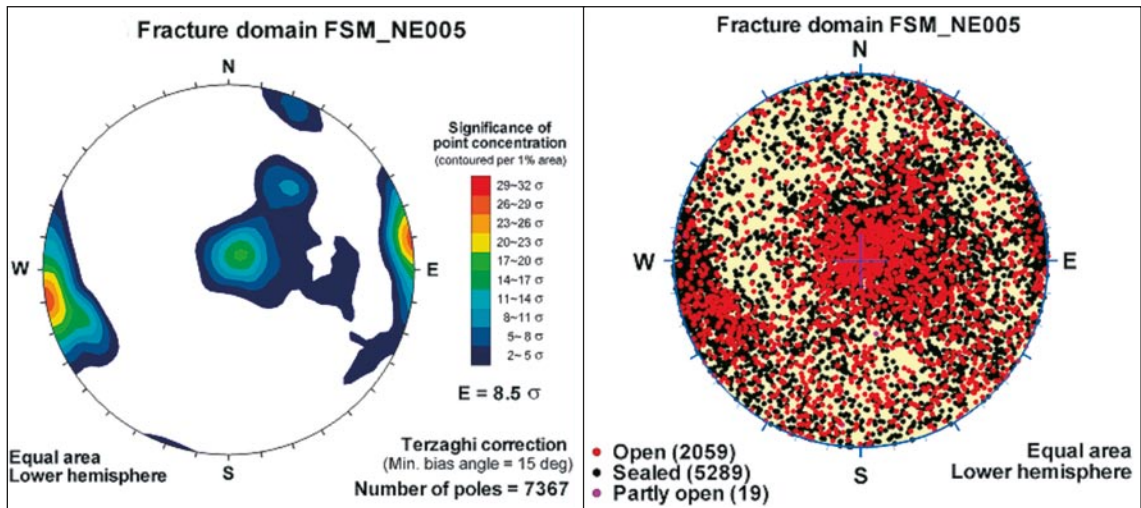


Figure 5-36. Summary of fracture orientation data from fracture domain FSM_NE005.

N–S striking deformation zones, moderate to steeply dipping

The north-south striking local major and regional deformation zones are dominated by ZSMNS001A–E and ZSMNS059A in the local model area (Figure 5-37). Both deformation zones have parallel strikes and dip 80–90° W. Details of these two and the other deformation zones are presented in Appendix 6 and more comprehensively in /Wahlgren et al. 2008/. Generally speaking these two zones and other members of this set of so called N-S striking structures have in fact strikes varying from NNW to NNE. They are steeply dipping with a tendency to dip to the west. However, two members in this group KLX04_DZ6b and KLX04_DZ6c, cf. Table 5-6 and Figure 5-38, are less steeply dipping, although their orientation and associated thickness are judged to be of low confidence. Both are based on a subdivision of an extensive and complex deformation sequence identified in the KLX04 core during the ESHI process. Drilling and outcrop investigations show that these deformation zones have a ductile origin and, similar to the NE-SW striking set, have been subjected to multiple phases of brittle reactivation.

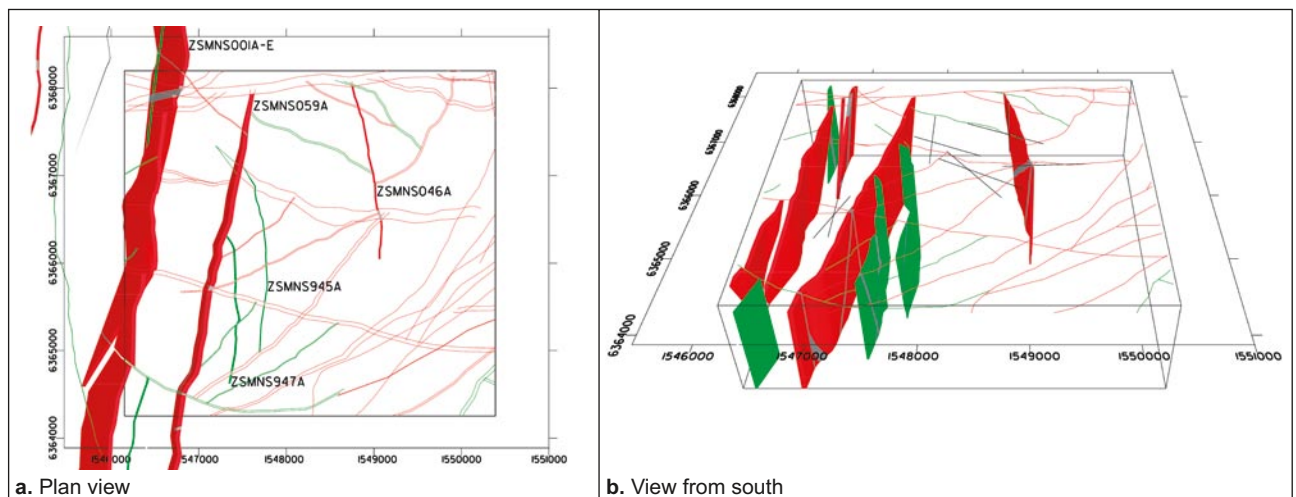


Figure 5-37. The main N-S striking structures encountered in the local model volume /Wahlgren et al. 2008/. All are sub vertical to steeply dipping to the west.

Kinematic studies identify strike-slip, predominantly sinistral displacements, although, in common with the NE-SW striking structures, this sense of movement has likely been reversed at a later stage. With the exception of ZSMNS001A–E and ZSMNS059A these deformation zones are narrow with thicknesses of 10 to 20 m with multiple thin discontinuous highly fractured cores. ZSMNS001A–E and ZSMNS059A are thicker, 45 m and 50 m, respectively. Both deformation zones are associated with highly fractured dolerite dykes that have been intercepted by the cored boreholes although they have not been identified during the surface mapping campaign. The magnetic susceptibility of the dolerites is in general lower than the average susceptibility of the country rock and the higher fracture frequency implies that the fractured dolerites are more susceptible to erosion than the normally fractured country rock. It follows that dolerites, like brittle deformation zones, are likely to be associated with topographic depressions and are unlikely to be clearly exposed at the ground surface. North of the investigated area, in the Götemar granite, dolerite dykes are observed with similar N-S strike directions. The other narrower deformation zones within this orientation set are possibly also associated with dolerite dykes, but in all cases they are likely to be very thin and discontinuous /Triumpf 2007/.

Immediately west of ZSMNS001A–E, the detailed lineament mapping suggests the presence of a series of smaller parallel striking structures with a higher frequency than observed to the east of ZSMNS001A–E.

A summary of all the available fracture orientation data from the three main N-S striking deformation zones in Laxemar is presented in Figure 5-39. For comparison the orientation data from fracture domain FSM_W (see Figure 5-57) are shown in Figure 5-40. It can be seen from Figure 5-39, that there are three pole maxima which correspond to a set of vertical fractures parallel to the deformation zones (i.e. striking NNE-SSW), a rather low density subvertical set at right angles to the deformation zones and a third, gently dipping to the south. It can be seen in Figure 5-40 that the fractures in the rock mass outside the three major deformation zones have a pole concentration striking more directly north-south and may represent a Riedel orientation related to the strike-slip system dominated by these major zones.

Table 5-6. N-S striking deformation zones in the local model volume not correlated with surface lineaments, as presented in Figure 5-38.

Zone ID	Orientation (degrees). Strike/dip, right hand rule	Estimated thickness (m)	Ductile	Brittle	Borehole intercept m.a.s.l.
KLX04_DZ6b	156/67	14		x	-874
KLX04_DZ6c	177/42	30	x	x	-935
KLX07_DZ13	348/65	10	x	x	-612
KLX21B_DZ10-12	192/80	10	x	x	-581

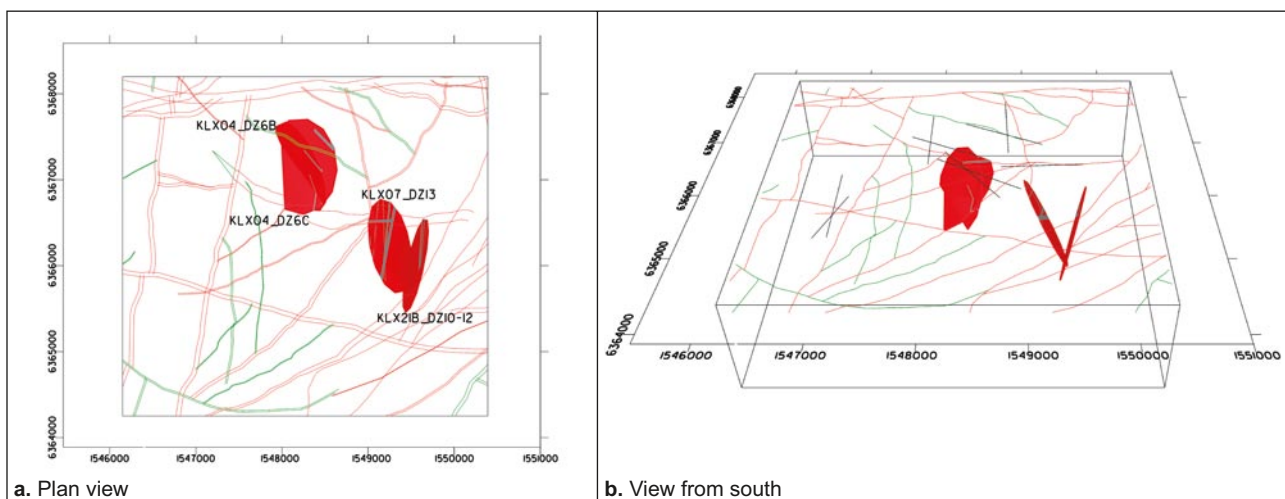


Figure 5-38. N-S striking deformation zones in the local model volume without associated surface lineaments, as listed in Table 5-6 /Wahlgren et al. 2008/.

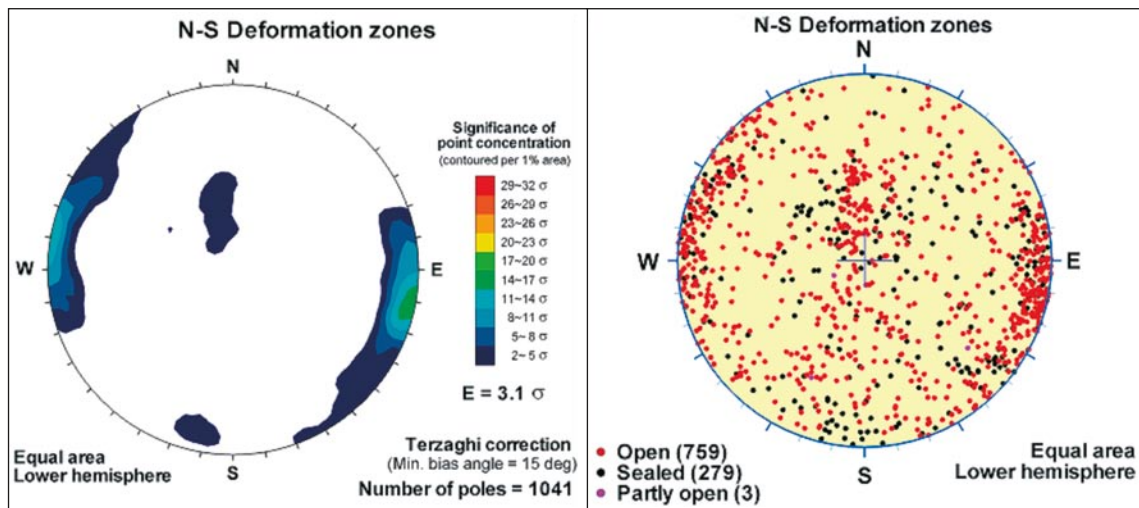


Figure 5-39. Summary of all available fracture orientation data (visible in BIPS) from the three main N-S striking deformation zones ZSMNS001C, ZSMNS046A and ZSMNS059A.

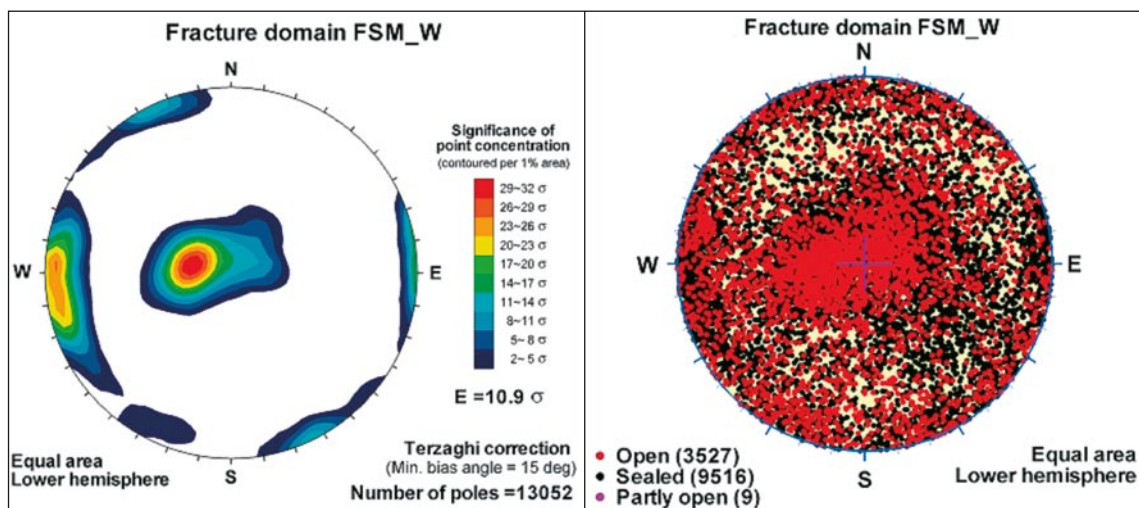


Figure 5-40. Summary of fracture orientation data from fracture domain FSM_W.

E-W and NW-SE striking, steep to moderately southward dipping deformation zones

This set of structures is dominated by ZSMEW002A, ZSMEW120A, ZSMEW900A–B and ZSMNW042A (Figure 5-41). ZSMNW042A is included in this group, which is otherwise dominated by the E-W structures since it has a similar character, size and inferred relationship with the regionally dominant ZSMEW002A.

By far the largest deformation zone in this group is ZSMEW002A (Mederhult zone) which is more or less parallel with the northern boundary of the local model area. This deformation zone has an estimated length of up to 30 km although with a highly variable thickness (20–200 m) as indicated by the regional topographic and geophysical data. This irregular surface expression of the deformation zone is shared by other members of this group, particularly in the case of ZSMNW042A in the south of the local model area. All of the main deformation zones that have been investigated by drilling show an original ductile fabric that has been very heavily overprinted by brittle reactivation. Alteration, dominated by red staining, is also common in this group of deformation zones. Similarly, the main members all dip moderately to steeply (55–65°) to the south. Three members of this group, presented in Table 5-7 and Figure 5-42, have no associated lineaments and have been modelled as discs. Other smaller members of the group have not been the focus of investigations and have been modelled with a vertical dip but are expected to have a similar dominantly brittle character.

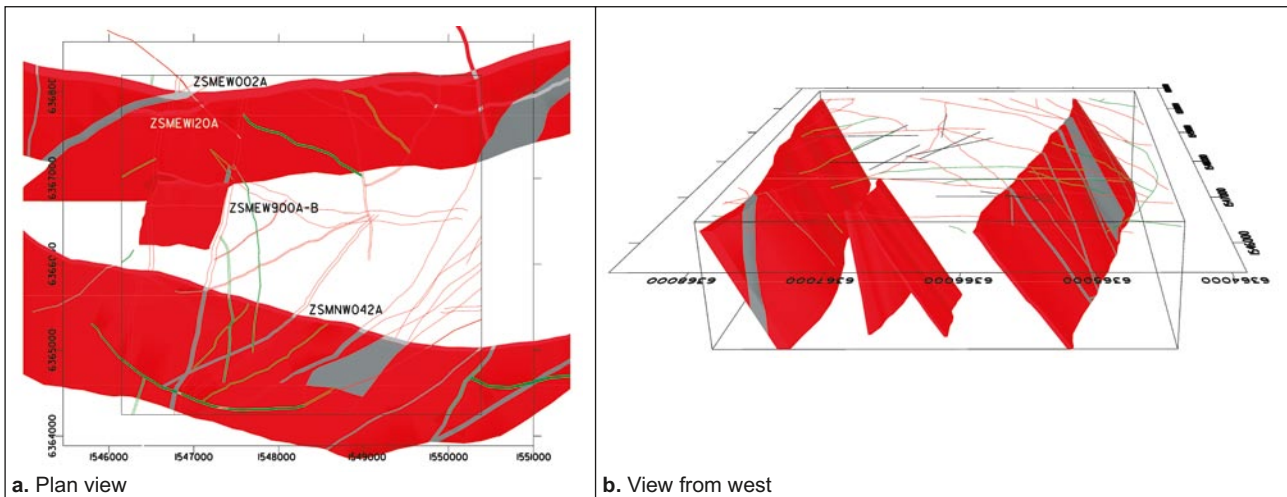


Figure 5-41. The main members of the E-W and NW-SE, steep moderately southward dipping deformation zones /Wahlgren et al. 2008/.

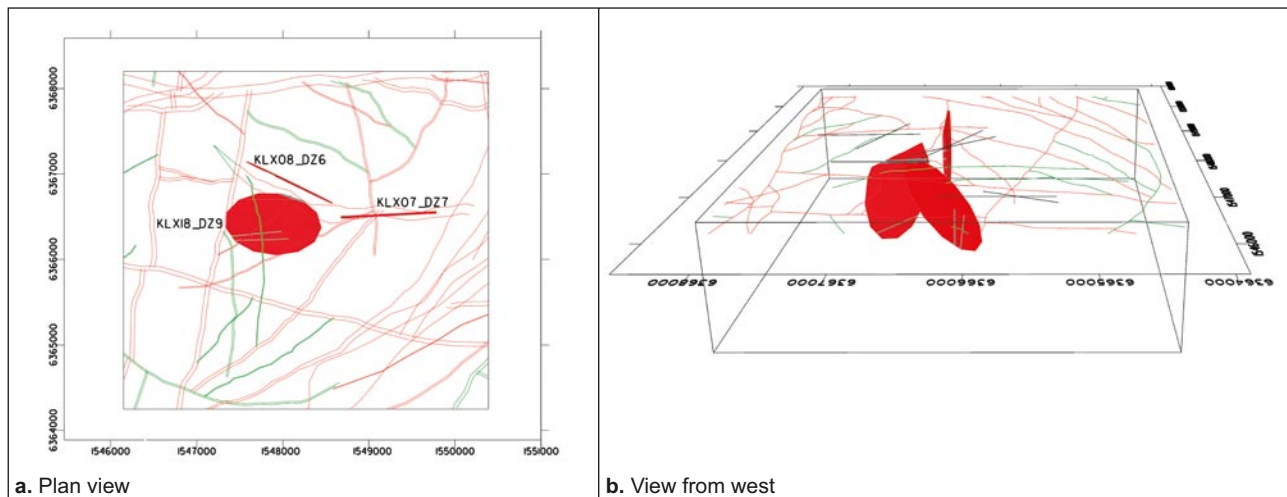


Figure 5-42. E-W, NW-SE, steep to moderately south dipping local major deformation zones in the local model volume without associated surface lineaments, as listed in Table 5-7 /Wahlgren et al. 2008/.

Table 5-7. E-W, NW-SE, steep to moderately south dipping local major and regional deformation zones in the local model volume without associated surface lineaments, as presented in Figure 5-42.

Zone ID	Orientation (degrees). Strike/dip, right hand rule	Estimated thickness (m)	Ductile	Brittle	Borehole intercept m.a.s.l.
KLX07_DZ7	267/90	30	x	x	-265
KLX18_DZ9	095/50	10	x	x	-450
KLX08_DZ6	296/89	10		x	-327

A summary of all the available fracture orientation data from the three main E-W deformation zones with steep southerly to subvertical dips is presented in Figure 5-43. It can be seen from this figure that there are three pole maxima which correspond to a set of vertical fractures sub-parallel to the deformation zones (i.e. striking WNW-ESE), a very weakly developed vertical set orthogonal to the deformation zones and a third, subhorizontal set.

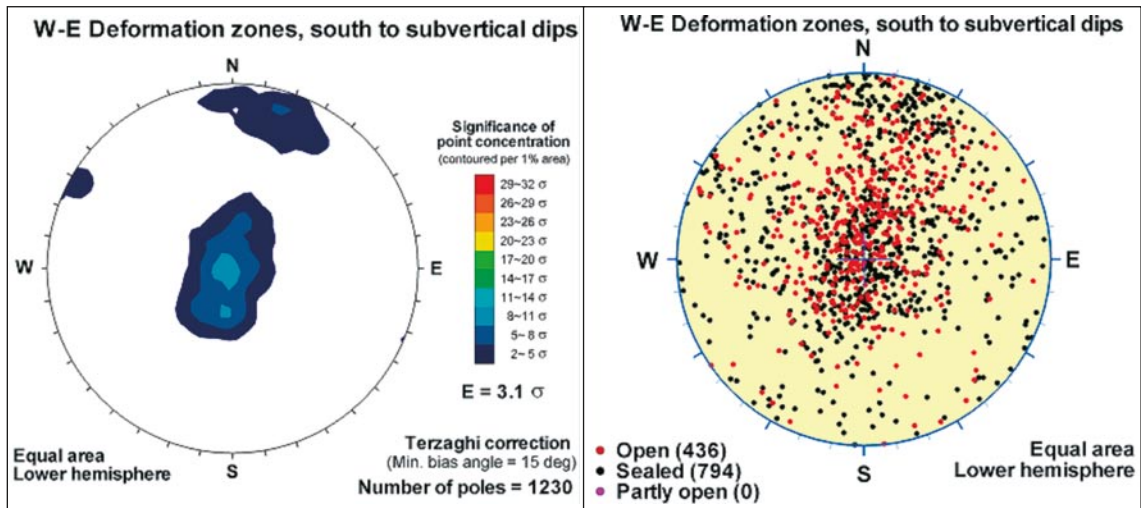


Figure 5-43. Summary of available fracture orientation data (visible in BIPS) from the three main E-W striking southerly to subvertically dipping deformation zones ZSMEW002A, ZSMEW900A/B and ZSMNW042A.

E–W and NW-SE striking, moderately northward dipping deformation zones

For the purposes of the local model description, this group is dominated by a single member, ZSMEW007A–C, Figure 5-44, although seismic reflection surveys and drilling results give evidence of sub-parallel, thinner deformation zones with a similar character at greater depths (Figure 5-45). In common, to a certain extent, with ZSMNW042A the deformation zone has a general east-west alignment that turns and becomes more NW-SE to the west. What singles out this deformation zone from essentially all other deformation zones in the local model volume is that it has a completely brittle origin and character with well developed breccias and characteristic red-green fault gouge locally concentrated in a 60 cm thick clayey core. As for all other deformation zones, a detailed description can be found in /Wahlgren et al. 2008/.

ZSMEW007A shares the wide irregular surface expression of the main deformation zones in the southward dipping E-W, NW-SE group. This surface expression is inferred to be linked to the dip of the zone, thickness variations (it has a mean thickness of 80 m) and complex geometric character. In common with the south dipping group, this deformation zone is strongly associated with alteration dominated by red staining, which, being more susceptible to weathering, may also help explain the topographic expression of the zone. In fact the distribution of red staining seen in the many borehole intercepts has been used as supporting evidence for the interpretation of the overall deformation zone dip. This red staining has been used in a similar fashion when establishing the southerly dip of ZSMNW042A.

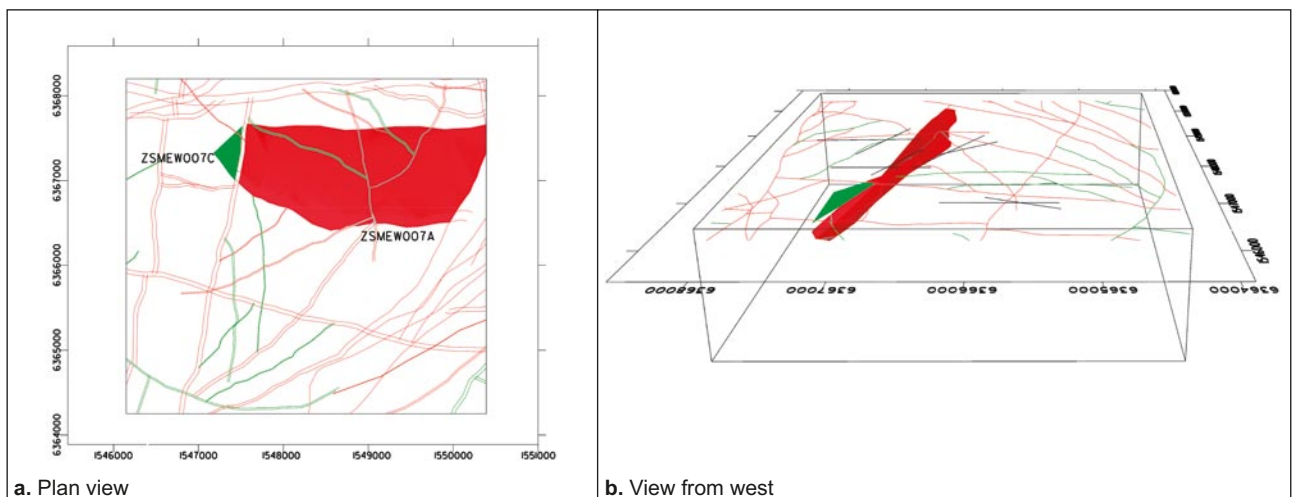


Figure 5-44. ZSMEW007A–C moderately dipping 45° to the north.

Other deformation zones, sub-parallel with ZSMEW007A and with a similar character are listed in Table 5-8 and shown in Figure 5-45. Associations with surface lineaments have not been established for these deformation zones. Surrounding boreholes show a lack of correlation which suggests that these deformation zones, despite their thickness, have a limited lateral extent. It could be argued that other cross-cutting deformation zones could generate offsets but such geometries and implied thicknesses should still be identifiable in the seismic profiling. In addition /Viola and Venvik Ganerød 2007a/ investigated the drill core from parts of KLX07A and proposed significant reductions in deformation zone thicknesses. For the current modelling work an overly conservative approach has possibly been adopted and the interpreted intercepts from ESHI intervals have been retained.

A summary of the available fracture orientation data from the main E-W deformation zones with moderately steep northerly dips is presented in Figure 5-46. For comparison fracture data specific to ZSMEW007A borehole intercepts and the broader fracture domain FSM_EW007 are included in Figure 5-47 and Figure 5-48, respectively.

Table 5-8. E-W to NW-SE striking, moderately northward dipping deformation zones in the local model volume not associated with surface lineaments, as presented in Figure 5-45.

Zone ID	Orientation (degrees). Strike/dip, right hand rule	Estimated thickness (m)	Ductile	Brittle	Borehole intercept m.a.s.l.
KLX07_DZ9	253/35, seismic reflector D /Juhlin et al. 2004/	10	x	x	-329
KLX07_DZ11	253/35, seismic reflector G /Juhlin et al. 2004/	30		x	-535
KLX07_DZ12	263/41	47		x	-548
KLX09_DZ10	263/37	25		x	-500
KLX10C_DZ3	300/35	10	x	x	-28
KLX10C_DZ7	323/39	10	x	x	-91

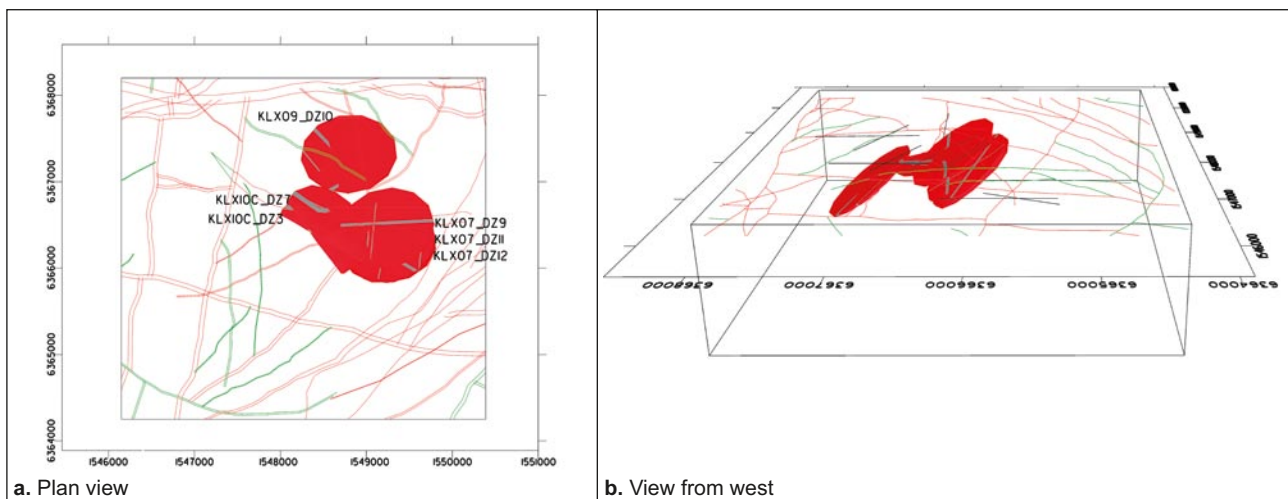


Figure 5-45. E-W, NW-SE, moderately northward dipping local major deformation zones in the local model volume without associated surface lineaments, listed in Table 5-8 /Wahlgren et al. 2008/.

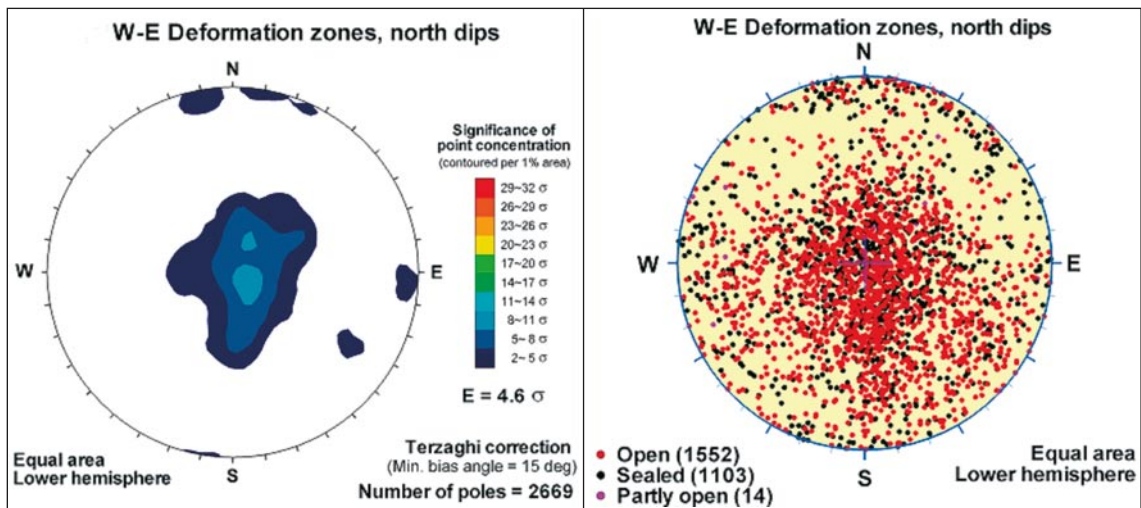


Figure 5-46. Summary of available fracture orientation data (visible in BIPS) from the main E-W and NW-SE striking, northerly dipping, deformation zones ZSMEW007A, KLX07A_DZ9, KLX07A_DZ11, KLX07A_DZ12 and KLX09_DZ10.

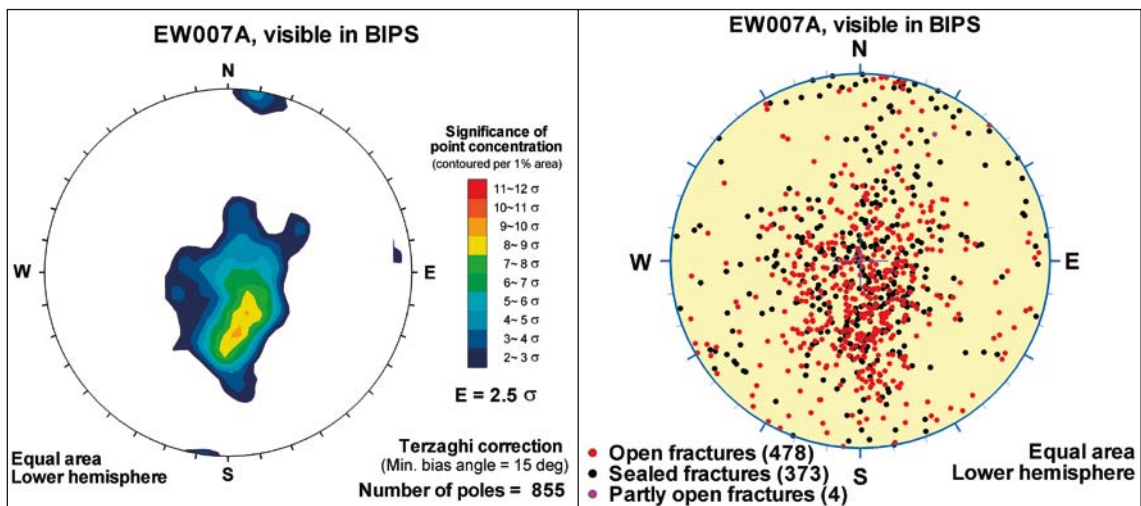


Figure 5-47. Summary of available fracture orientation data (visible in BIPS) from ZSMEW007A borehole intercepts.

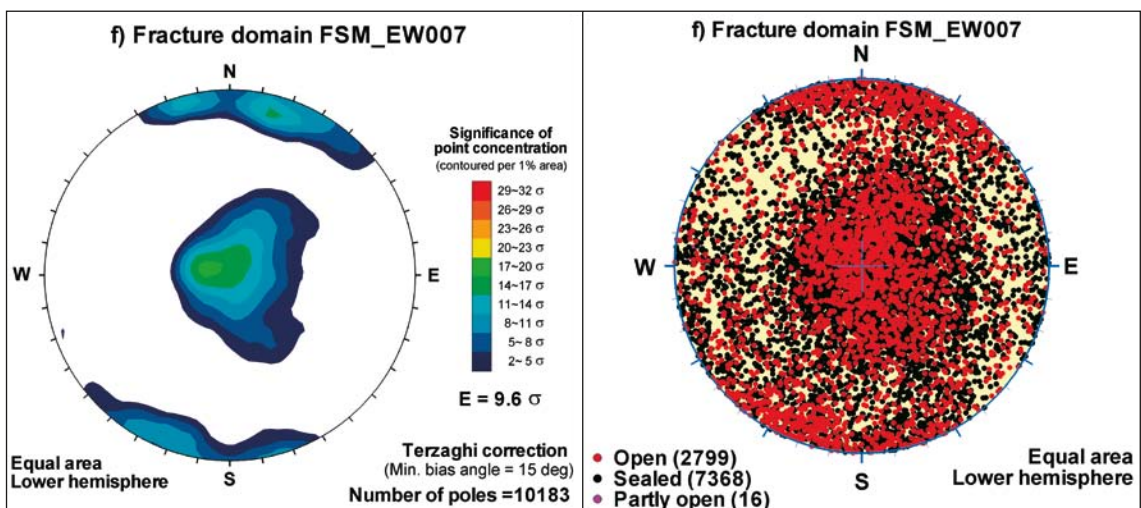


Figure 5-48. Summary of available fracture orientation data from fracture domain FSM_EW007.

Gently dipping deformation zones

It is not straightforward to identify the lateral extent of this type of deformation zone since often they do not have clearly identifiable outcrops. In addition, if such deformation zones are segmented and subsequently offset by movements along steeply dipping deformation zones, which is considered highly likely, the interpretation and estimation of their effective extents and ‘size’ is extremely difficult. It is noteworthy that although the Äspö HRL, CLAB and OKG underground facilities lie to the east of the regional Äspö shear zone, in a slightly different tectonic regime, no major gently dipping deformation zone was identified throughout the entire underground development at Äspö HRL, including the spiral, access ramp and shafts extending down to c. –450 m. However, gently dipping deformation zones are interpreted to occur in Laxemar but their sizes are judged to be small, extending from around the lower range of what is termed Local Major deformation zones (lower limit length of 1,000 m) to the MDZ size range (<1,000 m). Furthermore, no gently dipping local major or larger deformation zones were identified to outcrop in the Laxemar local model area.

The most suitable investigation method for the identification of extensive gently dipping deformation zones is seismic reflection surveying. The two main members in this group, ZSMEW946A and ZSMNW928A (Figure 5-49), are largely based on the results from such seismic reflection survey work /Juhlin et al. 2004/. The two underlying reflectors and their modelled geometries should in this context be taken to represent the upper boundaries of much thicker poorly defined and discontinuous series of smaller, gently dipping, thin, brittle deformation zones and mafic intrusions. Details on their interpretation are presented in /Wahlgren et al. 2008/ and other group members are listed in Table 5-9. Deformation zone ZSMNW928A is retained as being of medium confidence even though it has interpreted borehole intercepts, since its overall interpreted geometry is associated with uncertainty due to the difficulty of its interpretation. A review of the original interpretation of the seismic survey data /Wahlgren et al. 2008/, along with later available borehole data, lead to a reinterpretation of the reflector geometry with an uncertain correlation with borehole data. However, both the presented interpretation and an alternative interpreted orientation result in a structure that is located significantly below the depth of the potential storage volume /Wahlgren et al. 2008/.

Deformation zone ZSMEW946A, reflector M1, is more problematic since its modelled geometry cuts through the volume of interest at repository depth. Details of its character can be found in Appendix 6 and in /Wahlgren et al. 2008/. As stated above, the presented geometry of the zone marks the upper limit of what is judged to be a thicker discontinuous series of deformation zones and mafic intrusions rather than a single individual structure. The orientation of fine-grained diorite-gabbro in the associated rock domain is presented in Figure 5-50. As can be seen the mapped orientations of rock type boundaries are in general similar to the M1 reflector orientation.

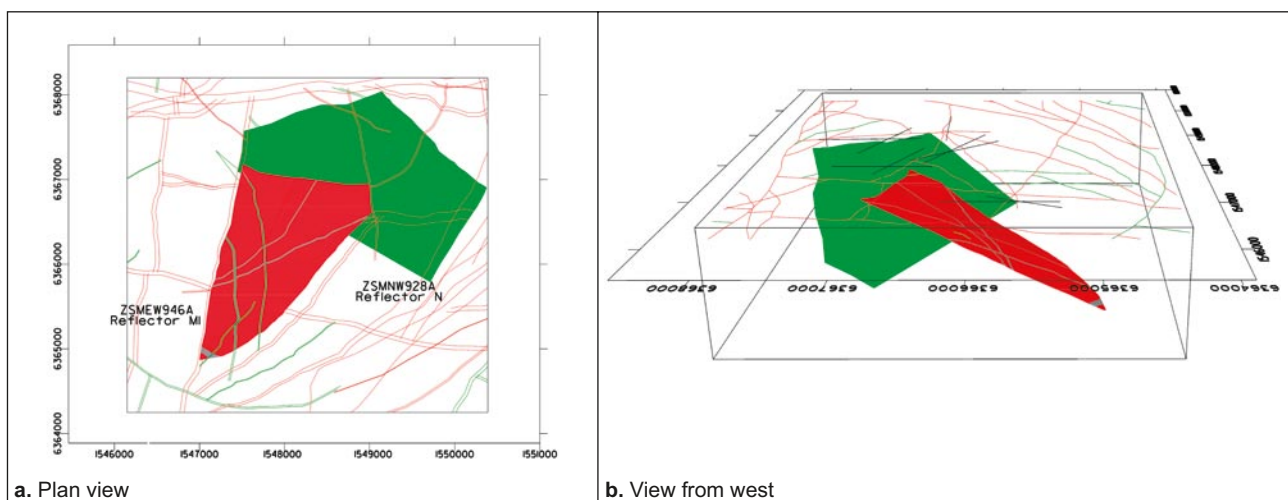


Figure 5-49. Gently dipping deformation zones ZSMEW946A (080/23°) and ZSMNW928A (120/28°) /Wahlgren et al. 2008/.

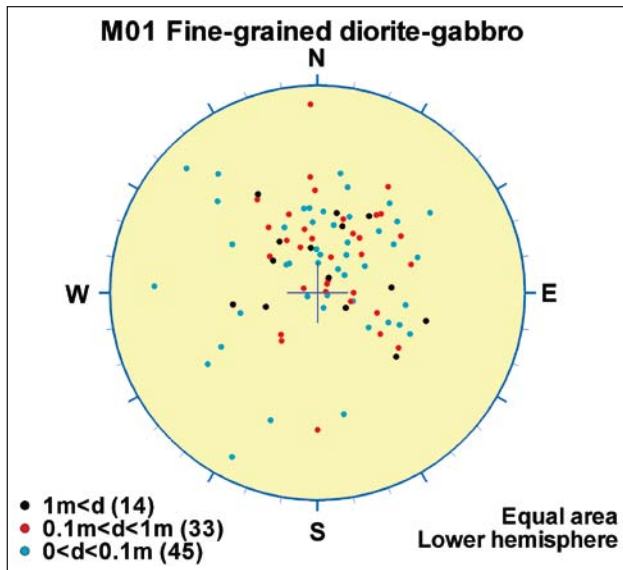


Figure 5-50. Mapped orientations of the fine-grained diorite-gabbro contacts as measured in all drill cores in RSMM01. The general orientation is similar to the M1 reflector series.

Additional members of this group, listed in Table 5-9, include KLX11_DZ11. This deformation zone lacks correlation with a ground surface lineament (Figure 5-51). Similar to other such deformation zones modelled in this manner it is modelled as a circular disc with a radius of 564 m, equivalent to an area of 1,000 m by 1,000 m square, and an attributed best estimate of true thickness, in this case 20 m. The modelled geometry is centred at an elevation of -439 m. Given that the elevation and orientation are similar to the M1 reflector geometry implies that KLX11_DZ11 can be taken as a potential member of this series. The deformation zone is brittle with markedly open fractures.

An additional seven discrete deformation zones without associated surface lineaments, with interpreted thicknesses of 10 m or more, are modelled as circular discs. These structures have been rated as having high confidence as to existence since they are all based on direct cored borehole evidence. However, essentially all their other assigned properties are generally judged to be of low confidence since the underlying individual judgement of orientation is of low confidence. This reflects the fact that dip directions in all directions have been observed, even though dips to the south and south east dominate. A summary of the available fracture orientation data from the gently dipping deformation zones listed in Table 5-9 is presented in Figure 5-52.

Table 5-9. Gently dipping local major deformation zones without associated surface lineaments, as presented in Figure 5-51.

	Orientation (degrees). Strike/dip, right hand rule	Estimated thickness (m)	Ductile	Brittle	Borehole intercept m.a.s.l.
KLX07_DZ10	225/28	10		x	-473
KLX08_DZ10	079/11	11		x	-770
KLX08_DZ1	000/18	27		x	-63
KLX09F_DZ1	178/19	14		x	+13
KLX03_DZ1b	121/21	10		x	-731
KLX03_DZ1c	125/13	10		x	-757
KLX09E_DZ2	295/14	22	x	x	-67
KLX11_DZ11	065/20	20		x	-439

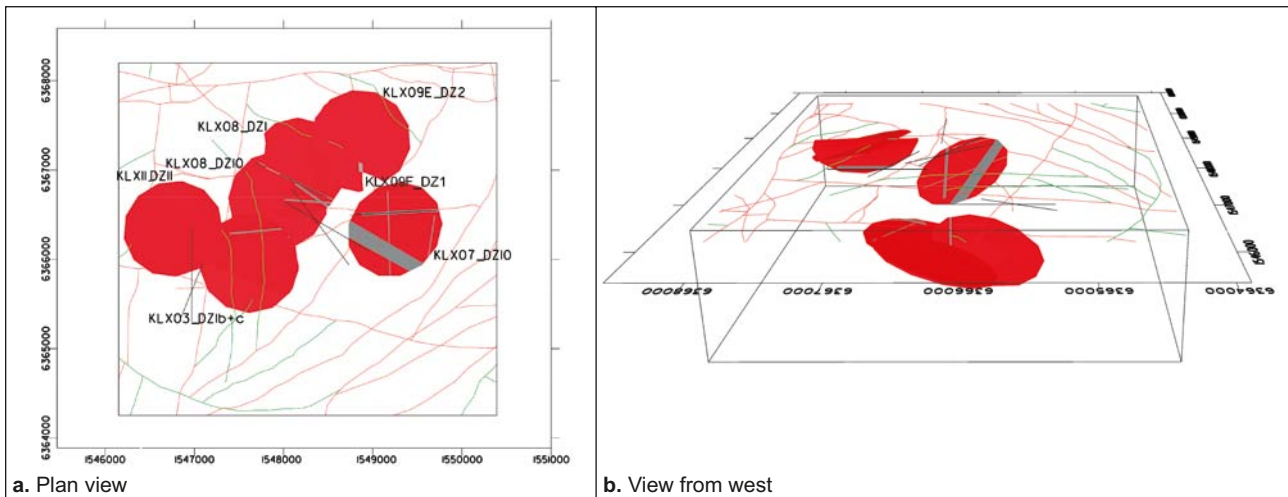


Figure 5-51. Gently dipping local major deformation zones not linked to surface lineaments, listed in Table 5-9 /Wahlgren et al. 2008/.

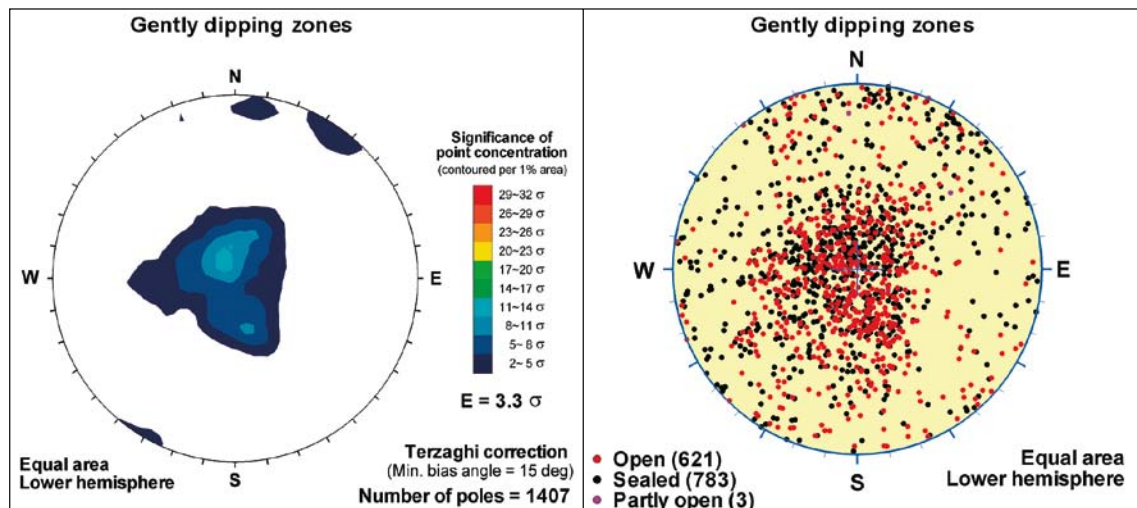


Figure 5-52. Summary of available fracture orientation data (visible in BIPS) from Gently dipping local major deformation zones KLX03_DZ1b, KLX03_DZ1c, KLX07A_DZ10, KLX08_DZ10, KLX08_DZ01, KLX09E_DZ2, KLX09F_DZ1, KLX11_DZ11.

5.5.5 Geometric model

As an aid to a better understand the modelled deformation zone geometries, a series of sections through the deterministic deformation zone model are presented in Figure 5-53, Figure 5-54 and Figure 5-55.

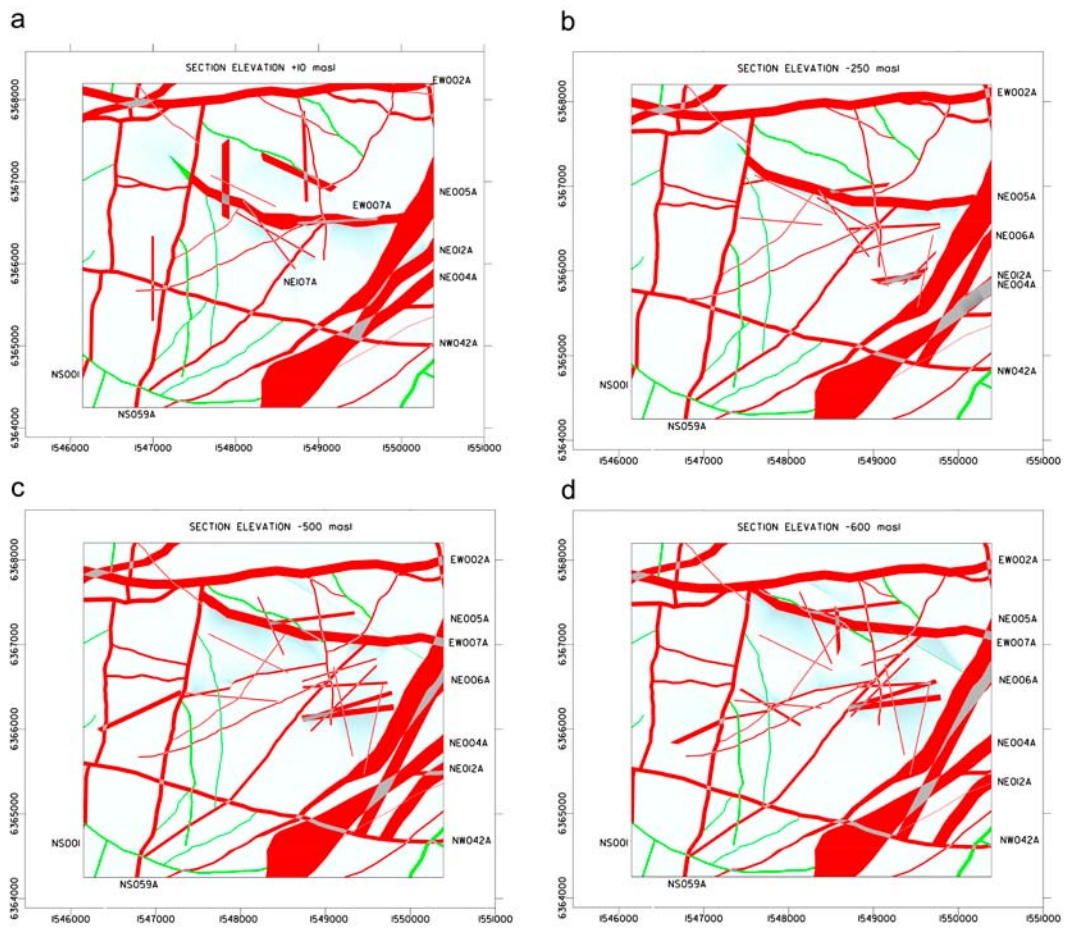


Figure 5-53. Horizontal sections through the local scale deformation zone model /Wahlgren et al. 2008/.
 a) Section elevation +10 m. b) Section elevation -250 m. c) Section elevation -500 m. d) Section elevation -600 m.

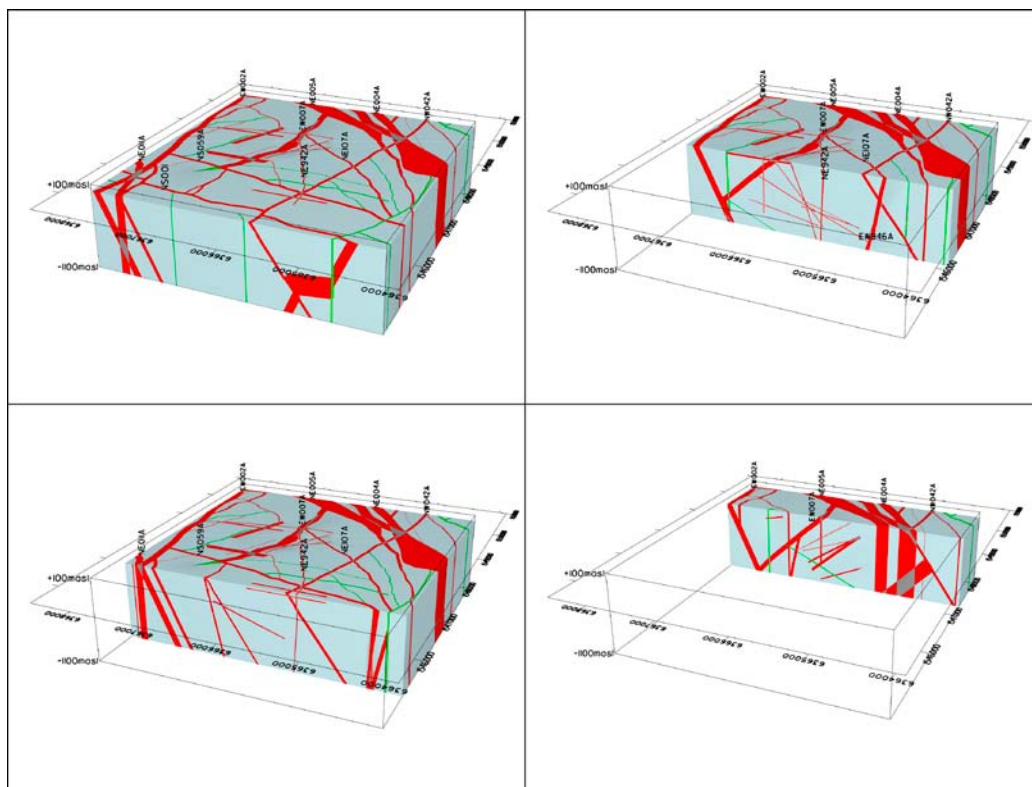


Figure 5-54. N-S sections, progressing eastwards through the local scale deformation zone model /Wahlgren et al. 2008/.

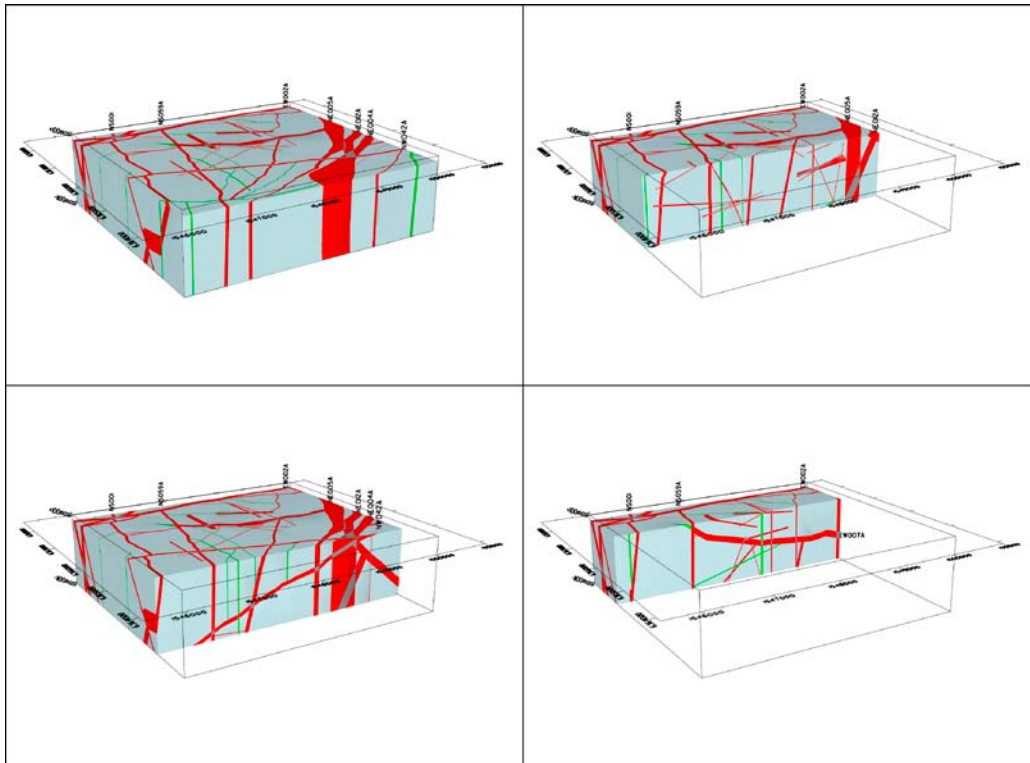


Figure 5-55. E-W sections, progressing northwards through the local scale deformation zone model /Wahlgren et al. 2008/.

5.6 Statistical model for fractures and minor deformation zones

The statistical model for fractures and minor deformation zones, hereafter referred to as the geological discrete-fracture network (DFN) model, is designed to describe rock fractures and minor deformation zones with an equivalent radius less than 564.2 metres (equal to the area created by a square fracture with a trace length of 1,000 m).

This section constitutes a summary of the results of the geological DFN modelling work undertaken during SDM-Site Laxemar. For a detailed description of the methodology, mathematical implementation, validation, and uncertainty surrounding the geological DFN, cf. /La Pointe et al. 2008/.

5.6.1 Division into fracture domains

Model version SDM-Site Laxemar represents a change in DFN modelling methodology compared with past site-descriptive models developed for Laxemar; fracturing is now described in terms of fracture domains instead of rock domains or specific lithologies. Fracture domains (abbreviated FSM throughout this section) provide a large-scale conceptual framework for describing spatial heterogeneity in rock fracturing. The goal behind identifying fracture domains is to find rock volumes with fracture characteristics such that the variability between volumes is larger than the variability within volumes /after Munier et al. 2003/, in line with standard geologic practice. As such, fracture domains should form the basic divisions over which spatial heterogeneity in rock fracturing is characterised; these domains may not necessarily correspond to the limits of other geologically-significant volumes such as those defined in the Rock Domain (RD) model (Section 5.4).

In Laxemar, the fracture orientation set definitions do not appear to change significantly across the local model domain. Rather, the relative intensity of fracture sets and the locations of deformation zones (Section 5.5) are used to delineate domains showing similar fracture intensity trends. Preliminary fracture domains were evaluated against the deformation zone model to make sure that the domains themselves were consistent with the current understanding of the geologic and tectonic history of Laxemar.

Fracture domains were identified and bounded using:

- a. The orientation and intensity of fractures by type: only sealed fractures, only open fractures, and all fractures combined;
- b. The orientation and intensity of regional and local scale lineaments derived from airborne laser mapping (Lidar) and high-resolution ground geophysics, as well as the deformation zones identified in the Laxemar local model area by the SDM-Site Laxemar deformation zone model (Section 5.5).

Fracture domains were identified by first examining fracture orientation data from boreholes, outcrops, and trenches for spatial trends in orientation and the relative intensity of pole clusters on contoured stereonet plots (Figure 5-56). Tentative fracture domains were hypothesised by combining observed intensity patterns with potential volume boundaries (regional and local deformation zones from the deformation zone model) and an understanding of the deformation history and tectonics in the Laxemar-Simpevarp region. The finalisation of the fracture domains occurs simultaneously with the fracture orientation analysis; the relative intensities of the fracture sets that are defined are used to finalise the fracture domain criteria.

The suitability of fracture domains as the primary framework for describing fracturing outside of deformation zones in Laxemar was evaluated through statistical analysis during geological DFN modelling /see La Pointe et al. 2008, cf. Section 4.4.4 therein/. Cross-tabulation and non-parametric ANOVA (Kruskal-Wallis) was used to test whether the variability in fracture intensity (P_{32}) was best captured as a function of lithology, rock domain, or fracture domain. The results indicated that, although there is a correlation between lithology and fracture intensity, the correlation between fracture domain and fracture intensity is much stronger. Intuitively, this makes quite a bit of sense; the fracture domains represent volumes of rock within which the character of brittle deformation has been strongly influenced by the strains imposed by stress along the deformation zones that make up the domain boundaries.

Six distinct fracture domains were identified in Laxemar within the local model volume (Figure 5-57). Their distinguishing properties are discussed later in this section. The full process of the identification of fracture domains, including the assignment of fractures to orientation sets and the treatment of relative set intensities, is described in detail in the SDM-Site Laxemar geological DFN report /La Pointe et al. 2008/.

The identified fracture domains in the cored boreholes of the focused volume in Laxemar are presented in Appendix 5.

Fracture domain FSM_EW007

This domain represents a volume of rock, approximately 250 m thick on the south side and 100 m thick on the north side of deformation zone ZSMEW007A, in which distinct fracture patterns were observed in cored borehole records. This domain features a reduced intensity of both N-S striking fractures and open subhorizontally dipping fractures (Figure 5-56). In this domain, most open fractures appear to strike in a WNW direction. Both fracture intensity and orientation have been interpreted as being affected by the E-W striking deformation zone ZSMEW007A. FSM_EW007 terminates against deformation zone ZSMNE005 in the east, and is assumed to terminate against zone ZSMNS059A in the west. The western termination is based on the increase in N-S striking fractures west of ZSMNS059A, as well as the dying-out of zone ZSMEW007A into a shorter structure of lower confidence.

Fracture domain FSM_NE005

This domain represents a volume of rock west of regional deformation zone ZSMNE005. This deformation zone represents one of several major belts of NE-SW trending ductile deformation that appear to have resulted from major crustal shortening in the Laxemar-Simpevarp region during the waning stages of the Svecokarelian orogeny. These ductile belts form the tectonic backbone of the Laxemar-Simpevarp region. Domain FSM_NE005 is characterised by a significant increase in the relative intensity of NS striking sealed fractures, relative to the rest of the Laxemar local model area (Figure 5-56). It is possible that the increased intensity of N-S striking fractures

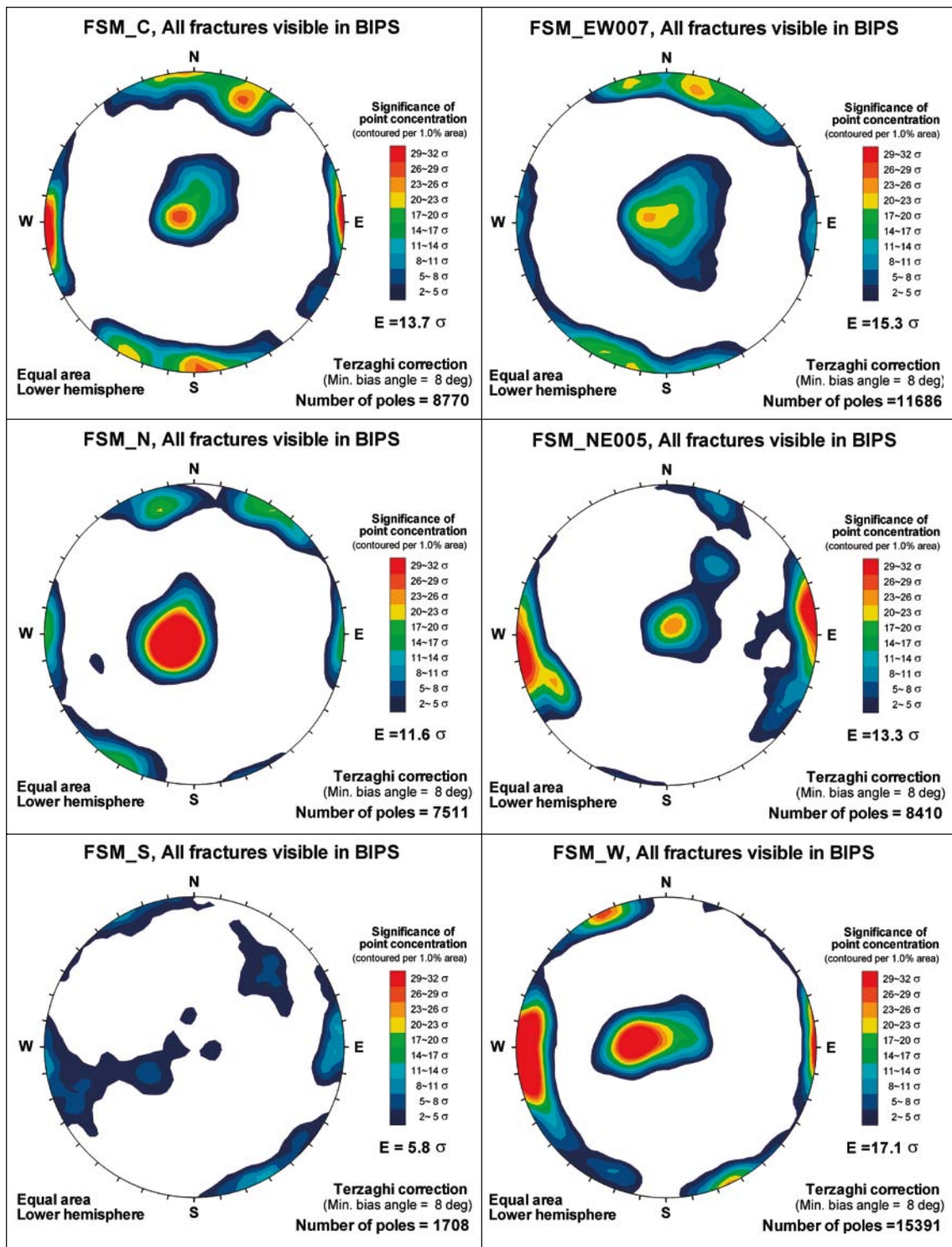


Figure 5-56. Kamb-contoured stereoplots illustrating all fractures visible in BIPS image logs from cored boreholes in different fracture domains. All plots are Terzaghi-weighted to compensate for sampling orientation bias.

represents brittle reactivation of shear structures originally formed in the ductile regime during N-S crustal shortening. FSM_NE005 is terminated against zone ZSMNE005A in the east, against zone ZSMNE107A in the west, (based on the patterns of fractures observed in boreholes on the west side of zone ZSMNE107A), and against zone ZSMNW042A in the south. The southern termination of FSM_NE005 is the most uncertain, due primarily to a paucity of data south of ZSMNW042A. The current geometry of FSM_NE005 is that it makes up the footwall of ZSMNW042A.

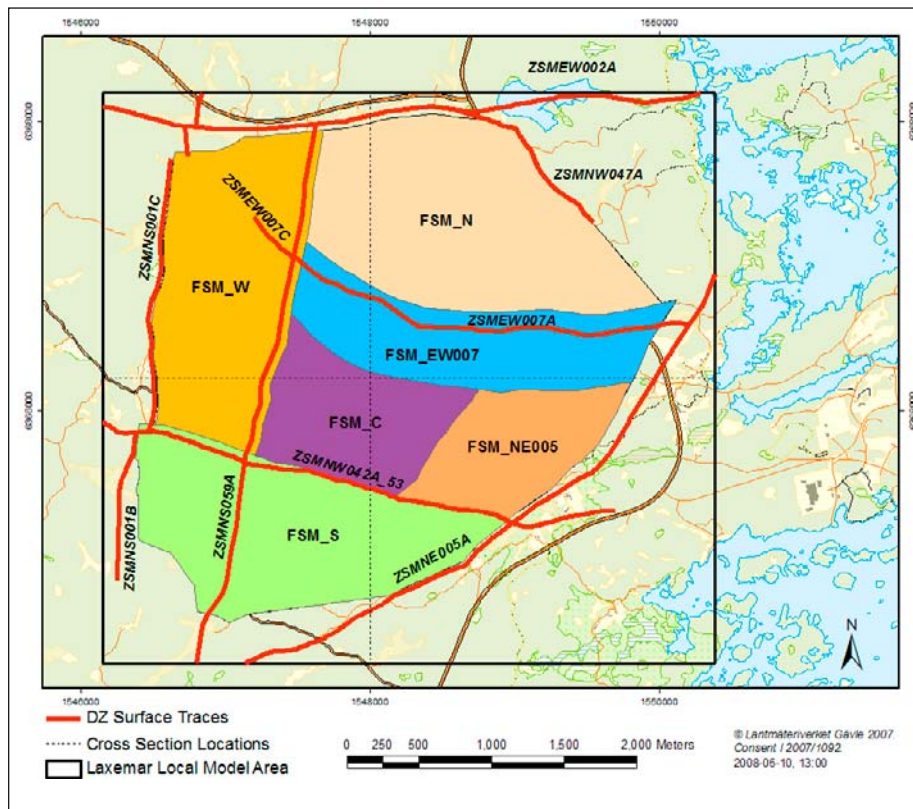


Figure 5-57. Surface projection of SDM-Site Laxemar fracture domains and bounding deformation zones in Laxemar (from /La Pointe et al. 2008/). The black box represents the limits of the Laxemar local model, while the colored polygons represent the surface limits of the fracture domains.

Fracture domain FSM_W

This domain represents the volume of rock between zones ZSMNS001C, ZSMNS059A, ZSMNW042A, and south of ZSMEW002A. Borehole data west of zone ZSMNS059A suggest dominant north-south fracture strikes. This dominance of north-south strike is noted in both subvertically and subhorizontally dipping fractures (Figure 5-56). Fractures that strike ENE and roughly parallel the NE-SW striking sinistral shear zones that make up the tectonic fabric of the Laxemar-Simpevarp region, are relatively subdued in intensity when compared with the rest of the Laxemar local model volume. This finding (largely from borehole data) is in agreement with surface kinematic investigation results /Viola and Venvik Ganerød 2007b/. Again, this domain fundamentally represents a crustal block isolated by the major ENE and N-S sinistral tectonic structures.

Fracture domain FSM_C

This domain represents a volume of rock south of FSM_EW007, north of zone ZSMNW042A, and bounded by zone ZSMNS059A on its western edge and ZSMNE107A and FSM_NE005 on its eastern edge. This fracture domain is dominated by sealed NS striking fractures in a fashion similar to FSM_W, and open WNW striking fractures (Figure 5-56). It is likely that the open WNW-striking fractures represent either primary fracturing (tension gashes) or brittle reactivation of older fractures in extension due to inferred NW-SE compression during the Caledonian orogeny and the present day. This may also explain the prevalence of NS striking sealed fractures (in compression for ~ 400 Ma).

Fracture domain FSM_N

This domain represents a volume of rock north of domain FSM_EW007 and east of ZSMNS059A. This fracture domain is dominated by subhorizontal fractures, but lacks the dominant open WNW fractures observed in FSM_C (Figure 5-56). The domain is bounded in the north by zones ZSMEW002A and ZSMNW047A.

Fracture domain FSM_S

This domain represents the rock volume south of zone ZSMNW042A (i.e. the hanging wall of the zone which dips to the south). The definition of this rock volume as a separate fracture domain is highly uncertain due to the lack of data from this volume of rock; the cored borehole KLX16A represents the only fracture data south of ZSMNW042A. In addition, the data from KLX16A is believed to have been strongly influenced by the adjacent zone ZSMNE107A. In this domain, the ENE and N-S to NNE striking fractures dominate (Figure 5-56), and there is a relative paucity of subhorizontal fractures compared with other fracture domains. If one regards zone ZSMNS059A (and the associated rock block representing FSM_W) as a restraint on the western edge of this domain, then the fracture pattern could be explained as Riedel shears (NS set) combined with the brittle reactivation along NE-SW striking shear zones (ENE set) parallel to the dominant regional tectonic fabric.

5.6.2 Modelling assumptions and data treatment

Orientation and intensity data from cored boreholes KLX06 and KLX09B have been excluded from the fracture set orientation modelling; these holes possess a total average uncertainty (Ω) greater than 10° . This exclusion is per the recommendations of the orientation uncertainty report /Munier and Stigsson 2007/. Also, data from cored boreholes KLX02 and KLX20A that are outside of the modelled fracture domains are excluded from the geological DFN modelling process.

The key assumptions required to generate the SDM-Site Laxemar GeoDFN model are as follows:

- Deterministic deformation zones constitute a distinct population of fractures different from the “background” fractures and minor deformation zones (MDZ). Therefore, the mathematical model for the background fractures and MDZ is a distinct model from the model describing the deformation zones;
- The length of a minor deformation zone trace or a linked fracture trace in outcrop is an accurate and appropriate measure of a single fracture’s trace length for the purpose of deriving the radius distribution of geologic structures;
- In past SDM at both Forsmark and Laxemar, the surface traces of deformation zones (DZ) longer than 1,000 m have been combined with outcrop fractures and lineaments from high-resolution geophysics and laser swath mapping in the 100 m – 1000 m range to calculate the fracture radius scaling exponent (k_r). This conceptual model has been colloquially termed the “tectonic continuum” in past reports. For SDM-Site Laxemar, the fracture size model is based solely on outcrop fractures and lineaments shorter than 1,000 m (surface traces of minor deformation zones, see /Wahlgren et al. 2008, cf. Section 3.12 therein/); deformation zone traces larger than 1,000 m were not included in the size model parameterisation (see /La Pointe et al. 2008, cf. Sections 3.1.3 and 3.4 therein/). This methodological change was made due to the desire to limit the range of fracture sizes modelled by the geological DFN (up to a maximum radius of 564.2 metres); it was viewed as inconsistent to include data from larger sizes;
- For purposes of modelling size (in terms of surface area), fractures can be approximated as planar, circular discs of zero thickness with a radius that can be described using a probability distribution. The actual fracture shape is not required to be circular; square, rectangular, or polyhedral-shaped fractures are fully acceptable, as long as they are simulated using a one-sided surface area which is equivalent to that of a disc of equal size;
- The geological DFN parameterisation uses a global orientation model that represents the average orientation of sets over all the fracture domains. The inherent assumption, which has been tested and is described in detail in the geological DFN summary report /La Pointe et al. 2008/ is that in Laxemar fracture domains principally differ, not in terms of fracture set orientations, but in terms of relative intensities of the identified orientation sets.

5.6.3 Derivation of statistical fracture model

The geological DFN model for SDM-Site Laxemar is composed of four distinct sub-models: the fracture domain model (previously discussed in Section 5.6.1), the fracture orientation model, the coupled fracture size/fracture intensity model, and the fracture spatial model. The mathematical and statistical derivations of these sub-models are described in detail in /La Pointe et al. 2008/; this section only presents a summary of the final model results.

DFN orientation model

Fracture orientation set modelling consists of the identification and parameterisation of fractures into sets as a function of their orientation in space (pole trend and plunge or dip and dip direction) and possibly of other geological factors. Though orientation is the primary key for classification, other parameters, such as lithology, fracture morphology, aperture, and fracture mineralogy can also be used to divide fractures into sets if they are found to possess statistically significant differences across the data record. The variability in orientation for each fracture set is defined using univariate Fisher hemispherical probability distributions /Fisher 1953/, and is expressed as a fracture set mean pole vector (trend, plunge), with an associated concentration parameter κ representing the dispersion of fracture poles around the mean pole vector, cf. Table 5-10.

DFN coupled size-intensity model

This sub-model describes the size of fractures, expressed as an equivalent radius r and the intensity, in terms of fracture area per unit volume (P_{32}), of the fractures observed in cored borehole records and on outcrops in Laxemar. Past modelling work, both at Forsmark /Fox et al. 2007/ and Laxemar /La Pointe and Hermanson 2006/ has suggested that fracture sizes are best characterised by a power law (Pareto distribution). The power law distribution is defined in terms of a size-scaling exponent (k_r , the distribution shape parameter) and a fracture minimum size (r_0 , the distribution location parameter) /Munier 2004, La Pointe et al. 2008/ All size-intensity model alternatives presented in the SDM-Site Laxemar geological DFN assume a power-law distribution for fracture radii; alternative distributions (lognormal, exponential) were not tested.

For the geological DFN, the coupled size-intensity modelling is based upon the volumetric fracture intensity (P_{32}), as derived from lineal fracture intensity (P_{10}) recorded in cored boreholes. Areal fracture intensity (P_{21}), as computed from the analysis of fracture traces mapped on detailed outcrops across the Laxemar local model area /Hermanson et al. 2008/, is used in conjunction with P_{32} values from boreholes to simultaneously match fracture size and intensity distributions to both outcrop and borehole data, so as to provide a model that is consistent at observational scales. Outcrop and lineament trace data are used to define the fracture radius scaling exponent (k_r), while the ratio of borehole fracture intensity to outcrop fracture intensity (P_{32OC} : the P_{32} necessary to reproduce the observed outcrop P_{21}) is used to calculate the minimum fracture size (r_0) /La Pointe et al. 2008/.

P_{32} is calculated analytically from P_{10} values observed in boreholes using a solution derived from stereological relationships between fracture orientation and fracture intensity /Wang 2005/. P_{32} is linearly related to P_{10} through the Wang conversion factor (C_{13}) for univariate Fisher orientation distributions which accounts for orientation bias due to linear sampling in a fashion similar to that of the classic Terzaghi correction. P_{32} values were computed on a set-by-set basis for each fracture domain using the global fracture set orientation definitions. The mathematical details of Wang's C_{13} are presented in /La Pointe et al. 2008, cf. Section 3.8.1 therein/. The arithmetic mean P_{32} value in a given fracture domain is used to determine matches between model parameters and observed fracture intensities.

Fracture size and fracture intensity, although separate properties, are mathematically related, since the value of intensity measured from geologic data always pertains to a specified size range. Thus, it is appropriate to combine the size and intensity models into one single sub-model. With a power-law model for fracture sizes, changes in observed fracture intensity can change the estimation of the size distribution parameters. Correspondingly, a change in the size parameters (k_r , r_0) will result in

Table 5-10. Global (across all fracture domains) orientation sets, SDM-Site Laxemar geological DFN model.

Fracture Set	Mean Pole		Fisher κ
	Trend (°)	Plunge (°)	
SH	335.10	87.10	7.20
ENE	340.30	0.50	9.90
WNW	24.10	3.10	7.50
N-S	269.10	1.70	7.30

a change of the intensity of fractures within a given size range; for example, increasing the value of the radius scaling exponent (k_r) while keeping the fracture intensity P_{32} and the size distribution minimum radius (r_0) the same will result in an increase in the intensity of smaller fractures and a corresponding decrease in the intensity of the larger fractures.

There are 29 different size-intensity model alternatives detailed in the SDM-Site Laxemar geological DFN; each alternative represents a different potential combination of assumptions and data treatments. A ranking process, described in detail in /La Pointe et al. 2008, cf. Section 3.8.2 therein/ and based on verification simulations performed relative to observed fracture data was used to select a recommended size-intensity model. The unlinked Base Model, the so-called BMU model alternative case, was selected as the recommended size-intensity model for SDM-Site Laxemar based on its performance in the verification cases. Conceptually, the BMU model case is based on the following assumptions:

- Fracture coupled size-intensity follows a power-law and can be described through a Pareto distribution /La Pointe et al. 2008, cf. Section 3.4 therein/;
- The fracture radius scaling exponent (k_r) does not vary as a function of fracture domain; it is conceptually acceptable to model the radius exponent as a function of fracture orientation set and not of lithology or fracture domain;
- For all fracture sets, the “Best Fit” radius exponent was used. It is possible to derive multiple radius scaling exponent fits from the surface mapping data; the Best Fit exponent effectively represents an ‘average’ value for k_r ;
- Fracture domains differ principally in terms of the observed mean volumetric fracture intensity (P_{32}) and the minimum radius (r_0); i.e. the size of the smallest fractures expected. This hypothesis complements the fracture domain model, where volumes are identified primarily on the basis of variations in fracture intensity by fracture set;
- Fracture intensity obeys Euclidean size-intensity scaling /La Pointe et al. 2008, cf. Section 3.6.1 therein/;
- Unlinked outcrop fracture traces are used in the parameterisation of the fracture radius scaling exponent /La Pointe et al. 2008, cf. Appendix A therein/.

The model parameterisations are presented below in Table 5-11. Note that the values presented in this table are for all fractures (open, partly open, and sealed).

The coupled size-intensity model can be difficult to understand; users are therefore strongly encouraged to consult the method-specific geological DFN report /La Pointe et al. 2008/ before attempting to use the model parameters presented in Table 5-11.

Table 5-11. BMU size-intensity parameters, SDM-Site Laxemar geological DFN model.

Fracture Set	k_r	r_{max}	FSM_C		FSM_EW007		FSM_N	
			r_0	P_{32}	r_0	P_{32}	r_0	P_{32}
ENE	3.00	564.20	0.37	1.72	0.32	1.98	0.46	1.38
NS	3.26	564.20	0.59	2.33	0.49	2.96	0.53	2.63
SH	3.31	564.20	0.33	2.66	0.23	4.42	0.22	4.62
WNW	2.80	564.20	0.08	2.53	0.07	2.90	0.08	2.67

Fracture Set	k_r	r_{max}	FSM_NE005		FSM_S		FSM_W	
			r_0	P_{32}	r_0	P_{32}	r_0	P_{32}
ENE	3.00	564.20	0.40	1.60	0.15	4.28	0.40	1.60
NS	3.26	564.20	0.36	4.30	0.27	6.09	0.42	3.60
SH	3.31	564.20	0.29	3.17	0.23	4.22	0.28	3.40
WNW	2.80	564.20	0.09	2.37	0.03	5.39	0.11	1.97

DFN spatial model

Spatial analysis quantifies how the location, size, termination, and fracture intensity of each set vary spatially. A spatial model makes it possible to extend local measurements of fracture intensity to other portions of the potential repository volume where there are no data. It also relates to the scaling of fracture intensity. Certain types of spatial models, such as Poissonian or fractal, imply that fracture intensity will increase, remain the same or decrease as a function of scale according to the particular governing equations. Scaling behaviour is important to quantify, as the scale at which fracture data are obtained may not be the scale at which they are used for subsequent modelling or calculations. In the SDM-Site Laxemar geological DFN, the spatial model consists of the following parameterisations and analyses:

- Correlation of fracture intensity to rock domains or host lithology, if possible.
- Analysis of fracture intensity scaling.
- Analysis of the spatial variability of fracture intensity.
- Evaluation of the depth-dependence of fracture intensity.
- Quantification of the termination relationships between fracture orientation sets.

A three-dimensional Poisson point process was judged as an adequate model for describing the location of fracture centres in space. Benchmark simulations /La Pointe et al. 2008, cf. Section 4.4.3 therein/ demonstrated that a Poissonian distribution of fractures whose size follows a power law will produce a one-dimensional fracture spacing pattern in boreholes that follows a Weibull distribution /Weibull 1951/. An analysis of fracture spacings from borehole data, conducted as part of the fracture intensity modelling, established that the spacing data from boreholes in Laxemar were indeed best fit using a Weibull probability distribution, indicating that the selection of a Poisson point process for modelling fracture centres is adequate and appropriate.

Fracture intensity scaling within the fracture domains in Laxemar was analysed in terms of the fractal mass dimension of outcrop fracture traces, and was found to be Euclidean to weakly fractal. The BMU size-intensity model alternative assumes Euclidean intensity scaling. A statistical analysis of fracture intensity and fracture properties from cored borehole data /La Pointe et al. 2008, cf. Section 4.4.4 therein/ suggested that use of fracture domains was a superior method of reducing the variability in fracture intensity to a corresponding subdivision into rock domains (cf. Section 5.4). The analysis also indicated weak correlations between bedrock lithology and fracture intensity, but no statistically significant correlations between fracture intensity and rock domain or depth were found.

Fracture intensity as a function of depth is summarised in Figure 5-58 and Figure 5-59. Fracture intensity as a function of orientation set and fracture domain does vary with depth, but the variability could not be linked to any observed geological or tectonic criteria and was not consistent (i.e. there was no systematic increase or decrease in fracture intensity with depth in a given fracture domain, or across the Laxemar local model volume as a whole).

In terms of the combined intensity of all fracture sets, the relatively straight CFI curves (Figure 5-58) suggest little depth-dependence of fracture intensity. All fracture domains except FSM_NE005 do show a gentle decrease in total fracture intensity below an elevation of approximately –700 to –800 m. Fracture domain FSM_W, however, shows an increase in the intensity of open fractures between a depth of approximately 380 and 480 m below the ground surface; the cause of this intensity spike is not immediately apparent from SDM-Site Laxemar modelling. There is also a zone in the upper 100 to 200 m of fracture domains FSM_N and FSM_W where the intensity of both open and all fractures appears to be enhanced (cf. Figure 5-59); this is most likely due to surface stress release effects.

The distribution of fracture intensity (P_{32}) in space within the Laxemar fracture domains can generally be modelled as a Gamma or Weibull probability distribution down to a minimum scale of approximately 9 m in most domains, and for most fracture sets except the ENE set. Table 5-12 illustrates at what scales the fracture domain fracture intensity can be represented as either a Gamma or a Weibull distribution. Full distribution parameters and a detailed explanation of the intensity methodology are presented in /La Pointe et al. 2008, cf. Sections 3.6.5 and 4.4.7 therein/.

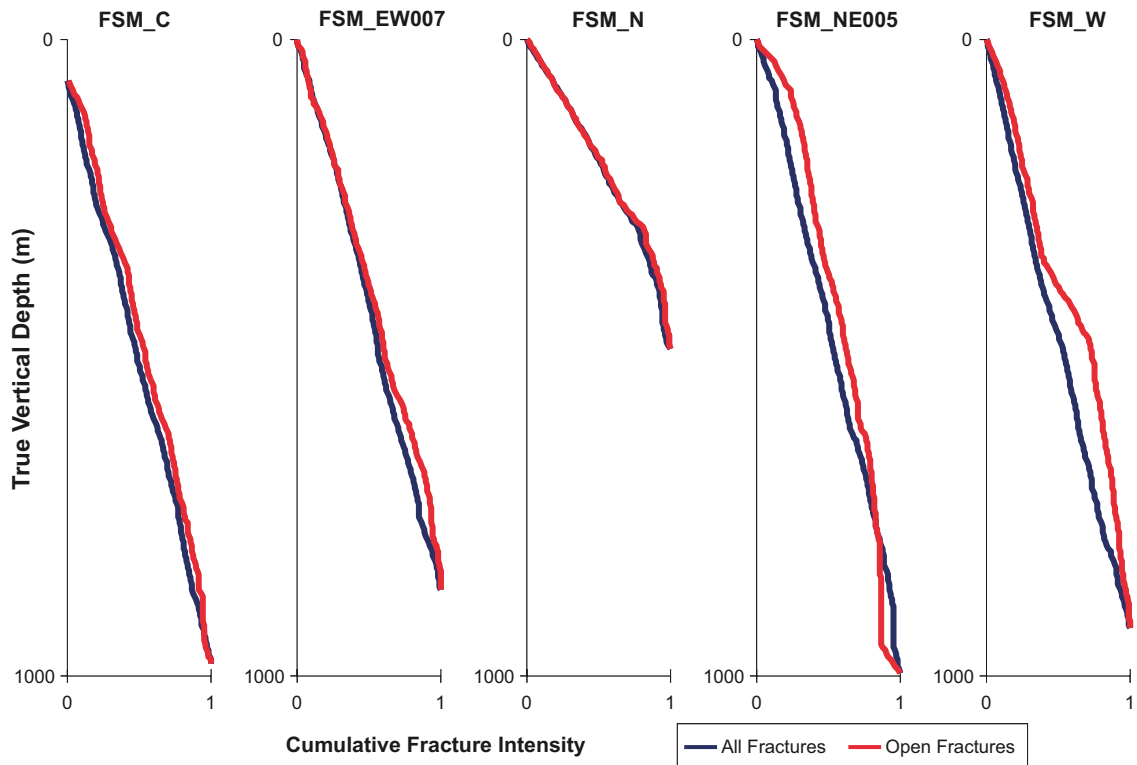


Figure 5-58. Cumulative fracture intensity (CFI) plots for all fracture sets combined, as a function of true vertical depth and fracture domain. CFI plots are useful for examining changes in fracture intensity; changes in the slope of the curve represent volumes of the bedrock within which there are increases or decreases in fracture intensity. CFI plots are focused on looking at domain-scale changes or at identifying mechanical layering.

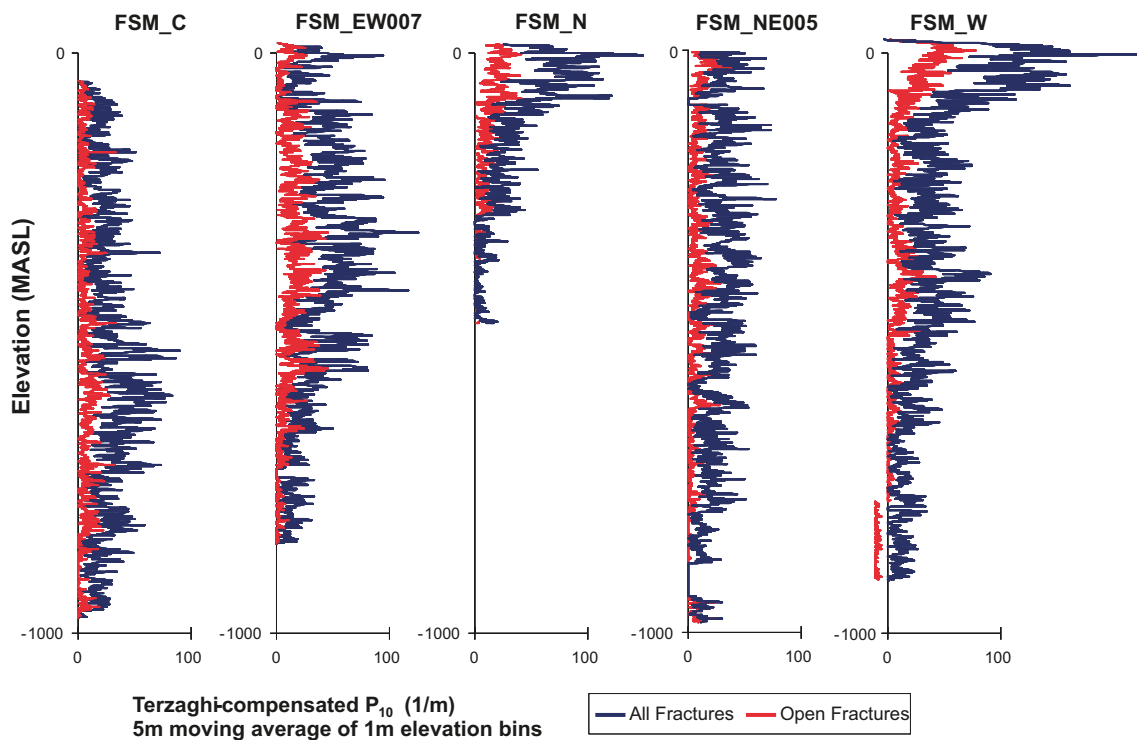


Figure 5-59. Plots of open fracture intensity (red) and total (purple) fracture intensity (P_{10}) as a function of elevation and fracture domain. The values plotted are Terzaghi-compensated P_{10} , calculated using the intensity of fractures in 1 m elevation intervals and plotted as a moving average of 5 elevation intervals.

Table 5-12. List of scales at which the variability of volumetric fracture intensity (P_{32}) can be modelled as a Gamma or Weibull distribution. In the SDM-Site Laxemar geological DFN, fracture P_{32} is a function of fracture domain and orientation set.

Set	Domain	Scale (m)
ENE	FSM_C	15
ENE	FSM_EW007	15
ENE	FSM_N	9
ENE	FSM_NE005	15
ENE	FSM_W	15
N-S	FSM_C	9
N-S	FSM_EW007	9
N-S	FSM_N	9
N-S	FSM_NE005	3
N-S	FSM_W	9
SH	FSM_C	9
SH	FSM_EW007	9
SH	FSM_N	3
SH	FSM_NE005	3
SH	FSM_W	9
WNW	FSM_C	9
WNW	FSM_EW007	9
WNW	FSM_N	9
WNW	FSM_NE005	3
WNW	FSM_W	9

Fracture terminations in the geological DFN model are expressed as a matrix. The columns of the matrix represent the target fracture set (the set that is being terminated against), while each row represents the orientation set being parameterised. Terminations are quantified as the percentage of traces belonging to one set that terminate against another set. A fracture trace is considered to ‘terminate’ against another fracture if its endpoint lies within 5 cm of another fracture trace without cutting across it, has been mapped in Sicada as terminating against another fracture in a ‘T’ or ‘Y’ intersection, and if the termination makes geological sense (i.e. if a fracture terminates against a lithological contact such as a dyke or vein, and the contact has then been fractured at a later date, the original intersection between the first fracture and the lithological contact is not termed an intersection). Matrices were computed for all fracture domains for which outcrop trace data existed, and a global average value computed.

In general, the fracture termination results suggest that, depending on outcrop, either the NS or ENE fracture set is the oldest set, followed by a younger WNW fracture set. At outcrops ASM000208 and ASM100235 /Hermanson et al. 2008, cf. Figure 5-3 and Figure 5-4 therein/, the ENE set shows distinct banding against an older NS set. At outcrops ASM000209 and ASM100234 /Hermanson et al. 2008, cf. Figure 5-3 and Figure 5-4 therein/ the relative timing is less-apparent; NS and ENE set fracturing may have been nearly contemporaneous at ASM100234. The relative timing of the SH set is almost impossible to determine from surface data alone. The termination relationships calculated from outcrop fracture mapping roughly correspond to the results of kinematics studies in Laxemar (Section 5.2.7); however, the geological DFN does not subdivide fractures in terms of sense-of-slip or timing of initial breakage versus later brittle re-activation. Further details regarding the terminations of fractures are available in /Hermanson et al. 2008, cf. Section 5.2 therein/.

Table 5-13 presents the global average fracture termination matrix for Laxemar. To determine the percentage of fractures in the ENE Set (row 1) that terminate against the NS set (column B), one reads the percentage from cell address B1 (25.53%). The percentages can be interpreted as a probability value; for a given fracture, in a given set, on a given outcrop or in a given fracture domain, where the percentage is considered equivalent to a probability that the fracture will terminate against another fracture.

Table 5-13. Termination matrix based on analysis of outcrop fracture traces, SDM-Site Laxemar geological DFN model.

	Fracture Set	A ENE	B N-S	C WNW	D SH	Bulk Termination
1	ENE	0.00%	25.53%	12.24%	6.54%	44.30%
2	N-S	11.82%	0.00%	11.58%	4.46%	27.86%
3	WNW	14.10%	26.87%	0.00%	5.95%	46.92%
4	SH	13.22%	20.66%	12.12%	0.00%	46.01%

Minor Deformation Zones in the Geological DFN

Minor deformation zones (MDZ) are included as components in the stochastic geological DFN model. Their orientations are specified by the univariate Fisher distributions previously discussed, and their sizes, in terms of the radius scaling exponent (k_r), are specified using the same power-law distributions as for stochastic fractures. MDZ termination relationships are assumed to follow the rules derived from outcrop studies; no additional information is available at the MDZ-scale to test this hypothesis.

A basic assumption concerning MDZ is that they represent larger structures than most of the fractures exposed between deterministic deformation zones in the cored boreholes. The SDM-Site Laxemar site descriptive model considers that all structures (fractures and MDZ) with a equivalent radius less than or equal to 564.2 m are treated stochastically in the geological DFN. However, the true size of the MDZ included in the cored borehole record in Laxemar is not known; as none of the MDZ can be traced to intercepts with other boreholes or identified uniquely at the ground surface in outcrop or by geophysics, their true size distribution is unknown. In particular, there are no data on the minimum size of MDZ.

An issue is that the power-law size-intensity scaling models used by the geological DFN model do not discriminate between MDZ and large fractures; the size-intensity model only gives the P_{32} of all structures in a certain size range. Therefore, the radius scaling exponent (k_r), which is derived from outcrop fracture maps and lineament traces, is used to describe both MDZ and large single fractures.

There are two possible alternatives to deal with the lack of information on the minimum size of MDZ-sized features without collecting additional data:

- Method 1: The P_{32} of MDZ can be used in conjunction with the various size-intensity alternative models to analytically determine a minimum size (r_{min}) of MDZ. This value will vary as a function of the radius scaling exponent (k_r) and the fitted mean P_{32} chosen for the specific size-intensity model alternative. The result of this implies that all structures between the fitted r_{min} value and the maximum size allowed for structures in the stochastic DFN model are MDZ. Data from the surface are only used to establish the radius scaling exponent, and not to determine the intensity of MDZ-sized structures.
- Method 2: One can assume that every surface lineament recorded by the detailed ground magnetic and Lidar surveys represents a MDZ. The minimum size (r_{min}) of the structures that created the surface lineaments can be estimated using the trace length ‘rollover effect’ on the area-normalised complementary cumulative number plots; the method is described below. As it is not possible to assign the lineaments to individual fracture domains without incurring substantial truncation effects, Method 2 produces r_{min} values that are global in scope. This method is described in detail in Section 5.5 of the geological DFN summary report /La Pointe et al. 2008/.

The recommendation of the geological DFN modelling team is to adopt a functional definition of 75 m as the minimum size of MDZ in Laxemar. This number is close to the values for the minimum MDZ size suggested by the trace length rollover effect /La Pointe et al. 2008, cf. Section 5.5 therein/, and is also equal to the radius of the smallest fracture viewed likely to be able to rupture a waste package during an earthquake /Fälth and Hökmark 2006/.

The frequency of MDZ in Laxemar is quantified by their P_{10} ; calculated as the number of MDZ intersecting a borehole, divided by the length of the borehole. A list of the minor deformation zones

identified in the cored borehole array is presented in /Hermanson et al. 2008, cf. Appendix 3 therein/ summarising the orientation and locations of MDZ quantified during the ESHI analysis. The length of borehole used in the P_{10} calculation is the total length (MD) of the borehole, minus the length of sections of boreholes inside deterministic (DZ) and minor deformation zones (MDZ).

Geological DFN modelling, however, also relies on P_{32} as the measure of fracture intensity. Therefore, for borehole MDZ intercept data to be useful in geological modelling, it is necessary to transform MDZ P_{10} to MDZ P_{32} . This is accomplished using the Wang approximation /La Pointe et al. 2008, cf. Section 3.5.1 therein/. The MDZ intercepts presented by /Hermanson et al. 2008/ were assigned to the fracture orientation sets developed for the geological DFN. For the purposes of geological DFN modelling, each borehole used the average C_{13} value over 3 m long intervals for each fracture set. The P_{32} of MDZ in Laxemar are presented below, organised by orientation set and fracture domain, in Table 5-14. FSM_S is not included in Table 5-14, as this fracture domain has generally been excluded from analyses due to a distinct lack of available data (only one single cored borehole). The P_{32} values presented for a single fracture set in a single fracture domain represent the arithmetic average of the P_{32} values calculated for that set for each individual borehole inside the fracture domain.

The P_{32} values presented in Table 5-14 are based solely on the P_{10} values observed during the ESHI and deformation zone modelling activities, and do not represent a fixed value for the minimum size (r_{min}) of MDZ. However, readers are strongly encouraged to consult /La Pointe et al. 2008, cf. Section 5.5 therein/; the choice of a minimum size for MDZ may have significant consequences in downstream models.

The length-thickness relationship of minor deformation zones (MDZ) has not been used in the geological modelling. Because of the difficulty of coupling shorter surface lineaments to subsurface structures away from boreholes and the issue of MDZ at depth, for which no size information at all is available, the use of length-thickness ratios from MDZ were viewed as adding more uncertainty to the geological model than geological understanding. The true thicknesses of MDZ, however, were calculated /cf. Wahlgren et al. 2008, cf. Section 3.12 therein/; the results are summarised in Figure 5-60.

Table 5-14. Number and intensity (P_{10} , P_{32}) of minor deformation zones (MDZ) in Laxemar as a function of fracture set and fracture domain.

Fracture Domain	Fracture Set	Number of MDZ	Total borehole length (m)	P_{10} (1/m)	Average P_{32} (m ² /m ³)
FSM_C	ENE	5	2,691.81	0.0019	0.0031
FSM_EW007	ENE	5	2,669.93	0.0019	0.0053
FSM_N	ENE	0	1,327.04	0.0000	0.0000
FSM_NE005	ENE	4	2,225.28	0.0018	0.0168
FSM_W	ENE	5	3,458.56	0.0014	0.0056
FSM_C	N-S	4	2,691.81	0.0015	0.0040
FSM_EW007	N-S	5	2,669.93	0.0019	0.0154
FSM_N	N-S	1	1,327.04	0.0008	0.0037
FSM_NE005	N-S	7	2,225.28	0.0031	0.0189
FSM_W	N-S	13	3,458.56	0.0038	0.0118
FSM_C	SH	15	2,691.81	0.0056	0.0096
FSM_EW007	SH	33	2,669.93	0.0124	0.0213
FSM_N	SH	26	1,327.04	0.0196	0.0234
FSM_NE005	SH	18	2,225.28	0.0081	0.0129
FSM_W	SH	41	3,458.56	0.0119	0.0219
FSM_C	WNW	4	2,691.81	0.0015	0.0048
FSM_EW007	WNW	2	2,669.93	0.0007	0.0019
FSM_N	WNW	3	1,327.04	0.0023	0.0078
FSM_NE005	WNW	1	2,225.28	0.0004	0.0069
FSM_W	WNW	5	3,458.56	0.0014	0.0038

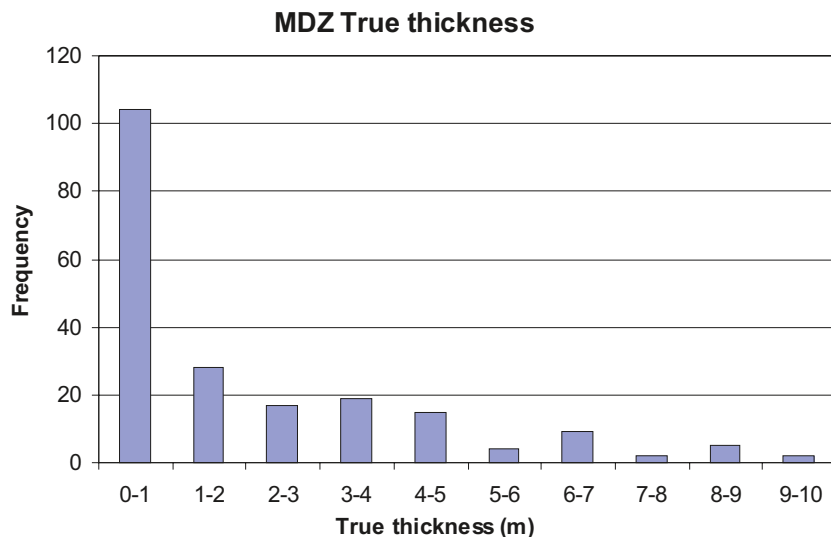


Figure 5-60. True thickness of MDZ in cored boreholes based on ESHI, excluding MDZ identified in cored borehole KLX27A /cf. Hermanson et al. 2008/.

The treatment of MDZ-sized lineaments is an issue in the geological DFN modelling. The methodology employed assumes that all lineaments shorter than 564.2 m represent geologic structures that are to be included in the stochastic geological DFN. A limited uncertainty analysis /La Pointe et al. 2008, cf. Section 6.1.2 therein/ was performed using the BMU size-intensity model alternative to determine what the effect would be on fracture intensity if only a fraction (50% and 75%) of the lineaments observed represented rock discontinuities (MDZ, long single fractures, fracture swarms, or sealed fracture networks). The uncertainty analysis was performed assuming two different fracture size ranges:

1. Expanded Full Perimeter Criteria (EFPC, cf. /Munier 2006, 2007/) size range of 2.7 to 564.2 m. The EFPC size range represents the population of fractures large enough to potentially make a full-perimeter intersection (i.e. cut completely through) of a canister deposition hole or repository tunnel. The intensity of fractures and MDZ in this size range directly affect the degree of utilisation in the potential repository.
2. The recommended MDZ size range of 75 – 564.2 m, the rationale for which was discussed earlier in this section. MDZ are considered a component of the stochastic fracture model (cf. Section 5.6.2).

The analysis indicated that, for the BMU model alternative, fracture intensity is relatively insensitive to the differences in the radius scaling exponent. Differences in P_{32} values approach, but are less than, one order of magnitude; this is on the same scale as the other conceptual uncertainties in the geological DFN model. The uncertainty has a larger effect on the MDZ size fraction (2.7–564.2 m) than on the EFPC size fraction (75–564.2 m).

As the number of lineaments decreases, the value of k_r increases, while the total fracture intensity as measured in cored boreholes remains constant. The effect is to decrease the relative intensity of larger fractures, and increase the intensity of smaller fractures. A second consequence is that the minimum size (r_0) of fractures becomes slightly larger as the number of lineaments that represent fractures decreases.

Depth dependencies in fracturing

The understanding of the properties of rock fracturing as a function of depth was evaluated during several different activities during SDM Site Laxemar, including during preparatory data compilation /Hermanson et al. 2008/, in the geological DFN model /La Pointe et al. 2008/, and in the hydrogeological DFN modelling.

Fracture orientation as a function of depth was evaluated by /Hermanson et al. 2008, cf. Appendix 5b therein/. It was found that although some variability in fracture orientations with depth was noted (specifically, of the location of the fracture set mean poles), the changes were neither regular enough nor spatially contiguous enough to be useful for predictive purposes. Past SDM work indicates that the spatial variability of fracture orientations is less important than the spatial variability of fracture intensity. In addition, uncertainty in the coupled fracture size-intensity models is far more significant than the uncertainty associated with fracture orientation variability.

There is insufficient data available to make firm conclusions as to whether the distribution of fracture sizes (and specifically, the minimum size r_0 and the radius scaling exponent k_r) is a function of vertical depth; the only direct information about fracture size comes from trace studies conducted at the ground surface. Hypotheses can be postulated based on data from other sites, but cannot be validated without the addition of underground information. There is little evidence in the literature to suggest that at cratonic sites such as Laxemar, there will be any systematic changes in the distribution of fracture sizes with depth.

Vertical depth was not found to be a useful discriminator for fracture intensity in the geological DFN model; no systematic, predictable relationship between fracture intensity and vertical depth was found during the development of the geological DFN model. This is not to say that there were no depth trends visible in the data analyzed: Figure 5-58 illustrates that, for domain FSM_NE005, the intensity of open fractures appears to decrease markedly below 100 m. However, the same figure also shows a corresponding increase in open fracture intensity at near-repository depths in fracture domain FSM_W. Some depth trends are also visible in domain FSM_C, where the intensity of open fractures does appear to decrease with increasing vertical depth. It is important to note, however, that the same trends are not observed when looking at the intensity of all fractures (open, partly open, and sealed) combined. Both the spatial analysis and the size-intensity model parameterisation efforts in the geological DFN modelling suggest that the differences of fracture intensity between fracture domains, or the differences inside and outside of deformation zones, are more important than the depth trend for the fracture population as a whole (i.e. open and sealed fractures).

The analysis of the intensity of MDZ recorded in the cored borehole array suggests that some near-surface (20 to 30 m depth) effects do occur; this is consistent with the sheet joints seen in the surface excavations at Forsmark /SKB 2008a/. However, the noted effect does not appear to extend much below a depth of 30 m. Once MDZ intensity has been normalised to compensate for the increased number of very shallow boreholes and the relative paucity of very deep boreholes, little difference (variabilities in MDZ P_{32} were on the order of $0.01 \text{ m}^2/\text{m}^3$) in average MDZ intensity is seen with depth.

5.7 Integrated geological model

This section provides a basic account of the interrelation between the various domains and deformation zones that are defined in the focused volume in Laxemar. The account is followed by a summary of the principal geological aspects that characterise the focused volume.

The geological modelling work for Laxemar has resulted in the production of three submodels, namely the rock domain model, deformation zone model and the geological DFN model. Each of the submodels focuses on the characterisation of a particular aspect of the bedrock environment. The submodels are complementary and only when taken together can they be considered to represent a complete geological description of the Laxemar site. The DFN model owes its basic analytical framework to the deformation zone and rock domain models and at the same time has provided feedback on the consistency of these models. The rock domain and deformation zone models owe their general structural framework to the general understanding of the development of the bedrock and its regional tectonic history reported by earlier workers. At the same time the rock domain and deformation zone studies themselves have provided feedback and have led to a more detailed understanding of the evolutionary model at a more local scale /cf. Söderbäck 2008/.

Figure 5-61 and Figure 5-62 provide integrations for the Laxemar local model volume of rock domains + deterministic deformation zones (with trace lengths longer than 1,000 m at the ground surface), and rock domains + deformation zones + fracture domains, respectively. As can be seen, the rock domains and the fracture domains do not coincide, since the variation in intensity of different fracture orientation sets, which is the prime basis for the delineation of the fracture domains, do not correlate with the defined rock domains. Instead, the fracture domains may consist of portions of different rock domains and the fracture domain boundaries coincide for the most part with deterministic deformation zones (Figure 5-62). Although the fracture orientation set definitions do not change appreciably in Laxemar, it is inferred that the variation in intensity between the defined fracture domains is not coincidental. Instead, it is inferred to be caused by the activation/reactivation of deformation zones and fractures due to variable stress fields acting as a result of large-scale orogenic processes that have affected the bedrock in the Laxemar-Simpevarp area during the geological evolution. The latter is supported by /Viola 2008/, who, despite the complex and polyphase brittle structural evolution in the Laxemar-Simpevarp area, was able to define conjugate fracture sets with different kinematics which were ascribed to different orogenic processes that have affected the bedrock.

All images have been extracted from the deterministic local scale geological models /Wahlgren et al. 2008/. Due to the difficulties in visualising the integration of the different geological models in fixed view figures, interactive 3D visualisations of the individual rock domain, deterministic deformation zone and fracture domain models, and a combined version integrating all three models are available as PDFs on the DVD attached to the printed report.

The focused volume for the localisation of a potential repository for the disposal of highly radioactive nuclear waste in Laxemar comprises the following rock domains and fracture domains (Figure 5-62):

- The part of rock domain RSMA01 that in principle occurs south of fracture domain FSM_EW007.
- RSMD01.
- RSMM01.
- FSM_W, FSM_C and FSM_NE005.

The following deformation zones are of prime importance for the integrated geological model and the focused volume for a potential repository (Figure 5-62):

- ZSMNS001C, which forms the western boundary for FSM_W and the focused volume.
- ZSMNW042A, which forms the southern boundary for FSM_W, FSM_C, FSM_NE005 and the focused volume.
- ZSMEW007A, which is surrounded by FSM_EW007, the latter of which forms the boundary between FSM_C and FSM_N. Furthermore, ZSMEW007A constitutes the northern boundary of the focused volume.
- ZSMNE005A, which forms the eastern boundary of FSM_NE005 and the focused volume.
- ZSMNS059A, which delimits FSM_W from FSM_C, FSM_EW007 and FSM_N east thereof.

Furthermore, the following deterministically modelled deformation zones, with a high confidence of existence and with trace lengths at the ground surface longer than 1,000 m, occur inside and intersect the focused volume that is being considered for a potential repository (cf. Figure 11-9 and for details Appendix 6):

- ZSMEW900A-B, moderately to steeply dipping to the south.
- ZSMNE944A, steeply dipping.
- ZSMNE942A, steeply dipping.
- ZSMNE107A, steeply dipping.
- ZSMNS046A, steeply dipping.

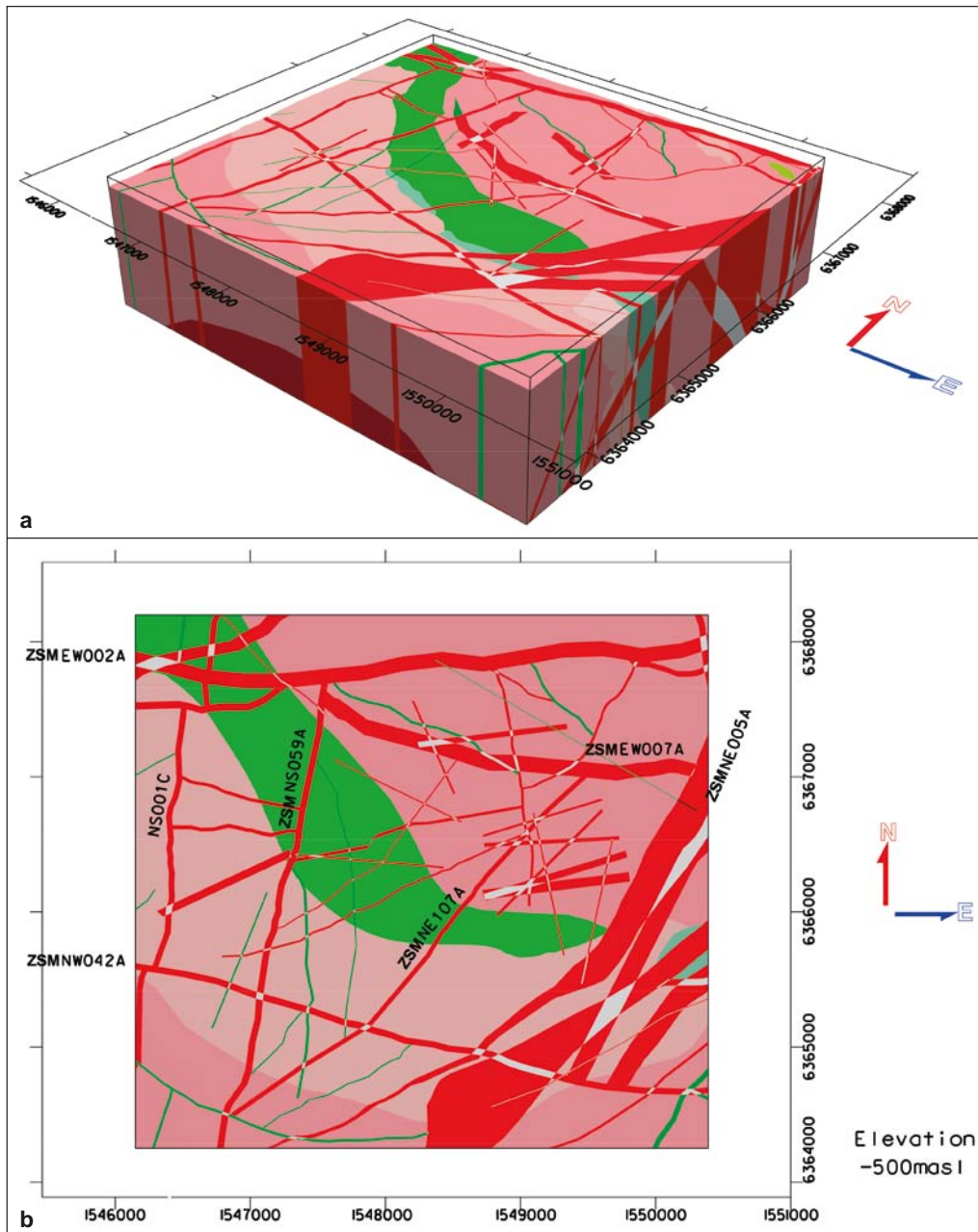


Figure 5-61. Integration of rock domains and deterministic deformation zones in the Laxemar local model volume. a) 3D view towards northwest. b) Horizontal section at -500 m. For explanation of rock domain and deformation zone colours, see Figure 5-30.

In addition, the gently south-dipping deformation zone ZSMEW946A (reflector M1), which does not outcrop within the focused area, intersects the volume of interest at repository depth. The presented geometry of ZSMEW946A is interpreted to mark the upper limit of a thicker discontinuous series of minor deformation zones and mafic intrusions rather than an individual structure.

In contrast to the correlation between deformation zones and fracture domain boundaries, rock domain boundaries and deformation zones do not correlate, except for the rock domains RSMP01 and RSMP02 (see Figure 5-25) which coincide with the primarily ductile deformation zones ZSMNE005A and ZSMNE004A, respectively (Figure 5-30).

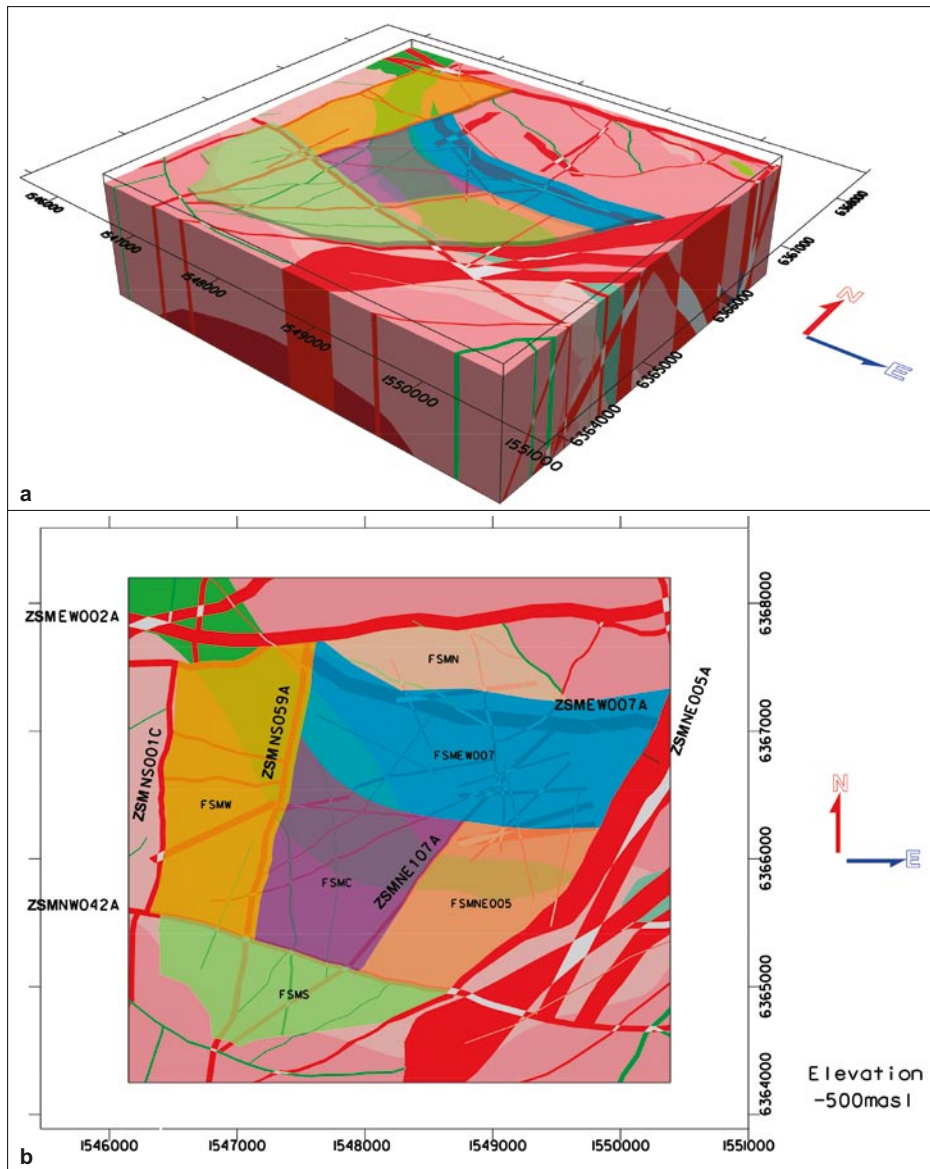


Figure 5-62. Integration of rock domains, fracture domains and deterministic deformation zones in the Laxemar local model volume. a) 3D view towards northwest. b) Horizontal section at -500 m.

The following points summarise the key geological aspects of the focused area/volume in Laxemar.

- The dominant rock types in the rock domains RSMD01 and RSMM01, that are in focus, are characterised by low quartz contents. The calculated quartz content for the quartz monzodiorite in RSMD01 is $13.0 \pm 3\%$, and the corresponding value for the Ävrö quartz monzodiorite in RSMM01 is $13.9 \pm 6.4\%$. Although very similar quartz contents, and overall mineralogical composition, the thermal and rock mechanical properties are different (cf. Chapters 6 and 7). The subordinate rock types fine-grained granite, fine-grained diorite-gabbro and pegmatite occur in similar amounts in both domains. Furthermore, dolerite dykes have been documented in three cored and a number of percussion boreholes that intersect the quartz monzodiorite in the RSMD01 domain. However, dolerite dykes are considered as a very subordinate rock type in the focused volume.
- The absolute majority of the deterministic deformation zones in Laxemar are steeply to vertically dipping. The most important exceptions are the approximately E-W oriented and south-dipping deformation zones ZSMEW002A, ZSMEW900A-B and ZSMNW042A, and the north-dipping ZSMEW007A. Except for ZSMEW007A which is strongly indicated to be entirely brittle in character, the remaining deterministic deformation zones, although commonly strongly overprinted by polyphase brittle deformation, are characterised by a ductile precursor.

- It is strongly suggested that the overall structural framework was formed when the bedrock still responded to ductile deformation. Since the majority of the deformation zones show signs of a ductile precursor and polyphase brittle reactivation, it is clear that the framework of ductile deformation zones has steered the stress release during the subsequent geological evolution in the brittle régime. Furthermore, the similarity between the orientation of small-scale ductile and brittle structures strongly suggests that the ductile anisotropy, although generally weakly developed in the rock domains outside deformation zones, has influenced the orientation of brittle structures during the geological evolution. A similar correlation exists between the orientation of the ductile structures and the orientation of subordinate rock types, particularly in the RSMD01 domain in the southern part of Laxemar. In addition, the similarity between the orientation of the fractures outside and inside deformation zones identified in ESHI suggests that they are related and that movements in the deformation zones have controlled the fracturing in the bedrock in the Laxemar local model volume.
- Different generations of fracture minerals have been recognised in Laxemar. Two generations are interpreted to predate the intrusions of the Götemar and Uthammar granites, one generation is associated with these intrusions, as well as generations that are interpreted to be related to both the Sveconorwegian and the Caledonian orogenies are documented, partly based on age dating results. Most fracture minerals show no distinctive variation with depth. The frequency of occurrence generally follows the variation in the total fracture frequency. Notable exceptions include calcite, pyrite, goethite and gypsum. Slightly smaller amounts of calcite in the uppermost 10–20 metres below ground surface are due to near surface dissolution. Oxidising conditions near the surface cause increase in goethite-bearing fractures at the expense of pyrite. Gypsum, which is indicated in a few boreholes, is restricted to open fractures in isolated sections of low fracture frequency and low transmissivity below an elevation of –350 m.
- Fracturing is described in terms of fracture domains instead of rock domains. Fracture domains provide a large-scale conceptual framework for describing spatial heterogeneity in rock fracturing. The fracture orientation set definitions do not change appreciably between fracture domains. However, the relative intensity of fracture sets and the location of deterministic deformation zones are used to delineate domains of similar fracture intensity trends.
- In general, the patterns of fracture orientations and relative fracture intensities inside the fracture domains in Laxemar are consistent with the orientations and timing of the regional deformation zones. The deformation zones work in conjunction with the regional stress field to produce unique intensity patterns in each fracture domain.

5.8 Verification and validation of models

5.8.1 Verification of lithology and alteration in KLX27A

All available data from Laxemar, including data from borehole KLX27A, have been used in the geometrical modelling of rock domains. However, data from the Boremap mapping of KLX27A were not used in the evaluation of primary data as reported in Section 5.2 and in /Wahlgren et al. 2008, cf. Chapter 3 therein/. Therefore, data from KLX27A can be utilised for verification purposes, applied here to the lithological homogeneity and degree and type of alteration in rock domain RSMD01. In Table 5-15, the prediction and outcome of the proportion of rock types in KLX27A is presented. As can be seen the outcome is very similar to the predicted proportion of rock types /Wahlgren et al. 2008, cf. Section 5.2.3 and Appendix 4 therein/. In Figure 5-63, the degree and type of alteration in KLX27A is presented. It is very similar to the overall alteration in the RSMD01 domain /Wahlgren et al. 2008, cf. Section 5.2.3 and Appendix 7 therein/. The outcome of the comparisons presented here, confirms the stability of the property assignment of the RSMD01 domain in the focused volume in Laxemar.

Predictions were also made of the lithological homogeneity, i.e. the proportions of different rock types in the borehole, prior to drilling of KLX11A and all subsequent longer cored boreholes. As can be seen in /Wahlgren et al. 2008, cf. Appendix 12 therein/, the outcomes are very similar to the predicted proportions, in particular for the boreholes that intersect the quartz monzodiorite in the RSMD01 domain, emphasising the homogeneous characteristics of this domain.

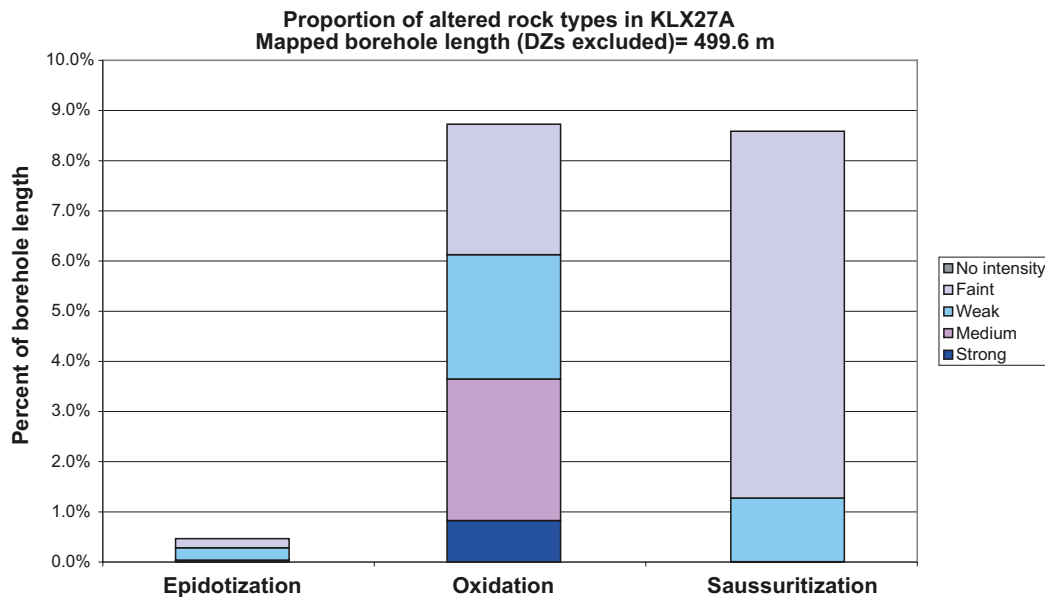


Figure 5-63. Histogram showing the degree and type of alteration in KLX27A.

Table 5-15. Proportion of rock types in KLX27A. Comparison of prediction made before drilling and the outcome.

KLX27A	Prediction	Outcome
Quartz monzodiorite	94.8%	93.5%
Fine-grained granite	1.8%	4.0%
Fine-grained diorite-gabbro	2.4%	2.3%
Pegmatite	1.0%	0.1%

5.8.2 Verification of geological DFN models and the results of a validation test

Both verification and partial validation were performed on the geological DFN model as part of SDM-Site Laxemar. Verification of the geological DFN modelling was conducted by building a series of small-scale DFN models using FracMan /Dershowitz et al. 1998/, conducting simulated sampling using the extent and geometries of actual outcrops, scanlines, and boreholes within the Laxemar local model volume. The verification was carried out not only for the recommended size-intensity model alternative (BMU), but also all for of the defined alternative models. The verification methodology and results are presented in /La Pointe et al. 2008, cf. Section 3.8 and Chapter 5 therein, respectively/.

The results of the verification simulations were used to develop rankings of the 29 different size-intensity model alternatives presented in the geological DFN. The significance of model rankings was evaluated using the Kruskal-Wallis non-parametric ANOVA tests /Kruskal and Wallis 1952/. As previously mentioned, the BMU model alternative was the best performing model, and was adopted as the recommended coupled size-intensity model for the SDM-Site Laxemar geological DFN simulations.

A partial validation of the geological DFN was performed /La Pointe et al. 2008, cf. Appendix G therein/ using fracture data from cored borehole KLX27A, which was not used in the SDM-Site Laxemar geological modelling. Borehole KLX27A is located in the southwest corner of the Laxemar local model area (cf. Figure 2-5), and is drilled through fracture domains FSM_S and FSM_W. The borehole is entirely inside rock domain RSMD01, and intersects the major northwest striking major deformation zone (ZSMNW042A) at approximately -170 m. The partial validation consisted of a blind prediction of KLX27A lineal fracture intensity (P_{10}) inside fracture domain FSM_W through stochastic simulation, followed by a comparison between the simulated and actual fracturing of FSM_W as seen in the borehole.

The results of the partial validation indicate that the geological DFN (assuming the BMU size-intensity alternative) overpredicts the total fracture intensity in KLX27A by a factor of 1.5 to 2.5 times. However the simulations did correctly predict the number of minor deformation zones intersected by KLX27A. In addition, a comparison of the simulation P_{10} results to values from boreholes elsewhere in FSM_W indicated a much better fit; the simulated P_{10} values were within a factor of 0.9 to 1.2 times the observed values.

An analysis of the orientation and fracture intensity patterns in KLX27A data and its neighbour, KLX19A, suggest that both boreholes are drilled into a volume of rock that is substantially different than the remainder of FSM_W. The total P_{10} in KLX27A is one-half the average P_{10} observed in domain FSM_W, the relative intensities of the global fracture sets are significantly different than elsewhere in FSM_W, and the mean pole vector of the N-S fracture set appears to be rotated 20°–30° clockwise, relative to the rest of domain FSM_W. All these characteristics point to the existence of a volume of rock in the footwall of deformation zone ZSMNW042A that is significantly different in terms of fracturing from the rest of domain FSM_W.

The partial validation performed using KLX27A data can in no way be used as an absolute proof of validity of the developed geological DFN. Notwithstanding, the exercise illustrates the predictive power of the model. A stringent validation of the model as a whole would necessitate coverage of all FSMs and also a much more rigorous statistical treatment.

5.9 Remaining uncertainties

Deterministic model for rock domains

Despite the significant increase in borehole data in the local model volume after model version Laxemar 1.2, the updating of the rock domain model mainly comprises minor adjustments and refinements compared with the Laxemar 1.2 rock domain model. The overall judgement of the SDM-Site rock domain model is that both the geometrical relationships between the rock domains and their property assignment are stable and well understood in the focused volume, covering southern and south-western Laxemar. However, it should be noted that the boundary between the RSMM01 and RSMA01 rock domains is not as well constrained as the boundary between the RSMM01 and RSMD01 domains. The uncertainty results from the similar porphyritic texture and grain size of the Ävrö quartz monzodiorite in RSMM01 and the Ävrö granite in RSMA01, the main difference being that in mineralogical composition. Furthermore, the uncertainty in the boundary between the RSMM01 and RSMA01 domains also relates to the appearance of diorite/gabbro which also characterises the RSMM01 domain. Uncertainty in the geometrical boundary between RSMM01 and RSMA01 is judged to lie within +/-100 m of the modelled boundary.

The uncertainty in the rock domain model relates to a certain degree to the orientation, but in particular to the spatial distribution of subordinate rock types, i.e. fine-grained granite, pegmatite and fine-grained diorite-gabbro (composite intrusions) and dolerites (including possible existence of additional dykes). In addition, the uncertainty also relates to the distribution and size of diorite/gabbro bodies and the proportion of Ävrö granodiorite in the RSMM01 domain, as well as the proportion of Ävrö quartz monzodiorite in RSMA01. These uncertainties have been addressed by the thermal modelling team using a stochastic simulation process.

The uncertainty in the alteration, classified as either faint, weak, medium or strong, of the intact rock, outside the deformation zones that intersect the rock domains, relates to the spatial distribution and the effect on e.g. thermal and rock mechanical properties. The effect may point in different directions, e.g. positive for the thermal conductivity and negative for the rock mechanical properties, cf. Sections 6.2 and 7.2, respectively. It should be noted that red staining (oxidation) is usually related to fracturing, whereas saussuritisation also affects rock portions unaffected by fracturing.

In the regional model volume, the uncertainty is high with regards to both the existence and geometry of rock domains, since only reconnaissance surface data and no subsurface information are available.

Deterministic model for deformation zones

Outside the local model area, i.e. in the regional model, uncertainty concerning the existence and geometry of possible deformation zones is generally higher. Although detailed information is available locally around the Äspö HRL, CLAB and OKG facilities, generally only reconnaissance surface data and no subsurface information are available outside the local model areas employed in the Simpevarp 1.2, Laxemar 1.2 and SDM-Site Laxemar model versions.

Drilling activities in Laxemar have focused on the interpreted major lineaments within the local model area and consequently not all possible local major deformation zones have been investigated by drilling. In particular there are only a few boreholes in southern Laxemar and this inevitably leads to a high degree of uncertainty in the existence and character of possible deformation zones in this area.

Overall there is relatively high confidence in the existence and position of the larger, layout determining deformation zones at the ground surface. However, their modelled positions at depth, away from the actual borehole intercepts, are more uncertain. In particular there is relatively high uncertainty in their character and variability in physical properties due to the inferred heterogeneity of the deformation zones and due to the limited number of borehole intercepts with zones. It is important to note when viewing the block models presented in Sections 5.5.5 and 5.7, and in particular the horizontal sections shown in Figure 5-53c, Figure 5-61b and Figure 5-62b, that although there is a relatively high degree of uncertainty in the exact position of any deformation zone at a specific depth, there is a much higher level of confidence in the general pattern of deformation zones at repository depth.

Uncertainty is quantified through the use of confidence classes and where appropriate spans of likely values of individual zone properties. True zone thickness and true zone lengths are needed to establish a reliable relationship between zone thickness and zone size in boreholes. Estimation of true thickness requires analysis of orientation of deformation zones in the drill core, which can be very difficult to establish and hence highly uncertain. This means that the extent, shape, and orientation of deformation zones exposed only in boreholes is regarded as very uncertain and difficult to estimate. Due to the possibility of gently dipping zones, identified only in boreholes, being vertically displaced by cross cutting steeply dipping zones, the lateral continuity and extent of this type of zone is highly uncertain. The tectonic history of Laxemar is complex and kinematic studies have not enabled clear a differentiation of the sequencing of brittle reactivation in the rock mass.

Statistical model for fractures and minor deformation zones

An analytical quantification of uncertainties in the geological DFN model is presented by /La Pointe et al. 2008, cf. Chapter 6 therein/. Uncertainties in the orientation model are fairly well-understood, and have been demonstrated in past SDM reports, cf. /Fox et al. 2007/, to have little effect on overall model stability and function. The primary impact of the uncertainties in the coupled size-intensity model is expected to be related to the degree of utilisation of the proposed repository footprint. The principal uncertainties in the size intensity model are:

Conceptual Uncertainties related to:

- whether or not the fracture size model is independent of the fracture domain;
- whether or not the distribution of fracture sizes changes with depth (i.e. is it acceptable to use data on fracture traces at the ground surface to describe the size distribution at repository depth);
- whether fracture intensity scales in a Euclidean manner or exhibits fractal characteristics; and
- whether a size model built atop linked or unlinked traces /La Pointe et al. 2008, cf. Appendix A therein/ is a more appropriate description of the rock mass in Laxemar. The linking of fracture traces was an attempt to better represent larger fractures observed on outcrop. The behaviour of a fracture as it approaches a free surface (such as the ground surface) becomes very complex; it is possible that ‘sequentially-located traces’ may in fact represent a single geologic structure in the subsurface.

Parameter Uncertainties related to:

- whether the chosen ‘average’ value for the radius scaling exponent (k_r) is the most appropriate description for fracture size, or whether one of the alternative (‘Upper’ and ‘Lower’) is applicable;

- whether there is a significant effect on the size-intensity model if only fractures marked as ‘open’ are included; and
- whether all, or just some, of the lineaments recorded during Lidar and high-resolution ground magnetic surveying are used to compute the radius scaling exponent (k_r).

Uncertainty in the geological DFN model is quantified in terms of fracture intensity (P_{32}), and specifically, as the ratio of P_{32} for the Base Case parameterisation (Base Model Unlinked, see Section 5.6) to the P_{32} for alternative model parameterisations. The ratio is a measure of how much the fracture intensity can vary depending on which coupled size-intensity alternative model is used. The implicit assumption in the uncertainty analysis is that the Base Case parameterisation (BMU alternative) is the most appropriate of the alternatives for describing fracture intensity at Laxemar. P_{32} ratios are computed for two ranges of fracture sizes: 2.7 – 564.2 m, which are roughly similar to fracture sizes considered in the Expanded Full Perimeter Criteria (EFPC), cf. /Munier 2006, 2007/, and the recommended MDZ size range of 75 – 564.2 m (cf. Section 5.6.3). The P_{32} ratios, as well as some brief comments, are presented in Table 5-16.

The additional uncertainties remaining in the geological DFN model are considered to be relatively minor, in terms of their effects on the degree of utilisation. However, it is possible that these uncertainties could have impacts on subsequent hydrogeological modelling and rock-mass stability during tunnel construction. These uncertainties include:

- Fracture termination relationships. Studies of surface fracture trace data indicate complicated relationships between conjugate fracture sets and multiple periods of brittle re-activation /Viola 2008/. It is likely that the termination analysis presented in the geological DFN is too simplified to accurately reproduce the truncation patterns actually seen in detailed fracture outcrops.
- Uncertainty in local variability of fracture orientation. The geological DFN utilises a global orientation model applicable to all fracture domains. Some borehole and outcrop data show clusters of fracture poles that could be considered ‘complementary’ fracture orientation sets. Again, the impact of this uncertainty on the degree of utilisation is expected to be small.
- Domain FSM_S is poorly characterised in terms of data density. Fracture orientation, size, intensity, and spatial models are therefore highly unconstrained for this domain, and consequently it was largely excluded from the geological DFN analyses. Model parameterisation (coupled size-intensity model, orientation model) is presented for this domain in the geological DFN summary report for completeness, /La Pointe et al. 2008/, but FSM_S has not undergone the same level of statistical analysis as the other fracture domains. Domain FSM_S is well outside the potential footprint for a repository at Laxemar; the geological DFN team judged that, due to the limited available data, it was impossible to conclude anything about the bulk properties of the domain with any real confidence.

Table 5-16. Summary of key uncertainties in the geological DFN and their expected impacts on downstream modelling.

Uncertainty	Range of the ratio of Alternative Model fracture intensity to Base Case (BMU) fracture intensity	Comments
Scaling Exponent Dependence on Fracture Domain Conceptual Uncertainty	0.14 to 2.79; generally ~ 0.15 – 0.22 for subhorizontal sets	Greatest variability is by set, not fracture domain.
Euclidean vs. Fractal Scaling Conceptual Uncertainty	0.77 to 1.67; 0.96 for subhorizontal sets	Varies by set
Linked vs. Unlinked Traces Conceptual Uncertainty	0.63 to 1.03; 1.03 for subhorizontal sets	Fairly minor impact, especially on subhorizontal fractures
Number of lineaments used in size-intensity model parameterisation	0.44 to 1.11; unable to test subhorizontal sets	Smaller than uncertainty in scaling exponent parameter fit
Scaling Exponent Parameter Uncertainty	0.35 – 1.51; 0.35 for subhorizontal sets	Not highly variable among different sets
Open vs. Sealed Parameter Uncertainty	0.05 to 0.10 for outcrops; 0.20 to 0.30 for boreholes; generally around 0.30 for subhorizontal set (borehole data)	Varies by set and domain

6 Bedrock thermal properties

The heat generated by the spent nuclear fuel will increase the temperature of all components of the KBS-3 repository: barriers, tunnels, seals and the host rock itself. To ensure the long-term sealing capacity and the mechanical function of the bentonite buffer surrounding each individual canister, a maximum bentonite temperature (currently 100°C) is prescribed in the design premises. This important requirement, which relates to the safety assessment, implies that the canisters cannot be deposited arbitrarily close to one another. Unnecessarily large distances between the canisters, on the other hand, will mean inefficient and unnecessarily costly use of the repository rock volume. In order to determine the minimum canister spacing required to meet the temperature criterion for all canister positions, including those in the least conductive parts of the different rock domains where near-field temperatures will be particularly high, it is necessary to establish an adequate description of the site's rock thermal properties and their spatial variation at the relevant canister scale. In this chapter the thermal modelling performed for Laxemar in order to establish a thermal site description that is adequate for the layout requirements as well as for thermo-mechanical simulations is presented.

The methodology employed for thermal modelling has been fundamentally revised compared with previous model versions, and has been documented in a separate strategy report /Back and Sundberg 2007/. The modelling involves stochastic simulation based on both the spatial statistical structure of rock types and the spatial distribution of thermal conductivities. By merging the realisations of the lithological and thermal simulations, a distribution of thermal properties is produced that takes into account the spatial variability both within and between different rock types. The realisations of thermal properties can be used for subsequent numerical temperature simulations for the thermal design of a repository, i.e. for determining the minimum canister and tunnel spacings required to meet the buffer temperature criterion and to perform layout optimisation. The strategy for such thermal dimensioning is described in /Hökmark et al. 2009/.

The thermal site description in this SDM-Site Laxemar report is based on a separate report /Sundberg et al. 2008a/, in which the thermal modelling is more comprehensively described.

6.1 State of knowledge at the previous model version

Thermal modelling of the Laxemar subarea has been performed in different stages and versions. Model version Laxemar 1.2 is reported in /Sundberg et al. 2006, SKB 2006a/ and model stage Laxemar 2.1 in /Wrafter et al. 2006, SKB 2006c/. Based on the modelling in version 1.2 /Sundberg et al. 2006/, thermal properties were reported for five rock domains, three of which could be considered to be volumetrically important, namely RSMA01, RSMM01 and RSMD01. In model stage 2.1, new data, together with limited modelling efforts, indicated rather similar mean thermal conductivities for the domains but considerably higher variability /Wrafter et al. 2006/.

It is important to point out that previous model versions were based on version Laxemar 1.2 of the geological rock domain model, which during the current SDM-Site Laxemar modelling underwent modification of importance to thermal properties modelling. This is particularly relevant for rock domains RSMA01 and RSMM01.

6.2 Evaluation of primary data

Sources of available data on thermal properties are identified in Appendix 3 (cf. Table A3-2 therein). A more complete description of primary data is given in /Sundberg et al. 2008a/.

6.2.1 Thermal conductivity from measurements

Laboratory measurements of the thermal conductivity and thermal diffusivity of water-saturated rock samples have been performed using the TPS (Transient Plane Source) method (see description in /Sundberg 2003a/). Summary statistics of thermal conductivity and thermal diffusivity for each rock type, irrespective of rock domain, are presented in Table 6-1 and are further described in /Sundberg et al. 2008a/. Ävrö granite has previously been recognised to be bimodal with respect to thermal conductivity /Wrafter et al. 2006/. This has led to the subdivision of Ävrö granite into two distinct rock types: Ävrö quartz monzodiorite (rock type name code: 501046) and Ävrö granodiorite (501056) (see /Wahlgren et al. 2008/ and Section 5.2.2). The former is quartz poor (usually < 15%) while the latter is quartz rich (usually > 20%). In the absence of modal analysis, a density of 2,710 kg/m³ has been used as a suitable threshold for distinguishing between the two rock types /Wahlgren et al. 2008/. Diorite-gabbro (501033) samples have yielded a wide range of thermal conductivity values, from 2.06 W/(m·K) to 3.65 W/(m·K), suggesting that more than one statistical population may be represented. A more extensive description is provided in /Sundberg et al. 2008a/.

The results of all thermal conductivity measurements are plotted against elevation in Figure 6-1. A comparison of data from different boreholes and different depths indicates little, if any, large-scale spatial variation in thermal conductivity for Ävrö granodiorite. However, for Ävrö quartz monzodiorite the differences in thermal conductivity between different parts of the local model volume may be larger. The mean thermal conductivity of quartz monzodiorite for surface samples is lower than that of borehole samples (for data from different boreholes, see /Sundberg et al. 2008a, cf. Tables 6-5 to Table 6-7 therein/).

The degree of alteration has been classified in the Boremap mapping as faint, weak, medium or strong, and is dominated by both oxidation and saussuritisation. The available data /Sundberg et al. 2008a/ indicate that the thermal conductivity of rock showing a weak or medium degree of alteration is generally higher than that of fresh rock. For Ävrö granodiorite, altered samples indicate a 4% higher thermal conductivity, whereas for quartz monzodiorite a 15% difference is noted. Little or no difference in thermal conductivity was noted between samples from drill core mapped as faintly altered and samples from core mapped as fresh, although this observation is based on only a few faintly altered samples. A possible explanation for the lack of a difference may be found in the fact that even samples mapped as “fresh” have undergone some degree of alteration /Drake and Tullborg 2006ab/.

Field measurements of thermal conductivity and thermal diffusivity on outcrops have been performed in Laxemar /Mossmark and Sundberg 2007/ and summarised and further evaluated in /Sundberg et al. 2008a/. The results indicate a mean thermal conductivity of 2.31 W/(m·K) for Ävrö quartz monzodiorite and a mean conductivity of 2.97 W/(m·K) for Ävrö granodiorite. The measurement scale of the field measurements is approximated to 0.2–0.5 m which is substantially larger than that for laboratory measurements, which is about 0.05 m.

Table 6-1. Measured thermal conductivity (W/(m·K)) of different rock types at room temperature (20°–25°C) using the TPS method /Gustafsson 1991/. The numbers of samples reflects the approximate relative volumetric importance of these rock types in the Laxemar-Simpevarp area.

Rock name	Name code	Mean	St. dev	Max	Min	Number of samples
Fine-grained dioritoid	501030	2.79	0.16	3.16	2.51	28
Quartz monzodiorite	501036	2.74	0.17	3.30	2.42	63
Ävrö quartz monzodiorite	501046	2.36	0.20	2.71	2.01	33
Ävrö granodiorite	501056	3.17	0.17	3.76	2.81	60
Fine-grained granite	511058	3.69	0.08	3.76	3.58	4
Granite	501058	3.01		3.11	2.89	3
Diorite-gabbro	501033	2.64	0.46	3.65	2.06	22
Fine-grained diorite-gabbro	505102	2.49	0.24	2.73	2.25	4

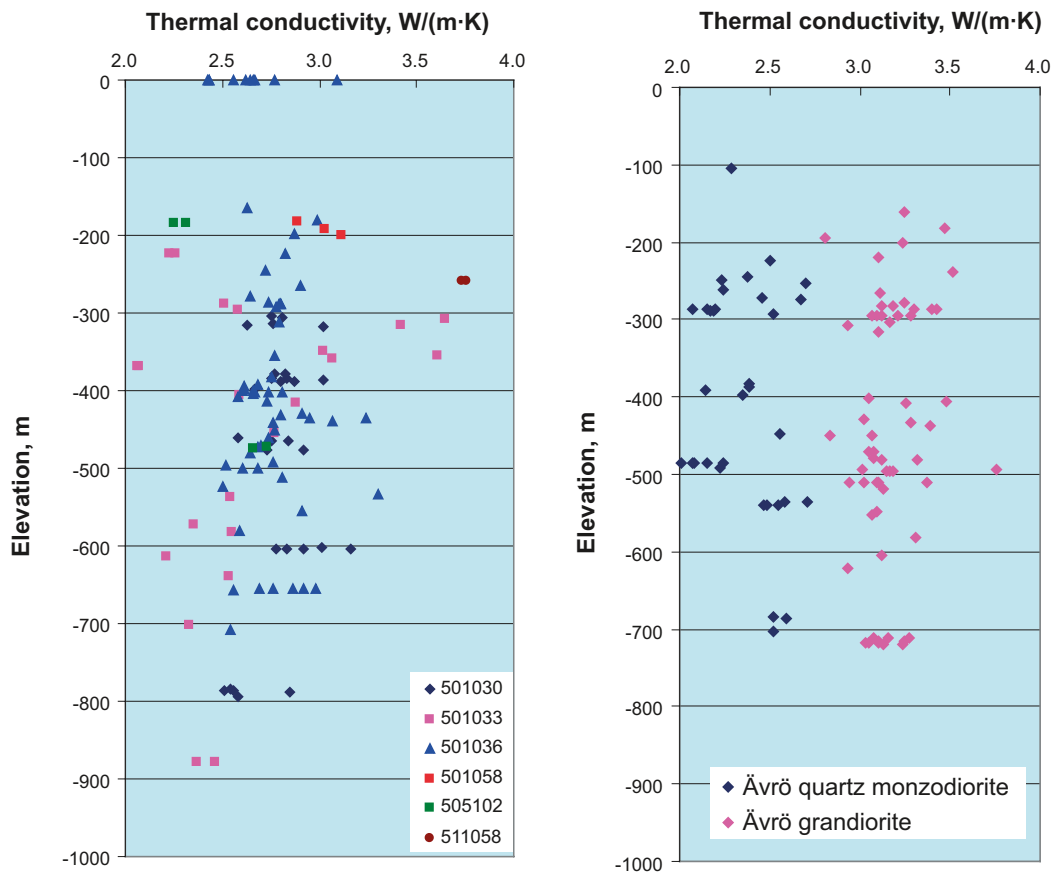


Figure 6-1. Thermal conductivity versus elevation for different rock types. Thermal conductivity measured using the TPS method. Data are from different boreholes. For rock type names, see Table 6-1.

The thermal conductivity of rock samples has also been calculated by the SCA method (Self Consistent Approximation) using mineral percentages derived from modal analyses and reference values of the thermal conductivity of different minerals, as described in /Sundberg 1988, Back and Sundberg 2007/. However, the results have higher uncertainties compared with measurements and have mainly been used for purposes of understanding the properties of altered rock types and for the thermal conductivity models for some rock types with sparse laboratory data.

6.2.2 Relationship between thermal conductivity and density

A relationship between density and measured (TPS) thermal conductivity for Ävrö granite in the Laxemar-Simpevarp area is well established /Sundberg 2003b, Sundberg et al. 2005, Wrafter et al. 2006, Sundberg et al. 2009/ (see Figure 6-2). The observed relationships are consistent with the results of theoretical calculations based on mineral composition /Sundberg et al. 2009/. For example, the high-density mafic rocks (e.g. gabbros) contain abundant pyroxene and amphibole (and in some cases chlorite), minerals which, compared to the feldspars, have relatively high thermal conductivities.

Establishing relationships between density and thermal conductivity allows a more reliable use of borehole density data for analysing the spatial correlation structure of thermal properties (Section 6.4.5). The relationship for different rock types is shown in Figure 6-2.

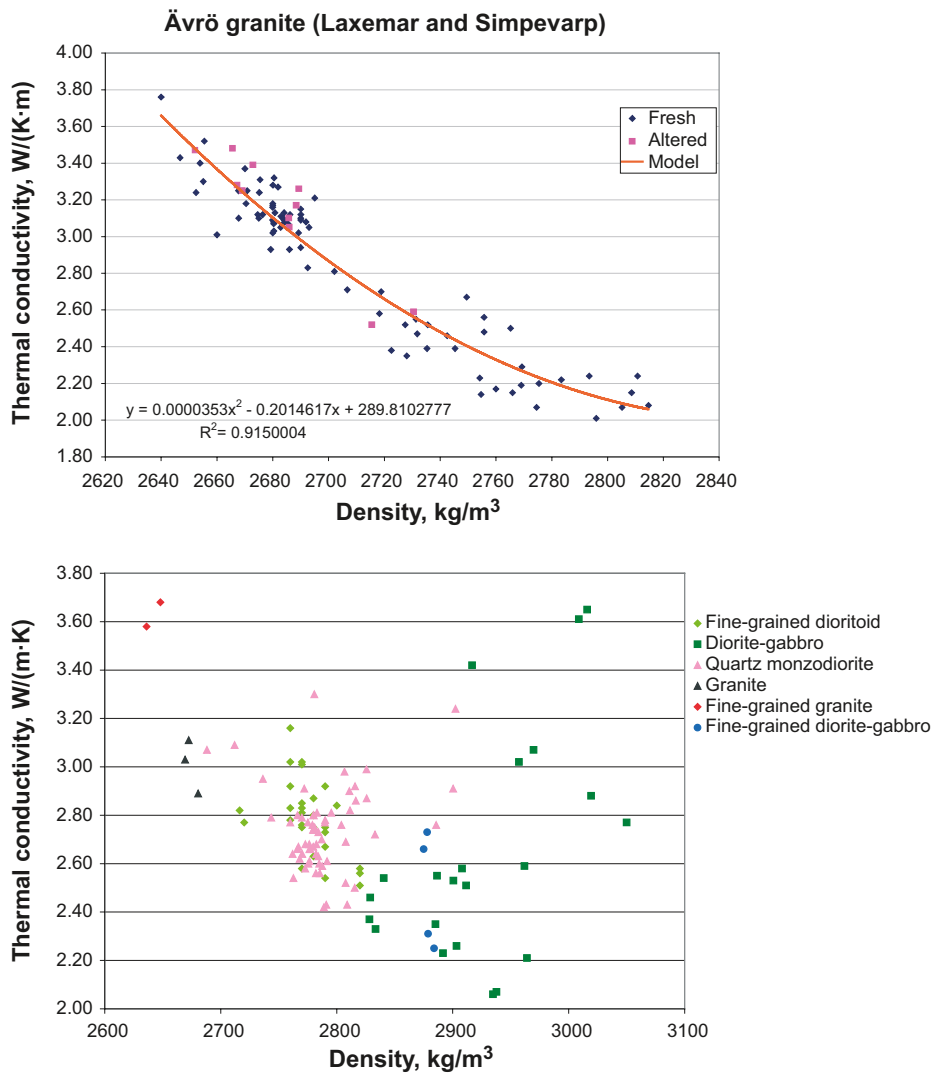


Figure 6-2. Relationships between density and thermal conductivity (TPS measurements) for Ävrö granite (above) and other rock types (below). Rocks with felsic and intermediate compositions show decreasing thermal conductivity with density, whereas mafic rocks display the opposite relationship. Ävrö granite comprises both Ävrö quartz monzodiorite (density > 2,710 kg/m³) and Ävrö granodiorite (density ≤ 2,710 kg/m³). The model for Ävrö granite is based on fresh samples only.

6.2.3 Measurement of anisotropy of thermal conductivity associated with foliation

In Laxemar, a faint to weak foliation, which is not uniformly distributed in the bedrock, is present and affects all rock types, see Section 5.2.4. The foliation implies a directional orientation of the minerals in the rock mass. The thermal conductivity is generally higher parallel to, and lower perpendicular to, the foliation plane.

Based on measurements of thermal conductivity at seven outcrop locations in Laxemar /Mossmark and Sundberg 2007/, the dip-corrected mean anisotropy factor has been estimated to 1.15 /Sundberg et al. 2008a/. No compensation has been made for possible uncertainties related to orientation of the strike of the foliation.

The mean anisotropy factor is of the same order of magnitude as that observed in Forsmark /Back et al. 2007/, a somewhat unexpected result given that the structural fabric in Forsmark is much more strongly developed than in Laxemar /Söderbäck 2008/. The measurements in Laxemar have been made in Ävrö quartz monzodiorite and Ävrö granodiorite. Since the foliation is similarly developed in other rock types, the results relating to anisotropy are judged to be valid for the entire Laxemar subarea. However, spatial variability in the anisotropy factor can be expected.

The orientation of the foliation varies throughout the Laxemar area which implies that the orientation of maximum and minimum anisotropy of thermal conductivity will also vary accordingly (Section 5.4.2). The foliation generally strikes east-west, but its dip varies considerably. In domain RSMA01, the foliation has a shallow to moderate dip to the north, whereas in domain RSMD01 the foliation is either subhorizontal or dips gently to the south. In the intervening domain RSMM01, the foliation displays variable dips both to the north and south.

6.2.4 Heat capacity

Heat capacity has been determined indirectly from thermal conductivity and diffusivity measurements using the TPS (Transient Plane Source) method, and directly by calorimetric measurement. In Table 6-2, results of both methods for the same samples are shown.

Differences in the heat capacity values of up to c. 20% are observed for individual rock samples. However, the average difference between the results of the two methods is less than 1%, which indicates that the calculated values based on TPS determinations, although more uncertain, do not suffer from bias. However, the higher precision calorimetric measurements have been used in the modelling when available.

The relationship between thermal conductivity and density is described in Section 6.2.2. To investigate if a corresponding relationship between heat capacity and density exists, density was plotted against both indirectly and directly determined heat capacity values. Figure 6-3, shows a consistent pattern of increasing heat capacity with increasing density for the calorimetric measurements. The pattern is much less consistent for the indirect determinations of heat capacity /Sundberg et al. 2008a, cf. Figure 3-24 therein/. One explanation for this is that these rocks are anisotropic which means that thermal diffusivity determinations vary according to the orientation of the plane of measurement.

6.2.5 Thermal conductivity vs heat capacity

In thermal modelling of Forsmark, a relationship between thermal conductivity and heat capacity was established /Sundberg et al. 2008b/. However, in Laxemar no obvious relationship between thermal conductivity and heat capacity exists. Therefore, the approach used for modelling heat capacity in Forsmark cannot be mimicked in Laxemar (Section 6.5.1).

6.2.6 Temperature dependence of thermal properties

The temperature dependence of thermal properties has been investigated by laboratory measurements, using the TPS-method, on samples of the dominant rock types, see Table 6-3. The temperature dependence for gabbro, based on literature data, is also included in the table for reference.

Table 6-2. Comparison between heat capacities (MJ/m³·K) calculated from TPS measurement and direct determination by the calorimetric method for the same samples.

Rock name	Diorite-gabbro	Quartz monzodiorite	Ävrö quartz monzodiorite	Ävrö granodiorite	Fine-grained diorite-gabbro	All rock types
Rock code	501033	501036	501046	501056	505102	
Calorimetric						
Mean	2.44	2.24	2.17	2.12	2.29	2.24
St. dev.	0.04	0.05	0.05	0.10		0.125
N	9	16	9	9	2	45
Max	2.52	2.34	2.26	2.25	2.30	2.52
Min	2.38	2.17	2.1	1.91	2.27	1.91
TPS						
Mean	2.37	2.22	2.19	2.13	2.20	2.23
St. dev.	0.22	0.10	0.13	0.17		0.164
N	9	16	9	9	2	45
Max	2.63	2.56	2.36	2.42	2.22	2.63
Min	1.91	2.08	1.99	1.89	2.17	1.89

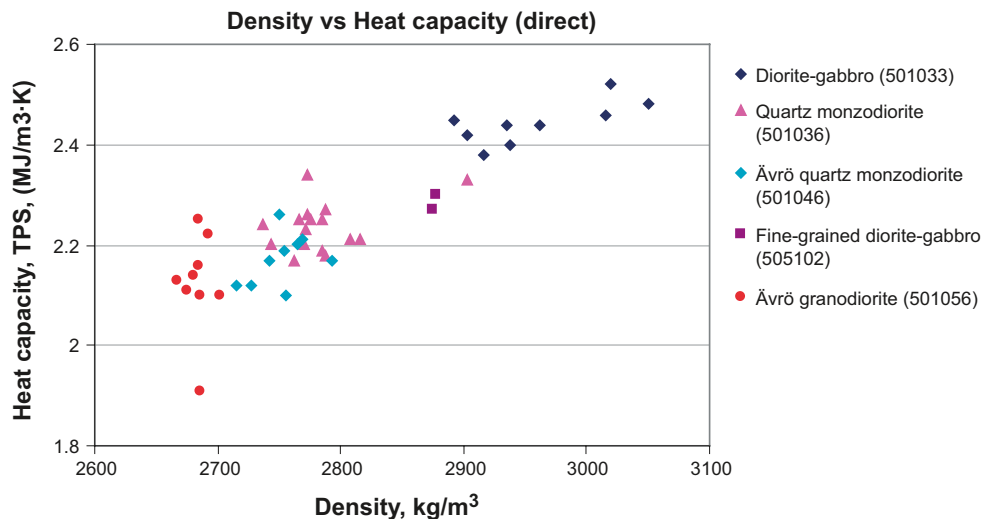


Figure 6-3. Density versus heat capacity (direct calorimetric measurements) for different rock types.

Table 6-3. Temperature dependence of thermal conductivity and heat capacity (per 100°C temperature increase) for different rock types. Mean values of temperature dependence calculated by linear regression. From /Sundberg et al. 2008a/.

Rock name	Mean temperature dependence		Number of samples
	Thermal conductivity	Heat capacity	
Fine-grained dioritoid (501030)	-3.4%	25.6%	11
Quartz monzodiorite (501036)	-1.1%	25.3%	5
Ävrö quartz monzodiorite (501046)	-2.9%	26.0%	8
Ävrö granodiorite (501056)	-6.8%	23.8%	5
Fine grained granite (511058) (estimated from similar rock types in Forsmark /Sundberg et al. 2008b/)	-10%	25%	
Gabbro (Literature data /Mottahgy et al. 2005/)	-3.1%	20.6%	1

6.2.7 Pressure dependence of thermal conductivity

The thermal conductivity is expected to be lower in stress-released samples than in samples at higher pressure (greater depths). However, if the samples are water saturated, the pressure influence up to 50 MPa appears to be low, approximately 1–2% according to /Walsh and Decker 1966/. All determinations of thermal conductivity performed in the site investigation programme have been made on water-saturated samples. The pressure dependence has therefore been neglected in the modelling.

6.2.8 Coefficient of thermal expansion

The coefficient of thermal expansion has been measured on samples from five different rock types, see Table 6-4. The mean values for the different rock types are rather similar. For more information see /Sundberg et al. 2008a/.

Table 6-4. Measured thermal expansion (m/(m·K)) on samples of different rock types in the Laxemar-Simpevarp area (interval of temperature: 20–80°C).

Rock code	Rock name	Arithmetic mean	St. dev.	Min	Max	No of samples
501030	Fine-grained dioritoid	$6.9 \cdot 10^{-6}$	$1.5 \cdot 10^{-6}$	$4.6 \cdot 10^{-6}$	$9.9 \cdot 10^{-6}$	17
501033	Diorite-gabbro	$7.4 \cdot 10^{-6}$	$1.0 \cdot 10^{-6}$	$5.9 \cdot 10^{-6}$	$8.3 \cdot 10^{-6}$	6
501036	Quartz monzodiorite	$7.3 \cdot 10^{-6}$	$1.1 \cdot 10^{-6}$	$5.8 \cdot 10^{-6}$	$9.3 \cdot 10^{-6}$	11
501046	Ävrö quartz monzodiorite	$7.1 \cdot 10^{-6}$	$1.4 \cdot 10^{-6}$	$4.3 \cdot 10^{-6}$	$9.1 \cdot 10^{-6}$	12
501056	Ävrö granodiorite	$7.3 \cdot 10^{-6}$	$1.9 \cdot 10^{-6}$	$4.5 \cdot 10^{-6}$	$1.2 \cdot 10^{-5}$	37

6.2.9 *In situ* temperature

Fluid temperature and vertical temperature gradients have been measured in most cored boreholes in Laxemar. Large differences in logged temperature at the same depth in different boreholes were noted in earlier model stages /Wrafter et al. 2006/. For this reason, the fluid loggings for each borehole have been evaluated with the objective of assessing their reliability. The criteria considered were 1) errors associated with logging probe and 2) time between drilling and logging. The evaluation of temperature data based on these criteria resulted in a number of “approved” boreholes, see /Sundberg et al. 2008a/. The results are presented in Table 6-5 and Figure 6-4. The measured temperatures at -500 m fall within the interval 14.7–14.9°C for the boreholes KLX02, KLX05, KLX08 and KLX18A. Comparison with results of Posiva flow logging indicates a generally good agreement between the two methods.

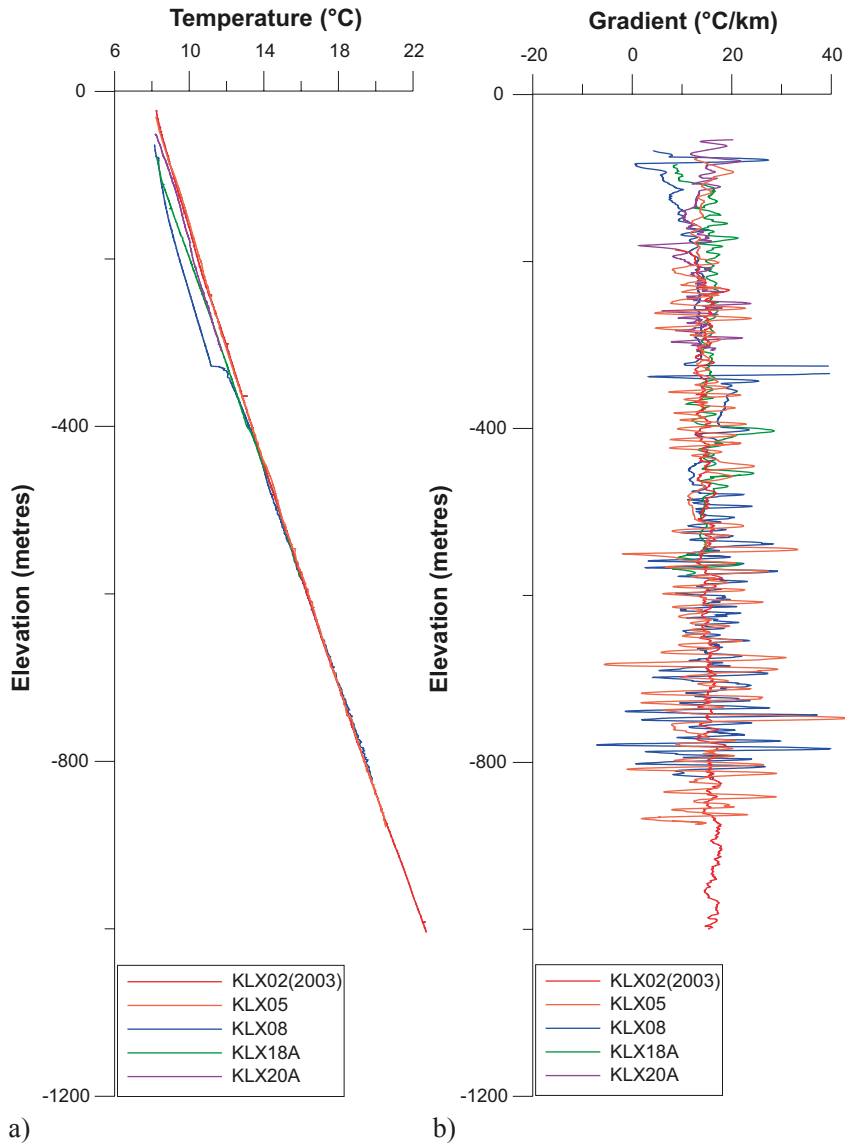


Figure 6-4. Summary of temperature (a) and gradient calculated for nine metre intervals (b) for five boreholes in Laxemar. Results from “approved” fluid temperature loggings only.

Table 6-5. Temperature (°C) for the “approved” boreholes in Laxemar, at three different elevations. Borehole inclinations are also included for the boreholes, given as lowest and highest angle. Temperature from Posiva flow logs (PFL) are given in parentheses.

Borehole	Temperature at –400 m	Temperature at –500 m	Temperature at –600 m	Inclination** (°)
KLX02 (2003)	13.4	14.8	16.3	83–85
KLX05	13.4 (13.1)	14.9 (14.7)	16.4 (16.3)	63–65
KLX08	13.2 (13.2)	14.7 (14.8)	16.3 (16.3)	56–60
KLX18A*	13.1 (13.1)	14.8 (14.7)	–	80–82
Arithmetic mean	13.3	14.8	16.3	

* KLX18A reaches a maximum vertical depth of about –580 m.

6.3 Strategy for thermal modelling

6.3.1 Conceptual model

The methodology employed for thermal modelling is based on stochastic simulation, and has been fundamentally revised compared with previous model versions. The new methodology is documented in a separate strategy report /Back and Sundberg 2007/. This methodology has also been implemented in the Forsmark site description, stage 2.2 /Back et al. 2007/ and stage 2.3 /Sundberg et al. 2008b/. The strategy for thermal modelling is based on a conceptual model which considers a range of properties, including lithology, alteration of rock types, thermal properties of rock types, spatial variability and correlation. The conceptual model explains the spatial variability of thermal conductivity in terms of lithological and mineralogical heterogeneity (variability), and also provides an explanation for anisotropy of thermal properties.

Thermal properties, especially thermal conductivity, vary significantly between different rock types but also within specific rock types. Much of this variability is a result of different mineralogical compositions of the igneous rock types, which is ultimately related to magma compositions. Compositional variability within a specific rock type is a result of variations in the mineral proportions caused, for example, by incomplete magmatic mixing and mingling processes. The “within rock type” variability is also a result of post-crystallisation processes such as hydrothermal alteration, but even the way in which rocks have been classified; for example, a particular rock type may include two or more subtypes that are difficult to distinguish from each other in hand specimen.

Based on the considerations above, the total variability of thermal properties within a rock domain depends on the lithology and the thermal properties of each rock type. The lower tail of the thermal conductivity distribution at a certain scale is determined by the fraction and size distribution of the thermally low-conductive rock types. This lower tail is important for the design of the repository.

The rock mass in Laxemar displays anisotropy in thermal properties. There are at least two main causes of thermal anisotropy to consider:

1. Anisotropy due to foliation (Section 6.2.3).
2. Anisotropy due to orientation of subordinate rock bodies.

The first type is a structural anisotropy caused by foliation within a rock type. Foliation implies a directional orientation of the minerals in the rock mass. The thermal conductivity is generally higher parallel to and lower perpendicular to the foliation plane.

The second type of anisotropy is a result of the preferential spatial orientation of bodies of subordinate rocks. Dykes of, for example, fine-grained granite and fine-grained diorite-gabbro may cause this type of thermal anisotropy in Laxemar, but its impact is considered to be minor.

6.3.2 Modelling approach

Introduction

The strategy /Back and Sundberg 2007/ for the thermal site descriptive modelling involves producing spatial statistical models of both rock types and thermal properties, and performing stochastic simulations to give spatial 3D realisations of thermal properties that are representative of the modelled rock domains /Back and Sundberg 2007/. These realisations are used to represent the rock domain statistically. The results of the thermal simulations are presented primarily at the 5 m scale, which is a relevant scale for the temperature development around a canister.

There are different objectives for which the modelling approach can be used. In this work, the focus is on description. Of special interest for the description are:

- to determine the lower percentiles of thermal conductivity,
- to model how the thermal conductivity varies with scale, and
- to produce realisations of the spatial distribution of thermal properties that can be used for subsequent modelling work, such as numerical temperature simulations for the thermal design of a repository (distances between canisters and tunnels).

For the thermal description, no consideration is given to parameterisation at specific locations in the rock mass; it is primarily the statistics of the rock domain that are of interest. The methodology for this type of problem is based on unconditional stochastic simulation (distributes simulated data spatially without honouring measurements at specific locations, i.e. no conditioning is applied). Large-scale spatial heterogeneity within a rock domain is dealt with by dividing the domain into lithologically more homogenous thermal subdomains. Due to the large rock volumes and computer limitations, conditional stochastic simulation with high resolution of an entire rock domain or subdomain is not feasible. Conditional simulation of small rock volumes at specific locations may be used for prediction purposes during the construction phase of a repository. The results of an example conditional simulation for a volume of rock in domain RSMM01 is reported in Section 6.5.1.

The focus of the modelling approach is on thermal conductivity, the main rock parameter influencing the temperature of the buffer surrounding the canister. In addition, the heat capacity distribution is modelled. The approach is based on the assumption of a Gaussian heat capacity distribution for each rock type (reclassified as TRCs; see below). The overall distribution of heat capacity for the rock domain is a product of the distributions for each rock type and the simulated realisations of the lithology.

Outline of the methodology

The methodology, outlined in Figure 6-5, is applied separately for each rock domain. The simulation scale (1) is defined first. This scale determines how lithological data (2) should be prepared and if a change of support (or upscaling) (5) is required for the thermal data (4). Support refers to the rock volume that the data values (measurements or simulated values) represent. A change of support is required if the measurement volume is significantly smaller than the desired simulation scale. The lithological data acquired from boreholes and mapping of the rock surface need to be reclassified into thermal rock classes, TRCs (3). The main reason is to simplify the lithological simulations, since only a limited number of classes can be handled.

The lithological data are used to construct models of the transitions between different TRCs, thus describing the spatial statistical structure of each TRC (7). The result is a set of transitional probability models that are used in the stochastic simulation of TRCs (8). These simulations generate a number of realisations of the spatial distribution of TRCs in each domain.

Based on the thermal data, a spatial statistical thermal conductivity model is constructed for each TRC (9). Such a model consists of both a statistical distribution and a variogram, i.e. a model describing spatial correlation. These models are used in the stochastic simulation of thermal conductivity (10), which results in a number of equally probable realisations of thermal conductivity for the studied TRCs.

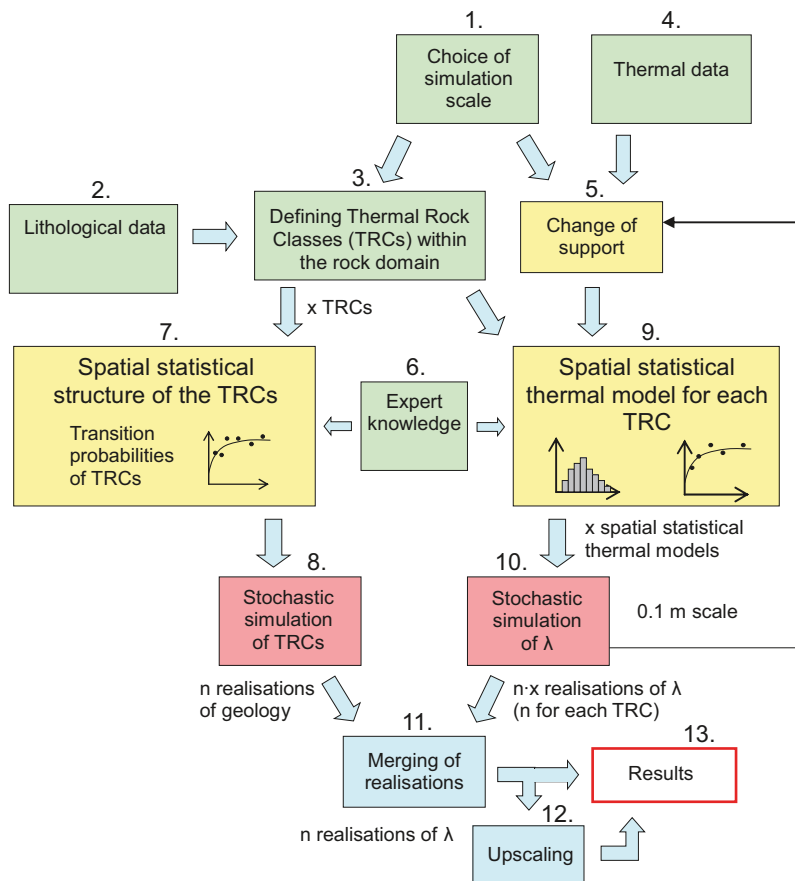


Figure 6-5. Schematic description of the approach for thermal conductivity modelling of a rock domain (λ denotes thermal conductivity; change of support = upscaling).

In the next step, the realisations of TRCs (lithology) and thermal conductivity are merged (11), i.e. each realisation of lithology is filled with simulated thermal conductivity values. The result is a set of realisations of thermal conductivity that considers both the difference in thermal properties between different TRCs, and the variability within each TRC. If the results are desired at a scale different from the simulation scale, upscaling of the realisations can be performed (12) to a scale not larger than the size of the simulation domain. In practice, upscaling should be made to a much smaller scale, preferably the canister scale. The results (13) can be presented in a number of ways, for example as 3D illustrations, histograms and statistical parameters for the rock mass, probabilities of encountering low thermal conductivity values, etc.

The methodology can also be used for other types of rock properties.

Adaptations of the modelling approach to Laxemar

The thermal modelling strategy outlined above is described in detail in /Back and Sundberg 2007/. However, there are some aspects of the modelling that need additional comments, primarily related to steps 5 through 10 in Figure 6-5. These include the establishment of thermal subdomains of the lithology and are described in /Sundberg et al. 2008a/.

Spatial statistical analysis of the Laxemar borehole data reveals that, with regard to lithology, the rock domains are often not homogeneous in a statistical sense. However, the stochastic simulations require statistical homogeneity. Therefore, where necessary, rock domains are divided into more lithologically homogenous subdomains and each subdomain is then modelled and simulated separately. These subdomains are denoted “thermal subdomains” to emphasise that they are defined from a thermal perspective. A thermal subdomain has no defined spatial boundaries; only its proportion of the given rock domain is defined. The proportion is estimated based on borehole lengths and

geological expertise. The number of realisations produced during simulation for each subdomain corresponds to the relative proportions of the subdomains within the domain. After simulation, all realisations for all subdomains are combined to form a single set of lithological realisations that represents the rock domain of interest.

6.3.3 Modelling assumptions

The modelling approach requires a number of assumptions in various steps of the modelling process. The most important ones are the following:

- Information in Sicada from Boremap and core samples used for thermal conductivity measurements are assumed to be representative of the rock domain;
- Water movements are not considered in the modelling;
- Rock stress is assumed to have no effect on the thermal properties (the effect is small in water-saturated rock /Walsh and Decker 1966/);
- The modelling is performed using effective values of thermal conductivity (isotropic assumption). This also applies to the upscaling methodology where effective values are calculated using the SCA approach, described in /Back and Sundberg 2007, cf. Section 2.3.4 therein/. Anisotropy is evaluated separately;
- It is assumed that the spatial statistical thermal model for a TRC (statistical distribution and variogram) is the same for all rock types that belong to that TRC;
- Spatial correlation in thermal conductivity between different parts of a rock type body is assumed not to be “broken” by the presence of a different type of rock separating these parts;
- In the lithological (TRC) simulations, it is assumed that the lengths/thicknesses of rock bodies follow an approximately geometric distribution;
- It is assumed that the thermal data represent the 0.1 m scale, which is the scale at which the initial simulations are performed (cells of cubic shape with 0.1 m sides);
- The 2 m scale is assumed to be sufficiently small to properly represent the subordinate rock types in the lithological simulations;
- The simulation volumes ($100 \times 100 \times 100 \text{ m}^3$ for scale 2 m) are assumed to be sufficiently large for the objectives of the simulations;
- For the purpose of lithological simulations, a rock domain is divided into thermal subdomains, each of which is assumed to be statistically homogeneous.

With the objectives of the thermal modelling in mind, all of these assumptions are considered to be reasonable. Information regarding the assumptions made for the lithological and the spatial statistical thermal models for each TRC is provided in the following sections.

6.3.4 Feedback from other disciplines

The SDM-Site Laxemar rock domain model /Wahlgren et al. 2008/ and Section 5.4, constitutes the basis for the description of thermal properties of the rock mass within the local model volume in Laxemar. Three key rock domains have been identified within the local model volume. These are the volumetrically important domains RSMA01, RSMD01 and RSMM01. The thermal properties of these three domains are evaluated here. Valuable cooperation with the geologists in the Laxemar modelling team has been established and maintained throughout the thermal modelling. Integration with geology was particularly comprehensive and important in the case of the geological interpretations used as input in the stochastic simulations of lithologies.

6.4 Geostatistical analyses and stochastic simulations

In this section, geostatistical analyses and simulations of both lithologies and thermal conductivity are summarised. For a more comprehensive description, see /Sundberg et al. 2008a/.

6.4.1 Thermal Rock Classes (TRC) – Definition, properties and proportions

Geological borehole data form the basis for the stochastic simulation of lithologies, an important component of the thermal modelling procedure. To keep the lithological simulations at a manageable level of complexity, the number of lithological classes should not exceed five. For this reason, the rock types are grouped into classes, called thermal rock classes (TRC). Rock types with similar thermal and lithological properties were assigned to the same class. A description of the eight TRCs defined is given in Table 6-6.

The code for a TRC is defined by using the last two or three digits of the rock code for the dominating rock type in that class. Ävrö granite has been divided into its constituent varieties, namely Ävrö quartz monzodiorite and Ävrö granodiorite, and forms the basis for two TRCs, 46 and 56 respectively. TRC 136, which comprises oxidised quartz monzodiorite, was defined in order to facilitate stochastic simulation of rock mechanics properties (Section 7.3). For thermal modelling purposes TRC 136 is assumed to be synonymous with TRC 36, so that both can be described by the same spatial statistical thermal model.

The TRCs defined for domains RSMA01, RSMD01 and RSMM01 together with the proportions of rock types are presented in Table 6-7 to Table 6-9. RSMA01 consists of five TRCs, while only four TRCs are selected for modelling of RSMD01 and RSMM01 since TRCs making up less than 1% of the volume are excluded. In addition, the 95% upper and lower confidence limits for TRC proportions in RSMA01, RSMD01 and RSMM01 are presented in the tables (for method and details see /Sundberg et al. 2008a/).

The most noticeable difference between the proportions estimated from the borehole data used for lithological simulations and the proportions estimated by the geological modelling team concerns TRC 58. The main reason for this is the exclusion from the lithological simulation data of fine-grained granite (511058) and pegmatite (501061) having borehole occurrences less than 1 m length. For all other TRCs, the estimates by the geological modelling team fall within the calculated 95% certainty limits.

Despite the relatively large number of boreholes in each domain, the high degree of lithological heterogeneity results in rather large uncertainties in the estimated proportions of TRCs.

Table 6-6. Classification of rock types into thermal rock classes (TRC). Dominant rock types in bold. For a more complete summary of thermal conductivity statistics, see Table 6-1.

TRC	Rock name (code)	Mean thermal conductivity (TPS)	Composition, mode of occurrence, etc	Present in rock domain
30	Fine-grained dioritoid (501030)	2.79	Intermediate composition	A
	Quartz monzodiorite (501036)	2.74		
33	Diorite-gabbro (501033)	2.64	Intermediate-mafic composition	M
	Fine-grained diorite-gabbro (505102)	2.49		
36	Quartz monzodiorite (501036)	2.70	Intermediate composition	D
	Fine-grained dioritoid (501030)	2.79		
56	Ävrö granodiorite (501056)	3.16	Felsic composition	A, M
	Granite (501058)	3.01		
46	Ävrö qtz monzodiorite (501046)	2.36	Intermediate composition	A, M
58	Fine-grained granite (511058)	3.69	Felsic composition; occur as dykes and small bodies	A, D, M
	Pegmatite (501061)			
102	Fine-grained diorite-gabbro (505102)	2.49	Intermediate-mafic composition; fine-grained diorite-gabbro occurs as dykes	A, D
	Diorite-gabbro (501033)	2.64		
	Dolerite (501027)			
136	Oxidised quartz monzodiorite (501036)	See TRC 36	Intermediate composition	D

Table 6-7. Proportions and confidence intervals for TRCs in domain RSMA01. Based on bore-holes located within domain RSMA01 in the central and southern part of Laxemar. Proportions based on geological model are from /Wahlgren et al. 2008/. Confidence intervals calculated from bootstrapping /Sundberg et al. 2008a/.

TRC	Rock name (code)	Mean proportion of TRC, 2 m borehole data	95% confidence intervals, 2 m borehole data	Proportion of TRC in 1,000 realisations, 2 m scale	Proportions based on geological model *
56	Ävrö granodiorite (501056), Granite (501058)	64.6%	55–76%	64.6%	} 88.7%
46	Ävrö quartz monzodiorite (501046)	26.2%	15–40%	27.1%	
58	Fine-grained granite (511058) Pegmatite (501061)	1.8%	0.6–2.8%	1.8%	3.6%
30	Fine-grained diorite (501030) Quartz monzodiorite (501036)	5.4%	0.3–11.3%	4.8%	5.2%
102	Fine-grained diorite-gabbro (505102) Diorite-gabbro (501033)	2.0%	1.2–2.8%	1.7%	2.5%

* In the geological model /Wahlgren et al. 2008/, proportions of Ävrö quartz monzodiorite and Ävrö granodiorite have not been estimated separately. Instead, both are included in Ävrö granite.

Table 6-8. Proportions and confidence intervals for TRCs in domain RSMD01. Proportions based on geological model are from /Wahlgren et al. 2008/. Confidence intervals calculated from bootstrapping /Sundberg et al. 2008a/.

TRC	Rock name (code)	Mean proportion of TRC, 2 m borehole data	95% confidence intervals, 2 m borehole data	Proportion of TRC in 1,000 realisations, 2 m scale	Proportions based on geological model *
36	Quartz monzodiorite (501036)	84.6%	80–89%	82.9%	} 89.1%
136	Oxidised quartz monzodiorite (501036)	8.4%	5.9–10.8%	9.9%	
58	Fine-grained granite (511058) Pegmatite (501061)	3.6%	1.1–8.9%	3.5%	
102	Fine-grained diorite-gabbro (505102), Diorite-gabbro (501033), Ävrö quartz monzodiorite (501046), Dolerite (501027)	3.4%	1.1–6.0%	3.7%	c. 4%
36+ 136	Quartz monzodiorite (501036)	93.0%	89–96%		Other: < 1%

* In the geological model /Wahlgren et al. 2008/, the proportion of quartz monzodiorite comprises both fresh and altered rock.

Table 6-9. Proportions and confidence intervals for TRCs in domain RSMM01. Proportions based on geological model are from /Wahlgren et al. 2008/. Confidence intervals calculated from bootstrapping /Sundberg et al. 2008a/.

TRC	Rock name (code)	Mean proportion of TRC, 2 m borehole data	95% confidence intervals, 2 m borehole data	Proportion of TRC in 1,000 realisations, 2 m scale	Proportions based on geological model *
33	Diorite-gabbro (501033), Fine-grained diorite-gabbro (505102),	16.9%	11.2–24.0%	16.7	18.0%
56	Ävrö granodiorite (501056), Granite (501058)	27.7%	15.4–41.4%	24.7	77%
46	Ävrö quartz monzodiorite (501046)	53.2%	35.6–68.0%	56.4	
58	Fine-grained granite (511058) Pegmatite (501061)	2.2%	0.5–4.7%	2.2	5.2%
					Other: < 1%

* In the geological model /Wahlgren et al. 2008/, proportions of Ävrö quartz monzodiorite and Ävrö granodiorite have not been estimated separately. Instead, both are included in Ävrö granite.

6.4.2 Geological heterogeneity and division into thermal subdomains

Rock domains RSMA01 and RSMM01 are lithologically more inhomogeneous than domain RSMD01. In order to capture the lithological heterogeneity present within the former two rock domains in the stochastic simulations, each domain was divided into thermal subdomains (Table 6-10), each of which was assumed to be statistically homogeneous. Each “subdomain” was then simulated separately.

Three thermal subdomains were defined for RSMA01. RSMM01 is the most lithologically heterogeneous of all the modelled rock domains and required division into 5 subdomains to adequately simulate this heterogeneity. It should be noted that the boundaries of the thermal subdomains have not been modelled deterministically; only the relative proportions of the subdomains are defined.

In contrast to RSMA01 and RSMM01, domain RSMD01 is lithologically quite homogenous, and subdivision into subdomains was judged to be unnecessary.

6.4.3 Spatial statistical models of lithology

The models of the spatial distribution of lithologies for each subdomain, or domain as in the case of RSMD01, are based on an analysis of data from the sub-vertical boreholes having a resolution of 2 m. Typical (mean) lens lengths and interactions of TRCs were calculated by transition probability analysis of the borehole data, performed using the T-PROGS code /Carle 1999/. Length refers to the dimensions of a TRC in a particular direction. Model parameters derived from this statistical analysis were modified in order to take geological interpretations into account. Geological interpretations, primarily of surface outcrop data, were also used to determine if the TRCs needed to be modelled with anisotropy in horizontal directions. For example, in domain RSMD01, fine-grained diorite-gabbro (TRC 102), which occurs as dyke-like bodies, was modelled with anisotropy. This rock type has the lowest mean thermal conductivity in RSMD01, and therefore the results of thermal modelling are more sensitive to how the rock type is modelled in the geological simulations. The other domains were modelled with the presumption of isotropy /Sundberg et al. 2008a/.

For rock domain RSMM01 only, spatial properties of TRCs for the 2 m resolution were scaled up so as to obtain model parameters for 4 m and 8 m resolutions. The upscaling was made through standard transition probability analysis, as described by e.g. /Davis 1986/. This was performed for the purpose of describing the size distribution of subordinate rock types.

In Table 6-11, the results of the spatial analysis are exemplified for 2 m data; see /Sundberg et al. 2008a/ for other domains and subdomains. Transition probabilities are presented as embedded probabilities of passing from one TRC to other TRCs irrespective of the lag distance; see /Back and Sundberg 2007, cf. Appendix B therein/ for more details.

Table 6-10. Thermal subdomains defined in rock domains RSMA01 and RSMM01. A subdomain’s proportion of a given domain is based on the borehole length assigned to each subdomain.

Rock domain	Subdomain	Chatacteristic rock type(s)	Dominant TRC	Proportion of domain
RSMA01	A1	Ävrö granodiorite	56	74%
	A2	Ävrö quartz monzodiorite	46	18%
	A3	Very heterogenous	30	8%
RSMM01	M1	Ävrö quartz monzodiorite,	46	38%
	M2	Ävrö quartz monzodiorite + high proportion diorite-gabbro	46	35%
	M3	Ävrö granodiorite	56	11%
	M4	Ävrö granodiorite + high proportion diorite-gabbro	56	10%
	M5	Ävrö granodiorite + high proportion fine grained granite	56	6%

Table 6-11. Proportions, transition probabilities and typical (mean) lengths for thermal subdomain A1, domain RSMA01, for 2 m data. Transition probabilities are shown as embedded probabilities of going from one TRC to other TRCs. Diagonal terms show the typical lengths of TRCs.

TRC	Proportion	Isotropic transition probabilities for TRCs (embedded) and typical lengths (m). (Lengths shown in bold)				
		TRC30	TRC 46	TRC 56	TRC 58	TRC 102
TRC 30	0.02	6.17	0.17	0.83	0.00	0.00
TRC 46	0.19	0.04	7.51	0.93	0.01	0.02
TRC 56	0.76	0.09	0.74	24.02	0.05	0.12
TRC 58	0.01	0.00	0.33	0.67	3.50	0.00
TRC 102	0.01	0.00	0.21	0.79	0.00	2.73

6.4.4 Stochastic simulations of lithology

Results

Unconditional stochastic simulations of the spatial distribution of TRCs at 2 m resolution were performed for each thermal subdomain or domain using the spatial properties derived from the analysis outlined in the previous section. The model dimensions were 100 m × 100 m × 100 m, i.e. a total of 125,000 cells. A total of 1000 realisations were produced for each rock domain. These were divided among the subdomains in proportion to the borehole length making up each subdomain (Table 6-12).

Figure 6-6, Figure 6-7 and Figure 6-8 give examples of realisations of the distribution of TRCs for the three modelled rock domains.

Table 6-12. Division of realisations among thermal subdomains in each rock domain

Rock domain	Thermal subdomain	Number of realisations, 2 m simulations
RSMA01	A1	741
	A2	179
	A3	80
RSMM01	M1	383
	M2	347
	M3	109
	M4	105
	M5	56
RSMD01	D	1,000

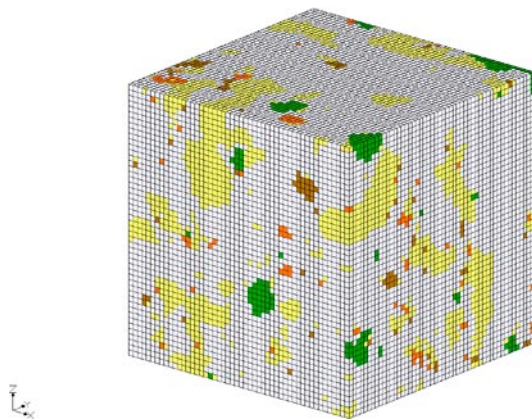


Figure 6-6. Visualisation of one realisation of the distribution of TRCs in subdomain A1 within domain RSMA01 with 2 m resolution (cell size). The simulated rock volume has dimensions 100×100×100 metres. The simulated TRCs are TRC30 (green), TRC46 (yellow), TRC56 (white), TRC58 (red) and TRC102 (brown).

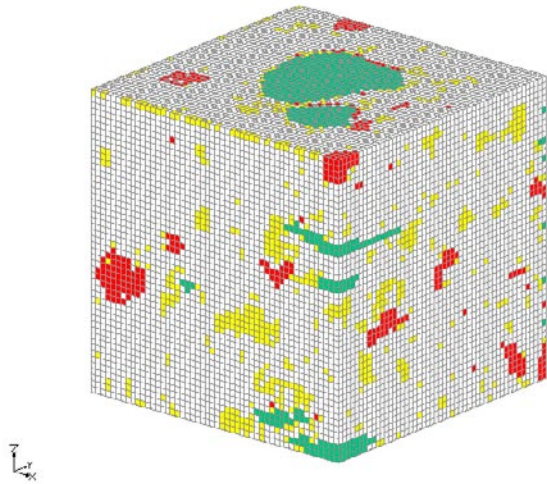


Figure 6-7. Visualisation of one realisation of the distribution of TRCs in domain RSMD01 with 2 m resolution (cell size). The simulated TRCs are TRC36 (white), TRC58 (red), TRC102 (green) and TRC136 (yellow). See also Figure 6-6.

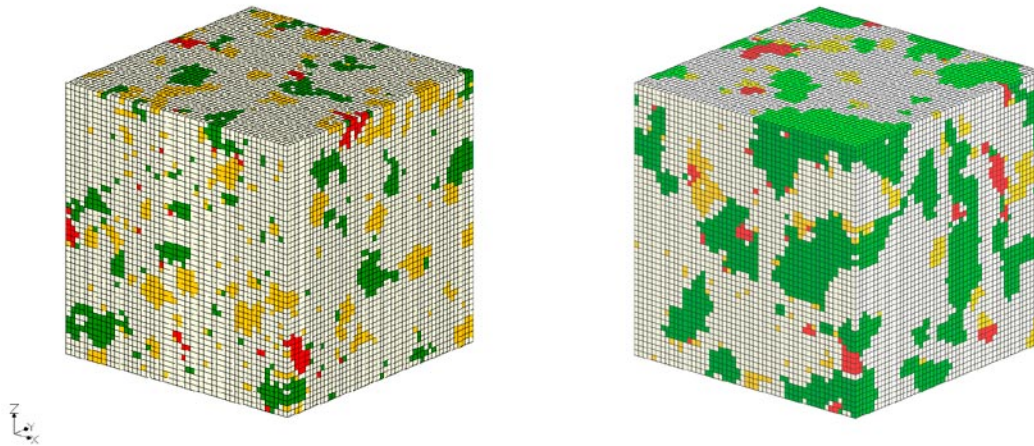


Figure 6-8. Visualisations of realisations of the distribution of TRCs in subdomain M1 (left) and sub-domain M2 (right) (both domain RSMM01) with 2 m resolution (cell size). The simulated TRCs are TRC33 (green), TRC46 (white), TRC56 (yellow) and TRC58 (red). See also Figure 6-6.

Analysis and verification of results

The statistical properties, i.e. the proportions of categories (TRCs), the typical lengths of categories and the spatial properties of categories are assumed to be stationary for all realisations. The relevance of the results of the simulations have been analysed and verified by means of statistical analysis with respect to the ability to reproduce:

- the proportions of the TRCs,
- typical (mean) lengths of TRCs calculated by transition probability analysis,
- the distribution of TRC lengths observed in borehole data.

The verification analysis was made by “drilling” simulated boreholes in the realisations as described in /Sundberg et al. 2008a/.

Proportions

The simulated TRC proportions have been analysed for domain RSMD01 and thermal subdomains A1, A2, A3 and M1. The simulations nearly exactly reproduce the proportions of the TRCs for all realisations and for all domains. Table 6-13 shows results of the proportions of TRCs in 10 randomly

selected realisations for subdomain A1. The corresponding tables for the other simulations can be found in /Sundberg et al. 2008a/.

Typical lengths

Results of the calculations of the typical lengths (m) for directions x, y and z are exemplified in Table 6-14 for TRC46 in subdomain A1. Results for the other TRCs, subdomains and domains can be found in /Sundberg et al. 2008a/.

It can be concluded that, for all domains and subdomains, the simulations are able to realistically reproduce the typical lengths calculated from transition probability analyses, but that there is in general a slight, in the order of 10%, overestimation of lengths. For shorter lengths close to the model resolution, overestimations are often greater and are believed to be due to discretisation effects. No directional bias was observed.

Distribution of lengths

A visual comparison was made of the histograms of lengths from the “simulated boreholes” with histograms of lengths observed in the actual borehole data, see /Sundberg et al. 2008a/. Although the borehole information is rather limited compared with the number of data from “simulated boreholes”, the visual comparison indicates that the T-PROGS code is able to reproduce – for all TRCs – the TRC length distributions that were registered in the borehole data.

6.4.5 Spatial statistical models of thermal conductivity

Approach

Spatial statistical thermal conductivity models at the 0.1 m scale are required for each TRC in order to perform simulations at the scale at which the measurement data apply. Upscaling is performed in two steps (from 0.1 m to 0.5 m, and 0.5 m to 2 m) in order to define thermal models for the 2 m scale, which is the scale used in the geological simulations. Two types of models are required for each TRC: a statistical distribution model and a model describing spatial correlation, i.e. a variogram model. The statistical distribution model represents heterogeneity in thermal conductivity, without consideration of anisotropy.

Table 6-13. Proportions of TRCs in 10 randomly selected realisations for subdomain A1.

Category	Proportions from input borehole data (%)	Proportions in randomly selected realisations (%)									
		1	2	3	4	5	6	7	8	9	10
TRC 30	2.4	2.4	2.4	2.4	2.4	2.4	2.4	2.4	2.4	2.4	2.4
TRC 46	19.2	19.2	19.2	19.2	19.2	19.2	19.2	19.2	19.2	19.2	19.2
TRC 56	76.0	75.9	75.9	75.9	75.9	75.9	75.9	75.9	75.9	75.9	75.8
TRC 58	1.3	1.3	1.3	1.3	1.3	1.3	1.3	1.3	1.3	1.3	1.3
TRC 102	1.2	1.2	1.2	1.2	1.2	1.2	1.2	1.2	1.2	1.2	1.2

Table 6-14. Typical lengths of TRC46 in x, y and z directions in subdomain A1.

Typical simulated length (m)*	Nominal value (m)*
$\mu_x=8.38$	7.51
$\mu_y=7.88$	7.51
$\mu_z=8.28$	7.51

* The typical simulated lengths are the mean lengths estimated from “simulated boreholes” through the simulated rock volumes. The nominal value is the typical length estimated from the transition probability analysis of the borehole data.

Once the thermal models for the 0.1 m scale are defined, the thermal models for the 2 m scale are fairly easily determined. Therefore, the focus of the presentation below is on the thermal models for the 0.1 m scale.

Spatial statistical models of thermal conductivity are based on the following data:

- data for describing the distribution of thermal conductivity are primarily TPS data for TRCs for which TPS data are plentiful, whereas for other TRCs, SCA values are used together with TPS data. Field measurement data and calculations from density loggings are also used to some extent,
- data for describing spatial correlation by means of variogram models are primarily density logging data supported by TPS data.

Statistical distribution models – 0.1 m scale

The statistical distribution models for each TRC are constructed from data values from the constituent rock types. For example, TRC 56 combines data from both Ävrö granodiorite (501056) and granite (501058). The data are weighted according to the relative proportions of each rock type, as well as the number of data values contributed by each rock type. Declustering was applied to most rock types to ensure that spatially clustered data do not produce bias in the statistics.

Thermal conductivity values determined from altered samples of the different rock types have been included in the data sets. For the common rock types, the relative amounts of data on altered samples are roughly equivalent to the proportion of the rock mass outside the deformation zones which has been mapped as altered to a degree of weak or higher; i.e. faint alteration excluded (see Section 5.2.3). Between 20 and 30% of the rock mass, lowest in domain RSMM01, highest in domain RSMA01, has been mapped as altered. Excluding faint alteration reduces these figures to 7 to 15%

Standard distribution models, e.g. normal, lognormal, were not used to describe the probability distributions of thermal conductivity since for most TRCs such models were not supported by the data. Distribution models are instead based on smoothing of the sample histograms, performed using an algorithm in the geostatistical software GSLIB /Deutsch and Journel 1998/. This algorithm uses a simulated annealing procedure that honours the sample data statistics, such as the mean and standard deviation. Smoothing is required because of relatively small data sets. The smoothing operation requires input regarding the maximum and minimum values. These values are derived mainly from a consideration of the following criteria: the range of the data for each TRC, and theoretical lower limits of thermal conductivity approximated from “extreme”, but possible, mineral compositions of each rock type, see also /Sundberg et al. 2008a, cf. Section 5.6.2 therein/.

Histograms and models for some TRCs are shown in Figure 6-9 to Figure 6-12 and commented in the following text. For a more comprehensive description, see /Sundberg et al. 2008a, cf. Section 5.6.2 therein/.

TRC 33 is present in rock domain RSMM01 only, where it makes up almost 20% of the rock volume. This TRC is dominated by diorite-gabbro (501033), but also includes subordinate amounts of fine-grained diorite-gabbro (505102). An analysis of various types of data from diorite-gabbro reveals a wide variation in properties and indicates, as the rock name suggests, that more than one distinct rock type is present. Based on density, two types have been defined for thermal modelling purposes. Histograms and statistics of thermal conductivity for the two types of diorite-gabbro are presented in Figure 6-9. Type A, the low-density variety, is characterised by low thermal conductivities (2.2–2.6 W/(m·K)). Type B, the high-density variety, is characterised by a wide range of thermal conductivity values from low to high (2.1–3.7 W/(m·K)).

Both fine-grained diorite-gabbro and diorite-gabbro type A are combined to form TRC 33A. Figure 6-10 shows the data distribution and the fitted model for TRC 33A. TRC 33B is defined by diorite-gabbro type B.

TRC 36 dominates rock domain RSMD01 and is comprised mainly of rock type quartz monzodiorite (501036), but also very minor amounts of fine-grained dioritoid (501030).

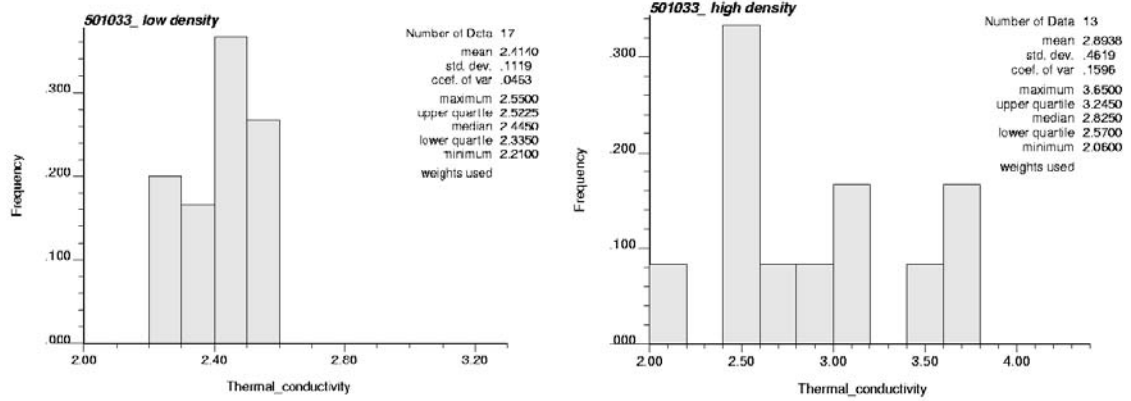


Figure 6-9. Histograms of thermal conductivity for diorite-gabbro (501033), type A (low density) and type B (high density) based on TPS and SCA values.

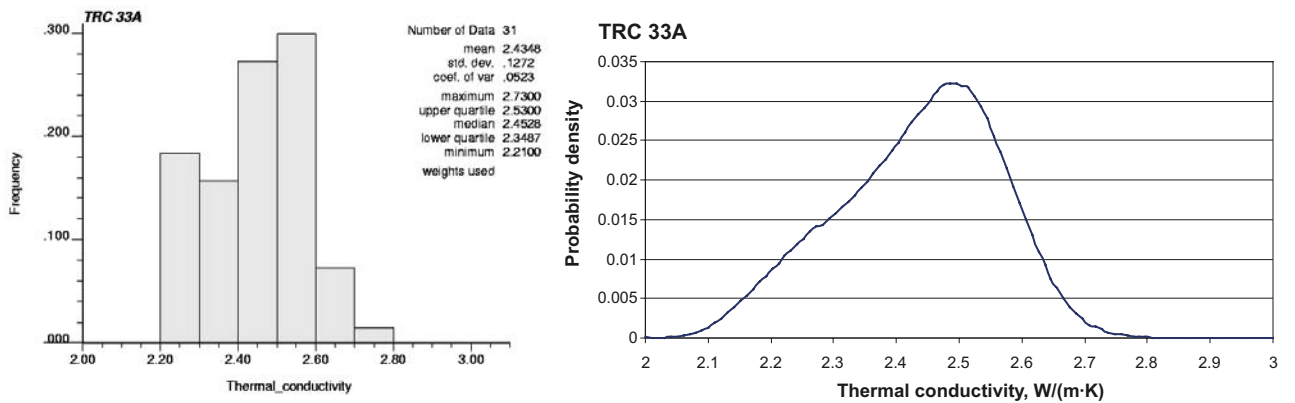


Figure 6-10. Histogram of thermal conductivity for TRC 33A (left) and statistical distribution model (right), based on smoothing of the data histogram and applied minimum value of 2.0 W/(m·K) based on a theoretical extreme composition.

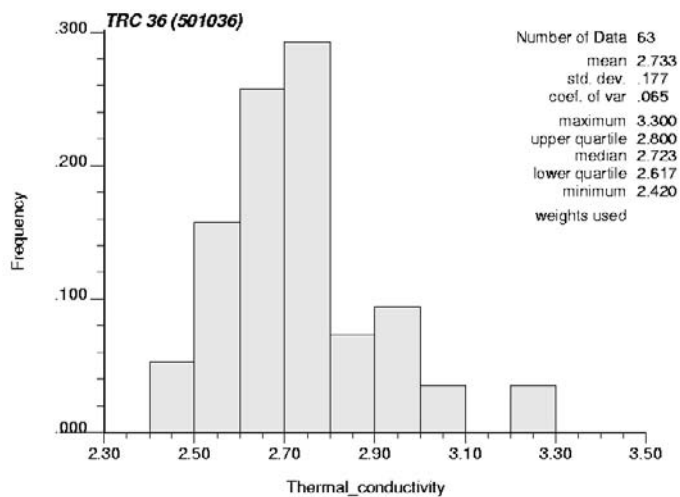


Figure 6-11. Histogram of TPS values for quartz monzodiorite (501036). Data weighted to take account of clustering.

TRC 46, present in domains RSMMA01 and RSMM01, is comprised of one rock type, namely Ävrö quartz monzodiorite (501046). A histogram and the statistics of thermal conductivity are presented in Figure 6-12. The statistical distribution model smoothens out the irregularities in the histogram caused by the small number of data. Relative to the TPS data, the smoothing operation has the greatest effect on the middle part of the distribution. In contrast, the lower tail of the data distribution is not influenced much by the smoothing procedure; the model follows the data closely and thus can be considered quite reliable for this part of the distribution

TRC 56 occurs in rock domains RSMMA01 and RSMM01. It is comprised of two rock types, Ävrö granodiorite (501056) and granite (501058). The latter is very subordinate in both rock domains. The distribution of measured conductivity values is described in Figure 6-12. Table 6-15 summarises the thermal conductivity statistics for each TRC.

Variogram models – 0.1 m scale

The spatial correlation of thermal conductivity within each TRC is modelled by a variogram. If possible, TPS data are used to construct sample variograms, but for most TRCs these data are not sufficiently abundant to enable construction of reliable variograms. Therefore, borehole density logs were used to study spatial correlation of thermal conductivity. A relationship between thermal conductivity and density has been established for some rock types (Section 6.2.2). Even for other rock types it is reasonable to assume that any spatial dependence in density, as indicated by a variogram, also reflects spatial dependence in thermal conductivity /Sundberg et al. 2008a/. The primary purpose of calculating variograms based on density logs is to estimate the range, i.e. the separation distance over which spatial dependence is apparent.

Table 6-15. Statistics of the distribution models used for simulation of each TRC and the thermal conductivity data on which the models are based.

TRC	Data			Model	
	Mean [W/(m·K)]	Standard deviation [W/(m·K)]	No. of data	Mean [W/(m·K)]	Standard deviation [W/(m·K)]
TRC 30	2.74	0.17	91	2.75	0.16
TRC 33A	2.43	0.13	31	2.43	0.13
TRC 33B	2.89	0.46	13	2.89	0.46
TRC 36	2.73	0.18	63	2.73	0.17
TRC 46	2.40	0.18	33	2.40	0.18
TRC 56	3.18	0.20	68	3.18	0.20
TRC 58	3.60	0.13	13	3.60	0.13
TRC 102	2.52	0.15	14	2.50	0.16

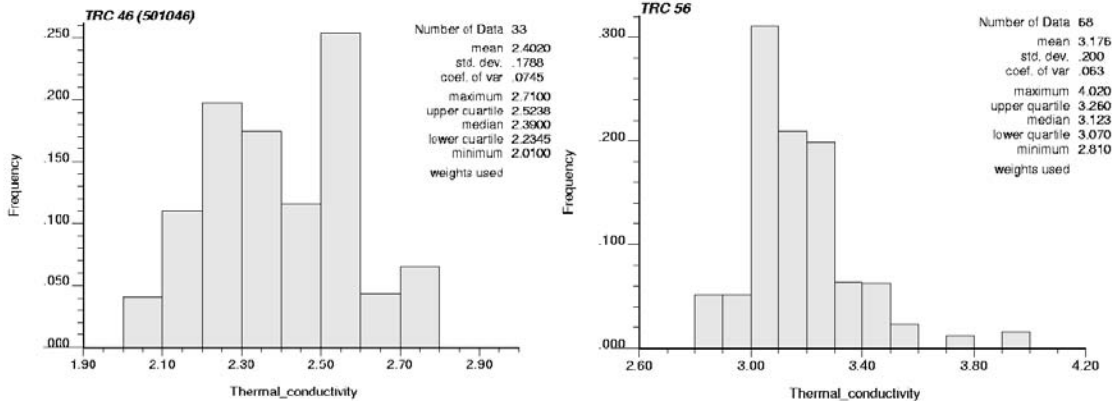


Figure 6-12. Histogram of thermal conductivity for TRC 46 (left) based on 33 TPS data for Ävrö quartz monzodiorite and for TRC 56 (right) based on data for Ävrö granodiorite (501056) and granite (501058); data values weighted.

The procedure followed in order to construct sample variograms for each TRC is described in /Sundberg et al. 2008a/. The variogram model for each TRC was chosen after an overall judgement of the sample variograms from individual boreholes. Given a choice between alternative variogram models, the one chosen was that giving the higher degree of spatial correlation, i.e. a lower nugget and a longer range. The nugget (small-scale variability at a scale smaller than measurement scale) was based, where possible, on TPS-data.

Examples of variograms for TRC 46, comprising Ävrö quartz monzodiorite, are shown in Figure 6-13. The variogram model for TRC 46 is to a large extent based on a small set of TPS data at small separation distances, and density loggings from subjectively selected boreholes.

The variograms models for each TRC are summarised in Table 6-16. A rock crystallised from magma that is well mixed and homogenous will have a long range. The rather homogenous quartz monzodiorite is a good example of this. More heterogeneous rock types such as Ävrö quartz monzodiorite and diorite-gabbro have shorter ranges. It should be noted that these models are applicable at the 0.1 m support only. For simulation at larger scales, the variogram models have to be scaled up appropriately (Section 6.4.6).

6.4.6 Stochastic simulations of thermal conductivity

Unconditional stochastic simulation of thermal conductivity was performed for each TRC using the geostatistical software GSLIB /Deutsch and Journel 1998/. Simulation was performed at three scales: 0.1 m, 0.5 m and 2 m. The purpose of the first two simulations was to perform “change of support” (upscaling) from the scale of thermal measurements (c. 0.1 m) to the 2 m scale.

The histogram of the upscaled values (2 m scale) defines the statistical distribution model for simulations at the 2 m scale. The variogram models for the 0.5 m and 2 m scales are modified from the model used for the 0.1 m scale by an upscaling algorithm /Journel and Huijbregts 1978/. The histograms and variograms used for modelling at 0.5 m and 2 m scales for each TRC are described in /Sundberg et al. 2008a, cf. Section 5.7 therein/.

Selected statistics based on the results of thermal simulations for all TRCs and sub-TRCs are presented in Table 6-17.

Verification of simulations was performed by analysing the extent to which the results could reproduce variogram models and distribution models, see /Sundberg et al. 2008a, cf. Appendices E and F therein/.

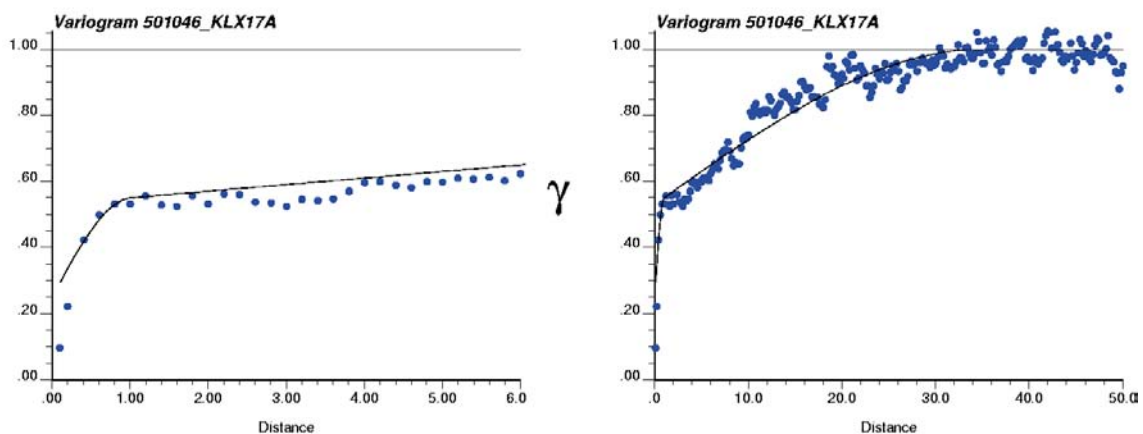


Figure 6-13. Variogram model for TRC 46 shown for two different distance scales. Model based on sample variograms for Ävrö quartz monzodiorite (501046) produced from density logging data from borehole KLX17A and a consideration of the TPS data. Nested variogram model fitted. Lag distance (x axis) in metres. The variogram is standardised to the variance of the measured data.

Table 6-16. Variogram model parameters for 0.1 m scale for each TRC. Semi-variance of variogram structures standardised to the variance of the measured data.

TRC	Based on rock type, code	Structure	Semi-variance	Range, m
TRC 30	501036	Nugget	0.33	
		Spherical	0.67	75
TRC 33A	501033 A	Nugget	0.10	
		Exponential	0.30	3
		Spherical	0.60	22
TRC 33B	501033 B	Nugget	0.18	
		Spherical	0.15	1
		Spherical	0.67	18
TRC 36	501036	Nugget	0.33	
		Spherical	0.67	75
TRC 46	501046	Nugget	0.25	
		Spherical	0.28	1
		Spherical	0.47	35
TRC 56	501056	Nugget	0.60	
		Spherical	0.20	2
		Spherical	0.20	50
TRC 58	511058	Nugget	0.40	
		Exponential	0.60	6
TRC 102	505102	Nugget	0.10	
		Spherical	0.90	1.5

Table 6-17. Thermal conductivity statistics, and variance reduction as a result of upscaling, for all simulated TRCs. Simulation at 2 m scale uses upscaled 0.5 m values as a distribution model.

TRC	Scale (m)	Source of data	Mean [W/(m·K)]	Standard deviation [W/(m·K)]	Variance reduction (%)
30	0.1	Simulations	2.747	0.163	
	2	Upscaled – 0.5 m realisations	2.746	0.130	36
33A	0.1	Simulations	2.434	0.130	
	2	Upscaled – 0.5 m realisations	2.433	0.105	35
33B	0.1	Simulations	2.893	0.462	
	2	Upscaled – 0.5 m realisations	2.884	0.361	39
36	0.1	Simulations	2.741	0.170	
	2	Upscaled – 0.5 m realisations	2.740	0.136	36
46	0.1	Simulations	2.401	0.179	
	2	Upscaled – 0.5 m realisations	2.399	0.124	52
56	0.1	Simulations	3.176	0.200	
	2	Upscaled – 0.5 m realisations	3.173	0.096	77
58	0.1	Simulations	3.605	0.135	
	2	Upscaled – 0.5 m realisations	3.604	0.074	70
102	0.1	Simulations	2.500	0.163	
	2	Upscaled – 0.5 m realisations	2.497	0.058	87

6.5 Thermal domain model

6.5.1 Domain modelling results

Thermal conductivity

The results of the final modelling steps are presented below for the three key rock domains, RSMA01, RSMM01 and RSMD01. First, the realisations of lithology (TRCs) and the realisations of thermal conductivity are merged. This provides the main output of the thermal modelling, that is, a set of 1000 realisations of thermal conductivity for each domain at the 2 m scale. Subsequently upscaling to larger scales is performed. Histograms and tables are used to illustrate the results of the thermal modelling for different scales. For domains with thermal subdomains, the proportions of the different subdomains are important for the domain properties, see Table 6-18.

Rock domain RSMA01

Domain RSMA01 consists of three thermal subdomains. Below, both the domain results and the results for some of the different thermal subdomains are presented.

Histograms of thermal conductivity for RSMA01 based on the 1000 realisations combined are shown in Figure 6-14. The lower tail is a result of the low-conductive rocks, mainly Ävrö quartz monzodiorite. Upscaling of the realisations to 5 m has the effect of smoothing the histogram, i.e. the bimodal distribution becomes unimodal.

Examples of 2D-slices through the 3D realisations for subdomain A1 are visualised in Figure 6-15. Subdomain A1 is dominated by the medium-high conductive Ävrö granodiorite. In subdomain A2 the low-conductive Ävrö quartz monzodiorite dominates whereas the subordinate subdomain A3 is lithologically heterogeneous.

Table 6-18. Proportions of the total number of realisations per domain assigned to the different thermal subdomains making up domains RSMA01 and RSMM01.

Domain	Sub domain	No. of lithological realisations	Percent of domain	Thermal realisations used
RSMA01	A1	741	74.1	1–741
	A2	179	17.9	742–920
	A3	80	8.0	921–1,000
RSMM01	M1	383	38.3	1–383
	M2	347	34.7	384–730
	M3	109	10.9	731–839
	M4	105	10.5	840–944
	M5	56	5.6	945–1,000

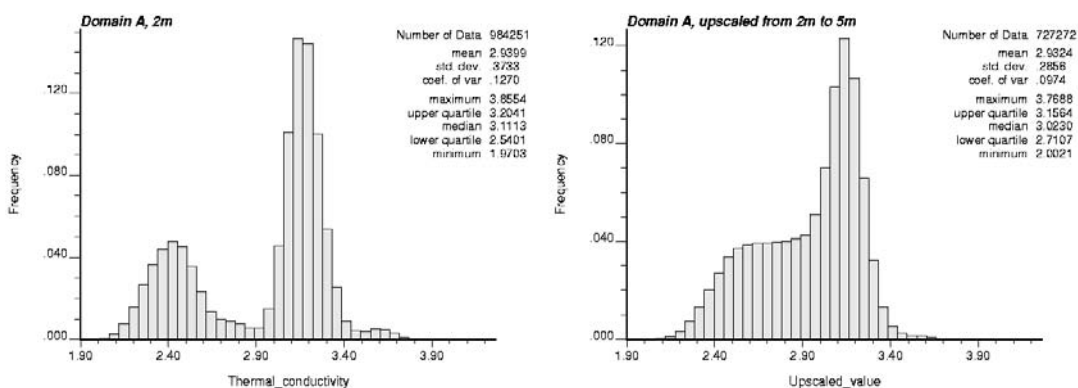


Figure 6-14. Histograms of thermal conductivity for domain RSMA01 simulated at 2 m scale (left) and upscaled to 5 m (right).

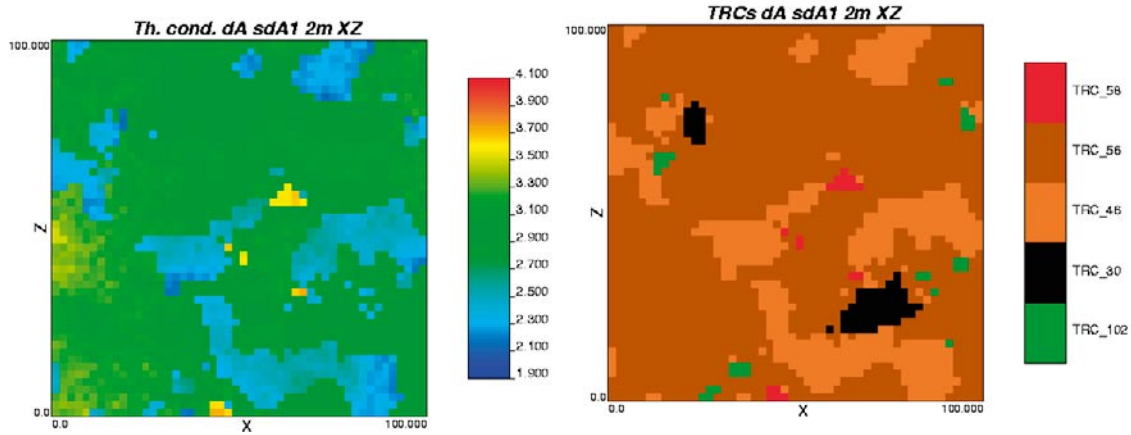


Figure 6-15. An example of a 2D visualisation of a realisation of thermal conductivity (slices in xz-plane) for thermal subdomain A1 simulated at the 2 m scale (left) and the corresponding realisation of lithology (TRC) (right).

Histograms of thermal conductivity for thermal subdomains A1 and A2 in RSMA01 are shown in Figure 6-16 and Figure 6-17 for the 2 m and 5 m scales. The proportions of high and low conductive rocks in each subdomain determine the shape of the histograms.

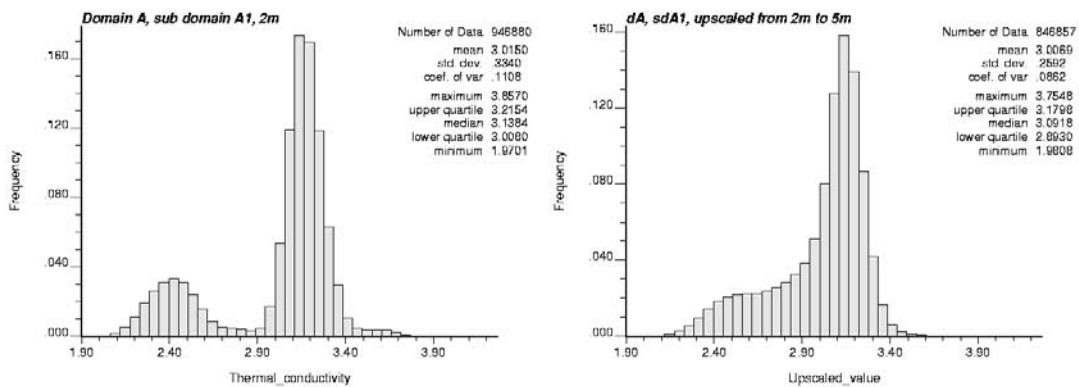


Figure 6-16. Histograms of thermal conductivity for thermal subdomain A1 in domain RSMA01 at the 2 m (left) and 5 m (right) scales.

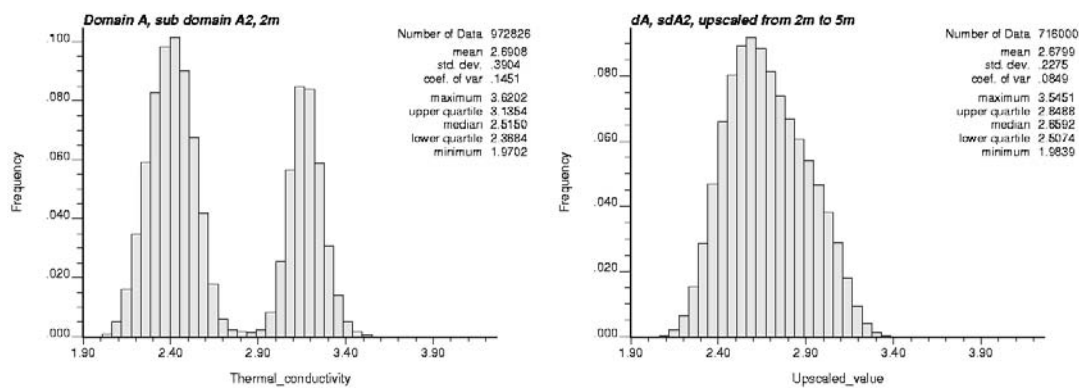


Figure 6-17. Histograms of thermal conductivity for thermal subdomain A2 in domain RSMA01 at the 2 m (left) and 5 m (right) scales.

Rock domain RSMM01

Rock domain RSMM01 consists of five thermal subdomains. Below, both the domain results and the results for some of the different thermal subdomains are presented. A histogram of the realisations combined is presented in Figure 6-18. The lower tail is a result of the low-conductive rocks, mainly Ävrö quartz monzodiorite and diorite-gabbro. Upscaling of the realisations to 5 m has the effect of smoothing the histogram.

Examples of 2D-slices through 3D realisations for subdomains M1 and M3 are visualised in Figure 6-19 and Figure 6-20, respectively. Subdomains M1 and M2 are dominated by the low conductive Ävrö quartz monzodiorite (TRC 46) and have low and high contents of diorite-gabbro (TRC 33), respectively. Subdomains M3 and M4 are dominated by the medium-high conductive Ävrö granodiorite (TRC 56) and have low and high contents of diorite-gabbro (TRC 33), respectively. Subdomain M5 is also dominated by Ävrö granodiorite (TRC 56) but has a rather high content of fine-grained granite (TRC 58). The estimated proportions of the subdomains are shown in Table 6-18.

Histograms of thermal conductivity at the 2 m and 5 m scales for thermal subdomains M1 and M3 are shown in Figure 6-21 and Figure 6-22, respectively.

A limited volume of rock within domain RSMM01 was simulated using conditional simulation with the objective of illustrating how the thermal modelling strategy can be used to predict the spatial distribution of thermal conductivity at specific locations. With conditional simulation, the data values at known locations are honoured. The simulations were conditioned on data, both TRCs and thermal conductivities, from a section of borehole KLX05. Each realisation provides an alternative equiprobable representation of the distribution of thermal conductivity in the simulated rock volume.

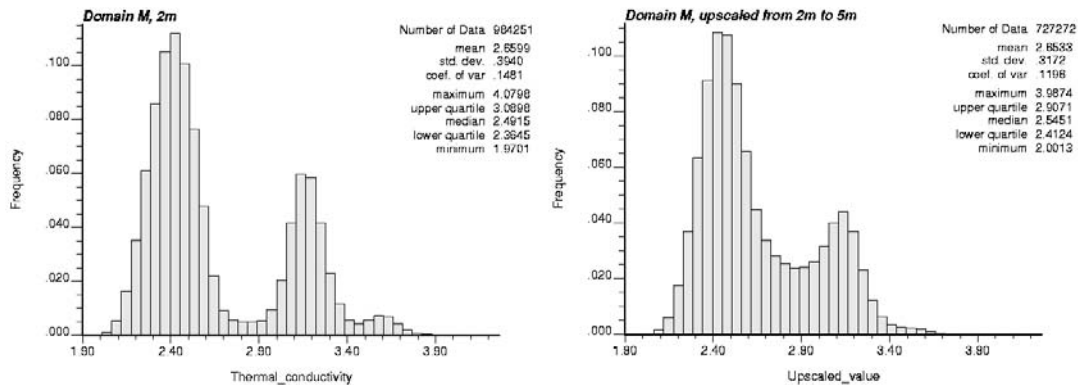


Figure 6-18. Histograms of thermal conductivity for domain RSMM01 simulated at 2 m scale (left) and upscaled to 5 m (right).

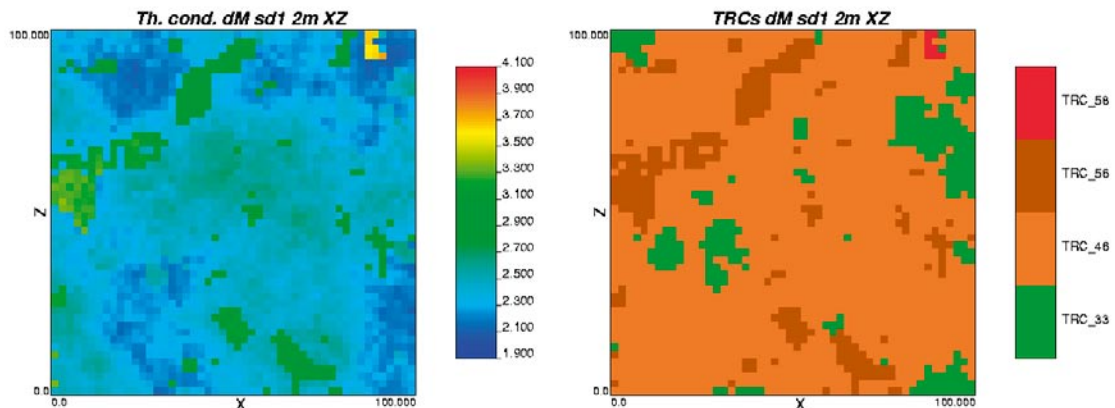


Figure 6-19. An example of a 2D visualisation of a realisation of thermal conductivity (slices in xz-plane) for thermal subdomain M1 simulated at the 2 m scale (left) and the corresponding realisation of lithology (TRC) (right).

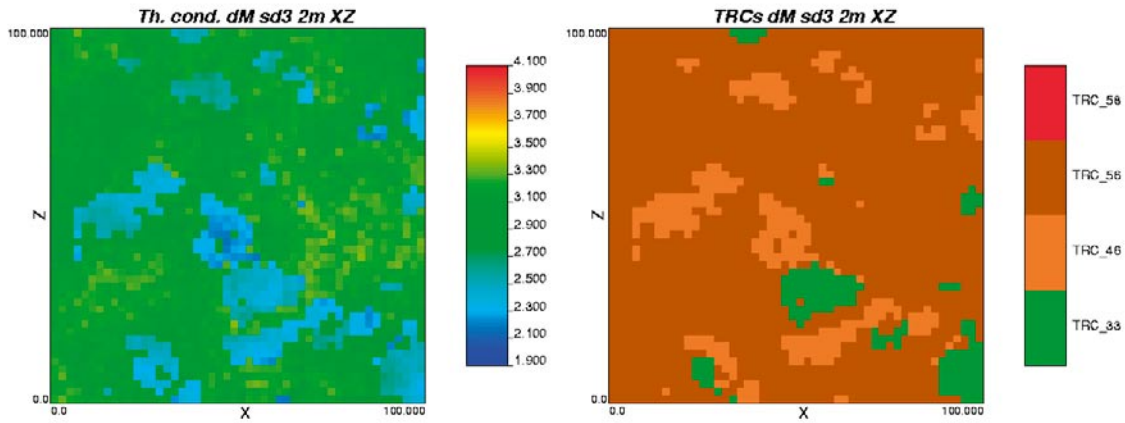


Figure 6-20. An example of a 2D visualisation of a realisation of thermal conductivity (slices in xz-plane) for thermal subdomain M3 simulated at the 2 m scale (left) and the corresponding realisation of lithology (TRC) (right).

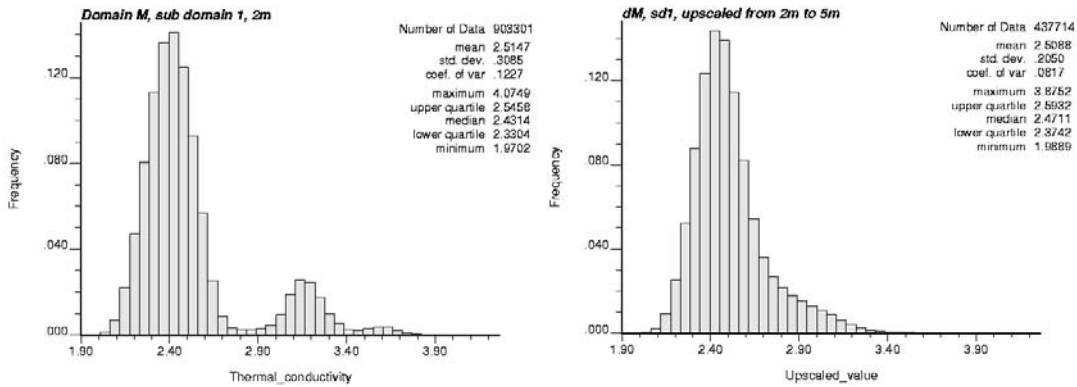


Figure 6-21. Histograms of thermal conductivity for thermal subdomain M1 in domain RSMM01 at the 2 m (left) and 5 m (right) scales.

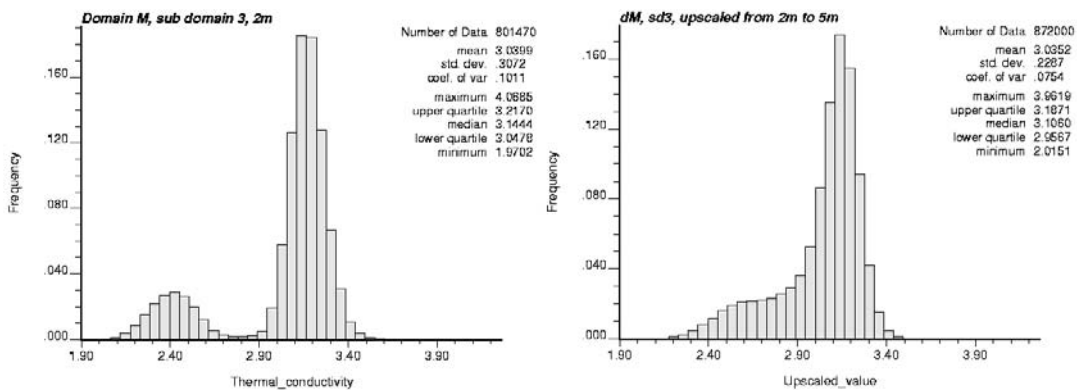


Figure 6-22. Histograms of thermal conductivity for thermal subdomain M3 in domain RSMM01 at the 2 m (left) and 5 m (left) scales.

An example of a 2D-slice through a 3D thermal realisation for the simulated volume is visualised in Figure 6-23. The corresponding realisation of lithologies is also presented. The differences between the realisations are a reflection of the spatial uncertainty. The results can be used for prediction purposes. For example, based on all the realisations, the probability that the thermal conductivity will be lower than a specified threshold value at any location can be estimated /Sundberg et al. 2008a/.

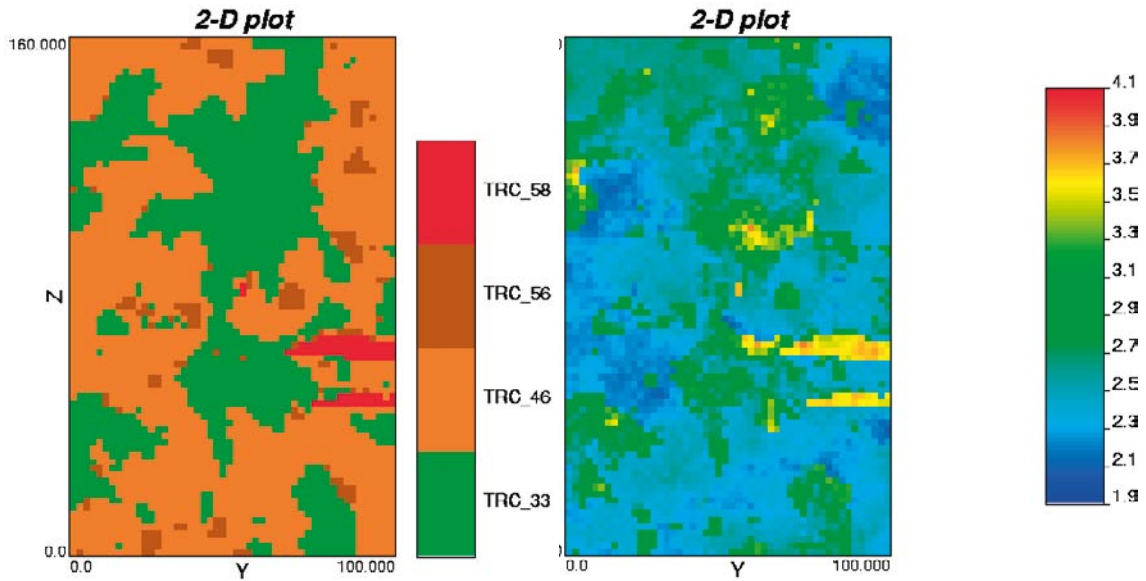


Figure 6-23. A slice (*yz*-plane) through a realisation of thermal conductivity for the simulated volume (right) and corresponding realisation of lithology (TRC) (left). The resolution of the simulation is 2 m. The realisation is derived from conditional simulation of a rock volume intersected by borehole KLX05.

Rock domain RSMD01

Domain RSMD01 was not divided into thermal subdomains. Examples of 2D-slices through the 3D realisations for the domain are visualised in Figure 6-24.

Histograms of thermal conductivity for all realisations are shown in Figure 6-25. Upscaling of the realisations to 5 m has the same smoothing effect on the histogram as for the other domains.

Heat capacity

Heat capacity has been modelled based on the TRC-distribution in each realisation together with a statistical distribution model of heat capacity for each TRC. The distribution models for the 2 m scale are based on normal distributions fitted to the measurement scale (0.1 m) data, which are then truncated at the mean \pm 2 standard deviations to give a variability which is considered to be more realistic for the 2 m scale.

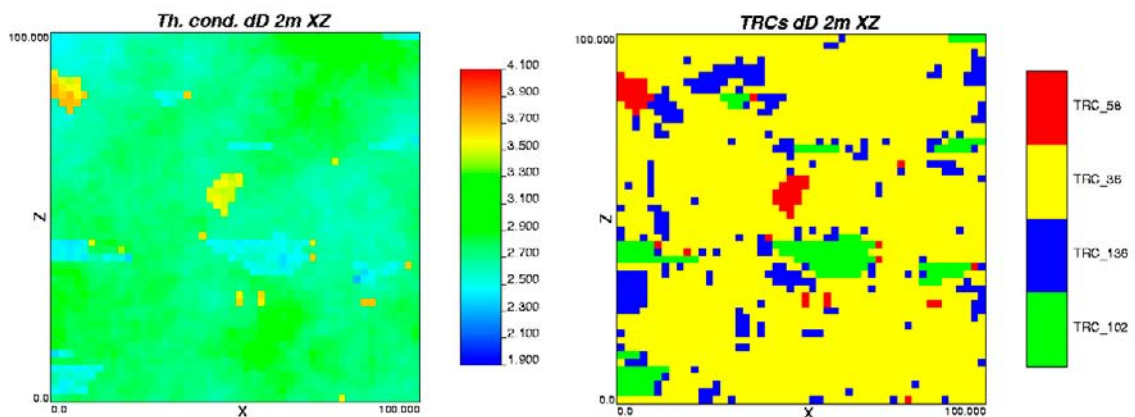


Figure 6-24. An example of a 2D visualisation of a realisation of thermal conductivity (slices in *xz*-plane) for domain RSMD01 simulated at the 2 m scale (left) and corresponding realisation of lithology (TRC) (right).

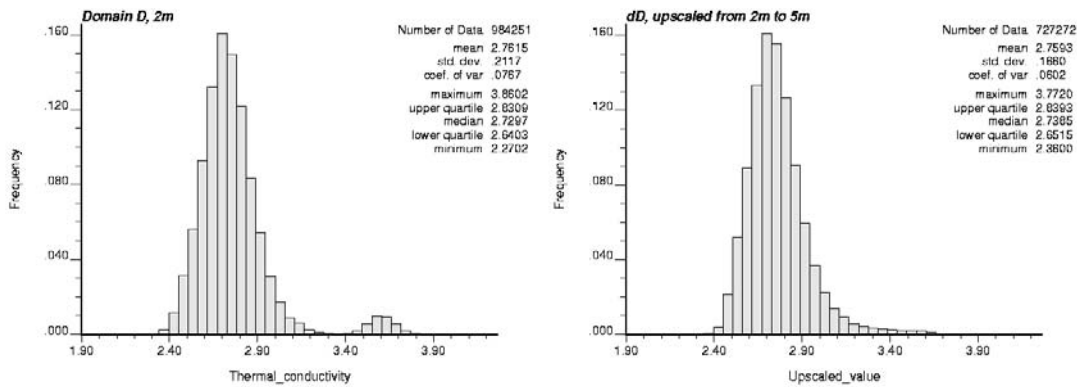


Figure 6-25. Histogram of thermal conductivity for domain RSMD01 simulated at the 2 m scale (left) and upscaled to 5 m (right).

The resulting frequency distributions of heat capacity at the 2 m scale for rock domains and thermal subdomains are shown, together with examples of visualisations, in /Sundberg et al. 2008a/. There are no dramatic differences in the mean heat capacity between the different domains. However, RSMM01 has a bimodal distribution and RSMD01 has an evident lower tail (Figure 6-26). The different subdomains show larger variations, especially in RSMM01; see /Sundberg et al. 2008a/. The means and standard deviations are summarised in Table 6-19.

Size distribution of TRCs

Based on the results of stochastic simulations of lithologies, it is possible to calculate the size distribution of subordinate rock types. However, a large number of simulations are required at several scales for this analysis. A summary of the results of the analysis carried out thus far is presented here.

Table 6-19. Heat capacity at the 2 m scale for different rock domains.

Domain	Mean (MJ/(m3-K))	Std (MJ/(m3-K))
RSMA01	2.16	0.06
RSMM01	2.21	0.12
RSMD01	2.23	0.06

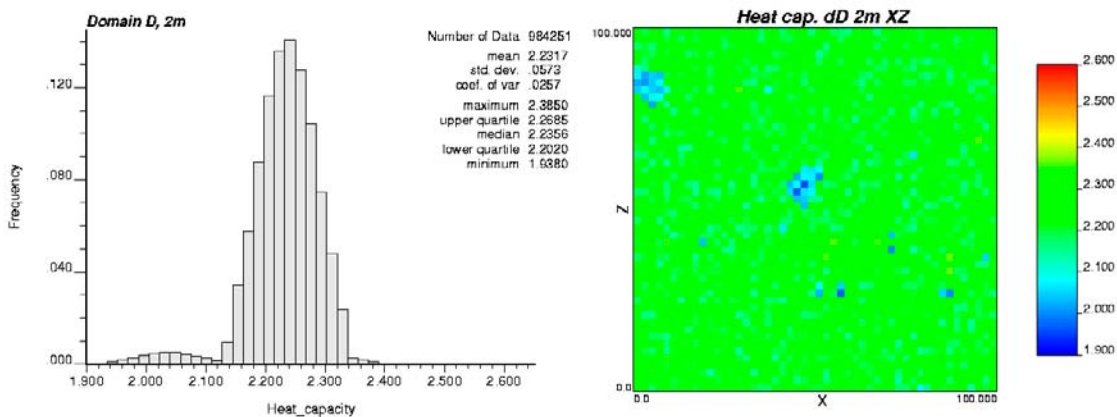


Figure 6-26. The distribution of heat capacities at the 2 m scale (left) and an example of a visualisation of the spatial distribution (right) for domain RSMD01.

To illustrate the information that can be obtained from a size-distribution analysis, the results of simulations at three scales, 2 m, 4 m and 8 m, have been analysed for TRC 33 (mainly diorite-gabbro) in domain RSMM01. This was performed by using an algorithm that calculates the volume of individual rock bodies in the lithological realisations generated by the stochastic simulations. In Figure 6-27, the size distributions of TRC 33 are shown.

6.5.2 Evaluation of results of domain modelling

The lower tail of the thermal conductivity distributions for each rock domain is of importance for the design of a repository. Therefore, the modelling results were analysed in detail in this respect. The results are presented in Figure 6-28 for rock domains RSMA01 and RSMM01. The plots illustrate how the lower percentiles increase when the scale increases. This is a way of describing how the variance reduction affects the lower percentiles and how sensitive they are to the choice of scale. Domain RSMD01 displays only slight scale dependence. The results are described in more detail in /Sundberg et al. 2008a/.

6.5.3 Summary of rock domain properties

Thermal conductivity

The main result of the thermal modelling is a set of realisations describing the spatial distribution of thermal properties at the 2 m scale for each of the three key rock domains, namely RSMA01, RSMM01 and RSMD01. The realisations are considered to be sufficiently realistic for use in future design work, most importantly as input to numerical temperature simulations for the design of the repository layout (e.g. distances between deposition holes). The strategy for thermal dimensioning is described in /Hökmark et al. 2009/.

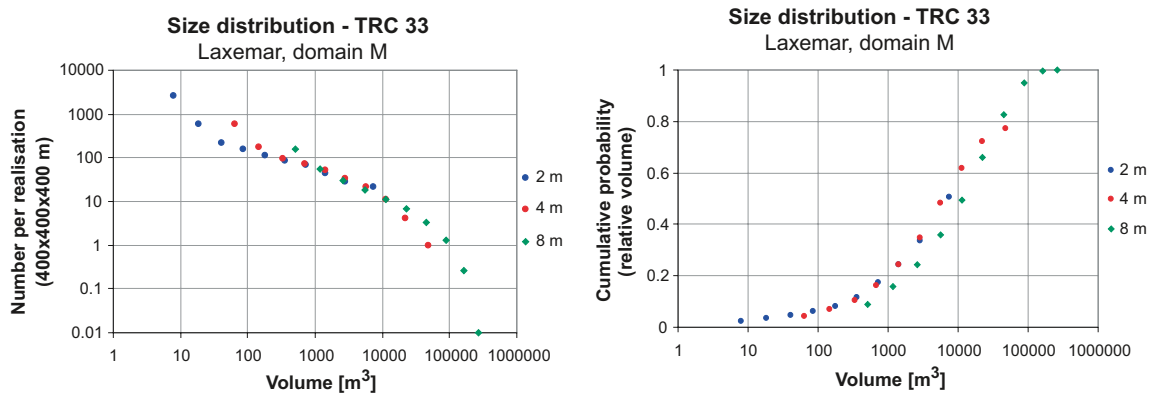


Figure 6-27. Size distribution of bodies of TRC 33 in domain RSMM01 in Laxemar; based on stochastic simulation at 2 m, 4 m and 8 m scales. A single realisation at 8 m scale represents a rock volume of 64,000,000 m³. In the figure on the left, the number of rock bodies is underestimated because bodies located at the boundaries of the simulation volume are ignored.

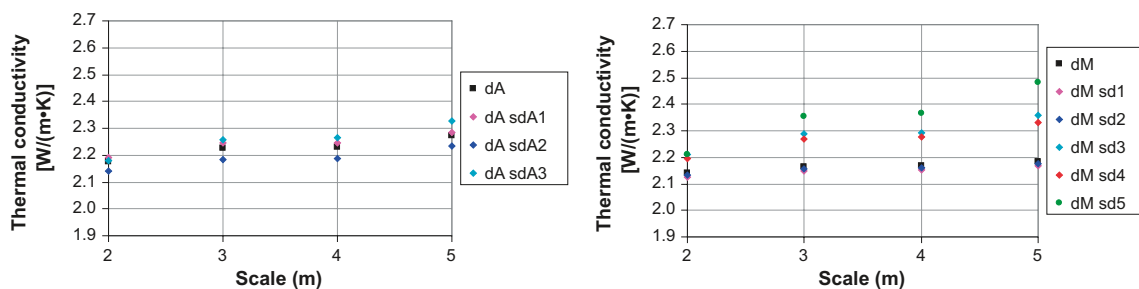


Figure 6-28. The 1-percentile (0.01 quantile) versus scale for domain RSMA01 (left), domain RSMM01 (right) and the corresponding thermal subdomains defined in Table 6-10.

The thermal conductivity at domain level for the 5 m scale is summarised in Table 6-20 for rock domains RSMA01, RSMM01 and RSMD01, respectively. RSMA01 has the highest mean thermal conductivity, and RSMM01 the lowest. In spite of the clear difference in mean thermal conductivity between RSMA01 and RSMM01, the 0.1 percentiles are rather similar for these two domains. This is largely an effect of the presence of low-conductive Ävrö quartz monzodiorite in both domains. The lithologically more homogeneous RSMD01 domain shows less variation in thermal conductivity and has low-percentiles that are significantly higher compared with the other two domains.

The thermal conductivity of altered rock is approximately 5–15% higher than fresh rock. The impact of alteration has been incorporated into the thermal modelling and is therefore reflected in the domain results.

The values in Table 6-20 are valid at 20°C. The thermal conductivity of the dominant rock types decreases by 0–10% per 100°C temperature increase (Table 6-3).

Thermal anisotropy

Anisotropy in thermal conductivity due to foliation of the Ävrö granite has been measured *in situ*. Field measurements indicate that thermal conductivity parallel to the foliation plane is higher, by a factor of approximately 1.15, than conductivity perpendicular to the foliation, see Section 6.2.3. The orientation of the foliation, as well as its degree of development, varies throughout the Laxemar area which implies that the orientation and magnitude of anisotropy of thermal conductivity will also vary correspondingly (Section 5.4.2). It should be noted that the domain modelling results presented in Section 6.5.1 and Table 6-20 assume isotropic conditions and thus do not take account of this anisotropy.

Heat capacity

The results for different domains are summarised in Table 6-21.

Thermal expansion coefficient

The mean measured coefficient of thermal expansion for five different rock types varies between $6.9 \cdot 10^{-6}$ and $7.4 \cdot 10^{-6}$ m/(m·K), see Section 6.2.8.

In situ temperature

The mean *in situ* temperatures measured at –400 m, –500 m and –600 m elevation, based on 4–5 boreholes, are estimated at 13.3°C, 14.8°C, and 16.3°C, respectively.

Table 6-20 Thermal conductivity (W/(m·K)) at the 5 m scale for the different rock domains in Laxemar based on simulations at the 2 m scale /Sundberg et al. 2008a/.

Statistical parameter	RSMA01 5 m scale	RSMM01 5 m scale	RSMD01 5 m scale
Mean	2.93	2.65	2.76
Standard deviation	0.29	0.32	0.17
0.1-percentile	2.16	2.11	2.41
1-percentile	2.27	2.19	2.48
2.5-percentile	2.34	2.23	2.50

Table 6-21 Heat capacity at the 2 m scale for different rock domains.

Domain	Mean (MJ/(m ³ ·K))	Std (MJ/(m ³ ·K))
RSMA01	2.16	0.06
RSMM01	2.21	0.12
RSMD01	2.23	0.06

6.6 Evaluation of uncertainties

6.6.1 Data uncertainty

The main data uncertainties are described below. A more detailed description is provided in /Sundberg et al. 2008a/.

Boremap data

Uncertainty in the location, orientation and diameter of the boreholes in space, and in the orientation of geological objects in the boreholes, as documented by /Munier and Stigsson 2007/, are judged to have little or no effect on the results of thermal modelling.

Fine-grained diorite-gabbro (505102), which occurs as dyke-like bodies throughout Laxemar, is commonly mixed with significant amounts of fine-grained granite. However, in the Boremap data, which is the basis for the lithological simulations, these occurrences have been recorded simply as fine-grained diorite-gabbro. The impact of this simplification on the thermal modelling results is that the lower tail percentiles of thermal conductivity in domain RSMD01 may be slightly underestimated.

Thermal conductivity and heat capacity

Assuming that the samples are isotropic, the TPS measurements are considered to be quite reliable, especially the thermal conductivity. However, if the samples have anisotropic thermal behaviour, which to some degree is the case in Laxemar, there may be some impact on the determinations, particularly of thermal diffusivity and on the calculated heat capacity. However, the heat capacity has also been determined directly by a calorimetric method and these measurements are considered to be more reliable.

Uncertainties are also associated with the anisotropic thermal conductivity of Ävrö granodiorite and Ävrö quartz monzodiorite, mainly due to few determinations and local variability in the orientation of the foliation. Uncertainties in the strike and dip of foliation in relation to the experimental configuration result in a potential underestimation of the anisotropy factor. However, after correction for the effect of a dipping foliation plane, the mean thermal anisotropy factor is judged to be quite reliable, but its spatial variability is particularly uncertain. It should be noted that the orientation of the foliation varies spatially throughout the Laxemar area which implies that the orientation of anisotropy of thermal conductivity will also vary correspondingly (Section 5.4.2).

Thermal expansion coefficient

Given the small number of sample locations, the representativeness of samples selected for thermal expansion measurements can be questioned. However, the variability both within and between different rock types is low.

Temperature

In the current model version, the reliability of temperature loggings has been evaluated in relation to calibration errors and disturbances from drilling. As a result of this evaluation, only “approved” boreholes have been used in the description. Although there are only a small number of reliable boreholes, the uncertainties are much smaller than in earlier model versions. The reliability of the estimated mean temperatures is strengthened by the temperature data from the Posiva flow logging in the same boreholes.

6.6.2 Model uncertainty

The thermal stochastic modelling primarily concerns thermal conductivity. There are several uncertainties associated with the different steps of this modelling. Here, a summary is given of the five uncertainties that are believed to be most important for the results at rock domain level, i.e. uncertainties associated with:

- the simulation scale,
- the simulation volume,

- the spatial statistical structure of TRCs (lithology),
- the spatial statistical thermal models, and
- the simulation technique.

A more detailed discussion is provided in /Sundberg et al. 2008a/.

The simulation scale

The effect of using a simulation scale of 2 m to represent subordinate rock types is not fully known. A discretisation error will affect the thermal modelling results for domains with rock bodies smaller than the simulation scale. However, in RSMA01 and RSMM01, TRCs critical to the lower tail of the thermal conductivity distribution are generally present at sizes much larger than the simulation scale. In RSMD01, one of the rock types impacting on the lower tail of the distribution is found as dyke-like bodies of fine-grained diorite-gabbro (TRC 102); a significant proportion of such bodies have a true thickness less than 2 m. However, the effects of discretisation diminish rapidly on upscaling, and have more or less disappeared in the results calculated for the 5 m scale.

The simulation volume

Theoretically, the limited simulation volumes affect the simulation results, but the effect decreases when the simulation volume increases. In Laxemar, the simulation volumes are $100 \times 100 \times 100 \text{ m}^3$. The choice of simulation volume was made with the following factors in mind: the large size of bodies of subordinate rock types, the long correlation lengths observed for some TRCs, and the requirements of the strategy for repository design work /Hökmark et al. 2009/.

There are two situations when the limited volume could be a problem with regard to describing a rock domain statistically: (1) when the lithological simulation volume is so small that the true properties of this limited rock volume deviate from the true domain or subdomain statistics, and (2) when the correlation lengths of thermal properties are similar to or longer than the length of the simulation volume.

For simulations at the 2 m scale, the first type of uncertainty is believed to be of minor importance. The second type of uncertainty is believed to be important mainly for domain RSMD01. Quartz monzodiorite (TRC 36), the main rock type in this domain, displays correlation lengths that are long ($> 100 \text{ m}$) in relation to the simulation volume. However, this is not believed to be critical for the simulation results presented here, since the greater part of the variance in thermal conductivity for quartz monzodiorite occurs within the scale represented by the simulation volume. Furthermore, the simulated spatial variability at scales of 2 – 10 m, which is the approximate range of scales relevant for temperature development around a canister, is rather insensitive to small to moderate changes in the model correlation length of this TRC.

It can be concluded that although there are uncertainties associated with the simulation volume, none of these are believed to have had any major impact on the thermal modelling results.

The spatial statistical structure of TRCs (lithology)

The models used for the lithological simulations are largely based on “best estimates” of uncertain parameters. There are several uncertainties associated with the developed models of the proportions and the spatial statistical structure of the TRCs (lithology). Most of these are coupled to the lack of knowledge concerning detailed geological characteristics, such as typical lengths of rock bodies, the true shape and orientation of rock bodies, trends in the statistics of the lithology within the rock domain, etc. This is particularly relevant for fine-grained diorite-gabbro (TRC 102), one of the rock types critical for the lower tail of the thermal conductivity distribution in domain RSMD01 /Sundberg et al. 2008a/. Hence, confidence in the lower tail of domain RSMD01 is somewhat lower than for other rock domains.

There are also uncertainties linked to the degree to which geological inhomogeneity has been reproduced in the lithological simulations. In the simulation volume, the proportions of TRCs are held constant in each realisation. In reality, the proportions are variable at the scale of the simulation

volume due to lithological heterogeneity. Geological heterogeneities within the domains RSMM01 and RSMA01 were dealt with by dividing the domains into subdomains, according to the strategy outlined in /Back and Sundberg 2007/. This is believed to have reduced the uncertainty significantly.

Uncertainties concerning the true proportions of rock types in the rock domains produce uncertainties in the lower tail of the thermal conductivity distribution at rock domain level. As a result of these uncertainties, the 1 percentile for the 2 m scale may be up to 0.02 W/(m·K) lower than predicted by the thermal model. This uncertainty is highest for RSMA01.

Due to the uncertainties in the TRC proportions, the uncertainties in the overall statistical distributions (the main body of the distribution, tails excluded) of thermal conductivity are much larger than in the lower tails of these distributions. This type of uncertainty is least for RSMD01 and largest for the lithologically more inhomogeneous RSMA01 and RSMM01 domains.

Furthermore, the estimated proportions of the different subdomains in a rock domain have rather large uncertainties since they are primarily based on the assumption that existing boreholes are representative.

The spatial statistical thermal models

Limited data for some TRCs result in uncertain spatial statistical thermal models. When data are few and show large variability, the shape of a statistical distribution cannot only be based on hard data. The distribution models are particularly uncertain as regards the tails of the distributions. Moreover, the lower limit of thermal conductivity for a TRC is usually not known and must be determined based on expert opinion. Therefore, the uncertainties in the shapes of the lower tails of the distribution models are translated into uncertainties in the estimates of low percentiles for the domain. This is only of importance for the TRCs with low thermal conductivities, in particular TRC 33A, 33B and 46. The variograms require even more data than the distribution models. It has been assumed that thermal conductivity exhibits a similar correlation structure to rock density. This is a reasonable assumption that allows the construction of variogram models, but the associated uncertainty is not known, at least not for all TRCs. However, given the total spatial variability in thermal conductivity present within a rock domain, this uncertainty has only a minor effect on the domain modelling results. Although the correlation structure influences the simulation results after upscaling, the absolute values of thermal conductivity are more important for the tails of the distributions.

An assessment of the spatial statistical thermal models for the dominant TRCs (TRC 46, 56 and 36) indicates that they are based on a rather large amount of data. In spite of the uncertainties, the spatial statistical thermal conductivity models are believed to be more reliable than in previous versions of the thermal site descriptive modelling. They do not rely on any particular statistical distribution and the correlation structure is explicitly included in the model, which was not the case in previous model versions.

The simulation technique

The simulation technique is a source of uncertainty. This uncertainty is closely related to the simulation scale and the simulation volume. The advantage of this uncertainty compared to the others is that it can easily be identified. The principle is simple: The result of a simulation is compared with the input models. Deviations indicate that there is uncertainty. This type of verification was performed both for the lithological and the thermal simulations. The conclusion is that the output of the thermal simulations resembles the input very well, but for the lithological simulations there is not an exact match as regards, for example, the length distribution of rock types. The reasons for this are the restricted simulation volumes (see above) and the simulation algorithms. This uncertainty is believed to have only a minor influence on the thermal modelling results.

6.6.3 Summary of uncertainties

Small uncertainties in the lower tail of the thermal conductivity distributions will have a significant impact on canister spacing. For this reason, the analysis of the uncertainties in the thermal model focus on the lower tail of the thermal conductivity distribution.

As regards the overall distribution (the main body of the distribution, tails excluded) of thermal conductivities for each rock domain, the highest confidence is placed in the results for rock domain RSMD01, because of its higher degree of homogeneity in geological and thermal properties compared with rock domains RSMM01 and RSMA01. The rather large uncertainties associated with the output of the geological simulations for RSMM01 and RSMA01, in particular the proportions of rock types and proportions of thermal subdomains, imply that the overall statistical distribution of thermal conductivity is also uncertain for these two rock domains. This is the aspect of the thermal model with the lowest confidence.

Confidence in the lower tails of the thermal conductivity distributions is generally high, slightly higher for rock domains RSMA01 and RSMM01 than for rock domain RSMD01. The uncertainties that do exist are primarily associated with uncertainties in the spatial statistical thermal models (distribution and spatial correlation models) for the critical TRCs. In contrast, the lower tails of the thermal conductivity distributions are not very sensitive to uncertainties in the rock type proportions and the spatial statistical structure of lithology (TRCs), although some impact on rock domain RSMD01 can be suspected.

Overall confidence in the thermal model is reinforced by the mutual consistency between understanding of the geology and the description of the thermal properties.

7 Rock mechanics

The rock mechanics model consists of two components, the model of mechanical characteristics and the model for *in situ* state of stress. The rock mechanics model is used in the repository design process to evaluate the stability of the various underground openings; rock caverns, tunnels and deposition holes. In the safety assessment the rock mechanics model is needed for analysis of long term changes in mechanical and hydrological conditions in and around the planned repository. This chapter provides a summary of the rock mechanics modelling results, presented in /Hakami et al. 2008/.

7.1 State of knowledge at previous model version

As part of the previous model version, Laxemar 1.2 /SKB 2006a/, a rock mechanics model was provided describing the mechanical properties and characteristics of intact rock, fractures, rock mass and rock stresses, as is also done in this current version. The main differences in the description relate to the incorporation of an increased number of laboratory tests, now including all rock types expected to have an occurrence larger than about 3% of a given rock domain and also including characterisation of oxidised rock. In the previous model version a large spread in the properties of Ävrö granite was observed, which is now mitigated by a division of the Ävrö granite into two separate rock types in the description. A further improvement in the description of intact rock is the simulation and visualisation of spatial variation of uniaxial compressive strength (UCS) for different rock domains.

The rock mass properties are currently estimated using roughly the same approach as in model version Laxemar 1.2. However, the characterisation of the rock (mass) in the deformation zones is now more comprehensive, compared with the previous version. Primarily, the increased amount of geological information has enabled a more elaborate rock mechanics description.

The stress model of version Laxemar 1.2 provided predictions for two different stress domains, domain I and domain II, with a fairly large uncertainty in the stress magnitudes. In this current version, following a similar approach, a stress model is provided only for the defined fracture domains of the focused volume. In this volume, additional stress measurement data have become available from the cored borehole KLX12A, which constitutes the main database for the updated stress model.

In total, 17 deep cored boreholes have been added in the focused volume of Laxemar since model version Laxemar 1.2 (see Section 2.3.1), which has significantly improved the possibilities for stress modelling and also for rock mass quality characterisation.

7.2 Evaluation of primary data

7.2.1 Laboratory tests of intact rock

For the description of intact rock it was judged most relevant to divide the Laxemar bedrock according to the “rock types” (each having a rock code in the databases) identified in the geological mapping and modelling (see Table 5-1). Thus, the defined rock domains have not been considered in the analysis of primary data on the intact rock. The rock type proportions and spatial variations in each rock domain are presented and discussed in Section 5.2.3 and the resulting spatial variation for strength properties is presented in Section 7.3.1.

To evaluate the strength of the intact rock, laboratory tests were performed on drill core samples. The results of these tests are used to characterise the rock types and to identify similarities and differences between them. Such results will be valuable in the design process, where stability analyses of different kinds are performed. Also in the safety assessment the mechanical properties are used as input to the estimation of the extent of thermal spalling around deposition holes.

Uniaxial compressive tests

In total, the test program included 145 uniaxial compressive tests on different rock types from 15 different boreholes (including two from the Simpevarp peninsula). The sampling location and results of these tests are shown in Figure 7-1. For each test the parameters determined are: uniaxial compressive strength (UCS), crack initiation stress, Young's modulus, Poisson's ratio and density. The results are exemplified by histograms of UCS for four different rock types shown in Figure 7-2. In most cases, where the number of tests is sufficient, the test results are seen to roughly follow a normal distribution.

To illustrate the rock mechanics basis for the previously discussed (cf. Sections 5.2.1, 5.2.2 and 6.2.1) division of the Ävrö granite (rock code 501044) into the two subvarieties Ävrö granodiorite (501056) and Ävrö quartz monzodiorite (501046), a diagram of UCS versus the wet density for all Ävrö granite samples is given in Figure 7-3. Note from Figure 7-2 and Figure 7-3 that there is a clear difference in the mean values of the two "new" rock type varieties, with Ävrö granodiorite being the stronger and Ävrö quartz monzodiorite being the weaker. Furthermore, a trend of lower UCS is seen for the oxidised samples of the Ävrö quartz monzodiorite and the quartz monzodiorite (not shown in the figures) compared with the unaltered samples.

During a uniaxial compression test the stress-strain curve will first increase linearly in a fully elastic mode after which the curve will start to deflect. The stress level at this deflection point is called the crack initiation stress and is clearly correlated to the peak stress value (the UCS), as may be concluded from the four cross-plot examples given in Figure 7-4. The coefficient of correlation is fairly similar, in the range of 0.52 to 0.57, depending on the rock type.

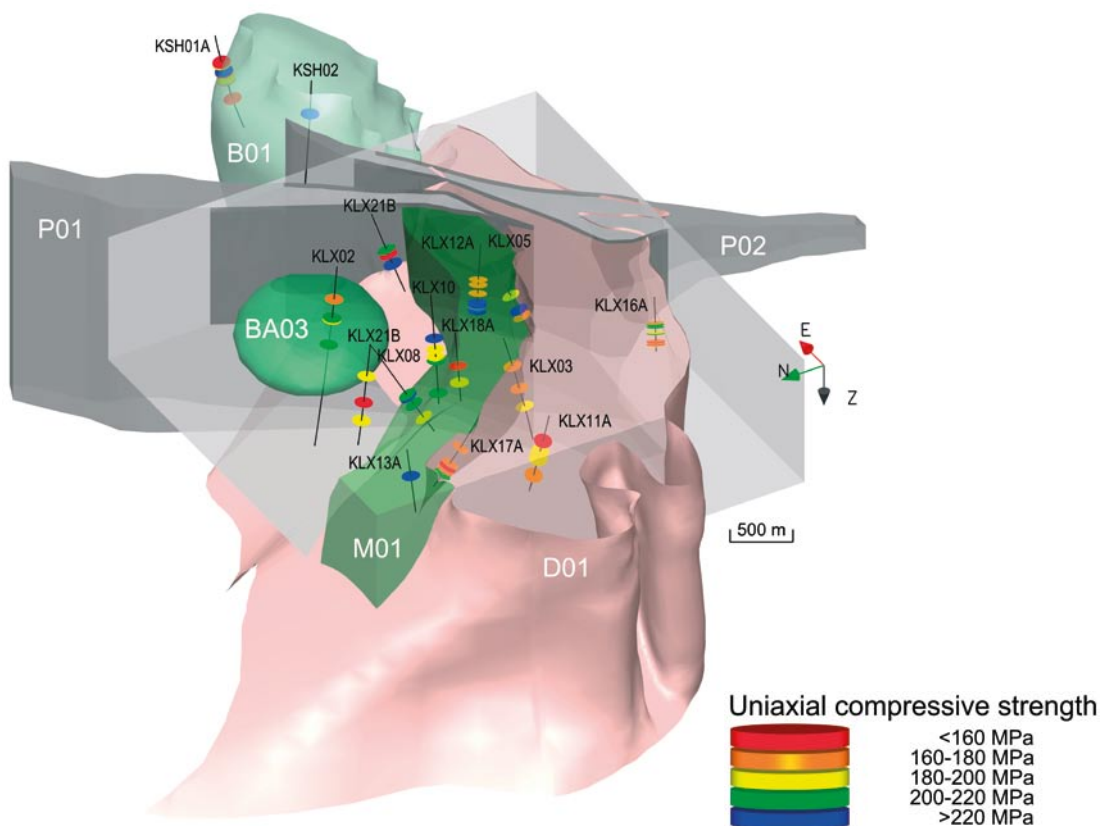


Figure 7-1. Location and results of the uniaxial compressive tests, a total of 145 tests in different rock types. Since the samples are situated close to one another, some sample locations are hidden. For a description of the rock domains indicated, see Section 5.4. (Rock domain RSMA01 is made transparent.) The grey box shows the Laxemar local model volume. Perspective view from the northwest.

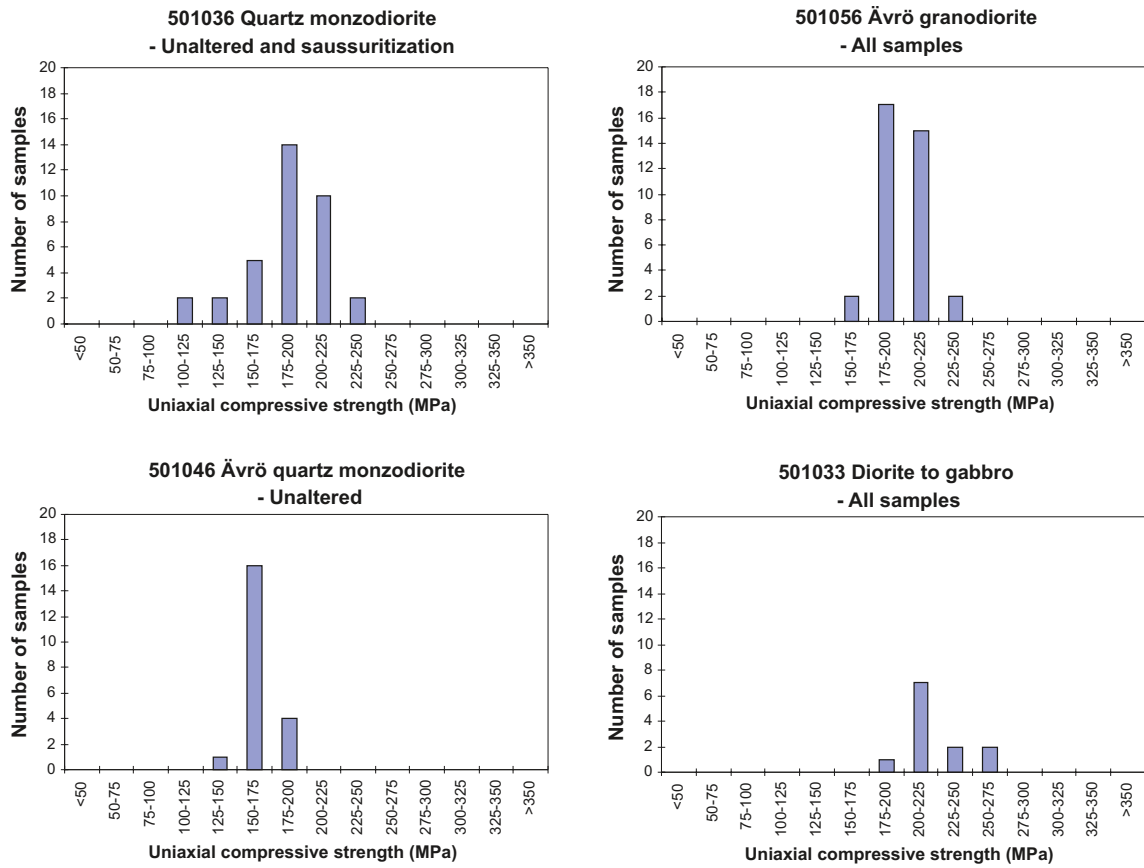


Figure 7-2. The frequency distribution of uniaxial compressive strength for the four most frequently occurring rock types.

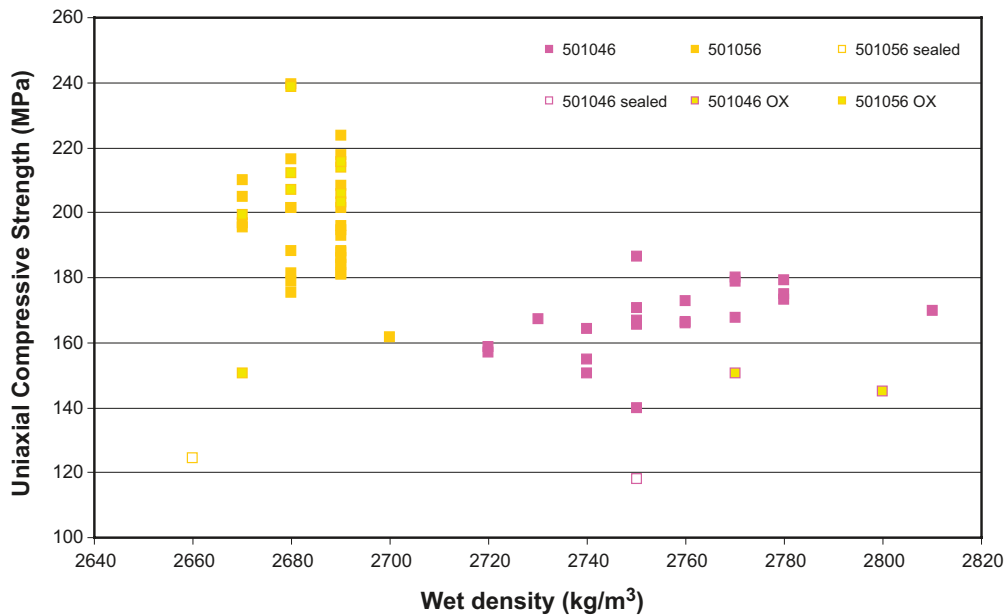


Figure 7-3. Uniaxial compressive strength versus wet density for Ävrö quartz monzodiorite (501046) and Ävrö granodiorite (501056). (OX = oxidised, Sealed = a pre-existing sealed fracture in the sample has been observed.)

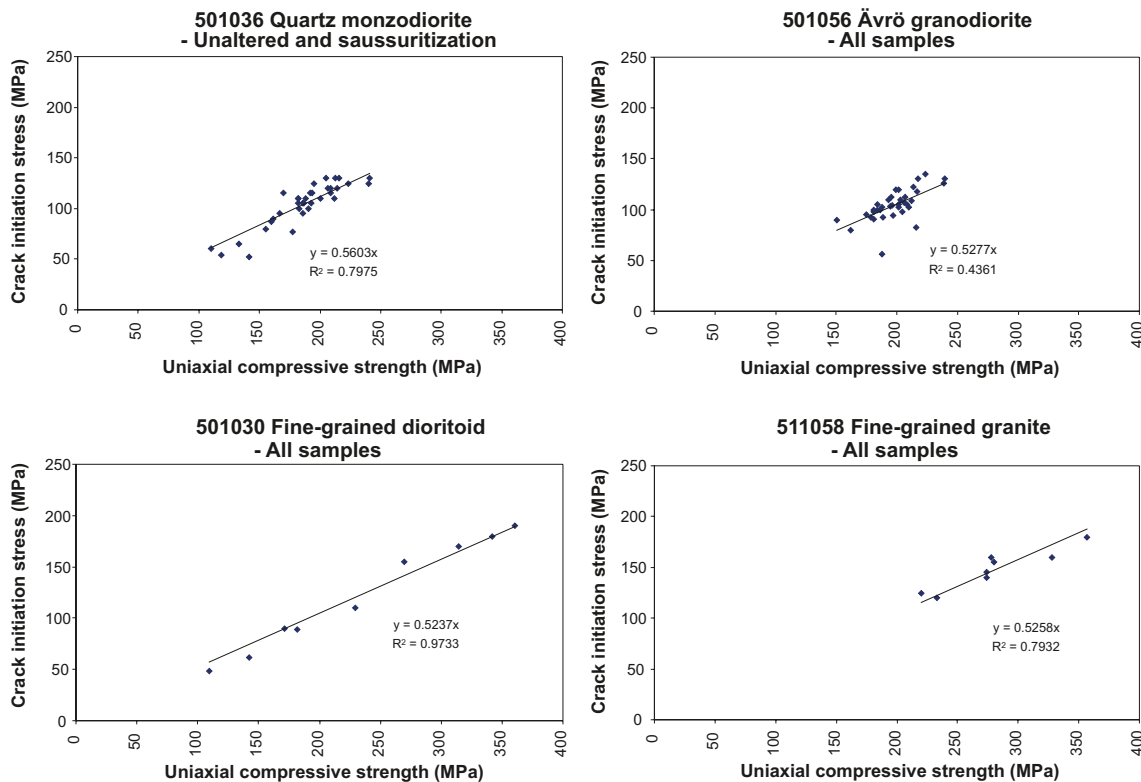


Figure 7-4. Cross-plot of the crack initiation stress and the uniaxial compressive strength of four rock types. The best fit linear functions passing through the origin, and the error coefficient, are shown in the diagrams.

Tensile tests

The tensile strength was tested by means of the indirect tensile test (Brazilian test) in the laboratory. The total number of successful tests was 192. The samples were often taken in batches of 10 located next to one another along a given core. The spatial spread of sampling points in the boreholes and test results are indicated in Figure 7-5, and some univariate statistics of the test results are presented in Table 7-1.

No difference in tensile strength is seen between the Ävrö granodiorite and the Ävrö quartz monzodiorite, both with a mean value of 13 MPa. The quartz monzodiorite is stronger having a tensile strength of about 16 MPa. A possible explanation to the difference in tensile strength is that the quartz monzodiorite is equigranular whereas the Ävrö granodiorite/Ävrö quartz monzodiorite is porphyritic, i.e. the quartz monzodiorite has a more uniform grain size distribution. The difference in tensile strength between rock types also fits well with the observed difference in porosity (Table 10-3). Of the rock types with statistically confirmed porosity measurements, rock type 501030 and 501036 have low porosities whereas rock types 501046 and 501056 have the highest porosities. A large part of pores are associated with grain boundaries and a correlation between porosity and tensile strength, governed by the mineral grain bonds, is therefore to be expected.

The influence of oxidation is again seen in the tensile tests on quartz monzodiorite. (No tensile tests are performed on oxidised Ävrö quartz monzodiorite). Oxidised rock shows increased porosity, cf. Table 10-3, which fits with the observed associated decrease in tensile strength, cf. Table 7-1

There is no evidence of a foliation of the core samples. Hence anisotropy is not considered to be relevant for tensile strength (or compressive strength) (cf. Section 5.2.3).

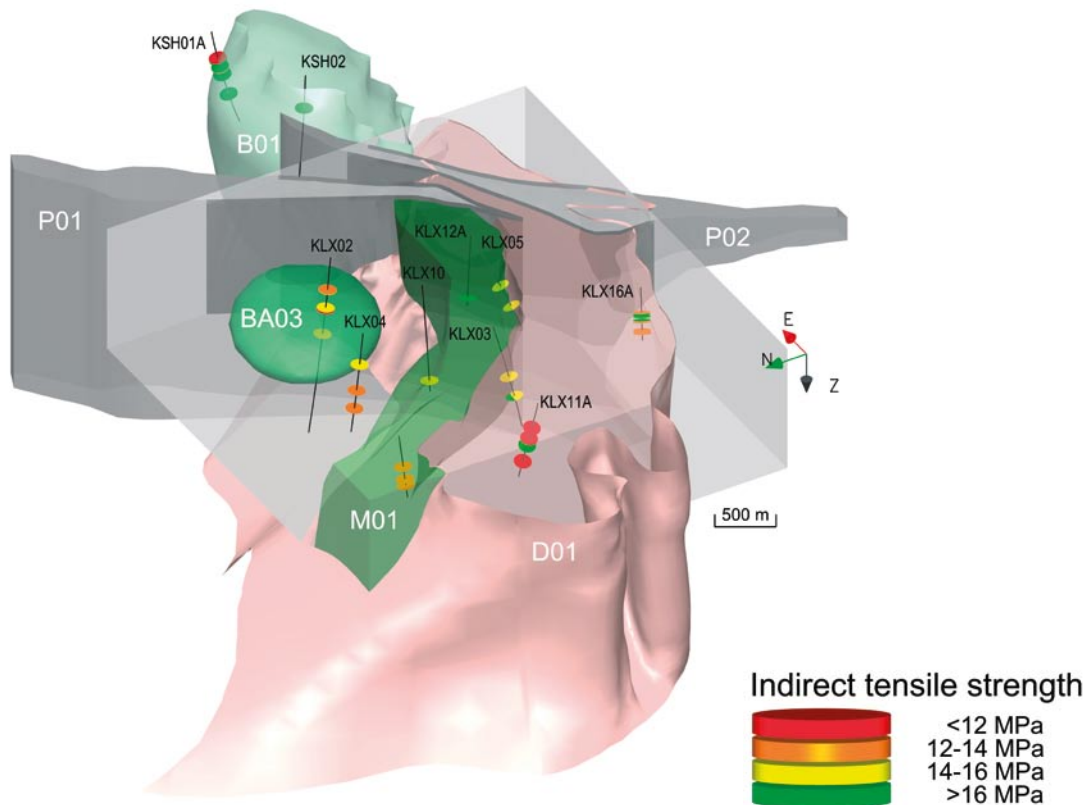


Figure 7-5. Location and results of the tensile strength tests ($N=192$). Since many of the samples are situated very close to one another, only some of them are visible in the figure. For a description of the rock domains indicated, see Section 5.4. The grey box shows the Laxemar local model volume. Perspective view from the northwest.

Table 7-1. Results from indirect tensile strength tests of samples for SDM-Site Laxemar.

Rock Type	No. of samples	Minimum σ_t (MPa)	Mean σ_t (MPa)	Maximum σ_t (MPa)	Std. dev. σ_t (MPa)
501030 Fine-grained dioritoid ¹⁾	24	13.8	19.0	24.1	2.3
501033 Diorite/gabbro ²⁾	10	14.9	15.7	17.1	0.7
501036 Quartz monzodiorite, unaltered and saussuritised	68	10.1	16.4	23.8	3.0
501036 Quartz monzodiorite, oxidised	10	11.2	13.7	17.6	2.1
501046 Ävrö quartz monzodiorite, unaltered ²⁾	28	9.4	13.0	15.5	1.2
501056 Ävrö granodiorite ¹⁾	52	9.3	12.9	16.4	1.5

1) Statistics includes some oxidised samples.

2) No oxidised samples tested.

Triaxial compressive tests

A total of 55 triaxial tests were performed (excluding samples where sealed fractures were identified). The different confining stresses used were 2, 7 and 10 MPa for all rock types with additional tests at 15 and 20 MPa confining stress for the three most frequently occurring rock types. Two examples of the results, in the form of stresses at failure, are shown in Figure 7-6. The best fit Hoek-Brown and Mohr-Coulomb failure envelope curves are also included in the figures. Both the uniaxial and triaxial test results, but not the tensile strength results, are used to fit the failure envelopes. As for the uniaxial strength (UCS), a difference is noted between the peak strength, at high confining stress, between Ävrö granodiorite and Ävrö quartz monzodiorite (c. 420 MPa and 320 MPa, respectively, at 20 MPa confinement). The different parameters determined from triaxial tests (cohesion and friction angle) are presented for each test in /Hakami et al. 2008/.

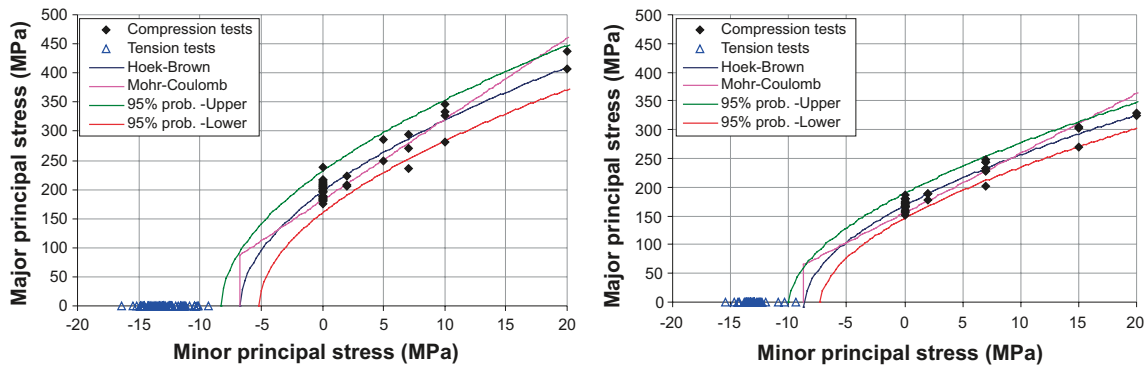


Figure 7-6. Hoek-Brown's and Coulomb's failure envelopes from uniaxial and triaxial tests for intact samples of (left) Ävrö granodiorite (501056) and (right) Ävrö quartz monzodiorite (501046). On the x-axis, the indirect tensile strength results are also shown, but they are not used for the curve fitting.

Microcrack volume measurements

To estimate the amount of microcracking of the samples (i.e. not the *in situ* rock), the non-linear volumetric strain recorded in hydrostatic triaxial compression tests was measured. Six samples of Ävrö granite from borehole KLX17A were tested in the site investigation and the results are presented in Figure 7-7. The results indicate a fairly linear increase of crack volume with depth, from about 0.01% in samples from -200 m elevation up to roughly 0.04% in samples from -500 m. This trend of increase is in accordance with the expected stress increase (see Section 7.3.5). The total porosity of the samples is about 0.3–0.4%.

However, one important circumstance in the interpretation of these results is the fact that the density of the six samples varies, such that the two samples from about -200 m are more dense. This means that according to the subdivision of Ävrö granite the two upper samples constitute Ävrö quartz monzodiorite while the other four samples are Ävrö granodiorite. These two varieties do not have the same mineral composition and also have slightly different mechanical properties. Therefore the limited number of triaxial tests with measurements of microcrack volume makes it impossible to draw strong conclusions about possible depth trends.

Nevertheless, the very small microcrack volumes measured on samples from all depths indicate that the stresses at these levels are not high enough to cause major damage to the drill core.

Another use of the microcrack volume measurements is that it provides an estimate of the difference in porosity between laboratory (de-stressed) samples and ambient *in situ* (confined) rock porosity, that is of importance in the determination of rock matrix pore water compositions (see Section 9.5.7).

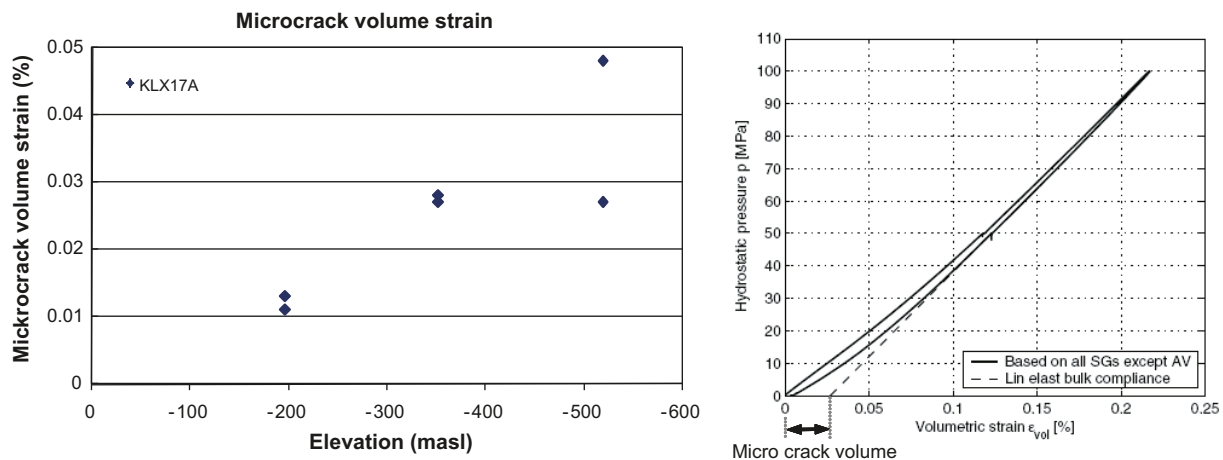


Figure 7-7. Measured microcrack volume versus depth for samples from borehole KLX17A (left). The two samples collected at shallow depth are Ävrö quartz monzodiorite and the other four samples are Ävrö granodiorite. An example of a test curve and definition of microcrack volume is shown to the right (Jacobsson 2007).

7.2.2 Laboratory tests of fractures

The strength and deformability of the natural rock fractures were studied using two methods; tilt tests and direct shear tests on fracture samples from the drill cores. In tilt tests, shearing is induced by the self-weight of the upper piece as the fracture sample is progressively tilted. Tilt tests were performed on 199 samples to obtain an overview of the variation in fracture properties. In direct shear tests, shearing is induced by actuators that apply load both parallel and perpendicular to the fracture plane. The size of each tested sample is about 55 mm in diameter. Direct shear tests were performed on 71 open fractures and 14 sealed fractures.

Some of the results from the tilts tests are shown in Figure 7-8 and from the direct shear tests in Figure 7-9. The results in the diagrams are grouped according to fracture orientation (different sets described in Section 5.6) of the tested samples and plotted versus the elevation of sample location. No particular depth dependence can be distinguished in the fracture mechanical properties. The roughness and the friction angle also seem to be quite similar regardless of the fracture orientation. Here one should bear in mind that there is probably a bias, or restriction, in the sampling towards the more frequent smaller size fractures (see further Section 7.4.2). The only difference related to orientation that is observed is a higher normal stiffness for the subhorizontal fracture set.

The core mapping characterisation parameters (fracture surface roughness, planarity and alteration categories) for the tested samples have been compared with the characterisation statistics of the entire fracture population. This comparison did not reveal any particular bias in the sampling. The clearly most frequent characteristics are “planar”, “rough” and “slightly altered” with chlorite and calcite as fracture infilling minerals (see also Sections 5.2.6 and 9.5.6). However, a study in some boreholes of the relatively few fractures that are classified as highly water bearing, the so called PFL-features (see Section 8.3.1), revealed that none of these fractures are among the mechanically tested fractures. According to /Rhén et al. 2008/, most of the PFL-features are mapped as crush, not as single fractures.

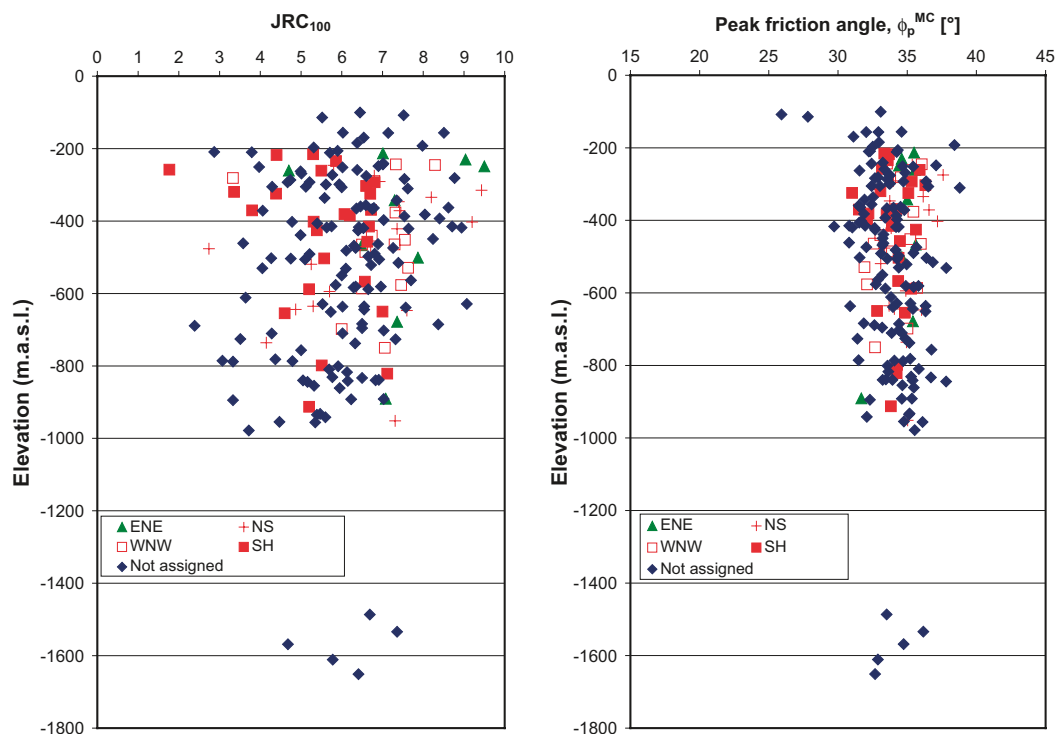


Figure 7-8. JRC_{100} and peak friction angle ϕ_p^{MC} versus depth derived from tilt tests on fractures of different orientation. The fracture sets are shown in the legend (SH = subhorizontal).

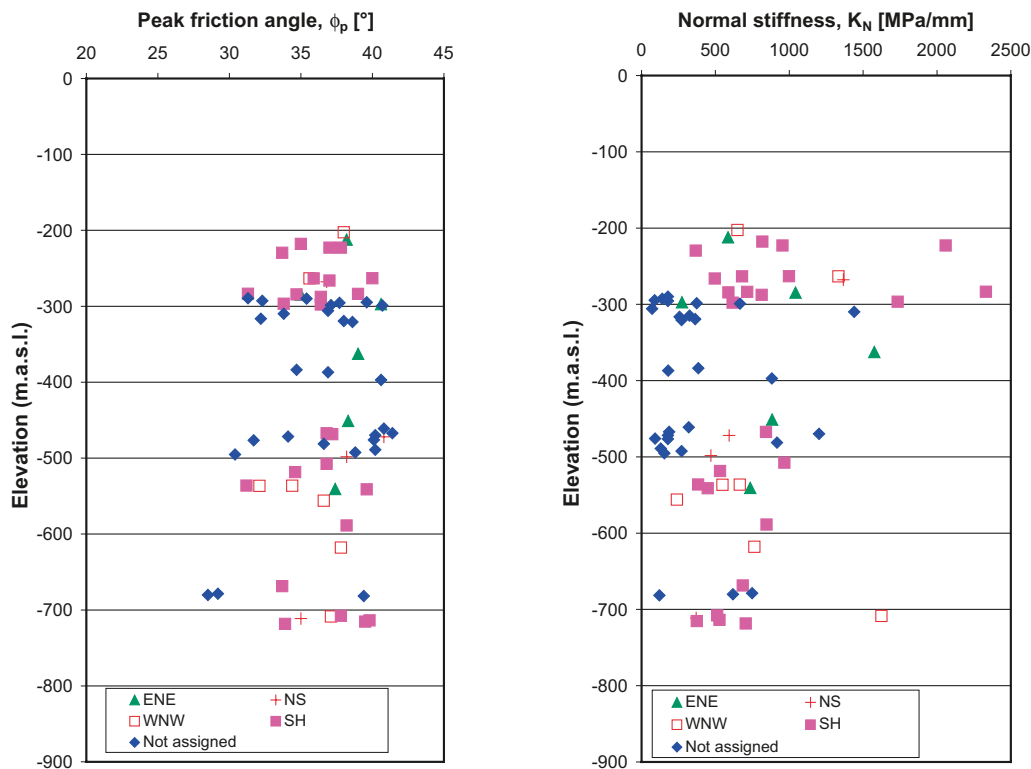


Figure 7-9. Peak and residual friction angle and normal stiffness K_N versus depth, determined from direct shear tests on fracture samples in the laboratory (constant normal load tests). The orientations of the tested fracture samples are shown in the legend (SH = subhorizontal).

7.2.3 Rock mass quality indices RMR and Q

The rock mass quality, from a rock engineering point of view, may be classified using empirical indices based on core mapping information. In this case characterisation has been performed using the RMR /Bienawski 1989/ and Q /Barton 2002/ systems (Figure 7-10 and Figure 7-11). The classification has been made, following the methodology outlined in /Röshoff et al. 2002/, for five deep subvertical boreholes in the Laxemar local model volume; KLX02, KLX03, KLX04, KLX05 and KLX12A. For the additional four boreholes KLX10, KLX11A, KLX15A and KLX19A, the Q and RMR values were estimated through an established correlation to the mapped RQD. The spread of Q and RMR values will depend slightly on the section length chosen (here 5 m sections), giving larger variability for shorter sections. Comparisons between different scales can be found in /Röshoff et al. 2002/.

The mean RMR value is about 80 in all fracture domains with a spread from about 60–90, i.e. the rock mass is rated as “Good” or “Very good”. The most frequent Q values inside the fracture domains of the focused volume are in the Q-class “Very good” quality rock. In the fracture domains FSM_N and FSM_EW007 the most frequent Q values indicate a “Good” rock quality. Inside deformation zones the variation of Q values is unsurprisingly large, ranging from “Very poor” to “Very good” depending on which 5 m section, of the total deformation zone section as defined by the geological single hole interpretation, that is studied. The RMR values give a rating in the range “Fair” to “Good”.

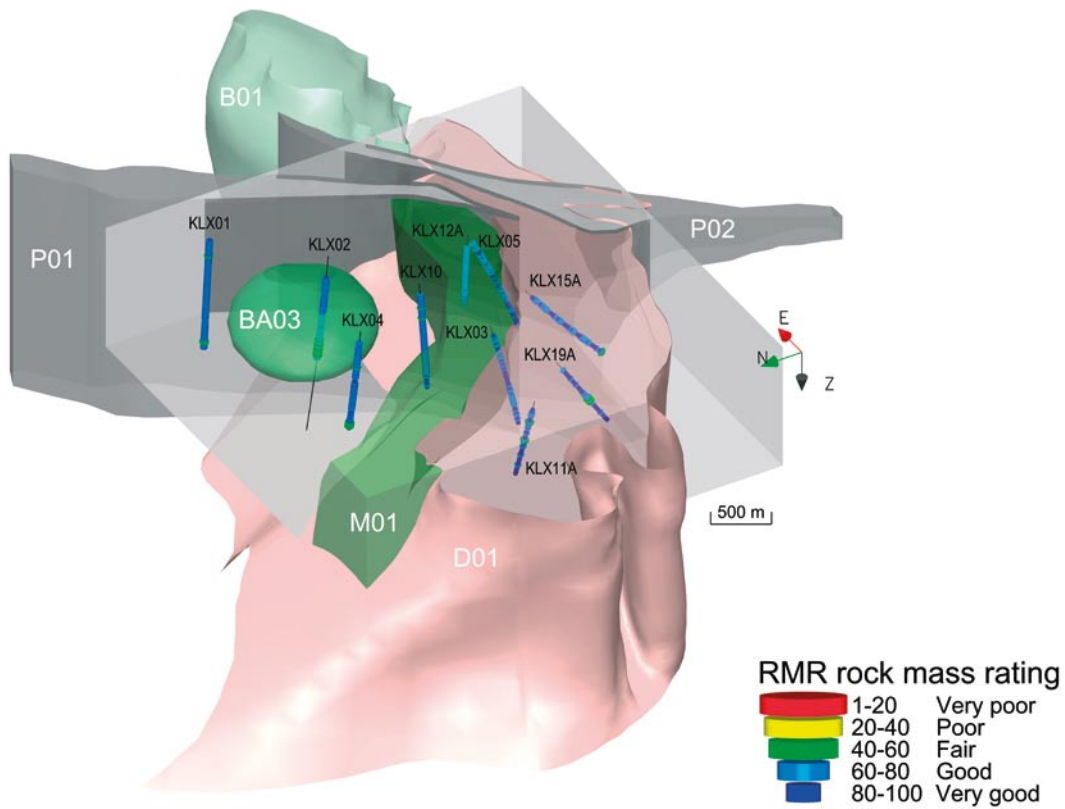


Figure 7-10. Location of the boreholes used for classification of the rock mass with RMR. Resulting RMR values for 5 m sections are marked along the boreholes. The grey box shows the Laxemar local model volume. Perspective view from the northwest.

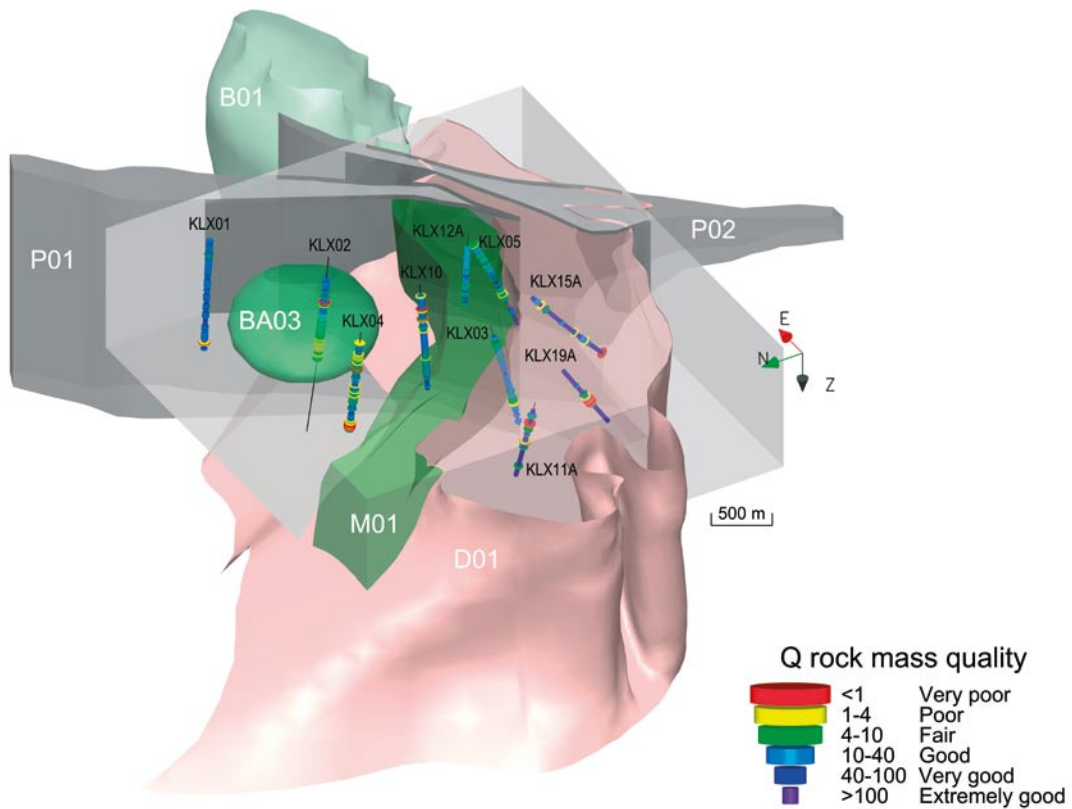


Figure 7-11. Location of the boreholes used for classification of the rock mass with Q system. Resulting Q values for 5 m sections are marked along the boreholes. The grey box shows the Laxemar local model volume. Perspective view from the northwest.

7.2.4 Stress data

Direct stress measurements have been performed using the overcoring method, hydraulic fracturing and hydraulic tests on pre-existing fractures (HTPF). Table 7-2 lists borehole locations and reporting of all direct measurement data that have been utilised in the stress modelling. Indirect input data to the stress model are observations of borehole breakouts and core dishing. Furthermore, the results from microcrack volume measurements (Section 7.2.1) and P-wave velocity measurements may be regarded as input to the stress modelling, since very high stress levels would lead to microcracking and lower P-wave velocities in the drill cores.

It should be noted that overcoring and hydraulic fracturing have been applied in only two boreholes within the local model volume. The largest amount of data is available from the Äspö Hard Rock Laboratory.

The results from the overcoring measurements from all boreholes (not older than 1996) are shown in Figure 7-12 as the principal stress magnitudes versus depth. The orientations of measured maximum principal stresses are found in the stereographic plot in the same figure.

Looking at all available data it may be considered that magnitudes and orientations are varied. Within the Laxemar local model volume there are two boreholes, KLX04 and KLX12A, where tests with the overcoring method have been carried out, and the results from these two boreholes are presented separately in Figure 7-13. From these diagrams a clear trend is seen for both orientation and magnitudes although the variation between single measurements is still quite significant. The direction of the maximum principal stress is NW-SE, as is to be expected given the acting tectonic forces in the region (Figure 3-3). In KLX12A the orientation of the major principal stress is consistently plunging slightly to SE, with the shallow data points plunging more than the deeper data. This may be an effect of the major deformation zone ZSNNW042 dipping south, or due to some minor sub-parallel zone located closer to KLX12A.

The results from hydraulic measurements relating to the minimum horizontal stress are shown in Figure 7-14. It can be seen that there is a general increase with depth, as expected, but also that there seems to be differences in the stress magnitude between the boreholes, and within a single borehole.

Table 7-2. Boreholes utilised for direct stress measurement by OverCoring (OC), Hydraulic Fracturing (HF) and Hydraulic Tests on Pre-existing Fractures (HTPF). Borehole locations are given in Figure 2-5.

Borehole name	Measurement method		
	OC	HF	HTPF
<i>Laxemar subarea</i>			
KLX04	P-05-69	–	–
KLX12A	P-07-123	P-07-232	P-07-232
<i>Simpevarp subarea</i>			
KAV04A	P-04-84	–	–
KSH01A	–	P-04-310	P-04-310
KSH02	P-04-23	–	–
<i>Older measurement in the Laxemar subarea</i>			
KLX02	–	PR U-97-27	–
<i>Äspö Hard Rock Laboratory</i>			
KA3759G	IPR-01-67	–	–
KF0093A01	R-02-26	IPR-02-02	–
KK0045G01	R-02-26	–	–
	IPR-01-67		
KA3376B01	IPR-03-16	–	–
KA2599G01	–	IPR-02-02	–
<i>Oskarshamn</i>			
KOV01 ¹⁾	IPR-02-18	IPR-02-01	–

1) Borehole in downtown Oskarshamn designed for testing of different logging equipments, about 30 km south of Laxemar.

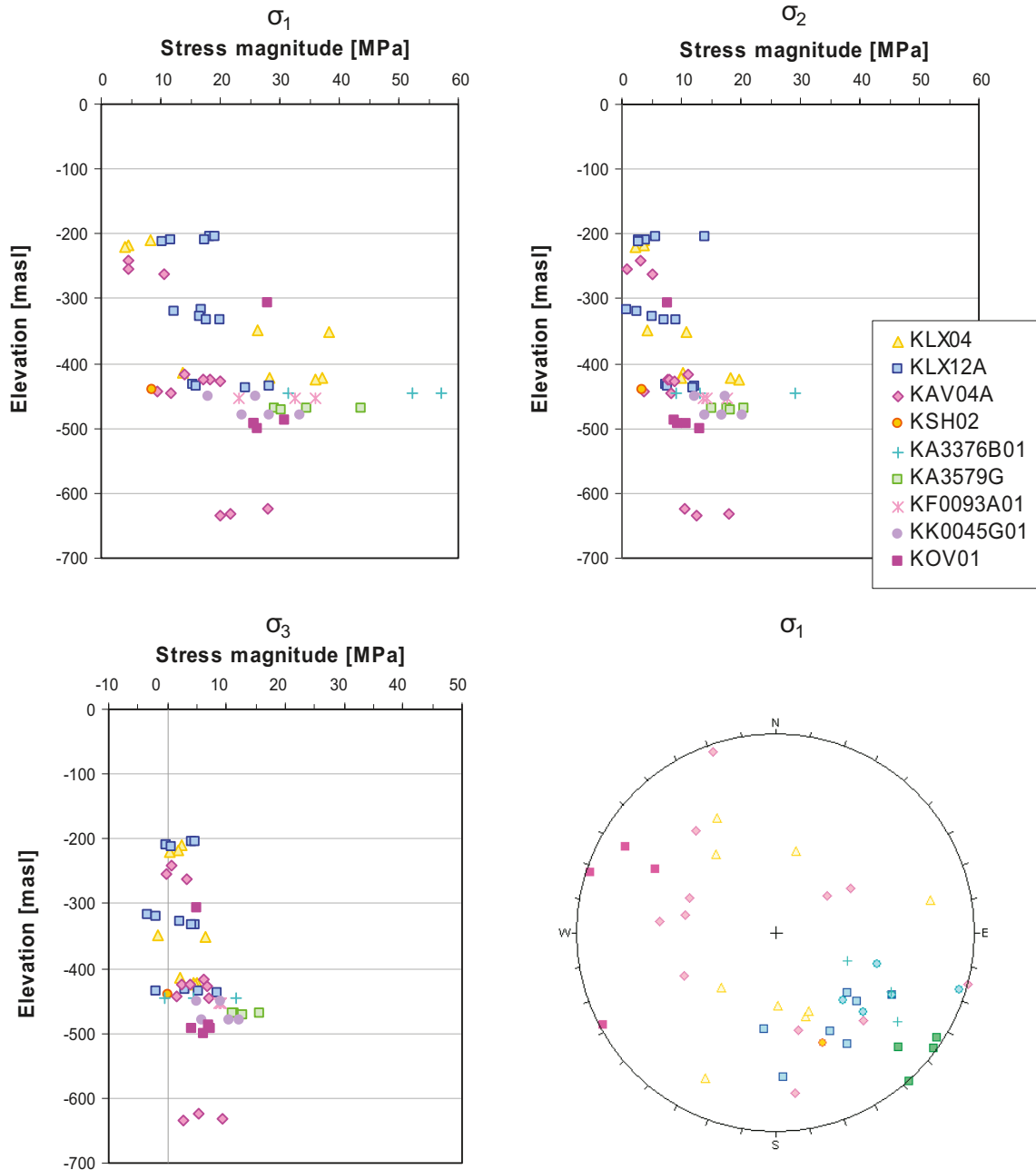


Figure 7-12. Principal stress magnitudes (σ_1 , σ_2 and σ_3) versus elevation from all utilized overcoring data in the region. The orientation of the maximum principal stress is shown in the pole plot in the lower right corner: Different boreholes are marked with different symbols (the same legend for all diagrams). Location of boreholes is shown in Figure 2-5.

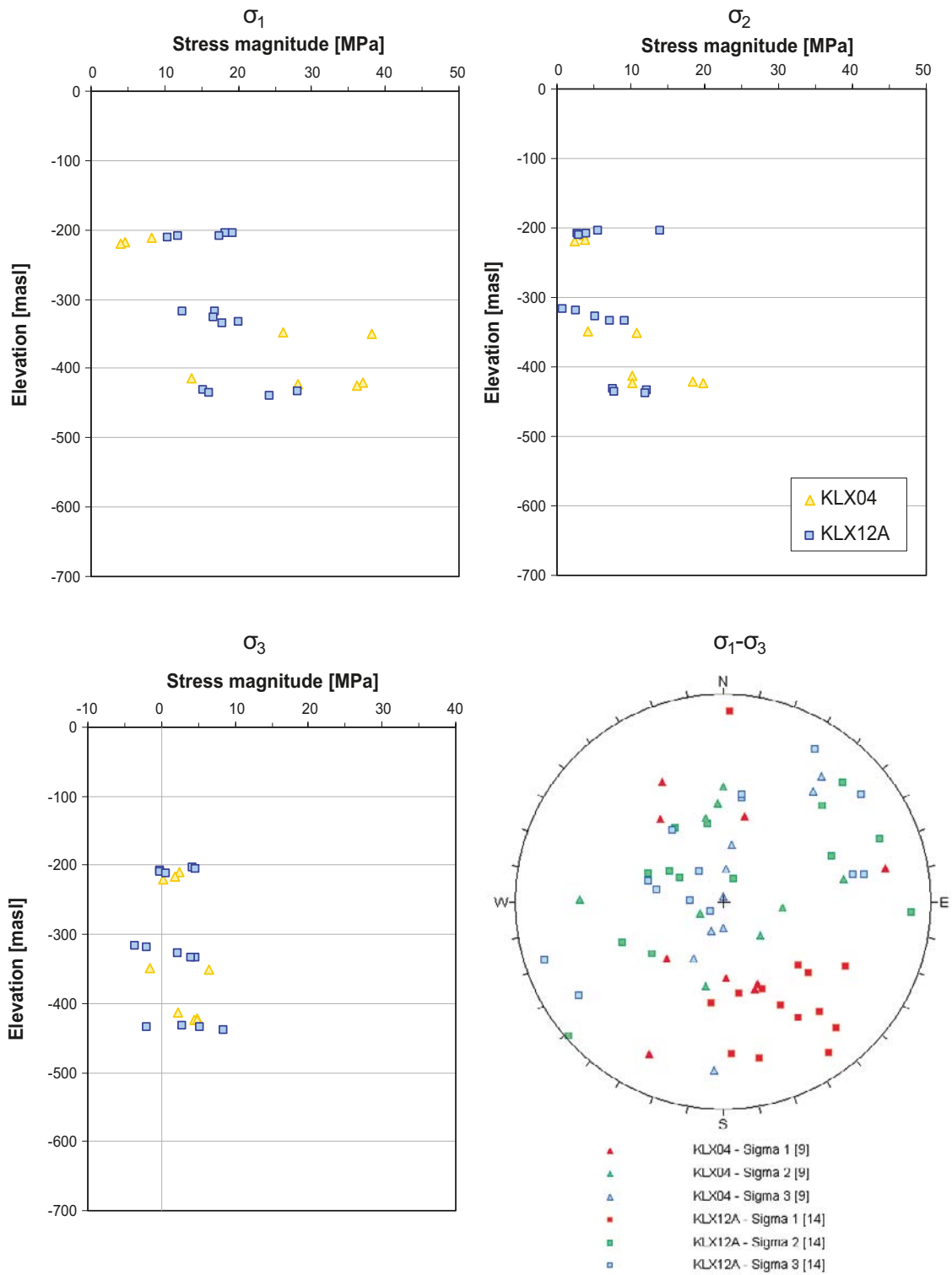


Figure 7-13. Overcoring measurement results in KLX04 and KLX12A versus elevation. Principal stresses (magnitude and orientation).

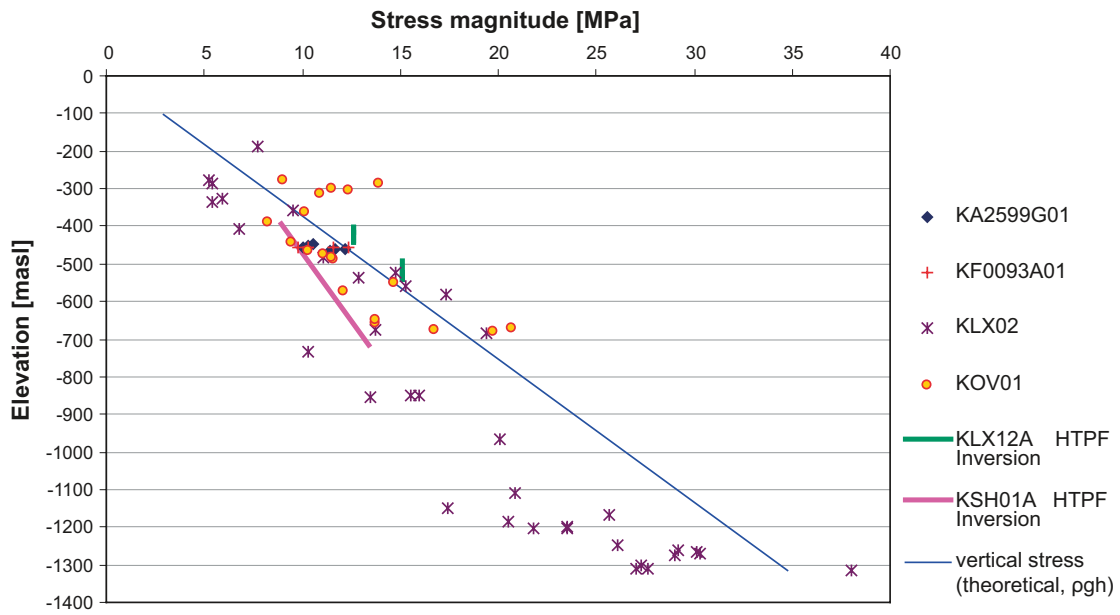


Figure 7-14. Results from hydraulic fracturing stress measurements – Minimum horizontal stress, σ_n . For KLX12A and KSH01A the results from an HTPF inversion of test results are also shown (KOV01 is located in Oskarshamn).

Very little core dinking is observed in the investigated drill cores in Laxemar. In total, only about 9 locations in 6 boreholes summing up to a total length of 3.5 m was characterised by core dinking, which should be compared to the total drill core length of 5,400 m analysed. Most of the core dinking occur associated with fine-grained granite veins /Hakami et al. 2008/.

Borehole breakouts are also very few. Breakouts were noted at 30 locations in 6 boreholes (of which 13 observations are associated with fractures), and most of them located deeper than 700 m (Figure 7-15). The orientation of the breakouts may be determined by use of the televiewer log. The mean azimuth of all breakouts (not associated with fractures) is 43.4° (Figure 7-15). For more details concerning breakouts, see /Hakami et al. 2008/. Most of the breakout occurrences are located in quartz monzodiorite with veins of fine-grained granite.

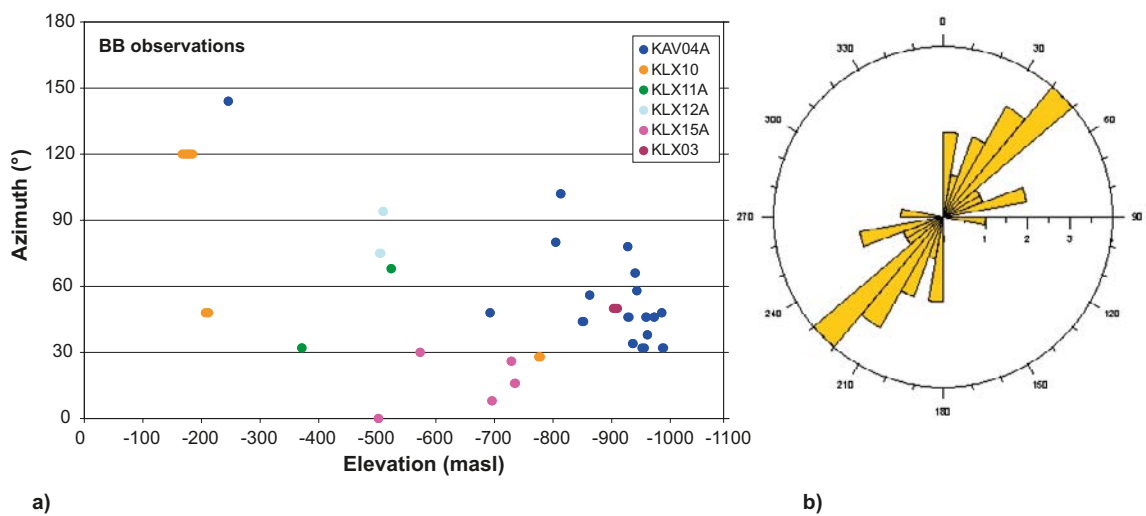


Figure 7-15. Results from the analysis of borehole geometry measurements by televiewer /Ringgaard 2009/ and /Hakami et al. 2008/. a) Plot showing azimuth for all the observed breakouts (including those associated with geological structures) as a function of elevation (borehole KLX12A ends at -560 m). b) Rose diagram for the 17 classical borehole breakouts not associated with geological structures in boreholes KAV04A, KLX03, KLX11A, KLX12A and KLX15A (Median = 46° and Mean = 43.4°).

7.3 Rock mechanics model

7.3.1 Intact rock properties

To select what rock types to include in the description, a criterion was established based on the expected rock type occurrence. It was decided that for rock types, or rock type varieties, that could be expected to constitute more than c. 3% of the repository volume, a separate description (parameter values) should be presented. Expected rock type proportions in each rock domain are described in Section 5.4.4 and can be found in /Wahlgren et al. 2008, cf. Appendices 4 and 11 therein/.

The modelling for the intact rock strength and deformability parameters is based directly on the laboratory test results. It was observed that data for all parameters seem to compose a bell-shaped frequency histogram and that the data fit quite well to a normal distribution /Hakami et al. 2008/. Therefore, truncated normal distribution functions were chosen as the most suitable models to be used for prediction of the parameters. The mean, standard deviation and minimum and maximum values were taken as equal to the actually observed test results, with some minor exceptions for cases where the number of tests was limited. All the parameter values for the models are given in Table 7-3 and the UCS models are also shown as probability functions in Figure 7-16. Furthermore, the uncertainty in the mean value of the distribution is quantified in Table 7-3 (see also Section 7.4.1). A great spread in the distribution for fine-grained dioritoid can be noted, probably due to spatial variations in rock type characteristics /Hakami et al. 2008/.

Table 7-3. Quantified parameters for models of strength and deformation properties for the different rock types in Laxemar.

Parameter	501030 Fine-grained dioritoid	501033 Diorite/gabbro	501036 Quartz monzodiorite – Unaltered	501046 Ävrö quartz monzodiorite – Unaltered	501056 Ävrö granodiorite	511058 Fine-grained granite
	Mean/stdev Min–Max Uncertainty in the mean	Mean/stdev Min–Max Uncertainty in the mean	Mean/stdev Min–Max Uncertainty in the mean	Mean/stdev Min–Max Uncertainty in the mean	Mean/stdev Min–Max Uncertainty in the mean	Mean/stdev Min–Max Uncertainty in the mean
Uniaxial compressive strength, UCS (MPa)	239/72 100–360 ±16%	225/20 200–270 ±5%	186 ¹⁾ /30 110–240 ±5%	167 ¹⁾ /11 140–190 ±3%	198/19 150–240 ±3%	280/45 210–350 ±11%
Crack initiation stress, σ_{ci} (MPa)	122/53 48–190 ±28%	130/14 105–155 ±6%	104 ²⁾ /22 52–130 ±7%	88 ²⁾ /19 50–110 ±9%	104/16 70–135 ±5%	148/20 110–180 ±9%
σ_{ci}/UCS ³⁾ (%)	52.4	57.3	56.0	52.8	52.8	52.6
Indirect tensile strength (MPa)	19/2.5 14–24 ±5%	16/1 15–17 ±4%	16.5 ⁴⁾ /3.0 10–23 ±4%	13 ⁴⁾ /1.2 10–16 ±4%	13/1.5 10–16 ±3%	–
Young's modulus (GPa)	80/8 70–97 ±5%	80/6 70–92 ±4%	76 ⁵⁾ /6.5 63–83 ±3%	71 ⁵⁾ /4 63–80 ±3%	72/5.5 60–83 ±3%	74/2.5 70–79 ±3%
Poisson's ratio (–)	0.26/0.05 0.17–0.33 ±3%	0.33/0.03 0.30–0.39 ±5%	0.29 ⁶⁾ /0.03 0.20–0.33 ±4%	0.28 ⁶⁾ /0.06 0.16–0.33 ±9%	0.25/0.05 0.15–0.34 ±7%	0.28/0.03 0.22–0.32 ±8%
Cohesion (MPa)	33/7 19–47 ±10%	30 ⁷⁾	26 ¹⁾ /3.5 19–33 ±4%	24 ¹⁾ /1.5 21–27 ±2.5%	24/2 20–28 ±2.5%	–
Friction angle (°)	53/0.8 51–54 ±1%	60 ⁷⁾	56 ⁸⁾ /0.3 56–57 ±0.2%	55 ⁸⁾ /0.3 55–56 ±0.2%	60/0.3 59–60 ±0.2%	–

1) For oxidised rock: mean uniaxial compressive strength and cohesion reduced by 7%.

2) For oxidised rock: mean crack initiation stress reduced by 8%.

3) From Best fit linear correlation curve shown in Figure 3-10 in /Hakami et al. 2008/. Crack initiation and UCS are correlated.

4) For oxidised rock: mean tensile strength reduced by 20%.

5) For oxidised rock: mean Young's modulus reduced by 14%.

6) For oxidised rock: mean Poisson's ratio increased by 8%.

7) Purely estimated valued used by the theoretical modelling.

8) For oxidised rock: no reduction of the friction angle applies.

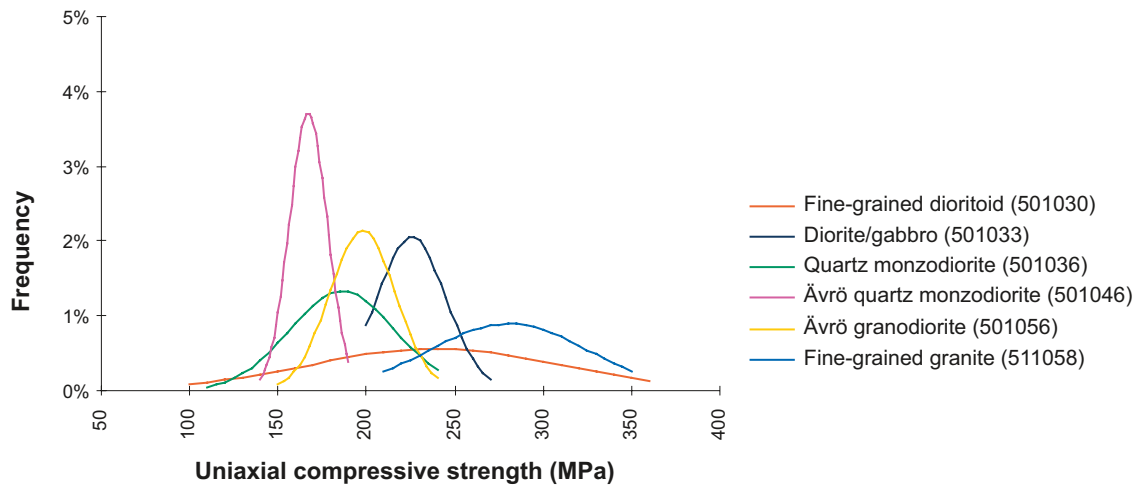


Figure 7-16. Models for frequency distributions of the different rock types for uniaxial compressive strength test samples; see Table 7-3, which gives the corresponding mean standard deviation and truncation values.

The models for the most frequently occurring rock types in Laxemar show that the strength is high but has a fairly large spread. The mean uniaxial compressive strength is 186 MPa for the fresh quartz monzodiorite (which is dominant in the southern rock domain RSMD01), 198 MPa for Ävrö granodiorite (dominating in domain RSMA01 in the north), 167 MPa for fresh Ävrö quartz monzodiorite and 225 MPa for diorite/gabbro which are mixed in domain RSMM01. The average Young's modulus for all the rock types is between 71 and 80 GPa.

A model for the spatial variation of UCS was established through variogram analysis. With support from the thermal model (see Sections 6.3 and 6.4), the assumption was made that there exists a correlation between UCS and the spatial variation of the density. Although the spread in the uniaxial compression test data is not optimal for variography (many lags missing), Figure 7-17 shows that there is a reasonable correspondence at short lag distances between the data and the model of spatial correlation derived from the density studies.

The simulations of the spatial variation of rock types were combined with the spatial model for the UCS within each rock type, and followed by simulations of UCS variation for the different rock domains /Hakami et al. 2008/. Figure 7-17 shows one example of horizontal sections (100×100 m) through a UCS simulation for each rock domain. (The cells in the visualisation are 2 m in size but the colour represents the ordinary small scale UCS values, as if representing a small sample located in the cell centre.)

7.3.2 Fracture properties

In a similar way as for the intact rock, the models for the single fracture properties were based on the direct shear laboratory test data. Some tests that were performed using a different version of the experimental set-up were calibrated such that the data could be used as a base for the description of the variation, see /Hakami et al. 2008/. Both peak and residual parameters were determined and the shear stiffness and dilatancy models vary with the normal stress. A selection of the main parameters of the models is given in Table 7-4. Since no significant differences related to fracture set were observed, the choice was to have one common model for all fractures. For a discussion of the model limitations, see Section 7.4.2.

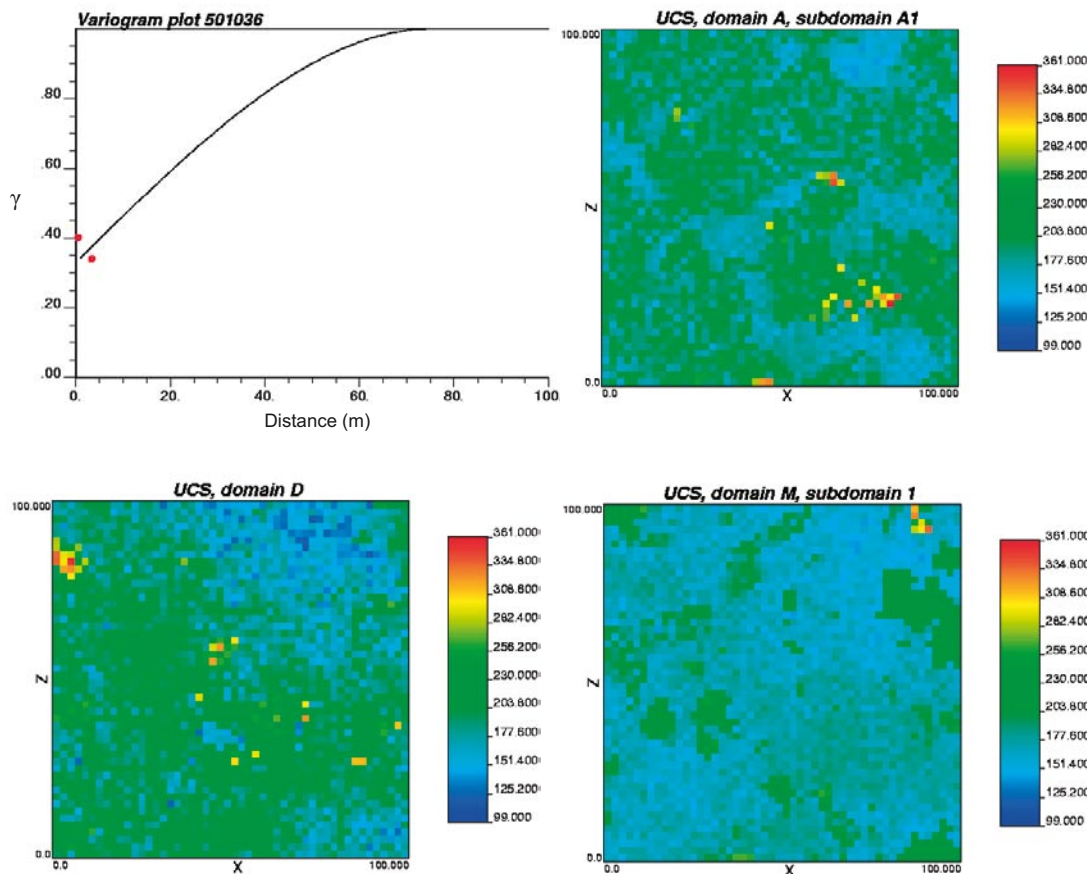


Figure 7-17. Model variogram and variogram data points (red) from the laboratory test data for quartz monzodiorite (upper left) and horizontal sections through simulations performed for the rock domains RSMA01(A), RSMM01(M) and RSMD01(D) /Hakami et al. 2008/.

Table 7-4. Summary of models for strength and deformation of fractures in Laxemar. The parameters are described as truncated normal distributions.

Parameter ¹⁾	Minimum	Mean	Maximum	Standard deviation
Normal stiffness K_N (MPa/mm)	72	721	4,003	655 ²⁾
Shear stiffness K_{SS} (MPa/mm)	11	26	49	9
Dilatancy angle, at 5 MPa (°)	2.5	8.3	15.4	2.9
Peak friction angle (°)	28.5	36.6	45.4	3.2
Peak cohesion (MPa)	0.3	0.9	2.5	0.4

1) Note that this is only a selection and that all values are shown in Table 4-9 in /Hakami et al. 2008/.

2) The distribution is much skewed towards high values, and thus the St. dev. Is high compared to the mean.

7.3.3 Rock mass properties – Fracture domains

The Laxemar local model volume has been divided into fracture domains, based on the similarities in fracturing (see Section 5.6). Since the rock mass mechanical properties are strongly governed by fracturing, it was a natural first step to divide the volume and associated data according to the defined fracture domains (The mechanical properties are of course also governed by the different rock types in the fracture domains and this is considered in the modelling, even though the description is made for the fracture domains). The available empirical data (see Section 7.2.3) were divided between fracture domains and, based on empirical relationships, six mechanical properties (i.e. deformation modulus, uniaxial compressive strength, Poisson's ratio, friction angle, cohesion and tensile strength) were estimated for each 5 m borehole section, based on empirical relationships.

The “theoretical” approach to the estimation of rock mass properties was to make numerical loading tests on rock blocks with simulated fracture networks. The fracture network was determined from simulations based on the DFN models given for each fracture domain (presented in Section 5.6). Thin tabular models of fractured rock were loaded in the y-direction to failure whilst the confining stress in the x-direction was held constant and the boundaries in the z-direction had no displacement, cf. Figure 7-18. Since the loaded blocks are thin the analyses may be regarded essentially as two-dimensional analyses. Ten geometrically different models were simulated for each calculation case. Different modes of confinement employed in the simulations enabled determination of the rock mass friction angle and cohesion. The mean values of the model parameters for intact rock and fractures already presented were used as input to the numerical analysis. The results of modelling in the current version are further presented in /Hakami et al. 2008/, while the methodology in general is discussed in /Olofsson and Fredriksson 2005/.

The results of the empirical and theoretical approach, for the estimation of two of the rock mass property parameters in the different fracture domains, are compared in Figure 7-19 (for other parameters and more details, see /Hakami et al. 2008/). It is indicated that the parameters for fracture domains FSM_C, FSM_W and FSM_NE005 are quite similar, and have slightly higher values than for the two remaining domains, FSM_N and FSM_EW007. Thus, based on the results from both the empirical and the theoretical approach, it was concluded that it would be sufficient to make one model for each of these fracture domain groups (see Table 7-5).

The spread in parameters is generally larger in the empirical approach and this is expected from the fact that the empirical approach uses a mean value of fracture frequency based on 5 m sections, whereas the theoretical model is based on fracture frequency for the entire section of a borehole that intersects the same fracture domain.

Note that the deformation zones observed in the ESHI (cf. Section 5.2.2), i.e. also the MDZs, are not included in the rock mass. The MDZs are not included in the ‘rock mass’ simulations made with the theoretical model, because the larger fracture sizes cannot be included in models at this scale. MDZ were also modelled separately in the empirical model approach (The position adopted in rock mechanics is thus different from that of hydrogeology, cf. Chapter 8). This means that the addition of MDZ compliance should not be forgotten if the rock mass response on a larger scale is to be analysed.

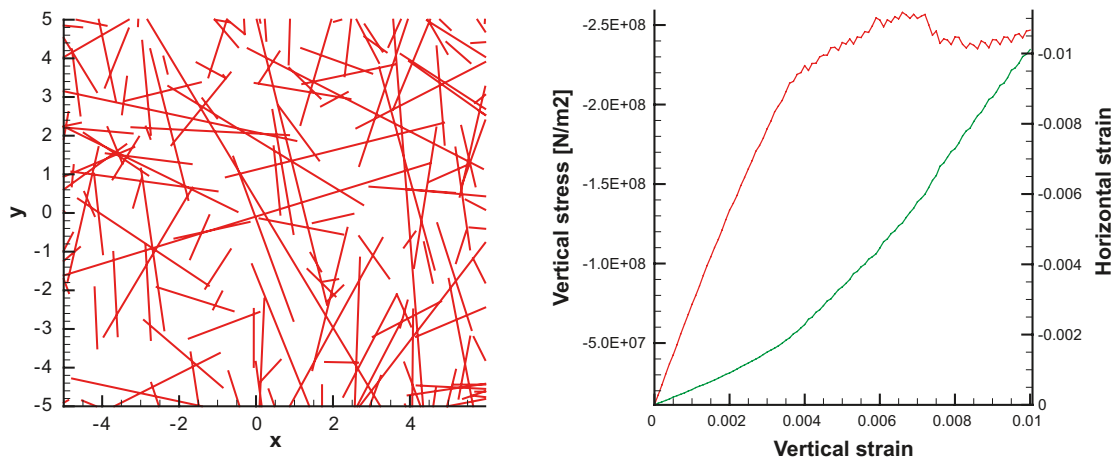


Figure 7-18. The theoretical approach for estimation of rock mass properties relies on numerical discrete element models (3DEC) of vertical (y-direction) loading of a fractured block ($10 \times 10 \times 1$ m) with horizontal confinement (x-direction) at different levels. An example of resulting stress strain curves (red = vertical, green = horizontal) is presented in the right diagram (confining stress 27 MPa).

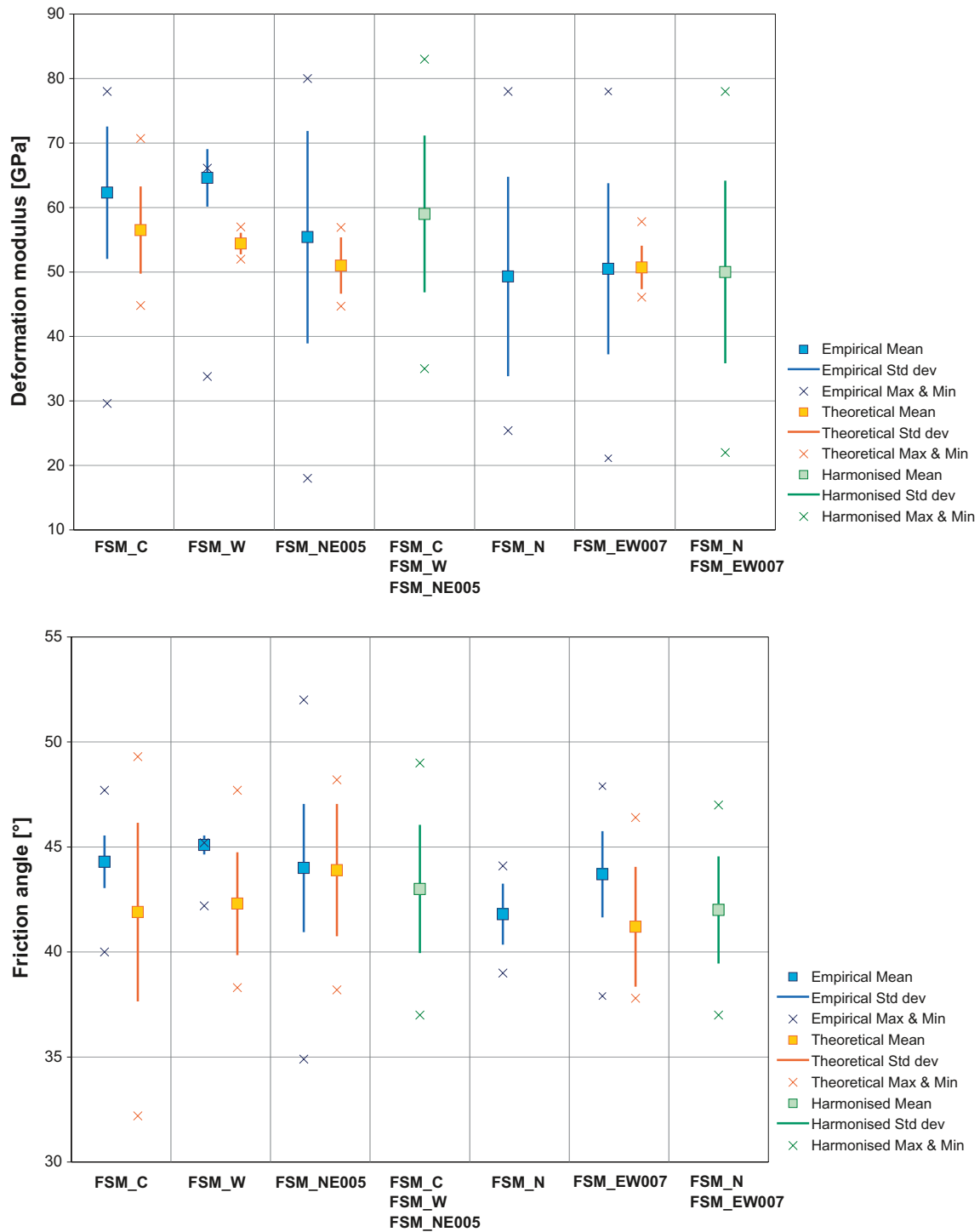


Figure 7-19. Comparison of the modelling results for deformation modulus (upper diagram) and Hoek-Brown friction angle (lower diagram) based on the empirical approach and the theoretical approach, respectively. The final “harmonised” model is also indicated in green (cf. Table 7-5) (No theoretical modelling performed for fracture domain FSM_N).

Table 7-5. Model for mechanical properties of the rock mass in the two groups of defined fracture domains.

Properties of the rock mass ¹⁾	FSM_C, FSM_W and FSM_NE005	FSM_N and FSM_EW007
	Mean/std. dev. Min-max Uncertainty of mean	Mean/std. dev. Min-max Uncertainty of mean
Deformation Modulus [GPa]	59/12 35–83 ±3%	50/14 22–78 ±3%
Poisson's ratio [-]	0.3/0.04 0.22–0.34 ±10%	0.3/0.03 0.24–0.36 ±10%
Uniaxial compressive strength (Hoek-Brown) [MPa]	51/14 23–79 ±14%	42/12 18–66 ±14%
Tensile strength (Hoek-Brown) [MPa]	1 0–8 ²⁾ 0.5–5 ³⁾	0.5 0.2–1.5 ²⁾ 0–2.5 ³⁾
Friction angle ⁴⁾ [°]	43/3 37–49 ±3%	42/2.5 37–47 ±3%
Cohesion ⁴⁾ [MPa]	18/2.5 13–23 ±7%	17/2 13–21 ±7%

1) The rock mass properties in the domains do not include the effects of DZ and MDZ, see text.

2) Minimum and maximum expected tensile strength (no Stand. dev given due to uncertainty in distribution).

3) The mean tensile strength is expected in this range, which describes the uncertainty.

4) For confinement stress between 10 and 30 MPa.

7.3.4 Rock mass properties – Deformation zones

The properties of the deformation zones have been estimated by two different approaches, the “empirical” and the “theoretical”. In the first case the properties are modelled in the same way as for the rock mass in fracture domains, using the Q and RMR from boreholes intersecting the deformation zones. In the theoretical approach, the starting point has been the description of deformation zones in the geological modelling expressed as fracture frequency, occurrence of crush and expected thickness of the deformation zones, see Section 5.5 and /Wahlgren et al. 2008/. This information is used to estimate the properties of large fracture planes whose properties are assumed to be applicable to the entire deformation zones.

When applying the results evaluated for the deformation zones, it is necessary to determine which description of the deformation zones is most appropriate for the specific case i.e. either as being sections of weaker *rock mass* or as a geometrically simplified large *fracture plane*. Depending on this choice the different estimated parameters, exemplified in Table 7-6, may be selected for the analysis.

7.3.5 Modelling of *in situ* state of stress

The strategy for the development of a model for the state of stress at the sites investigated by SKB is outlined in /Hakami et al. 2002/. This modelling has the following components: A study of the primary site-specific local scale and regional scale data (see Section 7.2.4), followed by an evaluation of the expected large scale variability in rock stress due to the presence and geometry of the major deformation zones, as given by the geological models. Furthermore, the small scale stress variability is assessed. Finally, the combined results form the basis for estimation of stress magnitudes and stress orientations in the focused volume for a possible future repository. A comprehensive presentation of the stress modelling is found in /Hakami et al. 2008/. The historical development and tectonics of the Laxemar-Simpevarp area is described in a specific report /Söderbäck 2008/, summarised in Chapter 3.

Table 7-6. Estimated mechanical properties of some of the deformation zones of various sizes. Using the empirical approach, the DZ is considered as a rock mass with weaker properties than the surrounding rock. The theoretical approach gives the parameters when considering the DZ as a single fracture plane with properties equivalent to the whole DZ. (More parameters and details are given in /Hakami et al. 2008/.)

Deformation zones	Empirical approach DZ modelled as rock mass			Theoretical approach DZ modelled as a single plane		
	RMR	Deformation modulus	Rock mass internal Friction angle ¹⁾	Normal stiffness	Shear stiffness	DZ plane friction angle
	[-]	E [GPa]	ϕ [°]	K_n [MPa/m]	K_s [MPa/m]	ϕ [°]
	Mean/std. dev. Min-max ²⁾	Mean/std. dev. Min-max ²⁾	Mean/std. dev. Min-max ²⁾			
ZSMEW007A	73.6/7.2 59.0–85.7	42.0/16.7 16.8–77.9	41.0/2.0 36.9–44.1	450	90	34.0
ZSMEW946A	67.7/7.7 61.2–78.9	29.8/14.5 18.2–52.9	40.5/2.2 38.5–43.3	2,960	470	34.0
ZSMNE107A	67.7/7.1 53.3–83.8	30.3/12.8 12.1–66.1	40.3/2.2 35.9–45.2	1,490	350	43.7
ZSMNE942A	72.5/6.3 53.6–79.2	38.9/12.2 10.9–54.4	41.6/1.7 36.6–44.1	2,730	510	34.0
ZSMNW042A	72.2/10.4 55.3–81.1	38.7/23.9 0–59.5	42.6/2.3 38.8–44.6	1,400	310	44.8
Other DZ	70.9/9.7 53.3–84.4	37.6/20.2 0–72.3	41.3/3.2 35.2–46.7	200–3,020 ³⁾	50–580 ³⁾	34–45.9 ³⁾
MDZ	72.9/9.0 50.8–83.8	40.4/20.4 0–66.1	42.4/2.6 36.2–47.8			

1) For confinement stress between 10 and 30 MPa.

2) Statistics made on all 5 m core sections from the borehole(s) intersecting each DZ (see text).

3) Range of values for 25 different DZ.

Evaluation of stress variability caused by major deformation zones

A large scale numerical model was set up, using a discrete element code (3DEC), where the major deformation zones were represented as large singular planar fracture planes intersecting a large rock block (Figure 7-20). This block (or slab) of rock was then compressed in a NW–SE direction, a direction assumed parallel to the crustal shortening that is currently ongoing in this part of the Fennoscandian shield (Figure 3-3). The compressive stresses predicted by this model have also been observed in direct measurements in Sweden in general and they correspond well to the orientation seen from the measurements in the Laxemar-Simpevarp area.

Depending on the amount of compression applied in the numerical model and depending on the geometrical and mechanical properties of the deformation zones, various amounts of slip and displacements will occur on the fracture planes. These slip movements will cause the stresses to redistribute accordingly (Figure 7-21). Different model cases, with different friction (24°–37°) and stiffness of the planes simulating deformation zones were analysed, but these variations did not result in major differences in the results /Hakami et al. 2008/.

Evaluation of spatial variability of local stress field

The smaller scale fractures in the fracture domains will also produce some variation in the stress field. This was demonstrated by the use of the same numerical models as were used for the estimation of rock mass properties (Section 7.3.3 and /Hakami et al. 2008/). The variability in magnitude and orientation of the stress in the elements of the mesh is considered to represent the variation in stress at the local scale at depth (scale of single overcoring measurements). A histogram of the distribution of maximum principal stress in the numerical model is shown in Figure 7-22. The mean stress magnitude is 27.2 MPa and the standard deviation is 3.4 MPa, i.e. 12.5% of the mean. (These analyses are the basis for the right column in Table 7-7 where the model results are presented).

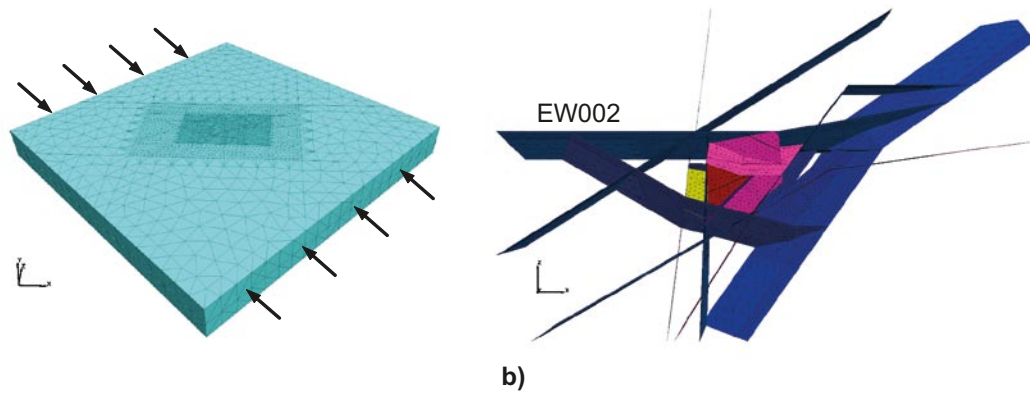


Figure 7-20. a) The geometry of the numerical model (3DEC) built to simulate stress variation at the site. The size of the block is $40 \times 40 \times 4$ km. The mesh is denser in the central parts where the Laxemar local model area is located. b) The major deformation zones at the site are included in the numerical model as fracture planes (plan view). The location and orientation of the zones is based on the deterministic deformation zone model (cf. Section 5.6).

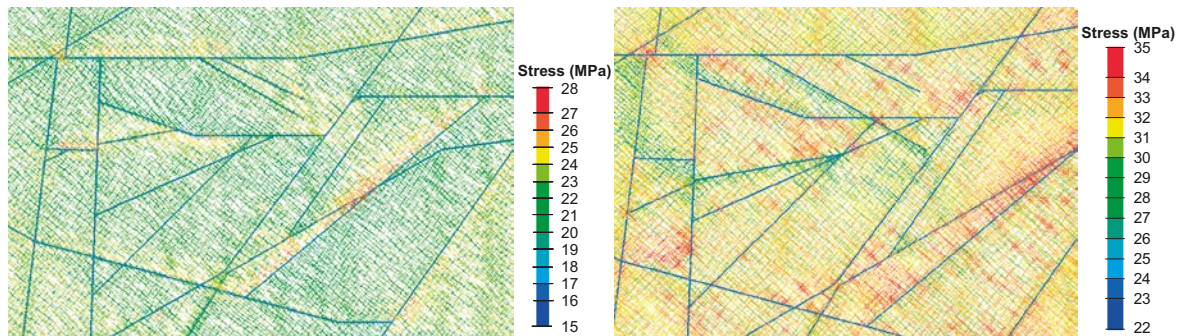


Figure 7-21. Example of results showing stress tensors coloured by magnitude of maximum principal stress in horizontal section at elevations of -400 m (left) and -600 m (right).

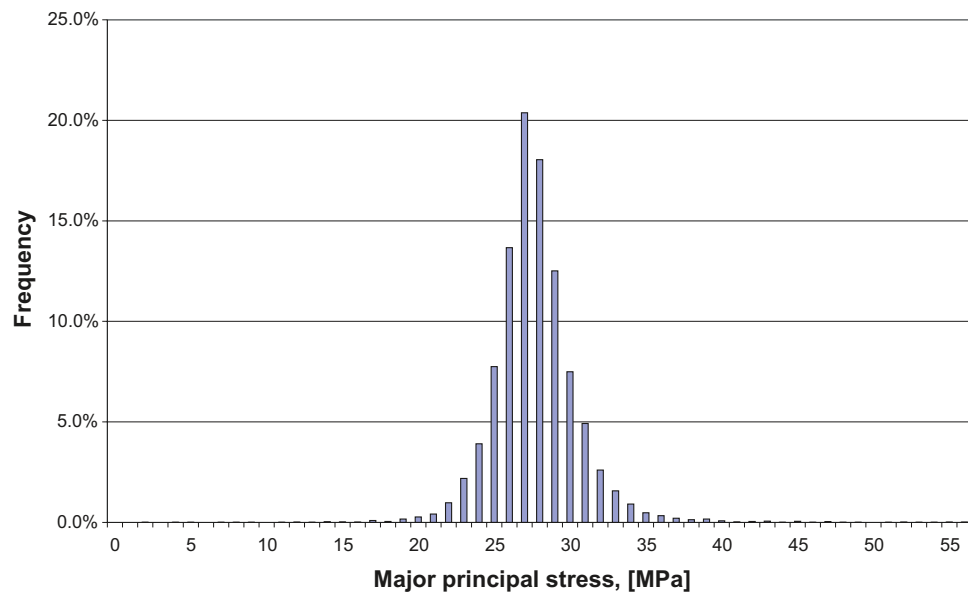


Figure 7-22. Distribution of the major principal stress in the numerical model (3DEC) simulating the stress variation due to fractures in the rock block. The histogram shows the summary of data from 5 numerical realizations, with different fracture networks in each, based on the same DFN.

Evaluation of stress limits based on borehole stability observations

A total number of 21 deep cored boreholes have been drilled in Laxemar (see Section 2.1.2 and Figure 2-5). If stresses are very high compared to the strength of the rock, a borehole will experience some failure in the borehole wall when the drilling is advancing. The borehole opening itself will cause tangential stresses at the borehole wall to become about three times higher than the *in situ* stress level. This may cause the rock in the wall to fail in the direction of the *in situ* minimum principal stress, a so-called borehole breakout. Therefore, the observation of borehole instabilities is of interest to the stress modelling, in particular since direct measurement data are scarce. The detailed borehole geometry can be studied from the televiewer logging data. The exact stress criteria for borehole breakouts are not known, but two criteria were employed; one empirical proposed by /Martin 2007/ and the Mogi-Coulomb criteria /Al-Ajmi and Zimmermann 2006/. Since almost no breakouts were observed along the boreholes, the assumption that stresses are at the limit of failure provides an upper limit for the actual stress level (see example of results in Figure 7-23). For further explanations of the assumptions made, see /Hakami et al. 2008/.

Model for the *in situ* stress at repository depth

The objective of the modelling is to provide a description to be used for stress prediction in the area of a planned future repository. The focused volume is located in fracture domains FSM_C, FSM_NE005, FSM_W and FSM_EW007 below the actual deformation zone ZSMEW007. Both the measurement data as such and the large scale numerical modelling of the influence of deformation zones on rock stresses show that it is possible that the stresses are not similar in the whole region. The measurements at Ävrö (KAV04A) and Simpevarp peninsula (KSH01A and KSH02) indicate lower stresses than the measurements at the Äspö laboratory (Figure 7-12). Some stress differences may therefore be expected between the Laxemar fracture domains, Simpevarp peninsula, Ävrö and Äspö, although it is quite uncertain how large this variation actually is. The distance between Laxemar, Simpevarp and Äspö laboratory, respectively, and the major deformation zones separating the areas was judged as a possible explanation for the differences seen in the data.

The focused volume is situated south of the deformation zones ZSMEW007A, north of ZSMNW042A and west of ZSM005A (the Äspö shear zone) (cf. Figure 5-30). In this volume only two boreholes provide overcoring data, KLX12A and the lower part of borehole KLX04. The overcoring data from KLX04 show a large spread in orientation and was therefore suspected to be influenced by the deformation zone located not far from the measurement points in the borehole. Therefore the data from borehole KLX12A were given most weight in the selection of most likely values in the model.

The results for the minimum horizontal stress do not differ significantly between the overcoring and the HTPF method in borehole KLX12A. A model with a most likely value lying between the results from the two methods was chosen, with the uncertainty span covering both, i.e. giving them equal weight.

For the maximum stress, the overcoring is considered more reliable than hydraulic fracturing data (classical interpretation of hydraulic fracturing). However, the overcoring data are supported by the HTPF inversion results which are in fair agreement with the overcoring results (Figure 7-23). It may be noted that the HTPF interpretation for KLX12A gave an interpretation for the major horizontal stress (the vertical stress was assumed vertical) at two depth levels, but for the lower level it was only possible to interpret an upper limit for the horizontal stress /Ask et al. 2007/. For the above given reasons the data from KLX12A was given most weight when selecting the most likely model for the major principal stress magnitude, but the data from the whole area was considered when the uncertainty span was estimated. The Äspö laboratory data are of special interest, since there are underground excavations at depth there. The individual stress data points from Äspö are fairly scattered (Figure 7-12), but using back-analysis in the TASQ tunnel of the Äspö laboratory (–460 m) the major principal stress magnitude is estimated to 25 MPa and 30 MPa (/Jonsson et al. 2009/ and /Andersson 2007/, respectively).

The problem of how to handle the depth trends, in particular since the measurements do not cover all depths, has been addressed. All measurement methods, both direct and indirect, including microcrack volume measurements (although these are very limited in number), indicate some kind of increase in stress with depth. The slight increase in core dishing and breakout occurrences with depth, also indicate that stresses do increase with depth (although these data are also limited and the observations may have other explanations such as temperature increase with depth). The stress

gradient obtained from the direct stress measurements varies from borehole to borehole and does not always follow linear trends. The measurements in the deepest borehole, KLX02 (Figure 7-14), are the most interesting for shedding light on this issue since the number of tests is quite large and cover the borehole depth with fairly continuous hydraulic fracturing measurements. Changes in the depth trend are seen in KLX02 but it is not possible to be certain about the reasons behind the variation, remembering the potential influence of MDZs, fractures and limitations in the measurement techniques employed. Therefore, it was judged that the most reasonable concept would be that, although locally variable, the best general prediction over large areas/volumes should be a stress magnitude model with a monotonic increase with depth. With the gradient chosen, based on the KLX12A overcoring data, the stress will not reach magnitudes that are expected to cause borehole breakouts above about c. -900 m. The additional mechanically stable deep boreholes in the Laxemar focused volume thus support this stress magnitude model, which is slightly lower than in the previous model version.

Looking at the orientation of the major principal stress from the measurements it can be seen that there is a slight variation between boreholes in the area, and also within single boreholes. They agree well in that the orientations are all consistently NW-SE, also in general in Simpevarp and Äspö. The value selected as the most likely for the final model is 135°. This value is supported by the mean (133°) and median (136°) values from breakout data that prevail in this model version. The KLX12A overcoring data gives a trend that is varying between measurement points, also indicating a plunge towards SE (see Figure 7-12. The three measurement levels have average trends of 145°, 150° and 163°, while the HTPF methods give average directions of 131° and 162° degrees, respectively. It is judged that for the whole focused volume an uncertainty span of ±15° (i.e. 120° to 150°) will cover the span of the expected mean value for the major stress orientation and, considering the uncertainty, a rounded-off most likely value of 135° is found appropriate for the description of the orientation of the major horizontal stress.

Table 7-7 and Table 7-8 present the final stress model, in Table 7-7 as functions of the depth in the interval -400 to -700 m, and in Table 7-8 as discrete values at three different depths. The model is only applicable to the so called focused volume, i.e. the fracture domains effectively bounded by the main deformation zones ZSMNS001C, ZSMEW007A, ZSMNW042A and ZSMNE005A. The uncertainty value gives span within which the mean stress (most likely value) is expected to fall. The uncertainty span for the mean maximum stress is 18–27 MPa at -500 m.

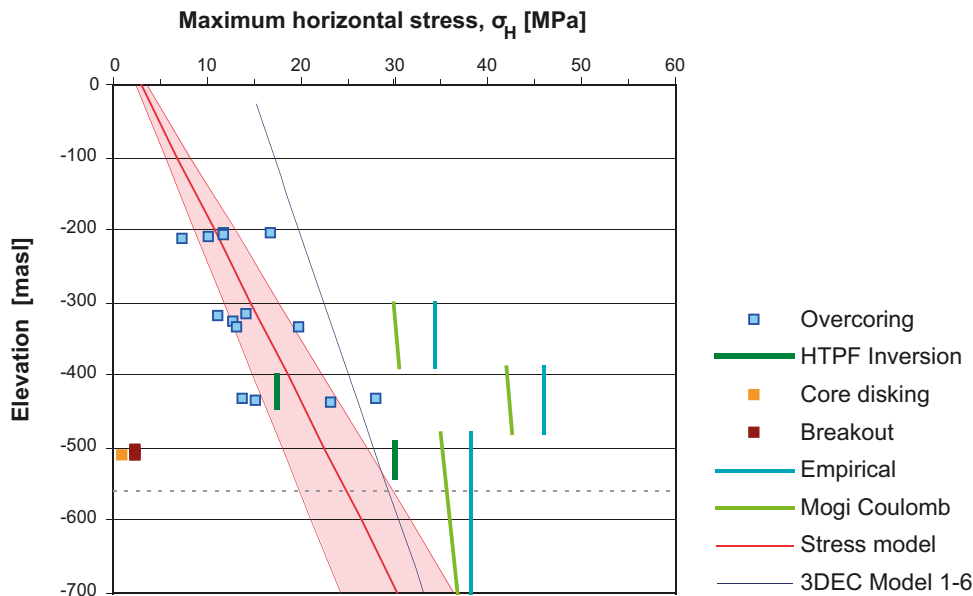


Figure 7-23. Comparison between direct and indirect stress data from KLX12A and the numerical model results along a scanline (fictive borehole) at approximately the same location as KLX12A – Maximum horizontal stress. The deepest HTPF measurement level result is determined as an upper limit value. Results of two models of the stress criterion for borehole breakout stress limits, “Empirical” and “Mogi-Coulomb”, are also given (see text). The changes with depth in these lines are due to changes in the dominant rock type. In KLX12A there is a very short length of core dishing and borehole breakouts, located in Ävrö quartzmonzonite associated with veins of fine-grained granite. The borehole ends at -560 m elevation.

Table 7-7. Stress model for domains FSM_C, FSM_W, FSM_NE005 and FSM_EW007, below ZSMEW007 (at –400 to –700 m elevation). The stress magnitude is modelled as a function of vertical depth, z (cf. Table 7-8).

Parameter	Most likely value (mean value)	Estimated uncertainty (in mean value)	Upper limit at 400 m depth based on the borehole stability analysis	Local stress variability (st. dev. of a normal dist. around the local mean value)
<i>Magnitude</i>				
Major horizontal stress, σ_H	0.039z + 3 MPa	± 20%	31–34 MPa ¹⁾	12%
Minor horizontal stress, σ_h	0.022z + 1 MPa	± 20%		13%
Vertical stress, σ_v	0.027z MPa	± 3%		15%
<i>Orientation</i>				
Major horizontal stress trend, σ_H	135°	± 15°		± 15°

1) Depending on the dominating rock type, lower value in RSMM01 and higher in RSMD01.

Table 7-8. Stress model for domains FSM_C, FSM_W, FSM_NE005 and FSM_EW007 below ZSMEW007. The stress magnitudes and orientations are given in terms of the uncertainty span for the mean stress values at three different depths (z) (cf. Table 7-7).

Vertical depth	400 m	500 m	600 m
<i>Magnitude, MPa</i>			
Major horizontal stress, σ_H	14.9–22.3	18.0–27.0	21.1–31.7
Minor horizontal stress, σ_h	7.8–11.8	9.6–14.6	11.4–17.0
Vertical stress, σ_v	10.5–11.1	13.2–14.0	15.7–16.7
<i>Orientation</i>			
Major horizontal stress trend, σ_H	120°–150°	120°–150°	120°–150°

The small scale variability, corresponding to overcoring data, is also described as a normal distribution around the mean value. The upper limit for the maximum principal stress, based on the borehole stability evaluation, is also given in Table 7-7.

7.4 Evaluation of uncertainties

7.4.1 Uncertainty in mechanical properties of intact rock

The main source of uncertainty associated with the intact rock properties in the *rock domains*, stems from the uncertainty in the estimation of rock type proportions in the domains (Section 5.4.4 and /Wahlgren et al. 2008, cf. Appendices 4 and 11 therein/). In particular, the uncertainty of proportions in rock domain RSMM01, where the spread in strength between existing rock types is large, makes the prediction of the strength distribution in that domain fairly inconclusive.

However, by considering the intact rock properties for each *rock type* separately, as in the intact rock models of Table 7-3, the main factor influencing the uncertainty in the rock strength estimation is the number of tests in each rock type, and therefore the overall confidence in the models is judged to be high. This applies to all determined parameters for intact rock and is based on several reasons. Firstly, the test methods used are standard methods, which mean that the parameters as such are well known and understood. A comparative study with tests performed at different laboratories has been carried out with satisfactory results. Secondly, the number of tests is large enough to enable sufficiently reliable statistics, at least for the fresh and most frequent rock types. Thirdly, the spatial distribution of the sampling points is reasonably good, from KLX11A in the west to KLX21B in the east of the local model volume. The intact rock models are also supported by previous modelling results from Simpevarp and the Äspö HRL.

7.4.2 Uncertainty in mechanical properties of fractures

The mechanical properties of single fractures have been modelled based on two types of tests; direct shear and normal stiffness tests on small fractures in drill cores in the laboratory, and so-called tilt tests, also performed on small fractures in drill cores. Due to the small diameter of the drill core (c. 52 mm), the sampling and testing procedures introduce limitations on the type of fractures that can be tested. Only fractures that may be considered as fairly mated (good fit between surfaces) and undisturbed by the drilling process were selected.

According to the geological DFN modelling (see Section 5.6), all sizes of single fractures exist, including very large structures. The largest fractures in the DFN are expected to appear in the geological single-hole interpretation as thin crush zones, or fractures with larger physical aperture, or possibly mapped as MDZs. There were no mechanical tests performed on these structures. Thus, it is important to keep in mind that the current mechanical descriptive model for fractures, as in Table 7-4, may be considered valid only for the frequently occurring smaller fractures of the population. Consequently, it is questionable whether the established mechanical properties are appropriate also for larger ‘fractures’ and the main hydraulic conductors in the rock between deterministic deformation zones, as established by PFL logs (Section 8.3.1).

The overall confidence in the mechanical properties of fractures is moderately high. The factor that enhances the confidence is the fairly large number of tests performed (71 direct shear tests) and that fairly consistent and reasonable results from the tests have been obtained. The circumstance that reduces the confidence is the inherent limitations associated with tests on the small drill core samples and inadequate knowledge regarding scale effects for the described parameters. No quantification of the uncertainty in the fracture parameters is made.

7.4.3 Uncertainty in mechanical properties for rock mass

Using both the empirical and the theoretical approaches, the properties of the rock mass in the fracture domains as well as inside interpreted deformation zones has been modelled. The overall confidence in the model of mechanical properties of the rock mass is high in relation to the fracture domains, i.e. the rock mass between interpreted deformation zones and excluding the effect of the MDZ. The uncertainty in the mean values for the fracture domain rock mass parameters has also been quantified in the description, see Table 7-5. These uncertainty estimates are judged partly based on the differences seen between the theoretical and the empirical approaches and partly on the 95% confidence span for the mean in the statistical treatment of the results.

However, the confidence in the rock mass properties inside the deformation zones is considered moderate, since the detailed internal structure of the deformation zones is assumed variable and highly complex and their large scale mechanical behaviour is not well known. The uncertainty calculation is based on empirical results and on the assumption that the very few boreholes intersecting a given zone are representative for the entire deformation zone along its extension. Furthermore, this statistical treatment assumes that the 5 m sections across the intersection are representative of the character of the zone, whereas in reality we expect differences along the extension of the deformation zones.

Therefore, care is recommended when interpreting and applying the presented model for deformation zones (Table 7-6). The appropriate choice of values will depend on the objective of the analysis. If the main interest is to obtain an estimate of the worst part of the section across the zone, modelled as rock mass, the value given as the minimum in the range obtained from the empirical approach is considered most relevant, whereas the mean value would represent a more appropriate estimate of the value of the mechanical properties of the whole zone thickness. Table 7-6 also presents an alternative mechanical model that could be useful when the deformation zones are treated as single planes. The uncertainty in the parameters of this latter model is fairly large.

7.4.4 Uncertainty in the stress model

Two different direct stress measurement methods have been applied in Laxemar. Overcoring was performed in KLX04 and KLX12A and hydraulic fracturing tests and HTPF in boreholes KLX02 and KLX12A. The results from the measurements in KLX12A, which is the only borehole located entirely within the focused volume, agree fairly well between the two different methods (Figure 7-23).

Considering the lack of borehole failures in the boreholes two different approaches have been employed to make an estimation of the expected upper limit for the *in situ* stresses. One utilises UCS and an empirical factor as an input and the other approach uses the friction angle and cohesion from the triaxial tests at the appropriate stress level. These two approaches gave similar results at repository depth (cf. the Mogi and Empirical results presented in Figure 7-23).

The overall uncertainty in the model for the mean stress magnitude ($\pm 20\%$) is fairly high. The reason for this is that the number of direct stress measurements that have been carried out is very limited and the area/volume where the model should apply is very large. There is a risk that the borehole selected for the stress measurements for some local reason has stresses that are not representative of the mean stress of the domain as a whole. However, the confidence in the upper limits for the stresses are higher because the number of deep cored boreholes within the Laxemar local model area is quite large and two independent approaches, giving similar results, have been applied to establish the estimates of the upper limit. Also, the uncertainty in the overall orientation of the maximum stress is low.

8 Bedrock hydrogeology

8.1 Context

8.1.1 Hydrogeological modelling in the SDM

The primary objectives of the bedrock hydrogeological model are to provide a general conceptual understanding of the groundwater flow system and to determine and justify the assignment of hydraulic properties, boundary and initial conditions. The evaluations are based on primary data and the model is derived to serve the needs of repository engineering, safety assessment and environmental impact assessment studies.

Three-dimensional, large-scale numerical flow models applied are used to underpin the development of the bedrock hydrogeological model. The flow models include 3D descriptions of the geometry of geological features (overburden, deterministic deformation zones and discrete fracture networks (DFN) to describe rock between deformation zones), transient hydrological and chemical boundary conditions, anisotropy and spatial heterogeneity in the hydraulic properties, density driven flow, advective transport and rock matrix diffusion of different water types (solutes). It has been suggested that an understanding of the hydrochemical evolution throughout geological time is a powerful means to subsequently predict the future development of groundwater flow and the chemical composition of the groundwater, see e.g. /NEA 1993, Bath and Lalieux 1999/. Testing and developing tools for coupled hydrogeological-hydrochemical modelling over time was also the focus of an international project based on multidisciplinary data from the Äspö Hard Rock Laboratory in Sweden /Laaksoharju and Wallin 1997, Wikberg 1998, Rhén and Smellie 2003/.

Figure 8-1 illustrates schematically the division of the groundwater system into hydraulic domains as used in the hydrogeological SDM for Laxemar. The groundwater system consists of three hydraulic domains, HSD, HCD and HRD, where:

- HSD (Hydraulic Soil Domain) represents the overburden.
- HCD (Hydraulic Conductor Domain) represents deformation zones.
- HRD (Hydraulic Rock mass Domain) represents the fracture domains in between the deformation zones.

The division into hydraulic domains constitutes the basis for the conceptual modelling, the planning of the site investigations and the numerical simulations carried out in support of the SDM. The flow models used in the SDM take into account the shoreline displacement in the Fennoscandian Shield during Holocene time, i.e. between 8000 BC and 2000 AD.

8.1.2 Model development

The development of the bedrock hydrogeological model of the Laxemar-Simpevarp area (including the Laxemar local model volume) is based on the bedrock geological model and the hydraulic investigations conducted in the cored boreholes (KLX in the Laxemar subarea, and in part KAS/KAV/KSH in the Simpevarp subarea) and percussion-drilled boreholes (HLX in the Laxemar subarea and HAS/HAV/HSB in the Simpevarp subarea). That is, the geometries of the hydraulic domains are consistent with the geometries of the geological features, and their hydraulic properties reflect the anisotropy and spatial variability observed in the hydraulic investigations.

Table 8-1 shows the cumulative number of boreholes providing hydraulic information about the bedrock in the Laxemar-Simpevarp area. The number of boreholes is shown in relation to the two investigation stages (ISI and CSI), the five model versions (Version 0, Simpevarp 1.1, Simpevarp 1.2 and Laxemar 1.2, and model version SDM-Site Laxemar) carried out during the period 2002–2008. Version Laxemar 1.2 represents the preliminary SDM and version SDM-Site Laxemar constitutes the principal contribution to the SDM of Laxemar from a hydrogeological point of view.

Hydrogeological description

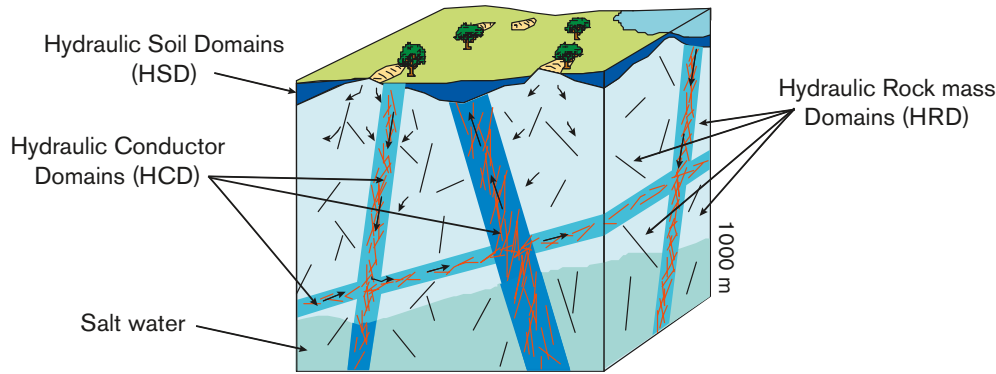


Figure 8-1. Cartoon showing the division of the crystalline bedrock and the overburden above it (Quaternary deposits mainly) into three hydraulic domains.

Table 8-1 also shows references to the major background reports in relation to each model version/ stage /Follin et al. 2004, 2005, 2006, Hartley et al. 2004c, 2005, 2006, 2007, Holmén 2008, Rhén et al. 1997c, 2006abc, 2008, 2009, SKB 2002, 2004, 2005a, 2006ac. The report /Rhén and Hartley 2009/ (not shown in Table 8-1) provides a detailed summary of the work described in these reports, i.e. the field investigations, the data analyses, the conceptual model development and the numerical modelling of groundwater flow and solute transport. This summary report constitutes the main hydrogeological reference for the SDM. However, sometimes a reference is given here to the specific background reports for the sake of clarity.

Table 8-1. The cumulative new (drilled during site investigation) number of boreholes providing hydraulic information about the bedrock in the Laxemar-Simpevarp area at the end of the five model versions carried out during the period 2002 through 2008. Kxx = core-drilled boreholes, Hxx = percussion-drilled boreholes (KLX and HLX: core-drilled boreholes percussion-drilled boreholes within Laxemar local model area). The reports listed in italics describe the hydraulic data collected and/or the hydrogeological modelling undertaken. The reports with underlined reference numbers summarise the development of the hydrogeological modelling along with the developments achieved within the other disciplines.

	Initial site investigation (ISI)			Complete site investigation (CSI)	
Desk top exercise	Training exercise	Preliminary SDM	Preliminary SDM	Feedback and strategy	Model verification and uncertainty assessment
Version 0	Version 1.1	Simpevarp Version 1.2	Laxemar Version 1.2	Laxemar Stage 2.1	Laxemar Stage 2.3 (version SDM-Site)
0 Kxx	0 Kxx ⁽¹⁾	4 Kxx ⁽²⁾	9 Kxx ⁽³⁾	11 KLX (25%) ⁽⁴⁾	44 KLX (100%) ⁽⁵⁾
0 Hxx	0 Hxx	3 Hxx	14 Hxx 3 KLX (7%) ⁽³⁾ 9 HLX(26%)	9 HLX (26%) ⁽⁴⁾	34 HLX (100%)
<i>R-02-35</i>	<i>R-04-25</i>	<i>R-05-08</i>	<i>R-06-10</i>	<i>R-06-110</i>	<i>R-08-78</i>
<i>TR-97-06</i>	<i>TR-97-06</i>	<i>R-06-20</i>	<i>R-06-21</i>	<i>R-07-57</i>	<i>R-08-91</i>
	<i>R-04-63</i>	<i>R-05-11</i>	<i>R-06-22</i>	<i>R-08-60</i>	
	<i>R-04-65</i>	<i>R-05-12</i>	<i>R-06-23</i>		
			<i>R-06-24</i>		

⁽¹⁾: Some old data from KLX01 and KLX02 were used besides earlier interpretations from the area.

⁽²⁾: Old data from KLX01, KLX02, KAV01, KAV02 and KAV03 also used besides the indicated three KSH holes and KAV01 with some new data.

⁽³⁾: KLX02–04. KLX02 included as some new tests were performed in that borehole. A few data from KLX05 and KLX06 were also available but these boreholes are not included here as the large amount of data became available later. Kxx also includes three KSH holes, KAV01, KAV04A, and KAV04B. Old data from KLX01 also used but not included in the numbers in the table.

⁽⁴⁾: KLX02–12 included but data not complete for all these boreholes at this stage. Old data from KLX01 also used. New HLX boreholes were not considered.

⁽⁵⁾: 19 core holes longer than 300 m and 25 shorter than 300 m.

As a means of approaching the issue of confirmatory testing, the strategy developed after the initial site investigation (ISI) stage, and described in detail by /Follin et al. 2007a, 2007b/, see Figure 8-2, has been employed. In practice, four kinds of data were used during the complete site investigation (CSI) stage:

- A. Hydraulic properties deduced from *single-hole hydraulic tests* (double-packer injection tests (PSS), difference flow logging pumping tests (PFL-f), and open-hole pumping tests (on a few occasions combined with impeller flow logging) (HTHB) /Rhén et al. 2008/).
- B. Groundwater level responses (point-water head drawdowns) in the bedrock in the depth interval 0 to c. 800 m observed during large-scale *interference (cross-hole) tests* /Rhén et al. 2009/.
- C. Present-day mean *natural groundwater levels* (point-water heads) observed in the Quaternary deposits and the bedrock down to an elevation of –600 m /Rhén et al. 2009/.
- D. Hydrochemical data (fracture water and matrix pore water) collected from the bedrock investigations (primarily the core-drilled boreholes) /Rhén et al. 2009/.

The general approach applied in the numerical modelling was to first parameterise the deformation zones and hydraulic rock (mass) domains hydraulically using fracture and inflow data from individual boreholes (A). Second, the successive confirmatory steps rely on using essentially the same groundwater flow and solute transport model in terms of grid discretisation and parameter settings for matching three types of independent field data (B–D). Using the three types of data, a unified conceptual description of the groundwater system has been attempted.

8.1.3 Main characteristics of relevance to the model

This section provides a brief summary of the primary hydrogeological characteristics of the Laxemar-Simpevarp area in general, and Laxemar in particular. Figure 8-3 shows a perspective view of the regional model area towards the north.

Overall, Laxemar is characterised by relatively distinct valleys, surrounded by undulating country dominated by exposed/shallow rock, the valleys coinciding with deformation zones.

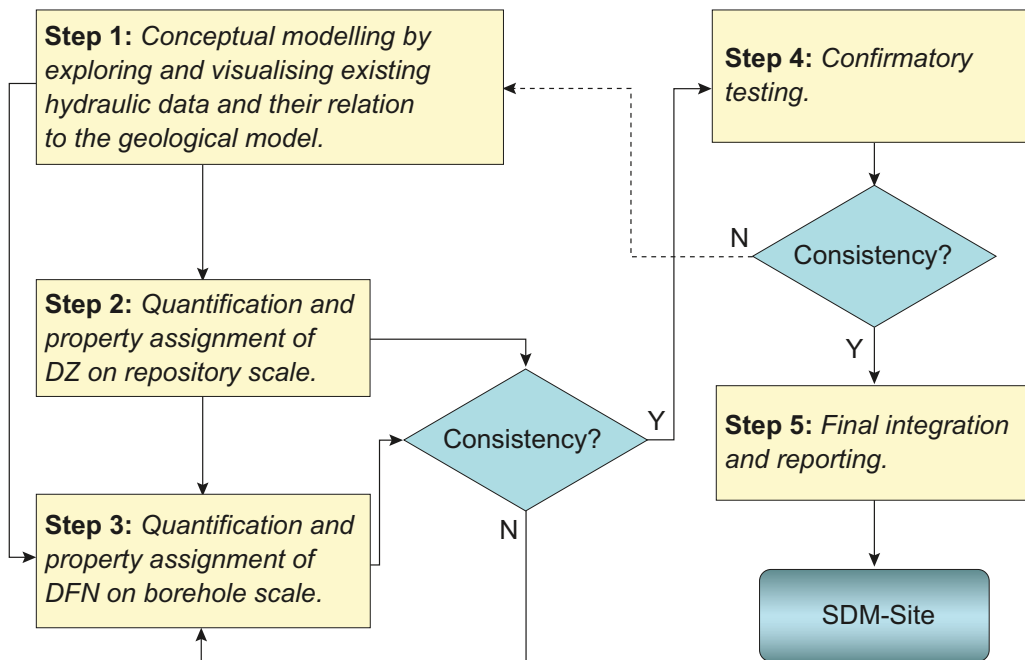


Figure 8-2. Flow chart of the five steps suggested for the hydrogeological modelling during the complete site investigation (CSI) stage. DZ = deformation zone, DFN discrete fracture network.

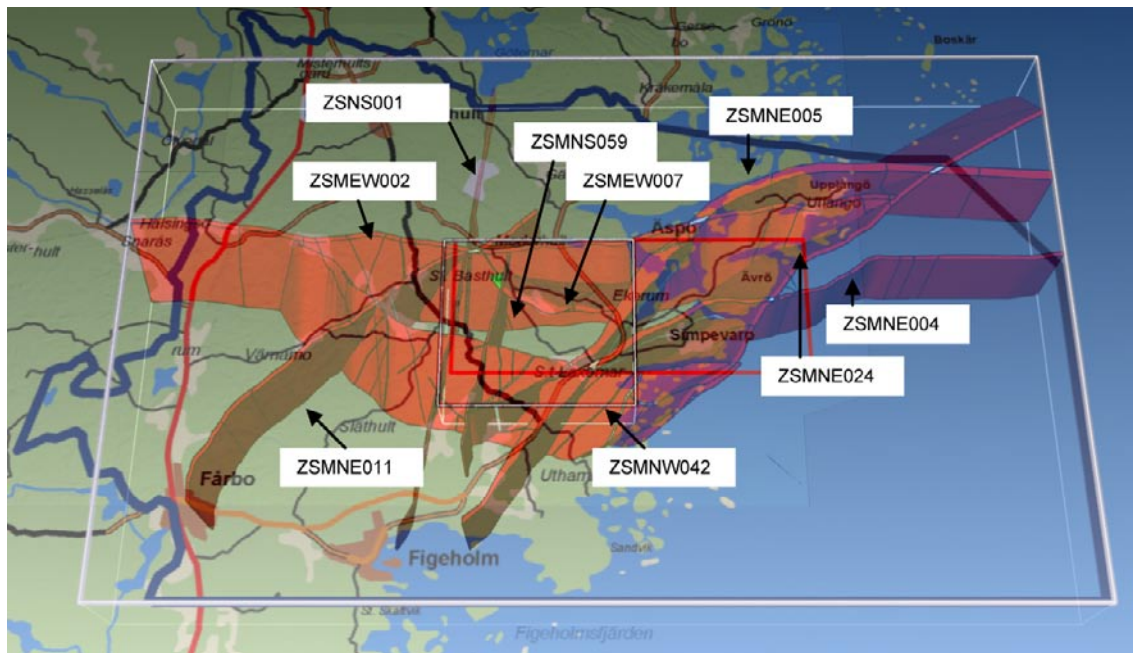


Figure 8-3. Perspective view of some of the main HCD (NE011A, EW002A, EW007A, NS001A;B;C;D;E, NS059A, NE005A, NE004A, NW042A and NE24A) within the Laxemar-Simpevarp regional model volume. The regional model boundaries for the groundwater flow model is shown as a blue line. The local model volume is outlined by the smaller box in white.

The regionally significant, principally ductile but also brittle, deformation zones ZSMNE011A and ZSMNE005A (Äspö shear zone) effectively bisects the local model area and define the area that bound Laxemar, Simpevarp being located east of ZSMNE005A. A further division of the local model area is introduced by the east-west trending ductile-brittle regional zone ZSMEW002A (Mederhult zone) and the equally east-west trending brittle zone ZSMEW007A, both of which run parallel to the essentially west to east regional hydraulic gradient. Zone ZSEWM007A and the ductile-brittle zone ZSMNW042A together with the north-south trending ductile-brittle zones ZSMNS001C and ZSMNS059A effectively outline an area which is denoted the “focused area”. All the above mentioned zones are interpreted as being steeply inclined, with the exception of the gently inclined ZSMEW007A (to the north) and ZSMNW042A (to the south). No major subhorizontal zone is interpreted in the Local model volume (including the focused volume), cf. Section 5.5.

The structural framework introduced by the deformation zones is paired with a relatively flat regional topographic gradient (in the order of 4%) which in the Laxemar-Simpevarp area is, on a local scale, intermittently broken by valleys and elevated areas, the latter which allow development of local scale flow cells below the elevated areas, cf. e.g. /Ericsson et al. 2006/.

The interpreted major principal horizontal stress σ_H in the area is oriented northwest (on average 135°), cf. Section 7.2.4. This implies that the principal stress direction is oriented oblique to ZSMEW002A, ZSMEW007A and ZSMNW042A, whereas zone ZSMNE005A runs parallel to the minor principal stress σ_h . The regional zones ZSMNE005A and ZSMEW002A are both of significant thickness (hundreds of metres), and are made up of ductile parts, essentially characterised by low to normal transmissivity, interlaced by brittle sections of significant transmissivity. The two north-south zones ZSMNS001C and ZSMNS059A are associated with dolerite dykes of low transverse hydraulic conductivity (properties established by measurement) hence attributed a local hydraulic barrier function. However, the rock flanking the dolerite dykes are associated with significant longitudinal (in direction of the zone plane) transmissivity, as established from interference tests in the southwest part of the focused area. With one notable exception (the centrally located ZSMEW007A) most of the interpreted deformation zones have been sampled with essentially one cored borehole intercept, and associated hydraulic characterisation. Based on experience from the nearby Äspö Hard Rock Laboratory and the few deformation zones with several borehole intercepts, the underlying assumption is that the distribution of hydraulic properties in the deformation zones is highly heterogeneous in nature, which is also indicated in Figure 5-29.

The hydraulic investigations carried out in the hydraulic rock domains (and the underlying fracture domains on which they are based, cf. Section 8.4.2) suggest that the frequency (or intensity) of conductive features detected by PFL (corresponding to features with transmissivities $> c. 10^{-9} \text{ m}^2/\text{s}$) varies spatially. Below -650 m there is less than one conductive feature per 100 m . In the interval -400 to -650 m there are between 6 to 22 conductive features per 100 m in the hydraulic rock domains designated as potential deposition volumes (mainly HRD_C and HRD_W, but also part of HRD_EW007, the latter which has a higher intensity of conductive fractures), with a slightly elevated intensity in the interval -150 to -400 m . In stark contrast, but not surprisingly, the corresponding intensity from ground surface down to -150 m is between 50–60 features per 100 m , reflecting effects due to stress release and abrasion from the latest glaciation.

In summary, and without taking into consideration applicable hydraulic boundary conditions and material properties of fractures, the rock below -650 m is characterised by a very low intensity of conductive fractures, and can be expected to be associated with a low flow rate, and possibly even near stagnant conditions. The near tenfold increase in conductive fracture intensity in the depth interval -400 to -650 m suggest higher flow rate and circulation in this interval, compared with that projected below -650 m .

8.2 State of knowledge at the previous model version

The state of hydrogeological knowledge and understanding reported in the preliminary site description of Laxemar /SKB 2006a/ can be summarised as follows:

- Hydraulic data from 9 cored boreholes (KSH01A, KSH02, KSH03A, KAV01, KAV04A, KAV04B and KLX02–04) and 14 percussion drilled boreholes (HSH01–03, HAV09–10, HLX10, HLX13, HLX14, HLX 18, HLX20, HLX22, HLX24, HLX25, HLX32) clearly demonstrated decreasing transmissivity with depth in the interpreted deterministic deformation zones and decreased hydraulic conductivity in the rock in between deformation zones.
- On average, a c. one order higher hydraulic conductivity is observed in deterministic deformation zones compared with the rock between the zones. This difference prevails from surface to a depth of c. $1,000 \text{ m}$.
- Regional simulations of the hydrogeological evolution during the Holocene indicated that the hydraulic boundary condition on the top surface of the model exert considerable impact on the results. A groundwater table used as a head boundary condition, located in some cases several metres below the ground surface, entails simulated results that are most compatible with measured hydrochemistry.
- The model calibration showed low sensitivity to a) use of alternative depth relationships in deformation zones and b) the extraction (elimination) of low-confidence deformation zones.
- Flow paths from (tracking particles in the flow direction) from a release area within the Laxemar local model volume at elevation -500 m discharge mostly within the Laxemar local model area and near the coast or in the larger valleys. Particle tracking also indicated that the recharge area of particles reaching the designated release area at elevation -500 m is located mostly within the Laxemar local model area but in some cases west thereof.

The main hydrogeological uncertainties, as concluded at the end of the ISI stage, are as listed below.

- There were only a limited number of cored boreholes, and hence very limited hydraulic test data available for the Laxemar subarea, and in particular in its southern and south-western parts.
- The confidence in the transmissivity assignment to individual deformation zones (HCD) was considered generally low and highly variable, because a) the confidence in their existence was considered low (deformation zones for the most part were interpreted from lineament data), and b) the limited number of tests and underlying borehole intercepts sustaining the parameterisation.
- The deformation zones (irrespective of their confidence of existence) were found to create a well-connected system, depending partly on their interpreted continuity and termination, and in part on the assumed homogeneous properties assigned along the lateral extent of the zones. The heterogeneity and spatial distribution of properties were found difficult to assess and assign to the flow model given the minute number of data. Preliminary tests indicated that heterogeneity within HCD had an effect on the calibrations and should be tested in the future.

- Decreasing trends in transmissivity with depth for HCD and in hydraulic conductivity with depth for HRD were noted. As in the case of spatial distribution within HCD, the depth trends were considered uncertain, given the limited amount of data available at the time.
- The assumption of a continuous distribution, from individual conductive features to large conductive zones within HRD, was in question. Further conceptual development, in part sustained by study of minor local deformation zones (MDZ), was expected to improve the basis for future modelling. Data and modelling indicated that HRD were anisotropic but less so than seen at Äspö HRL and the conclusion was that the assessed magnitude of the anisotropy was uncertain.
- The hydrogeological initial conditions were considered highly uncertain and time-dependent boundary conditions were considered uncertain, and as shown by subsequent work by /Hartley et al. 2007/, were considered highly decisive for the outcome of the palaeohydrogeological simulations.
- The size of the regional flow model was considered satisfactory but was later checked (and confirmed as being suitable) in /Holmén 2008/.

The feedback report concluding the ISI stage /SKB 2006b/ emphasised the need for additional data on hydraulic properties of hydraulic rock domains and their variability in the foreseen depositional volumes. Similarly, the need for additional data on hydraulic properties of deformation zones (HCD) was stressed. Data from the ISI stage also indicated that the southern part of the Laxemar local model area was less permeable than the northern part, providing one of the arguments for the focused area during CSI.

The early part of the CSI stage included continued focusing on sensitivity analysis which explored; the appropriateness of the western boundary of the regional model area, effects of Äspö HRL underground openings on the hydrogeological/hydrochemical conditions in Laxemar, sensitivity to palaeohydrogeological conditions.

The following principal conclusions were drawn:

- The comparative study /Holmén 2008/ using a large and a small regional model domain demonstrated that the weakly developed surface water divide employed for devising the western regional model boundary is in fact not a groundwater divide for the groundwater flow at greater depth. Hence, deep groundwater flow that passes below the weakly developed surface water divide in the large model will not be included in the small model. Given that the deep groundwater flow is not included in the small model, the latter will underestimate groundwater flow at the repository depth, and overestimate both lengths of flow paths as well as the breakthrough times of flow paths from the repository area. These differences (as established by results from the large and small models) are however small (within a factor of c. 1.5), since the deep groundwater flow missing in the small model is not large.
- As a consequence of this finding it was decided to retain the current (smaller) regional model domain, which is found more tractable for other simulation reasons.
- The underground openings of Äspö Hard Rock Laboratory only have a local effect on the groundwater situation. Typically, the simulations show influences in the areas around the islands of Äspö and Ävrö (including the islands of Hälö and Mjälén) and the eastern part of Laxemar local model area. The results showed the most sensitivity to selection of material properties of sea sediments in the bays around Äspö /Hartley et al. 2007/.
- The modelling of palaeohydrogeology in the Laxemar subarea is most sensitive to the hydrogeochemical conceptual model of the origin and composition of groundwater; in particular the initial distribution of salinity, and the depth dependency of the hydraulic conductivity /Hartley et al. 2007/. It was also concluded that different realisations of the hydrogeological DFN model generate a noticeable variability in the modelled groundwater composition and results for some boreholes may be significantly influenced by the presence of nearby transmissive deformation zones.
- Modelling based on near-surface data and interference test data from KLX09B–KLX09F boreholes showed a tendency toward distinctly more extensive and transmissive fracturing in the NW direction /Hartley et al. 2007/. It was also suggested that there is a possibility that the relationship between transmissivity and size may be different for different sets with strong correlations in subvertical sets parallel to the maximum *in situ* stress (NW), whereas features in other orientations (ENE and NS and subhorizontal) showed less strong correlations or may be spatially heterogeneous. However, it was concluded that it is not clear if such conclusions apply also at greater depth.

8.3 Evaluation of primary data

The hydrogeological investigations performed in the Laxemar-Simpevarp regional model area are summarised in Sections 2.1 and 2.3 and the data supporting the current model version are listed in Table A3-4 of Appendix 3. A summary of the evaluation of these data is presented below, cf. the detailed account in /R  n et al. 2008/.

8.3.1 Basic characteristics measured by the various hydraulic tests

The hydraulic characterisation of the more intensely fractured deformation zones and the less fractured bedrock in between, the so-called hydraulic rock domains is a cornerstone of the bedrock hydrogeological description. The adopted modelling approach combines a deterministic geometrical representation of the HCD with a stochastic geometrical representation of the HRD using a discrete fracture network (DFN) approach and the tectonic continuum hypothesis, see Figure 8-4.

The tectonic continuum hypothesis invokes that the size and intensity of fractures on multiple scales can be approximated through the use of a *single* power-law relationship, which by definition requires global fracture orientation sets. However, the density functions may vary between the sets. The orientations of the global fracture sets used in the hydrogeological DFN modelling within the Laxemar-Simpevarp regional model volume are assumed to be Fisher distributed.

Fracture intensity is intimately connected to the spatial arrangement of the fractures. The hydrogeological DFN modelling is based on the assumption that the spatial distribution of fracture centres of each fracture set within each fracture domain follows a Poisson process, which in turn implies a Euclidean scaling¹.

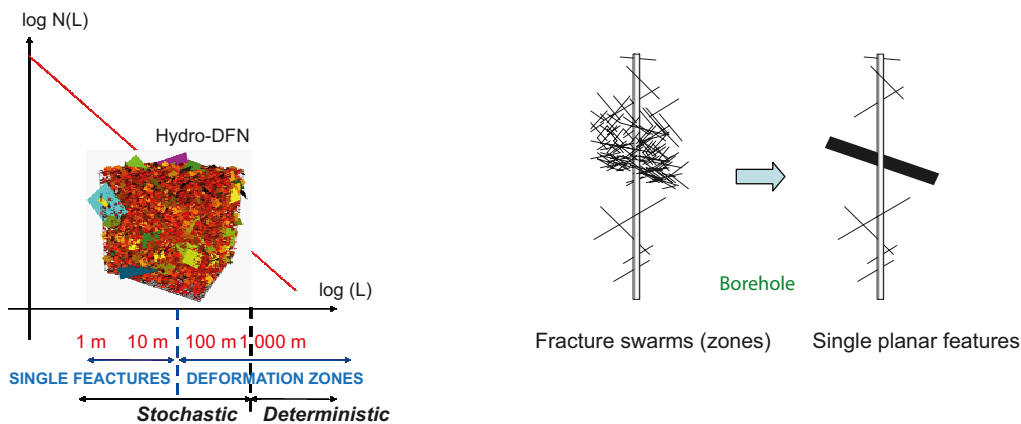


Figure 8-4. Left: The tectonic continuum hypothesis invokes that the frequency of fractures of different sizes can be approximated through the use of a single power-law density function. Structures up to $L = 1,000$ m ($r = 564.2$ m) are regarded as uncertain and are treated stochastically using the discrete fracture network (DFN) concept. The same distinction was used in the geological DFN modelling. Right: The fracture data collected between the upper and lower bounds of a deformation zone interval are lumped together to form a single planar feature. In the same fashion, all hydraulic data in the interval are also lumped together to form a single transmissivity value /SKB 2008a/.

¹ Euclidean scaling is a particular kind of a tectonic continuum where the number of fractures is linearly proportional to the dimensionality of the observation (length, area or volume). Thus, Euclidean scaling implies that doubling the scale (size) of observation, effectively doubles the number of fractures, i.e. constant fracture intensity.

The assumption of an Euclidean scaling was tested in the geological DFN modelling in parallel with other assumptions. Fracture intensity scaling was found Euclidian to weakly fractal and the recommended base model assumes Euclidian intensity scaling, cf. Section 5.6.3. It was also concluded that a three-dimensional Poisson process is adequate to describe the locations of fracture centres in space, as fracture locations following a Poisson process and paired with a power-law size distribution reproduces the fracture spacing (following a Weibull probability distribution) in the boreholes fairly well. In Section 5.6.3 it is also stated that fracture intensity model for *all fractures* generally can be described with a Weibull or Gamma probability distribution down to a minimum scale of approximately 9 m in most of the fracture domains (FSM) modelled geologically.

In effect, the primary geometrical concepts and statistical distributions of the global fracture sets defined in the geological DFN modelling are the same as those used in the hydrogeological DFN modelling:

- Fisher distributed fracture orientations.
- Set-specific power-law intensity (size) density functions.
- Poissonian fracture locations.

A key difference between the two DFN descriptions is in the data; the geological DFN modelling considers primarily the geometrical properties of *surface data* (outcrop data and lineament data) and borehole data representing *all fractures (open and sealed)*, whereas the hydrogeological DFN modelling focuses solely on the geometrical properties of *borehole data* representing two different sets of fracture data: (i) *potentially flowing fractures (open and partly open fractures)*, and (ii) *continuously flowing fractures* detected by the Posiva Flow Log method (so-called *PFL-f* features)².

The differences between the databases used by geology and hydrogeology impacted on how the DFN modelling was carried out. However, since the frequency of *potentially flowing fractures* constitutes a fraction of *all fractures*, the envisaged relationship between the associated power-law density functions can be illustrated as in Figure 8-5. Figure 8-5 implies that completely sealed features exist only among the small fractures (small features), whereas large features, i.e. deformation zones,

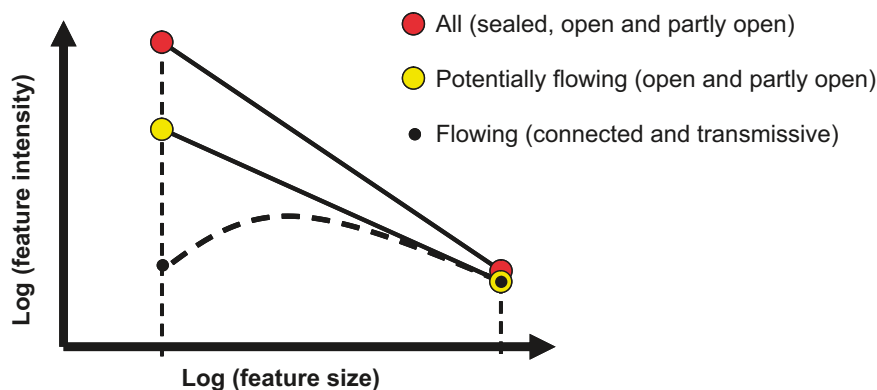


Figure 8-5. Cartoon showing the envisaged relationship between the density functions of *all*, *potentially flowing* and *flowing* features as a function of feature size. The flowing fractures detected with the PFL-f method are envisaged to be a subset of the flowing fractures in the hydrogeological DFN modelling work (modified after /SKB 2008a/).

² In the context of the SDM, ‘*all fractures*’ means that no distinction was made between fractures with regard to fracture aperture. Hence, *sealed* fractures were pooled with *partly open* and *open* fractures in the geological DFN modelling. In contrast, the hydrogeological DFN modelling focused, to begin with, on the properties of the ‘*potentially flowing fractures*’, which implies that the analysed fractures must be at least partly open. In order for a partly open or open fracture to be detected as a flowing fracture it must be (i) connected to a positive hydraulic boundary (either directly or indirectly via a network of other flowing fractures) and (ii) have a sufficient transmissivity relative to the measurement threshold of the test equipment used, cf. Section 8.3.3.

are all heterogeneous with regard to fractures within the deformation zones, i.e. there are generally a number of more or less open fractures that are connected that makes these large structures almost always flowing. Figure 8-5 shows also the conceived behaviour of the *continuously flowing fractures*, i.e. the *connected open fractures*. The *PFL-f fractures* are envisaged as a subset of the latter category, see Section 8.5.2.

A demonstration of the relevance of the notion illustrated in Figure 8-5 is shown for HRD_C in Figure 8-29.

8.3.2 Basic characteristics of the single-hole tests

The hydraulic parameterisation of the deformation zones and fracture domains to become HCD and HRD models is based on single-hole tests in boreholes. Difference flow logging pumping tests (PFL-f) and double-packer injection tests (PSS) were used in the deep, cored boreholes, whereas pumping tests in open holes (HTHB) were performed in the shallower, percussion-drilled boreholes. The lower measurement limits of the PFL-f and PSS tests make these methods superior to the HTHB test method, but they cannot be readily used in the percussion-drilled boreholes for technical reasons. Furthermore, the PFL-f and PSS test methods have different advantages and disadvantages. For this reason, they were run in parallel, in order to quantify the consequences for the site characterisation and subsequent hydrogeological discrete fracture network modelling and groundwater flow modelling.

The constituent parameters measured during the hydraulic tests are the flow rate, Q , and the pressure, p . Since these are correlated, the parameter studied is the specific capacity, $Q/\Delta p$, which has the same dimension as transmissivity, $T [L^2T^{-1}]$. The envisaged test conditions in fractured rock are shown in Figure 8-6. The specific capacity is dependent on several important aspects, among which the following are particularly noted:

- Q_{limit} ; the lower measurement limit of the flow rate for the test method.
- T_{bh} ; the transmissivity of the tested fracture intersecting the borehole. Evaluation of transmissivities (T_{bh}) can be affected by the hydraulic resistance close to the borehole (positive or negative skin factor), with either reduced or enhanced hydraulic communication between the borehole and the rock, respectively.
- C ; the connectivity of the tested fracture to other fractures away from the borehole. Some fractures are isolated, or are a part of an isolated cluster of fractures. Others are well connected and a part of the overall connected hydrogeological system.
- T/S ; the hydraulic diffusivity of the fracture system within the radius of influence.
- T/S ; the hydraulic diffusivity of the fracture system.
- t ; the duration of the hydraulic testing, i.e. the test time.
- ΔL ; the length of the test interval (test section).

The parameterisation of the deformation zones is fairly straightforward. All transmissivity data between the upper and lower bounds of a deformation zone interval, as determined in the single-hole geological interpretation are considered. That is, the transmissivity data from consecutive tests are integrated to form a single transmissivity value for that interval. This approach implies that the hydraulic thickness is assumed to be equal to the geological thickness. However, deformation zones associated with dolerite dykes have been attributed a hydrogeological thickness, incorporating conductive rock bordering the dolerite dyke. The in-plane heterogeneity of hydraulic properties within a deformation zone is studied by means of single-hole tests at different locations but also by way of PFL-f feature intensity along the intercepts of a given borehole with a deformation zone.

The hydraulic description of the hydraulic rock domains between the deformation zones is focused on the conductive fracture frequency (CFF) of continuously flowing fractures. This means that the connected fracture network situations such as cases D–F in Figure 8-6 were regarded as more important for the hydrogeological DFN modelling and the subsequent groundwater flow modelling and the hydrogeological site description than the disconnected (compartmentalised) network situations such as cases A–C. (Thus, cases A–C were not part of the hydrogeological DFN model calibration.)

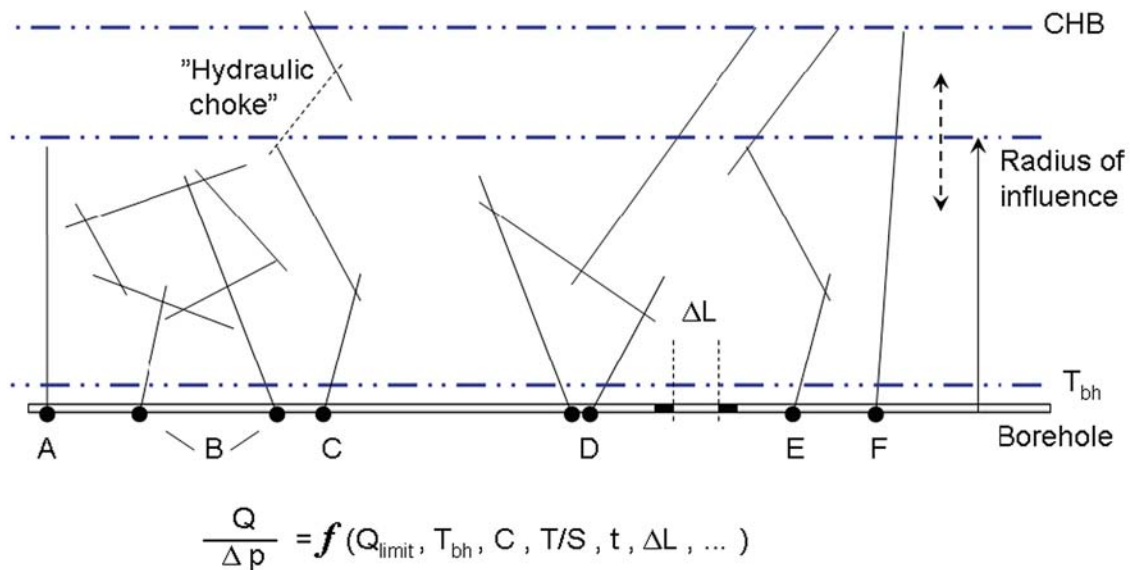


Figure 8-6. Cartoon showing a borehole with six different symbolic fracture network situations, cases A–F. The specific capacity, $Q/\Delta p$, measured along the borehole is dependent on several factors, e.g. the measurement limit, Q_{limit} , of the test method, the transmissivity of the fracture intersecting the borehole, T_{bh} , the fracture connectivity, C , the hydraulic diffusivity, T/S , of the fracture network, the test time, t , the length of the test section, ΔL , etc. The hydraulic characterisation of the fracture system varies depending on the method used as well as on the in situ conditions, e.g. the occurrence of “hydraulic chokes”. Cases A–C represent isolated fracture networks and cases D–F represent fracture networks connected to the overall hydrogeological system. The overall hydrogeological system for the latter is here indicated by a constant head boundary (CHB) suggesting a pseudo steady-state flow regime at long test times. The cartoon is rotated 90° to improve the readability /SKB 2008a/.

8.3.3 Evaluation of single-hole hydraulic tests

/Rhén et al. 2008/ provide a description of the hydrogeological interpretation of the single-hole hydraulic tests conducted in the core-drilled boreholes (PFL-f and PSS tests) and the percussion-drilled boreholes (HTHB tests) along with an extensive interdisciplinary comparison between the interpretation of geological and hydraulic data.

The PFL-f method uses a short test interval in the borehole and a long test time, whereas the PSS method employs the opposite test conditions, i.e. a long test interval and a short test time. Thus, the resolution of the PFL-f method is sufficient to study the transmissivity of individual fractures and the method can be used to evaluate the conductive fracture frequency (CFF) of continuously flowing networks, e.g. situations like cases D–F in Figure 8-6. However, the PFL-f method cannot identify situations with isolated fractures/clusters or “hydraulic chokes” such as in cases A–C. The PSS method, on the other hand, has great problems in distinguishing network situations like cases A–C from network situations like cases D–F, which means that using data from the PSS method alone for the hydrogeological DFN modelling could easily result in an over-prediction of fracture connectivity in the sparsely fractured bedrock in between the deformation zones. Due to this difference, the hydrogeological DFN modelling is based on the information acquired by the PFL-f method. This modelling is thoroughly explained in /Rhén et al. 2008/.

As PFL-f data have been correlated to the core log (Boremap), orientations of PFL-f features have been possible to assess. The correlation between the core log and the PFL-f data is reported in detail by /Forssman et al. 2005ab, Teurneau et al. 2008, Wikström et al. 2008abc, Forsmark et al. 2008/ and is briefly discussed in /Hermanson et al. 2008/. The uncertainties involved in the structural interpretations of PFL-f transmissivity data are explained in /Rhén et al. 2008/. Figure 8-7 through Figure 8-12 show examples of PFL-f transmissivity data and interpreted orientations from the core-drilled boreholes within the focused area, cf. /Rhén et al. 2008/ for other coreholes. The geological fracture domain (FSMxxxx) is shown by name and colour code. The deterministically modelled

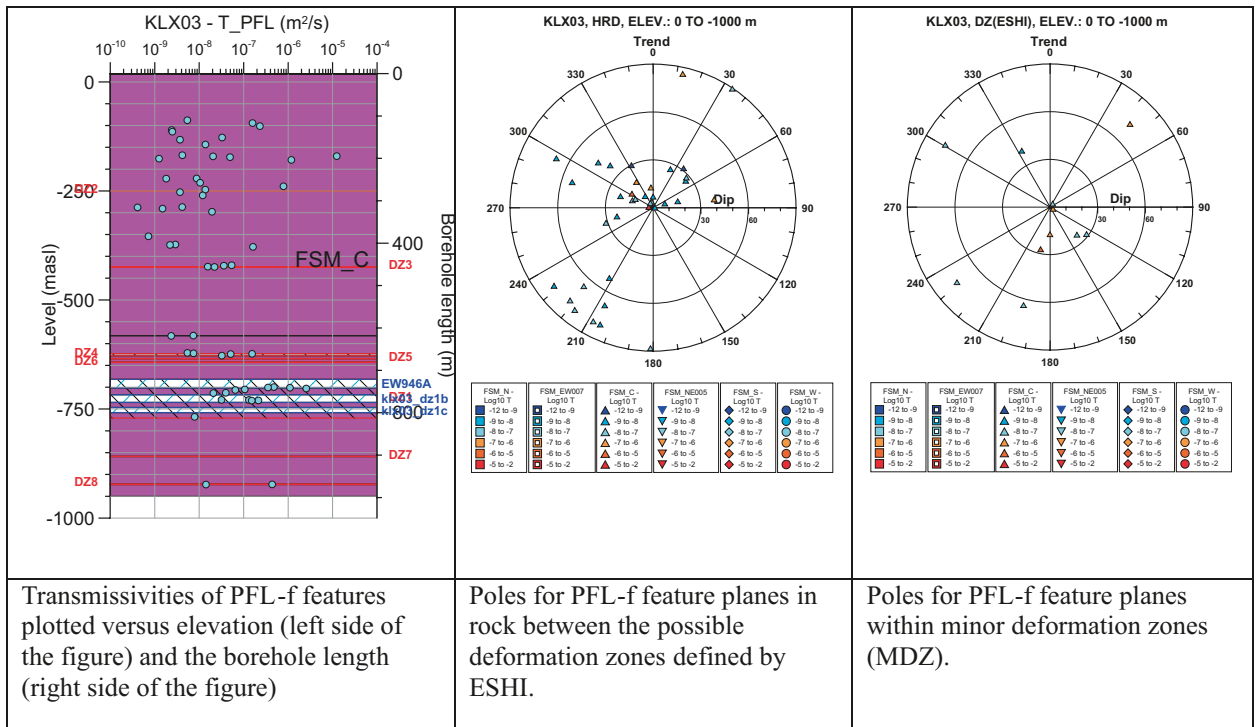


Figure 8-7. KLX03. PFL-f transmissivities vs. elevation, stereo net PFL-f features in rock between possible deformation zones (as interpreted from ESHI) and stereo net PFL-f features in MDZ (part of “possible deformation zones”) /Rhén et al. 2008/.

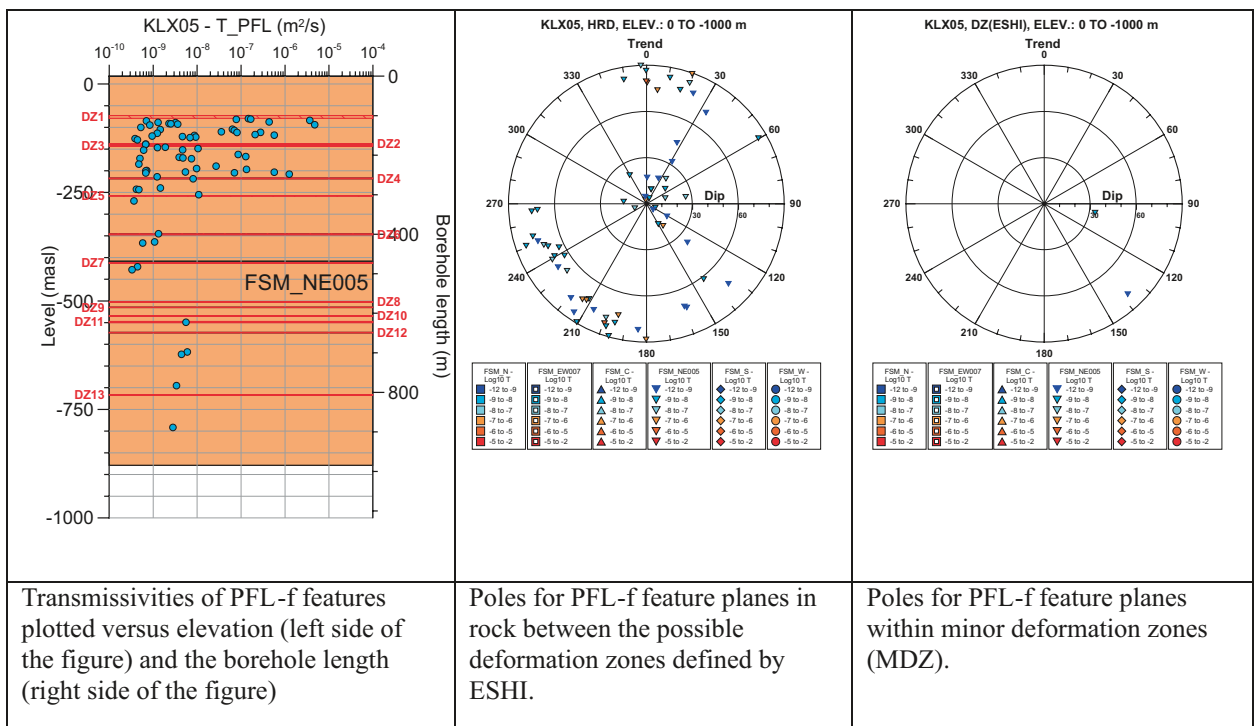


Figure 8-8. KLX05. PFL-f transmissivities vs. elevation, stereo net PFL-f features in rock between possible deformation zones (as interpreted from ESHI) and stereo net PFL-f features in MDZ (part of “possible deformation zones”). No PFL-f in MDZ or deterministically defined deformation zones exists in the hole /Rhén et al. 2008/.

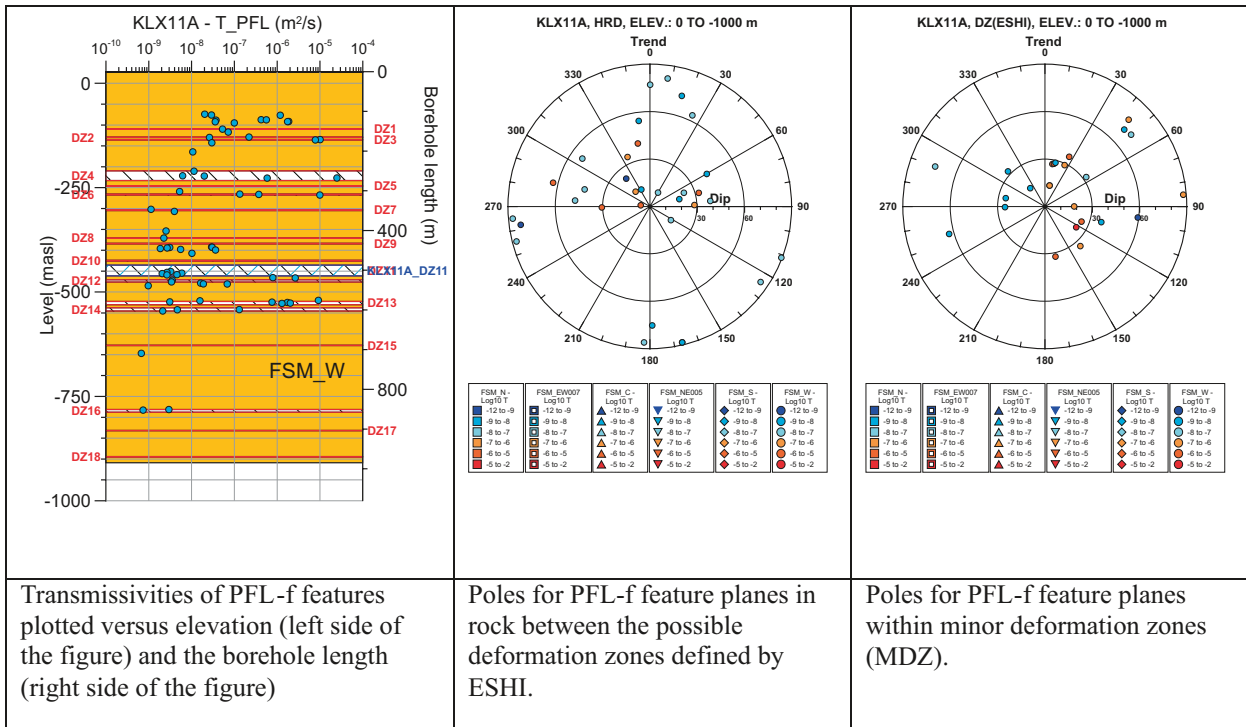


Figure 8-9. KLX11A. PFL-f transmissivities vs. elevation, stereo net PFL-f features in rock between possible deformation zones (as interpreted from ESHI) and stereo net PFL-f features in MDZ (part of “possible deformation zones”) /Rhén et al. 2008/.

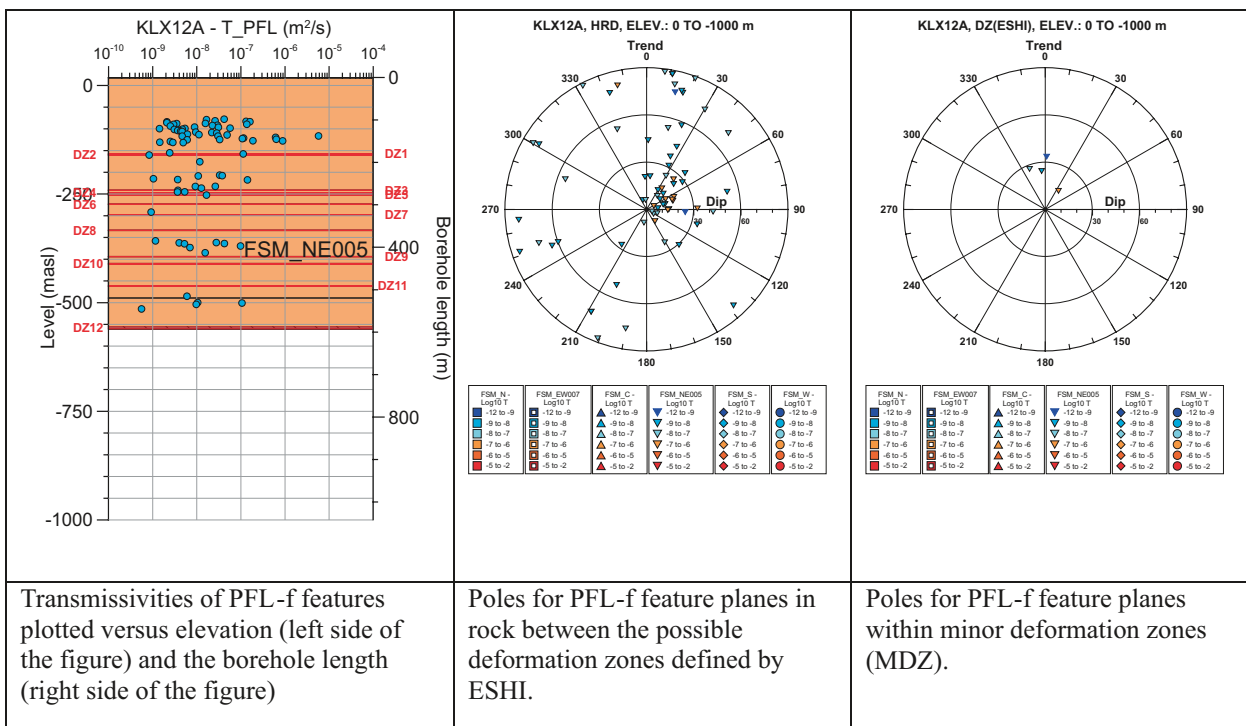


Figure 8-10. KLX12A. PFL-f transmissivities vs. elevation, stereo net PFL-f features in rock between possible deformation zones (as interpreted from ESHI) and stereo net PFL-f features in MDZ (part of “possible deformation zones”) /Rhén et al. 2008/.

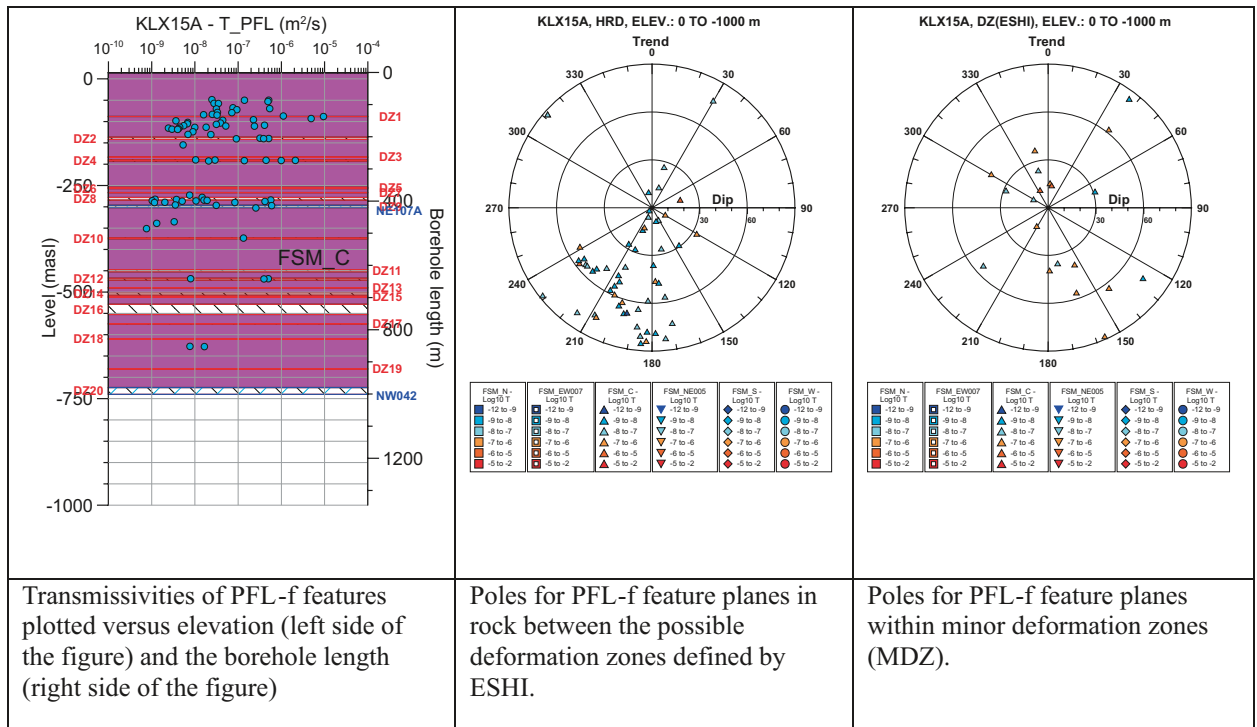


Figure 8-11. KLX15A. PFL-f transmissivities vs. elevation, stereo net PFL-f features in rock between possible deformation zones (as interpreted from ESHI) and stereo net PFL-f features in MDZ (part of “possible deformation zones”) /Rhén et al. 2008/.

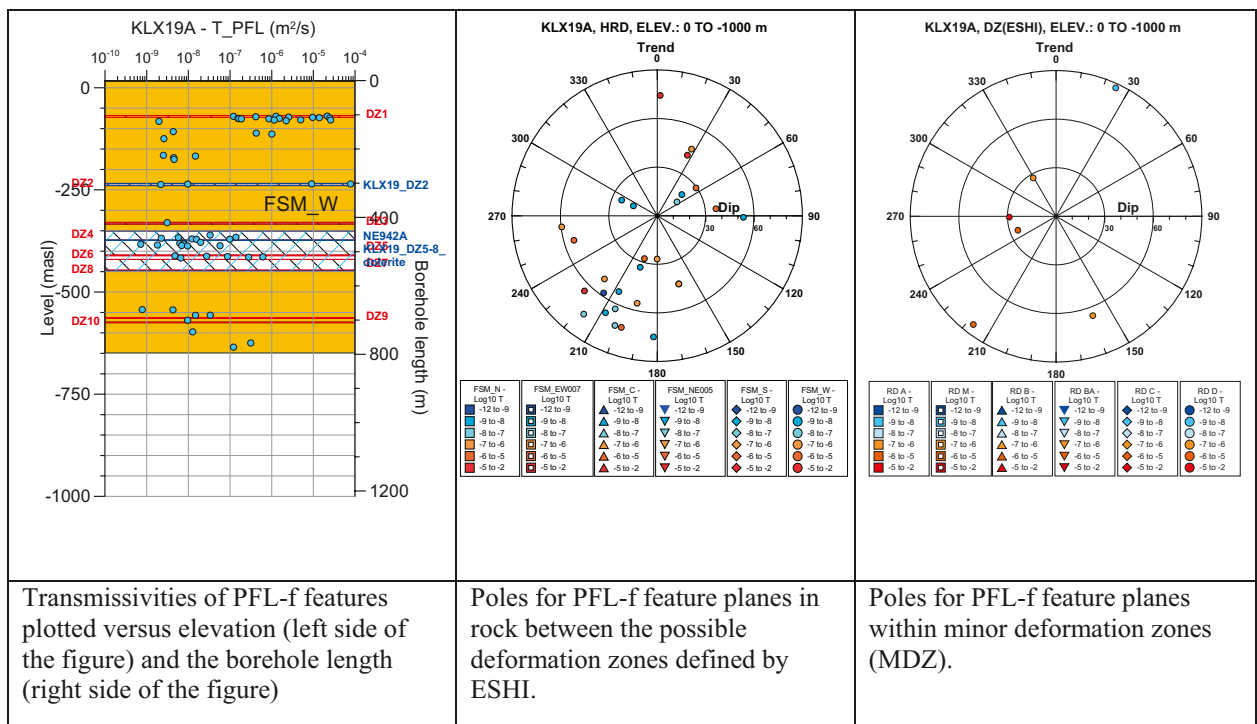


Figure 8-12. KLX19A. PFL-f transmissivities vs. elevation, stereo net PFL-f features in rock between possible deformation zones (as interpreted from ESHI) and stereo net PFL-f features in MDZ (part of “possible deformation zones”) /Rhén et al. 2008/.

deformation zones (DZ) are indicated by name: NNxxxx (leaving out the prefix ZSM-) and possible deformation zones by the names (DZx) given by the geological extended single-hole interpretation (ESHI). As can be seen in the figures, some of the possible deformation zones according to ESHI are modelled as deterministic and the rest are consequently considered to be minor deformation zones (MDZ) and part of the hydrogeological DFN model as discussed in Section 8.3.1, cf. Figure 8-4. Figure 8-13 summarises the mean PFL-f intensities and how these features are coupled to the geological mapping categories; certain, probable and possible, for open and partly open fractures, respectively, and for each cored borehole within the Laxemar local model area. Table 8-2 summarises fracture and PFL-f mapping of the cored boreholes.

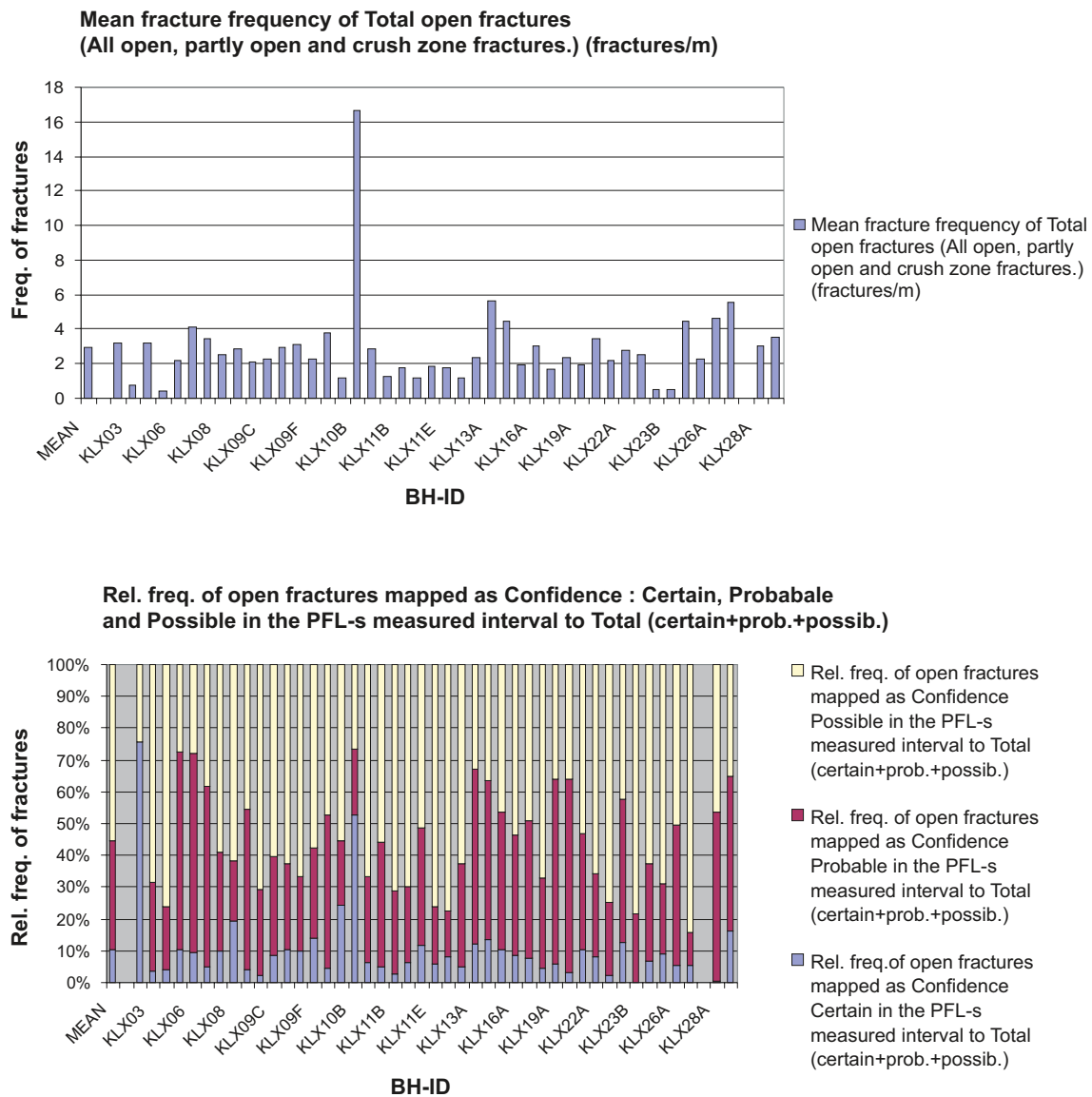


Figure 8-13. Top: Mean fracture frequency of total open fractures (All open, partly open and crush zone fractures (40 fractures/m assumed for crush zones)). Boreholes KLX02 through KLX29A (KLX27A data not included). Bottom: Relative frequency of mapped open fractures attributed confidence level “certain, probable and possible”. Boreholes KLX02 through KLX29A (KLX27A data excluded) /Hermanson et al. 2008/, see geometrical data in Table 8-2.

Table 8-2. Summary of sampled borehole lengths and numbers of fractures within Laxemar local model area at the time of data freeze Laxemar 2.3 according to different categories and the conductive PFL-f features in each of the boreholes measured with the PFL-f method.

Borehole	Top (m)	Bottom (m)	Length (m)	Total number of sealed	Number of all open ⁽¹⁾	Open ⁽¹⁾ and certain	Open ⁽¹⁾ and prob.	Open ⁽¹⁾ and poss.	Number of PFL-f
KLX02	205.82	1,005.83	800	853	2,208	1,608	3	597	87
KLX03	101.4	992.42	891	3,694	683	29	188	466	55
KLX04	101.43	986.22	885	3,458	2,019	85	402	1,532	129
KLX05	108.01	987.43	879	3,172	320	34	199	87	71
KLX06	101.79	987.52	886	4,184	1,048	108	649	291	186
KLX07A	101.98	827.56	726	4,131	2,388	135	1,349	904	240
KLX07B	19.8	192.75	173	658	522	55	161	306	80
KLX08	100.88	987.0	886	3,291	1,974	392	371	1,211	138
KLX09	102.00	871.45	769	2,699	1,959	84	984	891	68
KLX09B	12.6	97.6	85	381	172	5	46	121	44
KLX09C	15.5	117.0	102	457	226	19	71	136	36
KLX09D	12.91	117.91	105	493	310	38	82	190	41
KLX09E	13.87	114.4	101	654	280	27	68	185	34
KLX09F	9.9	146.53	137	683	316	47	89	180	43
KLX09G	22.3	92.58	70	449	266	13	128	125	42
KLX10A	102.13	993.21	891	3,239	594	149	120	325	191
KLX10B	10.73	43.5	33	229	506	270	103	133	24
KLX10C	9.75	139.75	130	1,101	375	25	101	249	25
KLX11A	101.53	985.12	884	4,278	1,074	54	420	600	66
KLX11B	4.18	94.26	90	249	156	4	41	111	37
KLX11C	5.66	115.73	110	308	125	8	30	87	41
KLX11D	12.55	112.54	100	445	187	22	69	96	49
KLX11E	2.00	115.28	113	453	202	12	36	154	37
KLX11F	3.37	113.38	110	293	120	10	17	93	24
KLX12A	102.13	597.25	495	1,814	1,154	55	378	721	77
KLX13A	101.22	589.58	488	1,650	2,047	247	1,127	673	155
KLX14A	17.14	167.5	150	675	613	88	302	223	72
KLX15A	77.58	971.02	893	3,471	1,686	181	727	778	78
KLX16A	20.39	420.63	400	2,489	1,191	107	446	638	78
KLX17A	68.45	693.85	625	3,320	1,049	81	455	513	47
KLX18A	101.35	604.79	503	1,954	1,104	57	309	738	151
KLX19A	100.73	794.3	694	1,510	1,200	72	695	433	60
KLX20A	100.9	448.09	347	1,376	920	27	562	331	55
KLX21B	100.85	850.68	750	4,187	1,654	177	601	876	59
KLX22A	13.53	94.9	81	371	223	18	58	147	43
KLX22B	13.4	93.37	80	346	195	4	45	146	28
KLX23A	19.28	94.28	75	135	40	5	18	17	17
KLX23B	14.88	44.88	30	19	14	0	3	11	4
KLX24A	18.36	93.46	75	400	307	23	93	191	41
KLX25A	13.82	43.82	30	165	68	6	15	47	8
KLX26A	15	94	79	311	307	18	134	155	25
KLX26B	15	43	28	50	155	9	16	130	17
KLX27A	70.38	640.61	570	2,048	863	137	405	321	50
KLX28A	16.97	75.4	58	241	164	1	87	76	36
KLX29A	7.1	54.42	47	230	163	27	79	57	27
Sum BH			16,456	66,614	33,147	4,573	12,282	16,292	2,916

⁽¹⁾: "Open" includes fractures mapped as open and partly open. Fractures that are judged to be open are assigned a confidence: certain, probable or possible.

The PSS, HTHB and PFL tests, cf. Section 8.3.2, have provided data for assessment of the HCD properties /Rhén et al. 2008/. The PSS data have also been compared with PFL data for same borehole sections and the results indicate similar estimates of the transmissivity for the same test sections, although the test and evaluation methods differ. However, the comparison also indicates the presence of clusters of hydraulically locally connected fractures that are not seen in long term tests, such as PFL tests, cf. Section 8.3.2 and /Rhén et al. 2008/. This may have an effect on groundwater flow modelling including underground tunnels but not on regional scale modelling of natural undisturbed conditions as shown in Sections 8.6 through 8.8. The flow dimension was also evaluated for tests in borehole KLX11A and nearly all tests have a flow dimension between 1.5 to 2.3, indicating that these tests are rather close to radial flow (flow dimension = 2), which is assumed by the evaluation methods employed for PSS and PFL /Rhén et al. 2008/.

8.3.4 Comparison between Laxemar and Äspö

Extensive investigations have been performed during the site investigation programme for the Äspö HRL, sited immediately east of the Laxemar local model area, cf. Figure 1-2. The investigations conducted during the site investigation for a deep repository differs to some extent from those for the Äspö HRL but some comparison can be made to indicate differences which can later provide guidance when using experiences from the tunnel excavations at Äspö HRL. It should be remembered that the siting of Äspö HRL was chosen to provide variable conditions suitable for an underground research laboratory and not to find suitable rock for a repository.

PSS tests were performed at test scales 3, 30 and 100 m during the site investigation programme for the Äspö HRL. During the site investigation for a deep repository the test scales have been 5, 20 and 100 m, respectively. In /Rhén et al. 2008/ test results from surface-drilled cored boreholes at Äspö of test scales 3 and 30 m are compared with tests in HRD_C, HRD_W and HRD_EW007 south of deformation zone ZSM_EW007, employing test scales of 5, 20 m. Data plotted include HRD and HCD in combination.

The conclusion drawn is that the hydraulic conductivity within the elevation interval –150 to –400 m is slightly lower in Laxemar compared with that of the Äspö data and lower within elevation interval –400 to –650 m in Laxemar compared with Äspö. Below –650 m the hydraulic conductivity in Laxemar is possibly lower than in Äspö, but the number of data points are limited at both sites. Above elevation –150 m the data are also too limited to draw any firm conclusion. However, HRD_EW007 is more conductive than HRD_C and HRD_W according to /Rhén et al. 2008/, which indicates that the hydraulic conductivity in HRD_EW007 may be similar to Äspö conditions.

8.3.5 Evaluation of hydraulic interference tests

Interference tests during the site investigations have been performed in a number of boreholes and a few of them are commented in /Rhén et al. 2009/. Some of these tests have been of fairly short duration (a day up to a few days) and involved only a few observation sections in boreholes, but some tests have employed both a long duration and involved several observation (monitoring) sections, and thus are of interest from the current flow modelling work point of view. The main focus of the interference tests has been to obtain support for the geologically interpreted geometry of the deformation zones but also to provide judgements of the hydraulic connectivity within and between major deformation zones and their hydraulic properties in terms of transmissivity and storage coefficient. The interference tests have mainly provided information down to 400–600 m depth, but occasionally deeper.

Two of the interference tests were chosen for model testing and calibration as their number of observation sections is fairly large, the pumping duration fairly long and as the tests were situated in two areas of interest for a possible deep repository. The two interference tests are here referred to as the HLX28 and the HLX33 interference tests, respectively, cf. Figure 8-14.

The HLX28 interference test focused on testing the characteristics of the HCD near HLX28, such as deformation zones; ZSMEW42A, ZSMNS001C, ZSMNS059A, KLX19_DZ5-8_dolerite and HLX28_DZ1. The interference test duration was c. 5 days.

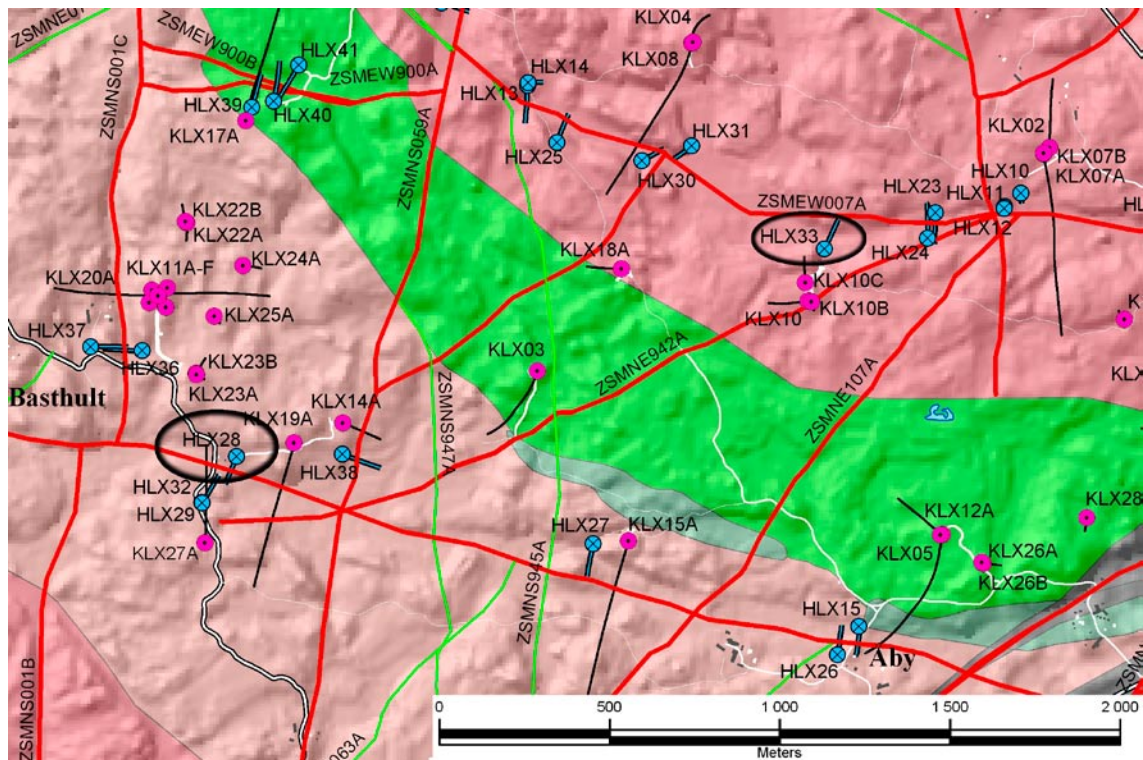


Figure 8-14. Location of interference tests with HLX33 and HLX28 employed as pumping boreholes. The borehole trajectories of the cored boreholes are shown as black lines. The background colour shows the rock domains, cf. Section 5.4.

The HLX33 interference test focused on testing the geometry and hydraulic character of the HCD ZSMEW007. The interference test duration was c. 40 days.

The modelling of the HLX28 and the HLX33 interference tests was reported in /Rhen et al. 2009/ and is commented on in Section 8.6.4.

8.4 Conceptual modelling

8.4.1 Deformation zones and associated hydraulic data

The deformation zone model developed for the preliminary SDM (model version Laxemar 1.2) /SKB 2006a/ was further elaborated and consolidated during the CSI stage, a work that is concluded as part of the SDM-Site Laxemar modelling based on data freeze Laxemar 2.3. The deformation zone model as implemented in the regional scale flow model is shown in Figure 8-15. The principal zones that are of relevance to groundwater flow and the hydrogeological situation, their geographical location, geometry and relationship to the current stress situation are reviewed in Section 8.1.3.

In the preliminary SDM /SKB 2006a/, 90 deformation zone intercepts representing 25 different deformation zones in the regional model area were investigated hydraulically. In SDM-Site Laxemar, these numbers are 158 and 57, respectively, which imply a more or less doubled information density. The transmissivity data acquired from the single-hole tests constitute the basis for assigning hydraulic properties to the deformation zones in the SDM.

The assignment of hydraulic properties to the different deformation zones in the preliminary SDM /SKB 2006a/ was based on depth trend regression analyses of available single-hole transmissivity data, or as step-wise depth trends determined for defined depth intervals (non-conditional assignment). In the flow modelling, a depth trend-based or step-wise change was applied as the base case, and the data adopted were adjusted (translated) to honour the measured borehole data of the individual deformation zones (conditional assignment) in the flow modelling /Hartley et al. 2006/.

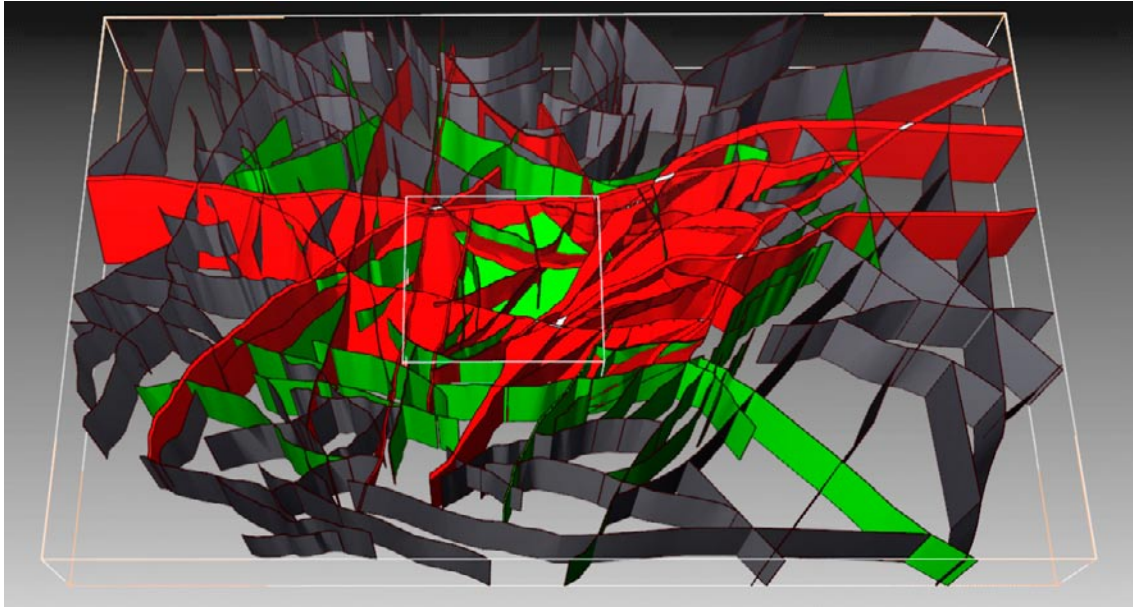


Figure 8-15. 3D visualisation of the regional model domain (large box with white line) and local model area (small box with white line) and the deformation zones included in the SDM-Laxemar deterministic deformation zone model. Colouring of zones according to judged confidence. Red: high confidence, green: medium confidence, grey: low confidence (cf. Section 5.5). Some of these deformation zones are modelled as multiple segments of a given numbered zone (e.g. ZSMxxxxxA, ZSMxxxxxB, etc) as indicated by the suffix capital letter.

Figure 8-16 shows a plot of the single-hole deformation zone transmissivity data used for the regional scale groundwater flow and solute transport modelling in the SDM. The transmissivity data are plotted versus vertical depth. Colour codes are used to distinguish the various identified main groups for defining trend functions /Rhén et al. 2008/. Figure 8-16 shows clearly evident depth trends in the transmissivity data, both overall, and for the identified groups, that spans 5 orders of magnitude from 10^{-3} to 10^{-8} m²/s near the surface, to 10^{-5} to 10^{-9} m²/s at a depth of -500 m. A slightly increased transmissivity is seen for orientation set EW compared with the NW-SE, NS and NE-SW sets. This is in part explained by the notably increased transmissivity of deformation zone ZSMEW007A foremost, cf. Figure 8-17.

The degree of heterogeneity within a HCD is exemplified and illustrated in Figure 8-17. Notable is a considerable lateral variability which spans over 2–5 orders of magnitude for a single HCD. Statistics of transmissivity (T) values of the HCD that have several borehole intercepts indicate that the standard deviation of $\text{Log}_{10}(T)$ is in the range 0.5 to 2 for an individual HCD, with a mean of c. 1 for all depth intervals tested, cf. /Rhén et al. 2008/. The estimated standard deviations are based on generally small samples and the highest standard deviations are based on very small samples and are not considered appropriate measures for the range of standard deviation of HCD transmissivity. For sensitivity study a standard deviation of $\text{Log}_{10}(T)$ equal to 1.4 was tested in the flow modelling, cf. Section 8.5.1.

Not surprisingly, the number of flowing features also increases when the total transmissivity of the HCD increases. The transmissivity distribution of the individual PFL-f features is, however, fairly similar, independent of the depth interval studied. Statistics of PFL-f features within HCD are presented in /Rhén et al. 2008/. A few HCD has several borehole intercepts and PFL-f data, and the Terzaghi corrected intensities ($P_{10\text{corr}}$) of the flowing features vary between c. 0.1 and 1.6 over the geologically defined thickness, indicating a considerable heterogeneity. Only 4 of 49 borehole intercepts (KLX27A excluded) of HCD within the local model volume have no PFL-features.

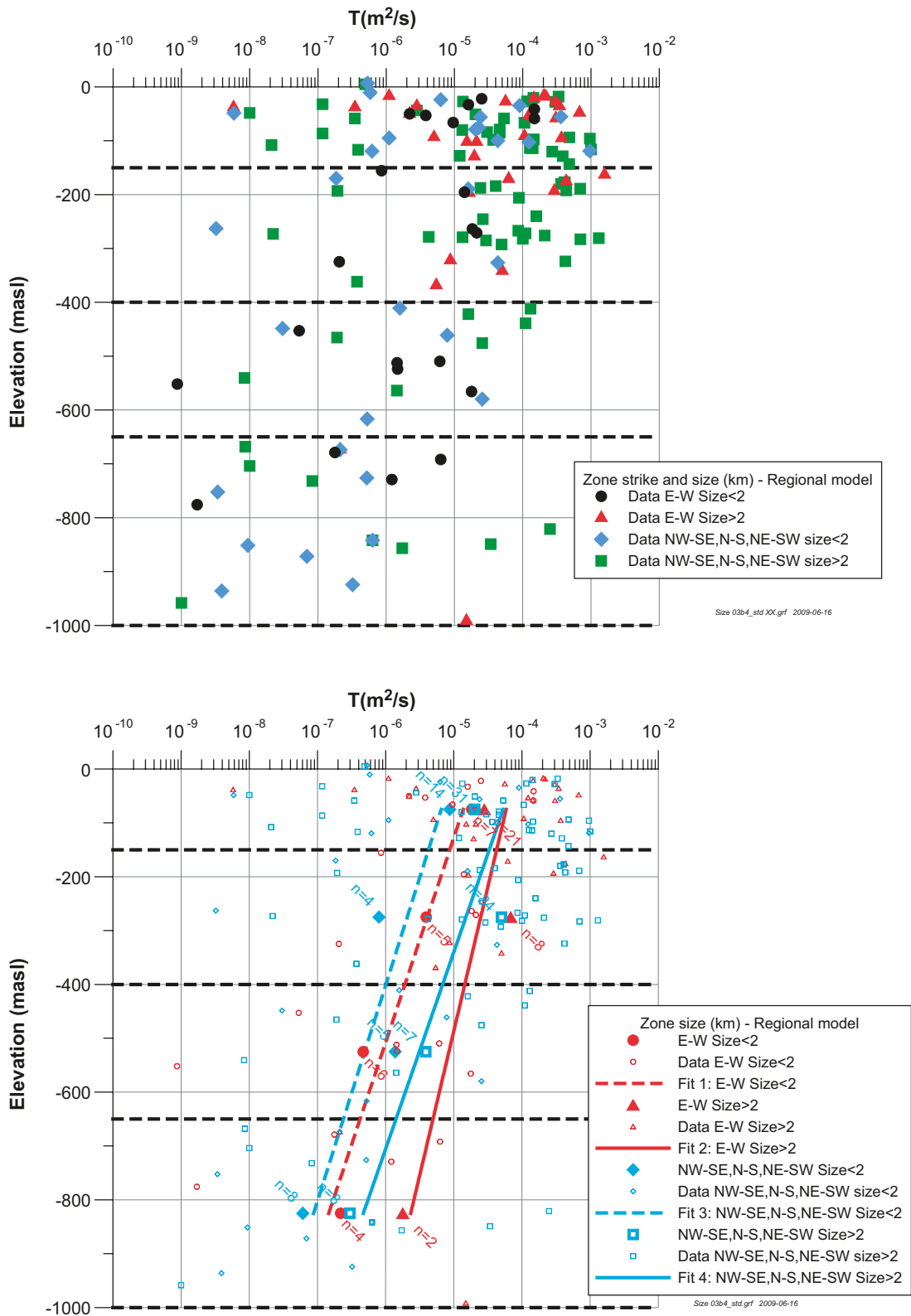


Figure 8-16. Deformation zone transmissivity (T) related to deformation zone orientations in the horizontal plane and size, versus elevation. Mean of $\log_{10}(T)$, plotted as well as the number of observations (n). Top: Data in regional model. Bottom: Regression line and data, regional model.

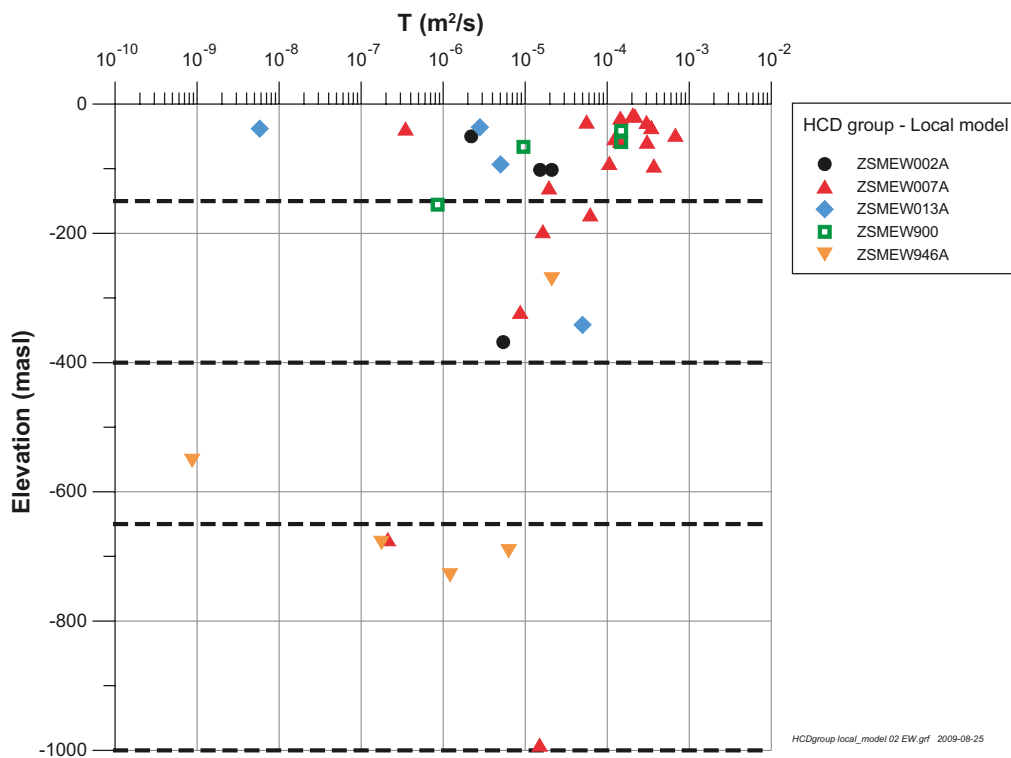
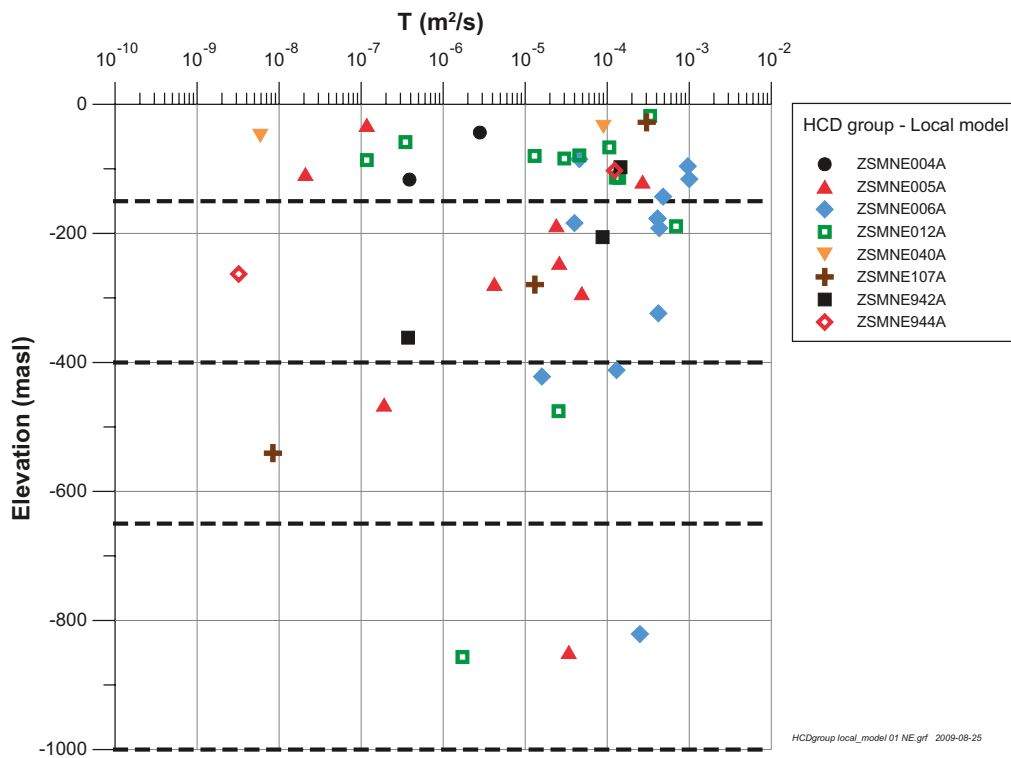


Figure 8-17. Deformation zone transmissivity (T) versus elevation, related to individual deformation zones. Two orientation groups plotted: NE (top) and EW (bottom), cf. /Rhén et al. 2008/ for other orientation groups.

The range for the estimated thickness of a HCD is c. 10–100 m, with mean around c. 20–40 m and a standard deviation of c. 20–40 m /Rhén et al. 2008/.

Dolerite dykes in Laxemar (associated with deformation zones ZSMNS001C, ZSMNS059A, klx19_dz5–8) are interpreted to be steep and to be mainly N-S oriented and are also expected to have a low hydraulic conductivity, but to be heavily fractured. However, the contacts between the dyke and the wall rock on either side of the dyke are fairly transmissive. The hydraulic conductivity of the dolerite core is estimated to be less than 10^{-9} m/s /Rhén et al. 2008/. The transmissivity of the flanking contacts or the dolerite-associated deformation zones is significantly higher, varying between $1.2 \cdot 10^{-5}$ m²/s and $4.8 \cdot 10^{-4}$ m²/s, suggesting significant anisotropy. Interference tests have indicated that these dolerite dykes can act as partial hydraulic barriers /Rhén et al. 2009/. It is however not known if these dykes can be considered as hydraulic barriers along the entire length of the deformation zones.

Mapping of the cored boreholes and mapping of zones in outcrop have shown that fault gouge is present in at least ZSMEW002A (KLX06), ZSMEW007A (observation in trench), ZSMNW042A (KLX27A) /Wahlgren et al. 2008/. This implies that these HCD can possibly exert some hydraulic barrier effect, possibly localised.

This implies that deformation zones ZSMNS001C, ZSMNS059A, klx19_dz5–8, ZSMEW002A and ZSMNW042A should be modelled with a lower permeability perpendicular to the plane of the HCD compared with the permeability along its plane.

The geological attributes of the deformation zones as mainly brittle or brittle-ductile, cf. Section 5.5, do not have hydraulic significance /Rhén et al. 2008/.

A number of subhorizontal deformation zones have been identified and one zone mentioned in Section 5.5.4, ZSMEW946A (reflector M), is of particular interest as it is within the volume of interest for a repository. This HCD does not seem to differ much from other HCD concerning magnitude of transmissivity and heterogeneity, cf. Figure 8-17. However, as indicated in Section 5.5.4 there is a complex series of zones below this structure.

In summary, the assessment of deformation zone transmissivity data shows:

- The range of transmissivity (T) is 10^{-9} to 10^{-3} m²/s for zone intercepts down to elevation –1,000 m.
- The variability of transmissivity within a HCD is assumed to be large and is based on a limited set of hydraulic tests performed in different parts of individual HCD. The variability (standard dev.) range of $\log_{10}(T)$ is c. 0.5 to 2.
- A clear trend of decreasing transmissivity with depth (cf. /Rhén et al. 2008/, that also shows confidence intervals for geometric mean transmissivity for the four depth zones > –150 m, –150 to –400 m, –400 to –650 m, < –650 m).
- A positive correlation between interpreted HCD “size” and transmissivity, but the variation is great. Size here corresponds to interpreted trace length at the surface /cf. Rhén et al. 2008/.
- Indications of transmissivity of HCD being dependent on the orientations of deformation zones. E-W zones appear more conductive than are zones of other orientations.
- Some HCD (associated with dolerite dykes and fault gouge infillings) are conceptualised as being anisotropic, less permeable across the HCD plane compared with along the plane.

8.4.2 Hydraulic rock domains and associated hydraulic data

PFL-f transmissivity data from 8 cored boreholes (KSH01A, KSH02, KAV01, KAV04A/B, KLX02–KLX04) were available for modelling in the preliminary SDM /SKB 2006a/ whereas PFL-f data from 45 cored boreholes, cf. Table 8-2, were available for the SDM-Site Laxemar modelling. As exemplified in Figure 8-7 through Figure 8-12, some of the PFL-f features are related to discrete fractures located between interpreted deformation zones and some are associated with interpreted deformation zones. Some of the deformation zones interpreted from the geological single-hole interpretation are modelled in the SDM as deterministic deformation zones and the remainder of the interpreted deformation zones are considered as minor deformation zones, cf. Sections 5.5 and 5.6.

Of all observed PFL-f features c. 25% are linked to deterministically modelled deformation zones and c. 10% can be linked to minor deformation zones (MDZ) and thus 65% are considered as single fractures in the remaining bedrock. The discrete nature of the PFL-f data in the rock between the deterministic deformation zones allows inferences about spatial variations in conductive fracture frequency.

Following the preliminary SDM, questions arose as to whether there existed grounds for a different subdivision of the rock than that coupled to rock domains, cf. Sections 5.4 and 5.6. /Hermanson et al. 2008/, in an interdisciplinary assessment, showed convincingly that a subdivision of the rock for DFN modelling purposes based on differences in fracture characteristics (primarily the relative intensity of fracture sets, the fracture orientation sets defined and assumed applicable throughout the local model volume) encapsulated better the variability in fracture properties, cf. Section 5.6.1.

/Rhén et al. 2008/ in a introductory study to the SDM hydrogeological DFN analysed transmissivity data subdivided both on the basis of rock domains and fracture domains. The statistical differences between the two were found to be subtle, but the subdivision based on fracture domains was retained to safeguard consistency with the division employed in the geological DFN, cf. Section 5.6. The latter subdivision contains 6 fracture domains referred to as FSM_N, FSM_NE005, FSM_EW007, FSM_C, FSM_W and FSM_S, respectively, cf. Section 5.6.1 and Figure 5-57, which are applicable within the local model volume. Subsequently, /Rhén et al. 2008/ in their subdivision of hydraulic data provided arguments for combining FSM_S, FSM_C and FSM_NE005 into one hydraulic rock domain denoted HRD_C. The remainder of fracture domains is without any further modification related to the corresponding hydraulic rock domains HRD_N, HRD_W, HRD_EW007, in all establishing four HRD within the local model volume, cf. Figure 8-18 and Figure 8-19.

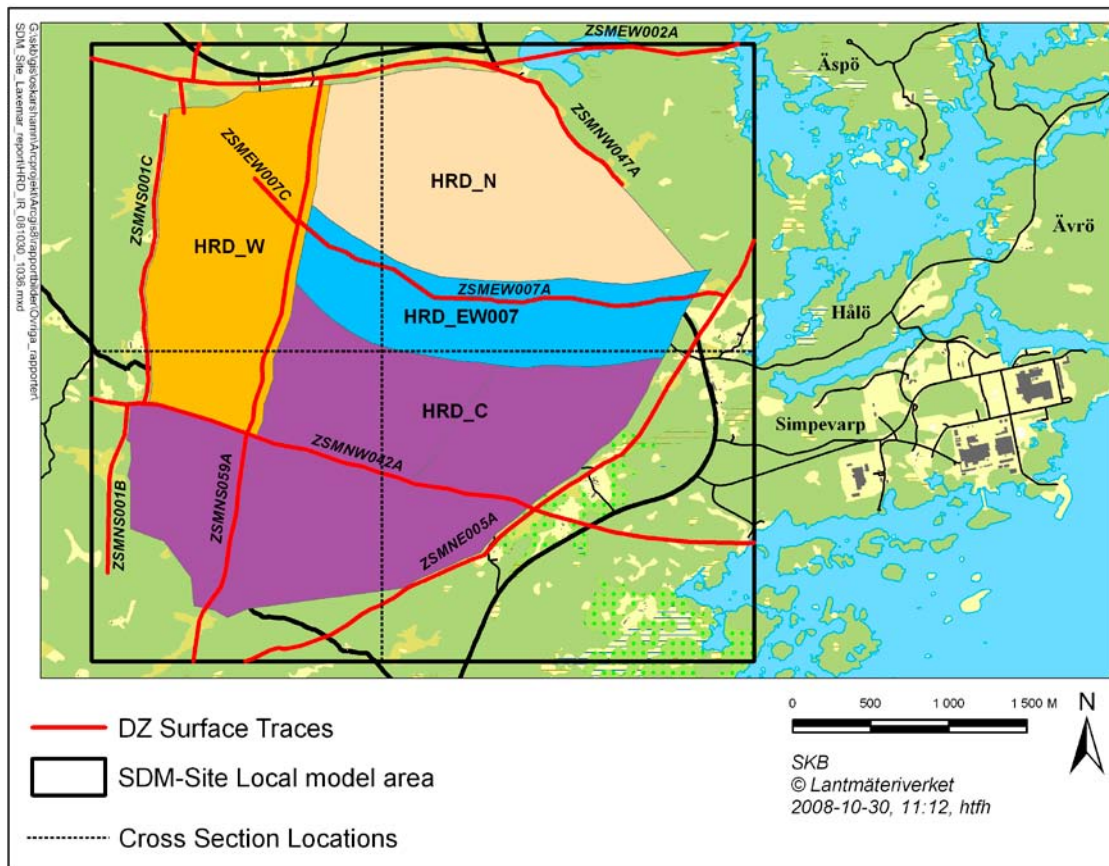


Figure 8-18. Subdivision of the local model volume into hydraulic rock domains based on the underlying division into fracture domains, cf. Section 5.6 and Figure 5-57.

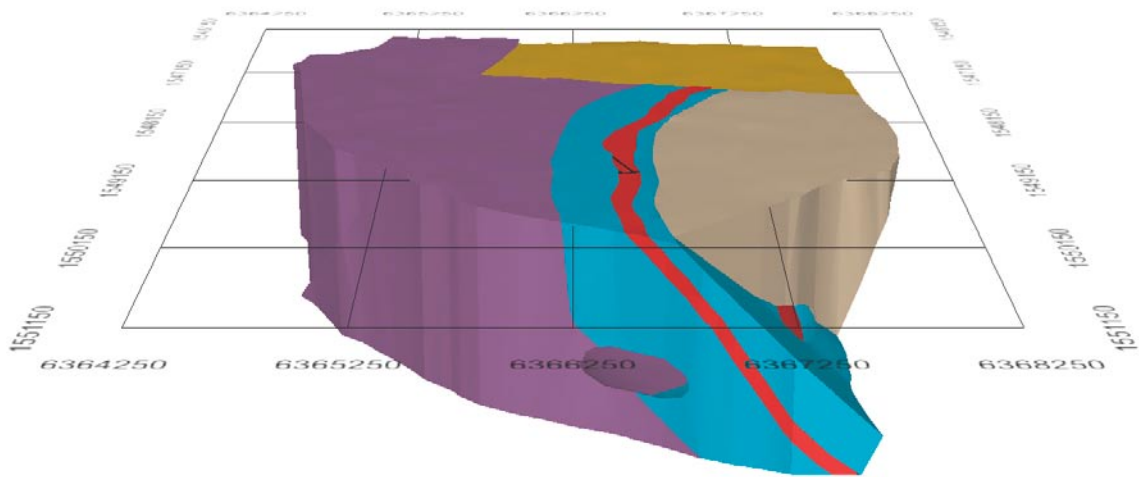


Figure 8-19. Illustration of the SDM Site Laxemar Hydraulic Rock Domain Model, 3D view looking westward.

Notable in the PFL-f data representative of the principal hydraulic rock domains acting as candidates for main potential disposal volumes (HRD_C and HRD_W), cf. Figure 8-9 to Figure 8-12, is a distinctly higher frequency of PFL features down to c. -200 m. This circumstance is seen in most Swedish crystalline sites. The situation between c. -200 and -600 m is characterised by a weak decrease of PFL-f intensity in the rock mass between interpreted deformation zones, and below c. -600 m the intensity of flowing features is very low. This characteristic depth dependence is best illustrated with an example based on HRD_C, cf. Figure 8-20 and conceptually illustrated in Figure 4-3.

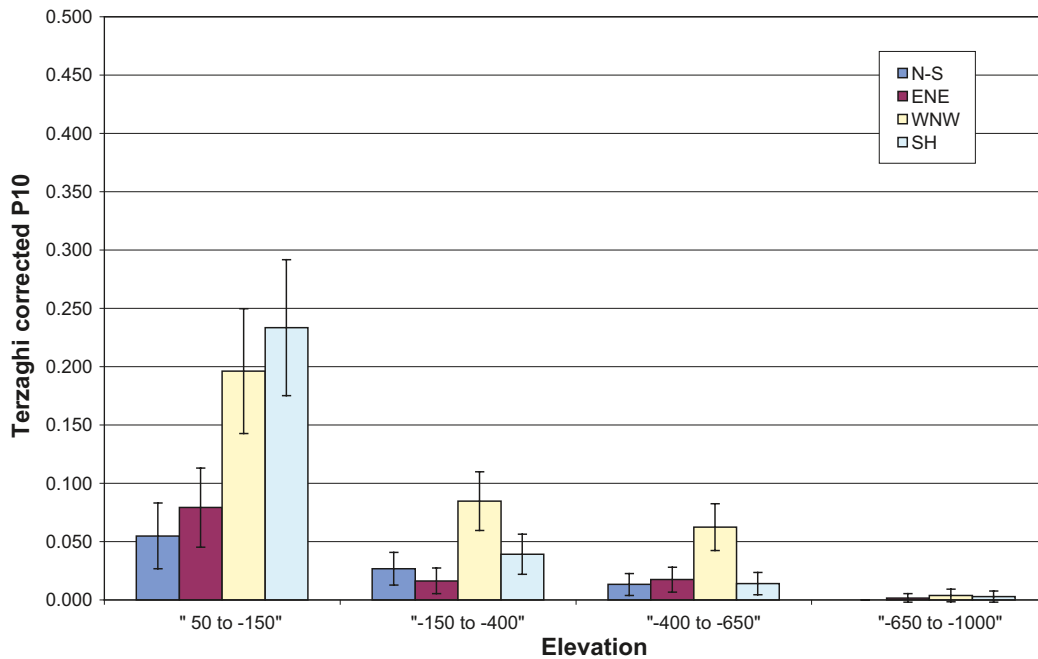


Figure 8-20. Variation of the Terzaghi-corrected fracture intensity for PFL-f features with depth for the fully characterised sections of boreholes penetrating Hydraulic Rock Domain HRD_C /Rhén et al. 2008/.

A careful scrutiny of the conductive fracture frequency and transmissivity data in primarily HRD_C and HRD_W entailed definition of the depth zones; 0 to –150 m, –150 to –400 m, –400 to –650 m and < –650 m, for the hydrogeological DFN modelling. The subdivision based on hydraulic rock domains and the superimposed division in depth zones has also been employed for presentation of basic hydraulic test data statistics in relation to defined hydraulic rock domains and depth zones, cf. Table 8-3 and Table 8-4. In the depth zone –400 to –650 m, the average spacing between conductive fractures in HRD_C is c. 9 m, which is slightly more than half of the corresponding average spacing in HRD_W. However, the average hydraulic conductivity is higher in HRD_W compared with HRD_C in this depth zone, indicating the effect of the differences in the transmissivity distributions, cf. Table 8-4.

In summary, the fracture domains defined geologically have been shown applicable also to the hydrogeological conceptual modelling, although with some minor adjustment and simplification. The conductive fracture frequency in the rock mass generally displays a very clear depth dependence below –150 m, but not always. The general picture of conductive fracture frequency and transmissivity distributions has helped define a depth zone subdivision applicable to hydrogeological DFN modelling within the entire local model volume.

Table 8-3. Summary of intensity statistics of flowing features detected by PFL for the borehole intervals outside of interpreted deterministic deformation zones. MDZ are included in these statistics, but the numbers of individual PFL features are summed up within an MDZ such that each is treated as one single feature. Modified after /Rhén et al. 2008/. $P_{10,corr}$ implies Terzaghi corrected intensity.

Domain	Depth Zone (m)	Length (m)	Count	PFL $P_{10,corr}$ (1/m)	PFL P_{10} (1/m)	
FSM_ EW007/	50 to –150	279	107	0.816	0.384	
	–150 to –400	1,001	241	0.550	0.241	
HRD_ EW007	–400 to –650	843	72	0.225	0.085	
	–650 to –1,000	213	0	0.000	0.000	
FSM_ NE005	50 to –150	371	167	0.820	0.451	
	–150 to –400	806	62	0.169	0.077	
	–400 to –650	615	17	0.071	0.028	
FSM_ HRD_ N/	–650 to –1,000	434	4	0.013	0.009	
	50 to –150	933	331	0.773	0.355	
	–150 to –400	608	115	0.339	0.189	
HRD_ N	–400 to –650	441	20	0.115	0.045	
	–650 to –1,000	177	9	0.082	0.051	
	50 to –150	204	48	0.350	0.235	
FSM_ C	–150 to –400	579	40	0.103	0.069	
	–400 to –650	1,040	51	0.129	0.049	
	–650 to –1,000	950	4	0.006	0.004	
FSM_ W/	50 to –150	1,282	379	0.499	0.296	
	HRD_ W	–150 to –400	904	33	0.078	0.037
	–400 to –650	677	23	0.060	0.034	
FSM_ S	–650 to –1,000	272	1	0.005	0.004	
	50 to –150	166	21	0.254	0.126	
	–150 to –400	65	20	0.655	0.308	
HRD_ C	–400 to –650	N/A	N/A	N/A	N/A	
	–650 to –1,000	N/A	N/A	N/A	N/A	
	50 to –150	741	236	0.564	0.319	
	–150 to –400	1,451	122	0.164	0.084	
HRD_ C	–400 to –650	1,655	68	0.107	0.041	
	–650 to –1,000	1,384	8	0.008	0.006	

Table 8-4. Select intensity and transmissivity statistics of flowing features detected by PFL for the borehole intervals outside of interpreted deterministic deformation zones. (Note that each MDZ is considered to be a single feature, even if it corresponds to several PFL within a borehole.). Modified after /Rhén et al. 2008/. $P_{10,corr}$ implies Terzaghi corrected intensity.

Domain	Depth Zone (m)	Length (m)	PFL $P_{10,corr}$ (1/m)	Sum T/L Length (m/s)	Min T (m ² /s)	Max T (m ² /s)
FSM_	50 to -150	279	0.816	3.1E-07	4.4E-10	3.2E-05
EW007/	-150 to -400	1,001	0.550	1.2E-07	3.1E-10	3.7E-05
HRD_	-400 to -650	843	0.225	1.2E-08	7.9E-10	1.8E-06
EW007	-650 to -1,000	213	0.000	0.0E+00	0.0E+00	0.0E+00
FSM_	50 to -150	371	0.820	2.4E-07	3.9E-10	1.4E-05
NE005	-150 to -400	806	0.169	4.0E-09	3.7E-10	1.2E-06
	-400 to -650	615	0.071	2.2E-09	3.3E-10	8.1E-07
	-650 to -1,000	434	0.013	1.6E-10	1.5E-09	6.1E-08
FSM_N/	50 to -150	933	0.773	6.7E-07	7.7E-10	6.5E-05
HRD_N	-150 to -400	608	0.339	2.1E-07	8.3E-10	3.6E-05
	-400 to -650	441	0.115	1.5E-08	1.1E-09	5.2E-06
	-650 to -1,000	177	0.082	4.1E-10	1.3E-09	2.6E-08
FSM_C	50 to -150	204	0.350	1.0E-07	2.4E-09	9.4E-06
	-150 to -400	579	0.103	3.4E-08	4.1E-10	1.2E-05
	-400 to -650	1,040	0.129	4.2E-09	3.9E-10	1.1E-06
	-650 to -1,000	950	0.006	7.3E-10	1.4E-08	4.4E-07
FSM_W/	50 to -150	1,282	0.499	2.8E-07	3.7E-10	4.6E-05
HRD_W	-150 to -400	904	0.078	2.9E-08	1.1E-09	1.0E-05
	-400 to -650	677	0.060	2.8E-08	6.7E-10	9.2E-06
	-650 to -1,000	272	0.005	1.4E-11	3.7E-09	3.7E-09
FSM_S	50 to -150	166	0.254	2.9E-07	1.3E-10	2.3E-07
	-150 to -400	65	0.655	1.9E-07	3.8E-09	1.0E-07
	-400 to -650	N/A	N/A	N/A	N/A	N/A
	-650 to -1,000	N/A	N/A	N/A	N/A	N/A
HRD_C	50 to -150	741	0.564	2.1E-07	3.9E-10	3.8E-05
	-150 to -400	1,451	0.164	2.4E-08	3.7E-10	1.2E-05
	-400 to -650	1,655	0.107	3.4E-09	3.3E-10	1.1E-06
	-650 to -1,000	1,384	0.008	5.5E-10	1.5E-09	4.4E-07

The conductive features form an anisotropic system; near surface subhorizontal and steeply dipping features with WNW strike dominate and below 100–200 m depth the relative intensity of the subhorizontal features decreases and steeply dipping conductive features with WNW strike dominate. Taking also the decrease by depth of the intensity of the flowing features into account, it is recognised that a large portion of the groundwater recharge is only flowing through the upper 200 m of rock, before discharging.

Results of block modelling of effective hydraulic conductivity made using the derived hydrogeological DFN are presented by /Rhén et al. 2008/ and are used to study scaling issues and the anisotropy of rock blocks of grid cells sizes of 5, 20 and 100 m, respectively, in the depth zone -400 to -650 m. It was found that K_{hmax}/K_{hmin} median value ratios were in the range 5–9 for HRD_C and HRD_EW007 and c. 2–4 for HRD_W. The ratio K_{hmax}/K_z was 1–1.6 for HRD_C and HRD_EW007 and c. 1–2 for HRD_W, for all grid sizes tested (K_h : Horizontal hydraulic conductivity, K_z : Vertical hydraulic conductivity). There seems to be a tendency that the anisotropy becomes more pronounced the larger the block size. The explanation is that the larger, but few, conductive fractures/features from a certain fracture set on average become more dominant for larger blocks, but are less influential in the smaller blocks.

The magnitude of the anisotropy calculated, as given above, is less than that found based on to observations made in the nearby Äspö HRL access tunnel, based on hydraulic testst in probe boreholes sampling subvertical fractures at the progressing tunnel face. It was found that the highest conductivity in the horizontal direction is WNW-NW, but also that the N-S direction showed high conductivity /Rhén et al. 1997c/. The ratio between the maximum and the minimum hydraulic conductivity in the horizontal plane was c. 100, which is considerably higher than the corresponding ratios estimated for the blocks of the Laxemar local model volume discussed above.

Evaluation of hydraulic data from the Prototype Repository at Äspö HRL shows results similar to those seen in the Äspö access tunnel, but also indicates that the most conductive fracture set is subvertical, with an approximate WNW strike /Rhén and Forsmark 2001/. It was also shown that the hydraulic conductivity was c. 100 times less in vertical boreholes compared with horizontal boreholes, indicating that subvertical fractures are the dominant conductive fractures at Äspö.

Anisotropy in Laxemar may be higher than indicated by the block modelling as the up-scaling from hydrogeological DFN to equivalent continuous porous medium (ECPM) block models has some tendency of averaging-out heterogeneity, but possibly also due to the fact that it is difficult to fully capture the true nature of anisotropy from a limited set of single-boreholes tests using the above procedure.

Out of 81 geologically mapped MDZ in the boreholes with PFL measurements (KLX27A excluded), 63 have one or several PFL-f features, indicating a considerable heterogeneity within MDZ. A large part of the MDZ are of quite limited thickness, cf. Figure 5-60, which probably is one explanation.

The hydraulic parameterisation of the hydrogeological DFN model, as presented by /Rhén et al. 2008/, is developed for the relevant hydraulic rock domains covering the focused volume; HRD_C, HRD_W and parts of HRD_EW007, which define the potential deposition volumes.

The main characteristics of the HRD can be summarised as follows:

- Transmissivity of PFL-f features ranges from c. $3 \cdot 10^{-10}$ to c. $6 \cdot 10^{-5}$ m²/s with a standard deviation of $\log_{10}(T)$ c. 1.
- A clear decreasing frequency of flowing features with depth but generally with a similar transmissivity distribution for each depth interval studied (as measured by PFL-f).
- As a consequence of the previous point – a resulting clear trend of decreasing hydraulic conductivity with depth.
- The mean hydraulic conductivity is c. 10 times lower in HRD than that of the HCD (test scale 100 m).
- The flowing features can be grouped in four orientation sets; steep ENE, WNW, N-S and a subhorizontal set.

8.4.3 The bedrock bordering the focused volume

The hydraulic parameterisation of the rock essentially covering the complete local model volume, is achieved by adding the parameterisation of HRD_N and HRD_EW007, cf. Figure 8-18. These two domains are either wedged between the two major deformation zones ZSMEW002A and ZSMEW007A (HRD_N) or essentially covering and flanking zone ZSMEW007A (HRD_EW007). Data collected in boreholes KLX02, KLX04, KLX06, KLX07A/7B, KLX08, KLX09, KLX10, KLX18A are principally used to inform these two hydraulic rock domains, in some instances sampling both HRD in the same borehole. Three representative examples of data are provided from KLX07A, KLX08 (HRD_EW007) and KLX09 (HRD_EW007/HRD_N) in Figure 8-21 through Figure 8-23, respectively. As a consequence of their close association to deformation zones, the frequency of PFL-f and also individual transmissivities of these HRD are notably higher than in the HRD making up the focused volume.

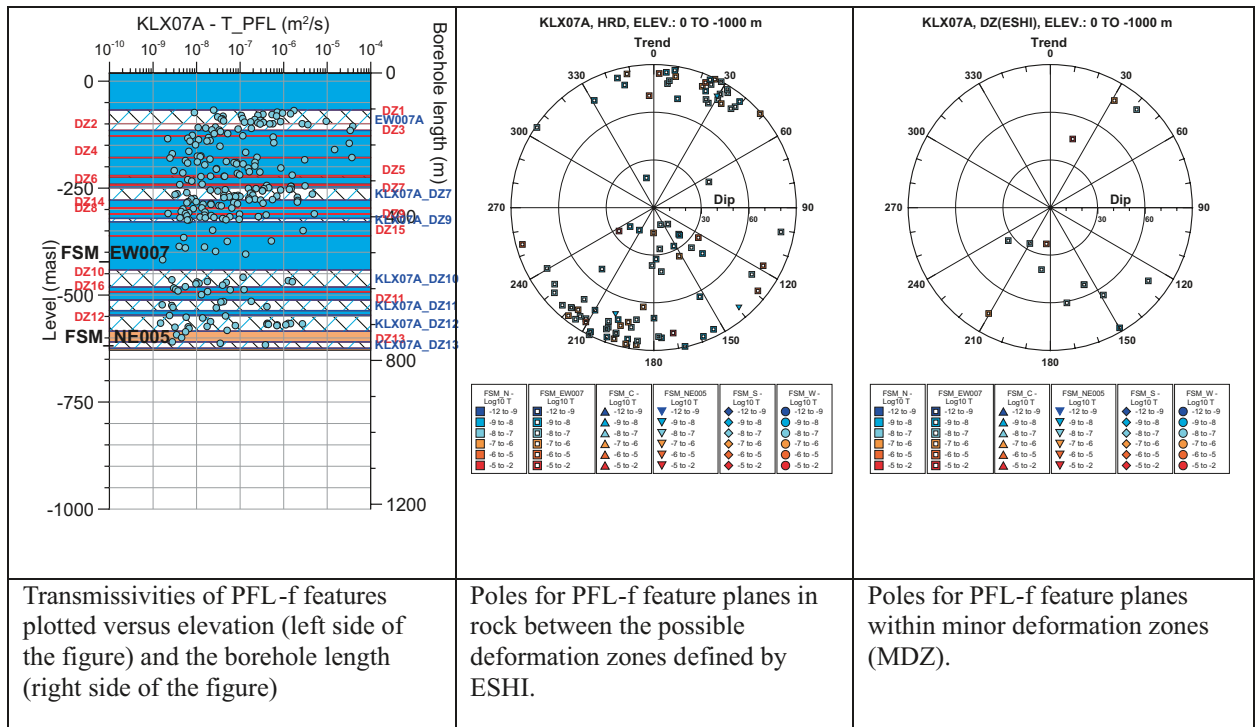


Figure 8-21. KLX07A. PFL-f transmissivities vs. elevation, stereo net PFL-f features in rock between possible deformation zones (as interpreted from ESHI) and stereo net PFL-f features in MDZ (part of “possible deformation zones”) /Rhén et al. 2008/.

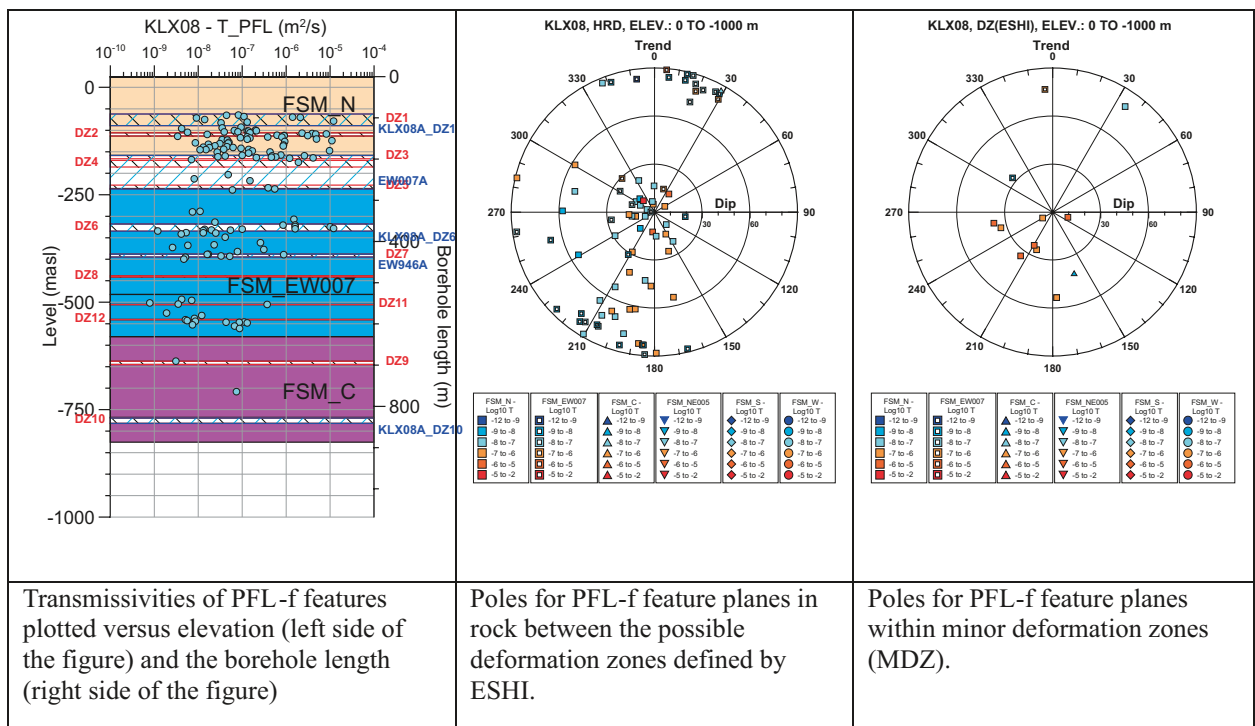


Figure 8-22. KLX08A. PFL-f transmissivities vs. elevation, stereo net of PFL-f features in rock between possible deformation zones (as interpreted from ESHI) and stereo net of PFL-f features in MDZ (part of “possible deformation zones”) /Rhén et al. 2008/.

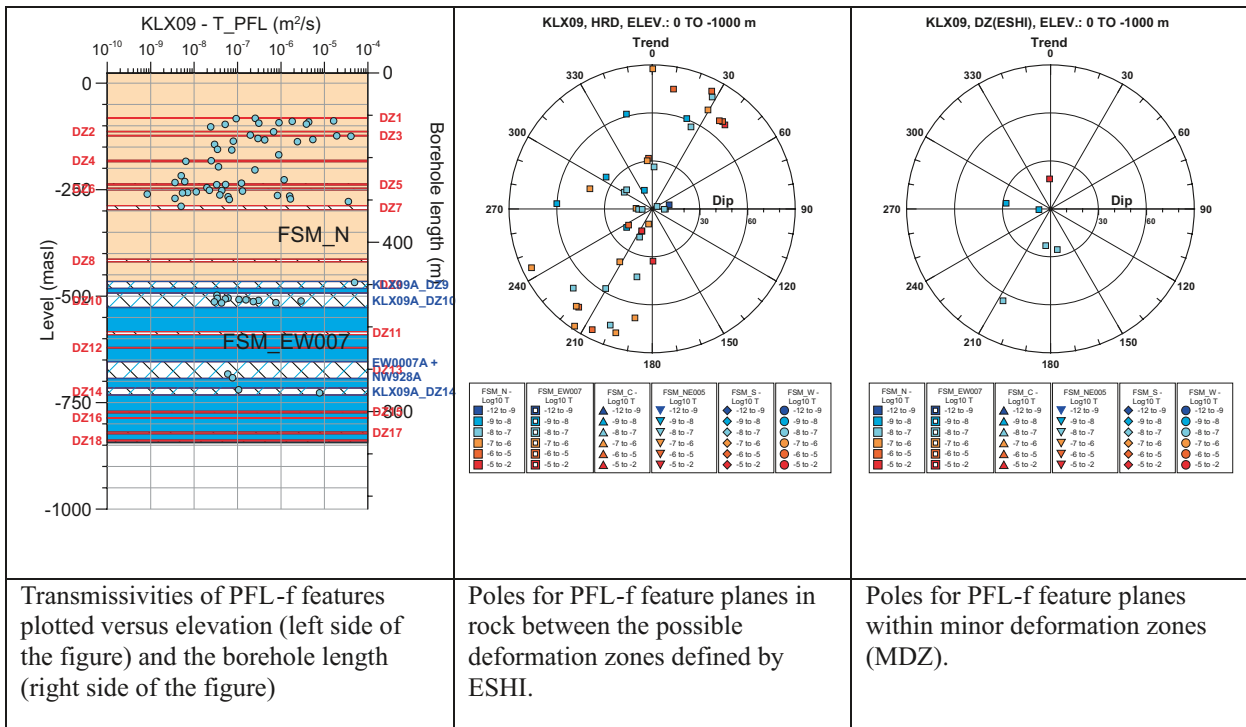


Figure 8-23. KLX09. PFL-f transmissivities vs. elevation, stereo net of PFL-f features in rock between possible deformation zones (as interpreted from ESHI) and stereo net of PFL-f features in MDZ (part of “possible deformation zones”, cf. /Rhén et al. 2008/).

The rock mass in the regional model, outside the defined FSMs, cf. Figure 5-57, is based on the material property assignments made in model version Laxemar 1.2 /SKB 2006a, Rhén et al. 2006abc/ and assessments of similarities between those regional HRD and the newly developed HRD inside the Laxemar local model volume, cf. /Rhén et al. 2008/.

8.4.4 The hydraulic soil domains (overburden)

Sandy-gravelly till is overlying the bedrock in almost the whole area. The hilly areas are dominated by shallow/exposed rock (Quaternary deposit depth less than c. 0.5 m), where groundwater recharge occurs. Groundwater discharge is conceptualised to take place in the low-altitude “valley” type areas. The latter are characterised by thicker overburden, possibly as thick as 50 m, including, from bedrock surface; till, glacial clay, postglacial sand/gravel and postglacial clay, cf. Section 4.3.2.

Conceptualisation and description of the overburden, its variable stratification and assignment of hydraulic conductivity is given in Section 4.2.2 and /Rhén et al. 2009/ (based on /Werner et al. 2008/), respectively.

8.4.5 Palaeohydrogeological conceptual model

The palaeoclimatological and geological development during the Quaternary is described in Section 3.2. Essential components of the palaeohydrogeological development shown in this section are the shoreline displacement and the different stages of the Baltic Sea. As discussed in Section 3.4, the groundwater evolution in Laxemar is expected to have been influenced by these climate changes and development of the Baltic Sea. The SDM-Site Laxemar shore level curve, cf. Figure 3-7, is used to map out in detail the shoreline changes with time in the Laxemar-Simpevarp area, cf. Figure 8-24 for an illustration of the denser saline Littorina water intrusion along larger valleys, mixing with older glacial and brackish groundwater. The figure also illustrates that the greater part of the Laxemar-Simpevarp area (central and western parts at higher elevations) has been exposed to Meteoric groundwater since the latest glaciation. It can be stated that the post-glacial Meteoric water has been infiltrating successively larger areas and has mixed and flushed out older waters in

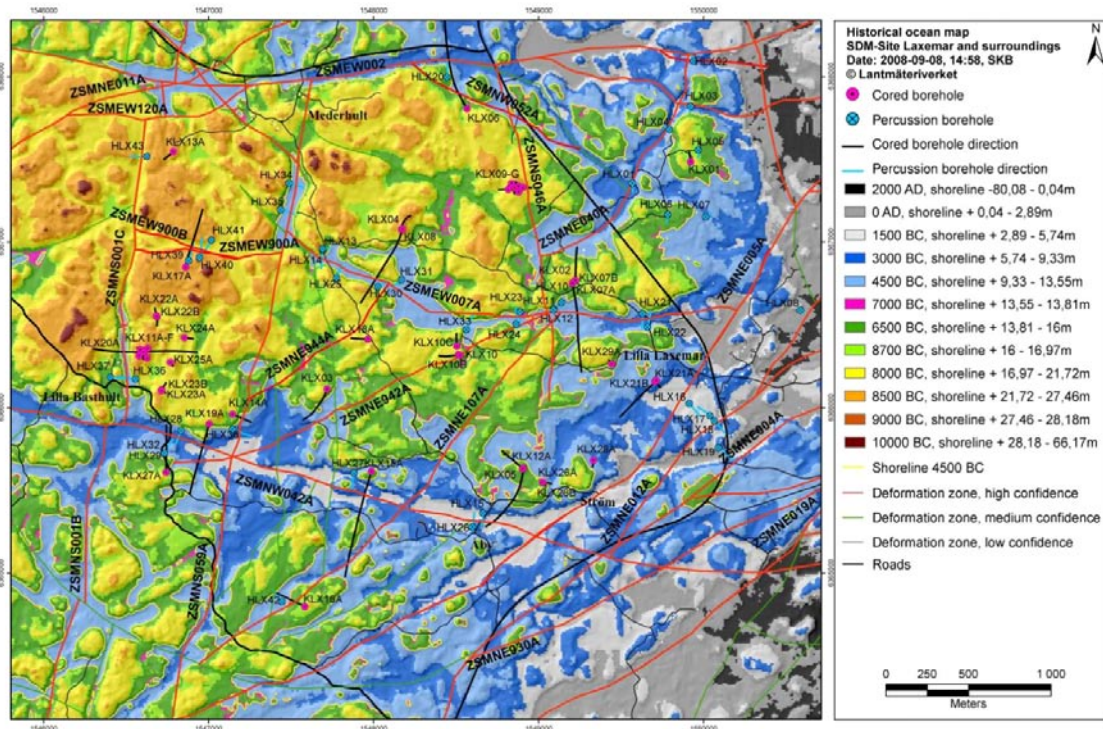


Figure 8-24. Shoreline changes in the Laxemar-Simpevarp area during the Littorina period (based on the SDM-Site Laxemar curve) -focus Laxemar local model area. The maximum salinity in the Baltic during the Littorina period occurred between 4500 BC and 3000 BC (Blue and grey areas indicate the coverage of the Littorina sea 4500–1500 BC) /Rhén et al. 2009/.

the upper part of the bedrock. The western part of the regional model area has never been exposed to Littorina sea water since it rose early above the sea, see /Rhén et al. 2009, cf. Chapter 4 therein/. However, some of the valleys in the west have an elevation indicating that Littorina water could have been present, but possibly the Littorina Sea water in such elongated coastal bays would have been diluted by freshwater provided by streams from the west.

Solute transport and reference waters

Coupled groundwater flow and solute transport is conceptualised in terms of the evolution of a number of groundwater constituents in order to understand the hydrochemical evolution in terms of the mixing of groundwaters of different origin. In the fracture water mixing takes place by the processes of advection, dispersion, diffusion (including rock matrix diffusion), while porewater composition is assumed to evolve only as a result of rock matrix diffusion. Groundwater composition is described in terms of mixtures of reference waters, consistent with the concept used for interpretation of hydrogeochemistry as described in Section 9.3. Fracture water is assumed to be a mixture of *Deep Saline Water*, *Glacial Melt Water*, *Littorina Sea Water* and *Altered Meteoric Water*. A fifth reference water is introduced in the palaeohydrogeological modelling, *Inter-glacial Porewater*, to illustrate some conceptual thinking on how the composition of the porewater may evolve in areas of the rock matrix remote from the connected flowing fracture system. This reference water is considered likely to be very old water residing primarily in the matrix composed of Meteoric and Brackish waters from periods before the Weichselian glaciation. Examples of such a reference water are considered to come from porewater samples obtained in rock of low fracture intensity found from about -400 m to -600 m elevation and below, and more than about 5 m from a water conducting fracture. Small proportions of *Inter-glacial Porewater* may enter the fractures by out-diffusion from the matrix giving a slight dilution of the 4 main fracture reference waters. The origin of this reference water is by its nature uncertain being subject to long-term transients – climate evolution and rock matrix diffusion. For the palaeohydrogeological modelling a base scenario is considered in which it is of freshwater Meteoric (Cl < 200 mg/L) type composition, with a more Brackish composition considered as a variant.

Palaeohydrogeological simulations start at 8000 BC at which time it is assumed that fracture and porewater is a mixture of *Deep Saline Water*, *Glacial Melt Water* and *Inter-glacial Porewater*, i.e. it enter the model via the definition of the initial condition. *Littorina Sea Water* and *Altered Meteoric Water* only enter the model via the boundary conditions that describe the evolution to the present-day. The numerical implementation of this development is described in Section 8.6.

8.5 Parameterisation of hydraulic conductor domains, and hydraulic rock domains

Here, the recommended parameterisation of the HCD and HRD for use in groundwater flow and solute modelling is described. The parameterisation of the hydraulic soil domains (HSD) is covered in Chapter 4.

8.5.1 Hydraulic conductor domains (HCD)

The Hydraulic Conductor Domains (HCD) are included in the flow model using their geometrical description provided by the Geology team and the hydraulic property assignment suggested in /Rhén et al. 2008/.

The majority of HCD are described by using generalised depth dependency relationships. The trend functions used are based on an exponential trend model:

$T=10^{(a+B*Z)}$, where Z is elevation in m (metres above sealevel).

The trend functions are assigned according to four main categories based on orientation and size according to Section 8.4.1. There are rather few HCD with several borehole intercepts down to c. 1,000 m depth such that a specific T versus depth trend function could be fitted (only 7, cf. /Rhén et al. 2008/). For the base case, transmissivity was assigned according to a depth trend defined for each HCD with no lateral heterogeneity (apart from some localised conditioning to measurement values).

The HCD are specified as surfaces defined by a set of points. For the purposes of the flow modelling, the HCD surfaces are triangulated based on an appropriate scale, 100 m was used. Transmissivity values were then associated with each triangle to represent the specified depth trend, or in the stochastic case, the transmissivities were sampled randomly from a log-normal distribution with a mean and standard deviation that varied with depth. The final step is to modify the transmissivities of any triangles within a specified distance of borehole intervals where a transmissivity has been interpreted. Again, a 100 m search radius was used around the measurement points. This process results in a discrete description of the HCD as triangulated surfaces, each with an assigned thickness, transmissivity (longitudinal and transverse), kinematic porosity and fracture surface area per unit volume, that may be used in either an ECPM or DFN flow model. For the ECPM approach used here, the ConnectFlow code, cf. Section 8.6.1, reads in each triangle, identifies which finite-elements are intersected by the HCD volume, and modifies the hydraulic properties accordingly to combine the background properties of the HRD with a representation of one or more HCD /see Marsic et al. 2001/).

The palaeohydrogeological simulations suggested that the HCD transmissivities reported in /Rhén et al. 2008/ should generally be reduced below -150 m. However, based on natural head measurements it was found that for a few specific HCD the transmissivity needed to be increased /Rhén et al. 2009/.

The distribution of the transmissivity in the HCD for the base case is shown in Figure 8-25 (for this case the standard deviation in $\text{Log}_{10}(T)$ is zero). For stochastic realisations with lateral heterogeneity, these values are used as the mean sampled value for a log-normal distribution with specified standard deviation, but truncated at ± 2 standard deviations. Equivalent plots for one example realisation of the HCD with spatial variability, standard deviation in $\text{Log}_{10}(T)=1.4$, is shown in Figure 8-26. In both cases, the heterogeneous transmissivity field is conditioned to measured values at the intercept with borehole intervals where measurements are available.

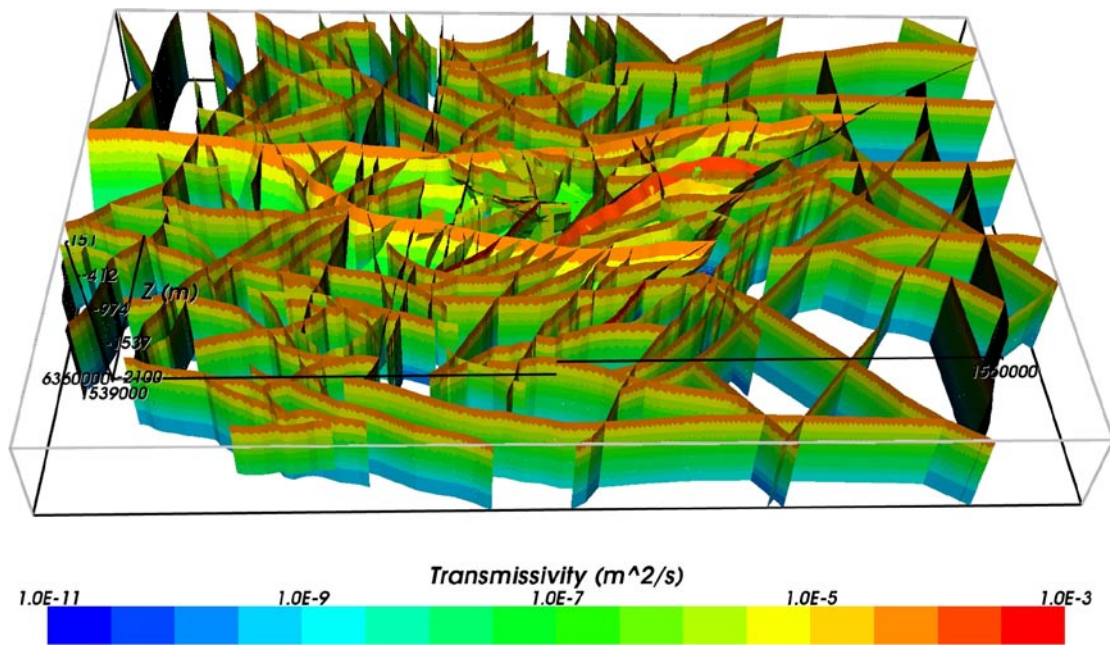


Figure 8-25. All HCD and their inferred depth dependent transmissivity. Here from an oblique view looking from the south. Regional model box in black for the groundwater flow simulations: 21x13 km² with bottom elevation at -2.3 km.

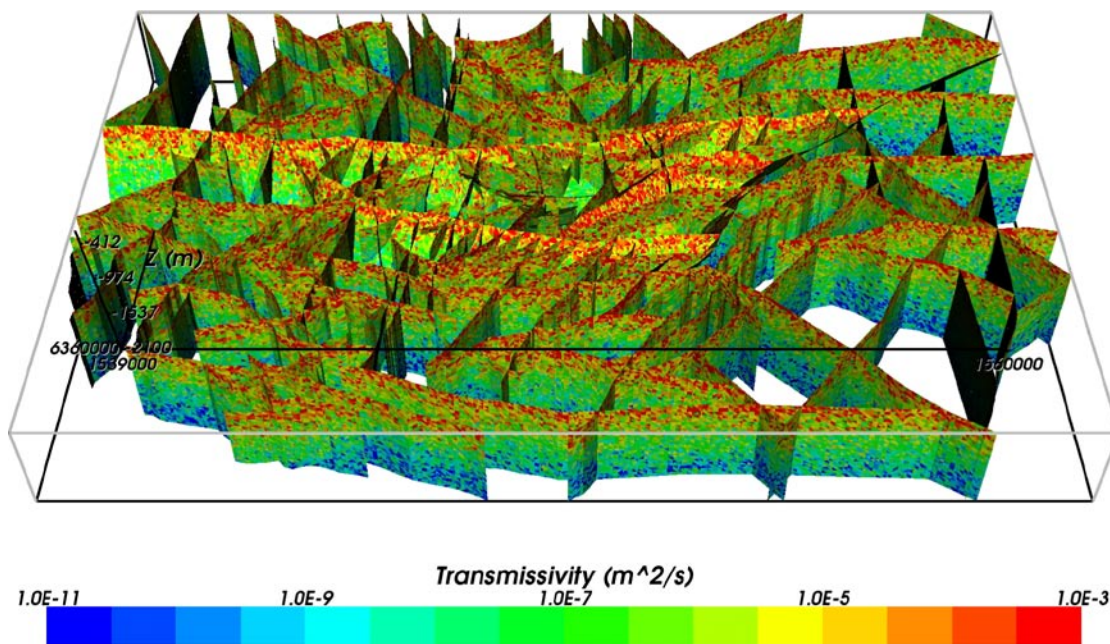


Figure 8-26. All HCD and their inferred depth dependent transmissivity for a case with spatial heterogeneity and a standard deviation in $\text{Log}_{10}(T)$ of 1.4. Here from an oblique view looking from the south. Regional model box in black for the groundwater flow simulations: 21x13 km² with bottom elevation at -2.3 km.

The transport properties; kinematic porosity and flow wetted surface area, a_r , are assigned to the deformation zones in the HCD model. There are measurements of the intensity of flowing features that could be used to estimate flow wetted surface for individual deformation zones and depth intervals. However, the uncertainties are large and a vast majority of the deformation zones have not been subject to measurement. The uncertainty in the kinematic porosity is probably even greater. Therefore, the chosen approach is to use the same generalised depth trends for these transport entities for all deformation zones.

Initially, the kinematic porosities, n_e , were calculated from $n_e = e_T/b_T$, using an interpreted HCD thickness b_T and transport aperture e_T , estimated from an empirical relationship with transmissivity, $e_T = a T^b$, where the constants a and b are obtained by fitting compiled results of tracer tests in crystalline rock /Rhén et al. 2008/. In the SDM-Site Laxemar hydrogeological flow modelling, a preliminary relation was used: $e_T = 0.705 T^{0.404}$ /Hjerne et al. 2009/, which compares with $e_T = 0.46 T^{0.5}$ /Dershowitz et al. 2003/ used in SDM-Site Forsmark. Typical transmissivities of the range 10^{-9} to 10^{-6} m²/s suggest that the values of transport aperture used in the hydrogeological flow modelling are 3–5 times higher than suggested by the formula used for Forsmark. This formulation for kinematic porosity is highly dependent on the interpreted transmissivity and thickness of zones. For the HRD, kinematic porosity was calculated based on the integrated fracture volume within a grid cell, and can be approximated by $n_e = e_t P_{10,corr,PFL}$, using the same relation between transport aperture and transmissivity for individual stochastic fractures. With this dependence on water-conducting fracture intensity used for the HRD, it was found that higher kinematic porosities were derived for the HRD than for the HCD, which is counter-intuitive. Since palaeohydrogeological simulations gave best results for higher kinematic porosities, the approach based on fracture intensity was used for both HCD and HRD. Since the corrected P_{10} values within HCD are about 3 times larger than for the HRD, the kinematic porosities for the HCD were based on typical kinematic porosities calculated for the HRD, multiplied by a factor of 3 giving a depth dependent kinematic porosity /Rhén et al. 2009, see Table 7-8 and Table 7-9 therein/.

The flow wetted surface area values were based on Terzaghi corrected P_{10} values obtained from PFL measurements /Rhén et al. 2008/. Hence, a_r is estimated by using the relationship $a_r = 2 \cdot P_{10,corr}(PFL-f)$.

8.5.2 Hydraulic Rock Domains (HRD)

The hydraulic rock domains are parameterised in terms of a stochastic DFN model, by calibration against available hydraulic data mainly from the PFL-tests. The hydrogeological DFN modelling is based on the assumption that:

$$P_{10,all} \geq P_{10,open} \geq P_{10,cof} \geq P_{10,PFL} \quad (8-4)$$

where $P_{10,cof}$ denotes the frequency of “connected open fractures”, a key property of any hydrogeological DFN model. The meaning of the different suffixes (*all*, *open*, *cof* and *PFL*) in Eq. (8-4) is explained in Figure 8-27.

To complete the parameterisation the following quantities are required; they are either estimated directly from the data or derived through the calibration process.

- The fracture surface area per unit volume of *open* fractures ($P_{32,open}$).
- The shape parameter k_r and the location parameter r_0 , assuming that the fracture size distribution follows a power-law distribution /Rhén et al. 2008/.
- The parameters relating transmissivity to fracture size. Three different kinds of correlations between fracture transmissivity and fracture size are considered as variants, as described in Table 8-5.

The hydrogeological DFN models allow the parameters described above to vary by fracture set, by depth zone and between different hydraulic rock domains.

The values of the power-law frequency distribution parameters (k_r and r_0) are not uniquely constrained by the methodology adopted and the data available. It is therefore necessary to consider several different combinations of parameters which allow the sensitivities to these parameters to be quantified in subsequent modelling. The combinations of the different parameters were based on the results reported in the preliminary SDM /SKB 2006a/.

A further uncertainty was how to identify the *open* (i.e. potential flowing) fractures in the data. In the base case, open fractures were assumed to correspond to any fracture classified as either open or partly open in the boreholes, and hence denoted ‘OPO’ fractures. A variant with a different classification of *open* fractures was used to assess this sensitivity, based on the restricted set of OPO fractures with either certain or probable classification during core mapping, and hence denoted ‘OPO-CP’ fractures. In short, four different combinations of values of the power-law frequency distribution parameters and $P_{32,open}$ were tested, cf. Figure 8-28.

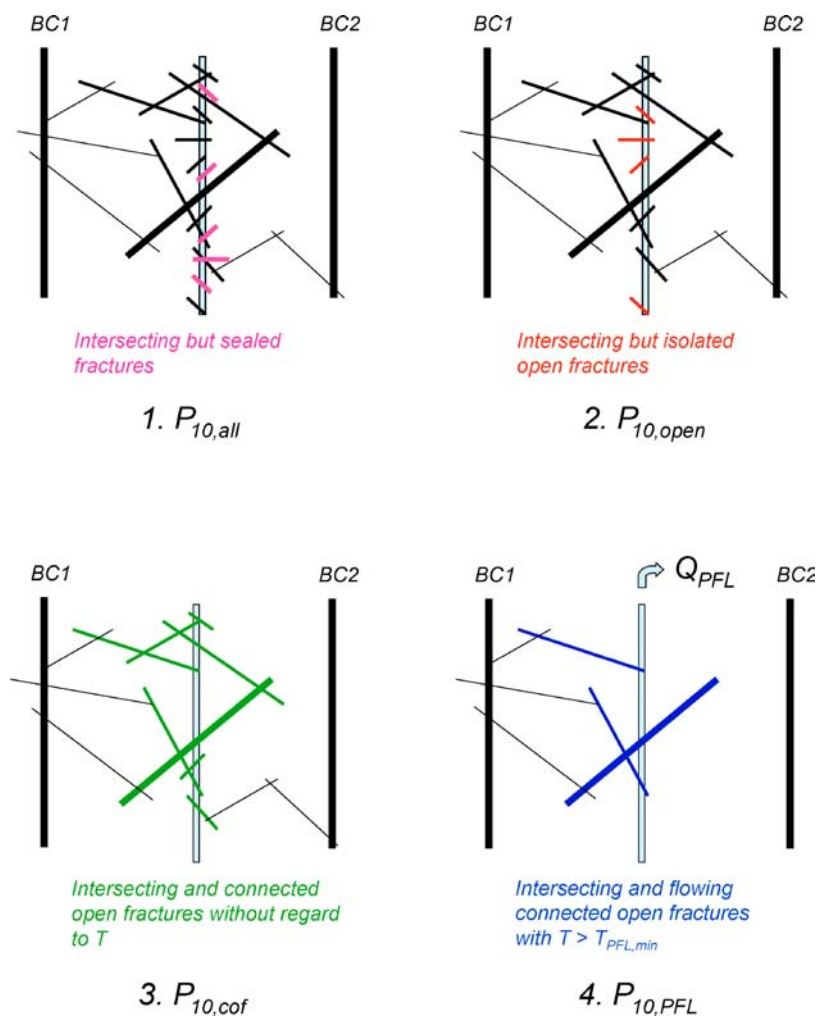


Figure 8-27. $P_{10,all}$ is the frequency of “all fractures” (sealed and open fractures) intersecting the borehole, $P_{10,open}$ is the frequency of “open fractures”, $P_{10,cof}$ is the frequency of “connected open fractures” and $P_{10,PFL}$ is the frequency of “flowing connected open fractures” identified with the PFL-f method. BC1 and BC2 represent hydraulic boundary conditions, e.g. the surface and/or nearby deformation zone which is connected to the surface. $P_{10,cof}$ cannot be measured but simulated values can be compared with the measured value of $P_{10,PFL}$.

Table 8-5. Transmissivity parameters used for all sets when matching measured PFL-f flow distributions. (Log base 10).

Type	Description	Relationship	Parameters
Correlated	Power-law relationship	$\log(T) = \log(a r^b)$	a, b
Semi-correlated	Log-normal distribution about a power-law correlated mean	$\log(T) = \log(a r^b) + \sigma_{\log(T)} N[0,1]$	$a, b, \sigma_{\log(T)}$
Uncorrelated	Log-normal distribution about a specified mean	$\log(T) = \mu_{\log(T)} + \sigma_{\log(T)} N[0,1]$	$\mu_{\log(T)}, \sigma_{\log(T)}$

The hydrogeological DFN simulations were repeated ten times (producing ten realisations) using the Monte Carlo method. For each HRD, a simulation model was constructed as a representative volume surrounding a notional vertical borehole with the volume sub-divided to 4 depth zones to represent the changes in fracture intensity and transmissivity with depth. For each of the variants considered, the hydrogeological DFN calibration was made in three stages:

- A check was made that the proposed DFN model could reproduce the measured intensity of *open* fractures in the boreholes. For each variant the fracture surface area per unit volume of rock, $P_{32,open}$ ($r \geq r_0$), was altered until a fair match between simulated and computed values of $P_{10,open,corr}$ was achieved, i.e.:

$$P_{32,open} \approx P_{10,open,corr} \quad (8-5)$$

- A connectivity calibration was made where the aim was to adjust the fracture size distribution parameters to obtain a match to the observed intensity of PFL-f features. This is a ‘fine-tuning’ of the power-law size parameters for each fracture set i to produce an accurate match between $P_{10,cof,corr}$ and $P_{10,PFL,corr}$, i.e.:

$$P_{10,cof,corr}^i \approx P_{10,PFL,corr}^i, \quad i \in (ENE, WNW, N-S, SubH) \quad (8-7)$$

- Flow simulations were carried out using three different kinds of relationships between fracture transmissivity and fracture size (see Table 8-5). These simulations used the power-law size parameters derived previously in the connectivity calibration.

Figure 8-28 shows the results of the connectivity calibration. Below -650 m elevation, the models predict very low mean connected open fracture intensities, but do not reproduce the zeros (no-flows) observed in the data for the N-S fracture set. Partly this is to be expected since a stochastic approach is being used and some realisations happen to have a small number of connected fractures intersecting the borehole. One way of reconciling the hydrogeological DFN model is to consider a depth variation in the hydraulic properties, such that fractures below -650 m elevation have a lower fracture transmissivity as well as intensity, chosen so that a number of the fractures simulated below -650 m elevation have transmissivities below the detection limit for the PFL-f method. This approach was adopted in the subsequent flow modelling.

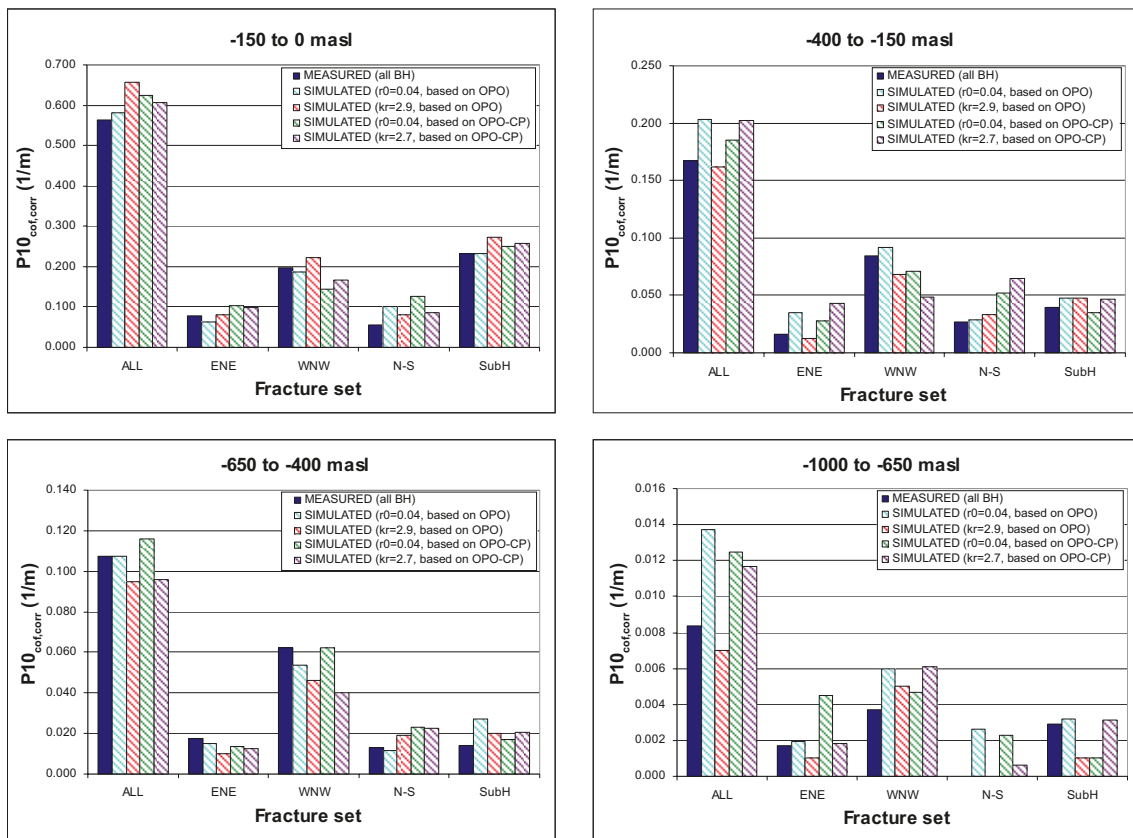


Figure 8-28. Comparison of the Terzaghi corrected connected open fracture intensities, $P_{10,cof,corr}$, for the individual fracture sets with the measured fracture intensities for PFL-anomalies for HRD_C. Four alternative geometrical fracture models were considered: k_r fixed with r_0 varying or r_0 fixed with k_r varying, and fracture intensity based on all open fractures (OPO); r_0 fixed with k_r varying or r_0 fixed with k_r varying, and fracture intensity based only fractures characterised as open with high certainty (OPO-CP).

Figure 8-29 shows plots of the fracture intensities of *all* fractures (taken from the geological DFN model), *open* fractures and *connected open fractures* as calculated in the connectivity analysis for HRD_C. The green lines represent the k_r -scaled (or r_0 fixed) model discussed in the geological DFN modelling and are based on the corrected linear borehole intensity of *all* fractures in the analysed boreholes $P_{10,all,corr}$. The red lines represent the k_r -scaled model used in the hydrogeological DFN modelling and are based on borehole intensity of *open* fractures $P_{10,open,corr}$. The blue lines represent the intensity of *connected open fractures* $P_{10,cof,corr}$ simulated in ten realisations of the hydrogeological DFN model. The parameter r_0 is set to the scale of observation, i.e. the borehole radius (0.038 m) and r_1 is set to 564.2 m ($L = 1,000$ m). Discrete features above this size are modelled deterministically in SKB's systems approach. Figure 8-29 confirms the expected consistency between the geological and hydrogeological k_r -scaled models, with a higher intensity of *all* fractures versus *open* fractures at all length scales, cf. Eq. (8-4). The curves representing the hydrogeological DFN honour the observed variation with depth of the total intensity of *open* and *PFL* fractures. This depth variation is not observed in the intensity of *all* fractures, which is the reason why there is only a single model representing the geological DFN. Interestingly, for the sparsely fractured rock at depths below about -150 m such distributions of intensity versus size for connected open fractures tend to be similar for each of the parameter variants considered in Figure 8-28. This is significant since it indicates that, despite the uncertainty in basic input, such as open fracture intensity and size distributions, the possible distributions of connected open fractures are constrained by the connectivity calibration, and hence giving some robustness in the resulting hydrogeological DFN models.

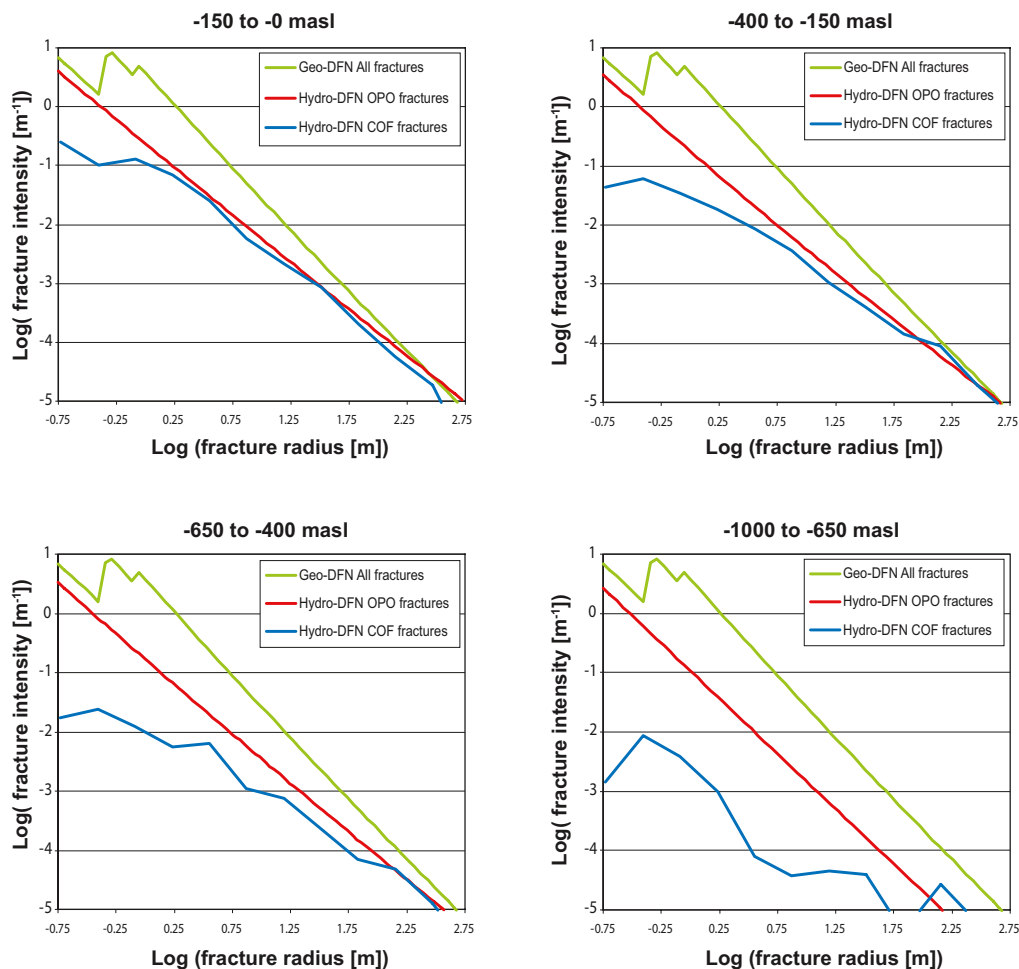


Figure 8-29. Comparison of the distributions of fracture intensity, P_{32} , with fracture size for 'all' fractures (as predicted by the geological DFN in green), that for 'open' fractures (as predicted by the hydrogeological DFN, OPO case, shown in red), and that for simulated 'connected open fractures' using the hydrogeological DFN connectivity analysis (shown in blue). Note that the jagged part of the geological DFN size distribution reflects the use of different r_0 parameters for each set.

To complete the hydrogeological DFN parameterisation, flow simulations were performed to calibrate a set of alternative relationships between fracture transmissivity and size that reproduced the numbers of inflows and the distribution of their magnitude as measured with the PFL-f tests. An example of a flow simulation is shown in Figure 8-30. The model configuration has zero head imposed on the vertical sides and top, a uniform 10 m drawdown in the vertical borehole, and hence there is an inflow at every fracture intersection with borehole. Only combinations of parameter values for open fracture intensity and power-law size distributions derived during the connectivity calibration step were considered in the flow modelling.

Three alternative relationships between fracture transmissivity and size were studied: direct correlation, semi-correlation and no correlation (see Table 8-5). By semi-correlation it was implied that the mean transmissivity of a fracture increases with its size, but there is a superimposed random component or spread of values for any given fracture size. This is perhaps the most realistic situation. Hence, in the flow calibration, the aim was to establish appropriate choices for the parameters for each relationship between fracture size and transmissivity that gives a match to the magnitude of the inflows. Four main calibration targets were used to quantify how well the model simulates the data:

- A histogram of the distribution of PFL-f specific flow-rates, Q/s , was compared using a bin size of half an order of magnitude.
- A histogram of the distribution of PSS (5 m scale) specific flow-rates, Q/s , within elevation -400 to -650 m, was compared using a bin size of half an order of magnitude.
- The total specific flow to the borehole, sum of PFL-f specific flow Q/s (calculated as an arithmetic average over the realisations).
- The specific inflow to 100 m borehole intervals for PFL-f and PSS (100 m scale) (calculated as a geometric mean over the realisations).
- The numbers of PFL-anomalies associated with each fracture set and the distribution of Q/s , for each set. This distribution is quantified in terms of the mean, plus/minus one standard deviation, minimum and maximum of $\text{Log}(Q/s)$.

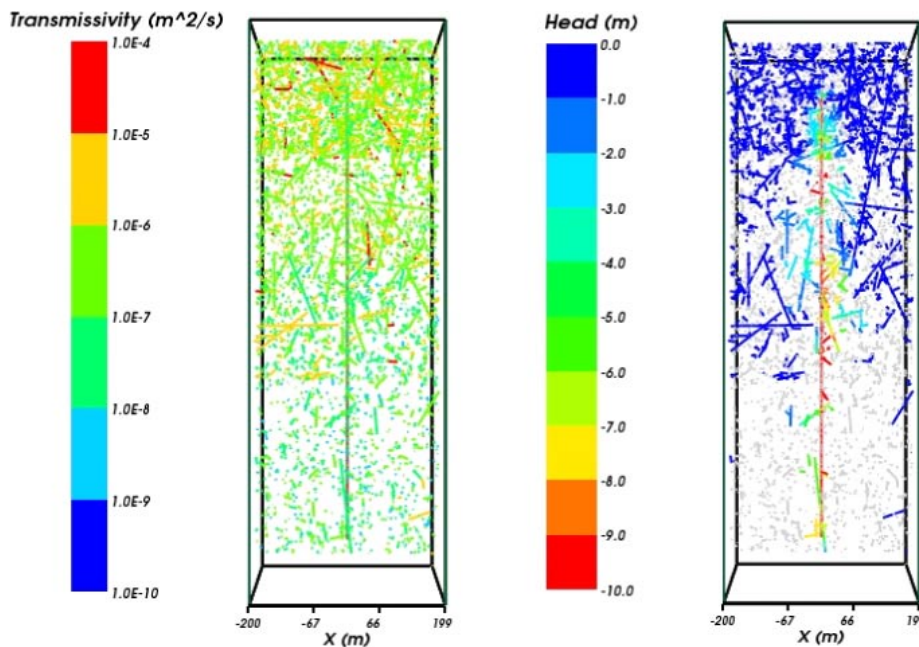


Figure 8-30. Vertical cross-section through one realisation of the hydrogeological DFN model of HRD C. Left: All open fractures coloured by transmissivity. The 1 km generic vertical borehole is in the middle of the figure. This figure indicates how the parameterisation changes the fracture intensity, fracture size, and fracture transmissivity with depth. Right: The connected open fractures coloured by drawdown with unconnected fractures coloured grey.

The resulting hydrogeological DFN parameterisations for HRD_C, HRD_W and HRD_EW007 are given in Table 8-6 to Table 8-8. The coefficients, exponents or standard deviations as appropriate to each transmissivity model reflect the rapid reduction in inflow magnitudes with depth observed in the PFL-f measurements.

Table 8-6. Description of the calibrated hydrogeological DFN input parameters for HRD_C with fixed $r_0=0.038$ m and intensity of open fractures based on OPO. (Orientation model, cf. Section 5.6.3).

Depth zone (m.a.s.l.)	Set	Orientation set pole: (trend, plunge), conc.	Fracture radius model power-law (k_r, r_0)	Intensity P_{32} (m^2/m^3) of open fractures	Transmissivity model T (m^2/s)
-150 to 0	ENE	(155.1,3.4), 9.6	(2.6, 0.038)	0.52	SC: ($6 \cdot 10^{-8}$, 0.5, 0.4) UC: ($2 \cdot 10^{-7}$, 0.6) C: ($2 \cdot 10^{-8}$, 0.9)
	WNW	(204,1.6), 12	(2.5, 0.038)	0.95	SC: ($2 \cdot 10^{-7}$, 0.6, 0.7) UC: ($1 \cdot 10^{-5}$, 0.9) C: ($5 \cdot 10^{-8}$, 1.1)
	N-S	(270.2,8.4), 7.8	(2.7, 0.038)	0.54	SC: ($2 \cdot 10^{-7}$, 0.6, 0.5) UC: ($1 \cdot 10^{-7}$, 0.7) C: ($6 \cdot 10^{-8}$, 1.2)
	SubH	(46.3,84.7), 12	(2.7, 0.038)	1.20	SC: ($1.5 \cdot 10^{-7}$, 0.7, 0.7) UC: ($3 \cdot 10^{-7}$, 0.8) C: ($6 \cdot 10^{-8}$, 1.0)
-400 to -150	ENE	(155.1,3.4), 9.6	(2.85, 0.038)	0.47	SC: ($1 \cdot 10^{-6}$, 0.7, 0.7) UC: ($2 \cdot 10^{-7}$, 0.7) C: ($5 \cdot 10^{-8}$, 1.4)
	WNW	(204,1.6), 12	(2.45, 0.038)	0.55	SC: ($8 \cdot 10^{-8}$, 0.3, 0.1) UC: ($3 \cdot 10^{-7}$, 0.6) C: ($2 \cdot 10^{-9}$, 1.3)
	N-S	(270.2,8.4), 7.8	(2.85, 0.038)	0.63	SC: ($1 \cdot 10^{-7}$, 0.7, 0.7) UC: ($2 \cdot 10^{-7}$, 0.4) C: ($3 \cdot 10^{-8}$, 1.0)
	SubH	(46.3,84.7), 12	(2.85, 0.038)	0.71	SC: ($1.5 \cdot 10^{-7}$, 0.8, 0.9) UC: ($8 \cdot 10^{-7}$, 1.4) C: ($3 \cdot 10^{-8}$, 1.1)
-650 to -400	ENE	(155.1,3.4), 9.6	(2.8, 0.038)	0.38	SC: ($5 \cdot 10^{-7}$, 0.5, 0.5) UC: ($2 \cdot 10^{-6}$, 0.8) C: ($3 \cdot 10^{-8}$, 0.7)
	WNW	(204,1.6), 12	(2.5, 0.038)	0.74	SC: ($2 \cdot 10^{-8}$, 0.6, 0.4) UC: ($1 \cdot 10^{-7}$, 0.9) C: ($3 \cdot 10^{-9}$, 0.9)
	N-S	(270.2,8.4), 7.8	(2.9, 0.038)	0.47	SC: ($1 \cdot 10^{-8}$, 0.4, 0.4) UC: ($8 \cdot 10^{-8}$, 0.4) C: ($1 \cdot 10^{-8}$, 0.5)
	SubH	(46.3,84.7), 12	(2.9, 0.038)	0.58	SC: ($3 \cdot 10^{-7}$, 0.6, 0.6) UC: ($2 \cdot 10^{-6}$, 0.9) C: ($1.5 \cdot 10^{-7}$, 0.9)
-1,000 to -650	ENE	(155.1,3.4), 9.6	(2.9, 0.038)	0.46	SC: ($5 \cdot 10^{-9}$, 0.6, 0.4) UC: ($1 \cdot 10^{-8}$, 0.4) C: ($5 \cdot 10^{-9}$, 0.6)
	WNW	(204,1.6), 12	(2.8, 0.038)	0.73	SC: ($5 \cdot 10^{-8}$, 0.6, 0.4) UC: ($5 \cdot 10^{-7}$, 0.4) C: ($5 \cdot 10^{-8}$, 0.6)
	N-S	(270.2,8.4), 7.8	(2.95, 0.038)	0.25	SC: ($5 \cdot 10^{-9}$, 0.6, 0.4) UC: ($1 \cdot 10^{-8}$, 0.4) C: ($5 \cdot 10^{-9}$, 0.6)
	SubH	(46.3,84.7), 12	(2.95, 0.038)	0.35	SC: ($1 \cdot 10^{-7}$, 0.6, 0.4) UC: ($2 \cdot 10^{-7}$, 0.4) C: ($1 \cdot 10^{-7}$, 0.6)

Table 8-7. Description of the calibrated hydrogeological DFN input parameters for HRD_W with fixed $r_0=0.038$ m and open fracture intensity based on OPO. (Orientation model, cf. Section 5.6.3).

Depth zone (m.a.s.l.)	Set	Orientation set pole: (trend, plunge), conc.	Fracture radius model power-law (k_r, r_0)	Intensity P_{32} (m^2/m^3) of open fractures	Transmissivity model T (m^2/s)
-150 to 0	ENE	(340.3,1.2), 15	(2.65, 0.038)	0.44	SC: ($5 \cdot 10^{-8}$, 0.7, 0.7) UC: ($8 \cdot 10^{-8}$, 1.1) C: ($4 \cdot 10^{-8}$, 1.2)
	WNW	(208.9,2.2), 10.9	(2.5, 0.038)	0.61	SC: ($1 \cdot 10^{-7}$, 0.8, 0.6) UC: ($6 \cdot 10^{-7}$, 1.1) C: ($3 \cdot 10^{-8}$, 1.3)
	N-S	(272.8,12), 11.5	(2.65, 0.038)	0.54	SC: ($1.5 \cdot 10^{-7}$, 0.7, 0.7) UC: ($4 \cdot 10^{-7}$, 1.0) C: ($2 \cdot 10^{-8}$, 1.0)
	SubH	(277.1,84.3), 11.1	(2.55, 0.038)	1.03	SC: ($1.5 \cdot 10^{-7}$, 0.7, 0.9) UC: ($1 \cdot 10^{-6}$, 0.9) C: ($1.5 \cdot 10^{-7}$, 1.0)
-400 to -150	ENE	(340.3,1.2), 15	(2.65, 0.038)	0.28	SC: ($1 \cdot 10^{-7}$, 0.5, 0.2) UC: ($1 \cdot 10^{-6}$, 0.4) C: ($3 \cdot 10^{-7}$, 0.5)
	WNW	(208.9,2.2), 10.9	(2.5, 0.038)	0.38	SC: ($3 \cdot 10^{-7}$, 0.5, 0.6) UC: ($6 \cdot 10^{-7}$, 0.8) C: ($1 \cdot 10^{-8}$, 1.0)
	N-S	(272.8,12), 11.5	(2.9, 0.038)	0.40	SC: ($1 \cdot 10^{-8}$, 0.5, 0.5) UC: ($1 \cdot 10^{-8}$, 0.5) C: ($2 \cdot 10^{-9}$, 0.5)
	SubH	(277.1,84.3), 11.1	(2.7, 0.038)	0.50	SC: ($1 \cdot 10^{-7}$, 0.7, 1.0) UC: ($1.5 \cdot 10^{-6}$, 1.4) C: ($8 \cdot 10^{-8}$, 1.2)
-650 to -400	ENE	(340.3,1.2), 15	(2.8, 0.038)	0.17	SC: ($3 \cdot 10^{-9}$, 0.6, 0.5) UC: ($2 \cdot 10^{-9}$, 0.5) C: ($1 \cdot 10^{-9}$, 0.6)
	WNW	(208.9,2.2), 10.9	(2.55, 0.038)	0.33	SC: ($3 \cdot 10^{-8}$, 0.6, 0.5) UC: ($2 \cdot 10^{-7}$, 0.3) C: ($2 \cdot 10^{-8}$, 0.7)
	N-S	(272.8,12), 11.5	(2.55, 0.038)	0.30	SC: ($3 \cdot 10^{-8}$, 0.4, 0.4) UC: ($2 \cdot 10^{-7}$, 0.3) C: ($1 \cdot 10^{-8}$, 0.6)
	SubH	(277.1,84.3), 11.1	(2.65, 0.038)	0.38	SC: ($5 \cdot 10^{-7}$, 0.4, 1.0) UC: ($1.5 \cdot 10^{-6}$, 1.2) C: ($1.2 \cdot 10^{-7}$, 1.2)
-1,000 to -650	ENE	(340.3,1.2), 15.0	(2.9, 0.038)	0.12	SC: ($5 \cdot 10^{-9}$, 0.6, 0.4) UC: ($1 \cdot 10^{-8}$, 0.6) C: ($5 \cdot 10^{-9}$, 0.6)
	WNW	(208.9,2.2), 10.9	(2.8, 0.038)	0.09	SC: ($5 \cdot 10^{-8}$, 0.6, 0.4) UC: ($5 \cdot 10^{-8}$, 0.6) C: ($5 \cdot 10^{-8}$, 0.6)
	N-S	(272.8,12), 11.5	(2.95, 0.038)	0.14	SC: ($5 \cdot 10^{-9}$, 0.6, 0.4) UC: ($1 \cdot 10^{-8}$, 0.6) C: ($5 \cdot 10^{-9}$, 0.6)
	SubH	(277.1,84.3), 11.1	(2.95, 0.038)	0.65	SC: ($1 \cdot 10^{-7}$, 0.6, 0.4) UC: ($8 \cdot 10^{-7}$, 0.6) C: ($1 \cdot 10^{-7}$, 0.6)

Table 8-8. Description of the calibrated hydrogeological DFN input parameters for HRD_EW007 with fixed $r_0=0.038$ m and open fracture intensity based on OPO. (Orientation model, cf. Section 5.6.3).

Depth zone (m.a.s.l.)	Set	Orientation set pole: (trend, plunge), conc.	Fracture radius model power-law (k_r , r_0)	Intensity P_{32} (m^2/m^3) of open fractures	Transmissivity model T (m^2/s)
-150 to 0	ENE	(162.8,1.4), 10.7	(2.70, 0.038)	0.55	SC: ($1 \cdot 10^{-7}$, 0.4, 0.4) UC: ($3 \cdot 10^{-7}$, 0.6) C: ($1 \cdot 10^{-7}$, 0.4)
	WNW	(25.3,0.2), 16.4	(2.3, 0.038)	1.01	SC: ($1 \cdot 10^{-7}$, 0.4, 0.4) UC: ($3 \cdot 10^{-7}$, 0.6) C: ($1 \cdot 10^{-7}$, 0.4)
	N-S	(88.9,3.9), 8.8	(2.65, 0.038)	0.33	SC: ($1 \cdot 10^{-6}$, 0.4, 0.4) UC: ($3 \cdot 10^{-6}$, 0.6) C: ($1 \cdot 10^{-6}$, 0.4)
	SubH	(138.7,81.3), 9.7	(2.75, 0.038)	1.72	SC: ($3 \cdot 10^{-7}$, 0.5, 0.5) UC: ($1.5 \cdot 10^{-6}$, 0.7) C: ($1.5 \cdot 10^{-7}$, 0.8)
-400 to -150	ENE	(162.8,1.4), 10.7	(2.8, 0.038)	0.60	SC: ($6 \cdot 10^{-8}$, 0.6, 0.6) UC: ($1 \cdot 10^{-6}$, 0.9) C: ($6 \cdot 10^{-8}$, 0.8)
	WNW	(25.3,0.2), 16.4	(2.35, 0.038)	1.15	SC: ($2 \cdot 10^{-8}$, 0.6, 0.6) UC: ($8 \cdot 10^{-8}$, 0.8) C: ($2 \cdot 10^{-8}$, 0.6)
	N-S	(88.9,3.9), 8.8	(2.6, 0.038)	0.54	SC: ($1.5 \cdot 10^{-7}$, 0.7, 0.7) UC: ($2 \cdot 10^{-6}$, 1.1) C: ($1.5 \cdot 10^{-7}$, 0.9)
	SubH	(138.7,81.3), 9.7	(2.8, 0.038)	0.82	SC: ($8 \cdot 10^{-8}$, 0.7, 0.9) UC: ($2 \cdot 10^{-7}$, 1.1) C: ($8 \cdot 10^{-8}$, 0.7)
-650 to -400	ENE	(162.8,1.4), 10.7	(2.95, 0.038)	0.69	SC: ($3 \cdot 10^{-8}$, 0.4, 0.4) UC: ($3 \cdot 10^{-8}$, 0.6) C: ($3 \cdot 10^{-8}$, 0.4)
	WNW	(25.3,0.2), 16.4	(2.50, 0.038)	1.43	SC: ($1 \cdot 10^{-7}$, 0.3, 0.3) UC: ($2 \cdot 10^{-7}$, 0.5) C: ($1 \cdot 10^{-7}$, 0.3)
	N-S	(88.9,3.9), 8.8	(2.95, 0.038)	0.64	SC: ($3 \cdot 10^{-7}$, 0.4, 0.4) UC: ($1 \cdot 10^{-6}$, 0.6) C: ($3 \cdot 10^{-7}$, 0.4)
	SubH	(138.7,81.3), 9.7	(2.95, 0.038)	0.92	SC: ($3 \cdot 10^{-8}$, 0.6, 0.4) UC: ($1 \cdot 10^{-7}$, 0.8) C: ($3 \cdot 10^{-8}$, 0.6)
-1,000 to -650	ENE	(162.8,1.4), 10.7	(2.9, 0.038)	0.33	SC: ($5 \cdot 10^{-9}$, 0.6, 0.4) UC: ($1 \cdot 10^{-8}$, 0.6) C: ($5 \cdot 10^{-9}$, 0.6)
	WNW	(25.3,0.2), 16.4	(2.8, 0.038)	0.89	SC: ($5 \cdot 10^{-8}$, 0.6, 0.4) UC: ($5 \cdot 10^{-8}$, 0.6) C: ($5 \cdot 10^{-8}$, 0.6)
	N-S	(88.9,3.9), 8.8	(2.95, 0.038)	0.21	SC: ($5 \cdot 10^{-9}$, 0.6, 0.4) UC: ($1 \cdot 10^{-8}$, 0.6) C: ($5 \cdot 10^{-9}$, 0.6)
	SubH	(138.7,81.3), 9.7	(2.95, 0.038)	0.80	SC: ($1 \cdot 10^{-7}$, 0.6, 0.4) UC: ($8 \cdot 10^{-7}$, 0.6) C: ($1 \cdot 10^{-7}$, 0.6)

An example of the comparison of inflows between model and data for HRD_C is given for the model using a semi-correlation between fracture size and transmissivity (Figure 8-31 to Figure 8-35). The match to the observed flow is poorest for the deepest depth zone (below –650 m elevation). However it should be noted that there are very few fractures carrying flow at this depth, so the distributions of PFL-f data or flows are not very well defined. Figure 8-35 shows bar and whisker plots that compare the measured and simulated inflows for the different fracture sets, normalised to appropriate borehole length sections. The numbers alongside the bars represent the Terzaghi weighted numbers of inflows above the detection limit per borehole section. Figure 8-35 shows that the inflows are dominated by the WNW and SubH fracture sets with a small contribution from the ENE set.

The matches for all three transmissivity models are reasonable above –650 m. The most significant difference in hydraulic characteristics between these 3 cases comes in the scale dependence of hydraulic conductivity, where the uncorrelated model has the least dependence. Considering the PSS measurement scale statistics (for 5, 20 and 100 m) (cf. /Rhén et al. 2008/), the uncorrelated model has less consistency with observations. It also predicts a factor 3 times higher kinematic porosity. An additional check on the plausibility of the chosen transmissivity parameters was to calculate the maximum transmissivity that could be generated for a stochastic fracture (<564.2 m radius) and make sure this did not greatly exceed the maximum transmissivity measured in the deterministically interpreted deformation zones (HCD). This was satisfied for all HRD and variants and ensures that when the hydrogeological DFN model is applied on the regional scale no anomalously high transmissivities are generated compared with field data.

To illustrate how the different transmissivity-size relationships compare they are plotted as log-log plots for the SubH set in HRD_C, cf Figure 8-36, based on the parameters given in Table 8-6. The semi-correlated and correlated models follow similar trends and also intercept the uncorrelated model for fractures of about 10 m radius. This is to be expected since fractures around 10–100 m form the body of the water-conducting network that gives the inflows in the simulations. There is less consistency between the transmissivity models below –650 m elevation as the distribution of inflows is poorly determined at these depths, there being so few data points to guide the calibration.

The similarity between the transmissivities for 10–100 m size fractures and the simulated inflow statistics for the different transmissivity relations (cf. /Rhén et al. 2008/) constitutes another illustration of the robustness of the hydrogeological DFN that comes from the model calibration steps, in this case the matching to inflow data. A further example of the stability of the flow characteristics predicted by the hydrogeological DFN is the consistency of upscaled hydraulic conductivities for 100 m blocks derived for each of the model variants considered (cf. /Rhén et al. 2008/).

Figure 8-37 shows an example of a realisation of the regional hydrogeological DFN model. The realisation is shown as 2 vertical cross-sections with only the connected open fractures and HCD displayed. The effect of the low connectivity below –650 m elevation is apparent, as is the higher fracture intensity associated with HRD_EW007 beneath KLX08 shown in the N-S section.

The definition of transport aperture for single fractures is part of the hydrogeological DFN and uses the same empirical function as used for the HCD, i.e. $e_i = 0.705 T^{0.404}$. The kinematic porosity used in the ECPM models can be calculated within a grid cell by summing up the area of water conducting fractures multiplied by transport aperture and dividing by the volume of the grid element.

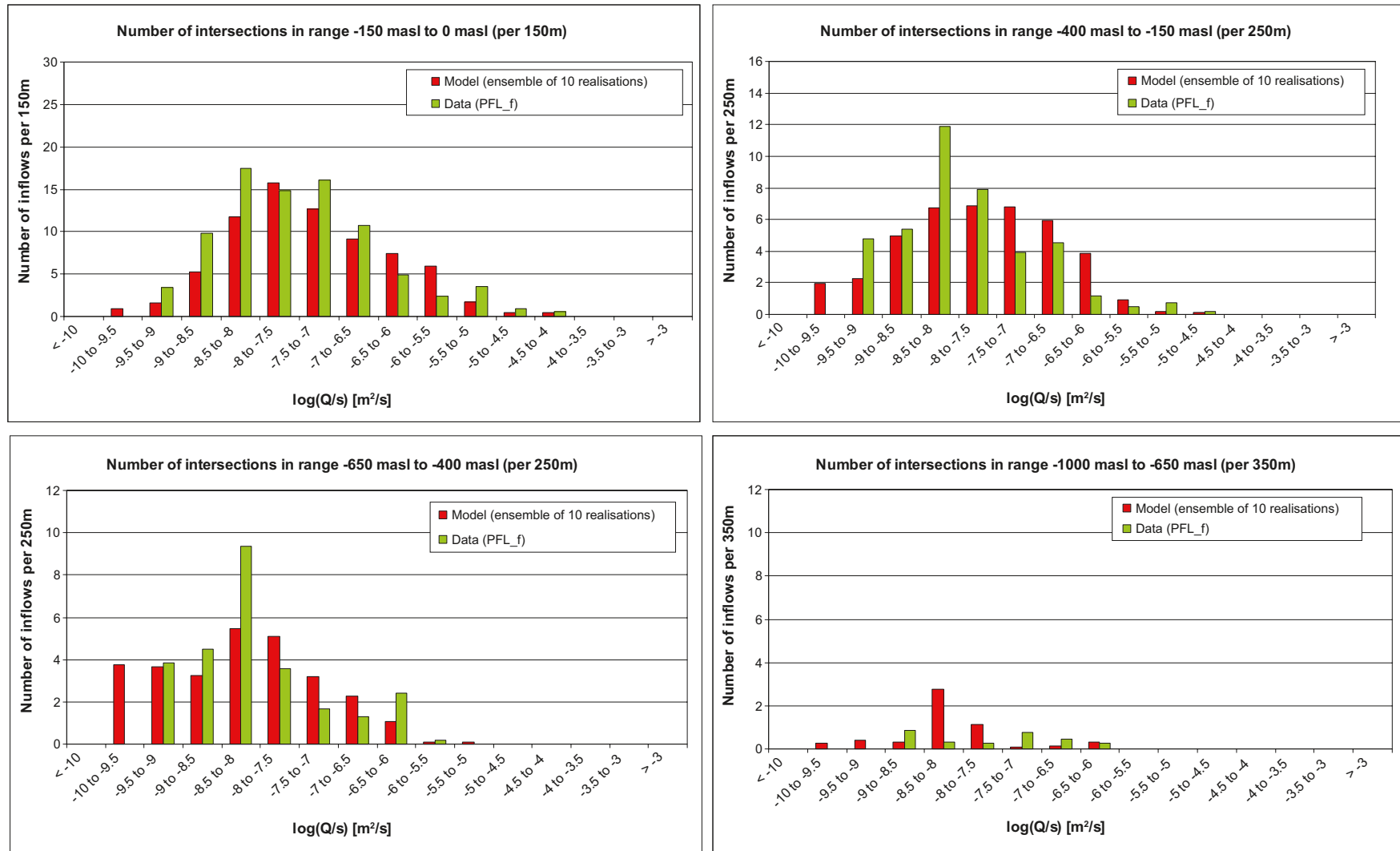


Figure 8-31. Histogram comparing the distribution of the magnitude of inflows divided by drawdown, Q/s , at abstraction boreholes in HRD_C. The model has a semi-correlated transmissivity, with r_0 fixed and open fracture intensity based on OPO fractures (see Table 8-6 for parameter values). The PFL-f measurements are treated as ensemble over all boreholes sections within HRD_C. The simulations represent the combined results of 10 realisations of the hydrogeological DFN model. The numbers of intersections are Terzaghi weighted and normalised to the length of borehole which is provided in the heading of each graph and have been Terzaghi corrected.

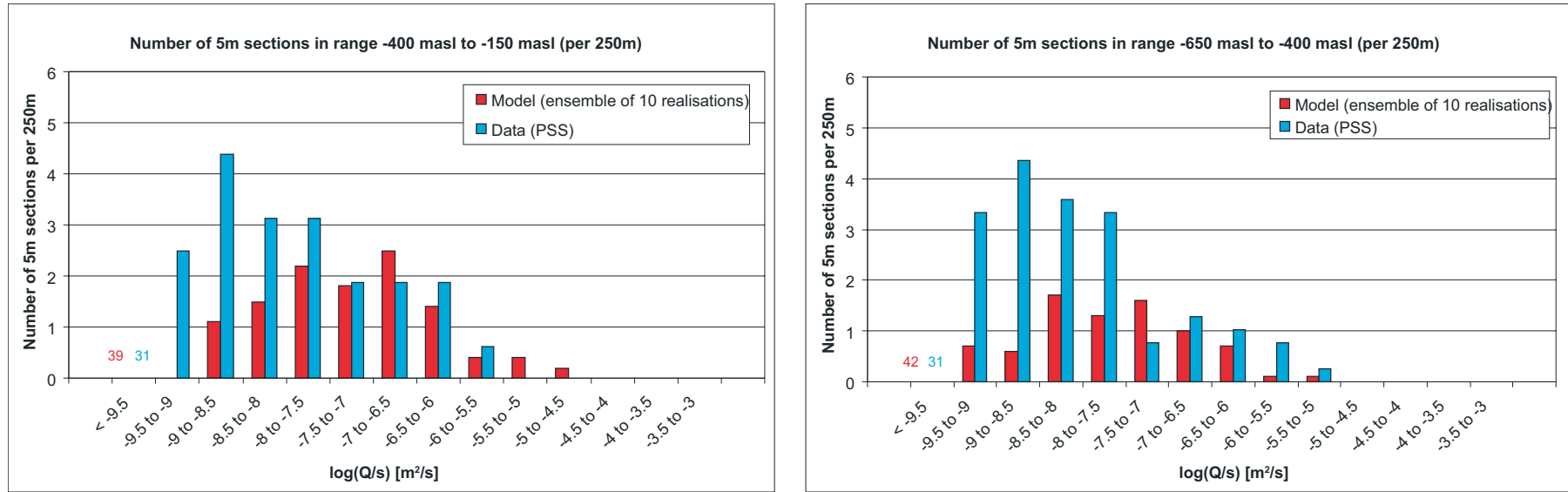


Figure 8-32. Histogram comparing the distribution of the magnitude of inflows divided by drawdown, Q/s , in 5 m sections at abstraction boreholes in HRD_C. The model has a semi-correlated transmissivity, with r_0 fixed and open fracture intensity based on OPO fractures. The PSS measurements are treated as ensemble over all boreholes sections within HRD_C. The simulations represent the combined results of 10 realisations of the hydrogeological DFN model. The numbers of intersections are normalised to the length of borehole which is provided in the heading of each graph.

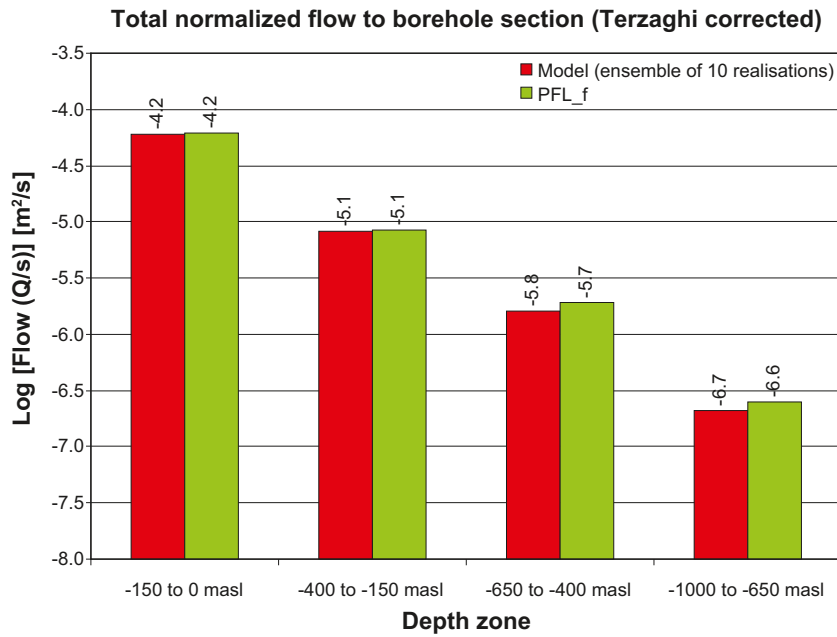


Figure 8-33. Comparison of the sum of individual flows, Q/s , for the PFL-f data from borehole sections within HRD_C against the hydrogeological DFN model. The model has a semi-correlated transmissivity, with r_0 fixed and open fracture intensity based on OPO fractures. For the model, the arithmetic mean is taken over 10 realisations. The flows are Terzaghi weighted and normalized to the borehole length indicated by the range on the horizontal axis.

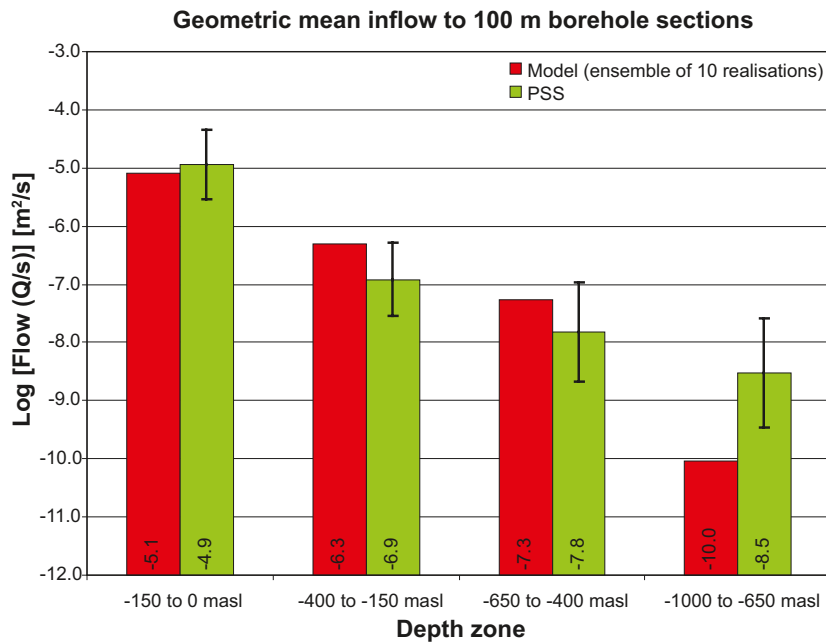


Figure 8-34. Comparison of the geometric mean of total flows, Q/s , to 100 m borehole intervals for the PSS data from borehole sections within HRD_C against the hydrogeological DFN model. The model has a semi-correlated transmissivity, with r_0 fixed and open fracture intensity based on OPO fractures. For the data, the geometric mean is shown as well as the 95% confidence interval in the mean. For the model, the mean value of total flow is taken over 10 realisations.

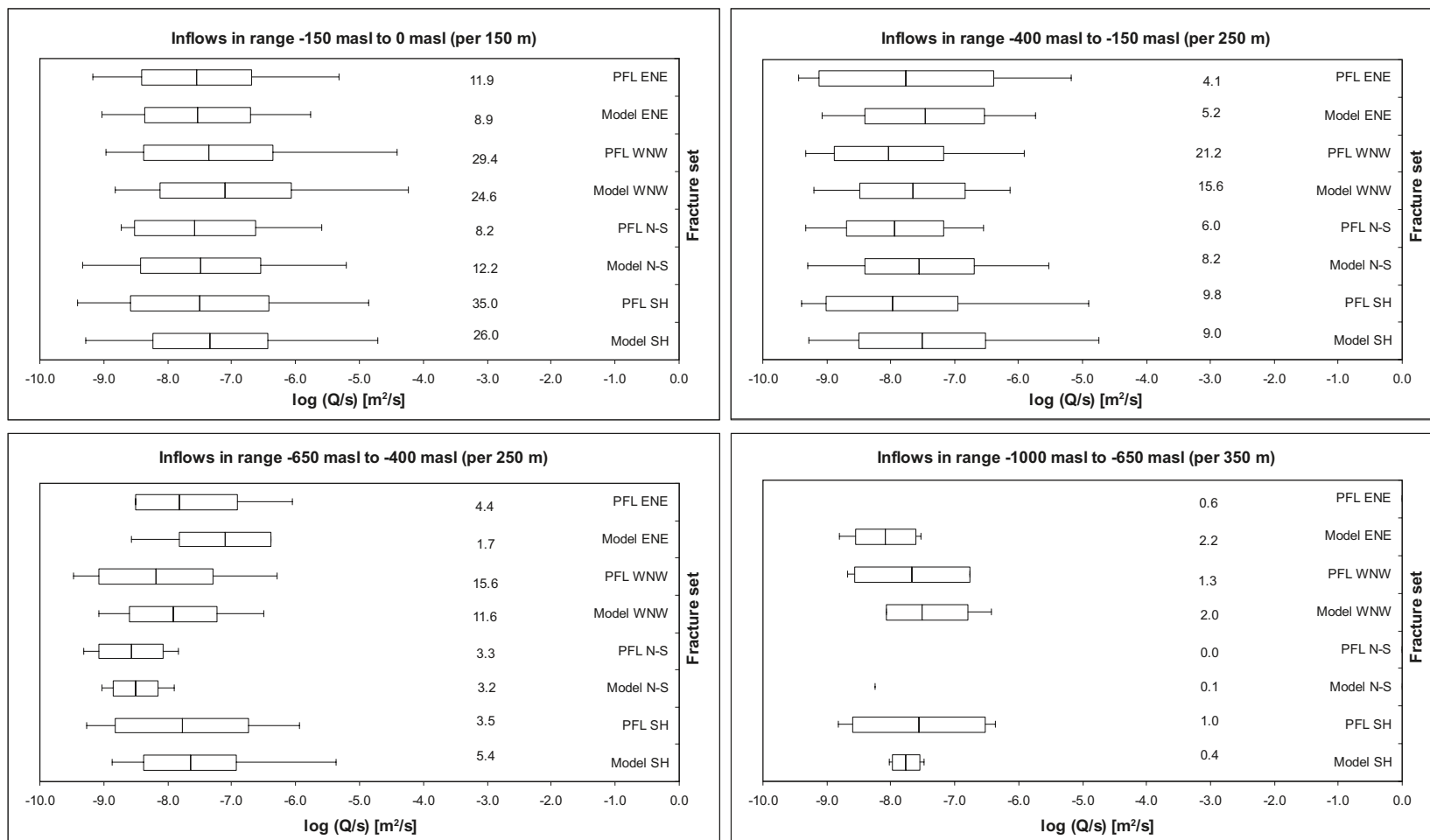


Figure 8-35. Bar and whisker plots comparing statistics taken over each fracture set for the individual inflows, Q/s , for the PFL-f data from borehole sections within HRD_C against statistics for an ensemble over 10 realisations of the hydrogeological DFN model. The model has a semi-correlated transmissivity, with r_0 fixed and P32 based on OPO fractures. The centre of the bar indicates the mean value, the ends of the bar indicate ± 1 standard deviation, the error bars indicate the minimum and maximum values and the value is the number of flowing fractures above the PFL-f detection limit per borehole section. For the data statistics are taken over the identified flow-features within each set. For the model, statistics are taken over the fractures generated within each set and over 10 realisations. The numbers of fractures are Terzaghi weighted and normalised to the length which is provided in the respective graph heading.

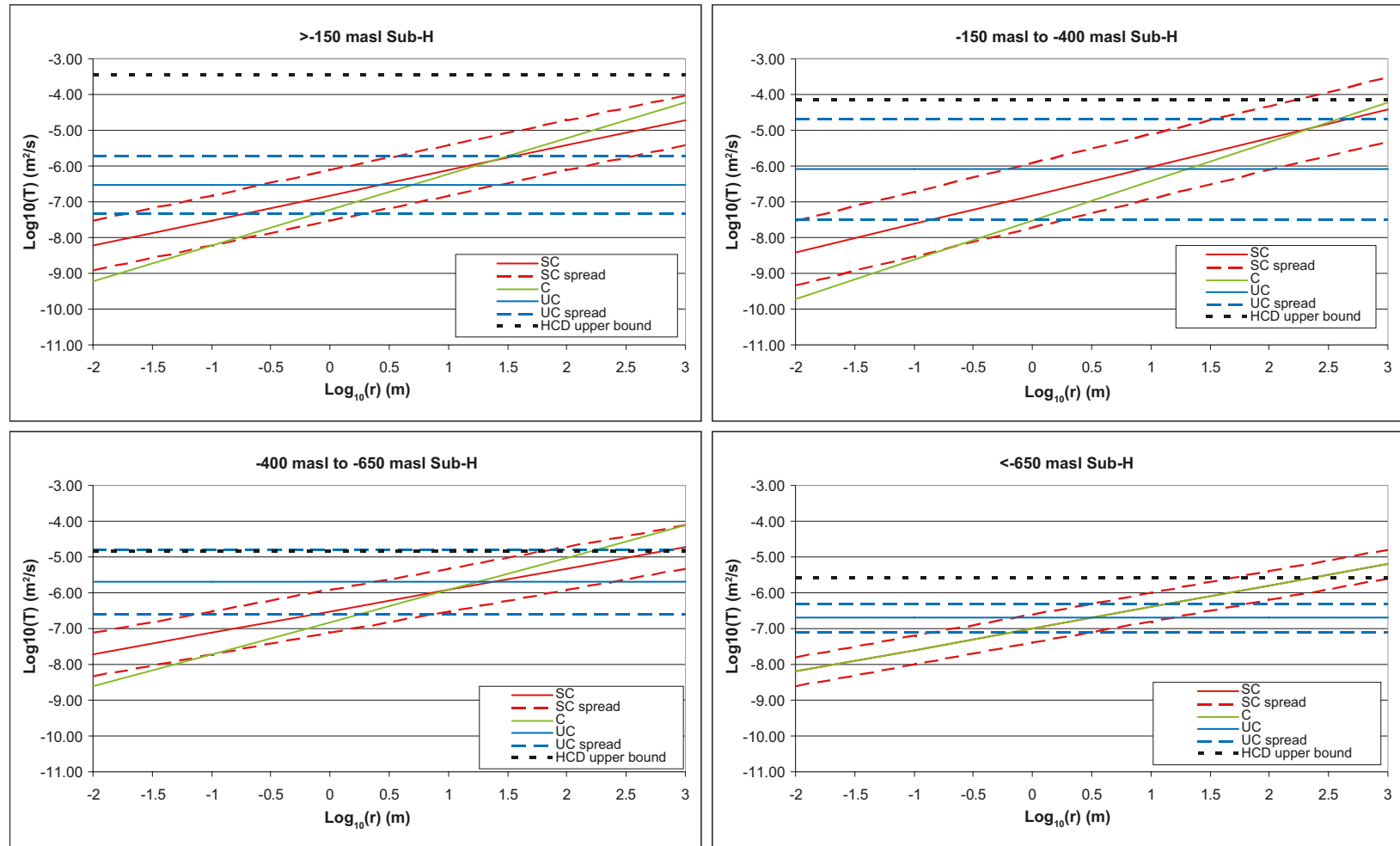


Figure 8-36. Comparison of the relationships between fracture transmissivity and fracture size in each depth zone for HRD_C. The plots are for the calibrated model with $r_0=0.038$ m and open fracture intensity based on OPO fractures. The plots show the central trend for each relationship together with lines at 1 standard deviation above and below the central trend. The dashed black line indicates the maximum value measured in the deterministically interpreted deformation zones (HCD).

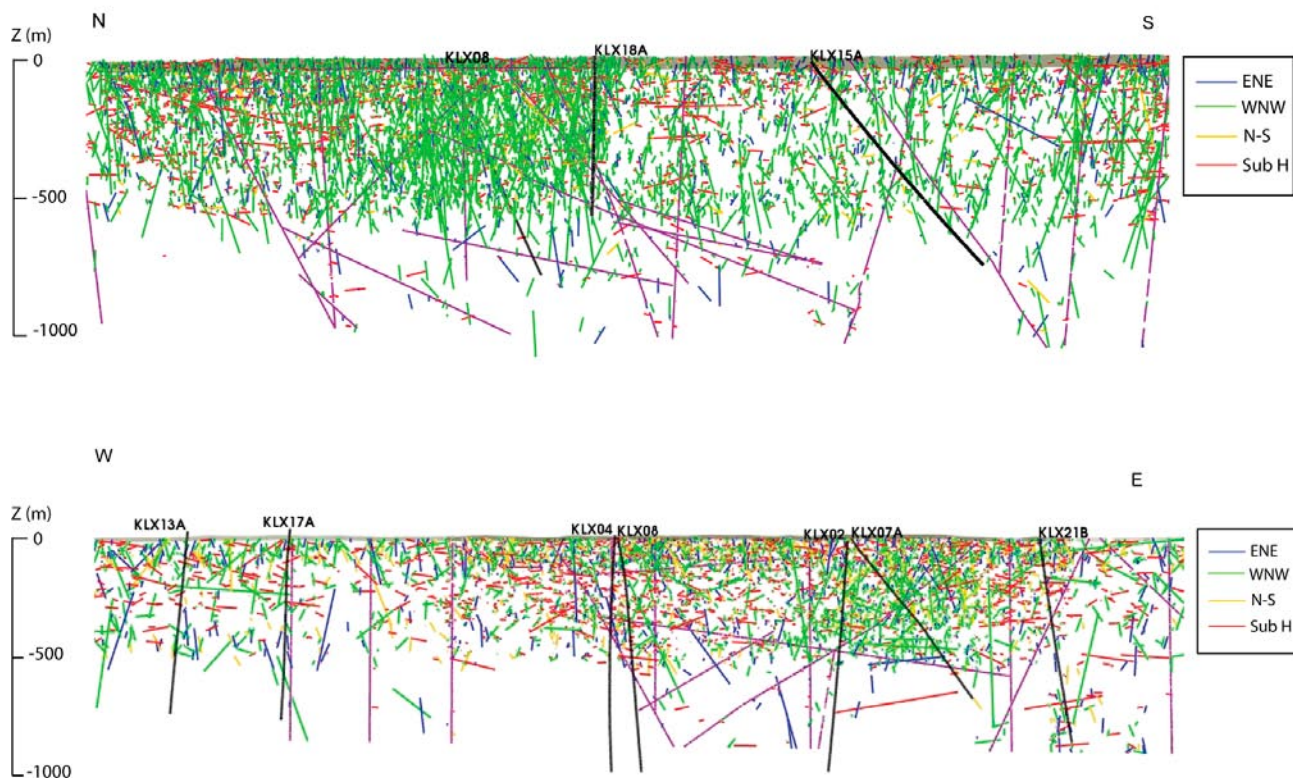


Figure 8-37. Traces of connected OPO fractures in the N-S Section A and the WNW-ESE Section B (see Figure 8-50) through the base case hydrogeological DFN simulation. The fractures are coloured according to orientation set (ENE – blue, WNW – green, N-S – yellow, subh – red). The HCD are shown in purple together with core drilled boreholes in the close proximity of the vertical section.

8.5.3 Hydraulic soil domains

The Quaternary deposits model consisting of 6 layers (Z1–Z6), cf. Section 4.3.2, was provided as a soil type indicator, horizon depth for the bottom of each layer, and the total Quaternary deposits thickness on a grid resolution for the data of 20 x 20 m. This detailed model was simplified in the regional groundwater flow modelling representing it by four element layers vertically, each of a constant 1 m thickness, with the horizontal extent of the hydrogeological grid element (40–120 m), to represent the HSD. The same hydraulic conductivity tensor was specified for each vertical stack of 4 grid elements, but varied horizontally from element-to-element, and was anisotropic with regard to horizontal and vertical components in order to represent the effective hydraulic properties of the Quaternary deposit layers, cf. /Rhén et al. 2009/ for details of the implementation.

8.5.4 Summary comparison of HRD hydraulic properties

Key hydraulic properties of the three HRD inside the focused volume are summarised by depth zone in Table 8-9 based on PFL flow measurements. The HRD are compared in terms of the corrected flowing fracture intensity (the bias of the orientation of the fractures relative to the boreholes is compensated for), the geometric mean transmissivity, the sum of transmissivities divided by borehole length, and the corrected fracture intensity multiplied by geometric mean transmissivity. The last two columns are alternative estimates of the bulk hydraulic conductivities of the bedrock based on arithmetic and geometric averages, respectively. HRD_EW007 has the highest flowing fracture intensity and the most gradual decrease with depth. HRD_W has least flowing fracture intensity and the most marked drop in intensity below –150 m. At repository depth, the flowing fracture intensity in HRD_EW007 is about twice that in HRD_C, which is nearly twice that in HRD_W. Geometric mean transmissivities are similar in HRD_EW007 and HRD_W and about three times higher than HRD_C. The variability in transmissivity, apparent from the difference between arithmetic and geometric mean estimates of bulk hydraulic conductivity, is greatest in HRD_W. HRD_C and HRD_W are similar in terms of geometric mean hydraulic conductivities, and about 3–5 times lower than HRD_EW007. HRD_W has the least fracture intensity, but the most variability.

Table 8-9. Summary of statistics of flowing features detected by PFL for the borehole intervals outside of interpreted deterministic deformation zones. MDZ are included in these statistics, but the transmissivity of individual PFL fractures are summed within an MDZ such that each is treated as a single feature.

Hydraulic Rock Domain	Depth Zone (m)	PFL $P_{10,corr}$ (m^{-1})	Geometric mean T (m^2/s)	Sum T/ Length (m/s)	$P_{10,PFL,corr} \times$ geometric mean T (m/s)
HRD_EW007	50 to -150	0.816	3.58E-08	3.1E-07	2.9E-08
	-150 to -400	0.550	3.0E-08	1.2E-07	1.7E-08
	-400 to -650	0.225	2.6E-08	1.2E-08	5.9E-09
	-650 to -1,000	N/A	N/A	N/A	N/A
HRD_W	50 to -150	0.499	4.39E-08	2.8E-07	2.2E-08
	-150 to -400	0.078	1.4E-08	2.9E-08	1.1E-09
	-400 to -650	0.060	2.9E-08	2.8E-08	1.7E-09
	-650 to -1,000	0.005	3.7E-09	1.4E-11	1.9E-11
HRD_C	50 to -150	0.564	3.33E-08	2.1E-07	1.9E-08
	-150 to -400	0.164	1.1E-08	2.4E-08	1.8E-09
	-400 to -650	0.107	8.5E-09	3.4E-09	9.1E-10
	-650 to -1,000	0.008	2.3E-08	5.5E-10	1.8E-10

8.5.5 Comparison between model and KLX27A data

KLX27A is a core-drilled borehole in the south-west corner of Laxemar. It is approximately 645 m long, inclined northwards, starting in HRD_C, crossing the ZSMNW042A deformation zone, and ending in HRD_W. About 408 m of the borehole is in HRD_W (excluding major deformation zones), only these latter data are used in the comparison study. Data from KLX27A were excluded from the data used to develop and calibrate the hydrogeological DFN model, and therefore it may be used to compare predictions of the Hydrogeological DFN model with the hydraulic properties observed in relevant parts of KLX27A. The comparison is presented in /Rhen et al. 2008a/.

The comparison between the model and the borehole data from KLX27A, demonstrates that a number of the observed hydraulic characteristics fall within the predicted variability, but some properties such as the intensity of PFL-f features below -400 m are exceptionally high in KLX27A. Considering the large spatial variability of occurrence of PFL-f features and the use of only one borehole for the comparison, the conditions for a statistically significant comparison cannot be expected to be fulfilled. It is therefore not possible to draw firm conclusions from the comparison, other than that the outcome of KLX27A confirms that HRD_W is characterised by a strong element of heterogeneity and is also probably more difficult to predict than HRD_C.

8.6 Regional scale flow model calibration

Forward model calibration consists of changing values of model input parameters in an attempt to match field observations within some acceptance criteria. By comparing the model predictions with different types of field data/measurements, the overall model development can be partially calibrated to improve the parameterisation, improve understanding of the hydrogeological system, and help build confidence in the hydrogeological conceptual model of the Laxemar-Simpevarp area, and Laxemar in particular. The general approach applied in SDM-Site Laxemar was to use essentially the same groundwater flow and solute transport model in terms of grid discretisation and parameter settings for matching all three types of field data referred to as data sets B, C and D, respectively, in Section 8.1.2.

8.6.1 Numerical modelling approach

The ConnectFlow code /Hartley and Holton 2004, Hartley et al. 2004ab, Hoch and Jackson 2004/ was used for the 3D groundwater flow and solute transport modelling carried out for SDM-Site Laxemar. The hydrogeological parameterisation is defined in terms of a hydrogeological DFN model and discretely modelled HCD, but this system is converted to an equivalent continuum porous

medium (ECPM) model for the confirmatory testing exercises, in order that processes such as rock matrix diffusion (RMD) can be represented. To become a meaningful activity in a highly heterogeneous and anisotropic medium such as the crystalline bedrock in the Laxemar-Simpevarp area, forward model calibration requires that the structural-hydraulic properties of the HCD and HRD are properly characterised and implemented in the ECPM model. The ECPM parameterisation is a two stage process. Firstly, transmissivities inferred from the hydraulic tests are used to parameterise the HCD and HRD models as described in Sections 8.5.1 and 8.5.2. Secondly, the geometrical and hydraulic properties of these two discrete models are transformed into ECPM hydraulic conductivities using a specified grid resolution (40 m within the focused volume and 120 m outside). It should be noted that the ECPM properties are not required in the migration simulations to be run in the safety assessment SR-Site, since these are carried out on a smaller scale than the simulations treated in the SDM. That is, the SR-Site groundwater pathway calculations explicitly employ the hydrogeological DFN without upscaling.

The calibrated model is referred to as the *deterministic base model simulation* in the SDM. The term *deterministic simulation* implies that standard deviation in $\text{Log}_{10}(T)$ was set to nought in Eq. (8-3) and that a *single realisation* of the hydrogeological DFN model of the HRD was used. Moreover, the hydrogeological DFN model assumed a semi-correlated relationship between fracture transmissivity and size.

8.6.2 Palaeohydrogeological modelling

Coupled groundwater flow and solute transport is modelled in terms of mass fractions of 5 reference waters (see Section 8.4.5). The chemical composition at any point and time is then described in terms of the mass fractions of these 5 reference waters. Using mass fractions as the transported entities makes the definition of boundary and initial conditions intuitive since they relate directly to the hydrogeochemical conceptual model of water origin. Likewise, it is useful to interpret the results in terms of the dilution or penetration of water of different origin. The reference waters contain both conservative and non-conservative species, but the flow modelling assumes a conservative behaviour of these species, i.e. no chemical reactions are involved in the modelling. However, it is the conservative species that are considered important in the flow calibration and the non-conservative species are simply used as indicators of relative changes in groundwater signatures by depth. The assumption is that reference water mixing is the dominant process for the evolution of the groundwater compositions below the uppermost part of the bedrock /Laaksoharju et al. 2009/. The formulation of the solute transport equations in terms of mass fractions is described in more detail in /Rhén et al. 2009/.

Inter-glacial porewater was introduced as a fifth reference water to illustrate some additional conceptual aspects on the evolution of porewater hydrogeochemistry, the interaction between porewater and fracture groundwater, and its implications for expected porewater sampling. The aim being to demonstrate that long-term transient processes associated with climate evolution and rock matrix diffusion into sparsely fracture rock give one possible explanation for the interpreted porewater chemistry. It is recognised that the interpretation of porewater chemistry is uncertain, in part due to few samples, and that the proposed explanations are non-unique, cf. Section 9.5.7 and /Laaksoharju et al. 2009/. The introduction of the fifth reference water is analogous to the corresponding introduction of the *Old Meteoric and Glacial Water* used in the palaeohydrogeological modelling of SDM-Site Forsmark /Follin et al. 2007c/, though a different range of compositions and formulation of the initial condition is considered for SDM-Site Laxemar.

Boundary conditions for palaeohydrogeological modelling

It is inferred that prior to 6500 BC the western part of the focused area, corresponding to HRD_W, would be close to the shoreline of a freshwater lake, whereas the eastern part, corresponding to HRD_C would be mostly covered by the lake. After 6500 BC, the lake gradually evolved into the Littorina Sea, and hence in the surface depressions corresponding to the major deformation zones ZSMEW002A (Mederhult zone), ZSMEW007A and ZSMNW042A there is denser, saline, surface water that will sink into the bedrock until it encounters groundwater of similar or higher density, i.e. *Deep Saline Water*. Salinity and density of the sea continued to increase, so the buoyancy force would increase until the Littorina maximum about 4500 to 3000 BC. The modelling has shown

that the lower salinity curve for the Baltic Sea shown in Figure 3-6 better captures the modelled groundwater evolution presented in Section 8.6.

One uncertainty in prescribing the hydrochemical boundary condition is which reference water composition to be used for the dilute water when sea water salinity was less than 100% of the Littorina reference water. After 4500 BC, *Littorina Sea Water* was diluted with *Altered Meteoric Water*. Before the Littorina maximum (4500 BC), the precursors to the Baltic were mainly a series of ice lakes, and so the dilute sea water was assumed to be *Glacial Melt Water* in origin. For simplicity in the numerical implementation of the boundary conditions, the same dilute groundwater composition was used above the shore level also prior to 4500 BC in the base case. A variant calculation was also considered where the dilute water prior to 4500 BC was *Altered Meteoric Water* instead. In which case, *Glacial Melt Water* was introduced into the palaeohydrogeological model only via the initial condition. /Rhén et al. 2009/ provides more details about the derivation of the boundary conditions.

Initial conditions for palaeohydrogeological modelling

The initial hydrochemical condition at 8000 BC is by its nature uncertain. However, combining our knowledge of the bedrock hydrogeology and the present-day hydrochemistry, constitute useful clues in guessing the initial conditions. In the deep bedrock below c. –650 m fracture transmissivities as well as the conductive fracture intensity are low, implying very long advective transport times, and the timescales for diffusion into the matrix blocks between the flowing fractures to be far longer than the current Holocene. The presence of *Deep Saline Water* and *Glacial Melt Water* in the fractures also suggests that the hydrochemical conditions at such depths have changed very little during the Holocene. Hence, the hydrochemical samples below c. –650 m can be used as indicators of appropriate initial conditions at depth, which can be extrapolated to higher elevations where post-glacial mixing may have taken place. Still, there are brackish-glacial groundwater samples collected at elevations up to c. –200 m, which suggest a persistence of hydrochemical composition over the timescale of interest. Above c. –150 m, the initial conditions are very uncertain since a younger post-glacial age is suggested by groundwater samples, but these also imply that the initial conditions are largely irrelevant at such shallow depth as the groundwater will have been replaced by later surface waters infiltrating according to the defined hydraulic boundary conditions. Hence, the approach used here is to consider the present-day groundwater samples below –650 m as being predominantly stable during the Holocene, and to use them to infer an initial hydrochemical composition and extrapolate this to shallower depths. Simple piecewise linear depth trends in the initial chemical composition are assumed.

The initial fracture water composition is assumed to be a mix of *Deep Saline*, *Glacial Melt Waters* and *Inter-glacial Porewater*. 100% Glacial Melt Water is assumed above –200 m, which gradually reduces to 0% *Glacial* and 100% *Deep Saline* at –2,100 m, with a small, <30%, fraction of *Inter-glacial Porewater* included at depths c. –1,000 m to give consistency with the measured concentrations of Cl and $\delta^{18}\text{O}$ measured at depth. The initial chemistry in the matrix is more difficult to define since there are relatively few porewater samples and conditions depend strongly on the distance of the samples from the nearest flowing fracture. The same profile of *Deep Saline Water* was assumed initially in the matrix as in the fractures, but the initial mass fractions of Glacial Melt Water and Inter-Glacial Porewater were calculated as a function of distance from the fracture surface (see examples in Figure 8-38), which results in a variation in initial profiles of $\delta^2\text{H}$ and $\delta^{18}\text{O}$ according to distance from the nearest water conducting fracture, which is one possible interpretation of the porewater samples (cf. Section 9.5.7). The conceptual interpretation is that during the Weichselian glaciation and subsequent melting, *Glacial Melt Water* will have infiltrated the fractures under high pressures and in-diffused into the matrix, but not have had time to diffuse into the larger matrix blocks at depth which in places are 10–100 m in size between flowing fractures. Hence, the porewater chemistry in the centre of matrix blocks at depth will not see the *Glacial Melt Water* whereas in areas of higher fracture intensity and close to the wall of flowing fractures, the porewater will be similar to the initial condition specified in the fracture water. The initial profile of matrix water was calculated allowing in-diffusion of the fracture water for an approximate time between 1,000–10,000 years; 5,000 years was used in the modelling.

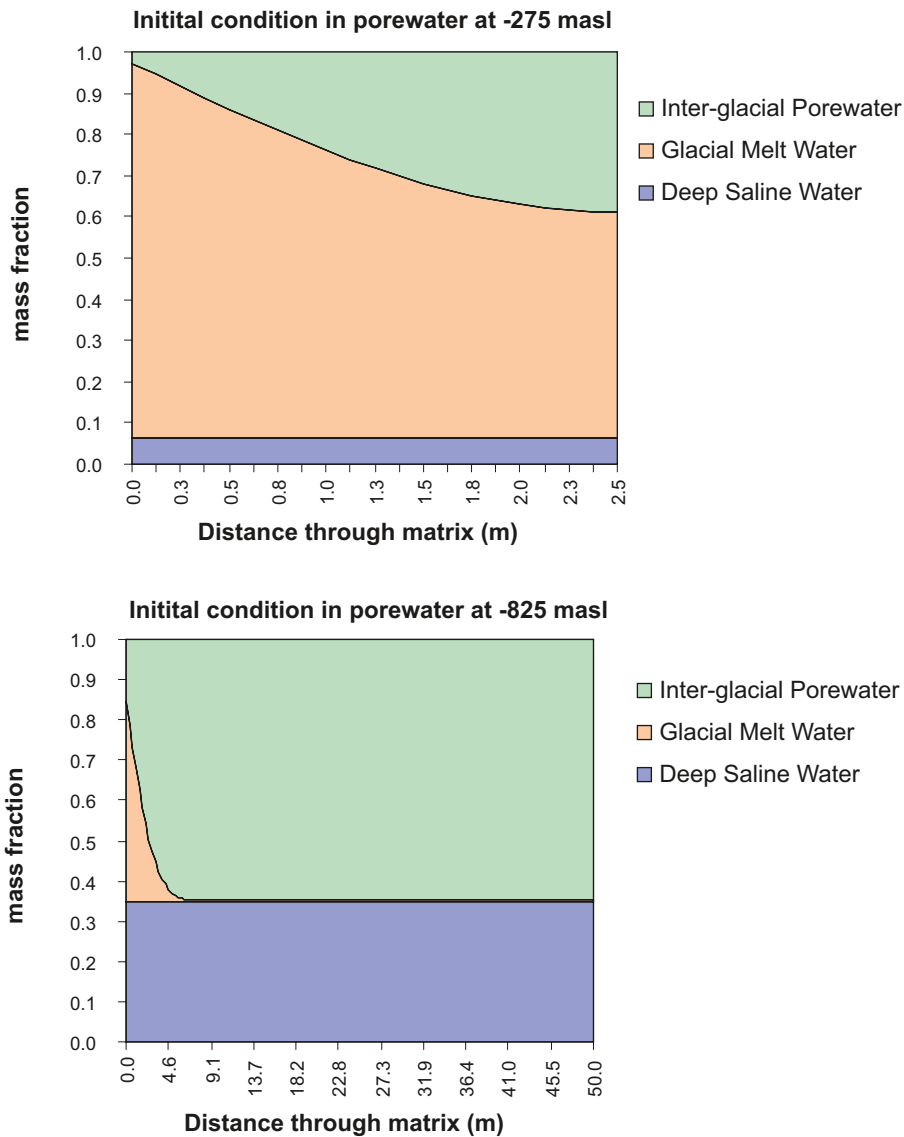


Figure 8-38. Examples of initial conditions in the matrix at two different depths for HRD_C. Profiles are shown as a function of distance from a water conducting fracture surface, so that 0 m is the equal to the initial condition in the fractures, and the right hand distance is the initial condition at the centre of a matrix block, the distance increasing with depth as flowing fracture intensity reduces.

8.6.3 Matching natural groundwater levels

Groundwater levels measured in open boreholes are available for the upper bedrock and Quaternary deposits to help confirm appropriate boundary conditions and hydraulic properties for the near-surface hydrogeology of the HSD and the uppermost parts of the HRD. Important issues such as the direction and magnitude of the hydraulic gradient between the bedrock and Quaternary deposits can be simulated and compared to such *in situ* data. In addition, groundwater levels in packed-off sections within the deep, core-drilled boreholes are also available for comparison. Since salinity increases with depth, so does the groundwater density. The groundwater levels measured in deep boreholes are therefore perceived as representing point-water heads /Rhén et al. 2009/. In order to understand vertical head gradients in a variable-density groundwater flow system, measured groundwater levels (point-water heads) are transformed into environmental heads, so that vertical flows are linearly proportional to the environmental head gradient. In a few packed-off sections there are some uncertainties as to whether the correct density adjustments have been made to the data in transformation from point-water heads to environmental water heads. Above -400 m elevation, this uncertainty is of low significance, and so the simulated and measured environmental head can be compared readily. Between -400 m and -800 m elevation, the measured environmental head is compared with the simulated environmental head, but the simulated point-water head is also calculated to quantify

the maximum possible uncertainty in the measured value due to inaccuracies in the interpreted density correction. The simulated heads are derived using the residual pressure and fluid density calculated at 2000 AD based on palaeohydrogeological simulations of the groundwater flow and solute transport evolution from 8000 BC to 2000 AD (see Section 8.6.6). As such, the simulations represent very long-term changes in head, but not the seasonal variations that affect measurements.

Figure 8-39 and Figure 8-40 show the results for the *deterministic base model simulation* for percussion drilled boreholes (HLX) and soil monitoring wells (SSM). The boreholes are ordered by bedrock elevation. The simulated groundwater levels are in both plots a bit higher than the measured levels; c. +0.3 m and +0.4 m of mean difference for the HLX holes and the SSM holes, respectively, within the focused volume. This magnitude of discrepancy is quite small considering that the simulations essentially predict the seasonally averaged groundwater levels, whereas the average fluctuations are about 1.6–1.8 m between recordings made at different dates. Simulations predict that the head gradient is directed downwards, i.e. recharge conditions, in about 60% of HLX holes.

Some examples of comparisons between simulated and measured environmental heads in core drilled boreholes are given in Figure 8-41 and Figure 8-42 for the *deterministic base model simulation*. Most of the core-drilled boreholes in the Laxemar subarea display a very gradual decrease in environmental head with depth, i.e. recharge conditions, as illustrated by the data and simulations of KLX10 and KLX12A in Figure 8-41. These boreholes are situated in the focused volume, involving HRD_C and HRD_EW007. The deepest measurements of environmental head in KLX10 illustrate the occasional sudden drop in measured environmental head at about –650 m associated with uncertainty in correcting the data for measured groundwater density.

Figure 8-42 gives an example of the environmental heads in KLX11A and KLX21B, in HRD_W and the eastern part of HRD_C, respectively, within the focused area. The gradual decrease in environmental head with depth is reproduced; although data suggests a higher gradient around –100 m in KLX11A associated with the subhorizontal HLX28_DZ1 minor deformation zone. The environmental head predicted in the upper 400 m of KLX21B is acceptable, and the sudden drop in measured environmental head below –400 m may result from problems in correcting for fluid density, as is predicted by the point-water head deviation. The mean difference between modelled and measured environmental head over all borehole packer intervals is calculated as 0.4 m, compared with average temporal variations of 1.2 m.

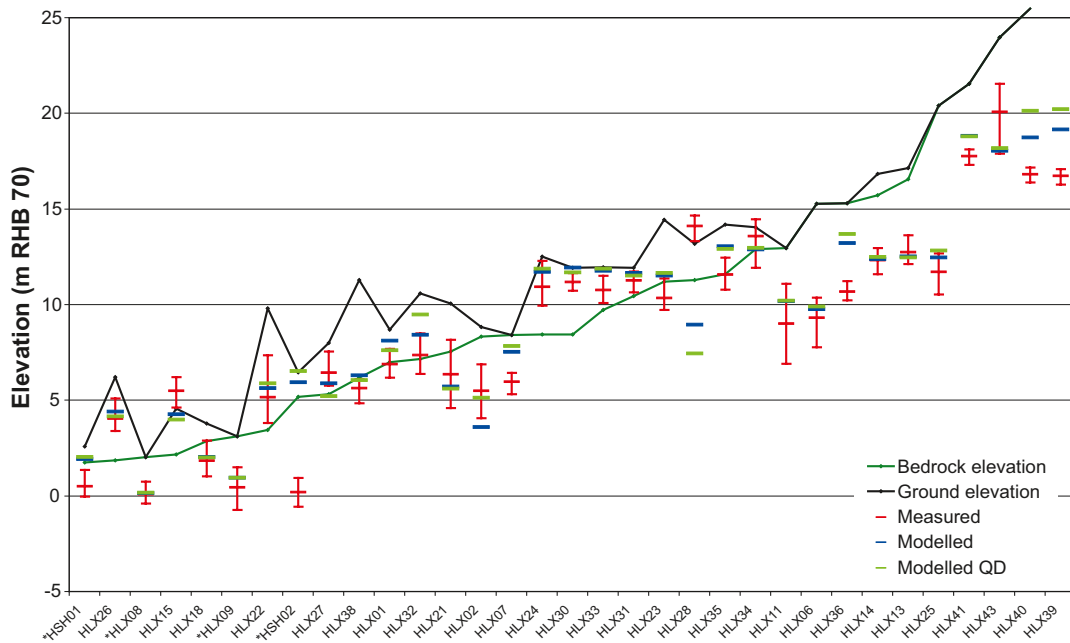


Figure 8-39. Comparison of the deterministic base model simulation (blue) with groundwater levels measured in the percussion-drilled boreholes (red). The boreholes are ordered by increasing bedrock elevation. The measured data are plotted as mean groundwater levels with error bars to show the range of the recordings over time. The simulated groundwater levels within the focused volume are on the average c. 0.3 m higher than the corresponding measured levels. For the model, values are also given for the QD (purple) at the same locations as the boreholes.

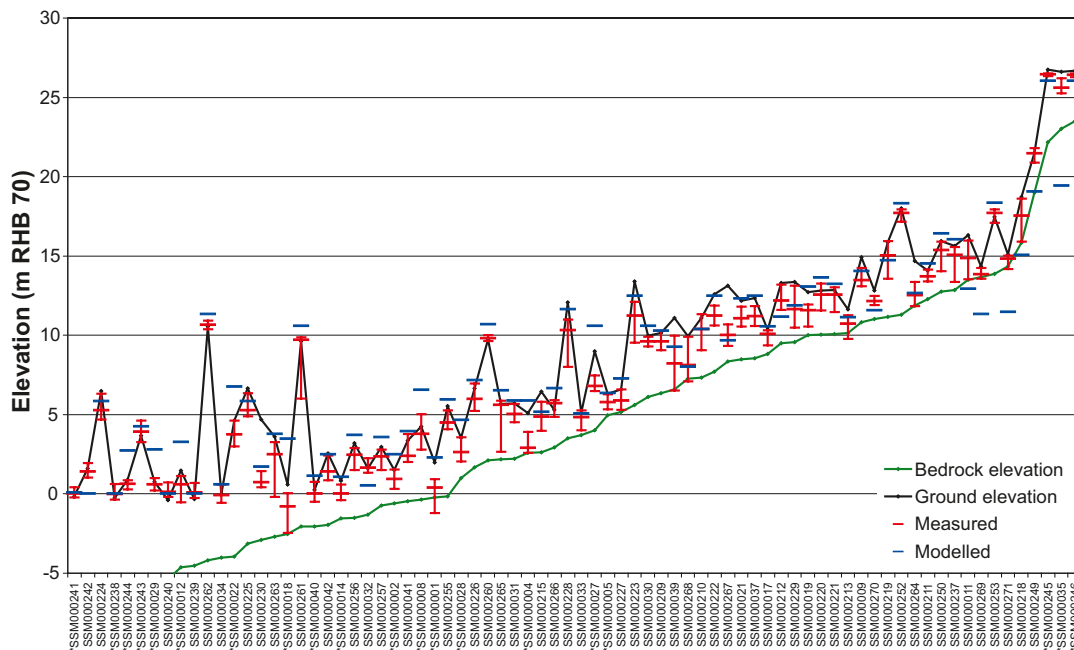


Figure 8-40. Comparison of the deterministic base model simulation with groundwater levels measured in the soil monitoring wells in the Quaternary deposits. The wells are ordered by bedrock elevation. The measured data are plotted as mean groundwater levels with error bars to show the range of the recordings over time. The simulated groundwater levels in the SSM boreholes within the focused volume are on the average c. 0.4 m higher than the corresponding measured levels.

8.6.4 Matching the interference tests in HLX33 (and HLX28)

The interference test in HLX33 is dominated by responses in HCD ZSMNEW007A. It requires an increase of a factor 50 in the effective transmissivity of the upper part of this zone to match both pointwater heads in the area and interference test drawdowns, but does not inform the hydraulic properties of the HRD.

The interference test in HLX28 is dominated mainly by hydraulic responses in the HCD. In this case, the minor deformation zone HLX28_DZ1 is mainly responsible for transmitting the response, while strong anisotropy in zones KLX19_DZ5–8 ZSMNS059A, ZSMNS001C and ZSMNW042A-west act to transmit the response longitudinally and also inhibit it transversely. This confirms the barrier effect of these zones. Some responses in the HRD are seen in this test, but these are generally in the close vicinity of the HCD. That is, the HCD are responsible for the primary responses, and the background fractures distribute these responses slightly further. If the HRD were too hydraulically conductive, then the responses in the HCD would be reduced since the background rock would provide additional water to replenish that pumped. Transient groundwater flow models suggest the hydraulic conductivity in the immediate vicinity of HLX28 is perhaps lower than interpreted in the hydrogeological DFN model for HRD_W.

8.6.5 Matching the drawdown due to inflow to Äspö hard rock laboratory (HRL)

The effects of inflows to the Äspö HRL facility on groundwater heads as seen in monitoring percussion boreholes surrounding the island of Äspö were extensively modelled in /Hartley et al. 2007/. There it was concluded that the measured drawdowns could be reproduced provided the Quaternary deposits in the bays around Äspö were of Gytjtja type (i.e. a vertical hydraulic conductivity of $5 \cdot 10^{-9} - 1 \cdot 10^{-8}$ m/s) to reduce recharge from the sea bed which otherwise restricted the zone of influence of pumping on the Laxemar-Simpevarp mainland. Another significant finding was that operation of the Äspö HRL facility has had little effect on the natural hydrochemistry measured in the Laxemar subarea, and hence it was not considered necessary to include pumping/drawdown induced by the Äspö HRL in the palaeohydrogeology simulations.

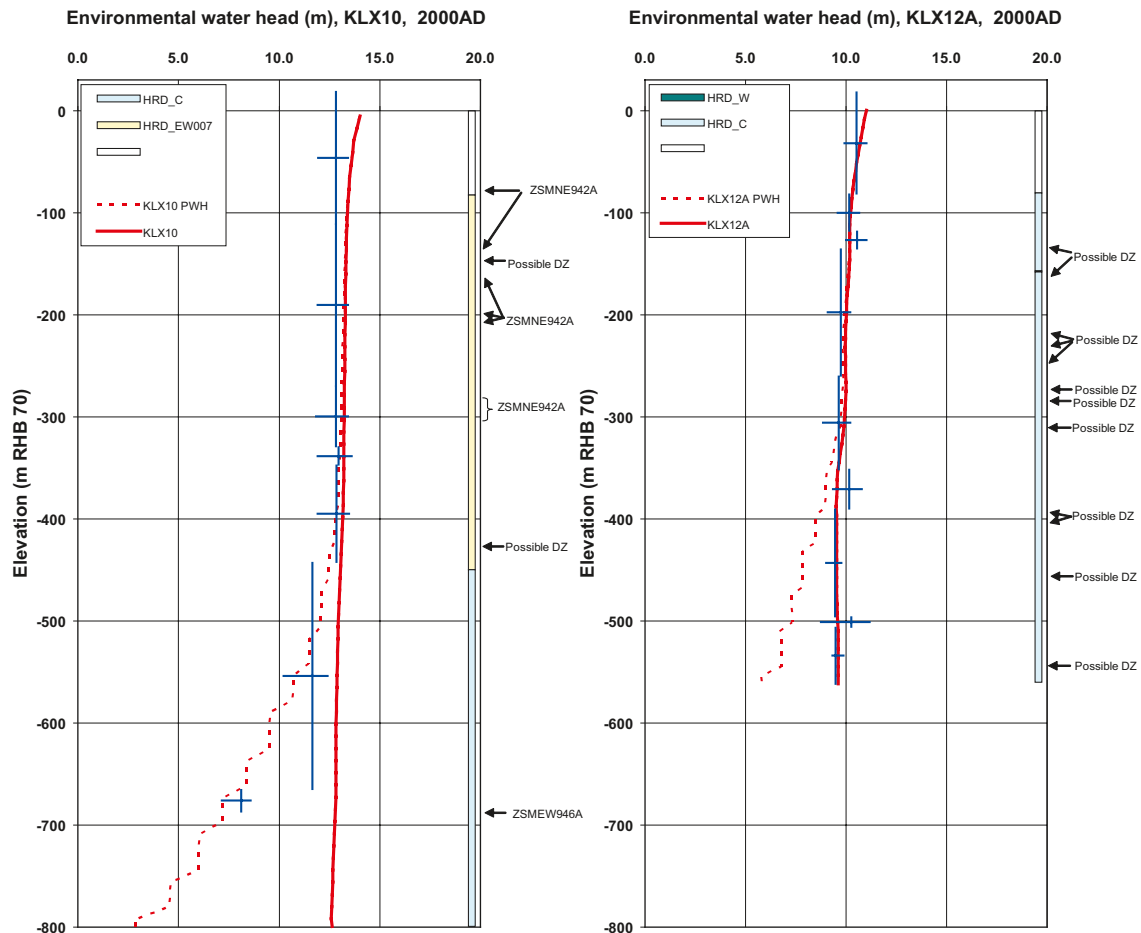


Figure 8-41. Examples of modelled environmental-water head (solid red line) and point-water head (dotted red line) in KLX10 and KLX12A in HRD_C for the base case compared with environmental-water heads (blue crossed lines, centre showing midpoint of the section, vertical line showing the extent of the section and horizontal line showing the temporal variation of the measured head) calculated from measured point-water head data in sections along the borehole. At the right hand side, the prevailing hydraulic rock domains are shown as coloured bars along the borehole. Detected fractures/deformation zones are indicated at their intersection depth along the borehole.

The SDM-Site Laxemar model of the HSD has largely Gyttja type sediments in the bays around Äspö, but there are a few places in the bays where the sediments beneath the sea are less tight allowing greater infiltration from the sea. In the SDM-Site Laxemar groundwater flow model it was found necessary to modify the remaining HSD to use Gyttja type in the bays around Äspö to confine the upper bedrock from sea water infiltration. Possibly this is just a consequence of using a coarser grid, 40 m, rather than the 20 m grid used to define the model of Quaternary deposits.

8.6.6 Matching hydrochemical data in cored boreholes

Modelling the evolution of the hydrological and hydrochemical conditions during the Holocene are essential parts of the site descriptive model. In this context, the calibration against measured hydrochemical profiles in cored boreholes is fundamental to the understanding of the hydrogeological processes in the fractured bedrock, since it addresses the impact of variable-density flow, and the solute (salt) transport interaction between the fracture system and matrix as this can have a considerable impact on how the flow rates and groundwater pathways evolve over time.

In general, the size of the hydrochemical database has increased significantly since the preliminary site description. In particular, this relates to porewater data, which were not available in the preliminary site description. However, in terms of reliable fracture water in core drilled boreholes, the hydrochemical database available for palaeohydrogeological modelling is still quite limited, see Table 8-10.

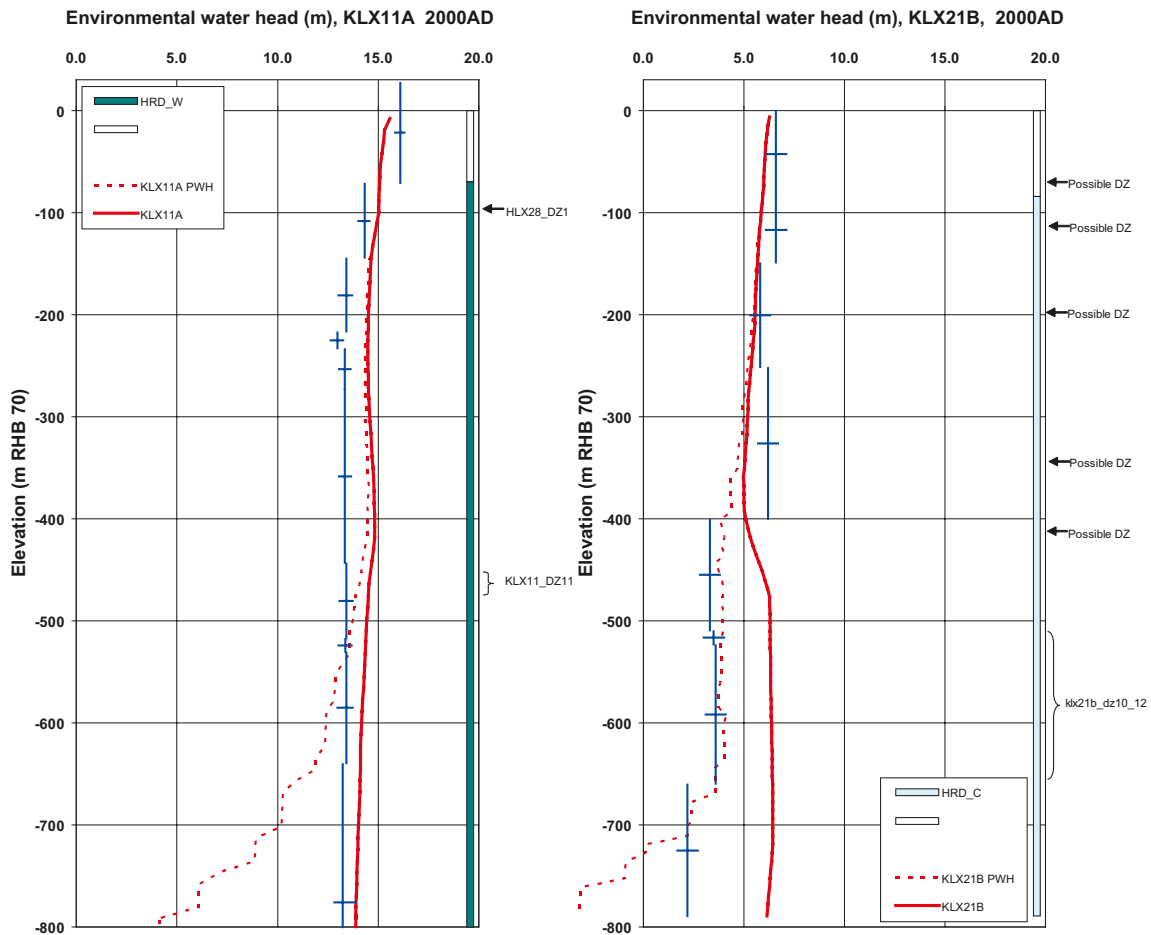


Figure 8-42. Examples of modelled environmental-water head (solid red line) and point-water head (dotted red line) in KLX11A in HRD_W and KLX21B in HRD_C for the base case compared with environmental-water heads (blue crossed lines, centre showing midpoint of the section, vertical line showing the extent of the section and horizontal line showing the temporal variation of the measured head) calculated from measured point-water head data in sections along the borehole. At the right hand side, the prevailing hydraulic rock domains are shown as coloured bars along the borehole. Detected fractures/deformation zones are indicated at their intersection depth along the borehole.

Table 8-10. Hydrochemical representativity of the 30 fracture water samples used for palaeo-hydrogeological modelling in the SDM-Site Laxemar flow modelling. The classification system (numbers and colours) is explained in Section 9.4.

Category	No. of samples used in SDM-Site Laxemar
1	3
2	4
3	46
4	31
5	0

Figure 8-43 through Figure 8-47 show an excerpt from the palaeohydrogeological comparisons made for the *deterministic base model simulation*. The *deterministic base model simulation* in the SDM generally predicts salinity about 200–300 m shallower than in the preliminary SDM, and significantly predicts brackish waters at repository depth, where they were fresh before. For example, the model predicts saline water from about –300 m in KLX03, see Figure 8-43, compared with –500 m in the preliminary SDM /Hartley et al. 2006, 2007/. The changes in current predictions of salinity beneath the Simpevarp peninsula and Äspö island relative to the preliminary SDM are far less /cf. Rhén et al. 2009, Hartley et al. 2007/, although there are some improvements at KAS06 and KSH03A, for example).

The chemical compositions of the reference waters are described in Chapter 9 (Table 9-1). Four main hydrochemical indicators were used in the palaeohydrogeological calibration:

- Cl – since it is conservative and indicates the locations of *Littorina Sea Water* and *Deep Saline Water*.
- Br/Cl ratio – since both are conservative and their ratio can be used to determine where the origin of saline water changes from a *Littorina Sea Water* to *Deep Saline Water* when the ratio increases from around 0.004 to 0.007, or more.
- $\delta^{18}\text{O}$ – since this is conservative over the timescales considered in the simulations and indicates any remnants of *Glacial Melt Water* when $\delta^{18}\text{O} < -13$ /Laaksoharju et al. 2009/.
- HCO_3 – because we model the infiltration of an *Altered Meteoric Water* into the bedrock. The HCO_3 is used as a signature for infiltrating post-glacial meteoric water (although it is a non-conservative species), this signature can also be traced by the low Cl content. The reference water composition of *Altered Meteoric Water* takes into account the major changes that meteoric water has undergone in the Quaternary deposits and the uppermost part of the bedrock such as organic decomposition and calcite dissolution. Mixing is important for the groundwater components in Altered Meteoric Water but still HCO_3 content can also be dependent on reactions.

Figure 8-44 shows the results for the boreholes located in HRD_C. The predicted depth of infiltration of post-glacial meteoric water indicated by HCO_3 varies between about –300 m and –700 m which is consistent with the limited *in situ* data available; although perhaps about 100 m too deep. The simulated transition from fresh to brackish water between –200 m to –600 m indicated by Cl reflects the data, although the porewater salinity is over-predicted below –600 m. The model predicts a transition from marine saline water to non-marine at –200 m to –500 m, which is consistent with what can be inferred from the data. The flow model predicts a lens of brackish-glacial water between –500 m and –1,000 m in HRD_C, whereas the data only has glacial signature in KLX03 at about –400 m. The simulations demonstrate that the enriched $\delta^{18}\text{O}$ in the porewater is preserved below –650 m, as found from the measurements in KLX03.

Figure 8-45 and Figure 8-46 present the comparison of simulated and measured hydrochemistry in HRD_W recharge and discharge areas, respectively. The comparison is reasonable in discharge areas (KLX11A and KLX19A) for all 4 hydrochemical indicators, but the model over-predicts post-glacial meteoric flushing in the recharge areas around KLX13A and KLX17A. The top 400 m of KLX13A is intersected by 6 minor deformation zones. These may prevent vertical flushing of post-glacial meteoric water by deflecting it horizontally, or the associated increase in water conducting fracture intensity may enhance the retardation effect of rock matrix diffusion. Similarly, the upper 200 m of KLX17A is intersected by the gently dipping zones ZSMEW900A/B and 6 additional minor deformation zones in the top 500 m. Still, the predictions of salinity in both the fracture water and porewater are good in these recharge areas.

Figure 8-47 shows that the hydrochemical comparison for boreholes in HRD_EW007 is generally good. The depleted Oxygen-18 in KLX08 fracture water suggesting a lens of brackish-glacial waters around –400 m to –500 m is predicted, about 100 m deeper, as is the enriched $\delta^{18}\text{O}$ in porewater below –600 m. It should be noted that the simulated porewater compositions shown here are the average over the matrix blocks. For large matrix blocks, hydrochemistry in the porewater may vary greatly according to the distance to a water conducting fracture. Good agreements were also achieved for boreholes in the lower lying areas to the north of the focused area, and to the east around Äspö, Ävrö and the Simpevarp peninsula /see Rhén et al. 2009/ which have been subject to post-glacial meteoric infiltration for less time.

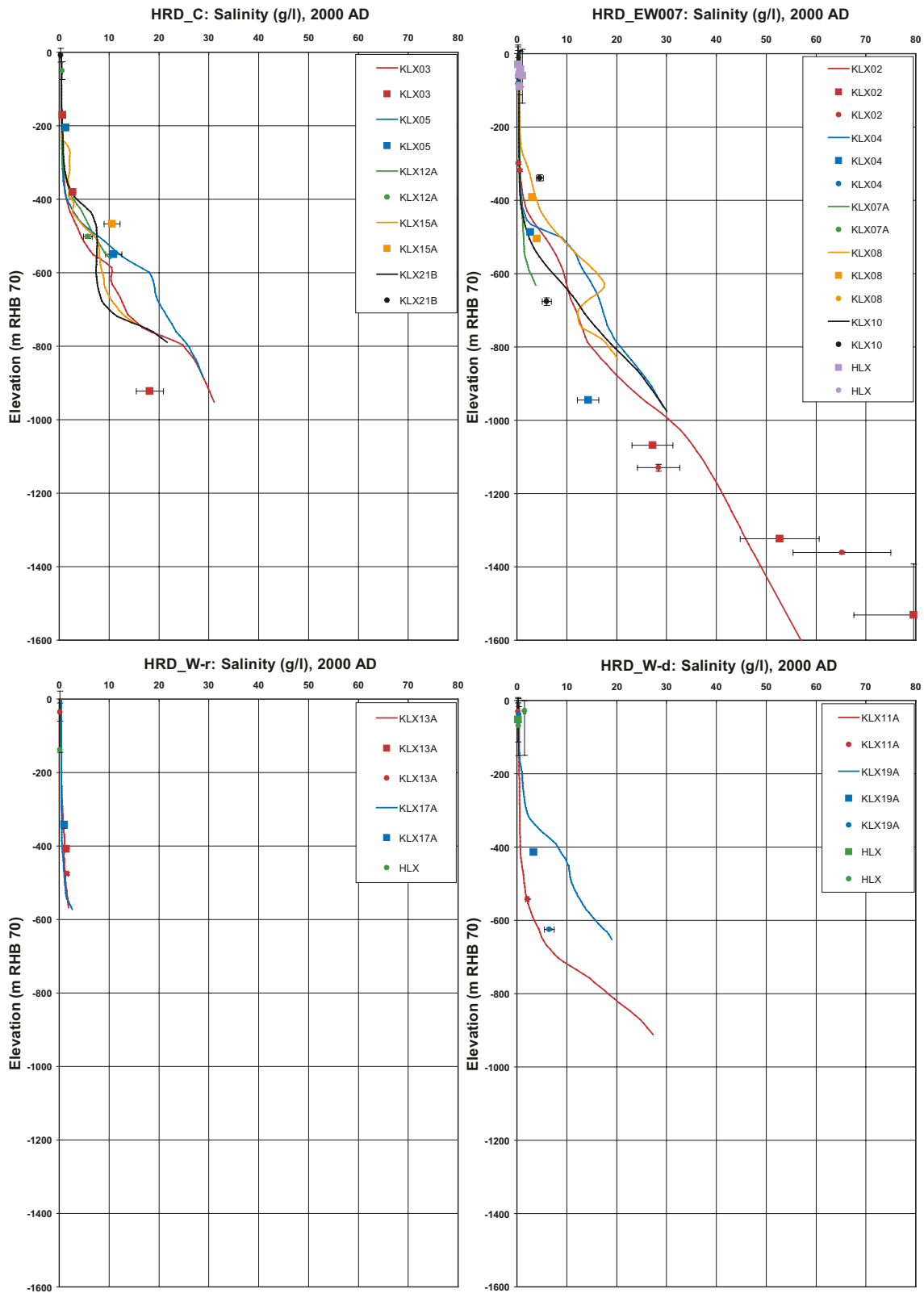


Figure 8-43. Comparison between the deterministic base model simulation (lines) and measured salinity concentrations (TDS) in the fracture system (squares for Category 1–3, diamonds for Category 4 data) for different groups of calibration boreholes. The error bars on the measured data indicate the laboratory analytical error.

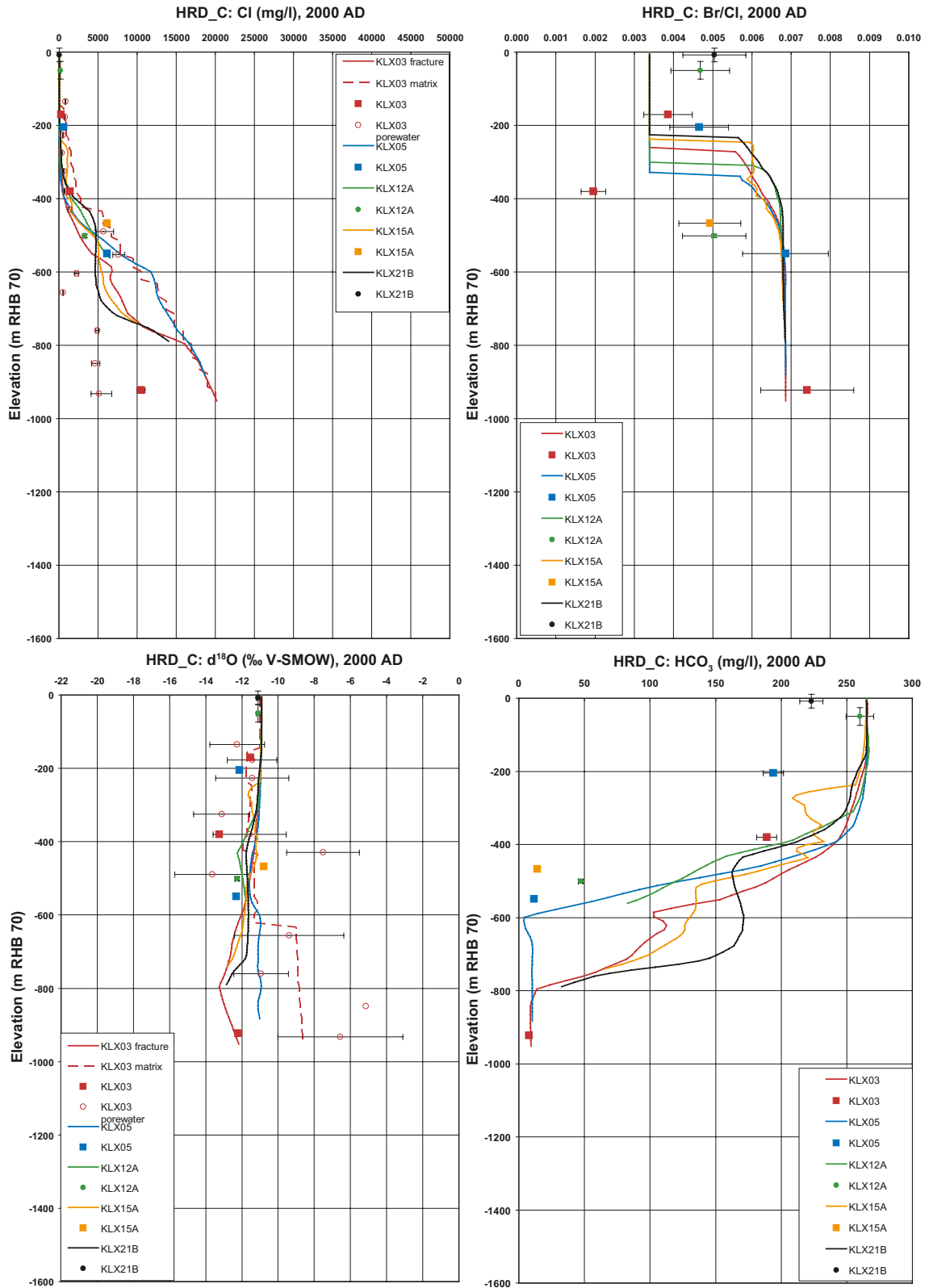


Figure 8-44. Comparison between the deterministic base model simulation (fracture water: solid lines; porewater = dashed lines) and measured concentrations of Cl, Br/Cl, $\delta^{18}\text{O}$ and HCO_3 (squares for Category 1–3, diamonds for Category 4, circles for porewater data) for boreholes in HRD_C. The error bars on the measured data indicate the laboratory analytical error.

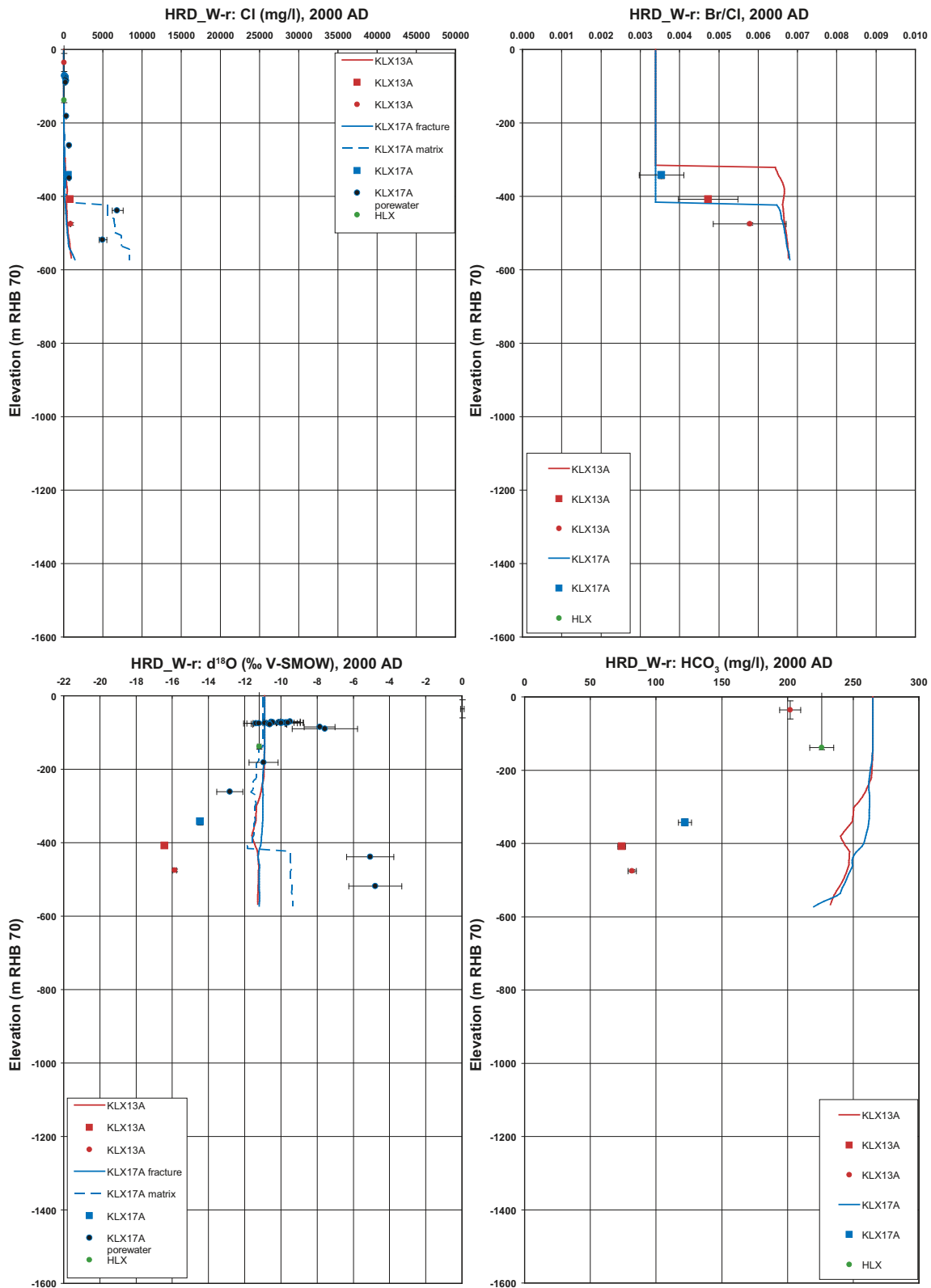


Figure 8-45. Comparison between the deterministic base model simulation (fracture water: solid lines; porewater = dashed lines) and measured concentrations of Cl, Br/Cl, $\delta^{18}\text{O}$ and HCO_3 (squares for Category 1–3, diamonds for Category 4, circles for porewater data) for boreholes in “HRD_W-recharge”. The error bars on the measured data indicate the laboratory analytical error.

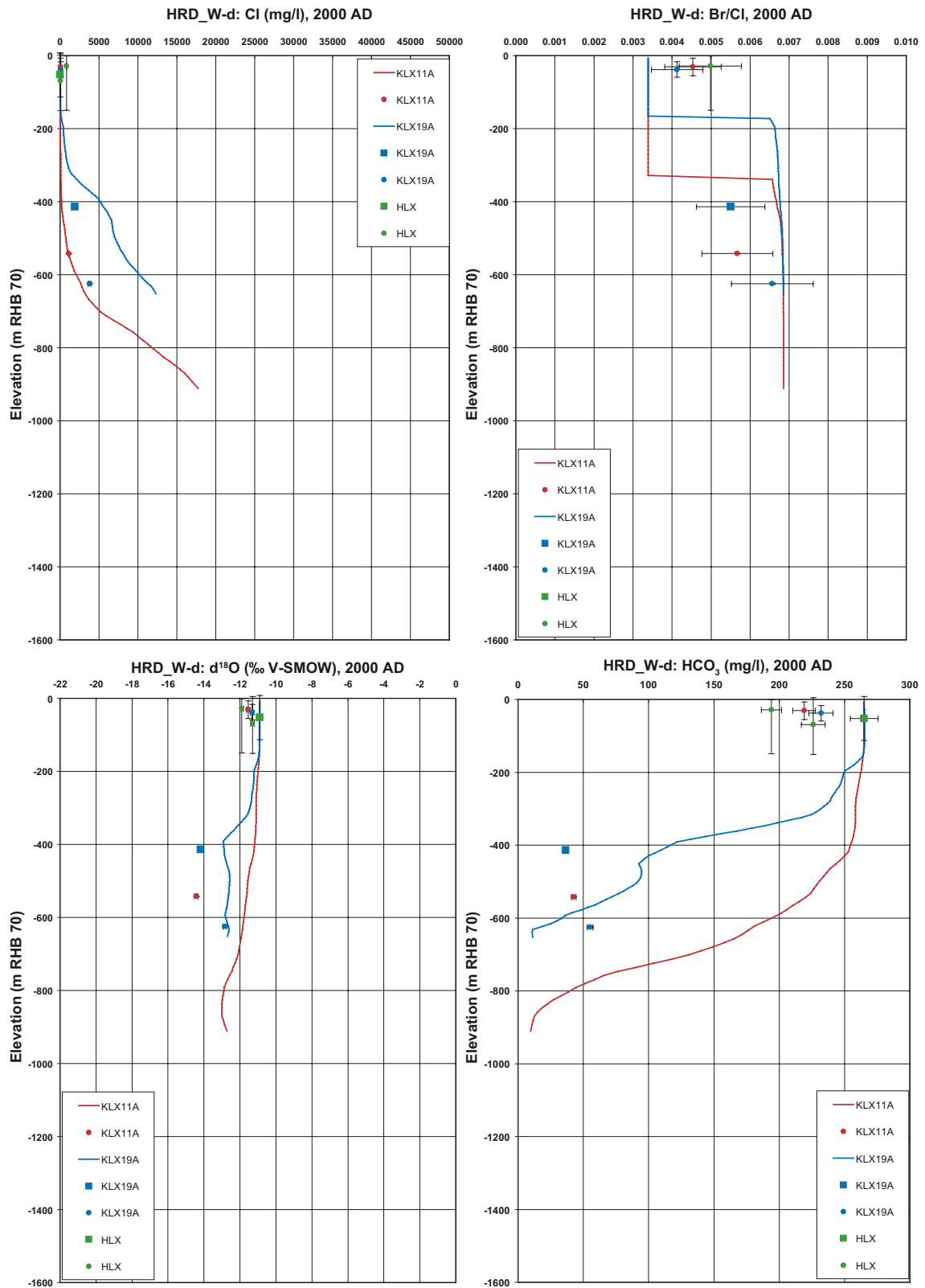


Figure 8-46. Comparison between the deterministic base model simulation (fracture water: solid lines; porewater = dashed lines) and measured concentrations of Cl, Br/Ci, $\delta^{18}\text{O}$ and HCO_3 (squares for Category 1–3, diamonds for Category 4, circles for porewater data) for boreholes in “HRD_W-discharge”. The error bars on the measured data indicate the laboratory analytical error.

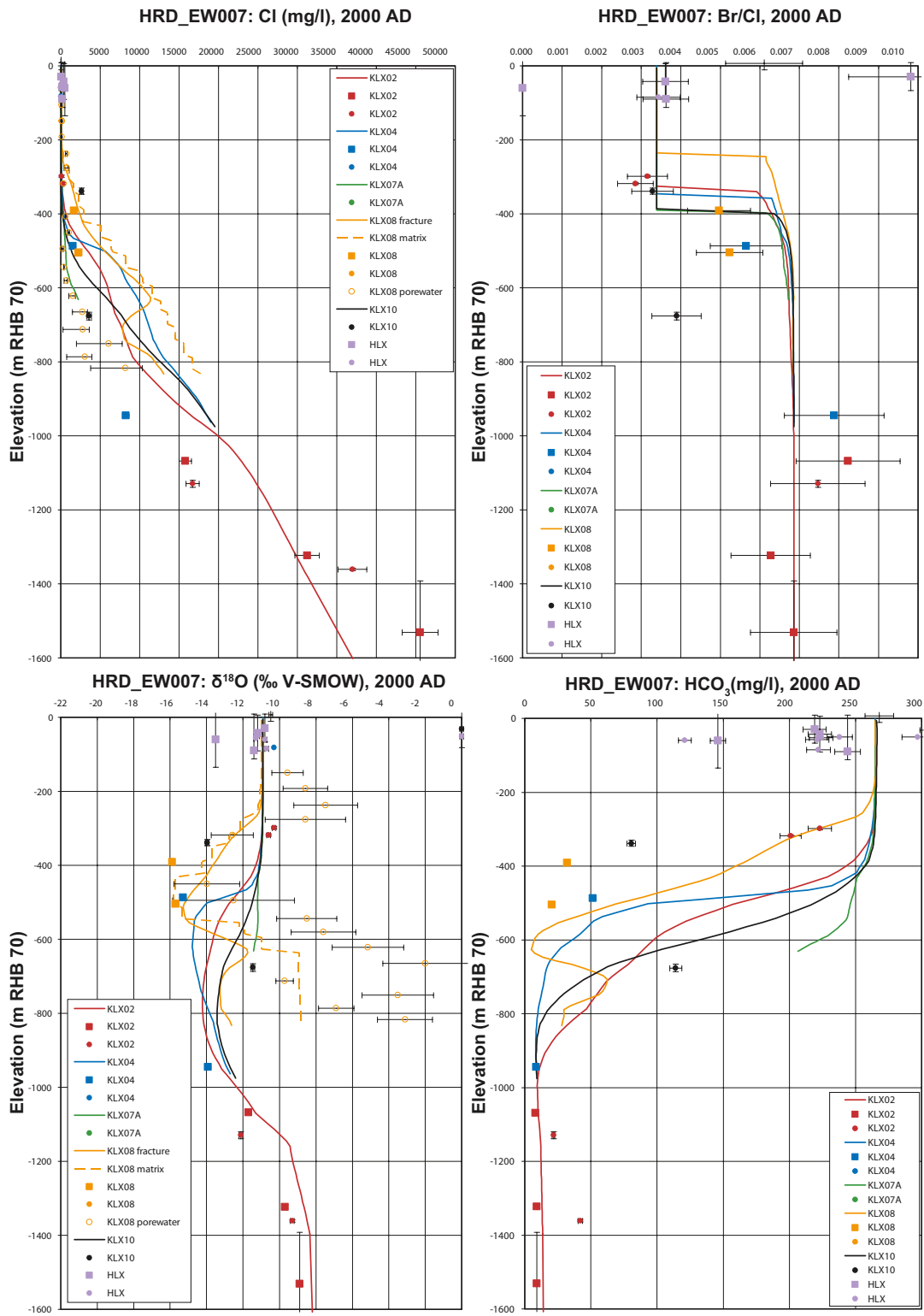


Figure 8-47. Comparison between the deterministic base model simulation (fracture water: solid lines; porewater = dashed lines) and measured concentrations of Cl, Br/Cl, $\delta^{18}\text{O}$ and HCO_3 (squares for Category 1–3, diamonds for Category 4, circles for porewater data) for boreholes in HRD_EW007. The error bars on the measured data indicate the laboratory analytical error.

8.6.7 Comment in relation to outcome of LPT (HLX28)

A long-term pumping and tracer test (LPT) was started 20th January 2009 with borehole HLX28 as pumping borehole and HLX32:2, HLX37:1, HLX38:3, KLX11A:3, KLX20A:5, and KLX27:6 as tracer injection sections (KLXxx:Y, Y is the number of the packed-off observation section), cf. Figure 8-48. The purpose of the test is to verify and shed light upon:

- HCD HLX28 DZ1 and its hydraulic contact with HCD ZSMNW042,
- ZSMNW042A and its hydraulic contact with ZSMNS001C and ZSMNS059A, respectively,
- The barrier effect coupled to the dolerite dykes ZSMNS001C and ZSMNS059A,
- The hydraulic contact between HRD and HLX28_DZ1 and ZSMNW042A.
- The approximate transport properties for HCD HLX28_DZ1 and ZSMNW042A and the indications for transport properties for the coupled system with ZSMNS001C and ZSMNS059A using tracer injections in packed-off borehole sections; HLX32:2, HLX37:1, HLX38:3, KLX11A:3, KLX20A:5 and KLX27:6, respectively.

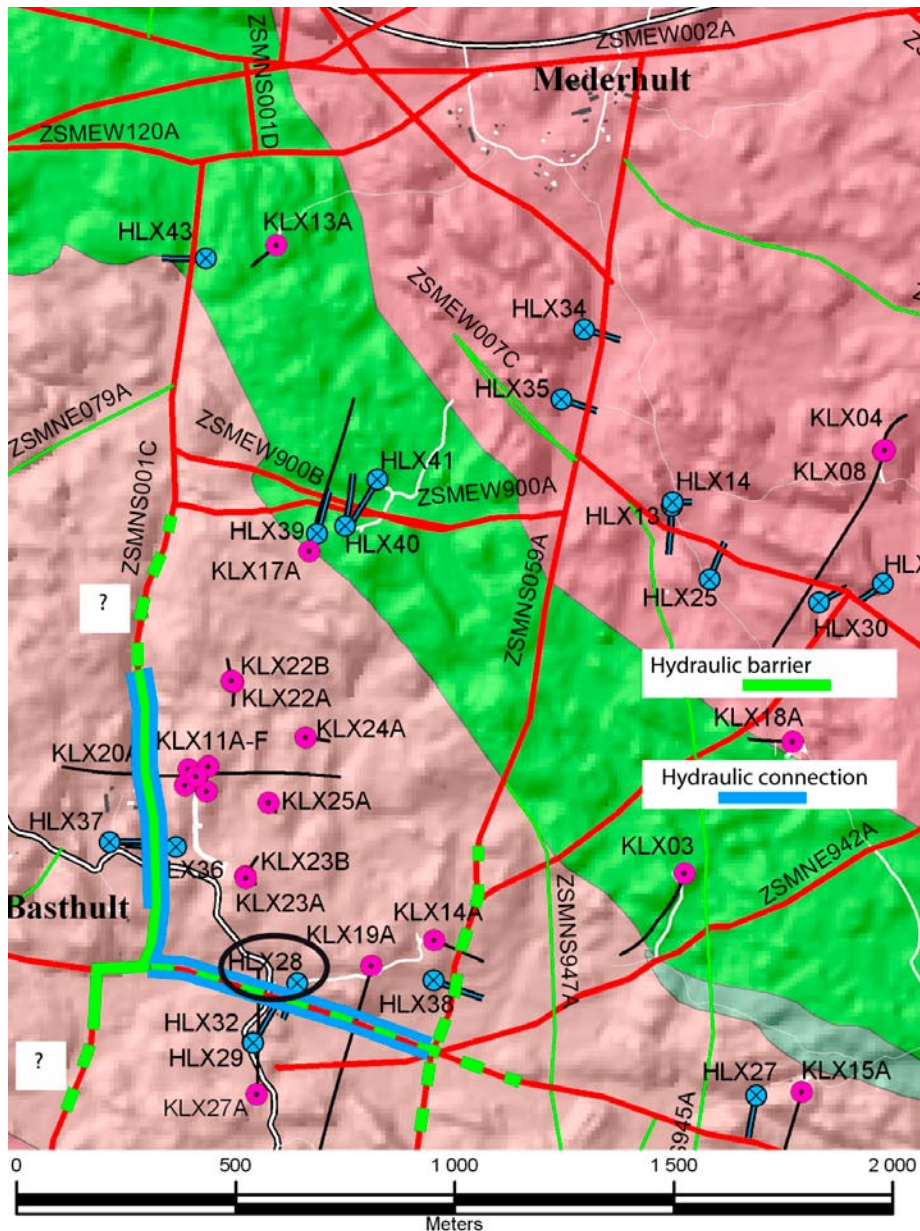


Figure 8-48. LPT tests with HLX28 as pumping borehole.

The test was finished May 2009 and only preliminary results are available.

The pressure response was monitored in 257 borehole sections during the test within the Laxemar local model area. The responses in KLX20A and HLX37 after two months of pumping clearly demonstrated the barrier effect of ZSMNS001. Responses in KLX03 and KLX14A, although rather small in KLX03 and the two eastern-most sections in KLX14A, showed that ZSMNS059A is not a complete hydraulic barrier. The reason may be that as the dyke is thin, it is locally permeable and/or that some deformation zones intersecting ZSMNS059A, e.g. ZSMNW042A, actually are not cross-cut by the dolerite dyke in such way that it prohibits pressure responses to be transmitted through the deformation zone. The responses south of ZSMNW042 in KLX27A are small, indicating that the suggested barrier effect attributed to fault gouge is a reasonable assessment. The response in KLX19A below the possible dolerite dyke, klx19_dz5-8 is small, as previously seen in other tests, and thus provides evidence for interpretation that this local zone acts as a barrier to flow across it.

8.7 Resulting bedrock hydrogeological model

The bedrock in the Laxemar-Simpevarp area has been extensively characterised with both single-hole and cross-hole (interference) tests. Single-hole constant-head injection tests and difference flow logging tests have been used in parallel to characterise the fracture properties close to the boreholes, whereas the interference tests have been used for larger-scale studies. Hydrochemical data and natural groundwater environmental head measurements have provided a basis for confirmatory testing of the hydrogeological interpretation using groundwater flow and solute transport simulations. The interpretation of the data and the simulations have formed the hydrogeological conceptual model, and the schematic 3D cross-section in Figure 8-49 summarises the key components of the conceptual model of the bedrock hydrogeology in the focused volume at Laxemar.

The general conclusions from these investigations are:

- the intensity of flowing fractures decreases with increasing depth,
- the upper part of the rock has more subhorizontal fracturing and slightly higher mean fracture transmissivities than the deeper parts,
- E-W zones have slightly higher transmissivities than other zones,
- WNW fractures have generally higher intensity and hence are more likely to be connected than fracture sets of other orientations,
- there is considerable spatial heterogeneity in hydraulic properties of both the deformation zones and bedrock in between, especially in the western part of the focused volume has lower fracture intensity but with slightly higher transmissivities than other parts of the volume.

Concerning the deterministically modelled deformation zones the following hydrogeological model has been suggested:

- the key interpreted characteristics are:
 - a clear trend of decreasing transmissivity with depth,
 - a positive correlation between interpreted “size” and transmissivity. Size here corresponds to interpreted trace length on the surface,
 - indications that the transmissivity of HCD is dependent on the orientations of deformation zones with E-W zones appearing more conductive than zones of other orientations,
 - significant lateral heterogeneity with a suggested standard deviation of $\text{Log}_{10}(T)$ of 1.4,
- in general the primary assessed transmissivity models for the HCD (based on the hydraulic test results) complies with the confirmatory model testing performed, however, with a general slight reduction in transmissivity (1/3) below –150 m elevation,
- in a few HCD larger corrections of the transmissivities were applied. In 3 HCD, ZSMEW007A, ZSMNE107A and ZSMNS001C, the longitudinal transmissivity (transmissivity along the zone plane) was increased significantly (a factor 3–50) above –400 m elevation, while the transmissivity of ZSMNE944A was reduced slightly compared to initial assessment,

- for consistency with the parameterisation of kinematic porosity in the HRD, a parameterisation of kinematic porosity formulated in terms of the flowing fracture intensity within the HCD and transport aperture of single fractures is recommended (rather than a formulation based on interpreted HCD transmissivity and thickness). Palaeohydrogeological calibration confirms the appropriateness of such a definition of kinematic porosity,
- the role of N-S dolerite dykes associated with ZSMNS001A-C and ZSMNS059A (along with some other dolerite affected minor HCD) as localised flow barriers appears confirmed by discontinuities in natural head measurements in core drilled boreholes. A similar effect arising from clayey fracture infill or fault gouge in ZSMEW002A and ZSMNW042A-west also seems to be confirmed by the natural head data. These behaviours are also confirmed by modelling these structures as strongly anisotropic, i.e. large contrast between longitudinal (in plane) transmissivity and transverse transmissivity. Particle tracking has shown that this has significant impact on groundwater flow patterns in at least the western part of the Laxemar subarea.

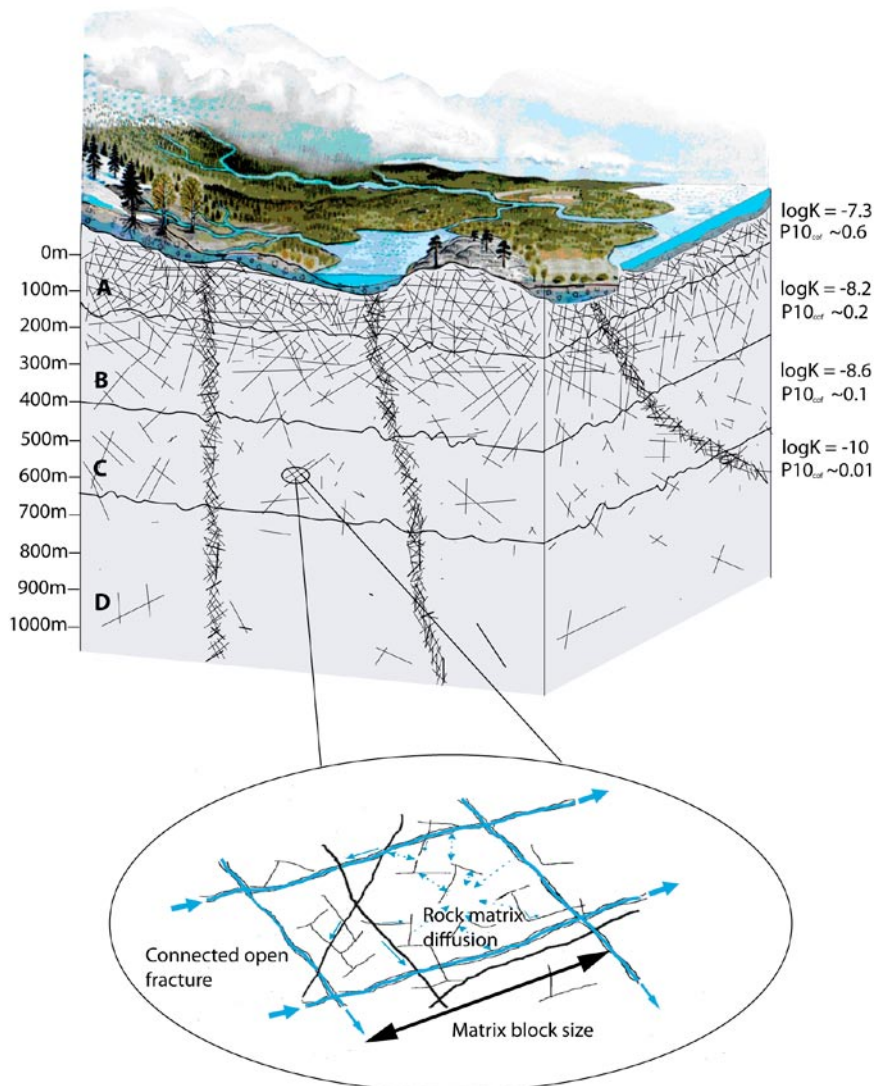


Figure 8-49. Schematic 3D cross-section summarising the hydrogeological conceptual model of the bedrock within the focused volume in Laxemar. Flow in the upper most depth zone **A** is dominated by subhorizontal and WNW fracturing. Solute transport is advection dominated with matrix block sizes of about 2 m, and about 1,000 years for hydrochemical equilibrium between fractures and matrix. WNW fractures dominate flow in **B-D**. In **B**, advective solute transport is retarded significantly by RMD with matrix block sizes of about 5 m and chemical signatures in the matrix lagging 1,000s of years behind the fractures. RMD dominates solute transport in **C** with a few sparse areas of significant advection. Matrix block sizes are around 10 m, and matrix hydrochemistry lags 10,000s of years behind fractures. There is very little advection in **D** with matrix block sizes of about 100 m and 100,000s of years lag between matrix and fracture hydrochemistry.

Concerning the bedrock in between the deterministically modelled deformation zones, the following hydrogeological model has been suggested:

- regional scale groundwater flow and solute transport simulation tests of palaeohydrogeology, natural head measurements and hydraulic interference test data have confirmed that hydrogeological properties implied by the hydrogeological DFN model base case /Rhén et al. 2008/ (based on all open and partly open fractures and semi-correlated transmissivity model) provide an appropriate description of the hydrogeological situation in the bedrock. Only relatively minor modifications were considered necessary to obtain acceptable comparisons between the flow model results and field data,
- a slight reduction (1/3) in hydraulic conductivity below –150 m elevation improved the palaeohydrogeological calibration,
- Sensitivity studies suggest a slight increase (a factor 3) in hydraulic conductivity above –150 m elevation was beneficial to both the natural head and palaeohydrogeology calibration to measured hydrochemistry, although such a change was not included in the base case model,
- basing kinematic porosity on connected fracture intensity and transport aperture as calculated by the hydrogeological DFN model was confirmed as being appropriate for the palaeohydrogeological simulations, although it was necessary to include the contribution to kinematic porosity from small fractures down to the $r=0.28$ m scale by increasing the hydrogeological DFN-based kinematic porosity by a factor of 5,
- fracture surface area per unit volume used to parameterise rock matrix diffusion (RMD) of solute transport based on the average intensity of flowing fractures detected by the PFL method proved appropriate in the palaeohydrogeological calibration. This confirms the decreasing intensity of flowing features with depth as indicated by the hydrogeological DFN model.

An important aspect of solute transport is the relative magnitude of advective transport to rock matrix diffusion. Where advection in the fractures is rapid then there is little time for solute to diffuse transversely into the matrix (porewater), and hence there is little retardation of the solute mixing front. Where advection is reduced, then a greater relative proportion of solute diffuses into the matrix as the solute moves through the fractures, and hence the advance of the mixing front is retarded. Rates of advection are governed by fracture intensity, transmissivity, hydraulic gradient and kinematic porosity. As concluded in Section 8.4.2, the key parameter controlling volumetric flux through a rock volume in Laxemar is the intensity of water conducting fractures. Rates of diffusion are governed by diffusivity, concentration gradients and matrix porosity. The total exchange of solute with the matrix within a rock volume scales linearly with flowing fracture area per unit volume, i.e. fracture intensity. Therefore, both transport processes, advection and RMD, scale in proportion to the same key parameter and hence their ratio is relatively uniform, and in consequence the variability in the solute mixing front is likely to be much less than the variability in hydraulic material properties.

Combining the interpretation of hydraulic characteristics of the bedrock from /Rhén et al. 2008/ with the understanding gained from simulating the palaeohydrogeological evolution /Rhén et al. 2009/, the hydrogeological situation for groundwater flow and solute transport is summarised in Table 8-11. This description focuses on the balance between advective solute transport and the effect of RMD as suggested by the measured hydrochemical data. This balance will be affected by the natural hydraulic gradients present during the current climatic period, and changes during periods of elevated gradient, e.g. during deglaciation.

Table 8-11. Schematic summary of groundwater flow and solute transport characteristic under the current temperate climate conditions.

Depth zone	General characteristics
> –150 m	Advection dominated – high groundwater flow rates with subhorizontal fracturing giving $K_h > K_v$ in many areas. Flushed by post-glacial meteoric water. High fracture intensity is high, with matrix blocks 1–2 m in size, which gives equilibrium between fracture and matrix on timescales of ~1,000 years.
–150 m to –400 m	Some advection, but rock matrix diffusion (RMD) provides retardation of post-glacial meteoric penetration. Fracture intensity is generally much lower, reducing advection and matrix blocks typically ~5 m in size, and so matrix lags behind fractures by 1,000s of years. In more fractured areas, enhanced access to matrix counters enhanced flux, and so mixing fronts are relatively uniform.
–400 m to –650 m	Low advection. Solute mixing front greatly retarded by RMD because advective flow rates are low. Fracture intensity is lower still, with typical matrix blocks ~10 m in size, and so matrix hydrochemistry lags behind fractures ~10,000 years. Expect some differences between fracture and porewater chemistry.
< –650 m	Very low advection. RMD dominates Fracture intensity very low, with typical matrix blocks ~100 m in size, and so matrix hydrochemistry lags behind fractures ~100,000 years. Expect substantial differences between fracture and porewater chemistry.

8.7.1 Visualisations in support of hydrochemistry interpretation

Based on the palaeohydrogeological model calibrated against chemical samples collected in boreholes, predictions were made of the present-day 3D spatial distribution of hydrochemical constituents between the boreholes. Examples of the palaeohydrogeological cross-sections identified in Figure 8-50 are shown in Figure 8-51 and Figure 8-52. Figure 8-51 shows the distribution of Cl (indicating salinity) and $\delta^{18}\text{O}$ (indicating remnants of *Glacial Melt Water*) on horizontal sections at –500 m. It can be seen that continuous lenses of brackish-glacial water exist along the low-lying E-W valleys associated with the Laxemarån river valley (ZSMNW042A) in the south, the Mederhult zone (ZSMEW002A) to the north, and beneath zone ZSMEW007A in the centre of the Laxemar subarea. There are also smaller localised lenses of brackish-glacial water throughout the focused volume that are a result of spatial heterogeneity, and hence may vary in position and magnitude according to the particular realisation of HRD and HCD hydraulic properties. The model predicts that boreholes KLX01, KLX02, KLX03, KLX04, KLX05, KLX08, KLX15A, KLX19A all either intersect or are very close to lenses of brackish water at this depth. There are areas of less saline water predicted in the centre of HRD_C and especially HRD_W which are not intersected by any boreholes with chemical sampling. *Glacial Melt Water* is present in similar areas, especially the large continuous lens of depleted $\delta^{18}\text{O}$ water beneath zone ZSMEW007A, gently dipping to the north.

As an example of simulated hydrochemistry on a vertical section, Figure 8-52 shows the composition of fracture groundwater in terms of mass fractions of *Littorina Sea Water*, *Glacial Melt Water*, *Altered Meteoric Water* and *Deep Saline Water* on the WNW-ESE Section B (see Figure 8-50). This shows that *Littorina Sea Water* is generally below 10% throughout the Laxemar subarea, persisting at the level of just a few percent at the present-day. It does enter the fracture system in the lower lying areas (below about 15 m for the present-day topography) during the Littorina maximum, but gets displaced by post-glacial meteoric infiltration once the land has risen above sea level. This contrasts with the clear *Littorina Sea Water* signature seen at Forsmark /Follin et al. 2007c/, which persists mainly due to the lower topography and hydraulic gradients. *Altered Meteoric Water* generally penetrates to –200 m to –400 m in the Laxemar subarea, a little deeper in HRD_W. Continuous lenses of remnant *Glacial Melt Water* in HRD_EW007 exist beneath the northwardly gently dipping zone ZSMEW007A and further east beneath lower lying areas, centred on repository depth, –500 m. Highly saline (>600 mg/l of Cl) non-marine water associated with *Deep Saline Water* starts at about –500 m.

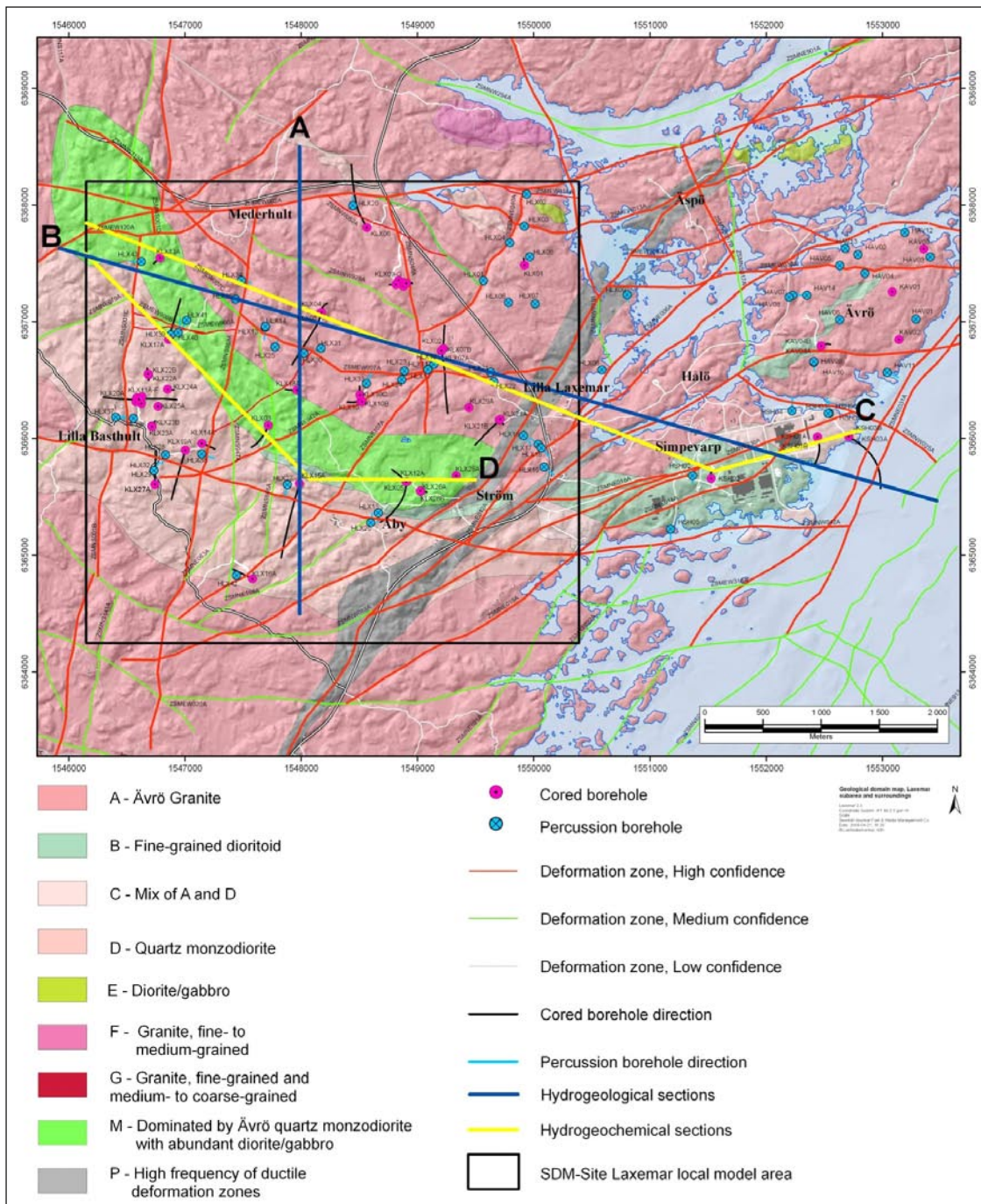


Figure 8-50. Sections A and B (blue lines) correspond to hydrogeological Sections 5 and 7, respectively, in /Rhén et al. 2009/. Sections C and D (yellow lines) correspond to hydrochemical Sections 3 and 5, respectively, in /Laaksoharju et al. 2009/.

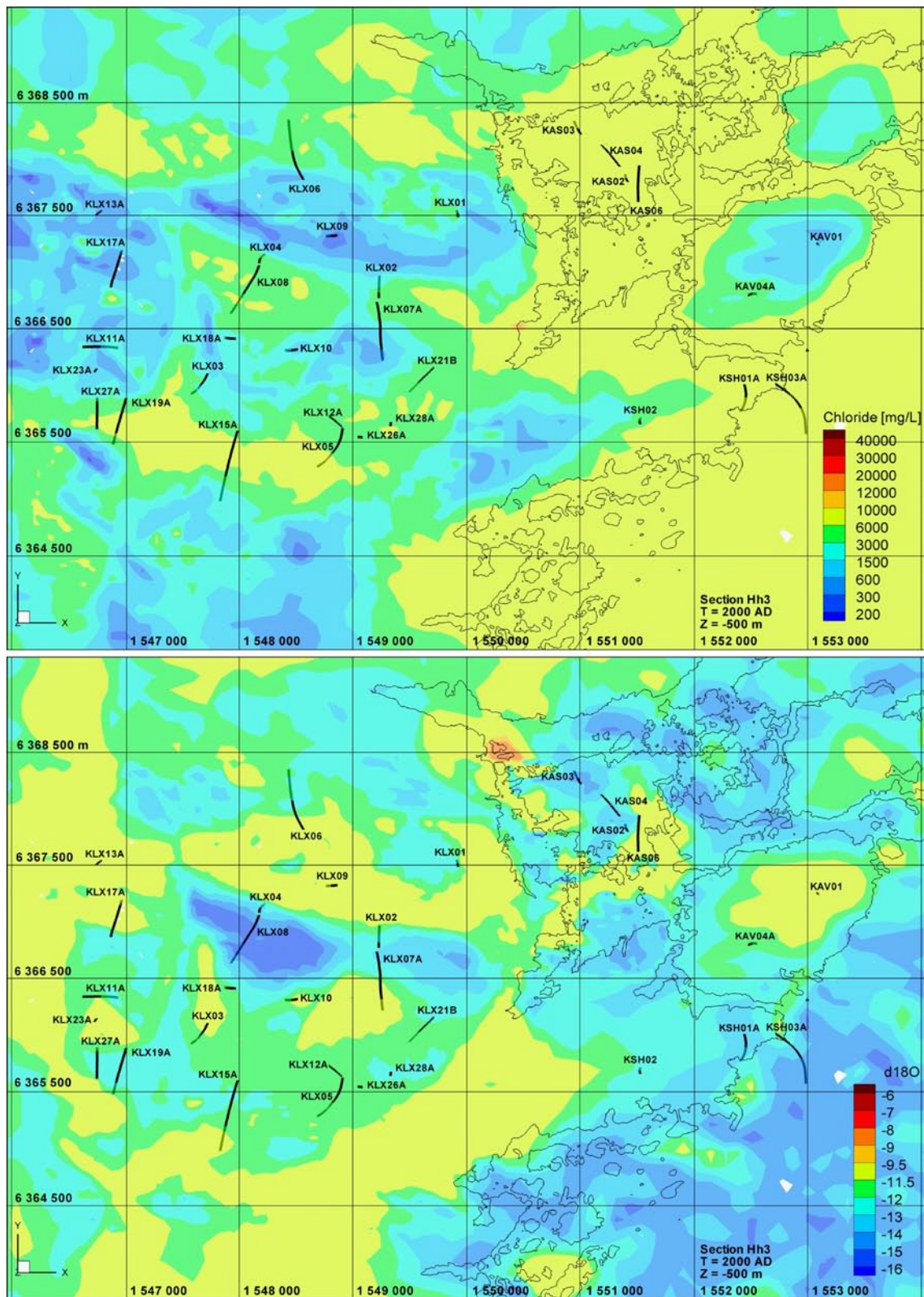


Figure 8-51. Distribution of Cl (top) and $\delta^{18}O$ (bottom) predicted on a horizontal slice at -500 m covering the Laxemar-Simpevarp area in the deterministic base model simulation.

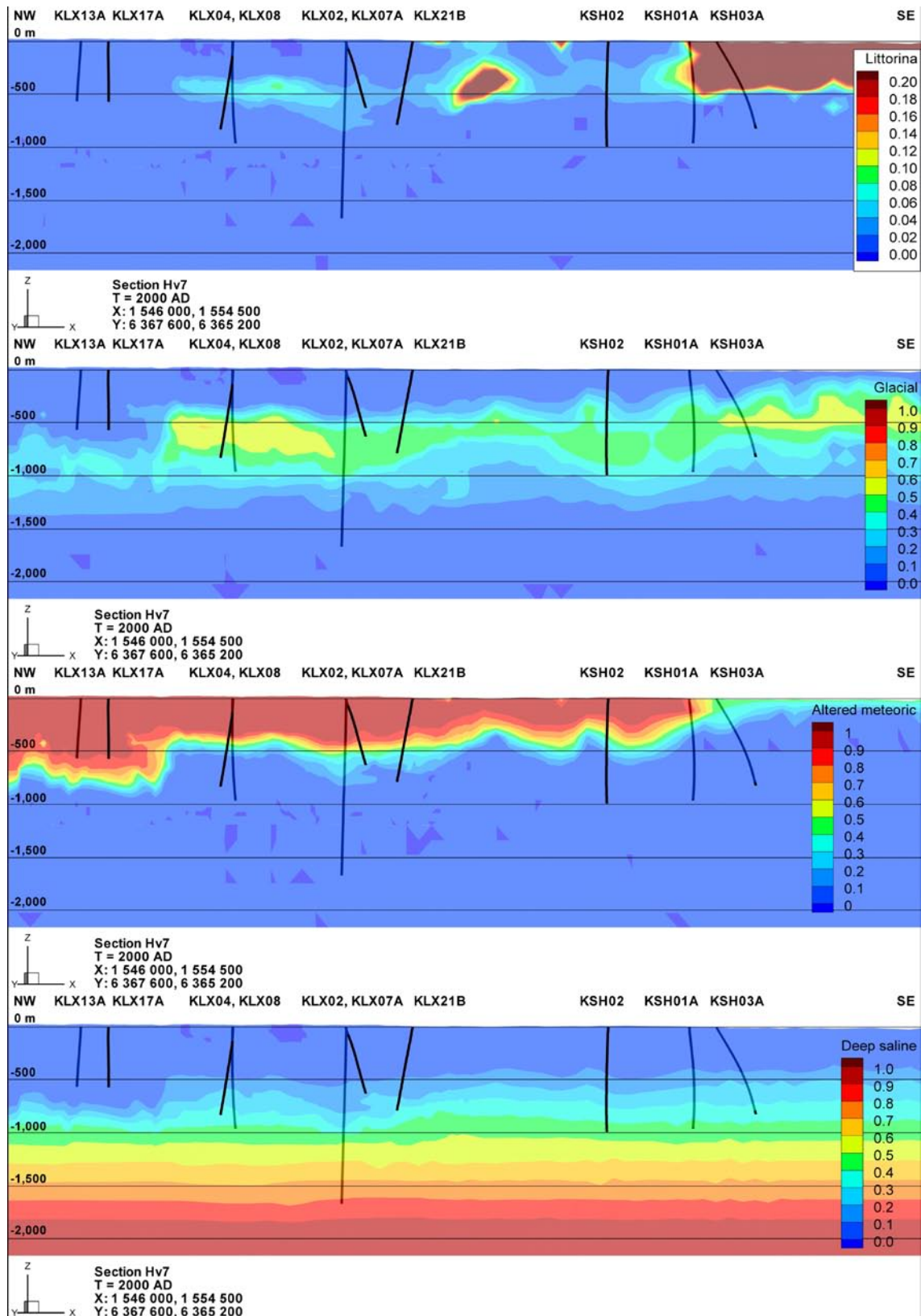


Figure 8-52. Distribution of mass fractions reference waters: Littorina Sea Water (on a scale 0–0.2), Glacial Melt Water, Altered Meteoric Water, and Deep Saline Water (top to bottom) predicted by the deterministic base model simulation on vertical WNW-ESE Section B through the Laxemar-Simpevarp area, cf. Figure 8-50.

8.7.2 Visualisations for interpretation of flow and solute transport

Particle tracking is a useful tool for interpretation of groundwater flow paths and calculation of solute transport flow-path properties. Figure 8-53 through Figure 8-55, show particle tracks for the *deterministic base model simulation* when particles are released at elevation –500 m in HRD_C, HRD_W and HRD_EW007, respectively. In HRD_C the particles generally head south toward ZSMNW042A or east toward ZSMNE005A and ZSMNE006A where they reach the bay near Äspö, with a few particles continuing further south east to the Baltic south of the Simpevarp peninsula. For HRD_W, the flow-paths are hemmed in by the dolerite dykes associated with ZSMNS001C and ZSMNS059, and hence most particles discharge to the south in ZSMNW042A. For HRD_EW007, most particles follow ZSMEW007A eastward to discharge either in ZSMNE005A or in ZSMNE006A where they reach the bay near Äspö.

Figure 8-56 ranks the HCD according to their importance for particle tracking, and shows that ZSMNE005A, ZSMNW042A-east and ZSMNE006A form the downstream path for 40–50% of particles. ZSMNE012A, ZSMNE004A, ZSMNE107A, ZSMNS059A and ZSMNE942A all encounter about 20–30% of the particles.

Backward pathlines were also used to identify areas of recharge relevant to the focus volume. The main recharge area for HRD_C is the low hills south of zone ZSMEW007A within HRD_C itself. South of ZSMNW042A, the recharge areas are some low hills further south, again very localised. For HRD_W, the recharge area is also within the HRD lying toward the north, near high topography around ZSMEW900A. HRD_EW007 gets recharge from the same low hills as HRD_C to the south of ZSMEW007, and from some hills slightly to the north. In summary, all recharge areas affecting the repository area at 2000 AD are localised, predominantly within the Laxemar subarea. Hence, flow and chemistry boundary conditions far west of the Laxemar subarea have limited influence on the focused volume.

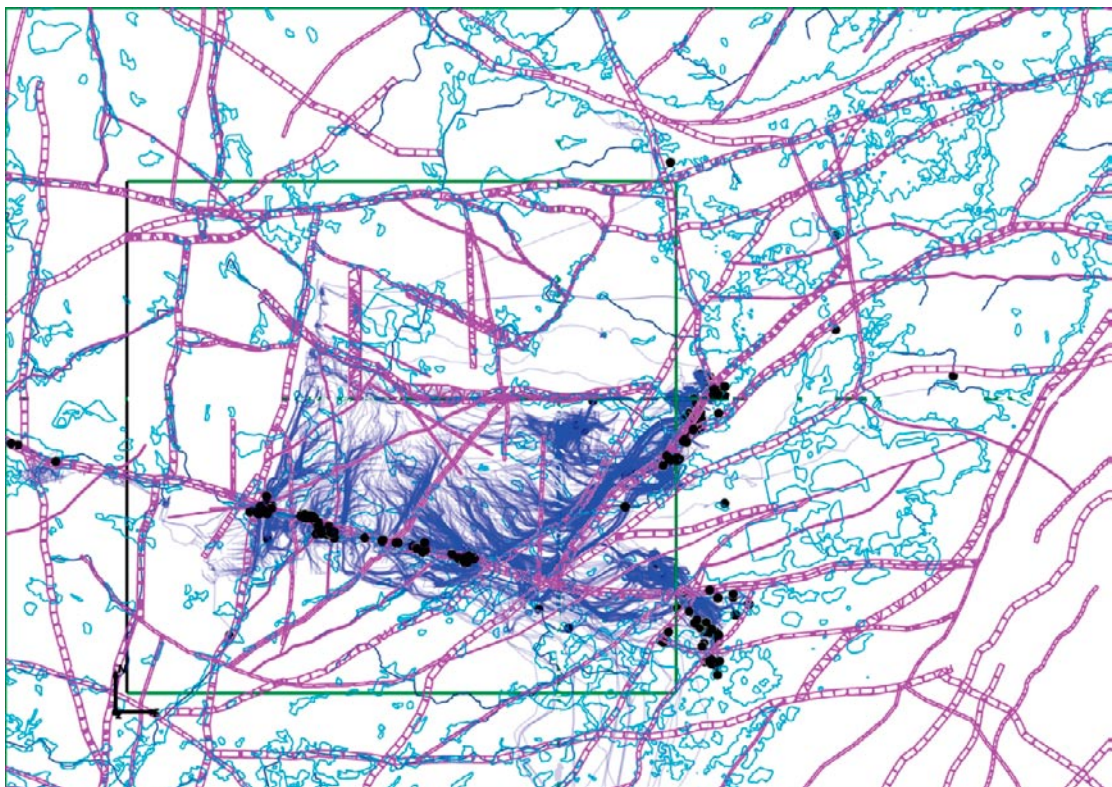


Figure 8-53. Pathlines for the base case model. Pathlines starting in HRD_C are shown in blue with the exit locations (discharge) in black. HCD at 0 m (purple), surface water bodies (cyan), streams (blue), and the local model area (green) are superimposed.

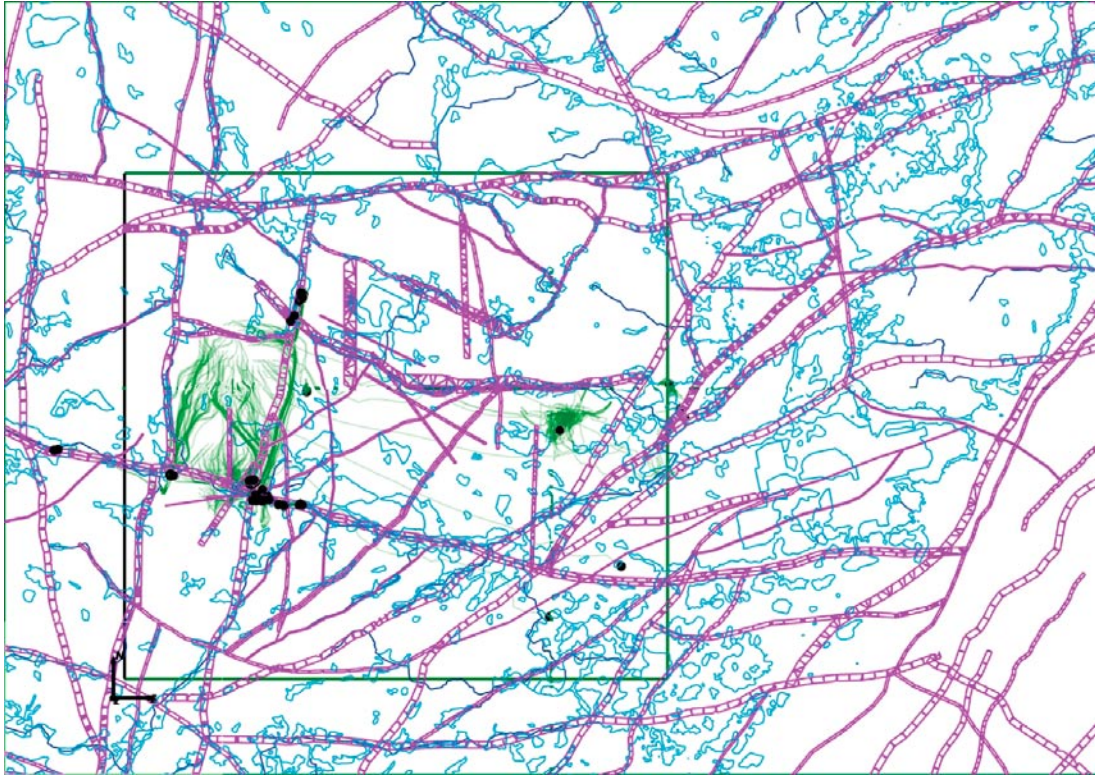


Figure 8-54. Pathlines for the base case model. Pathlines starting in HRD_W are shown in green with the exit locations (discharge) in black. HCD at 0 m (purple), surface water bodies (cyan), streams (blue), and the local model area (green) are superimposed.

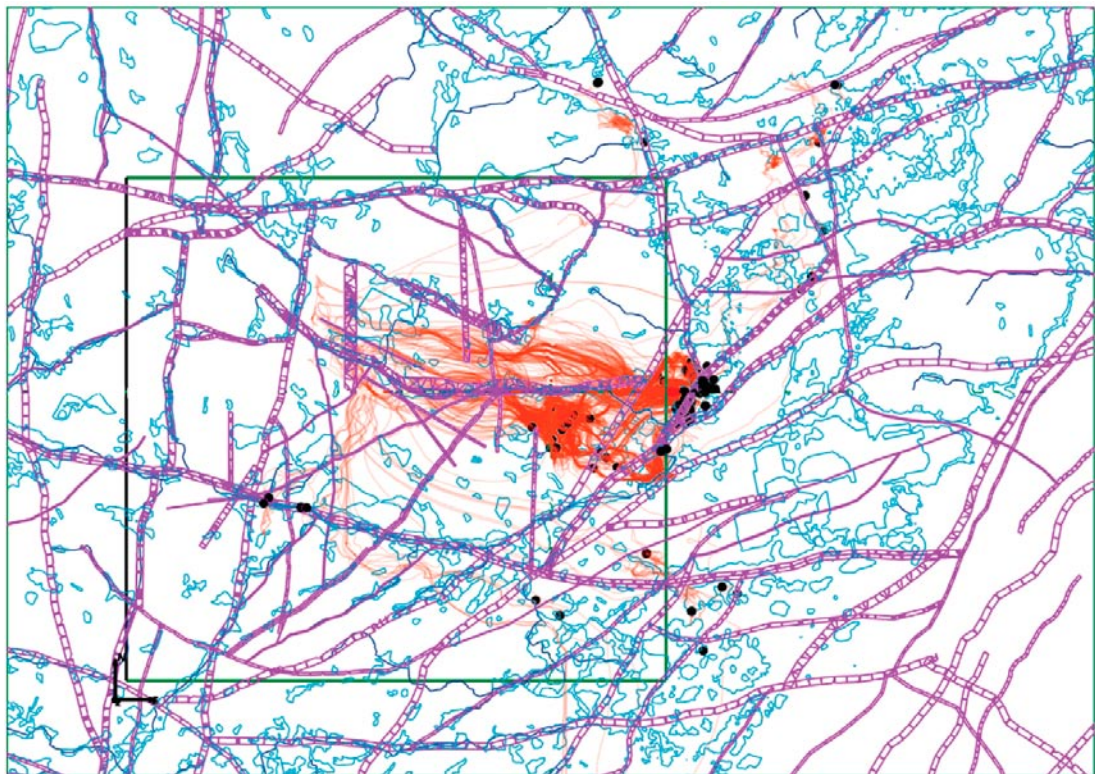


Figure 8-55. Pathlines for the base case model. Pathlines starting in HRD_EW007 are shown in red with the exit locations (discharge) in black. HCD at 0 m (purple), surface water bodies (cyan), streams (blue), and the local model area (green) are superimposed.

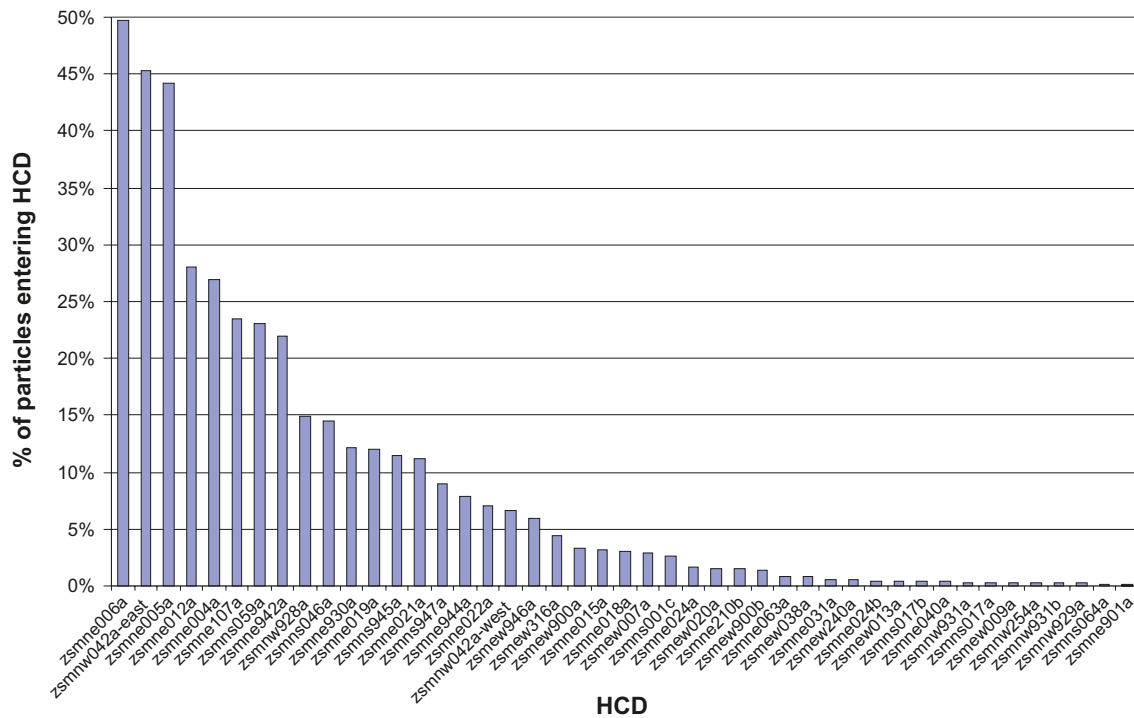


Figure 8-56. Histogram showing the percentage of particles that enter each HCD along pathlines started at the 2,142 locations in the focused area for the base case. The HCD are ordered accordingly. Thus, almost 50% of particles enter ZSMNE006A. A particle may enter several HCD, and so the percentages add to >100%.

8.7.3 Average vertical flux rates versus depth

Table 8-12 presents the arithmetic average discharge and recharge through a series of depth-distributed surfaces corresponding to the ground surface topography of the local model area extended to also cover the Simpevarp subarea, as extracted from the SDM-Site Laxemar base case model groundwater flow simulation. The average recharge is based on the downward flow rate at 2000 AD divided by the extended local model area as defined above. Correspondingly, the average discharge is based on the upward flow rate. The Darcy velocities are based on the velocity components in each cell, sorted on HCDs and HRDs. The bulk bedrock Darcy velocity in the near surface bedrock between deformation zones at a depth of 20 m is in the order of 60 mm/year where the corresponding velocity at repository depth is 0.16 mm/year, i.e. about a factor 380 lower. At repository depth (500 m) the Darcy velocity in HCD is about 0.6 mm/year, which is 4 times higher than in the HRD at the corresponding depth.

Table 8-12. Summary of arithmetic average discharge and recharge through a series of depth-distributed surfaces corresponding to the ground surface topography of an area corresponding to the local model area extended to also cover the Simpevarp subarea, as extracted from the SDM-Site Laxemar base case model groundwater flow simulation. The geometric means of the magnitude of the Darcy velocity vector for points in each plane are given for the entire bedrock, outside of the deformation zones, and inside the deformation zones.

Vertical depth below ground surface [m]	Average discharge [m/year]	Average recharge [m/year]	Geometric mean Darcy velocity [m/year]	Geometric mean Darcy velocity outside deformation zones [m/year]	Geometric mean Darcy velocity in deformation zones (m/year)
1	$4.96 \cdot 10^{-2}$	$1.86 \cdot 10^{-1}$	$1.3 \cdot 10^0$	$9.7 \cdot 10^{-1}$	N/A
20	$4.38 \cdot 10^{-2}$	$4.57 \cdot 10^{-2}$	$6.6 \cdot 10^{-2}$	$5.8 \cdot 10^{-2}$	$8.8 \cdot 10^{-2}$
100	$2.21 \cdot 10^{-2}$	$2.35 \cdot 10^{-2}$	$4.5 \cdot 10^{-2}$	$3.7 \cdot 10^{-2}$	$6.2 \cdot 10^{-2}$
180	$6.93 \cdot 10^{-3}$	$6.52 \cdot 10^{-3}$	$6.1 \cdot 10^{-3}$	$4.2 \cdot 10^{-3}$	$1.2 \cdot 10^{-2}$
340	$1.82 \cdot 10^{-3}$	$1.95 \cdot 10^{-3}$	$1.7 \cdot 10^{-3}$	$1.0 \cdot 10^{-3}$	$4.0 \cdot 10^{-3}$
500	$3.21 \cdot 10^{-4}$	$3.15 \cdot 10^{-4}$	$2.9 \cdot 10^{-4}$	$1.6 \cdot 10^{-4}$	$6.4 \cdot 10^{-4}$
660	$8.36 \cdot 10^{-5}$	$9.37 \cdot 10^{-5}$	$5.5 \cdot 10^{-5}$	$2.6 \cdot 10^{-5}$	$1.5 \cdot 10^{-4}$
780	$4.10 \cdot 10^{-5}$	$4.02 \cdot 10^{-5}$	$1.4 \cdot 10^{-5}$	$8.5 \cdot 10^{-6}$	$2.8 \cdot 10^{-5}$

8.8 Parameter sensitivity analysis

The sensitivity of the simulated groundwater pressure and solute transport to a number of uncertain parameters and model settings is illustrated in /Rhén et al. 2009/. Some variant case simulations were used to illustrate the development of the model calibration. For example, a variant to show why it had been necessary to modify the transmissivity of some HCD; and a variant to show why the hydraulic conductivity of the bedrock below -150 m had been reduced. An interesting variant was to demonstrate that by increasing the horizontal hydraulic conductivity above -150 m elevation, motivated by a possible slightly higher transmissivity in the dominant subhorizontal fracturing in the upper bedrock, resulted in an improved match to both the natural groundwater heads and hydrochemistry. Another variant calculation was used to demonstrate how important the interpreted anisotropy in some HCD, i.e. the dolerite-dykes, together with ZSMNW042A-west and ZSMEW002A, is in reproducing the “jumps” in observed environmental head observed across these zones. For solute transport, additional variants were considered to assess the sensitivity to boundary and initial conditions. One variant considered the sensitivity to the non-marine water prior to the Littorina period, considering either a meteoric or glacial composition, which had very little effect on present-day hydrochemistry. A second variant considered a deeper initial profile for *Deep Saline Water*, which resulted in a similar salinity, but of slightly increased marine composition, about 5–10% in the Laxemar subarea, rather than 0–5%. A third variant considered a different initial porewater composition with the *Inter-glacial Porewater* being brackish of mixed meteoric and marine composition, with $Cl=5,000$ mg/l, which resulted in only slight differences to the fracture water composition, but lower and perhaps more realistic salinity of the porewater.

The sensitivity considered most important to test by numerical modelling was the spatial variability in the hydraulic properties due to the interpreted high lateral heterogeneity in HCD transmissivity, $\text{Log}_{10}(T)$ of 1.4, and the observed variability in flowing fracture statistics between boreholes. Groundwater flow and solute transport calculations were performed for 10 variant cases each based on 1 realisation of the HRD, varying spatially according to the stochastic nature of the hydrogeological DFN model, and 1 realisation of lateral heterogeneity in the HCD transmissivity. These 10 realisations were used to quantify the stochastic variability in predicted point-water heads in percussion drilled boreholes (see Figure 8-57), the environmental heads in core drilled boreholes (see Figure 8-58), and of hydrochemical constituents (see Figure 8-59). Figure 8-57 indicates that

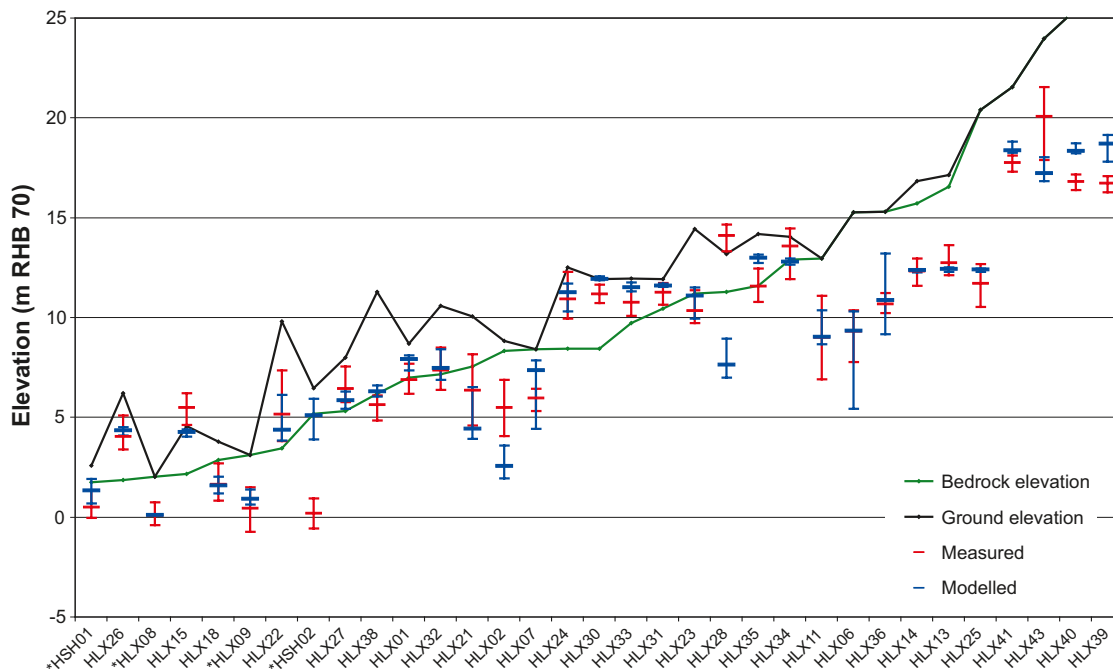


Figure 8-57. Comparison of measured heads in percussion drilled boreholes (HLX) for 10 stochastic realisations of HCD and HRD. For the model, the minimum, maximum and median value in the bedrock is shown in blue. The field data are plotted as mean point water heads in the bedrock with error bars to show the range of values at different measurement times. Boreholes marked by a * are outside the local model area.

the point-water heads in some percussion drilled boreholes, such as HLX06, are highly dependent on spatial variability of the hydraulic conductivity and so discrepancies between model predictions and measurements can be explained by spatial heterogeneity. For others, such as HLX40, the effect of spatial variability is small, and hence perhaps other parameters should be considered to improve the match. Two examples, of the sensitivity of environmental head to spatial variability are shown in Figure 8-58. These are typical and demonstrate how the measurement values generally fall within the range predicted with spatial variability, indicating that the calibration on heads is probably as good as can be achieved given the magnitude of variability in the bedrock hydraulics. Similarly, the variability in simulated hydrochemical constituents is exemplified by KLX08 in Figure 8-59. This indicates that the depth to a particular hydrochemical signature can vary by as much as 200 m between realisations, and can make the difference between the existence or not of a pocket of glacial water within a particular borehole. It is noted that the results for the *deterministic base model simulation* tends to result in less flushing by post-glacial infiltration than in the majority of realisations with heterogeneous HCD. In two-dimensions, one would expect the ensemble mean flow-rates in a zone to be given by the geometric mean transmissivity, but in three-dimensions the flow-rate will be slightly enhanced by variability if zones are thick compared to element sizes used. Hence, the hydrochemistry results with spatial variability suggest that high flow channels within the HCD have enhanced connectivity via high flow channels in the surrounding HRD.

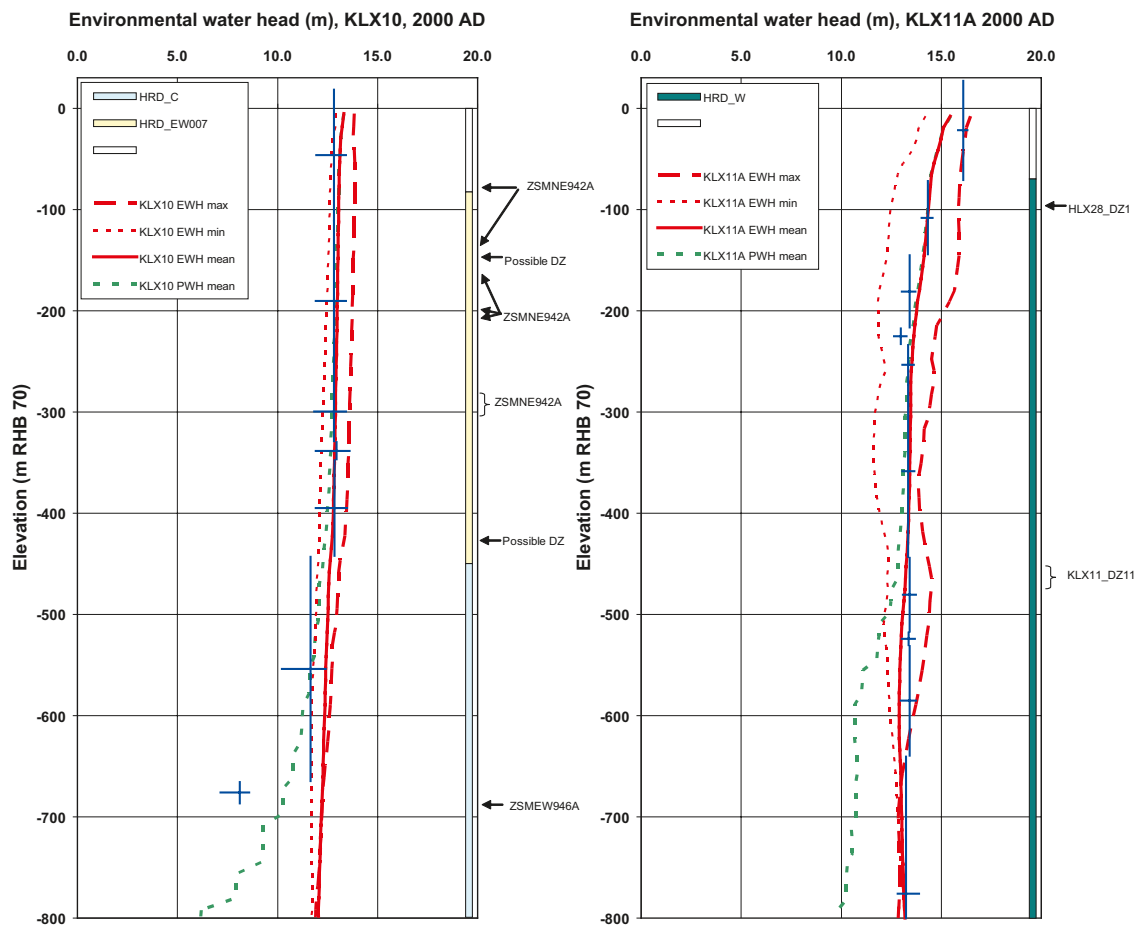


Figure 8-58. Examples of stochastic variability of modelled environmental-water head for 10 realisations of HCD and HRD (mean: solid red line; min: dotted red line; max: dashed red line) and point-water head (mean: dotted green line) in KLX10 in HRD_C and KLX11A in HRD_W compared with observed environmental-water heads (blue crossed lines, centre showing midpoint of the section, vertical line showing the extent of the section and horizontal line showing the temporal variation of the measured head) calculated from measured point-water head data in sections along the borehole. At the right hand side, the prevailing hydraulic rock domains are shown as coloured bars along the borehole. Detected fractures/deformation zones are indicated at their interpreted intersection depths in the borehole.

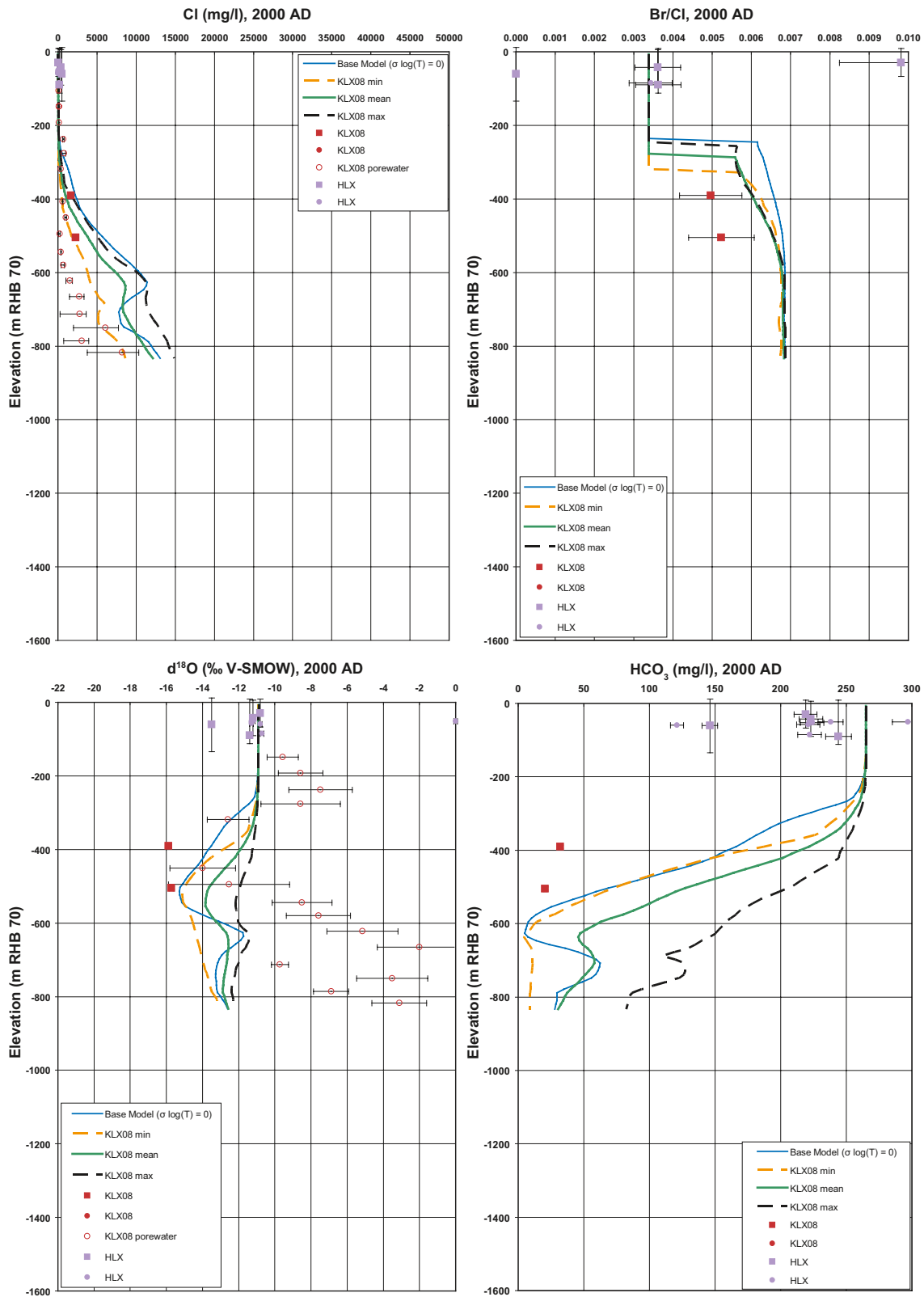


Figure 8-59. Examples of stochastic variability of Cl, Br/Cl, $\delta^{18}O$ and HCO_3 in the fracture system for 10 realisations of HCD and HRD (mean: solid green line; min: dashed orange; max: dashed black; base case: solid blue) compared with data in KLX08. Square symbols are used for hydrochemistry Category 1–3 data, circles are used for the porewater data, and small diamond symbols for the hydrochemistry Category 4 data. The error bars on the data only indicate the laboratory analytical error.

The effect of spatial heterogeneity on particle tracking was also considered in terms of the variability in exit locations for the 10 realisations of HCD/HRD. The results are presented in Figure 8-60 and indicate the same key areas of discharge as the *deterministic base model simulation*, but there are also quite a lot of additional minor discharge areas that occur when spatial heterogeneity is considered. ZSMNS001D, ZSMEW002, ZSMNW254, ZSMNE021A all appear as being possible discharge areas when a stochastic modelling approach is used. Hence, it is recommended that multiple realisations also are considered in any future modelling.

The other important sensitivity for particle tracking is the effects of hydraulic anisotropy interpreted for some HCD, i.e. the dolerite-dykes, together with ZSMNW042A-west and ZSMEW002A. A variant without such anisotropy revealed that the main difference is that particles starting in HRD_W generally exit further to the east. Particles starting in the northern part of HRD_W around ZSMEW900A seem to enter ZSMEW007A and discharge many kilometres further east, demonstrating the strong influence of the dolerite dykes on solute transport in HRD_W. Based on back tracing particle tracks upstream from the focused volume it is concluded that the relevant recharge areas change only subtly with the low hills in HRD_W becoming more important, but the majority of recharge to the focused volume remains within the Laxemar local model area. There is slightly more, perhaps a few percent, of back traced particles that originate several kilometres to the WSW of the Laxemar subarea around zone ZSMNS009A.

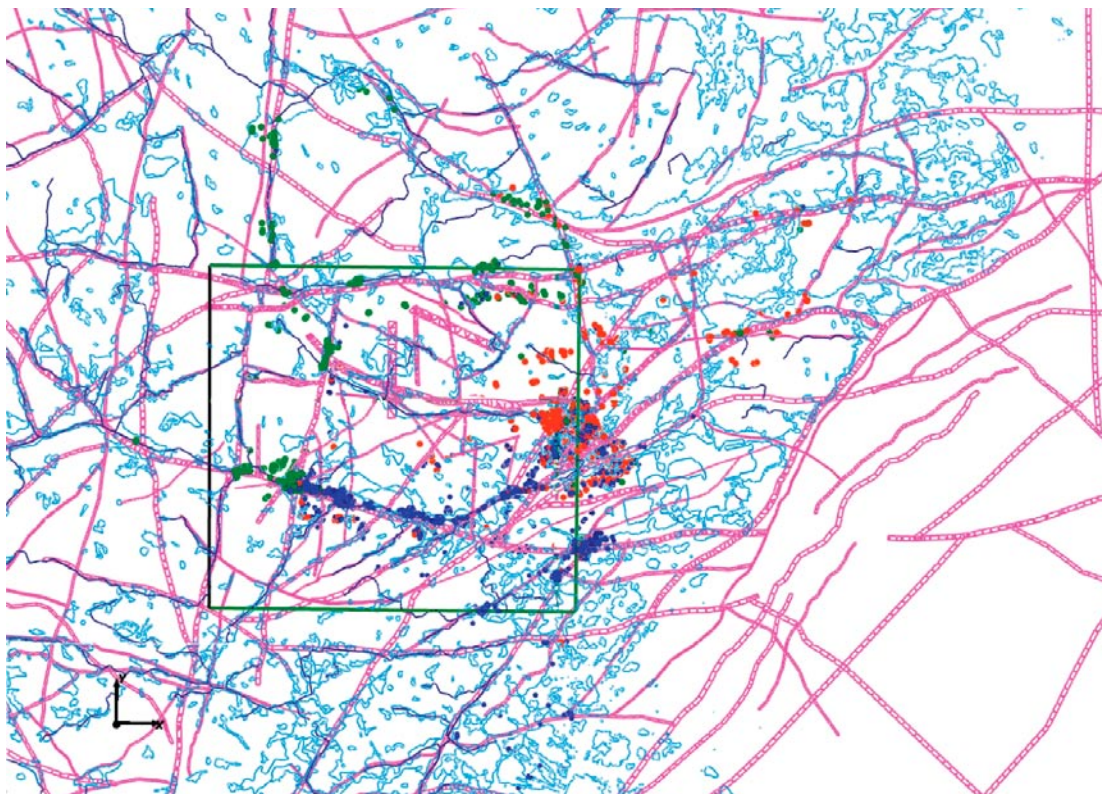


Figure 8-60. Particle exit locations of pathlines released in HRD_C (blue), HRD_EW007 (red) and HRD_W (green) for 10 realisations of the HRD and HCD. HCD on a slice at 0 m (purple), surface waterbodies (cyan), streams (blue), and the local model area (green) are superimposed.

8.9 Confidence and remaining uncertainties

The parameter assessments of the hydrogeological model based on single-hole tests was tested using several types of data; drawdown-cone caused by Äspö HRL, interference tests, natural point-water head measurements and hydrochemical data. These tests with the regional groundwater flow model resulted in a few suggested changes of the parameterisation (e.g. generally a decrease by factors around 1/3 for some transmissivities or hydraulic conductivities of HCD and HRD, respectively, assessed by single-hole tests) but in general the initial parameterisation was satisfactory. The transport parameters used for the hydrogeological modelling within the SDM are considered uncertain but provides reasonable matches to data available. In Chapter 10 and especially in Sections 10.5.3 and 10.8 the uncertainties involved in the transport of solutes are discussed. There are however also other remaining uncertainties that are discussed below.

8.9.1 Groundwater levels in the bedrock aquifer

The calculated environmental heads in the deeper part of the core drilled boreholes, based on the point-water heads under natural (undisturbed) conditions, are uncertain due to difficulties to collect representative water density of the formation water. Due to this it was judged that adjustments of hydraulic properties below c. –600 m elevation should not be made based on just data representing natural head conditions. It is judged that this shortage in the data quality has not had any severe consequences for the calibration but contributes to the uncertainty of assessed properties below c. –600 m elevation.

8.9.2 Structural model (HCD)

Within the focused volume several of the deformation zones (HCD) are intersected by one or more boreholes. It was observed that there is a large variability of hydraulic properties within some of the deformation zones, indicating that heterogeneity is likely to be large within the HCD. As a consequence most assessments of hydraulic properties for an individual HCD in the present model must be considered very uncertain, although the general depth trends of mean transmissivity seem to be justified by the tests made with the regional groundwater flow model. The assessed heterogeneity of the transmissivity used in the modelling (as a large-scale variation) has support in data but must still be considered uncertain.

One should also observe that within the Laxemar local model volume the numbers of borehole intercepts with deformation zones are more limited below –150 m elevation compared with above, and the total number of intercepts is a smaller compared with the regional data set. Therefore, the assessment of trend functions of the transmissivity with depth for the HCD is uncertain (but the uncertainty is quantified as confidence limits of geometric mean, cf. /Rhén et al. 2008/).

Outside the local model area there are only hydraulic tests available east of the local model area, providing data for estimating properties of HCD. As there are no data for large part of the regional model volume, the assessed properties within the regional volume outside the Laxemar local model volume are obviously highly uncertain.

The existence of dolerite dykes and their possible function as hydraulic barriers have been proven by cross-hole test results. However, it is not known if the most obvious example, ZSMNS001, acts as a barrier along its whole extent. The other dolerite dykes proven to exist seem to be possible local hydraulic barriers but it is considered very uncertain if they are barriers over longer distances. The thickness observed in boreholes is limited and may indicate that one should not expect barrier effect of similar character to ZSMNS001 seen in south-western part of the focused area. The geological description also indicates that possibly other dolerite dykes than observed in boreholes may exist, but they are perhaps relatively thin and may just act as highly local hydraulic barriers.

Some HCD, lacking surface outcrop (lineament) and being intercepted only by borehole, are modelled with assumed radius of 564 m. The size and character of these HCD should be considered uncertain.

8.9.3 Hydraulic rock domain (HRD) model

The investigations have been extensive but also covered a large area (volume) including both the Laxemar local model area and the Simevarp subarea, cf. Chapter 1. As a consequence there are fairly large distances between boreholes even within the focused area and there are limited data to assess spatial distributions of hydraulic properties; and defining subvolumes (HRD) with different properties, as well as depth dependencies. One should therefore expect that there can be a considerable variation in the properties within the hydraulic rock domains in the focused volume. Especially below elevation –650 m, data on the conductive fractures are sparse and the hydrogeological DFN models below that elevation should be considered uncertain.

Hydrogeological DFN models with three different types of transmissivity distributions have been developed but only the transmissivity model that is considered to be the conceptually most reasonable based on all open fractures has been tested in the regional groundwater flow modelling. It remains to test the other hydrogeological DFN models developed on a regional scale to assess how they behave relative to the hydraulic tests available for testing out the groundwater flow model.

The developed hydrogeological DFN models show anisotropic conditions that vary mainly by depth (horizontal and WNW conductive fractures dominate near surface and by depth the intensity of the horizontal set decreases). The magnitude of the ratio between maximum and minimum permeability estimated from block modelling of the hydrogeological DFN models is considerably less than that observed in the nearby Äspö HRL and possibly suggests the anisotropy within the Laxemar local model volume being underestimated. Still, the main directions for maximum and minimum permeability in the horizontal plane are consistent, and give the right indications of how the anisotropy changes with depth.

The hydrogeological DFN includes conductive features from decimetre scale to features with radius of 564 m, where the largest can be assumed to be MDZ. Data have shown that the geologically mapped MDZ must be hydraulically heterogeneous, but so far the all hydrogeological DFN features are modelled homogenous. Modelling the largest hydrogeological DFN features as heterogeneous features may thus appear more conceptually appropriate, but has not been tested yet.

Outside the local model volume there are only a few hydraulic tests east of the Laxemar local model area relevant for calibrating the hydrogeological DFN models. The assessed hydrogeological DFN properties within the regional volume outside the Laxemar local model volumes are obviously highly uncertain.

8.9.4 Compartmentalised fracture networks at repository depth

As described in Section 8.5, the calibration of the hydrogeological DFN model considers the connected conductive fractures on a large scale, since it is based on the results of PFL logging established during long-term pumping. The comparison of the PFL test results with results of transient PSS tests in the corresponding boreholes indicate that there probably exist local, fairly low-transmissive (generally less than c. 10^{-8} m²/s), fracture networks (compartmentalised networks) that are not, or at least poorly, connected to the “global hydraulically connected fracture system” tested by the PFL logging /Rhén et al. 2008/. The role of compartmentalised networks, if existent, needs to be addressed in future modelling.

9 Bedrock hydrogeochemistry

9.1 Introduction

The overall objectives of the hydrogeochemical description for the Laxemar-Simpevarp area are to establish a detailed understanding of the hydrogeochemical conditions at the site and to provide descriptions that fulfil the needs identified by the safety assessment group during the site investigation phase /Ström et al. 2008/. Understanding current undisturbed hydrochemical conditions at the proposed repository site is crucial when predicting future changes in groundwater chemistry that may be of relevance to the long-term integrity of the currently planned SKB repository system, in particular what may affect copper corrosion and/or bentonite degradation processes. Therefore, the following variables are of particular interest for the hydrogeochemical site descriptive modelling and also needed in the safety analysis: pH, Eh, sulphur species, iron, manganese, potassium, carbonate, phosphate, nitrogen species (e.g. ammonia), total dissolved solids (TDS) and the main cations, isotopes (stable and radioactive), colloids, fulvic and humic acids, organic material (including acetate) and microorganisms. In addition, dissolved gases (e.g. carbon dioxide, methane and hydrogen) are of interest because of their likely participation in microbial reactions /Laaksoharju et al. 2008a/.

The work has involved the development of descriptive and mathematical models for groundwaters including integration and interaction with such models developed in the geological and hydrogeological work (cf. Chapters 5 and 8, respectively). In this report, the groundwaters have been interpreted with respect to their *composition, origin and evolution*, requiring close integration with geological, climatological and hydrogeological information. Past climate changes are one of the major driving forces for long-term hydrogeochemical changes (hundreds to thousands of years) and are, therefore, of fundamental importance for understanding the palaeohydrogeological, palaeohydrogeochemical and present evolution of groundwater in the crystalline bedrock of the Fennoscandian Shield. Despite these changes, the alkalinity and redox buffer capacities of the bedrock are controlled by relatively fast and reversible processes which occur on time scales of hundreds of years. Hence, the pH and Eh variability of the contacting groundwaters are restricted to a narrow and stable range provided that appropriate alkalinity and redox buffer capacities are present. The methodology adopted is described in detail elsewhere /e.g. Smellie et al. 2002, Laaksoharju et al. 2008b/ and the specific hydrogeochemical methodology used within the SKB site investigation programme is published in a special issue of Applied Geochemistry /Gascoyne and Laaksoharju 2008/. At all stages of the studies, collaboration with HydroNet, SurfaceNet and RetNet groups has been stressed.

Further to the groundwater studies, detailed investigations of matrix porewaters have been carried out. In addition, the importance of mineralogy has been underlined in site understanding, for example, as input to the geochemical equilibrium modelling. From a palaeohydrogeological viewpoint, geochemical and mineralogical information from fracture minerals, altered rock and the reference rock matrix has been compiled in /Drake et al. 2008/, where analyses of these data are restricted to the pH and redox buffering capacity of the host rock. The major findings from the fracture mineral and matrix porewater investigations have been integrated into the overall site description. Subsequently, studies of microbes and related chemical reactions have been integrated with the redox modelling of the site.

Important feedback from SR-Can /SKB 2006d/ and Insite (the international review group established by the authorities) and Sierg (SKB's independent international review group) was integrated into the modelling. The list of critical issues established by the authorities represents an important input to the investigations, aiming to improve various aspects of the site descriptive model and site understanding. Of the issues proposed, some were addressed already in version 1.2 /SKB 2006d/, but additional data during development of model version SDM-Site Laxemar facilitated further consideration (cf. /Laaksoharju et al. 2009/).

9.2 State of knowledge at the previous model version

Hydrogeochemical model versions 1.1 and 1.2 for the Simpevarp subarea are reported in /Laaksoharju et al. 2004, SKB 2004b/, and subsequent hydrogeochemical model versions 1.2 and 2.1 for the Laxemar subarea are reported in /SKB 2006ef/. No full SDM was produced for model step Laxemar L2.1 but it included feedback from the SR-Can study and Insite/Sierg reviews. Preliminary work based on data freezes Laxemar L2.2 and Laxemar L2.3 (August 31, 2007), and partial information from the Extended data freeze Laxemar 2.3 (November 30, 2007), was carried out during 2007 and resulted in an updated category assessment of the analytical data delivered in early February 2008.

The earlier Laxemar hydrogeochemical model versions 1.2 and 2.1 /SKB 2006ef/ concluded that the complex groundwater evolution and patterns in the Laxemar-Simpevarp area are a result of many integrated factors such as: a) the present-day topography and proximity to the Baltic Sea, b) past changes in hydrogeology related to glaciation/deglaciation, land uplift and repeated marine/lake water regressions/transgressions (excluding the western part of the Laxemar subarea which was never completely submerged because of higher topography), and c) organic or inorganic alteration of the groundwater composition caused by water/rock interactions and microbial processes. The chemistry of the sampled groundwaters reflects to various degrees processes related to modern and ancient water/rock interactions and mixing.

In /SKB 2006f/ the 2.1 models and site understanding were consolidated. The models were updated and further understanding achieved concerning the spatial variability, origin, evolution and major reactions of the groundwaters, the microbial contents and their depth variation, and the contents of colloids and gases. In addition, porewater composition and its interaction with fracture groundwaters was further quantified and uncertainties in the mixing calculations identified (cf. Section 4.9 and /SKB 2006f, cf. Appendix 7 therein/). Furthermore, the studies of fracture fillings and especially the isotopic signatures in calcite have supported the conceptual understanding of the Laxemar subarea (cf. Section 4.8 and /SKB 2006f, cf. Appendix 1 therein/), and the detailed mineral investigations were used as direct input to the hydrogeochemical modelling /SKB 2006f/.

9.3 Conceptual model

9.3.1 Major concepts

Initially, it is necessary to explain the sample coding used in this report to differentiate generally between an approximate borehole length or borehole elevation, and more specifically when designating accurately a depth interval or sample location. The sample coding used is as follows:

- A specific sample from a single borehole location is prefixed by the borehole number followed by the elevation in metres, i.e. KLX02:–455 m elevation. This coordinate refers to the mid point of the corresponding packed-off section in the borehole.
- A specific depth interval is labelled as ‘–404 to –420 m elevation’.
- An approximate depth or depth interval is labelled ‘about or approximately 500 m depth’ or ‘about or approximately 500 to 700 m depth’.
- Any location related to borehole length is signified specifically as ‘432 m borehole length’ (i.e. KLX02:432 m borehole length), or generally as ‘about or approximately 500 m borehole length’ or ‘about or approximately 500 to 700 m borehole length’.
- Repository depth refers to ‘–400 to –700 m elevation’.

The nomenclature of the groundwater types used in this chapter depends on the purpose of the modelling and a distinction can be made between the following:

1. *Current groundwater types*, i.e. these are the types that are now used to distinguish different waters as measured *in situ* today. The nomenclature of these present water types is related to the perceived main origin of these waters (i.e. meteoric, Littorina, glacial meltwaters etc) but their compositions have subsequently been altered by mixing and reactions.

2. *Origins of current groundwater types.* This relates to the chemical composition of the real groundwater end members, i.e. the ‘actual’ precipitation, the ‘real’ glacial meltwater, the ‘best estimate’ Littorina sea water, etc. ‘End member’ therefore refers to a modern or older water type which constitutes an important component to the presently measured groundwaters in the Laxemar-Simpevarp area. The end-member compositions identified and used for the site modelling are listed in Table 9-1 and described in detail by /Gurban 2009, Gimeno et al. 2009/.

The description of the current groundwater types in the Laxemar (and Simpevarp) subarea is based on the salinity content of the water (e.g. Fresh, Brackish, Saline and Highly Saline). Brackish groundwaters may be subdivided into Brackish Glacial, Brackish Marine and Brackish Non-marine, mainly based on $\delta^{18}\text{O}$ and marine indicators such as magnesium and chloride-bromide ratios. As a consequence, the same groundwater type can be described in some samples as, for example, Brackish Glacial or a mixture of Glacial and Brackish Non-marine with subordinate Littorina water.

The names of the water types used in the different evaluations and modelling activities based on /Smellie et al. 2008/ and documented in /Gimeno et al. 2009, Gurban 2009, Molinero et al. 2009, Hallbeck and Pedersen 2008 and Laaksoharju et al. 2009/ are as follows:

1. *Palaeohydrogeochemical description:* Highly Saline, Old Meteoric \pm Old Glacial, Last Deglaciation, Littorina and Present Meteoric.
(Note: ‘ \pm Old Glacial’ means that the Old Meteoric water may or may not contain an Old Glacial component; Last deglaciation means ‘the final stage of the last phase of ice sheet coverage’).
2. *Mixing end members (M3) modelling:* Deep Saline, Glacial, Littorina and Altered Meteoric. (Old Meteoric + Glacial was tested as a modelling alternative at an early stage by /Gurban 2009/).
3. *Site descriptive model:* Highly Saline, Saline, Brackish Marine, Brackish Non-marine, Transition (mixture between marine and non-marine water), Brackish Glacial, Mixed Brackish and Fresh.

To understand, interpret and conceptualise the groundwater evolution, the following issues need to be considered:

1. *The ‘original’ composition of the water present in the bedrock:* This is essentially unknown, but evidence from fracture groundwaters and matrix porewaters indicates that resident groundwaters prior to the last deglaciation were a mixture of old meteoric \pm old glacial and saline in type as a function of depth. Note that the uncertainty in recognising groundwater components older than the last deglaciation increases considerably with age (cf. /Smellie et al. 2008/).
2. *Effects of the last deglaciation:* Includes incursion of glacial meltwater.
3. *Introduction of more recent groundwater types (post glacial):* Because the studied site is situated close to the Baltic Sea coast, it is evident that both fresh meteoric water and brackish marine sea waters of different salinities may have played important roles. Fresh meteoric waters from very different climates (e.g. ranging from temperate to cold) may also have been recharged repeatedly.
4. *Factors influencing groundwater flow that largely determine the resulting groundwater chemistry:* These include topography, bedrock hydraulic conductivity, interconnection of different fractures and fracture networks, density differences and potential glacial loading and unloading.
5. *The reactions taking place in the soil cover and bedrock which modify the original signature of the recharge water:* Examples are redox reactions mostly mediated by microbial activity involving oxygen consumption, and reactions with manganese, iron, sulphide and carbon. In addition, water-rock reactions such as ion exchange, calcite dissolution/precipitation, and silicate weathering will have occurred, together with mixing and also diffusion (e.g. exchange with matrix porewater).

As a result of the extensive site investigations in Sweden and Finland, it is clear that the hydrogeochemical evolution of fracture groundwater results from advective mixing and water-rock interactions driven by past and present changes in the climate /e.g. Laaksoharju and Wallin 1997, Laaksoharju et al. 1999, Pitkänen et al. 1999/. Many of the evaluation and modelling steps used within ChemNet are focused on discriminating these effects by using different modelling approaches such as mixing, reactions and transport modelling. These issues are addressed and discussed in detail in /Laaksoharju et al. 2009/.

Table 9-1. End-member compositions used for the SDM-Site Laxemar site descriptive hydrogeochemistry modelling.

Parameter	Deep Saline	Littorina	Glacial	Old Meteoric + Glacial**	Altered Meteoric Laxemar #10231
pH (units)	8	7.6	----	----	8.17
Alkalinity(mg/L)	14.1	92.5	0.12	0.12	265.0
Cl (mg/L)	47,200	6,500	0.5	0.5	23.0
SO ₄ ²⁻ (mg/L)	906.0	890	0.5	0.5	35.8
Br (mg/L)	323.66	22.2	----	----	----
Ca (mg/L)	19,300	151	0.18	0.18	11.2
Mg (mg/L)	2.12	448	0.1	0.1	3.6
Na (mg/L)	8,500	3,674	0.17	0.17	110.0
K (mg/L)	45.5	134	0.4	0.4	3.0
Si (mg/L)	2.9	3.94	----	----	7.0
δ ² H (‰ VSMOW*)	-44.9	-37.8	-158.0	-118	-76.5
δ ¹⁸ O (‰ VSMOW*)	-8.9	-4.7	-21.0	-16.0	-10.9

* Vienna Standard Mean Ocean Water.

** Tested as a modelling alternative at an early stage /Gurban 2009/.

---- No data available.

9.3.2 Model input

Rock domains, deformation zones and fracture domains

A fundamental understanding of the geology, including the rock domains, fracture domains and deformation zones, is important for the characterisation and interpretation of the hydrogeochemistry. The different groundwater types identified in the upper and intermediate parts of the bedrock display a complex mixing pattern governed by the palaeo and present hydrology and the structural geology. At greater depths, water-rock interactions with dissolution and precipitation of minerals will affect the water composition, such that over a long time period the chemical composition of the rock and fracture minerals will leave a specific imprint in the groundwater.

The construction of a conceptual hydrogeochemical model for the Laxemar subarea is very much related to the hydrogeological and geological models of the area. Figure 8-51 presents a geological map of the Laxemar-Simpevarp area showing the deterministically modelled rock domains and deformation zones (cf. Chapter 5 for details), the locations of the percussion and cored boreholes, and the positions of the cross-sections used in the hydrogeochemical site description (cf. Section 9.6). The dominant rock types in Laxemar consist of porphyritic Ävrö granite, porphyritic Ävrö quartz monzodiorite and equigranular quartz monzodiorite. The rock domains refer to rock volumes in which specific rock units have been distinguished on the basis of similar composition, grain size, degree of bedrock homogeneity and degree and style of ductile deformation. Deformation zones refer to parts of the bedrock along which there is a concentration of strain and damage.

Three dominating rock domains are identified within the local model, namely RSMA01, RSMM01 and RSMD01 (cf. Section 5.4). Rock domain RSMMA01 dominates in the northern, eastern and southernmost part of the Laxemar local model area/volume. South and south-west of the northern part of the RSMA01 domain, the local model area/volume is occupied by the RSMM01 domain. Rock domain RSMM01 is characterised by Ävrö quartz monzodiorite with a much higher proportion of diorite/gabbro than in the other rock domains. The model volume south of the RSMM01 domain is occupied by the RSMD01 domain which is dominated by quartz monzodiorite. Narrow and elongated domains between the RSMM01 and RSMD01 domains are characterised by fine-grained dioritoid.

To further facilitate site description and model development, the bedrock between the deformation zones has been divided into several fracture domains based on geological criteria (cf. Chapter 5.6) and /Wahlgren et al. 2008/.

The identified deformation zones in the Laxemar regional model area can be grouped as follows:

- Northeast-southwest striking, moderate to steeply dipping.
- North-south striking, moderate to steeply dipping.
- East-west to northwest-southeast striking, steep to moderate dip to the south.
- East-west to northwest-southeast striking moderate dip to the north.
- Gently dipping.

The groundwater types identified in Laxemar occur in the basement rock independently of the rock domains in the area. However, the occurrence and relation of groundwaters to their spatial location with respect to some key deformation zones show a variation which in some areas can be related to the deformation zones.

Hydrogeology

Details of the near-surface hydrogeology are described in /Werner et al. 2008/, of the bedrock hydrogeology in /Rhén et al. 2008, Rhén et al. 2009/ and in Chapter 8, and both are summarised in /Laaksoharju et al. 2009/. Analysis has shown that with only a slight modification of the fracture domains (FSMs), they can be correlated closely to hydraulic rock domains (HRDs) (cf. Figure 8-18).

General character

Groundwater recharge in the Laxemar subarea is generally associated with high altitude areas, whereas groundwater discharge is located in low altitude areas (valleys, water courses and depressions, such as the Mederhult depression). The degree of surface runoff (overland flow) may be large, as there are extensive areas with exposed or very shallow bedrock. However, there is often a thin layer of Quaternary deposits and/or vegetation present in the areas mapped as exposed bedrock, which may act to reduce the degree of surface runoff.

The regional groundwater flow in the Laxemar-Simpevarp area is driven by topography with a general gradient from the high elevated areas in the west to the Baltic Sea in the east. The flow pattern is largely governed by the mutual connections of the deformation zones which characterise the region. On a regional scale, the Laxemar subarea is predominantly subjected to recharge conditions and the Simpevarp subarea is an area of mainly groundwater discharge. The topography also results in localised areas of recharge/discharge (supported by particle track modelling) which represent groundwater circulation cells of varying depth and extent, and therefore of varying groundwater ages. There is a diminishing effect of groundwater circulation down to a depth about 1,000 m, and below about 1,200 m the groundwater is effectively stagnant. /Rhén et al. 2008/.

Bedrock hydraulic conductivity

Lateral and vertical groundwater flow through the bedrock of the Laxemar subarea is dependent on the hydraulic properties of the water conductive open connected fractures and deformation zones in combination with the differences in hydraulic gradient which exert the driving force for flow. Advective flow is greatest in the upper bedrock, less at intermediate levels, and least at greater depths. From compilations of hydraulic borehole measurements, all tests indicate that the hydraulic conductivity decreases with depth and that most of this decrease occurs in the upper 100 to 200 m of the bedrock. At the 100 m test scale, the bedrock above elevation -150 m has a geometric mean hydraulic conductivity of about $2 \cdot 10^{-7}$ m/s for the entire data set (local model volume; HCD+HRD). For the depth zone -150 to -400 m, the geometric mean hydraulic conductivity is about $2 \cdot 10^{-8}$ m/s for the entire data set (HCD+HRD), and between deformation zones (HRD) is about $0.8 \cdot 10^{-8}$ m/s for the local model volume. The tendency is that the hydraulic conductivity decreases in both the deformation zones and in the rock between the deformation zones with increasing depth (for details, see Section 8.5).

Fracture intensity

Determination of the intensity of open fractures formed part of the hydraulic DFN modelling phase (cf. Section 8.5.2 and /Laaksoharju et al. 2009/), and according to the resulting model the following depth zones have been recognised: 0 to –150 m, –150 to –400 m, –400 to –650 m and < –650 m. These generally conform to the different groundwater depth intervals derived from the hydrochemical evaluation.

9.3.3 Working hypothesis on the past groundwater evolution

The present working hypothesis for the hydrogeochemical site conceptual model recognises that climatic and hydraulic changes responsible for the present groundwater chemistry are not restricted to post glacial time. During the last deglaciation (i.e. the last phase of ice sheet coverage), glacial water was injected into the bedrock under high hydraulic pressure and is still present as a major component at intermediate depths. At greater depths, old highly saline waters (partly mixed with old glacial waters) or older meteoric waters dominate. Also recognised at shallow to intermediate depths is a relict meteoric water, probably of a warm climate origin, preserved in the rock matrix porewater in less fractured, less hydraulically conductive parts of the bedrock. The age of this component is unknown, but possibilities include certainly pre-Holocene and perhaps pre-Pleistocene or even further back in time. Importantly, the hydrochemistry of the Laxemar subarea cannot be explained without recognising this older component. Therefore, the present groundwaters are the result of complex mixing and reactions over a long period of geological time determined largely by the hydrogeological properties of the host bedrock. The following major water types, in chronological order, are now recognised: *Highly Saline Water* > *Saline Water* > *Brackish Non-marine Water* > *Last Deglaciation Meltwater* > *Brackish Marine (Littorina/Baltic) Water* > *Fresh Water* /Laaksoharju et al. 2008a/. (Note that the water types are given in order of decreasing age and ‘Last Deglaciation’ (i.e. the final stage of the last phase of ice sheet coverage) refers to the period 18,000 to 12,000 BC).

Figure 9-1 illustrates the conceptualisation of the Laxemar groundwater system from before the last phase of the ice sheet coverage (c. 25,000 years ago) to the present day. Two different scenarios are shown: a) the upper series representing areas not covered by the Littorina Sea transgression, and b) the lower series representing areas submerged by the Littorina Sea for a period long enough to influence the groundwater. A tentative distribution of groundwater types and salinity gradients in Laxemar prior to the recharge of meltwater from the last deglaciation immediately before the Holocene is the starting point for both scenarios. It is inferred that old meteoric waters, comprising components derived probably from both temperate and cold climate events, were residing in the crystalline bedrock at this time and most likely with sufficient residence time to interact with the minerals. Assuming there were favourable salinity gradients established, old meteoric waters could have been exposed to diffusion dominated mixing with deeper, more saline groundwaters, if there existed a high density contrast that would have prevented advective mixing. During the last deglaciation period the bedrock was flushed by glacial meltwater and it is assumed that it penetrated to great depths as indicated by $\delta^{18}\text{O}$ signatures recorded in groundwaters at about 1,000 m depth. However, these signatures may also reflect relicts of one or more older glaciations.

Subsequently, Laxemar was partly covered by brackish marine water during the Littorina Sea transgression stage, and this water is assumed to have had a maximum salinity of about 6,500 mg/L Cl /Pitkänen et al. 1999, 2004/. This salinity (twice the present salinity of the Baltic Sea) prevailed at least from 4500 to 3000 BC. Fresh water streams discharging into the elongated east-west coastal bays probably diluted the Littorina water, thereby limiting the density driven infiltration into the bedrock below these bays and resulting in a weak Littorina signature in the groundwater. An alternative or an additional process is that the Littorina signature was diluted in the bedrock as a result of meteoric water infiltration driven by land uplift. In any case, the Littorina component is present today in the Laxemar subarea at depths of about 500 to 600 m as recorded in a few samples (e.g. from KLX15A, cf. Figure 9-21). In the Simpevarp subarea the Littorina signal is more prominent and is found at depths between about 200 to 600 m (cf. Figure 9-20).

The uplift and shoreline displacement in the Laxemar-Simpevarp area suggest that extensive meteoric water recharge dominated during the last 6,000 years as illustrated in Figure 9-1. This is confirmed by the $\delta^{18}\text{O}$ signatures in the groundwater, especially in the western and central parts of the Laxemar-Simpevarp area. This flushing process commenced during uplift of the land above sea

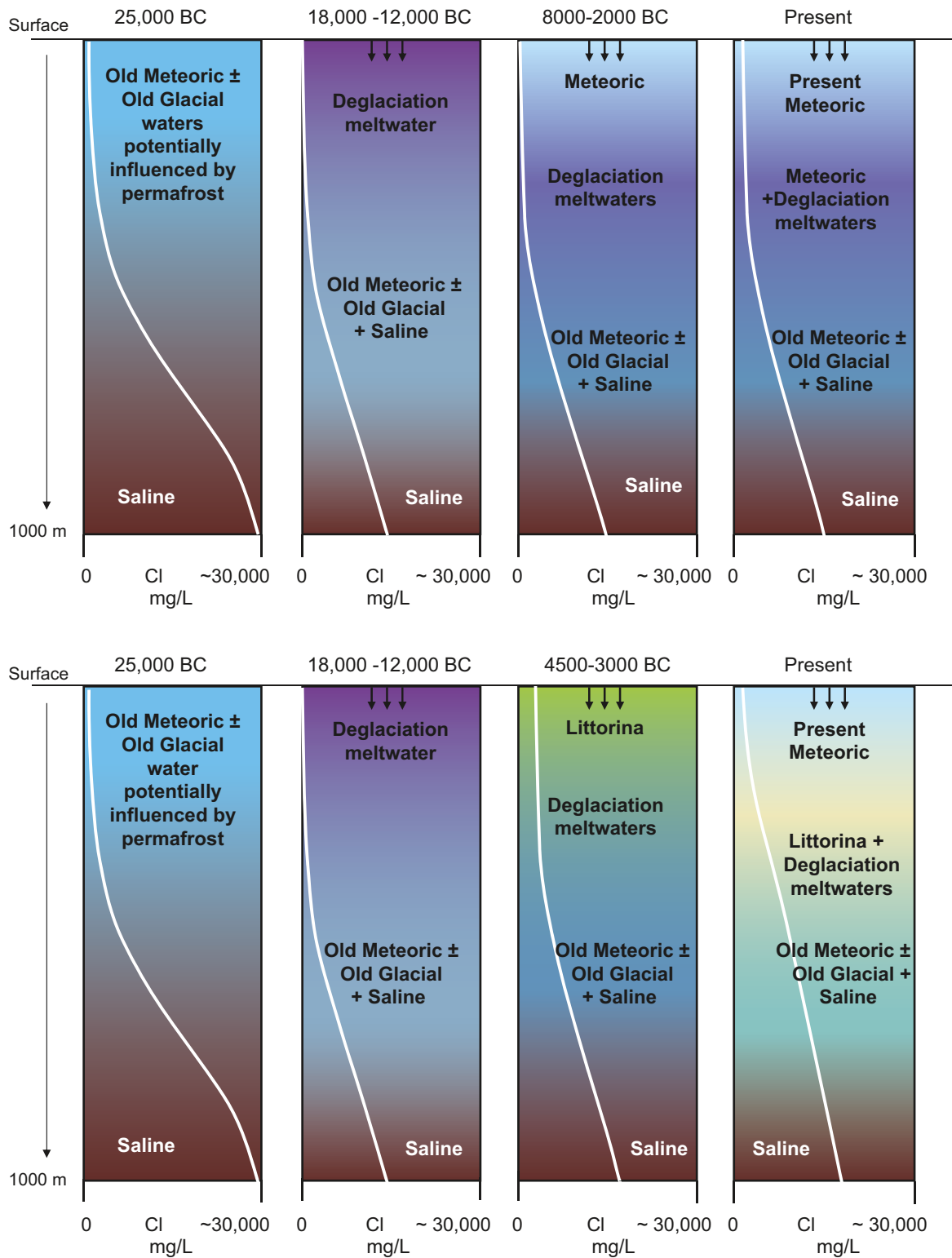


Figure 9-1. Sketch showing tentative salinities and groundwater-type distributions versus depth for the hydraulically conductive zones in the Laxemar subarea. Two different scenarios are outlined; the upper series representing areas not covered by the Littorina Sea and the lower series representing areas submerged by the Littorina Sea for a period long enough to influence the groundwater. The upper series shows from left to right: 1) the situation prior to the last deglaciation, 2) last deglaciation and intrusion of Late Weichselian meltwater, 3) meteoric recharge, and 4) the present situation. The lower series shows: 1) the situation prior to the last deglaciation, 2) last deglaciation and intrusion of Late Weichselian meltwater, 3) intrusion of brackish marine (Littorina Sea) water, and 4) the present situation.

level with the establishment of hydraulic gradients, and continues to the present day (Figure 9-1). Today, this meteoric water is being mixed with minor portions of glacial water and brackish marine waters, indicated by the $\delta^{18}\text{O}$ values and Mg concentrations as well as the Br/Cl ratios which are still present in the basement.

The above description is valid generally for the Laxemar subarea bedrock. Further discussions on the conceptual understanding of the development of the Laxemar-Simpevarp area are described in /Laaksoharju et al. 2009, Tröjbom et al. 2008/.

9.4 Hydrogeochemical data

The SDM-Site Laxemar hydrochemistry evaluation is based on the 'Extended data freeze Laxemar' 2.3 of November 30th, 2007. These data were compiled and their quality checked in February 2008, and the resulting 'internal' dataset was used both for the hydrogeochemical modelling and for delivery to HydroNet. Minor edits and updates were carried out in May 2008 and this version represents the final dataset used in the SDM-Site Laxemar hydrogeochemistry modelling. Additional data, for example, from borehole KLX27A, were compiled in October 2008 but only used for comparison purposes and as partial support in the construction of the conceptual visualisations. All datasets are stored in the Simon database.

The datasets used in the SDM-Site Laxemar hydrochemistry evaluation include all relevant data from the Laxemar and Simpevarp subareas together with available information from Äspö HRL (before the tunnel construction). The Sicada database contains complete hydrogeochemical analyses including microbes, colloids and gas analysis, and porewater analyses from bedrock samples. Quality assessment of the Laxemar-Simpevarp data is documented in /Smellie and Tullborg 2009/ together with reference to earlier evaluated Äspö and Ävrö data. Groundwater data from other Nordic sites and SFR (Final Repository for Radioactive Operational Waste) have been used on occasions for comparison /e.g. Gimeno et al. 2009/.

9.4.1 Borehole groundwater chemistry data

The locations of the percussion and cored boreholes in the Laxemar subarea are shown in Figure 2-5; a total of 46 cored and 43 percussion boreholes have been drilled. Twenty cored boreholes and 19 percussion boreholes were sampled for hydrochemical evaluation, and of the cored boreholes 6 were sampled also for gases, 5 for microbes and 4 for colloids.

Table 9-2 summarises the type and number of samples included in the dataset for the Laxemar and Simpevarp subareas and the data freeze at which they were delivered /Gimeno et al. 2009/.

9.4.2 Quality assured data

The Extended data freeze Laxemar 2.3 groundwater dataset has been evaluated systematically with respect to quality, and an assignment of different categories made regarding their value for further hydrogeochemical interpretation work /Smellie and Tullborg 2009/. This was based on an integrated geological, hydrogeological and hydrochemical approach. A separate small-scale feasibility study of some selected borehole sections was made to determine the possibility of further quantifying the effects from drilling and pumping /Gascoyne and Gurban 2009/, but this did not affect the categorisation of the dataset. The classification into the various categories for the cored boreholes is presented in Table 9-3 in terms of the most important criteria that apply for different categories. The number of samples and the allocated category are listed in Table 9-2 and the complete tables are stored in the SKB model database Simon.

The highest quality data (categories 1 and 2) are required, for example, for geochemical equilibrium calculations, modelling of redox conditions, and for specialised studies on microbes, organics and colloids. These data, together with category 3 and category 4 (with caution) data, adequately address the overall site understanding (e.g. groundwater distribution, origin and evolution and its integration with hydrogeology). Category 5 data should be used with considerable caution in the context of both hydrogeochemistry and hydrogeology, in particular the tube sample data. For details see /Smellie et al. 2008, Laaksoharju et al. 2009/.

Table 9.2. Number of sampling points and types of sample categories included in the final ‘Extended data freeze Laxemar 2.3’ for the Laxemar-Simpevarp area. The different rows indicate the number of new samples delivered at each data freeze (2.1, 2.2 and 2.3) or updated existing samples between one data freeze and the next (2.1–2.2 and 2.2–2.3). No supplementary data from existing samples in Laxemar 2.1 and 2.2 were added after the final ‘Extended data freeze Laxemar 2.3’. The numbers in the table indicate the total number of sampling points and then after the slash, the number of these samples which have category 1, 2, 3, or 4. (Perc Bhs: percussion boreholes; Cored Bhs: cored boreholes; NSGW: near surface groundwaters; Precip: precipitation).

Data freeze		Perc Bhs	Cored Bhs	Tube sampling	NSGW	Sea water	Lake water	Stream water	Precip
Laxemar 2.1	Äspö	14/5	137/21						
	Ävrö		61/3						
	Laxemar	15/5	122/12	35/2	45/39				
	Simpevarp	10/2	15/3	10/0	53/38	54/31	230/186	553/335	
Laxemar 2.1–2.2	Ävrö	9/4	4/0						
	Laxemar	5/3	39/7	64/0	4/4				
	Simpevarp		11/5	20/0	37/22	289/124	17/15	38/32	2/2
Laxemar 2.2	Ävrö		3/0						
	Laxemar	14/6	49/4	46/5					
	Simpevarp		10/2		68/60	67/29	34/34	64/63	3/3
Laxemar 2.2–2.3	Laxemar	3/3	26/6	17/2					
	Simpevarp		2/2		8/6	4/2	2/2	6/6	3/3
Laxemar 2.3	Laxemar	1/1	46/9	4/0					
	Simpevarp				27/21	24/11	13/13	33/31	1/1
Total		71/29	525/74	196/9	242/190	438/197	296/250	694/467	9/9

Table 9-3. Classification criteria for cored boreholes /Smellie et al. 2008, Laaksoharju et al. 2009, Smellie and Tullborg 2009/.

Cored boreholes Aspects/conditions	Category				
	1	2	3	4	5
Drilling water (≤ 1%)	x	x	x	x	x
Drilling water (≤ 5%)		x	x	x	x
Drilling water (≤ 10%)			x	x	x
Drilling water (> 10%)				x	x
Time series (adequate)	x	x	x	x	x
Time series (inadequate)			x	x	x
Time series (absent)				x	x
Suitable section length	x	x	x	x	x
Sampling during drilling				x	x
Sampling using PLU hydraulic testing equipment			x	x	x
Tube sampling					x
Charge balance ± 5% (± 10% for < 50 mg/L Cl)	x	x	x	x	x
Major ions (complete)	x	x	x	x	x
Major ions (incomplete)			x	x	x
Environmental isotopes (complete)	x	x	x	x	x
Environmental isotopes (incomplete)		x	x	x	x
Hydraulic effects (short-circuiting)					x

Table 9-4. Number of samples from percussion and cored boreholes allocated to each category up to and including the “Extended data freeze Laxemar 2.3”.

Category	1	2	3	4	5
Percussion boreholes	0	0	6	12	3
Cored boreholes	2	3	18	23	242

9.5 Explorative analysis and modelling

Explorative analysis involves an initial general examination of the groundwater data using traditional geochemical approaches to describe the data and provide an early insight and understanding of the site, i.e. the construction of a preliminary conceptual model for the area /SKB 2002/ (cf. Section 9.3.5). Based on this hydrochemical framework, selected data are further evaluated using different modelling approaches such as visualisation, mixing modelling, equilibrium modelling, redox modelling and evaluation of microbes, colloids and gases /Laaksoharju et al. 2009/.

Studies of fracture fillings, composition of the porewaters in the bedrock and groundwater residence times also constitute important information for the site description /Drake and Tullborg 2009a, Waber and Smellie 2008, Waber et al. 2009/. The background data, the explorative analysis and the modelling are detailed in /Gimeno et al. 2009, Hallbeck and Pedersen 2008/. The most important results are described in this section.

During the explorative analyses of the groundwaters it became apparent that a subdivision of the sampled groundwaters into six major groundwater types would facilitate the description and interpretation of the figures and diagrams. The major groundwater types distinguished are: *Fresh, Brackish Glacial, Brackish Marine, Brackish Non-marine, Saline and Highly Saline*. In addition, two groundwater types were included to accommodate important mixing processes resulting from anthropogenic and/or natural processes: a) a shallow near-surface '*Mixed Brackish*' type mainly comprising fresh and brackish glacial (sometimes with a weak marine component) groundwaters, and b) a deeper '*Transition*' water type mainly comprising degrees of mixing between brackish glacial or brackish non-marine groundwaters with a brackish marine water component. This subdivision into different groundwater types corresponds to the division used in the conceptual visualisation (cf. Section 9.6). The main chemical and isotopic character of each groundwater type, and their respective colour coding used for plotting and in the site descriptive visualisations, are detailed in /Laaksoharju et al. 2009/ and summarised in the box on the opposite page.

9.5.1 Initial data evaluation and visualisation

Addressed are the major ions and isotopes for site understanding; some minor ions of relevance to the repository safety case (e.g. phosphate) and the trace elements (including REEs, uranium and radium) are briefly mentioned. The redox sensitive elements are discussed in Section 9.5.3 under 'The redox system'.

For the visualisation and interpretation of primary data, widespread use has been made of scatter plots to separate the different groundwater groups, to demonstrate depth variations of the major ions and to help derive the origin and major ion evolution trends of the different groundwater systems. Three-dimensional presentations of the same data also have been used to quickly locate and relate the data from the various boreholes to achieve a better understanding of the lateral distribution of the different groundwater types.

The role of fracture domains, hydraulic rock domains and chemical trends

Based on earlier experience from the Forsmark site investigations, the Laxemar subarea has been subdivided into rock domains, fracture domains and hydraulic domains (cf. Chapters 5 and 8). Analysis has shown that with only a slight modification of the fracture domains, they can be correlated closely with the hydraulic rock domains (cf. Figure 8-18). To determine whether these domains can be demarcated by differences in hydrochemistry, both fracture domains and hydraulic rock domains have been compared using chloride, magnesium and $\delta^{18}\text{O}$. These are considered the most important hydrochemical signatures to describe the groundwaters based on the conceptual understanding of the Laxemar-Simpevarp area. Essentially, this comparison shows identical patterns between both domain types and therefore the hydraulic domains were selected for further evaluation.

The chloride trends indicate some differences between the hydraulic rock domains (cf. Figure 8-18 for their location). In general, at depths greater than about 200 m domain HRD_C indicates a somewhat higher salinity than domains HRD_W and HRD_EW0007. Magnesium shows the greatest increase in domain HRD_C at about 500 to 550 m depth, and weaker increases in domains HRD_EW0007 and particularly HRD_W at about 200 to 400 m depth, respectively. Oxygen-18 shows most depletion at about 400 m depth in domains HRD_W and HRD_EW0007, whilst domain HRD_C, in comparison, shows a small peak of more enriched oxygen-18 values at about 600 m /Laaksoharju et al. 2009/.

Fresh

Water type: Fresh (< 200 mg/L Cl; < 1.0 g/L TDS); Mainly meteoric in origin, i.e. Na(Ca)-HCO₃(SO₄) in type, $\delta^{18}\text{O} = -11.5$ to -9.8 ‰ VSMOW.

Mixed Brackish (*Not a specific groundwater type*)

Waters of mixed Fresh \pm Brackish Glacial (\pm Brackish Marine) origin (200–2,000 mg/L Cl; 1.0–3.5 g/L TDS); it is usually sampled at 20–150 m depth and may be the result of natural and/or anthropogenic mixing during drilling activities and sampling.

Brackish Glacial

Water type: Brackish Glacial (200–10,000 mg/L Cl; < 1.0–18 g/L TDS); $\delta^{18}\text{O} \leq -13.0$ ‰ VSMOW). Last Deglaciation meltwater + Brackish Non-marine to Saline component; Ca-Na-Cl (SO₄); Mg < 25 mg/L; $\delta^{18}\text{O} < -13.0$ ‰ VSMOW.

(It may also occur with a weak marine (Littorina) component in the Simpevarp subarea; Na-Ca-Cl (SO₄); Mg > 25 mg/L; $\delta^{18}\text{O} < -13.0$ ‰ VSMOW).

Brackish Marine

Water type: Brackish Marine (2,000–6,000 mg/L Cl; 3.5–10 g/L TDS; Mg > 100 mg/L); variable Littorina Sea component (\pm modern Baltic Sea) + Last Deglaciation meltwater \pm Brackish Non-marine to Saline component; Na-Ca-Mg-Cl-SO₄; $\delta^{18}\text{O} > -13.0$ ‰ VSMOW

Transition zone (*Not a specific groundwater type*)

Transition type representing a mixture of Brackish Glacial and/or Brackish Non-marine groundwaters with a variable component of Brackish Marine. These waters range from 2,000–10,000 mg/L Cl and from 25–100 mg/L Mg; $\delta^{18}\text{O} > -13.0$ ‰ VSMOW. They may be the result of natural and/or anthropogenic mixing during drilling activities and sampling.

Brackish Non-marine

Water type: Brackish Non-marine (3,000–10,000 mg/L Cl; 5–18 g/L TDS; Mg < 25 mg/L); Old Meteoric \pm Old Glacial \pm Last Deglaciation meltwater \pm Saline component, i.e. Na-Ca-Cl (SO₄) in type, $\delta^{18}\text{O} > -13.0$ ‰ VSMOW.

Saline

Water type: Saline (10,000–20,000 mg/L Cl; 18–35 g/L TDS; Old Meteoric \pm Old Glacial \pm Last Deglaciation meltwater \pm Highly saline component, i.e. Ca-Na-Cl (SO₄) in type, $\delta^{18}\text{O} = -13.0$ to -10.0 ‰ VSMOW.

Highly Saline

Water type: Highly Saline (> 20,000 mg/L Cl; > 35 g/L TDS); Ca-Na-Cl (SO₄) in type; $\delta^{18}\text{O} > -10.0$ ‰ VSMOW.

The observed differences between the hydraulic rock domains may warrant some consideration when describing the hydrochemistry of the Laxemar subarea. More important, however, is the relation of the hydrochemistry to the different deformation zones that have provided the majority of the hydrochemical data. This has been addressed by plotting groundwater data sampled from known deformation zones with the possibility of establishing changes in composition at different elevation levels from the same zone. However, no such changes were observed, possibly due to the limited available data.

Depth trends of key major ions.

The major ions of Cl, Mg and $\delta^{18}\text{O}$ are plotted against elevation in Figure 9-2 showing the variation in composition with depth of the different groundwater types which are colour coded. Also presented in each plot are the near-surface soil pipe groundwater samples (NSGW) to provide a reference to the hydrochemical end-member composition entering the upper bedrock system.

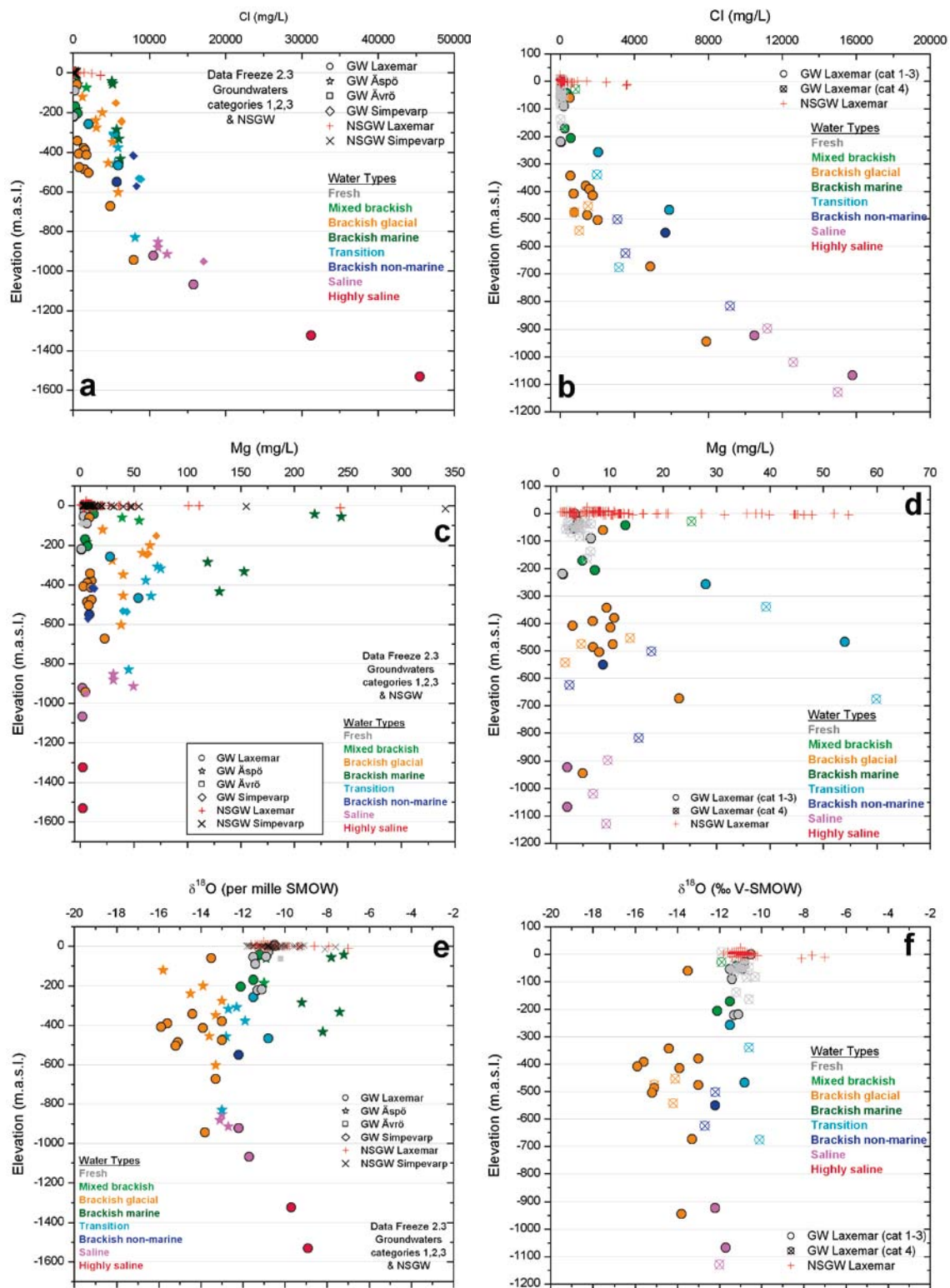


Figure 9-2. Distributions of chloride (a, b), magnesium (c, d) and $\delta^{18}O$ (e, f) in the Laxemar-Simpevarp area (left-hand figures) and the Laxemar subarea (right-hand figures), respectively. The scales along the chloride, magnesium and elevation axes have been increased in the Laxemar subarea plots to better visualise the groundwaters at shallow to intermediate depths.

In general terms, with respect to pH all groundwaters lie within the range of 7.5 to 8.6. As expected, pCO_2 in equilibrium with these waters decreases with depth due to water/rock interactions and/or mixing with saline groundwaters, and most groundwaters are in equilibrium with calcite /Gimeno et al. 2009/. However, groundwaters mostly of brackish glacial water type show variable pH, but essentially at equilibrium with calcite apart from one exception with higher pH and pCO_2 . Studies of

fracture filling calcites (cf. /Drake and Tullborg 2009a/ and Section 9.5.6, and Section 5.2.6) indicate only minor recent changes (either precipitation or dissolution), in accordance with the recorded close to equilibrium conditions.

For the important major ions, Figure 9-2a, c and e presents chloride, magnesium and $\delta^{18}\text{O}$ groundwater data representing the Laxemar-Simpevarp area, and Figure 9-2b, d and f represents similar compositional data from just the Laxemar subarea for comparison. Figure 9-2a shows a range of chloride from less than 200 mg/L to about 8,000 mg/L, which generally characterises the upper approximately 600 m depth. With increasing depth there is a rapid and systematic increase to a maximum of 45,000 mg/L at about 1,500 m depth sampled from borehole KLX02 in the Laxemar subarea. For magnesium (Figure 9-2c), a decrease ranging from about 250 to 50 mg/L is observed from close to the bedrock surface to about 600 m depth, and this can be directly correlated to variable amounts of brackish marine (Littorina) type groundwaters when present (this is particularly clear from the Äspö data). From about 600 to 900 m depth there is a further decrease in magnesium to well below 25 mg/L, with the exception of the Äspö data which still show groundwaters with about 50 mg/L Mg to depths just under 900 m. Below about 1,000 m depth magnesium is less than 5 mg/L.

The $\delta^{18}\text{O}$ data (Figure 9-2e and f) is influenced in the upper approximately 600 m on the one hand by depleted values associated with the brackish glacial groundwaters ($\delta^{18}\text{O} \leq -13.0\text{‰}$ VSMOW), and on the other hand by enriched values associated especially with brackish marine groundwaters, but also with recharge meteoric groundwaters ($\delta^{18}\text{O} \geq -13.0\text{‰}$ VSMOW). This results in a wide variation in $\delta^{18}\text{O}$ from within 50 m of the bedrock surface ($\delta^{18}\text{O} = -3.5$ to -7‰ VSMOW) and this variation further broadens with increasing depth to about 550 m to include more depleted values at around $\delta^{18}\text{O} = -16\text{‰}$ VSMOW. At about 600 m the range in $\delta^{18}\text{O}$ decreases dramatically and from here there is a gradual enrichment with increasing depth to about $\delta^{18}\text{O} = -9\text{‰}$ VSMOW at the maximum depths sampled.

Attempts also have been made to visualise these groundwater data in three dimensions to obtain a feel for the spatial distribution of the chemical species laterally across the Laxemar-Simpevarp area /Laaksoharju et al. 2009/. Figure 9-3 shows the vertical chloride distributions which mirror that described in Figure 9-2a and b, except this time it is possible not only to see how many salinity data there are at potential repository depths in the Laxemar subarea (indicated as two marked horizontal

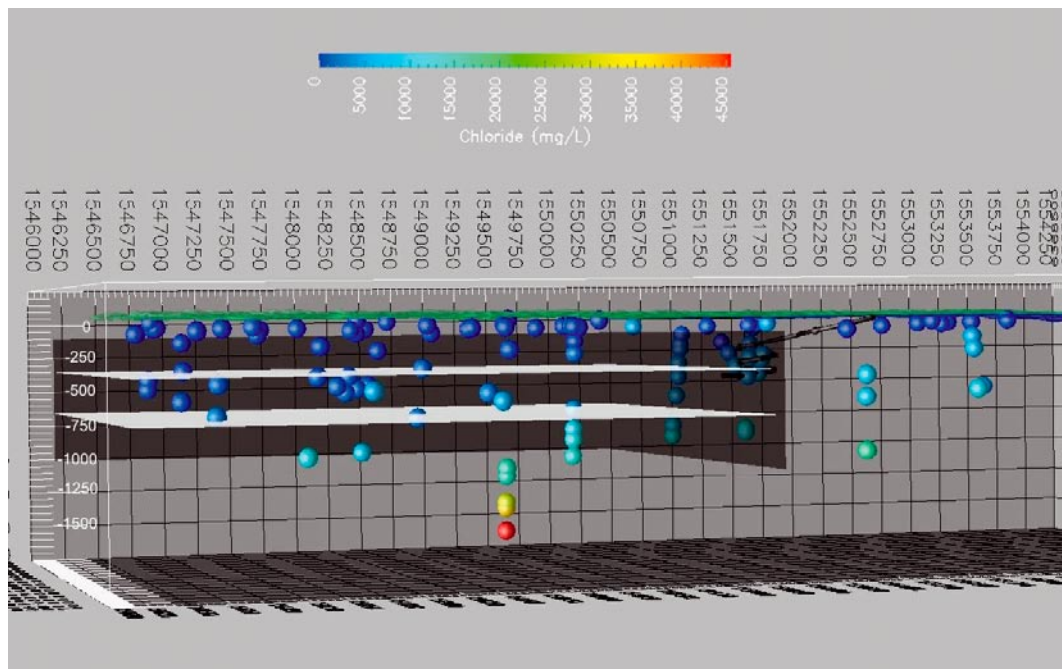


Figure 9-3. Three-dimensional visualisation of chloride concentrations and their lateral and vertical distribution across the Laxemar-Simpevarp area. The deepest borehole corresponds to KLX02. Also shown are the two marked horizontal levels (in white) representing the potential range of repository depths in the Laxemar subarea (at approximately -400 to -700 m elevation).

levels between -400 to -700 m elevation), but also the higher levels of salinity further to the east, illustrating the large scale discharge features characterising the Simpevarp subarea. The salinity profile shown in KLX02 provides the only deep groundwater input to site understanding, and may well reflect the deep groundwater chemistry within the Laxemar-Simpevarp area as a whole.

Depth trends of supporting major ions, together with phosphate and DOC

Supporting major ions include sodium, calcium, potassium, sulphate, bicarbonate, strontium and barium, together with phosphate and dissolved organic carbon (DOC); some of these are highlighted in Figure 9-4.

The distribution of *calcium* in the Laxemar subarea generally shows similarities to that of *sodium* in that both increase with depth and chloride content. Calcium (Figure 9-4a) shows a weak increase to about 500 mg/L in the upper bedrock, extending to depths of about 450 m, associated with groundwater types ranging from fresh, mixed brackish and brackish glacial. From about 500 m to greater depths, higher calcium concentrations relate to transition and brackish to saline non-marine groundwaters, and a lower compositional range relates to with the brackish glacial types. For sodium, these trends are stronger and commence at much shallower depths than indicated by calcium.

Not evident from these elevation plots, but indicated when plotting sodium versus calcium /SKB 2006f, Gimeno et al. 2009/, is the transition at about 600 m from a Na-Ca Cl type groundwater to a deeper and more evolved Ca-Na Cl type groundwater, accompanied by a decrease to very low magnesium values. In the Simpevarp subarea this transition is also evident, but occurs at deeper levels in the bedrock, due perhaps to the greater density penetration of a marine water component (i.e. sodium source) at this low topographic coastal location during the Littorina Sea transgression.

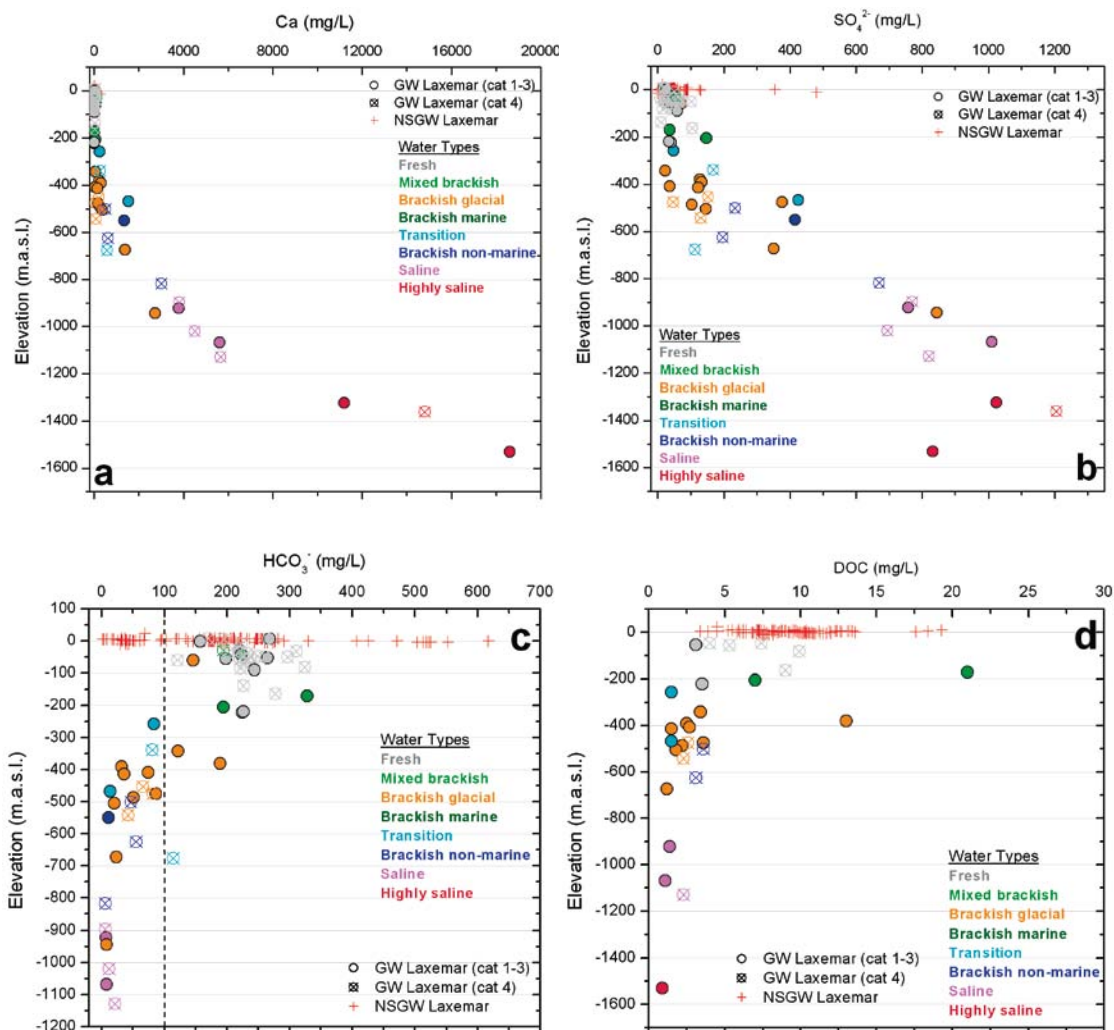


Figure 9-4. Depth distributions in the Laxemar subarea of calcium (a), sulphate (b), bicarbonate (c) and DOC (d).

Potassium contents (not plotted) associated with the fresh and mixed brackish groundwaters are < 6 mg/L in the uppermost 250 m, and variable up to a maximum of 15 mg/L in the 250 to 500 m interval characterised by brackish glacial, brackish non-marine and transition groundwater types. Potassium and magnesium both increase in brackish groundwaters with a marine component. Below about 550 m to the maximum depths sampled, there is a gradual and steady increase in potassium from about 7 mg/L to a maximum of about 30 mg/L corresponding to increasing chloride.

Most of the **sulphate** contents appear to be uniformly less than 100 mg/L in the upper approximately 200 m and less than 200 mg/L down to about 450 m depth (Figure 9-4b). A marked increase to just over 400 mg/L occurs from about 450 to 550 m depth, and from here continues to increase steadily to about 1,000 to 1,200 mg/L at 1,000 to 1,200 m depth, where a maximum value of just over 1,000 mg/L SO₄ is reached before decreasing to about 830 mg/L at greater depths. This behaviour is in agreement with the hypothesis of these groundwaters being in equilibrium with gypsum, as suggested by the model calculations /Gimeno et al. 2009/.

Isotopic studies show that the original $\delta^{34}\text{S}$ isotopic signature is significantly modified by microbial sulphate reduction. This is most prominent down to about 300 to 400 m depth depending on location. At greater depths, the sulphate content increases and the origin of this sulphate can be attributed mostly to dissolution of sulphate minerals (gypsum), although some of marine origin may still be present.

Bicarbonate contents (Figure 9-4c) are variable from about 150 to 320 mg/L in the first approximately 250 m of bedrock, and even more so in the overburden sediments which show extreme ranges in composition from close to zero to just over 600 mg/L HCO₃. In both cases, this illustrates environments where the carbonate system and the microbial production of CO₂ are very active /Gimeno et al. 2009/. Concentrations and variability then decrease from about 200 to 600 m after which very low values (< 10 mg/L HCO₃) continue to the maximum depths sampled. This is in contrast with the brackish to saline non-marine groundwaters which show values ranging from about 60 to < 10 mg/L HCO₃ with increasing depth.

The content of **DOC** (Dissolved Organic Carbon; Figure 9-4d) appears to be within the 1 to 7 mg/L range, apart from some higher values in the upper bedrock which may be influenced by anthropogenic activities. From about 250 to 600 m depth the DOC, with one exception, consistently lies within the range of about 1.5 to 3.5 mg/L, and at greater depths at about 1.0 to 1.5 mg/L. Possible contamination at these depths is supported by the anomalous tritium trends (cf. Section 9.5.8).

The distribution of **strontium** with increasing depth and salinity is closely similar to that of calcium (cf. Figure 9-4a). However, the Ca/Sr ratio is not constant and shows a wide and variable range in the shallow groundwaters as a result of weathering of the different rocks and minerals. At greater depth the ratio seems to stabilise and in groundwaters with salinities higher than approximately 4,000 mg/L the Ca/Sr ratio shows almost constant values, an observation made also at Forsmark and Olkilouto. Interestingly, at all three sites the ratios agree with each of the respective brine end members, which may suggest that in the deeper, more saline groundwaters, both calcium and strontium are mostly derived from the saline end member and controlled by mixing /Gimeno et al. 2008, 2009/.

Strontium isotope ratios (⁸⁷Sr/⁸⁶Sr) show a large variation in the near surface groundwaters (0.711 to 0.732) /Tröjbom et al. 2008, Laaksoharju et al. 2009/. Especially high ratios in samples with low strontium contents support the influence by different weathering processes noted above, whereas low ratios in samples with higher strontium contents indicate possible marine sources. For groundwaters at depths below 50 m, the range is, with a few exceptions, much narrower (0.715 to 0.717) which overlaps with the values measured in the host rock /Drake and Tullborg 2009a/. In general, all the Laxemar groundwater types show fairly similar strontium isotope ratios and this is interpreted as being the result of homogenisation due to water-rock interactions, mainly ion exchange processes /Peterman and Wallin 1999/.

Barium, in contrast to strontium, does not show a clear trend with depth or salinity; most values fall within the 0–200 µg/L range with a small increase to about 400 mg/L at about 500 m depth. The lack of any marked trend suggests some type of mineralogical control on the behaviour of barium. Two different barium minerals have been detected in fracture coatings in the area; barite (barium sulphate) which seems to be in equilibrium in most groundwaters, and harmotome (a Ba-zeolite) /Drake and Tullborg 2009a/.

Phosphate concentrations (PO_4^{3-}) in the Laxemar-Simpevarp groundwaters are low; the highest variability and contents are associated with the near surface groundwaters (with maximum values close to 30 mg/L) and some fresh shallow groundwaters (up to 0.1 mg/L). These higher values are probably related to anthropogenic phosphate (e.g. fertilizer) or to the decomposition of organic matter in the overburden or in the recharge zone. The only documented phosphate mineral in the area is apatite which is present as an accessory phase in the bedrock. Concentrations of phosphate in deeper groundwaters are mostly below 0.05 mg/L or even below the detection limit.

Depth trends of minor and trace elements

Heavy trace elements

Heavy trace elements such as Mo, As, Cr, Co, Cu, Pb, V and Ni have been analysed in a number of sampled sections. However, in common with Forsmark, there were major difficulties surrounding their evaluation involving the introduction of different post glacial groundwater types and contamination resulting from drilling and sampling activities (cf. discussion in /Smellie et al. 2008, Laaksoharju et al. 2009/).

Rare earth elements

Rare earth elements (REEs) are usually evaluated collectively due to their similar chemical behaviour and as such are excellent indicators of origin, oxidation state etc. In general, the total REE concentrations in the Laxemar groundwaters vary from below the detection limit to 4.5 $\mu\text{g/L}$, and most of the groundwaters analysed for REEs lack data above the detection limit for the complete series /Laaksoharju et al. 2009/.

Most of the analysed samples consist of brackish glacial waters sampled mainly about 300 to 600 m depth together with: a) two shallower samples (about 25 to 330 m depth) of fresh and mixed-brackish water composition ($\text{Cl} < 250 \text{ mg/L}$), and b) two of the deepest saline non-marine samples (about 700 m) corresponding to a transition to saline non-marine type (about 700 m), and highly saline waters (about 1,300 m). Interestingly, the highly saline types showed the lowest REE contents.

In general, the dissolved REE patterns show the same distribution as the fracture filling minerals and the wall rock, indicating that the REEs are mainly derived from these phases and that leaching has been fairly uniform for all REEs. For instance, the slightly negative Eu anomalies found in the fracture fillings derive from the wall rock signature /cf. Drake et al. 2006/ and the less common positive Eu anomalies, and some LREE enrichments, could be derived from some calcites /Drake and Tullborg 2009a/. However, slight HREE enrichment can be found in some waters as a result of complexation with carbonate species which by far are the most important species.

Major groundwater evolution trends

Br/Cl versus elevation

The Br/Cl percentage weight ratio versus elevation (Figure 9-5a) shows a wide range of Br/Cl values in the overburden soil pipes (0.002 to 0.012). In the upper bedrock, a narrow range of Br/Cl values (about 0.0035 to 0.005) occurs within this more dynamic hydraulic system down to about 250 m. This is followed by a steady increase in the Br/Cl percentage weight ratio from 0.0045 to 0.008 at about 400 to 800 m depth, which represents a gradual decrease in hydraulic conductivity (and therefore groundwater flow). Following this, the Br/Cl weight ratio maintains similar values to about 1,200 m before decreasing to about 0.007 at greater depths characterised by very low flow and stagnant groundwater conditions. This decrease helps to underline the uniqueness of these deep, highly saline evolved groundwaters at depths greater than about 1,200 m, suggesting closed system conditions.

The brackish glacial groundwaters do not deviate from the overall trend to about 1,000 m which is not unexpected as these glacial waters would have been highly diluted (i.e. insignificant Br and Cl compared to the pre-existing bedrock groundwaters) when introduced during the last deglaciation.

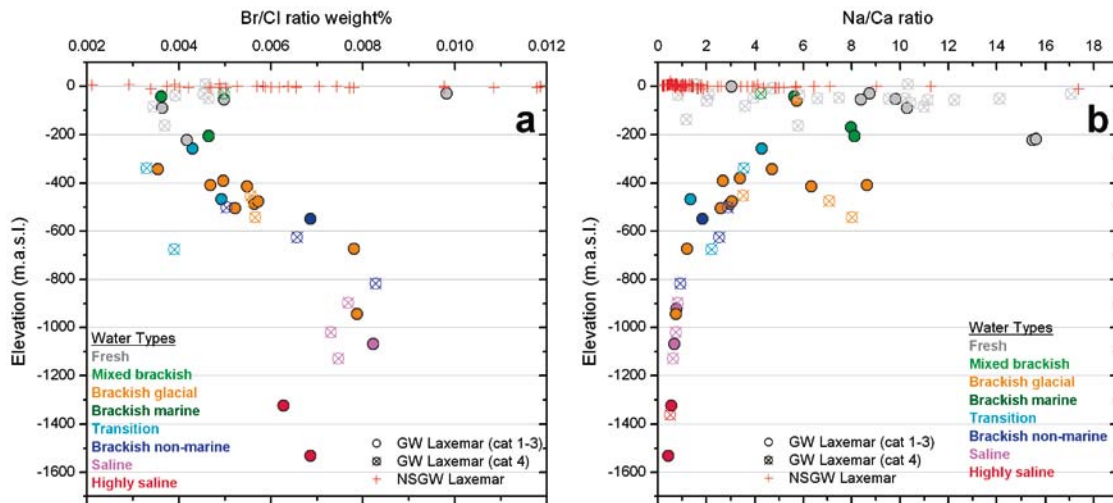


Figure 9-5. Plot of Br/Cl (a) and Na/Ca (b) versus elevation for groundwaters in the Laxemar subarea.

Na/Ca versus elevation

Figure 9-5b illustrates clearly at about 400 m depth the change from a Na-Ca-Cl to a Ca-Na-Cl type groundwater, indicating an increasing deep saline component and a corresponding decrease in influence from downward advective flow circulation. As noted above, the upper bedrock sodium may partly reflect some marine (i.e. Littorina Sea) influence.

Ca/Mg versus Br/Cl

Figure 9-6, plotting Ca/Mg versus Br/Cl, provides an opportunity to interpret further the nature of the Laxemar groundwaters. The figure differentiates: a) a small group of residual modern marine waters (Baltic Sea) in the overburden, b) most of the fresh groundwaters circled in grey, c) most of the brackish glacial groundwaters circled in orange, d) the deepest most highly saline groundwaters

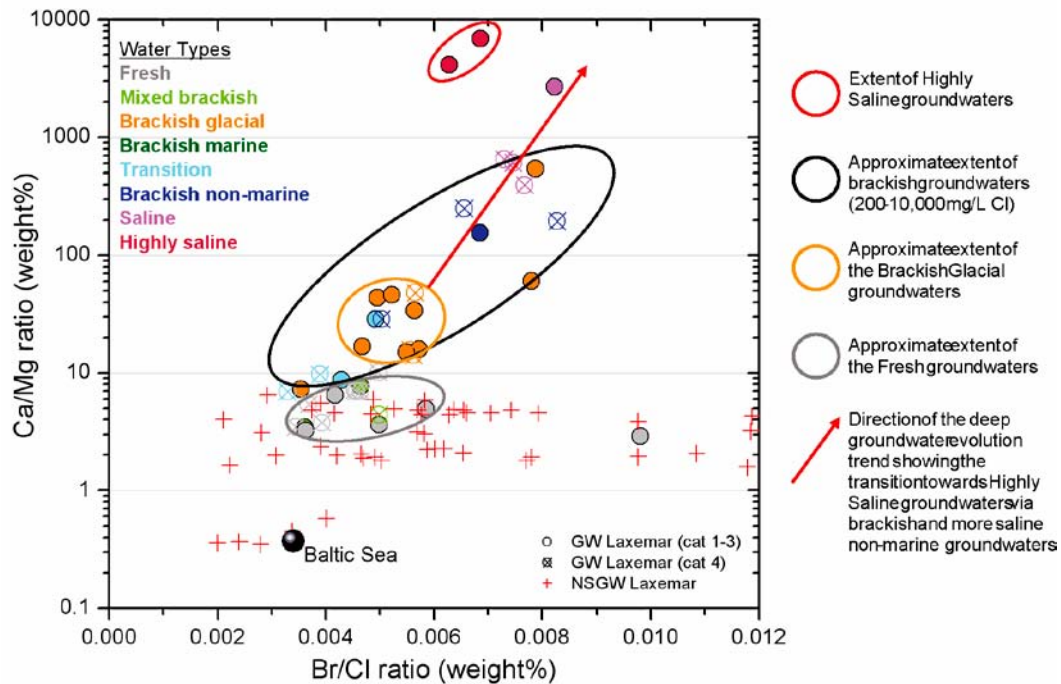


Figure 9-6. Plot of Ca/Mg versus Br/Cl for the Laxemar subarea showing the depth trend in the deeper bedrock groundwaters (i.e. > 600 m depth) from brackish to saline non-marine groundwaters to highly saline groundwater types.

circled in red, and e) the position of the two transition samples influenced by a weak Littorina Sea component. The red arrow shows a potential evolution pathway in the deeper bedrock groundwaters (i.e. > 600 m depth) via brackish to saline non-marine groundwater types. Much of the data along this pathway (i.e. to depths of about 1,000 m) represent groundwaters that contain an increasing component of the highly saline non-marine (or mixed non-marine/old marine) groundwater type. However, this highly saline groundwater type deviates significantly from the evolution trend indicated, reflecting the rapid change from low flow conditions (i.e. saline groundwaters to about 1,000 m depth) to very low flow to near-stagnant groundwater conditions (i.e. highly saline groundwaters to at least 1,500 m depth) indicated in KLX02 to occur at depths greater than about 1,200 m /Ekman 2001/.

Accompanying the overall increase in salinity to about 1,000 m depth is the change from a Na-Ca-Cl groundwater at shallower depths, to a Ca-Na-Cl groundwater at greater depths. This is clearly shown above in Figure 9-5b and by plotting Na/Cl versus Br/Cl /Laaksoharju et al. 2009/.

The general character of these highly saline groundwaters has also been studied /Laaksoharju et al. 2009, Gimeno et al. 2009/ and the following observations can be made:

- Ca-Na-Cl groundwaters of deep origin are common throughout the Laxemar-Simpevarp area and are particularly well described in Laxemar.
- True brines (> 100 g/L TDS) have not yet been accessed despite drilling KLX02 to about 1,700 m depth in Laxemar. In this deep borehole, advective mixing is prevalent to about 1,000 m depth, and diffusion processes probably dominate at depths greater than 1,200 m where closed stagnant conditions prevail.
- The highly saline groundwaters show significant water-rock interaction enrichment with increasing depth (e.g. indicators such as Li, Cs and ^{18}O and ^2H /Laaksoharju et al. 2009/). Given the depths and the low flow to stagnant hydraulic conditions of these groundwaters, the increased mineralisation suggests an affinity to a non-marine source rather than a surface-derived post glacial marine source, although an ancient non-marine/old marine mixing origin cannot be excluded.
- Certain element ratios (e.g. Ca/Na, Ca/Mg and Br/Cl ratios) reveal similarities between the Laxemar and other studied deep groundwaters in the Canadian Precambrian Shield area /Laaksoharju et al. 2009/.
- Although permafrost conditions almost certainly occurred in Laxemar down to depths of about 200 to 300 m, there is no convincing hydrochemical evidence to date that might indicate that residual fluids from freeze-out processes have influenced the composition of the present-day deep groundwaters /Laaksoharju et al. 2009/.
- The long-term hydrochemical stability of the highly saline groundwater environment associated with low flow to stagnant hydraulic conditions is supported by ^{36}Cl dating which indicates ages in the range of hundreds of thousands of years.

9.5.2 Supplementary data from borehole KLX27A

Supplementary groundwater data from the cored borehole KLX27A became available after the 'Extended data freeze Laxemar 2.3'. This borehole, drilled in the southwestern part of the Laxemar subarea, is 650 m long and represents the last drilled borehole within the Oskarshamn site investigation programme (cf. Figure 2-5).

Groundwater sampling for complete chemical characterisation (CCC) was performed in the borehole at section 641.5 to 646.03 m borehole length (elevation -559 to -567 m). Because the section sampled falls within the intended repository depth interval, the results are of great importance for the site description. The time-series data recorded indicate stability and, together with a low drilling fluid content (< 0.1%), the sampled section is regarded as representative. Considerable effort was made to obtain high quality Eh measurements but this was unfortunately not successful due to equipment failure and extreme weather conditions. Nevertheless, reducing conditions are indicated even though stable Eh values were not achieved.

The groundwater sampled is brackish glacial (Na-Ca-Cl-SO₄) in type (Cl = 1,700 mg/L, Na = 973 mg/L, Ca = 125 mg/L, SO₄ = 106 mg/L). Bicarbonate is low (13 mg/L) which excludes carbon-14 analyses of the inorganic carbon. Tritium is, as expected, below detection (< 0.8 TU) and stable isotope analyses show a depleted δ¹⁸O signature (−14.7‰ VSMOW). The groundwater composition of KLX27A is typical for the deeper, brackish glacial groundwaters and therefore in agreement with the present understanding of the site.

9.5.3 Mixing calculations

Multivariate Mixing and Mass-balance (M3) modelling is based on four end members (Deep saline, Glacial, Littorina and Altered Meteoric); the background and application of the modelling is presented and discussed in /Laaksoharju et al. 2009, Gimeno et al. 2009, Gurban 2009/. In general, the modelled results support: a) independent interpretations based on measured ions and isotopes in the groundwaters, b) indications of major features, such as the groundwater type classification (cf. Section 9.5) , and c) the penetration depth or location of the different end-member water types predicted by using hydrogeological modelling (cf. Chapter 8 and Section 9.7). In Figure 9-7, the M3 mixing proportions are shown as scatter plots indicating the end-member contributions of Deep Saline, Glacial, Littorina Sea and Altered Meteoric water in relation to the groundwater types and depth.

Figure 9-7a shows the mixing proportions of Deep Saline water. Taking the different subareas separately, the first general conclusion that can be drawn is that the different groundwater types are very well correlated with the M3 mixing proportions for this end member (also observed for the remaining end-member distributions, cf. Figures 9-7b,c and d). The depth trend of the Deep Saline end member is clearly represented by the Laxemar subarea groundwaters. Here, the different groundwater types evolve towards the saline and highly saline waters with increasing depth by an increased percentage of the Deep Saline end member from proportions > 35% up to almost 100% (deepest samples taken from borehole KLX02). These saline and highly saline waters are found below repository depths (−400 to −700 m elevation) in the focused volume. The other locations also show a percentage increase of Deep Saline with depth, but only up to a maximum of 30% in Äspö and 40% in the Simpevarp subarea. The slightly higher Deep Saline percentage for the same depth (about 1,000 m) in Simpevarp (40%) compared to Äspö and Laxemar (30–35%) is an interesting observation, reflecting the discharge nature of the groundwaters near the coast.

In Figure 9-7b the Glacial end member corresponds to the depleted δ¹⁸O signatures indicative of an influx of cold climate water such as glacial meltwater from the last deglaciation. This glacial signature is clearly seen in the plots of the different areas and the agreement with the groundwater types defined is also good. Orange coded samples, which correspond to the brackish glacial groundwater type, have the highest glacial contribution (up to 55%) followed by the transition waters (turquoise code), and both are mainly found at repository depths in the focused volume. The rest of the groundwater types have Glacial mixing proportions of less than 30%.

Groundwaters with important Littorina Sea water end-member signatures (Figure 9-7c) are only detected in a few samples from Äspö and Simpevarp. The percentage of Littorina in the Laxemar groundwaters is very low and close to the detection limit of the M3 method (0.1 mixing units). Only boreholes KLX01, KLX10 and KLX15A show slight influences of brackish marine water, with less than 15% of Littorina component in the focused volume and at repository depths. Independent evaluation of Littorina signatures based on chloride and bromide support this low marine water signature in the system. This may reflect that the penetration of Littorina Sea water has been less important at Laxemar due to the palaeogeographical history of the area /Laaksoharju et al. 2009/, or that it has already been flushed out.

The groundwater samples with an Altered Meteoric end-member portion > 80% correspond generally to groundwaters with measurable tritium contents (restricted to the first 100 to 200 m). As expected, the resulting ‘fresh’ and ‘mixed brackish’ waters show large proportions of the Altered Meteoric end member. There is an important amount of Altered Meteoric end member at the repository level in the Laxemar subarea between 30 to 60% for most of the samples (Figure 9-7d).

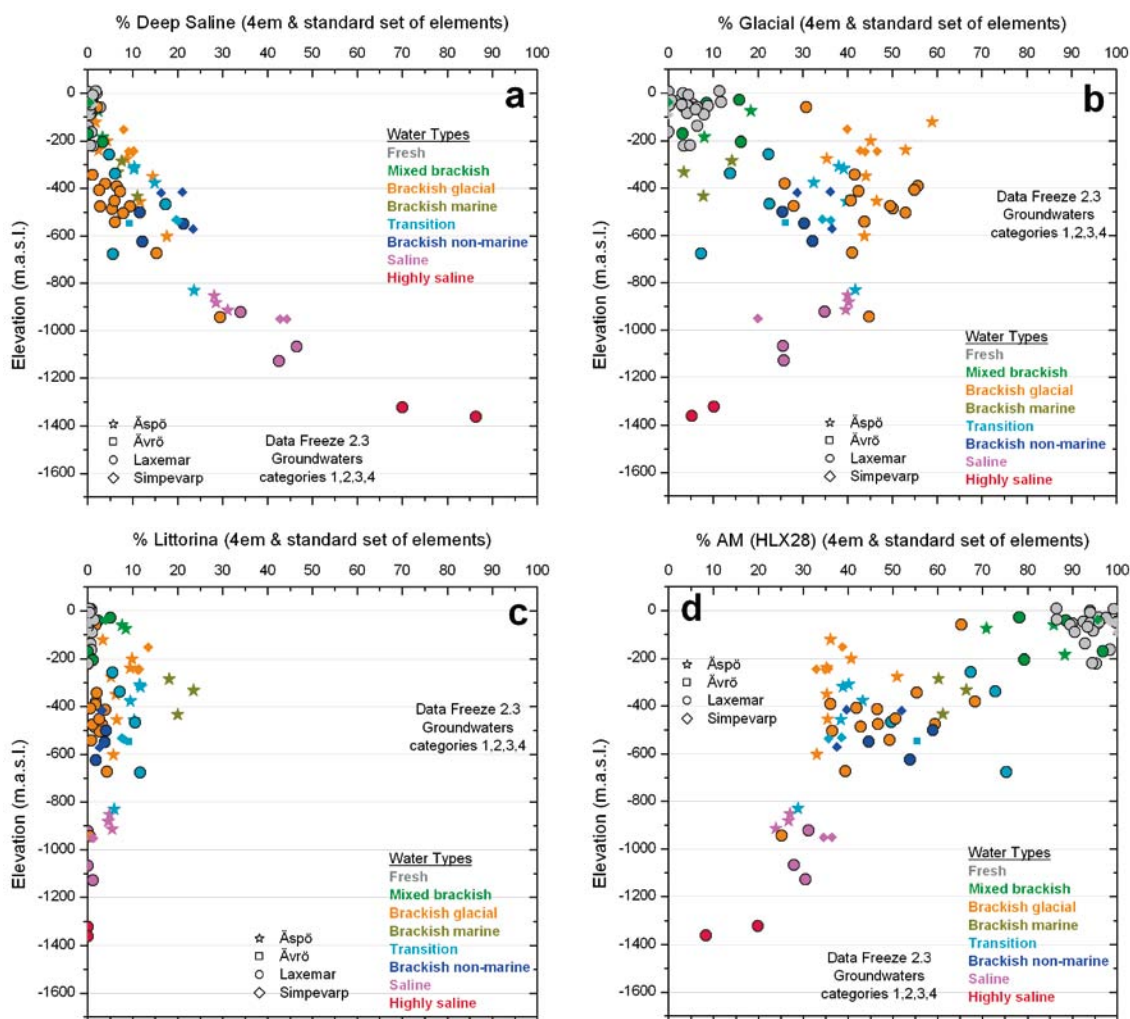


Figure 9-7. Computed M3 mixing proportions of: a) Deep Saline, b) Glacial, c) Littorina Sea and, d) recent Altered Meteoric groundwater, all plotted versus depth (elevation) and for current groundwater types.

9.5.4 The redox system

To evaluate the groundwater redox system in the Laxemar-Simpevarp area an integrated modelling approach has been applied by combining hydrogeochemical, mineralogical and microbiological information. The major aim has been to: a) confirm or support the redox potential field measurements, and b) confirm the redox pair(s) believed to control the redox conditions in the groundwater. This is detailed in /Gimeno et al. 2009/ and summarised in /Laaksoharju et al. 2009/.

The number of samples with representative and complete data for the analysis of the redox system (Eh values, Fe^{2+} , S^{2-} , Mn, $\text{NO}_3\text{-NO}_2\text{-NH}_4$, U, microbial and mineralogical data) is few and data are scarce, especially the potentiometric Eh measurements at depths exceeding 500 m. Nevertheless, all available groundwater redox potential data in the Laxemar-Simpevarp area clearly show reducing conditions (Figure 9-8a), even taking into account all the possible perturbations of the original redox environment during drilling and sampling /Laaksoharju et al. 2009/. This indicates the ability of microbial and water-rock interaction processes to create very reducing conditions, even in the shallowest parts of the system most sensitive to perturbation.

With regard to the behaviour of redox-sensitive elements, the general trends observed in the dissolved concentrations of iron, sulphur, manganese and nitrogen species are described below. Moreover, the controls on their dissolved contents are interpreted with the support of speciation-solubility calculations /Gimeno et al. 2009/.

The surface and near surface system

In the near surface groundwaters, dissolved Fe^{2+} and S^{2-} contents from the Laxemar-Simpevarp area do not deviate from the ranges found in similar groundwaters from other sites in the Fennoscandian Shield. Dissolved Fe^{2+} in the soil pipe groundwaters (Figure 9-8b) display values in the range 0.1 to 9 mg/L, which are compatible to values in the near surface groundwaters from Forsmark and Olkiluoto /cf. Pitkänen et al. 2004/. Speciation-solubility calculations show that most of the near surface groundwaters are in equilibrium or oversaturated with respect to siderite (FeCO_3). This suggests effective precipitation of siderite and its involvement in the control of dissolved Fe^{2+} .

Maximum contents of dissolved sulphide are close to 1 mg/L (Figure 9-8c) and most values are less than < 0.2 mg/L. For the majority of groundwaters with sulphide contents greater than 0.04 mg/L, the speciation-solubility calculations indicate equilibrium with respect to ‘amorphous’ FeS. This underlines its effective precipitation in the presence of microbial sulphate reduction in these groundwaters, as also deduced from $\delta^{34}\text{S}$ values by /Tröjlbom et al. 2008/ (Figure 9-9).

Dissolved manganese contents in the near surface groundwaters (Figure 9-8d) range from < 0.1 to 2 mg/L. The higher concentrations are consistent with the existence at very shallow levels of reducing environments with effective Mn(II) mobilisation due both to inorganic processes (e.g. weathering of amphiboles, biotites or chlorites) and to manganese reduction of organic matter by MRB (Manganese Reducing Bacteria) using the manganese sources in the soil minerals. The dissolved manganese seems to be mainly limited by the precipitation of rhodochrosite (MnCO_3), which

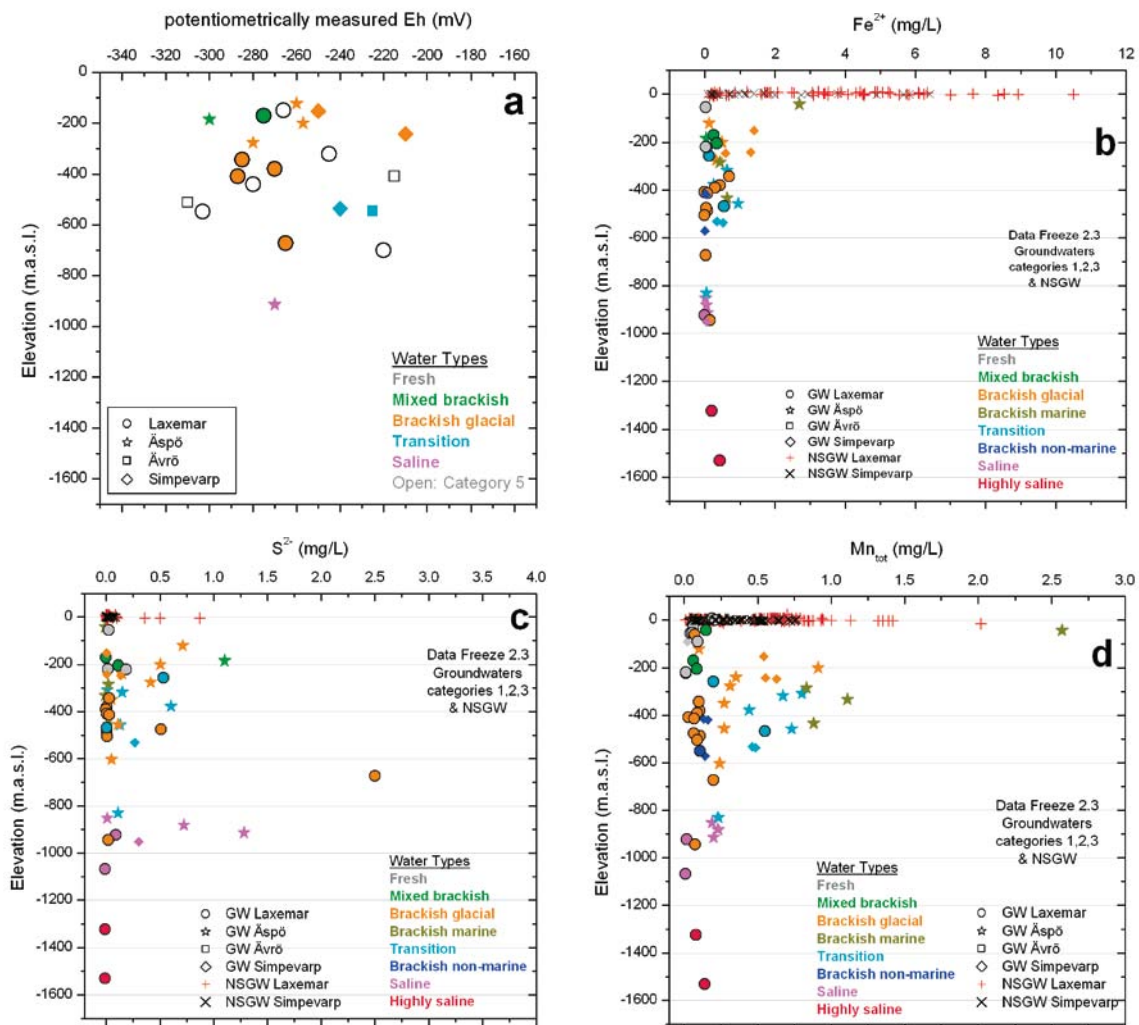


Figure 9-8. Distribution of potentiometric Eh (a), Fe^{2+} (b), S^{2-} (c) and Mn_{tot} (d) with depth in the Laxemar-Simpevarp area groundwaters. (Categories 1-3 are represented by coloured symbols and open unfilled symbols represent category 5 samples).

is the only manganese mineral reaching equilibrium in these waters. Although rhodochrosite has not been detected so far in the overburden, its control on dissolved manganese contents is feasible in this environment in which the biogenic CO₂ input and the aluminosilicate and calcite weathering reactions can produce an important increase in alkalinity.

For dissolved nitrogen, available analytical data include values for nitrate, nitrite and ammonium (the latter shown in Figure 9-10a). The concentrations of nitrate and nitrite show in common with ammonium the greatest variability and largest concentrations in the near surface groundwaters. This variability is associated with the oxic/anoxic transition.

Maximum nitrate contents reach 5.5 mg/L with most samples under 1 mg/L. For nitrite, with only one exception at 0.37 mg/L, all contents are clearly under 0.05 mg/L, and those of ammonium are generally below 3.5 mg/L. The total dissolved nitrogen (N_{total}) contents in the near surface system are mainly derived from the atmospheric pool and from the degradation of organic matter /Tröjbom et al. 2008/, although some contribution from weathering of potassium-rich silicates containing ammonium is also possible. Moreover, cation exchange reactions involving NH₄⁺ can participate in the behaviour of dissolved ammonium in the near surface groundwaters. Nitrogen contents show a large temporal variability, possibly related to seasonal variation in biological activity, where the main dissolved species are generally ammonium and/or dissolved organic nitrogen.

Dissolved uranium in the near surface groundwaters (Figure 9-10b) shows the greatest range and also the highest values (up to 13 µg/L). This is attributed to the oxidising to mildly reducing conditions and the availability of bicarbonate for complexation. For example, both near surface groundwaters and deeper groundwaters with bicarbonate contents lower than 25 mg/L show uranium contents lower than 1 µg/L. However, irrespective of uranium content, the near surface groundwaters show low ²³⁴U/²³⁸U activity ratios (close to 1) which can be indicative of oxidising to mildly reducing conditions /Laaksoharju et al. 2009/.

The deeper groundwater system

In the deeper groundwater system, dissolved Fe²⁺ concentrations decrease roughly down to about 700 m depth (Figure 9-8b). At greater depth, at least to about 1,000 m, the values are lower than 0.2 mg/L, after which the deepest, most highly saline samples reach values of 0.5 mg/L at -1,560 m elevation. For dissolved S²⁻, there is a large number of samples with significant sulphide contents (e.g. > 0.2 mg/L), but no clear evolution trend with depth (Figure 9-8c). As a general observation there are increased values (S²⁻ > 0.2 mg/L) mainly at Äspö and Ävrö compared to only a few in Laxemar. However, ongoing sulphate reduction is occurring in groundwaters at shallow and intermediate depths (cf. Section 9.5.8), supported by enriched δ³⁴S values and decreased sulphate contents (Figure 9-9).

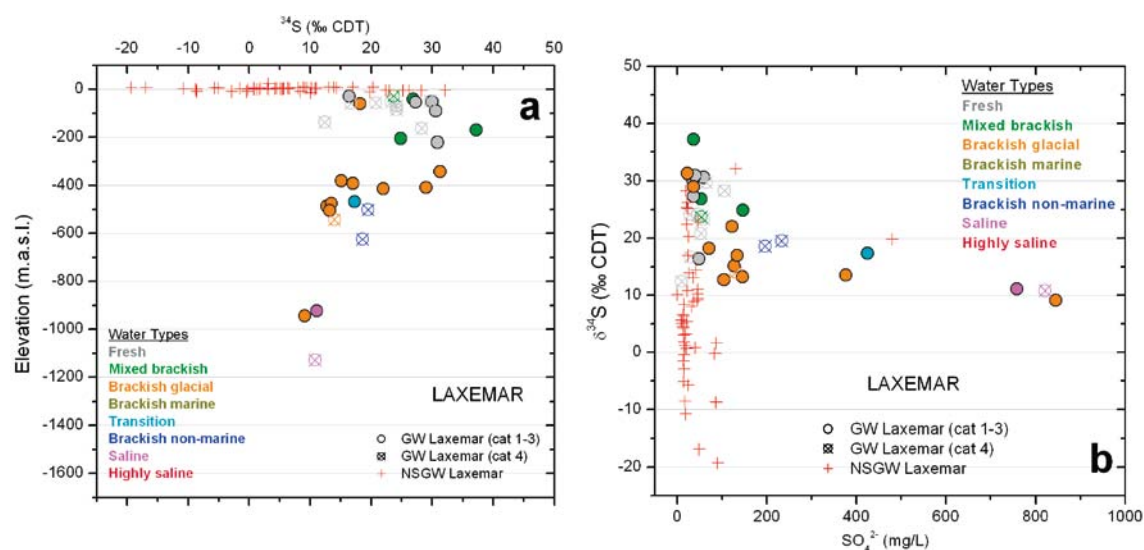


Figure 9-9. δ³⁴S versus elevation (a) and sulphate (b), in groundwaters from the Laxemar subarea.

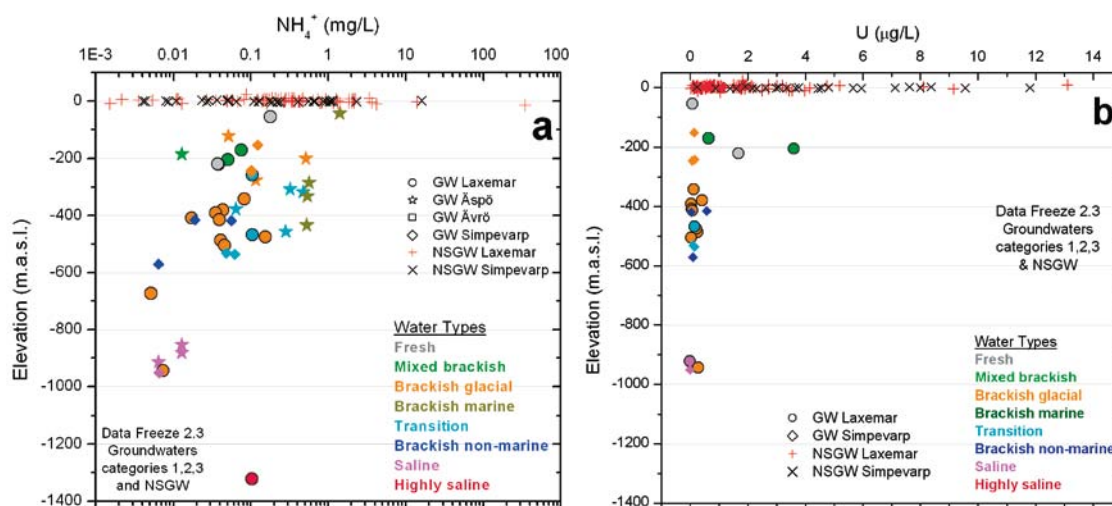


Figure 9-10. Concentrations of NH_4^+ (a) and uranium (b) versus elevation in groundwaters from the Laxemar-Simpevarp area.

Speciation-solubility calculations indicate that siderite saturation indices decrease with increasing depth and chloride content, showing that this phase is not an important control on dissolved Fe^{2+} concentrations in this part of the system. With regard to $\text{Fe}(\text{II})$ monosulphides, equilibrium occurs down to about 600 m depth mainly in groundwaters from Simpevarp and Äspö, but also in some groundwaters from Laxemar. This equilibrium, with respect to the amorphous and metastable iron monosulphides found in most Simpevarp groundwaters (including the near surface waters), indicates a presently continuous supply of H_2S produced by SRB (Sulphate Reducing Bacteria) activity combined with the presence of $\text{Fe}(\text{II})$ supplied by IRB (Iron Reducing Bacteria) activity (cf. Section 9.5.4) or dissolution of $\text{Fe}(\text{II})$ minerals (cf. Gimeno et al. 2009). Pyrite of biogenic origin has also been identified in the bedrock fractures (cf. Section 9.5.6).

Dissolved manganese concentrations in groundwaters from the Laxemar-Simpevarp area vary from below detection to more than 2.5 mg/L (Figure 9-8d). Overall, its concentration with depth shows a similar pattern to that of the dissolved Fe^{2+} contents, with large and variable values in the brackish groundwaters in the upper approximately 500 m of the bedrock, and very low values in the deeper, more saline waters. This roughly parallel behaviour could indicate the ‘simultaneous’ control of both elements by iron phases (i.e. oxyhydroxides, clays). The highest manganese contents found in the Simpevarp-Äspö subareas for some deep brackish groundwaters between about 200 and 500 m depth, probably reflect residual input from recharged Littorina waters, in common with that described for the Forsmark, Olkiluoto and Finnsjön areas /Gimeno et al. 2008/.

The variability range and content of dissolved nitrogen species drastically decrease in the deeper groundwater system due to the general reducing conditions (Figure 9-10a). Consequently, extremely low contents of nitrate and nitrite have been observed, comparable with other crystalline environments in the Canadian Shield /Gascoyne 2004/, Olkiluoto /Pitkänen et al. 2004/ and Forsmark /Gimeno et al. 2008/. Shallow groundwaters of meteoric origin in Laxemar-Simpevarp also show this character indicating the development of an anoxic environment at an early stage in the groundwater evolution. Ammonium contents also decrease with depth in the Laxemar-Simpevarp area with the largest variability occurring in the upper 500 m of the bedrock where groundwaters with a clear Littorina component show the highest values (also recorded at Forsmark and Olkiluoto).

The uranium contents in the groundwaters show a decreasing trend with depth and bicarbonate content. Measured uranium contents are about 1 $\mu\text{g/L}$ or lower in all groundwaters from depths greater than about 300 m in accordance with the low Eh recorded (< -240 mV). The low uranium contents are accompanied by $^{234}\text{U}/^{238}\text{U}$ activity ratios typically > 2 supporting reducing conditions /Laaksoharju et al. 2009/. In the Forsmark area, some groundwaters with bicarbonate contents above 30 mg/L and Eh above approximately -200 mV show uranium contents exceeding 10 $\mu\text{g/L}$ at depths between about 250 and 640 m, cf. /Smellie et al. 2008/. This is attributed to the presence of an easily dissolved uranium phase present along some of the water-conducting fractures. Such uranium phases seem not to be present, or at least much less frequent and accessible in the fracture system at depth in Laxemar.

9.5.5 Characterisation of microorganisms, colloids and gases

Microorganisms

There is no obvious trend with depth concerning the diversity of the microorganisms found in the groundwaters at Laxemar. The highest stacked most probable number (MPN) values are found in borehole KLX03:–380 m elevation and in KLX15A and KLX17A at –467 and –548 m elevation respectively (Figure 9-11) /Hallbeck and Pedersen 2008/. The microbial populations consist of autotrophic and heterotrophic acetogens, and iron-, manganese- and sulphate-reducing bacteria. In KLX03:–380 m elevation both autotrophic and heterotrophic methanogens are found, and this diversity distribution is common to most of the samples but with different values. However, there are some exceptions to this pattern; the shallow samples in KLX08:–150 m, KSH01A:–153 and KLX03:–171 m elevation have no MRB and low MPN in general, and there are no SRB indicated in KLX03:–171 and KLX03:–922 m elevation. The deepest sample at –922 m elevation has a very high salinity which could have been a problem in the culturing, so the presence of SRB at depth cannot be excluded. The dominating group of organisms in all sections is the acetogens which produce acetate, either from organic compounds in combination with production of hydrogen gas, or in an autotrophic way from carbon dioxide and hydrogen gas. Acetate is an excellent carbon and energy source for most microorganisms. Autotrophic production of acetate from hydrogen and carbon dioxide has been suggested as a basis for subsurface ecosystems that are independent of organic material supply from photosynthesis /Pedersen 2001/.

The most important findings from the microbiological investigations at Laxemar are:

- Sulphate-reducing bacteria are present at all depths sampled, but show wide variations in population levels.
- Iron- and manganese-reducing bacteria are present at all depths, except for low population levels of manganese-reducers in samples from both the shallowest and deepest groundwaters.
- Acetogens are the dominating physiological group of microorganisms.
- Measured Eh correlates with the number of sulphate-reducing bacteria for a subset of samples from intermediate depths. This suggests that the $\text{SO}_4^{2-}/\text{S}^{2-}$ -system, catalysed by sulphate-reducing bacteria, plays an important role in determining the redox state of the system at these depths (Figure 9-12).

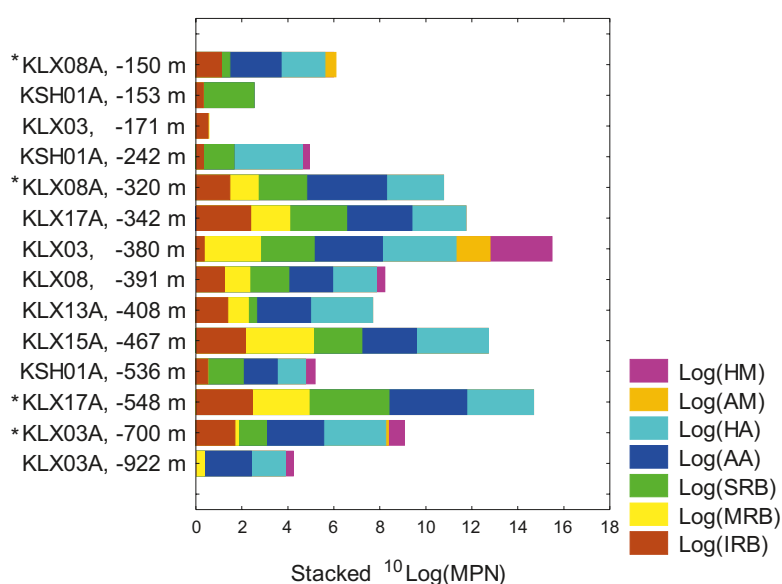


Figure 9-11. Stacked \log^{10} MPN values showing the proportions of the different cultivable bacteria for samples from Laxemar and Simpevarp sorted by depth. IRB = iron-reducing bacteria, MRB = manganese-reducing bacteria, SRB = sulphate-reducing bacteria, AA = autotrophic acetogens, HA = heterotrophic acetogens, AM = autotrophic methanogens, HM = heterotrophic methanogens. * indicate that the groundwaters sampled were not representative for the sampled depth /Smellie and Tullborg 2009/.

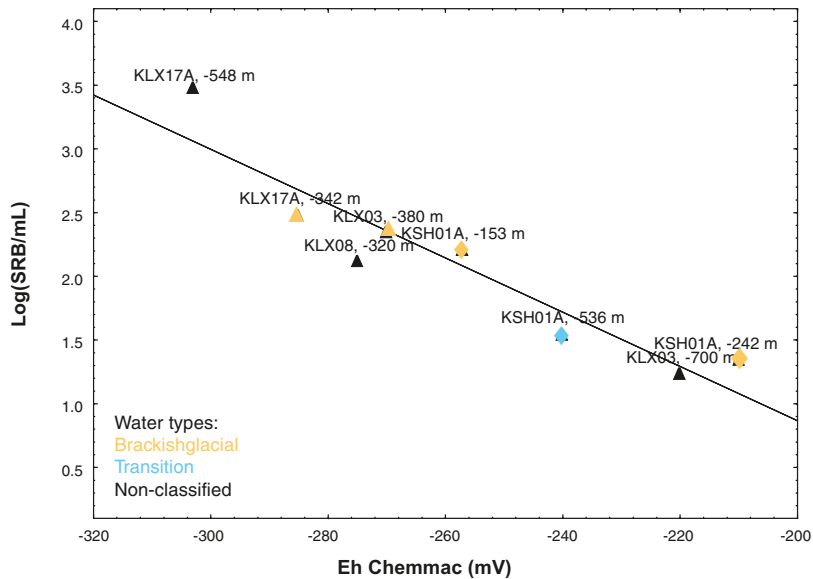


Figure 9-12. The relation between the number of sulphate-reducing bacteria and measured Eh. Some data are excluded, i.e. KLX03: -171 m, KLX03: -922 m, KLX08: -150 m and KLX13A: -408 m elevation, where only very low numbers of SRB could be identified, and KLX15A: -467 m elevation where matching Eh values are not available. Statistics: $^{10}\text{Log}(\text{SRB}) = -171 - 41 \times E_h$, $r = -0.94$, significant at $p=0.0006$, $n=8$. Data from the 'Extended data freeze Laxemar 2.3'.

Colloids

Different methods to characterise colloids were used during the site investigation: a) filtration method, b) fractionation method, c) laser-induced breakdown colloid detection (LIBD) /Berg et al. 2006/, used for some samples during the last sampling campaign in Laxemar, and d) colloid analysis by means of submicro-filtration plus scanning electron microscopy and energy-dispersive spectroscopy (SEM/EDS) /Nilsson and Degueldre 2007/.

Both inorganic and organic colloids exist and these were measured at Laxemar; the results of the organic colloid analyses are presented in /Hallbeck and Pedersen 2008/. Microorganisms should also be considered as colloids as there are many groundwater examples $\leq 1 \mu\text{m}$ in size. In addition, a recent study of groundwater in the Äspö HRL tunnel identified a variety of viruses (i.e. phages); these are protein particles, approximately 200 nm in diameter that can infect microbial cells. The major conclusions from the colloid characterisation are listed below /Hallbeck and Pedersen 2008/:

- The number of colloids found in the Laxemar-Simpevarp groundwaters is approximately in the order of $10^6/\text{mL}$ and the measured concentrations are in agreement with measurements from other crystalline groundwater environments. Because the colloid samples come from a system which is disturbed following drilling and sampling, the measured populations can indicate maximum values.
- A decrease in colloid content versus depth is indicated.
- The filtration and fractionation method showed that the colloids are composed mostly of iron and sulphur. LIBD in combination with EDX on the other hand show that the colloids are composed mostly of aluminium, silica and iron; this may partly be due to contamination from drilling debris. Both inorganic and organic colloids exist in Laxemar and some colloids are probably microbes and potentially even viruses (phages).

Gases

The major dissolved gases in groundwaters from the Fennoscandian Shield and the Laxemar-Simpevarp area are nitrogen, carbon dioxide, helium, methane and argon. Nitrogen followed by helium are present in greatest amounts, with nitrogen and carbon dioxide being most common in the more shallow groundwaters and helium in the deeper parts of the system. Other gases present

are methane, argon, hydrogen and traces of higher hydrocarbons with up to three carbon atoms. The available data indicate that the total gas content is less than would be expected in Fennoscandian Shield groundwaters. This indicates either an open, high out-flux system, or low in-flux of gases from below (geogases). Although their concentrations generally increase with depth, in particular helium (cf. Section 9.5.8), the gases are not oversaturated at the depths from which they were sampled. There are few samples taken for gas analyses and the isotopic composition of important gases like hydrogen and methane is missing. The description of the origin of gases should therefore be considered as preliminary.

9.5.6 Studies of fracture fillings

Background

Water/mineral reactions (that may or may not involve biogenic activity) are important for the hydro-geochemical understanding and detailed description of the groundwater environment for two main reasons: a) recent water/mineral interactions with groundwaters influence the present groundwater chemistry (e.g. dissolution/precipitation of calcite, oxidation/production of pyrite, ion exchange etc), and b) the distribution and chemical/isotopic composition of certain minerals (e.g. calcite, pyrite and Fe-oxyhydroxide) provide information on former physico-chemical conditions which are important for the description of the long-term stability of the site. Fracture minerals, and to some extent the adjacent bedrock, participate most actively in water/mineral interactions. Furthermore, fracture minerals may serve also as a redox and pH buffer in the case of recharging oxidising groundwaters (e.g. during glaciations and deglaciations). The most common fracture minerals in the crystalline rocks at Laxemar are chlorite, calcite, epidote, quartz, clay minerals, pyrite and hematite. The results of the fracture mineral investigations from Laxemar-Simpevarp, including the palaeohydrogeological studies, are reported in /Drake and Tullborg 2009a/ and summarised below (cf. also Section 5.2.6).

The following sequence of fracture mineral generations has been established:

Generation 1 is an epidote- and quartz-rich mylonite formed during the early geological history of the area. The mylonites are mainly associated with deformation zones, are often accompanied by wall rock alteration, and have a minimum age close to ca 1,773 Ma when the rock cooled below about 500°C.

Generation 2 is a cataclasite which occurs in at least two different varieties, sometimes with semi-ductile features suggesting formation close to 300 to 350°C. Both were formed during the early geological history of the area, although both have experienced later reactivation. The cataclasites are mainly associated with deformation zones and the older ductile shear zones have influenced the orientation of many *Generation 2* structures.

Generation 3 consists of a sequence of at least three different mineral parageneses in sealed fractures, and occasionally of greisen. Major minerals are calcite, quartz, chlorite, fluorite, pyrite, muscovite, epidote, prehnite and laumontite. The latter three either replace or transect each other in chronological order. *Generation 3* is related to the intrusions of the Götemar and Uthammar granites (ca 1,450 Ma), as supported by $^{40}\text{Ar}/^{39}\text{Ar}$ plateau ages /Drake et al. 2009b/, but may also include some older fracture mineralisations.

Generation 4 mainly includes calcite, adularia, laumontite, chlorite, quartz, illite and hematite which are found in thin sealed fractures cross-cutting *Generation 3* fillings. *Generation 4* is interpreted as Sveconorwegian in age as indicated by a $^{40}\text{Ar}/^{39}\text{Ar}$ plateau age on adularia (989 Ma). Furthermore, N-S oriented ca 900 Ma dolerites in the westernmost part of Laxemar support activity in the area during that period of time.

The oldest *Generation 5* fillings (calcite dominated) were probably formed in relation to the Caledonian orogeny as a result of the circulation of warm brine fluids at about 80 to 145°C at ca 440 to 400 Ma ago. Other minerals include adularia, fluorite, pyrite, gypsum (possibly originally anhydrite), barite, zeolites, hematite, clay minerals, chlorite, chalcopyrite, galena, sphalerite and REE-carbonate. These fillings precipitated from organic-rich fluids, probably influenced by descending waters from overlying sediments. The relatively high formation temperatures may also have been influenced by subsidence due to thick overlying sediments. Younger fillings of *Generation 5*

precipitated during gradually lower temperatures as the overlying sedimentary successions were successively eroded, shown by the changing stable isotope compositions and chemical compositions, which grade into Generation 6 signatures.

Generation 6 consists of low temperature fracture coatings which may have been precipitated recently, i.e. during the Quaternary. These include clay minerals, calcite and goethite above the redox front, and pyrite below. Generation 6 minerals are not easily distinguished from the youngest Generation 5 fillings, which have overlapping stable isotope signatures and trace element compositions. The stable isotope composition of these minerals (mainly calcite) shows that they may have been precipitated from groundwaters with similar signatures as the present-day groundwater at the site.

Wall rock alteration is common and most noticeable as red staining adjacent to fractures filled with hydrothermal minerals. The red colour is due to hematite dissemination and is associated with fractures sealed with mineralisations of Generations 1, 2 and 3; this is detailed in /Drake et al. 2008, Drake and Tullborg 2009a/ and summarised in /Laaksoharju et al. 2009/.

Studies of calcite, pyrite, gypsum and barite

Isotope systematics have resulted in the identification of three general types of calcite /Drake and Tullborg 2009b/: a) hydrothermal calcite (Generation 3 and 4), b) warm brine-type calcite originating from a fluid influenced by organic material (Generation 5a), and c) low temperature calcite precipitated from different groundwaters under present-day ambient temperatures (Generation 5b and 6).

The isotope record, the chemistry, and the fluid inclusions in the analysed fracture minerals show gradually changing signatures with time, such as successively lower temperatures, increased organic and microbial influence, and higher $^{87}\text{Sr}/^{86}\text{Sr}$ ratios (larger proportion of radiogenic Sr). The conclusions are summarised below and detailed in /Drake and Tullborg 2009a/:

- The hydrothermal Generation 3 and 4 calcite and pyrite show inorganic $\delta^{13}\text{C}$, $\delta^{18}\text{O}$ and $\delta^{34}\text{S}$ signatures, T_h at about 195–370°C and variable salinities. The large variation in salinity, trace element chemistry and T_h suggest formation over a long time span related to the intrusions of the Göttemar and Uthammar granites. In addition, it is suggested that the Generation 4 fillings are hydrothermal in origin, with inorganic signatures similar to those of Generation 3. However, formation temperatures were slightly lower during this less significant event, which may have been caused by fluid circulation in relation to the intrusion of dolerite dykes during the Sveconorwegian period.
- Palaeozoic Generation 5a calcites show organic $\delta^{13}\text{C}$ signatures, T_h of 80–145°C, high salinities and lower $^{87}\text{Sr}/^{86}\text{Sr}$ (also in gypsum), and lower $\delta^{18}\text{O}$ than the present groundwater. High manganese contents and partial LREE enrichment also suggest organic and possibly microbial influence. Formation from descending organic-rich fluids influenced by Palaeozoic sediments or Palaeozoic sea water is a possible scenario for formation of these ‘warm brine’ calcites.
- Late Palaeozoic to recent, possibly Quaternary, Generation 5b/6 calcite and pyrite show organic and microbial influence at temperatures below 110°C, occasionally with closed system signatures. The $\delta^{18}\text{O}$ and $^{87}\text{Sr}/^{86}\text{Sr}$ values show that some of these calcites may have formed from fluids in equilibrium with waters similar to present ambient groundwaters. Formation from waters with different $\delta^{18}\text{O}$ values and salinities, such as fresh and brackish groundwaters, is indicated, and also suggested by different crystal morphologies of calcite. The frequency of low $\delta^{13}\text{C}$ and biogenically (and microbial) modified $\delta^{34}\text{S}$ decreases with depth, and the microbially influenced $\delta^{13}\text{C}$ is found deeper in the recharge area (Laxemar subarea) than in the discharge area (Simpevarp subarea).
- Major hydrological/hydrochemical fluctuations during recent low temperature conditions have been observed, but the amounts of produced or dissolved minerals during these conditions have been relatively small at depths greater than about 100 m. Most of the fracture fillings in the area are very old (Proterozoic to Palaeozoic) and the signatures of most of the generations suggest precipitation during a long time span with varying conditions; this is typical for several of the fracture mineral generations. Late Palaeozoic calcite is difficult to separate from recent calcites as they are usually found in the same fracture systems, indicating that these fractures have been intermittently water conducting from the Palaeozoic onwards. However, the exact position of the flow channels may have varied along the fracture planes.

Changes in pH and redox conditions

Different mineralogical and geochemical indicators, such as the distribution of Fe(II)/Fe(III) minerals and behaviour of redox sensitive elements like cerium and uranium, can be studied in order to reveal possible redox front development, for example, in the near-surface bedrock environment. In addition, although calcite is not redox sensitive *sensu stricto*, there is a secondary relationship due to interactions between the biosphere and the bicarbonate. Two different studies focused on the Precambrian and recent redox features identified in the fractures and in the wall rock, have been carried out in Laxemar and the results are summarised in /Drake and Tullborg 2009a/:

1. Hydrothermally altered, red-stained (supposedly oxidised) wall rock samples have been compared with fresh rock nearby, and differences in mineralogy, mineral and whole rock chemistry (especially the reducing capacity) have been determined /Drake et al. 2008/.
2. The position of the recent near surface redox front has been investigated based on mineralogical, geochemical and uranium series disequilibrium analyses of mineral coatings along open fractures /Drake et al. 2009a/.

The results from the hydrothermally altered and potentially oxidised wall rock, which is mainly related to the Generation 3 fracture minerals, show that the red-stained rock adjacent to the fractures displays major changes in mineralogy. Biotite, plagioclase and magnetite have been altered and chlorite, K-feldspar, albite, sericite, prehnite, epidote and hematite have been formed. However, the changes in chemistry are moderate with K-enrichment, Ca-depletion and constant Fe_{tot} documented. The Fe^{3+}/Fe_{tot} ratio in the oxide phase is higher in the red-stained samples, whereas the Fe^{3+}/Fe_{tot} ratio in the silicate phase is largely similar to that in the wall rock and the unaltered reference samples. Because most of the Fe is hosted in the silicate phase, the decrease in reducing capacity (Fe^{2+}), if any, in the red-stained wall rock, is very small and not as high as macroscopic observations suggest. The increase in porosity in the red-stained rock may result in increased sorptivity and diffusion close to the fracture.

With respect to a recent near surface redox front, borehole studies show at what depths oxidising groundwater within the last 1 Ma generally has been reduced by, for example, fracture minerals \pm organic redox buffer. These investigations show that the redox front in Laxemar is generally positioned at about 15–20 m depth, depending locally on the bedrock hydraulic properties. The main features of the redox front are generally observed in the fracture mineralogy and geochemistry (Figure 9-13), and as a shift with increasing depth from: a) mainly goethite to mainly pyrite, b) positive cerium anomalies to slightly negative or insignificant cerium anomalies, and c) mobilisation and removal of uranium to mainly deposition.

Leaching of calcite in open fractures in the upper approximately 20–30 m bedrock further supports infiltration of very dilute recharge waters which probably have had relatively low pH and may at least partly have been charged with oxygen. Scattered goethite occurrences down to about 80 m and occasional signs of uranium removal at about 35–55 m depth, generally correlate with borehole sections of high fracture transmissivity (and/or high fracture frequencies) facilitating local downward percolation of oxidising groundwaters to greater depth. Removal of uranium during oxidising conditions within the last 300 ka, a period including both glaciations and interstadials, is not indicated in the analysed samples below about 55 m depth. Although penetration of glacial waters to much greater depths has been confirmed in the Laxemar-Simpevarp area /SKB 2006f/, this study conforms to the modelling carried out by /Guimerà et al. 1999/ and the conclusions drawn by /Gascoyne 1999/ in that these glacial waters were not oxidising at repository depths. This is supported by present-day observations which show that oxygen in recharge waters is generally consumed within the upper approximately 20 m (\pm 5 m) and to slightly greater depths in bedrock with increased hydraulic conductivity ($\geq 1 \cdot 10^{-7}$ m/s).

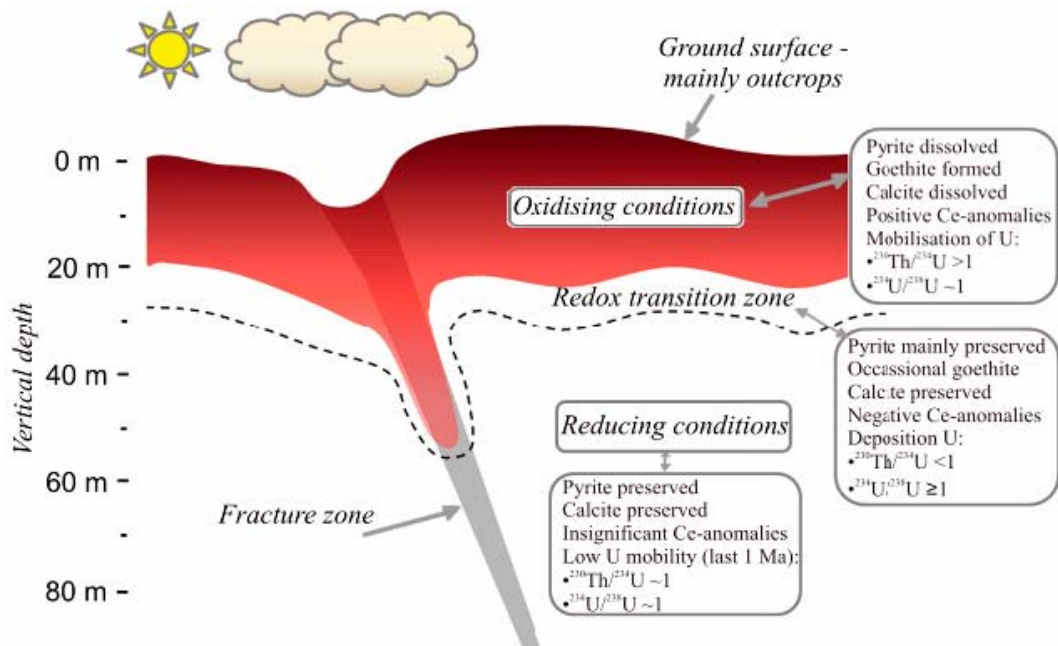


Figure 9-13. Tentative sketch of the near-surface redox front in Laxemar. The different fields represent the depth intervals where mineralogical, chemical and uranium series disequilibrium analyses of fracture coatings indicate recent oxidising conditions, reducing conditions or a transition zone in between. The study is based on a limited number of samples and deeper penetration of oxidising groundwaters along specific channels in highly transmissive fracture zones may occasionally have lasted for short periods of time. Figure from /Drake et al. 2009a/.

Concerning the available redox and pH buffer capacity provided by the fracture minerals present along the groundwater pathways, the following conclusions can be made:

- The most efficient pH buffer is calcite which is present in most of the fractures and deformation zones although in lower amounts in the upper approximately 10–20 m of the bedrock.
- The main inorganic redox buffer is Fe(II), which is present in chlorite, biotite and clay minerals and pyrite grains. This redox buffer has only been significantly decreased in the very near surface fractures (upper 20 metres), but may be partly reduced also in the upper approximately 50 m of bedrock.
- Despite earlier oxidising hydrothermal events and potential increased introduction of oxidising glacial meltwater during the Quaternary glaciations, there is a large redox buffer capacity still present in the fracture and wall rock minerals. Any potential build up of reducing capacity in the fracture minerals during recent periods of reducing groundwater conditions is difficult to estimate. Processes that could contribute to an increase in redox capacity include the production of Fe^{2+} and Mn^{2+} that may either precipitate (e.g. co-precipitation with calcite) or be sorbed on mineral surfaces due to ion exchange. In addition, iron sulphides may be formed due to bacterial activity of sulphate reducers. However, it can be concluded that the amounts of recent (Quaternary) minerals formed is probably small.

9.5.7 Porewater composition in bedrock

Background

The term 'porewater' as used here refers to the water in the connected pore space of the rock matrix that is accessible for diffusion-dominated interactions with groundwater circulating in nearby (micro-) fractures /Waber and Smellie 2008/.

Rock matrix porewater has been analysed from three boreholes in the Laxemar subarea (KLX03, KLX08 and KLX17A) that were drilled to about 1,000 m borehole length at different locations (Figure 5-30). In addition to systematic sampling along each drillcore, a continuous profile of porewater samples was collected at shallow depth in borehole KLX17A for some 20 m along the borehole from a water-conducting fracture zone down into the adjacent rock matrix. This was used to investigate the most recent (i.e. Holocene to Pleistocene) interaction between porewater and fracture groundwater. Differential flow logging has been performed on all three boreholes but unfortunately only a few reliable CCC (Complete Chemical Characterisation) groundwater analyses exist from nearby water-conducting fracture zones. No drillcore samples exist from any of the upper 100 m percussion drilled part of the boreholes.

Porewater composition

The chemical and isotopic composition of porewater extracted from drillcore material depends on the location of the three boreholes and the porewater samples with respect to the hydraulic domains and the occurrence of deformation zones /Laaksoharju et al. 2009, Waber et al. 2009/. The vertical occurrence of distinct porewater compositions is similar in boreholes KLX03 and KLX17A, but these differ from that in borehole KLX08. Porewater data show (Figure 9-14) a distinction between bedrock characterised by high fracture transmissivity and a high frequency of water-conducting fractures at shallow to intermediate depth, and bedrock characterised by low fracture transmissivity and a low frequency of water-conducting fractures at greater depth. In the more transmissive shallow to intermediate depth interval, porewater is of a general Na-HCO₃ chemical type with Cl contents of less than 1,500 mg/kgH₂O, and a range of oxygen isotope compositions (Figure 9-15) similar to that of present-day Baltic Sea water ($\delta^{18}\text{O}$ about -8‰ VSMOW) down to about 430 m depth in KLX03 and KLX17A and to about 620 m depth in KLX08. Cold climate signatures ($\delta^{18}\text{O} < -13\text{‰}$ VSMOW) are observed far from the nearest water-conducting fractures at depths of about 325 m (20–50 m distant) and 490 m (50–100 m distant) in borehole KLX03, close to a fracture at a depth of 350 m (0–5 m distant) in borehole KLX17A, and adjacent to water-conducting fractures at depths of 460 m (50–100 m distant) and 490 m (10–20 m distant) in borehole KLX08 (Figure 9-15 and Figure 9-16).

In all three boreholes, a change in porewater composition occurs below the dilute Na-HCO₃ type to a porewater with elevated chloride contents and of a general Na-Ca-SO₄ chemical type. This porewater type was encountered over a depth interval of about 120 m and there are compositional differences between boreholes KLX03 and KLX17A where this type of porewater occurs between about 430–550 m depth, compared with KLX08 where it occurs between about 620–750 m depth. The change coincides with a marked decrease in hydraulic conductivity, in the frequency of water-conducting features and, in boreholes KLX03 and KLX08, the transition zone from Ävrö granite to quartz monzodiorite. In boreholes KLX03 and KLX17A, Cl contents range from 5,000 to 7,600 mg/kgH₂O (Figure 9-14) and are associated with strongly variable $\delta^{18}\text{O}$ values of between about -4‰ to -13‰ VSMOW (Figures 9-15 and 9-16). In borehole KLX08, Cl contents range from 2,500 to 6,000 mg/kgH₂O with associated $\delta^{18}\text{O}$ values from -2‰ to -10‰ VSMOW. The Na-Ca-SO₄ type porewater appears to have a restricted vertical distribution roughly coinciding with the proposed repository depth.

More dilute porewater of Na-HCO₃ type (borehole KLX03) and Na-Ca-Cl-(HCO₃) type (borehole KLX08) occur again below the depth interval of the Na-Ca-SO₄ type porewater. Here, Cl contents vary between about 500 to 3,000 mg/kgH₂O and associated $\delta^{18}\text{O}$ values of between about -8‰ to -11‰ VSMOW. Towards the bottom of boreholes KLX03 and KLX08 at depths of about 930 m and 820 m, respectively, the Cl contents increase again to more than 5,000 mg/kgH₂O in KLX03 and more than 8,000 mg/kgH₂O in KLX08. The oxygen isotope composition of these deep Na-Ca-Cl-(HCO₃) to Na-Ca-Cl type porewaters is generally enriched in ¹⁸O compared to the more shallow porewaters (Figure 9-15 and Figure 9-16).

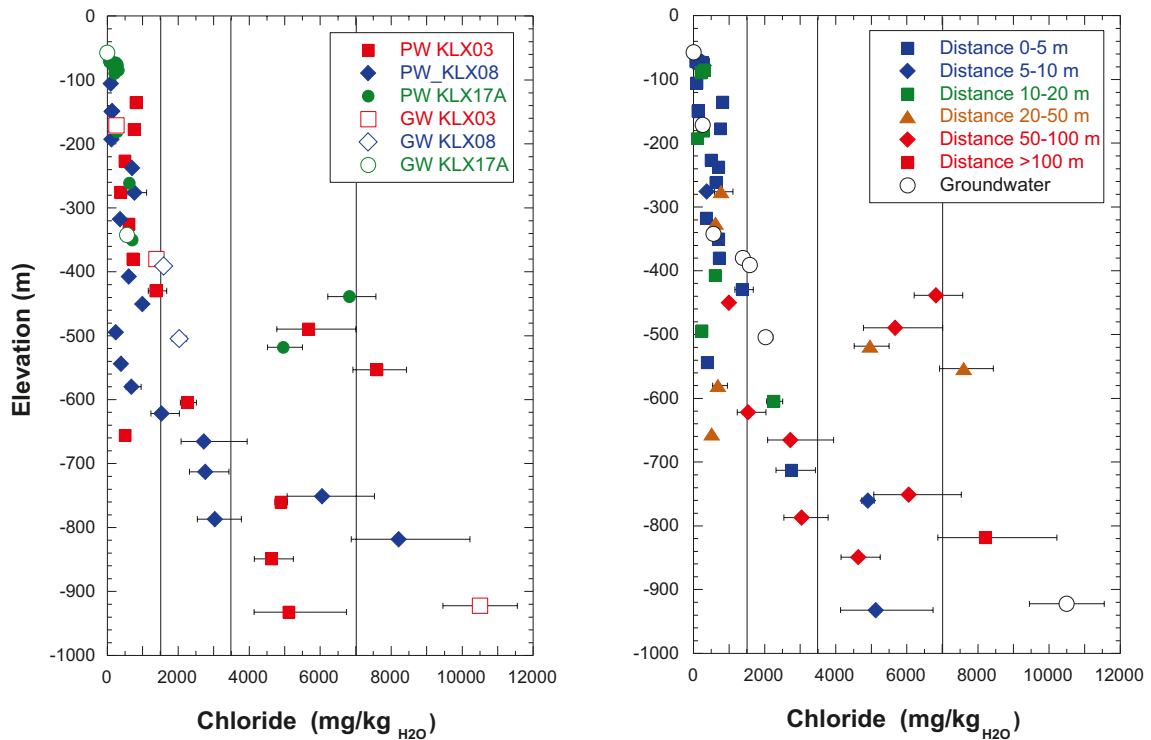


Figure 9-14. Chloride concentration in porewaters (PW, closed symbols) and related Category 1–3 groundwaters from boreholes KLX03, KLX08 and KLX17A in the Laxemar subarea on the left, compared with the distance of the porewater samples in one dimension from the nearest water-conducting fracture on the right. Fracture groundwater data from /Laaksoharju et al. 2009/.

Relationship between porewater and fracture groundwater

In boreholes KLX03 and KLX17A, generally equal chloride contents and oxygen isotope compositions are observed for porewaters and fracture groundwaters in the transmissive shallow to intermediate depth interval down to at least about 380 m for porewater samples located within less than 5 m from the nearest water-conducting fracture in the borehole. For such samples, a close to steady state situation is established for those components between the porewater and fracture groundwater of present-day origin and, at intermediate depths, cold climate infiltration. However, a transient state is still established even at shallow depths for samples more distant from a water-conducting fracture, for example, shown by the chloride content and isotope composition of two samples from borehole KLX17A at about 90 m depth (Figures 9-14 and 9-15). No fracture groundwater data exist at this 0–380 m depth interval in borehole KLX08 to compare with the porewater data.

At intermediate levels, different relationships for Cl values and $\delta^{18}\text{O}$ values prevail between porewater and fracture water depending on borehole location, distance of the porewater sample to the next water-conducting fracture, and fracture groundwater evolution. For samples located close to water-conducting fractures, a steady-state situation is established for both natural tracers in KLX17A, but only for ^{18}O in KLX03 between about 380–430 m depth where fracture groundwater data are available. In borehole KLX08, a transient state with respect to both Cl and ^{18}O is established down to about 500 m depth, while a close to steady state situation is suggested for ^{18}O .

Towards greater depth, fracture groundwater data are limited to one single analysis in borehole KLX03 at about 920 m depth. This porewater has a lower chloride content (Figure 9-14) and is enriched in ^{18}O compared with the fracture groundwater (Figures 9-15 and 9-16) and a transient state is established. Similar observations would also be expected for the large 500 to 900 m interval, which includes the zone with Na-Ca-SO₄ type porewater and from where fracture groundwater data are missing.

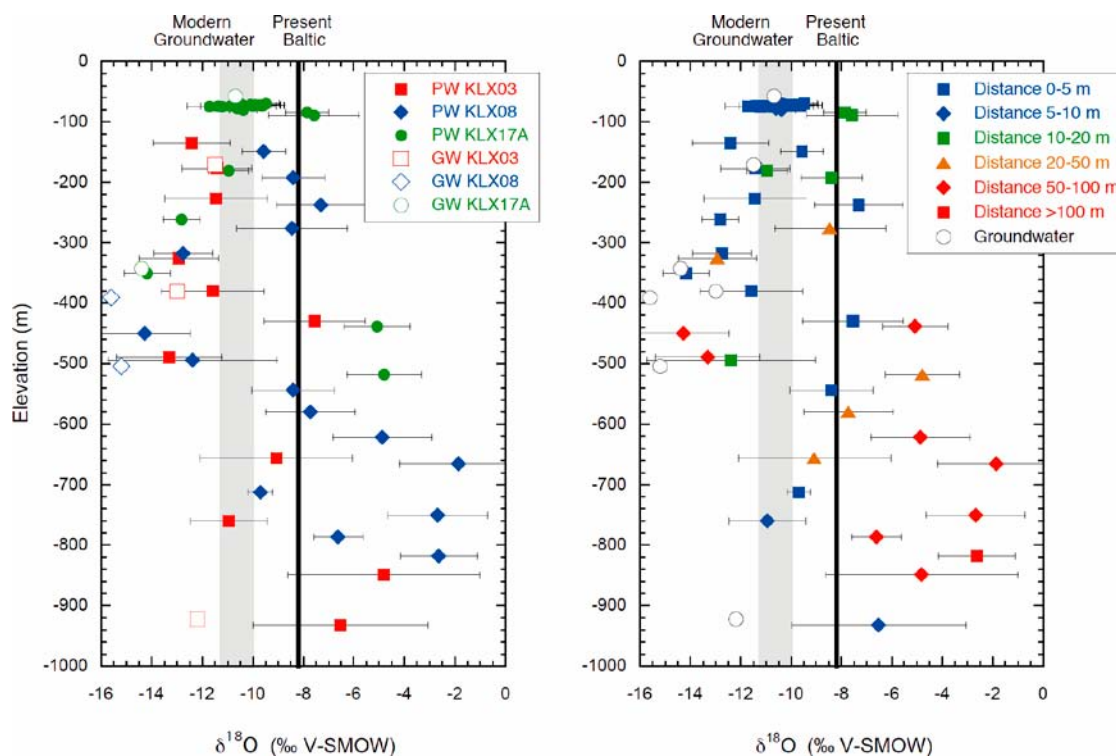


Figure 9-15. Oxygen isotope composition, $\delta^{18}\text{O}$, of porewater (PW, closed symbols) and related groundwater (GW, open symbols, category 1–3 data) from boreholes KLX03, KLX08 and KLX17A in the Laxemar subarea on the left, compared with the distance of the porewater samples from the next water-conducting fracture on the right. Fracture groundwater data from /Laaksoharju et al. 2009/.

Solute transport in the rock matrix

The interpretation of porewater data in a broader hydrogeological context requires knowledge of the solute transport properties of the various rock types. For the porewater samples such information was derived from measurements and modelling of the chloride concentration time series obtained from the out-diffusion experiments /Waber et al. 2009/. This exercise showed that neither the water-loss porosity (i.e. the connected porosity where solute transport can occur in the rock matrix), nor the calculated Cl^- pore diffusion coefficient, show a clear correlation with sample depth, and only a slight tendency towards decreasing values with increasing depth is observed. This is also observed for the effective diffusion coefficient of Cl^- calculated from these data /Laaksoharju et al. 2009/.

For the samples analysed for porewaters in the Laxemar subarea, differences in concentration between porewater samples and fracture groundwaters are especially observed if the distance to the nearest water-conducting fracture can be assumed to exceed 5–10 m. Keeping in mind the limitations of borehole investigations to roughly one dimension, and the relatively high fracture frequency at shallow depths, such a situation may have been established at shallow depths in borehole KLX08 and for two samples in borehole KLX17A, but more probably so below about 500 m depth in all three boreholes. The chemical and isotopic signatures preserved in such samples have been established a long time ago by palaeowaters which differed in composition from the fracture groundwaters sampled today, and are characterised by having very long residence times in the bedrock of several tens to hundreds of thousands of years (cf. Section 9.5.8). Combined with diffusion being identified as the dominant transport process, it can be concluded that given enough time, matrix diffusion of solutes is efficient over at least decametres in the intact rock matrix /Waber et al. 2009/.

With diffusion being identified as the dominant solute transport process in the rock matrix, the chemical and isotopic concentration of the porewater sample can be brought into an evolutionary context as a function of time (or space) using the fracture groundwaters as boundary conditions for the diffusion domain /Laaksoharju et al. 2009, Waber et al. 2009/.

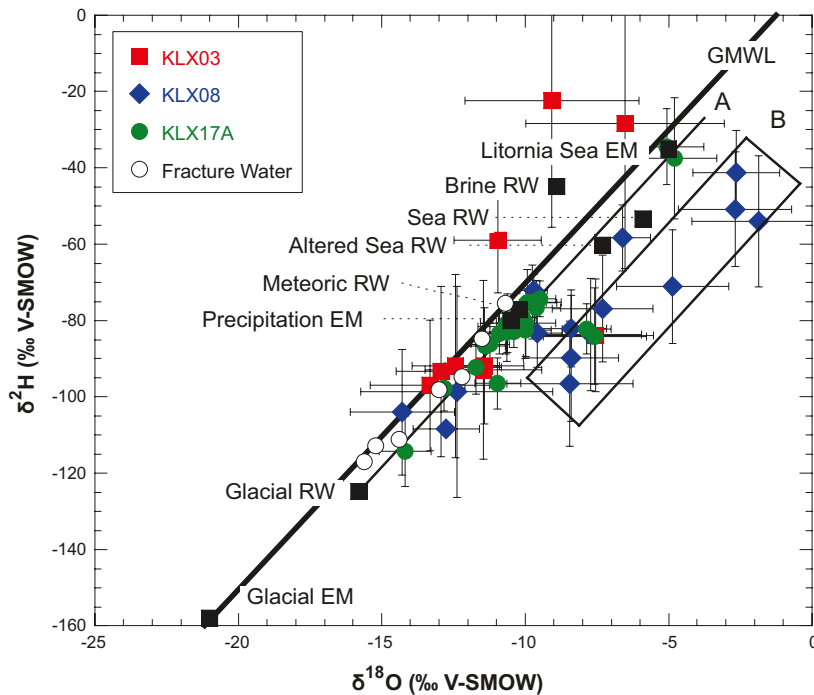


Figure 9-16. $\delta^{18}\text{O}$ vs $\delta^2\text{H}$ diagram of porewater from the different boreholes in the Laxemar subarea. Note trend 'A' which covers most samples of porewater in KLX03 and KLX17A defined by the 'Littorina Sea Water' to 'Glacial Reference Water' end-member compositions as used in the fracture groundwater modelling. Rectangle 'B' generally indicates the greater scatter/deviation of the KLX08 porewaters from the GMWL, possibly representing different climatic conditions compared with KLX03 and KLX17A. The isotope compositions of end member (EM) and reference fracture (RW) groundwaters are given for comparison. (GMWL = Global Meteoric Water Line). Fracture groundwater data and end-member compositions from /Laaksoharju et al. 2009/ and Table 9-1, respectively.

Palaeohydrogeological evolution

The porewater of most of the samples is of meteoric origin as indicated by their oxygen and hydrogen isotope compositions that plot to the right of the Global Meteoric Water Line, GMWL (Figure 9-16). The majority of porewater samples from boreholes KLX03 and KLX17A, and a few samples from borehole KLX08 that in one dimension are far from the nearest water-conducting fracture in this borehole, plot close to a line defined by the fracture groundwater 'Littorina Sea Water' to 'Glacial Reference Water' end-member compositions as used in the fracture groundwater modelling (cf. Table 9-1). A somewhat smaller range is covered by most of the porewater samples from borehole KLX08, and three samples located far from the nearest water-conducting fracture in KLX17A (2 samples) and KLX03 (1 sample), which all plot further to the right of the GMWL. Even allowing for the analytical uncertainties and possible superimposition of different events during diffusion in the rock matrix, the variable isotope compositions preserved in the porewaters may represent: a) different periods of warm and cold (palaeo-) climatic signatures, or b) different diffusion pathways (i.e. different distances to the nearest water-conducting fracture) that may have influenced the isotopic signatures.

Modelling of the shallow bedrock system has been carried out on the fracture profile from borehole KLX17A /Waber et al. 2009/. The results have been interpreted as showing that the isotope signature enriched in ^{18}O and ^2H (together with the low chloride) and preserved in the samples most distant (> 15 m) from the water-conducting zone, have been established before the Weichselian glaciation and should, therefore, represent a warm climate origin (Eemian Interglacial or older). This is in accordance with the fracture groundwater scenario outlined in Section 9.3.4. With respect to the other enriched samples which plot to the right of the GMWL (Figure 9-16) and including porewaters sampled closer to the water-conducting fracture, it may be argued that these represent warm climate signatures introduced more recently in the Holocene during post glacial time. This possibility is still under discussion.

The close to a steady-state situation established in boreholes KLX03 and KLX17A down to about 380 m depth between porewaters sampled close to a water-conducting fracture and the fracture groundwaters, indicates that over short distances the exchange between porewater and fracture groundwater occurred relatively rapidly. The recorded low Cl⁻ concentrations, combined with isotope signatures similar to those of modern shallow groundwater and, with increasing depth, of a cold climate to glacial component, indicates that these porewaters have preserved signatures of the most recent climatic changes (i.e. Holocene). A similar explanation appears to account for the samples from borehole KLX08 in this depth interval. Signatures in the circulating fracture groundwaters of the most recent cold climate or glacial origin are preserved in the porewaters below these depths, down to about 350 m in KLX17A and down to at least 500 m in KLX08.

Most prominent is the change in chemical and isotopic composition of the porewater in the Ävrö granite over a depth interval of about 120 m, starting at about 430 m depth in boreholes KLX03 and KLX17A and about 620 m depth in borehole KLX08, i.e. at depths probably close to the maximum penetration of the fracture brackish glacial groundwaters. Geochemical model calculations show that the mineralisation and isotopic composition of this Na-Ca-SO₄ porewater type cannot be explained by interaction with a known type of fracture groundwater or more advanced interaction with the Ävrö granite, but must originate from different processes /Waber et al. 2009/. There are two possible sources to the measured Ca-Na-SO₄ waters in Laxemar discussed in /Laaksoharju et al. 2009/: a) freeze-out mirabilite formation at shallow depths during permafrost (with subsequent breakdown and migration of Na-SO₄ waters to greater depths), and b) dissolution of old fracture gypsum (and migration of Ca-SO₄) during the last deglaciation whereupon glacial rebound may have reactivated sealed fracture systems of Palaeozoic age. Other potential hydrochemical evidence for permafrost influence (e.g. boron isotope systematics) is presented and discussed in /Laaksoharju et al. 2009/.

General conclusions

- Solute transport in the intact rock matrix appears to be dominated by diffusion, and matrix diffusion was identified to occur at least over several decametres into the rock matrix.
- The chloride and stable isotope signatures preserved in porewater reflect the evolution of fracture groundwater at a specific location and vary as a function of borehole location, porewater sample depth and distance from the nearest water-conducting fracture.
- Porewaters are generally of a dilute Na-HCO₃ type with Cl concentrations below 1,500 mg/kg_{H₂O} down to about 420 m depth in KLX03 and KLX17A and down to about 620 m depth in KLX08. The associated isotope signatures suggest a meteoric influence from climatic conditions similar to those prevailing today in all boreholes and also from the Holocene temperature maximum in borehole KLX08.
- Cold climate influence from the latest glaciation occurs in some porewater samples collected close to fractures down to about 350 m depth in boreholes KLX03 and KLX17A and down to about 500 m depth in borehole KLX08.
- A steady-state situation between pore water and fracture groundwater for both Cl concentration and isotope signatures is only established in some locations at shallow levels (to about 350 m depth) whereas transient states prevail for at least one of the natural tracers at intermediate levels.
- A distinct change in chemical and isotopic composition of the porewater to a highly mineralised Na-Ca-SO₄ type is observed between about 430–530 m in boreholes KLX03 and KLX17A and between about 620–750 m in borehole KLX08. Compatible fracture groundwater compositions have not been observed and the porewater signatures appear to have evolved a long time ago (before the Last Glacial Maximum) from fracture groundwater possibly influenced by freeze-out processes.
- In general terms, the porewater data indicate a change with increasing depth from waters of temperate meteoric origin, to glacial waters and finally to saline waters (i.e. a progressive change from dilute Na-HCO₃ to a saline Na-Ca-Cl type porewater) with a highly mineralised Na-Ca-SO₄ type porewater observed within a narrow depth interval at intermediate depths.

(Note: The data presented and discussed in this section are based on primary borehole length measurements taken in the field and the elevation data calculated in Sicada. Adjusted elevation data based on single-hole interpretation measurements would only minimally modify the results, and therefore in this context are regarded to be unimportant for plotting purposes).

9.5.8 Groundwater residence time

A key factor in understanding past and present groundwater evolution in the Laxemar-Simpevarp area is to constrain the average residence time for each of the major groundwater types. This can be approached qualitatively in terms of the major and trace element compositions of the groundwaters, i.e. in a broad sense based on aspects of water-rock reaction kinetics (cf. /Laaksoharju et al. 2009/ and discussion in Section 9.5.1). On a more quantitative level, because of their known half-lives decay character, the radioactive isotopes of ^3H ($t_{1/2} = 12.3$ y), ^{14}C ($t_{1/2} = 5,730 \pm 40$ y), ^{36}Cl ($t_{1/2} = 301,000$ y) and non-radioactive ^4He , have been used in the hydrochemical evaluation /Laaksoharju et al. 2009/; the results are summarised below.

Short residence times

Figure 9-17a shows tritium (^3H) versus elevation and includes category 1 to 5 data from percussion and cored boreholes from the Laxemar-Simpevarp area. The category 5 samples show a wide scatter of tritium activity contents with no obvious depth trend which is attributed mainly to a large percentage of drilling fluid and the influence of open hole conditions prior to, and during tube sampling. The category 1 to 4 groundwater samples, in contrast, show a characteristic decrease in tritium to a depth of about 100 to 150 m, which represents the penetration limit of modern fresh meteoric groundwater. The persistent tritium contents (1–4 TU) with increasing depth are due to various sources of contamination which are discussed in detail in Section 3 and also in /Smellie and Tullborg 2009/. Despite the problems with contamination from short-circuiting and sampling activities, and the possible introduction of tritium from contaminated drilling fluid, it is notable that there exist a large number of groundwater samples at all depths with little or no tritium (< 0.8 TU; Figure 9-17a). This underlines the heterogeneity of the flow system present in the Laxemar subarea.

Radiocarbon (^{14}C) extends the range of detection up to 35,000 years for groundwater residence time. Theoretically, this range should cover comfortably the period since the last deglaciation (cf. Figure 9-1), in particular confirmation of the Littorina Sea transgression. However, radiocarbon dating is complex and a major problem has been to constrain the ^{14}C input signature to the bedrock. The carbon isotope system is discussed in detail in /Laaksoharju et al. 2009/ and only the main results are summarised below.

Considering the general $^{14}\text{C}_{\text{TIC}}$ evolution versus depth (Figure 9-17 b), the near surface recharge waters with high ^{14}C (about 100 pmC), low HCO_3^- (< 60 mg/L; cf. Figure 9-4c) and atmospheric $\delta^{13}\text{C}$ ($> -8\text{‰}$), will increase their HCO_3^- due to microbial degradation of organic material of variable age which, in turn, leads to dissolution of calcite with low or no ^{14}C . This sequence of reactions is described in detail by /Gimeno et al. 2009/ and supported by geochemical modelling. The reactions indicate that shallow groundwaters with short residence times (modern tritium contents) show high HCO_3^- contents (200 to 350 mg/L), organically influenced $\delta^{13}\text{C}$ -values ($< -10\text{‰}$) and, most importantly, a diluted ^{14}C signal (50 to 80 pmC).

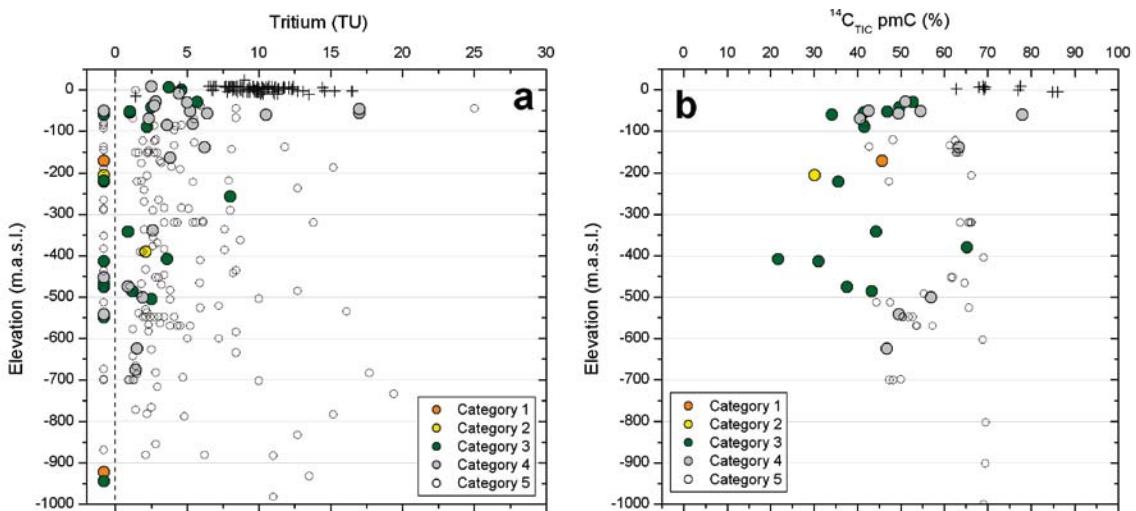


Figure 9-17. Tritium (a) and $^{14}\text{C}_{\text{TIC}}$ (b) versus elevation based on category 1 to 5 data from percussion and cored boreholes from the Laxemar subarea. Data below zero reflect values under detection limit (0.8 TU).

Because bicarbonate decreases with depth, ^{14}C analyses from depths greater than 600 m are rare and those present are from samples of dubious quality (i.e. not category 1–3 samples).

Long residence times

Helium-4 concentrations in groundwater have been measured and comparison with calculations of residence time based on helium production (in turn based on uranium and thorium concentrations in the host rock) have yielded unrealistically old ages and the reasons for this are discussed in /Gascoyne and Gurban 2009, Laaksoharju et al. 2009/. Nevertheless, gas analyses from the Laxemar-Simpevarp area generally show increasing helium with depth indicating longer residence times with increasing depth.

Chlorine-36 has been measured in selected groundwaters from the Laxemar-Simpevarp area ranging from the present Baltic Sea to near-surface recharge groundwaters, to deeper brackish marine (Littorina) and brackish non-marine groundwaters, and finally to saline groundwaters sampled from close to maximum depths /Gascoyne and Gurban 2009/. The variations of $^{36}\text{Cl}/\text{Cl}$ with chloride content for the Laxemar-Simpevarp samples are shown in Figure 9-18, together with data from Forsmark /Laaksoharju et al. 2008b, Smellie et al. 2008/, older data from Äspö and Laxemar subarea /Louvat et al. 1999/ and data from Olkiluoto /Pitkänen et al. 1996/. Despite the relatively few analyses from each site, a common pattern is indicated: a) high but variable values in the recharge waters with low chloride contents, b) Baltic Sea samples with relatively low $^{36}\text{Cl}/\text{Cl}$ ratios, c) Littorina influenced samples showing the lowest $^{36}\text{Cl}/\text{Cl}$ ratios, and d) highest values at greater depth in the brackish non-marine and saline groundwaters. In these last-mentioned groundwaters the $^{36}\text{Cl}/\text{Cl}$ starts to approach secular equilibrium with the host bedrock.

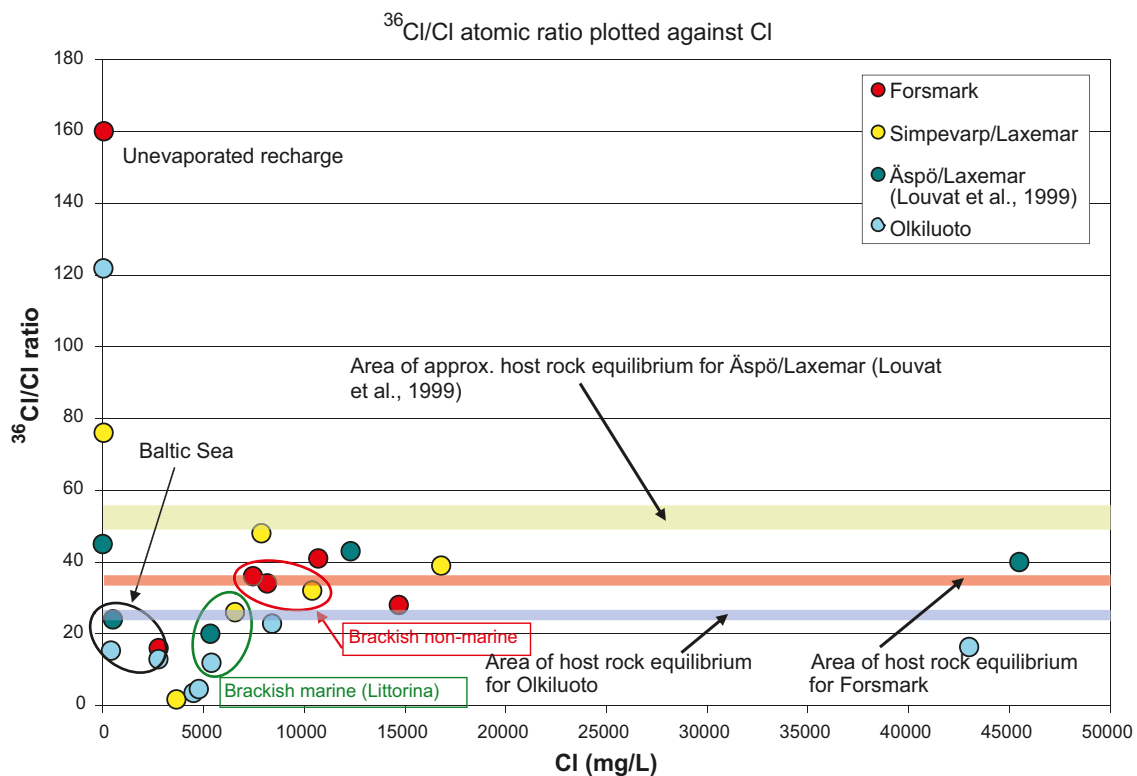


Figure 9-18: $^{36}\text{Cl}/\text{Cl}$ ratio versus Cl (modified from /Smellie et al. 2008/). In red are the Forsmark samples, in yellow are the Laxemar-Simpevarp data, in green the Äspö-Laxemar data from /Louvat et al. 1999/ and in light turquoise the Olkiluoto data from /Gascoyne 2001/. Also indicated are the respective host rock equilibrium for each of the three sites, as indicated by the coloured horizontal bars.

Conclusions

In summary, there is a range of quantitative (isotopic) evidence based on depth relationships that are generally supported by hydrochemical signatures (e.g. stable isotopes) and hydrogeological observations. This evidence shows:

- Recent to young fresh groundwaters, some showing signs of mixing, characterise the upper approximately 100 to 150 m of the bedrock. At these depths, because the hydraulic system is more dynamic, climatic changes have resulted in the cyclic introduction and flushing out of different groundwater types over tens of thousands of years, such that residence times for individual groundwater types seem relatively short, i.e. probably some hundreds to a few thousand years. The heterogeneity of the system is demonstrated by the scattered occurrence of tritium free waters sampled in the upper 100 m and also measurements of cold climate signatures retained in a few sampling points. Groundwaters referred to as brackish glacial in type are generally mixtures of glacial waters and temperate climate meteoric water of post glacial origin based on their $^{14}\text{C}_{(\text{TIC})}$ content. The saline component in these waters may be Littorina Sea waters or older saline waters depending on location. The glacial component, assumed to be related to the last phase of ice sheet coverage, is generally low in bicarbonate and very low in $^{14}\text{C}_{(\text{TIC})}$.
- The $^{14}\text{C}_{(\text{TIC})}$ analyses support that the groundwater carbon inventory is mainly post glacial. Input of organic and inorganic carbon compounds of post glacial origin is detectable to a depth of approximately 500 m with a corresponding decrease in bicarbonate. At depths greater than 500 m the bicarbonate content is very small.
- Significantly older groundwaters, found at depths greater than about 600 to 1,000 m, are characterised initially by brackish non-marine groundwaters which become successively more mineralised with increasing depth (to saline in type) by water/rock interactions, mixing with (unknown) deep saline water, and exchange with the rock matrix porewater. Hydraulic conditions at these depths and preliminary ^{36}Cl data indicate very low groundwater flow or close to stagnant conditions and suggest residence times that appear to be at least several hundreds of thousands of years.
- The presence of highly saline groundwaters ($> 20,000$ mg/L Cl) in the Laxemar subarea from depths greater than 1,400 m suggest still older groundwaters residing under effectively stagnant groundwater conditions.

9.5.9 Evaluation of uncertainties in field data and interpretation methods

During every phase of the hydrogeochemical investigation programme, i.e. drilling, sampling, analysis, evaluation and modelling etc, uncertainties are introduced which have to be accounted for, addressed fully and clearly documented to provide confidence in the end result /Smellie et al. 2002, Laaksoharju et al. 2008ab/. Many of the uncertainties are difficult to judge since they are consequences of expert judgement and not mathematical modelling. There is no undisturbed groundwater sampled prior to drilling and therefore evaluation of many of the uncertainties associated with sampling are based on indirect (e.g. short circuiting) or direct indications (e.g. drilling water content).

The sampling, analytical and modelling uncertainties are addressed and quantified in /Smellie et al. 2002, Nilsson 2009, Laaksoharju et al. 2008a, Bergelin et al. 2008, Gimeno et al. 2009, Gurban 2009/. Uncertainties associated with the effects of borehole perturbations and temporal and spatial variability are discussed below.

Effects of borehole perturbations

It is well known that site characterisation activities (mainly drilling activities) introduce perturbations in the system that can impact on the hydrochemistry of the groundwater samples collected at the site /Smellie and Tullborg 2009/. It is of interest, therefore, to perform scoping calculations in order to evaluate how much disturbance can be allowed for a given groundwater sample at repository depth, and still meet, for example, the SKB suitability criteria /Molinero et al. 2008/.

For Forsmark it can be concluded that the suitability criteria related to TDS and PH would be fulfilled always for the groundwaters, even for complete disturbance of the sample. The Ca+Mg criteria could be surpassed in the case of dilutions higher than 90 percent of the native groundwater sample.

Furthermore, cation exchange processes have an effect by lowering the Ca+Mg concentrations in the groundwater, compared with a pure conservative mixing. Similar results can be assumed for Laxemar although the groundwaters are more dilute when compared with Forsmark.

The oxygen consumption capacity of the granite bedrock has also been evaluated by using reactive transport modelling. The modelling was made for the Forsmark site /Molinero et al. 2008/ but the results are not site specific and can therefore be applied to conditions at Laxemar. It was shown that a hypothetical contamination event by atmospheric oxygen at repository depth would be consumed in a relatively short period of time (about 1 year) if the maximum amounts of reported pyrite are included in the model. However, the model results have proved to be sensitive to uncertain parameters such as the exact mineralogical composition and the specific reactive surface area of such minerals. An interesting conclusion is that in the base case considered in the model, the oxygen intrusion in a borehole would only affect a very short distance into the bedrock (of about 1 cm). The modelling documented in /Molinero et al. 2008/ supports these conclusions when the oxidising influence from drilling water on the groundwater composition was considered small. This is not unrealistic as the initially introduced drilling waters in Forsmark were not strongly oxidising as attempts to reduce oxidation (e.g. by flushing with nitrogen gas) formed part of the routine procedure during drilling. From another standpoint, the measured downhole redox potential (Eh) values support further the reductive capacity of the groundwater system. For example, in one borehole, after re-installation of the equipment (due to pump failure) the negative redox potential was re-established after 1–7 days indicating that possible oxygen contamination was consumed during this time period /Laaksoharju et al. 2009/.

Temporal and spatial variability

Temporal and spatial variability are important in order to address how well the sampled groundwaters represent the described rock volume.

Temporal variability of the groundwater character has been assessed by: a) comparing the electrical conductivity values measured shortly after drilling with the results obtained during hydraulic logging, b) evaluating open borehole values collected during hydrochemical logging (tube sampling), and c) by studying the time-series data during hydrochemical sampling and during subsequent monitoring /cf. Gimeno et al. 2009, Gurban 2009/. Figure 9-19 illustrates a case in which sections sampled for complete chemical characterisation (CCC) in borehole KLX03 are compared with results from the resistivity logging and tube sampling.

The measurements were conducted during a time period of more than two years (June 2004–November 2006). Most of the samples obtained without pumping plot closer to the electrical conductivity values even though pumping during, for example, the CCC sampling, is at a low flow rate. Exceptions include samples from about 750 m borehole length (–701 m elevation) where some plot close to the electrical conductivity values obtained during pumping. This indicates sampling in, or close to, a transition zone between brackish and saline groundwaters /cf. Smellie et al. 2008, Gurban 2008/. In conclusion, the large amount of data from different measurements and time periods can be used to indicate the temporal variability of the groundwater in the bedrock.

To address the spatial variability, 3D plots can be used to show how the measured samples vary in the 3D bedrock volume. To address the possible groundwater variability between the boreholes, coupled 3D modelling has to be used /Auvé et al. 2006/. In this case, the methodology used combines results from the hydrogeological modelling with a mixing and reaction-path simulation using PHREEQC. This coupling provides the theoretical but detailed compositional character of the groundwaters in a rock volume (constituted by a grid with about one million points) that represents the whole regional area (for details cf. /Gimeno et al. 2008/).

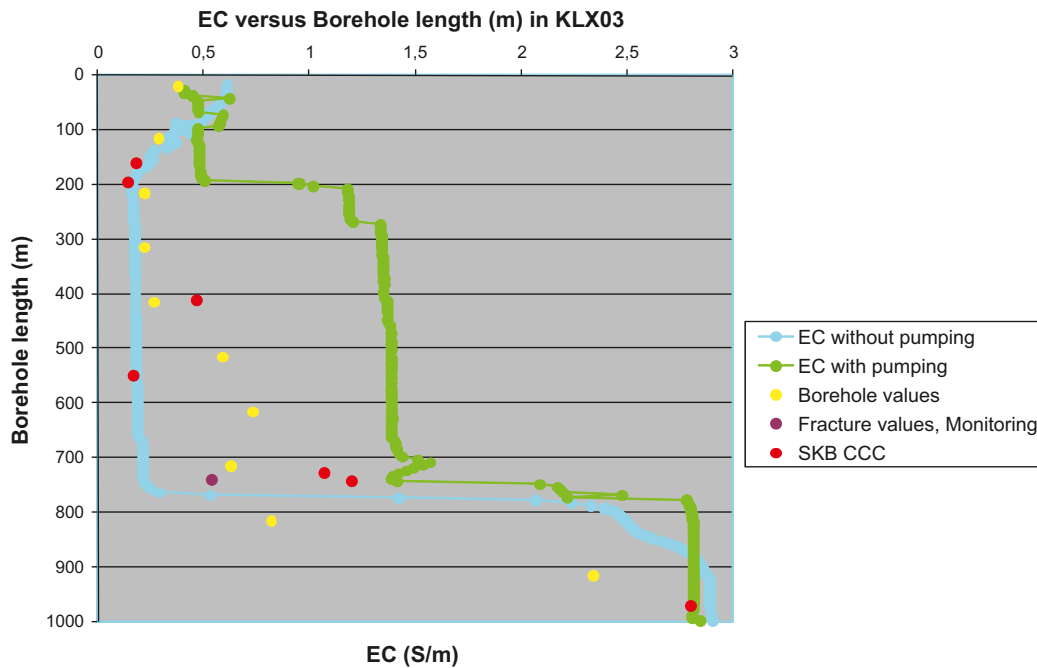


Figure 9-19. Electrical conductivity measurements made during hydraulic logging of the freshly drilled borehole KLX03. The borehole values are compared with the conductivity of the samples taken after the hydraulic logging: 1) in the open borehole tube sampling (yellow dots), 2) with time series (red circles) taken during the complete chemical sampling (CCC) from fractures, and 3) the monitoring sections (brown) taken during the monitoring programme.

9.6 Hydrogeochemical site description

9.6.1 Background

The main aim of the hydrogeochemical site descriptive model is to present an understanding of the site based on measurements and model contributions described in the previous sections. The site descriptive model is a combination of a quantitatively derived hydrogeochemical model (e.g. based on site measurements) and a qualitatively derived hydrogeochemical model (e.g. more descriptive, process-oriented conceptual model). The main objective is to describe the chemical composition and distribution of the groundwater and porewater in the bedrock and the groundwater close to the interface between bedrock and the overburden, and the hydrogeochemical processes involved in its origin and evolution. This description is based primarily on measurements of the groundwater composition, but also incorporates the use of available geological and hydrogeological site descriptive models. The description also serves as the basis for possible hydrogeochemical simulations of the palaeohydrogeochemical evolution of the site and also to predict future changes.

In this section, the Laxemar subarea hydrogeochemical site descriptive model, and its extension to the Simpevarp subarea, is presented together with a concluding summary of the main hydrogeochemical properties and characteristics of the Laxemar-Simpevarp area.

9.6.2 Hydrogeochemical visualisation

Background

The Laxemar subarea 2D visualisation in /Laaksoharju et al. 2009/ is based on the selection of five cross-sections that best represent the integration of geological and hydrogeological understanding, and the available hydrochemical data. Presented below are two of the most illustrative examples which correspond to cross-sections C and D in Figure 8-50 and presented in Figure 9-20 and Figure 9-21, respectively. Note that the legend included in Figure 9-20, describing the different groundwater types, also relates to Figure 9-21.

To provide a more realistic visualisation of groundwaters in a fractured crystalline rock environment (i.e. to avoid giving a porous medium impression to the bedrock), the groundwater types are shown confined to the major water-conducting fractures and deformation zones. The various groundwater types within these zones are colour coded and the transition from one groundwater type to another is indicated as being gradual and diffuse.

The orientation of cross-section C in Figure 9-20 approximates to the west to east regional groundwater flow direction, and it also includes the Simpevarp subarea. This provides the opportunity to visualise changes in groundwater chemistry from recharge conditions to the west to discharge at the coastal margin to the east. Furthermore, this section is closely similar to the corresponding hydrogeological cross-section B used in the hydrogeological modelling, cf. Figure 8-50, therefore allowing direct comparison between simulated (i.e. modelled) and measured values of, for example, Cl and $\delta^{18}\text{O}$.

Groundwaters

In the west and central part of the Laxemar subarea (Figure 9-20, NW-SE part of the cross-section), which exemplifies largely recharge conditions, the upper bedrock (down to about 100–250 m) is characterised by fresh, recharge waters. Some mixed type groundwaters are also present where the fresh waters have been influenced locally by brackish and glacial components and sometimes by a weak marine component derived from residual groundwaters in the overburden. From about 250 m to 900 m depth, brackish groundwaters (200 to 10,000 mg/L Cl) dominate, comprising mixtures of brackish non-marine groundwaters with waters introduced during and after the last deglaciation. Of the latter types, brackish glacial groundwaters of variable distribution and salinity (and referred to as ‘a series of heterogeneous lenses’) are common in the Laxemar subarea, especially in the central, west and northwestern parts. They occur mostly at about 300 to 600 m depth interval, but deeper occurrences are observed in borehole KLX04 down to about 900 m depth and much shallower occurrences above 100 m. These shallow occurrences, together with other examples in the area at depths less than 250 m, may reflect preserved isolated pockets or lenses of glacial-type water in rock volumes of lower hydraulic conductivity. For the ‘anomalous’ deep occurrence in borehole KLX04, it can not be excluded that if some of the other boreholes had been drilled to greater depths (> 1,000 m), they also may have intercepted brackish glacial groundwaters.

In the southeastern parts of the Laxemar subarea, of lower topography and closer to the coast, some of the groundwaters between about 250 to 600 m depth show weak Littorina signatures.

The majority of observations, both hydrochemical and hydrogeological, indicate that at about 600 m there is a change from intermediate to low flow conditions that persist to about 900 m. Within this approximate 600 to 900 m interval, which is dominated by brackish non-marine groundwaters, minor glacial components are observed but these may not necessarily represent the last deglaciation.

The transition from brackish non-marine to saline groundwaters occurs at about 900 m and continues to about 1,200 m. This saline type also appears to include minor glacial components even though chlorine-36 dating supports a very old age for these groundwaters (hundreds of thousands of years, cf. Section 9.5.13). Finally, at about 1,200 m and only observed in borehole KLX02, there is a transition to highly saline groundwaters with very low flow to effectively stagnant conditions where there is no evidence of glacial influence as indicated from stable isotope data.

This described stratification of different groundwaters in Laxemar correlates generally with the hydrogeological depth zones employed in the hydrogeological DFN model (cf. Section 9.3.3 and Section 8.5), i.e. at elevations of 0 to –150 m, –150 to –400 m, –400 to –650 m, and > –650m.

In the Simpevarp subarea (Figure 9-20, W-E part of the cross-section), these general groundwater compositional stages are also evident but appear to occur at shallower depths, i.e. brackish glacial groundwaters at about 100 to 300 m depth, the transition from brackish non-marine to saline groundwaters at about 500 m, and saline to highly saline groundwaters at about 900 to 1,000 m depth. This probably reflects discharge conditions close to the Baltic Sea coastline as supported by the hydrogeological model /Rhén et al. 2009/. Another aspect that differentiates the Simpevarp subarea from the Laxemar subarea is the presence of a stronger Littorina Sea signature in Simpevarp since this area is topographically low, was submerged for a much longer time period by the Littorina Sea, and subsequent flushing has been less efficient and is still on-going.

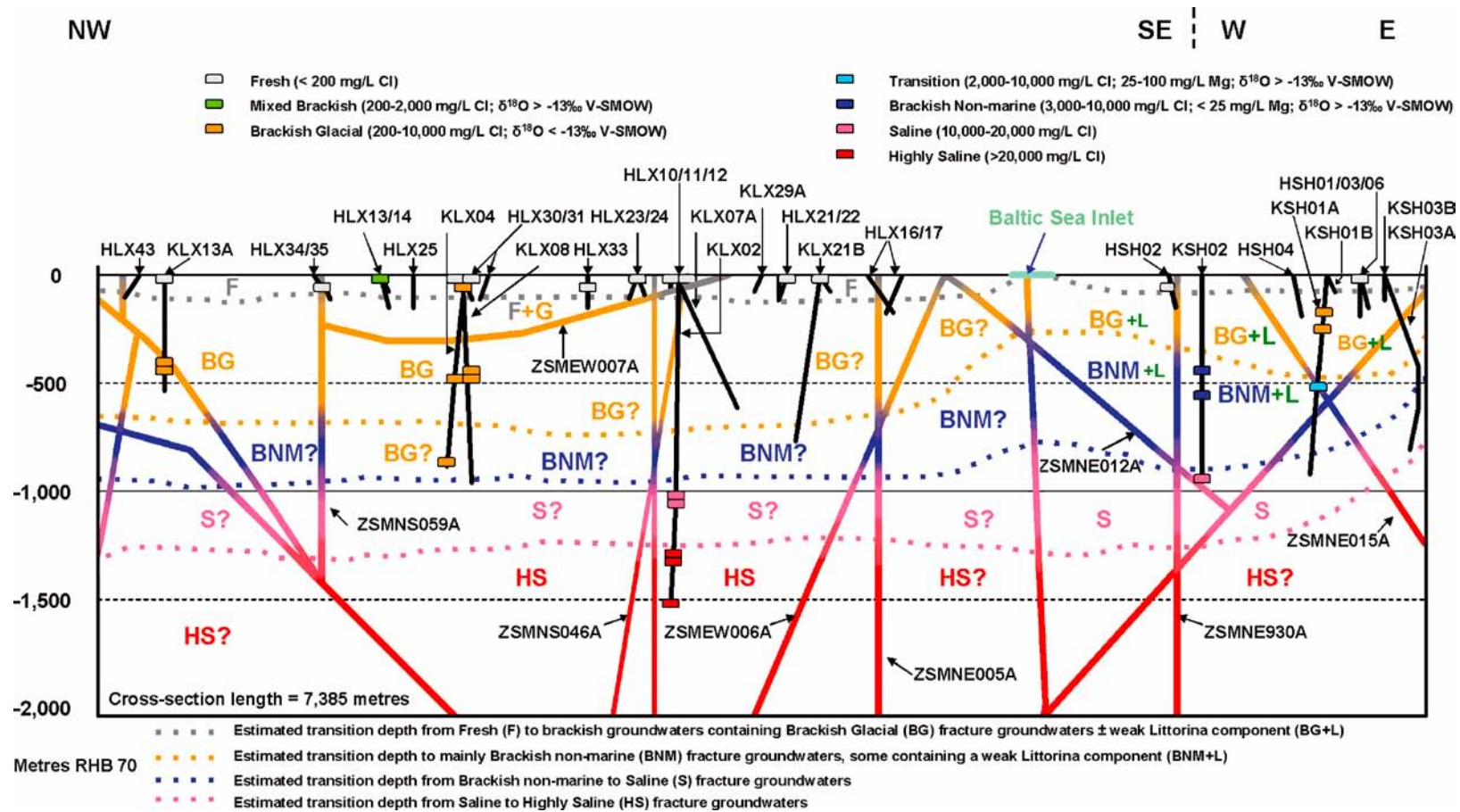


Figure 9-20. Approximately NW-SE/W-E cross-section through the Laxemar-Simpevarp area (cf. cross-section C in Figure 8-50 for location). The visualisation is based on a 0 to -1,100 m RHB 70 vertical scale. Shown are: a) the location of the boreholes and the borehole sections which have undergone hydrogeochemical sampling, b) the main fracture groundwater types (colour coded) which characterise the site, and c) the chloride distribution with depth along the major deformation zones. The dotted lines in different colours represent the approximate depths of penetration of the various fracture groundwater types along hydraulically active deformation zones. The main regional groundwater flow direction is from the west (recharge) to the east (discharge), approximately parallel to the section. (Cross-section length = 7,385 metres).

The location of the brackish glacial groundwaters which characterise the central part of the Laxemar subarea visualised in Figure 9-20 is based on few measured data. The extent of the brackish glacial groundwaters is largely derived from Figure 9-21 (NW-SE part of the cross-section) and an additional cross-section (cf. /Laaksoharju et al. 2009/; cross-section #2 in Section 6.2) which traverses the central and western part of the Laxemar subarea, providing a much better spatial coverage of the groundwater chemistry. Noticeable is the dominance of the brackish glacial groundwaters and their distribution both laterally and vertically.

Figure 9-21 (cross-section D in Figure 8-50) was chosen also to cover the west and southern part of the Laxemar subarea (W-E part of the cross-section), in particular the southeastern part where a weak Littorina component resides in borehole KLX15A (associated with both brackish non-marine and brackish glacial groundwaters denoted by BNM+L/BNM+L and BG+L/BG+L, respectively) and a very weak component in borehole KLX12A (associated with a brackish non-marine groundwater). The increased salinity trend to shallower depths to the east is similar to that shown in Figure 9-20 and represents a groundwater discharge feature towards the Baltic Sea coast in the Simpevarp subarea.

Porewaters

Porewater data are available from three boreholes, KLX03, KLX08 and KLX17A, and are presented and described in Section 9.5.7. Because of limited data, it is not possible to accurately establish the lateral spatial distribution of the porewater chloride compositions, and the vertical distribution is very much influenced by the nearest deformation zone. These porewater data are therefore visualised independently along the three investigated boreholes, two of which (boreholes KLX17A and KLX03) are shown in Figure 9-21. Of importance is that the changes in the chloride content with depth described for the different groundwater types in Section 9.6.1 are qualitatively supported by the porewater data, which in turn are influenced by the decrease in hydraulic conductivity (i.e. decrease in the frequency of open, water-conducting fractures) with depth.

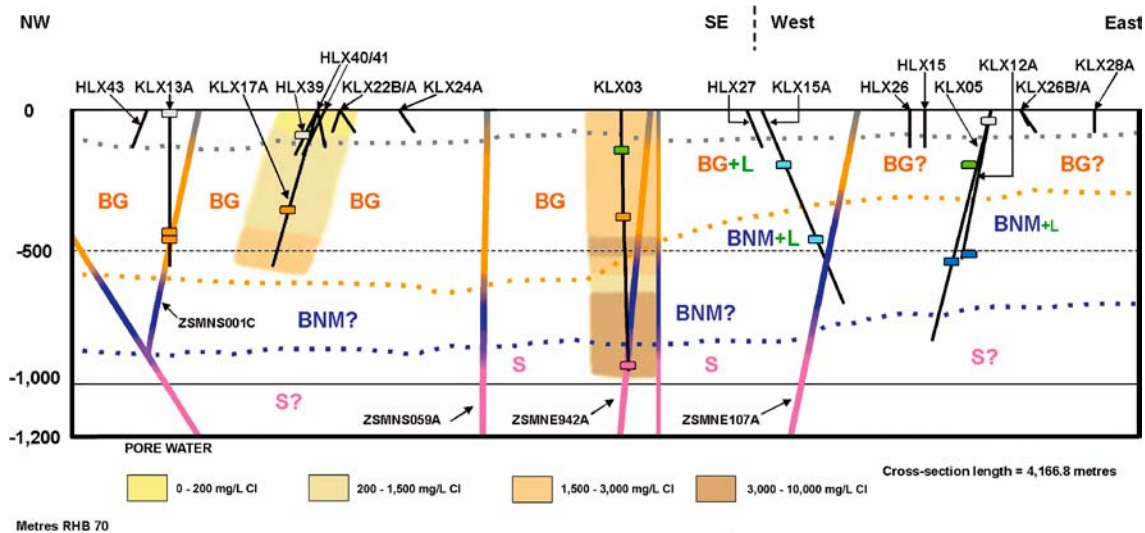


Figure 9-21. Approximately NNW-SSE/W-E cross-section through west central Laxemar to its eastern margin (cf. cross-section D of Figure 8-50 for location). The visualisation is based on a 0 to -1,100 m RHB 70 vertical scale. Shown are: a) the location of the boreholes and the borehole sections which have undergone hydrochemical sampling, b) the main fracture groundwater types (colour coded) which characterise the site, c) the chloride distribution with depth along the major deformation zones, and d) the porewater chloride variation along boreholes KLX17A and KLX03. The dotted lines in different colours represent the approximate depths of penetration of the various fracture groundwater types along hydraulically active deformation zones. The main regional groundwater flow direction is from the west (recharge) to the east (discharge), approximately parallel to the section. (Cross-section length = 4,167 metres).

9.6.3 Summary of hydrogeochemical characteristics

The main characteristics of the Laxemar groundwaters are:

- The 0–20 m depth interval is hydrogeologically active (residence times in the order of years to decades) and dominated by modern recharge meteoric water or Fresh groundwater (< 200 mg/L Cl) of Na-Ca-HCO₃ (SO₄) type showing large variations in pH and redox conditions.
- The 20–250 m depth interval is dominated by Fresh-Mixed Brackish-Brackish Glacial groundwaters of Na-Ca-HCO₃ (SO₄) to Na-Ca-Cl-HCO₃ type, showing a transition to stable reducing conditions with increasing depth. The residence times of the groundwaters are in the order of decades to several thousands of years.
- The 250–600 m depth interval is dominated by Brackish Glacial–Brackish Non-marine–Transition groundwaters of Na-Ca-Cl-(HCO₃) type. Redox conditions are reducing and low Eh values (–245 to –303 mV) are typically controlled by the interplay between the iron and especially the sulphur systems. The significant portions of glacial waters in this depth interval, and the equally significant increase of non-marine groundwaters with depth, indicate that groundwaters older than the last deglaciation at around 14,000 years ago are becoming increasingly important.
- The 600–1,200 m depth interval is dominated by Brackish Non-marine–Saline (± Brackish Glacial and Transition) groundwaters of Na-Ca Cl-(SO₄) to Ca-Na Cl-(SO₄) type. These groundwaters show very low magnesium values and are clearly reducing (–220 to –265 mV). Interpretation of chlorine-36 measurements suggests long residence times of hundreds of thousands of years; this is supported hydrogeologically by low flow to near stagnant conditions.
- The pH values are between 7.2 and 8.6 in the groundwaters and do not show any clear variation trend with depth. It is mainly controlled by calcite dissolution-precipitation reactions and, probably, by microbial activities. Of secondary importance is the influence of other common chemical processes, such as aluminosilicate dissolution-precipitation or cation exchange.

9.7 Consistency with the hydrogeological model

Close integration of hydrogeochemistry and hydrogeology is a necessary prerequisite to achieve site understanding. Hydrogeology requires hydrogeochemical information, for example, salinity distributions, groundwater end-member compositions, and palaeohydrogeochemical input to help constrain initial model conditions. Hydrogeology, on the other hand, can provide the groundwater flow description related to the hydraulically constrained geological framework so that the spatial distribution of hydrochemical signatures (laterally and vertically) can be interpreted and visualised. In the SDM-Site Laxemar site descriptive modelling, the following steps have helped the interaction between hydrogeochemistry and hydrogeology.

1. **Palaeo-conceptual model** construction for the site based on available Quaternary geological information. The model was used to set the boundary conditions for the hydrogeochemical and hydrogeological modelling.
2. **Parameter values and modelling results** such as major ions and isotopes and M3 mixing proportions were delivered to the hydrogeologists and used for flow model calibrations and comparisons.
3. **Collaboration** in the form of regular discussions focused on modelled output of boundary conditions and their relevance to the conceptual site modelling, and to the development of the palaeohydrogeological and palaeohydrogeochemical conceptual models.
4. The **Hydrogeochemical site descriptive model** is based on a common nomenclature of groundwater types and understanding of groundwater flow established through discussion and interaction.
5. **Comparison** – the output from the hydrogeological modelling was compared with measured hydrogeochemical parameters such as Cl, ¹⁸O, mixing proportions of the different water types calculated using the M3 code and with the overall general hydrogeochemical understanding concerning the origin, residence times and penetration depths and occurrences of the different water types in the bedrock.

Interaction and integration between hydrogeochemistry and hydrogeology has been a common goal since the initiation of the site investigation programme in Laxemar. Important at this early stage was the use of a generalised palaeo-conceptual site model by the two disciplines which essentially was shared (Section 9.3.4). As investigations progressed, hydrogeochemistry provided some insight into the present and past evolution of the different groundwater types within the approximate 0–1,000 m bedrock interval sampled in Laxemar. In turn, these observations provided an important platform for interaction with the hydrogeological modelling programme (cf. Chapter 8 and /Rhén and Hartley 2009, Laaksoharju et al. 2009/). From a hydrogeochemical perspective, the present hydrogeochemical site descriptive model sections shown in Figures 9-20 and 9-21 are the result of close interaction with hydrogeology, where input concerning confirmation of flow directions, flow properties and possibilities to maintain different water types in the bedrock has been of great importance in supporting the modelling results. Quantitative agreement between the models was achieved by comparisons between predicted and measured groundwater constituents as discussed in Chapter 8 and in /Rhén et al. 2009, Laaksoharju et al. 2009/.

Coupled modelling of groundwater flow and reactive solute transport was applied to quantitatively integrate hydrogeological and hydrochemical understanding /Molinero et al. 2009/. Exemplifying the Laxemar hydrochemical data, Figure 9-22 shows the comparison between: 1) computed results from conservative transport simulations, and 2) computed results of reactive transport simulations and measured values of pH and HCO_3^- concentrations. The results suggest that these two variables can be regarded as reactive indicators of the groundwater processes. Figure 9-22 is a qualitative illustration of the ability of coupled reactive transport numerical models to reproduce the hydrochemical behaviour of the groundwater system. The modelling takes into account matrix diffusion effects and the predictions of hydrochemically conservative elements such as Cl and $\delta^{18}\text{O}$ are in good agreement /Molinero et al. 2009/.

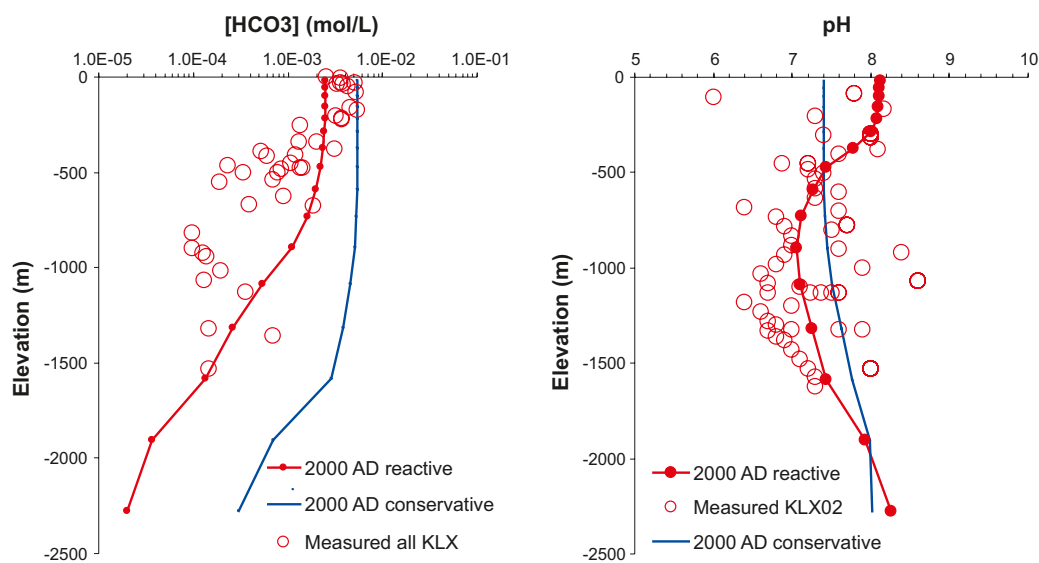


Figure 9-22. Computed and measured concentrations of HCO_3^- (left) and pH (right) along a vertical profile located in the middle of the model domain. Computed results of a conservative transport run (blue) and a reactive transport run (red) are plotted to evaluate the influence of the geochemical processes on the dissolved concentrations. This modelling is based on the Laxemar 1.2 hydrogeological flow model version.

9.8 Confidence and uncertainty in the integrated hydrogeochemical model

An assessment of the confidence and remaining uncertainties in the geochemical model /Laaksoharju et al. 2009/ has revealed that confidence in the understanding and description of the current spatial distribution of groundwater composition generally is high. Furthermore, the uncertainties in the processes affecting the current water composition at the sampled locations are generally sufficiently bounded, whereas there are larger uncertainties as to whether the process understanding is sufficient for predicting the groundwater composition during a future glaciation.

The upper approximately 150 to 200 m of bedrock comprising a mixture of young recharging groundwaters are fairly well characterised with corresponding low uncertainties. At greater depths (particularly to about 500 m depth) the main uncertainties are associated with low quality hydrochemical data (e.g. short-circuiting problems) and a spatial lack of hydrochemical data, both laterally (particularly in the case of the porewater), and at depths greater than 700 m (particularly in the case of the fracture groundwater), such that a large degree of expert judgement has been used to extrapolate the hydrochemistry. However, these uncertainties were reduced with the realisation that at depths greater than about 700 m, the fracture groundwater and porewater chemistries increase fairly uniformly in salinity and laterally appear to be quite homogeneous.

9.8.1 Current groundwater evolution and composition

The main processes determining the overall geochemical evolution of the Laxemar-Simpevarp area groundwater systems are mixing and reaction processes. Mixing has taken place between different types of waters (end members) over time, making the discrimination of the main influences complex. In addition to mixing processes and the effects of their superimpositions, different chemical reactions have taken place in the system due to the interaction between groundwaters, minerals and/or microbial activity (e.g. aluminosilicate and carbonate dissolution/precipitation, cation exchange, gypsum dissolution, main redox reactions, etc). Some elements (Cl and/or $\delta^{18}\text{O}$) behave conservatively in groundwater, whilst others are affected by chemical reactions to differing degrees, especially the redox sensitive elements.

The overburden (near surface/shallow system down to about 250 m depth) is dominated by water-rock interactions between the recharging meteoric water and the soil, till sediments and bedrock. Weathering and potential calcite dissolution under acidic conditions in the near-surface bedrock environment is promoted and controlled by biogenic input of carbon dioxide. This gives rise to pH values usually above 7, calcium concentrations mostly between 50 and 200 mg/L, and bicarbonate concentrations up to 600 mg/L in the near surface waters (down to about 20 m depth). Concentrations then decrease to very low values at great depths. However, bicarbonate locally reaches values up to 100 to 200 mg/L in some of the brackish glacial groundwaters hosted in the upper approximate 500 m.

In the intermediate to deep bedrock system (250–1,200 m depth), groundwater mixing processes usually dominate and the effects of reactions between the groundwaters and the minerals in the fracture fillings are superimposed on mixing signatures. There are traces of downward advective movement of groundwater to maximum depths of about 1,200 m. Below this depth, low flow and near stagnant conditions prevail and solute transport is increasingly diffusion controlled.

It is envisaged that prior to the latest glaciation, there existed a concentration profile extending from dilute meteoric waters in the near surface of the bedrock to highly saline, brine-type compositions at about 1,000 m depth and deeper. These highly saline groundwaters, as today, indicate high contents of chloride, calcium, sodium, potassium and sulphate, low values of magnesium and bicarbonate, a more or less constant Ca/Sr ratio, and enriched oxygen-18 signatures. Then, with the onset of the latest glaciation/deglaciation, the input of dilute waters (meteoric or glacial meltwaters) over time modified the pre-existing concentration profile from the surface to depth. The cold climate signature depleted the oxygen-18 signature and waters with low p_{CO_2} and high pH values entered the system. These different mixtures promoted calcite precipitation and cation exchange due to dilution, i.e. lead to a decrease of calcium and increase of sodium in the groundwaters.

The next major event is the input of a marine component (Littorina Sea) into the bedrock following several diagenetic processes during its passage through marine sediments. This water then passed into the bedrock down to different depths depending on the coastal proximity (more in Simpevarp and Äspö than in Laxemar), on the rock hydraulic properties, and on the salinity of the pre-existing groundwaters (i.e. glacial to brackish glacial waters with depleted oxygen-18 signatures). Eventually, the higher density of these Littorina waters displaced the previous dilute waters and the result was groundwaters more enriched in oxygen-18, magnesium, sulphate, bicarbonate and silica. Calcite will have precipitated and the cation exchange will have produced the decrease of sodium and the increase of calcium in the waters. Finally, the continuous input of meteoric waters will have produced a superimposed dilution profile which is more marked in the recharge areas such as in Laxemar.

Modelled groundwater mineral equilibrium features are supported by mineralogical and microbial observations. The pH buffering capacity in Laxemar at depths greater than about 100 m appears to be controlled by the carbonate system, and modelling indicates that this water is in equilibrium with calcite.

According to data analyses and modelling of the redox system, reducing conditions currently prevail at depths greater than about 20 m. Most of the Eh values determined in the Laxemar subarea are in the brackish glacial groundwaters at depths between about 00 and 700 m. The iron and the sulphur systems are very important for the control of redox processes in the Laxemar-Simpevarp area groundwaters. Iron (II) and (III) minerals are widely distributed in the studied systems and the presence of IRB has been documented. However, the bioenergetic calculations and the redox modelling approach performed from a partial equilibrium assumption for iron reduction and sulphate reduction processes indicate that sulphate reduction is the thermodynamically favoured process.

All the data indicate that the system has retained a significant reducing capacity to the present day. The key role played by SRB in the stabilisation of these reducing conditions is supported by several lines of evidence, including the microbially influenced $\delta^{34}\text{S}$ values found in pyrites from the Laxemar-Simpevarp area at shallow to intermediate depths, and the low $\delta^{13}\text{C}$ values found in calcites from fracture fillings from the same area. The importance of SRB at great depths (> about 700 m) in the Laxemar subarea remains unclear.

9.8.2 Overall confidence

The following aspects of the hydrogeochemical model are associated with the highest confidence:

- The origin, major end members and major processes affecting the present water composition at the sampled locations.
- Current spatial distribution of groundwater types in the context of the controlling processes at the site, even if the heterogeneity of the flow system makes it difficult to predict with confidence the precise distribution in the absence of confirmatory measurements.
- Existence of a redox transition zone detected in the fracture minerals.

The main reasons for this confidence are the many consistent time and spatial data to support the description concerning the origin, most of the major end members and major processes. Integration with hydrogeology supports the palaeohydrogeological description of the site. Various considerations such as reactive modelling, interpretation of different isotope ratios (Sr, S, C) buffer capacity measurements (Eh, pH) and microbial data support the process understanding.

The following aspects are associated with the lowest confidence:

- Understanding of measured levels of sulphide and ability to predict sulphide production.
- Undisturbed detailed groundwater composition at repository depth.
- Buffer capacity regarding Ca and Mg content under dynamic flow conditions.
- Detailed spatial variability and groundwater types associated with different rock domains. The results indicate poor correlation, possibly due to too few samples. The description is focussing on divisions into groundwater types.

The implications of these uncertainties need to be assessed in subsequent safety analysis within SR-Site.

10 Bedrock transport properties

The main objective of the investigations and modelling of the bedrock transport properties is to present a detailed description of site-specific transport conditions that can be used to support the selection of processes and parameters in models developed by safety assessment and others for radionuclide transport and for predicting future groundwater composition. In addition, the results of the transport properties modelling are used as qualitative and/or quantitative input to transport modelling within the site descriptive hydrogeological and hydrogeochemical modelling. This chapter contains a summary of the transport properties site descriptive model, which is presented in detail by /Crawford and Sidborn 2009/.

10.1 State of knowledge at previous model version

The present site descriptive model for transport properties for the Laxemar subarea has undergone major revisions since version Laxemar1.2 /SKB 2006a/, and model stage 2.1 /SKB 2006c/. Earlier versions were in part hampered by the lack of site-specific data from laboratory measurement for, in particular, sorption properties and effective diffusivities measured by through-diffusion. The earlier focus on the Simpevarp subarea /SKB 2004a, 2005a/ also meant that much of the earlier sampling was directed towards boreholes drilled on the Simpevarp peninsula. Since the rock types found in the Simpevarp subarea are geochemically similar to those in Laxemar, material properties data from both subareas are now pooled together in the SDM-Site Laxemar site descriptive model. This is necessitated by the fact that a large number of samples used in the laboratory programme were obtained from the earlier Simpevarp boreholes and to neglect such data would considerably weaken the statistical basis for the recommendation of material properties for specific rock types (principally this affects the fine-grained dioritoid rock type 501030). Hydrogeological properties of different parts of the focused area were also less well characterised in previous versions, which limited the possibilities of making well-supported estimations of flow-related transport properties. The maturation of the geological, hydrogeological and hydrogeochemical site understanding throughout the different model versions has been instrumental in shaping the current conceptual understanding of site-specific transport processes.

It should be noted that throughout the various model iterations, the focus has been upon the development of a retardation model based upon rock types as outlined in the methodology report /Widestrand et al. 2003/, rather than a description based upon geological rock-, fracture-, or hydrogeological rock domains. Also, the parameterisation of different fractures types is related to the presence or absence of specific secondary minerals lining the fracture surfaces and there is no strict modelling demarcation between fractures resident in the HRD and those in the HCD. Deformation zones are posited to consist of a subpopulation of fractures corresponding to the above, although with additional structures referred to as deformation zone sub-elements in the retardation model.

10.2 Evaluation of primary data

The different methods used in the laboratory programme for establishing material retention properties are described in /Widestrand et al. 2003/. The primary data evaluation for the retardation model is presented in detail in /Selnert et al. 2009/ and are summarised in /Crawford and Sidborn 2009/. The flow-related transport properties evaluation including a full account of primary data evaluation is also given in /Crawford and Sidborn 2009/. The following subsections give only a brief overview of the primary data evaluation and the reader is directed to the relevant reference reports for more detailed review and explanations.

10.2.1 Data and models from other disciplines

/Selnert et al. 2009/ have summarised and evaluated data and descriptions from geology, hydrogeology and hydrogeochemistry with the aim of identifying and describing relevant materials and conditions for bedrock transport analyses. The corresponding evaluations in previous model versions guided the sample selection and focus of much of the laboratory investigations which are reported in the current model version. A great deal of supporting information was assembled from the geology site descriptive modelling /Wahlgren et al. 2008/ to aid in the creation of a retardation model that encompasses relevant rock and alteration types, as well as key fracture classes and deformation zones found in the focused area. Information from hydrogeochemistry was used in the selection of five synthetic water types for use in laboratory sorption studies to reflect the range of evolving groundwater conditions expected during the lifespan of the possible repository.

Information and models provided by hydrogeology were used in the construction of a conceptual transport pathway model described in detail in /Crawford and Sidborn 2009/. The input consisted primarily of hydrogeological DFN model parameters as well as model parameters describing deformation zone hydrogeological properties. The hydrogeological models were then used to make quantitative estimates of flow-related transport properties and advective travel times for transport from a hypothetical repository.

10.2.2 Transport data

Transport data obtained from the laboratory programme include effective diffusivities for solute transport in the rock matrix, matrix porosities, the specific surface area of internal micro-surfaces, cation exchange capacities (CEC), and radionuclide specific sorption properties of rock in contact with synthetic groundwater of varying composition.

The effective diffusivity is quantified through the formation factor, F_f , which is the ratio of effective diffusivity to the free diffusivity of a solute at infinite dilution in water ($F_f = D_e/D_w$). The formation factor is, by definition, a purely geometric entity that depends on the porosity, tortuosity, and constrictivity of the porous space available for solute diffusion within the rock. Formation factors are obtained by through-diffusion experiments in the laboratory using a tritiated water tracer as well as by *in situ* and laboratory electrical resistivity measurements. On the order of 36,000 *in situ* measurements of effective diffusivity obtained from high spatial resolution geophysical logging in the site investigation boreholes are reported in the Sicada database. From the laboratory programme there are 42 resistivity-based formation factor measurements and 90 through-diffusion measurements available.

Rock matrix porosity data consist of 333 measurements based on a gravimetric water re-saturation technique used to quantify site-scale variation and 3 measurements using PMMA-resin (polymethylmethacrylate) impregnation for the study of heterogeneous porosity distributions in individual samples of specific rock types.

The surface area of the rock matrix porosity was measured by means of the BET-measurement technique. In all, 197 measurements of surface area were made using crushed rock samples and 6 measurements using intact core pieces.

Sorption properties of rock samples were measured using a batch measurement technique for 2 different crushed rock size fractions, different solutes representing a range of sorption chemistries, and up to 5 different synthetic groundwater types (a total of 263 individual measurements for matrix rock, 85 measurements for fracture filling materials, and 88 measurements for deformation zone materials). Batch sorption measurements were also performed on 6 whole core pieces and 85 samples of scraped fracture coatings. Cation exchange capacities (CEC) were measured for 9 different crushed matrix rock samples, 1 deformation zone sample, and 5 fracture coatings sampled by scraping.

All data obtained from the transport properties laboratory programme are reported in the Sicada database and are described in detail by /Selnert et al. 2009/. A summary of the data is also given in /Crawford and Sidborn 2009/.

10.3 Conceptual model

In the event of canister failure, radionuclides may escape and migrate to the surrounding rock through the bentonite buffer and/or backfilling material surrounding the canister emplacement. The radionuclides may then be transported into fractures intersecting the deposition hole, into the disturbed zone around the excavated volume, and into fractures intersecting the tunnels.

Radionuclides that reach the rock volume are transported by the groundwater flowing in fractures within the rock. In low porosity crystalline rock, all long-range transport is expected to occur by way of channelised advective flow hosted in fractures and other connected conductive structures (e.g. flow channelling within variable aperture fractures, enlarged fracture intersections, within fault step-overs, crush zones, etc). For the description of transport properties, the rock matrix is considered to comprise the host rock minerals as well as all grain boundary pores and micro-fractures that contribute to diffusive and sorptive retention properties. The definition of the rock matrix excludes features with advective flows as well as diffusive open fractures of sufficient size to be included in the hydrogeological DFN model (Section 8.5.2).

Owing to the low permeability of the rock, the water residing in the porosity of the rock matrix is considered to be immobile, and long-range transport through the rock mass itself can be neglected over the timescales relevant for safety analysis. Radionuclides may be transported by advective pathways through the fractured rock until they reach the near surface bedrock where additional transport processes and pathways in unconsolidated Quaternary geologic materials and surface aquatic systems are considered (see Chapter 4). It is thought that radionuclides will principally be transported via a sequence of pathways featuring successively increasing flow in the stochastically modelled background fractures and minor deformation zones within the defined hydraulic rock domains until they encounter flow paths in the large, deterministically defined deformation zones from where they may be transported to the near surface. Implicit in this conceptual model is the conjecture of transport in a dual porosity system where there is a clear demarcation between advective and diffusive domains. This is a modelling simplification. In reality, a hierarchy of spatial scales exists for transport within the bedrock, which results in a continuum of behaviour spanning the different size realms from the largest fractures to the smallest pore spaces.

There are a number of processes that act to retard the transport of solutes in such a way that they are transported at a slower rate than the groundwater within which they are carried. Certain nuclides may sorb on the surfaces of the fractures through which they are transported. From the fractures they may also migrate into pore spaces within the rock matrix by molecular diffusion. As flow is commonly channelised, there may be regions of effectively stagnant water within the fractures into which nuclides can migrate by molecular diffusion and then subsequently migrate into the rock matrix. The interior of the rock matrix contains stagnant “porewater” in which the radionuclides can be sequestered in aqueous form, and micro-surfaces upon which they can sorb. A key parameter governing the extent of matrix interaction and consequently transport retardation is the flow-wetted surface to flow ratio, or F-factor.

A schematic illustration of a possible transport flow path is depicted in Figure 10-1 for a stochastic fracture typical of the different hydraulic rock domains in Laxemar. Such fractures generally feature a thin fracture coating of secondary mineralisation and possibly an alteration rim of limited thickness.

Nine different fracture types have been identified in Laxemar. These differ only in the types of secondary minerals present in the fracture coating and the estimated thickness of the alteration rim. The classification is based partly on the different geochronological epochs of alteration that are thought to have occurred at the site, and partly on the potential for the different secondary minerals to influence transport processes. By far the most commonly occurring fracture mineral in open fractures is calcite, often found in combination with chlorite and various clay minerals, cf. Section 9.5.6. Pyrite, hematite, and epidote are also relatively common although not nearly to the same extent.

In principal, the systems of fractures found within deformation zones are conceptualised to be similar to the singular fractures found in the hydraulic rock domains, although with added micro-structural complexity and with different proportions of type-fractures. Fractures within the larger deterministic deformation zones are considered to have layers of hydrothermal and tectonic alteration that extend from the fracture surface to some distance into the host rock. In some cases,

the rock between successive fractures is completely altered leaving no intervening fresh rock at all. In some fractures, there may also be large amounts of particulate infilling materials (fault gouge) and breccia pieces, cf. Figure 10-1. During the evolution of the bedrock, the fractures may have been sealed by secondary mineral precipitates and reactivated in different cycles. Therefore, the fracture coatings are not necessarily distributed evenly on both surfaces of the fracture.

The rock matrix porosity consists of micro-fractures and grain boundary pores. Micro-fracturing is most intense at fracture surfaces and has a tendency to decrease with distance into the undisturbed rock matrix. The porosity near fracture surfaces is frequently dominated by micro-fracturing. The undisturbed matrix porosity, on the other hand, is often dominated by grain-boundary pores and is pervasively distributed throughout the rock mass. That the matrix porosity is well-connected over significant distances is supported by a considerable body of evidence that includes palaeo-hydrogeochemical signatures of relict diffusive exchange with flowing groundwater (cf. Section 9.5.7 and /Laaksoharju et al. 2009/), *in situ* measurements of site-specific formation factors /Crawford and Sidborn 2009/, as well as other supporting laboratory and *in situ* experiments /Löfgren et al. 2007/.

Sorption can take place on the external fracture surfaces in contact with flowing water or within the micro-porous structure of the rock matrix. Since the diffusion-accessible mineral surface area within the rock matrix can be orders of magnitude greater than that of the external fracture surfaces in contact with flowing water, the sorption of radionuclides can give an enormously increased retardation effect over that of matrix diffusion alone. Owing to alteration processes, the pore spaces immediately adjacent to fracture surfaces often feature considerably larger sorptive surface area than the more deeply lying rock and this can give rise to a strong increase in sorptivity at the fracture surface. This is supported by measurements of BET-surface areas /Brunauer et al. 1938/ of site-specific fracture coatings and altered materials.

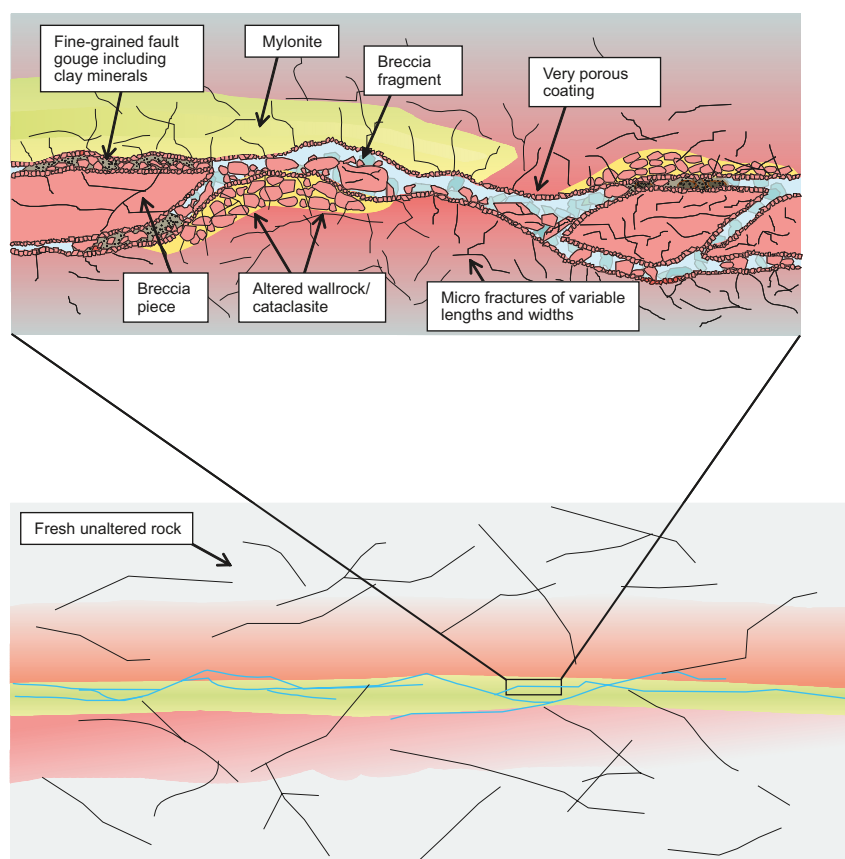


Figure 10-1. Schematic illustration of a transport path in cross-section. The pathway is characteristic of a typical fracture possibly hosted in a minor deformation zone. The fracture is filled with a discontinuous coating of secondary minerals in addition to particulate infill material and breccia fragments. Based on a conceptual model taken from /Andersson et al. 2002b/.

Transported radionuclides are usually in the form of ionic, charged species and will tend to associate with mineral surfaces that possess a net charge of opposite sign. In the present context this is what is referred to as a sorption process. Such interactions are well described in the scientific literature /e.g. Stumm and Morgan 1996/ and the most important mechanisms for this interaction are thought to be ion-exchange and surface complexation. The surface charge of minerals is usually described as having a *permanent* component which is independent of groundwater composition, and a *variable* component which changes with the groundwater composition, e.g. /Langmuir 1997/. The variable component of the surface charge arises due to surface functional groups which are basically oxide groups that can be protonated and deprotonated with the consequence that the variable surface charge is sensitive to the pH of the contacting groundwater. From the surface chemistry literature, e.g. /Stumm and Morgan 1996/, it is known that most of the minerals that comprise granitic rock will have a net negative surface charge at all reasonable groundwater pH values.

Solutes that sorb by a surface complexation mechanism can form covalent bonds with the reactive surface groups, whereas solutes that sorb by way of ion-exchange associate with permanently charged sites in a purely electrostatic interaction. Different ion-exchanging solutes have different hydrated charge densities and therefore can associate more or less closely with these charged sites thereby giving rise to different affinities for association amongst different solution components. Ion exchange in the context of solute transport in geologic media refers to the tendency of certain cations to replace others that are bound to permanently charged sites at the mineral surface due to these differences in sorption affinity.

In many cases, the sorbed solutes cannot completely balance the total surface charge and therefore other cations in solution are attracted towards the surface. At some distance, the more closely bound cations shield the residual charge of the surface from less closely bound cations to such an extent that only the potential gradient normal to the surface limits the movement of the less closely bound cations. For these cations, transport parallel to the surface is relatively unhindered whereas movement normal to the surface is restricted by electrostatic forces. The volume these cations occupy is referred to as the diffuse double layer or electrical double layer (EDL) /Stumm and Morgan 1996/. The physical extent of the EDL varies as a function of ionic strength in the groundwater which can have consequences for the mobility of ionic solutes in very dilute groundwater and narrow pore spaces. Potential effects are so-called anion exclusion and EDL-mediated surface diffusion. These are described and accounted for in safety assessment as transport model variants.

In the safety assessment framework, that provides the basis for identification of the retention parameters in the site descriptive model for transport, retention of radionuclides is assumed to be caused primarily by diffusion and sorption. For modelling purposes, these are assumed to be reversible linear processes. Transport retardation of solutes by matrix diffusion is modelled as a homogeneous Fickian process characterised by an effective diffusivity, D_e , and sorption is modelled using a constant partitioning ratio, K_d , which is a function of groundwater chemistry and rock type. Together with the rock matrix porosity, θ_m , the diffusion and sorption parameters can be combined to describe the solute retention properties of the rock matrix.

The use of a Fickian model for solute diffusion in combination with a linear model of sorption (as implied by the K_d concept) are modelling simplifications of what is in reality a complex, coupled reactive transport process. However, there is a broad scientific consensus that the use of these modelling simplifications is adequate for the goals of safety assessment, provided that appropriate parameter values are selected for the prevailing conditions, e.g. /NEA 1999/. More details concerning the overall modelling approach and justification of modelling assumptions (including caveats on the use of the K_d concept) can be found in /Crawford and Sidborn 2009/.

Generally, these simplifications are justified on the basis that the transported radionuclides are considered to be extremely dilute, trace components within the groundwater. The mechanisms by which radionuclides are postulated to interact with the rock matrix (i.e. diffusion and sorption) are also applicable to the transport of other solutes dissolved in the groundwater and are considered to be part of the suite of chemical reactive processes that affect groundwater composition.

10.4 Transport properties of the bedrock

10.4.1 Overview of rock domains and fracture domains

For the site descriptive modelling of bedrock transport properties, attention is focused on the rock domains RSMA01, RSMD01, and RSMM01, as these are volumetrically the most significant domains both in the local model volume and the focused volume.

A full account of the proportions of different rock types and classes of alteration can be found both in Section 5.2.3. For the purposes of parameterising the material properties of the rock, however, it can be stated that the rock in RSMA01 is dominated by Ävrö granite, whereas the major rock type in RSMD01 is an equigranular, medium-grained quartz monzodiorite, and that in RSMM01 is Ävrö quartz monzodiorite.

Slightly more than 50% of the fractures mapped in boreholes KLX02-KLX29A (excluding KLX27A) are sealed. There is a greater intensity of open and partly open fractures in the upper part of the bedrock, but this decreases with increasing depth. Based on detailed studies of fracture mineralogy and wall rock alteration /Drake and Tullborg 2009a/ (summarised in Section 9.5.6), /Eklund and Mattsson 2008/, the most common fracture minerals in Laxemar are calcite and chlorite mostly found in combination and frequently together with other minerals.

Calcite is present in 78% of the mapped sealed fractures and in 48% of the mapped open fractures, while chlorite is present in 76% of the open fractures and in 33% of the sealed fractures. Calcite generally covers on the order of 10–20% of the fracture surface and only rarely the whole fracture surface. Chlorite, on the other hand, usually covers the whole fracture surface, but is also usually overlain by other fracture minerals, most typically calcite.

Clay minerals occur in roughly 34% of the mapped open fractures although only about 2% of sealed fractures. However, according to /Drake and Tullborg 2009a/ the clay mineral content is probably underestimated since most mapped chlorite bearing fractures also contain clay, while hematite is overrepresented due to its propensity to discolour or stain other minerals such as chlorite and feldspar. Hematite is present in about 14% of the open fractures. Water conducting fractures are frequently characterised by non-cohesive and clayish fracture coatings and contain fine grained filling materials (i.e. fault gouge).

Red-stained, hydrothermally altered rock is a common feature adjacent to fractures in the Laxemar area. Almost 50% of the sealed fractures in the Laxemar subarea are bordered by red-stained wall rock. Red-stained rock is commonly thought to represent a distinct zone of altered, oxidised rock although detailed analyses are not routinely performed. The hydrothermal alteration frequently reaches further into the rock from the fracture surface than is directly evident from the red-staining, as can often be seen from biotite and plagioclase alteration. This is described in more detail in /Selnert et al. 2009/.

Based on the characterisation of different fracture mineralisations and theoretical potential for influencing transport properties, nine major fracture types have been identified. These are summarised in Table 10-1.

Table 10-1. Classification of basic fracture types within retardation model. Fracture mineral abbreviations in bold text are dominant for the given fracture class.

Type	Fracture coating	Thickness	Wall rock alteration
A	Chl+Ca ± Py/CPy ± Other	0.2–1 mm	≤ 10 mm
B	Ep ± Pr ± Ad ± Chl ± Ca ± Qz	0.5–1 mm	≤ 20 mm
C	Hm ± Other	0.5–5 mm	≤ 50 mm
D	Lau ± Ca ± Chl	0.2–2 mm	≤ 20 mm
E	Chl + Ca	0.2–0.5 mm	≤ 10 mm (oxidation and saussuritisation)
F	Clay ± other	0.2–5 mm	≤ 50 mm
G	Chl ± other	~ 0.2 mm	≤ 50 mm
H	No mineral	n/a	≤ 10 mm (oxidation, saussuritisation, and epidotisation)
I	Ca ± other	~ 0.2 mm	≤ 10 mm

Note: fracture mineral abbreviations are: Adularia (Ad), calcite (Ca), chlorite (Chl), chalcopyrite (Cpy), epidote (Ep), hematite (Hm), laumontite (Lau), prehnite (Pr), pyrite (Py), quartz (Qz).

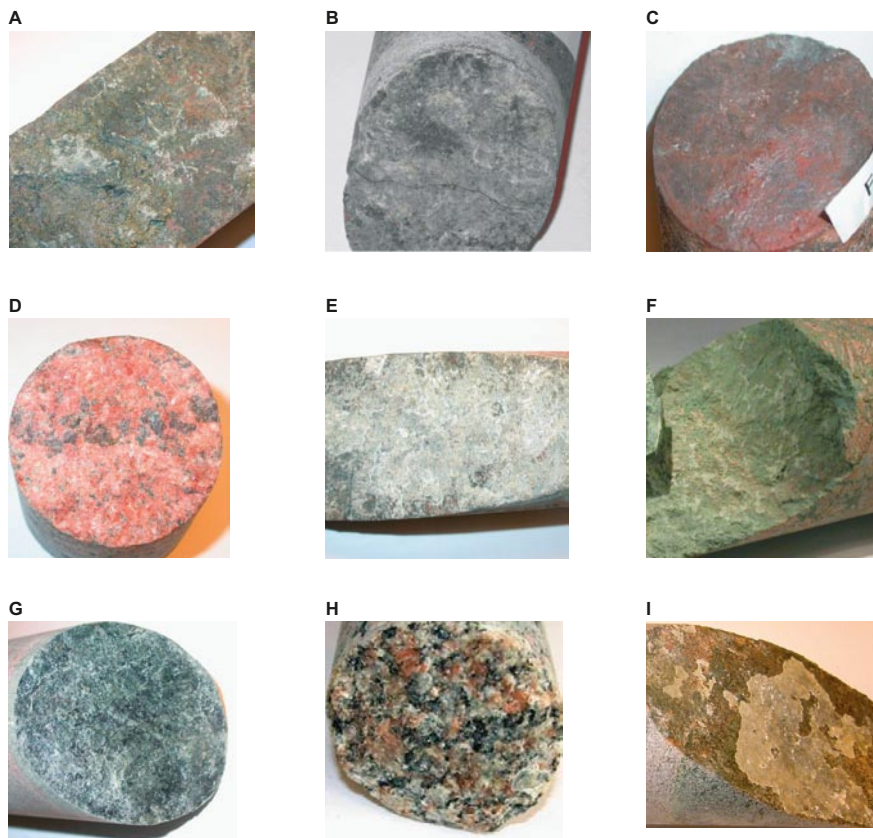


Figure 10-2. Typical appearance of the surface coating minerals associated with the basic fracture types considered in the retardation model. The predominant mineralogy of the different fracture types is described in Table 10-1.

Some typical examples of the appearance of some of these fractures can be seen in Figure 10-2 and the relative abundance of the different fracture types as a function of depth in Laxemar is shown in Figure 10-3.

For the retardation model five additional, recurring structural elements have been identified as being characteristic of deformation zones. These are distinct from the single fracture classes described above which also populate the deformation zones. These structural elements are described in Table 10-2.

Synthesis of a generalised model for deformation zones is difficult owing to their complexity and spatial variability. This is further complicated by the fact that their structure is usually only known through interpretation of a small number of one-dimensional borehole intercepts. Much of the complexity of deformation zones arises through cycles of reactivation during different geological events. They therefore display a wide spectrum of alteration types, brittle and ductile features formed at different stages of their geological history.

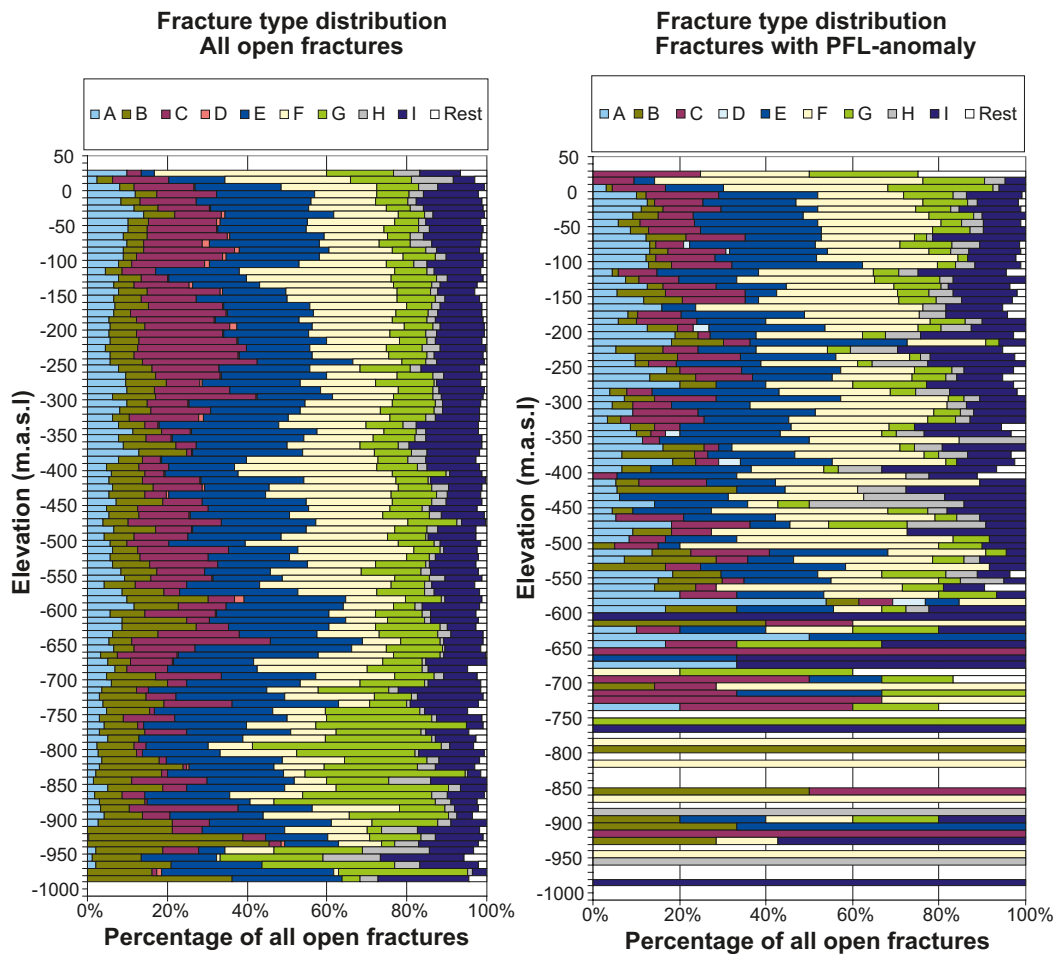


Figure 10-3. Relative abundance of different fracture types at different depths in Laxemar. (Left) data for open fractures, (Right) data for fractures associated with flowing features (identified by PFL-f). The apparent change of fracture mineralogy below 700 m reflects the scarcity of data available at this depth rather than a systematic change in mineral distribution.

Table 10-2. Main identified structural elements residing in deformation zones that have been included in the retardation model.

- 1) **Fault rock/gouge (strongly tectonised and partly incohesive material).**
Generally, altered rock fragment, mineralogy partially depending on host rock together with chlorite, saussurite and clay.
- 2) **Chlorite (green gouge, primarily close to mafic rock types).**
Chlorite ± corrensite.



- 3) **Porous episyenitic wall rock.**
Prehnite, adularia, quartz, calcite \pm laumontite, epidote, hematite. Quartz dissolution and redistribution sometimes occurs.



- 4) **Cataclisite (with mylonitic banding).**
Altered rock fragments sealed with epidote, adularia, quartz, hematite \pm laumontite in various proportions.



- 5) **Oxidized wall rock (medium to strong alteration).**
Hydrothermally altered host rock, with a mineralogy related to initial rock type. Red staining due to small hematite grains, K-feldspar, saussurite, plagioclase, quartz, chlorite is common in granitic variants.



10.4.2 Representative transport property data

In the following sections, a brief summary is given of the parameter values thought to be representative of the material properties of the major rock types found in Laxemar. The parameter values are based on the measurement data obtained in the transport properties laboratory programme summarised in /Crawford and Sidborn 2009/ and described in detail in /Selnert et al. 2009/. For the rock matrix porosity and formation factor, there is a very good sample support that allows best estimate parameter values (i.e. the central tendency of the measurement data) to be assessed with a relatively high degree of confidence. For sorption, however, the lower numbers of samples for particular solute/rock type/water combinations means that the data should be applied with caution. More detailed quantification of sorption K_d variability and uncertainty with respect to additional considerations of variable porewater chemistry and mineralogical composition will be made within the safety assessment SR-Site. The sorption data given in this section are therefore based purely on the values reported from the laboratory programme without additional thermodynamic interpretation, modelling, correction, or analysis.

Formation factors which are presented in the retardation model (Table 10-3) are based on *in situ* resistivities as well as through-diffusion measurements performed in the laboratory. Since *in situ* formation factors derived from resistivity measurements are obtained under approximately natural stress conditions and are generally lower than laboratory measured values, a good case could be made for using these as a cautiously conservative choice in transport modelling. However, it could also be argued that the through-diffusion technique is the method that best simulates the actual physical process to be studied (i.e. solute diffusion in the porewater) and that the electrical resistivity technique may be influenced by artefacts that are not, as yet, fully understood which give rise to the empirical deviation of roughly a factor of two when comparing the methods. It is noted also that the empirically observed deviation between electrically-based and through-diffusion methods is so consistent and conserved between different investigations that there are good arguments for using a simple empirical correction even in the absence of a full mechanistic explanation of the effect. In some situations, it is not entirely clear if the *in situ* data are “exactly” comparable for different spatial locations owing to residual uncertainties concerning relative sample sizes (i.e. influencing estimated statistical distributions), porewater compositions, and the possible influence of undetected open fractures within the sampled *in situ* rock volume.

Table 10-3. Representative transport parameters for the main rock types (>2%) within rock domains RSMA01, RSMD01, RSMM01, and RFMBA03. Data are given for porosity, formation factor, BET-surface area, and cation exchange capacity (CEC) as determined within the laboratory programme. Rock type codes are explained in Table 5-1.

	501030	501033	501036	501046	501056	501058	505102	511058
Porosity (vol%), non-DZ								
unaltered rock only	0.20±0.22	n/a	0.19±0.19	0.36±0.14	0.30±0.10	n/a	0.16±0.06	0.24±0.07
altered rock only	0.79±0.56	n/a	n/a	0.15	0.55±0.33	n/a	n/a	0.64
all rock	0.23±0.26	0.06	0.19±0.19	0.35±0.14	0.32±0.15	0.61	0.16±0.06	0.27±0.19
Porosity (vol%), DZ								
unaltered rock only	0.16±0.13	n/a	0.25	0.33±0.08	0.43±0.18	n/a	0.46±0.50	0.15±0.08
altered rock only	0.47	n/a	0.87±0.35	0.94±0.62	0.36±0.25	n/a	n/a	n/a
all rock	0.19±0.19	n/a	0.75±0.40	0.63±0.52	0.40±0.20	0.76	0.46±0.50	0.15±0.08
Formation factor (<i>in situ</i>)†								
unaltered rock only	(6.0±5.3)·10 ⁻⁶	(1.2±0.6)·10 ⁻⁵	(9.7±5.9)·10 ⁻⁶	(2.1±1.9)·10 ⁻⁵	(2.2±1.9)·10 ⁻⁵	(1.2±1.0)·10 ⁻⁵	(1.3±1.1)·10 ⁻⁵	(1.2±1.0)·10 ⁻⁵
altered rock only	(3.2±4.2)·10 ⁻⁵	(1.7±0.7)·10 ⁻⁵	(9.3±6.1)·10 ⁻⁶	(2.6±2.2)·10 ⁻⁵	(3.1±2.8)·10 ⁻⁵	(1.5±1.5)·10 ⁻⁵	(1.8±0.9)·10 ⁻⁵	(4.6±11)·10 ⁻⁵
all rock	(8.1±9.2)·10 ⁻⁶	(1.2±0.6)·10 ⁻⁵	(9.7±5.9)·10 ⁻⁶	(2.1±1.9)·10 ⁻⁵	(2.3±2.1)·10 ⁻⁵	(1.3±1.0)·10 ⁻⁵	(1.4±1.2)·10 ⁻⁵	(1.9±2.5)·10 ⁻⁵
Formation factor (lab)								
	3.1·10 ⁻⁵	n/a	6.1·10 ⁻⁵	4.6·10 ⁻⁴	7.0·10 ⁻⁵	n/a	9.8·10 ⁻⁵	4.4·10 ⁻⁵
BET (m²/g)								
	0.043	0.03	0.022	0.04	0.039	n/a	n/a	n/a
CEC (cmol/kg)*								
	1.0±0.6	n/a	1.0±0.7	0.9±0.7	<1.0	n/a	n/a	n/a

Notes: Entries given as "n/a" in the table signify data "not available".

The term "DZ" and "non-DZ" refer to rock samples taken from within or outside of deformation zones, respectively.

(†) Formation factors derived from *in situ* measurements are empirically corrected for measurement bias (reduced by 50%) and are for "rock matrix" (i.e. ≥ 0.5 m distant from the nearest mapped, open fracture). The data for rock domains includes rock from the HRD and HCD (deterministic deformation zones) considered together.

(*) 1 cmol/kg = 1 meq/100 g.

The above discussion is not meant to indicate a belief that the one method is more reliable than the other. A detailed discussion concerning the issues related to use of the electrical resistivity measurement technique can be found in /Crawford and Sidborn 2009/ where the use of *in situ* formation factors derived from borehole resistivity logging is discussed with particular emphasis given to Laxemar. In the current SDM-Site Laxemar modelling, the formation factor data derived from *in situ* measurements are presented along with through-diffusion based measurements as alternative bases for retardation model parameterisations.

Material properties of individual rock types

The data compiled in Table 10-3 to Table 10-7 comprise values for material property parameters preliminarily recommended for modelling of radionuclide transport under site-specific conditions and relate to the bulk rock matrix. Full details concerning the rationale used in the selection of data can be found in /Selnert et al. 2009/.

Owing to the heterogeneity of the bedrock in Laxemar, *in situ* formation factors are given where values are classified as “unaltered rock only”, “altered rock only”, and “all rock” where both altered and unaltered rock are lumped together. Furthermore, the data sets consider rock within the hydraulic rock domains (HRD) and hydraulic conductor domains (HCD) taken together as a single group.

Since much of the reported sorption data are based on very small sample numbers (in some cases as few as one or two measurements), these should be considered to be order of magnitude estimates only. It should be noted that negative values occasionally arise due to the aqueous mass balance technique used to discriminate sorption on the geological samples and sorption on the surface of containment vessel walls which is quantified using separate blanks spiked with the groundwater/solute mix. Although not strictly related to the instrumental level of detection it still can be considered as part of the overall limit of quantitative detection inherent in the method. In such cases, which typically involve weakly sorbing solutes, the presence or absence of sorption is not possible to distinguish with statistical certainty. Since negative K_d values are not physically meaningful, the presence of negative K_d values in the data tables should be taken to signify that the true K_d value is lower than the limit of statistical quantification, although not necessarily zero. This is discussed in more detail in /Crawford and Sidborn 2009/

The reduced selection of nuclides in certain cases is due to the difficulty of performing a full set of measurements for every rock type/groundwater combination and represents an economic and logistic compromise where only the main rock types 501036 (Quartz monzonite to monzodiorite) and 501046 (Ävrö quartz monzodiorite) are subjected to the full suite of measurements. The detailed rationale for this is outlined in /Widestrand et al. 2003/.

Generally there are no significant differences in the retardation properties of the different rock types (for explanation of rock codes given below, cf. Table 5-1). The minor differences that are observed are:

- Of the rock types with statistically confirmed porosity measurements, rock type 501030 and 501036 have low porosities whereas rock types 501046 and 501056 have the highest porosities. The porosities of the altered samples, both inside and outside of deformation zones, are higher than unaltered samples (defined here to be rock without strong or medium alteration). A possible exception is for rock type 501056 (Ävrö granodiorite) within deformation zones where the opposite is observed, cf. Table 10-3. It is noted, however, that visual discrimination of alteration is more subjective and difficult for the naturally red-coloured rock types such as the Ävrö granodiorite compared to the more greyish rock types. Ambiguity in visual discrimination of alteration should therefore be acknowledged as an uncertainty which affects the basis for conclusions concerning the impact of alteration on porosity.
- Rock type 501046 appears to have a higher formation factor than the other rock types based on laboratory through-diffusion measurements. When comparing *in situ* formation factors based on resistivity logs, however, there is no noticeable difference. The laboratory diffusion data for this rock type is based on a sample group taken from borehole KSH01 (–858.6 to –858.84 m elevation interval) and may not be statistically representative for the site.

- *In situ* formation factor data for the “altered rock only” category is typically based on much smaller numbers of measurements than “unaltered rock only” and “all rock”. This, in combination with the existence of significant skewness in the underlying distributions makes it difficult to make robust comparisons of unaltered and altered rock.
- *In situ* formation factor data for rock type 501058, 505102, and 511058 are based on very small sample sizes and are therefore associated with a greater degree of uncertainty than the other rock types.
- Rock type 501056 appears to have lower sorptivity than the other rock types. The reported data, however, are based on a single sample measured in triplicate and therefore may not be representative for the site.
- The CEC values appear to be very similar for the different rock types. It should be noted that the uncertainty associated with the CEC values is roughly $\pm 50\%$ since the CEC is immediately above the detection limit for crushed rock. Thus, any quantitative correlation with BET surface area or sorptivity is masked by the uncertainty of the CEC measurement.

In addition to the above issues, it should also be noted that the shifting of focus on different areas during the investigation process has led to an uneven distribution of samples with regard to the current Laxemar local model volume. Approximately half of all laboratory measurement samples are sourced from the Simpevarp subarea and the other half has a biased overrepresentation of samples from rock domain RSMA01 and fewer samples from RSMD01.

Table 10-4. Sample K_d values (m^3/kg) measured for the main rock types (where available) within all rock domains. Data are given as the mean \pm standard deviation for sorption measurements using fresh (Type I) groundwater. Rock type codes are explained in Table 5-1.

	501030	501036	501046	501056	511058
Cs(I)	0.25 \pm 0.098	0.15 \pm 0.13	0.16 \pm 0.0031	(5.3 \pm 3.9) $\cdot 10^{-2}$	(9.8 \pm 0.93) $\cdot 10^{-2}$
Sr(II)	(3.0 \pm 0.94) $\cdot 10^{-2}$	(2.5 \pm 0.72) $\cdot 10^{-2}$	(1.9 \pm 0.16) $\cdot 10^{-2}$	(1.3 \pm 0.89) $\cdot 10^{-2}$	(2.3 \pm 0.17) $\cdot 10^{-2}$
Ln-Ac(III)	0.12 \pm 0.017	0.17 \pm 0.066	0.15 \pm 0.006	0.22 \pm 0.036	0.11 \pm 0.023
Ra(II)	n/a	0.24 \pm 0.0093	0.16 \pm 0.024	n/a	n/a
Ni(II)	n/a	0.35 \pm 0.03	0.37 \pm 0.066	n/a	n/a
Np(IV/V)*	n/a	(5.5 \pm 0.8) $\cdot 10^{-3}$	(3.3 \pm 0.024) $\cdot 10^{-3}$	n/a	n/a
U(IV/VI)*	n/a	(5.0 \pm 0.78) $\cdot 10^{-3}$	(2.9 \pm 0.043) $\cdot 10^{-3}$	n/a	n/a

Notes: Entries given as “n/a” in the table signify data “not available”.
Ln-Ac(III) signifies trivalent lanthanides and actinides as a group (assuming analogous behaviour).
(*) the redox status of Np and U during the laboratory measurements was unclear.

Table 10-5. Sample K_d values (m^3/kg) measured for the main rock types (where available) within all rock domains. Data are given as the mean \pm standard deviation for sorption measurements using marine (Type II) groundwater. Rock type codes are explained in Table 5-1.

	501030	501036	501046	501056	511058
Cs(I)	n/a	n/a	n/a	(1.3 \pm 0.14) $\cdot 10^{-3}$	n/a
Sr(II)	n/a	n/a	n/a	(3.3 \pm 0.7) $\cdot 10^{-3}$	n/a
Ln-Ac(III)	n/a	n/a	n/a	1.0 \pm 0.25	n/a
Ra(II)	n/a	n/a	n/a	n/a	n/a
Ni(II)	n/a	n/a	n/a	n/a	n/a
Np(IV/V)*	n/a	n/a	n/a	n/a	n/a
U(IV/VI)*	n/a	n/a	n/a	n/a	n/a

Notes: Entries given as “n/a” in the table signify data “not available”.
Ln-Ac(III) signifies trivalent lanthanides and actinides as a group (assuming analogous behaviour).
(*) the redox status of Np and U during the laboratory measurements was unclear.

Table 10-6. Sample K_d values (m^3/kg) measured for the main rock types (where available) within all rock domains. Data are given as the mean \pm standard deviation for sorption measurements using saline (Type III) groundwater. Rock type codes are explained in Table 5-1.

	501030	501036	501046	501056	511058
Cs(I)	$(3.4 \pm 1.6) \cdot 10^{-2}$	$(2.4 \pm 1.8) \cdot 10^{-2}$	$(2.9 \pm 0.27) \cdot 10^{-2}$	$(5.5 \pm 1.1) \cdot 10^{-3}$	$(1.4 \pm 0.053) \cdot 10^{-2}$
Sr(II)	$(3.0 \pm 2.2) \cdot 10^{-3}$	$(2.9 \pm 1.7) \cdot 10^{-3}$	$(2.6 \pm 0.7) \cdot 10^{-4}$	$(3.9 \pm 7.2) \cdot 10^{-4}$	$(3.2 \pm 0.26) \cdot 10^{-3}$
Ln-Ac(III)	0.83 \pm 0.46	1.4 \pm 0.76	1.5 \pm 0.31	0.34 \pm 0.11	0.82 \pm 0.16
Ra(II)	n/a	$(7.7 \pm 0.39) \cdot 10^{-3}$	$(8.1 \pm 1.9) \cdot 10^{-3}$	n/a	n/a
Ni(II)	n/a	$(8.4 \pm 0.73) \cdot 10^{-2}$	$(6.6 \pm 0.42) \cdot 10^{-2}$	n/a	n/a
Np(IV/IV)*	n/a	$(3.8 \pm 0.24) \cdot 10^{-3}$	$(3.8 \pm 0.24) \cdot 10^{-3}$	n/a	n/a
U(IV/VI)*	n/a	$(1.2 \pm 0.16) \cdot 10^{-2}$	$(4.0 \pm 0.23) \cdot 10^{-3}$	n/a	n/a

Notes: Entries given as "n/a" in the table signify data "not available".
 Ln-Ac(III) signifies trivalent lanthanides and actinides as a group (assuming analogous behaviour).
 (*) the redox status of Np and U during the laboratory measurements was unclear.

Table 10-7. Sample K_d values (m^3/kg) measured for the main rock types (where available) within all rock domains. Data are given as the mean \pm standard deviation for sorption measurements using brine (Type IV) groundwater. Rock type codes are explained in Table 5-1.

	501030	501036	501046	501056	511058
Cs(I)	n/a	$(4.9 \pm 0.44) \cdot 10^{-3}$	n/a	$(5.9 \pm 4.4) \cdot 10^{-3}$	n/a
Sr(II)	n/a	$(-4.1 \pm 4.9) \cdot 10^{-4}$ **	n/a	$(1.5 \pm 2.0) \cdot 10^{-3}$	n/a
Ln-Ac(III)	n/a	0.41 \pm 0.072	n/a	0.34 \pm 0.31	n/a
Ra(II)	n/a	n/a	n/a	n/a	n/a
Ni(II)	n/a	n/a	n/a	n/a	n/a
Np(IV/IV)*	n/a	n/a	n/a	n/a	n/a
U(IV/VI)*	n/a	n/a	n/a	n/a	n/a

Notes: Entries given as "n/a" in the table signify data "not available".
 Ln-Ac(III) signifies trivalent lanthanides and actinides as a group (assuming analogous behaviour).
 (*) the redox status of Np and U during the laboratory measurements was unclear.
 (**) some negative values reported signifying that sorption could not be statistically verified.

Table 10-8. Sample K_d values (m^3/kg) measured for the main rock types (where available) within all rock domains. Data are given as the mean \pm standard deviation for sorption measurements using brackish, non-marine (Type V) groundwater. Rock type codes are explained in Table 5-1.

	501030	501036	501046	501056	511058
Cs(I)	n/a	$(6.1 \pm 1.1) \cdot 10^{-2}$	$(3.3 \pm 0.33) \cdot 10^{-2}$	$(2.5 \pm 0.16) \cdot 10^{-2}$	n/a
Sr(II)	n/a	$(3.1 \pm 1.1) \cdot 10^{-3}$	$(3.7 \pm 0.86) \cdot 10^{-3}$	$(3.7 \pm 0.26) \cdot 10^{-3}$	n/a
Ln-Ac(III)	n/a	1.2 \pm 0.23	1.1 \pm 0.47	1.0 \pm 0.19	n/a
Ra(II)	n/a	n/a	$(4.0 \pm 0.53) \cdot 10^{-2}$	n/a	n/a
Ni(II)	n/a	n/a	$(5.7 \pm 0.18) \cdot 10^{-2}$	n/a	n/a
Np(IV/IV)*	n/a	n/a	$(-1.7 \pm 2.4) \cdot 10^{-4}$ **	n/a	n/a
U(IV/VI)*	n/a	n/a	$(3.5 \pm 0.29) \cdot 10^{-3}$	n/a	n/a

Notes: Entries given as "n/a" in the table signify data "not available".
 Ln-Ac(III) signifies trivalent lanthanides and actinides as a group (assuming analogous behaviour).
 (*) the redox status of Np and U during the laboratory measurements was unclear
 (**) some negative values reported signifying that sorption could not be statistically verified

Material properties of fractures

The data compiled in Table 10-9 through Table 10-16 comprise values for material property parameters preliminarily recommended for modelling of radionuclide transport under site-specific conditions and concern material properties of specific fracture types. According to the available data, the presence of different fracture mineralisations cannot be related to specific rock types, rock domains, or fracture domains with statistical certainty. In spite of this, there do appear to be minor variations in the relative frequency of various fracture types between different fracture domains. This, however, is only qualitatively established and may not be representative of the entire rock volume owing to the small number of investigation boreholes and the possibility of sampling bias.

As previously mentioned, 9 different classes of fracture (“fracture types”) have been included in the retardation model (see Table 10-1). A thin layer of fracture coating with a thickness in the range of 0.1–5 mm has been identified in all fracture types with the exception of fracture type H (no coating). Due to their limited thickness and their generally friable nature it has not been possible to make porosity or effective diffusivity measurements on samples of fracture coating materials. There are, however, data from the LTDE-SD project /Widestrand et al. (in prep)/ for fracture Type E that indicates an increased porosity in chlorite/calcite layers of 3–5% which is also supported by PMMA-measurements showing increased porosity in fracture coatings /Penttinen et al. 2006/. It is therefore likely that these layers have a higher porosity and consequently, a higher effective diffusivity (i.e. formation factor) than the intact wall rock.

The measured BET surface areas of the fracture material are significantly higher than the corresponding BET surface areas of rock matrix samples. They vary from 2 m²/g to 24 m²/g, which is roughly 100–300 times higher than the corresponding range for the underlying matrix rock. With regard to the CEC measurements, it is found that the fracture coatings (for Type A and C) have CEC values 10 to 40 times higher than the corresponding values for the rock matrix. This indicates that fracture coatings in general have substantially enhanced retention properties as compared to the intact rock matrix itself.

The large differences in the BET surface area of intact rock and fracture filling materials are not always accompanied by a comparable divergence in estimated K_d values, although most particularly for ion exchanging solutes such as Cs(I). In this particular case, however, the variability of the K_d values is in general agreement with the known ion-exchange behaviour of Cs(I) in association with clay minerals so this is not altogether unexpected. For solutes that sorb by way of a surface complexation mechanism a closer agreement is expected. Although there appears to be a clear correlation between BET surface area and sorptivity generally when comparing different size fractions of crushed rock, it is very difficult to observe a consistent correlation with surface area when comparing the relative sorptivity of matrix rock and fracture coating materials.

For the timescales characteristic of safety assessment it is realistic to assume that these fracture coatings constitute an equilibrium storage capacity and it is generally not necessary to model the full multilayer diffusive transport problem. Generally, the presence of fracture coatings has little impact on the residence time distribution of transported radionuclides at later times and the effect is only relevant for very early breakthrough under typical safety assessment conditions and for the interpretation of tracer test data. In /Crawford and Sidborn 2009/ scoping calculations are made which indicate significantly enhanced retardation of early arriving solute for F-factors in the low to mid-range ($\sim 10^4$ y/m) assuming transport parameters that are typical for these materials.

Retardation parameters for the identified fracture types are given in Table 10-9 to Table 10-16. Owing to the shortage of measurement data for certain fracture types using Laxemar site specific samples, data have been imported from other sources in some cases. These specific cases are annotated in the property tables where appropriate.

Table 10-9. Retardation model parameters for fracture type A, cf. Table 10-1.

Fracture coating: Calcite +Chlorite +Pyrite ±Chalcopyrite ±other					
Thickness	0.2–1 mm				
Porosity (vol%)	n/a				
Formation factor	n/a				
BET surface area (m ² /g)	15±9				
CEC (cmol/kg)	40±13				
Sorption, K _d (m ³ /kg)	Water type (I–V)				
	fresh	marine	saline	brine	Type V
Cs(I)	3.2	n/a	n/a	n/a	n/a
Sr(II)	0.16	n/a	n/a	n/a	n/a
Ln-Ac(III)	0.88±0.16	n/a	n/a	n/a	n/a
% of all open fractures	7%				
% of transmissive fractures	10%				
Wall rock alteration	≤ 10 mm				

Notes: Entries given as “n/a” in the table signify data “not available”.

Table 10-10. Retardation model parameters for fracture type B, cf. Table 10-1.

Fracture coating: Epidote ± Prehnite ± Adularia ±chlorite ±quartz ±calcite					
Thickness	0.5–1 mm				
Porosity (vol%)	n/a				
Formation factor	n/a				
BET surface area (m ² /g)	6±2				
CEC (cmol/kg)	n/a				
Sorption, K _d (m ³ /kg)	Water type (I–V)				
	fresh	marine	saline	brine	Type V
Cs(I)	0.26±0.007	n/a	(2.9±2.0)·10 ⁻²	(1.6±0.01)·10 ⁻²	n/a
Sr(II)	0.11±0.08	n/a	(9.6±8.8)·10 ⁻⁴	(1.7±0.5)·10 ⁻⁴	n/a
Ln-Ac(III)	0.34±0.13	n/a	1.3±0.54	0.13±0.01	n/a
% of all open fractures	8%				
% of transmissive fractures	5%				
Wall rock alteration	~ 20 mm				

Notes: Entries given as “n/a” in the table signify data “not available”.

Table 10-11. Retardation model parameters for fracture type C, cf. Table 10-1.

Fracture coating: Hematite +Clay ±Chlorite ±other					
Thickness	0.5–1 mm				
Porosity (vol%)	n/a				
Formation factor	n/a				
BET surface area (m ² /g)	13±11				
CEC (cmol/kg)	12–24				
Sorption, K _d (m ³ /kg)	Water type (I–V)				
	fresh	marine	saline	brine	Type V
Cs(I)	0.35±0.05	n/a	0.19±0.18	1.1·10 ⁻²	n/a
Sr(II)	0.38±0.15	n/a	(1.7±0.06)·10 ⁻³	7.4·10 ⁻⁴	n/a
Ln-Ac(III)	0.38±0.43	n/a	0.93±0.96	0.56	n/a
% of open fractures	10%				
% of transmissive fractures	9%				
Wall rock alteration	≤ 50 mm				

Notes: Entries given as “n/a” in the table signify data “not available”.

Table 10-12. Retardation model parameters for fracture type D, cf. Table 10-1.

Fracture coating: Laumontite ±calcite ±chlorite						
Thickness	0.2–2 mm					
Porosity (vol%)	n/a					
Formation factor	n/a					
BET surface area (m ² /g)*	0.42±0.02					
CEC (cmol/kg)*	18±5					
Sorption, K _d (m ³ /kg)*	Water type (I–V)					
	fresh	marine	saline	brine	Type V	
Cs(I)	0.29±0.14	(1.6±0.24)·10 ⁻²	(1.6±0.3)·10 ⁻²	(4.1±0.4)·10 ⁻³	n/a	
Sr(II)	(5±2)·10 ⁻²	(1.3±3.8)·10 ⁻⁴	(0.4±3.3)·10 ⁻⁴	(0.31±5)·10 ⁻⁴	n/a	
Ln-Ac(III)	1.0±0.4	1.3±2.1	1.2±0.14	2.1±0.4	n/a	
% of all open fractures	0.3%					
% of transmissive fractures	0.3%					
Wall rock alteration	≤ 20 mm					

Notes: Entries given as “n/a” in the table signify data “not available”.

(*) material property data imported from Forsmark model for corresponding fracture type (E) /Byegård et al. 2008/.

Table 10-13. Retardation model parameters for fracture type E, cf. Table 10-1.

Fracture coating: Chlorite +Calcite ±oxidised walls ±saussuritised walls						
Thickness	0.2–0.5 mm					
Porosity (vol%)*	3–5%					
Formation factor	n/a					
BET surface area (m ² /g)	2.2					
CEC (cmol/kg)	n/a					
Sorption, K _d (m ³ /kg)	Water type (I–V)					
	fresh	marine	saline	brine	Type V	
Cs(I)	n/a	n/a	n/a	n/a	n/a	
Sr(II)	n/a	n/a	n/a	n/a	n/a	
Ln-Ac(III)	n/a	n/a	n/a	n/a	n/a	
% of all open fractures	23%					
% of transmissive fractures	20%					
Wall rock alteration	≤ 10 mm					

Notes: Entries given as “n/a” in the table signify data “not available”.

(*) material property data imported from LTDE-SD experiment for corresponding fracture type /Widstrand et al. in prep/.

Table 10-14. Retardation model parameters for fracture type F, cf. Table 10-1.

Fracture coating: Clay +Chlorite ±calcite						
Thickness	0.2–5 mm					
Porosity (vol%)	n/a					
Formation factor	n/a					
BET surface area (m ² /g)	24					
CEC (cmol/kg)	n/a					
Sorption, K _d (m ³ /kg)	Water type (I–V)					
	fresh	marine	saline	brine	Type V	
Cs(I)	3.2±0.5	n/a	3.0±1.5	n/a	n/a	
Sr(II)	0.16±0.02	n/a	(3.3±0.97)·10 ⁻³	n/a	n/a	
Ln-Ac(III)	1.2±0.2	n/a	9.3±1.9	n/a	n/a	
% of all open fractures	21%					
% of transmissive fractures	27%					
Wall rock alteration	≤ 50 mm					

Notes: Entries given as “n/a” in the table signify data “not available”.

Table 10-15. Retardation model parameters for fracture type G, cf. Table 10-1.

Fracture coating: Chlorite ±other					
Thickness	~ 0.2 mm				
Porosity (vol%)	0.9%				
Formation factor	n/a				
BET surface area (m ² /g)*	7.9				
CEC (cmol/kg)*	13±2				
Sorption, K _d (m ³ /kg)*	Water type (I–V)				
	fresh	marine	saline	brine	Type V
Cs(I)	0.4±0.08	n/a	(1.7±0.14)·10 ⁻²	n/a	n/a
Sr(II)	(3.8±0.5)·10 ⁻²	n/a	(5.1±2.3)·10 ⁻³	n/a	n/a
Ln-Ac(III)	1.2±0.34	n/a	9.5±2.7	n/a	n/a
Ra(II)	1.7±0.2	n/a	(2.9±0.29)·10 ⁻²	n/a	n/a
Ni(II)	1.0±0.5	n/a	1.2±0.5	n/a	n/a
Np(V/VI)**	0.21±0.008	n/a	(4.7±0.7)·10 ⁻³	n/a	n/a
U(IV/VI)**	(4.0±0.2)·10 ⁻²	n/a	3.5±0.3	n/a	n/a
% of all open fractures	11%				
% of transmissive fractures	7%				
Wall rock alteration	≤ 50 mm				

Notes: Entries given as “n/a” in the table signify data “not available”.

(*) material property data assumed to be the same as for deformation zone element 2 (see Table 10-19).

(**) the redox status of Np and U during the laboratory measurements was unclear.

Table 10-16. Retardation model parameters for Fracture Type H (material properties assumed to be same as for rock types specified in Table 10-3 to Table 10-8) , cf. Table 10-1.

Fracture coating: None	
Thickness	n/a
Porosity (vol%)	see Table 10-3
Formation factor	see Table 10-3
BET surface area (m ² /g)	see Table 10-3
CEC (cmol/kg)	see Table 10-3
Sorption, K _d (m ³ /kg)	refer to appropriate data sets in Table 10-4 to Table 10-8
% of all open fractures	3%
% of transmissive fractures	4%
Wall rock alteration	≤ 10 mm

Notes: Entries given as “n/a” in the table signify data “not available”.

Table 10-17. Retardation model parameters for Fracture Type I, cf. Table 10-1.

Fracture coating: Calcite ±other					
Thickness	~ 0.2 mm				
Porosity (vol%)	n/a				
Formation factor	n/a				
BET surface area (m ² /g)	n/a				
CEC (cmol/kg)	n/a				
Sorption, K _d (m ³ /kg)	Water type (I–V)				
	fresh	marine	saline	brine	Type V
Cs(I)	n/a	n/a	n/a	n/a	n/a
Sr(II)	n/a	n/a	n/a	n/a	n/a
Ln-Ac(III)	n/a	n/a	n/a	n/a	n/a
% of all open fractures	11%				
% of transmissive fractures	13%				
Wall rock alteration	≤ 10 mm				

Notes: Entries given as “n/a” in the table signify data “not available”.

Material properties of deterministically modelled deformation zones

As described in Section 5.5, deformation zones are usually characterised as consisting of a transition zone and a core. Transmissive fractures, if they are present, are often found in the transition zone, close to the wall rock. The deformation zone core is commonly, although not necessarily, found to have substantially reduced hydraulic conductivity in a direction normal to its strike. The hydrogeological properties of the deformation zone core are, however, complex since the core is typically characterised by both an increased intensity of fracturing (usually associated with increased flow) and also often been subjected to intense compression and shear which can give rise to compact aggregations of fault gouge and breccia (usually associated with restricted flow).

There are a number of different possibilities for the modelling of deformation zones in a radionuclide transport perspective. One possibility is to define effective retention parameters for the zone in its entirety, where the zone is simply represented as a region of higher retention capacity and transmissivity. Another possibility is to partition the deformation zone into high and low transmissive elements. Implicit in this approach is the need to assign limited diffusion depths for different deformation zone sub-elements to avoid double counting of storage capacities. Some of the different possibilities available are illustrated in Figure 10-4.

Independently of which model is adopted for use in transport calculations, there are some overarching issues which should be considered when parameterising deformation zones:

- the vast majority of borehole sections mapped as having strong or medium oxidation are found within deformation zones. In addition, four separate categories of altered rock have been distinguished as recurrent structural elements within, or in close proximity to deformation zones. Retardation parameters for these elements are given in Table 10-18 to Table 10-21,
- a deformation zone consists of a high frequency of open and sealed fractures. Retardation parameters for open fractures are found in Table 10-9 to Table 10-16,
- both the frequency and distribution of transmissive fractures vary between different deformation zones although the transmissivity ranges are broadly similar for all fracture types described in the retardation model.

Table 10-18 to Table 10-21 give recommended data for the different rock types that are specific to deformation zones.

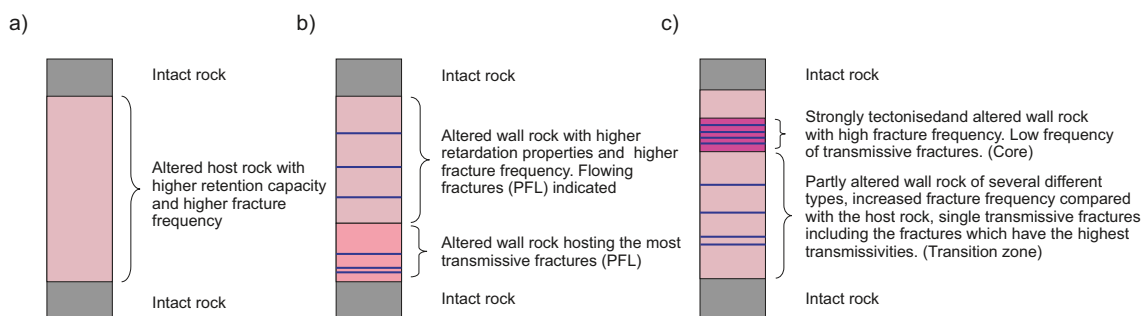


Figure 10-4. Schematic illustration of different alternatives for describing a deformation zone retardation model; a) deformation zone considered as a single unit with higher retention capacity than the surrounding rock; b) the deformation zone divided into a high and low transmissive unit; c) variation including core zone, the latter also divided into a high and low transmissive unit.

Table 10-18. Retardation model parameters for Category 1, Fault rock/gouge (strongly tectonised and partly incohesive material), cf. Table 10-2.

Mineral content	Altered rock fragments, mineralogy partially dependent on host rock. Generally chlorite, saussurite, and clay together with rock fragments				
Porosity (vol%)	3%				
Formation factor	n/a				
BET surface area (m ² /g)	24.1				
CEC (cmol/kg)	n/a				
Sorption, K _d (m ³ /kg)	Water type (I–V)				
	fresh	marine	saline	brine	Type V
Cs(I)	5.1	n/a	0.6±0.03	n/a	n/a
Sr(II)	0.14	n/a	(1.8±0.1)·10 ⁻³	n/a	n/a
Ln-Ac(III)	2.5	n/a	2.6±1.7	n/a	n/a

Notes: Entries given as “n/a” in the table signify data “not available”.

Table 10-19. Retardation model parameters for Category 2, Chlorite (primarily in close proximity to mafic rock types), cf. Table 10-2.

Mineral content	Chlorite ±corrensite				
Porosity (vol%)*	12%				
Formation factor	n/a				
BET surface area (m ² /g)	8				
CEC (cmol/kg)	13±2				
Sorption, K _d (m ³ /kg)	Water type (I–V)				
	fresh	marine	saline	brine	Type V
Cs(I)	0.4±0.08	n/a	(1.7±0.14)·10 ⁻²	n/a	n/a
Sr(II)	(3.8±0.5)·10 ⁻²	n/a	(5.1±2.3)·10 ⁻³	n/a	n/a
Ln-Ac(III)	1.2±0.34	n/a	9.5±2.7	n/a	n/a
Ra(II)	1.7±0.2	n/a	(2.9±0.29)·10 ⁻²	n/a	n/a
Ni(III)	1.0±0.5	n/a	1.2±0.5	n/a	n/a
Np(IV/V)*	0.21±0.008	n/a	(4.7±0.7)·10 ⁻³	n/a	n/a
U(IV/VI)*	(4.0±0.2)·10 ⁻²	n/a	3.5±0.3	n/a	n/a

Notes: Entries given as “n/a” in the table signify data “not available”.

(*) determined by C¹⁴-PMMA impregnation.

(**) the redox status of Np and U during the laboratory measurements was unclear.

Table 10-20. Retardation model parameters for Category 3, Porous, episyenetic (vuggy) wall rock, cf. Table 10-2.

Mineral content	Prehnite, adularia, quartz, calcite ±laumontite, epidote, hematite. Occasional signs of quartz dissolution.				
Porosity (vol%)	6%				
Formation factor*	1.1·10 ⁻³ (through-diffusion)				
BET surface area (m ² /g)	13				
CEC (cmol/kg)	n/a				
Sorption, K _d (m ³ /kg)	Water type (I–V)				
	fresh	marine	saline	brine	Type V
Cs(I)	0.69±0.13	n/a	0.12±0.032	n/a	n/a
Sr(II)	(6.5±0.13)·10 ⁻²	n/a	(3.9±1.0)·10 ⁻³	n/a	n/a
Ln-Ac(III)	0.52±0.01	n/a	1.3±1.1	n/a	n/a

Notes: Entries given as “n/a” in the table signify data “not available”.

(*) sample taken from outside deformation zone, although for an interval defined as “crush” in the boremap.

Table 10-21. Retardation model parameters for Category 4, Cataclasite (with mylonitic banding), cf Table 10-2.

Mineral content	Epidote, adularia, quartz, hematite ±laumontite (strong variations in mineralogy)				
Porosity (vol%)	3±2%				
Formation factor	7.6·10 ⁻³				
BET surface area (m ² /g)	15±8				
CEC (cmol/kg)	n/a				
Sorption, K _d (m ³ /kg)	Water type (I–V)				
	fresh	marine	saline	brine	Type V
Cs(I)	0.76±0.19	n/a	(8.5±0.8)·10 ⁻²	n/a	n/a
Sr(II)	(3.3±0.4)·10 ⁻²	n/a	(1.0±0.37)·10 ⁻²	n/a	n/a
Ln-Ac(III)	0.44±0.08	n/a	5.6±1.0	n/a	n/a
Ra(II)	1.9±1.1	n/a	0.19±0.021	n/a	n/a
Ni(II)	0.9±0.5	n/a	0.52±0.11	n/a	n/a
Np(IV/V)*	0.23±0.01	n/a	(8.1±1.2)·10 ⁻²	n/a	n/a
U(IV/VI)*	(5.9±0.3)·10 ⁻³	n/a	5.8±0.44	n/a	n/a

Notes: Entries given as “n/a” in the table signify data “not available”.

(*) the redox status of Np and U during the laboratory measurements was unclear.

Table 10-22. Retardation model parameters for Category 5, Strongly oxidised wall rock, cf. Table 10-2.

Mineral content	Hydrothermally altered host rock with mineralogy roughly corresponding to initial rock type. Red staining from small hematite grains, K-feldspar, saussurite, plagioclase, quartz. Chlorite is quite common in granitic variants.				
Porosity (vol%)	0.7±0.4%				
Formation factor	(1.5±1.3)·10 ⁻⁴ (through-diffusion)				
BET surface area (m ² /g)	0.6				
CEC (cmol/kg)	n/a				
Sorption, K _d (m ³ /kg)	Water type (I–V)				
	fresh	marine	saline	brine	Type V
Cs(I)	n/a	n/a	(1.7±0.13)·10 ⁻²	(4.9±1.6)·10 ⁻⁴	(1.1±0.1)·10 ⁻²
Sr(II)	n/a	n/a	(-0.3±6)·10 ⁻⁴ *	(-0.5±3)·10 ⁻⁴ *	(4.0±0.53)·10 ⁻³
Ln-Ac(III)	n/a	n/a	0.17±0.03	0.26±0.016	1.7±0.4

Notes: Entries given as “n/a” in the table signify data “not available”.

(*) some negative values reported signifying that sorption could not be statistically verified.

Parameterisation of effective diffusive properties using *in situ* resistivity data

There is some evidence to suggest /Crawford and Sidborn 2009/ that the effective diffusivities of borehole core samples measured in the laboratory may be biased by stress release and mechanical damage induced during drilling and sample preparation. In particular, the laboratory measurements of microcrack volume indicating an increase with core sampling depth discussed already in Chapter 7 and in /Hakami et al. 2008/ are indicative of mechanical damage resulting from the increased force required for drilling at increasing depth (owing to the increased stress from the load of the overlying bedrock). Although similar effects can arise in the immediate few centimetres surrounding an investigation borehole, it is thought that this should not have a large impact on the *in situ* data to the same extent as in the laboratory based measurements. The reasons for this are discussed in more detail in /Crawford and Sidborn 2009/. Since *in situ* measurements of resistivity can be used to measure the formation factor of the rock under “relatively” undisturbed conditions this would suggest that the *in situ* data may be more reliable for use in transport modelling. Figure 10-5 shows a typical comparison of formation factors derived from *in situ* and laboratory measurement data (including both resistivity and through-diffusion measurement data) for borehole KLX04.

As can be seen from Figure 10-5, the laboratory based measurements appear to be in reasonable parity with the *in situ* data when the entire data set along a borehole is considered. This is very different to the situation in Forsmark where it was found that the *in situ* method gave values roughly an order of magnitude less than the laboratory measurement data.

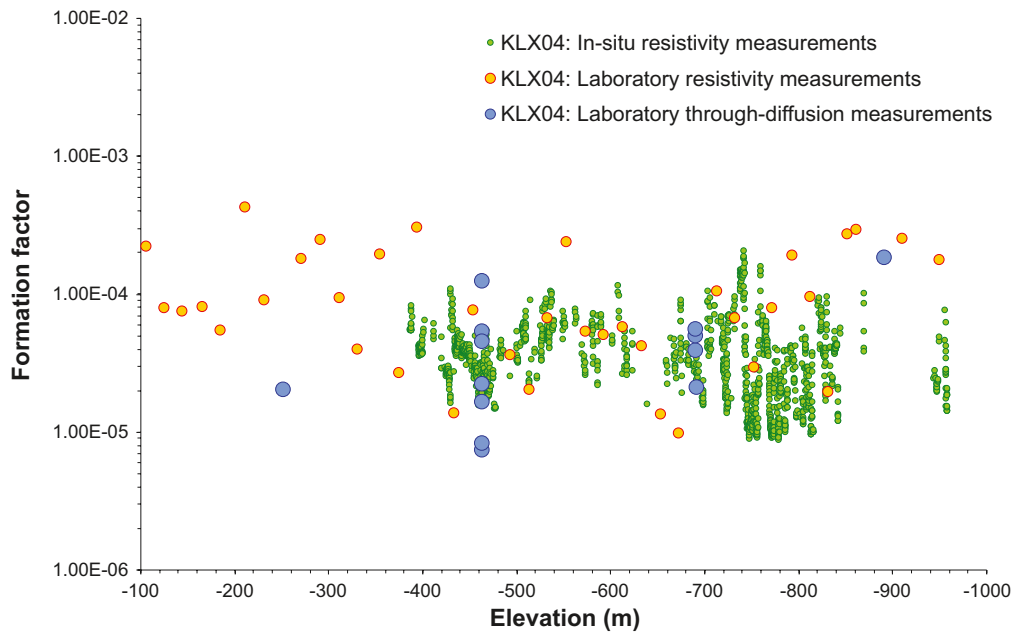


Figure 10-5. Comparison of formation factors derived from *in situ* resistivity measurements in KLX04 (green markers) with corresponding data from electrical resistivity measurements on core samples in the laboratory (orange markers) and through-diffusion measurements (blue markers). The resistivity data are plotted “as is” without additional empirical correction for the known methodological bias for the resistivity method compared to the through-diffusion method.

Although there appears to be very good correspondence between the laboratory and *in situ* data for KLX04, it is not clear whether the *in situ* data are accurately estimated owing to uncertainty concerning the porewater composition and the agreement is likely to be purely coincidental. Reasons for this are discussed in more detail in chapter 11.8 and in /Crawford and Sidborn 2009/.

A perceptible depth trend, although weak in magnitude, can be seen for the *in situ* formation factor data when considering the entire Laxemar data set. This is illustrated in Figure 10-6 below where the formation factor data for all Laxemar boreholes are plotted as 10 m moving averages. The plotted data are for rock matrix where only values more than 0.5 m distant from the nearest mapped open fracture are included. It should be noted that strong deviations from the general trend are seen at discontinuities in the data set, although this is an artefact inherent to the calculation of moving averages that include discontinuous sequences of data. It is inconclusive, however, whether the apparent depth variation can be credited to the increasing *in situ* stresses with greater depths or whether it is an artefact related to uncertainty in the assumed matrix porewater conductivity profiles. A quantitative parameterisation of the retardation model with depth-dependent formation factors has therefore not been considered in this work since the overall trend is weak, may not be representative of different rock volumes, and is possibly an artefact.

There are good mechanistic reasons for expecting a compression of the matrix pore spaces *in situ* /Crawford and Sidborn 2009/. Reductions in effective diffusivity under increasing stress have also been reported by /Skagius and Neretnieks 1986/ in re-confined samples at pressures up to 35 MPa. Similar results were obtained by /Bradbury and Green 1986/ at confining pressures up to 16 MPa. Results from *in situ* diffusion experiments reported by /Birgersson and Neretnieks 1990/ in the Stripa project, however, were inconclusive with regard to compression of pore spaces under *in situ* stress conditions (estimated to be ~ 15 MPa at the 360 m level in the Stripa mine).

In situ diffusion experiments reported by /Vilks et al. 2003, 2004/ at the (Canadian) AECL Underground Research Laboratory showed no evidence for a decreasing effective diffusivity with increasing depth. The experiments were carried out at different depth levels (240 m, 300 m, 420 m) corresponding to an interval of 30–60 MPa maximum stress. Stress redistribution in the nearest centimetre adjacent to the borehole wall, giving a locally decreased effective diffusivity, was identified as a confounding factor complicating the interpretation of the results. For the shallowest depth

(30 MPa), however, the *in situ* results were found to be identical to effective diffusivities measured in the laboratory in re-confined samples subjected to the same stress magnitude. This may suggest that borehole wall damage effects might not be prevalent in boreholes drilled in Laxemar owing to the generally lower *in situ* stresses encountered in the bedrock.

In spite of these complicating issues, the generally lower values obtained for formation factors measured *in situ* (cf. Table 10-3) suggest that the use of these data are a defensibly conservative choice. There are, however, a number of additional issues related to the interpretation of laboratory versus *in situ* measurements which are necessary to consider before recommending these data for general use in modelling. Although most of the uncertainties are reasonably well bounded, the *in situ* formation factor data are presented here as an alternative parameterisation rather than recommending the use of one data set over the other.

The principal uncertainty which could affect the applicability of the data concerns the physical nature of the measurement bias in the electrical method that gives a difference by about a factor of two between formation factors measured by through-diffusion and electrical methods under laboratory conditions. Although an investigation is currently underway to resolve this issue, it is not currently clear whether the empirical correction factor derived for the resistivity method in the laboratory can be assumed to be roughly the same for the generally lower (and variable) porewater salinities encountered in the *in situ* rock. For this reason the data are presented here in an uncorrected form for the comparisons in Figure 10-5 and Figure 10-6. If the *in situ* formation factors are to be used in transport modelling, it is preliminarily recommended that they be divided by a factor of two to account for the methodological bias (this has already been done for the data presented in Table 10-3).

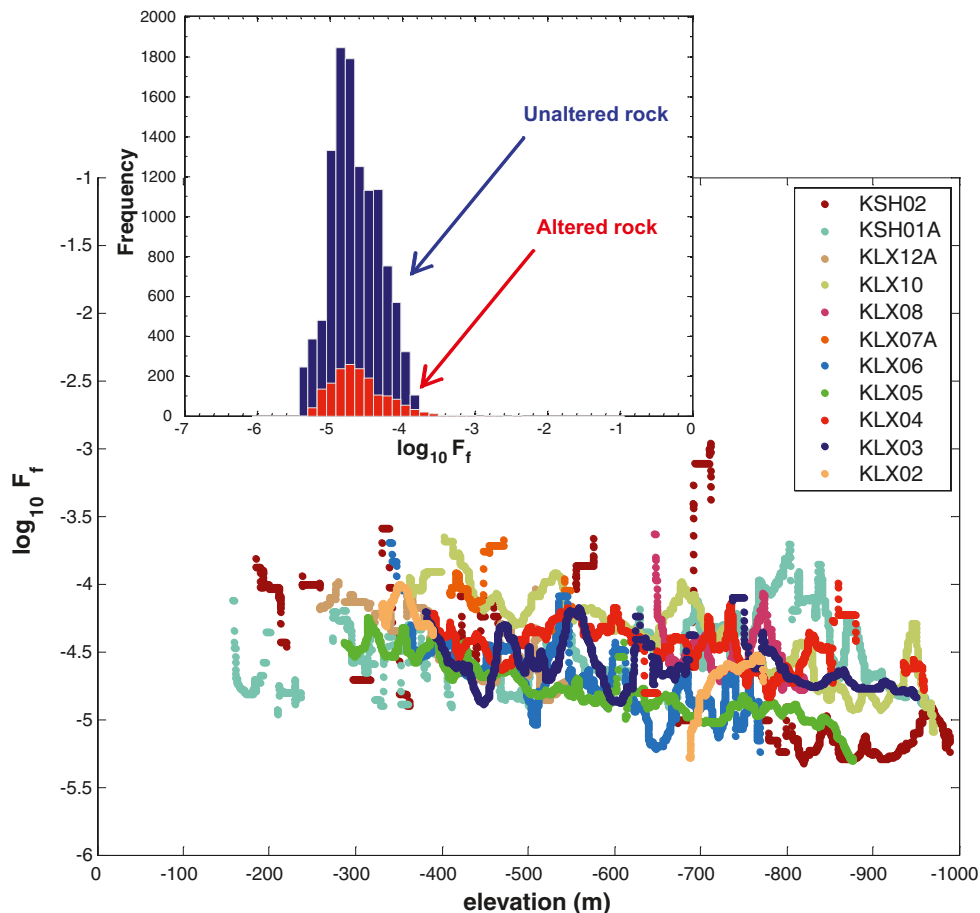


Figure 10-6. Depth dependency of formation factors derived from *in situ* resistivity measurements in all investigation boreholes for unaltered rock (10 m running averages of raw, uncorrected data from Sicada for all rock types). The overall distribution of formation factors is also given as a histogram (inset) where a comparison is made showing very little quantitative difference between the data flagged as belonging to altered rock and that for unaltered rock.

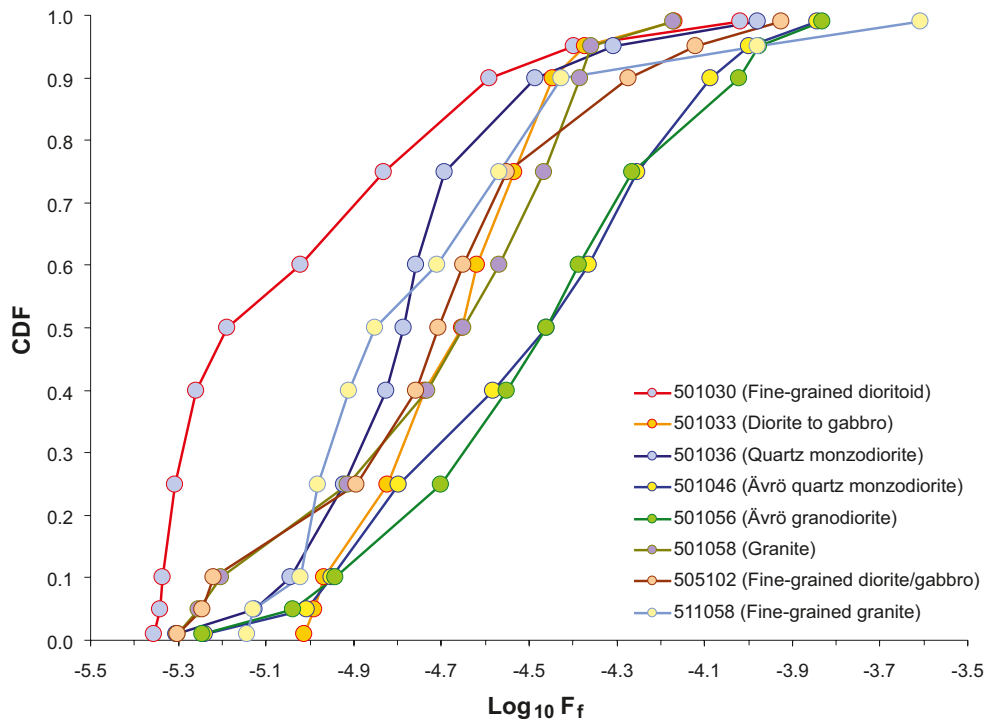


Figure 10-7. Empirical percentiles for *in situ* matrix formation factors (uncorrected), specified according to rock type (all borehole data obtained from the Laxemar-Simpevarp area) and plotted as a cumulative distribution function, CDF.

Some representative data sorted by rock type are plotted in Figure 10-7 for all borehole data obtained from the Laxemar-Simpevarp area. As can be seen from the plotted data, there does not appear to be very large systematic differences between the different rock types given the overall statistical dispersion in the data. Possible exceptions are rock type 5010046 (Ävrö quartz monzodiorite) and 501056 (Ävrö granodiorite) which appear to have slightly elevated formation factors, and rock type 501030 (fine grained dioritoid) which appears to have a somewhat lower formation factor than most of the other rock types. It is also noted that the unusual shape of the cumulative distribution curve for the fine grained dioritoid (data from KSH01A and KSH02) might be a result of data censoring of the lower tail of the distribution. It is speculated in /Crawford and Sidborn 2009/ that this could be due to a more prominent surface conduction bias in the formation factors estimated for this rock type.

10.4.3 Application of the retardation model

The quantitative descriptions of the identified fracture types including selected retardation parameters are given in Table 10-9 to Table 10-16. The corresponding descriptions of and data for deformation zones are presented in Table 10-18 to Table 10-21. It is intended that the different fracture types and deformation zone structural elements can be used in a modular fashion for constructing integrated models of radionuclide transport along flow paths within the rock.

It should be noted that the data in the retardation model is given for different fracture classes and deformation zone elements hosted in specific rock types. Although it is possible to define additional subdivisions in the data based on concepts of rock domains, fracture domains, and hydraulic rock domains this has not been pursued for the Laxemar transport properties site descriptive model. The main motivation for this is the strategy set out for the retardation model site descriptive model /Widstrand et al. 2003/ which prescribes a mineralogy-based approach. Some supplementary data sets are compiled in /Crawford and Sidborn 2009/ for *in situ* formation factors organised according to rock domain (RSM), fracture domain (FSM), and hydraulic rock domain (HRD) where feasible. Owing to incomplete coverage, however, data are not available for all FSM and HRD domains defined by geology and hydrogeology, respectively.

In this section, the material property data are characterised in the form of mean values \pm standard deviation of the measurement data. The full sorption data set in the Sicada database will be subsequently used as a basis for selection of site-specific data which will be used for stochastic parameterisation of transport models. /Crawford and Sidborn 2009/ provide additional statistics for the relevant material property parameters.

This section should be regarded as a proposal for how to formulate a descriptive and semi-quantitative retardation model based on the available database. The proposals for the selection of data are given, however, with acknowledgement of the qualitative and quantitative uncertainties in the retention parameters derived. This caveat implies that the model does not provide exact and detailed guidelines on how to “dress” the geological and hydrogeological models with transport parameters using the retardation model tables. The retardation model should be regarded as an overview of the interpreted site-specific information on retardation parameters, intended to provide a basis for the formulation of alternative parameterisations or necessary simplifications within safety assessment modelling.

10.5 Flow-related transport properties

10.5.1 Conceptualisation of flow paths

As discussed previously, long-range solute transport in fractured rock takes place in advective flow channels hosted within fractures and deformation zones. Matrix diffusion coupled with sorption has been identified as the main retardation process that limits the rate at which solutes are transported along these flow paths. The greater the surface area in contact with flowing water (the so called “flow-wetted surface”, or *FWS*) for a given water flow rate, the greater the interaction will be with both the fracture surface and the rock matrix. Within SDM-Site the flow-wetted surface to flow ratio is referred to as the “F-factor” /Andersson et al. 1998/ or “hydrodynamic transport resistance”. The F-factor is a key parameter governing the transport of radionuclides within fractured rock.

In the analyses presented in SDM-Site, transport is conceptualised to occur along advective flow paths in a multi-compartment system. The three compartments assumed in the transport model are:

1. The non-engineered near field (NNF).
2. The immediate far field (IFF).
3. The distant far field (DFF).

In this model, the non-engineered near field (NNF) is assumed to comprise approximately the first few metres or so from a canister position intersected by one or more low transmissivity fractures to the nearest significant conductive structure within the fracture domain containing the hypothetical repository. The distance of 10 m assumed in the scoping calculations made in /Crawford and Sidborn 2009/ is arbitrary although thought to be a reasonable order of magnitude estimate of the average distance for a “typical” transport path in the NNF that might dominate radionuclide transport from a hypothetical repository.

The immediate far field (IFF) is assumed to comprise the first 100 m in the fracture domain containing the hypothetical repository. The choice of 100 m is purely intended for illustrative purposes and may not necessarily coincide with forthcoming repository layout designs. Since fractures featuring high transmissivities are likely to be avoided when selecting canister deposition holes, typical flow paths within the IFF should, on average, have higher transmissivities than flow paths within the NNF and therefore these have been treated separately. The IFF has flow properties corresponding to the hydraulic rock domains parameterised in the hydrogeological DFN supplied by hydrogeology (/Rhén et al. 2008/ and Section 8.5.2).

The distant far field in the present context is taken to comprise the deterministic deformation zones surrounding the repository volume. The hydrogeological properties of these zones are also described in /Rhén et al. 2008, 2009/ and Section 8.4.

A conceptual illustration of the possible sequence of flow paths extending from a canister position to the near surface is shown in Figure 10-8. Transport pathways in surface systems and the top 100 m of the bedrock aquifer are neglected in the scoping calculations since these upper regions of the rock are not expected to contribute significantly to the overall hydrodynamic transport resistance of migration pathways. The term “near surface” is therefore taken to represent the upper bedrock aquifer at depths shallower than 100 m.

The demarcation of the transport system into a three-stage compartment is used here purely for illustrative purposes and for making scoping calculations to account for where the main hydrodynamic transport resistances are encountered in the bedrock. In safety assessment, the hydrogeological models and material properties parameter tables are used directly in an integrated model to simulate radionuclide migration in the bedrock without the need for compartmentalisation in the fashion employed here.

Transport from a hypothetical repository at elevation -500 m to the near surface (which is taken to be at an elevation of -100 m) is considered for the analyses of hydrodynamic transport resistance presented here. Most of the hydrodynamic transport resistance is encountered at greater depths within the repository volume and the lower reaches of the deterministic deformation zones. Therefore, the neglect of possible highly transmissive features (e.g. horizontal sheet joints, etc) in the upper part of the bedrock does not substantially influence the estimated overall F-factors.

Within safety assessment, alternative scenarios of radionuclide transport are considered. One of these is the possibility of a deliberate or accidental anthropogenic intrusion. In such a situation, transport via the deterministic deformation zones may be bypassed completely. Although this is discussed briefly in /Crawford and Sidborn 2009/, no specific calculations are made for such flow paths, as these are considered to be more of a safety assessment character and not strictly part of the site descriptive model.

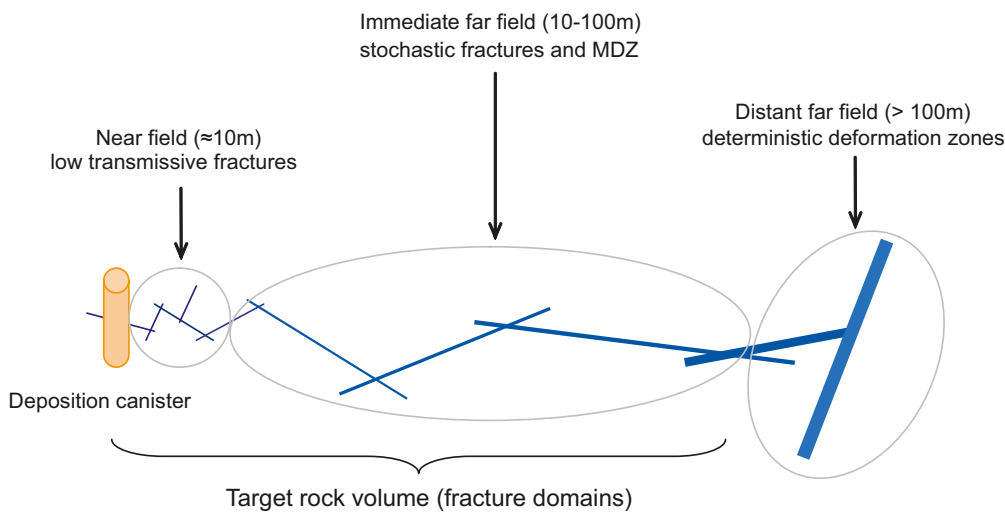


Figure 10-8. Illustration of a potential flow path from a hypothetical repository to the near surface (defined here as depth shallower than 100 m). Transport is conceptualised to occur along a sequence of flow paths featuring increasing transmissivity.

10.5.2 F-factor estimation

In the overall modelling strategy, F-factor estimations are made for each sub-compartment of the hypothetical transport path assuming a pre-defined set of reference conditions. In the calculations presented here, a local hydraulic gradient of 1% is assumed as a reference condition for each sub-compartment. This allows comparisons to be made of the relative importance of different compartments given different scenarios for the local hydraulic gradient. The relevant F-factor for the complete transport path is given by the sum of the F-factors for each compartment assuming that transport occurs through a sequence of connected flow paths as outlined previously. As described in /Crawford and Sidborn 2009/, the F-factor for the whole flow path or individual compartments can be linearly rescaled to give estimates for different hydraulic gradients. Based on topographical considerations, a hydraulic gradient of about 4% is thought to be a reasonably representative estimate for the regional flow system at repository depth. To facilitate simplified comparisons with the corresponding calculations for Forsmark presented in /Crawford 2008/, however, a value of 1% has been assumed in the scoping calculations. This figure is assumed *a priori* as a reference hydraulic gradient for each of the sub-compartments in the flow-related transport properties modelling evaluation.

The F-factors thus calculated are considered to be simple comparative estimates of the hydrodynamic resistance characterising typical flow paths in each sub-compartment and should not be taken to be realistic F-factors for safety assessment purposes. There are, for example, good reasons to specify different hydraulic gradients within different model sub-compartments, which could mean as much as order of magnitude variations in the calculated F-factors. It should be clearly noted that the forgoing discussion concerning appropriate local hydraulic gradients does not affect larger, regional scale simulations where the hydraulic boundary conditions are well characterised. In such simulations and those to be used in safety assessment, spatially variable local gradients arise naturally due to the distribution of differently conductive elements in the hydrogeological model and do not need to be considered explicitly. This can be seen in the results for the particle tracking described in Section 10.5.3 where the local hydraulic gradient can be seen to vary considerably over the length of a typical transport path. In the particular example shown in Figure 10-18, the local hydraulic gradient (described as hydraulic potential in the paleosimulations due to the additional effect of variable fluid density) varies from less than 0.1% to nearly 4%, although with an average $\sim 0.3\%$.

The central best estimate F-factor for typical flow paths in the NNF is roughly 10^5 yr/m, although values could range from as little as 10^3 yr/m to as much as 10^7 yr/m. These estimates, however, are dependent on different assumptions of path length, hydraulic gradient, and fracture transmissivity which in turn are highly constrained by the, as yet, largely undetermined repository layout and acceptance/rejection criteria for individual canister holes. The values discussed here should therefore be considered as speculative, “what if” type calculations rather than prognostic F-factors for an actual repository.

Stochastic realisations of the hydrogeological DFN model within a hypothetical voxel of side length 100 m indicate that the fractured rock is relatively well connected hydraulically although with a certain degree of anisotropy along different axes (for different orientations of the applied hydraulic boundary conditions). Figure 10-9 shows the probability of existence (referred to as the percolation probability) of at least one hydraulically connected structure spanning the modelled domain for 100 stochastic realisations of the hydrogeological DFN for HRD_C shown here as a typical example.

Hydraulically connected DFN realisations were converted to an equivalent pipe network and the path of least transport resistance, PLTR was calculated for each realisation using graph theory for the case of neutrally conductive fracture intersections as well as highly conductive fracture intersections. An example of typical F-factor ranges calculated using this method is given in the left-hand image in Figure 10-10 for a 1% hydraulic gradient applied along the EW axis assuming the semi-correlated (SC), fracture size-transmissivity model and a 100 m transport distance. Corresponding results for the same rock volume, although obtained using the particle tracking capabilities of Napsac/ConnectFlow (and only considering (non-enhanced) neutrally conductive fracture intersections) are shown in the right hand-image of the same figure.

The voxel calculations made using the hydrogeological DFN generally gave F-factors in the range of about 10^3 – 10^5 yr/m (on average $\sim 10^4$ yr/m) with only very minor differences between the various hydraulic rock domains at the Laxemar site.

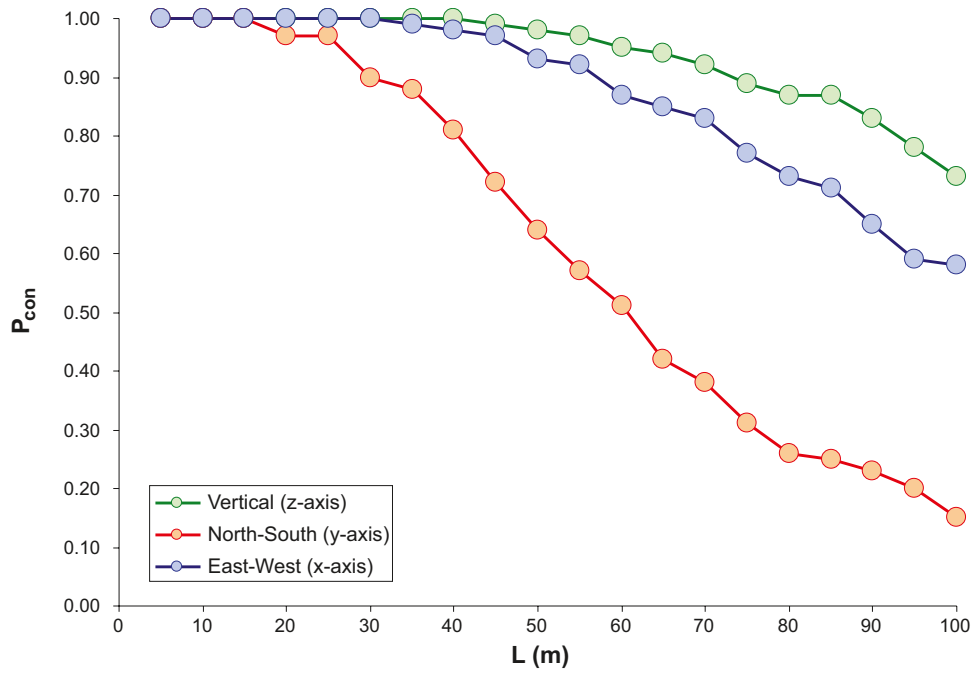


Figure 10-9. Results of connectivity analysis for HRD_C (-400 m to -650 m) based on 100 stochastic realisations of the hydrogeological DFN model. The percolation probability for the existence of at least one or more conductive structures is plotted as a function of distance for the three principal axes of the model (The percolation threshold is stochastically defined as the point where the percolation probability is 50%).

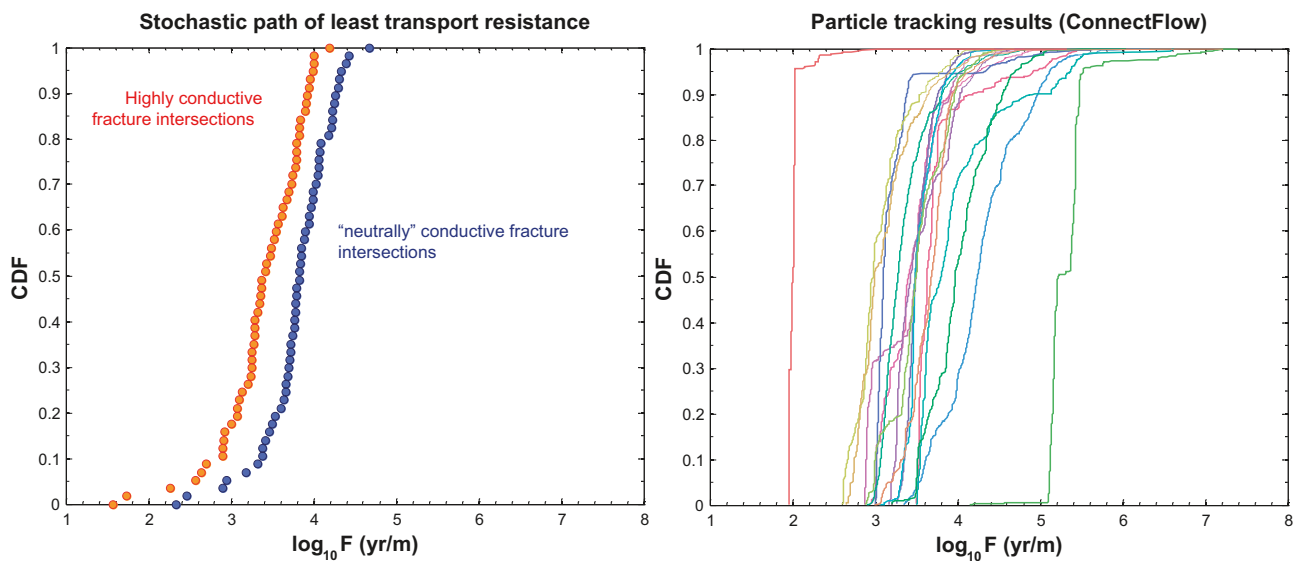


Figure 10-10. The left-hand image shows typical F -factor ranges (given as a cumulative distribution) for paths of least transport resistance in the immediate far-field (100 stochastic realisations of the hydrogeological DFN for HRD_C in the depth zone -650 m to -400 m). The right hand image shows typical particle tracking results obtained using ConnectFlow (20 stochastic realisations) for the same rock volume, although considers neutrally conductive fracture intersections only. The calculations are based on a 100 m transport distance and a semi-correlated fracture length-transmissivity (SC) model with a 1% hydraulic gradient applied along the EW axis.

Based on the hydrogeological description of deformation zones presented in /Rhén et al. 2008/, a simple analytical estimate can be made for the F-factor of typical flow paths found within the deterministic deformation zones. Here, two different modelling approaches have been adopted. The first modelling approach is based upon a simplified 2D representation of the zone where the flow-wetted surface is assumed to be comprised of the two surfaces bounding the zone and borehole measured transmissivities are assumed to correspond to point samplings of the transmissivity of the 2D flow structure. The other approach uses statistics of flow channel (PFL) frequencies together with estimated hydraulic conductivities over the thickness of the deformation zone in a 3D (streamtube) representation. Both model representations assume a depth dependency in hydraulic transmissivity or conductivity that can be described as a power law or exponential decrease. It can be argued that the 2D approach tends to overestimate the flow connectivity of the system and underestimates the available flow wetted surface thereby possibly underestimating the potential hydrodynamic transport resistance. The 3D representation, on the other hand, assumes that the flow in the zone samples the entire flow-wetted surface in an uncorrelated manner, which could give an overestimate of the hydrodynamic resistance.

For radionuclide release at an elevation of –500 m within the deformation zone and a hydraulic gradient of 1%, typical F-factors for transport to the near surface (–100 m) are estimated to be roughly in the same ranges as those calculated for the hydraulic rock domains. Since a large amount of the variation in F-factors estimated for the HCD relates to differences in underlying modelling assumptions in the 2D and 3D representations, it is not possible to determine with certainty whether the dominant hydrodynamic transport resistance is related to the hydraulic rock domains (in the depth zone –650 m to –400 m where the hypothetical repository is assumed to be situated) or deformation zones comprising the HCD /Crawford and Sidborn 2009/. In /Crawford and Sidborn 2009/ scoping calculations are also presented for advective transport times along typical flowpaths where a number of different transport aperture-transmissivity relations have been considered. The scoping calculations indicate advective transport times for the composite transport paths from a hypothetical repository to the near surface ranging from as little as few years to slightly more than a century with the bulk of the advective travel time being accumulated in the deterministic deformation zones. These are expected to have a substantially larger kinematic porosity than hydraulic rock domains and are therefore found to dominate the advective transport times in the simplified scoping analyses.

The F-factor is calculated in hydrogeological models as the pathline integrated inverse of the transport aperture and fluid velocity product. In an ECPM representation it is calculated as the formally equivalent, pathline integrated ratio of specific flow-wetted surface and Darcy flux. Since there is an inverse relation between transport aperture and flow velocity, the choice of transport aperture does not have a direct impact upon the calculation of the F-factor owing to mutual cancellation of aperture terms. This is predicated upon the use of flow statistics of the rock being used as a primary basis for calculations. In SDM-Site Laxemar, flows are considered to be a primitive since they are directly observable in boreholes and are used to condition the properties of the hydrological DFN. Transport apertures and advective travel times are then derived which are statistically consistent (via various empirical power laws) with the modelled transmissivities and flowrates. The uncertain value of the transport aperture is only an issue for the calculation of F-factors if one works back from physical apertures to derive hydrogeologic properties. The consequences of the various assumptions underlying the derivation of F-factors and advective travel times are, however, discussed in more detail in /Crawford and Sidborn 2009/.

10.5.3 Particle tracking results from paleohydrogeological simulations

Particle tracking calculations performed in conjunction with ECPM simulations of the regional hydraulic model using Connect Flow indicate somewhat larger F-factors than the three-compartment scoping calculations would otherwise suggest. Some typical ECPM particle tracking results for solute release within the focus volume at –500 m elevation are shown in Figure 10-11. These are based upon the trajectories of particles calculated for a flow field frozen in time at the conclusion of the paleohydrogeological simulations described in /Rhén et al. 2009/.

The distribution of F-factors for particles released within HRD_C is given in Figure 10-12 for the particles which arrived at the surface exit locations. The corresponding distribution of advective travel times is given in Figure 10-13.

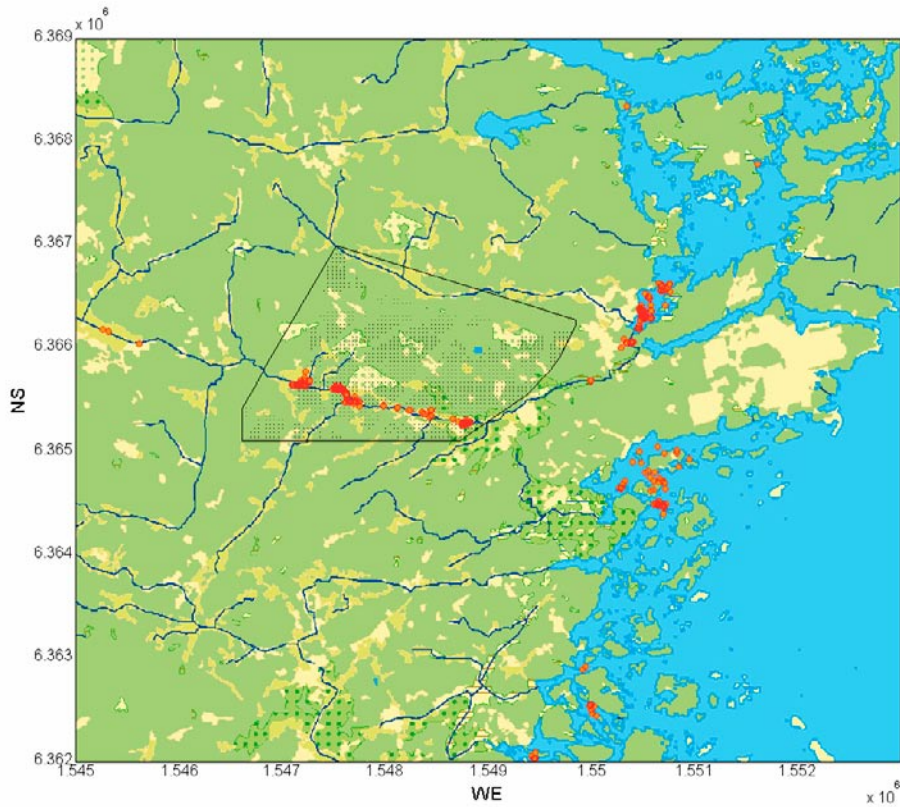


Figure 10-11. Visualisation of surface exit locations (red markers) for particles released at -500 m within HRD_C (polygon outline). The small grey markers within the release area correspond to the actual release locations considered in the particle tracking calculations.

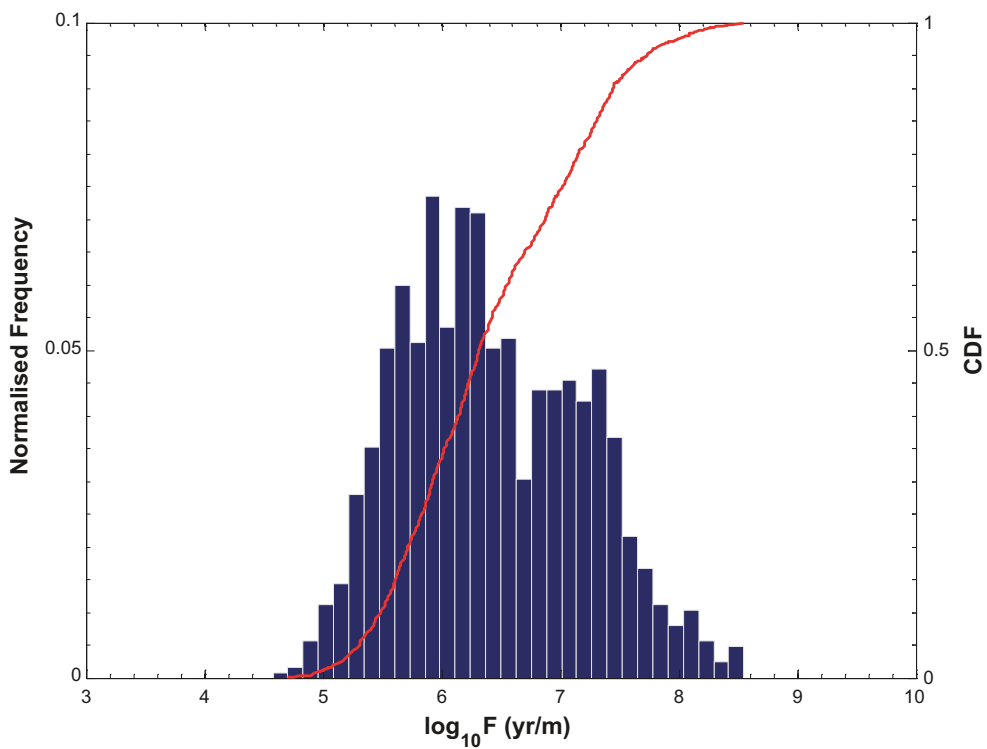


Figure 10-12. F-factor (yr/m) distribution at release locations calculated with ConnectFlow for solute release at -500 m elevation within HRD_C (based on the regional scale Base Case simulations simulation /Rhén et al. 2009/). The simulated data are shown as a histogram and empirical cumulative distribution function (CDF).

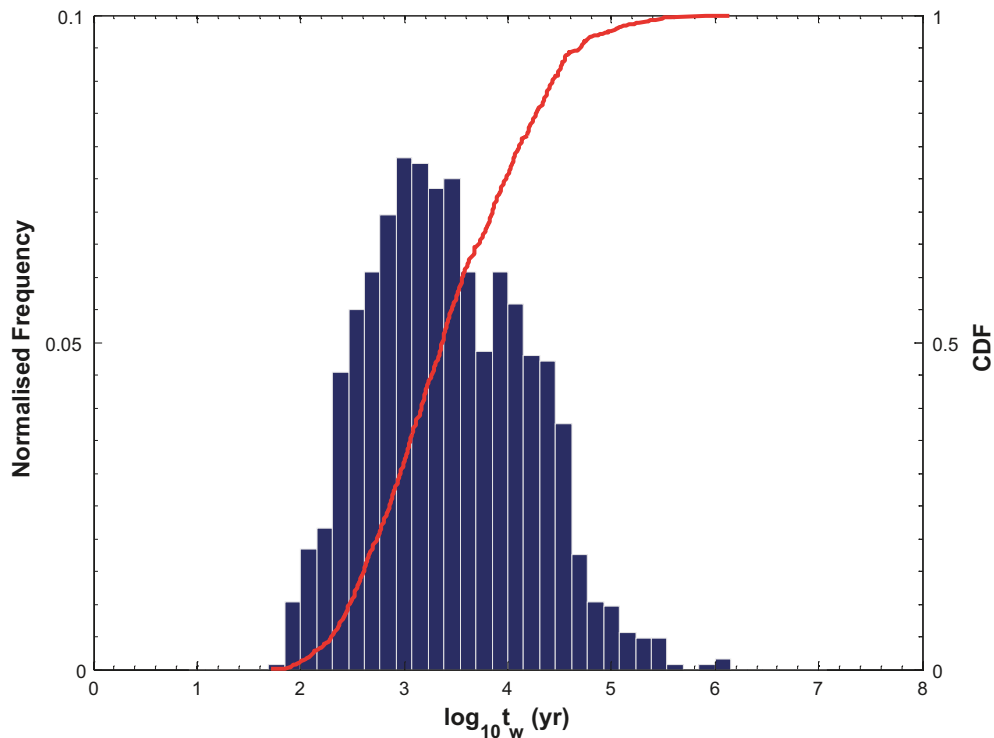


Figure 10-13. Advective travel time, t_w at release locations calculated with *ConnectFlow* for solute release at -500 m elevation within *HRD_C* (based on the regional scale Base Case simulation /Rhén et al. 2009). The simulated data are shown as a histogram and empirical cumulative distribution function (CDF).

The single particle track shown in Figure 10-14 is a typical example of a transport path from the hypothetical release area.

It is interesting to note that the particle follows an initially upwards trajectory before turning and following a downwards trajectory beneath the elevation of the hypothetical repository until it reaches deformation zone ZSMNE005A at roughly -700 m elevation whereupon it tracks roughly NE via an intermediate HRD volume (external to *HRD_C*) and deformation zone ZSMNE004A before exiting to the surface via deformation zone ZSMNE006A.

Figure 10-15 shows the path integrated value of the F-factor plotted against the transport path length, with the different structural elements encountered by the particle colour coded and labelled.

In the case of this specific particle release location, most of the hydrodynamic resistance appears to be encountered within the HCD accounting for roughly 80% of the total F-factor accumulated along the transport path. A large part of the F-factor accumulated by the particle occurs at depths below the release location where the HCD exhibits relatively low hydraulic conductivity. Certain particles, however, migrate via near vertical transport paths and only encounter HCD structures in the top 100–200 m of the bedrock. In these cases, the bulk of the F-factor is accumulated within the HRD and the near surface HCD structures make a negligible contribution to the cumulative F-factor for the migration path.

The corresponding cumulative advective travel time for the particle is shown in Figure 10-16 as a function of migration path length.

As can be seen in Figure 10-16, the advective travel time for the particle shown is dominated by transport in the deterministic deformation zones with only about 10% attributable to transport in the hydraulic rock domains. Since the advective travel time is equal to the product of the F-factor and average transport half-aperture along a pathline, the close correspondence between the appearance of Figure 10-15 and Figure 10-16 is to be expected. The relation between the F-factor and advective travel times can be shown more clearly by making a cross-plot comparison as in Figure 10-17.

The difference in local hydraulic potential encountered by the particle is shown in Figure 10-18 as a function of migration path length, while the cross-plot of hydraulic potential difference versus local mean hydraulic conductivity (for an assumed *in situ* temperature of 12°C) is shown in Figure 10-19. For most of the migration path the local hydraulic gradient is less than that assumed in the scoping calculations (1%) described previously. There is, however, a short interval where the hydraulic gradient is significantly higher than 1%. The cross plot of hydraulic potential versus hydraulic conductivity (and elevation) does not give any indication of depth dependency.

For groundwater recharge pathways characterised by low F-factors (less than about 10^5 yr/m), the matrix retardation of an intruding meteoric water mixing front is very weak or non-existent. Here, the advective transport time dominates the transport of salt with transport times varying from as little as a few years up to perhaps some hundreds of years for very high transport apertures. In a safety assessment perspective and also for the transport of salt in the paleosimulations, this is very fast and for all practical purposes can be considered to be an almost instantaneous transport process.

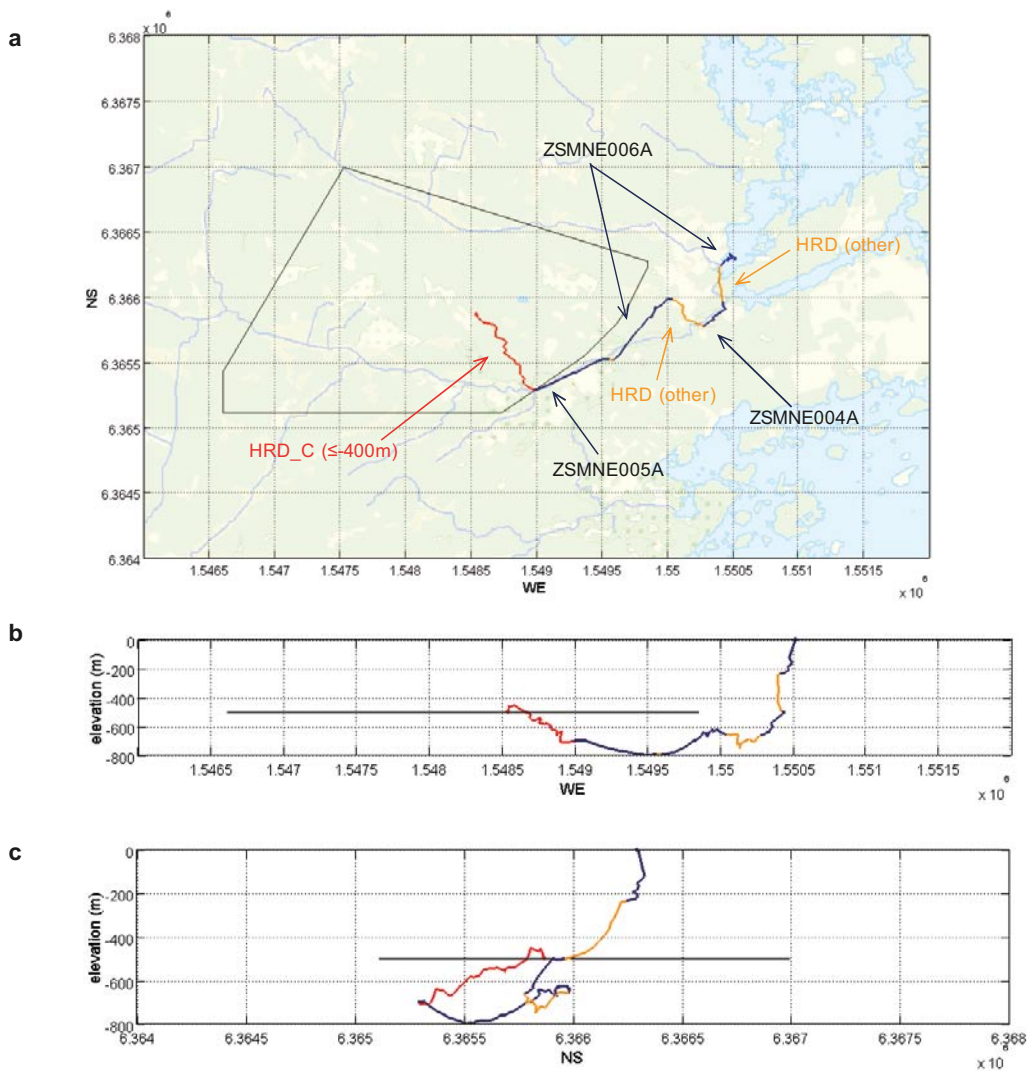


Figure 10-14. The transport path taken by a single particle seen from above (a) as well as a cross-sectional view from a vantage point facing South (b) and facing West (c). The path line is coloured with regard to structural encountered by the particle on its way to the surface exit location, i.e. red for HRD_C (≤ -400 m), dark blue for deterministic deformation zones, and orange for subsidiary HRD volumes as defined in the ECPM model. The outline of the particle release area is shown as a grey polygon at -500 m elevation.

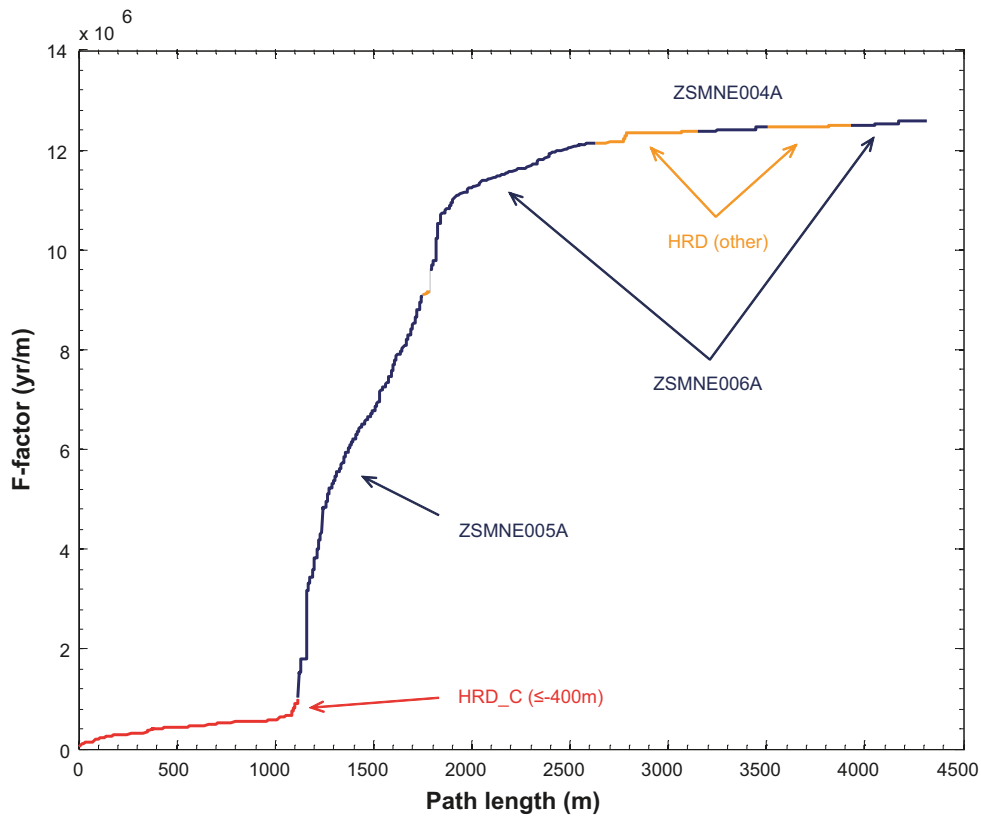


Figure 10-15. Cumulative F-factor as a function of migration path length for an individual particle representing a typical transport path. Different structural elements encountered by the particle along its migration path are colour-coded and labelled in the figure.

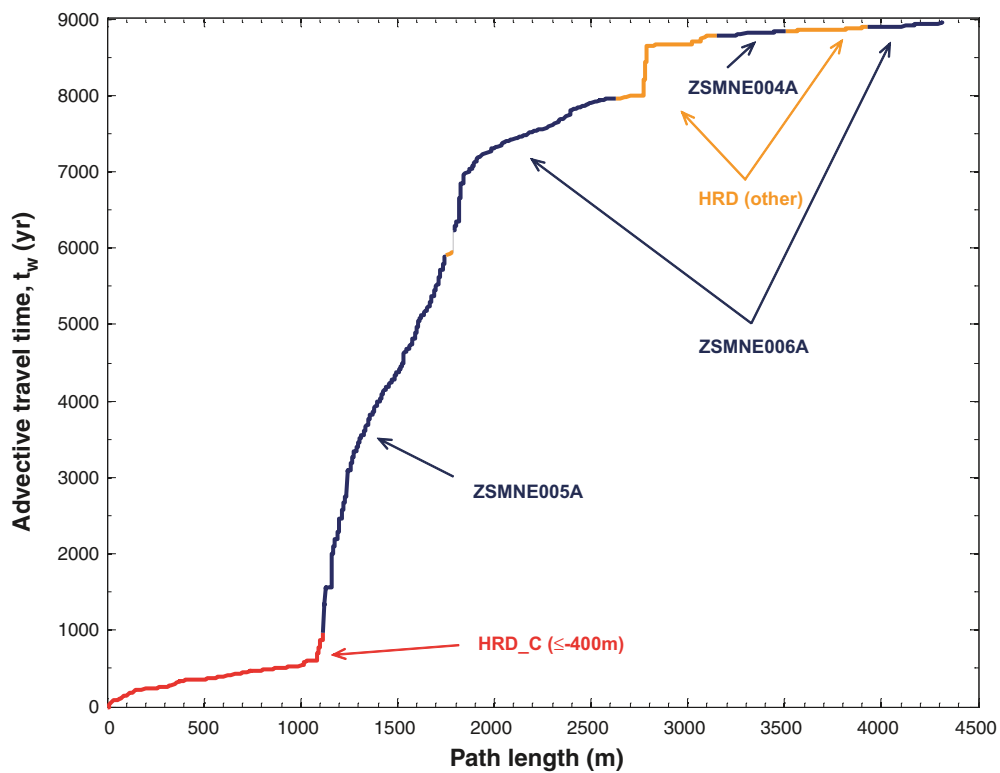


Figure 10-16. Cumulative advective transport time as a function of migration path length for an individual particle representing a typical transport path. Different structural elements encountered by the particle are colour-coded and labelled in the figure.

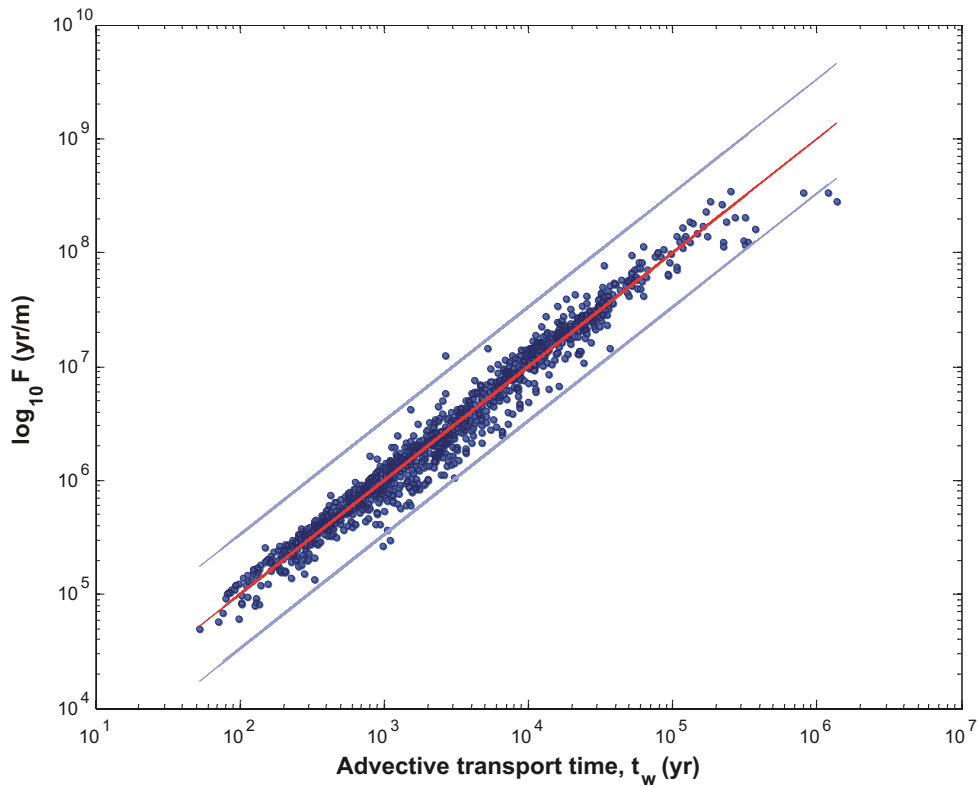


Figure 10-17. Cross plot showing the correlation between the pathline integrated F -factor and advective travel time. The red trend line shows the relation between F -factor and advective travel time for an average transport aperture of 2 mm. The upper and lower trend lines bounding the data correspond to transport apertures of 0.6 mm and 6 mm, respectively.

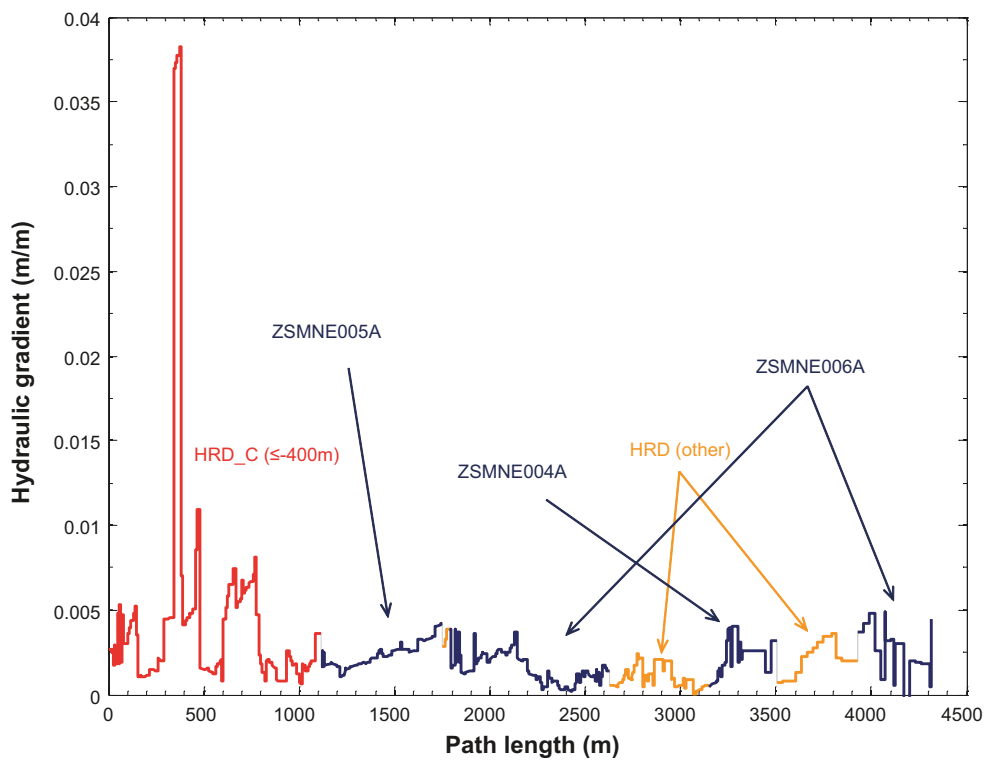


Figure 10-18. Local hydraulic gradient (m/m) experienced by the particle as a function of migration path length. Different structural elements encountered by the particle are colour-coded and labelled in the figure.

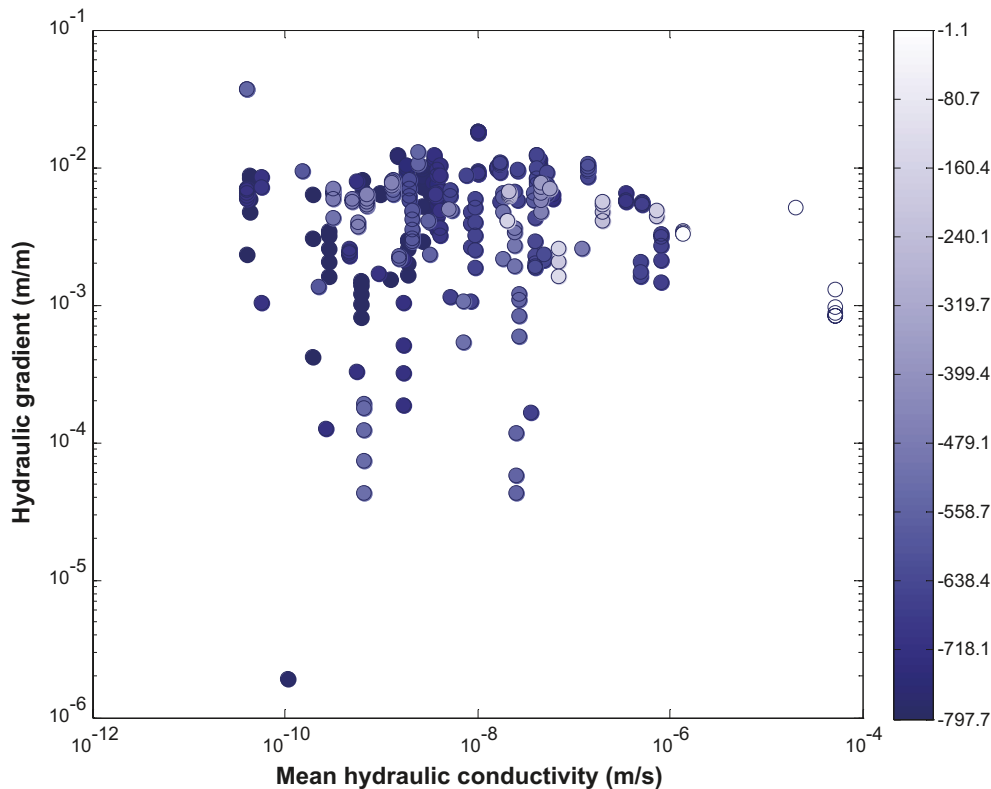


Figure 10-19. Cross-plot of the local hydraulic gradient (m/m) experienced by the particle along its migration path versus the local mean hydraulic conductivity (m/s) of the bedrock at that location. The symbols are shaded according to elevation (m) as specified in the colour bar at the right-hand side of the figure.

This is essentially a flushing regime whereby saline water initially resident in the fracture system can be rapidly displaced by intruding meteoric water in an almost plug-flow manner. In these cases, the meteoric water mixing front is sharp and its penetration depth into the fracture system is governed entirely by the advective travel time for the recharge. Since the advective travel time is much less than the paleosimulation time-span for all reasonable transport apertures, the kinematic porosity has no discernable effect on the present-day salt distribution for F-factors of this magnitude.

Although the matrix diffusion retardation of the mixing front is very weak in these cases the impact on salt inventory in the rock matrix can, nonetheless, be large in the vicinity of fractures since salt can still diffuse out of the rock matrix into the dilute, fast-flowing water in the fractures. The impact on the overall matrix salt inventory, however, also depends upon the volumetric intensity of flow-bearing fractures since the diffusive penetration depth associated with a 10,000 yr contact time is expected to be at most a couple of metres for the estimated effective diffusivity of the rock matrix. If the fracture intensity is very high, the total amount of salt mobilised from the rock matrix may be very large, whereas if the fracture intensity is low, the total amount of salt mobilised might be small.

For groundwater recharge pathways characterised by very high F-factors (exceeding about $\sim 5 \cdot 10^6$ y/m), on the other hand, the matrix retardation effect is sufficiently strong that the downwards rate of propagation of the mixing front should be relatively unchanged by the kinematic porosity. Here, the meteoric water mixing front is sharp and typically has a width less than about 10% of the recharge path length. In these cases, the meteoric water never reaches great depths and since the fracture water remains saline there is little tendency for leaching of salt from the matrix downstream of the mixing front. Although the retardation of the mixing front by matrix diffusion is described as being strong, the overall impact of matrix diffusion on the salt inventory in the rock matrix can be shown to be very weak.

For recharge pathways featuring intermediate F-factors in the range $\sim 5 \cdot 10^5$ to $\sim 5 \cdot 10^6$ yr/m, the transport aperture can have a non-negligible effect on the depth of propagation of the mixing front if the associated advective travel times are roughly of the same magnitude or greater than the

paleosimulation time itself. Here, the matrix retardation effect gives a diffuse, almost linear mixing front with a width roughly of the same scale as the recharge path length. The kinematic porosity can modify the location of the mixing front termination point and the apparent mixing front width if the advective travel time is sufficiently long that less than a pore volume flows through the system during the paleosimulation time-span (which would be the case for advective travel times greater than about 10,000 yr).

A more detailed discussion concerning advective transport times, matrix diffusion, and the consequences for salt transport and for sorbing and non-sorbing radionuclides in safety assessment can be found in /Crawford and Sidborn 2009/.

10.5.4 Flow channelling

A number of different forms of flow channelling have been considered, both in the evaluation of typical F-factors for flow paths from the repository and with regard to the consequences for radionuclide migration when propagated forward in the transport models. These are discussed in detail in /Crawford and Sidborn 2009/ although a short summary of some of the main issues is given below.

One main type of flow channelling considered occurs on the scale of the fracture network itself and arises due to the tendency of heterogeneous fracture networks to exhibit poor hydraulic connectivity and form preferential flow paths. This type of flow channelling is internalised in the description of the hydrogeological DFN and emerges spontaneously in individual realisations of the model.

Other types of flow channelling occur on much smaller spatial scales and are not explicitly incorporated in the models supplied by hydrogeology. These additional flow channelling effects are of some importance since they could potentially give rise to flow censoring effects in borehole investigations and lead to biases in the synthesis of hydrogeological DFN models. Specifically there are two issues; 1) flowing channels may be completely missed owing to their limited width and the low probability of a direct borehole intersection, and 2) those flowing features that are identified may appear to support lower flow rates than in actuality owing to the low transmissivity of structures in which they are hosted. These are referred to in the following paragraphs as “Type 1” and “Type 2” flow censoring effects, respectively.

The most common type of small-scale flow channelling phenomenon, referred to here as “in-plane” flow channelling, relates to the tendency for preferential flow paths to form within variable aperture fractures where *in situ* normal stresses and shearing history result in partial closure due to variable surface asperity contacts. These specific types of flow channels are dynamic in nature and cannot be considered as physical pipes. Their existence and distribution is strongly influenced by the hydrogeologic boundary conditions. Scoping calculations detailed in /Crawford 2008/ indicate that such flow channels should be sufficiently well-connected hydraulically throughout the pore space of fractures that, for the most part, they will be readily identified from investigation boreholes without significant censoring effects.

This projection is based on consideration of the fact that fracture transmissivity appears to decrease strongly with increasing surface contact fractions up to the percolation limit which occurs at a contact area fraction of about 50%. For highly compressed fractures approaching the percolation threshold, the maximum censoring effect would amount to an underestimation of the flow channel frequency of about 50% if the probability of a borehole randomly intersecting a physically closed section of the fracture is considered. It is noted, however, that such fractures are also the least likely to support flows above the detection limit. For less compressed fractures, which are also more likely to exhibit non-negligible flows, the censoring effect is expected to be substantially less. This simple analysis, however, assumes that fracture filling materials do not fill the void flow space to such an extent that the underlying assumptions of the scoping calculations are violated.

Other categories of “pipe-like” flow channels such as those hosted within fault step-overs, shears and fracture jogs may be less likely to be observed directly by an investigation borehole given their limited physical dimensions. Similarly, fast flow channels possibly hosted at and along fracture intersections enlarged by tectonic events and hydrothermal weathering would most likely not be directly intersected by investigatory boreholes. The probability of detecting such features is then largely dependent on the permeability of surrounding fractures with which they are hydraulically connected.

Since such pipe-like flow channels are of finite length and hosted as sub-structures within fractures, they generally cannot form continuous (i.e. unbroken) flow paths through the fracture domains. Such features therefore need to be relatively well connected to the wider fracture network via in-plane flow channels hosted in single fractures in order for flow to occur.

Generalised radial flow analysis of PSS hydraulic responses in packed off borehole sections suggest that most flowing features (> 90%) on a 5 m test scale are associated with flow dimensions greater than 1.5 and only a small fraction exhibit smaller flow dimensions symptomatic of approximately linear flow channelling /Rhén et al. 2008/. Although it is likely that some flow channels are missed, this result is in general consistent with the notion of a hydraulically well-connected flow space within fractures.

Although this appears to suggest that “Type 1” flow censoring effects as described above might not occur, it is not possible to rule out the presence of calcite dissolution features in partially annealed fractures containing large amounts of readily solubilised calcite fracture fillings. Such features could form fast, persistent flowpaths of narrow extent and may not be easily identifiable from borehole investigations.

In the transient analyses reported by /Rhén et al. 2008/ (see also, Section 8.3.3), roughly 20% of the 5 m test sections gave indications of positive skin effects or recharge boundaries which could be interpreted to be indicative of strongly transmissive, nearby flow channels hosted in less transmissive features (i.e. where the borehole happens to intersect a less transmissive region of the flow space). It is therefore not possible to strictly rule out “Type 2” flow censoring effects in the available hydrogeological data set although it appears likely that this only influences a minority of identified features.

Based on this reasoning, it is speculated that network-scale flow channelling effects probably dominate, although the other more localised flow channelling effects described above are also likely to be present in Laxemar. Resolution of this issue may not be possible until the construction of an underground opening since many aspects of flow channelling cannot be properly quantified from a surface based site investigation. From a tunnel, for example, it is sometimes possible to directly observe individual flow channels and statistics of fracture trace lengths which can be used to partially validate the choice of power law slope which is treated as a fitting parameter in the hydrogeological DFN modelling based upon borehole data. It should be noted, however, that even *in situ* observations are subject to substantial bias effects owing to stress redistribution and excavation damage which can have an impact on the distribution and extent of flow channelling observed in a tunnel.

Nevertheless, it is possible to approximately calculate the likely spatial distribution of different kinds of specific flow channel features from the geological information used in construction of DFN models. Scoping calculations of the possible existence of highly conductive fracture intersections, for example, have been made in the main background report /Crawford and Sidborn 2009/ using the hydrogeological DFN model provided by hydrogeology. In a forward modelling perspective, it is found that such features should not have a significant detrimental impact on transport properties, provided they do not form a contiguous flow path through the rock (see, for example, Figure 10-10).

On balance it is thought that although flow channelling might lead to the underestimation of the frequency of flow bearing features, it will probably make little difference to the order of magnitude of the hydrodynamic transport resistance provided that there is reasonable confidence in the transmissivity model for hydrologic features parameterised within the hydrogeological DFN. Since it is thought that Type 2 flow censoring effects might only affect a small minority of PFL-tested sections, this seems a reasonable conjecture. It is also supported by cross-plot comparisons of transmissivities derived from PFL measurements and those obtained from transient PSS analysis which show reasonable order of magnitude correspondence indicating that the assumption of radial flow dimension in PFL testing does not lead to significant errors /Rhén et al. 2008/.

The consequences of flow channelling phenomena have also been considered within a forward modelling perspective for the transport of solutes. Several model alternatives based upon the assumption of narrow flow channels are discussed in the following section.

10.6 Transport of radionuclides

Coupling of the F-factor estimates from the hydrogeological modelling with the retardation model allows for the prediction of typical transport times for key radionuclides. The transport models described in this section consider advectively dominated flow and transport along a single flow path with diffusion and sorption within the rock matrix. Here, a flow path is considered to be a simple set of serially connected flow channels which may be narrow in width (on the order of cm to some tens of cm). In a full hydrogeological simulation of the transport problem as would be used in safety assessment, however, flow paths would be expected to bifurcate and join with other flow paths over different length scales giving rise to a distribution of F-factors and advective transport times. Such calculations are more of a safety assessment character and are not treated here (although it is noted that the distribution of different flow paths is obtained automatically from simulations of the full hydrogeological model as would be implemented in safety assessment). A full account of the transport modelling scoping calculations can be found in /Crawford and Sidborn 2009/.

If flow channels are narrow as expected, the one-dimensional description of matrix diffusion customarily used in safety assessment calculations is inaccurate and may underestimate radionuclide retardation. For this reason, three main scenarios are considered for the SDM-Site Laxemar radionuclide transport modelling. These are:

1. (Base model) Advective flow coupled with 1D diffusion/sorption within the rock matrix.
2. (Model Alternative 1) Advective flow in a narrow channel coupled with 1D diffusion/sorption in the rock matrix plus diffusion into a stagnant zone of limited extent and subsequent 1D diffusion/sorption within the rock matrix.
3. (Model Alternative 2) Advective flow in a narrow channel coupled with 2D radial diffusion/sorption in the rock matrix.

Along channelised flow paths hosted within fractured rock there may be “in-plane” stagnant zones as well as large numbers of open fractures, which although non-flowing, intersect the flow path. It is possible for transported radionuclides to diffuse into these regions and access additional surface area for mass transfer to the rock matrix. To avoid the possibility of double counting of matrix storage capacities and to improve modelling transparency, only in-plane diffusion accessible surface is considered in the present analysis. In the scoping calculations for model alternative 1, a flow channel width of 10 cm is assumed with a stagnant zone 1 m in extent within the plane of the fracture along 50% of the flow path (forthwith referred to as a 10:1 in-plane stagnant zone).

For model alternative 2, a channel width of 10 cm is considered without stagnant zones. In this case the diffusion front of solute migrating in the rock matrix will start to take on a noticeably radial character after it has diffused a distance into the rock matrix roughly comparable to the channel width. The 2D, radial diffusion of solutes can result in a substantially enhanced rate of diffusive uptake compared with that which would be predicted on the basis of the base case model incorporating 1D diffusion. The basic features of the base case model and both model alternatives are illustrated in Figure 10-20.

For the assumed hydraulic properties used in the estimation of the flow-related transport properties, it was not possible to unambiguously determine whether the bulk of the accumulated F-factor for transport resides in the HRD (immediate far-field) or HCD (distant far-field). Furthermore, it is noted that the ECPM calculations made using ConnectFlow generally give larger F-factors than those obtained using the simplified scoping models. Although part of this discrepancy can be related to the slightly higher hydraulic gradients in the scoping calculations than those that arise naturally in the fully integrated hydrogeological model, much of the difference appears to be due to the way in which the flow is distributed over the specific flow-wetted surface in an ECPM or streamtube representation (where full mixing over the discretisation volume is assumed). In the calculations presented in this section, an F-factor of 10^4 yr/m is assumed as a representative case. This is roughly the mid-range of typical F-factors calculated in the scoping calculations for composite flowpaths from a hypothetical repository to the near surface as described in /Crawford and Sidborn 2009/.

In the calculations presented here, simplified fractures are considered with rock matrix material properties roughly corresponding to the rock found in HRD_C while the impact of fracture coatings is neglected. It is likely that this simplification is conservative, since the increased hydrogeological and micro-structural complexity found within complex fractures featuring fracture coatings (and

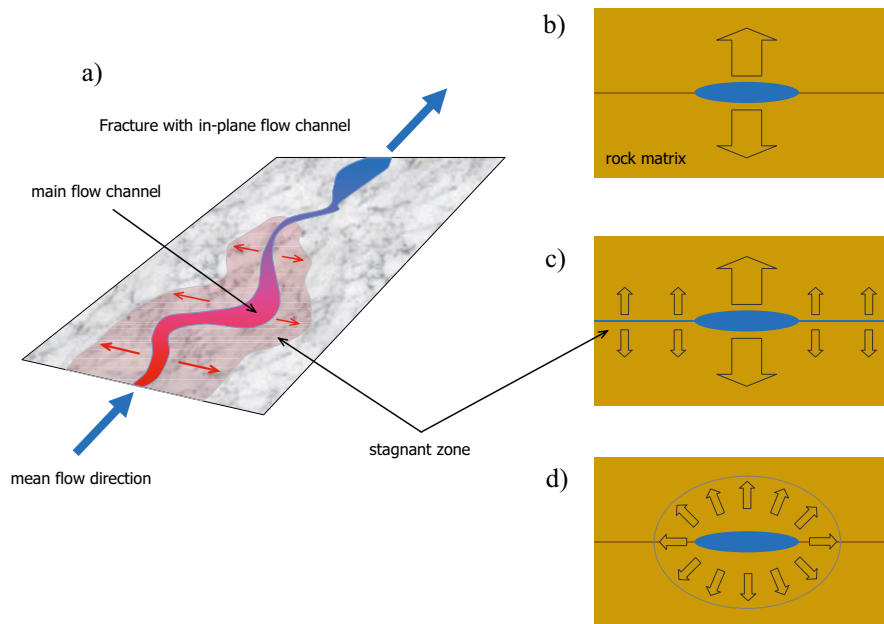


Figure 10-20. Schematic view (a) of a fracture hosting an in-plane flow channel of limited width with possible stagnant zones flanking the main flow channel. On the right hand side of the figure is a conceptual illustration of the diffusive mass transfer process corresponding to the base model (b), model alternative 1 (c), and model alternative 2 (d).

flowing features hosted in deformation zones) should, on balance, give rise to substantially greater retardation properties if fully considered in the analysis.

Figure 10-21 shows an example of typical residence times calculated for the different transport models assuming saline groundwater chemistry, a flow path F-factor of 10^4 yr/m, and a solute recovery fraction of 50% (i.e. the transport time for the first 50% of arriving solute). Here, a rock matrix formation factor $F_r \approx 1.1 \cdot 10^{-5}$ is assumed, which is typical of the mix of rock types found in HRD_C (based on data from *in situ* measurements) and the impact of sorption K_d value on the radionuclide transport time is calculated. Approximate, illustrative time limits for quantitative and qualitative safety analysis are shown as the red, broken and unbroken, horizontal lines in the figures. These may not necessarily conform to safety assessment time limits considered in SR-Site, although are loosely based on guidelines contained in /SSI 2005/.

Transport times longer than 10^7 yr (graduated, background shading) are considered to be of academic interest only and are included here to illustrate the relative scaling of recovery times implied by the modelled retardation processes. In addition, to give an appreciation of the time scales involved, some significant events in Earth's geological history are indicated on the time axis. Since these events have taken place in the past, they are intended to be interpreted in a relative sense with regard to the estimated transport times.

To illustrate the combined impact of K_d uncertainty and fundamental modelling assumptions for specific solutes, the span of transport times vs. K_d is plotted as a rectangular polygon in the figures. The lower left hand vertex of each polygon is the transport time of the model giving the fastest breakthrough using the lowest reported K_d value, whereas the upper right hand vertex corresponds to the transport time of the model giving the slowest breakthrough time for the maximum reported K_d value. Since there are too few measurements of sorption on individual rock types to give a sufficiently reliable span of K_d uncertainty, the depicted K_d ranges consider a pooling of data for all the main rock types (501030, 501036, 501046, 501056, and 511058) compiled in /Selnert et al. 2009/, see Table 5-1 for applicable rock type codes. It should be noted that the results presented in Figure 10-21 assume constant groundwater hydrogeochemical conditions which will not necessarily be the case, particularly over the very long time spans indicated. Since the K_d for specific solutes is often sensitive to changes in groundwater chemical composition, the estimated transport times shown here should be regarded as merely illustrative.

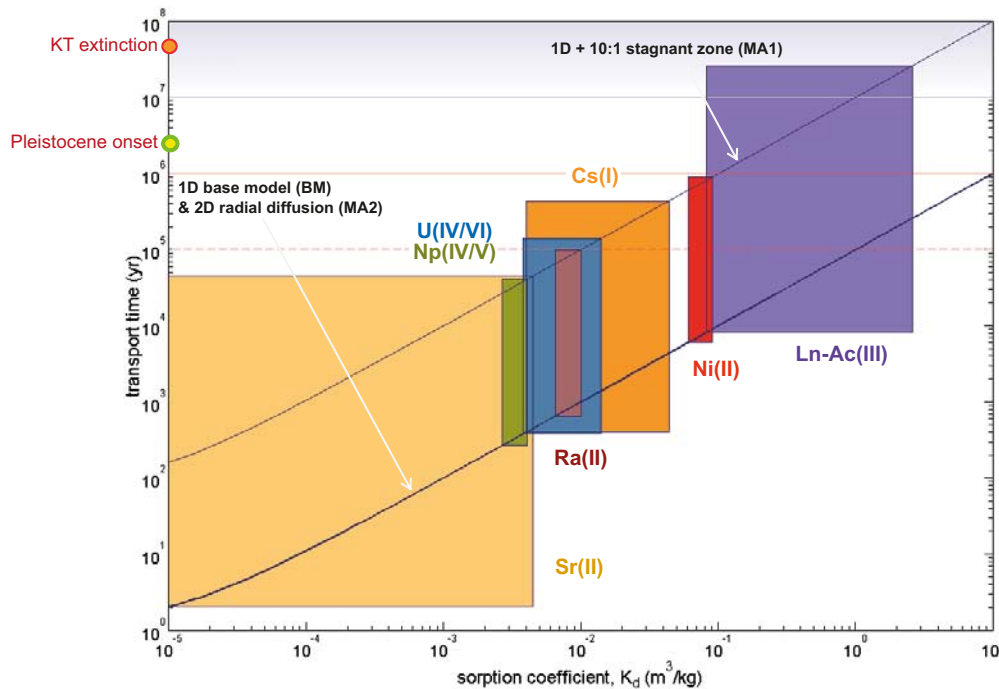


Figure 10-21. Typical radionuclide transport times (blue curves) as a function of sorption K_d for a recovery fraction of 50%, an F-factor of 10^4 yr/m, formation factor of $1.1 \cdot 10^{-5}$, and a maximum rock matrix depth of 2 m. Shaded polygons represent approximate range of variability for individual nuclides under saline conditions (see text for explanation). Relative timescales associated with various significant events in Earth's geological past are indicated on the time-axis.

Provided the groundwater composition is relatively constant, the estimated transport times for very strongly sorbing solutes (i.e. $K_d \gg 1 \text{ m}^3/\text{kg}$) are so long that the solutes could be considered, for all practical purposes, immobile. In such cases, colloidal and possibly bacterial siderophore¹ transport mechanisms may dominate the releases to the biosphere. For colloids, this will be particularly the case if sorption is deemed to be irreversible. In the case of reversible sorption, however, scoping calculations presented in /Crawford and Sidborn 2009/ indicate a negligible effect on radionuclide transport for the natural colloid concentrations to be found in groundwater at repository depth.

Bacteria capable of excreting siderophores have been cultivated from deep groundwater samples obtained at the Äspö HRL /Johnsson et al. 2006/, although it is not currently known whether there is a non-negligible background concentration of these complexing agents within the groundwater from repository depth at the Laxemar site (owing to the difficulty of directly identifying these by routine chemical analysis). Given that reducing conditions normally prevail at these depths, however, it is not thought that siderophores should be present in sufficient concentrations to detrimentally impact radionuclide sorption. Investigations at the Äspö HRL have confirmed that these substances are not present in the reducing groundwaters found at repository depth /Essén et al. 2007/.

The transport simulation results indicate a large spread in transport times for specific solutes with differing sorption properties. For weakly or non-sorbing solutes, an F-factor of 10^4 yr/m gives a sufficiently poor matrix retardation effect that the advective travel time has a strong influence upon the uncertainty of the travel time. For larger F-factors, say $F \geq 10^6$ yr/m (for example), the matrix residence time is so large that the advective travel time has only a minor impact and can be neglected. The impact of uncertain transport apertures on advective travel times and the overall transport residence time distribution is discussed in more detail in /Crawford and Sidborn 2009/.

¹ Bacterial siderophores are strong complexing substances released by certain bacteria, usually under oxidising conditions (i.e. when Fe(III) availability is low) by those bacteria that use the Fe(II/III) redox couple as an oxidant. These complexing agents can also bind certain radionuclides very strongly resulting in reduced apparent sorption on geological materials.

The range of variability of measured K_d values for specific solutes is about 1–2 orders of magnitude. Some solutes such as Ra(II) and Ni(II) have reduced ranges of apparent K_d variability due to the lower number of samples. Other solutes such as Sr(II) have poorly constrained lower K_d bounds owing to their generally weak sorption and relatively high measurement limits. Np and U are a special case owing to their sensitivity to redox conditions and the possibility that fully reducing conditions may not have been achieved in the laboratory. It is noted that the lower measured bounds for the sorption of U and Np may be biased by the presence of mobile, oxidised forms which may not always exist under repository conditions at depth.

Uncertainty concerning individual material property parameters (i.e. K_d and D_e) are propagated linearly with the uncertainty in predicted transport time being proportional to the uncertainty in these parameters. Since the transport time is approximately proportional to the square of the F-factor, on the other hand, the same relative level of uncertainty in this parameter has a substantially larger impact on predicted transport times. If the F-factor, for example, is reduced by a factor of 10 the transport time decreases roughly by a factor of 100.

Additional variability in estimated transport times follows if further consideration is given to the different assumptions made during transport modelling. The three different models described above represent hypothetical consequences of different modelling assumptions. It is not known whether the assumption of a 10:1 in-plane stagnant zone in model alternative 1 is a reasonable estimate of the average stagnant zone width potentially existing along typical flow paths within the rock. If the assumption is correct, this would give transport times increased by nearly two orders of magnitude compared with the base case scenario lacking stagnant zones (for the magnitude of the F-factor considered here). For an F-factor of 10^4 yr/m, the radial diffusion model (model alternative 2) does not give substantially different residence times compared with the base model. However, for higher F-factors (in excess of 10^5 y/m) substantially increased retention times are obtained using this model.

A detailed account of the modelling and additional results for marine, brine, and fresh water end-members can be found in /Crawford and Sidborn 2009/.

10.7 Field-scale confirmatory testing of transport properties

An important element of the Laxemar site descriptive modelling has been the integration of field-scale testing within the modelling work. These tests serve a multitude of functions for the different topic areas of interest. For transport properties site descriptive modelling, tracer tests are used to verify connectivity as well as to demonstrate retention of transported solutes. This section gives a brief overview of the tracer tests that have been performed within the Laxemar site investigation, their main results, and consequences for site descriptive modelling and safety assessment. Here, the focus is on the tracer tests that have most relevance for the transport properties site descriptive modelling. These consist of multiple well tracer tests and a series of single well injection withdrawal tests (SWIW). The locations of the boreholes in which tests were conducted are indicated in Figure 10-22. Results of tracer dilution tests are not discussed in this section, although they are discussed in the background report /Crawford and Sidborn 2009/ in connection with flow related transport properties modelling.

10.7.1 Multiple well tracer tests

Three multiple well tracer tests have been performed in Laxemar. Two of these used only non-sorbing tracers, and the third used a mixture of non-sorbing and sorbing tracers.

The first test /Gustafsson and Ludvigson 2005/ took the form of a pumping test with Rhodamine WT injection in a borehole section in KLX02 and withdrawal in borehole HLX10. No tracer breakthrough was detected after two weeks of pumping, possibly owing to a more complicated flow geometry than initially assumed. Indirect pumping responses in the injection borehole KLX02, indicated that more than one fracture/fracture zone was involved in the transport. A possible interpretation suggested that the flow path connecting the two boreholes is considerably longer than the initially estimated 260 m, and that a pumping period longer than two weeks would be required to obtain a breakthrough curve.

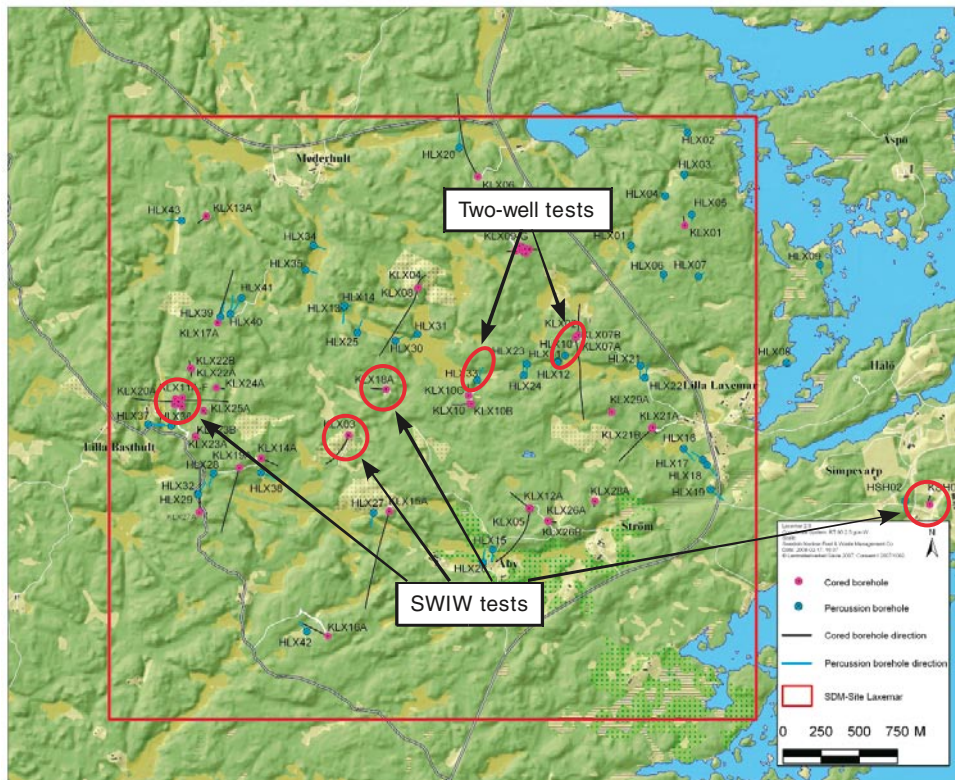


Figure 10-22. Borehole locations for tracer tests used in the SDM-Site Laxemar transport properties evaluation.

The second test /Svensson et al. 2008/ involved uranine injection in soil well SSM000228 and withdrawal pumping in borehole HLX33 at an estimated 204 m linear distance. A uranine tracer mass recovery of 33% was obtained in the withdrawal borehole HLX33 after 760 hours of sampling, and the tracer recovery data was evaluated using a simple one-dimensional advection-dispersion model, assuming a constant fluid velocity and negligible transverse dispersion. The third tracer test /Lindquist et al. 2008/ involved injection of various non-sorbing and sorbing tracers in K LX15A with pumping recovery in HLX27 at a distance of roughly 140 m. In this test, the tracer recovery data was evaluated using the same modelling approach described above as well as a more elaborate model including matrix diffusion.

A so-called “long term pumping” (LPT) test using a suite of different non-sorbing tracers injected in a number of percussion-drilled (HLX27A, HLX32, HLX37, HLX38) and core drilled (KLX11A, KLX20A) boreholes surrounding a central pumping borehole (HLX28) is currently underway in south-western Laxemar. Information from this tracer test, although not reported as part of SDM-Site Laxemar, will provide additional input to future hydrogeological modelling.

10.7.2 Single well injection-withdrawal (SWIW) tests

A number of single well injection-withdrawal (SWIW) tests have been performed in various borehole locations during the site investigation at Laxemar. This tracer test is based on the injection of sorbing and non-sorbing tracers over a short period of time, typically 1–2 hours, followed by a 10–20 hours chaser period during which only water is injected. The injection of chaser water has the effect of pushing the tracer out radially in a ring in the formation surrounding the tested section. After the end of the chaser phase, the flow is reversed and tracer recovered in the same borehole from which it was initially injected.

The technique is attractive for the purposes of the site investigation, since it can be used to perform tracer tests within transmissive structures found at repository depth in which it would be very difficult to perform standard dipole or multiple well tracer tests from the surface. An additional advantageous feature of the SWIW technique is that the reversal of flow during the experiment theoretically reduces the impact of advective dispersion and flow dimension on the residence time distribution of recovered tracer, thereby potentially simplifying the mechanistic interpretation.

In total, six SWIW tests have been performed in Laxemar in different types of structures, at different depths and transmissivity ranges, with the aim of characterising the transport properties of a variety of flowing structures typical of those that might be encountered in the vicinity of a repository. A summary of the individual tests is given in Table 10-23.

10.7.3 Evaluation of tracer test data, interpretation and consequences for safety assessment

In the evaluation of the different tracer tests, it was generally found that an adequate fit of the overall peak shape and height could be obtained using a standard transport model based on the advection-dispersion equation with linear sorption /Gustafsson and Nordqvist 2005, Gustafsson et al. 2006, Thur et al. 2007ab, Svensson et al. 2008/. Using the tracer recovery data, the longitudinal dispersivity and a linear retardation factor were estimated in a first round of inverse modelling using the SUTRA numerical simulation code /Voss and Provost 2002/. This approach, however, was found to consistently underestimate the long-term tailing of mainly the non-sorbing tracers. The specification of a matrix diffusion/sorption term in a second round of modelling gave considerably better fits to the tailing portions of the breakthrough curves for the SWIW tests of uranine. For sorbing tracers, however, this approach generally gave worse fits than the advection-dispersion model. The breakthrough data from the two-well test between SSM000228 and HLX33 was evaluated with the advection-dispersion model only.

The data evaluation gives indications of a diffusion-mediated retardation process for non-sorbing tracers. The retention of sorbing tracers, however, appears to be less affected by diffusion.

From the fitted matrix interaction parameters derived in the extended SWIW test data evaluation /Nordqvist 2008/, it is possible to compare the “apparent” formation factor observed during the tracer tests with that recommended for use in safety assessment. Since the matrix interaction parameter is a lumped parameter that includes the combined effects of matrix diffusion and sorption,

Table 10-23. Summary of basic features of SWIW tests performed in Laxemar.

Borehole	Elevation (m)	T (m ² /s)	Type	Rock and fracture coating description, cf. Table 5-1 for rock type codes
KSH02	-417	1.0·10 ⁻⁶	1 fracture	Fine-grained dioritoid (501030) calcite coating moderately altered
KSH02	-571	5.2·10 ⁻⁷	DZ (3-4 flowing features)	Granite, fine-to medium grained (531058) calcite, chlorite coating slightly altered
KLX03	-701	4.5·10 ⁻⁶	DZ (3-4 flowing features)	Fine-grained diorite-gabbro (505102) chlorite, clay minerals coating slightly altered
KLX18A	-447	4.3·10 ⁻⁸	DZ (3-4 flowing features)	Granite to quartz monzodiorite (501044) calcite, chlorite coating 1 fracture slightly altered, 2 unaltered
KLX11A	-466	3.4·10 ⁻⁶	2 fractures	Quartz monzonite to monzodiorite (501036) chlorite coating slightly altered
KLX11A	-542	1.4·10 ⁻⁷	DZ (2 flowing features)	Quartz monzodiorite (501036) calcite, chlorite coating slightly altered

there is a need to additionally specify the porosity of the rock and sorption K_d (for the sorbing tracers) to estimate the apparent formation factor. This then gives an indication of the amount of mass transfer enhancement that is observed in a tracer experiment compared with that expected on the basis of independent measurements. The apparent mass-transfer enhancement factor is shown in Figure 10-23 for the various SWIW tracer tests performed. Since the SWIW tests are not associated with a well-defined observation scale, the results are plotted against the transmissivity of the tested section.

One aspect of the data interpretation that should be noted is that the two tests that show the largest difference in apparent diffusive mass transfer enhancement factors between Cs^+ and uranine, namely KSH02 (-571 m) and KLX11A (-542 m), are also the only tests with quantitatively determined matrix retardation factors. With the exceptions of these two tests, the matrix interaction parameter for Cs^+ is only qualitatively estimated (i.e. reported in the form of a retention parameter greater than a specified detection limit). Since these other tests also exhibit the poorest model fit for Cs^+ , it may be reasonable to question the estimated strong matrix interaction parameters reported in these particular cases for Cs^+ .

An interesting feature of the test data reinterpretation presented in Figure 10-23 is that the diffusive mass transfer enhancement factor (at least for those tests with quantitatively determined Cs^+ matrix retardation factors) seems to be larger for non-sorbing tracers than sorbing tracers. This trend has also been shown to be consistent across all SWIW tracer tests evaluated in Forsmark /Crawford 2008/, and cannot readily be explained in terms of uncertainty concerning the sorption K_d value used in the evaluation.

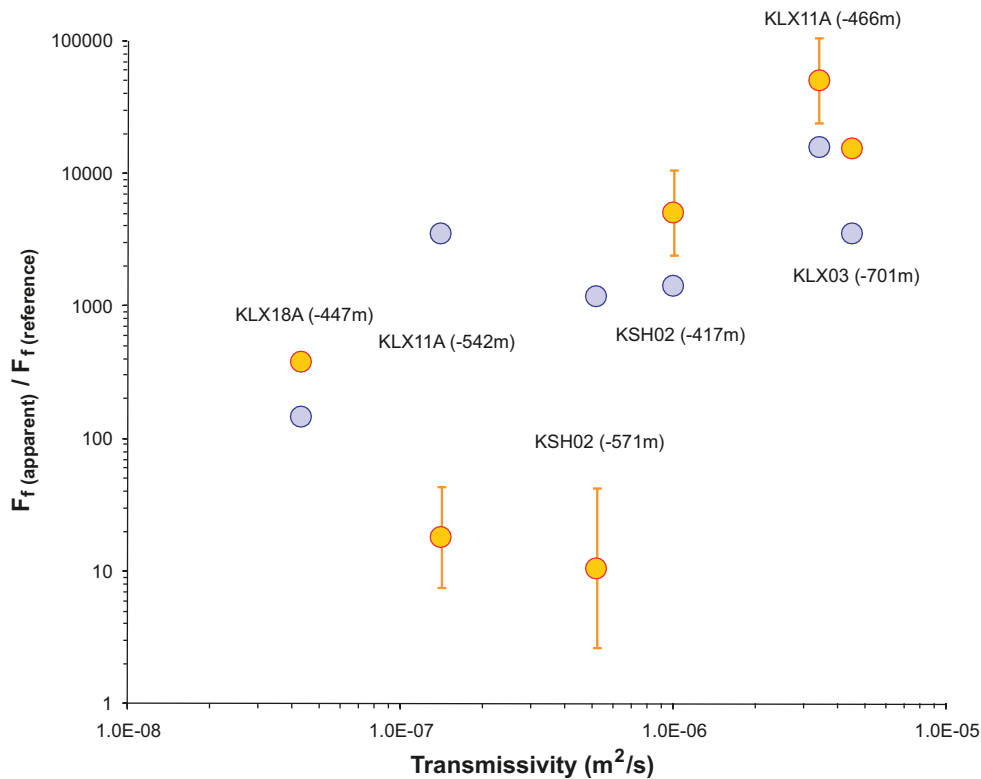


Figure 10-23. Apparent diffusive mass transfer enhancement factors for SWIW tracer tests carried out in Laxemar plotted against transmissivity of the tested flow path (assuming reference formation factors typical for the host rock in the test section, based on through diffusion measurements). Data are shown for both Cs^+ (orange shaded symbols) and non-sorbing Uranine tracer (blue shaded symbols). The plotted data are geometric means with error bars where a range of possible K_d values has been considered. It should be noted that in some cases, owing to the small ranges of reported K_d values for specific rock types, the error bars for Cs^+ are not visible against the larger circular markers.

The results of this analysis indicate that there is an apparent enhancement of diffusive mass transfer of the non-sorbing tracer to the immobile zone that is considerably larger than can be justified on the basis of uncertain laboratory derived measurement values. With the exception of the test performed in KLX18A, the apparent formation factor of uranine is sufficiently high as to be nearly commensurate with that for free diffusion in water. Even making allowances for very large increases in formation factors at the fracture surfaces, or in association with fault gouge material, cannot satisfactorily explain the degree of apparently enhanced diffusive uptake of uranine. An alternative explanation is that transport occurs within a complex fracture featuring substantially greater flow-wetted surface than the single fracture plane assumed in the simulations. The increase in flow-wetted surface required, however, seems larger than what is realistic for the flow structures considered (i.e. by an order of magnitude or more).

In Forsmark it was suggested that the apparently enhanced diffusivity of non-sorbing tracers might be related to non-Gaussian dispersion within flow channels featuring tapered apertures (i.e. non-equilibrium diffusion between flow streamlines). If true, this would suggest that tracers with differing sorptive properties probe different parts of the immobile zone, with the mass transfer of non-sorbing tracers dominated by diffusion between neighbouring flow streamlines, whereas the mass transfer of sorbing tracers is dominated by mass transfer directly to the rock matrix or fracture coating along the flow-wetted surface of the advective flow path.

An alternative explanation for the observed effect could be inaccurate accounting for background levels of uranine at the site derived from drilling fluids. As far as can be discerned, however, the background concentrations of uranine have been correctly accounted for in the data evaluations and this does not appear to be an issue. Other concerns related to the presence of background flows in strongly heterogeneous formations which could flush away significant amounts of the non-sorbing tracer do not appear to be a problem since a very high tracer recovery (>80%) was obtained in all tests.

Additional modelling work with more detailed consideration of hydrodynamic processes on the timescale of tracer tests may need to be done if these issues are deemed to warrant further resolution.

10.8 Evaluation of uncertainties

The key uncertainties in the transport properties site descriptive model can be divided into two main categories; a) uncertainties related to assessment of the hydrodynamic transport resistance, and b) uncertainties related to material properties parameters used in transport modelling. Based on the outcome of the simulation studies using alternative transport models discussed in Section 10.6, a third category could also be considered where the form of the transport model employed (e.g. the concept of 1D diffusion with/without a stagnant zone, 2D radial diffusion formulation, etc) may have a large impact on predictions made within safety assessment. However, since the model alternatives considering channelling effects seem to suggest a strongly positive impact on radionuclide transport retardation relative to the models commonly used in safety assessment studies, this is not considered to be a critical uncertainty in the same sense as a) and b). It should be noted that this consideration of flow channelling is an issue related to forward propagation in transport modelling and should not be confused with impacts of flow channelling arising during inverse modelling for the purposes of flow model parameterisation. Additional issues related to this are discussed further below.

With regard to the hydrodynamic transport resistance of the rock, the main uncertainty appears to be the properties of the network of small, less transmissive fractures that might connect individual canister positions with major flow paths in the hydraulic rock domains. Since these are dependent on additional considerations of repository design that are not strictly part of the site descriptive model, this uncertainty has been dealt with by means of generic scoping calculations of a “what if?” character in the transport properties evaluation.

Scoping calculations suggest that flow censoring effects arising due to the low probability of narrow flow channels being directly intersected by investigation boreholes may not be a significant issue for the estimation of hydrodynamic resistance within the hydraulic rock domains (HRD). If correct, then the main uncertainties concerning the flow properties of the hydraulic rock domains are already covered by the corresponding discussion of uncertainties given in Chapter 8 for the hydrogeological

modelling. Generally, the stochastic hydrogeological DFN simulations suggest that flowing structures should occur relatively frequently within the hypothetical repository volume (i.e. HRD_C in the depth zone -400 m to -650 m) and when they do occur they have properties which are broadly consistent with what would be expected *à priori*, based on the ranges of transmissivity of flowing fractures and structures identified in the borehole investigations. It is not possible to fully account for the influence of compact aggregations of fracture filling minerals, nor “calcite erosion features” in partially annealed fractures from surface based borehole investigations.

Owing to the highly heterogeneous nature of deformation zones, it is not possible to properly account for the possibility of pipe-like flow channels in these structures that may not be readily observed from a limited number of borehole intercepts. If the hydrodynamic transport resistance was to be overwhelmingly dominated by the properties of the hydraulic rock domains this might not be a significant problem as uncertainties concerning the hydrogeological description of the deformation zones would then not have a large impact upon safety assessment transport calculations. Since the estimated ranges of hydrodynamic transport resistance appear to be similar in both the hydraulic rock domains and deformation zones, this could also be a potential uncertainty. F-factors calculated for transport of radionuclides along flow paths from a hypothetical repository to the near surface are very sensitive to the radionuclide release location relative to major flow paths as well as local hydraulic gradients encountered within the repository rock volume. Large-scale simulations made using ConnectFlow indicate that if full credit is taken for these effects, average F-factors might be increased compared with those estimated using scoping calculations incorporating more pessimistic assumptions. There are, however, differences between transport modelling approaches using discrete fracture networks and ECPM (or streamtube representations) that make it difficult to completely reconcile the differences when comparing results from different models.

With regard to the material properties parameterisation of the rock, by far the largest uncertainty is associated with the sorption partitioning ratio, K_d , evaluated for the different radionuclides within the laboratory investigation. It is also noted that the sorption behaviours of only a small number of solutes have been investigated. These have been selected to reflect a broad range of different chemical behaviours, although should not be considered to be the only solutes of interest which is acknowledged here as a significant uncertainty for safety assessment studies of radionuclide transport. On the other hand, the porosity and effective diffusivity (or formation factor) of the rock matrix appear to be relatively well constrained for the main rock types even though they also have associated uncertainties. There does not appear to be strong evidence for *in situ* compression of pore spaces in the unaltered matrix rock given other uncertainties in the estimation of *in situ* formation factors. The apparent depth dependency observed in the formation factor logs is possibly an artefact of uncertain porewater composition rather than related to increasing *in situ* stresses at greater depths. It is possible, however, that core damage effects may have an impact on formation factors determined in the laboratory (giving overestimated values). For this reason, *in situ* formation should be considered a more conservative choice for parameterisation of transport models in safety assessment. An exception to this is possibly the more fine grained rock types (e.g. rock type 501030) where surface conduction bias may censor the lower tail of the formation factor distribution. In these cases, laboratory based measurements might be the more conservative choice.

For sorption partitioning ratios (K_d), it is important to firstly acknowledge that a major uncertainty concerns the use of empirically established measurement values to represent what is, in reality, a complex mechanistic process with strong dependency on groundwater chemistry, sorptive surface area, and relative quantities of specific accessory minerals (e.g. biotite, chlorite, hematite). Although the largest uncertainty appears to be related to groundwater composition, there are differences between radionuclides which sorb by way of different mechanisms, and some radionuclides are more sensitive than others to small changes in these different variables. For the ranges of groundwater compositions likely to be encountered by migrating radionuclides, however, it should be possible to choose appropriate K_d values for specific rock types which are capable of predicting radionuclide transport times of sufficient accuracy for use in safety assessment.

Uncertainties coupled to the laboratory measurement data for sorption relate to a number of issues regarding data interpretation and representativity of crushed rock samples for *in situ* conditions. One of the major uncertainties related to the use of crushed rock samples is the creation of additional surface area (principally external particle surfaces) for sorption. This is further complicated by the possible enrichment of more strongly sorbing mineral phases (e.g. biotite) in the smallest size fractions.

Comparative measurements have indicated, however, that the larger size fractions, on the order of a couple of mm sieve size, have internal surface areas reasonably close to the values obtained using monolithic borehole core samples and therefore can be assumed to be approximately representative of the *in situ* rock. For this reason, the sorption data reported from the laboratory programme for matrix rock samples are based on the largest crushed size fraction (1–2 mm) and longest contact time (180 days) to minimise any effects related to diffusive disequilibrium. In spite of these precautions there are still indications from recent studies of Cs electromigration that even the 2 mm crushed size fraction may have a sorptive surface area greater than that of intact monoliths /André et al. 2008/ and therefore may give overestimates of the sorption K_d .

Additional uncertainties relate to possible alteration of the chemical composition of contacting water used in the sorption experiments owing to mineral weathering reactions as well as slow changes in the mineralogy of the crushed rock samples themselves. The difficulty in maintaining a well defined redox state in the contacting water, for example, was found to be a particular problem for the measurement of U and Np sorption. It is also uncertain which mechanism or mixture of mechanisms are responsible for the apparent time dependency frequently associated with solute uptake in the laboratory sorption measurements. This could be a result of slow weathering reactions as discussed above, diffusive processes, or possibly a combination of effects. It has been found, however, that the magnitude of the kinetic effect and its relation to particle size is not fully consistent with a purely diffusive uptake mechanism. It is therefore currently unclear whether the time dependency is an inherent characteristic and relevant, or an artefact and therefore not representative of *in situ* rock sorptive properties.

11 Current understanding of the site

This chapter presents an integrated description of the understanding of Laxemar at the completion of the surface-based site investigation programme. The description and understanding of Laxemar are founded on a substantial amount of site-specific data, especially from the focused volume, i.e. the south-western part of Laxemar (Figure 11-1).

Surface investigations have included geological mapping and the compilation of bedrock and Quaternary geological maps as well as various ground geophysical investigations, for example high resolution magnetic measurements, that have provided information for the identification and characterisation of deformation zones. A large number of surface ecological investigations have provided data on both abiotic and biotic characteristics in the larger Laxemar-Simpevarp area. In addition, a monitoring programme which is still on-going, has provided time-series data for, e.g. meteorological parameters and water levels in lakes, streams and in the Baltic Sea.

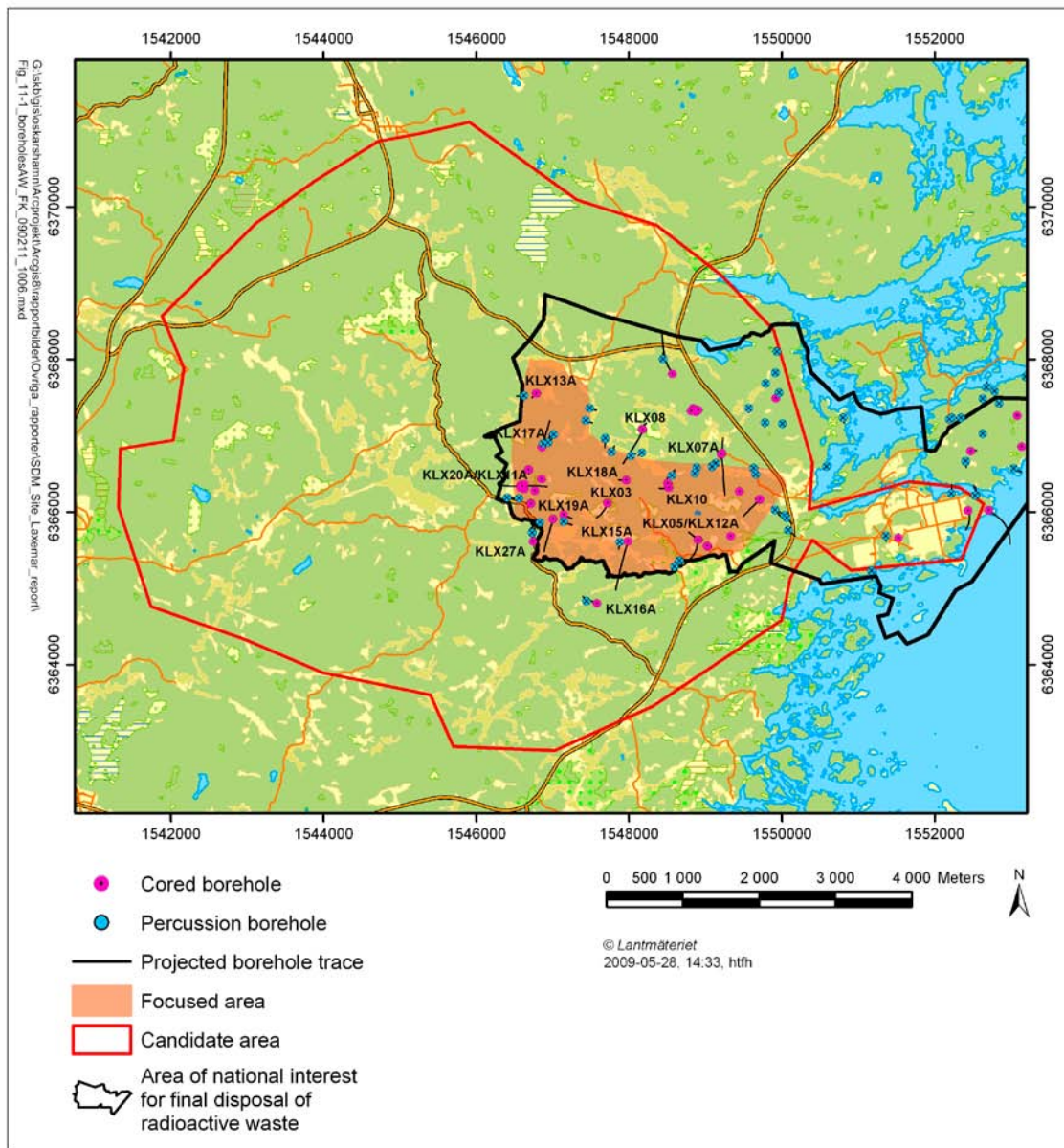


Figure 11-1. The Laxemar-Simpevarp candidate area with the focused area in Laxemar marked with light brown colour and the location of the main drill sites.

Borehole data in support of the Laxemar site description come from 46 core-drilled boreholes ranging in depth from about 100 m to 1,000 m (KLX02 is the longest with a length of about 1,700 m). Notable is that small amounts of data exist from the uppermost parts of telescope-drilled (usually the upper approximately 100 m portions) of the cored boreholes. The database also contains results from investigations in 43 percussion-drilled boreholes and some 189 monitoring wells in the Quaternary deposits (i.e. the so-called soil monitoring wells).

In addition to results from standardised borehole measurements (e.g. drilling logs, image logs, core logs, geophysical logs and hydraulic tests) in cored and percussion holes, information from more specialised investigations has also been collected. These specialised investigations include resistivity logging for establishing the *in situ* formation factor (diffusivity), measurements of groundwater flow, cross-hole interference tests and investigations of rock matrix porewater. Rock stress measurements from overcoring, hydraulic fracturing, hydraulic tests on pre-existing fractures and studies of borehole breakouts and other types of fallout structures in the borehole wall have been performed in several of the boreholes. Furthermore, the database include data from several types of laboratory investigations carried out on samples of intact rock material and selected fracture samples from these boreholes. The soil monitoring wells have provided time-series data on groundwater levels and water chemistry, as well as information on the stratigraphy of the Quaternary deposits in the area. Time-series data of hydraulic head have also been acquired in the bedrock by means of multi-packer systems in the cored boreholes, and in some cases also in percussion holes.

11.1 The surface system

The description of the surface system is in itself multi-disciplinary, given that it relies on the integrated understanding of meteorology, hydrology, oceanography, hydrogeochemistry, Quaternary geology and ecology in the Laxemar-Simpevarp area. The derived integrated understanding of the surface system is described in Chapter 4 and is further detailed in /Söderbäck and Lindborg 2009/. In this section only a brief summary of the surface description is provided, and with a particular focus on aspects of common importance to the surface and bedrock systems.

11.1.1 Evolution during the Quaternary

The character of the current surface system is strongly influenced by the climate evolution during the Quaternary period. The Quaternary climate was characterised by large and sometimes rapid changes in global temperature, during which the Laxemar-Simpevarp area was covered by glaciers at least three (but probably more) times. Preserved information older than the latest glacial phase (or stade) is rare in Sweden in general, and consequently the duration and extent of early Quaternary glaciations is poorly known. The latest glacial, the Weichselian started c. 115,000 years ago. It was characterised by colder periods (stadials) interrupted by milder interstadials. During the first two cold periods, the Laxemar-Simpevarp area was most probably free of ice but hosted a tundra climate. During the two early Weichselian interstadials the climate was probably colder than today and the Laxemar-Simpevarp area was sparsely forested. The onset of the latest glacial coverage in the area is not known, whereas the timing of the last deglaciation is rather well established. The largest extent of the Weichselian ice sheet was reached c. 18,000 years ago and, according to glaciological models, the ice cover thickness in the Laxemar-Simpevarp region at that time was about 2.4 km.

All Quaternary deposits in the Laxemar-Simpevarp area have probably been deposited during or after the latest deglaciation. However, the possibility of the occurrence of older deposits cannot be excluded and there are indications of older deposits in neighbouring areas. The ice sheet in the area moved from the north-west during the latest glaciation and deposited the glacial till. There are several glaciofluvial deposits, with a northerly strike, in the investigated area. These deposits were formed when stones, gravel and sand were transported by the melt water within tunnels under the ice sheet. During continued retreat of the ice, glacial clay was deposited at the floor of the fissure valleys, which are characteristic of the Laxemar-Simpevarp area.

The Baltic Sea completely covered the Laxemar-Simpevarp area after the latest deglaciation c. 12,000 BP. Land uplift was fastest during the first few thousand years following the deglaciation and has subsequently decreased to the present rate of 1 mm/year, cf. Figure 3-7. The development

of the Baltic Sea after the latest deglaciation has been characterised by an ongoing shoreline displacement. The interaction between isostatic recovery of the Earth's crust and eustatic sea level variations has caused a varying depth of the straits connecting the Baltic Sea with the Atlantic Ocean by way of the North Sea, which in turn has caused varying salinity throughout the postglacial Holocene epoch. Between 4500 to 3000 BC, during the middle of the Littorina Sea stage, the salinity of the Baltic Basin was almost twice that of today's Baltic, offshore Laxemar, cf. Figures 3-5 and 3-6.

The shoreline displacement has had a significant impact on the distribution and redeposition of fine-grained Quaternary deposits. The most exposed areas have been subjected to wave washing and currents. Consequently, sand and gravel have been eroded from older deposits, transported and redeposited at more sheltered locations. Periods of erosion have occurred also at sheltered locations, which have resulted in the erosion of fine-grained deposits such as glacial clay. In the coastal areas of Laxemar, clay gyttja has been deposited in the long and narrow valleys when these were shallow bays. The shoreline displacement continuously transforms seafloors to new terrestrial areas or to freshwater lakes. Newly formed areas are successively, and also currently, exposed to erosion, whereas sheltered bays with conditions favourable for deposition of clay gyttja have formed in other areas. Lakes and wetlands are successively covered by fen peat, which at some locations is then covered by bog peat.

Investigations to evaluate the occurrence of seismic activity during and after the Weichselian glaciation in and around the Laxemar-Simpevarp area have been carried out. None of the morphological lineaments recognised have been inferred to represent late- or post-glacial faults. Furthermore, no deformational features in Quaternary deposits have been unambiguously related to seismic activity. There is no geomorphological evidence in the Laxemar-Simpevarp area for major historic earthquakes.

The development of the ecosystems after the deglaciation at Laxemar-Simpevarp is strongly correlated not only to climate changes and shoreline displacement, but also to human activities.

11.1.2 Description of the surface system

The landscape and topography in the Laxemar-Simpevarp area forms part of the so-called sub-Cambrian unconformity (peneplain) with an overall gentle gradient dipping approximately 4% towards the Baltic Sea. Notwithstanding this, the landscape is variable on a smaller scale with recurrent transitions between hilly areas (mostly barren outcropping bedrock or covered by a very thin soil cover) and valleys filled with sediments, some of which are fissure valleys. Areas with thicker overburden are found in the southern part of the Laxemar subarea.

Quaternary deposits

The distribution of Quaternary deposits is mainly related to the local bedrock morphology where the higher situated areas show thin overburden, and long and narrow valleys show considerably thicker overburden, including more fine-grained water-laid sediments, cf. Figure 11-2. Some 58% (of which 34% is till coverage) of the area is covered by Quaternary deposits and some 42% corresponds to outcrop bedrock or very thin soil cover. Stratigraphical investigations indicate that the overburden formed in conjunction with the end of the latest glaciation, but older units cannot be excluded. In more elevated areas the thickness of Quaternary deposits generally is less than one or a few metres. The total thickness of Quaternary deposits in the valleys is often several metres with maximum overburden depths of more than 30 metres, as established in boreholes, and in places perhaps as thick as 50 m, according to geophysical measurements. Available results also show that the different stratigraphical units in general are thicker in valleys in the off-shore parts of the area, compared with valleys on land.

Lakes

The lakes in the area are relatively small (0.03 to 0.24 km² in area) and shallow, with average and maximum depths in the range of 1–4 m and 2–11 m, respectively. All lakes are located above sea level, which implies that no sea-water intrusion takes place. Wetlands cover up to 18% of the delineated catchment areas.

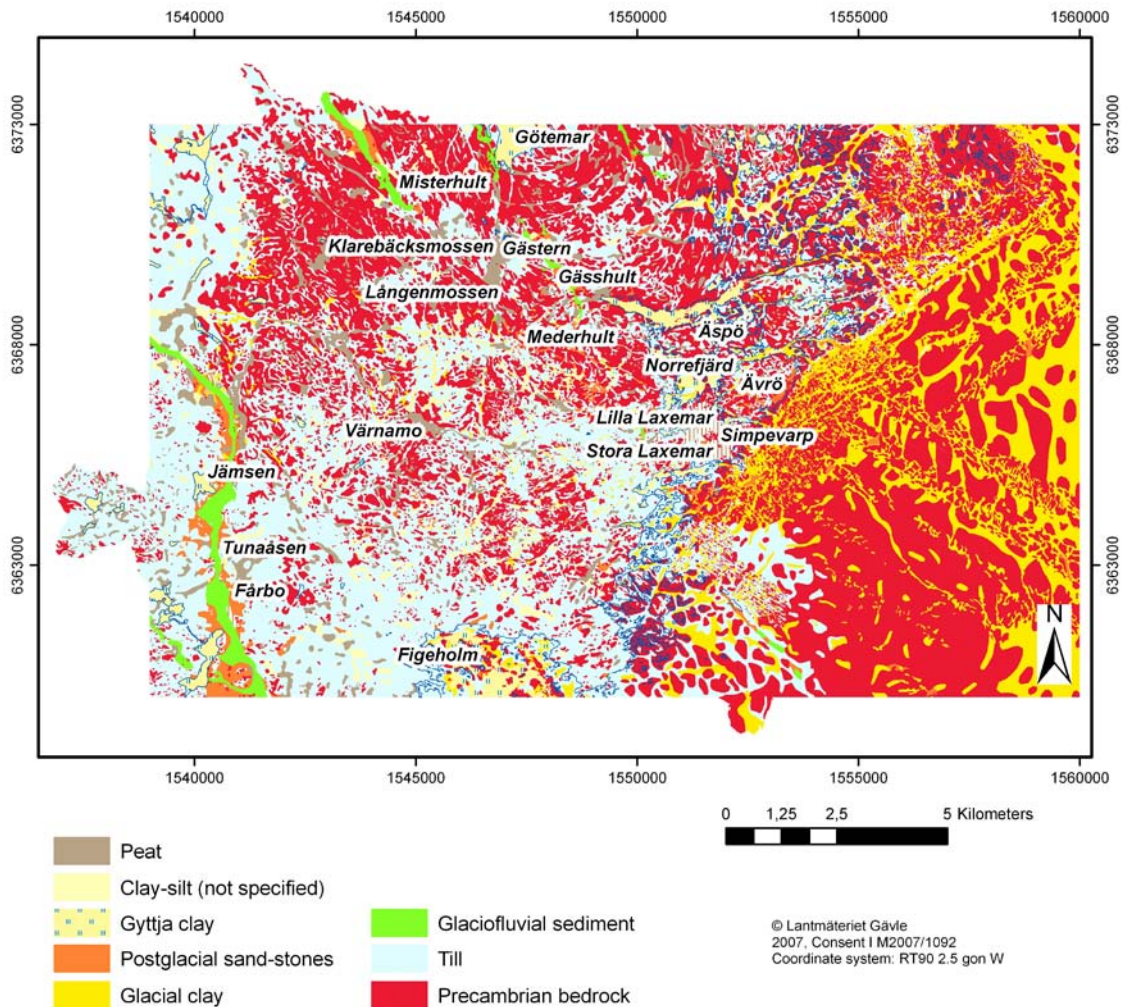


Figure II-2. Geographical distribution of Quaternary deposits and outcrop bedrock in the Laxemar-Simpevarp area. Modified after /Sohlenius and Hedenström 2008/.

Hydraulic properties of Quaternary deposits

The sandy-gravelly till, which overlies the bedrock in the whole area, is characterised by a relatively high hydraulic conductivity (c. $4 \cdot 10^{-5}$ m/s), close to an order of magnitude higher values than those associated with deposits in the deepest parts of the larger valleys, mostly associated with deformation zones. Furthermore, there exist indications of an anisotropic hydraulic conductivity, with an anisotropy ratio (K_h/K_v) in the order of 15–30, reflecting the stratigraphy of the overburden. However, this should be treated with caution since the test scales differ between different investigations. Generic data are also used in support of the estimates of hydrogeological properties of Quaternary deposits other than till. Observations of hydraulic head suggest a clear hydraulic coupling between the bedrock and the overburden. Areas of recharge are located in the elevated parts of western Laxemar, and in areas even further to the west, whereas local discharge areas in Laxemar are located mainly along the major east-west trending valleys, with the bulk of the flow being concentrated in the overburden and the uppermost 10 metres of the bedrock. The principal areas of regional discharge are associated with the shallow bays along the coast.

Hydrogeochemistry

The two important factors governing the hydrogeochemistry of the surface system in the Laxemar-Simpevarp area are the characteristic topography and the post-glacial shoreline displacement. Elevated areas are influenced by atmospheric deposition and weathering processes in the Quaternary deposits and in the upper parts of the bedrock, the latter driven by free H^+ ions generated by degradation of

biogenic carbon. In areas of low elevation, close to the coast, marine remnants in the Quaternary deposits influence the hydrogeochemistry. In essence, regional scale hydrogeochemical characteristics are governed by meteoric recharge and subsequent flushing. The hydrochemistry of near coastal groundwater samples indicates discharge of deeper groundwaters.

The Ecosystems

The location of the Laxemar-Simpevarp area close to the Baltic Sea (Figure 11-3) means that the seashore is a characteristic feature in the east, together with coniferous forests, shallow lakes, various types of wetland with interlaced patches of agricultural land, the latter primarily concentrated in the valleys. Terrestrial vegetation is strongly influenced by the distribution and characteristics of the Quaternary deposits and by human land use. Forests cover the major parts of the Laxemar-Simpevarp main catchment, whereas wetlands cover less than 1%. The agricultural land covers close to 9% of the land area of the main catchments. As noted above, the lakes in the area are all shallow and classified as mesotrophic brown-water lakes, which implies moderate nutrient concentrations, high concentration of organic carbon and brown water, the latter indicating high input of organic matter.

Confidence

Generally, the site descriptive model for the surface system is associated with a high degree of confidence. The main reasons for this confidence are the relative wealth of site investigation data, the well-defined domains of the overburden, the consistent typical stratigraphy and the fact that the bedrock surface is well-exposed within the model area. Uncertainties associated with the sub-models have been thoroughly evaluated, and descriptions and model results are, in most cases, consistent with regional/generic data and/or with the results from alternative models. Considerable efforts have been made to establish an integrated description of the overburden and the superficial bedrock. Notable is the relatively high degree of hydraulic connectivity between these two entities. The principal remaining uncertainties are associated with the description of the spatial distribution of the thickness of the



Figure 11-3. View (looking northwest) of the focused area in Laxemar. In the foreground (lower right) is the Clab facility on the Simpevarp peninsula. Cleared stripes in the forest are clearings for the main power lines connecting to the nuclear power plants.

overburden and the hydraulic properties of the shallow bedrock and those of the Quaternary deposits along valleys. Even though the general groundwater flow pattern is considered well-established, it is difficult to establish the exact location of discharge points of deep groundwater due to heterogeneous hydraulic property distributions of the coastal subvertical deformation zones that are considered to be associated with groundwater discharge. Other remaining uncertainties concern the description of the spatial distribution of the chemical composition in the deep Quaternary deposits, as well as process estimates (plant uptake, transpiration etc) and effects of microbiological processes. Finally, some discharge measurements are questionable.

11.1.3 Human population and land use

With archaeological methods it is possible to identify traces of some 300–400 generations that have lived in the Laxemar-Simpevarp region since the last deglaciation. Recent investigations have shown that the region was highly exploited during Early Stone Age (9000–4000 BC) /Söderbäck 2008/. During the Late Stone Age (4000–1800 BC), the practise of agriculture and raising livestock increased, in addition to hunting, gathering and fishing. The Bronze Age (1800–550 BC) is represented in the region by many graves, cairns, circles of stones and piles with stone sherds (known as *skärvstenshögar* in Swedish). In strong contrast, there is an almost complete lack of typical graves and characteristic site-names from the Iron Age (300 BC–1100 AD), suggesting that the region was almost deserted during this period. It is not possible to reconstruct the land use and living conditions of the population during the medieval period (1100–1550 AD) since there are no written sources available from that period.

The number of crofters' settlements and population density increased moderately in the Laxemar-Simpevarp region during the late 16th to the late 18th century, partly due to partitioning of farms. The population in the region increased dramatically until the end of the 19th century, followed by a gradual decrease in population during the 20th century.

The present-day population density within the Laxemar-Simpevarp area is about one third of the average population density of the County of Kalmar (to which the area belongs) and less than half the population density of Sweden. One out of five properties in the region is a vacation house. The land use is dominated by forestry. Agriculture in the area is limited and arable and grazing land comprise less than 10% of the total land area.

11.2 Rock domains and their associated thermal and rock mechanical properties

The lithology of the investigated site, i.e. the types and occurrences of dominant rock types and associated subordinate rock types, govern the degree of homogeneity of the investigated rock volume and the potential for mineral resources. Through its mineralogical characteristics it also sets the limits on the mechanical and thermal properties. In the site descriptive model the lithology is described by rock domains, which are defined on the basis of similarities in composition, grain size, homogeneity, and the style and degree of ductile deformation of the rock.

11.2.1 Rock crystallisation and cooling history

The bedrock that currently forms the ground surface in the Laxemar-Simpevarp area was formed and crystallised at great depth. Geochronological data strongly suggest that both the dominant and subordinate rock types that form the bedrock were emplaced and crystallised c.1.8 Ga ago during the waning stages of the Svecokarelian orogeny. A close temporal and genetic relationship between the different rock types is also evidenced by magma-mingling and magma-mixing processes, exemplified by the occurrence of enclaves, hybridisation and diffuse transitional contacts between different rock types. Additional rock-forming events occurred at c. 1.45 Ga ago, which gave rise to the Götemar and Uthamar granites north and south of Laxemar, respectively, and at c. 0.9 Ga when mafic magma intruded and formed dolerite dykes in the area.

In a regional structural context, the bedrock in the Laxemar-Simpevarp area is dominated by well-preserved intrusive rocks, although a non-uniformly developed, faint to weak foliation occurs. The area is cross-cut by low-grade ductile shear zones in which the rocks are affected by a high degree of ductile strain. This anisotropy was established at an early stage (shortly after the formation of the bedrock) in the geological evolution of the area and constitutes a regional structural framework that has had important implications for the spatial distribution of younger brittle reactivation in the bedrock.

Geochronological data indicate that the bedrock in the Laxemar-Simpevarp area passed through the brittle-ductile transition in the crust sometime between 1.76 and 1.62 Ga. Thus the c. 1.45 Ga Götemar and Uthammar granites were emplaced into a cold brittle crust, see also Section 3.1.2.

11.2.2 Rock composition and ductile deformation

A substantial amount of geological and geophysical data, both at the surface and from depth in the form of information from cored and percussion boreholes underpin the SDM-Site Laxemar rock domain model. Surface data are the basis for establishing a bedrock geological map (Figure 5-1 and Figure 11-4) with its distribution of rock units. Joint analysis and evaluation of the surface and borehole data are used in the projection of rock domains from the surface to depth.

Rock types

The dominant rock types in the focused volume are (from south to north), equigranular quartz monzodiorite, porphyritic Ävrö quartz monzodiorite (with inhomogeneously distributed bodies of diorite-gabbro) and porphyritic Ävrö granite. The mineralogical composition of the equigranular quartz monzodiorite and the porphyritic Ävrö quartz monzodiorite is similar, e.g. the quartz content is c. 13% in both rock types. The porphyritic Ävrö granite in northern Laxemar has a higher content of quartz (c. 22%, mean value) and potassium feldspar and lower content of mafic minerals.

Ductile deformation

From a structural point of view, the bedrock in Laxemar is dominated by well-preserved intrusive rocks. However, a faint to weak foliation, which is not uniformly distributed in the bedrock in the local model volume, is present. Based on the mapping of the boreholes, c. 80% of the bedrock in Laxemar has been documented as massive, i.e. does not contain any ductile anisotropy. It has been inferred that the non-uniformly distributed, faint to weak foliation in Laxemar defines an irregular antiformal configuration with a subhorizontal to gently westward plunging fold axis. The most spectacular and characteristic ductile, structural features in Laxemar are low-grade ductile to brittle-ductile shear zones that vary in thickness from decimetres up to tens of metres. The most prominent ones are those flanking Laxemar in the northwest and in the southeast (Figure 11-5).

Subordinate rock types and alteration

Important subordinate rock types throughout Laxemar comprise fine-grained granite, fine-grained diorite-gabbro and pegmatite. Subordinate rock types occur as dyke-like bodies, patches and small irregular intrusions. Dolerite is encountered in a number of cored and percussion boreholes in western Laxemar but has not been observed in outcrop. Although only one dolerite occurrence is indicated in the bedrock map, cf. Figure 5-1, an additional 21 lineaments that possibly could be related to dolerite dykes have been identified based on an interpretation of the detailed ground magnetic data and digital elevation models. The hydraulic significance of the dolerite dykes is discussed in Section 11.5.2. Although there are a number of thicker occurrences of subordinate rocks in boreholes, the majority of the subordinate rock types have thicknesses less than 0.1 m, cf. Figure 5-7. Furthermore, the majority of the occurrences of fine-grained granite and fine-grained diorite-gabbro are subhorizontally to moderately dipping and have a dominant NE-SW strike, although a general spread between N-S and E-W occurs. The pegmatites display similar strike orientations, but are dominated by steep to subvertical dips.

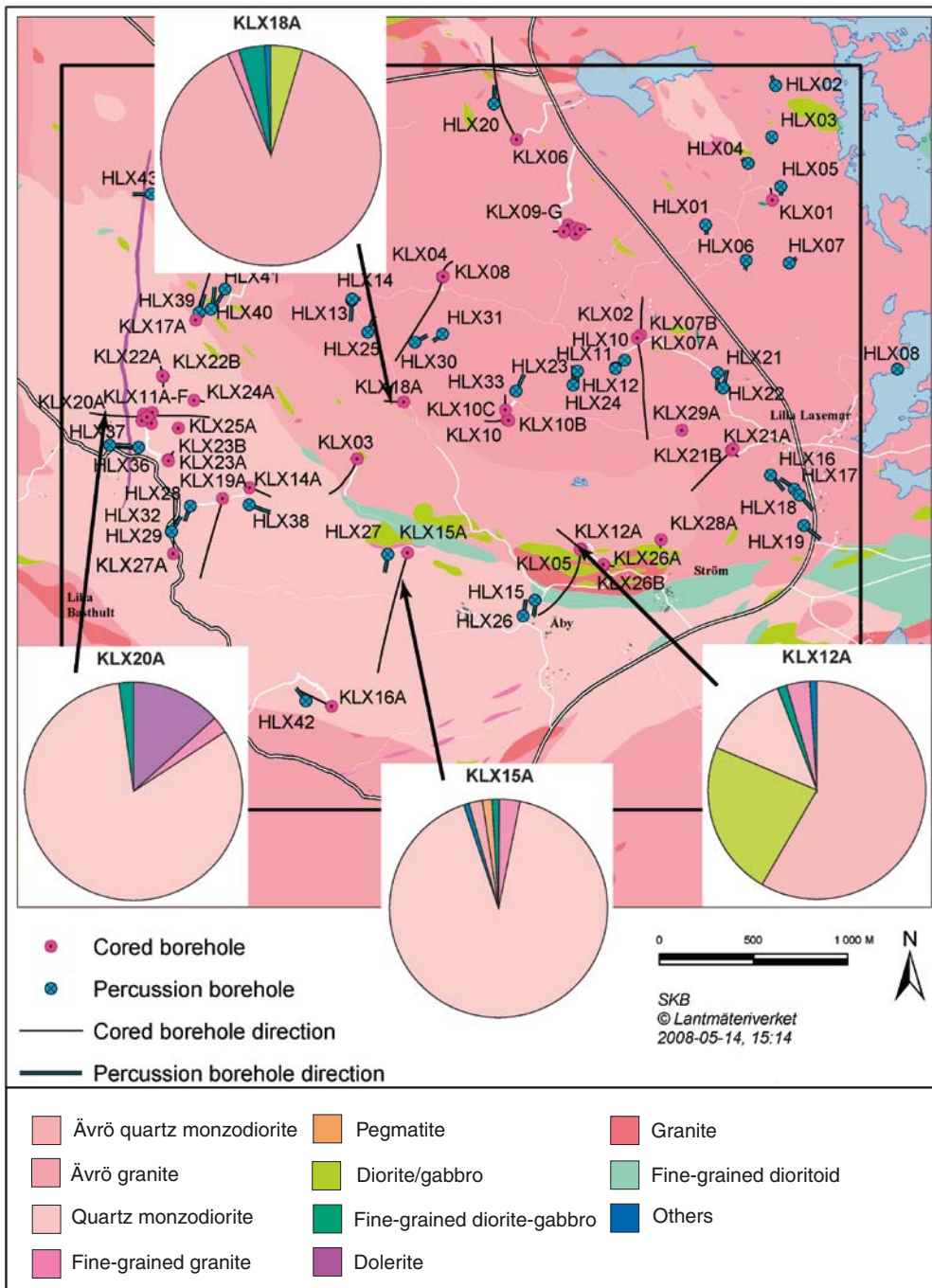


Figure 11-4. Geological map of the bedrock in the Laxemar local model area and its immediate surroundings. Pie charts show the percentage (volume) of different rock types in some typical cored boreholes. Distributions of rock types in boreholes are based on information in /Wahlgren et al. 2008, cf. Appendix 4 therein/.

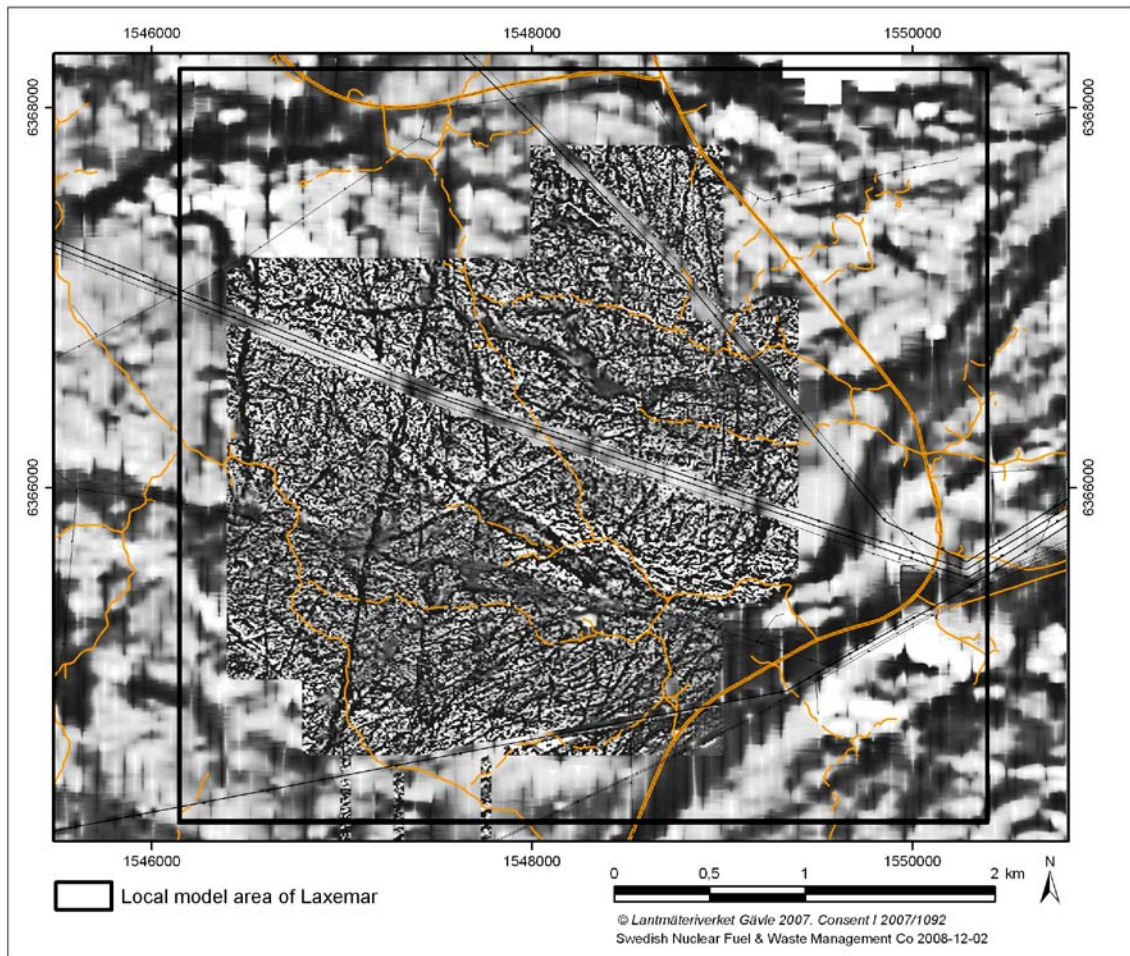


Figure 11-5. Magnetic anomaly map showing the low grade ductile deformation zones (darker lineations on the map, cf. Figure 5-19), and in particular the prominent NE-striking ductile shear zones in the NW and SE corners of the map. The image is a combination of NS-delineated aerial and detailed ground magnetic surveys. Yellow lines correspond to roads. Figure reproduced from /Wahlgren et al. 2008/.

The degree of alteration in the bedrock in between the deformation zones that are identified in the extended geological single-hole interpretation (ESHI) is in general classified as faint to weak and, although inhomogeneously distributed, affects approximately 20–25% of the bedrock. Red staining (oxidation), which is secondary in character and fracture-controlled, is by far the most abundant type of alteration in the Ävrö granite and Ävrö quartz monzodiorite (cf. Figure 5-5). The quartz monzodiorite displays a much higher degree of saussuritisation and epidotisation than the Ävrö granite and Ävrö quartz monzodiorite. The saussuritisation is more primary in character than the red staining and is interpreted to be a late-stage magmatic alteration. The red staining has been demonstrated to increase the thermal conductivity and decrease the uniaxial compressive strength (cf. Sections 6.2 and 7.3).

11.2.3 Rock domain model

The focused volume is made up of three principal rock domains, from north to south; RSMA01, RSMM01 and RSMD01, cf. Figure 5-24 through 5-26 and Figure 11-6. The delineation is primarily made on the basis of the characteristics of rock types and structural overprinting. For a detailed review, cf. Section 5.4.

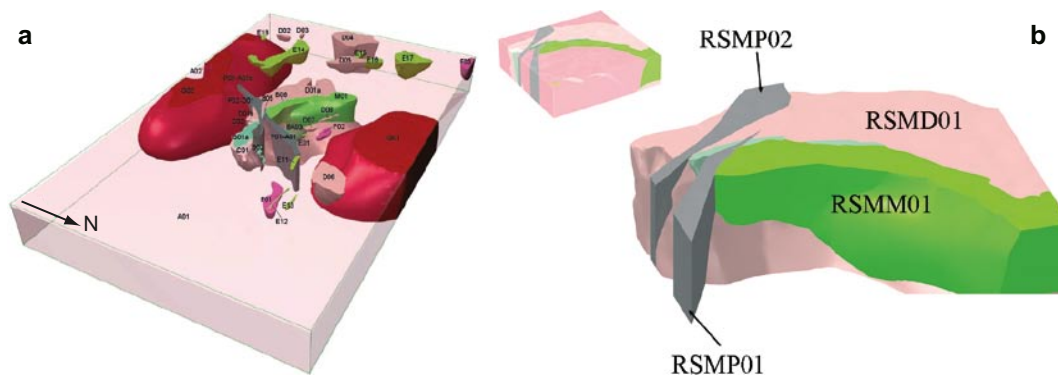


Figure 11-6. a) Rock domains in the regional model (view from the NE), the Götemar and Uthamar granites seen in red in the north and south, respectively. Volumes coloured pink correspond to Ävrö granite, cf. Figure 5-1 b) Blow-up of central part of the model (view from the NNE). Rock domain RSMA01 corresponds to transparent parts of modelled volume. Figures after /Wahlgren et al. 2008/.

Rock domains in the focused volume

The focused volume in Laxemar is dominated by the rock domains RSMD01, RSMM01 and RSMA01. The RSMD01 domain is strongly dominated by equigranular, medium-grained quartz monzodiorite (c. 89% of the domain volume). Subordinate rock types include fine-grained granite (5%), fine-grained diorite-gabbro (2%), dolerite (2%) and pegmatite (1.5%). Dolerite, mostly associated with deformation zones, is considered to constitute a very subordinate rock type and is not expected to be evenly distributed throughout the domain. The subordinate rock types, except pegmatite, display the same gentle dips as the foliation (dominantly to the south). The major part (c. 75%) of the RSMD01 domain is judged to be composed of fresh unaltered rocks

The RSMM01 domain, dominated by Ävrö quartz monzodiorite (including granodioritic to granitic compositions) constitutes c. 75% of the domain, but is characterised by a much higher proportion of variably distributed diorite/gabbro (c. 16%) than the other rock domains. The most important subordinate rock types and their proportions are similar to those of the RSMD01 domain. The major parts (c. 85%) of the RSMM01 domain is fresh unaltered rock.

Ävrö granite, a porphyritic rock that varies in composition between quartz monzodiorite (Ävrö quartz monzodiorite), granodiorite (Ävrö granodiorite) and granite, is the dominant (c. 88%) rock type in the central and southern parts of the RSMA01 domain. Typical subordinate rock types are fine-grained granite (3%), fine-grained diorite-gabbro (2%), fine-grained dioritoid (3%) and quartz monzodiorite (2.5%). Granite, pegmatite and diorite/gabbro occur in minor amounts, i.e. less than 1% each. The major part (c. 70%) of the RSMA01 domain constitutes fresh unaltered rock.

The subordinate rock types fine-grained granite, i.e. fine-grained diorite-gabbro and pegmatite show variable correlation to the non-uniformly distributed foliation in the rocks in all three rock domains. The difference in mineralogical composition of the dominant rock types is reflected in the rock mechanical properties and in the thermal conductivity, the latter is generally lower in the quartz monzodiorite than in the Ävrö granodiorite, cf. Section 11.2.5 and Section 11.2.6, respectively.

Rock domains outside the focused volume

Rock domains defined outside the focused volume include RSMB01 (dominated by fine-grained diorite) found on the Simpevarp peninsula, east of Laxemar. Furthermore, domains RSMP01/P02, which are associated with a high concentration of low-grade ductile shear zones, occur immediately east of the focused volume, cf. Figure 5-24.

Confidence

The confidence in the overall geometry of the rock domains defined in the focused volume is considered high, although the precise geometries of the individual rock domain boundaries at depth are not completely established. Furthermore, the descriptions of properties and character of the

dominant rock types making up the rock domains in the focused volume are judged to be of high confidence since the character of the rock types that represent the domains is very well established, cf. /Wahlgren et al. 2008/.

The overall judgement of the SDM-Site Laxemar rock domain model is that both the geometrical relationships between the rock domains and their property assignment are stable and well understood in the focused volume. However, for natural reasons an uncertainty exists in the exact position of the rock domain boundaries at depth in between the fix points in the boreholes. Furthermore, the uncertainty in the rock domain model relates to a certain degree to the orientation, but in particular to the spatial distribution of subordinate rock types, i.e. fine-grained granite, pegmatite and fine-grained diorite-gabbro (composite intrusions). In addition, the uncertainty also relates to the distribution and size of diorite/gabbro bodies and the proportion of Ävrö granodiorite in the RSMM01 domain, as well as the proportion of Ävrö quartz monzodiorite in RSMA01. The uncertainties that relate to the spatial distribution of rock types have been addressed in the thermal modelling using stochastic simulation (cf. Section 6.4).

11.2.4 Mineral resources

The Laxemar-Simpevarp area may be considered as sterile with regard to ore and metallic mineralisation. Furthermore, there is no potential for industrial minerals. For a comprehensive description of the ore potential in the Laxemar-Simpevarp area, see /Lindroos 2004/.

11.2.5 Thermal properties

The thermal conductivity of the bedrock has been assessed from field measurements, by laboratory measurements on drill core samples, by calculations based on mineral composition from modal analyses, and by established relationships between bedrock density and thermal conductivity. The heat capacity has been determined from calorimetric measurements and also indirectly from measurements of thermal conductivity and diffusivity on drill core samples.

Thermal conductivity and heat capacity

The dominant rock types in the RSMM01 and RSMD01 domains within the focused volume have mineralogical compositions that imply low values of thermal conductivity, while the dominant granitic to granodioritic rock in the RSMA01 domain has higher thermal conductivity. Measurements at the centimetre scale show mean values in individual boreholes in the range 3.06 to 3.32 W/(m·K) for the medium-grained and more quartz-rich Ävrö granodiorite (sub-variety of the Ävrö granite), the dominant rock type in rock domain RSMA01. The quartz-poor Ävrö quartz monzodiorite that dominates rock domain RSMM01, has a significantly lower thermal conductivity in the range 2.18 to 2.44 W/(m·K) (based on data from two boreholes only). The measured thermal conductivity of quartz monzodiorite, which dominates rock domain RSMD01, shows average values in the order of 2.63 to 2.84 W/(m·K). Measured and calculated conductivities also indicate that rocks affected by alteration (oxidation) have higher thermal conductivity than their unaltered equivalents (some 10–15% higher). Field and laboratory measurements have also revealed the presence of anisotropy in the thermal conductivity, which can be largely attributed to foliation/lineation. The thermal conductivity parallel to foliation is estimated to be on average 15% higher than perpendicular to the foliation. Anisotropy due to the orientation of subordinate rock bodies has been taken into account in the thermal modelling of RSMD01.

The variability in thermal conductivity within each rock type, and between rock types, is considered in the upscaling of thermal conductivity from rock type level to rock domain level by the use of spatial statistical models of lithology and thermal conductivity, cf. Figure 11-7. These models build on the grouping of rock types with similar thermal conductivity into thermal rock classes (TRC). The distribution of TRCs is simulated and combined with simulations of the distribution of thermal conductivity within each TRC to obtain the resulting distribution of thermal conductivity within a given rock domain. The impact of the degree of heterogeneity within the dominant rock domains is illustrated by the realisations at the 2 m scale shown in Figure 11-7.

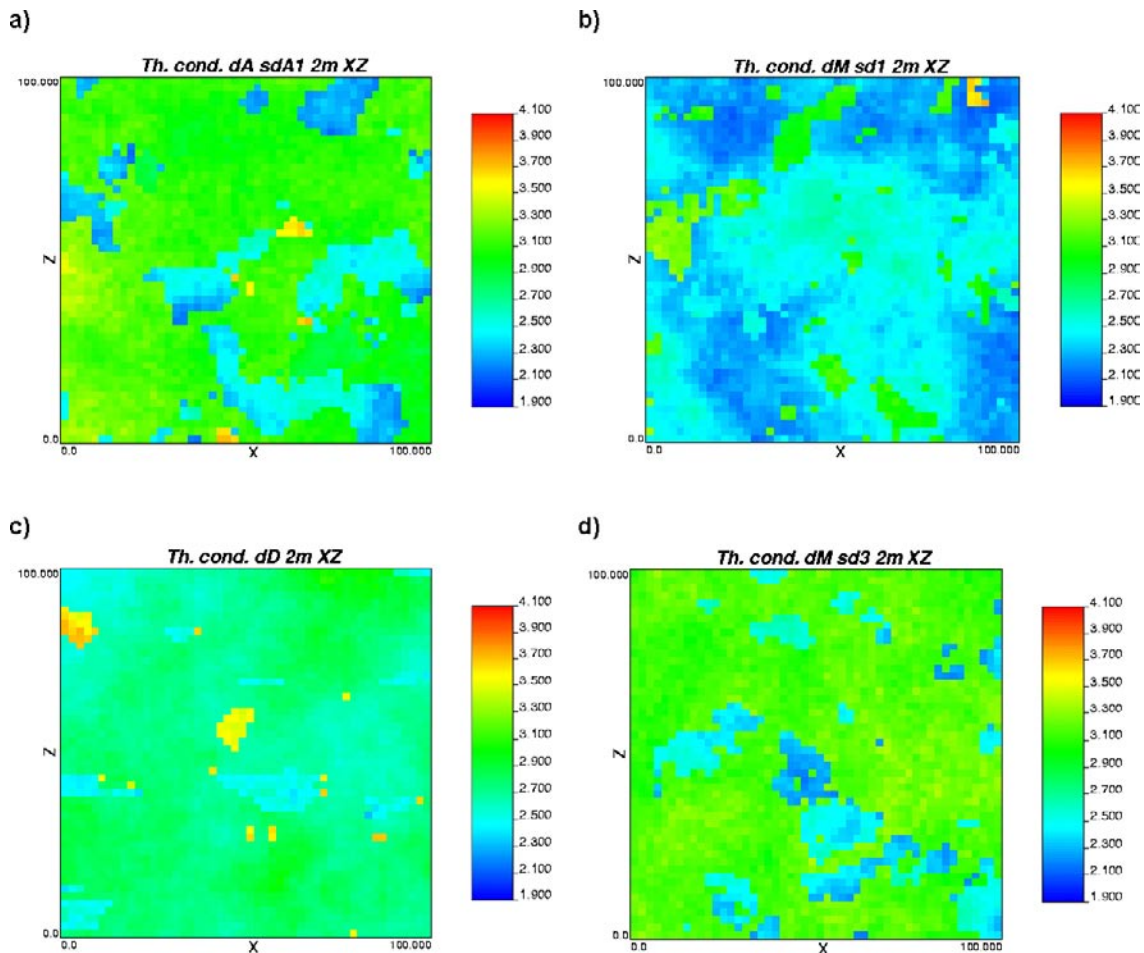


Figure 11-7. 2D sections from individual 3D simulations exemplifying the spatial distribution of thermal conductivity ($W/(m \cdot K)$) of various rock domains. The resulting distribution of thermal conductivity considers the spatial variability in conductivity both within and between TRCs. a) RSMA01 – subdomain A1, dominated by the medium-high conductive Ävrö granodiorite (TRC 56). b) RSMM01 – subdomain M1 is dominated by low conductive Ävrö quartz monzodiorite (TRC 46) with variable content of diorite-gabbro (TRC 33), c) RSMD01 – due to its relative homogeneity no thermal subdomain were defined, d) RSMM01 – subdomain M3 is dominated by medium-high conductive Ävrö granodiorite (TRC 56) with variable content of diorite-gabbro (TRC 33).

The mean value of the thermal conductivity from the stochastic simulations is c. 2.9, 2.7 and 2.8 $W/(m \cdot K)$ at the 5 m scale at a temperature of 20°C for rock domains RSMA01, RSMM01 and RSMD01, respectively. In the latter two of these rock domains, lithological heterogeneity is accounted for through the introduction of thermal subdomains, as many as five in the case of RSMM01. The impact of poorly conductive rock, mainly Ävrö quartz monzodiorite and diorite-gabbro, is particularly obvious in RSMM01, a feature displayed by the pronounced bimodality in the resulting histogram (Figure 11-8). The lower tail of the thermal conductivity distribution influences the spacing of canisters in the repository layout. The 2.5 percentile of the thermal conductivity distribution is estimated to be 2.34, 2.22 and 2.50 $W/(m \cdot K)$ for domains RSMA01, RSMM01 and RSMD01, respectively (5 m scale).

The mean value of the heat capacity in rock domains RSMA01, RSMM01 and RSMD01 assessed from measurements and from simulated TRC-distributions is fairly constant throughout the modelled rock volume and amounts to 2.16, 2.21 and 2.23 $MJ/(m^3 \cdot K)$, respectively. These values are valid for the 2 m scale and at a temperature of 20°C.

The *in situ* temperature constitutes the initial temperature condition for a repository. The current mean temperature at –500 m elevation is estimated at 14.8°C, based on measurements in boreholes KLX02, KLX05, KLX08 and KLX11A.

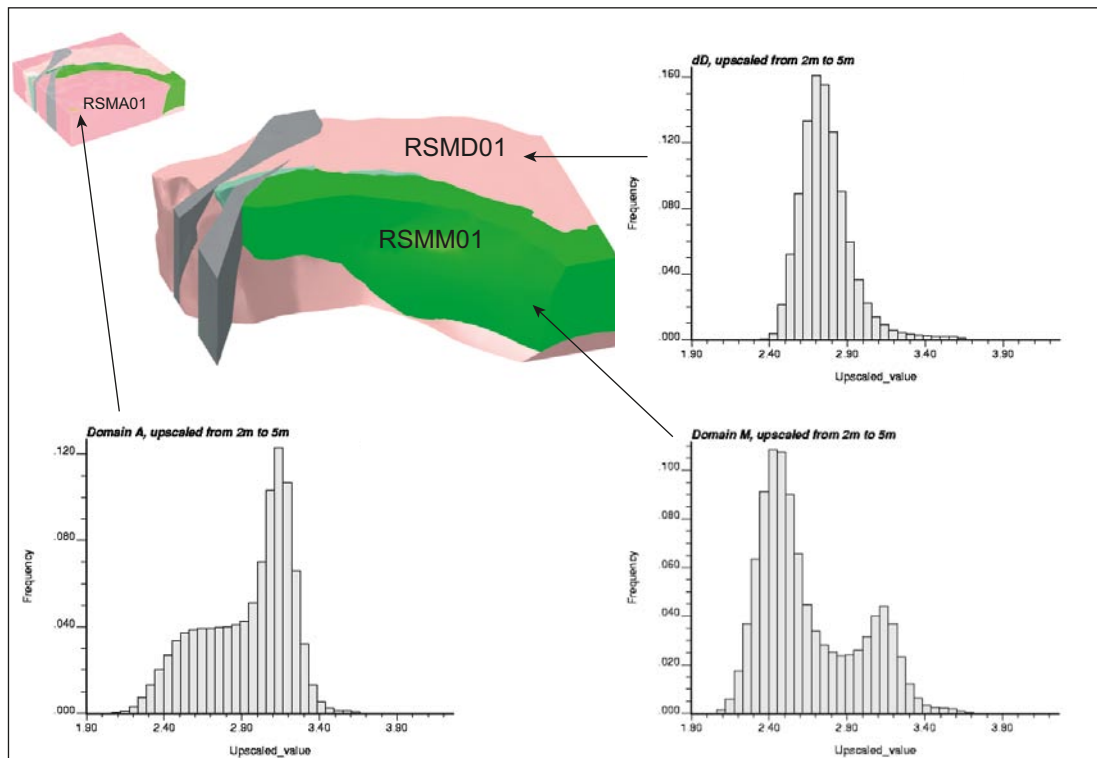


Figure 11-8. Modelled thermal conductivity at the 5 m scale for rock domains RSMA01, RSMM01 and RSMD01. The lower tails of the distributions are to a large extent characteristic of the rock types Ävrö quartz monzodiorite, diorite-gabbro and quartz monzodiorite (different for each domain). Modified after Figure 5-25 and Figures 6-16 to 6-18.

Confidence

Rock domains RSMA01 and RSMM01 are both characterised by heterogeneity in rock type distribution and both show similar values for the lower tail percentiles. Rock domain RSMD01 on the other hand is more homogeneous and shows higher values for the lower tail percentiles, the latter implying shorter canister spacing. The confidence in the overall distribution of thermal conductivity is high for RSMD01, because of its homogeneity. The confidence in the lower tails of the distributions, which is important for the thermal dimensioning of the layout of the repository, is generally high, although slightly higher for RSMA01 and RSMM01 than for RSMD01. Overall confidence in the thermal model is reinforced by its consistency with the rock domain model.

11.2.6 Strength and other mechanical properties of intact rock

Lithology also affects the thermal expansion, mechanical strength and deformation properties of intact matrix rock. The assessment of thermal expansion, mechanical strength and deformation properties is based on results from measurements on samples from the dominant rock types in RSMA01, RSMM01 and RSMD01.

Thermal expansion

The mean value of the measured thermal expansion coefficient for the dominant rock types in the identified rock domains at Laxemar (diorite-gabbro, quartz monzodiorite, Ävrö quartz monzodiorite, Ävrö granodiorite) vary between $7.1 \cdot 10^{-6}$ – $7.4 \cdot 10^{-6}$ m/(m·K). Domain modelling has not been performed and given the small differences in measured values, thermal expansion appears well constrained.

Strength and deformation modulus

The mean uniaxial compressive strength (UCS) and Young's modulus (E) of the dominant rock types in the rock domains RSMA01, RSMM01 and RSMD01 show that these rock types are medium strong to strong (167–225 MPa) and stiff (deformation modulus > 70 GPa), cf. Table 7-3. The UCS of the corresponding altered varieties is some 10% lower. The crack initiation stress is shown to be 52–57% of the uniaxial peak stress (i.e. of the UCS).

Confidence

The confidence in the derived mechanical properties of the rock mass is in general high, due to the large amount of data in support of the model and only minor changes in values caused by the addition of new data during the various modelling stages. Furthermore, the results are consistent with the understanding of the geology of the site. The confidence in the strength and deformation properties of the separately described rock types of rock domains RSMA01, RSMM01 and RSMD01 is dependent on the number of tested samples, but is generally considered to be high. On the rock domain level, the uncertainty in proportions of different rock types in rock domain RSMM01, where the spread in strength between existing rock types is wide, makes the prediction of strength distribution in this domain fairly inconclusive.

11.3 Deformation zones, fracture domains and fractures

11.3.1 Origin and reactivation throughout geological time

The focused volume in Laxemar is well bounded by major deformation zones, and in particular the major shear zones east and west of the area. Five sets of deformation zones have been identified with a high confidence of existence in Laxemar, cf. Figure 5-32. These comprise NE-SW and N-S striking, moderately to steeply dipping zones, E-W to NW-SE striking zones with steep to moderate dip to the south, E-W to NW-SE striking zones with moderate dip to the north and gently dipping zones, cf. Section 5.5.4. Although more or less strongly overprinted by polyphase brittle deformation (reactivation), the vast majority of the zones were originally formed when the bedrock still responded to stress in a ductile manner. This implies that the gross structural framework was established early in the geological evolution of the Laxemar-Simpevarp area, cf. Section 11.2.1. Apart from zone ZSMEW007A in central Laxemar, very few zones are interpreted to only display brittle deformation. Examples of deformation zones that are dominated by ductile deformation, i.e. that only display minor brittle overprinting, are the NE-trending set of zones that make up the Äspö shear zone system, i.e. ZSMNE004A and ZSMNE005A, in the easternmost part of Laxemar. A corresponding NE-trending zone occurs west of Laxemar (ZSMNE011A), and, consequently, Laxemar is interpreted to be bounded both in the east and west by deformation zones of predominantly ductile character, cf. Figure 11-5 and Figure 11-9.

Low-temperature geochronological data, dating of fracture minerals, kinematic data and consideration of the regional tectonic context have been utilised to establish a conceptual understanding of the formation and reactivation of deformation zones from the waning stages of the Svecokarelian orogeny, c. 1.80 to 1.75 Ga, until the Quaternary. The conceptual understanding suggests that the majority of the deformation zones had formed and had possibly also been reactivated during Palaeoproterozoic time, i.e. prior to 1.6 Ga, and have been reactivated in conjunction with orogenic events during the remainder of the Proterozoic and the Phanerozoic (cf. Figure 5-27). Available data indicate that tectonic reactivation and/or hydrothermal alteration has occurred in deformation zones in the Laxemar-Simpevarp area in conjunction with the intrusions of the 1.45 Ga Götömar and Uthammar granites, as well as the 1,100–900 Ma Sveconorwegian, and 510–400 Ma Caledonian orogenies. Apart from the tectonic activities, which are presumed to have waned with time, the effects of deposition (loading) of sediments and subsequent erosion (unloading) and exhumation of the crystalline basement are of significance. Examples of loading events in south-eastern Sweden are the formation of sedimentary basins and accompanying deposition of sediments on the crystalline basement after c. 900 Ma and c. 400 Ma, caused by erosion of the Sveconorwegian and Caledonian mountain ranges, respectively. Further examples of loading events that have affected south-eastern Sweden are the development of a passive continental margin during the Early Palaeozoic and repeated glaciations during the Quaternary period.

The ductile deformation zones are the oldest structures in the Laxemar-Simpevarp area. Kinematic data indicate that NE- and N-S-trending zones are characterised by sinistral movements, whereas E-W zones display more complex kinematics /Lundberg and Sjöström 2006/. The kinematic data suggest that the ductile deformation zones formed in response to bulk crustal shortening in an approximately N-S direction. There is a lack of reliable ductile, kinematic data from the regional, inclined E-W striking deformation zones. However, during the N-S directed bulk shortening suggested by the kinematic indicators on the NE trending deformation zones, the E-W trending zones, which as noted above have a moderate dip, would be reactivated in a reverse, dip-slip sense. An alternative interpretation with a bulk crustal shortening in approximately NE-SW direction has been proposed by /Viola 2008/. However, an approximately N-S bulk crustal shortening direction is favoured since this is in accordance with the regional geological context within the Svecokarelian orogen, cf. Section 3.1.2.

The unravelling of the subsequent brittle deformation is based on the definition of conjugate fracture sets (cf. Section 5.2.7 and /Viola 2008/). Two episodes of compression with shortening in direction c. NNW-SSE and NNE-SSW generated conjugate fractures coated with epidote and quartz. These are interpreted to be related to the latest stages of the Svecokarelian and possibly Gothian orogenies, respectively. Accordingly, the movements along the deformation zones would be predicted to be similar to those formed in the ductile regime. Dating of adularia and biotite using $^{40}\text{Ar}/^{39}\text{Ar}$ has revealed that the bedrock in the Laxemar-Simpevarp area was indeed affected by the Sveconorwegian orogeny, which is supposed to have caused an overall c. E-W bulk crustal shortening in the area. Conceptually, and in contrast to the earlier history, this implies that movements along the NE-SW and NW-SE oriented steep zones would be dextral and sinistral, respectively, and the N-S oriented zones were subjected to compression and characterised by dip-slip movement if not too steeply inclined. However, the crustal shortening was followed by late Sveconorwegian c. E-W extension/transtension, manifested by the intrusion of late Sveconorwegian N-S trending dolerite dykes in reactivated zones. Data also demonstrate that the bedrock was affected by the Caledonian orogeny, as indicated by e.g. $^{40}\text{Ar}/^{39}\text{Ar}$ adularia ages. From a conceptual point of view, the Caledonian NW-SE shortening direction would give rise to, for example, compressional conditions in NE-SW oriented zones and sinistral movements in N-S trending zones. Although reactivation of zones and fractures has been demonstrated in the Laxemar-Simpevarp area during the Sveconorwegian and Caledonian orogenic events, there remains an uncertainty regarding to what extent zones/fractures formed or were reactivated in conjunction with these events. Permian NE-SW transtension has also been indicated in the area along reactivated suitably oriented, moderately to gently dipping fractures, as well as NE-SW and NNW-SSE shortening events in the Ordovician limestones on the island of Öland. The latter could tentatively be far-field effects of the Alpine orogeny. Each of these orogenies may have caused reactivation of pre-existing deformation zones and fractures, which consequently complicate the understanding of the geological evolution.

The possible reactivation of fractures and deformation zones due to loading of sedimentary successions after, for example, the Sveconorwegian and Caledonian orogenies is not clear. The same applies to possible effects of loading due to the glaciations and subsequent unloading due to ice retreat during the Quaternary. The rock stresses in Laxemar are of similar magnitude as for crystalline bedrock in Sweden. Sheet jointing due to stress release is not a common feature in the Laxemar-Simpevarp area. However, exceptions are found in the younger Götömar granite (e.g. as seen in the Kråkemåla quarry).

11.3.2 Deterministic deformation zones

It is strongly indicated that the overall structural framework was formed when the bedrock still responded to ductile deformation. Given that the majority of deformation zones show signs of poly-phase brittle reactivation, this suggests that the framework of ductile deformation zones has steered the stress release during the subsequent geological evolution in the brittle regime, cf. Sections 5.5.1 and 5.5.2.

The developed deterministic deformation zone model constitutes an integration of the current understanding of the deformation history in the region. This was developed from available magnetic lineament, seismic reflection and refraction data as available from the surface, as well as data on fracture orientation, fracture mineralogy and alteration, as available from surface measurements

and, in particular, from cored boreholes. Lineaments associated with magnetic and electromagnetic anomalies derived from both high-resolution ground magnetic data and aerial survey data across the focused area and its immediate surroundings, in combination with topographical data, including high resolution Lidar data (detailed digital elevation model (DEM)), are the main surface data that support the occurrence of steeply dipping deformation zones of length $\geq 1,000$ m (Figure 11-9). The various lineament indications are combined, and ultimately form the basis of the map of linked coordinated lineaments (Figure 5-18). The magnetic anomalies stem from alteration/oxidation of minerals (magnetite) in the deformation zone resulting in reduced magnetic susceptibility (compare Figure 11-5 and Figure 5-19). This alteration has its correspondence at depth in the geophysical anomaly pattern caused by the possible deformation zones identified in the geological single-hole interpretation of boreholes.

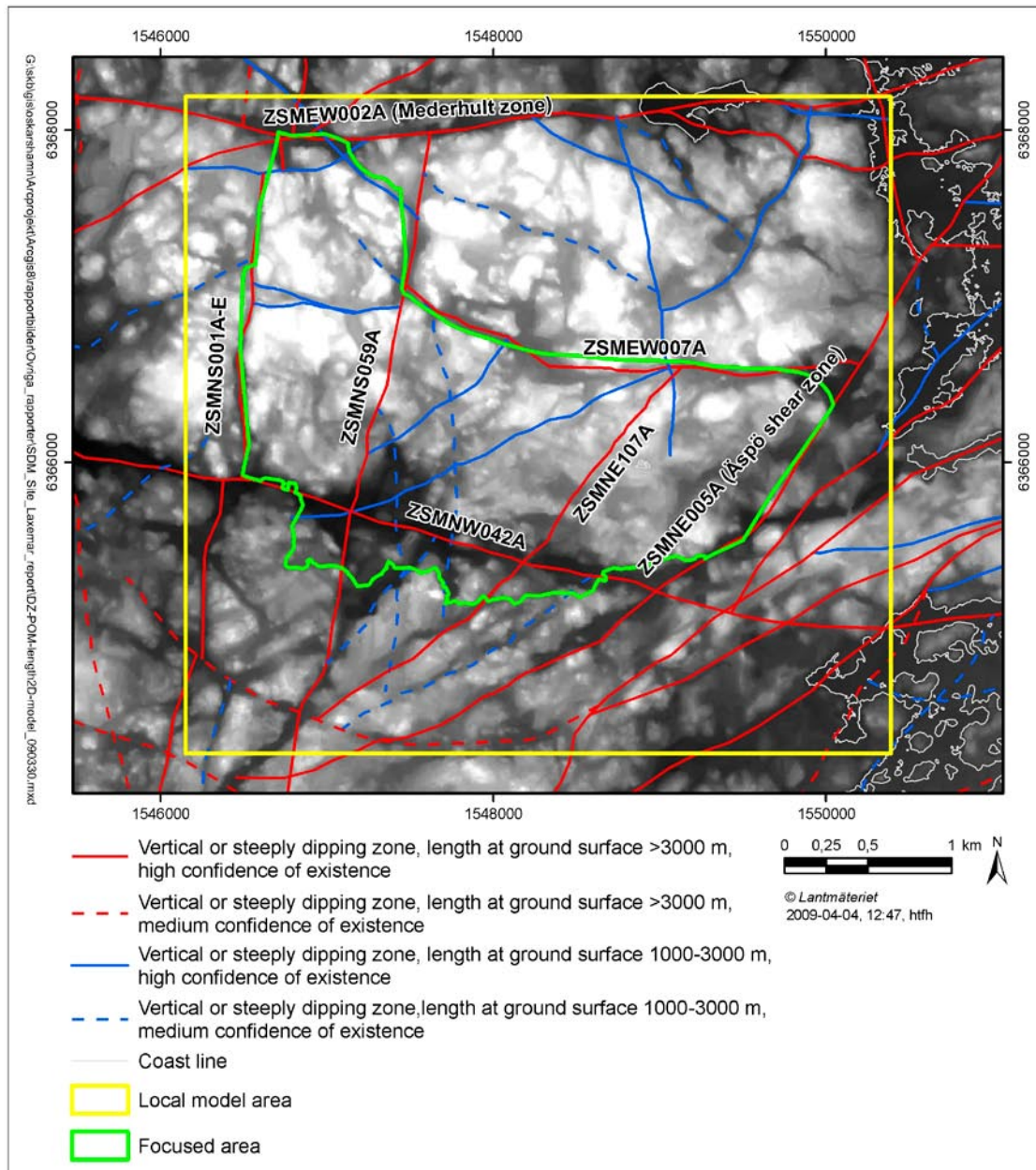


Figure 11-9. Map of modelled deterministic deformation zones within the local model area. Confidence attributed to steeply dipping deformation zones longer than 1,000 m is given as established by combining various geophysical techniques with targeted boreholes. The underlying map shows topography as given by the digital elevation model (DEM), 10 m resolution.

Interpretation of the geometry of deterministic deformation zones devoid of borehole intercepts is in principle possible from the shape of geophysical anomaly patterns, in places also supported by escarpments in the topography, and/or the pattern of the refraction seismic anomalies. However, as a rule, the interpreted deformation zones that lack borehole intercepts are assumed to be vertical. Deformation zones identified in the extended single-hole interpretation (ESHI) with an estimated true thickness greater than 10 m and without an associated lineament on the ground surface are modelled deterministically as circular discs of finite size, cf. Section 5.5.3.

Geometrical constraints on the occurrence of gently dipping deformation zones are provided by seismic reflection and borehole data. The gently south-dipping reflector M1, cf. Section 5.5.4 and /Juhlin et al. 2004/, marks the upper limit of what is judged to be a thicker discontinuous series of minor deformation zones and spatially associated mafic intrusions rather than a singular structure. A correlation has been established between the geometry of this reflector and the geometry of the subordinate rock type fine-grained diorite-gabbro and the inherent foliation, suggesting that this subordinate rock type has steered the development of the gently dipping inferred deformation zone which relates to the M1 reflector. No major subhorizontal or gently dipping zone has been interpreted, whereas a number of gently dipping minor deformation zones have been documented (cf. Figure 5-22 and Section 11.3.3). However, these are interpreted to be of limited extent.

The local model contains a total of 70 deterministically modelled deformation zones, of which 47 are associated with either interpreted surface outcrop or multiple intercepts in boreholes, and 23 are associated with deformation zones based on singular borehole intercepts devoid of surface expression (modelled as circular discs of finite size). The majority (> 75%) of these interpreted deterministic deformation zones are judged to be of high confidence in terms of their existence. The geological and geophysical data which form the basis for interpretation of each individual deformation zone are provided in /Wahlgren et al. 2008, cf. Table 5-5 and Appendix 14 therein/. Only 8 deformation zones longer than 3 km in the local model volume intersect the margins and surface of the focused volume (ZSMNS001B and ZSMNS001C, ZSMEW007B and ZSMEW007C are counted as two singular deformation zones, respectively), and another 21 deformation zones in the size range 1 to 3 kms (of which 10 are devoid of surface expression), intersect the margins of the defined focused volume in the depth interval -400 to -600 m. A compilation of properties of the latter deformation zones is provided in Appendix 6.

Most zones do not have one distinct single core surrounded by a symmetric transition zone distributed on either side of the deformation zone. Rather, several narrow cores are more common in the thicker zones. The cores are distinguished from the transition zones by e.g. very high fracture frequency, strong hydrothermal alteration (e.g. red staining), and the occurrence of cohesive (e.g. cataclasites, cemented breccias) or non-cohesive rocks (e.g. breccia, fault gouge).

The regional model contains 171 deformation zones that are modelled deterministically, of which 40 are also part of the local model. The number of high confidence deformation zones in the regional model is 33 (19%). The regional model contains 68 deformation zones with a length of 3 km or more.

Hydraulic interference tests have provided support for the established deterministic deformation zone model, particularly in the central and southwest parts, cf. Section 11.6.2 and Section 8.3.3.

Confidence

The confidence in the existence and location of deterministic deformation zones that are important for the layout of a repository is high in the local model volume, but the uncertainty in their location increases towards depth, and away from borehole intercepts. Notwithstanding, the overall pattern of deformation zones at repository depth is considered well known. Furthermore, the orientation and extent of deformation zones based only on a single borehole, without identifiable surface expression and represented by finite discs in the model, is generally medium to low. The possible occurrence of yet undetected deformation zones longer than 3,000 m is judged unlikely. It is furthermore considered that the deterministic model of deformation zones has reached an acceptable level of stability, in particular with regards to the local model volume. Other uncertainties in the deterministic deformation zone model are associated with the geometries of deformation zones not intercepted by boreholes, although this concerns mostly the regional model beyond the local model boundary.

Furthermore, there exists an uncertainty regarding the heterogeneity of the properties of deformation zones, both along strike and down dip, given that most zones are only intercepted by one borehole. The geometry, especially true thicknesses, of deterministic deformation zones is difficult to assess, since deformation zones, in particular those that are mainly brittle in character, rarely are exposed at the ground surface. Finally, the true extent of gently dipping zones known only in boreholes is associated with uncertainty, given the possibility of their being displaced along cross-cutting vertical deformation zones. Uncertainty is qualified by the use of confidence classes and, where appropriate, spans of likely values of individual zone properties, see /Wahlgren et al. 2008, cf. Appendix 14 therein/.

It is important to note that the cross-plot between deformation zone true thickness and zone size presented in Figure 5-28 is based solely on data from the deformation zone model; it does not include data for structures shorter than 1,000 m in trace length (MDZ, cf. Section 11.3.3). There are insufficient data on feature size in the population of minor deformation zones (MDZ) to determine if the thickness-size relationship is valid at smaller scales. Consequently, there exists a risk that a structure observed in a cored borehole and classified as an MDZ may in fact actually represent a previously undetected deformation zone (length > 1,000 m). It is very difficult to associate specific probability to this risk due to the fact that structure thickness may vary in space, a size-intensity probability model has not been fitted to the deformation zone model and that the relationship between length and thickness has not been established for MDZ. It is also noted that some of the deterministic deformation zones based on a single intercept may in fact represent features smaller than the 1,000 m cut-off between deterministic deformation zones and MDZ.

11.3.3 Minor deformation zones

Minor deformation zones (MDZ) are assumed to affect the positioning of individual canister deposition holes. In Laxemar, MDZ are interpreted to have a size < 1,000 m, and are consequently modelled stochastically as part of the geological and hydrogeological discrete fracture network (DFN) models, cf. Sections 5.6.3 and 8.5.2, respectively. The description of minor deformation zones, as a component of the stochastic geological DFN model, is based primarily on the trace length distribution of Lidar and high-resolution ground-magnetic lineaments combined with the measured intensity of MDZ in boreholes from the ESHI process. Data from 3D seismic reflection/refraction surveys were not used in the parameterisation of MDZ.

An overall premise for the modelling is that all linked lineaments < 1,000 m are assumed to constitute MDZ. This assumption was tested in a targeted MDZ study where 18 linked lineaments of MDZ size were explored by short cored boreholes, which identified them as brittle-ductile features, associated with increased fracturing, and in places by crush and mylonites and by enhanced transmissivity. The study concluded that not all linked lineaments can be conclusively identified as being of practical importance (primarily with regards to hydraulic conductivity). Furthermore, it was evident that it is not easy to correlate a linked lineament with a corresponding intercept in a borehole, even over the limited depths involved in the study. The uncertainty regarding whether a lineament reflects a structural feature (MDZ) in the bedrock was further explored as part of the geological DFN modelling (Section 5.9), and was shown to be less important than other conceptual and parameter uncertainties of the geological DFN parameterisation /La Pointe et al. 2008/.

In total, 243 MDZ were recorded in the Laxemar cored borehole data set; however there was only sufficient information available to assign orientations to 211 of the 243 MDZ. Approximately 50% of the MDZ were interpreted as being brittle, 16% as ductile and 34% as being ductile-brittle in character. A large proportion (65%) of the MDZ was associated with subordinate rock types; specifically, 45% of the MDZ were associated with fine-grained granite. The median thickness of the MDZ identified in boreholes is 1 m, where 51% have true thicknesses smaller than 1 m, cf. Figure 5-60. Approximately 70% of the MDZ belong to the subhorizontally- to gently dipping set. Subvertical orientation sets of the MDZ are found to be comparable with those of the local major deformations zones, and ultimately, with the fracture orientation patterns of the fracture domains, cf. Section 11.3.4.

Spacings between MDZ in the deeper boreholes at Laxemar are in the order of 120–200 m, which is in agreement with similar observations in deeper boreholes at the Äspö HRL (75–200 m), with somewhat shorter distances seen in the Äspö access tunnel (75–100 m).

The size distribution of MDZ is not well known. However, attempts to constrain the minimum size of MDZ relative to their intensity in boreholes /La Pointe et al. 2008, cf. Section 5.5 therein/ suggest a minimum size (radius) between 63 and 125 m, as a function of fracture domain and fracture set. A minimum size of 75 m is recommended as a functional definition for the size transition between fracture and MDZ.

The hydraulic significance of MDZ is discussed in Section 11.5.2.

Confidence

The uncertainty regarding the existence and character of MDZ is quite large and is nearly impossible to address without additional data that only can be obtained during underground construction and from additional surface mapping efforts at larger (10 m–1,000 m) scales. Nevertheless, it is believed that the uncertainty is quantified inside the general size-intensity uncertainty of the geological DFN and its various alternative models. It will likely never be possible to predict the locations and geometries of every MDZ at the site scale, but significant insight can be gained through stochastic simulation. The understanding and treatment of MDZ will continue to evolve in conjunction with development of e.g. detailed scale models when commencing underground construction.

11.3.4 Fracture domains, fractures and geological DFN model

Analyses of fracture data have indicated that fracturing in the rock between deterministic deformation zones in the local model volume can be described using four fracture sets; a subvertically dipping, NS striking set that appears to be the oldest; an ENE-WSW striking subvertically dipping set; a WNW-ESE striking subvertically dipping set; and a subhorizontally to moderately dipping set of fractures that generally strike NS to NNW (SH set). Open and partially open fractures make up some 30% of the fracture population in the cored boreholes. The ensuing geological DFN model, builds on the subdivision into fracture domains, and is designed to describe fractures and minor deformation zones with an equivalent radius less than the equivalent to that of a square fracture of trace length 1,000 m).

Fracture domains

Fracture domains were identified by examining fracture orientation data from boreholes, outcrops, and trenches for spatial trends in orientation and the relative intensity of pole clusters (Figure 5-56). Tentative fracture domains were delineated by combining observed fracture set orientation and set-relative intensity patterns with potential volume boundaries (regional and local major deformation zones from the deformation zone model) and an understanding of the deformation history and tectonics in the Laxemar-Simpevarp region. The relative intensities of the fracture sets defined were used to complete the fracture domain criteria. There is no direct correspondence between fracture domains and rock domains (Section 5.7); fracture domain boundaries are defined by the deformation zone model, which by in large cut across multiple rock domains. The statistical analysis of fracture intensity patterns /La Pointe et al. 2008, cf. Section 4.4.4 therein/ did suggest some correlation of fracture intensity to host rock lithology, but not to rock domain.

Altogether six fracture domains were identified, cf. Section 5.6 (Figure 5-57) and Figure 11-10. Those of primary interest for hosting a repository are FSM_C, FSM_W, FSM_NE005 and parts of FSM_EW007, cf. Section 5.6.1 and Figure 5-57 for details on the tectonic context.

- Fracture domain FSM_EW007 represents an approximately 250 m thick volume of rock distributed unevenly on either side, and excluding, deformation zone ZSMEW007A and features a reduced intensity of both N-S striking and open subhorizontal fractures, although most open fractures appear to belong to the WNW set. Both fracture intensity and orientation have been interpreted as being affected by the E-W striking deformation zone ZSMEW007A.
- Fracture domain FSM_NE005 represents a rock volume immediately west of the regional deformation zone ZSMNE005A, being one of several major belts of NE-SW trending ductile deformation in the region, cf. Section 11.3.1. Domain FSM_NE005 is characterised by a significant increase in the relative intensity of N-S striking sealed fractures.
- Fracture domain FSM_C is the volume of rock immediately south of FSM_EW007 and north of deformation zone ZSMNW042A. This domain is dominated by sealed N-S striking fractures in a fashion similar to FSM_W, and open WNW striking fractures.
- Fracture domain FSM_W represents the volume of rock bounded by deformation zones ZSMNS001C, ZSMNS059A, ZSMNW042A, and ZSMEW002A, cf. Figure 11-9 and Figure 11-10. Borehole data suggest dominant north-south fracture strikes in both subvertically dipping and subhorizontal fracture sets. The third set of fractures strikes ENE, shows a relatively weak intensity and is roughly parallel to the NE-SW striking sinistral shear zones which form the overall tectonic fabric of the region.

An additional two domains, FSM_N (north of FSM_EW007) and FSM_S (hanging wall of deformation zone ZSMNW042A) complete the fracture domains interpreted within the local model volume. Overall, patterns of relative fracture intensity inside each domain appear to correspond well to the tectonic history forming the base of the deterministic deformation zone modelling. The subdivision into these fracture domains is further supported by the estimated hydraulic properties of the bedrock between deformation zones, cf. Section 11.5.2.

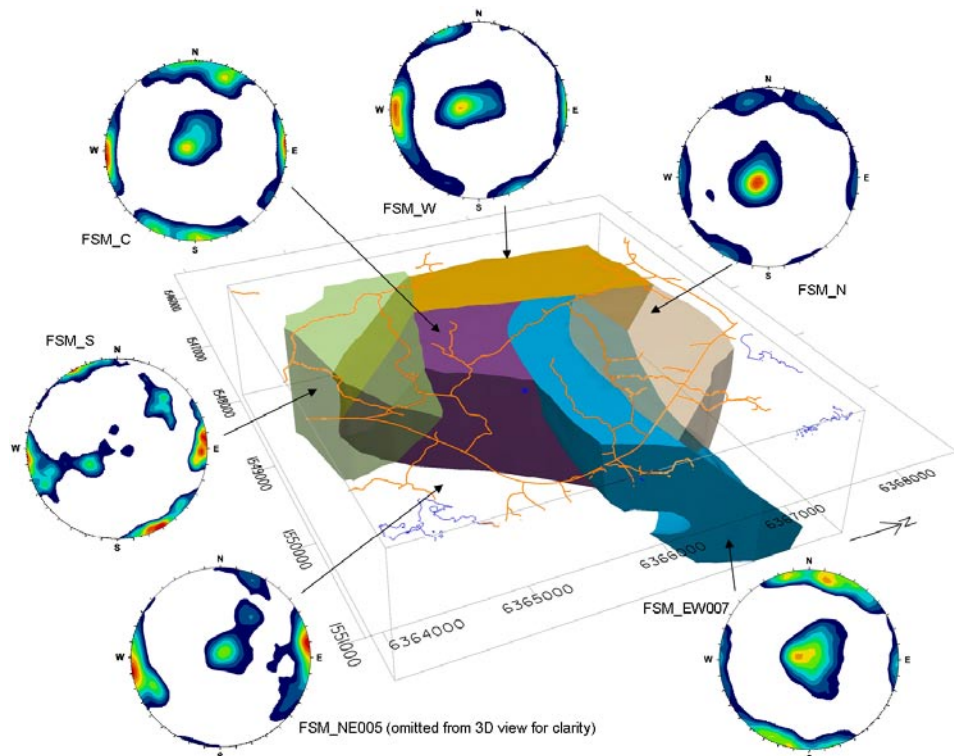


Figure 11-10. Perspective view of fracture domains with pole diagrams of associated fracturing. Note that fracture domain FSM_NE005 has been cut away from the figure so as to better show the behaviour of FSM_C (which contains the target repository volume) at depth. Perspective view from the southeast, see also Figure 5-57.

At depths greater than about 100 m, no or very weak depth dependency in the intensity of fractures (whether open, open + sealed) is noticed, cf. Section 5.6.3. Depth dependencies in fracturing are more readily apparent in the upper 100 m, cf. Section 11.7.1. As further explained in Section 11.5.2, a clear decrease with depth in the intensity of flowing fractures is seen in the PFL logging data from cored boreholes.

Geological discrete fracture network models

Fractures and MDZ with interpreted sizes less than 1,000 m long are treated stochastically through geological DFN models. The geological DFN, which is a statistical representation of the orientations, sizes, intensities, and locations of bedrock fractures, incorporates both open and sealed fractures in its parameterisation. The assumption is that sealed fractures should be treated as potential planes of weakness or containing flow paths that could potentially be accessed in the future due to changes in the *in situ* stress field, groundwater chemistry or short-circuiting effects induced by underground construction.

Geological DFN model parameterisations have been produced for the six fracture domains identified within the local model volume at Laxemar. The assumptions and components of the geological DFN modelling are detailed in Sections 5.6.2 and 5.6.3.

The coupled fracture size/fracture intensity model is the key component of the geological DFN; it describes both the size of fractures, expressed as equivalent radius and the intensity in terms of fracture area per unit volume (P_{32}). A total of 29 different size-intensity model alternatives have been produced as part of the geological Laxemar DFN; each alternative represents a different potential combination of conceptual assumptions and data treatments (Section 5.6.3).

Based on verification simulations with subsequent comparison with observed fracture data and subsequent ranking, a recommended size-intensity model was selected, cf. Section 5.6.3, which is based on Euclidian scaling, a 3D Poisson point process fracture centre location model, size parameterised from unlinked outcrop fracture traces, a global (i.e. the same value for all fracture domains) value for the radius scaling exponent k_r , and fracture domain-dependent minimum fracture size (r_o).

Confidence

The orientations, geological controls, and intensity (P_{32}) of rock fractures are considered fairly well-constrained, although there is a relative lack of data from sub-repository depths when compared to the rock volumes above the typical repository horizon. In general, these three parameters are known with moderate (intensity) to high (geologic control, orientation) confidence. The most uncertain aspect of the geological DFN is the size model, especially with regards to the size of large (> 10 m) fractures and MDZ. This includes the conceptual uncertainty that it might not be appropriate to use fracture trace data from the ground surface to describe fracture traces at repository depths which can only be tested underground.

The sizes of large fractures and MDZ are constrained by lineament maps based on high-resolution ground magnetic and Lidar data. The orientations of Lidar and high-resolution ground magnetic lineaments are fairly certain, but information on the dip and dip direction of most of the structures suggested by lineaments is weak. There is very little information available on the size distribution of subhorizontally to gently dipping MDZ. The available data come from surface outcrops; the abundance of borehole data is not helpful in this particular case. Information on sizes in the range 10 m to ~ 100 m is also missing. Lineament maps only cover fractures and deformation zones down to ~ 100 m in length, while the outcrops generally only sample structures up to a maximum of ~ 10 m in length. The resolution of indirect assessment using geophysics is not sufficient to address this deficiency. The uncertainty in size is quantified through uncertainty analysis, which produces ratios of P_{32} for various size-intensity model alternatives, and by a verification case ranking of alternative models, cf. detailed discussion in Section 5.9.

The primary effect of the uncertainty in the geological DFN model is on the volume of rock found to be suitable for canister deposition holes once repository construction begins (referred to as “degree of utilisation”). The degree of utilisation will be controlled primarily by the intensity of fractures larger than approximately 3 m in radius (Section 5.6.3). The uncertainty has been bracketed by the inclusion of parameters for multiple competing size-intensity model alternatives in the geological DFN reporting, cf. a more comprehensive discussion in /La Pointe et al. 2008, cf. Section 6.3 therein/.

11.3.5 Fracture mineralogy

Detailed studies /Drake et al. 2006, Drake and Tullborg 2009a/ of fracture mineralogy and wall rock alteration have provided information on the type and abundance of fracture minerals in Laxemar. Calcite and chlorite are by far the most common fracture minerals, and these are especially frequent in the open fractures. Other common minerals are clay minerals, pyrite, hematite, epidote, adularia, quartz and prehnite. Rare occurrences (in less than 1% of the fractures) of, for example, zeolites, gypsum, fluorite, muscovite, chalcopyrite, are also observed.

Different generations of fracture minerals have been recognised at Laxemar (Section 5. 2.6 and 9.5.6), and their relative age relationships are distinguished using various techniques. The absolute ages of some of these generations have also been established. The relative and absolute age determinations have been used in the establishment of the geological evolution of the site, cf. Section 3.1.2. The oldest fracture mineralisations in the area are associated with mylonites and subsequently cataclasites formed as a result of reactivation of the mylonites. The mylonites, and probably most of the cataclasites, are older than the intrusions of the 1.4 Ga Göttemar and Uthammar granites north and south of the area, respectively, cf. Figure 11-6. The subsequent generation of fracture minerals was formed during a prolonged event with gradually lower formation temperatures in conjunction with the Göttemar and Uthammar granites. These fillings are associated with intense wall rock alteration, such as red staining, sericitisation, saussuritisation and greisen (close to the Göttemar granite) which is typical for the Laxemar-Simpevarp area. Fracture minerals which are suggested to be related to far-field effects of the Sveconorwegian orogeny (c. 1,100–900 Ma) are also documented, although this event has not been very significant in the area.

The occurrence of Lower Cambrian sandstone inside a few subvertically-dipping near-surface fractures at Laxemar indicates that the bedrock surface is close to the sub-Cambrian peneplain. The orientation of fractures which contain minerals interpreted to be related to the Caledonian orogeny (510–400 Ma) corresponds to the orogenic bulk shortening direction. Fracture fillings of similar mineralogy as the Caledonian fracture fillings were precipitated intermittently in open bedrock fractures from the late Palaeozoic during a gradual lowering of temperature, ranging to ambient temperatures similar to present conditions. A combination of calcite $\delta^{18}\text{O}$ values and crystal morphologies indicate formation from waters with different $\delta^{18}\text{O}$ values and salinities (fresh and brackish water). Fracture coatings in currently water conducting fractures often consist of clay minerals, calcite, chlorite, and wall rock fragments. The amount of potentially very young (Quaternary) fracture minerals is very small compared with older fracture minerals. The most common fracture minerals in open fractures (chlorite and calcite) show no distinctive variation with depth (Figure 5-13) and the frequency of these minerals generally follows the variation in total fracture frequency. Clays are the third most frequent minerals in open fractures and their frequency follows the variation in frequency of open fractures with depth, although the relative frequency is commonly higher in interpreted deformation zones. Most other minerals show no significant variation with depth.

Pyrite is a common mineral in open fractures at most depths, although there is a clear decrease in pyrite occurrences near the surface. This decrease is correlated with an increase in the number of goethite-bearing fractures (Figure 5-14). This mineral distribution trend is interpreted as being an effect of oxidising conditions near the surface (Figure 9-13). Open fractures without any visible mineral coating and with fresh wall rock surfaces are relatively rare in Laxemar, although there is an increase of this fracture type towards the ground surface (Figures 4-18 and 5-15). Occasional larger occurrences at greater depths are generally associated with deformation zones.

11.3.6 Mechanical properties of deformation zones and fractures

The strength and deformability properties of the natural rock fractures at laboratory scale are found to be essentially independent of fracture orientation and fracture orientation set, with the sole exception being a higher normal stiffness for the subhorizontal fracture set. Since no significant differences related to fracture set are observed, the choice is to employ one common model for all the fractures in all fracture domains (Table 7-4).

The average deformation moduli for rock inside deformation zones are in the order of 30–45 GPa, with rock inside minor deformation zones (MDZ) attributed an average modulus towards the higher end of this range. The deformation moduli of the deformation zones (Table 7-6), are roughly 65% of the corresponding strength of the fractured rock mass (Table 7-5), cf. Figure 11-11.

Confidence

The confidence in the mechanical properties of individual fractures is considered moderately high given the relatively large number of samples, and relative stability of results when adding new data. However, given that the samples analysed are somewhat biased towards individual fractures of smaller size, uncertainty remains regarding the mechanical behaviour of large-scale fractures.

The confidence in the mechanical properties of individual fractures is considered moderately high given the relatively large number of samples, and the relative stability of results when adding new data. However, given that the fracture samples analysed are biased towards individual fractures and given the size of tested fracture samples, uncertainty remains regarding the behaviour of the fractures at their full scale and also regarding the behaviour of more complex larger fractures.

11.4 Rock stress

11.4.1 Stress evolution

The stress evolution is closely related to the deformational history of the site. According to the established conceptual understanding (cf. Chapter 3 and Section 11.3.1), the different sets of deformation zones in Laxemar had formed and had already been subjected to reactivation more than 400 million years ago in response to stress conditions caused by different tectonic events along active continental margins.

The early establishments of these geological structures, and their response to subsequent tectonic events and loading and unloading cycles, connected with the burial and denudation of sedimentary rocks and glaciation and deglaciation, have most likely played a role in the evolution of the stress in the bedrock in Laxemar.

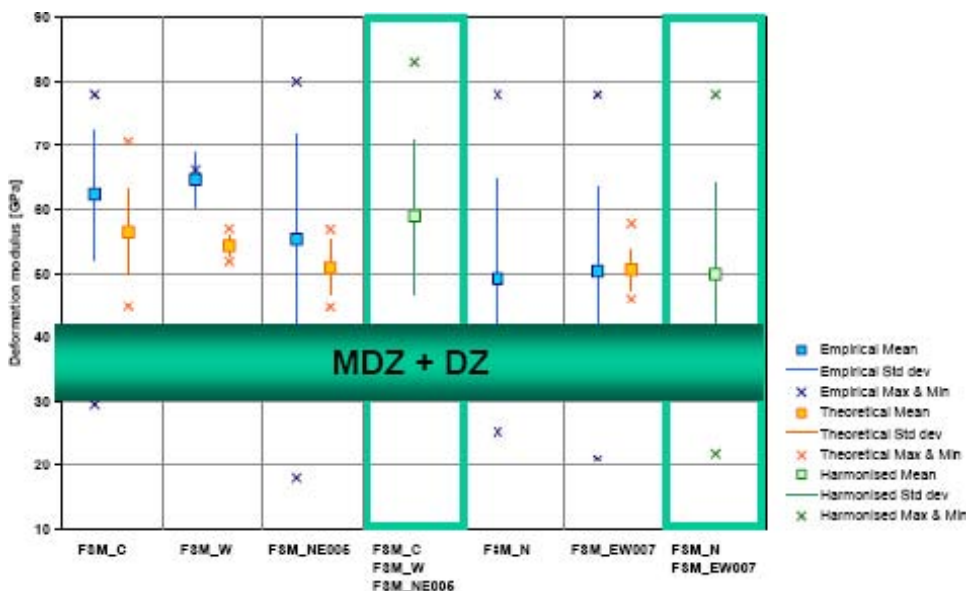


Figure 11-11. Comparison of the modelling result for the deformation modulus of fracture rock mass of defined fracture domains with that of deformation zones as established using the empirical approach and the theoretical approaches.

The current stress regime is dominated by the ongoing North-Atlantic ridge spread resulting in a NW–SE orientation of the major horizontal stress. The stress magnitude in the bedrock within the focused volume is assumed to be characterised by the measurements in borehole KLX12A, which suggest a steady increase in rock stress with depth.

11.4.2 Stress model

The assessment of the *in situ* stress state in Laxemar is based on both direct measurement and indirect observations. Data from direct overcoring measurements, hydraulic fracturing and hydraulic jacking of pre-existing fractures are available from two boreholes, KLX04 in fracture domains FSM_N and KLX12A in fracture domain FSM_C. To these data collection points should also be added measurements in a significant number of boreholes in the Simpevarp subarea and also at the Äspö HRL. Indirect observations of core dinking (N=9), borehole breakouts (N=17) and micro fallouts (N=26) from six boreholes (Section 7.2.4) indicate that only very minor portions of the rock show evidence of stress-driven damage.

Direct measurements as well as indirect observations all indicate a general orientation of the major principal stress in the sector of $N135 \pm 15^\circ$ (Figure 11-12).

The stress model for the focused volume in Laxemar (Section 7.3.5 and Figure 11-13) is developed based on data from overcoring measurements and evaluations of indirect observations combined with the understanding of the geological conditions at the site. The stress model indicates a major horizontal stress in the focused volume (valid for FSM_C, FSM_W and FSM_NE005) at –500 m elevation of c. 22 MPa and c.12 MPa for the minor horizontal stress, cf. Figure 11-13 and Table 7-8. The measured maximum stress levels at the Äspö HRL range from 27 to 30 MPa at a depth of 450 m and may be considered as an upper bound for the stress magnitudes, see Figure 11-13, also coinciding with the upper uncertainty bound presented.

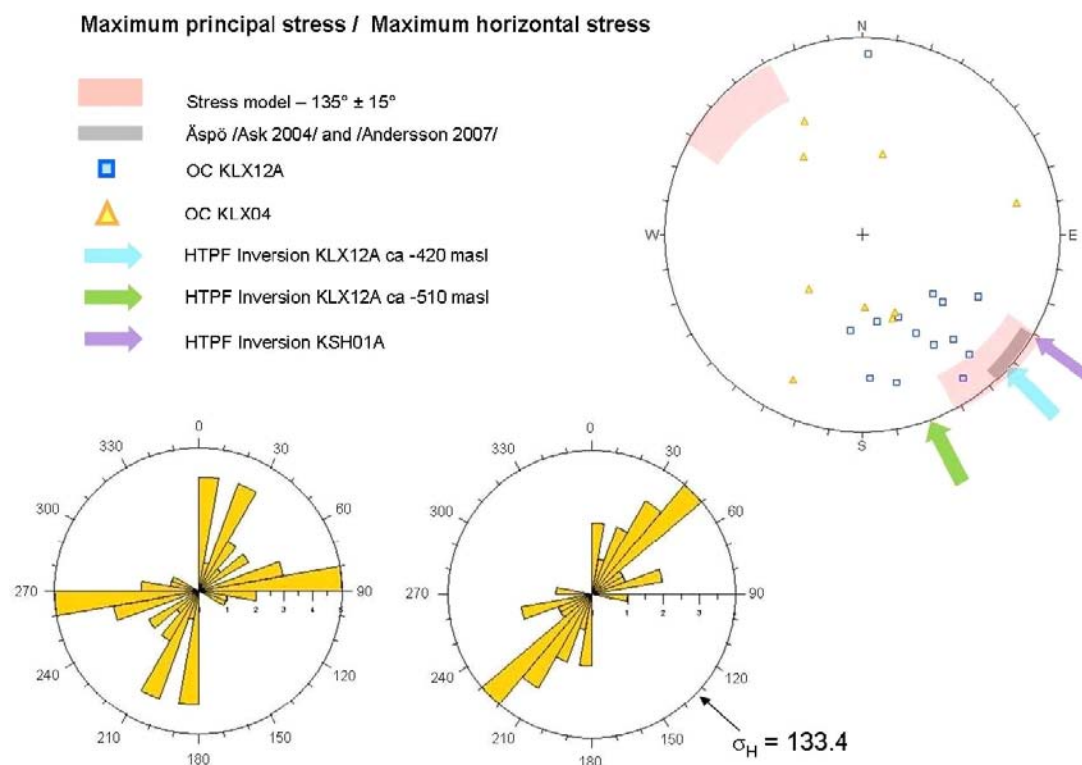


Figure 11-12. Orientation of major principal stress from direct measurements by overcoring (OC) together with the orientation of major horizontal stress from inversion of hydraulic jacking of pre-existing fractures (HTPF) and from indirect observations of micro fallouts (lower left, N=26) and borehole breakouts (lower right, N=17). The locations of borehole breakouts are predominantly concentrated to depths below –500 m, cf. Figure 7-15.

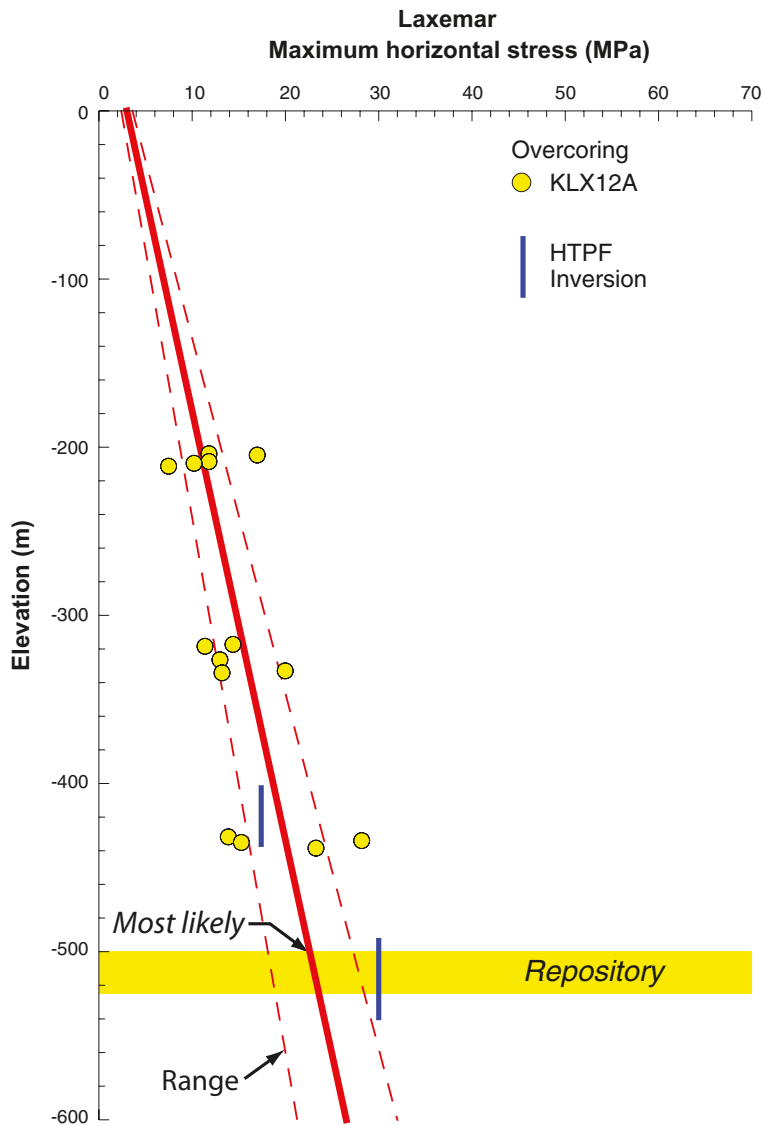


Figure 11-13. Model for the maximum horizontal stress (most likely value) and its uncertainty span as a function of depth, and underlying results from direct measurements in KLX12A (cf. Section 7.3.5).

All the stress measurements and indirect stress observations suggest increase of stress with depth and that the minor horizontal stress magnitude is approximately equal to the vertical stress, and that the maximum horizontal stress is approximately 2.5 to 3 times the vertical stress.

Confidence

The confidence in the orientation of the rock stresses is high given the consistent picture provided by the direct and indirect stress data from Laxemar and its environs, which also is consistent with the ongoing North-Atlantic ridge spread. Furthermore, the confidence in the absolute stress magnitudes is considered moderately high. This is based on the comparable values obtained from overcoring and HTPF measurements, further substantiated by the results of indirect observations. However, the confidence in the upper stress magnitude is even higher given the large number of deep boreholes in Laxemar, and given the minute amount of borehole breakouts.

11.5 Bedrock hydraulic properties

11.5.1 Evolution

Geological data from Laxemar, including the dating of fracture minerals, indicate that a large proportion of the fractures at the site are sealed (average ~70%). As noted above, the majority of the fractures can be regarded as ancient structures, especially in the deeper parts of the bedrock in the focused volume, i.e. fracture domains FSM_C and FSM_W and FSM_NE005. The youngest generation of calcite occurs in fractures and fracture zones that are currently hydraulically conductive, including depths below –500 m elevation, and may have precipitated during a long period including the present. The last major reactivation occurred over the Caledonian orogeny, some 510–400 Ma ago. Many conductive fractures have remained conductive ever since, although the distribution of conductive flow paths may have varied over time in the fractures and networks of fractures. The mineralogy of the conductive fractures (as seen in PFL-logs) does not stand out as different in relation to other fractures mapped as open, which makes tracing of the evolution of “conductivity” over time difficult, if not impossible. Based on these observations and indications, it is conceptually inferred that the hydraulic properties of the fractures can be correlated with both the brittle deformational history that formed and reactivated the fractures, and to the formation of fracture minerals during different periods in the past. There exists an apparent correlation with the current stress field and the fact that the WNW fracture set stands out as preferentially conductive. However, the processes that occurred during the past 1,800 million years most likely overshadow an apparent coupling to the current stress field, which has existed for approximately the past 12 million years.

11.5.2 Hydraulic properties of deformation zones and hydraulic rock domains

Detailed information on the position (and apparent thickness) of deterministically modelled deformation zones and conductive fractures in between deformation zones combined with results of high-resolution inflow measurements in 44 core-drilled boreholes and pumping tests in 30 percussion-drilled boreholes provide the basis for the assignment of hydraulic properties of deformation zones and hydraulic rock domains in Laxemar. These data constrain locations of interconnected flowing fractures with high certainty and provide values of the integrated (effective) transmissivity for the connected fractures down to c. 10^{-9} m²/s. Results of single-hole injection tests, and a number of multiple-hole interference tests of varying temporal and spatial coverage, complement the database.

Deformation zones

Analyses of the hydraulic data have revealed that all deformation zones, taken as a whole, irrespective of orientation (strike and dip), are characterised by a decrease in transmissivity with depth, with a contrast of c. 300 times for the uppermost 1,000 metres of the bedrock (Figure 8-16 and Figure 11-14). The range for the transmissivity of individual deformation zone intercepts range from about 10^{-8} to 10^{-3} m²/s with geometric mean values at –500 m varying from $5 \cdot 10^{-7}$ to 10^{-5} m²/s for the four deformation zone groups, E-W zones appearing more transmissive. The lateral heterogeneity at a given elevation cannot be assessed on a zone by zone basis given that the number of data from each zone is low. However, the lateral heterogeneity at each depth interval, as assessed from an ensemble of the pooled hydraulic data of all zones compiled in Figure 11-14, is substantial (the standard deviation range of $\log^{10}(T)$ is 0.5 to 2), cf. Section 8.4.1. This suggests the possibility of developed channelised flow within the deformation zone through the individual hydraulically connected, fractures of the zones.

An additional indication of heterogeneity on smaller scales is evident in the variability in flow-log data as measured across individual borehole intercepts with deformation zones, cf. an example in Figure 11-14. Only very weak evidence exists of regional scale anisotropy induced by variable transmissivity of deformation zones of different orientation, cf. Figure 8-16. A partial hydraulic barrier effect is foremost attributed to the existence of dolerite associated with deformation zones ZSMNS001C and ZSMNS059A, as established by *in situ* measurements, which could affect the regional flow patterns to some extent, cf. Section 8.8. The possible existence of additional smaller dolerite dykes has been inferred by geometrical and geophysical analogy, cf. Section 5.2.1, but the effects of these shorter dolerites on groundwater flow, if they do exist, are assumed negligible and local, cf. Section 8.9. An additional alternative manifestation of partial barrier effects within the focused area is attributed to the interpreted existence of fault gouge associated with deformation zone ZSMNW042A in the south, cf. Section 8.7.

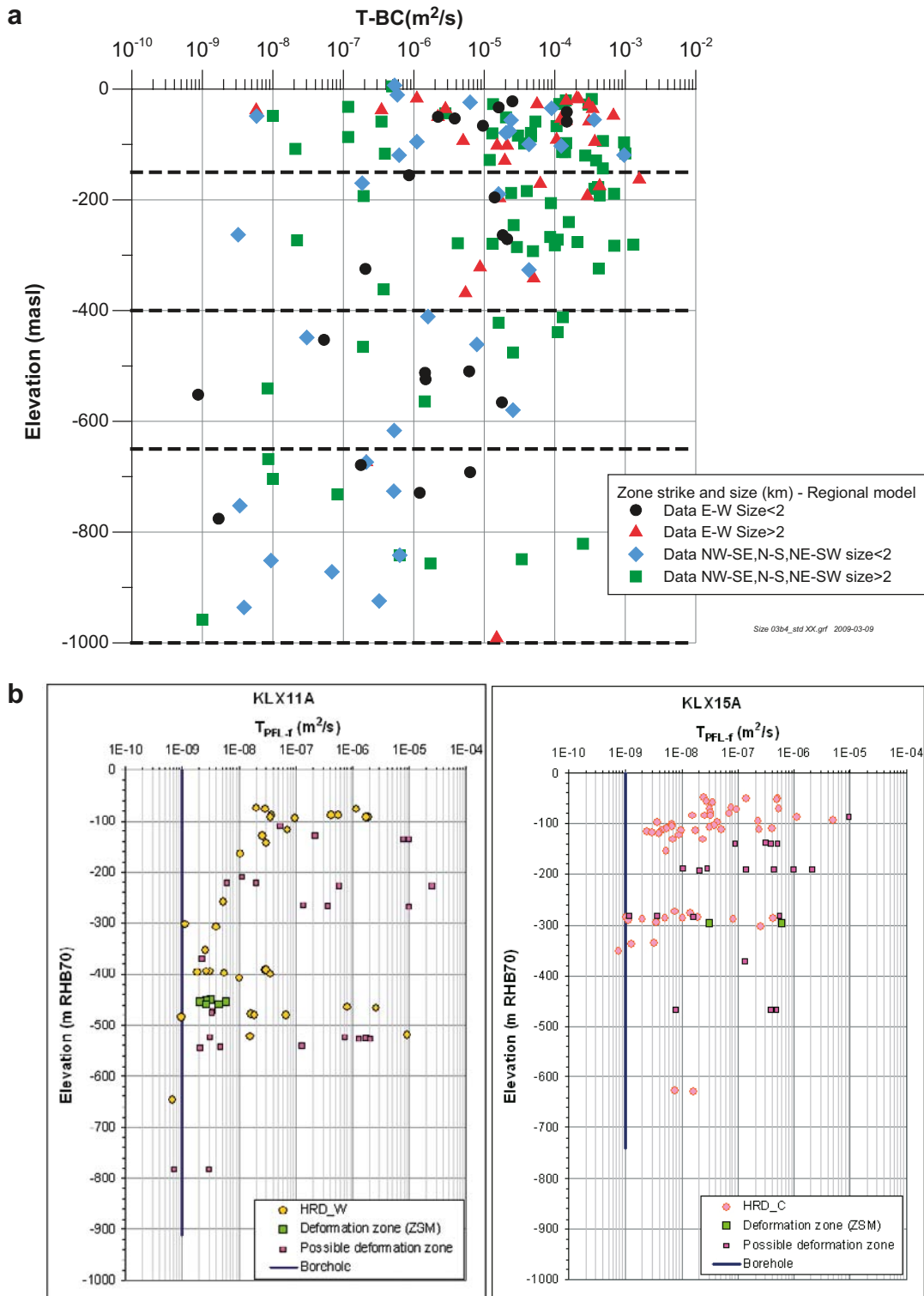


Figure 11-14. Measured transmissivities in fractures in a) deformation zones and b) in fracture domains in boreholes in the focused volume; KLX11A (HRD_W) and KLX15A (HRD_C), see also Sections 8.4.1 and 8.3.3.

The finding from the Äspö HRL that thicker dykes of fine-grained granites (“aplites”) in general are more permeable than other rock types, is also seen in Laxemar. However, thin veins of fine-grained granite, that completely dominate, do not seem to make the rock more permeable than implied by the average hydraulic conductivity of the rock mass /Rhén et al. 2008/.

Hydraulic rock domains

On average, the hydraulic conductivity of the Laxemar rock mass between deterministic deformation zones is about one order of magnitude lower than that of the rock within deterministic deformation zones. The bedrock in between deformation zones has been divided into hydraulic rock domains, cf. Section 8.4.2 and Figure 8-18, which in turn are directly related to the underlying fracture domains defined geologically. The hydraulic characterisation of the rock in between deformation zones therefore renders support for the division into different fracture domains. For example, as can be seen from the measured data, the hydraulic rock domain HRD_C, despite being made up of fracture domains FSM_C, FSM_NE005 and FSM_S, has relatively uniform hydraulic properties (Table 8-3 and Table 8-4) which justifies the merger into one hydraulic rock domain. Overall, the planned future deposition volumes are targeted on HRD_C and HRD_W, and partly in HRD_EW007, cf. Figure 8-18 and 8-19. Analysis of hydraulic data, mainly the frequency of conductive structures identified by flow logging, from all four hydraulic rock domains indicates a need to further subdivide the rock into four depth zones (Table 8-3 and 8-4). In the depth zone 0 to -150 m, the frequency of flowing fractures is high, whereas in the interval -150 to -450 m through -450 to -650 m, the corresponding frequency in HRD_C, although highly variable, suggests a general decrease with depth. At -650 m elevation, a dramatic decrease in the frequency of flowing fractures occurs. A similar picture is also valid for HRD_W, although the frequency of flowing features in this case is generally lower.

In the depth zone -400 to -650 m, the average spacing between conductive fractures in HRD_C is c. 9.4 m, which is close to half of the corresponding average spacing in HRD_W, and about twice that of HRD_EW007. However, the lower conductive fracture intensity in the rock mass of HRD_W is balanced by a factor 8 higher mean hydraulic conductivity ($K=2.8 \cdot 10^{-8}$ m/s as established from PFL measurements) for the same depth zone compared with HRD_C, cf. Table 8-4.

The geometric and hydraulic properties of fractures in the rock between the deterministically modelled deformation zones are represented and quantified by hydrogeological DFN models calibrated against corrected open fracture frequency ($P_{10,corr}$), the corrected flowing fracture frequency ($P_{10,PFL,corr}$) and the spatial distribution of inflow expressed as the specific capacity (Q/s) recorded with the Posiva Flow Log (PFL-f). The principal focus of this calibration is on data from hydraulic rock domains HRD_C, HRD_W and HRD_EW007 (Section 8.5.2). The scaling approach used in the hydrogeological DFN modelling resembles the r_0 -fixed model presented as an alternative in the geological DFN modelling. Whereas the geological DFN modelling is based on the corrected frequency of all fractures $P_{10,all,corr}$, the hydrogeological DFN focuses on the corrected frequencies of open fractures $P_{10,open,corr}$, and flowing fractures $P_{10,PFL,corr}$.

The division into hydraulic rock domains honours the variation in the intensity and size of open fractures with depth within the domains of principal interest, HRD_C and HRD_W, as well as the remainder of hydraulic rock domains. An example realisation of the integrated hydrogeological DFN model in a local model context is given in Figure 11-15.

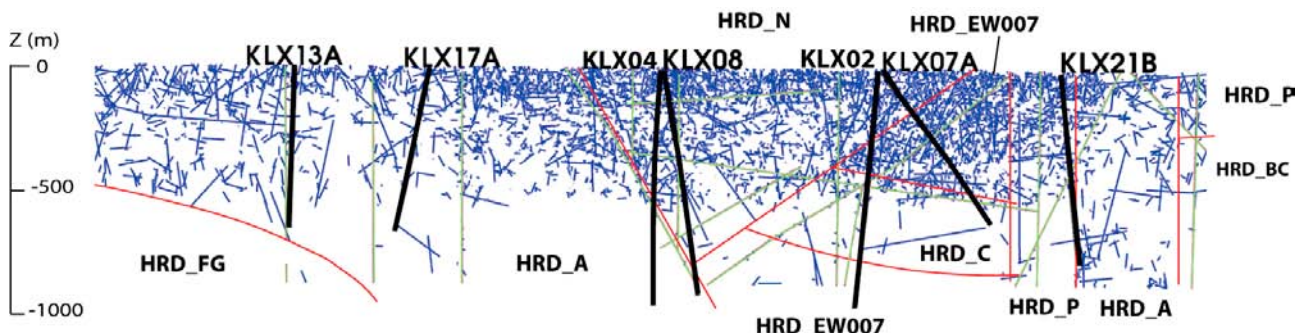


Figure 11-15. Example realisation of the hydrogeological DFN-model showing all open and connected fractures in a NW-SE cross-section through central Laxemar, cf. Profile B in Figure 8-50. Cored boreholes, deterministically modelled deformation zones and subdivision in hydraulic rock domains are also indicated in black, green and red, respectively. Section length = 4,300 m.

Uncertainties in the hydraulic properties of the connected fracture network are handled by three alternative assumptions concerning the possible relationships between fracture transmissivity and fracture size, cf. Section 8.5.2. Although it is difficult to establish which of these models that best reflect reality, all three models give similar ranges of transmissivities for fractures in the size range 10–100 m. For this reason, the three models are likely to show similar flow characteristics. It should be noted that the groundwater flow and solute transport simulations employed in this work use solely the semi-correlated transmissivity-size model.

Hydraulic characteristics of minor deformation zones

Included in the hydrogeological DFN are conductive structures corresponding to MDZ, cf. Section 11.3.3 for a discussion of the geological basis and understanding of MDZ.

Hydraulic testing in boreholes using the PFL-f technique indicates that only a portion (c. 60%) of the geologically defined MDZ are associated with a conductive fracture. For HRD_C the fraction of conductive MDZ is about 39%, whereas the corresponding fraction of OPO (open or partly open) fractures that have an associated PFL-f feature is about 7%. The corresponding numbers for HRD_W are 69% and 17%. Consequently, a MDZ is significantly more likely to be associated with a PFL-f feature than an OPO fracture.

In the hydrogeological DFN, each feature is assumed to have constant transmissivity throughout. Employing this interpretation, there exist only two reasons why a feature in the hydrogeological DFN does not have a PFL-f feature associated with it; it is either not hydraulically significant (e.g. because its transmissivity is less than the measurement limit), or alternatively, the feature is not part of the connected network. In generalised terms, MDZ should be hydrogeologically significant features provided that they are connected (assuming they have constant transmissivity throughout). Furthermore, it is noted that the reason for the decrease with depth in the proportion of flowing MDZ (measureable by the PFL method) is the decrease in intensity with depth that results in diminishing connectivity of water-conducting features. Consequently, the reason why not all MDZ are hydraulically significant is in part attributed to the sparsity of fracturing at depth, and the effect of vertical rock stress given that the majority of MDZ are gently inclined.

Additional hydrogeological characteristics of MDZ include:

- the intensity of open fractures is around 4 times higher within MDZ than in the surrounding rock.
- the intensity of PFLs in MDZ is also about 4 times higher compared with the surrounding rock.

The higher intensity of PFL fractures within the MDZ follows from the intensity of open fractures being higher, i.e. MDZ constitute a more concentrated variety of the naturally fractured rock. Given that a large number of geologically defined MDZ are thinner than 1 m, and the overall average intensity of PFL fractures in MDZ is about 0.5 m^{-1} , a significant proportion of thin MDZ may not contain a flowing fracture detected by PFL

Confidence

In general, there is a medium to high confidence in the bedrock hydrogeological model of the site and the assigned hydraulic properties, including the general trend of decreasing hydraulic conductivity with depth in hydraulic rock domains and deformation zones, the distribution and statistics associated with flowing fractures (at least down to –500 m), differences and similarities between the defined HRD and underlying rock types, and a weak (most likely somewhat underestimated) hydraulic anisotropy. The main reasons for this assertion are the wealth of data in the main domains HRD_C and HRD_W within the local model volume. The stability over time of the hydraulic conductivity assignment to the hydraulic rock domains is difficult to assess given that fracture domain-based hydraulic rock domains, and subdivision into depth zones were introduced subsequent to model version Laxemar 1.2. However, with regards to the parameterisation of the deformation zones a relative stability has been maintained, even though the database has increased. Furthermore, consistency has been established with geology through hydraulic confirmation of a few geologically defined deformation zones by interference tests and with rock mechanics through anisotropic hydraulic conditions which are consistent with the rock stress variation with depth.

The hydraulic property distribution of HRD_C appears to be rather homogeneous, which was manifested in a relatively easy and straight forward calibration of the corresponding hydrogeological DFN model. In contrast, HRD_W was more difficult to calibrate, partly attributed to the availability of less data to constrain this HRD, but possibly also attributable to a higher degree of heterogeneity. The comparison of predictions of conductive fracture frequency and transmissivity distribution in KLX27A with the measured outcome, cf. Section 8.5.5, showed that different c. 200 m intervals within this single borehole spanned the extremes predicted by the model. This suggests a higher degree of variability, and hence lower predictability, associated with the hydraulic characteristics of HRD_W compared with HRD_C. Further constraints on hydraulic properties can only be achieved by additional data, either from additional surface boreholes or from investigations during underground construction.

Lower confidence is attributed in property assignment of deformation zones with no or just one hydraulic observation and also to the description of spatial variability and anisotropy within individual deformation zones.

The apparent contradiction that among the MDZ, being the largest amongst stochastic features, only a fraction (39–69% depending of which HRD) is detected by PFL, can be reconciled by neglecting (hydraulically) many of the thin geologically interpreted MDZ, as well as considering the reduction in fracture connectivity with depth. An alternative explanation, yet untested by the hydrogeological DFN model, is the manifestation of heterogeneity within the MDZ structure planes. It cannot be ruled out that the two effects also are active in parallel. It is projected that inclusion of heterogeneous distribution of hydraulic properties within MDZ would entail reduced upscaled block hydraulic conductivities in the regional flow model.

The aspects associated with lower confidence and remaining uncertainty are handled by employing bounding estimates or alternative models, as described previously.

11.6 Groundwater

11.6.1 Evolution during the Quaternary

Several groundwater types which are now present in the bedrock can be associated with past climatic events in the late Pleistocene, including inter-glaciations, glaciations, deglaciations, and associated changes in the shoreline in conjunction with transgressions and regressions. Among these, the latest glaciation (last phase of the ice sheet coverage) and post-glacial period are the most important for the groundwater development in the Fennoscandian shield, especially in terms of land uplift and shoreline displacement as well as the development of the Baltic Basin. There is even recognition of an old, dilute meteoric water (preserved as porewater) evolving very slowly by diffusive mixing over several climate cycles, possibly dating as far back as the Pleistocene or even the Tertiary.

The description of post-glacial development, cf. Section 9.3.4, reveals that when the continental ice melted and retreated from the Laxemar-Simpevarp area about 12,000 BC, glacial melt water invaded the bedrock under considerable pressure. The exact penetration depth is unknown and is also dependent on the geometry and heterogeneity of the system. However, according to results of hydrogeological modelling simulating the effects of the ice at the ice margin, penetration to typical repository depth and below is possible /Jaquet and Siegel 2006/. Furthermore, chemical and isotopic data from matrix porewater support this estimate of penetration, cf. Section 9.5.7 and 11.6.2. Laxemar was exposed after deglaciation to both the Baltic Ice Lake and the Yoldia Sea, cf. Figure 3-5. The former was fresh (lacustrine) and the latter represented an influx of seawater from the west during warmer conditions following deglaciation, and is considered to have been dilute brackish. Neither signature is measurable in present Laxemar groundwaters, attributed to short exposure in times and limited hydraulic and diffusional driving forces. The subsequent Ancylus Lake (8800 to 7500 BC) was lacustrine followed by the brackish Littorina Sea (7500 to 4000 BC) with a salinity twice that of the current Baltic Sea. During the Littorina Sea stage, the salinity was considerably higher than at present, reaching 9 to 14‰ in the period 4500 to 3000 BC. The effect of the Littorina Sea on the Laxemar bedrock and groundwater was partly balanced by the shoreline displacement, cf. Figure 3-7, allowing only penetration of the more dense (although diluted) brackish Littorina seawater in low lying parts of Laxemar, resulting in a density driven intrusion that affected the groundwater in more conductive parts of the bedrock.

Concurrently, as the Laxemar-Simpevarp region emerged from the sea, starting c. 9500 BC, recharge of meteoric water of lower density formed a freshwater cushion on top of the older waters. As a result of the relatively sharp escarpment in the coastal topography east of Laxemar, combined with early deglaciation of Laxemar, invasion of saline water during the Holocene is limited, and geographically constrained locally.

Quaternary evolution has affected the groundwater chemistry in Laxemar. Although most effects are post-glacial, there exist groundwater and porewater indications of a pre-Pleistocene, dilute interglacial component of mixed meteoric and marine origin that infiltrated during earlier temperate climates. The hydrogeochemistry of the Laxemar-Simpevarp area cannot be explained without recognising this older component. The present groundwater compositions therefore are a result of mixing and reactions over a long period of geological time. The interfaces between different water types are not sharp, and reflect more the inherent variability in the structural-hydraulic properties of the bedrock and variability in hydraulic gradient.

11.6.2 Groundwater composition and water rock interactions

Explorative analyses of groundwater chemistry data measured on samples from cored boreholes, percussion boreholes and soil boreholes, and hydrogeochemical modelling are vital components in the evaluation of the hydrogeochemical conditions at Laxemar in terms of the origin of the groundwater and the processes that control its water composition.

The many consistent temporal and spatial data support the description concerning the groundwater origins, most of the major end members and the major hydrochemical processes. Chemical reaction modelling, the use of different isotope ratios (of the elements Sr, S, C, B, Cl, O, H and the U-decay series) and measurements of Eh, pH and microbe population data have contributed to process understanding. Matrix porewater compositions and input from fracture mineralogical studies have provided palaeohydrogeological evidence and lend further support to the process understanding of the site.

In general, the groundwater composition supports the occurrence of different hydrogeological regimes in the regional scale model volume, but above all, their subdivision in depth zones. Preservation of certain isotopic signatures of groundwaters sampled below –600 m suggests older ages and consequently longer groundwater residence times of these more highly saline waters. Furthermore, integration with hydrogeology supports the palaeohydrogeological description of the site.

Groundwater in fractures

Hydrogeologically, the Laxemar subarea is an area of groundwater recharge and shows classical systematic changes in groundwater chemistry with depth which accompany increasingly lower hydraulic conductivity values and lower groundwater flow rates in the bedrock. Although such changes entail greater water/rock interactions, the major groundwater feature is that the groundwater composition is mainly a result of transport (mixing) of groundwaters of different origins (deep groundwater, glacial water, Littorina Sea water and meteoric water). The groundwater compositions are, or have been, modified by reactions ranging from fast (e.g. redox reactions catalysed by microorganisms, ion exchange, calcite equilibrium) to long-term water/rock reactions such as aluminosilicate equilibrium at depth. Despite these changes, the alkalinity and redox buffer capacity provided by the bedrock (cf. Figure 9-13) and microbial metabolisms, are driven by comparatively fast reactions (hundreds of years). Hence, the pH and Eh variability of the groundwaters is restricted to a narrow and stable range. The pH values are between 7.2 and 8.6 in the groundwaters and do not show any clear trend with depth. The control of pH is mainly exerted by calcite dissolution-precipitation reactions and, probably, microbial activities. Influence of other common chemical processes, such as aluminosilicate dissolution-precipitation or cation exchange, are probably of secondary importance.

The main fracture groundwater types which characterise the Laxemar-Simpevarp area are shown in Figure 11-16. Post glacial meteoric water is dominant in the bedrock down to approximately 150 m and is present as a decreasing component at intermediate depth. Because only part of the Laxemar subarea was covered by the Littorina Sea, postglacial marine waters are rare in the bedrock in Laxemar, especially in the central part and towards the west and north-west. Weak Littorina

signatures are found in groundwaters to the south-east close to the Simpevarp subarea at various depths between 200 and 680 m in some boreholes. Clear evidence of glacial water components is commonly present in the approximately 300 to 600 m depth interval, especially in the western and central parts of the area. These waters with the largest glacial component are usually low in chloride (1,000–2,500 mg/L). Decreasing hydraulic conductivity of the deformation zones with depth is reflected in the different mixing/reaction environments, and increasing residence times of the groundwater. At depths greater than 1,200 m, low flow and stagnant conditions prevail.

The dissolved oxygen is consumed in the shallow, upper part (approximately upper 50 m) of the bedrock, generally resulting in reducing groundwater conditions already at these depths. Redox-sensitive species such as iron and manganese are generally present in low concentrations in the deeper groundwaters at Laxemar (less than 1 mg/L Fe²⁺ and 0.5 mg/L Mn²⁺) compared with the near-surface waters (up to 10 mg/L Fe²⁺ and below 2.0 mg/L Mn²⁺). However, Fe and Mn-reducing bacteria are identified at all depths analysed for microbes. Easily accessible Fe-oxyhydroxides and Mn-oxides on the fracture walls are rare, if present at all, below 100 to 150 m, and the relatively low Eh (-275 mV) measured at shallow depths (~170 m) indicate that Fe- and Mn-reducers are active in the control of the redox system, mainly in the very upper part of the bedrock (potentially down to around 100 m). At greater depths between 170 to 500 m, measured Eh values are well below -200 mV and seem to correlate with the number of sulphate-reducing bacteria. Furthermore, high δ³⁴S_(SO₄) values and correspondingly low sulphate contents occur together, which emphasises the importance of sulphate reduction at depths between 100 m and at least 500 m. At still greater depths, less information is available on the redox system. Taking into consideration that the system below 600 m is much less dynamic, and thus nutrition may be limiting microbial activity, lower sulphide production is assumed at these depths. Nevertheless, dissolved sulphide has been measured in several borehole sections sampled below 550 m. This general lack of data indicates that the redox system is less well characterised at these depths. The major groundwater features are summarised in Figure 11-17.

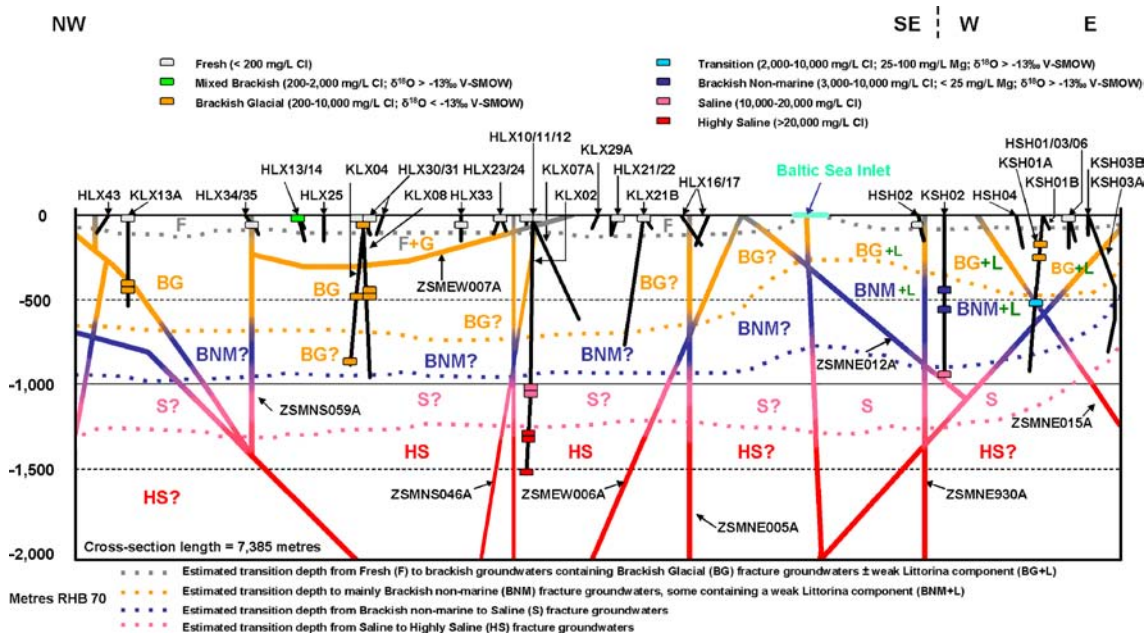


Figure 11-16. Approximately NW-SE/W-E cross-section through the Laxemar-Simpevarp area (see Profile C in Figure 8-50 for location). Shown are: a) the location of the boreholes and the borehole sections (coloured rectangles) that have undergone hydrochemical sampling, b) the main fracture groundwater types (colour coded) which characterise the site (HS = Highly saline, S = Saline, BNM = Brackish non-marine, BG = Brackish glacial, L = Littorina), and c) the chloride distribution with depth along the major deformation zones. The dotted lines in different colours represent the approximate depths of penetration of the various fracture groundwater types along hydraulically active deformation zones. The main regional groundwater flow direction is from the west (recharge) to the east (discharge), approximately parallel to the section. Cross-section length = 7,385 metres.

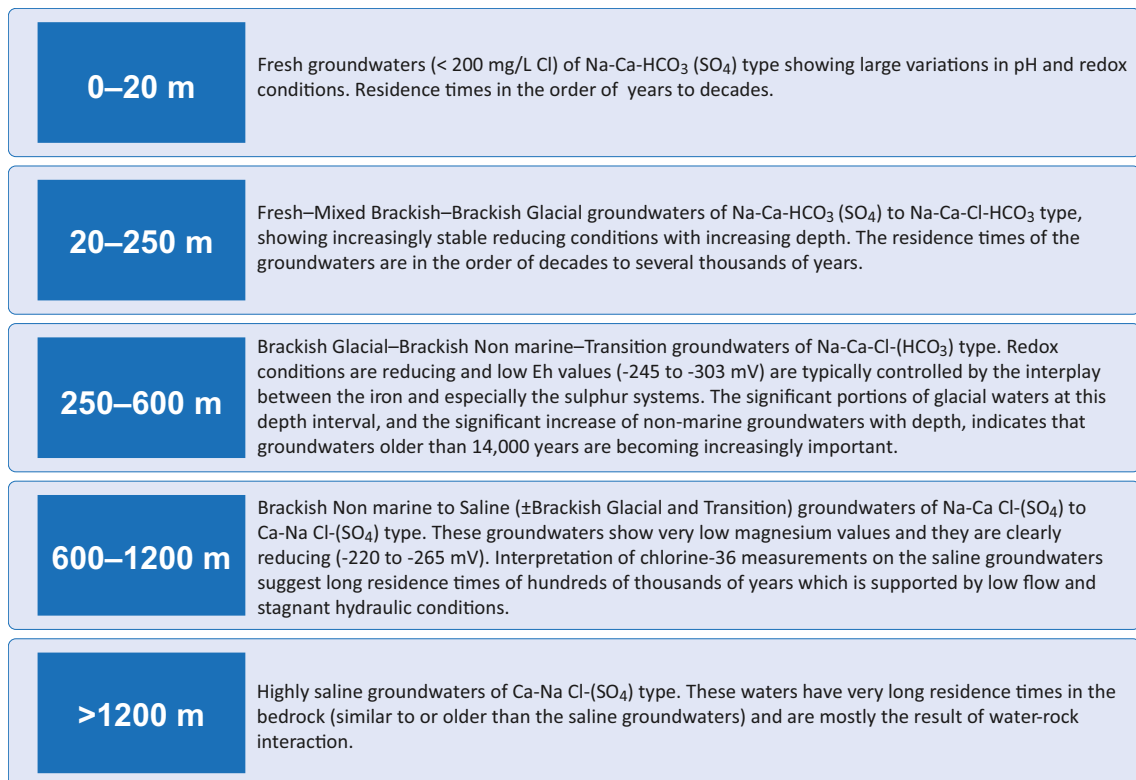


Figure 11-17. Major groundwater features and their applicable depth intervals. NB. The above depth intervals presented differ slightly from the depth zones introduced by hydrogeology in Chapter 8.

The measured colloid content decreases with depth (for example, the colloid content is less than 20 µg/L at depths greater than 350 m) which is to be expected due to the increasing ionic strength which destabilises the colloids. The measured gas contents in the groundwater are 50–110 mL/L and dominated by N₂. The helium and argon contents increase with depth indicating a possible input from deep-seated gas sources.

The succession of groundwater stratification at Laxemar, as described above, correlates closely with the depth zones of the hydrogeological DFN model (see Section 8.5.2). This applies in particular to the marked difference in groundwater composition above and below –250 m. Overall, the above succession also applies to the more coastal Simpevarp subarea, although the compositional stages occur at shallower depths and the Littorina signature is more pronounced.

In summary:

- 1) Today's groundwater types and chemistry reflects the change in climate during the latest glaciation and the post-glacial period. Significant components of glacial waters have been retained in the bedrock at intermediate depth especially in the Laxemar subarea.
- 2) Stable reducing conditions and neutral pH prevail in the groundwaters below approximately 100 m depth.
- 3) Despite repeated intrusions of glacial meltwater, the buffer capacity of the fracture minerals and the wall rock has not been exhausted and are expected to provide a significant buffer capacity to assure stable redox and pH conditions during future changes in groundwater recharge (cf. Figure 9-13).

Composition of rock matrix porewater

Matrix porewater composition and isotopic signatures in Laxemar are found to be closely correlated to variations in hydraulic properties of the bedrock, cf. Section 9.5.7. At shallow to intermediate depths (down to about –430 m), the porewater is generally of Na-Ca-HCO₃ type with a low chloride

content and an $\delta^{18}\text{O}$ signature ranging from slightly more enriched than present-day meteoric recharge to a more depleted cold water signature, cf. Section 9.5.7. Below this dilute water, a transition zone occurs (from -450 to -550 m) with porewaters of Na-Ca-SO₄ type with significantly higher chloride concentrations and highly variable $\delta^{18}\text{O}$ signatures. The vertical distribution of these sulphate rich groundwaters located at approximate repository depth seems restricted. The general similarity of the chloride and $\delta^{18}\text{O}$ values of porewaters and fracture groundwaters at shallow to intermediate depth indicate a steady state situation between the two. In contrast, the porewaters in the noted transition zone at repository depth, and also at greater depth, are characterised by lower chloride contents and enrichment of $\delta^{18}\text{O}$ relative to fracture groundwaters, suggesting a transient state. This latter observation indicates insufficient time for the fracture groundwaters to have equilibrated with the matrix porewaters, and is consistent with the hydrogeological interpretation of a lower conductive fracture frequency and lower hydraulic conductivity below about -600 m, where there is low groundwater turnover (cf. Sections 11.5.2 and 8.5.2).

Confidence

There is a generally high confidence in the description and understanding of the current spatial distribution of groundwater composition, as established mainly from the consistency between analyses and modelling of chemical data, and in part from the agreement with hydrogeological and structural geological understanding of the Laxemar-Simpevarp area. Furthermore, the existence of a near-surface redox reaction zone (also known as the redox front) is well established. The common occurrence and preservation over geological time of calcite, chlorite and pyrite suggests that there exists a buffering capacity against the effects of penetration of dilute groundwater. One important remaining uncertainty concerns the variability in sulphide concentrations measured in the on-going monitoring programme. Initial drilling and pumping may have disturbed the system, or may have facilitated sulphate reduction. However, this issue remains to be resolved.

11.6.3 Groundwater flow and consistency with groundwater signatures

The palaeo-evolution of groundwater composition in Laxemar-Simpevarp during the last c. 10,000 years, i.e. during the Holocene, has been simulated in the palaeo-hydrogeological modelling work (see Section 8.6 and 8.7 and further detailed in /Rhén et al. 2009, Rhén and Hartley 2009/). The simulated results are compared with measured chemical data on a borehole basis in Section 8.6.4 and in terms of plan view and vertical sections in Section 8.7.1.

The presence and mixtures of different reference waters in the bedrock at 8000 BC define the initial conditions for the palaeohydrogeological simulations. These conditions have been derived on the basis of analyses of present-day water composition in fractures and matrix porewater, which support the existence of deep saline and glacial melt water in the fracture waters, and an inter-glacial porewater originating as a slowly evolving water over several climatic cycles, prior to the Holocene. To ensure differences in composition over time between fracture water and matrix porewater, an initial condition consisting of a mix of inter-glacial porewater and deep saline was prescribed for the matrix porewater, cf. Figure 8-26.

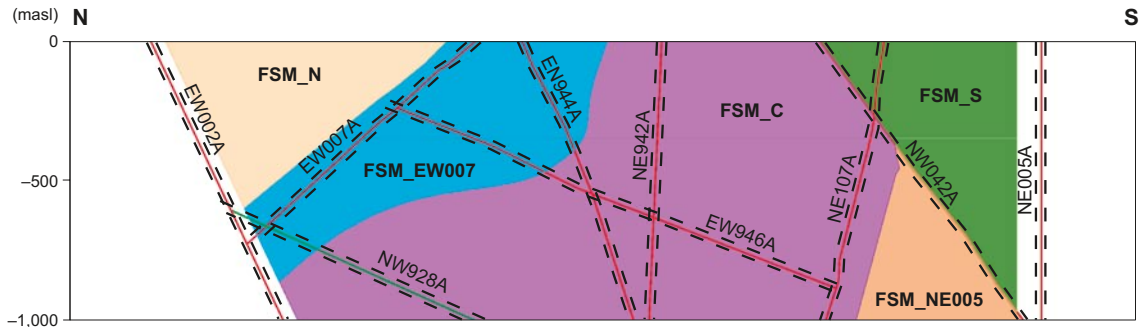
The results of the simulations with the three-dimensional hydrogeological flow model show fair agreement with measured concentrations of Cl, Br/Cl, $\delta^{18}\text{O}$ and HCO₃ in the borehole fracture water of HRD_C and HRD_W, cf. Section 8.6.4. The model also predicts well the preservation of Inter-glacial porewater below -650 m in HRD_C, as seen in enriched $\delta^{18}\text{O}$. Results for HRD_W predict well the retention of Deep saline water in deep porewaters, as well as lower salinity in the fracture water compared to porewater, which is consistent with measured data.

The model predicts relatively continuous thick lenses of brackish-glacial water centred at repository depth along the low lying E-W valleys associated with the Laxemarån river valley (ZSMNW042A) in the south, the Mederhult zone (ZSMEW002A) to the north, and beneath zone ZSMEW007 in the centre of the Laxemar subarea, cf. Section 8.7.1. There are also smaller localised lenses of brackish-glacial water throughout the focused area that are a result of spatial heterogeneity, and hence may vary in position and magnitude according to the particular realisation of hydraulic properties in hydraulic rock domains and deformation zones. The above finding is compatible with the hydrogeochemical description, cf. Section 9.6.2, although there the positioning of the brackish-

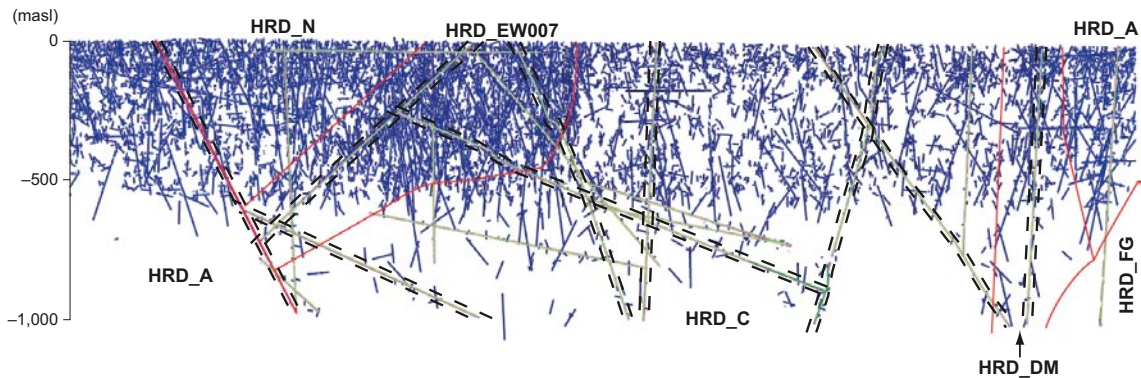
glacial water is somewhat higher, between c. –300 and –600 m. A conceptual model illustration of the present-day distribution of brackish-glacial water is illustrated in Figure 11-18, to be compared with the hydrogeochemical site descriptive model presented in Figure 11-16.

The simulation results show no significant traces (< 10%) of relict Littorina signatures within the Laxemar subarea, but modelled traces of Littorina water are seen superficially near the coast in the Simpevarp subarea, east of Laxemar. These results are compatible with measured hydrogeochemistry and the hydrogeochemical conceptualisation where the lower topography of Simpevarp is emphasised, resulting in a longer submersion by the Littorina Sea, and subsequent flushing having been less efficient and being still on-going, cf. Section 11.6.2.

Fracture domain model



Conceptual hydrogeological DFN model (connected open fractures)



Conceptual distribution of modelled groundwater end-members

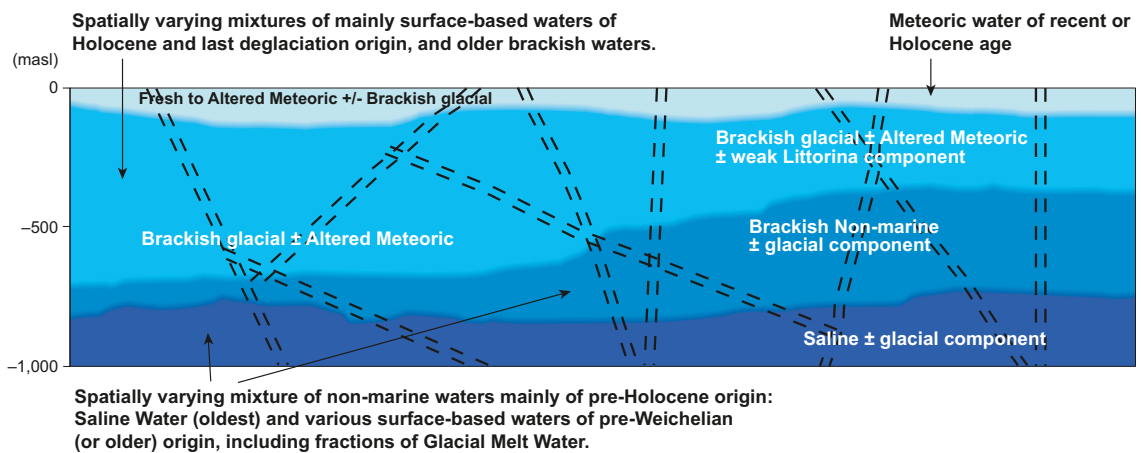


Figure 11-18. Comparison of conceptual models for fracture domains, hydraulic DFN and associated hydraulic rock domains and the present-day distribution of different groundwater types along the N-S section given by Profile A through the local model volume. The relationship between the profile and the hydrogeochemical conceptual section in Figure 11-16 is given by Figure 8-50. The length of the section is ~ 4,300 m.

Performed sensitivity analyses show that the results for the interval –150 to –600 m are highly dependent on the hydraulic and solute transport parameters (fracture surface area in particular) and initial conditions. In this depth range, the measured hydrogeochemistry is relatively uniform with regard to simulated heterogeneity (i.e. local hydraulic conductivity and PFL feature intensity). The magnitude of fracture-matrix solute exchange is governed by the ratio between available specific fracture surface area to groundwater volumetric flux (cf. the F-factor discussed in Section 11.8.2) such that when the fracture intensity (and specific surface area) is increased for a given volumetric flux, then solute transport is retarded more effectively by rock matrix diffusion. However, in the heterogeneous model, for a given hydraulic gradient, an increased intensity entails both increased volumetric flux and higher surface area in similar proportions. This implies that the two principal factors governing the effects of matrix diffusion cancel out, resulting in a homogenisation of the simulated fracture groundwater chemistry in relation to the simulated heterogeneity. The main effect of increased fracture intensity is that a greater proportion of the overall porewater storage capacity equilibrates with the chemistry in the fractures during a given time period. Furthermore, the results of various combinations of heterogeneity in hydraulic rock domains and deformation zones indicate a vertical variability (shift) in modelled bounds in fracture groundwater composition in the order of 50–100 m.

Overall, the parameterisation of deformation zones and hydraulic rock domains put forward, cf. Section 8.5, is found to be robust. Improvement to the calibration on head, drawdown and hydrogeochemistry is achieved when reducing by 1/3 the transmissivity of deformation zones below –150 m and when increasing by a factor 3 the horizontal hydraulic conductivity of hydraulic rock domains above –150 m.

11.7 Surface – bedrock interactions

Unified descriptions of the geological, hydrogeological, hydrogeochemical and transport properties of the superficial bedrock down to c. 100 m depth have been devised. Central in this presentation are a set of common schematic conceptual geological sections on which discipline-wise conceptualisation is superimposed, cf. Section 4.4.

11.7.1 Rock types and fracturing

Notable is the observation that the rock types and even the degree of alteration seen in the superficial bedrock are the same as at typical repository depth. Fracture intensity in the upper 100 m of the bedrock, between deterministic deformation zones, indicates a slight gradual increase in the frequency of open fractures from c. –100 m towards the ground surface. This increase in open fracture intensity appears to be coupled to a corresponding decrease in the intensity of sealed fractures, suggesting that some of the open fractures constitute reactivated sealed fractures. Furthermore, there is a tendency for an increase of subhorizontal to gently dipping open fractures towards the ground surface, suggesting in part that they are caused by stress release, and representing sheet joints, see Section 4.4.1. Contrastingly, depth trends in the intensity of fracturing at depths greater than –100 m is weak, cf. Section 5.6.3, which, however, stands in contrast to the indication of a decrease with depth seen in the intensity of flowing fractures, as established by PFL-f, cf. Section 11.5.2. Anisotropy exhibits a systematic change with depth with the subhorizontal fracture set becoming less important at depth, while the vertical sets remain important.

11.7.2 Hydraulic properties and surface-bedrock interactions

The bedrock shows a general decrease in hydraulic conductivity with depth in both deformation zones and the rock mass between deformation zones, cf. Section 8.5. The properties of the upper 50–150 m are interpreted as anisotropic, where the subhorizontal fracture set has a higher horizontal hydraulic conductivity than the vertical fracture set, cf. discussion in Section 8.4.2. It is suggested that the uppermost 5–10 m of the bedrock is more fractured and permeable due to the influence of the latest glaciation, and particularly so on the lee side of south-eastern rock slopes, as the ice sheet moved from NW towards SE. Although data to support the latter is scarce, observation of deforma-

tion zones in trenches excavated in Laxemar indicate a heavily weathered and fractured near-surface rock /Sohlenius et al. 2006/. In these areas, the near-surface bedrock is expected to be characterised by increased hydraulic conductivity.

Groundwater discharge from the superficial rock and Quaternary deposits to the surface waters is strongly influenced by the geometry and the hydrogeological properties of the Quaternary deposits overlying the glacial till which is found throughout the area, cf. Section 11.1.2. This process is also affected by the horizontal extent and the hydrogeological properties of the upper rock (including the deformation zones) and the high-conductive Quaternary deposits overlying the rock in the valleys. The large valleys in Laxemar constitute areas of groundwater discharge to the surface, but also constitute horizontal groundwater flow channels along the superficial rock/Quaternary deposits system, where ultimately groundwater discharge to the surface is facilitated in areas where there are no layers of glacial clay and postglacial sediments on top of the till, cf. Figure 11-19. Typical flow situations across valley, along valley, and across lake that were analysed by numerical modelling are detailed in Section 4.3.3.

11.7.3 Hydrogeochemistry and redox buffering

The hydrogeochemistry observed today in the surficial parts of the groundwater system (i.e. extending down to about -250 m) is partly a consequence of the palaeohydrological past. In higher elevated areas, meteoric recharge has had a great influence on the observed hydrogeochemistry, which is usually characterised by dilute fresh water of low ionic strength. The meteoric recharge in the western parts of the area gives rise to two different groundwater flow movements or (sub-)systems; a) a shallow young groundwater system which partly discharges towards the east, and b) a deeper/older groundwater pathway which merges with an overall regional flow at greater depth (below -250 m) discharging further to the east, cf. the associated conceptual hydrogeochemical model of the superficial bedrock presented in Figure 4-26.

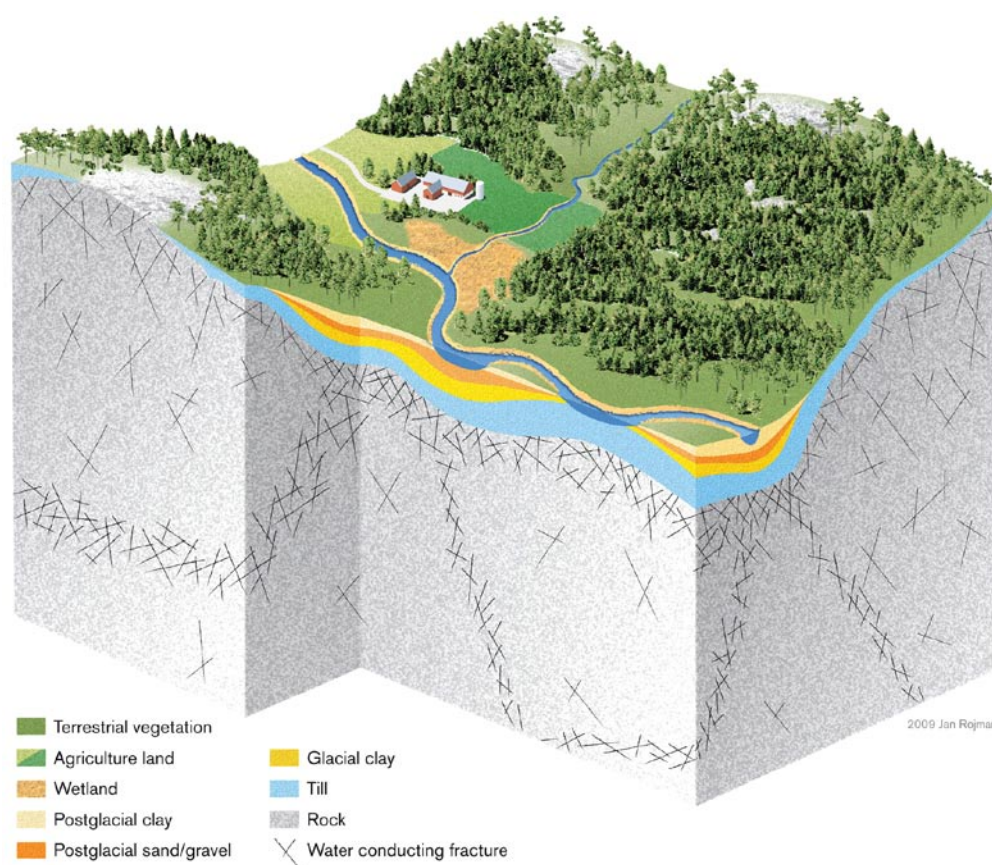


Figure 11-19. Schematic perspective view of a typical large valley in Laxemar showing a simplified stratigraphy of Quaternary deposits in cross-section.

Recharge to the deeper parts of the bedrock is probably augmented in the close vicinity of deformation zones in the more inland parts of the Laxemar-Simpevarp area. The low-elevated eastern part constitutes discharge areas for the regional flow, and groundwater discharge from deeper levels is associated with deformation zones located below lakes and brackish coastal basins and bays.

Possibly the most important characteristic of the superficial rock is its reducing capacity. The clear evidence for a developed redox front has been established from fracture minerals analyses, element chemistry and U-series isotopes, as explained in Section 9.5.6. It is located at a depth of about 15–20 m, somewhat deeper in deformation zones. The existence of the redox front also emphasises the importance of the superficial bedrock for consuming oxygen and maintaining reduced conditions at greater depth, which is imperative for canister integrity.

Confidence

The available geological and hydrogeological data for the superficial bedrock are quite sparse. Despite the relatively large number of boreholes, the information from cored boreholes in the upper 100 m is quite limited. As a consequence the quantification of fracture frequency and hydraulic properties of the superficial rock has a high associated uncertainty. This is due to the fact that most of these boreholes are percussion drilled to c. 100 m depth to e.g. host pumps for the PFL flow logging. A high confidence is attributed to chemical and mineralogical evidence for the existence and relative stability of the redox front. Evidence for this front is provided by a series of mutually independent observations and analyses, which are also consistent with data and overall interpretation of the deeper bedrock system. Furthermore, a general consistency has been established on a regional scale between the surface hydrogeochemistry and deep hydrogeochemistry models.

11.8 Transport properties

11.8.1 Properties of the rock matrix

Properties

The development of the retardation model relies to a large extent on interaction with other disciplines; primarily geology and hydrogeochemistry. Specifically, geology provides lithological and structural models in which the rock types, fractures and deformation zones are described, as well as the mineralogical compositions of intact and altered materials. Hydrogeochemical information is used as a basis for the selection of water compositions in laboratory measurements of retardation parameters. Furthermore, hydrogeochemical data together with results from mineralogical and geochemical analyses of fracture materials are important inputs to the conceptual development of the site-specific retardation model and understanding of the retention processes at the site. Tracer tests in the form of weak dipole and single well injection-withdrawal tests (SWIW) have been performed in a number of boreholes with the aim of confirming the existence of field-scale retardation and to assess the utility of the retardation models to predict solute transport. Although it is not possible to extract data that can be used directly for parameterisation of transport models used in safety assessment, the tracer tests by and large confirm retardation and give results that are broadly consistent with the current understanding of field scale transport processes.

The input data for the retardation model consist of laboratory measurements of formation factors for solute transport in the rock matrix, matrix porosities, specific surface areas of internal micro-surfaces, cation exchange capacities (CEC), and sorption properties of rock in contact with synthetic groundwater of varying composition. *In situ* measurements of the rock formation factor obtained from high spatial resolution geophysical logging in the site investigation boreholes are also used.

Retardation properties

The main parameters of interest are the immobile zone porosity, θ_m , the effective diffusivity, D_e , and the linear equilibrium sorption coefficient, K_d . These material property parameters are evaluated, interpreted and presented in the form of a retardation model. In the three-dimensional spatial representation of Laxemar, the retardation model is used to parameterise the various geological elements

described in the geological site descriptive model. These elements consist of the rock mass containing varying proportions of different site-specific rock types, key fracture classes (Table 10-1) and various deformation zone micro-structural components (Table 10-2).

The limited data available for the different rock masses indicate that there are generally no significant differences in the retardation properties between the rock types present in the rock domains RSMA01A, RSMM01A and RSMD01A, all contained within the focused volume. Furthermore, taking the variation in the parameter values into account, there are very few indications of significant differences between the different rock types. As far as key fracture classes are concerned, either a thin layer of fracture coating or no coating at all have been identified as being of importance. On safety assessment timescales, fracture coatings generally give rise to very slightly enhanced transport retardation relative to that provided by the intact wall rock, so the absence of fracture coatings is therefore indicative of a relatively lower degree of retardation. The difference, however, is very small and only relevant for very early arrival of transported radionuclides /Crawford and Sidborn 2009/.

Although the overall ranges of formation factors estimated for different rock types are similar, there does appear to be some support for Ävrö quartz monzodiorite and Ävrö granodiorite having slightly elevated formation factors, and fine-grained dioritoid having slightly lower formation factors than other rock types. There is considerable uncertainty in the *in situ* formation factors estimated for Laxemar bedrock owing to the generally low ionic strength porewater found at repository depth and also due to uncertainty concerning porewater compositions in a number of boreholes where *in situ* resistivity measurements were performed. Although generally lower formation factors can be expected under *in situ* conditions owing to stress effects, uncertainty in the porewater composition means that it cannot be robustly determined whether the decrease in formation factor with increasing depth in Laxemar is related to this circumstance or constitutes an artefact resulting from inaccurate estimates of porewater compositional trends.

The BET surface areas (of the fracture coatings and filling materials) have been measured to be significantly higher than corresponding BET surface areas of samples from the rock mass, indicating that these materials may have potentially enhanced retention properties relative to the rock matrix. The large differences observed between the BET surface areas measured for fracture-coating materials and intact rock, however, are generally not accompanied by a corresponding 1:1 variation with respect to sorptivity. However good a qualitative indicator, the high BET surface areas measured for fracture materials can therefore not be interpreted as being a directly proportional measure of increased sorptivity of the fracture material relative to the host rock.

The deformation zone structural elements, for which retardation properties have been tabulated, are all comparatively heterogeneous in their structure. From the material properties data, these structural elements could be identified as potentially strong sinks for radionuclides transported from a repository. This, however, should also be considered in the context of the possibly lower hydrodynamic transport resistance of these zones and their increased micro-structural complexity including additional diffusion-accessible surface area (see next section).

Confidence

Generally, there is a low and relatively well quantified uncertainty in diffusivity. Uncertainty in sorption is only semi-quantitatively established and is high for many species and specific groundwater compositions. Sorptivities of certain radionuclides in contact with specific groundwaters and rock types are not known, or are not supported by sufficiently large sample sizes to be considered statistically quantified. Sorptivities of U and Np under strongly reducing conditions are likely to be underestimated owing to difficulties in maintaining appropriately low redox conditions in the laboratory. There is uncertainty in the distribution and thickness of altered rock surrounding flow paths. The importance of this, however, depends on the differences in the material properties of these materials relative to unaltered rock. The data suggest that altered rock is generally associated with increased retention for most radionuclides and therefore this uncertainty can be bounded (i.e. retardation is underestimated if alteration is neglected in transport calculations).

11.8.2 Flow-related properties

Solute transport in fractured rock over longer distances is conceptualised to occur along advective flow paths hosted within fractures and deformation zones. Matrix diffusion coupled with sorption has been identified as the main retardation process that limits the rate at which solutes are transported along these flow paths. The flow-wetted surface to flow ratio (alternatively known as the “F-factor” or “hydrodynamic transport resistance”) is a key parameter governing the transport of radionuclides within fractured rock. While the retardation effect, and consequently, typical solute residence times, scale approximately linearly with rock matrix diffusivity (D_e) and sorption coefficient (K_d), it can be shown to scale quadratically with the F-factor. A given level of uncertainty in the F-factor therefore has a substantially larger impact on solute transport than a similar relative uncertainty in the rock matrix properties parameterisation.

The F-factor depends on groundwater flow and its distribution within the rock. The main source of input data used as a basis for assessing the transport resistance is thus the site-specific hydrogeological properties which are generated from models which represent the major deformation zones deterministically and the less fractured rock within the hydraulic rock domains outside these zones, stochastically, cf. Section 8.5. For the hydraulic rock domains, the stochastic description is based upon the hydrogeological DFN. The description of the deterministic deformation zones, on the other hand, is based upon two different, although complementary approaches for representing the hydrogeological properties of these features, cf. Section 10.5.2.

Indication of the ranges of transport resistance

Using the hydrogeological DFN as input, numerical simulations were carried out of flow and migration in a cubic volume of side length 100 m with a hydraulic potential difference applied over opposing faces, cf. Section 10.5. The aim of the simulations was not to model the actual F-factor distribution for transport of radionuclides from an individual canister position, but rather to give an indication of F-factors associated with typical flow paths in hydraulic rock domains that could host a potential repository. This is important to bear in mind as an individual canister hole presents a cross-sectional area considerably less than the 10,000 m² face of the simulation volume. Transport from any particular canister location is therefore strongly dependent upon additional considerations of local fracture network connectivity and represents a sub-sampling of the typical F-factor distributions calculated for the rock volume as a whole. In addition to F-factors for typical flow paths in the rock, an assessment was also made of the frequency with which they can be expected to occur. This is an important measure of transport potential in the bedrock as it reflects directly upon the number of canister positions that can be expected to be in near contact with major flow paths. From the simulations it is concluded that F-factors close to the source (here termed “the non-engineered near field”) are difficult to evaluate as they are highly dependent on selection/rejection criteria for transmissive fractures intersecting the deposition holes. Typical F-factors in the range of about 10³–10⁷ yr/m are calculated for fractures in the transmissivity range from 10⁻⁸–10⁻¹⁰ m²/s depending on underlying assumptions, which include typical path length and representative local hydraulic gradient. It is generally found that HRD_C at repository depth (here taken to correspond to the depth zone -400 m to -650 m) is relatively well connected hydraulically although there is some anisotropy in the connectivity. HRD_W appears to be somewhat less well connected hydraulically and exhibits considerably less anisotropy.

Median F-factors for “typical” flow paths in the 100 m scale are found to be on the order of 10⁴ yr/m (with an approximate range of 10³ to 10⁵ yr/m) for both HRD_C and HRD_W assuming a semi-correlated fracture size-transmissivity relation. Flowpaths are typically comprised of small numbers of spatially clustered fractures, although there are a statistically significant number of realisations featuring single fractures that span the entire simulation volume. Simulations of HRD_EW007 indicate similar F-factor magnitudes despite a somewhat higher hydraulic connectivity than other hydraulic rock domains at repository depth. HRD_W has a slightly lower hydraulic connectivity than HRD_C, although here too it is found that the F-factor ranges are roughly the same as those estimated for other hydraulic rock domains.

A simple analytical model has been used to estimate typical F-factors in the deterministic deformation zones, based on the exponential and power law models of transmissivity decrease with depth provided by hydrogeology, cf. Chapter 8, and a 1% hydraulic gradient. Only very minor differences are observed in the estimated F-factors for deformation zones of different strike orientation and dip (the small differences in F-factor magnitudes calculated for different deformation zone orientations is related only to transport path length since the mathematical model describing zone effective transmissivity is not influenced by zone orientation). Depending upon various modelling assumptions, F-factor ranges of about 10^3 yr/m to 10^5 yr/m seem reasonable. The range of variability estimated for the deformation zones largely reflects underlying differences between assumptions in the models rather than true stochastic variability. Therefore it is not possible to give a single best estimate for F-factors characterising typical flowpaths in the deformation zones. The results indicate a considerable level of uncertainty in the hydrodynamic resistance provided by the deformation zones and in some cases F-factors are estimated that are comparable to or larger than those estimated for the HRD.

Effects of channelised flow

The existence of distinct physical flow channels in existing fractures may have an impact upon interpretation of borehole data in that a borehole may hit or miss (censoring) such channels. This can lead to the underestimation of the true frequency of channels that carry flow in the bedrock and their associated hydraulic properties. Some channels take the form of physical pipe-like structures (e.g. enlarged fracture intersections) whereas others are more dynamic in nature and depend upon spatially variable fracture apertures and hydraulic boundary conditions (e.g. in-plane flow channels). Channelised flow of a dynamic nature also occurs on a fracture network-scale and is strongly influenced by fracture network connectivity and hydraulic boundary conditions (e.g. large-scale preferential flowpaths and hydraulic compartmentalisation). Flow channels may be very narrow in width and unlikely to be intersected directly by a borehole. Therefore the permeability of the surrounding fracture pore space becomes very important for identification of these features and interpretation of their hydraulic properties. Six different, potentially important sub-classes of flow channels have been considered in the transport properties evaluation detailed in /Crawford and Sidborn 2009/. The uncertainties introduced by some of the different forms of channelised flow can be reasonably well constrained by scoping simulations. Its overall effect does not appear to be sufficiently severe that it would cast doubt on the utility of the hydrogeological models produced within SDM-Site Laxemar.

It is also concluded that additional physical mechanisms enhancing solute uptake, such as diffusion into stagnant zones with concomitant matrix diffusion, may increase transport retardation substantially. Channelised flow may therefore possibly have an overall beneficial effect. For the ranges of F-factors estimated in the flow related transport properties evaluation, however, it appears that radial diffusion from flow channels of limited extent does not give greatly enhanced retardation as compared with a simplified 1D matrix diffusion formulation.

Confidence

Uncertainty in hydrogeological DFN parameters and the role of channelised flow phenomena may lead to underestimation of flow channel frequency in the focused volume. However, the overall F-factors for typical flow paths through the repository volume should not be greatly different, provided that the fracture transmissivity model is deemed reasonable (i.e given an approximately correct order of magnitude in flow predictions).

The hydrogeological DFN parameters for fractures within the repository volume can only be properly constrained by statistical analysis and mapping of open fractures in tunnels. During underground investigations of fracture trace lengths, frequencies of flowing fractures in tunnels and couplings between rock mechanical properties and fracture transmissivities should be studied to more fully ascertain the extent of different channelised flow phenomena including the possible existence of fast, persistent flow paths in the bedrock. This will lead to more reliable models for solute transport from the repository volume, particularly over the first few tens of metres from canister positions which may have the greatest impact on overall radionuclide release rates. Nevertheless, it is judged that the current hydrogeological DFN model, with its alternative descriptions of the transmissivity size correlation, provides adequate bounds on the uncertainty of the flow-related transport properties.

11.9 Overall confidence

The uncertainty and confidence in the SDM-Site Laxemar site descriptive model have been assessed and the results are documented in detail in /SKB 2009/. This assessment comprised exploration of confidence in the site characterisation data base, key remaining issues and their treatment, handling of alternatives, consistency between disciplines and the main reasons for confidence and lack of confidence in the model. The outcome of the assessment is summarised below.

11.9.1 Data usage

In general, only a few data have been omitted from the modelling work, mainly because they are judged to be less relevant and reliable than the data considered. These omissions are judged to have little negative impact on confidence. Poor precision in the measured data are, in general, judged to have limited impact on uncertainties in the site descriptive model. There is poor precision in determining the position of some boreholes at depth in three-dimensional space as well as in the orientation of BIPS images in some boreholes, resulting in uncertainties in the orientation of objects, for example fractures, mapped in the borehole. These problems are identified, quantified and considered in the modelling work, and they affect uncertainty, but have little negative impact on confidence.

Measurement bias in the data and bias due to poor representativity are much reduced compared with earlier model versions, but some bias still remains.

11.9.2 Key remaining issues and their handling

Some uncertainties remain in the Laxemar site descriptive model. Most of the uncertainties concerning properties and processes inside the focused volume are quantified or at least bounded by alternative models or assumptions (cf. Section 11.9.3). These uncertainties are propagated to repository engineering and safety assessment for further assessment of the impact on repository layout and long-term safety.

There exists a risk of inadvertently misjudging structures based on a single borehole intercept as a MDZ, when in fact it should be of size $> 1,000$ m and consequently modelled deterministically. As discussed in Section 11.3.2 it is very difficult to quantify this risk, but it can be explored in any future modelling.

The existence of a near-surface redox reaction zone appears to be well-established, based on the chemistry of the shallow groundwater samples and fracture mineralogy in the superficial bedrock. Furthermore, the common occurrence of calcite suggests that there is buffering capacity against dilute groundwater. However, uncertainties concerning quantification of the redox and alkalinity buffering capacity of flow paths in the rock of the focused volume are still not bounded. Complementary studies to reduce the uncertainties are currently in progress. One concerns a more quantitative evaluation of the amount of different minerals along fractures, and the other aims to provide more detailed information bearing on the significance and origin of fractures that lack a mineral coating or filling and wall-rock alteration.

Another key remaining uncertainty concerns concentrations of sulphide in the groundwater. Time series data from the ongoing monitoring programmes are judged to be sufficient to allow assessment of the undisturbed sulphide concentrations. This assessment is done jointly at Laxemar and Forsmark.

It is judged that other remaining uncertainties in the investigated rock volume can only be reduced significantly by additional data from underground, e.g. the uncertainty in size distribution and size-intensity models for the subhorizontal fracture set, including gently dipping minor deformation zones. These uncertainties and their suggested treatment are addressed in /SKB 2009/.

Uncertainties outside the focused volume (which embeds the proposed repository volume) are more substantial, but are judged to be of less importance for the design and long-term safety of a potential repository. Additional surface-based boreholes outside the focused volume would only marginally decrease uncertainty.

11.9.3 Handling of alternatives

Many of the previous hypotheses proposed during earlier versions of the SDM work have now been discarded or handled by bounding assumptions. Nevertheless, four hypotheses are retained with alternative models developed and propagated, where necessary, to repository engineering/design and to safety assessment.

Fracture size and intensity modelling in the geological DFN. Effectively, some 29 alternative and internally ranked models have been produced. These include: fractal or Euclidean scaling for fracture size-intensity, fracture size scaling exponent (k_r , as a global parameter or function of fracture domain), fracture size calculated using linked or unlinked outcrop traces, fracture intensity (P_{32}) on open fracture intensity or total fracture intensity, and fracture size calculated using bounding trace length scaling exponents ('Upper' or 'Lower') instead of the 'Best Fit' exponent.

Hydraulic properties and connectivity of the fracture network at a scale smaller than the deterministic deformation zones in the context of the correlation between fracture size and transmissivity. In contrast to the situation after version Laxemar 1.2 of the site descriptive model, there is now a multitude of data in support of the hydrogeological description. The PFL-data are used specifically to capture the effects of connected fractures, and all deep PFL-tested boreholes show a consistent picture. The orientation of conductive fractures is generally consistent with the orientation of the current minimum principal stress. However, it is not currently possible to resolve uncertainty in the potential correlation between fracture size and transmissivity, and the three alternatives "full correlation", "semi-correlation" and "no correlation" need to be retained and propagated to SR-Site. The alternatives have no implications for engineering and need not be considered in the design work.

Alternative hypotheses regarding groundwater composition and processes. There is a good understanding of the current spatial distribution of groundwater composition and the existence of a near-surface redox reaction zone appears to be well established, even though there are uncertainties in the data interpretation. The common occurrence of calcite suggests that there is buffering capacity against dilute groundwater, but quantification is uncertain. The uncertainties are sufficiently well bounded concerning conditions at the present day, whereas there are larger uncertainties as to whether the process understanding is sufficient for predicting the groundwater composition during a glaciation. Even though current understanding suggests that there is sufficient buffering capacity in the bedrock, SR-Site may have to handle the alternative possibility that dilute waters generated during ice-melting will reach repository levels. To some extent, future treatment of this uncertainty is dependent on the outcome of a currently ongoing study aiming at quantifying the occurrences of different fracture minerals.

Effects of connectivity, complexity and channelling on distribution of flow (F-factor). Details of the flow field in the fracture plane are uncertain. In SR-Can, channelling was handled by dividing the transport resistance obtained from the hydrogeological DFN model by a factor of 10, whereas SDM-Site explores a multitude of channelling hypotheses. The bounding estimates of the influence of channelling assessed in SDM-Site will be propagated to SR-Site.

11.9.4 Consistency between disciplines

Another prerequisite for confidence is consistency (i.e. no conflicts) between the different discipline model interpretations. Furthermore, confidence is enhanced if aspects of the model are supported by independent evidence from different disciplines. The assessment revealed that essentially all identified interactions between the different disciplines are considered in the site descriptive modelling work. Furthermore, the interdisciplinary feedbacks provide qualitative and independent data support to the different discipline-specific descriptions and thus enhance overall confidence.

11.9.5 Confidence statement

Generally, it is judged that key aspects of the Laxemar site descriptive model, i.e. information needed for repository design and safety assessment, have a high level of confidence, even if details of the spatial variability remain unknown. The overall reason for this confidence is the relative wealth of data from the focused volume and the consistency between independent data from different disciplines. Nevertheless, some aspects still have lower levels of confidence. The lack of confidence is handled by providing wide uncertainty ranges, bounding estimates or alternative models.

12 Conclusions

12.1 Fulfilment of objectives

Bearing in mind the overall objective of the site descriptive modelling work at Laxemar and the Laxemar-Simpvarp area, it can be concluded that an integrated description of the site, based on available complete site investigation data, has been developed and documented. The description is supported by a large amount of data and the results of analyses and modelling that are mutually supporting and consistent. This demonstrates that a fundamental understanding of the current state of conditions and the on-going processes in Laxemar and the Laxemar-Simpevarp area has been achieved, from the surface down to below the potential repository depth. In addition, the properties of the site can be explained in the context of an understanding of past evolution, throughout geological history.

Concerning the specific objectives of the site descriptive modelling work, it is concluded that all data in data freeze Laxemar 2.3 have been analysed, and the results provide, together with knowledge from previous modelling work, the basis for the site-descriptive model of the Laxemar-Simpevarp area, and of Laxemar in particular. Models of the geology /Wahlgren et al. 2008/, thermal properties /Sundberg et al. 2008a/, rock mechanics properties /Hakami et al. 2008/ and hydrogeological properties /Rhén et al. 2008/ have been documented separately and delivered to repository engineering. Data that became available after data freeze Laxemar 2.3 have, to a lesser degree, been assessed in terms of comparison and or partial validation, or at least commented upon, in relation to these models.

The final site descriptive model builds on an integrated geological model in 3D into which other discipline-specific models have been integrated successfully without any conflicting interpretations. A systematic assessment of confidence in the model, including treatment of uncertainties and evaluation of alternative interpretations, has been carried out /SKB 2009/. This assessment was conducted in cooperation with representatives of repository engineering and safety assessment. It addressed the feedback obtained from the work with the preliminary repository layout step D1 and from the safety assessment SR-Can, as well as the feedback obtained on earlier versions of the site description. The overall outcome of this assessment is that the properties of importance for both repository constructability and long-term safety are bounded sufficiently, and that data from underground now bears the prime potential to further reduce uncertainties in the focused volume. Uncertainties outside the focused volume, particularly west thereof, are larger but judged to be of less importance.

12.2 Key remaining issues

Remaining issues where the uncertainties are still not bounded sufficiently concern a quantitative evaluation of the redox and alkalinity buffering capacity of flow paths in the rock in the focused volume. In addition, the reason for increasing sulphide concentrations with time in some borehole sections sampled during the on-going monitoring programme is currently being investigated.

12.3 Implications for the underground construction phase

If Laxemar is selected as a site for the final repository there are a number of issues that are judged to require further study prior to and during the underground construction phase in order to decrease the uncertainties in the description of the focused volume, cf. /SKB 2009/. The most important of these are summarised below:

- The uncertainties in size distribution and size-intensity models for fractures at repository depth can only be reduced by data collected underground.
- Uncertainties in stress magnitudes will be further reduced and constrained by observations and measurements of deformation and back analyses during the construction phase.

- A more detailed description of the bedrock and the thermal conductivity distributions from underground investigations will enable thermal optimisation of the repository, if deemed required.
- There is little point in carrying out hydraulic tests in additional surface-based boreholes. The next step in confidence building would be to predict conditions based on information collected from underground tunnels. Tunnel (and underground borehole) data will provide information about the fracture size distribution of relevant fracture sets at the relevant depths. Furthermore, underground work will also provide possibilities for short-range interference tests at relevant depths.
- Uncertainties in the understanding of chemical processes will be reduced by assessing the effects of drawdown and inflows on, for example, groundwater chemistry and fracture minerals during excavation.
- The hydrogeological DFN parameters for fractures within the repository volume can only be properly constrained by using open fracture statistics from tunnels and inflow distribution measured in underground boreholes. These data will help test and improve current models which are based on surface outcrop and surface borehole data.
- Information on the frequency of flowing fractures collected underground in tunnels and investigations of couplings between mechanical properties and fracture transmissivities is expected to provide information on the extent of in-plane channelled flow, which may improve the models for solute transport.

13 References

- Al-Ajmi A M , Zimmerman R W, 2006.** Stability analysis of vertical boreholes using the Mogi-Coulomb failure criterion. *Int. J. Rock Mech.* 43 (8).
- Andersson M, Nilsson C-A, 1992.** Markgeokemiska kartan 3-7, F-H. SGU. Rapporter och meddelanden nr 73. Kartor i skalan 1:1 miljon (in Swedish).
- Andersson J, Hermanson J, Elert M, Gylling B, Moreno L, Selroos J-O, 1998.** Derivation and treatment of the flow-wetted surface and other geosphere parameters in the transport models FARF31 and COMP23 for use in Safety Assessment. SKB TR-98-60, Svensk Kärnbränslehantering AB.
- Andersson J, Ström A, Svemar C, Almén K-A, Ericsson L-O, 2000.** What requirements does the KBS-3 repository make on the host rock? Geoscientific suitability indicators and criteria for siting and site evaluation. SKB TR-00-12, Svensk Kärnbränslehantering AB.
- Andersson J, Christiansson R, Hudson J, 2002a.** Site Investigations Strategy for Rock Mechanics Site Descriptive Model. SKB TR-02-01, Svensk Kärnbränslehantering AB.
- Andersson P, Byegård J, Dershovitz W, Doe T, Hermanson J, Meier P, Tullborg E L, Winberg A, 2002b.** TRUE Block Scale Project. Final Report. 1. Characterisation and model development. SKB TR-02-13, Svensk Kärnbränslehantering AB.
- Andersson J, Berglund J, Follin S, Hakami E, Halvarson J, Hermanson J, Laaksoharju M, Rhén I, Wahlgren C-H, 2002c.** Testing the methodology for site descriptive modelling. Application for the Laxemar area. SKB TR-02-19, Svensk Kärnbränslehantering AB.
- Andersson J, 2003.** Site descriptive modelling – strategy for integrated evaluation. SKB R-03-05, Svensk Kärnbränslehantering AB.
- Andersson J, Franzén F, Lingman A, Sandström O, 2005.** Recipientundersökningar vid kärnkraftverket vid Oskarshamn. Sammanställning av resultat från undersökningar av fisksamhällen och mjukbottenfauna 1962–2001. *Finno* 2005:8, Fiskeriverket (in Swedish).
- Andersson J C, 2007.** Äspö Hard Rock Laboratory. Äspö Pillar Stability Experiment, Final report. Rock mass response to coupled mechanical thermal loading. SKB TR-07-01, Svensk Kärnbränslehantering AB.
- André M, Neretnieks I, Malmström M, 2008.** Measuring sorption coefficients and BET surface areas on intact drillcore and crushed granite samples. *Radiochimica Acta* 96(1–5), 1–5.
- Ask D, Cornet F, Brunet C, Fontbonne F, 2007.** Stress measurements with hydraulic methods in borehole KLX12A. Oskarshamn site investigation. SKB P-07-232, Svensk Kärnbränslehantering AB.
- Auqué, L F, Gimeno M J, Gómez J B, Puigdomenech I, Smellie J, Tullborg E-L, 2006.** Groundwater chemistry around a repository for spent nuclear fuel over a glacial cycle. Evaluation for SR-Can. SKB TR-06-31, Svensk Kärnbränslehantering AB.
- Back P-E, Sundberg J, 2007.** Thermal Site Descriptive Model. A Strategy for the Model Development during Site Investigations. Version 2.0. SKB R-07-42, Svensk Kärnbränslehantering AB.
- Back P E, Wrafter J, Sundberg J, Rosén L, 2007.** Thermal properties. Site descriptive modelling Forsmark – stage 2.2. SKB R-07-47, Svensk Kärnbränslehantering AB.
- Bath A, Lalieux P, 1999.** Technical summary of the SEDE Workshop on the use of hydrogeochemical information in testing groundwater flow models. In: Use of hydrogeochemical information in testing groundwater flow models, Technical summary and proceedings of an NEA Workshop, Borgholm, Sweden, 1–3 September 1997 (organised by the NEA Co-ordinating Group on Site Evaluation and Design of Experiments for Radioactive Waste Disposal (SEDE)). OECD/NEA, Radioactive Waste Management, pp. 13–30.
- Barton N, 2002.** Some new Q-value correlations to assist in site characterisation and tunnel design, *I.J. Rock Mech. & Min. Eng.*, Vol. 39, pp 185–216.

- Berg C, Bergelin A, Wacker P, Nilsson A-C, 2006.** Forsmark site investigation. Hydrochemical characterisation in borehole KFM08A. Results from the investigated section at 683.5–690.6 (690.8) m. SKB P-06-63, Svensk Kärnbränslehantering AB.
- Bergelin A, Nilsson K, Lindquist A, Wacker P, 2008.** Oskarshamn site investigation. Complete chemical characterisation in borehole KLX27A. Results from borehole section 641.5 to 650.6 m. SKB P-08-77, Svensk Kärnbränslehantering AB.
- Bergman B, Juhlin C, Palm H, 2001.** Reflektionsseismiska studier inom Laxemarområdet. SKB R-01-07, Svensk Kärnbränslehantering AB.
- Bergman T, Sohlenius G, 2007.** Oskarshamn site investigation. Petrographic analysis of gravel and boulders in till from the Laxemar area. SKB P-07-30, Svensk Kärnbränslehantering AB.
- Berglund S, Selroos J-O, 2004.** Transport properties site descriptive model – Guidelines for evaluation and modelling. SKB R-03-09, Svensk Kärnbränslehantering AB.
- Beunk F F, Page L M, 2001.** Structural evolution of the accretional continental margin of the Paleoproterozoic Svecofennian orogen in southern Sweden. *Tectonophysics* 339, 67–92.
- Bienawski Z T, 1989.** Engineering rock mass classifications. John Wiley & Sons.
- Birgersson L, Neretnieks I, 1990.** Diffusion in the Matrix of Granitic Rock: Field Test in the Stripa Mine. *Water Resources Research* 26(11), 2833–2842.
- Bosson E, Gustafsson L-G, Sassner M, 2008.** Numerical modelling of surface hydrology and near-surface hydrogeology at Laxemar-Simpevarp. Site descriptive modelling, SDM-Site Laxemar. SKB R-08-72, Svensk Kärnbränslehantering AB.
- Bradbury M, Green A, 1986.** Investigations into the factors influencing long range matrix diffusion rates and pore space accessibility at depth in granite. *J. Hydrol.*, 89, pp. 123–139.
- Brunauer S, Emmet P, Teller E, 1938.** Adsorption of gases in multimolecular layers. *Journal of the American Chemical Society* 60, 309–319, doi:10.1021/ja01269a023.
- Brunberg A-K, Blomqvist P, 2000.** Post-glacial, land rise-induced formation and development of lakes in the Forsmark area, central Sweden. SKB TR-00-02, Svensk Kärnbränslehantering AB.
- Brunberg A-K, Carlsson T, Brydsten L, Strömberg M, 2004.** Oskarshamn site investigation. Identification of catchments, lake-related drainage parameters and lake habitats. SKB P-04-242, Svensk Kärnbränslehantering AB.
- Byegård J, Selnert E, Tullborg E L, 2008.** Site descriptive modelling of transport properties. Retardation model Forsmark 2.3. SKB R-08-98, Svensk Kärnbränslehantering AB.
- Bödvarsson R, Lund B, Roberts R, Slunga S, 2006.** Earthquake activity in Sweden. Study in connection with a proposed nuclear waste repository in Forsmark or Oskarshamn. SKB R-06-67, Svensk Kärnbränslehantering AB.
- Bödvarsson R, 2008.** Swedish National Seismic Network (SNSN) – A short report on recorded earthquakes during the second quarter of the year 2008. SKB P-08-60, Svensk Kärnbränslehantering AB.
- Carle S F, 1999.** T-PROGS: Transition Probability Geostatistical Software. Version 2.1. Hydrologic Sciences Graduate Group. University of California, Davis.
- Caine J S, Evans J P, Forster C B, 1996.** Fault zone architecture and permeability structure. *Geology* 24 (11), 1025–1028.
- Crawford J, 2008.** Bedrock transport properties Forsmark. Site descriptive modelling. SDM-Site Forsmark. SKB R-08-48, Svensk Kärnbränslehantering AB.
- Crawford J, Sidborn M (eds) 2009.** Bedrock transport properties Laxemar. Site descriptive modelling. SDM Site Laxemar. SKB R-08-94, Svensk Kärnbränslehantering AB.
- Cruden A R, 2008.** Emplacement mechanisms and structural influences of a younger granite intrusion into older wall rocks – a principal study with application to the Götemar and Uthammar granites. Site-descriptive modelling. SDM-Site Laxemar. SKB R-08-138, Svensk Kärnbränslehantering AB.

- Davis J C, 1986.** Statistics and data analysis in geology. Wiley & Sons.
- Dershowitz W, Lee G, Geier J, Foxford T, La Pointe P, Thomas A, 1998.** FRACMAN, Interactive discrete feature data analysis, geometric modelling and exploration simulation. User documentation, version 2.6. Golder Associates, Inc. Redmond, Washington, USA.
- Dershowitz W, Winberg A, Hermanson J, Byegård J, Tullborg E-L, Andersson P, Mazurek M, 2003.** Äspö Hard Rock Laboratory. Äspö Task Force on modelling of groundwater flow and transport of solutes – Task 6C – A semi-synthetic model of block scale conductive structures at the Äspö HRL. SKB IPR-03-13, Svensk Kärnbränslehantering AB.
- Deutsch C, Journel A, 1998.** GS-LIB: Geostatistical Software Library and User's Guide. Second edition. Oxford University Press, New York.
- Drake D, Tullborg E-L, 2006a.** Mineralogical, chemical and redox features of red-staining adjacent to fractures – Results from drill core KSH01A+B and KSH03A+B. SKB P-06-01, Svensk Kärnbränslehantering AB.
- Drake D, Tullborg E-L, 2006b.** Mineralogical, chemical and redox features of red-staining adjacent to fractures – Results from drill core KLX04. SKB P-06-02, Svensk Kärnbränslehantering AB.
- Drake H, Tullborg E-L, 2006c.** Oskarshamn site investigation. Fracture mineralogy, Results from drill core KSH03A+B. SKB P-06-03, Svensk Kärnbränslehantering AB.
- Drake H, Sandström B, Tullborg E-L, 2006.** Mineralogy and geochemistry of rocks and fracture fillings from Forsmark and Oskarshamn: Compilation of data for SR-Can. SKB R-06-109, Svensk Kärnbränslehantering AB.
- Drake H, Tullborg E-L, 2007a.** Paleohydrogeology of the Simpevarp area, southeastern Sweden, as evidenced by stable isotopes in fracture minerals. In: T.D. Bullen and Y. Wang (Editors), Water-rock Interaction: Proceedings of the 12th International Symposium on Water-Rock Interaction, Kunming, China, 31 July–5 August 2007. Taylor & Francis, London, UK, 723–726.
- Drake H, Tullborg E-L, 2007b.** Oskarshamn site investigation. Fracture mineralogy, Results from drill cores KLX03, KLX04, KLX06, KLX07A, KLX08 and KLX10A. SKB P-07-74, Svensk Kärnbränslehantering AB.
- Drake H, Page L, Tullborg E-L, 2007.** Oskarshamn site investigation, 40Ar/39Ar dating of fracture minerals. SKB P-07-27, Svensk Kärnbränslehantering AB.
- Drake H, Tullborg E-L, Annersten H, 2008.** Red-staining of the wall rock and its influence on the reducing capacity around water conducting fractures. Applied Geochemistry 23, 1898–1920.
- Drake H, Tullborg E-L, 2009a.** Fracture mineralogy Laxemar. SKB R-08-99, Svensk Kärnbränslehantering AB.
- Drake H, Tullborg E-L, 2009b.** Paleohydrogeological events recorded by stable isotopes, fluid inclusions and trace elements in fracture minerals in crystalline rock, Simpevarp area, SE Sweden. Applied Geochemistry 24, 715–732.
- Drake H, Tullborg E-L, MacKenzie A B, 2009a.** Detecting the near-surface redox front in crystalline bedrock using fracture mineral distribution, geochemistry and U-series disequilibrium. Applied Geochemistry, 24, 1023–1039.
- Drake H, Tullborg E-L, Page L, 2009b.** Distinguished multiple events of fracture mineralisation related to far-field orogenic effects in Paleoproterozoic crystalline rocks, Simpevarp area, SE Sweden. Lithos 110, 37–49.
- Döse C, Strähle A, Rauséus G, Samuelsson E, Olsson O, 2008.** Revision of BIPS-orientations for geological objects ion boreholes from Forsmark and Laxemar. SKB P-08-37, Svensk Kärnbränslehantering AB.
- Eklund S, Mattsson K-J, 2008.** Oskarshamn site investigation. Quantitative mapping of fracture minerals in Laxemar. SKB P-08-38, Svensk Kärnbränslehantering AB.
- Ekman L, 2001.** Project Deep Drilling KLX02. Phase 2. Methods, scope, summary and results. Summary Report. SKB TR-93-06, Kärnbränslehantering AB.

- Elhammer A, Sandkvist Å, 2005.** Oskarshamn site investigation – Detailed marine geological survey of the sea bottom outside Simpevarp. SKB P-05-35, Svensk Kärnbränslehantering AB.
- Enachescu C, Wolf P, Rohs S, van der Wall R, 2008.** Hydraulic injection tests in borehole KLX27A, Subarea Laxemar. Oskarshamn site investigation, SKB P-08-27, Svensk Kärnbränslehantering AB.
- Engdahl A, Ternsell A, Hannu S, 2006.** Oskarshamn site investigation – Chemical characterisation of deposits and biota. SKB P-06-320, Svensk Kärnbränslehantering AB.
- Engdahl A, Rådén R, Borgiel M, Omberg L-G, 2008.** Oskarshamn and Forsmark site investigations. Chemical composition of suspended material, sediment and pore water in lakes and seabays. SKB P-08-81, Svensk Kärnbränslehantering AB.
- Ericsson L O, Holmén J, Rhén I, Blomquist N, 2006.** Storregional grundvattenmodellering – fördjupad analys av flödesförhållanden i östra Småland. Jämförelse av olika konceptuella beskrivningar. SKB R-06-64, Svensk Kärnbränslehantering AB (in Swedish).
- Essén S, Johnsson A, Bylund D, Pedersen K, Lundström U, 2007.** Siderophore production by *Pseudomonas stutzeri* under anaerobic conditions. *Applied and Environment Microbiology* 73(18), 5857–5864.
- Fisher R, 1953.** Dispersion on a sphere, *Royal Society of London Proceedings* 217: 295–305.
- Follin S, Stigsson M, Berglund S, Svensson U, 2004.** Variable-density groundwater flow simulations and particle tracking – numerical modelling using DarcyTools. Preliminary site description of the Simpevarp area – version 1.1. SKB R-04-65, Svensk Kärnbränslehantering AB.
- Follin S, Stigsson M, Svensson U, 2005.** Variable-density groundwater flow simulations and particle tracking – Numerical modelling using DarcyTools. Preliminary site description Simpevarp subarea – version 1.2. SKB R-05-11, Svensk Kärnbränslehantering AB.
- Follin S, Stigsson M, Svensson U, 2006.** Hydrogeological DFN modelling using structural and hydraulic data from KLX04, Preliminary site description, Laxemar subarea – version 1.2. SKB R-06-24, Svensk Kärnbränslehantering AB.
- Follin S, Johansson P-O, Levén J, Hartley L, Holton D, McCarthy R, Roberts D, 2007a.** Updated strategy and test of new concepts for groundwater flow modelling in Forsmark in preparation of site descriptive modelling stage 2.2. SKB R-07-20, Svensk Kärnbränslehantering AB.
- Follin S, Levén J, Hartley L, Jackson P, Joyce S, Roberts D, Swift B, 2007b.** Hydrogeological characterisation and modelling of deformation zones and fracture domains, Forsmark modelling stage 2.2. SKB R-07-48, Svensk Kärnbränslehantering AB.
- Follin S, Johansson P-O, Hartley L, Jackson P, Roberts D, Marsic N, 2007c.** Hydrogeological conceptual model development and numerical modelling using CONNECTFLOW. Forsmark modelling stage 2.2. SKB R-07-49, Svensk Kärnbränslehantering AB.
- Forsmark T, Wikström M, Forssman I, Rhén I, 2008.** Correlation of Posiva Flow Log anomalies to core mapped features in KLX17A, KLX18A, KLX19A, KLX20A and KLX21B. Oskarshamn site investigation. SKB P-07-215, Svensk Kärnbränslehantering AB.
- Forssman I, Zetterlund M, Forsmark T, Rhén I, 2005a.** Correlation of Posiva Flow Log anomalies to core mapped features in KSH01A, KSH02A and KAV01. SKB P-05-65, Svensk Kärnbränslehantering AB.
- Forssman I, Zetterlund M, Forsmark T, Rhén I, 2005b.** Correlation of Posiva Flow Log anomalies to core mapped features in KLX02, KLX03, KLX04, KAV04A and KAV04B. SKB P-05-241, Svensk Kärnbränslehantering AB.
- Fox A, La Pointe P, Öhman J, Hermanson J, 2007.** Forsmark modelling stage 2.2. Statistical geological discrete fracture network model for the Forsmark site, stage 2.2. SKB R-07-46, Svensk Kärnbränslehantering AB.
- Fredén C (ed), 2002.** Berg och jord. Sveriges Nationalatlas. Third edition. 208 pp (in Swedish).

- Fredriksson R, 2004.** Oskarshamn site investigation – Inventory of the soft-bottom macrozoobenthos community in the area around Simpevarp nuclear power plant. SKB P-04-17, Svensk Kärnbränslehantering AB.
- Fälth B, Hökmark H, 2006.** Seismically induced shear displacement on repository host rock fractures. Results of new dynamic discrete fracture modelling. SKB R-06-48, Svensk Kärnbränslehantering AB.
- Gascoyne M, 1999.** Long-term maintenance of reducing conditions in a spent nuclear fuel repository. A re-examination of critical factors. SKB R-99-41, Svensk Kärnbränslehantering AB.
- Gascoyne M, 2001.** ³⁶Cl in Olkiluoto groundwaters: Evidence for intrusion of Litorina seawater. POSIVA OY Working Report 2001-20.
- Gascoyne M, 2004.** Hydrogeochemistry, groundwater ages and sources of salts in a granitic batholith on the Canadian Shield, southeastern Manitoba. *Applied Geochemistry* 19, 519–560.
- Gascoyne M, Laaksoharju M (ed), 2008.** High-level radioactive waste disposal in Sweden: Hydrogeochemical characterisation and modelling of two potential sites. *Applied Geochemistry*, 23:7.
- Gascoyne M, Gurban I, 2009a.** Application of the Drilling Impact Study (DIS) to Laxemar groundwaters In: B. Kalinowski (ed) 2009. Background complementary hydrogeochemical studies Model, Site descriptive modelling, SDM-Site Laxemar. SKB R-08-111, Svensk Kärnbränslehantering AB.
- Gascoyne M, Gurban I, 2009b.** Determination of residence time based on ⁴He and ³⁶Cl of Laxemar groundwaters. In: B Kalinowski (ed), 2009. SKB R-08-111, Svensk Kärnbränslehantering AB.
- Gimeno M J, Auqué L F, Gómez J B, Acero P, 2008.** Water-rock interaction modelling and uncertainties of mixing modelling. SKB R-08-111, Svensk Kärnbränslehantering AB.
- Gimeno M J, Auqué L F, Gómez J B, Acero P, 2009.** Water-rock interaction modelling and uncertainties of mixing modelling SDM-Site Laxemar-Simpevarp. In: Kalinowski B, (ed), 2009. Background complementary hydrogeochemical studies. SKB R-08-111, Svensk Kärnbränslehantering AB.
- Greger M, 2004.** Uptake of nuclides by plants. SKB TR-04-14, Svensk Kärnbränslehantering AB.
- Gustafsson S, 1991.** Transient plane source techniques for thermal conductivity and thermal diffusivity measurements of solid materials. *Rev. Sci. Instrum.* 62, p 797–804. American Institute of Physics, USA.
- Gustafsson B, 2004a.** Millennial changes of the Baltic Sea salinity. Studies of the sensitivity of the salinity to climate change. SKB TR-04-12, Svensk Kärnbränslehantering AB.
- Gustafsson B, 2004b.** Sensitivity of the Baltic Sea salinity to large perturbations in climate. *Climate Research* 27, 237–251.
- Gustafsson E, Ludvigson J-E, 2005.** Combined interference test and tracer test between KLX02 and HLX10. SKB P-05-20, Svensk Kärnbränslehantering AB.
- Gustafsson E, Nordqvist R, 2005.** Oskarshamn site investigation. Groundwater flow measurements and SWIW tests in boreholes KLX02 and KSH02. SKB P-05-28, Svensk Kärnbränslehantering AB.
- Gustafsson E, Nordqvist R, Thur P, 2006.** Groundwater flow measurements and SWIW test in borehole KLX03. SKB P-05-246, Svensk Kärnbränslehantering AB.
- Guimerà J, Duro L, Jordana S, Bruno J, 1999.** Effects of ice melting and redox front migration in fractured rocks of low permeability. SKB TR-99-19, Svensk Kärnbränslehantering AB.
- Gurban I, 2008.** Forsmark Site: M3 modelling and 2D visualisation of the hydrochemical parameters in Forsmark groundwater data 2.2 and 2.3. In: Kalinowski B (ed), 2008. Background complementary hydrogeochemical studies. SKB R-08-87, Svensk Kärnbränslehantering AB.
- Gurban I, 2009.** M3 modelling of the hydrochemical parameters of Laxemar-Simpevarp groundwaters. In: Kalinowski B (ed), 2009. Background complementary hydrogeochemical studies. SKB R-08-111, Svensk Kärnbränslehantering AB.

- Hakami E, Hakami H, Cosgrove J, 2002.** Strategy for a Rock Mechanics Site Descriptive Model. Development and testing of an approach to modelling the state of stress. SKB R-02-03, Svensk Kärnbränslehantering AB.
- Hakami E, Fredriksson A, Lanaro F, Fredriksson A, Wrafter J, 2008.** Rock mechanics Laxemar, Site descriptive modelling. SDM-Site Laxemar. SKB R-08-57, Svensk Kärnbränslehantering AB.
- Hallbeck L, Pedersen K, 2008.** Explorative analyses of microbes, colloids, and gases together with microbial modelling. Site descriptive modelling. SDM-Site Laxemar. SKB R-08-109, Svensk Kärnbränslehantering AB.
- Harrström J, Thur P, 2009.** Groundwater flow measurements in permanently installed boreholes. Test campaign no. 4 2008, Oskarshamn site investigation, SKB P-09-XX, in prep, Svensk Kärnbränslehantering AB.
- Hartley L J, Holton D, 2004.** CONNECTFLOW (Release 8.0). Technical summary document, Serco Assurance Report SA/ERRA C/TSD02V1.
- Hartley L J, Hoch A R, Cliffe K A, Jackson C P, Holton D, 2004a.** NAMMU (Release 8.0). Technical summary document, Serco Assurance Report SA/ENV/0626.
- Hartley L J, Holton D, Hoch A R, 2004b.** NAPSAC (Release 8.0). Technical summary document, Serco Assurance Report SA/ERRA-N/TSD02V1.
- Hartley L, Worth D, Gylling B, Marsic N, Holmén J, 2004c.** Preliminary site description: Groundwater flow simulations. Simpevarp area (version 1.1) modelled with CONNECTFLOW. SKB R-04-63, Svensk Kärnbränslehantering AB.
- Hartley L, Hoch A, Hunter F, N Marsic 2005.** Regional hydrogeological simulations – Numerical modelling using ConnectFlow. Preliminary site description Simpevarp subarea – version 1.2. SKB R-05-12, Svensk Kärnbränslehantering AB.
- Hartley L, Hunter F, Jackson P, McCarthy R, Gylling B, Marsic N, 2006.** Regional hydrogeological simulations using CONNECTFLOW. Preliminary site description Laxemar subarea – version 1.2. SKB R-06-23, Svensk Kärnbränslehantering AB.
- Hartley L, Jackson P, Joyce S, Roberts D, Shevelan J, Swift B, Gylling B, Marsic N, Hermanson J, Öhman J, 2007.** Hydrogeological Pre-Modelling Exercises: Assessment of impact of the Äspö Hard Rock Laboratory; Sensitivities of Palaeo-Hydrogeology; Development of a Local Near-Surface Hydro-DFN for KLX09B-F. Site descriptive modelling. SDM-Site Laxemar. SKB R-07-57, Svensk Kärnbränslehantering AB.
- Hermanson J, Fox A, Öhman J, Rhén I, 2008.** Compilation of data used for the analysis of the geological and hydrogeological DFN models. Site descriptive modelling. SDM-Site Laxemar. SKB R-08-56. Svensk Kärnbränslehantering AB.
- Hjerne C, Nordqvist R, Harrström J, 2009 (in prep).** Compilation and analyses of results from cross-hole tracer tests with conservative tracers. SKB R-09-28, Svensk Kärnbränslehantering AB.
- Holmén J, 2008.** Premodelling of the importance of the location of the upstream hydraulic boundary of a regional flow model of the Laxemar-Simpevarp area. Site descriptive modelling. SDM-Site Laxemar. SKB R-08-60, Svensk Kärnbränslehantering AB.
- Hoch A R, Jackson C P, 2004.** Rock-matrix diffusion in transport of salinity. Implementation in CONNECTFLOW. SKB R-04-78, Svensk Kärnbränslehantering AB.
- Hökmark H, Sundberg J, Kristensson O, Lönnqvist M, Hellström G, 2009.** Strategy for thermal dimensioning of the final repository for spent nuclear fuel. SKB R-09-04, Svensk Kärnbränslehantering AB.
- Ingvarson N H, Palmeby A S L F, Svensson L O, Nilsson K O, Ekfeldt T C I, 2004.** Oskarshamn site investigation – Marine survey in shallow coastal waters, Bathymetric and geophysical investigation 2004. SKB P-04-254, Svensk Kärnbränslehantering AB.
- Isaaks E H, Srivastava R M, 1989.** Applied Geostatistics, Oxford University Press, New York, 1989.
- Jacobsson L, 2007.** Borehole KLX17A. Microcrack volume measurements and triaxial compression test on intact rock. Oskarshamn site investigation. SKB P-07-140, Svensk Kärnbränslehantering AB.

- Jaquet O, Siegel P, 2003.** Groundwater flow and transport modelling during a glaciation period. SKB R-03-04, Svensk Kärnbränslehantering AB.
- Jaquet O, Siegel P, 2006.** Regional groundwater flow model for a glaciation scenario. Simpevarp subarea – version 1.2. SKB R-06-100, Svensk Kärnbränslehantering AB.
- Janson T, Magnusson J, Bergvall M, Olsson R, Cuisiat F, Skurtveit E, Grimstad E, 2006.** Final repository for spent nuclear fuel. Underground design Laxemar Layout D1. SKB R-06-36, Svensk Kärnbränslehantering AB.
- Johnsson A, Arlinger J, Pedersen K, Ödegaard-Jensen A, Albinsson Y, 2006.** Solid-aqueous phase partitioning of radionuclides by complexing compounds excreted by subsurface bacteria. *Geomicrobiology Journal* 23, 621–630.
- Johansson R, 2006.** A comparison of two independent interpretations of lineaments from geophysical and topographic data from the Simpevarp area. SKB R-06-53, Svensk Kärnbränslehantering AB.
- Jonsson M, Bäckström A, Feng Q, Berglund J, Johansson M, Mas Ivars D, Olsson M, 2009.** Studies of factors that affect and controls the Excavation Damage/Disturbed Zone. Äspö Hard Rock Laboratory. SKB R-09-17, Svensk Kärnbränslehantering AB.
- Journel A G, Huijbregts C J, 1978.** Mining geostatistics. Academic Press, London.
- Juhlin C, Bergman B, Palm H, 2004.** Oskarshamn site investigation. Reflection seismic studies performed in the Laxemar area during 2004. SKB P-04-215, Svensk Kärnbränslehantering AB.
- Koistinen T, Stephens M B, Bogatchev V, Nordgulen O, Wennerström M, Korhonen J, 2001.** Geological map of the Fennoscandian Shield, scale 1:2 000 000. Geological Surveys of Finland, Norway and Sweden and the North-West Department of Natural Resources of Russia.
- Korhonen K, Kuivamäki A, Ruotoistenmäki T, Paananen M, 2005.** Interpretation of lineaments from airborne geophysical and topographic data. An alternative model within version Laxemar 1.2 of the Oskarshamn modelling project. SKB P-05-247, Svensk Kärnbränslehantering AB.
- Kruskal W H, Wallis W A, 1952.** Use of ranks in one-criterion variance analysis. *Jour. Am. Stat. Assoc.* 47, 583–634.
- Kumblad L, Kautsky U, Næslund B, 2006.** Transport and fate of radionuclides in aquatic environments – the use of ecosystem modeling for exposure assessments of nuclear facilities. *Journal of Environmental Radioactivity* 87, 107–129.
- Laaksoharju M, Wallin B (eds), 1997.** Evolution of the groundwater chemistry at the Äspö Hard Rock Laboratory. Proceedings of the second Äspö International Geochemistry Workshop, June 6–7, 1995. Äspö HRL. SKB ICR-97-04, Svensk Kärnbränslehantering AB.
- Laaksoharju M, 1999.** Groundwater Characterisation and Modelling: Problems, Facts and Possibilities. Dissertation TRITA-AMI-PHD 1031; ISSN 1400-1284; ISRN KTH/AMI/PHD 1031-SE; ISBN 91-7170-. Royal Institute of Technology, Stockholm, Sweden. SKB TR-99-42, Svensk Kärnbränslehantering AB.
- Laaksoharju M, Tullborg E-L, Wikberg P, Wallin B, Smellie J, 1999.** Hydrogeochemical conditions and evolution at Äspö HRL, Sweden. *Applied Geochemistry* Vol. 14, #7, 1999, Elsevier Science Ltd., pp 835–859.
- Laaksoharju M (ed) 2004.** Hydrogeochemical evaluation for Simpevarp model version 1.2. Preliminary site description of the Simpevarp area. SKB R-04-74, Svensk Kärnbränslehantering AB.
- Laaksoharju M, Smellie J, Tullborg E-L, Gimeno M, Molinero J, Gurban I, Hallbeck L, 2008a.** Hydrogeochemical evaluation and modelling performed within the site investigation programme. *Applied Geochemistry* 23:7. Elsevier.
- Laaksoharju M, Smellie J, Tullborg E-L, Gimeno M, Gurban I, Hallbeck L, Molinero J, Waber N, 2008b.** Bedrock hydrogeochemistry Forsmark. Site descriptive modelling. SDM-Site Forsmark. SKB R-08-47, Svensk Kärnbränslehantering AB.
- Laaksoharju M, Smellie J A T, Tullborg E-L, Wallin B, Drake H, Gimeno M, Hallbeck L, Molinero J, Nilsson A-C, Waber N, 2009.** Bedrock hydrogeochemistry Laxemar, Site descriptive modelling, SDM-Site Laxemar. SKB R-08-93, Svensk Kärnbränslehantering AB.

- Lagerbäck R, Sundh M, Svantesson S-I, 2006.** Oskarshamn site investigation – Searching for evidence of late- or postglacial faulting in the Oskarshamn region. Results from 2005. SKB P-06-160, Svensk kärnbränslehantering AB.
- Langmuir D, 1997.** Aqueous environmental geochemistry. Prentice Hall, New Jersey.
- La Pointe P, Hermanson J, 2006.** Statistical model of fractures and deformation zones. Preliminary site description Simpevarp subarea, version 1.2. SKB R-05-28, Svensk Kärnbränslehantering AB.
- La Pointe P, Fox A, Hermanson J, Öhman J, 2008.** Site Descriptive Modelling. SDM-Site Laxemar. Geological discrete fracture network model for the Laxemar site. SKB R-08-55, Svensk Kärnbränslehantering AB.
- Lindquist A, Hjerne C, Nordqvist R, Ludvigson J-E, Harrström J, Carlsten S, 2009 (in prep).** HLX27 confirmatory hydraulic interference test and tracer test in Laxemar, Oskarshamn site investigation, SKB P-08-96, Svensk Kärnbränslehantering AB.
- Lindqvist G, 2004a.** Oskarshamn site investigation. Refraction seismic measurements in the water outside Simpevarp and Ävrö and on land on Ävrö. SKB P-04-201, Svensk Kärnbränslehantering AB.
- Lindqvist G, 2004b.** Oskarshamn site investigation. Refraction seismic measurements in Laxemar. SKB P-04-134, Svensk Kärnbränslehantering AB.
- Lindqvist G, 2004c.** Oskarshamn site investigation. Refraction seismic measurements in Laxemar autumn 2004. SKB P-04-298, Svensk Kärnbränslehantering AB.
- Lindqvist G, 2005.** Oskarshamn site investigation. Refraction seismic measurements in Laxemar spring 2005. SKB P-05-155, Svensk Kärnbränslehantering AB.
- Lindqvist G, 2006.** Oskarshamn site investigation. Refraction seismic measurements in Laxemar spring 2006. SKB P-06-49, Svensk Kärnbränslehantering AB.
- Lindqvist G, 2007.** Oskarshamn site investigation. Refraction seismic measurements in Laxemar spring 2007. SKB P-07-131, Svensk Kärnbränslehantering AB.
- Lindroos H, 2004.** The potential for ore, industrial minerals and commercial stones in the Simpevarp area. SKB R-04-72, Svensk Kärnbränslehantering AB.
- Louvat D, Michelot J, Aranyossy J, 1999.** Origin and residence time of salinity in the Äspö groundwater system. Applied Geochemistry 14, 917-925.
- Lundberg E, Sjöström H, 2006.** Oskarshamn site investigation. Kinematic analysis of ductile and brittle/ductile shear zones in Simpevarp and Laxemar subarea. SKB P-06-118, Svensk Kärnbränslehantering AB.
- Lundin L, Lode E, Stendahl J, Björkvald L, Hansson J, 2005.** Oskarshamn site investigation – Soils and site types in the Oskarshamn area. SKB R-05-15, Svensk Kärnbränslehantering AB.
- Lundin L, Lode E, Stendahl J, 2006.** Oskarshamn site investigation – Extended soil chemistry in three site types. SKB P-06-321, Svensk Kärnbränslehantering AB.
- Lundin L, Snäll S, Jonsson E, Hannu S, Selnert E, Engdahl A, 2007.** Oskarshamn site investigation – Characterization of soil samples from three valleys in the Laxemar area. SKB P-07-222, Svensk Kärnbränslehantering AB.
- Lundqvist L, 2006.** Inledande kulturhistoriska studier i Simpevarpsområdet: Småland, Misterhults socken, Oskarshamn kommun. SKB R-06-65, Svensk Kärnbränslehantering AB (in Swedish).
- Löfgren A, Lindborg T, 2003.** A descriptive ecosystem model – a strategy for model development during site investigations. SKB R-03-06, Svensk Kärnbränslehantering AB.
- Löfgren M, Crawford J, Elert M, 2007.** Tracer tests – possibilities and limitations. Experiments from SKB fieldwork: 1977–2007. SKB R-07-39, Svensk Kärnbränslehantering AB.
- Löfgren A (ed) 2008.** The terrestrial ecosystems at Forsmark and Laxemar. Site descriptive modelling. SDM-Site. SKB R-08-01, Svensk Kärnbränslehantering AB.
- Marsic N, Hartley L, Jackson P, Poole M, 2001.** Development of hydrogeological modelling tools based on NAMMU. SKB R-01-49, Svensk Kärnbränslehantering AB.

- Martin C D, 2007.** Quantifying in-situ stress magnitudes and orientations at Forsmark for Design Step D2. SKB R-07-26, Svensk Kärnbränslehantering AB.
- Mattsson H, Triumf C-A, 2007.** Oskarshamn site investigation. Detailed ground geophysics at Laxemar, spring 2007. Magnetic total field. SKB P-07-168, Svensk Kärnbränslehantering AB.
- Miliander S, Punakivi M, Kyläkorpi L, Rydgren B, 2004.** Simpevarp site description: Human population and human activities. SKB R-04-11, Svensk Kärnbränslehantering AB.
- Mjöfors K, Johansson M-B, Nilsson Å, 2007.** Input and turnover of forest tree litter in the Forsmark and Oskarshamn areas. SKB R-07-23, Svensk Kärnbränslehantering AB.
- Molinero J, Arcos D, Duro L, 2008.** Contribution to ChemNet activities. Forsmark model 2.2–2.3. In: Kalinowski B (ed), 2008. Background complementary hydrogeochemical studies. SKB R-08-87, Svensk Kärnbränslehantering AB.
- Molinero J, Salas J, Arcos D, Duro L, 2009.** Integrated hydrogeological and geochemical modelling of the Laxemar-Simpevarp area during the recent Holocen (last 8000 years). In: Kalinowski B (ed), 2009. Background complementary hydrogeochemical studies, Site descriptive modelling. SDM-Site Laxemar. SKB R-08-111, Svensk Kärnbränslehantering AB.
- Morosini M, Jenkins C, Simson S, Albrecht J, Zetterlund M, 2007.** Oskarshamn site investigation. Hydrogeological characterization of deepest valley soil aquifers and soil-rock transition zone at Laxemar, 2006. Subarea Laxemar. SKB P-07-91, Svensk Kärnbränslehantering AB.
- Mossmark F, Sundberg J, 2007.** Oskarshamn site investigation. Field Measurements of Thermal Properties. Multi Probe Measurements in Laxemar. SKB P-07-77, Svensk Kärnbränslehantering AB.
- Mottaghy D, Schellschmidt R, Popov Y A, Clauser C, Kukkonen I T, Nover G, Milanovsky S, Romushkevich R A, 2005.** New heat flow data from the immediate vicinity of the Kola super-deep borehole. Vertical variation in heat flow confirmed and attributed to advection. *Tectonophysics* 401, 119–142.
- Munier R, Stenberg L, Stanfors R, Milnes A G, Hermanson J, Triumf C-A, 2003.** Geological Site Descriptive Model. A strategy for the model development during site investigations. SKB R-03-07, Svensk Kärnbränslehantering AB.
- Munier R, 2004.** Statistical analysis of fracture data, adapted for modelling Discrete Fracture Networks-Version 2. SKB R-04-66, Svensk Kärnbränslehantering AB.
- Munier R, 2006.** Using observations in deposition tunnels to avoid intersections with critical fractures in deposition holes. SKB R-06-54, Svensk Kärnbränslehantering AB.
- Munier R, 2007.** Demonstrating the efficiency of the EFPC criterion by means of Sensitivity analyses. SKB R-06-115, Svensk Kärnbränslehantering AB.
- Munier R, Stigsson M, 2007.** Implementation of uncertainties in borehole geometries and geological orientation data in Sicada. SKB R-07-19, Svensk Kärnbränslehantering AB.
- NEA, 1993.** Palaeohydrogeological methods and their application. Workshop Proceedings, Paris, France, 9–10 November, 1992. Co-ordinating Group on Site Evaluation and Design of Experiments for Radioactive Waste Disposal – SEDE, OECD-NEA.
- NEA, 1999.** Confidence in models of radionuclide transport for site-specific assessments. In: Synthesis and Proceedings from the third GEOTRAP Workshop, OECD-NEA Radioactive Waste Management, Carlsbad, New Mexico, USA, 14–17 June 1999.
- Nilsson G, 2004.** Oskarshamn site investigation – Investigation of sediments, peat lands and wetlands. Stratigraphical and analytical data. SKB P-04-273, Svensk Kärnbränslehantering AB.
- Nilsson A-C, Degueldre D, 2007.** Granitic groundwater colloids sampling and characterisation. Forsmark site investigation. SKB P-07-169, Svensk Kärnbränslehantering AB.
- Nilsson A-C, 2009.** Quality of hydrochemical analyses in data freeze Laxemar 2.3. In: B. Kalinowski (ed) 2009. Background complementary hydrogeochemical studies Model , Site descriptive modelling, SDM-Site Laxemar. SKB R-08-111, Svensk Kärnbränslehantering AB.
- Nordén S, Andersson E, Söderbäck B, 2008.** The limnic ecosystems at Forsmark and Laxemar-Simpevarp. Site descriptive modelling. SDM-Site. SKB R-08-02, Svensk Kärnbränslehantering AB.

- Nordqvist R, 2008.** Evaluation and modelling of SWIW tests performed within the SKB site characterisation programme. SKB R-08-104, Svensk Kärnbränslehantering AB.
- Nyman H, Sohlenius G, Strömgren M, Brydsten L, 2008.** Oskarshamn site investigation – Depth and stratigraphy of regolith. SKB R-08-06, Svensk Kärnbränslehantering AB.
- Olofsson I, Fredriksson A, 2005.** Strategy for a numerical Rock Mechanics Site descriptive Model. SKB R-05-43, Svensk Kärnbränslehantering AB.
- Olsson T, Stanfors R, Sigurdsson O, Erlström M, 2007.** Oskarshamn site investigation. Identification and characterisation of minor deformation zones based on lineament interpretation. SKB P-06-282, Svensk Kärnbränslehantering AB.
- Ottosson P, 2006.** Nulägesbeskrivning av rekreation och friluftsliv i Oskarshamn. SKB P-06-114, Svensk Kärnbränslehantering AB.
- Pedersen K, 2001.** Diversity and activity of microorganisms in deep igneous rock aquifers of the Fennoscandian Shield. In: Fredrickson J K and Fletcher M (eds), *Subsurface microbiology and biogeochemistry*. New York: Wiley-Liss Inc., 97–139.
- Penttinen L, Siitari-Kauppi M, Ikonen J, 2006.** Oskarshamn site investigation. Determination of porosity and micro fracturing using the ¹⁴C-PMMA technique in samples taken from Oskarshamn area. SKB P-06-62, Svensk Kärnbränslehantering AB.
- Persson K S, Sjöström H, 2003.** Late-orogenic progressive shearing in eastern Bergslagen, central Sweden. *GFF* 125, 23–36.
- Persson Nilsson K, Bergman T, Eliasson T, 2004.** Oskarshamn site investigation. Bedrock mapping 2004 – Laxemar subarea and regional model area. Outcrop data and description of rock types. SKB P-04-221, Svensk Kärnbränslehantering AB.
- Persson T, Lenoir L, Taylor A, 2006.** Bioturbation in different ecosystems at Forsmark and Oskarshamn. SKB R-06-123, Svensk Kärnbränslehantering AB.
- Persson H, Stadenberg I, 2007.** Distribution of fine roots in forest areas close to the Swedish Forsmark and Oskarshamn nuclear power plants. SKB R-07-01, Svensk Kärnbränslehantering AB.
- Peterman Z, Wallin B, 1999.** Synopsis of strontium isotope variations in groundwater at Äspö Hard Rock Laboratory, Southern Sweden. *Applied Geochemistry* 14:7, 953–962.
- Pitkänen P, Snellman M, Vuorinen U, 1996.** On the origin and chemical evolution of groundwater at the Olkiluoto site. Posiva Oy, Report POSIVA-96-04.
- Pitkänen P, Luukkonen A, Ruotsalainen P, Leino-Forsman H, Vuorinen U, 1999.** Geochemical modelling of groundwater evolution and residence time at the Olkiluoto site. Posiva Tech Rep. (98-10), Posiva, Helsinki, Finland.
- Pitkänen P, Partamies S, Luukkonen A, 2004.** Hydrogeochemical interpretation of baseline groundwater conditions at the Olkiluoto site. Posiva Tech. Rep. (2003-07), Posiva, Helsinki, Sweden.
- Pusch R, 1974.** Densitet, vattenhalt och portal – Förslag till geotekniska laboratorieanvisningar, Del 7. Byggnadsforskningens informationsblad B5:1973. Byggnadsforskningsrådet.
- Pässe T, 2001.** An empirical model of glacio-isostatic movements and shore-level displacement in Fennoscandia. SKB R-01-41, Svensk Kärnbränslehantering AB.
- Pöllänen J, Pekkanen J, Väisäsvaara J, 2008.** Difference flow logging in borehole KLX27A Subarea Laxemar. Oskarshamn site investigation. SKB P-08-22, Svensk Kärnbränslehantering AB.
- Rhén I (ed), Bäckblom G (ed), Gustafson G, Stanfors R, Wikberg P, 1997a.** Äspö HRL – Geoscientific evaluation 1997/2. Results from pre-investigations and detailed site characterization. Summary report. SKB TR 97-03, Svensk Kärnbränslehantering AB.
- Rhén I, Gustafson G, Wikberg P, 1997b.** Äspö HRL – Geoscientific evaluation 1997/4. Results from pre-investigations and detailed site characterization. Comparison of predictions and observations. Hydrogeology, groundwater chemistry and transport of solutes. SKB TR 97-05, Svensk Kärnbränslehantering AB.

- Rhén I (ed), Gustafson G, Stanfors R, Wikberg P, 1997c.** Äspö HRL – Geoscientific evaluation 1997/5. Models based on site characterization 1986–1995. SKB TR 97-06, Svensk Kärnbränslehantering AB.
- Rhén I, Forsmark T, 2001.** Äspö Hard Rock Laboratory, Prototype repository, Hydrogeology, Summary report of investigations before the operation phase. SKB IPR-01-65, Svensk Kärnbränslehantering AB.
- Rhén I, Smellie J A T, 2003.** Task force modelling of groundwater flow and transport of solutes, Task 5 summary report. SKB TR-03-01, Svensk Kärnbränslehantering AB.
- Rhén I, Follin S, Hermanson J, 2003.** Hydrological Site Descriptive Model – a strategy for its development during site investigations. SKB R-03-08, Svensk Kärnbränslehantering AB.
- Rhén I, Forsmark T, Forsman I, Zetterlund M, 2006a.** Hydrogeological single-hole interpretation of KSH01, KSH02, KSH03, KAV01 and HSH01–03, Preliminary site description, Simpevarp subarea – version 1.2. SKB R-06-20, Svensk Kärnbränslehantering AB.
- Rhén I, Forsmark T, Forsman I, Zetterlund M, 2006b.** Hydrogeological single-hole interpretation of KLX02, KLX03, KLX04, KAV04A and KAV04b, Preliminary site description, Laxemar subarea – version 1.2. SKB R-06-21, Svensk Kärnbränslehantering AB.
- Rhén I, Forsmark T, Forsman I, Zetterlund M, 2006c.** Evaluation of hydrogeological properties for Hydraulic Conductor Domains (HCD) and Hydraulic Rock Domains (HRD), Laxemar subarea – version 1.2. SKB R-06-22, Svensk Kärnbränslehantering AB.
- Rhén I, Forsmark T, Hartley L, Jackson C P, Roberts D, Swan D, Gylling B, 2008.** Hydrogeological conceptualisation and parameterisation, Site descriptive modelling. SDM-Site Laxemar. SKB R-08-78, Svensk Kärnbränslehantering AB.
- Rhén I, Hartley L, 2009.** Bedrock hydrogeology Laxemar, Site descriptive modelling, SDM-Site Laxemar. SKB R-08-92, Svensk Kärnbränslehantering AB (in prep).
- Rhén I, Forsmark T, Hartley L, Jackson C P, Joyce S, Roberts D, Swift B, Marsic N, Gylling B, 2009.** Bedrock Hydrogeology: model testing and synthesis, Site descriptive modelling. SDM-Site Laxemar. SKB R-08-91, Svensk Kärnbränslehantering AB.
- Ringgaard J, 2009.** Mapping of borehole breakouts. Processing of acoustical televiewer data from KAV04A, KLX10, KLX11A, KLX12A, KLX15A and KLX18A. SKB P-09-31, Svensk Kärnbränslehantering AB.
- Roos P, Engdahl A, Karlsson S, 2007.** Oskarshamn and Forsmark site investigations. Analysis of radioisotopes in environmental samples. SKB P-07-32, Svensk Kärnbränslehantering AB.
- Rudmark L, Malmberg-Persson K, Mikko H, 2005.** Oskarshamn site investigation – Investigation of Quaternary deposits 2003–2004. SKB P-05-49, Svensk Kärnbränslehantering AB.
- Röshoff K, Lanaro F, Jing L, 2002.** Strategy for a Rock Mechanics Site Descriptive Model. Development and testing of the empirical approach. SKB R-02-01, Svensk Kärnbränslehantering AB.
- Selnert E, Byegård J, Widestrand H, Carlsten S, Döse C, Tullborg E-L, 2009.** Bedrock Transport Properties. Data Evaluation and Retardation Model, Site descriptive modelling, SDM-Site Laxemar. SKB R-08-100, Svensk Kärnbränslehantering AB.
- Sheppard M I, Sheppard S C, Grant C, 2007.** Solid/liquid partition coefficients to model trace element critical loads for agricultural soils in Canada. *Canadian Journal of Soil Science* 87, 189–201.
- Sitch S, Smith B, Prentice I C, Arneth A, Bondeau A, Crameer W, Kaplans J O, Levis S, Lucht W, Sykes M T, Thonicke K, Venevsky S, 2003.** Evaluation of ecosystem dynamics, plant geography and terrestrial carbon cycling in the LPJ Dynamic Global Vegetation Model. *Global Change Biology* 9, 161–185.
- Skagius K, Neretnieks I, 1986.** Diffusivity measurements and electrical resistivity measurements in rock samples under mechanical stress. *Water Resour. Res.* 22(4), pp. 570–580.
- SKB, 2000.** Förstudie Oskarshamn – Slutrapport. Svensk Kärnbränslehantering AB (in Swedish).

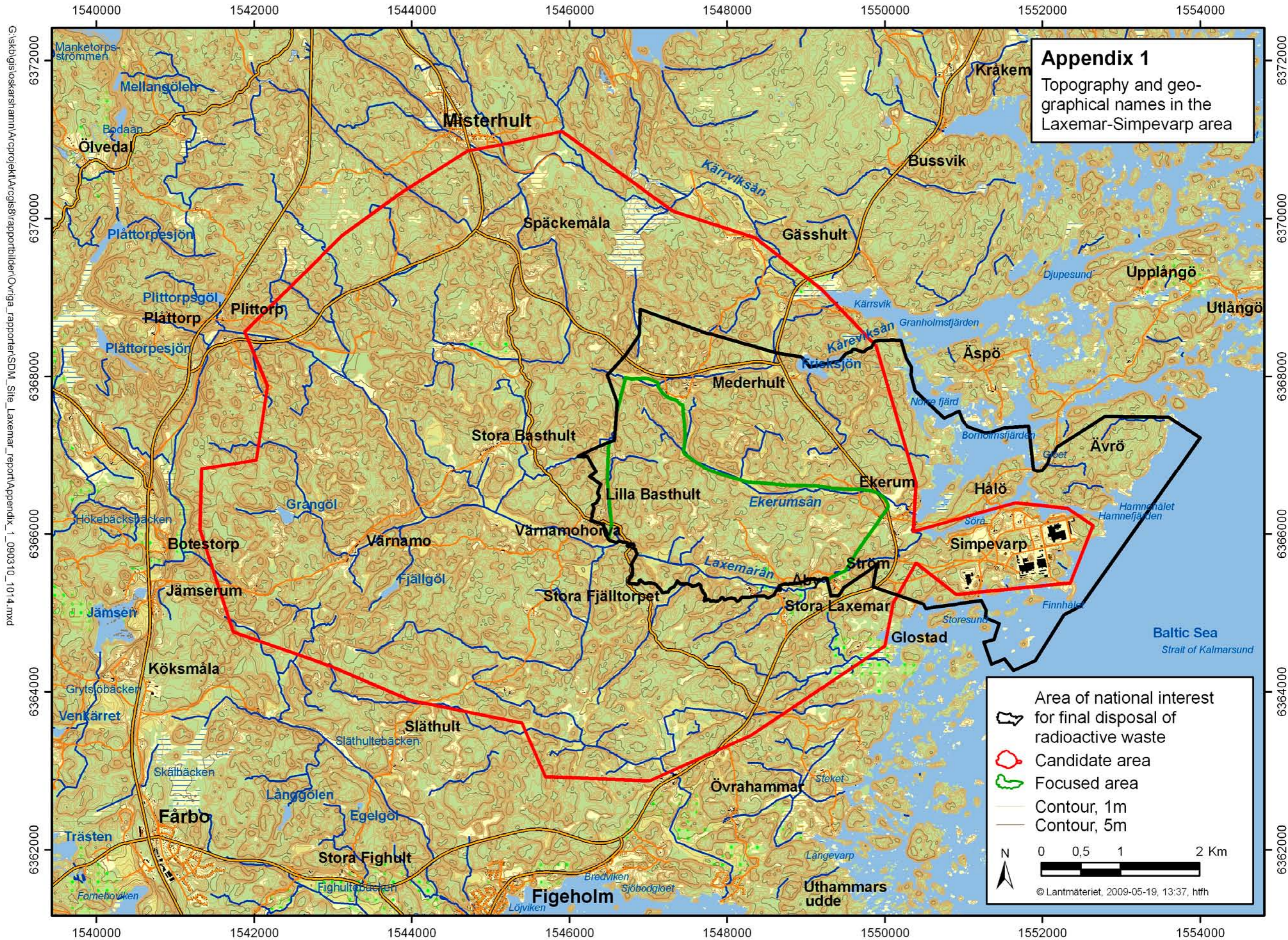
- SKB, 2001.** Geovetenskapligt program för platsundersökning vid Simpevarp. SKB R-01-44, Svensk Kärnbränslehantering AB.
- SKB, 2002.** Simpevarp – site descriptive model version 0. SKB R-02-35, Svensk Kärnbränslehantering AB.
- SKB, 2004a.** Preliminary site description Simpevarp area – version 1.1. SKB R-04-25, Svensk Kärnbränslehantering AB.
- SKB, 2004b.** Hydrogeochemical evaluation for Simpevarp model version 1.2. Preliminary site description of the Simpevarp area. SKB R-04-74, Svensk Kärnbränslehantering AB.
- SKB, 2005a.** Preliminary site description. Simpevarp subarea – version 1.2. SKB R-05-08, Svensk Kärnbränslehantering AB.
- SKB, 2005b.** Evaluation of site investigation data as a basis for focusing of continued site investigations at Laxemar. SKB P-05-264, Svensk Kärnbränslehantering AB (in Swedish).
- SKB, 2006a.** Preliminary site description. Laxemar subarea – version 1.2. SKB R-06-10, Svensk Kärnbränslehantering AB.
- SKB, 2006b.** Programme for further investigations of bedrock, soil, water and environment in Laxemar subarea. Oskarshamn site investigation. SKB R-06-29, Svensk Kärnbränslehantering AB.
- SKB, 2006c.** Preliminary site description Laxemar stage 2.1. Feedback for completion of the site investigation including input from safety assessment and repository engineering. SKB R-06-110, Svensk Kärnbränslehantering AB.
- SKB, 2006d.** Long-term safety for KBS-3 repositories at Forsmark and Laxemar - a first evaluation. Main report of the SR-Can project. SKB TR-06-09, Svensk Kärnbränslehantering AB.
- SKB, 2006e.** Hydrogeochemical evaluation. Preliminary site description Laxemar subarea – version 1.2. SKB R-06-12, SKB, Svensk Kärnbränslehantering AB.
- SKB, 2006f.** Hydrogeochemical evaluation. Preliminary site description Laxemar subarea – version 2.1. SKB R-06-70, Svensk Kärnbränslehantering AB.
- SKB, 2007a.** Priorities in selection a site for a repository in Oskarshamn. SKB R-07-21, Svensk Kärnbränslehantering AB (in Swedish).
- SKB, 2008a.** SDM-Site Forsmark. Site descriptive modelling. SKB TR-08-05, Svensk Kärnbränslehantering AB.
- SKB, 2008b.** Programme for long-term observations of geosphere and biosphere after completed site investigation. Oskarshamn site investigation. SKB R-07-59 (in prep), Svensk Kärnbränslehantering AB.
- SKB, 2009.** Confidence Assessment. Site descriptive modelling. SDM-Site Laxemar. SKB R-08-101, Svensk Kärnbränslehantering AB.
- Smellie J, Laaksoharju M, Tullborg E-L, 2002.** Hydrogeochemical site descriptive model – a strategy for the model development during site investigations. SKB R-02-49, Svensk Kärnbränslehantering AB.
- Smellie J, Tullborg E-L, Nilsson A-C, Gimeno M, Sandström B, Waber N, Gascoyne M, 2008.** Explorative analysis of major components and isotopes, SDM-Site Forsmark. SKB R-08-84, Svensk Kärnbränslehantering AB.
- Smellie J, Tullborg E-L, 2009.** Documentation related to categorisation of the extended data freeze Laxemar 2.3 groundwater samples. In: Kalinowski B (ed), 2009. Background complementary hydrogeochemical studies. SKB R-08-111, Svensk Kärnbränslehantering AB.
- Sohlenius G, Bergman T, Snäll S, Lundin L, Lode E, Stendahl J, Riise A, Nilsson J, Johansson T, Göransson M, 2006.** Oskarshamn site investigation – Soils, Quaternary deposits and bedrock in topographic lineaments situated in the Laxemar subarea. SKB P-06-121, Svensk Kärnbränslehantering AB.
- Sohlenius G, Hedenström A, 2008.** Description of the regolith in the Laxemar-Simpevarp area. Site descriptive modelling, SDM-Site Laxemar. SKB R-08-05, Svensk Kärnbränslehantering AB.

- SSI, 2005.** Statens strålskyddsinstitutets allmänna råd om tillämpning av föreskrifterna (SSI FS 1998:1) om skydd av människors hälsa och miljön vid slutligt omhändertagande av använt kärnbränsle och kärnavfall. SSI FS 2005:5, Statens strålskyddsinstitutets författningssamling.
- Stanfors R, Olsson P, Stille H, 1997.** Äspö HRL – Geoscientific evaluation 1997/3. Results from pre-investigations and detailed site characterization. Comparison of predictions and observations. Geology and mechanical stability. SKB TR 97-04, Svensk Kärnbränslehantering AB.
- Stenberg L, Håkanson N, 2007.** Revision of borehole deviation measurements in Oskarshamn. Oskarshamn site investigation. SKB P-07-55, Svensk Kärnbränslehantering AB.
- Stephens M B, Fox A, La Pointe P, Simeonov A, Isaksson H, Hermanson J, Öhman J, 2007.** Site descriptive modelling, Forsmark stage 2.2. Geology. SKB R-07-45, Svensk Kärnbränslehantering AB.
- Sternbeck J, Land M, Nilsson Ö, 2006.** ²¹⁰Pb and ¹⁴C dating of sediments and peat. Accumulation rates of carbon, nitrogen and phosphorus. Oskarshamn and Forsmark site investigations. SKB P-06-301, Svensk kärnbränslehantering AB.
- Sterner R W, Elser J J, 2002.** Ecological Stoichiometry. Princeton University Press, Princeton, USA.
- Streckeisen A, 1976.** To each plutonic rock its proper name. Earth Science Reviews 12, 1–33.
- Ström A, Andersson J, Skagius K, Winberg A, 2008.** Site descriptive modelling during characterization for a geological repository for nuclear waste in Sweden. Applied Geochemistry, vol. 23, pp. 1747–1760.
- Strömberg M, Brydsten L, 2008.** Digital elevation models of Laxemar-Simpevarp. SDM-Site Laxemar. SKB R-08-63, Svensk Kärnbränslehantering AB.
- Stumm W, Morgan J J, 1996.** Aquatic Chemistry: Chemical equilibria and rates in natural waters. 3rd ed. Wiley, New York.
- Sundberg J, 1988.** Thermal Properties of Soils and Rocks. Publ. A 57, Dissertation. Geologiska institutionen, Chalmers University of Technology, and University of Göteborg.
- Sundberg J, 2003a.** A strategy for the model development during site investigations version 1.0. SKB R-03-10, Svensk Kärnbränslehantering AB.
- Sundberg J, 2003b.** Thermal properties at Äspö HRL. Analysis of distribution and scale factors. SKB R-03-17, Svensk Kärnbränslehantering AB.
- Sundberg J, Back P-E, Bengtsson A, Ländell M, 2005.** Oskarshamn site investigation. Thermal modelling of the Simpevarp area – Supporting document for thermal model version 1.2. SKB R-05-24, Svensk Kärnbränslehantering AB
- Sundberg J, Wrafter J, Back P-E, Ländell M, 2006.** Thermal modelling, Preliminary site description Laxemar subareas – version 1.2. R-06-13, Svensk Kärnbränslehantering AB.
- Sundberg J, Wrafter J, Back P E, Rosén L, 2008a.** Thermal properties Laxemar. Site descriptive modelling. SDM-Site Laxemar. SKB R-08-61, Svensk Kärnbränslehantering AB.
- Sundberg J, Wrafter J, Ländell M, Back P E, Rosén L, 2008b.** Thermal properties Forsmark. Modelling stage 2.3. Complementary analysis and verification of the thermal bedrock model. SKB R-08-65, Svensk Kärnbränslehantering AB.
- Sundberg J, Back P-E, Ericsson L O, Wrafter J, 2009.** A method for estimation of thermal conductivity and its spatial variability in igneous rocks from in situ density logging. International Journal of Rock Mechanics and Mining Sciences, 46, 1023–1028.
- Svensson N-O, 1989.** Late Weichselian and early Holocene shore displacement in the central Baltic, based on stratigraphical and morphological records from eastern Småland and Gotland, Sweden. LUNDQUA 25, 181 pp.
- Svensson T, Ludvigson J-E, Walger E, Thur P, Gokall-Norman K, Wass E, 2008.** Oskarshamn site investigation. Combined hydraulic interference- and tracer test in HLX33, SSM000228, and SSM000229. SKB P-07-187, Svensk Kärnbränslehantering AB.

- Söderbäck B (ed), 2008.** Geological evolution, palaeoclimate and historic development of the Forsmark and Laxemar-Simpevarp areas. Site descriptive modelling SDM-Site. SKB R-08-19, Svensk Kärnbränslehantering AB.
- Söderbäck B, Lindborg (eds), 2009.** Surface system Laxemar-Simpevarp. Site descriptive modelling. SDM-Site Laxemar. SKB R-09-01, Svensk Kärnbränslehantering AB.
- Teurneau B, Forsmark T, Forssman I, Rhén I, 2008.** Correlation of Posiva Flow Log anomalies to core mapped features in KLX05, KLX06, KLX07A–B and KLX08. Oskarshamn site investigation. SKB P-07-212, Svensk Kärnbränslehantering AB.
- Thunehed H, Triumf C-A, 2005.** Oskarshamn site investigation. Detailed ground geophysical survey at Laxemar. Magnetic total field and resistivity. SKB P-05-188, Svensk Kärnbränslehantering AB.
- Thunehed H, Triumf C-A, 2006.** Oskarshamn site investigation. Detailed ground geophysics at Laxemar, autumn/winter 2005/2006. Magnetic total field and resistivity. SKB P-06-137, Svensk Kärnbränslehantering AB.
- Thur P, Gustafsson E, 2007.** Groundwater flow measurements in KLX21B. Oskarshamn site investigation. SKB P-07-199, Svensk Kärnbränslehantering AB.
- Thur P, Nordqvist R, Gustafsson E, 2007a.** Oskarshamn site investigation. Groundwater flow measurements and SWIW test in borehole KLX11A. SKB P-07-180, Svensk Kärnbränslehantering AB.
- Thur P, Nordqvist R, Gustafsson E, 2007b.** Oskarshamn site investigation. Groundwater flow measurements and SWIW test in borehole KLX18A. SKB P-06-287, Svensk Kärnbränslehantering AB.
- Thur P, 2008.** Groundwater flow measurements in permanently installed boreholes. Test campaign no. 3 2007, Oskarshamn site investigation. SKB P-08-31, Svensk Kärnbränslehantering AB.
- Triumf C-A, 2003.** Oskarshamn site investigation. Identification of lineaments in the Simpevarp area by the interpretation of topographical data. SKB P-03-99, Svensk Kärnbränslehantering AB.
- Triumf C-A, Thunehed H, Kero L, Persson L, 2003.** Oskarshamn site investigation. Interpretation of airborne geophysical survey data. Helicopter borne survey data of gamma ray spectrometry, magnetics and EM from 2002 and fixed wing airborne survey data of the VLF-field from 1986. SKB P-03-100, Svensk Kärnbränslehantering AB.
- Triumf C-A, 2004a.** Joint interpretation of lineaments in the eastern part of the site descriptive model area. Oskarshamn site investigation. SKB P-04-37, Svensk Kärnbränslehantering AB.
- Triumf C-A, 2004b.** Oskarshamn site investigation. Joint interpretation of lineaments. SKB P-04-49, Svensk Kärnbränslehantering AB.
- Triumf C-A, 2004c.** Oskarshamn site investigation. Gravity measurements in the Laxemar model area with surroundings. SKB P-04-128, Svensk Kärnbränslehantering AB.
- Triumf C-A, 2007.** Oskarshamn site investigation. Assessment of probable and possible dolerite dykes in the Laxemar sub-area from magnetic total field data and digital elevation models. SKB P-07-223, Svensk Kärnbränslehantering AB.
- Triumf C-A, Thunehed H, 2007.** Oskarshamn site investigation. Co-ordinated lineaments longer than 100 m at Laxemar. Identification of lineaments from LIDAR data and co-ordination with lineaments in other topographical and geophysical data. SKB P-06-262, Svensk Kärnbränslehantering AB.
- Tröjbom M, Söderbäck B, 2006.** Chemical characteristics of surface systems in the Simpevarp area. Visualisation and statistical evaluation of data from surface water, shallow groundwater, precipitation and regolith. SKB R-06-18, Svensk Kärnbränslehantering AB.
- Tröjbom M, Söderbäck B, Kalinowski B, 2008.** Hydrochemistry of surface water and shallow groundwater, Site descriptive modelling, SDM-Site Laxemar. SKB R-08-46, Svensk Kärnbränslehantering AB.
- Tullborg E-L, Drake H, Sandström B, 2008.** Palaeohydrogeology: A methodology based on fracture mineral studies. Applied Geochemistry 23, 1881–1897.

- Vilks P, Cramer J, Jensen M, Miller N, Miller H, Stanchell F, 2003.** In situ diffusion experiment in granite: Phase I. *J. Contam. Hydrol.*, 61, pp. 191–202.
- Vilks P, Miller N, Jensen M, 2004.** In-situ diffusion experiment in sparsely fractured granite. In: *Scientific Basis for Nuclear Waste Management XXVII*, Hanchar J, Stroes-Gascoyne S, Browning L (eds.). *Mater. Res. Soc. Symp. Proc.* 824.
- Viola G, Venvik Ganerød G, 2007a.** Oskarshamn site investigation. Structural analysis of brittle deformation zones in the Simpevarp-Laxemar area, Oskarshamn, southeast Sweden. SKB P-07-41, Svensk Kärnbränslehantering AB.
- Viola G, Venvik Ganerød G, 2007b.** Oskarshamn site investigation. Structural characterisation of deformation zones (faults and ductile shear zones) from selected drill cores and outcrops from the Laxemar area – results from Phase 2. SKB P-07-227, Svensk Kärnbränslehantering AB.
- Viola G, 2008.** Ductile and brittle structural evolution of the Laxemar-Simpevarp area: an independent analysis based on local and regional constraints. SKB R-08-124, Svensk Kärnbränslehantering AB.
- Viola G, Venvik Ganerød G, 2008.** Oskarshamn site investigation. Structural characterisation of deformation zones (faults and ductile shear zones) from selected drill cores from the Laxemar area. SKB P-08-07, Svensk Kärnbränslehantering AB.
- Viola G, Venvik Ganerød G, Wahlgren C-H, 2009.** Unravelling 1.5 Gyr of brittle deformation history in the Laxemar-Simpevarp area, southeast Sweden: a contribution to the Swedish site investigation study for the disposal of highly radioactive nuclear waste. *Tectonics*, in press.
- Vollmer F, 1995.** C program for automatic contouring of spherical orientation data using a modified Kamb method, *Computers and Geosciences* 21, 31–49.
- Voss C I, Provost A M, 2002.** SUTRA. A model for saturated-unsaturated, variable-density groundwater flow with solute or energy transport. *Water-Resources Investigation Report 02-4231*, U.S. Geological Survey, Reston, Va.
- Waber H N, Smellie J A T, 2008.** Characterisation of porewater in crystalline rocks. *Applied Geochemistry* 23, 1834–1861.
- Waber H N, Gimmi T, Smellie J A T, deHaller A, 2009.** Porewater in the rock matrix. Site descriptive modelling. SDM-Site Laxemar. SKB R-08-112, Svensk Kärnbränslehantering AB (in prep).
- Wahlgren C-H, Bergman T, Persson Nilsson K, Eliasson T, Ahl M, Ekström M, 2005.** Oskarshamn site investigation. Bedrock map of the Laxemar subarea and surroundings. Description of rock types, modal and geochemical analyses, including the cored boreholes KLX03, KSH03 and KAV01. SKB P-05-180, Svensk Kärnbränslehantering AB.
- Wahlgren C-H, Hermanson J, Curtis P, Triumpf C-A, Drake H, Tullborg E-L, 2006a.** Geological description of rock domains and deformation zones in the Simpevarp and Laxemar subareas. Preliminary site description Laxemar subarea – version 1.2. SKB R-05-69, Svensk Kärnbränslehantering AB.
- Wahlgren C-H, Bergman T, Ahl M, Ekström M, 2006b.** Oskarshamn site investigation. Modal and geochemical analyses of drill core samples 2006 and updated bedrock map of the Laxemar subarea. Classification of rock types in KLX08, KLX10, KLX11A, KLX12A, KLX18A and KLX20A. SKB P-06-279, Svensk Kärnbränslehantering AB.
- Wahlgren C-H, Bergman T, Ahl M, Ekström M, 2006c.** Oskarshamn site investigation. Modal and geochemical analyses of drill core samples 2005. Classification of rock types in KLX03, KLX04, KLX06, KLX07A, KLX07B, KLX08 and KLX10. SKB P-06-07, Svensk Kärnbränslehantering AB.
- Wahlgren C-H, Bergman T, Ahl M, Ekström M, Page L, Söderlund U, 2007.** Oskarshamn site investigation. Modal and geochemical analyses of drill core samples 2007 and ⁴⁰Ar/³⁹Ar dating of a dolerite. Classification of rock types in KLX15A, KLX16A, KLX19A, KLX20A and KLX21B. SKB P-07-191, Svensk Kärnbränslehantering AB.
- Wahlgren C-H, Curtis P, Hermanson J, Forsberg O, Öhman J, Fox A, La Pointe P, Drake H, Triumpf C-A, Mattsson H, Thunehed H, Juhlin C, 2008.** Geology Laxemar. Site descriptive modelling. SDM-Site Laxemar. SKB-R-08-54, Svensk Kärnbränslehantering AB.

- Wang X, 2005.** Stereological Interpretation of Rock Fracture Traces on Borehole Walls and Other Cylindrical Surfaces. Virginia Polytechnic Institute and State University, doctoral dissertation.
- Walsh J B, Decker E R, 1966.** Effect of pressure and saturating fluid on the thermal conductivity of compact rock. *J. Geophys. Res.*, 71, pp. 3053–3061.
- Weibull W, 1951.** A statistical distribution function of wide applicability. *Journal of Applied Mechanics* 18, pp. 293–305.
- Werner K, Bosson E, Berglund S, 2006.** Description of climate, surface hydrology, and near-surface hydrogeology. Preliminary site description Laxemar subarea - version 1.2. SKB R-05-61, Svensk Kärnbränslehantering AB.
- Werner K, 2008.** Description of surface hydrology and near-surface hydrogeology at Laxemar-Simpevarp. Site descriptive modelling, SDM-Site Laxemar. SKB R-08-71, Svensk Kärnbränslehantering AB.
- Werner K, Öhman J, Holgersson B, Rönnback K, Marelus F, 2008.** Meteorological, hydrological and near-surface hydrogeological monitoring data and near-surface hydrogeological properties data from Laxemar-Simpevarp. Site descriptive modelling, SDM-Site Laxemar. SKB R-08-73, Svensk Kärnbränslehantering AB.
- Westman P, Wastegård S, Schoning K, Gustafsson B, 1999.** Salinity change in the Baltic Sea during the last 8 500 years: evidence causes and models. SKB TR 99-38, Svensk Kärnbränslehantering AB.
- Whicker F W, Schultz V, 1982.** Radioecology: Nuclear Energy and the Environment. CRC Press, Boca Raton, Florida.
- Widestrand H, Byegård J, Ohlsson Y, Tullborg E L, 2003.** Strategy for the use of laboratory methods in the site investigations programme for the transport properties of the rock. SKB R-03-20, Svensk Kärnbränslehantering AB.
- Widestrand H, Byegård J, Selnert E, Skålberg M, Gustafsson E, (in prep).** Äspö Hard Rock Laboratory, Long Term Sorption Diffusion Experiment (LTDE-SD), Supporting laboratory program – Sorption diffusion experiments and rock material characterisation. Äspö Hard Rock Laboratory. SKB IPR-09-08, Svensk Kärnbränslehantering AB.
- Wijnbladh E, Aquilonius K, Floderus S, 2008.** The marine ecosystems at Forsmark and Laxemar-Simpevarp. Site descriptive modelling. SDM-Site. SKB R-08-03, Svensk Kärnbränslehantering AB.
- Wikberg P, 1998.** Äspö Task Force on modelling of groundwater flow and transport of solutes. Plan for modelling Task 5 : Impact of the tunnel construction on the groundwater system at Äspö, a hydrological-hydrochemical model assessment exercise. SKB HRL-98-07, Svensk Kärnbränslehantering AB.
- Wikström M, Forsmark T, Teurneau B, Forssman I, Rhén I, 2008a.** Correlation of Posiva Flow Log anomalies to core mapped features in KLX09, KLX09B–G, KLX10, KLX10B–C and KLX11A–F. Oskarshamn site investigation. SKB P-07-213, Svensk Kärnbränslehantering AB.
- Wikström M, Forsmark T, Zetterlund M, Forssman I, Rhén I, 2008b.** Correlation of Posiva Flow Log anomalies to core mapped features in KLX12A, KLX13A, KLX14A, KLX15A and KLX16A. Oskarshamn site investigation. SKB P-07-214, Svensk Kärnbränslehantering AB.
- Wikström M, Forsmark T, Forssman I, Rhén I, 2008c.** Correlation of Posiva Flow Log anomalies to core mapped features in KLX22A–B, KLX23A–B, KLX24A, KLX25A, KLX26A–B, KLX27A, KLX28A and KLX29A. Oskarshamn site investigation. SKB P-07-216, Svensk Kärnbränslehantering AB.
- Wrafter J, Sundberg J, Ländell M, Back P, 2006.** Thermal modelling. Site descriptive modelling. Laxemar 2.1. SKB R-06-84, Svensk Kärnbränslehantering AB.



Nomenclature

This appendix contains explanations to acronyms and technical terms used by SKB which occur in this report. Definition of terms that are of basic importance for the modelling and description of the Laxemar-Simpevarp area are provided in Section 1.6.5.

1D	One-dimensional.
2D	Two-dimensional.
3D	Three-dimensional.
3DEC	3 Dimensional Distinct Element Code; numerical modelling tool used to estimate rock mass mechanical properties and <i>in situ</i> stress variability due to deformation zones.
AA	Autotrophic Acetogens – microorganisms that produce acetate from inorganic sources.
AD	Anno Domini.
ASMxxxxxx	Bedrock surface exposure, either in a trench or outcrop, upon which detailed geologic mapping has been performed.
AM	Autotrophic Methanogens – microorganisms that produce methane from inorganic sources.
AMS	Anisotropy of Magnetic Susceptibility; laboratory method to determine orientation of ductile structures in the bedrock as well as degree and character of ductile strain.
³⁹ Ar	Isotope formed as a result of induced neutron activation of ³⁹ K.
⁴⁰ Ar	Radiogen isotope formed from ⁴⁰ K.
ATP	Adenosine-Tri-Phosphate.
BAT type Filter Tip	The BAT GMS (Bengt-Arne Torstensson Ground Water Monitoring System) type Filter Tip provides, together with various BAT probes, a system for groundwater measurement/logging of pore pressures and groundwater levels, <i>in situ</i> measurement of soil permeability and for discrete sampling of groundwater and soil gas.
BC	Before Christ.
BET	Brunauer Emmet Teller; A method for determining the specific surface area, available for sorption, of a solid material by use of gas adsorption.
BIPS	Borehole Imaging Processing System; down-hole video camera system providing oriented images of the borehole wall.
BMU	Base Model, Unlinked. A set of conceptual assumptions representing an alternative model case in the geological DFN. The BMU case was found to be the best-performing alternative during DFN model verification, and was thus recommended for use as the preferred DFN conceptual assumptions for SDM Site Laxemar.
Boremap	SKB's core mapping methodology including inspection of both the drill core and the oriented images of the borehole provided by BIPS.
Candidate area	See definition in Section 1.6.5.
Candidate volume	See definition in Section 1.6.5.
¹³ C	Heavy stable carbon isotope.
CCC	Complete Chemical Characterisation; a defined set of various sampling and analyses including on-line, long-term Chemmac measurements of Eh, pH, electrical conductivity, dissolved oxygen and water temperature.
CCN	Complementary Cumulative Number plot: A type of plot in which the number of data values greater than or equal to a specific value are plotted as a function of the value.
CDF	Cumulative Density Function. A function that quantifies the cumulative probability of a distribution. It is the probability that the value of a randomly selected value is less than a specified value.
CDP	Common Data Point lines along which reflection seismic data have been projected for stacking and interpretation.
CDT	Canyon Diablo Troilite; standard used for sulphur isotope data ($\delta^{34}\text{S}$).
CEC	Cation Exchange Capacity; a measure of sites in a material that are available for ion exchange.
CFF	Conductive Fracture Frequency.
Chemmac	A measurement system that allows on-line, long-term measurements of chemical and physical parameters in the unbroken sample water line both at the ground surface and at depth down-hole. Eh, pH and water temperature are measured and logged simultaneously by electrodes and sensors downhole as well as at the surface. Dissolved oxygen and electrical conductivity are measured at the surface.
³⁶ Cl	Radioactive isotope of chlorine (half-life = 301,000 years).
ConnectFlow	Numerical modelling tool for simulation of groundwater flow.
CPM	Continuous Porous Medium.

CSI	Complete Site Investigation stage.
D_e	Effective diffusivity of the rock matrix
DEM	Digital Elevation Model.
DFF	Distant Far Field; a coined term used in the transport modelling report to represent transport paths within the hydraulic conductor domain from approximately repository elevation to the near surface which may or may not include subsequent transport paths in the surface system and biosphere.
DFN	Discrete Fracture Network. A statistical model of the geometry of fractures in a rock volume.
DIC	Dissolved Inorganic Carbon.
DOC	Dissolved Organic Carbon.
DP	Dissolved Phosphorus.
DZ	Deformation zone.
EC	Electrical Conductivity.
ECPM	Equivalent Continuous Porous Medium.
EDL	Electrical double layer; a term used to describe the variation of electric potential near a mineral surface in an aqueous solution. The charge is counteracted by ionic charges of opposite sign attracted to the surface of the mineral giving rise to a diffuse layer of ions which differs in composition to that of the bulk solution.
EDS	Energy-Dispersive Spectroscopy.
EDX	Energy-Dispersive X-ray analysis; method used together with LIBD to analyse the composition of colloids.
Eh	Redox potential (usually expressed in mV).
EIA	Environmental Impact Assessment.
EM	Electromagnetic data.
ESHI	Extended single-hole interpretation. A re-assessment and updating of the original single-hole interpretation (SHI), see below).
F_r	Formation factor defined as the ratio of effective diffusivity (D_e) to the free diffusivity of a solute at infinite dilution in water (D_w).
F-factor	Hydrodynamic transport resistance expressed as the flow-wetted surface to flow ratio.
Focused area	See definition in Section 1.6.5.
Focused volume	See definition in Section 1.6.5.
FSM	Identification code prefix for a deterministically modelled fracture domain at Laxemar-Simpevarp; for definition of fracture domain, see Section 1.6.5.
FWS	Flow Wetted Surface; the surface area of a fracture in contact with flowing groundwater.
GIS	Geographic Information System.
GMWL	Global Meteoric Water Line.
GSLIB	Geostatistical Software Library: a package of software tools used for geostatistical analysis and stochastic simulation of thermal conductivity.
^3H	Tritium (Radioactive hydrogen isotope, half-life = 12.43 years).
HA	Heterotrophic acetogens – microorganisms that produce acetate from organic sources.
HAV	Percussion-drilled borehole at Ävrö island (part of Simpevarp subarea).
HCD	Hydraulic Conductor Domain; at Laxemar-Simpevarp equivalent to deterministic deformation zone.
^4He	Helium-4 (Heavy isotope of helium).
HF	Hydraulic Fracturing; method for measurement of <i>in situ</i> rock stresses.
HLX	Percussion-drilled borehole at Laxemar.
HM	Heterotrophic Methanogens – microorganisms that produce methane from organic sources.
HRD	Hydraulic Rock Domain; at Laxemar equivalent to fracture domain or amalgamation of two or more fracture domains.
HREE	Heavy Rare Earth Elements.
HRL	Hard Rock Laboratory.
HSH	Percussion-drilled borehole at the Simpevarp peninsula (part of Simpevarp subarea).
HTHB	Equipment used for hydraulic characterisation in boreholes by open hole pumping test. Swe: <i>Hydrotestutrustning för hammarborrhål</i> .
HTPF	Hydraulic Tests on Pre-existing Fractures; method for measurement of <i>in situ</i> rock stresses.
SH fracture set	Subhorizontal fracture set.
IFF	Immediate far field; a coined term used in the transport modelling report to represent transport paths directly outside the disturbed zone of the rock surrounding a hypothetical repository within the hydraulic rock domain and extending to the onset of the hydraulic conductor domain.
Insite	INdependent Site Investigation Tracking & Evaluation; SKI's international advisory group on site investigation issues.
IRB	Iron-reducing bacteria.

ISI	Initial Site Investigation stage.
ISIS	Software used in stochastic geological DFN modelling.
Isometric view	A form of graphical projection, more specifically, a form of axonometric projection. It is a method of visually representing three-dimensional objects in two dimensions, in which the three coordinate axes appear equally foreshortened and the angles between any two of them are 120°.
Karstic erosion feature	A pipe-like flow channel of narrow extent (cm to dm width) speculated to form within the plane of calcite annealed fractures. Although their existence has not been conclusively demonstrated nor disproved at the Laxemar site, such flow channels could potentially form fast and persistent flowpaths in the rock due to reactive transport feedback effects that enhance the transmissivity of the channel. Since these are thought to be hosted in otherwise partially annealed fractures, they are not likely to be identified from borehole investigations owing to the low probability of direct intersection with an investigation borehole.
K_d	Sorption partitioning coefficient; defined operationally as the ratio of sorbed and dissolved solute. Although generally taken to be representative of linear equilibrium sorption, it is an empirical quantity that is not strictly dependent upon any specific mechanistic reasoning or reactive process and is therefore of a conditional nature.
KLX	Core-drilled borehole at Laxemar.
KSH	Core-drilled borehole on the Simpevarp peninsula (part of Simpevarp subarea).
K-T extinction	Cretaceous-Tertiary extinction event; a large-scale mass extinction of animal (the conclusion of the age of the dinosaurs and the rise of modern mammals) and plant species in a geologically short period of time, approximately 65.5 million years ago, which marked the end of the Mesozoic era and beginning of the Cenozoic era.
LSM	Line along the ground surface along which data have been acquired in the Laxemar-Simpevarp area, for example seismic refraction profiles.
LIBD	Laser-induced breakdown colloid detection; method used together with EDX to analyse the composition of colloids.
LIDAR	Light Detection and Ranging. An optical remote sensing technology that measures properties of scattered light to find range and/or other information about a feature. Unless otherwise stated, in SKB SDM reporting, LIDAR is synonymous with ALSM (Airborne Laser Swath Mapping), which is a technique for creating high-resolution elevation models of the ground surface from dense clouds of laser range data collected by helicopters or fixed-wing aircraft.
LPJ-GUESS	Dynamic vegetation model.
LREE	Heavy Rare Earth Elements.
M3	Multivariate mixing and mass balance calculation programme.
m.a.s.l.	Metres above sea level, cf. Section 2.5.
MD	Measured depth; the length between the start of the borehole and a subsurface feature, as measured along the drill path.
MDZ	Minor Deformation Zone; deformation zone with a trace length at the ground surface shorter than 1,000 m. Modelled stochastically as part of DFN model.
MIKE SHE	Numerical modelling tool for surface hydrogeological modelling.
MPN	Most Probable Number of cells method; statistical cultivation method for counting the most probable number of cells of different cultivable metabolic groups of microorganisms.
MRB	Manganese-Reducing Bacteria.
NEP	Net Ecosystem Production; the difference between gross primary production and total ecosystem respiration.
NNF	Non-engineered near field; a coined term used in the transport modelling report to represent transport paths outside of the engineered repository although within the disturbed zone of the repository and including the first few metres of conductive flowpaths initially encountered by radionuclides transported from a capsule position.
NPP	Net Primary Production; the production of organic material in ecosystems.
NRB	Nitrate-Reducing Bacteria.
^{18}O	Heavy stable isotope of oxygen.
OC	Overcoring; method for measurement of rock stresses.
Oversite	The SSI international expert group.
P_{10}	Linear fracture intensity (1D) expressed as fracture intercept per unit length (m^{-1}). Generally calculated from the number of fractures intersecting a borehole or scanline.
$P_{10\text{corr}}$	Terzaghi corrected linear fracture intensity (m^{-1}).
$P_{10,\text{PFL},\text{corr}}$	Terzaghi corrected linear intensity of flowing fractures (m^{-1}).
$P_{10,\text{o},\text{corr}}$	Terzaghi corrected linear intensity of open fractures (m^{-1}).
P_{21}	Areal fracture intensity (2D) expressed as fracture trace length per unit area (m/m^2). Generally calculated by summing the lengths of all fracture traces observed in a specific area.
P_{32}	Volumetric fracture intensity (3D) expressed as fracture area per unit volume (m^2/m^3).
PCA	Principal Component Analysis; statistical method for analysing groundwater compositions.
pCO_2	Partial pressure of carbon dioxide.

PDB	Standard according to Pee Dee Belemnite Formation (used for 13C as well as for 18O, especially for carbonates).
PFL	Posiva Flow Log; equipment used for hydraulic characterisation in boreholes by difference flow logging pumping tests.
PFL fracture	Flowing fracture detected by PFL-f.
PFL-f	Difference flow logging pumping tests.
PSM	Point at the ground surface where data have been acquired, for example observation points during bedrock mapping.
PHREEQC	Numerical modelling tool for chemical speciation, batch-reaction, one-dimensional transport, and inverse geochemical calculations.
pmC	Percent modern Carbon.
POC	Particulate Organic Carbon.
POP	Particulate Organic Phosphorus.
PMMA	Poly-methylmethacrylate; a resin used in a method for determining heterogeneous porosity distributions in rock samples.
P-report	SKB report series for results of the site investigations at Forsmark and Laxemar-Simpevarp.
PSE	Preliminary Safety Evaluation.
PSS	Pipe String System; equipment used for hydraulic characterisation in boreholes by double-packer injection tests.
Q	An empirical system of rock mass classification used in tunnel design and engineering. The Q-factor for a given rock type is calculated as a function of RQD, joint roughness, number of joint sets, joint alteration, ground water conditions and a stress reduction factor (SRF).
QA	Quality Assurance.
RAMAC	Borehole radar measurement system with dipole and directional antennae that provides information on the character of the rock mass around the borehole.
REEs	Rare Earth Elements.
REX	Åspö large-scale redox experiments.
RSM	Identification code prefix for a deterministically modelled rock domain at Laxemar-Simpevarp; for definition of rock domain, see Section 1.6.5.
RHB 70	Coordinate system used for elevation; see Section 2.5.
RMR	Rock Mass Rating; an empirical system for classifying rocks based on material properties (uniaxial compressive strength), RQD value, joint spacing and orientation, joint surface properties, and the groundwater conditions.
RT 90	Coordinate system used for X and Y-directions; see Section 2.5.
RU	Rock Unit; see definition in Section 1.6.5.
RVS	Rock Visualisation System; SKB's tool for modelling and visualisation of the 3D geometry of geological entities.
RQD	Rock Quality Designation, a parameter to quantify the fracturing of drill cores.
³⁴ S	Stable isotope of sulphur.
SCA	Self Consistent Approximation; method for calculation of thermal conductivity using mineral composition and reference values of thermal conductivity of different minerals.
SDM	Site Descriptive Model.
SEM	Scanning Electron Microscope.
SFR	Repository for low- and intermediate level radioactive waste at Forsmark.
SHI	Single-hole interpretation; an integrated interpretation of geological and geophysical data from a borehole that gives rise to an essentially 1D model for rock units and possible deformation zones along the borehole.
Sicada	Site characterisation database: SKB's database for primary site investigation data.
Sierg	Site Investigation Expert Review Group; SKB's international expert group.
Simon	SKB's database for site descriptive models.
SKB	Swedish Nuclear Fuel and Waste Management Company.
SKBdoc	SKB's internal documentation database.
SKI	Swedish Nuclear Power Inspectorate.
SOC	Soil organic carbon.
SP	Self Potential.
⁸⁷ Sr	Radiogenic strontium isotope, produced by decay of ⁸⁷ Rb.
⁸⁶ Sr	Stable isotope of strontium.
SRB	Sulphate-Reducing Bacteria.
SSI	Swedish Radiation Protection Authority.
SSM	Soil borehole in Laxemar-Simpevarp.
SWIW	Single Well Injection and Withdrawal; method for single-hole tracer test.

TCM	Tectonic Continuum Model; alternative DFN size model based on the assumption that fractures with traces on the scale of metres are part of the same fracture population as lineaments or deformation zones with traces on the scale of kilometres.
TDS	Total Dissolved Solids.
TIC	Total Inorganic Carbon.
TNC	Total Number of Cells.
TOC	Total Organic Carbon.
ToC	Top of Casing (shown in WellCAD plots).
T-PROGS	Transition Probability Geostatistic Software: provides a transition probability-based geostatistical approach to stochastic simulation of spatial distributions of categorical variables.
TPS	Transient Plane Source; laboratory method for measurement of thermal conductivity and thermal diffusivity of rock samples.
TRC	Thermal Rock Class; Group of rock types with similar thermal and lithological properties.
TU	Tritium Units.
θ_m	Rock matrix porosity; for the puposes of transport modeling in the site investigation this is determined by a gravimetric water resaturation technique (SS-EN 1936) involving equilibration of a core sample in water followed by a drying step at 70°C.
UCS	Uniaxial Compressive Strength.
USD	Uranium-Series Decay analyses.
VLF	Very Low Frequency; electromagnetic geophysical method that makes use of radio transmissions at very low frequencies as plane-wave sources.
VSMOW	Vienna Standard Mean Ocean Water, refers to the "ocean standard" available at IAEA in Vienna. (IAEA, 1995. Reference document, TEC DOC-825, 165 p.).
VSP	Vertical Seismic Profiling.
WellCad	Software for integrated display of SICADA borehole data from in diagrams.
ZSM	Identification code prefix for a deterministically modelled deformation zone at Laxemar-Simpevarp; for definition of deformation zone, see Section 1.6.5.

Appendix 3

Table A3-1. Available bedrock geological and geophysical data and their handling in the SDM-Site Laxemar geological modelling.

Available data Data specification	Ref	Usage in SDM-Site Analysis/Modelling
Data from core-drilled boreholes		
Technical data in connection with drilling (KSH01A, KSH01B, KSH02, KSH03A, KSH03B, KAV01, KAV04A, KAV04B, KLX03, KLX04, KLX05, KLX06, KLX07A, KLX07B, KLX08, KLX09, KLX09B-F, KLX09G, KLX10, KLX10B, KLX10C, KLX11A, KLX11B-F, KLX12A, KLX13A, KLX14A, KLX15A, KLX16A, KLX17A, KLX18A, KLX19A, KLX20A, KLX21B, KLX22A, KLX22B, KLX23A, KLX23B, KLX24A, KLX25A, KLX26A, KLX26B, KLX27A, KLX28A, KLX29A)	P-03-113 P-04-151 P-04-233 P-05-25 P-05-167 P-05-111 P-05-233 P-05-234 P-06-14 P-06-222 P-06-265 P-06-297 P-06-116 P-06-306 P-06-283 P-06-305 P-07-195 P-08-21 P-07-221 P-07-98 P-07-202 P-07-134 P-08-24	Siting and orientation of boreholes in modelling work.
Radar and BIPS-logging, and interpretation of radar logs (KSH01A, KSH01B, KSH02, KSH03A, KSH03B, KAV01, KAV04A, KAV04B, KLX03, KLX04, KLX05, KLX06, KLX07A, KLX07B, KLX08, KLX09, KLX09B-F, KLX09G, KLX10, KLX10B, KLX10C, KLX11A, KLX11B-F, KLX12A, KLX13A, KLX14A, KLX15A, KLX16A, KLX17A, KLX18A, KLX19A, KLX20A, KLX21B, KLX22A, KLX22B, KLX23A, KLX23B, KLX24, KLX25, KLX26A, KLX26B, KLX27A, KLX28A, KLX29A)	P-03-109 P-03-120 P-03-73 P-04-195 P-04-218 P-04-239 P-04-275 P-04-48 P-04-66 P-05-231 P-05-240 P-05-30 P-05-82 P-05-161 P-06-156 P-06-159 P-06-167 P-06-260 P-06-48 P-06-50 P-06-99 P-07-117 P-07-12 P-07-13 P-07-57 P-07-58 P-08-30	Data used in borehole mapping (BIPS) and in single-hole interpretation (radar logging) with focus on the identification of brittle deformation zones. Input for both rock domain and DZ modelling.
Geophysical logging (KAV01, KAV01, KAV04A, KAV04B, KLX03, KLX04, KLX05, KLX06, KLX07A, KLX07B, KLX08, KLX09, KLX09B, KLX09D, KLX09F, KLX09G, KLX10, KLX10B, KLX10C, KLX11A, KLX11B, KLX12A, KLX13A, KLX14A, KLX15A, KLX16A, KLX18A, KLX19, KLX20, KLX21B, KLX22A, KLX22B, KLX23A, KLX23B, KLX24, KLX25, KLX26A, KLX26B, KLX27A, KLX28, KLX29A, KSH01A, KSH01B, KSH02, KSH03A, KSH03B)	P-03-16 P-03-111 P-04-232 P-04-50 P-04-202 P-04-306 P-04-280 P-05-31 P-05-144 P-05-228 P-05-270 P-06-20 P-06-154 P-06-197 P-06-198	Data used in borehole mapping and in single-hole interpretation. Input for both rock domain and DZ modelling.

Available data Data specification	Ref	Usage in SDM-Site Analysis/Modelling
	P-06-290 P-06-307 P-06-314 P-06-315 P-07-15 P-07-56 P-07-152 P-08-03	
Interpretation of geophysical logs (KAV01, KAV04A, KAV04B, KLX01, KLX02, KLX03, KLX04, KLX05, KLX06, KLX07A, KLX07B, KLX08, KLX09A, KLX09B, KLX09D, KLX09F, KLX09G, KLX10, KLX10B, KLX10C, KLX11A, KLX11B, KLX12A, KLX13A, KLX14A, KLX15A, KLX16A, KLX17A, KLX18A, KLX19A, KLX20A, KLX21B, KLX22A, KLX22B, KLX23A, KLX23B, KLX24A, KLX25A, KLX26A, KLX26B, KLX27A, KLX28A, KLX29A, KSH01A, KSH01B, KSH02, KSH03A, KSH03B)	P-04-214 P-04-217 P-04-27 P-04-28 P-04-77 P-05-34 P-05-189 P-05-259 P-05-44 P-06-124 P-06-157 P-06-162 P-06-253 P-06-264 P-06-292 P-06-317 P-06-65 P-07-114 P-07-21 P-07-25 P-07-75 P-07-97 P-08-04	Used in single-hole interpretation. Input for both rock domain and DZ modelling.
Boremap mapping (KAV01, KAV04, KLX02, KLX03, KLX04, KLX05, KLX06, KLX07A, KLX07B, KLX08, KLX09, KLX09B, KLX09C, KLX09D, KLX09E, KLX09F, KLX09G, KLX10, KLX10B, KLX10C, KLX11A, KLX11B, KLX11C, KLX11D, KLX11E, KLX11F, KLX12A, KLX13A, KLX14A, KLX15A, KLX16A, KLX17A, KLX18A, KLX19A, KLX20A, KLX21B, KLX22A, KLX22B, KLX23A, KLX23B, KLX24A, KLX25A, KLX26A, KLX26B, KLX27A, KLX28A, KLX29A, KSH01A, KSH01B, KSH02, KSH03A, KSH03B)	P-04-01 P-04-02 P-04-129 P-04-130 P-04-131 P-04-132 P-05-185 P-05-22 P-05-224 P-05-23 P-05-24 P-05-263 P-06-236 P-06-237 P-06-238 P-06-240 P-06-241 P-06-242 P-06-243 P-06-244 P-06-255 P-06-256 P-06-257 P-06-42 P-06-51 P-06-82 P-07-71 P-07-157 P-07-158 P-07-159 P-07-210 P-07-211 P-07-218 P-08-39	Rock type, ductile deformation in the bedrock, fracture statistics. Data used in identification of rock units and brittle deformation zones in single-hole interpretation. Input for rock domain, DZ and DFN modelling.
Mineralogical and geochemical analyses of rock types and fracture fillings (KLX03, KLX04, KLX06, KLX07A, KLX07B, KLX08, KLX09, KLX10, KLX11A, KLX12A, KLX13A, KLX15A, KLX16A, KLX18A, KLX19A, KLX20A, KLX21B, KLX26A, KLX26A, KSH01, KSH02, KSH03, KAV01)	P-04-102 P-04-250 P-05-174 P-05-180 P-06-01 P-06-02 P-06-03	Mineralogical and geochemical properties of rock types and fracture fillings. Input for rock domain, DZ and DFN modelling.

Available data Data specification	Ref	Usage in SDM-Site Analysis/Modelling
	P-06-04 P-06-07 P-06-279 P-07-03 P-07-74 P-07-191 P-08-11 P-08-12 P-08-41 P-08-42 P-08-44	
Characterisation of brittle deformation zones (KSH03A, KLX03, KLX04, KLX06, KLX07A, KLX07B, KLX08, KLX09, KLX10, KLX11A, KLX12A, KLX13A, KLX15A, KLX16A, KLX17A, KLX18A, KLX19A, KLX20A, KLX21B)	P-07-41 P-07-227 P-08-07 R-08-124	Input for DZ modelling and geological evolution.
Single-hole interpretation (KAV01, KAV04A, KAV04B, KLX01, KLX02, KLX03, KLX04, KLX05, KLX06, KLX07A, KLX07B, KLX08, KLX09, KLX09B, KLX09C, KLX09D, KLX09E, KLX09F, KLX09G, KLX10, KLX10B, KLX10C, KLX11A, KLX11B, KLX11C, KLX11D, KLX11E, KLX11F, KLX12A, KLX13A, KLX14A, KLX15A, KLX16A, KLX17A, KLX18A, KLX19A, KLX20A, KLX21B, KLX22A, KLX22B, KLX23A, KLX23B, KLX24A, KLX25A, KLX26A, KLX26B, KLX27A, KLX28A, KLX29A, KSH01A, KSH01B, KSH02, KSH03A, KSH03B)	P-04-133 P-04-231 P-04-308 P-04-309 P-04-32 P-05-38 P-06-128 P-06-129 P-06-174 P-06-175 P-06-176 P-07-153 P-07-155 P-07-156 P-07-161 P-07-208 P-07-209 P-07-66 P-07-67 P-07-68 P-07-69 P-07-70 P-08-05 P-08-06 P-08-48	Interpretation used in rock domain, DZ and DFN modelling.
Calculation of Fracture zone index (KSH01)	P-03-93	Input for DZ modelling.
Radar and BIPS-logging, and interpretation of radar logs (HSH01, HSH02, HSH03, HAV09, HAV10, HAV11, HAV12, HAV13, HLX10, HLX13, HLX15, HLX17, HLX18, HLX19, HLX20, HLX21, HLX22, HLX23, HLX24, HLX25, HLX26, HLX27, HLX28, HLX30, HLX31, HLX32, HLX33, HLX34, HLX35, HLX36, HLX37, HLX38, HLX39, HLX40, HLX41, HLX42, HLX43)	P-03-15 P-04-195 P-04-275 P-04-279 P-04-297 P-04-48 P-05-231 P-05-240 P-06-159 P-06-260 P-07-12 P-07-58	Data used in borehole mapping (BIPS) and in single-hole interpretation (radar logging) with focus of identification of brittle deformation zones. Input for both rock domain and DZ modelling.
Geophysical logging (HAV09, HAV10, HLX13, HLX15, HLX17, HLX18, HLX19, HLX20, HLX21, HLX22, HLX23, HLX24, HLX25, HLX26, HLX27, HLX28, HLX30, HLX31, HLX32, HLX33, HLX34, HLX35, HLX36, HLX37, HLX38, HLX39, HLX40, HLX41, HLX43, HSH01, HSH02, HSH03)	P-03-15 P-04-202 P-04-240 P-04-280 P-04-306 P-04-50 P-05-228 P-05-270 P-06-197 P-06-290 P-06-315	Data used in borehole mapping and in single-hole interpretation. Input for both rock domain and DZ modelling.

Available data Data specification	Ref	Usage in SDM-Site Analysis/Modelling
Interpretation of geophysical logs (HSH01, HSH02, HSH03, HAV09, HAV10, HLX13, HLX15, HLX17, HLX18, HLX19, HLX20, HLX21, HLX22, HLX23, HLX24, HLX25, HLX26, HLX27, HLX28, HLX30, HLX31, HLX32, HLX33, HLX34, HLX35, HLX36, HLX37, HLX38, HLX39, HLX40, HLX41, HLX43, Percussion drilled part of KSH01A)	P-04-28 P-04-214 P-04-217 P-04-27 P-04-284 P-05-34 P-05-259 P-06-264 P-06-292 P-06-65 P-07-25	Used in single-hole interpretation. Input for both rock domain and DZ modelling.
Boremap mapping (HLX13, HLX15, HLX17, HLX18, HLX19, HLX20, HLX21, HLX22, HLX23, HLX24, HLX25, HLX26, HLX27, HLX27, HLX28, HLX30, HLX31, HLX32, HLX33, HLX34, HLX35, HLX36, HLX37, HLX38, HLX39, HLX40, HLX41, HLX42, HLX43, HSH01, HSH02, HSH03, HAV09, HAV10, HAV11, HAV12, HAV13)	P-04-02 P-05-104 P-05-163 P-05-83 P-05-164 P-05-279 P-05-162	Data mainly used for identification of rock units and DZ in single-hole interpretation. Input for rock domain and DZ modelling. Problem with recognition of rock types and mineral coatings along fractures. Also underestimation of the amount of fractures inferred solely on the basis of BIPS images.
Single-hole interpretation (HAV09, HAV10, HLX13, HLX15, HLX17, HLX18, HLX19, HLX20, HLX21, HLX22, HLX23, HLX24, HLX25, HLX26, HLX27, HLX28, HLX30, HLX31, HLX32, HLX33, HLX34, HLX35, HLX36, HLX37, HLX38, HLX39, HLX40, HLX41, HLX42, HLX43, HSH01, HSH02, HSH03)	P-04-231 P-04-309 P-04-32 P-06-128 P-06-129 P-06-174 P-06-175 P-07-153 P-07-155 P-07-156 P-07-161 P-07-209 P-07-67 P-08-05 P-08-06	Interpretation used in rock domain and DZ modelling.
Calculation of Fracture zone index (HSH01)	P-04-26	
Bedrock mapping – outcrop data	P-03-06 P-04-102 P-04-221 P-05-47 P-06-121	Rock type, rock type distribution, ductile deformation in the bedrock, fracture statistics, and identification of deformation zones at surface. Input for rock domain, DZ and DFN modelling.
Bedrock geological map	P-04-102 P-05-180 P-06-279	Input for rock domain modelling.
Mineralogical and geochemical analyses of rock types	P-04-102 P-05-47 P-05-180	Mineralogical and geochemical properties of rock types. Input for rock domain modelling.
Petrophysical and <i>in situ</i> gamma-ray spectrometric data of rock types	P-03-97 P-04-294 P-06-100 IPR-06-32	Input for rock domain modelling.
U-Pb, ⁴⁰ Ar/ ³⁹ Ar, (U-Th)/He geochronological data of bedrock and fracture minerals (including samples from drill cores)	P-04-102 P-07-27 P-07-160 P-07-191 R-01-60 PR 25-95-04	Input for conceptual understanding of the geological modelling work.
Characterisation of deformation zones	P-05-181 P-06-118 P-06-282 P-07-41 P-07-227	Focused lineament investigations, MDZ studies and outcrop structural investigations. Input for DZ modelling.

Available data Data specification	Ref	Usage in SDM-Site Analysis/Modelling
Detailed bedrock mapping	P-04-102 P-04-274 P-04-35 P-05-260 P-06-06 P-07-29 P-04-244	Fracture statistics (orientation, length) and identification of brittle and ductile features at surface. Input for rock domain, DZ and DFN modelling.
Digital orthorectified aerial photographs and digital terrain model	P-02-02	Input for lineament identification and subsequent DZ modelling.
Methodology for construction of digital terrain models	P-04-03	
Aerial orthophotos and laser scanning (LIDAR)	P-05-223	Detailed elevation model and orthophotos. Input for lineament identification and subsequent DZ modelling.
Marine geological survey	P-05-35	Input for lineament interpretation and subsequent DZ modelling.
Helicopterborne geophysical data (magnetic, VLF, EM and gamma-ray spectrometry)	P-03-25	Base data for identification of lineaments and subsequent DZ modelling.
Electric soundings	P-06-21 P-07-88	
High-resolution seismic reflection data	P-03-71 P-03-72 P-04-52 P-04-204 P-04-215 R-01-07 TR-02-04	Identification of seismic reflectors in the bedrock that may correspond to deformation zones or boundaries between different types of bedrock. Input for DZ modelling.
Seismic refraction data	P-04-134 P-04-201 P-04-298 P-05-155 P-05-179 P-06-49 P-07-131	Identification of low velocity anomalies in the bedrock that may correspond to deformation zones. Input for DZ modelling.
Ground geophysical data (magnetic and EM data)	P-03-06 P-03-66 P-04-211 P-05-188 P-06-137 P-07-168	Input for DZ modelling. Assessment of possible dolerite dykes.
Gravity data (profiles)	P-04-128	Geophysical modelling. Input for rock domain modelling.
Interpretation of topographic, bathymetric and helicopterborne geophysical data including alternative lineament interpretation	P-03-99 P-04-37 P-04-49 P-05-188 P-05-247 R-06-53 P-07-223	Identification of lineaments. Input for DZ modeling. Assessment of dolerite dykes – input to rock domain modelling.
Previous models		
RVS-modelling Ävrö	R-01-06	DZ modelling.
Laxemar	TR-02-19	Methodology test.
Simpevarp site descriptive model versions 0, 1.1, 1.2	R-02-35 R-04-25 R-05-08	Comparison and updating of models.
Laxemar site descriptive model versions 1.2, 2.1	R-06-10 R-06-110 R-05-45 R-05-69	Comparison and updating of models.
Äspö Hard rock Laboratory	IPR-03-34	DZ modelling.

Table A3-2. Available bedrock rock thermal data and their handling in the SDM-Site Laxemar thermal modelling.

Available data Data specification	Ref	Usage in SDM-Site Analysis/Modelling
Data from core-drilled boreholes		
Fluid temperature and density logging		
	<i>Results</i>	<i>Interpretation</i>
KLX02	P-03-111	P-04-214
KLX03	P-04-280	P-05-34
KLX04	P-04-306	P-05-34
KLX05	P-05-144	P-05-189
KLX07A	P-05-228	P-05-259
KLX08	P-05-270	P-06-65
KLX10	P-06-20	P-06-162
KLX11A	P-06-197	P-06-157
KLX12A	P-06-198	P-06-253
KLX13A	P-06-307	P-06-317
KLX15A	P-07-152	P-07-114
KLX16A	P-07-56	P-07-97
KLX17A	P-06-315	P-07-25
KLX18A	P-06-290	P-06-292
KLX19A	P-06-314	P-07-21
KLX20A	P-06-290	P-06-292
KLX21B	P-07-15	P-07-75
Temperature data from Posiva flow-logging		
KLX05	P-05-160	Description of natural temperature variations with depth. For comparison with fluid temperature loggings.
KLX08	P-05-267	
KLX18A	P-06-184	
Boremap mapping		
KLX02	P-04-231	Major and subordinate rock type distribution. Data used as input to stochastic simulation of lithologies. Data also used for rock type identification of drill core samples used for thermal and density measurements.
KLX03	P-04-275	
KLX04	P-04-239	
KLX05	P-05-185	
KLX07A	P-05-263	
KLX08	P-06-42	
KLX10	P-06-51	
KLX11A	P-06-237	
KLX12A	P-06-242	
KLX13A	P-06-255	
KLX15A	P-07-157	
KLX16A	P-07-211	
KLX17A	P-07-158	
KLX18A	P-06-238	
KLX19A	P-07-210	
KLX20A	P-06-241	
KLX21B	P-07-218	
Laboratory measurements of density		
KAV01	P-04-58	Data used for investigation of relationship between density and thermal conductivity. For Ävrö granite samples, density is used to differentiate Ävrö quartz monzodiorite from Ävrö granodiorite.
KAV04A	P-04-271	
KSH01A	P-04-56	
KSH02	P-04-57	
KA2599G01	R-02-27	
KLX02	P-04-259	
KLX03	P-05-94, P-07-61	
KLX04	P-04-268	
KLX05	P-05-127, P-07-61	
KLX06	P-05-130	
KLX07A	P-05-207, P-07-61	
KLX08	P-06-30	
KLX10	P-06-35, P-07-61	
KLX11A	P-06-268, P-07-61	
KLX12A	P-06-71	
KLX13A	P-06-274	
KLX16A	P-07-141	

Available data Data specification	Ref	Usage in SDM-Site Analysis/Modelling	
Laboratory measurements of thermal properties			
KAV01	P-04-55	Estimation of thermal conductivity, thermal diffusivity and specific heat capacity.	
KAV04A	P-04-270		
KSH01A	P-04-53		
KSH02	P-04-54		
KA2599G01	R-02-27		
KLX02	P-04-258		
KLX03	P-05-93, P-07-62		
KLX04	P-04-267		
KLX05	P-05-126, P-07-62		
KLX06	P-05-129		
KLX07A	P-05-208, P-07-62		
KLX08	P-06-31		
KLX10	P-06-36, P-07-62		
KLX11A	P-06-269, P-07-62		
KLX12A	P-06-72		
KLX13A	P-06-275		
KLX16A	P-07-144		
Modal analyses			
KAV01	P-04-55	Estimation of thermal conductivity from mineralogical composition of the bedrock. Impact of alteration on mineralogy and thermal conductivity.	
KAV04A	P-04-270		
KSH01A	P-04-53		
KSH02	P-04-54		
KLX01	Sicada database		
KLX02	P-04-258		
KLX03	Sicada database, field note 676		
KLX04	P-04-267		
KLX03, KLX04, KLX06, KLX07A, KLX08, KLX10	P-06-07		
KLX08, KLX10, KLX11A, KLX12A, KLX18A, KLX20A	P-06-279		
KLX05, KLX07A, KLX10, KLX11A KLX12A	P-07-62		
KLX15A, KLX16A, KLX19A	P-07-191		
Laboratory tests of thermal expansion			
KAV01	P-04-61	Estimation of the thermal expansion coefficient.	
KAV04A	P-04-272		
KSH01A	P-04-59		
KSH02	P-04-60		
KLX02	P-04-260		
KLX03	P-05-95		
KLX04	P-04-269		
KLX05, KLX07A, KLX10, KLX12A	P-07-63		
Surface data			
Laboratory tests of thermal properties – surface samples	P-05-169		Estimation of thermal conductivity, thermal diffusivity and specific heat capacity.
Modal analyses – surface samples	P-04-102, P-05-180		
Small-scale field measurements of thermal properties	P-07-77		
Models			
Geological model	R-08-54	Rock domain model, definition of deformation zones, description of alteration, foliation, and orientation of subordinate rock bodies, which are used as input for thermal modelling.	

Table A3-3. Available mechanical and stress data and their handling in the SDM-Site Laxemar rock mechanics modelling.

Available data Data specification	Ref	Usage in SDM-Site Analysis/Modelling
Laboratory tests on intact rock		
Uniaxial compressive strength (UCS) tests	P-04-207 P-04-209 P-04-255 P-04-261 P-05-90 P-06-32 P-06-37 P-06-73 P-06-270 P-06-300 P-07-143 P-07-217	Characterisation of the intact rock; Empirical determination of the rock mass mechanical properties by means of Q and RMR; Theoretical determination of the rock mass mechanical properties by means of numerical modelling.
Triaxial compressive strength tests	P-04-208 P-04-210 P-04-262 P-05-96 P-05-128 P-06-40 P-06-76 P-06-272	Characterisation of the intact rock; Empirical determination of the rock mass mechanical properties by means of Q and RMR; Theoretical determination of the rock mass mechanical properties by means of numerical modelling.
Triaxial compressive test and microcrack volume measurement	P-07-140	
Indirect tensile strength tests	P-04-62 P-04-63 P-04-256 P-04-263 P-05-91 P-06-38 P-06-74 P-06-271 P-06-276 P-06-299 P-07-142	Characterisation of the intact rock; Theoretical determination of the rock mass mechanical properties by means of numerical modelling.
Laboratory tests on fractures		
Tilt tests on fractures	P-03-107 P-04-10 P-04-42 P-04-44 P-04-265 P-05-02 P-06-34	Characterisation of the fracture properties and of the rock mass by Q and RMR.
Shear tests on open fractures, method I	P-05-05 P-05-06 P-05-07	Characterisation of the fractures – strength and stiffness; Theoretical determination of the rock mass mechanical properties by means of numerical modelling.
Shear tests on open fractures, method II	P-04-257 P-04-264 P-05-92	
Shear tests on open fractures, method III	P-05-146 P-06-39 P-06-75	
Shear tests on sealed fractures, method III	P-05-209 P-06-277	

Available data Data specification	Ref	Usage in SDM-Site Analysis/Modelling
Direct stress measurements		
Overcoring (OC)	P-04-23 P-04-84 P-05-69 P-07-123 R-02-26 IPR-01-67 IPR-02-18 IPR-03-16	Estimation of the <i>in situ</i> stress field.
Hydraulic fracturing (HF)	P-04-310 P-07-232 PR U-97-27 IPR-02-01 IPR-02-02	Estimation of the <i>in situ</i> stress field.
Hydraulic fracturing on pre-existing fractures (HTPF)	P-04-310 P-07-232	Estimation of the <i>in situ</i> stress field.
Indirect stress data		
Borehole breakout	P-04-280 P-06-198 P-09-31	Estimation of the <i>in situ</i> stress field.

Table A3-4. Available data on hydrogeology and their handling in the SDM-Site Laxemar hydro-geological modelling.

Available data Data specification	Ref	Usage in SDM-Site Analysis/Modelling
<i>Geometrical and topographical data</i>		
Digital Elevation Model (DEM)	P-04-03 P-04-254 R-05-38 R-05-35	Basic input to flow and mass transport models, descriptions and modelling of the marine ecosystem.
<i>Geological data</i>		
Map and model of Quaternary deposits in the terrestrial part and sea bottom of the Simpevarp regional model area	R-08-05 R-08-06	
Rock types	R-08-54	
Bedrock model, geometry	P-06-282 P-07-223 R-08-54 R-09-01	
<i>Cored borehole data</i>		
Wireline tests coreholes, drilling information)	P-03-113 P-04-151 P-04-233 P-05-25 P-05-111 P-05-167 P-05-233 P-05-234 P-06-14 P-06-116 P-06-222 P-06-265 P-06-283 P-06-305 P-06-306 P-07-98 P-07-134 P-07-195 P-07-202	Borehole data and (prel) transmissivity distribution in large scale.
Difference flow logging	P-03-70 P-03-110 P-04-213 P-04-216 P-05-67 P-05-68 P-05-74 P-05-160 P-05-225 P-05-267 P-06-58 P-06-164 P-06-183 P-06-184 P-06-185 P-06-199 P-06-229 P-06-245 P-06-246 P-06-318 P-07-17 P-07-20 P-07-24 P-07-34 P-07-64 P-07-72 P-07-87 P-07-116 P-07-176 P-08-22 IPR-01-06 R-01-52	Conductive parts of the borehole, Statistics of conductive fractures.

Available data Data specification	Ref	Usage in SDM-Site Analysis/Modelling
Correlation Difference flow logging and core mapping	P-05-65 P-05-241 P-07-212 P-07-213 P-07-214 P-07-215 P-07-216	Conductive parts of the borehole. Base for orientation of conductive fractures for usage in the hydrogeological DFN.
Hydraulic injection tests, pumping tests (single hole)	P-04-247 P-04-288 P-04-289 P-04-290 P-04-291 P-04-292 P-05-16 P-05-184 P-05-192 P-05-222 P-05-273 P-06-148 P-06-182 P-06-201 P-06-225 P-07-48 P-07-49 P-07-79 P-07-80 P-07-90 P-07-94 P-07-99 P-07-120 P-07-192 P-07-193 P-08-27 P-08-57	Transmissivity distribution along the borehole in different scales.
Percussion hole data		
Drilling and hydraulic tests	P-03-114 P-04-150 P-04-234 P-04-235 P-04-236 P-05-55 P-05-190 P-05-194 P-05-237 P-05-275 P-06-291	
Hydraulic tests	P-03-56 P-04-212 P-04-287 P-06-147 P-06-319	Hydraulic test data for the bedrock.
Standpipes in QD deposits data		
Drilling	P-03-80 P-04-22 P-04-46 P-04-121 P-04-317 P-05-49 P-06-121 P-06-248 P-07-91	Standpipes geometri used in the flowmodelling. Description of stratigraphical distribution and total depth of overburden in the terrestrial parts of the Simpevarp and Laxemar subareas.

Available data Data specification	Ref	Usage in SDM-Site Analysis/Modelling
Interference tests		
Interference tests using percussion and core holes	P-04-287 P-05-20 P-05-193 P-06-145 P-06-151 P-07-18 P-07-39 P-07-173 P-07-182 P-07-183 P-07-185 P-07-186 P-07-187 P-08-15 P-08-16 TR-01-11	Infer connectivity between deformation zones and estimate transmissivity and (if possible) storage coefficient for deformation zones.
Other borehole, construction, tunnel data and models		
Hydraulic tests in areas Äspö, Ävrö, Hälö, Simpevarp, Mjälén and Laxemar areas	TR-97-02 TR-97-03 TR-97-05 TR-97-06 TR-02-19 R-98-55 IPR-00-28 IPR-01-44 IPR-01-52 IPR-01-65 IPR-03-13 SICADA database	Previous made evaluations compared to new data and for assessment of properties not known or with few data from SI.
Other hydraulic data	R-04-09 TR-98-05	Previous made evaluations compared to new data and for assessment of properties not known or with few data from SI.
Meteorological and hydrological data		
Regional data		
Meteorological and hydrological data from surrounding stations prior to and during the site investigations	TR-02-03 R-99-70 R-08-73	General description of hydrology, comparison with site investigation data.

Table A3-5. Available hydrogeochemical data and their handling in the SDM-Site Laxemar hydrogeochemical modelling.

Available data Data specification	Ref	Usage in SDM-Site Analysis/Modelling
Surface water data		
Precipitation, running water, soil pipes, sea water samples	P-08-10 P-06-324 P-06-325 P-06-155	Delineation and general characteristics of Meteoric water end-member and surface water recharge.
Precipitation gauges	P-05-175 P-05-118	Discharge pattern in surface areas.
SMM-drillcores	P-04-75 P-04-14 P-04-13	Explorative analyses and modelling.
Surface water sampling		Characterisation and description of spatial and temporal variability of surface water chemistry.
Shallow groundwater – soil pipes		
Shallow groundwater sampling	P-08-90 P-06-13 P-06-325 P-03-80	Description of the input of shallow groundwater end-member to the bedrock.
Groundwater – cored and percussion boreholes		
Cored boreholes – intermediate to deep groundwater	P-08-91 P-08-82 P-08-77 P-08-69 P-07-188 P-07-189	Explorative analyses which involves manual evaluation and mathematical modelling such as PHREEQC, M3 and coupled transport modelling. The results providing the basis to the conceptual model of the site. The use of the data in the specific modelling approaches are described in SKB R-08-93.
Complete chemical sampling and characterisation (class 4 and 5) and Hydrochemical logging	P-07-164 P-07-149 P-07-126 P-07-73 P-07-37 P-06-310 P-06-311 P-06-312	Description of groundwater types and their distribution at various depth intervals.
KSH01, KSH02, KSH03A, KAV01, KAV04, KLX01, KLX02, KLX03, KLX04, KLX05, KLX06, KLX07A, KLX08, KLX09, KLX10, KLX11A, KLX12A, KLX13A, KLX15A, KLX16A, KLX17A, KLX18A, KLX19A, KLX20A, KLX21B, KLX27A		Regional and spatial distribution of groundwater types.
Percussion boreholes	P-06-308 P-06-280 P-06-259 P-06-180 P-06-181 P-06-142 P-06-47 P-06-17 P-06-16 P-06-08 P-05-244 P-05-230 P-05-226 P-05-198 P-05-195 P-05-85 P-05-54 P-05-89 P-05-88 P-05-05 P-04-304 P-04-299 P-04-281 P-04-220 P-04-219 P-04-51 P-04-12 P-03-89 P-03-88 P-03-113	Chemical character of all the the roundwater types.

Available data Data specification	Ref	Usage in SDM-Site Analysis/Modelling
<i>Hydrochemical monitoring</i>		
Hydrochemical monitoring programme for core and hammer drilled boreholes 2007. KLX04, KLX05, KLX07A, KLX08, KLX10, KLX12A, KLX13A, KLX15A, KLX18A, KLX19A, KLX20A HLX43, HLX39, HLX38, HLX37, HLX35, HLX32, HLX28	P-08-90 P-08-88 P-07-167 P-07-47 P-07-219 P-06-313 P-06-127 P-06-57 P-05-282 P-05-205	Chemical changes during time series sampling and, variability check.
<i>Porewater data</i>		
KLX08, KLX3, KLX17A	P-08-43 P-06-77 P-06-12 P-06-163	Delineate the porewater chemistry and isotope compositions. Used for studies of interaction between the fracture water and porewater support to the general palaeo understanding of the site. Important input for the hydrogeological modelling.
<i>Microbial, colloidal and gas data</i>		
Sampling of microbes, colloids and gases	P-08-83 P-08-09 P-08-08	General and detail description of microbes, colloids and gases. Redox reaction support, and important input to safety assessment.
<i>Fracture mineral data</i>		
Open and closed fractures	P-08-44 P-08-12 P-08-11 P-07-74 P-05-174	Mineral characterisation. Identification of redox-sensitive minerals. Estimation of redox-capacity and redox sensitive minerals. Origin and age determination of calcite fracture fillings. Support for the palaeo understanding of the site.

Table A3-6. Available data for bedrock transport properties and their handling in the SDM-Site Laxemar bedrock transport model.

Available data Data specification	Ref	Usage in SDM-Site Analysis/Modelling
Material properties data		
Laboratory measurements of porosity, effective diffusivity (formation factor), BET-surface areas, and sorption	P-07-179 (P-05-106 and P-06-286 now obsolete)	Assignment of corresponding material property parameters in retardation model.
Laboratory measurements of rock formation factors by AC electrical resistivity method	P-05-19 P-05-75 P-06-289 P-07-203	Comparative measurements of formation factors used in retardation model.
<i>In situ</i> measurements of formation factors by AC electrical resistivity method	P-05-27 P-05-105 P-05-143 P-06-288	Comparative measurements and alternative parameterisation for rock formation factors used in retardation model.
Quantitative distribution of fracture minerals	P-08-38	Development of "fracture type" classifications used in retardation model.
PMMA-measurements of porosity distribution and heterogeneity	P-06-62	Porosity estimation for deformation zone structural elements used in retardation model. Supporting argumentation for existence of increased porosity in vicinity of fracture surfaces.
Pore water characterisation and diffusion experiments	P-04-249 P-06-12 P-06-77 P-06-163 P-08-43 R-08-112	Supporting argumentation for the existence of a connected rock matrix porosity and qualitative assessment of uncertainty related to <i>in situ</i> formation factors.
Rock matrix permeability measurements	P-07-204	Supporting argumentation for existence of <i>in situ</i> compression of pore spaces.
Microcrack volume measurements	P-07-140	Supporting argumentation for existence of <i>in situ</i> compression of pore spaces.
Confirmatory testing data		
Groundwater flow monitoring in permanently installed boreholes using tracer dilution method	P-06-61 P-07-181 P-08-31 R-08-103	Measurement of <i>in situ</i> flow rates under non-pumped conditions and estimations of local hydraulic gradients.
Groundwater flow measurements using tracer dilution method and SWIW tests	P-05-28 P-06-287 P-07-26 P-07-180 P-07-199 R-08-104	Partial confirmation of the existence of retardation processes consistent with premises of transport model. Tracer dilution data used to provide estimates of local hydraulic gradients.
Multiple well tracer tests	In prep.	Partial confirmation of the existence of retardation processes consistent with premises of transport model. Tracer dilution data used to provide estimates of local hydraulic gradients.

Table A3-7. Available abiotic data for the surface system and their handling in the SDM-Site Laxemar surface systems modelling.

Available data Data specification	Ref	Usage in SDM-Site Analysis/Modelling
Geometrical and topographical data		
Digital Elevation Model (DEM)	P-04-03 P-04-254 R-05-38	Basic input to flow and mass transport models, descriptions and modelling of the marine ecosystem.
Surveying of streams	P-06-05	Description of stream characteristics. Input to quantitative water flow modelling (MIKE SHE).
Geological data		
Map of Quaternary deposits in the terrestrial part of the Simpevarp regional model area	P-04-22 P-05-49	Description of surface distribution of Quaternary deposits in the terrestrial part of the regional model area.
Maps of Quaternary deposits covering a large part of the sea bottom in the regional model area	TR-99-37 P-04-254 P-05-35 P-06-296 R-08-06	Description of surface distribution of Quaternary deposits at the sea floor.
Map of soils in the terrestrial part of the Simpevarp regional model area	P-04-243 R-05-15	Distribution of soil types in the regional model area.
Deposits on the bottom of watercourses	P-05-40	Evaluation of the map of Quaternary deposits.
Stratigraphical studies in machine cut trenches	P-05-47 P-05-49 P-06-121	Stratigraphy and total depth of Quaternary deposits.
Stratigraphy and total depth of Quaternary deposits from the sea and lake floors	R-02-47 P-04-254 P-04-273 P-05-35 P-06-144 R-08-05	Description of stratigraphical distribution and total depth of Quaternary deposits at the sea and lake floors.
Drilling and sampling of Quaternary deposits	P-03-80 P-04-22 P-04-121 P-04-317 P-05-49 P-06-121 P-06-248 P-07-91	Description of stratigraphical distribution and total depth of overburden in the terrestrial parts of the Simpevarp and Laxemar subareas.
Helicopter borne survey data	P-03-100	Description of surface distribution of Quaternary deposits in parts of the Simpevarp regional model area.
Resistivity measurements	P-03-17 P-06-284	Total depth of Quaternary deposits.
Refraction seismic	P-04-134 P-04-201 P-04-298 P-05-155 P-06-49	Total depth of Quaternary deposits.
Chemical and mineralogical analyses of Quaternary deposits	R-02-47 R-04-72 P-04-273 R-05-15 P-05-35 P-05-49 R-06-18 P-06-121 P-06-301 P-06-320 P-06-321 P-07-30 P-07-222	Chemical and mineralogical properties of Quaternary deposits.
Physical analyses of Quaternary deposits	R-02-47 P-04-17 P-04-243 P-04-273 R-05-15 P-05-49 P-06-121 P-07-91	Physical properties of Quaternary deposits.

Available data Data specification	Ref	Usage in SDM-Site Analysis/Modelling
Dating of sediment and peat	P-06-250 P-06-301	Accumulation rates of sediment and peat.
Meteorological data		
Regional data		
Meteorological data from surrounding stations prior to and during the site investigations	TR-02-03 R-99-70 P-05-227 P-06-19 P-07-38 P-07-172	General description of meteorology, comparison with site investigation data.
Site investigation data		
Meteorological data from the stations on Äspö (Sep. 2003-Aug. 2007) and in Plittorp (Jul. 2004–Aug. 2007); Sicada data up to Dec. 2007 are used	P-05-227 P-06-19 P-07-38 P-07-172	Description of meteorology and comparison with data from surrounding stations. Input to quantitative water flow modelling (MIKE SHE).
Hydrological data		
Regional data		
Hydrological data from surrounding hydrological stations prior to and during (Sicada data only) the site investigations	R-99-70 TR-02-03	General description of hydrology. Comparison with site investigation data.
Site investigation data		
Investigation of potential locations for hydrological stations	P-03-04	Size of catchment areas for manual and automatic surface-water discharge measurements.
Geometrical data and descriptions of catchment areas, lakes and streams	P-04-242	Delineation and general characteristics of catchment areas, lakes and streams. Input to quantitative water flow modelling (MIKE SHE).
Manual discharge measurements in streams	P-04-13 P-04-75 P-04-246	Description of spatial and temporal variability of surface-water discharge.
Monitoring of surface-water discharges in streams	P-05-227 P-06-19 P-07-38 P-07-172	Description of spatial and temporal variability of surface-water discharge. Calculation of specific discharge. Calibration of quantitative water flow models (MIKE SHE).
Monitoring of surface-water levels in lakes and the sea	P-05-227 P-06-19 P-07-38 P-07-172	Description of spatial and temporal variability of surface-water levels. Input to quantitative water flow modeling (MIKE SHE).
Characterisation of streams, including vegetation, bottom substrate and technical encroachments	P-05-40	Description of streams and land improvement and drainage operations.
Field checks of streams and land improvement and drainage operations	P-05-70 P-05-238	Description of streams and land improvement and drainage operations. Input to quantitative water flow modelling (MIKE SHE).
Hydrogeological data		
Hydrogeological inventory in the Oskarshamn area	P-04-277	General description of hydrogeology, water operation permits and land improvement and drainage operations.
Inventory of private wells	P-03-05	General description of private wells.
Monitoring of groundwater levels in the QD and point-water heads in the rock	P-05-205 P-05-282 P-07-219 P-08-28	Conceptual hydrogeological model. Calibration of quantitative water flow models (MIKE SHE).
Geological data from drilling in QD and installation of groundwater monitoring wells	P-03-80 P-04-46 P-04-121 P-04-317 P-05-167 P-06-121 P-06-248 P-07-91	Conceptual hydrogeological model.
Hydraulic conductivity from slug tests in groundwater monitoring wells	P-04-122 P-04-318 P-06-149 P-06-150 P-06-248 P-07-91	Conceptual hydrogeological model. Hydrogeological parameterisation of the QD.

Available data Data specification	Ref	Usage in SDM-Site Analysis/Modelling
Hydraulic conductivity from particle-size distribution curves	P-04-273 P-05-47 P-05-49 P-06-121 P-07-91	Conceptual hydrogeological model. Hydrogeological parameterisation of the QD.
Hydraulic conductivity and storage-properties data from single-hole and interference tests in groundwater monitoring wells	P-07-173	Conceptual hydrogeological model. Hydrogeological parameterisation of the QD.
Hydraulic interference and tracer tests in percussion boreholes and groundwater monitoring wells	P-06-151 P-07-187	Conceptual hydrogeological model.
Groundwater flow velocities from tracer dilution tests in groundwater monitoring wells	P-07-197	Conceptual hydrogeological model.
<i>Oceanographical data</i>		
Regional oceanographical data	TR-97-14 R-99-70 TR-02-03 TR-08-02	Description of coastal basins. Quantitative modelling.
<i>Chemistry data</i>		
Surface water sampling	P-04-13 P-04-14 P-04-75 P-05-118 P-05-175 P-06-155 P-06-324	Characterisation and description of spatial and temporal variability of surface water chemistry.
Shallow groundwater	P-03-80 P-04-46 P-04-121 P-04-317 P-06-13 P-06-248 P-06-325 P-07-222	Characterisation of the chemistry in shallow groundwater.
Chemical composition of biota and deposits	P-06-250 P-06-320 P-07-32	Modelling.
Overburden	P-03-80 P-04-46 P-04-121 P-04-243 P-04-273 P-04-317 P-06-250 P-06-301 P-06-320 P-07-222	Characterisation of the chemistry of the Quaternary deposits.
Sediment, suspended material and pore water	P-08-81	Modelling.

Table A3-8. Available biotic data for the surface system and their handling in the SDM-Site Laxemar surface system modelling.

Available data Data specification	Ref	Usage in SDM-Site Analysis/Modelling
<i>Terrestrial biota</i>		
Compilation of existing information 2002	R-02-10	Description.
Bird population survey	P-04-21 P-05-42 P-06-298 P-07-226	Description, modelling.
Mammal population survey	P-04-04 P-04-237 R-05-36 P-07-122 P-07-136	Description, modelling.
Amphibians and reptiles	P-04-36	Description, modelling.
Mammal ecological data and carbon budget	R-05-36	Description, modelling.
Vegetation inventory	P-04-20	Description.
Vegetation mapping	P-03-83	Description, modelling.
LAI-index and tree stand data	TR-06-29	Description, modelling.
Litter fall and litter decomposition	R-07-23	Description, modelling.
Dead wood	P-05-87	Description.
Successional birch habitats	P-04-315	Description.
Biomass and Net Primary Productivity (NPP) of the vegetation	R-08-01 P-05-80	Description, modelling.
Fine root biomass, turnover and depth	R-06-121 R-07-01 TR-07-11	Description, modelling.
Data from soil mapping	R-05-15 P-04-243	Description, modelling.
Respiration measurements	P-06-278 TR-06-28 TR-07-13 R-06-125	Description, modelling.
Bioturbation	R-06-123	Description, modelling.
Ecosystem modelling	R-06-121 R-08-01	COUP model. LPJ-GUESS model.
Wetlands; Their properties and function	TR-04-08	Description.
<i>Limnic biota</i>		
Limnic producers	P-04-253 P-05-40 P-05-173 P-06-232	Description, modelling.
Habitat borders	P-04-242	Description.
Limnic consumers	P-04-253 P-04-251 P-04-252 P-06-232 P-06-251	Description, modelling.
Ecosystem modelling	R-08-02	
<i>Marine biota</i>		
Compilation of existing information 2002	R-02-10	Description.
Light penetration depth	P-04-13	Description.
Zooplankton, phytoplankton	P-04-253	Description, modelling.
Bacteria	P-06-232	
Identification of dominating species	P-03-68	Description.
Macrophyte communities	P-03-69	Description, modelling.
Soft bottom infauna	P-04-17	Description, modelling.

Available data Data specification	Ref	Usage in SDM-Site Analysis/Modelling
Bottom fauna	P-04-17 P-04-82 P-04-252 P-05-45 P-06-303	Description, modelling.
Reed	P-04-316	Description, modelling.
Fish sampling	P-04-19	Description, modelling.
Fish population estimates	P-05-57 P-06-10	Description, modelling.
Bird population survey	P-04-21 P-05-42 P-06-298 P-07-226	Description.
Spatial distribution of marine organisms	R-07-50	Modelling.
Ecosystem modelling	R-08-03	
<i>Humans and land use</i>		
Humans and land use	R-04-11	Description, modelling.

Table A3-9. Reports in the SKB P, IPR, ICR, R, and TR-series referenced in Tables 1 through 8.

P-02-02	Wiklund S. Digitala ortofoton och höjdm modeller. Redovisning av metodik för platsundersökningsområdena Oskarshamn och Forsmark samt förstudieområdet Tierp Norra (in Swedish).
P-02-05	Mattsson H, Triumf C-A, Wahlgren C-H. Prediktering av förekomst av finkorniga granitgångar i Simpevarpsområdet.
P-03-04	Lärke A, Hillgren R. Rekognoscering av mätplatser för ythydrologiska mätningar i Simpevarpsområdet (in Swedish).
P-03-05	Morosini M, Hultgren H. Inventering av privata brunnar i Simpevarpsområdet, 2001-2002 (in Swedish).
P-03-06	Wahlgren C-H, Persson L, Danielsson P, Berglund J, Triumf C-A, Mattsson H, Thunehed H. Oskarshamn site investigation. Geologiskt underlag för val av prioriterad plats inom området väster om Simpevarp.
P-03-07	Curtis P, Elfström M, Stanfors R. Oskarshamn site investigation Compilation of structural geological data covering the Simpevarp peninsula, Ävrö and Hälö.
P-03-15	Nilsson P, Gustafsson C. Simpevarp site investigation. Geophysical, radar and BIPS logging in borehole KSH01A, HSH01, HSH02 and HSH03.
P-03-16	Nielsen U T, Ringgaard J. Simpevarp site investigation. Geophysical borehole logging in borehole KSH01A, KSH01B and part of KSH02.
P-03-17	Thunehed H, Pitkänen T. Simpevarp site investigation. Electrical soundings supporting inversion of helicopterborne EM-data. Primary data and interpretation report.
P-03-25	Rønning H J, Kihle O, Mogaard J O, Walker P. Simpevarp site investigation. Helicopter borne geophysics at Simpevarp, Oskarshamn, Sweden.
P-03-31	Green M. Platsundersökning Simpevarp. Fågelundersökningar inom SKB:s platsundersökningar 2002 (in Swedish).
P-03-36	Curtis P, Elfström M, Stanfors R. Oskarshamn site investigation. Visualization of structural geological data covering the Simpevarp peninsula, Ävrö and Hälö.
P-03-56	Ludvigson J-E, Levén J, Jönsson S. Oskarshamn site investigation. Hydraulic tests and flow logging in borehole HSH03.
P-03-63	Byström S, Hagthorpe P, Thunehed H. Oskarshamn site investigation. QC-report concerning helicopter borne geophysics at Simpevarp, Oskarshamn, Sweden.
P-03-66	Triumf C-A. Oskarshamn site investigation. Geophysical measurements for the siting of a deep borehole at Ävrö and for investigations west of CLAB.
P-03-67	Borgiel M. Makroskopiska organismers förekomst i sedimentprov. En översiktlig artbestämning av makroskopiska organismer (in Swedish).
P-03-68	Tobiasson S. Tolkning av undervattensfilm från Forsmark och Simpevarp (in Swedish).
P-03-69	Fredriksson R, Tobiasson S. Simpevarp site investigation. Inventory of macrophyte communities at Simpevarp nuclear power plant. Area of distribution and biomass determination.
P-03-70	Rouhiainen P, Pöllänen J. Oskarshamn site investigation. Difference flow measurements in borehole KSH01A at Simpevarp.
P-03-71	Vangkilde-Pedersen T. Oskarshamn site investigation. Reflection seismic surveys on Simpevarpshalvön 2003 using the vibroseismic method.
P-03-72	Juhlin C. Oskarshamn site investigation. Evaluation of RAMBØLL reflection seismic surveys on Simpevarpshalvön 2003 using the vibroseismic.
P-03-73	Aaltonen J, Gustafsson C, Nilsson P. Oskarshamn site investigation. RAMAC and BIPS logging and deviation measurements in boreholes KSH01A, KSH01B and the upper part of KSH02.
P-03-74	Barton N. Oskarshamn site investigation. Q-logging of KSH 01A and 01B core.
P-03-80	Ask H. Installation of four monitoring wells, SSM000001, SSM000002, SSM000004 and SSM000005 in the Simpevarp subarea.
P-03-83	Boresjö Bronge L, Wester K. Vegetation mapping with satellite data of the Forsmark, Tierp and Oskarshamn regions.
P-03-87	Wacker P. Oskarshamn site investigation. Hydrochemical logging in KSH01A.
P-03-88	Berg C. Hydrochemical logging in KSH02. Oskarshamn site investigation.
P-03-89	Berg C. Hydrochemical logging in KAV01. Oskarshamn site investigation.
P-03-90	Fridriksson G, Öhr J. Assessment of plant biomass of the ground, field and shrub layers of the Forsmark area.
P-03-93	Lindqvist L, Thunehed H. Oskarshamn site investigation. Calculation of Fracture Zone Index (FZI) for KSH01A.
P-03-97	Mattsson H, Thunehed H, Triumf, C-A. Oskarshamn site investigation. Compilation of petrophysical data from rock samples and in situ gamma-ray spectrometry measurements.
P-03-99	Triumf C-A. Oskarshamn site investigation. Identification of lineaments in the Simpevarp area by the interpretation of topographical data.
P-03-100	Triumf C-A, Thunehed H, Kero L, Persson L. Interpretation of airborne geophysical survey data. Helicopter borne survey data of gamma ray spectrometry, magnetics and EM from 2002 and fixed wing airborne survey data of the VLF-field from 1986. Oskarshamn site investigation.

- P-03-106 **Chryssanthakis P, Tunbridge L.** Borehole: KSH01A. Determination of P-wave velocity, transverse borehole core. Oskarshamn site investigation.
- P-03-107 **Chryssanthakis P.** Borehole: KSH01A. Results of tilt testing. Oskarshamn site investigation.
- P-03-109 **Aaltonen J, Gustafsson C.** RAMAC and BIPS logging in borehole KSH02.
- P-03-110 **Rouhiainen P, Pöllänen J.** Oskarshamn site investigation – Difference flow measurements in borehole KSH02 at Simpevarp.
- P-03-111 **Nielsen U T, Ringgaard J, Horn F.** Geophysical borehole logging in boreholes KSH02 and KLX02.
- P-03-113 **Ask H, Morosini M, Samuelsson L-E, Stridsman H.** Oskarshamn site investigation – Drilling of cored borehole KSH01.
- P-03-114 **Ask H, Samuelsson L-E.** Oskarshamn site investigation – Drilling of three flushing water wells, HSH01, HSH02 and HSH03.
- P-03-120 **Aaltonen J, Gustafsson C.** RAMAC logging in boreholes KAV01 and KLX02.
- P-04-01 **Ehrenborg J, Stejskal V.** Oskarshamn site investigation. Boremap mapping of core drilled boreholes KSH01A and KSH01B.
- P-04-02 **Nordman C.** Oskarshamn site investigation. Boremap mapping of percussion boreholes HSH01-03.
- P-04-03 **Brydsten L.** A method for construction of digital elevation models for site investigation program at Forsmark and Simpevarp.
- P-04-04 **Cederlund G, Hammarström A, Wallin K.** Surveys of mammal populations in the areas adjacent to Forsmark and Oskarshamn. Results from 2003.
- P-04-10 **Chryssanthakis P.** Oskarshamn Site Investigation – Borehole KSH02, Results of tilt testing.
- P-04-11 **Chryssanthakis P, Tunbridge L.** Borehole: KSH02A Determination of P-wave velocity, transverse borehole core. Oskarshamn site investigation.
- P-04-12 **Wacker P, Berg C, Bergelin A.** Complete hydrochemical characterisation in KSH01A. Results from four investigated sections, 156.5–167.0, 245.0–261.6, 586.0–596.7 and 548.0–565.4 metres.
- P-04-13 **Ericsson U, Engdahl A.** Surface water sampling at Simpevarp 2002–2003. Oskarshamn site investigation.
- P-04-14 **Ericsson U.** Sampling of precipitation at Äspö 2002–2003.
- P-04-17 **Fredriksson R.** Inventory of the soft-bottom macrozoobenthos community in the area around Simpevarp nuclear power plant. Oskarshamn site investigation.
- P-04-19 **Engdahl A, Ericsson U.** Fish sampling in connection with geophysical measurements at Simpevarp 2003.
- P-04-20 **Andersson J.** Vegetation inventory in part of the municipality of Oskarshamn.
- P-04-21 **Green M.** Bird surveys in Simpevarp 2003. Oskarshamn site investigation.
- P-04-22 **Rudmark L.** Investigation of Quaternary deposits at Simpevarp peninsula and the islands of Ävrö and Hälö. Oskarshamn site investigation.
- P-04-23 **Sjöberg J.** Overcoring rock stress measurements in borehole KSH02. Oskarshamn Site Investigation.
- P-04-26 **Lindqvist L, Thunehed H.** Oskarshamn site investigation. Calculation of Fracture Zone Index (FZI) for HSH01.
- P-04-27 **Mattsson H.** Oskarshamn site investigation. Interpretation of borehole geophysical data from the percussion drilled part of the borehole KSH01A.
- P-04-28 **Mattsson H, Thunehed H.** Interpretation of geophysical borehole data from KSH01A, KSH01B, KSH02 (0-100 m), HSH01, HSH02 and HSH03 and compilation of petrophysical data from KSH01A and KSH01B.
- P-04-32 **Mattsson H, Stanfors R, Wahlgren C-H, Stenberg L, Hultgren P.** Geological single-hole interpretation of KSH01A, KSH01B, HSH01, HSH02 and HSH03. Oskarshamn site investigation.
- P-04-35 **Hermanson J, Hansen L, Wikholm M, Cronquist T, Leiner P, Vestgård J, Sandah K-A.** Detailed fracture mapping of four outcrops at the Simpevarp peninsula and Ävrö. Oskarshamn site investigation.
- P-04-36 **Andrén C.** Oskarshamn site investigation, Amphibians and reptiles in SKB special area of investigation at Simpevarp.
- P-04-37 **Triumf C-A.** Joint interpretation of lineaments in the eastern part of the site descriptive model area. Oskarshamn site investigation.
- P-04-42 **Chryssanthakis P.** Oskarshamn Site Investigation – Borehole KAV01, Results of tilt testing.
- P-04-43 **Chryssanthakis P, Tunbridge L.** Borehole: KAV01 Determination of P-wave velocity, transverse borehole core. Oskarshamn site investigation.
- P-04-44 **Chryssanthakis P.** Oskarshamn Site Investigation – Borehole KLX02, Results of tilt testing.
- P-04-45 **Chryssanthakis P, Tunbridge L.** Borehole: KLX02 Determination of P-wave velocity, transverse borehole core. Oskarshamn site investigation.
- P-04-46 **Ask H.** Drilling and installation of two monitoring wells, SSM 000006 and SSM 000007 in the Simpevarp subarea.
- P-04-48 **Gustafsson J, Gustafsson C.** Oskarshamn site investigation. RAMAC and BIPS logging in boreholes KSH03A, KSH03B, HAV09, HAV10 and BIPS in KAV01. Revised April 2006.
- P-04-49 **Triumf C-A.** Oskarshamn site investigation. Joint interpretation of lineaments.

- P-04-50 **Nielsen U T, Ringgaard J, 2004.** Geophysical borehole logging in borehole KSH03A, KSH03B, HAV09 and HAV10.
- P-04-51 **Berg C.** Hydrochemical logging in KSH03A.
- P-04-52 **Juhlin C, Bergman B, Palm H, Tryggvason A.** Oskarshamn site investigation. Reflection seismic studies on Ävrö and Simpevarpshalvön, 2003.
- P-04-53 **Adi-Zarrabi B.** Drill hole KSH01A Thermal properties: heat conductivity and heat capacity determined using the TPS method and mineralogical composition by modal analysis.
- P-04-54 **Adi-Zarrabi B.** Drill hole KSH02 Thermal properties: heat conductivity and heat capacity determined using the TPS method and mineralogical composition by modal analysis.
- P-04-55 **Adi-Zarrabi B.** Drill hole KAV01 Thermal properties: heat conductivity and heat capacity determined using the TPS method and mineralogical composition by modal analysis.
- P-04-56 **Savukoski M, Carlsson L.** Drill hole KSH01A. Determining of porosity by water saturation and density by buoyancy technique.
- P-04-57 **Carlsson L.** Drill hole KSH02. Determining of porosity by water saturation and density by buoyancy technique. Oskarshamn site investigation.
- P-04-58 **Carlsson L.** Drill hole KAV01. Determining of porosity by water saturation and density by buoyancy technique. Oskarshamn site investigation.
- P-04-59 **Åkesson U.** Drill hole: KSH01A. Extensometer measurement of the coefficient of thermal expansion of rock.
- P-04-60 **Åkesson U.** Drill hole: KSH02. Extensometer measurement of the coefficient of thermal expansion of rock.
- P-04-61 **Åkesson U.** Drill hole: KAV01. Extensometer measurement of the coefficient of thermal expansion of rock. Oskarshamn site investigation.
- P-04-62. **Jacobsson L.** Oskarshamn Site Investigation – Drill hole KSH01A, Indirect tensile strength tests.
- P-04-63 **Jacobsson L.** Oskarshamn Site Investigation – Drill hole KSH02, Indirect tensile strength tests.
- P-04-66 **Gustafsson J, Gustafsson C.** Oskarshamn site investigation. RAMAC logging with directional radar antenna in boreholes KSH01A, KSH01B and KSH02. Revised April 2006.
- P-04-75 **Ericsson U, Engdahl A.** Surface water sampling in Oskarshamn – Subreport October 2003 to February 2004.
- P-04-77 **Mattsson H, Thunehed H.** Oskarshamn site investigation. Interpretation of geophysical borehole data and compilation of petrophysical data from KSH02 (80–1,000 m) and KAV01.
- P-04-82 **Borgiel M.** Sampling and analyses of brackish water phyto-benthic plant and animal communities in the Grepen area. A method study.
- P-04-84 **Sjöberg J.** Overcoring rock stress measurements in borehole KAV04. Oskarshamn site investigation.
- P-04-102 **Wahlgren C-H, Ahl M, Sandahl K-A, Berglund J, Petersson J, Ekström M, Persson P-O.** Oskarshamn site investigation. Bedrock mapping 2003 – Simpevarp subarea. Outcrop data, fracture data, modal and geochemical classification of rock types, bedrock map, radiometric dating.
- P-04-110 **Rouhiainen P, Pöllänen J.** Oskarshamn site investigation. Difference flow measurements in borehole KSH02 at Simpevarp.
- P-04-121 **Johansson T, Adestam L.** Drilling and sampling in soil. Installation of groundwater monitoring wells.
- P-04-122 **Johansson T, Adestam L.** Slug tests in groundwater monitoring wells in soil in the Simpevarp area.
- P-04-128 **Triumf C-A.** Gravity measurements in the Laxemar model area with surroundings.
- P-04-129 **Ehrenborg J, Stejskal V.** Oskarshamn site investigation. Boremap mapping of core drilled borehole KLX02.
- P-04-130 **Ehrenborg J, Stejskal V.** Oskarshamn site investigation. Boremap mapping of core drilled borehole KAV01.
- P-04-131 **Ehrenborg J, Stejskal V.** Oskarshamn site investigation. Boremap mapping of core drilled borehole KSH02.
- P-04-132 **Ehrenborg J, Stejskal V.** Oskarshamn site investigation. Boremap mapping of core drilled boreholes KSH03A and KSH03B.
- P-04-133 **Mattsson H, Stanfors R, Wahlgren C-H, Carlsten S, Hultgren P.** Oskarshamn site investigation. Geological single-hole interpretation of KSH02 and KAV01.
- P-04-134 **Lindqvist G.** Refraction seismic measurements in Laxemar. Oskarshamn site investigation
- P-04-150 **Ask H, Samuelsson L-E.** Drilling of two flushing water wells, HAV09 and HAV10.
- P-04-151 **Ask H, Morosini M, Samuelsson L-E, Stridsman H.** Oskarshamn site investigation – Drilling of cored borehole KSH02.
- P-04-185 **Chryssanthakis P.** Simpevarp Site Investigation – Drill hole: KSH01A, The normal stress and shear tests on joints.
- P-04-195 **Gustafsson J, Gustafsson C.** RAMAC and BIPS logging in boreholes KAV04A, KAV04B, HLX13 and HLX15.
- P-04-201 **Lindqvist G.** Refraction seismic measurements in the water outside Simpevarp and Ävrö and on land on Ävrö. Oskarshamn site investigation.
- P-04-202 **Nielsen U T, Ringgaard J.** Geophysical borehole logging in borehole KAV04A, KAV04B, HLX13 and HLX15.

- P-04-204 **Schmelzbach C, Juhlin C.** 3D processing of reflection seismic data acquired within and near the array close to KAV04A on Ävrö, 2003.
- P-04-206 **Chryssanthakis P, Tunbridge L.** Borehole: KAV04A. Determination of P-wave velocity, transverse borehole core.
- P-04-207 **Jacobsson L.** Oskarshamn Site Investigation – Drill hole KSH01A, Uniaxial compression test of intact rock.
- P-04-208 **Jacobsson L.** Oskarshamn Site Investigation – Drill hole KSH01A, Triaxial compression test of intact rock.
- P-04-209 **Jacobsson L.** Oskarshamn Site Investigation – Drill hole KSH02, Uniaxial compression test of intact rock.
- P-04-210 **Jacobsson L.** Oskarshamn Site Investigation – Drill hole KSH02, Triaxial compression test of intact rock.
- P-04-211 **Thunehed H, Triumf C-A, Pitkänen T.** Geophysical profile measurements over interpreted lineaments in the Laxemar area.
- P-04-212 **Svensson T.** Oskarshamn site investigation. Pumping tests and flow logging in boreholes KSH03 and HSH02.
- P-04-213 **Rouhiainen P, Pöllänen J.** Oskarshamn site investigation – Difference flow measurements in borehole KAV01 at Ävrö.
- P-04-214 **Mattsson H.** Interpretation of geophysical borehole data and compilation of petrophysical data from KSH03A (100–1,000 m), KSH03B, HAV09, HAV10 and KLX02 (200–1,000 m).
- P-04-215 **Juhlin C, Bergman B, Palm H.** Reflection seismic studies performed in the Laxemar area during 2004.
- P-04-216 **Pöllänen J, Sokolnicki M.** Difference flow measurements in borehole KAV04A and KAV04B.
- P-04-217 **Mattsson H.** Interpretation of geophysical borehole data and compilation of petrophysical data from KAV04A (100–1,000 m), KAV04B, HLX13 and HLX15.
- P-04-218 **Carlsten S.** Oskarshamn site investigation. Geological interpretation of borehole radar reflectors in KSH01, HSH01-03, KAV01 and KSH02.
- P-04-219 **Berg C.** Hydrochemical logging in KLX04A.
- P-04-220 **Berg C.** Hydrochemical logging in KAV04A.
- P-04-221 **Persson Nilsson K, Bergman T, Eliasson T.** Bedrock mapping 2004 – Laxemar subarea and regional model area. Outcrop data and description of rock types.
- P-04-231 **Hultgren P, Stanfors R, Wahlgren C-H, Carlsten S, Mattsson H.** Geological single-hole interpretation of KSH03A, KSH03B, KLX02, HAV09 and HAV10.
- P-04-232 **Nielsen U T, Ringgaard J, Horn F.** Geophysical borehole logging in borehole KAV01.
- P-04-233 **Ask H, Morosini M, Samuelsson L-E, Ekström L, Håkansson N.** Drilling of cored borehole KSH03.
- P-04-234 **Ask H, Samuelsson L-E.** Drilling of two percussion boreholes, HLX13 and HLX14.
- P-04-235 **Ask H, Samuelsson L-E, Zetterlund M.** Percussion drilling of boreholes HLX15, HLX26, HLX27, HLX28, HLX29 and HLX32 for investigation of lineament NW042.
- P-04-236 **Ask H, Samuelsson L-E.** Percussion drilling of borehole HLX20 for investigation of lineament EW002.
- P-04-237 **Ignell H.** Investigations on mammals – bats. Investigation of the fauna of mammals in selected places within SKB investigation area. Oskarshamn site investigation.
- P-04-239 **Gustafsson J, Gustafsson C.** RAMAC and BIPS logging in borehole KLX04.
- P-04-240 **Nielsen U T, Vangkilde-Pedersen T, Ringgaard J.** Oskarshamn site investigation. Geophysical borehole logging in borehole HLX17, HLX18 and HLX19.
- P-04-242 **Brunberg A-K, Carlsson T, Brydsten L, Strömberg M.** Identification of catchments, lake-related drainage parameters and lake habitats. Oskarshamn site investigation.
- P-04-243 **Lundin L, Björkvald L, Hansson J, Stendahl J.** Surveillance of soils and site types in the Oskarshamn area.
- P-04-244 **Berglund J.** Scan line fracture mapping. Subarea Laxemar and passage for tunnel.
- P-04-246 **Morosini M, Lindell L.** Compilation of measurements from manually gauged hydrological stations, October 2002–March 2004. Oskarshamn site investigation.
- P-04-247 **Ludvigson J, Levén J, Källgården J, Jönsson S.** Single-hole injection tests in borehole KSH02. Oskarshamn site investigation.
- P-04-249 **Waber N, Smellie J.** Borehole KSH02: Characterisation of matrix pore water (Feasibility Study). Oskarshamn site investigation.
- P-04-250 **Drake H, E-L Tullborg.** Oskarshamn site investigation. Fracture mineralogy and wall rock alteration. Results from drill core KSH01A+B.
- P-04-251 **Engdahl A, Ericsson U.** Sampling of freshwater fish. Description of the fish fauna in four lakes.
- P-04-252 **Ericsson U, Engdahl A.** Benthic macro invertebrates. Results from sampling in the Simpevarp area 2004.
- P-04-253 **Sundberg I, Svensson J-E, Ericsson U, Engdahl A.** Phytoplankton and zooplankton. Results from sampling in the Simpevarp area 2003-2004. Oskarshamn site investigation.
- P-04-254 **Ingvanson N, Palmeby A, Svensson O, Nilsson O, Ekfeldt T.** Oskarshamn site investigation. Marine survey in shallow coastal waters Bathymetric and geophysical investigation 2004.

- P-04-255 **Jacobsson L.** Borehole KLX02. Uniaxial compression test of intact rock.
- P-04-256 **Jacobsson L.** Drill hole KLX02. Indirect tensile strength test.
- P-04-257 **Jacobsson L.** Borehole KLX02 Normal stress and shear tests on joints.
- P-04-258 **Adi-Zarrabi B.** Drill hole KLX02. Thermal properties: heat conductivity and heat capacity determined using the TPS method and mineralogical composition by modal analysis.
- P-04-259 **Savukoski M.** Drill hole KLX02. Determining of porosity by water saturation and density by buoyancy technique. Oskarshamn site investigation.
- P-04-260 **Åkesson U.** Drill hole: KLX02. Extensometer measurement of the coefficient of thermal expansion of rock. Oskarshamn site investigation.
- P-04-261 **Jacobsson L.** Borehole KLX04A Uniaxial compression test of intact rock.
- P-04-262 **Jacobsson L.** Borehole KLX04A Triaxial compression test of intact rock.
- P-04-263 **Jacobsson L.** Drill hole KLX04A: Indirect tensile strength test.
- P-04-264 **Jacobsson L.** Borehole KLX04A Normal stress and shear tests on joints.
- P-04-265 **Chryssanthakis P.** Borehole KLX04A Tilt testing.
- P-04-266 **Chryssanthakis P, Tunbridge L.** Borehole KLX04A Determination of P-wave velocity, transverse borehole core.
- P-04-267 **Adi-Zarrabi B.** Drill hole KLX04A Thermal properties: heat conductivity and heat capacity determined using the TPS method and Mineralogical composition by modal analysis.
- P-04-268 **Savukoski M.** Drill hole KLX04. Determining of porosity by water saturation and density by buoyancy technique. Oskarshamn site investigation.
- P-04-269 **Åkesson U.** Drill hole KLX04. Extensometer measurement of the coefficient of thermal expansion of rock.
- P-04-270 **Adi-Zarrabi B.** Drill hole KAV04A. Thermal properties; heat conductivity and heat capacity determined using the TPS method and mineralogical composition by modal analysis.
- P-04-271 **Savukoski M.** Drill hole KAV04A. Determining of porosity by water saturation and density by buoyancy technique. Oskarshamn site investigation.
- P-04-272 **Åkesson U.** Drill hole: KAV04A. Extensometer measurement of the coefficient of thermal expansion of rock. Oskarshamn site investigation.
- P-04-273 **Nilsson G.** Investigation of sediments, peat lands and wetlands. Stratigraphical and analytical data.
- P-04-274 **Cronquist T, Forssberg O, Maersk Hansen L, Jonsson A, Koyi S, Leiner P, Sävås J, Vestgård J.** Detailed fracture mapping of two outcrops at Laxemar.
- P-04-275 **Gustafsson J, Gustafsson C.** Oskarshamn site investigation. RAMAC and BIPS logging in boreholes KLX03, HAV11 to HAV13 and HLX21 to HLX25. Revised April 2006.
- P-04-277 **Nyborg M, Vestin E, Wilén P.** Oskarshamns site investigation. Hydrogeological inventory in the Oskarshamn area.
- P-04-279 **Gustafsson J, Gustafsson C.** Oskarshamn site investigation. RAMAC and BIPS logging in boreholes HLX17, HLX18 and HLX19.
- P-04-280 **Nielsen U T, Horn F.** Geophysical borehole logging in borehole KLX03, HLX21, HLX22, HLX23, HLX24 and HLX25.
- P-04-281 **Wacker P, Berg C.** Water sampling in KSH02A. Summary of water sampling analysis in connection with Pipe String System (PSS) and Single Well Injection Withdrawal (SWIW) measurements.
- P-04-284 **Mattsson H, Keisu M.** Oskarshamn site investigation. Interpretation of geophysical borehole data from HLX17, HLX18 and HLX19.
- P-04-287 **Rahm N, Enachescu C.** Hydraulic testing of percussion drilled lineament boreholes on Ävrö and Simpevarp, 2004.
- P-04-288 **Rahm N, Enachescu C.** Hydraulic injection tests in borehole KLX02, 2003. Sub-area Laxemar.
- P-04-289 **Rahm N, Enachescu C.** Hydraulic injection tests in borehole KSH01A, 2003/2004. Sub-area Simpevarp.
- P-04-290 **Rahm N, Enachescu C.** Hydraulic injection tests in borehole KSH03, 2004, Sub-area Simpevarp.
- P-04-291 **Rahm N, Enachescu C.** Hydraulic injection tests in borehole KAV04A, 2004. Sub-area Simpevarp.
- P-04-292 **Rahm N, Enachescu C.** Hydraulic injection tests in borehole KLX04, 2004. Sub-area Laxemar.
- P-04-294 **Mattsson H, Thunehed H, Triumf C-A.** Compilation of petrophysical data from rock samples and in situ gamma-ray spectrometry measurements. Stage 2 – 2004 (including 2002).
- P-04-297 **Gustafsson J, Gustafsson C.** Oskarshamn site investigation. RAMAC and BIPS logging in boreholes HLX10, HLX26, HLX27 and HLX28.
- P-04-298 **Lindqvist, G.** Refraction seismic measurements in Laxemar autumn 2004. Oskarshamn site investigation.
- P-04-299 **Berg C, Wacker P.** Hydrochemical logging in KLX03A.
- P-04-304 **Berg C.** Hydrochemical logging in KAV04A. Results from isotope determinations (3H, d2H and d18O). Oskarshamn site investigation
- P-04-306 **Nielsen U T, Ringgaard J, Horn F.** Geophysical borehole logging in boreholes KLX04, HLX26, HLX27 and HLX28,
- P-04-308 **Carlsten S, Hultgren P, Mattsson H, Stanfors R, Wahlgren C-H.** Geological single-hole interpretation of KAV04A, KAV04B, KLX01 and HLX15.

- P-04-309 **Carlsten S, Hultgren P, Mattsson H, Stanfors R, Wahlgren C-H.** Oskarshamn site investigation. Geological single-hole interpretation of KLX04, HLX21, HLX22, HLX23, HLX24 and HLX25.
- P-04-310 **Lindfors U.** Hydraulic fracturing and HTPF rock stress measurements in borehole KSH01A. Oskarshamn site investigation.
- P-04-315 **Alling V, Andersson P, Fridriksson G, Rubio Lind C.** Estimation of biomass and primary production of birch. Birch biotopes in Forsmark and Oskarshamn.
- P-04-316 **Alling V, Andersson P, Fridriksson G, Rubio Lind C.** Biomass production of Common reed (*Phragmites australis*), infauna, epiphytes, sessile epifauna and mobile epifaunal, Common reed biotopes in Oskarshamn's model area.
- P-04-317 **Johansson T, Adestam L.** Drilling and sampling in soil. Installation of groundwater monitoring wells in the Laxemar area.
- P-04-318 **Johansson T, Adestam L.** Slug tests in groundwater monitoring wells in soil in the Laxemar area.
- P-05-02 **Chryssanthakis P.** Borehole KLX03A. Tilt testing. Oskarshamn site investigation.
- P-05-03 **Chryssanthakis P, Tunbridge L.** Borehole KLX03A. Determination of P-wave velocity, transverse borehole core.
- P-05-05 **Jacobsson L.** Oskarshamn Site Investigation – Drill hole KAV01, Normal loading and shear tests on joints.
- P-05-06 **Jacobsson L.** Oskarshamn Site Investigation – Drill hole KSH01A, Normal loading and shear tests on joints.
- P-05-07 **Jacobsson L.** Oskarshamn Site Investigation – Drill hole KSH02, Normal loading and shear tests on joints.
- P-05-16 **Rahm N, Enachescu C.** Pumping tests and water sampling in borehole KLX04, 2004. Sub-area Laxemar.
- P-05-18 **Gustavsson E, Gunnarsson M.** Oskarshamn site investigation. Laboratory data from the site investigation programme for the transport properties of the rock. Boreholes KSH01A, KSH02 and KLX02.
- P-05-20 **Gustafsson E, Ludvigson J-E.** Combined interference test and tracer test between KLX02 and HLX10.
- P-05-22 **Ehrenborg J, Stejskal V.** Boremap mapping of core drilled boreholes KAV04A and KAV04B.
- P-05-23 **Ehrenborg J, Dahlin P.** Boremap mapping of core drilled borehole KLX04.
- P-05-24 **Ehrenborg J, Dahlin P.** Boremap mapping of core drilled borehole KLX03.
- P-05-25 **Ask H, Morosini M, Samuelsson L-E, Ekström L, Håkansson N.** Drilling of cored borehole KAV04.
- P-05-19 **Thunehead H.** Resistivity measurements on samples from KLX02. Oskarshamn site investigation.
- P-05-27 **Löfgren M, Neretnieks I.** Oskarshamn site investigation. Formation factor logging *in situ* and in the laboratory by electrical methods in KSH01A and KSH02. Measurements and evaluation of methodology.
- P-05-28 **Gustafsson E, Nordqvist R.** Groundwater flow measurements and SWIW tests in boreholes KLX02 and KSH02.
- P-05-30 **Gustafsson J, Gustafsson C.** Oskarshamn site investigation. RAMAC and BIPS logging in borehole KLX06. Revised April 2006.
- P-05-31 **Nielsen U T, Ringgaard J, Horn F.** Oskarshamn site investigation. Geophysical borehole logging in borehole KLX06.
- P-05-34 **Mattsson H, Thunehead H, Keisu M.** Interpretation of geophysical borehole measurements and compilation of petrophysical data from KLX01, KLX03, KLX04, HLX21, HLX22, HLX23, HLX24, HLX25, HLX26, HLX27 and HLX28.
- P-05-35 **Elhammer A, Sandkvist Å.** Detailed marine geological survey of the sea bottom outside Simpevarp.
- P-05-38 **Carlsten S, Hultgren P, Mattsson H, Stanfors R, Wahlgren C-H.** Oskarshamn site investigation. Geological single-hole interpretation of KLX03, HLX26 and HLX27.
- P-05-40 **Carlsson T, Brunberg A-K, Brydsten L, Strömberg M.** Characterisation of running waters, including vegetation, substrate and technical encroachments.
- P-05-42 **Green M.** Bird monitoring in Simpevarp 2002-2004.
- P-05-44 **Mattsson H.** Interpretation of geophysical borehole measurements from KLX06.
- P-05-45 **Fredriksson R.** Inventory of the marine fauna attached to hard substrates in the Simpevarp area. Oskarshamn site investigation.
- P-05-47 **Bergman T, Malmberg Persson K, Persson M, Albrecht J.** Oskarshamn site investigation. Characterisation of bedrock and quaternary deposits from excavations in the southern part of Laxemar subarea.
- P-05-49 **Rudmark L, Malmberg-Persson K, Mikko H.** Investigation of Quaternary deposits 2003-2004.
- P-05-54 **Berg C.** Hydrochemical logging in KSH03A. Results from isotope determinations (³H, dD, d18O and d37Cl). Oskarshamn site investigation.
- P-05-55 **Ask H, Samuelsson L-E, Zetterlund M.** Percussion drilling of boreholes HLX21, HLX22, HLX23, HLX24, HLX25, HLX30, HLX31 and HLX33 for investigation of lineament EW007.
- P-05-57 **Enderlein O.** The abundance of nightly pelagic fish in the Baltic Sea outside Simpevarp nuclear power station. Oskarshamn site investigation.

- P-05-65 **Forssman I, Zetterlund M, Forsmark T, Rhén I.** Oskarshamn site investigation. Correlation of Posiva Flow Log anomalies to core mapped features in KSH01A, KSH02A and KAV01.
- P-05-67 **Rouhiainen P, Pöllänen J, Sokolnicki M.** Difference flow logging of borehole KLX 03. Subarea Laxemar.
- P-05-68 **Rouhiainen P, Sokolnicki M.** Difference flow logging of borehole KLX04.
- P-05-69 **Sjöberg J, Perman F.** Overcoring rock stress measurements in borehole KLX04. Oskarshamn site investigation.
- P-05-70 **Svensson J.** Fältundersökning av diskrepanser gällande vattendrag i GIS-modellen. Platsundersökning Oskarshamn.
- P-05-74 **Sokolnicki M, Rouhianien P.** Oskarshamn site investigation. Difference flow logging of borehole KLX06. Sub-area Laxemar.
- P-05-75 **Thunehed H.** Resistivity measurements and determination of formation factors on samples from LX04 and KSH02.
- P-05-80 **Löfgren A.** Estimation of biomass and net primary production in field and ground layer, and biomass in litter layer of different vegetation types in Forsmark and Oskarshamn. Oskarshamn/Forsmark site investigation.
- P-05-82 **Gustafsson J, Gustafsson C.** Oskarshamn site investigation. RAMAC and BIPS logging in boreholes KLX05 and HLX32.
- P-05-83 **Sigurdsson O.** Oskarshamn site investigation Simplified Boremap mapping of percussion boreholes HLX15, HLX26, HLX27, HLX28 and HLX32 on lineament NW042.
- P-05-85 **Berg C.** Hydrochemical logging in KLX06. Oskarshamn site investigation.
- P-05-87 **Andersson J.** Investigation of the amount of dead wood. Oskarshamn site investigation.
- P-05-88 **Berg C.** Hydrochemical logging in KLX04 Results from isotope determinations (3H, δD and $\delta 18O$).
- P-05-89 **Berg C.** Hydrochemical logging in KLX03 Results from isotope determinations (3H, δD and $\delta 18O$).
- P-05-90 **Jacobsson L.** Borehole KLX03A. Uniaxial compression test of intact rock. Oskarshamn site investigation,
- P-05-91 **Jacobsson L.** Drill hole KLX03A. Indirect tensile strength test. Oskarshamn site investigation.
- P-05-92 **Jacobsson L, Flansbjerg M.** Borehole KLX03A. Normal loading and shear tests on joints. Oskarshamn site investigation.
- P-05-93 **Adi-Zarrabi B.** Drill hole KLX03A. Thermal properties: heat conductivity and heat capacity determined using the TPS method. Oskarshamn site investigation.
- P-05-94 **Savukoski M.** Drill hole KLX03. Determining of porosity by water saturation and density by buoyancy technique. Oskarshamn site investigation.
- P-05-95 **Åkesson U.** Drill hole KLX03. Extensometer measurement of the coefficient of thermal expansion of rock. Oskarshamn site investigation.
- P-05-96 **Jacobsson L, 2005.** Borehole KLX03A. Triaxial compression test of intact rock. Oskarshamn site investigation.
- P-05-104 **Sigurdsson O.** Oskarshamn site investigation. Simplified Boremap mapping of percussion boreholes HLX17, HLX18 and HLX19.
- P-05-105 **Löfgren M, Neretnieks I.** Formation factor logging in-situ by electrical methods in KLX03 and KLX04.
- P-05-106 **Börjesson S, Gustavsson E.** Laboratory data from the site investigation programme for the transport properties of the rock. Data delivery for data freeze Laxemar 2.1. Oskarshamn site investigation.
- P-05-111 **Ask H, Morosini M, Samuelsson L-E, Ekström L, Håkanson N.** Drilling of cored borehole KLX04.
- P-05-118 **Ericsson U, Engdahl A.** Oskarshamn site investigation – Surface water sampling at Simpevarp 2004.
- P-05-126 **Adi-Zarrabi B.** Drill hole KLX05A. Thermal properties: heat conductivity and heat capacity determined using the TPS method. Oskarshamn site investigation.
- P-05-127 **Savukoski M.** Drill hole KLX05. Determining of porosity by water saturation and density by buoyancy technique. Oskarshamn site investigation.
- P-05-128 **Jacobsson L.** Borehole KLX06A. Triaxial compression test of intact rock. Oskarshamn site investigation.
- P-05-129 **Adi-Zarrabi B.** Drill hole KLX06A. Thermal properties: heat conductivity and heat capacity determined using the TPS method. Oskarshamn site investigation.
- P-05-130 **Liedberg L.** Drill hole KLX06. Determining of porosity by water saturation and density by buoyancy technique. Oskarshamn site investigation.
- P-05-143 **Löfgren M, Pettersson M.** Formation factor logging in situ by electrical methods in KLX05 and KLX06. Oskarshamn site investigation.
- P-05-144 **Nielsen U T, Ringgaard J, Dahl J F.** Oskarshamn site investigation. Geophysical borehole logging in boreholes KLX05 and HLX32.
- P-05-146 **Jacobsson L, Flansbjerg M.** Borehole KLX06A. Normal loading and shear tests on joints. Oskarshamn site investigation.
- P-05-155 **Lindqvist G.** Oskarshamn site investigation. Refraction seismic measurements in Laxemar spring 2005.
- P-05-160 **Sokolnicki M, Rouhiainen P.** Difference flow logging of borehole KLX05. Subarea Laxemar. Oskarshamn site investigation.

- P-05-161 **Gustafsson J, Gustafsson C.** Oskarshamn site investigation. RAMAC directional logging in borehole KLX05 and RAMAC and BIPS logging in borehole HLX20. Revised April 2006.
- P-05-162 **Sigurdsson O.** Oskarshamn site investigation. Simplified Boremap mapping of percussion boreholes HAV11, HAV12 and HAV13.
- P-05-163 **Sigurdsson O.** Oskarshamn site investigation. Simplified Boremap mapping of percussion borehole HLX20 on lineament EW002.
- P-05-164 **Sigurdsson O.** Oskarshamn site investigation. Simplified Boremap mapping of percussion boreholes HLX13, HLX21, HLX22, HLX23, HLX24, HLX25, HLX30, HLX31 and HLX33 on lineament EW007.
- P-05-167 **Ask H, Morosini M, Samuelsson L-E, Ekström L, Håkanson N.** Drilling of cored borehole KLX03.
- P-05-169 **Dinges C.** Laxemar, surface samples. Thermal properties: heat conductivity and heat capacity of surface samples determined using the TPS method. Oskarshamn site investigation.
- P-05-173 **Aquilonius K.** Vegetation in lake Frisksjön.
- P-05-174 **Drake H, Tullborg E-L.** Fracture mineralogy and wall rock alteration. Results from drill cores KAS04, KA1755A and KLX02.
- P-05-175 **Ericsson U.** Precipitation at Simpevarp 2004. Oskarshamn site investigation.
- P-05-179 **Mattsson H, Triumf C-A, Lindqvist G.** Oskarshamn site investigation. Re-interpretation of the refraction seismic profiles 277, 280 and 506 by use of Wavepath Eikonal Traveltime Tomography. A comparison with the traditional interpretation technique.
- P-05-180 **Wahlgren C-H, Bergman T, Persson Nilsson K, Eliasson T, Ahl M, Ekström M.** Bedrock map of the Laxemar subarea and surroundings. Description of rock types, modal and geochemical analyses, including the cored boreholes KLX03, KSH03 and KAV01.
- P-05-181 **Braathen A, Nordgulen Ö.** Oskarshamn site investigation. Structural investigations of deformation zones (ductile shear zones and faults) around Oskarshamn – a pilot study.
- P-05-184 **Rahmn N, Enachescu C.** Pumping tests and hydraulic injection tests in borehole KLX06.
- P-05-185 **Ehrenborg J, Dahlin P.** Oskarshamn site investigation. Boremap mapping of core drilled borehole KLX06.
- P-05-188 **Thunehed H, Triumf C-A.** Oskarshamn site investigation. Detailed ground geophysical survey at Laxemar. Magnetic total field and resistivity.
- P-05-189 **Mattsson H, Keisu M.** Interpretation of geophysical borehole measurements from KLX05.
- P-05-190 **Ask H, Zetterlund M.** Percussion drilling of boreholes HLX16, HLX17, HLX18 and HLX19.
- P-05-192 **Rahm N, Enachescu C.** Hydraulic injection tests in borehole KLX03, 2005. Subarea Laxemar.
- P-05-193 **Morosini M, Ludvigson J-E.** Hydraulic characterisation of deformation zone EW007, Subarea Laxemar.
- P-05-194 **Sigurdsson O, Ekström L.** Percussion drilling of boreholes HSH04, HSH05, HSH06, HAV11, HAV12, HAV13 and HAV14.
- P-05-195 **Berg C.** Hydrochemical logging in KLX05. Oskarshamn site investigation.
- P-05-198 **Nilsson A-C.** Översikt över provhanterings- och analysrutiner för vattenprov. Platsundersökningar i Forsmark och Oskarshamn
- P-05-205 **Nyberg G, Wass E, Askling P.** Groundwater monitoring program. Report for December 2002 – October 2004. Oskarshamn site investigation-
- P-05-207 **Liedberg L.** Drill hole KLX07A. Determining of porosity by water saturation and density by buoyancy technique. Oskarshamn site investigation.
- P-05-208 **Adi-Zarrabi B.** Drill hole KLX07A. Thermal properties: heat conductivity and heat capacity determined using the TPS method. Oskarshamn site investigation.
- P-05-209 **Jacobsson L, Flansbjer M.** Borehole KLX07A. Shear tests on sealed joints. Oskarshamn site investigation.
- P-05-222 **Rahm N, Enachescu C.** Hydraulic injection tests in borehole KLX05, 2005. Subarea Laxemar.
- P-05-223 **Nyborg M.** Oskarshamn site investigation. Aerial photography and airborne laser scanning Laxemar-Simpevarp. The 2005 campaign.
- P-05-224 **Ehrenborg J, Dahlin P.** Oskarshamn site investigation. Boremap mapping of core drilled boreholes KLX05.
- P-05-225 **Sokolnicki M, Rouhianien P.** Oskarshamn site investigation. Difference flow logging of borehole KLX07A and KLX07B. Sub-area Laxemar.
- p-05-226 **Berg C.** Hydrochemical logging in KLX07a. Oskarshamn site investigation.
- P-05-227 **Lärke A, Hillgren R, Wern L, Jones J, Aquilonius K.** Hydrological and meteorological monitoring at Oskarshamn during 2003–2004. Oskarshamn site investigation.
- P-05-228 **Nielsen U T, Ringgaard J, Fris Dahl J.** Oskarshamn site investigation. Geophysical borehole logging in boreholes KLX07A, KLX07B, HLX20, HLX34 and HLX35.
- P-05-230 **Berg C.** Hydrochemical logging in KLX08. Oskarshamn site investigation.
- P-05-231 **Gustafsson J, Gustafsson C.** Oskarshamn site investigation. RAMAC and BIPS logging in boreholes KLX07A, KLX07B, HLX34 and HLX35 and deviation logging in boreholes KLX07B, HLX34 and HLX35. Revised April 2006.
- P-05-233 **Ask H, Morosini M, Samuelsson L-E, Ekström L, Håkansson N.** Oskarshamn site investigation. Drilling of cored borehole KLX05.

- P-05-234 **Ask H, Morosini M, Samuelsson L-E, Ekström L, Håkansson N.** Oskarshamn site investigation. Drilling of cored borehole KLX06.
- P-05-237 **Sigurdsson O, Ask H, Zetterlund M.** Percussion drilling of boreholes HLX34 and HLX35.
- P-05-238 **Bosson E, Berglund S.** Kontroll och inmätning av diken i potentiella utströmningsområden i Laxemar. Valideringstest av yhydrologisk modellering (in Swedish, with Abstract in English).
- P-05-240 **Gustafsson J, Gustafsson C.** Oskarshamn site investigation. RAMAC, BIPS and deviation logging in boreholes KLX08, HLX30 and HLX33.
- P-05-241 **Forssman I, Zetterlund M, Forsmark T, Rhén I.** Correlation of Posiva Flow Log anomalies to core mapped features in KLX02, KLX03, KLX04, KAV04A and KAV04B.
- P-05-244 **Berg C.** Hydrochemical logging in KLX06. Results from isotope determinations (3H, dD and d18O). Oskarshamn site investigation.
- P-05-247 **Korhonen K, Kuivamäki A, Ruotoistenmäki T, Paananen M.** Interpretation of lineaments from airborne geophysical and topographic data. An alternative model within version Laxemar 1.2 of the Oskarshamn modelling project.
- P-05-259 **Mattsson H, Keisu M.** Oskarshamn site investigation. Interpretation of geophysical borehole measurements from KLX07A, KLX07B, HLX20, HLX32, HLX34 and HLX35.
- P-05-260 **Forsberg O, Cronquist T, Hansen L, Vestgård J.** Oskarshamn site investigation. Detailed outcrop mapping at the drill site of KLX09 in Laxemar.
- P-05-263 **Ehrenborg J, Dahlin P.** Oskarshamn site investigation. Boremap mapping of core drilled boreholes KLX07A and KLX07B.
- P-05-267 **Sokolnicki M, Pöllänen J.** Difference flow logging of borehole KLX08. Subarea Laxemar. Oskarshamn site investigation.
- P-05-270 **Nielsen U T, Ringgaard J.** Oskarshamn site investigation. Geophysical borehole logging in boreholes KLX08, HLX30, HLX31 and HLX33.
- P-05-273 **Rahm N, Enachescu C.** Hydraulic injection tests in borehole KLX07A, 2005 Laxemar.
- P-05-275 **Ask H.** Percussion drilling of boreholes HLX36 and HLX37 for investigation of lineament NS001.
- P-05-279 **Sigurdsson O.** Oskarshamn site investigation. Simplified Boremap mapping of percussion boreholes HLX34 and HLX35 on lineament NS059 and of percussion boreholes HLX36 and HLX37 on lineament NS001.
- P-05-279 **Sigurdsson O.** Oskarshamn site investigation. Simplified Boremap mapping of percussion boreholes HLX34 and HLX35 on lineament NS059 and of percussion boreholes HLX36 and HLX37 on lineament NS001. Revised March 2008.
- P-05-282 **Nyberg H, Wass E.** Oskarshamn site investigation. Groundwater monitoring program – Report for November 2004–June 2005.
- P-06-01 **Drake H, Tullborg E-L.** Oskarshamn site investigation. Mineralogical, chemical and redox features of red-staining adjacent to fractures. Results from drill cores KSH01A+B and KSH03A+B.
- P-06-02 **Drake H, Tullborg E-L.** Oskarshamn site investigation. Mineralogical, chemical and redox features of red-staining adjacent to fractures. Results from drill core KLX04.
- P-06-03 **Drake H, Tullborg, E-L.** Oskarshamn site investigation. Fracture mineralogy. Results from drill core KSH03A+B.
- P-06-04 **Drake H, Tullborg E-L.** Oskarshamn site investigation. Fracture mineralogy of the Götemar granite. Results from drill cores KKR01, KKR02 and KKR03.
- P-06-05 **Strömgren M, Brydsten L, Lindgren F.** Oskarshamn site investigation. Measurements of brook gradients.
- P-06-06 **Cronquist T, Forsberg O, Hansen L, Koyi S, Vestgård J, Wikholm M.** Oskarshamn site investigation. Detailed outcrop mapping on drillsite KLX11.
- P-06-07 **Wahlgren C-H, Bergman T, Ahl M, Ekström M.** Oskarshamn site investigation. Modal and geochemical analyses of drill core samples 2005. Classification of rock types in KLX03, KLX04, KLX06, KLX07A, KLX07B, KLX08 and KLX10.
- P-06-08 **Bergelin A, Berg C, Wacker P.** Complete chemical characterisation in KLX03. Results from four investigated borehole sektionen: 193.5–198.4 m, 408.0–415.3 m, 735.5–748.0 m, 964.5–975.2 m. Oskarshamn site investigation.
- P-06-10 **Adill A, Andersson J.** Estimation of fish community biomass in Borholmsfjärden, NW Baltic Proper. Oskarshamn site investigation.
- P-06-12 **Waber N, Smellie J.** Borehole KLX03: Characterisation of pore water Part 1: Methodology and analytical data. Oskarshamn site investigation.
- P-06-13 **Ericsson U, Engdahl A.** Sampling of shallow ground water at Simpevarp 2004. Oskarshamn site investigation.
- P-06-14 **Ask H, Morosini M, Samuelsson L-E, Ekström L, Håkansson N.** Oskarshamn site investigation. Drilling of cored boreholes KLX07A and KLX07B.
- P-06-16 **Berg C.** Hydrochemical logging in KLX07A. Results from isotope determinations (3H, dD and d18O). Oskarshamn site investigation.
- P-06-17 **Berg C.** Hydrochemical logging in KLX05A. Results from isotope determinations (3H, dD and d18O). Oskarshamn site investigation.
- P-06-19 **Lärke A, Hillgren R, Wern L, Jones J.** Oskarshamn site investigation. Hydrological and meteorological monitoring at Oskarshamn, November 2004 until June 2005.

- P-06-20 **Nielsen U T, Ringgaard J, Fris Dahl J.** Oskarshamn site investigation. Geophysical borehole logging in borehole KLX10.
- P-06-21 **Thunehed H, Pitkänen T.** Oskarshamn site investigation. Transient electromagnetic soundings at Laxemar and the regional surroundings. Estimations of depth to saline groundwater.
- P-06-30 **Savukoski M.** Borehole KLX08. Determining of porosity by water saturation and density by buoyancy technique. Oskarshamn site investigation.
- P-06-31 **Adl-Zarrabi B.** Borehole KLX08 Thermal conductivity and thermal diffusivity determined using the TPS method. Oskarshamn site investigation.
- P-06-32 **Jacobsson L.** Borehole KLX08. Uniaxial compression test of intact rock. Oskarshamn site investigation.
- P-06-34 **Chryssanthakis P.** Borehole KLX10. Tilt testing. Oskarshamn site investigation.
- P-06-35 **Savukoski M.** Borehole KLX10. Determining of porosity by water saturation and density by buoyancy technique. Oskarshamn site investigation.
- P-06-36 **Adl-Zarrabi B.** Borehole KLX10. Thermal conductivity and thermal diffusivity determined using the TPS method. Oskarshamn site investigation.
- P-06-37 **Jacobsson L.** Borehole KLX10. Uniaxial compression test of intact rock. Oskarshamn site investigation.
- P-06-38 **Jacobsson L.** Drill hole KLX10. Indirect tensile strength test. Oskarshamn site investigation.
- P-06-39 **Jacobsson L, Flansbjerg M.** Borehole KLX10. Normal loading and shear tests on joints. Oskarshamn site investigation.
- P-06-40 **Jacobsson L.** Borehole KLX10. Triaxial compression test of intact rock. Oskarshamn site investigation.
- P-06-42 **Dahlin P, Ehrenborg J.** Oskarshamn site investigation. Boremap mapping of core drilled borehole KLX08.
- P-06-47 **Berg C, Gustavsson E.** Hydrochemical logging in KLX09. Oskarshamn site investigation.
- P-06-48 **Dahlin P, Ehrenborg J.** Oskarshamn site investigation. Boremap mapping of core drilled borehole KLX08.
- P-06-49 **Lindqvist G.** Oskarshamn site investigation. Refraction seismic measurements in Laxemar spring 2006.
- P-06-50 **Gustafsson J, Gustafsson C.** Oskarshamn site investigation. RAMAC and BIPS logging in boreholes KLX10 and HLX31.
- P-06-51 **Dahlin P, Mattsson K, Ehrenborg J.** Oskarshamn site investigation. Boremap mapping of telescopic drilled borehole KLX10.
- P-06-58 **Sokolnicki M.** Oskarshamn site investigation. Difference flow logging of borehole KLX10. Sub-area Laxemar.
- P-06-61 **Askling P, Andersson P.** Groundwater flow measurements in permanent installed boreholes. Test campaign no. 1, 2005. Oskarshamn site investigation.
- P-06-62 **Penttinen L, Siitari-Kauppi M, Ikonen J.** Quantitative mapping of fracture minerals in Laxemar. Oskarshamn site investigation.
- P-06-65 **Mattsson H, Keisu M.** Oskarshamn site investigation. Interpretation of geophysical borehole measurements from KLX08, HLX30, HLX31 and HLX33.
- P-06-71 **Savukoski, M.** Borehole KLX12A. Determining of porosity by water saturation and density by buoyancy technique. Oskarshamn site investigation.
- P-06-72 **Adl-Zarrabi B.** Borehole KLX12A. Thermal properties of rocks using calorimeter and TPS method. Oskarshamn site investigation.
- P-06-73 **Jacobsson L.** Borehole KLX12A. Uniaxial compression test of intact rock. Oskarshamn site investigation.
- P-06-74 **Jacobsson L.** Drill hole KLX12A. Indirect tensile strength test. Oskarshamn site investigation.
- P-06-75 **Jacobsson L, Flansbjerg M.** Borehole KLX12A. Normal loading and shear tests on joints. Oskarshamn site investigation.
- P-06-76 **Jacobsson L.** Borehole KLX12A. Triaxial compression test of intact rock. Oskarshamn site investigation.
- P-06-77 **Waber N, Smellie J.** Borehole KLX03: Characterisation of pore water. Part 2: Rock properties and diffusion experiments. Oskarshamn site investigation.
- P-06-82 **Petersson J, Skogsmo G, Berglund J, Strähle A.** Oskarshamn site investigation. Comparative geological logging with the Boremap system: 9.6–132.2 m of borehole KLX07B.
- P-06-99 **Gustafsson J, Gustafsson C.** Oskarshamn site investigation. RAMAC, BIPS and deviation logging in boreholes KLX09B, KLX09C, KLX09D, KLX09E, KLX09F and KLX09G.
- P-06-100 **Mattsson H.** Oskarshamn site investigation. The magnetic anisotropy of rocks across two major deformation zones in the Laxemar and Simpevarp area.
- P-06-116 **Ask H, Morosini M, Samuelsson L-E, Ekström L, Håkansson N.** Oskarshamn site investigation. Drilling of cored borehole KLX10.
- P-06-117 **Stanfors R.** Review of existing information from the Äspö HRL area, with focus on hydraulically important minor structures.

- P-06-118 **Lundberg E, Sjöström H.** Oskarshamn site investigation. Kinematic analysis of ductile and brittle/ductile shear zones in Simpevarp and Laxemar subarea.
- P-06-121 **Sohlenius G, Bergman T, Snäll S, Lundin L, Lode E, Stendahl J, Riise A, Nilsson J, Johansson T, Göransson M.** Oskarshamn site investigation. Soils, Quaternary deposits and bedrock in topographic lineaments situated in the Laxemar subarea.
- P-06-124 **Mattsson H, Keisu M.** Oskarshamn site investigation. Interpretation of geophysical borehole measurements from KLX09.
- P-06-127 **Wacker P.** Hydrochemical monitoring programme for core drilled boreholes 2005. Summary of analyses from water sampling. Oskarshamn site investigation.
- P-06-128 **Carlsten S, Hultgren P, Mattsson H, Stanfors R, Wahlgren C-H.** Oskarshamn site investigation. Geological single-hole interpretation of KLX05, HLX15, HLX18, HLX19 and HLX32.
- P-06-129 **Carlsten S, Hultgren P, Mattsson H, Stanfors R, Wahlgren C-H.** Oskarshamn site investigation. Geological single-hole interpretation of KLX06, HLX13, HLX17 and HLX28.
- P-06-137 **Thunehed H, Triumf C-A.** Oskarshamn site investigation. Detailed ground geophysics at Laxemar, autumn/winter 2005/2006. Magnetic total field and resistivity.
- P-06-142 **Nilsson K.** Hydrochemical logging in KLX12A. Oskarshamn site investigation.
- P-06-144 **Sohlenius G, Hedenström A, Nyman H.** Characterisation of Quaternary deposits in Lake Frisksjön and Skettkärrret. Oskarshamn site investigation.
- P-06-145 **Enachescu C, Böhner J, Rohs S.** Hydraulic interference tests, pumping borehole KLX07A Subarea Laxemar.
- P-06-147 **Rohs S.** Flow logging in boreholes HLX21, HLX35 and HLX38 Subarea Laxemar.
- P-06-148 **Harrström J, Ludvigson J, Hjerne C.** Hydraulic injection tests in borehole KLX12A Subarea Laxemar.
- P-06-149 **Johansson T, Göransson M.** Oskarshamn site investigation. Slug tests in groundwater monitoring wells SSM000222–SSM000230 in soil – Subarea Laxemar.
- P-06-150 **Svensson J, Zetterlund M.** Oskarshamn site investigation. Complementary slug tests in groundwater monitoring wells February 2006 – Subareas Laxemar and Simpevarp.
- P-06-151 **Morosini M, Wass E.** Oskarshamn site investigation. Hydraulic interference and tracer testing of a rock-soil aquifer system between HLX35 and HLX34, SSM000037, SSM000222 and SSM000223 – Subarea Laxemar.
- P-06-154 **Nielsen U T, Ringgaard J, Fris D.** Oskarshamn site investigation. Geophysical borehole logging in borehole KLX09.
- P-06-155 **Ericsson U, Engdahl A.** Surface water sampling at Simpevarp 2005.
- P-06-156 **Gustafsson J, Gustafsson C.** Oskarshamn site investigation. RAMAC and BIPS logging in borehole KLX11A.
- P-06-157 **Mattsson H.** Oskarshamn site investigation. Interpretation of geophysical borehole measurements from KLX11A. Revised September 2006.
- P-06-159 **Gustafsson J, Gustafsson C.** Oskarshamn site investigation. RAMAC, BIPS and deviation logging in boreholes KLX11B, KLX11C, KLX11D, KLX11E, KLX11F, KLX18A, KLX20A, HLX38 and HLX40 and BIPS and deviation logging in KLX19A.
- P-06-162 **Mattsson H.** Oskarshamn site investigation. Interpretation of geophysical borehole measurements and petrophysical data from KLX10.
- P-06-163 **Waber N, Smellie J.** Borehole KLX08. Characterisation of pore water. Part 1: Methodology and analytical data. Oskarshamn site investigation.
- P-06-164 **Väisäsvaara J, Heikkinen P, Kristiansson S, Pöllänen J.** Oskarshamn site investigation. Difference flow logging of borehole KLX09. Sub-area Laxemar.
- P-06-167 **Gustafsson J, Gustafsson C, Friborg J.** Oskarshamn site investigation. RAMAC and BIPPS logging in boreholes KLX10B, KLX10C and KLX12A.
- P-06-174 **Carlsten S, Hultgren P, Mattsson H, Stanfors R, Wahlgren C-H.** Oskarshamn site investigation. Geological single-hole interpretation of KLX10, HLX20 and HLX36.
- P-06-175 **Carlsten S, Hultgren P, Mattsson H, Stanfors R, Wahlgren C-H.** Oskarshamn site investigation. Geological single-hole interpretation of KLX07A, KLX07B, HLX34 and HLX35.
- P-06-176 **Carlsten S, Strähle A, Hultgren P, Mattsson H, Stanfors R, Wahlgren C-H.** Oskarshamn site investigation. Geological single-hole interpretation of KLX08.
- P-06-180 **Lindquist A, Nilsson K.** Hydrochemical logging in KLX11A. Oskarshamn site investigation.
- P-06-181 **Nilsson K.** Hydrochemical logging in KLX20A. Oskarshamn site investigation
- P-06-182 **Harrström J, Ludvigson J, Hjerne C.** Single-hole injection tests in borehole KLX10.
- P-06-183 **Kristiansson S.** Oskarshamn site investigation. Difference flow logging of borehole KLX20A. Sub-area Laxemar.
- P-06-184 **Sokolnicki M, Kristiansson S.** Difference flow logging of borehole KLX18A Subarea Laxemar. Oskarshamn site investigation.
- P-06-185 **Väisäsvaara J, Heikkinen P, Kristiansson S, Pöllänen J.** Oskarshamn site investigation. Difference flow logging of borehole KLX12A. Sub-area Laxemar.
- P-06-197 **Nielsen U T, Ringgaard J.** Oskarshamn site investigation. Geophysical borehole logging in boreholes KLX11A, HLX36 and HLX37.

- P-06-198 **Nielsen U T, Ringgaard J.** Oskarshamn site investigation. Geophysical borehole logging in boreholes KLX12A, KLX09G, KLX10B and KLX10C.
- P-06-199 **Sokolnicki M, Väisäsvaara J.** Oskarshamn site investigation. Difference flow logging of borehole KLX09B–F. Sub-area Laxemar.
- P-06-201 **Enachescu C, Rohs S, Wolf P.** Hydraulic injection tests in borehole KLX11A Subarea Laxemar.
- P-06-222 **Ask H, Morosini M, Samuelsson L-E, Ekström L, Håkansson N.** Oskarshamn site investigation. Drilling of cored borehole KLX08.
- P-06-225 **Enachescu C, Rohs S, van der Wall R.** Hydraulic injection tests in borehole KLX18A Subarea Laxemar.
- P-06-229 **Väisäsvaara J, Leppänen H, Kristiansson S, Pöllänen J.** Oskarshamn site investigation. Difference flow logging of borehole KLX09G, KLX10B and KLX10C. Sub-area Laxemar.
- P-06-232 **Andersson E, Karlsson S, Söderbäck B, Wijnblad E.** Biomass of benthic and planktonic bacteria in Laxemar and Forsmark and biomass of Reed (*Phragmites australis*) in Lake Frisksjön. Oskarshamn and Forsmark site investigation.
- P-06-236 **Mattsson K-J, Eklund S.** Oskarshamn site investigation. Boremap mapping of core drilled MDZ boreholes KLX09G, KLX10B and KLX10C.
- P-06-237 **Rauséus G, Mattsson K-J, Eklund S, Ehrenborg J.** Oskarshamn site investigation. Boremap mapping of core drilled borehole KLX11A.
- P-06-238 **Mattsson K-J, Eklund S.** Oskarshamn site investigation. Boremap mapping of core drilled borehole KLX18A.
- P-06-240 **Rauséus G, Mattsson K-J, Ehrenborg J.** Oskarshamn site investigation. Boremap mapping of core drilled borehole KLX09.
- P-06-241 **Rauséus G, Ehrenborg J.** Oskarshamn site investigation. Boremap mapping of core drilled borehole KLX20A.
- P-06-242 **Rauséus G, Ehrenborg J.** Oskarshamn site investigation. Boremap mapping of core drilled borehole KLX12A.
- P-06-243 **Mattsson K-J, Eklund S, Ehrenborg J.** Oskarshamn site investigation. Boremap mapping of core drilled MDZ boreholes KLX22A, KLX22B, KLX23A and KLX23B.
- P-06-244 **Mattsson K-J, Rauséus G, Eklund S, Ehrenborg J.** Oskarshamn site investigation. Boremap mapping of core drilled DFN boreholes KLX11B–KLX11F.
- P-06-245 **Väisäsvaara J, Pekkanen J.** Oskarshamn site investigation. Difference flow logging of borehole KLX13A. Sub-area Laxemar.
- P-06-246 **Kristiansson S, Pöllänen J, Väisäsvaara J, Kyllönen H.** Oskarshamn site investigation. Difference flow logging of borehole, KLX22A–B, KLX23A–B, KLX24A, KLX25A, Sub-area Laxemar.
- P-06-248 **Johansson T, Göransson M, Zetterlund M, Jenkins K, Rönnback K.** Oskarshamn site investigation. Hydrogeological characterization in bogs, lakes and sea bays.
- P-06-250 **Kaislahti Tillman P, Risberg J.** Holocene sedimentary environmental changes at sites PSM002118 and PSM002123 offshore Simpevarp. Oskarshamn site investigation.
- P-06-251 **Andersson R.** Electrofishing in two streams in the Simpevarp area. A study of the movement of migratory fish species. Oskarshamn site investigation.
- P-06-253 **Mattsson H.** Oskarshamn site investigation. Interpretation of geophysical borehole measurements from KLX12A. Revised January 2008.
- P-06-255 **Rauséus G, Mattsson K-J, Ehrenborg J.** Oskarshamn site investigation. Boremap mapping of telescopic drilled borehole KLX13A.
- P-06-256 **Mattsson K-J, Rauséus G, Ehrenborg J.** Oskarshamn site investigation. Boremap mapping of core drilled MDZ boreholes KLX26A and KLX26B.
- P-06-257 **Mattsson K-J, Rauséus G, Ehrenborg J.** Oskarshamn site investigation. Boremap mapping of core drilled MDZ boreholes KLX24A and KLX25A.
- P-06-259 **Nilsson K.** Hydrochemical logging in KLX12A. Results from isotope determinations (^3H , $\delta^2\text{H}$, $\delta^{18}\text{O}$, $^{87}\text{Sr}/^{86}\text{Sr}$ and $\delta^{34}\text{S}$). Oskarshamn site investigation.
- P-06-260 **Gustafsson J, Gustafsson C.** Oskarshamn site investigation. RAMAC, BIPS and deviation logging in boreholes KLX13A, KLX14A, KLX22A, KLX22B, KLX23A, KLX23B, KLX24A, KLX25A, KLX26A, KLX26B, HLX39 and HLX41.
- P-06-262 **Triumf C-A, Thunehed H.** Oskarshamn site investigation. Co-ordinated lineaments longer than 100 m at Laxemar. Identification of lineaments from LIDAR data and co-ordination with lineaments in other topographical and geophysical data.
- P-06-264 **Mattsson H, Keisu M.** Oskarshamn site investigation. Interpretation of geophysical borehole measurements from KLX09G, KLX10B, KLX10C, HLX36 and HLX37.
- P-06-265 **Ask H.** Oskarshamn site investigation. Core drilling of short boreholes KLX09B, KLX09C, KLX09D, KLX09E and KLX09F for discrete fracture network investigation (DFN).
- P-06-268 **Savukoski M.** Borehole KLX11A. Determining of porosity by water saturation and density by buoyancy technique. Oskarshamn site investigation.
- P-06-269 **Adl-Zarrabi B.** Borehole KLX11A. Thermal properties of rocks using calorimeter and TPS method. Oskarshamn site investigation.
- P-06-270 **Jacobsson L.** Borehole KLX11A. Uniaxial compression test of intact rock. Oskarshamn site investigation.

- P-06-271 **Jacobsson L.** Drill hole KLX11A. Indirect tensile strength test. Oskarshamn site investigation.
- P-06-272 **Jacobsson L.** Borehole KLX11A. Triaxial compression test of intact rock. Oskarshamn site investigation.
- P-06-274 **Liedberg L.** Borehole KLX13A. Determining of porosity by water saturation and density by buoyancy technique. Oskarshamn site investigation.
- P-06-275 **Adi-Zarrabi B.** Borehole KLX13A. Thermal properties of rocks using calorimeter and TPS method. Oskarshamn site investigation.
- P-06-276 **Jacobsson L.** Drill hole KLX13A. Indirect tensile strength test. Oskarshamn site investigation.
- P-06-277 **Jacobsson L, Flansbjer M.** Borehole KLX13A. Shear tests on sealed joints. Oskarshamn site investigation.
- P-06-278 **Lundkvist E.** Production and respiration measurements in different vegetation types. Comparisons between a young pine stand, a wet forest, a fen, and an agricultural field. Oskarshamn site investigation.
- P-06-279 **Wahlgren C-H, Bergman T, Ahl M, Ekström M.** Oskarshamn site investigation. Modal and geochemical analyses of drill core samples 2006 and updated bedrock map of the Laxemar subarea. Classification of rock types in KLX08, KLX10, KLX11A, KLX12A, KLX18A and KLX20A.
- P-06-280 **Lindquist A.** Hydrochemical logging in KLX13A. Oskarshamn site investigation
- P-06-282 **Olsson T, Stanfors R, Sigurdsson O, Erlström M.** Oskarshamn site investigation. Identification and characterization of minor deformation zones based on lineament interpretation.
- P-06-283 **Ask H.** Oskarshamn site investigation. Core drilling of short boreholes KLX11B, KLX11C, KLX11D, KLX11E and KLX11F for discrete fracture network investigation (DFN).
- P-06-284 **Thunehed H.** Vertical electric sounding and inversion of helicopter-borne EM measurements. Oskarshamn site investigation.
- P-06-286 **Gustavsson E.** Data report from the laboratory investigations of the transport properties of the rock. Data delivery for data freeze Laxemar 2.2. Oskarshamn site investigation.
- P-06-287 **Thur P, Nordqvist R, Gustafsson E.** Groundwater flow measurements and SWIW test in borehole KLX18A. Oskarshamn site investigation.
- P-06-288 **Löfgren M.** Formation factor logging in situ by electrical methods in KLX07A, KLX08, KLX10 and KLX12A. Oskarshamn site investigation.
- P-06-289 **Thunehed H.** Resistivity measurements on samples from KSH01, KSH02, KLX02, KLX04 and KLX11A. Oskarshamn site investigation.
- P-06-290 **Nielsen U T, Ringgaard J.** Oskarshamn site investigation. Geophysical borehole logging in boreholes KLX20A, KLX18A, KLX11B, KLX09B, KLX09D, KLX09F, HLX38, HLX39, HLX40 and HLX41.
- P-06-291 **Ask H.** Percussion drilling of boreholes HLX38, HLX39, HLX40, HLX41, HLX42 and HLX43 for lineament investigation.
- P-06-292 **Mattsson H, Keisu M.** Oskarshamn site investigation. Interpretation of geophysical borehole measurements from KLX18A, KLX20A, KLX09B, KLX09D, KLX09F, KLX11B, HLX38, HLX39, HLX40, HLX41 and interpretation of petrophysical data from KLX20A.
- P-06-295 **Berglund J, Nyborg M, Triumf C-A.** Oskarshamn site investigation. Lineaments longer than 10 m in two sub areas of Laxemar. Identification of short lineaments from LIDAR and magnetic total field data.
- P-06-296 **Kenczek C, Sunesson N.** Bottenypsklassificering i Borholmsfjärden och vattenkemi i grunda fjärdar i SKB:s platsundersökningsområde. Platsundersökning Oskarshamn.
- P-06-297 **Ask H.** Oskarshamn site investigation. Core drilling of 13 short boreholes (KLX09G, KLX10B, KLX10C, KLX22A, KLX22B, KLX23A, KLX23B, KLX24A, KLX25A, KLX26A, KLX26B, KLX28A and KLX29A) for investigation of minor deformation zones (MDZ).
- P-06-298 **Green M.** Bird monitoring in Simpevarp 2002–2006. Oskarshamn site investigation.
- P-06-299 **Jacobsson L.** Drill hole KLX05. Indirect tensile strength. Oskarshamn site investigation.
- P-06-300 **Jacobsson L.** Boreholes KLX05 and KLX13A. Uniaxial compression test of intact rock. Oskarshamn site investigation.
- P-06-301 **Sternbeck J, Land M, Nilsson Ö.** 210Pb and 14C dating of sediments and peat. Accumulation rates of carbon, nitrogen and phosphorus. Oskarshamn and Forsmark site investigations.
- P-06-303 **Wijnblad E, Plantman P.** Primary production and respiration in shallow phyto-benthic communities. Oskarshamn site investigation.
- P-06-305 **Ask H, Morosini M, Samuelsson L-E, Ekström L, Håkansson N.** Oskarshamn site investigation. Drilling of cored borehole KLX12A.
- P-06-306 **Ask H, Morosini M, Samuelsson L-E, Ekström L, Håkansson N.** Oskarshamn site investigation. Drilling of cored borehole KLX11A.
- P-06-307 **Nielsen U T, Ringgaard J.** Oskarshamn site investigation. Geophysical borehole logging in boreholes KLX13A, KLX14A, KLX22A, KLX22B, KLX23A, KLX23B, KLX24A, KLX25A, KLX26A and KLX26B.
- P-06-308 **Bergelin A, Nilsson K, Lindquist A, Wacker P.** Complete chemical characterisation in KLX08. Results from four investigated borehole sections: 197.0–206.6 m, 396.0–400.9 m, 476.0–485.6 m, 609.0–618.5 m. Oskarshamn site investigation.
- P-06-310 **Lindquist A.** Hydrochemical logging in KLX19A. Oskarshamn site investigation.
- P-06-311 **Nilsson K.** Hydrochemical logging in KLX09. Results from isotope determinations ($\delta^3\text{H}$, $\delta^2\text{H}$ and $\delta^{18}\text{O}$). Oskarshamn site investigation.

- P-06-312 **Nilsson K.** Hydrochemical logging in KLX20A Results from isotope determinations (3H, d2H and d18O). Oskarshamn site investigation.
- p-06-313 **Askling P, Nilsson K.** Hydrochemical monitoring programme for core drilled boreholes, June–July 2006. Summary of analyses from summer water sampling and parts of winter sampling. Oskarshamn site investigation.
- P-06-314 **Nielsen U T, Ringgaard J.** Oskarshamn site investigation. Geophysical borehole logging in boreholes KLX19A, KLX28A and KLX29A.
- P-06-315 **Nielsen U T, Ringgaard J.** Oskarshamn site investigation. Geophysical borehole logging in boreholes KLX17A and HLX43.
- P-06-317 **Mattsson H, Keisu M, Thunehed H.** Oskarshamn site investigation. Interpretation of geophysical borehole measurements from KLX13A, KLX14A, KLX22A, KLX22B, KLX23A, KLX23B, KLX24A, KLX25A, KLX26A and KLX26B.
- P-06-318 **Väisäsvaara J.** Oskarshamn site investigation. Difference flow logging of borehole KLX14A. Sub-area Laxemar.
- P-06-319 **Rohs S, van der Wall R, Wolf P.** Flow logging in boreholes HLX14, HLX20, HLX27, HLX28, HLX32, HLX33, HLX37, HLX39 and HLX43 Subarea Laxemar.
- P-06-320 **Engdahl A, Ternsell A, Hannu S.** Chemical characterisation of deposits and biota. Oskarshamn site investigation.
- P-06-321 **Lundin L, Lode E, Stendahl J.** Extended soil chemistry in three site types. Oskarshamn site investigation.
- P-06-324 **Ericsson U, Engdahl A.** Sampling and analysis of precipitation at Simpevarp 2005. Oskarshamn site investigation.
- P-06-325 **Ericsson U, Engdahl A.** Sampling and analysis of shallow ground water at Simpevarp 2005. Oskarshamn site investigation.
- P-07-03 **Janson T, Ljunggren B, Bergman T.** Oskarshamn site investigation. Modal analyses on rock mechanical specimens. Specimens from borehole KLX03, KLX04, KQ0064G, KQ0065G, KF0066A and KF0069A.
- P-07-12 **Gustafsson J, Gustafsson C.** Oskarshamn site investigation. RAMAC, BIPS and deviation logging in boreholes KLX17A and HLX43.
- P-07-13 **Gustafsson J, Gustafsson C.** Oskarshamn site investigation. RAMAC, BIPS and deviation logging in boreholes KLX19A, KLX28A and KLX29A.
- P-07-15 **Nielsen U T, Ringgaard J.** Oskarshamn site investigation. Geophysical borehole logging in borehole KLX21B.
- P-07-17 **Pöllänen J.** Oskarshamn site investigation. Difference flow logging of borehole, KLX28 and KLX29A, Sub-area Laxemar.
- P-07-18 **Enachescu C, Wolf P, Rohs S, van der Wall R.** Hydraulic interference tests, pumping borehole KLX08 Subarea Laxemar.
- P-07-20 **Kyllönen H, Leppänen H.** Oskarshamn site investigation. Difference flow logging of borehole KLX19A. Sub-area Laxemar.
- P-07-21 **Mattsson H, Keisu M.** Oskarshamn site investigation. Interpretation of geophysical borehole measurements from KLX19A, KLX28A and KLX29A.
- P-07-24 **Väisäsvaara J, Kristiansson S, Sokolnicki M.** Oskarshamn site investigation. Difference flow logging of borehole KLX11A. Sub-area Laxemar.
- P-07-25 **Mattsson H, Keisu M.** Oskarshamn site investigation. Interpretation of geophysical borehole measurements from KLX17A and HLX43.
- P-07-26 **Nordqvist R.** Extended evaluation of SWIW-tests in KSH02, a method study.
- P-07-27 **Drake H, Page L, Tullborg E-L.** Oskarshamn site investigation. ⁴⁰Ar/³⁹Ar dating of fracture minerals.
- P-07-29 **Forsberg O, Cronquist T, Vestgård J, Bergkvist L, Hermanson J, Öhman J, Pettersson A, Koyi S, Bergman T.** Oskarshamn site investigation. Detailed outcrop mapping in trenches.
- P-07-30 **Bergman T, Sohlenius G.** Petrographic analysis of gravel and boulders in till from the Laxemar area. Oskarshamn site investigation.
- P-07-32 **Roos P, Engdahl A, Karlsson S.** Analysis of radioisotopes in environmental samples. Oskarshamn and Forsmark site investigations.
- P-07-34 **Pöllänen J.** Oskarshamn site investigation. Difference flow logging of borehole KLX17A. Sub-area Laxemar.
- P-07-38 **Sjögren J, Hillgren R, Wern L, Jones J, Engdahl A.** Hydrological and meteorological monitoring at Oskarshamn, July 2005 until December 2006.
- P-07-39 **Enachescu C, Rohs S, Wolf P.** Hydraulic interference tests, pumping borehole KLX20A Subarea Laxemar.
- P-07-41 **Viola G, Venvik Ganerod G.** Oskarshamn site investigation. Structural analysis of brittle deformation zones in the Simpevarp-Laxemar area, Oskarshamn, southeast Sweden.
- p-07-47 **Berg C, Nilsson A-C.** Hydrochemical monitoring of percussion- and core drilled boreholes. Results from water sampling and analyses during 2006.
- P-07-48 **Enachescu C, Rohs S, Wolf P.** Hydraulic injection tests in borehole KLX08, 2006 Subarea Laxemar.
- P-07-49 **Enachescu C, Rohs S.** Hydraulic injection tests in borehole KLX20A, 2006 Subarea Laxemar.

- P-07-56 **Nielsen U T, Ringgaard J.** Oskarshamn site investigation. Geophysical borehole logging in borehole KLX16A.
- P-07-57 **Gustafsson J, Gustafsson C.** Oskarshamn site investigation. RAMAC, BIPS and deviation logging in boreholes KLX21A and KLX21B.
- P-07-58 **Gustafsson J, Gustafsson C.** Oskarshamn site investigation. RAMAC, BIPS and deviation logging in boreholes KLX16A and HLX42.
- P-07-61 **Liedberg L.** Borehole KLX03, KLX05, KLX07A, KLX10 and KLX11A. Determination of porosity by water saturation and density by buoyancy technique. Oskarshamn site investigation.
- P-07-62 **Adi-Zarrabi B.** Borehole KLX03, KLX05, KLX07, KLX10 and KLX11A. Thermal properties of rocks using calorimeter and TPS method, and mineralogical composition by modal analysis. Oskarshamn site investigation.
- P-07-63 **Åkesson U.** Boreholes KLX07A, KLX10, KLX05 and KLX12A. Extensometer measurement of the coefficient of thermal expansion of rock. Oskarshamn site investigation.
- P-07-64 **Sokolnicki M, Kristiansson S.** Oskarshamn site investigation. Difference flow logging of borehole KLX11B-F. Sub-area Laxemar.
- P-07-66 **Carlsten S, Mattsson K-J, Curtis P, Hultgren P, Stanfors R, Thunehed H, Wahlgren C-H.** Oskarshamn site investigation. Geological single-hole interpretation of KLX22A–B, KLX23A–B, KLX24A, KLX25A and KLX26A–B.
- P-07-67 **Carlsten S, Strähle A, Hultgren P, Thunehed H, Stanfors R, Wahlgren C-H.** Oskarshamn site investigation. Geological single-hole interpretation of KLX09 and HLX37.
- P-07-68 **Carlsten S, Strähle A, Hultgren P, Mattsson H, Wahlgren C-H.** Oskarshamn site investigation. Geological single-hole interpretation of KLX12A, KLX09G, KLX10B and KLX10C.
- P-07-69 **Carlsten S, Strähle A, Hultgren P, Keisu M, Wahlgren C-H.** Oskarshamn site investigation. Geological single-hole interpretation of KLX11A.
- P-07-70 **Carlsten S, Strähle A, Hultgren P, Mattsson H, Wahlgren C-H.** Oskarshamn site investigation. Geological single-hole interpretation of KLX18A and KLX20A.
- P-07-71 **Sigurdsson O.** Oskarshamn site investigation. Simplified Boremap mapping of percussion drilled telescope boreholes KLX08, KLX09, KLX10, KLX11A, KLX19A and KLX21B.
- P-07-72 **Pöllänen J.** Oskarshamn site investigation. Difference flow logging of borehole, KLX26A and KLX26B, Sub-area Laxemar.
- P-07-73 **Lindquist A.** Hydrochemical logging in KLX21B. Oskarshamn site investigation.
- P-07-74 **Drake H, Tullborg E-L.** Oskarshamn site investigation. Fracture mineralogy. Results from drill cores KLX03, KLX04, KLX06, KLX07A, KLX08 and KLX10A.
- P-07-75 **Mattsson H, Keisu M.** Oskarshamn site investigation. Interpretation of geophysical borehole measurements from KLX21B.
- P-07-77 **Mossmark F, Sundberg J.** Field measurements of thermal properties. Multi probe measurements in Laxemar. Oskarshamn site investigation.
- P-07-79 **Enachescu C, Rahm N.** Method evaluation of single hole hydraulic injection tests at site investigations Oskarshamn.
- P-07-80 **Ludvigson J-E, Hansson K, Hjerne C.** Method evaluation of single-hole hydraulic injection tests at site investigations in Forsmark.
- P-07-87 **Väisäsvaara J.** Oskarshamn site investigation. Difference flow logging of borehole KLX16A. Sub-area Laxemar.
- P-07-88 **Thunehed H.** Oskarshamn site investigation. Comparison between measurements of Total Dissolved Solids and Transient Electromagnetic Soundings in the regional model area.
- P-07-90 **Enachescu C, Böhner J, Wolf P.** Pumping tests and hydraulic injection tests in borehole KLX19A, 2007 Subarea Laxemar.
- P-07-91 **Morosini M, Jenkins C, Simson S, Albrecht J, Zetterlund M.** Oskarshamn site investigation. Hydrogeological characterization of deepest valley soil aquifers and soil-rock transition zone at Laxemar, 2006 – Subarea Laxemar.
- P-07-94 **Enachescu C, Böhner J, van der Wall R.** Hydraulic injection tests in borehole KLX21B Subarea Laxemar.
- P-07-97 **Mattsson H, Keisu M.** Oskarshamn site investigation. Interpretation of geophysical borehole measurements from KLX16A.
- P-07-98 **Ask H, Morosini M, Samuelsson L-E, Ekström L, Håkansson N.** Oskarshamn site investigation. Drilling of cored borehole KLX18A.
- P-07-99 **Enachescu C, Rohs S.** Hydraulic injection tests in borehole KLX13A Subarea Laxemar.
- P-07-114 **Mattsson H, Keisu M.** Oskarshamn site investigation. Interpretation of geophysical borehole measurements from KLX15A.
- P-07-116 **Sokolnicki M, Pöllänen J.** Oskarshamn site investigation. Difference flow logging of borehole KLX21B. Sub-area Laxemar.
- P-07-117 **Gustafsson J, Gustafsson C.** Oskarshamn site investigation. RAMAC, BIPS and deviation logging in borehole KLX15A.
- P-07-119 **Waber N, Smellie J.** Borehole KLX08. Characterisation of pore water. Part 1: Methodology and analytical data. Oskarshamn site investigation.

- P-07-120 **Enachescu C, Rohs S, Wolf P.** Hydraulic injection tests in borehole KLX16A, 2007 Subarea Laxemar.
- P-07-122 **Truvé J.** Surveys of mammal populations in the areas adjacent to Forsmark and Oskarshamn. Results from 2007, compared with results from 2002/2003. Oskarshamn and Forsmark site investigation.
- P-07-123 **Lindfors U, Perman F.** Overcoring rock stress measurements in borehole KLX12A. Oskarshamn site investigation.
- P-07-126 **Lindquist A.** Hydrochemical logging in KLX16A. Oskarshamn site investigation.
- P-07-131 **Lindqvist G.** Oskarshamn site investigation. Refraction seismic measurements in Laxemar spring 2007.
- P-07-134 **Ask H, Morosini M, Samuelsson L-E, Ekström L, Håkansson N.** Oskarshamn site investigation. Drilling of cored borehole KLX20A.
- P-07-136 **Cederlund G, Lemel J.** Älgstammens ålderssammansättning och reproduktion i Oskarshamn. Platsundersökning Oskarshamn.
- P-07-140 **Jacobsson L.** Borehole KLX17A. Microcrack volume measurements and triaxial compression test on intact rock. Oskarshamn site investigation.
- P-07-141 **Savukoski M.** Borehole KLX16A. Determining of porosity by water saturation and density by buoyancy technique. Oskarshamn site investigation.
- P-07-142 **Jacobsson L.** Borehole KLX16A. Indirect tensile strength test. Oskarshamn site investigation.
- P-07-143 **Jacobsson L.** Borehole KLX16A. Uniaxial compression test of intact rock. Oskarshamn site investigation.
- P-07-144 **Adl-Zarrabi B.** Borehole KLX16A. Thermal properties of rocks using TPS method. Oskarshamn site investigation.
- P-07-149 **Bergelin A, Nilsson K, Lindquist A, Wacker P.** Complete chemical characterisation in KLX13A. Results from two investigated borehole sections: 432.0-439.2 m, 499.5-506.7 m. Oskarshamn site investigation.
- P-07-152 **Nielsen U T, Ringgaard J.** Oskarshamn site investigation. Geophysical borehole logging in borehole KLX15A.
- P-07-153 **Carlsten S, Mattsson K-J, Strähle A, Curtis P, Hultgren P, Mattsson H, Stanfors R, Wahlgren C-H.** Oskarshamn site investigation. Geological single-hole interpretation of KLX28A and KLX29A.
- P-07-155 **Carlsten S, Mattsson K-J, Strähle A, Curtis P, Hultgren P, Mattsson H, Stanfors R, Wahlgren C-H.** Oskarshamn site investigation. Geological single-hole interpretation of KLX14A and HLX43.
- P-07-156 **Carlsten S, Strähle A, Hultgren P, Mattsson H, Stanfors R, Wahlgren C-H.** Oskarshamn site investigation. Geological single-hole interpretation of KLX13A, HLX39 and HLX41.
- P-07-157 **Mattsson K-J, Dahlin P.** Oskarshamn site investigation. Boremap mapping of telescopic drilled borehole KLX15A.
- P-07-158 **Mattsson K-J, Dahlin P.** Oskarshamn site investigation. Boremap mapping of telescopic drilled borehole KLX17A.
- P-07-159 **Mattsson K-J, Dahlin P.** Oskarshamn site investigation. Boremap mapping of core drilled MDZ boreholes KLX28A and KLX29A.
- P-07-160 **Page L, Söderlund P, Wahlgren C-H.** Oskarshamn site investigation. $^{40}\text{Ar}/^{39}\text{Ar}$ and (U-Th)/He geochronology of samples from the cored boreholes KSH03A, KSH03B, KLX01, KLX02 and the access tunnel to the Äspö Hard Rock Laboratory.
- P-07-161 **Carlsten S, Mattsson K-J, Strähle A, Hultgren P, Mattsson H, Wahlgren C-H.** Oskarshamn site investigation. Geological single-hole interpretation of KLX19A and HLX38.
- P-07-167 **Askling P, Nilsson K.** Hydrochemical monitoring programme for core drilled boreholes 2006. Summary of analyses from water sampling. Oskarshamn site investigation.
- P-07-168 **Mattsson H, Triumf C-A.** Oskarshamn site investigation. Detailed ground geophysics at Laxemar, spring 2007. Magnetic total field.
- P-07-172 **Sjögren J, Hillgren R, Wern L, Jones J, Engdahl A.** Hydrological and meteorological monitoring at Oskarshamn, January 2007 until August 2007.
- P-07-173 **Gokall-Norman K, Ludvigson J-E.** Oskarshamn site investigation. Hydraulic pumping- and interference tests in soil monitoring wells on Laxemar, spring of 2007.
- P-07-176 **Pöllänen J, Sokolnicki M, Väisäsvaara J.** Oskarshamn site investigation. Difference flow logging of borehole KLX15A. Sub-area Laxemar.
- P-07-179 **Selnert E, Byegård J, Widestrand H.** Laboratory measurements within the site investigation programme for the transport properties of the rock. Final Report. Oskarshamn site investigation.
- P-07-180 **Nordqvist R.** Extended evaluation of SWIW-tests in KSH02, a method study.
- P-07-181 **Askling P, Andersson P.** Groundwater flow measurements in permanent installed boreholes. Test campaign no. 2, 2006.
- P-07-182 **Morosini M, Jönsson S.** Pump- and interference testing of percussion drilled section of cored boreholes KLX09, KLX11A, KLX12A, KLX13A, KLX18A, KLX19A and KLX39 Subarea Laxemar.

- P-07-183 **Walger E, Ludvigson J-E, Svensson T, Thur P, Harrström J.** Hydraulic interference in KLX06, KLX14A, KLX15A, KLX16A, KLX17A, KLX18A, KLX19A, KLX21B, KLX22A, KLX22B, KLX23A, KLX23B, KLX26A and KLX26B, Laxemar subarea.
- P-07-185 **Thur P, Walger E, Ludvigson J-E.** Hydraulic interference in HLX34, HLX27, and HLX42 in the Laxemar subarea.
- P-07-186 **Harrström J, Walger E, Ludvigson J, Morosini M.** Hydraulic interference tests HLX27, HLX28 and HLX32, Subarea Laxemar.
- P-07-187 **Svensson T, Ludvigsson J-E, Walger E, Thur P, Gokall-Norman K, Wass E, Morosini M.** Combined interference- and tracer test in HLX33, SSM000228, and SSM000229, Subarea Laxemar.
- P-07-188 **Lindquist A.** Hydrochemical logging in KLX19A. Oskarshamn site investigation.
- P-07-189 **Lindquist A.** Hydrochemical logging in KLX121B. Oskarshamn site investigation.
- P-07-191 **Wahlgren C-H, Bergman T, Ahl M, Ekström M, Page L, Söderlund U.** Oskarshamn site investigation. Modal and geochemical analyses of drill core samples 2007 and ⁴⁰Ar/³⁹Ar dating of a dolerite. Classification of rock types in KLX15A, KLX16A, KLX19A, KLX20A and KLX21B.
- P-07-192 **Enaschescu C, Rohs S, van der Wall R, Wolf P.** Hydraulic injection tests in borehole KLX15A, 2007 Subarea Laxemar.
- P-07-193 **Enaschescu C, van der Wall R, Wolf P.** Hydraulic Injection Tests in Borehole KLX17A, 2007 Subarea Laxemar.
- P-07-195 **Ask H, Morosini M, Samuelsson L-E, Tiberg L.** Oskarshamn site investigation. Drilling of cored borehole KLX13A.
- P-07-197 **Asking P.** Oskarshamn site investigation. Groundwater flow measurements in soil wells SSM000243, SSM000244, SSM000261, SM000262 and SSM000263, spring 2007 – Subarea Laxemar.
- P-07-202 **Ask H, Morosini M, Samuelsson L-E, Tiberg L.** Oskarshamn site investigation. Drilling of cored borehole KLX19A.
- P-07-199 **Thur P, Gustafsson E.** Groundwater flow measurements in borehole KLX21B. Oskarshamn site investigation.
- P-07-203 **Thunehed H.** Complementary resistivity measurements on samples from KLX03, KLX04, KLX05, KLX10, KLX12A and KLX13A. Oskarshamn site investigation.
- P-07-204 **Vilks P.** Rock matrix permeability measurements on core samples from borehole KLX03. Oskarshamn site investigation.
- P-07-208 **Carlsten S, Mattsson K-J, Stråhle A, Curtis P, Hultgren P, Mattsson H, Wahlgren C-H.** Oskarshamn site investigation. Geological single-hole interpretation of KLX16A.
- P-07-209 **Carlsten S, Mattsson K-J, Stråhle A, Hultgren P, Mattsson H, Wahlgren C-H.** Oskarshamn site investigation. Geological single-hole interpretation of KLX17A and HLX42.
- P-07-210 **Mattsson K-J, Dahlin P, Ehrenborg J.** Oskarshamn site investigation. Boremap mapping of telescopic drilled borehole KLX19A.
- P-07-211 **Mattsson K-J, Dahlin P, Lundberg E.** Oskarshamn site investigation. Boremap mapping of core drilled borehole KLX16A.
- P-07-212 **Teurneau B, Forsmark T, Forssman I, Rhén I.** Oskarshamn site investigation. Correlation of Posiva Flow Log anomalies to core mapped features in KLX05, KLX06, KLX07A-B and KLX08.
- P-07-213 **Wikström M, Forsmark T, Teurneau B, Forssman I, Rhén I.** Oskarshamn site investigation. Correlation of Posiva Flow Log anomalies to core mapped features in KLX09, KLX09B–G, KLX10, KLX10B–C and KLX11A–F.
- P-07-214 **Wikström M, Forsmark T, Zetterlund M, Forssman I, Rhén I.** Oskarshamn site investigation. Correlation of Posiva Flow Log anomalies to core mapped features in KLX12A, KLX13A, KLX14A, KLX15A and KLX16A.
- P-07-215 **Forsmark T, Wikström M, Forssman I, Rhén I.** Oskarshamn site investigation. Correlation of Posiva Flow Log anomalies to core mapped features in KLX17A, KLX18A, KLX19A, KLX20A, KLX21B.
- P-07-216 **Wikström M, Forsmark T, Forssman I, Rhén I.** Oskarshamn site investigation. Correlation of Posiva Flow Log anomalies to core mapped features in KLX22A–B, KLX23A–B, KLX24A, KLX25A, KLX26A–B, KLX27A, KLX28A and KLX29A.
- P-07-217 **Jacobsson L.** Boreholes KLX17A, KLX18A and KLX21B. Uniaxial compression test of intact rock. Oskarshamn site investigation.
- P-07-218 **Mattsson K-J, Dahlin P, Lundberg E.** Oskarshamn site investigation. Boremap mapping of telescopic drilled borehole KLX21B.
- P-07-219 **Nyberg H, Wass E.** Oskarshamn site investigation. Groundwater monitoring program – Report for July 2005 to December 2006.
- P-07-221 **Ask H, Morosini M, Tiberg L.** Oskarshamn site investigation Drilling of cored borehole KLX17A.
- P-07-222 **Lundin L, Snäll S, Jonsson E, Hannu S, Selner E, Engdahl A.** Characterization of soil samples from three valleys in the Laxemar area. Oskarshamn site investigation.
- P-07-223 **Triumpf C-A.** Oskarshamn site investigation. Assessment of possible dolerite dykes in the Laxemar subarea from magnetic total field data and digital elevation models.
- P-07-226 **Green M.** Bird monitoring in Simpevarp 2002–2007. Oskarshamn site investigation.
- P-07-227 **Viola G, Venvik Ganerod G.** Oskarshamn site investigation. Structural characterisation of deformation zones (faults and ductile shear zones) from selected drill cores and outcrops from the Laxemar area- Results from Phase 2.

- P-07-232 **Ask D, Cornet F, Brunet C, Fontbonne F.** Stress measurements with hydraulic methods in borehole KLX12A. Oskarshamn site investigation.
- P-08-03 **Nielsen U T, Ringgaard J.** Oskarshamn site investigation. Geophysical borehole logging in borehole KLX27A.
- P-08-04 **Mattsson H.** Oskarshamn site investigation. Interpretation of geophysical borehole measurements from KLX27A.
- P-08-05 **Carlsten S, Mattsson K-J, Strähle A, Hultgren P, Mattsson H, Wahlgren C-H.** Oskarshamn site investigation. Geological single-hole interpretation of KLX15A and HLX30, HLX31 and HLX33.
- P-08-06 **Carlsten S, Mattsson K-J, Strähle A, Curtis P, Thunehed H, Wahlgren C-H.** Oskarshamn site investigation. Geological single-hole interpretation of KLX21B and HLX40.
- P-08-07 **Viola G, Venvik Ganerod G.** Oskarshamn site investigation. Structural characterization deformation zones (faults and ductile shear zones) from selected drill cores from Laxemar area, Oskarshamn, southeast Sweden.
- P-08-08 **Pedersen K.** Microorganisms in groundwater from boreholes KLX13A and KLX17A: numbers, viability, and metabolic diversity. Results from three sections: 432.0–439.2 m in KLX13A and 416.0–437.5 m and 642.0–701.1 m in KLX17A. Oskarshamn site investigation.
- P-08-09 **Pedersen K.** Microorganisms in groundwater from borehole KLX15A - numbers, viability, and metabolic diversity. Results from one section: 623.00–634.51 m in KLX15A. Oskarshamn site investigation.
- P-08-10 **Ericsson U, Engdahl A.** Monitoring of surface water chemistry 2006. Oskarshamn site investigation.
- P-08-11 **Drake H, Tullborg E-L.** Oskarshamn site investigation. Mineralogy in water conducting zones. Results from drill cores KLX13A and KLX17A with additional fracture mineralogical data from drill cores KLX14A, KLX19A, KLX20A and KLX26A.
- P-08-12 **Drake H, Tullborg E-L.** Oskarshamn site investigation. Fracture mineralogy. Results from drill core KLX15A.
- P-08-15 **Enachescu C, Rohs S, van der Wall R.** Evaluation of hydraulic interference tests, pumping borehole KLX19A Subarea Laxemar.
- P-08-16 **Enachescu C, Rohs S, van der Wall R, Wolf P, Morosini M.** Evaluation of hydraulic interference tests, pumping borehole KLX27A Subarea Laxemar.
- P-08-21 **Ask H.** Oskarshamn site investigation. Core drilling of short borehole KLX14A.
- P-08-22 **Pöllänen J, Pekkanen J, Väisäsvaara J.** Oskarshamn site investigation. Difference flow logging of borehole, KLX27A, Sub-area Laxemar.
- P-08-24 **Ask H, Morosini M, Tiberg L.** Oskarshamn site investigation Drilling of boreholes KLX21A and KLX21B.
- P-08-27 **Enachescu C, Wolf P, Rohs S, van der Wall R.** Hydraulic injection tests in borehole KLX27A, 2008 Subarea Laxemar.
- P-08-28 **Nyberg H, Wass E.** Oskarshamn site investigation. Groundwater monitoring program – Report for January-August 2007.
- P-08-30 **Gustafsson J, Gustafsson G.** Oskarshamn site investigation. RAMAC, BIPS and deviation logging in borehole KLX27A.
- P-08-31 **Thur P.** Groundwater flow measurements in permanently installed boreholes. Test campaign no. 3 2007. Oskarshamn site investigation.
- P-08-38 **Eklund S, Mattsson K-J.** Quantitative mapping of fracture minerals in Laxemar. Oskarshamn site investigation.
- P-08-39 **Mattsson K-J, Eklund S.** Oskarshamn site investigation. Boremap mapping of telescopic drilled borehole KLX27A.
- P-08-41 **Drake H, Tullborg E-L.** Oskarshamn site investigation. Mineralogy in water conducting zones. Results from boreholes KLX03, KLX04, KLX06, KSH01A+B, KSH02 and KSH03A.
- P-08-42 **Drake H, Tullborg E-L.** Oskarshamn site investigation. Mineralogy in water conducting zones. Results from boreholes KLX07A+B and KLX08.
- P-08-43 **Waber N, Smellie J.** Borehole KLX17A Characterisation of pore water. Part 1 Methodology and analytical data. Oskarshamn site investigation.
- P-08-44 **Drake H, Tullborg E-L.** Oskarshamn site investigation. Detecting the near surface redox front in crystalline rock. Results from drill cores KLX09B–G and KLX11B–F.
- P-08-48 **Carlsten S, Mattsson K-J, Strähle A, Mattsson H, Wahlgren C-H.** Oskarshamn site investigation. Geological single-hole interpretation of KLX27A.
- P-08-57 **Enachescu C, Lenné S, Rohs S, van der Wall R.** Transient evaluation of PFL pumping tests. Sub-area Laxemar and Simpevarp.
- P-08-69 **Bergelin A, Nilsson K, Lindquist A, Wacker P.** Complete chemical characterisation in KLX15A. Results from the investigated borehole section: 623.0 to 634.5 m. Oskarshamn site investigation.
- P-08-77 **Bergelin A, Nilsson K, Lindquist A, Wacker P.** Complete chemical characterisation in borehole KLX27A. Results from borehole section 641.5 to 650.6 m. Oskarshamn site investigation.
- P-08-81 **Engdahl A, Rådén R, Borgiel M, Omberg L-G.** Chemical composition of suspended material, sediment and pore water in lakes and sea bays. Oskarshamn and Forsmark site investigation.

- P-08-82 **Nilsson K, Thur P.** Water sampling in KLX11A and KLX19A. Summary of analyses from water sampling during pumping in connection with Single Well Injection Withdrawal (SWIW) tests and Pipe String System (PSS) measurements
- P-08-83 **Pedersen K.** Microorganisms in groundwater from borehole KLX27A – numbers, viability, and metabolic diversity. Results from one section: 641.50–650.56 m in KLX27A.
- P-08-88 **Nyberg G, Wass E.** Groundwater Monitoring Program. Report for September 2007-September 2008. Oskarshamn site investigation.
- P-08-90 **Ericsson U.** Monitoring of shallow ground water chemistry, 2006. Oskarshamn site investigation.
- P-08-91 **Harrström J, Nilsson K.** Hydrogeochemical analyses in percussion boreholes in Simpevarp and Laxemar in 2003, 2005 and 2006. Oskarshamn site investigation.
- P-08-96 **Lindquist A, Hjerne C, Nordqvist R, Ludvigson J-E, Harrström J, Carlsten S.** Oskarshamn site investigation. Confirmatory hydraulic interference test and tracer test in Laxemar.
- P-09-31 **Ringgaard J.** Mapping of borehole breakouts. Processing of acoustical televiewerdata from KAV04A, KLX10, KLX11A, KLX12A, KLX15A and KLX18A.
- PR-25-87-03 **Talbot C, Riad L.** Natural fractures in the Simpevarp area.
- PR 25-87-04 **Nisca D.** Aerogeophysical interpretation. Bedrock and tectonic analysis.
- PR-25-88-12 **Kornfält K-A, Wikman H.** The rocks of the Äspö island. Description to the detailed maps of solid rocks including maps of 3 uncovered trenches.
- PR 25-89-13 **Stenberg L, Sehlstedt S.** Geophysical profile measurements on interpreted regional aeromagnetic lineaments in the Simpevarp area.
- PR 25-89-15 **Munier R.** Brittle tectonics on Äspö, SE Sweden.
- PR-25-89-17 **Bjarnason B, Klasson H, Leijon, B, Strindell L, Öhman T.** Rock stress measurements in boreholes KAS02, KAS03 and KAS05 on Äspö.
- PR-25-89-23 **Rydström H, Gereben L.** Regional geological study – Seismic refraction survey.
- PR 25-94-39 **Stanfors R, Rhén I, Forsmark T, Wikberg P.** Evaluation of the fracture zone EW-1, based on the cored boreholes KA1755A, KA1751, KA1754A and KAS04.
- PR 25-95-04 **Wikman H, Kornfält K-A.** Updating of a lithological model of the bedrock of the Äspö area.
- PR-25-95-21 **Munier R.** Studies of the geological structures at Äspö. Comprehensive summary of results.
- PR U-097-27 **Ljunggren C, H Klasson.** Drilling KLX02 - Phase 2 Lilla Laxemar Oskarshamn – Deep hydraulic fracturing Rock stress measurements in Borehole KLX02, Laxemar.
- IPR-99-17 **Sundberg J, Gabrielsson A.** Laboratory and field measurements of thermal properties of the rock in the prototype repository at Äspö HRL.
- IPR-00-28 **Andersson P, Ludvigson J-E, Wass E, Holmqvist M.** TRUE Block Scale. Tracer Test Stage. Interference tests, dilution tests and tracer tests, phase A.
- IPR-01-06 **Rouhiainen P.** Difference flow measurements in borehole KLX02 at Laxemar.
- IPR-01-44 **Andersson P, Ludvigsson J-E, Wass E.** TRUE Block Scale project. Preliminary characterisation stage. Combined interference tests and tracer tests. Performance and delivery evaluation.
- IPR-01-52 **Andersson P, Ludvigsson J-E, Wass E, Holmqvist M.** True Block Scale, Detailed characterisation stage, Interference tests and tracer tests PT-1 PT-4.
- IPR-01-65 **Forsmark T, Rhén I.** Summary report of investigations before the operation phase. Prototype Repository (D27).
- IPR-01-67 **Klasson H, Persson M, Ljunggren C.** Overcoring rock stress measurements at the Äspö HRL. Prototype Repository: Borehole KA3579G (Revised data) and K-tunnel: Borehole KK0045G01.
- IPR-02-01 **Rummel F, Klee G, Weber U.** Äspö Hard Rock Laboratory. Rock Stress measurements in Oskarshamn. Hydraulic fracturing and core testing in borehole KOV01.
- IPR-02-02 **Klee G, Rummel F.** Äspö Hard Rock Laboratory. Rock Stress measurements at the Äspö HRL. Hydraulic fracturing in boreholes KA2599G01 and KF0093A01.
- IPR-02-03 **Collin M, Börgesson L.** Äspö Hard Rock Laboratory. Prototype Repository. Instrumentation of buffer and backfill for measuring THM processes.
- IPR-02-18 **Klasson H, Lindblad K, Lindfors U, Andersson S.** Äspö Hard Rock Laboratory. Overcoring rock stress measurements in borehole KOV01, Oskarshamn.
- IPR-03-13 **Dershowitz W, Winberg A, Hermanson J, Byegård J, Tullborg, E-L, Andersson P, Mazurek M.** Äspö Hard Rock Laboratory. Äspö Task Force on modelling of groundwater flow and transport of solutes. Task 6c. A semi-synthetic model of block scale conductive structures at the Äspö HRL.
- IPR-03-16 **Sjöberg J.** Äspö Hard Rock Laboratory. Äspö Pillar Stability Experiment. 3D overcoring rock stress measurements in borehole KA3376B01 at Äspö HRL.
- IPR-03-34 **Berglund J, Curtis P, Eliasson T, Ohlsson T, Starzec P, Tullborg E-L.** Äspö Hard Rock Laboratory – Update of the geological model 2002.
- IPR-06-32 **Mattsson H.** The magnetic anisotropy of rocks across the deformation zone NE-1 at the Äspö HRL.
- ICR-01-04 **Byegård J, Widstrand H, Skålborg M, Tullborg E-L, Siitari-Kauppi M.** First TRUE Stage. Complementary investigations of diffusivity, porosity and sorptivity of Feature A-site specific geologic material.
- R-97-13 **Carbol P, Engkvist I.** Compilation of radionuclide sorption coefficients for performance assessment.
- R-98-05 **Axelsson C-L, Mærsk Hansen L.** Update of structural models at SFR nuclear waste repository, Forsmark, Sweden

- R-98-55 **Follin S, Årebäck M, Axelsson C-L, Stigsson M, Jacks G.** Förstudie Oskarshamn. Grundvattnets rörelse, kemi och långsiktiga förändringar (in Swedish).
- R-98-56 **Bergman T, Isaksson H, Johansson R, Lindén A H, Lindgren J, Lindroos H, Rudmark L, Wahlgren C-H.** Förstudie Oskarshamn. Jordarter, bergarter och deformationszoner.
- R-99-04 **Bergman T, Follin S, Isaksson H, Johansson R, Lindén A H, Lindroos H, Rudmark L, Stanfors R, Wahlgren C-H.** Förstudie Oskarshamn. Erfarenheter från geovetenskapliga undersökningar i nordöstra delen av kommunen.
- R-99-70 **Lindell S, Ambjörn C, Juhlin B, Larsson-McCann S, Lindquist K.** Available climatological and oceanographical data for site investigation program.
- R-00-45 **Bergman T, Rudmark L, Wahlgren C-H, Johansson R, Isaksson H.** Förstudie Oskarshamn. Kompletterande geologiska studier.
- R-01-06 **Markström I, Stanfors R, Juhlin C.** Äspölaboratoriet RVS-modellering, Ävrö Slutrapport (in Swedish).
- R-01-07 **Bergman B, Juhlin C, Palm H.** Reflektionsseismiska studier inom Laxemarområdet.
- R-01-15 **Munier R, Hermanson J.** Metodik för geometrisk modellering. Presentation och administration av platsbeskrivande modeller.
- R-01-37 **Landström O, Tullborg E-L, Eriksson G, Sandell Y.** Effects of glacial/post-glacial weathering compared with hydrothermal alteration – implications for matrix diffusion.
- R-01-52 **Ludvigson J-E, Hansson K, Rouhiainen P.** Methodology study of Posiva difference flow meter in borehole KLX02 at Laxemar.
- R-01-60 **Åhäll K-I.** Åldersbestämning av svårdaterade bergarter i sydöstra Sverige.
- R-02-06 **Boresjö Bronge L, Wester K.** Vegetation mapping with satellite data of the Forsmark and Tierp regions.
- R-02-10 **Berggren J, Kyläkorpi L.** Ekosystemen i Simpevarpsområdet Sammanställning av befintlig information (in Swedish).
- R-02-10 **Berggren J, Kyläkorpi L.** Ekosystemen i Simpevarpsområdet – Sammanställning av befintlig information (In Swedish: Ecosystems in the Simpevarp area – A list of available information).
- R-02-26 **Janson T, Stigsson M.** Test with different stress measurement methods in two orthogonal bore holes in Äspö HRL.
- R-02-27 **Sundberg J.** Determination of thermal properties at Äspö HRL. Comparison and evaluation of methods and methodologies for borehole KA 2599 G01.
- R-02-35 **SKB.** Simpevarp – site descriptive model version O.
- R-02-37 **Röshoff K, Cosgrove J.** Sedimentary dykes in the Oskarshamn-Västervik area – A study of the mechanism of formation.
- R-02-42 **Alm E, Sundblad K.** Fluorite-calcite-galena-bearing fractures in the counties of Kalmar and Blekinge, Sweden.
- R-02-47 **Risberg J.** Holocene sediment accumulation in the Äspö area. A study of a sediment core.
- R-03-07 **Munier R, Stenberg L, Stanfors R, Milnes A G, Hermanson J, Triumf C-A.** Geological Site Descriptive Model. A strategy for the development during site investigations.
- R-03-10 **Sundberg J.** Thermal Site Descriptive Model. A strategy for the model development during site investigations. Version 1.0.
- R-04-09 **Smellie J.** Recent geoscientific information relating to deep crustal studies.
- R-04-11 **Miliander S, Punakivi M, Kyläkorpi L, Rydgren B.** Human population and activities at Simpevarp.
- R-04-12 **Kyläkorpi L.** Tillgänglighetskartan (/Map of accessibility).
- R-04-16 **Laaksoharju M, Smellie J, Gimeno M, Auqué L, Gómez J, Tullborg E-L, Gurban I.** Hydrogeochemical evaluation of the Simpevarp area, model version 1.1.
- R-04-25 **SKB.** Preliminary site description. Simpevarp area – version 1.1.
- R-04-66 **Munier R.** Statistical analysis of fracture data, adapted for modelling Discrete Fracture Networks-Version 2.
- R-04-72 **Lindroos H.** The potential for ore, industrial minerals and commercial stones in the Simpevarp area.
- R-04-74 **SKB.** Hydrogeochemical evaluation for Simpevarp model version 1.2. Preliminary site description of the Simpevarp area
- R-05-08 **SKB.** Preliminary site description. Simpevarp subarea – version 1.2.
- R-05-12 **SKB.** Preliminary safety evaluation for the Simpevarp subarea – Based on data and site descriptions after the initial site investigation stage.
- R-05-15 **Lundin L, Lode E, Stendahl J, Björkvald L, Hansson J.** Soils and site types in the Oskarshamn area. Oskarshamn site investigation.
- R-05-36 **Truvé J, Cederlund G.** Mammals in the areas adjacent to Forsmark and Oskarshamn. Population density, ecological data and carbon budget.
- R-05-38 **Brydsten L, Strömberg M.** Digital elevation models for site investigation programme in Oskarshamn. Site description version 1.2.
- R-05-45 **Hermanson J, Forsberg O, Fox A, La Pointe P.** Statistical model of fractures and deformation zones. Preliminary site description, Laxemar subarea, version 1.2.
- R-05-54 **Nyman H.** Depth and stratigraphy of Quaternary deposits. Preliminary site description Laxemar subarea – version 1.2

- R-05-61 **Werner K, Bosson E.** Description of climate, surface hydrology, and near-surface hydrogeology. Preliminary site description Laxemar subarea – version 1.2.
- R-05-69 **Wahlgren C-H, Hermanson J, Curtis P, Triumph C-A, Drake H, Tullborg E-L.** Geological description of rock domains and deformation zones in the Simpevarp and Laxemar subareas. Preliminary site description Laxemar subarea – version 1.2.
- R-06-06 **SKB.** Preliminary safety evaluation for the Laxemar subarea – Based on data and site descriptions after the initial site investigation stage.
- R-06-10 **SKB.** Preliminary site description, Laxemar subarea – version 1.2.
- R-06-11 **Lindborg T (ed).** Description of surface systems, Preliminary site description Laxemar subarea – version 1.2.
- R-06-12 **SKB.** Hydrogeochemical evaluation. Preliminary site description, Laxemar subarea – version 1.2.
- R-06-18 **Tröjbom M, Söderbäck B.** Chemical characteristics of surface systems in the Simpevarp area. Visualisation and statistical evaluation of data from surface water, precipitation, shallow groundwater, and regolith.
- R-06-35 **SKB.** Final repository for spent nuclear fuel. Underground design for Simpevarp, Layout D1.
- R-06-36 **SKB.** Final repository for spent nuclear fuel. Underground design Laxemar, Layout D1.
- R-06-53 **Johansson R.** A comparison of two independent interpretations of lineaments from geophysical and topographic data from the Simpevarp area.
- R-06-109 **Drake H, Sandström B, Tullborg E-L.** Mineralogy and geochemistry of rocks and fracture fillings from Forsmark and Oskarshamn. Compilation of data for SR-Can.
- R-06-110 **SKB.** Preliminary site description Laxemar stage 2.1. Feedback for the completion of the site investigation including input from safety assessment and repository engineering.
- R-06-121 **Karlberg L, Gustafsson D, Jansson P-E.** Modelling carbon and water flows in terrestrial ecosystems in the boreal zone – examples from Oskarshamn.
- R-06-123 **Persson T, Lenoir L, Taylor A.** Bioturbation in different ecosystems at Forsmark and Oskarshamn.
- R-06-125 **Tagesson, T.** Calibration and analysis of soil carbon efflux estimates with closed chambers at Forsmark and Laxemar.
- R-07-01 **Persson, H, Stadenberg I.** Distribution of fine roots in forest areas close to the Swedish Forsmark and Oskarshamn nuclear power plants.
- R-07-23 **Mjöfors K, Johansson, M-B, Nilsson Å, Hyvönen R.** Input and turnover of forest tree litter in the Forsmark and Oskarshamn areas.
- R-07-50 **Carlén I, Nikolopoulos A, Isaeus, M.** Spatial modelling of marine organisms in Forsmark and Oskarshamn. Including calculation of physical predictor variables.
- R-08-01 **Löfgren A (ed).** The terrestrial ecosystems at Forsmark and Laxemar. Site descriptive modelling. SDM-Site.
- R-08-02 **Nordén S, Andersson E, Söderbäck B.** The limnic ecosystems at Forsmark and Laxemar. Site descriptive modelling, SDM-Site.
- R-08-03 **Wijnbladh E, Aquilonius K, Floderus S.** The marine ecosystems at Forsmark and Laxemar. Site descriptive modelling, SDM-Site.
- R-08-05 **Solenius G, Hedenström A.** Description of regolith at Laxemar-Simpevarp. Site descriptive modelling, SDM-Site.
- R-08-06 **Nyman H, Sohlenius G, Strömberg M, Brydsten L.** Oskarshamn site investigation – Depth and stratigraphy of regolith.
- R-08-103 **Nordqvist R, Gustafsson E, Andersson P, Thur P.** Groundwater flow and hydraulic gradients in fractures and fracture zones at Forsmark and Oskarshamn.
- R-08-104 **Nordqvist R.** Evaluation and modelling of SWIW tests performed within the SKB site characterisation programme.
- R-08-112 **Waber N, Gimmi T, Smellie J, de Haller A.** Porewater in the rock matrix. Site descriptive modelling. SDM Site Laxemar.
- R-08-124 **Viola G.** Ductile and brittle structural evolution of the Laxemar-Simpevarp area: an independent analysis based on local and regional constraints.
- R-08-138 **Cruden A R.** Emplacement mechanisms and structural influences of a younger granite intrusion into older wall rocks – a principal study with application to the Götemar and Uthammar granites. Site descriptive modelling. SDM-Site Laxemar.
- TR-93-06 **Eliasson T.** Mineralogy, geochemistry and petrophysics of red coloured granite adjacent to fractures.
- TR-94-02 **Wersin P, Spahiu K, Bruno J.** Time evolution of dissolved oxygen and redox conditions in a HLW repository.
- TR 95-13 **Landström O, Tullborg E-L.** Interactions of trace elements with fracture filling minerals from the Äspö Hars Rock laboratory.
- TR-97-02 **Stanfors R, Erlström M, Markström I.** Äspö HRL – Geoscientific evaluation 1997/2. Overview of site characterisation 1986–1995.
- TR-97-03 **Rhén I (ed), Bäckblom G (ed), Gustafson G, Stanfors R, Wikberg P.** Äspö HRL – Geoscientific evaluation 1997/1. Results from pre-investigations and detailed site characterization. Summary report
- TR-97-05 **Rhén I, Gustafson G, Wikberg P.** Äspö HRL – Geoscientific evaluation 1997/4. Results from pre-investigations and detailed site characterization. Comparison of predictions and observations. Hydrogeology, groundwater chemistry and transport of solutes.

- TR-97-06 **Rhén I (ed), Gustafson G, Stanfors R, Wikberg P.** Äspö HRL – Geoscientific evaluation 1997/5. Models based on site characterization 1986–1995.
- TR-97-14 **Engqvist A.** Water exchange estimates derived from forcing for the hydraulically coupled basins surrounding Äspö island and adjacent coastal water.
- TR-97-20 **Ohlsson Y, Neretnieks I.** Diffusion data in granite. Recommended values.
- TR-98-05 **Juhlin C, Wallroth T, Smellie J, Eliasson T, Ljunggren C, Leijon B, Beswick J.** The Very Deep Hole Concept: Geoscientific appraisal of conditions at great depth.
- TR-98-18 **Byegård J, Johansson H, Skálberg M, Tullborg E-L.** The interaction of sorbing and non-sorbing tracers with different Äspö rock types. Sorption and diffusion experiments in the laboratory scale.
- TR-99-37 **Brydsten L.** Change in coastal sedimentation conditions due to positive shore displacement in Öregrundsgrepen.
- TR-00-12 **Andersson J, Ström A, Svemar C, Almén K-A, Ericsson L-O.** What requirements does the KBS-3 repository make on the host rock? Geoscientific suitability indicators and criteria for siting and site evaluation.
- TR-01-11 **Ekman L.** Project Deep Drilling KLX02 – Phase 2. Methods, scope of activities and results. Summary.
- TR-02-03 **Larsson-McCann S, Karlsson A, Nord M, Sjögren J, Johansson L, Ivarsson M, Kindell S.** Meteorological, hydrological and oceanographical information and data for the site investigation program in the community of Oskarshamn.
- TR-02-04 **Juhlin C, Bergman B, Cosma C, Keskinen J, Enescu.** Vertical seismic profiling and integration with reflection seismic studies at Laxemar, 2000.
- TR-02-19 **Andersson J, Berglund J, Follin S, Hakami E, Halvarson J, Hermanson J, Laaksoharju M, Rhén I, Wahlgren C-H.** Testing the methodology for site descriptive modelling. Application for the Laxemar area.
- TR-04-08 **Kellner E.** Wetlands – different types, their properties and functions.
- TR-06-09 **SKB.** Long-term safety for KBS-3 repositories at Forsmark and Laxemar – a first evaluation. Main report of the SR-Can project.
- TR-06-28 **Tagesson T.** Seasonal variation and controlling factors of soil carbon effluxes in six vegetation types in southeast of Sweden.
- TR-06-29 **Tagesson T.** Indirect estimations and spatial variation in leaf area index of coniferous, deciduous and mixed forest stands in Forsmark and Laxemar.
- TR-07-11 **Persson H Stadenberg I.** Growth dynamics of fine roots in a coniferous forest site close to Forsmark in the central part of Sweden.
- TR-07-13 **Tagesson T.** Soil carbon effluxes in ecosystems of Forsmark and Laxemar.
- TR-08-02 **Engqvist A.** Validation of coastal oceanographic models at Laxemar-Simpevarp. Site descriptive modelling, SDM-Site Laxemar.
- SKI 98:41 **Xu S, Wörman A.** Statistical patterns of geochemistry in crystalline rock and effect of sorption kinetics on radionuclide migration.

Appendix 4

Table A4-1. Borehole length, elevation, inclination and bearing of all telescopic and conventionally core-drilled boreholes in the Laxemar-Simpevarp area. These borehole parameters are provided for TOC (Top Of Casing, corresponding to Length = 0 m). Furthermore, both the elevation uncertainty and radial uncertainty (see illustration in Figure 2-6) are presented.

Borehole	Length (m)	Elevation (m in RHB70)	Elevation uncertainty (m)	Inclination (degrees from horizontal)	Bearing (degrees RT 90)	Radius uncertainty (m)
KLX01	0.00	16.77	0.00	-85.30	348.73	0.00
KLX01	517.86	-500.00	2.46	-86.80	355.16	27.10
KLX01	1,077.99	-1,059.35	4.76	-87.00	351.83	56.42
KLX02	0.00	18.40	0.00	-85.00	357.30	0.00
KLX02	520.80	-500.00	3.33	-83.49	0.73	27.26
KLX02	1,700.50	-1,669.83	12.88	-81.90	4.70	89.00
KLX03	0.00	18.49	0.00	-74.93	199.04	0.00
KLX03	535.29	-500.00	4.44	-76.21	212.76	16.81
KLX03	1,000.42	-952.21	8.07	-76.57	244.69	31.42
KLX04	0.00	24.09	0.00	-84.76	0.93	0.00
KLX04	526.60	-500.00	1.87	-84.65	34.60	16.54
KLX04	993.49	-964.00	3.73	-82.60	63.33	31.21
KLX05	0.00	17.63	0.00	-65.22	190.19	0.00
KLX05	574.26	-500.00	2.42	-64.67	219.95	15.37
KLX05	1,000.16	-883.26	4.23	-63.91	241.73	26.86
KLX06	0.00	17.68	0.00	-65.20	329.65	0.00
KLX06	592.54	-500.00	5.35	-53.54	349.49	10.55
KLX06	994.94	-787.99	10.63	-38.09	355.91	17.79
KLX07A	0.00	18.47	0.00	-60.04	174.18	0.00
KLX07A	678.34	-500.00	7.86	-52.46	174.43	11.90
KLX07A	844.73	-631.27	9.65	-51.78	174.87	14.82
KLX07B	0.00	18.38	0.00	-85.15	174.33	0.00
KLX07B	200.13	-180.99	0.05	-84.79	178.34	0.51
KLX08	0.00	24.31	0.00	-60.51	199.17	0.00
KLX08	608.45	-500.00	3.53	-58.85	212.22	8.99
KLX08	1,000.41	-832.82	5.91	-56.96	212.75	15.03
KLX09	0.00	23.45	0.00	-84.94	267.41	0.00
KLX09	527.24	-500.00	1.17	-83.06	265.88	9.11
KLX09	880.38	-850.62	1.94	-83.09	272.93	15.21
KLX09B	0.00	23.61	0.00	-89.83	21.25	0.00
KLX09B	100.22	-76.60	0.01	-89.74	224.99	0.34
KLX09C	0.00	23.75	0.00	-59.52	160.39	0.00
KLX09C	120.05	-78.26	0.12	-57.22	169.55	0.91
KLX09D	0.00	23.10	0.00	-60.25	270.15	0.00
KLX09D	121.02	-80.57	0.07	-57.76	272.20	1.50
KLX09E	0.00	22.16	0.00	-59.96	338.90	0.00
KLX09E	120.00	-81.06	0.11	-58.20	346.08	0.83
KLX09F	0.00	19.57	0.00	-59.74	90.67	0.00
KLX09F	152.30	-109.96	0.09	-56.63	101.39	0.91
KLX09G	0.00	19.63	0.00	-61.08	85.41	0.00
KLX09G	100.10	-66.90	0.06	-58.43	93.67	1.03
KLX10	0.00	18.28	0.00	-85.19	250.80	0.00
KLX10	522.13	-500.00	1.08	-83.36	263.61	8.32
KLX10	1,001.20	-975.79	2.03	-83.41	275.30	15.95
KLX10B	0.00	18.15	0.00	-59.97	170.32	0.00
KLX10B	50.25	-25.05	0.05	-58.68	168.62	0.73
KLX10C	0.00	16.93	0.00	-60.03	352.43	0.00
KLX10C	146.25	-108.25	0.09	-57.38	0.42	0.97
KLX11A	0.00	27.14	0.00	-76.77	89.84	0.00

Borehole	Length (m)	Elevation (m in RHB70)	Elevation uncertainty (m)	Inclination (degrees from horizontal)	Bearing (degrees RT 90)	Radius uncertainty (m)
KLX11A	553.99	-500.00	2.55	-70.97	90.22	7.98
KLX11A	992.29	-910.99	4.79	-68.22	95.61	14.29
KLX11B	0.00	27.27	0.00	-89.93	136.16	0.00
KLX11B	100.20	-72.92	0.01	-89.48	185.99	0.24
KLX11C	0.00	27.19	0.00	-60.73	159.34	0.00
KLX11C	120.15	-77.13	0.05	-59.41	166.16	0.65
KLX11D	0.00	25.57	0.00	-59.00	268.70	0.00
KLX11D	120.35	-75.29	0.08	-54.98	275.50	1.01
KLX11E	0.00	22.65	0.00	-60.92	336.17	0.00
KLX11E	121.30	-82.05	0.13	-58.14	345.25	0.65
KLX11F	0.00	24.46	0.00	-61.14	88.61	0.00
KLX11F	120.05	-79.39	0.06	-59.00	98.48	0.65
KLX12A	0.00	17.74	0.00	-75.31	315.92	0.00
KLX12A	538.84	-500.00	0.20	-75.38	309.56	3.65
KLX12A	602.29	-561.39	0.22	-75.44	307.29	4.04
KLX13A	0.00	24.15	0.00	-82.24	224.48	0.00
KLX13A	528.28	-500.00	1.22	-83.00	227.88	9.15
KLX13A	595.85	-567.07	1.37	-83.22	229.00	10.33
KLX14A	0.00	16.35	0.00	-49.96	111.95	0.00
KLX14A	176.27	-113.36	0.18	-44.57	114.80	1.06
KLX15A	0.00	14.59	0.00	-54.42	198.83	0.00
KLX15A	672.75	-500.00	1.32	-48.10	193.17	4.47
KLX15A	1,000.43	-739.99	1.96	-46.81	190.38	6.77
KLX16A	0.00	18.85	0.00	-64.98	294.37	0.00
KLX16A	433.55	-371.44	0.89	-63.22	295.11	6.96
KLX17A	0.00	27.63	0.00	-61.34	11.21	0.00
KLX17A	613.85	-500.00	10.20	-56.39	15.86	26.77
KLX17A	701.08	-572.47	11.74	-56.00	14.89	30.92
KLX18A	0.00	21.01	0.00	-82.11	271.40	0.00
KLX18A	528.36	-500.00	0.66	-79.88	276.03	3.82
KLX18A	611.28	-581.60	0.77	-79.69	278.11	4.43
KLX19A	0.00	16.87	0.00	-57.55	197.13	0.00
KLX19A	616.43	-500.00	5.94	-56.28	194.79	10.70
KLX19A	800.07	-652.63	7.73	-56.03	193.63	13.89
KLX20A	0.00	27.24	0.00	-50.03	270.60	0.00
KLX20A	457.92	-311.34	4.06	-41.04	281.69	5.75
KLX21B	0.00	10.68	0.00	-70.86	225.05	0.00
KLX21B	547.11	-500.00	0.49	-68.42	224.72	11.47
KLX21B	858.78	-789.36	0.77	-67.94	222.97	18.24
KLX22A	0.00	21.97	0.00	-60.34	179.19	0.00
KLX22A	100.45	-64.44	0.16	-58.95	185.80	0.60
KLX22B	0.00	21.57	0.00	-61.25	343.97	0.00
KLX22B	100.25	-65.35	0.11	-58.63	351.15	1.20
KLX23A	0.00	22.26	0.00	-61.36	28.73	0.00
KLX23A	100.15	-64.46	0.11	-58.47	33.73	0.42
KLX23B	0.00	22.32	0.00	-60.85	121.36	0.00
KLX23B	50.27	-21.28	0.07	-59.45	121.94	0.24
KLX24A	0.00	21.29	0.00	-59.15	98.41	0.00
KLX24A	100.17	-63.68	0.10	-56.60	99.73	0.77
KLX25A	0.00	22.84	0.00	-59.46	145.73	0.00
KLX25A	50.24	-20.19	0.05	-58.22	146.22	0.25
KLX26A	0.00	15.63	0.00	-60.45	93.47	0.00
KLX26A	101.14	-71.80	0.06	-59.14	96.60	0.81
KLX26B	0.00	15.82	0.00	-60.01	137.42	0.00
KLX26B	50.37	-27.76	0.02	-59.59	139.60	0.27

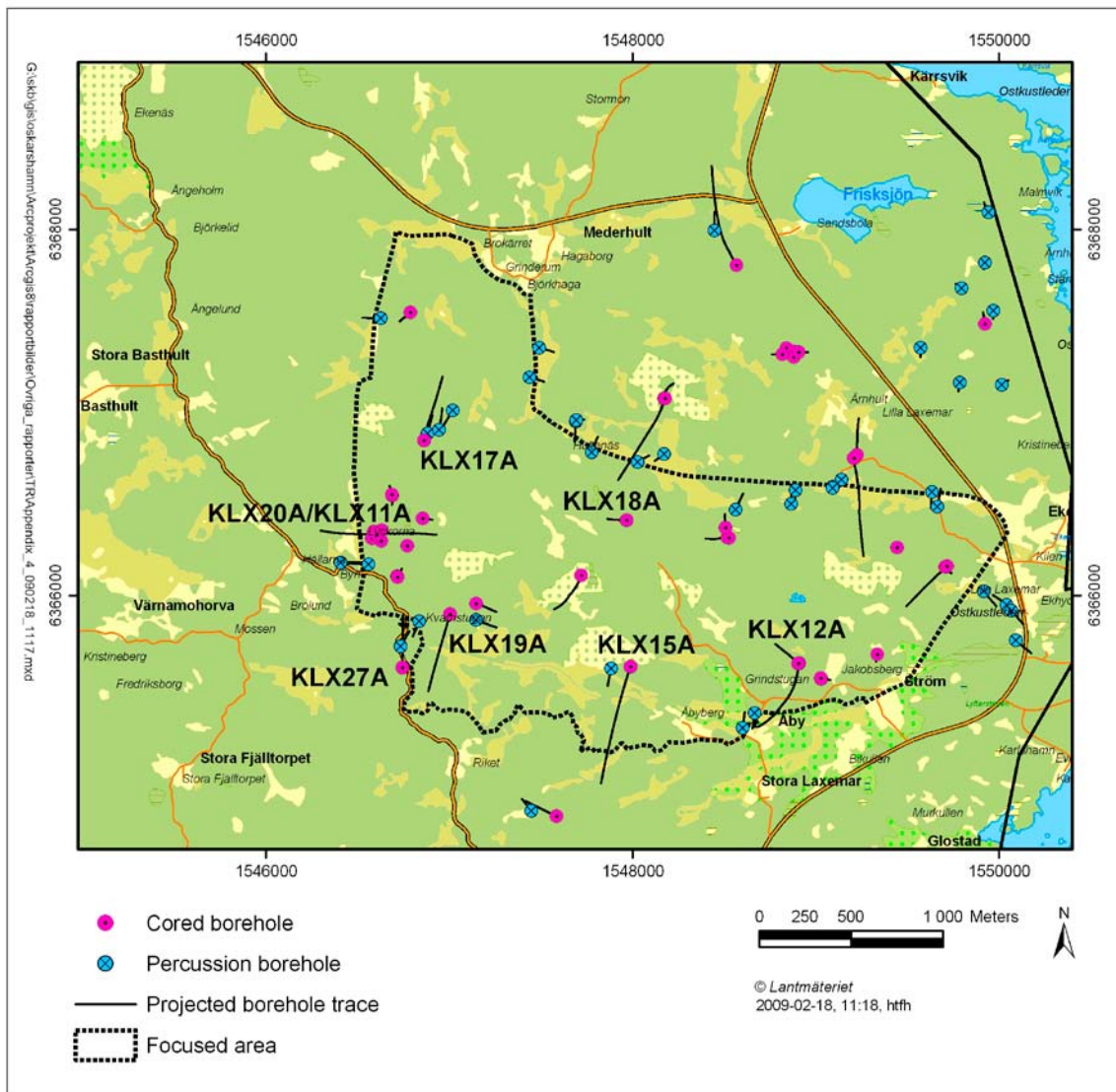
Borehole	Length (m)	Elevation (m in RHB70)	Elevation uncertainty (m)	Inclination (degrees from horizontal)	Bearing (degrees RT 90)	Radius uncertainty (m)
KLX27A	0.00	16.98	0.00	-65.37	0.73	0.00
KLX27A	574.82	-500.00	0.94	-62.51	0.12	2.39
KLX27A	650.56	-566.94	1.08	-61.44	0.97	2.73
KLX28A	0.00	10.05	0.00	-60.06	189.70	0.00
KLX28A	80.23	-58.84	0.05	-58.18	187.00	1.09
KLX29A	0.00	13.63	0.00	-60.91	321.21	0.00
KLX29A	60.25	-38.64	0.06	-59.33	323.84	0.45
KSH01A	0.00	5.32	0.00	-80.44	173.60	0.00
KSH01A	519.51	-500.00	0.66	-75.79	186.15	7.98
KSH01A	1,003.00	-963.12	1.42	-68.30	207.52	17.13
KSH01B	0.00	5.20	-	-87.88	177.76	-
KSH01B	100.25	-94.98	-	-87.88	177.76	-
KSH02	0.00	5.48	0.00	-85.63	330.68	0.00
KSH02	506.47	-500.00	0.20	-86.63	9.21	3.14
KSH02	1,001.11	-993.74	0.40	-86.42	41.23	6.20
KSH03A	0.00	4.15	0.00	-59.21	125.80	0.00
KSH03A	596.89	-500.00	10.31	-57.97	152.28	27.30
KSH03A	1,000.70	-825.68	18.12	-46.19	180.49	47.58
KSH03B	0.00	4.08	-	-64.31	128.54	-
KSH03B	100.86	-86.89	-	-64.07	132.75	-
KAV01	0.00	14.10	0.00	-89.20	225.61	0.00
KAV01	514.30	-500.00	-	-87.20	137.04	-
KAV01	757.31	-742.52	-	-85.80	141.61	-
KAV04A	0.00	10.35	0.00	-84.91	77.03	0.00
KAV04A	511.90	-500.00	0.20	-85.13	79.67	9.88
KAV04A	1,004.00	-990.26	0.40	-85.46	101.69	20.46
KAV04B	0.00	10.35	-	-89.84	134.27	-
KAV04B	101.03	-90.68	-	-89.84	134.27	-

Table A4-2. Borehole length, elevation, inclination and bearing of all percussion-drilled boreholes in the bedrock in Laxemar. These borehole parameters are provided for TOC (Top Of Casing, corresponding to Length = 0 m) and borehole bottom. Furthermore, both the elevation uncertainty and radial uncertainty (see illustration in Figure 2-6) are presented. N.B. Borehole KLX21A is a percussion–drilled hole for a telescopic cored hole that was not realised.

Borehole	Length (m)	Elevation (m in RHB70)	Elevation uncertainty (m)	Inclination (degrees from horizontal)	Bearing (degrees RT 90)	Radius uncertainty (m)
HLX01	0.00	8.90	0.00	-59.40	177.73	0.00
HLX01	100.63	-78.15	3.23	-59.10	181.63	5.33
HLX02	0.00	9.04	0.00	-59.30	327.30	0.00
HLX02	132.00	-109.08	8.30	-67.40	339.73	6.93
HLX03	0.00	10.45	0.00	-63.10	187.73	0.00
HLX03	100.00	-81.94	5.70	-70.41	191.73	5.23
HLX04	0.00	10.36	0.00	-65.20	303.73	0.00
HLX04	125.00	-107.72	7.51	-73.87	312.48	6.54
HLX05	0.00	15.71	0.00	-59.90	175.73	0.00
HLX05	100.00	-72.47	4.41	-60.46	198.06	5.23
HLX06	0.00	15.48	0.00	-58.60	182.73	0.00
HLX06	100.00	-70.71	3.68	-63.81	185.62	5.38
HLX07	0.00	8.61	0.00	-60.80	49.73	0.00
HLX07	100.00	-81.85	5.84	-70.26	60.59	5.23
HLX08	0.00	2.22	0.00	-47.80	122.30	0.00
HLX08	40.00	-26.31	2.47	-45.10	125.98	2.93
HLX09	0.00	3.31	0.00	-61.30	166.30	0.00
HLX09	151.00	-131.86	6.70	-65.90	169.53	7.90
HLX10	0.00	11.74	0.00	-68.69	176.67	0.00
HLX10	85.00	-67.45	3.98	-68.69	176.67	9.56
HLX11	0.00	13.15	0.00	-68.49	23.16	0.00
HLX11	70.00	-51.97	3.00	-68.49	23.16	7.24
HLX12	0.00	12.67	0.00	-83.88	167.15	0.00
HLX12	31.00	-18.16	0.35	-83.88	167.15	2.37
HLX13	0.00	17.39	0.00	-58.07	184.18	0.00
HLX13	200.20	-148.60	7.16	-54.37	184.85	9.56
HLX14	0.00	17.11	0.00	-68.65	89.87	0.00
HLX14	115.90	-90.41	2.49	-67.77	91.29	6.07
HLX15	0.00	4.81	0.00	-58.37	184.65	0.00
HLX15	151.90	-120.97	5.99	-54.55	195.88	7.28
HLX16	0.00	3.65	0.00	-58.10	139.90	0.00
HLX16	202.20	-168.00	19.06	-58.10	139.90	32.00
HLX17	0.00	3.35	0.00	-59.49	310.94	0.00
HLX17	202.20	-176.29	8.75	-65.40	304.77	7.90
HLX18	0.00	4.04	0.00	-57.60	135.91	0.00
HLX18	181.20	-148.56	3.37	-57.20	139.67	8.35
HLX19	0.00	5.95	0.00	-57.90	130.04	0.00
HLX19	202.20	-162.89	5.74	-56.19	129.73	9.50
HLX20	0.00	11.18	0.00	-60.38	0.41	0.00
HLX20	202.20	-164.60	18.03	-60.38	0.41	32.00
HLX21	0.00	10.31	0.00	-56.99	185.54	0.00
HLX21	150.30	-108.92	9.32	-48.94	181.93	7.81
HLX22	0.00	10.06	0.00	-59.44	13.45	0.00
HLX22	163.20	-118.74	14.27	-47.10	9.04	8.54
HLX23	0.00	14.69	0.00	-58.18	182.89	0.00
HLX23	160.20	-115.78	8.24	-50.83	180.60	7.94
HLX24	0.00	12.77	0.00	-58.39	358.69	0.00
HLX24	175.20	-126.96	12.29	-47.66	355.35	9.01
HLX25	0.00	20.66	0.00	-58.59	17.94	0.00
HLX25	202.50	-160.26	11.49	-67.26	24.91	7.68
HLX26	0.00	6.48	0.00	-60.42	12.37	0.00
HLX26	151.20	-115.78	11.51	-48.50	6.98	7.58
HLX27	0.00	8.25	0.00	-59.41	191.00	0.00

Borehole	Length (m)	Elevation (m in RHB70)	Elevation uncertainty (m)	Inclination (degrees from horizontal)	Bearing (degrees RT 90)	Radius uncertainty (m)
HLX27	164.70	-124.59	11.50	-48.04	189.73	8.29
HLX28	0.00	13.42	0.00	-59.49	201.38	0.00
HLX28	154.20	-112.81	9.01	-51.41	201.31	7.56
HLX29	0.00	10.70	0.00	-56.96	22.34	0.00
HLX29	12.90	-0.11	0.46	-56.96	22.34	0.98
HLX30	0.00	12.18	0.00	-61.04	55.82	0.00
HLX30	163.40	-134.51	3.92	-68.61	62.25	1.16
HLX31	0.00	12.16	0.00	-58.76	231.77	0.00
HLX31	133.20	-104.44	4.94	-63.25	233.79	5.49
HLX32	0.00	10.84	0.00	-58.67	28.59	0.00
HLX32	162.60	-121.19	9.45	-51.60	31.37	8.10
HLX33	0.00	12.20	0.00	-58.81	21.77	0.00
HLX33	202.10	-166.17	5.72	-65.76	25.74	1.36
HLX34	0.00	14.29	0.00	-59.73	101.07	0.00
HLX34	151.80	-112.10	4.95	-53.37	106.06	2.44
HLX35	0.00	14.44	0.00	-60.13	102.22	0.00
HLX35	151.80	-111.90	7.60	-52.62	108.44	7.18
HLX36	0.00	15.56	0.00	-59.02	270.61	0.00
HLX36	199.80	-144.81	11.17	-49.59	274.74	2.21
HLX37	0.00	15.19	0.00	-59.25	86.18	0.00
HLX37	199.80	-150.98	5.74	-52.87	92.78	1.35
HLX38	0.00	11.53	0.00	-59.46	110.04	0.00
HLX38	199.50	-149.50	10.91	-48.02	107.66	1.79
HLX39	0.00	27.04	0.00	-59.35	14.29	0.00
HLX39	199.30	-144.48	0.28	-61.12	15.60	2.63
HLX40	0.00	25.74	0.00	-59.82	11.03	0.00
HLX40	199.50	-132.51	14.29	-44.77	4.73	3.23
HLX41	0.00	21.80	0.00	-59.15	208.29	0.00
HLX41	199.50	-137.87	11.96	-48.15	211.60	3.21
HLX42	0.00	12.88	0.00	-57.21	321.51	0.00
HLX42	152.60	-114.86	0.66	-54.95	320.77	0.42
HLX43	0.00	24.20	0.00	-50.51	268.55	0.00
HLX43	170.60	-113.13	5.83	-58.16	268.46	3.23
HSH01	0.00	2.86	0.00	-69.99	4.99	0.00
HSH01	200.00	-140.76	44.31	-30.50	334.93	0.00
HSH02	0.00	6.65	0.00	-80.09	186.10	0.00
HSH02	201.00	-179.28	12.07	-57.53	173.63	0.00
HSH03	0.00	2.52	0.00	-79.49	218.94	0.00
HSH03	201.00	-195.11	0.00	-79.49	218.94	0.00
HSH04	0.00	2.86	0.00	-59.00	359.77	0.00
HSH04	236.20	-199.61	0.01	-59.00	359.77	0.00
HSH05	0.00	2.72	0.00	-57.95	180.87	0.00
HSH05	200.20	-166.97	0.00	-57.95	180.87	0.00
HSH06	0.00	2.35	0.00	-57.77	2.14	0.00
HAV09	0.00	2.17	-	-68.02	178.68	-
HAV09	200.20	-183.48	-	-68.02	178.68	-
HAV10	0.00	2.23	-	-68.47	35.08	-
HAV10	100.00	-90.80	-	-68.47	35.08	-
HAV11	0.00	2.38	-	-59.61	113.47	-
HAV11	220.50	-187.82	-	-59.61	113.47	-
HAV12	0.00	9.40	-	-58.79	0.27	-
HAV12	157.80	-125.55	-	-58.79	0.27	-
HAV13	0.00	2.21	-	-58.81	0.08	-
HAV13	142.20	-119.43	-	-58.81	0.08	-
KLX21A	0.00	10.69	0.00	-50.72	134.83	0.00
KLX21A	75.00	-47.54	0.05	-50.95	134.09	1.18

WellCAD composites for cored boreholes in the focused volume

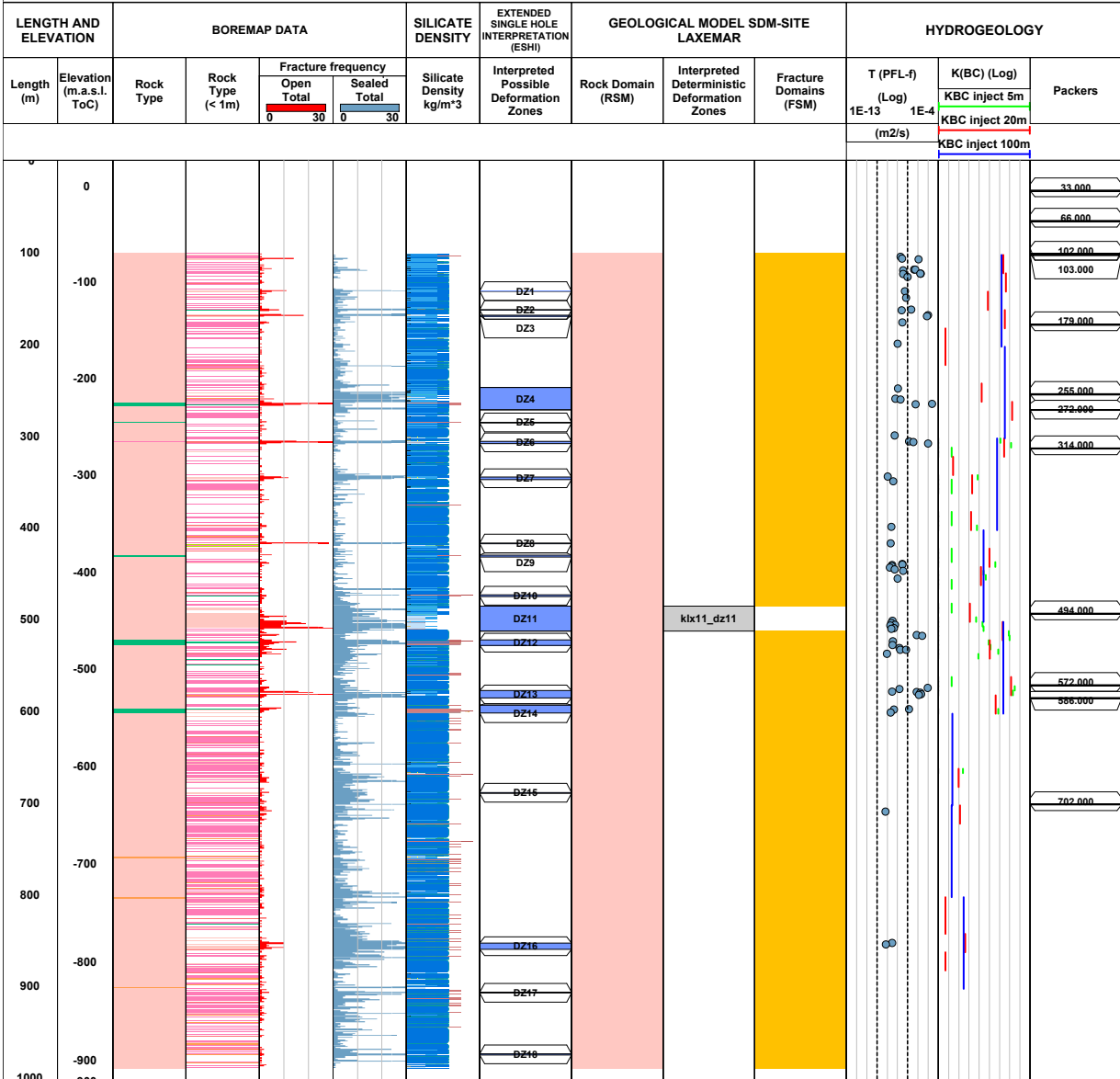


Title COMPOSITE LOG for cored borehole KLX11A



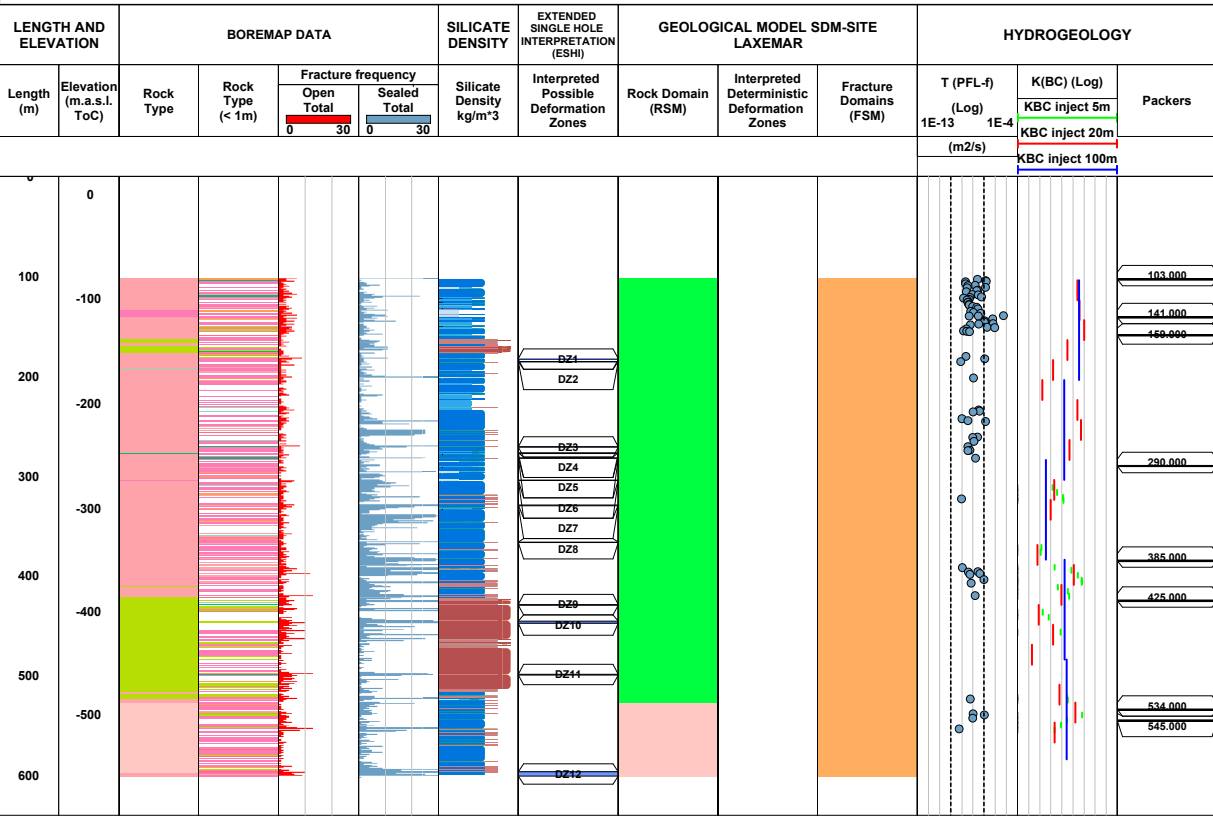
Site LAXEMAR
Borehole KLX11A
Diameter [mm] 76
Length [m] 992.290
Bearing ToC [°] 89.84
Coordinate System RT90-RHB70
Northing ToC [m] 6366339.72
Easting ToC [m] 1546608.49
Elevation [m.a.s.l.ToC] 27.14
Inclination ToC [°] -76.76
Drilling Start Date 2005-11-24 06:00:00
Drilling Stop Date 2006-03-02 11:00:00
Surveying Date 2005-11-09 10:15:00
Plot Date 2009-02-03 23:05:00

ROCK TYPE LAXEMAR Fine-grained granite Pegmatite Quartz monzodiorite Fine-grained diorite-gabbro	SILICATE DENSITY dens<2680 2680<dens<2730 2730<dens<2800 2800<dens<2890 dens>2890	ROCK DOMAIN (RSM) RSM01	DEFORMATION ZONE FROM ESHI DZ FRACTURE DOMAINS (FSM) FSM W
DEFORMATION ZONE (ZSM) DZ (In BH)			



Title COMPOSITE LOG for cored borehole KLX12A				
	Site	LAXEMAR	Elevation [m.a.s.l.ToC]	17.74
	Borehole	KLX12A	Inclination ToC [°]	-75.30
	Diameter [mm]	76	Drilling Start Date	2005-11-10 09:30:00
	Length [m]	602.290	Drilling Stop Date	2006-03-04 14:48:00
	Bearing ToC [°]	315.92	Surveying Date	2005-10-31 12:15:00
	Coordinate System	RT90-RHB70	Plot Date	2009-02-03 23:05:00
Northing ToC [m]	6365630.78			
Easting ToC [m]	1548904.44			

ROCK TYPE LAXEMAR	SILICATE DENSITY	ROCK DOMAIN (RSM)	DEFORMATION ZONE FROM ESHI
Fine-grained granite	dens<2680	RSM001	DZ
Ävrö granite	2680<dens<2730	RSMM01	FRACTURE DOMAINS (FSM)
Quartz monzodiorite	2730<dens<2800		FSM NE005
Diorite / Gabbro	2800<dens<2890		
Fine-grained dioritoid	dens>2890	DEFORMATION ZONE (ZSM)	
Fine-grained diorite-gabbro			

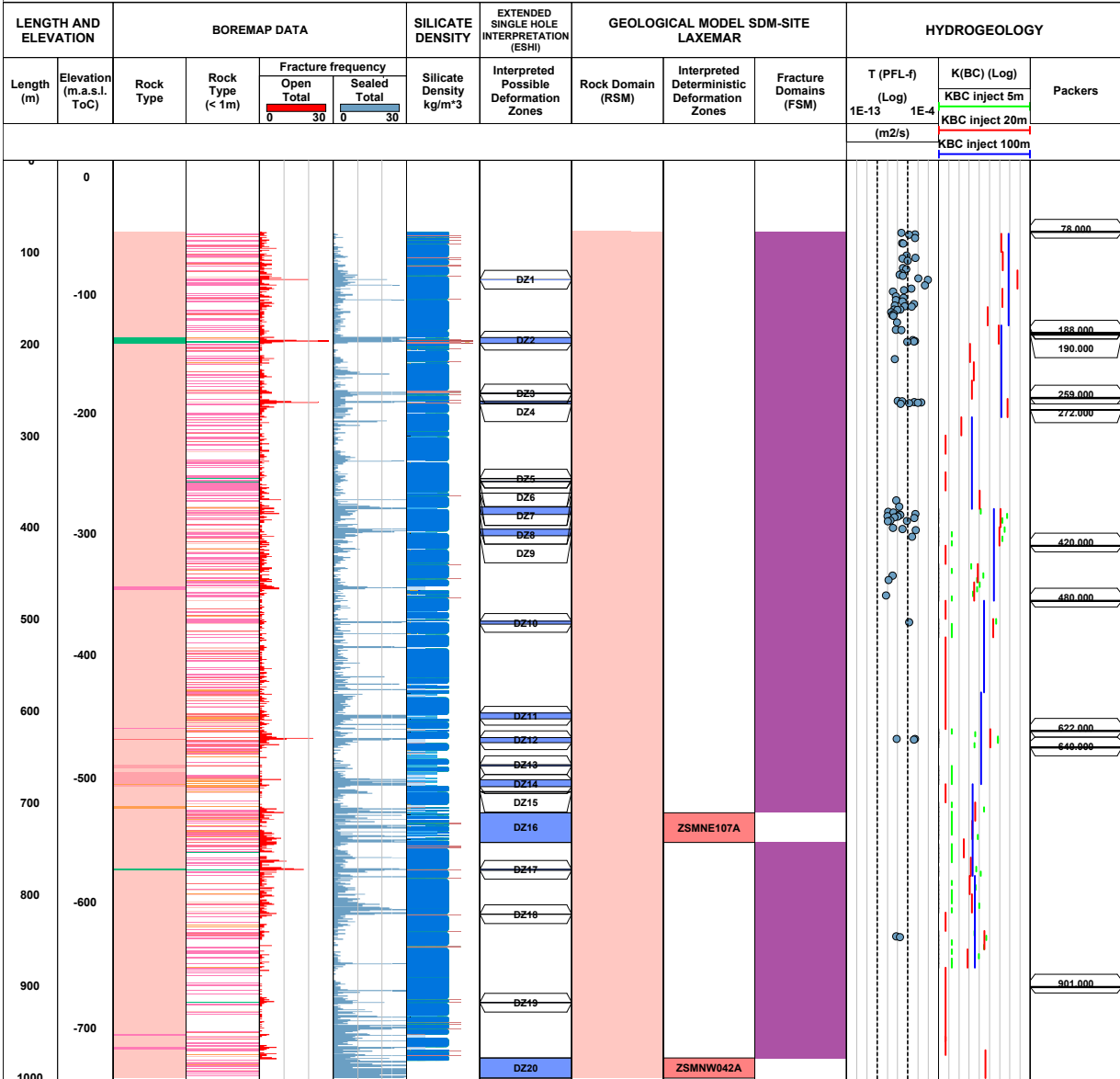



Title COMPOSITE LOG for cored borehole KLX15A



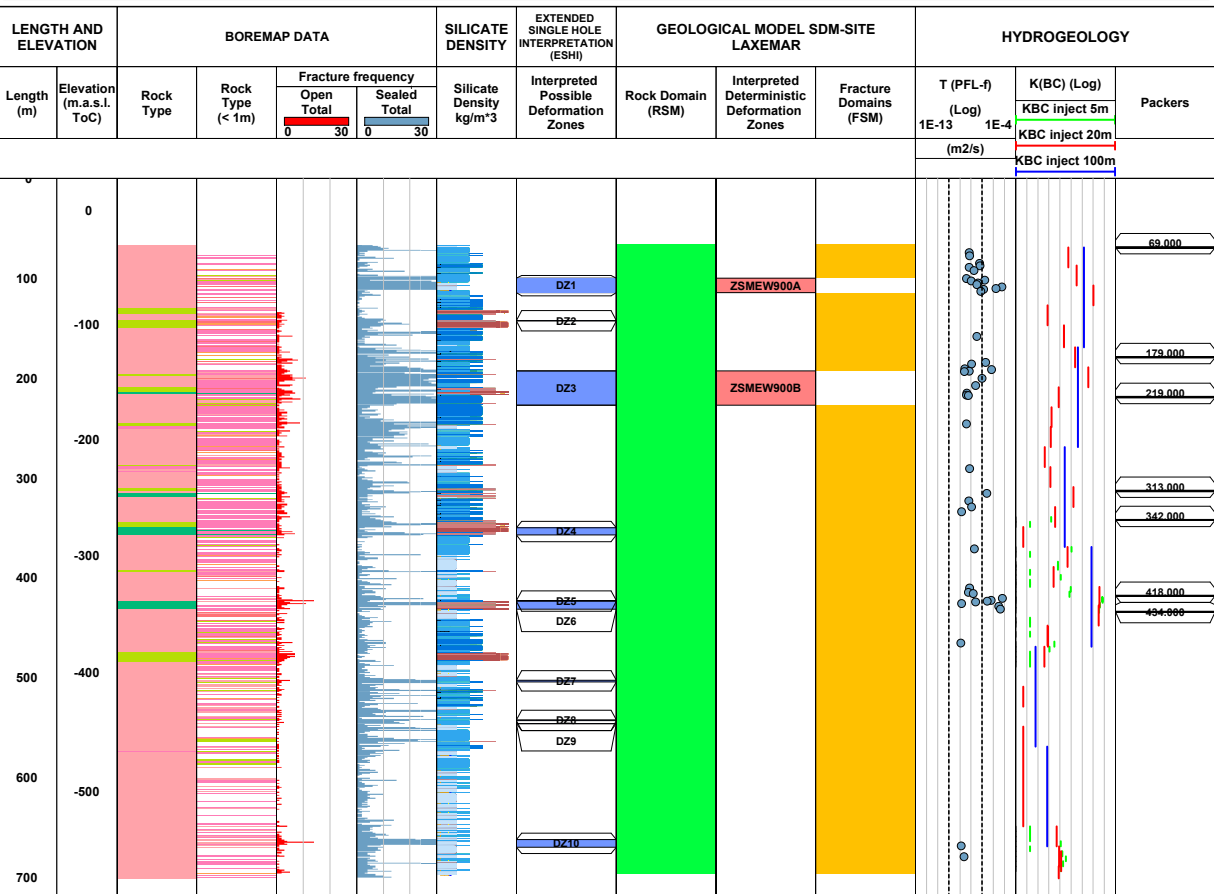
Site	LAXEMAR	Elevation [m.a.s.l.ToC]	14.59
Borehole	KLX15A	Inclination ToC [°]	-54.41
Diameter [mm]	76	Drilling Start Date	2007-01-17 10:30:00
Length [m]	1000.430	Drilling Stop Date	2007-02-25 20:00:00
Bearing ToC [°]	198.83	Surveying Date	2007-01-02 12:45:00
Coordinate System	RT90-RHB70	Plot Date	2009-02-04 23:05:12
Northing ToC [m]	6365614.17		
Easting ToC [m]	1547987.47		


ROCK TYPE LAXEMAR Fine-grained granite Pegmatite Granite Ävrö granite Quartz monzodiorite Fine-grained diorite-gabbro	SILICATE DENSITY dens<2680 2680<dens<2730 2730<dens<2800 2800<dens<2890 dens>2890	ROCK DOMAIN (RSM) RSM01	DEFORMATION ZONE FROM ESHI DZ FRACTURE DOMAINS (FSM) FSM C
		DEFORMATION ZONE (ZSM) DZ (ZSM)	



Title COMPOSITE LOG for cored borehole KLX17A				
	Site	LAXEMAR	Elevation [m.a.s.l.ToC]	27.63
	Borehole	KLX17A	Inclination ToC [°]	-61.33
	Diameter [mm]	76	Drilling Start Date	2006-09-13 06:00:00
	Length [m]	701.080	Drilling Stop Date	2006-10-23 09:30:00
	Bearing ToC [°]	11.21	Surveying Date	2006-08-16 16:03:00
	Coordinate System	RT90-RHB70	Plot Date	2009-02-04 23:05:12
	Northing ToC [m]	6366848.75		
Easting ToC [m]	1546862.09			

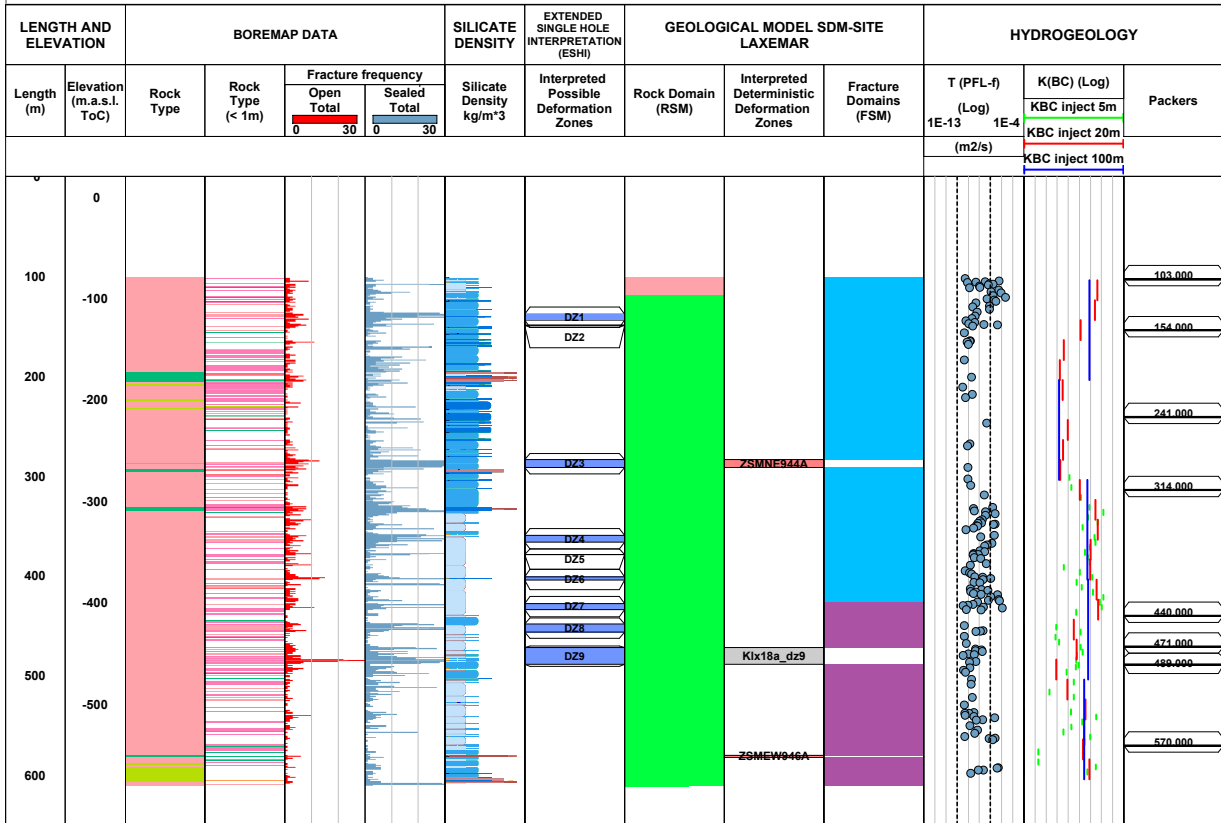
ROCK TYPE LAXEMAR	SILICATE DENSITY	ROCK DOMAIN (RSM)	DEFORMATION ZONE FROM ESHI
Fine-grained granite	dens<2680	RSMM01	DZ
Åvrö granite	2680<dens<2730		FRACTURE DOMAINS (FSM)
Diorite / Gabbro	2730<dens<2800		FSM W
Fine-grained diorite-gabbro	2800<dens<2890		
	dens>2890	DEFORMATION ZONE (ZSM)	
		DZ (ZSM)	




Title COMPOSITE LOG for cored borehole KLX18A				
	Site	LAXEMAR	Elevation [m.a.s.l.ToC]	21.01
	Borehole	KLX18A	Inclination ToC [°]	-82.10
	Diameter [mm]	76	Drilling Start Date	2006-03-29 10:00:00
	Length [m]	611.280	Drilling Stop Date	2006-05-02 12:22:00
	Bearing ToC [°]	271.40	Surveying Date	2006-02-22 11:15:00
	Coordinate System	RT90-RHB70	Plot Date	2009-02-04 23:05:12
	Northing ToC [m]	6366413.39		
Easting ToC [m]	1547966.35			

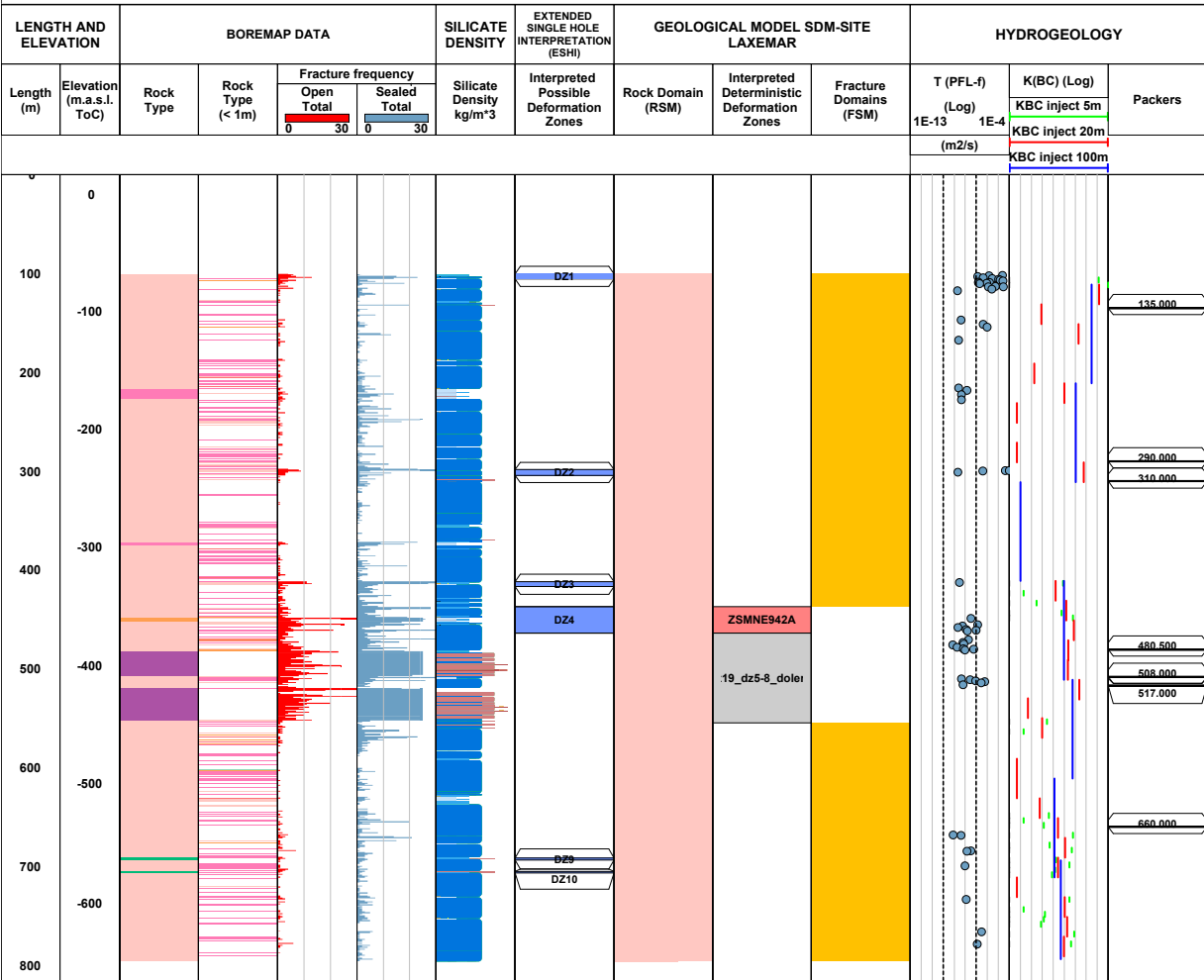
ROCK TYPE	LAXEMAR	SILICATE DENSITY	ROCK DOMAIN (RSM)	DEFORMATION ZONE FROM ESHI
	Fine-grained granite			
	Åvrö granite			
	Diorite / Gabbro			
	Fine-grained diorite-gabbro			

DEFORMATION ZONE (ZSM)	
	DZ (ZSM)
	DZ (In BH)

















Title COMPOSITE LOG for cored borehole KLX19A				
	Site	LAXEMAR	Elevation [m.a.s.l.ToC]	16.87
	Borehole	KLX19A	Inclination ToC [°]	-57.54
	Diameter [mm]	76	Drilling Start Date	2006-06-03 11:00:00
	Length [m]	800.070	Drilling Stop Date	2006-09-20 17:27:00
	Bearing ToC [°]	197.13	Surveying Date	2006-05-22 13:39:00
	Coordinate System	RT90-RHB70	Plot Date	2009-02-04 23:05:12
	Northing ToC [m]	6365901.42		
Easting ToC [m]	1547004.62			

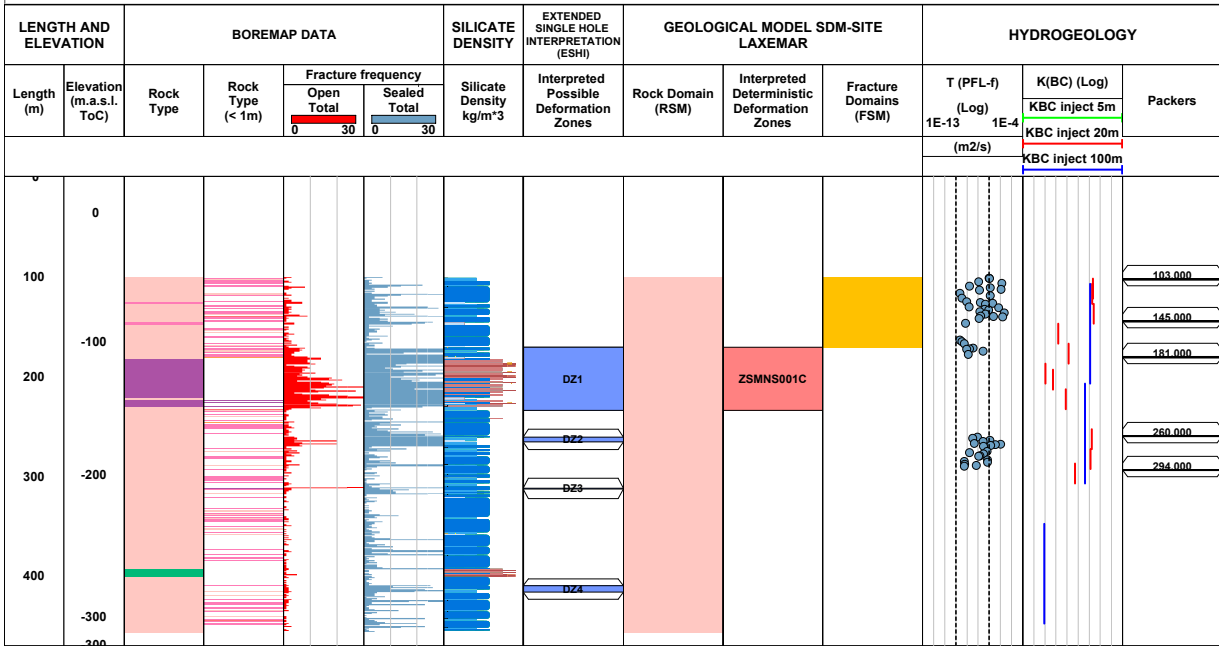
ROCK TYPE LAXEMAR	SILICATE DENSITY	ROCK DOMAIN (RSM)	DEFORMATION ZONE FROM ESHI
Dolerite	dens<2680	RSMD01	DZ
Fine-grained granite	2680<dens<2730		FRACTURE DOMAINS (FSM)
Pegmatite	2730<dens<2800		FSM W
Quartz monzodiorite	2800<dens<2890		
Fine-grained diorite-gabbro	dens>2890	DEFORMATION ZONE (ZSM)	
		DZ (ZSM)	
		DZ (In BH)	



Title COMPOSITE LOG for cored borehole KLX20A

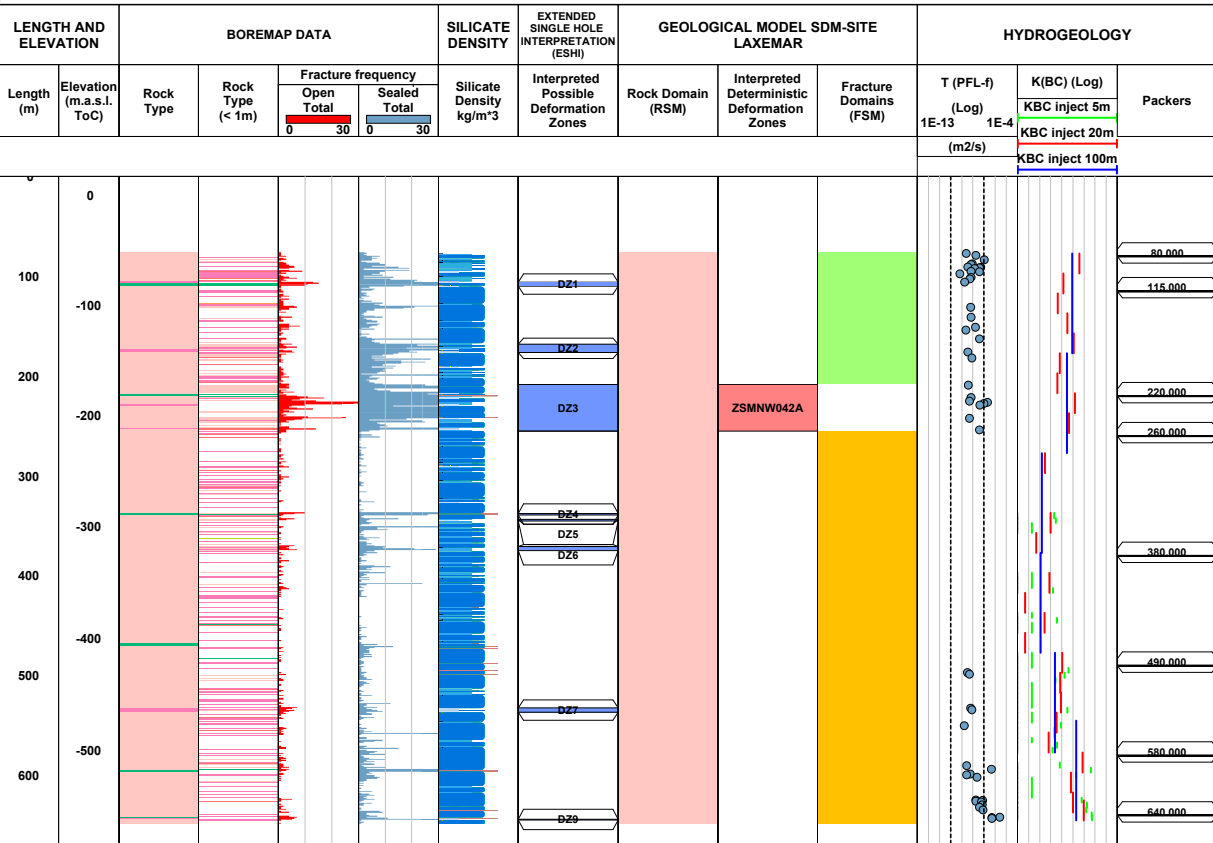
	Site	LAXEMAR	Elevation [m.a.s.l.ToC]	27.24
	Borehole	KLX20A	Inclination ToC [°]	-50.02
	Diameter [mm]	76	Drilling Start Date	2006-03-25 06:00:00
	Length [m]	457.920	Drilling Stop Date	2006-04-24 13:20:00
	Bearing ToC [°]	270.60	Surveying Date	2006-05-09 09:15:00
	Coordinate System	RT90-RHB70	Plot Date	2009-02-04 23:05:12
	Northing ToC [m]	6366334.57		
	Easting ToC [m]	1546604.89		

ROCK TYPE LAXEMAR	SILICATE DENSITY	ROCK DOMAIN (RSM)	DEFORMATION ZONE FROM ESHI
 Dolerite	 dens<2680	 RSM D01	 DZ
 Fine-grained granite	 2680<dens<2730		FRACTURE DOMAINS (FSM)
 Quartz monzodiorite	 2730<dens<2800		 FSM W
 Fine-grained diorite-gabbro	 2800<dens<2890		
	 dens>2890	DEFORMATION ZONE (ZSM)	
		 DZ (ZSM)	



Title COMPOSITE LOG for cored borehole KLX27A				
	Site	LAXEMAR	Elevation [m.a.s.l.ToC]	16.98
	Borehole	KLX27A	Inclination ToC [°]	-65.36
	Diameter [mm]	76	Drilling Start Date	2007-10-08 14:00:00
	Length [m]	650.560	Drilling Stop Date	2007-11-21 11:30:00
	Bearing ToC [°]	0.73	Surveying Date	2007-09-07 13:30:00
	Coordinate System	RT90-RHB70	Plot Date	2009-02-04 23:05:12
Northing ToC [m]	6365608.29			
Easting ToC [m]	1546742.63			

ROCK TYPE LAXEMAR	SILICATE DENSITY	ROCK DOMAIN (RSM)	DEFORMATION ZONE FROM ESHI
Fine-grained granite	dens<2680	RSM01	DZ
Quartz monzodiorite	2680<dens<2730		FRACTURE DOMAINS (FSM)
Fine-grained diorite-gabbro	2730<dens<2800		FSM W
	2800<dens<2890		FSM S
		DEFORMATION ZONE (ZSM)	
		DZ (ZSM)	



Properties of deformation zones modelled to intersect the focused volume between –400 and –600 masl

The geological and hydrogeological properties of the thirty seven (37) deformation zones that have been modelled to intersect the Laxemar focused volume between –400 to –600 m elevation are summarized in the tables in this appendix. Six (6) of these zones are gently dipping and thirty-one (31) zones are steeply dipping structures. Eight (8) of the steeply dipping zones have a trace length at the ground surface that is longer than 3,000 m (ZSMNE005A, ZSMNE011A ZSMNE107A, ZSMNS001C (with the inclusion of sections A to E), ZSMNS059A, ZSMEW002A, ZSMNW042A and ZSMEW007A (with the inclusion of section C). Nineteen (19) zones are devoid of any identified ground surface expression. No local minor deformation zones (trace length of < 1,000 m) are included in the deterministic model.

Transmissivities assigned to the deformation zones are:

Measured T (sum T(PFL-f)): Summed-up measured T from PFL-f for individual boreholes intercepting the deformation zone in the given depth interval.

Model T: Calibrated T value of zone extracted from the ConnectFlow base case model for the given depth interval.

The tables in this appendix provide basic data concerning the deformation zones intersecting the focused volume. A more comprehensive geological of all deformation zones intersecting the local model volume can be found in Appendix 14 /Wahlgren et al. 2008/.

Contents

Format for zone property descriptions

NE-SW Striking deformation zones, steeply dipping

Deformation zone ZSMNE005A
Deformation zone ZSMNE011A
Deformation zone ZSMNE063A
Deformation zone ZSMNE107A
Deformation zone ZSMNE108A
Deformation zone ZSMNE942A
Deformation zone ZSMNE944A

N-S Striking deformation zones, steeply dipping

Deformation zone ZSMNS001A-E
Deformation zone ZSMNS046A
Deformation zone ZSMNS059A
Deformation zone ZSMNS945A
Deformation zone ZSMNS947A
Deformation zone KLX04_dz6b
Deformation zone KLX04_dz6c
Deformation zone KLX07_dz13
Deformation zone KLX21B_dz10-12
Deformation zone KLX28_dz1

E-W to NW-SE striking deformation zones, steep to moderately southward dipping

Deformation zone ZSMEW002A
Deformation zone ZSMEW120A
Deformation zone ZSMEW900A-B
Deformation zone ZSMNW042A
Deformation zone ZSMNW119A
Deformation zone KLX07_dz7
Deformation zone KLX08_dz6
Deformation zone KLX18_dz9

E-W to NW-SE striking deformation zones, steep to moderately northward dipping

Deformation zone ZSMEW007A-C
Deformation zone KLX07_dz9
Deformation zone KLX07_dz11
Deformation zone KLX07_dz12
Deformation zone KLX10C_dz3
Deformation zone KLX10C_dz7

Gently dipping deformation zones

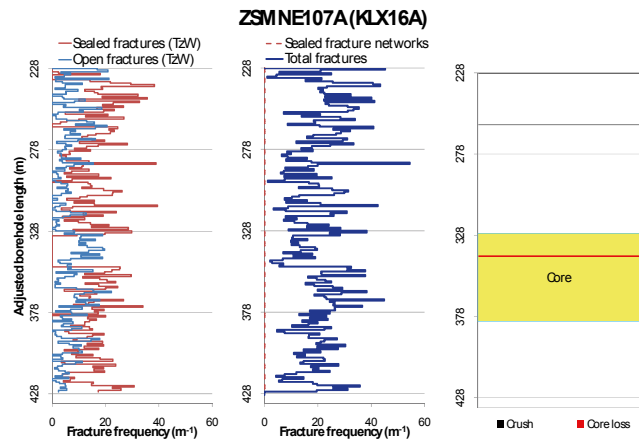
Deformation zone ZSMEW946A
Deformation zone KLX03_dz1b
Deformation zone KLX03_dz1c
Deformation zone KLX07_dz10
Deformation zone KLX08_dz10
Deformation zone KLX11_dz11

Format for zone property descriptions

Deformation zone: <i>Zone name</i>	
<p style="text-align: center;">Borehole intersections (metres along borehole)</p> <p>Borehole name: <i>intersection depth.</i> ESHI= <i>Extended Single Hole Interpretation</i> DZ_x= <i>Numbered possible deformation zone from ESHI</i></p>	<p><i>Figure showing the location of the zone, relevant boreholes and the local model boundary.</i></p>
<p style="text-align: center;">Deformation style, alteration and geometry</p> <p>Deformation style: <i>statement of evidence for a ductile and/or brittle zone character.</i></p> <p>Alteration: <i>type of alteration.</i></p> <p>Strike/dip (right-hand-rule): <i>modelled average zone orientation.</i></p> <p>Trace length at ground surface: <i>x.x km, not limited by the model boundary. Sometimes referred to as the 'geological length'.</i></p> <p>Model thickness / model thickness span : <i>x m / x-x m</i></p> <p>Measured thickness (-400 to -600 m elevation): <i>x m</i></p> <p>Comment:</p>	
Fractures in the deformation zone	
<p><i>Terzaghi corrected, borehole specific, fracture orientations within the modelled zone boundaries.</i></p>	
<p>Elevation: <i>-x to -x m (RHB 70)</i></p>	
Transmissivity (m²/s)	
<p>General dip of PFL-features, elevation -400 to -600m: <i>x</i> Measured T (sum T(PFL-f)), elevation -400 to -600m: <i>x</i> Number of PFL-features, elevation -400 to -600m: <i>x</i> Model T, elevation -400 to -500m: <i>x.x E-6</i> Model T, elevation -500 to -600m: <i>x.x E-7</i></p>	

Deformation zone: *Zone name*

Terzaghi corrected, selected borehole specific, fracture frequencies within the modelled zone boundaries. Deformation core zone marked in yellow. Position of crush and core-loss, not included in fracture frequency calculations, shown in grey and red respectively. All depths refer to adjusted values after borehole surveying.



Fracture frequency, P₁₀ (number of fractures/m), were calculated for 1-m bins, starting from (adjusted) SEC_UP of the DZ. The lowest bin is constrained by the (adjusted) SEC_LOW, and may therefore be smaller than 1 m.

Example: A DZ defined between 100.5 m to 103.0 m, will be resolved into three bins: 100.5 to 101.5 m, 101.5 to 102.5 m, and 102.5 to 103.0 m.

Partly open fractures are included in the data set “open fractures”. The Terzaghi-weighted P₁₀ for a 1-m bin is calculated as

$$P_{10} = \frac{\sum_n \frac{1}{\sin(\max[\alpha, \alpha_{\min}])}}{L}, \text{ minimum bias angle, } \alpha_{\min} = 15^\circ \Leftrightarrow \text{Max TzW} = 3.86,$$

Where L = 1 m, and n is the number of fractures inside the bin. The minimum bias angle is used to avoid artificial weights for small angles, where the effects of non-zero borehole radius are not negligible. The Terzaghi weighing is not implemented for sealed networks and crush zones, as TW concerns geometric bias owing to orientation of planar features versus scan line (borehole); the orientation of a sealed nw or crush zone, itself, is generally unclear (even if fractures inside are defined).

P₁₀ for a sealed nw or crush zone is calculated by: 1000 [mm/m]/d [mm], where d is the piece-length of rock between fractures, in the unit m. It is superimposed onto the DZ 1-m bins, by fractional section length inside each bin.

Example: A crush with piece length 10 mm extends from 99.0 m to 102.0m. The crush has a P₁₀ of 100 [1/m]. The first bin (ex. above) 100.5 to 101.5 m, will have a crush P₁₀ of 100 [1/m], while the second bin, 101.5 to 102.5 m will have a crush P₁₀ of 50 [1/m], as only half of the second bin contains crush.

Crush P₁₀ is not shown explicitly, but included in the total frequency = Open (TzW) + Sealed (TzW) + crush + sealed nw.

In the third graph, the SEC_UP/SEC_LOW is shown for DZ core, crush, and core-loss. These reflect actual lengths – not binned.

Deformation zone: Zone name

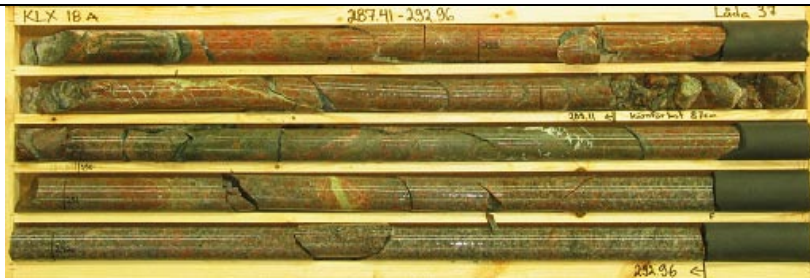


Photo of drill core from part of the deformation zone. Generally part of a core zone if such has been identified. The depth numbers shown at the top of each core box are generally unadjusted measurements (not based on detailed borehole geometry survey) since photography was performed at an early stage prior to the down-hole survey.

Engineering characteristics

Transition part of zone:

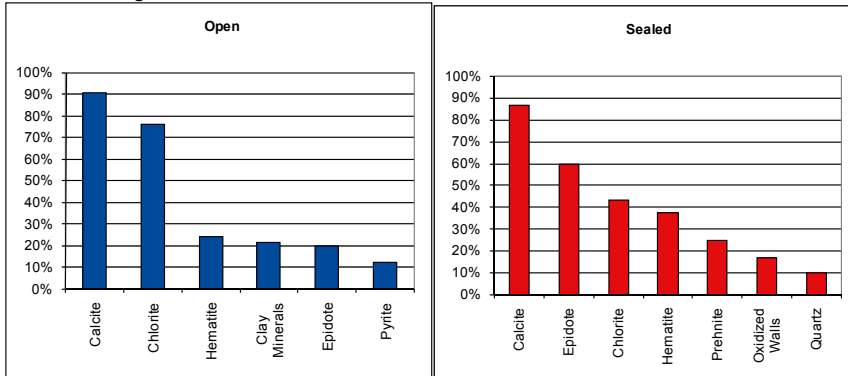
Frequency of open fractures: $x.x \text{ m}^{-1}$

Std dev: $x.x$

Frequency of sealed fractures: $x.x \text{ m}^{-1}$

Std dev: $x.x$

Mineral coatings



Fault core:

Percentage of fault core: fault core percentage of DZ/DZs, $x \%$

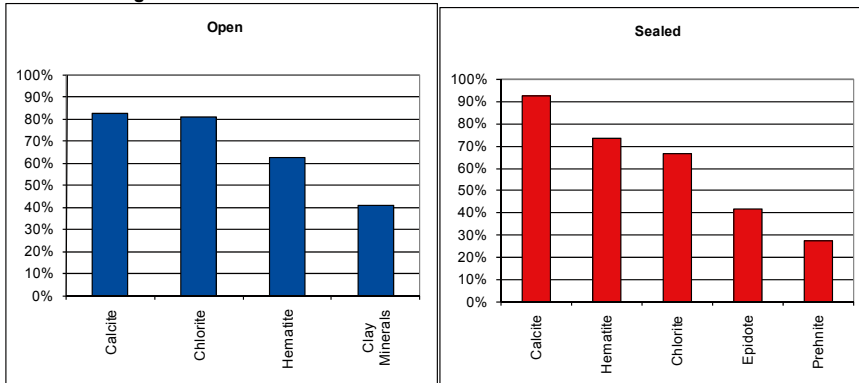
Frequency of open fractures: $x.x \text{ m}^{-1}$

Std dev: $x.x$

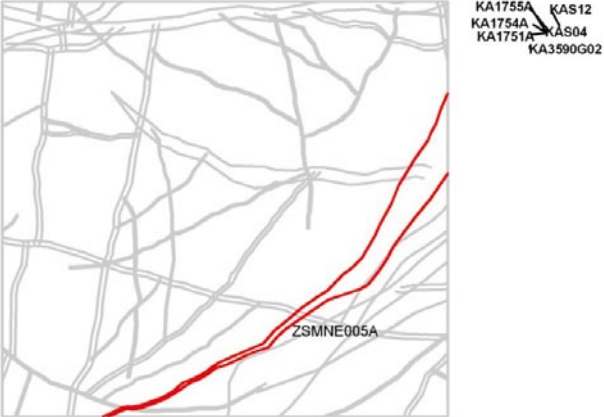
Frequency of sealed fractures: $x.x \text{ m}^{-1}$

Std dev: $x.x$



Mineral coatings




NE-SW striking deformation zones, steeply dipping

Deformation zone ZSMNE005A		
<p>Borehole intersections (metres along borehole)</p> <p>HLX09: no data HLX16: no data HLX17: no data KA1751A: 110-114 m KA1754A: 90-115 m KA1755A: 95-140 m KA3590G02: 19-30 m KAS04: 131-437 m KAS12: 19-286 m KAS17: no data KA2598A: no data KA3600F: no data KA3510A: no data KA2563A: no data</p>		
<p>Deformation style, alteration and geometry</p> <p>Deformation style: ductile and brittle</p> <p>Alteration: red staining. Evidence from bounding outcrops</p> <p>Strike/dip (right-hand-rule): 060/90</p> <p>Trace length at ground surface: 16 km</p> <p>Model thickness / model thickness span : 250 m / 10-300 m</p> <p>Measured thickness (-400 to -600 m elevation): no data</p> <p>Comment: no data obtained during the current site investigation within the local model volume.</p>		
Fractures in the deformation zone		
KA1751A	KA1754A	KA1755A
<p>Elevation: -247 to -247.2 m (RHB 70) no data</p>	<p>Elevation: -277 to -288 m (RHB 70) no data</p>	<p>Elevation: -269.9 to -285.6 m (RHB 70) no data</p>
<p>Transmissivity (m²/s)</p> <p>General dip of PFL-features, elevation -400 to -600m: no data</p> <p>Measured T (sum T(PFL-f)), elevation -400 to -600m: no data</p> <p>Number of PFL-features, elevation -400 to -600m: no data</p> <p>Model T, elevation -400 to -500m: 1.49E-6</p> <p>Model T, elevation -500 to -600m: 8.27E-7</p>	<p>Transmissivity (m²/s)</p> <p>General dip of PFL-features, elevation -400 to -600m: no data</p> <p>Measured T (sum T(PFL-f)), elevation -400 to -600m: no data</p> <p>Number of PFL-features, elevation -400 to -600m: no data</p> <p>Model T, elevation -400 to -500m: 1.49E-6</p> <p>Model T, elevation -500 to -600m: 8.27E-7</p>	<p>Transmissivity (m²/s)</p> <p>General dip of PFL-features, elevation -400 to -600m: no data</p> <p>Measured T (sum T(PFL-f)), elevation -400 to -600m: no data</p> <p>Number of PFL-features, elevation -400 to -600m: no data</p> <p>Model T, elevation -400 to -500m: 1.49E-6</p> <p>Model T, elevation -500 to -600m: 8.27E-7</p>

Deformation zone ZSMNE005A		
KA3590G02	KAS04	KAS12
Elevation: -461.2 to -468.8 m (RHB 70) no data	Elevation: -100.7 to -357.4 m (RHB 70) no data	Elevation: -13 to -259.6 m (RHB 70) no data
Transmissivity (m²/s)	Transmissivity (m²/s)	Transmissivity (m²/s)
General dip of PFL-features, elevation -400 to -600m: no data Measured T (sum T(PFL-f)), elevation -400 to -600m: no data Number of PFL-features, elevation -400 to -600m: no data Model T, elevation -400 to -500m: 1.49E-6 Model T, elevation -500 to -600m: 8.27E-7	General dip of PFL-features, elevation -400 to -600m: no data Measured T (sum T(PFL-f)), elevation -400 to -600m: no data Number of PFL-features, elevation -400 to -600m: no data Model T, elevation -400 to -500m: 1.49E-6 Model T, elevation -500 to -600m: 8.27E-7	General dip of PFL-features, elevation -400 to -600m: no data Measured T (sum T(PFL-f)), elevation -400 to -600m: no data Number of PFL-features, elevation -400 to -600m: no data Model T, elevation -400 to -500m: 1.49E-6 Model T, elevation -500 to -600m: 8.27E-7
Engineering characteristics		
Fracture orientation: 220/85, 110/80, 250/30, 025/20 Fracture frequency: 9 m ⁻¹ (limited dataset) Crush zone: no data Fracture filling: Calcite, chlorite, epidote, hematite, quartz Percentage of fault core: no data		

Deformation zone ZSMNE011A	
<p>Borehole intersections (metres along borehole)</p> <p>None</p>	
<p>Deformation style, alteration and geometry</p> <p>Deformation style: brittle and ductile</p> <p>Alteration: red staining</p> <p>Strike/dip (right-hand-rule): 050/90</p> <p>Trace length at ground surface: 10.5 km</p> <p>Model thickness / model thickness span : 100 m / 50-150 m</p> <p>Measured thickness (-400 to -600 m elevation): no data</p> <p>Comment:</p>	
Fractures in the deformation zone	
<p>No data</p>	 <p>Outcrop PSM004118 brittle ductile deformation associated with ZSMNE011A.</p>
Transmissivity (m²/s)	
<p>General dip of PFL-features, elevation -400 to -600m: no data</p> <p>Measured T (sum T(PFL-f)), elevation -400 to -600m: no data</p> <p>Number of PFL-features, elevation -400 to -600m: no data</p> <p>Model T, elevation -400 to -500m: 1.49E-6</p> <p>Model T, elevation -500 to -600m: 8.27E-7</p>	
Engineering characteristics	
<p>No borehole intercepts</p>	

Deformation zone ZSMNE063A	
<p style="text-align: center;">Borehole intersections (metres along borehole)</p> <p>None</p>	
Deformation style, alteration and geometry	
<p>Deformation style: brittle and ductile (no direct evidence- inferred association with other NE-SW trending deformation zones)</p> <p>Alteration: oxidation</p> <p>Strike/dip (right-hand-rule): 040/90</p> <p>Trace length at ground surface: 1.1 km</p> <p>Model thickness / model thickness span : 10 m / 5-20 m</p> <p>Measured thickness (-400 to -600 m elevation): no data</p> <p>Comment:</p>	
Fractures in the deformation zone	
Transmissivity (m²/s)	
<p>General dip of PFL-features, elevation -400 to -600m: no data</p> <p>Measured T (sum T(PFL-f)), elevation -400 to -600m: no data</p> <p>Number of PFL-features, elevation -400 to -600m: no data</p> <p>Model T, elevation -400 to -500m: 2.26E-7</p> <p style="padding-left: 100px;">Model T, elevation -500 to -600m: 1.37E-7</p>	
Engineering characteristics	
<p>Fracture orientation: 220/85, 100/65, 250/30, 025/20 (no direct evidence- inferred association with other NE-SW trending deformation zones)</p> <p>Fracture frequency: no data</p> <p>Crush zone: no data</p> <p>Fracture filling: no data</p> <p>Fault core: no data</p>	

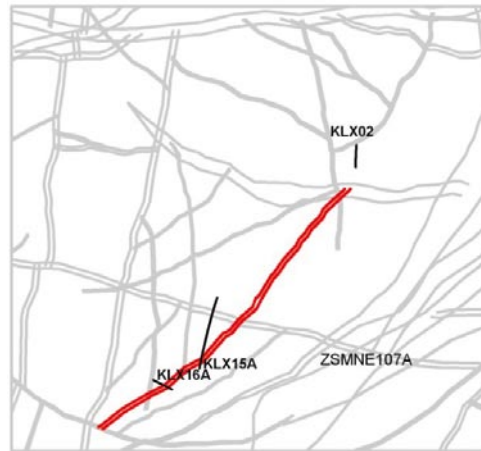
Deformation zone ZSMNE107A

Borehole intersections (metres along borehole)

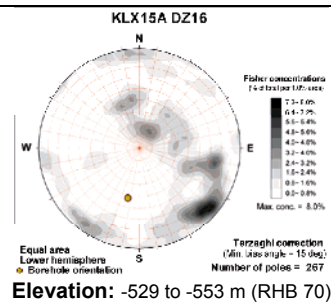
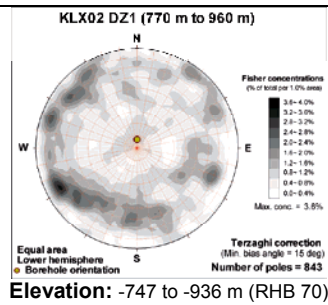
HLX10: - m (no data)
 KLX02: 770-960 m (ESHI DZ1 770-960 m)
 KLX15A: 711-744 m (ESHI DZ16 711-744 m)
 KLX16: 228-434 m (ESHI DZ9 228-231 m, DZ10 252-254 m, DZ11 259-266 m, DZ12 327-434 m)

Deformation style, alteration and geometry

Deformation style: ductile and brittle
Alteration: red staining and saussuritisation.
Strike/dip (right-hand-rule): 225/80
Trace length at ground surface: 3.1 km
Model thickness / model thickness span : 35 m / 10-40 m
Measured thickness (-400 to -600 m elevation): 15 m (KLX15A DZ16)
Comment: length- possible break at ZSMNW042A that would give an interpretation as two separate structures would halve the length.



Fractures in the deformation zone



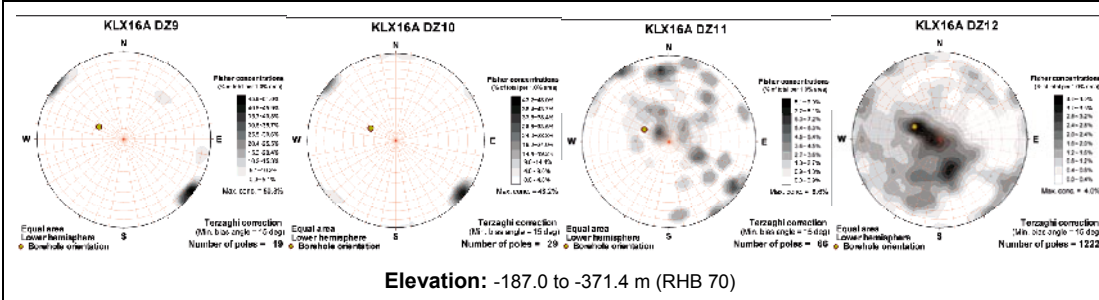
Transmissivity (m²/s)

General dip of PFL-features, elevation -400 to -600m: no data
 Measured T (sum T(PFL-f)), elevation -400 to -600m: no data
 Number of PFL-features, elevation -400 to -600m: no data
 Model T, elevation -400 to -500m: 1.49E-6
 Model T, elevation -500 to -600m: 8.27E-7

Transmissivity (m²/s)

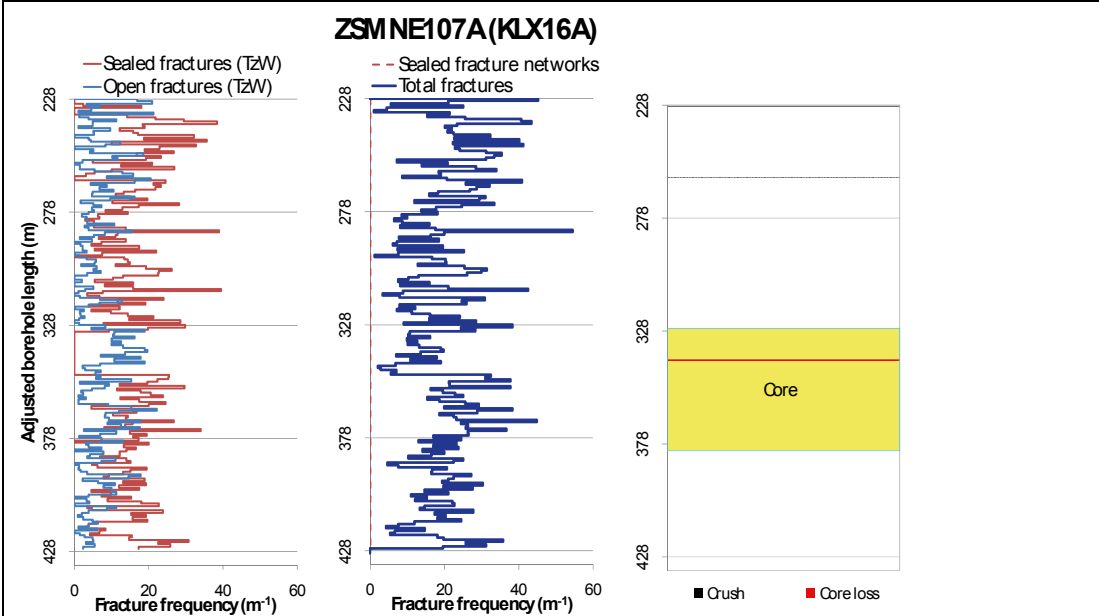
General dip of PFL-features, elevation -400 to -600m: No PFL-f
 Measured T (sum T(PFL-f)), elevation -400 to -600m: 0
 Number of PFL-features, elevation -400 to -600m: 0
 Model T, elevation -400 to -500m: 1.49E-6
 Model T, elevation -500 to -600m: 8.27E-7

Deformation zone ZSMNE107A



Transmissivity (m^2/s)

General dip of PFL-features, elevation -400 to -600m: no data
 Measured T (sum T(PFL-f)), elevation -400 to -600m: no data
 Number of PFL-features, elevation -400 to -600m: no data
 Model T, elevation -400 to -500m: $1.49E-6$
 Model T, elevation -500 to -600m: $8.27E-7$



Deformation zone ZSMNE107A



KLX16A 335-345 m borehole length. Part of DZ12 including core zone.

Engineering characteristics

Transition part of zone:

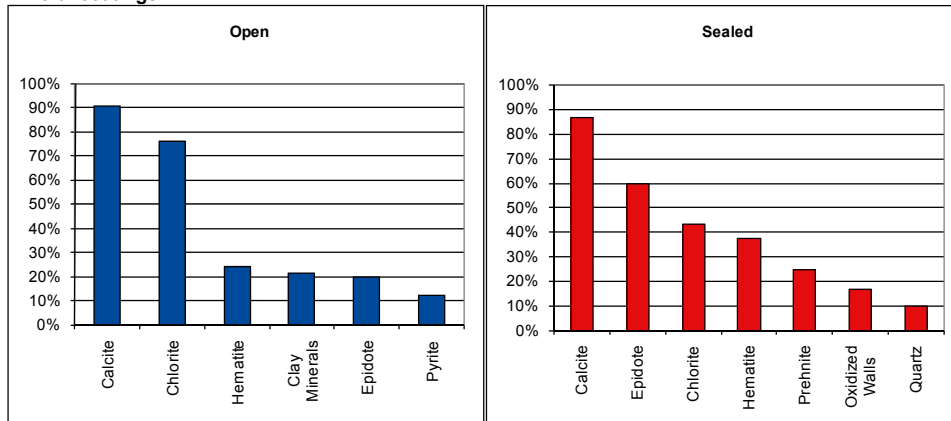
Frequency of open fractures: 3.2 m^{-1}

Std dev: 0.5

Frequency of sealed fractures: 24.3 m^{-1}

Std dev: 5.2

Mineral coatings



Deformation zone ZSMNE107A

Fault core:

Percentage of fault core: 18 %

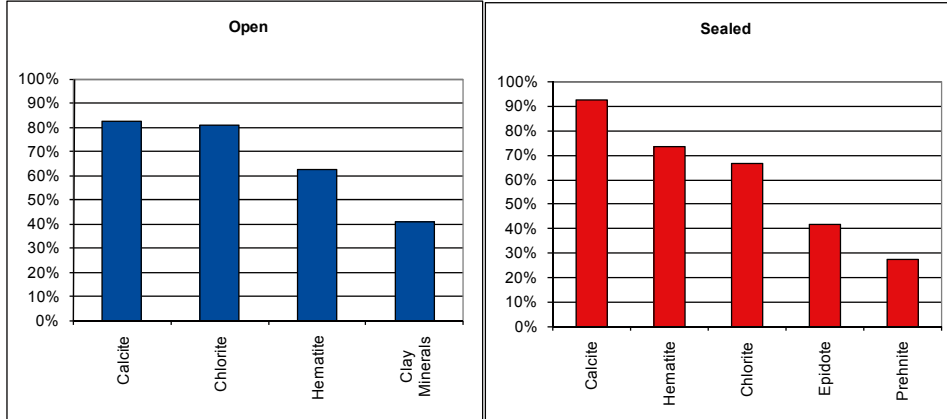
Frequency of open fractures: 6.0 m⁻¹


Std dev: 3.0

Frequency of sealed fractures: 55.8 m⁻¹

Std dev: 54.3

Mineral coatings

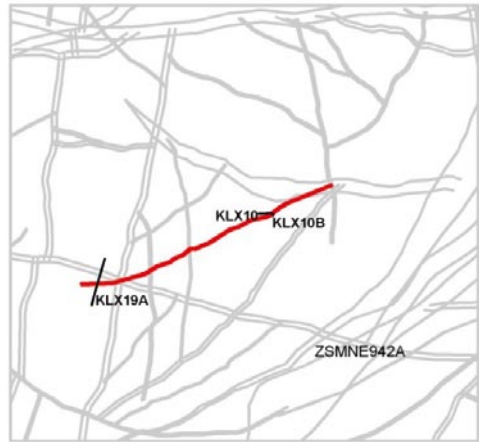


Deformation zone ZSMNE108A	
<p>Borehole intersections (metres along borehole)</p> <p>None</p>	
<p>Deformation style, alteration and geometry</p> <p>Deformation style: ductile and brittle</p> <p>Alteration: red staining.</p> <p>Strike/dip (right-hand-rule): 060/90</p> <p>Trace length at ground surface: 1.8 km</p> <p>Model thickness / model thickness span : 10 m / 5-50 m</p> <p>Measured thickness (-400 to -600 m elevation): no data</p> <p>Comment: character and properties are based on other similar trending deformation zones</p>	
Fractures in the deformation zone	
No borehole intercepts	
<p>Transmissivity (m²/s)</p> <p>General dip of PFL-features, elevation -400 to -600m: no data</p> <p>Measured T (sum T(PFL-f)), elevation -400 to -600m: no data</p> <p>Number of PFL-features, elevation -400 to -600m: no data</p> <p>Model T, elevation -400 to -500m: 2.26E-7</p> <p>Model T, elevation -500 to -600m: 1.37E-7</p>	
Engineering characteristics	
No borehole intercepts	

Deformation zone ZSMNE942A

Borehole intersections (metres along borehole)

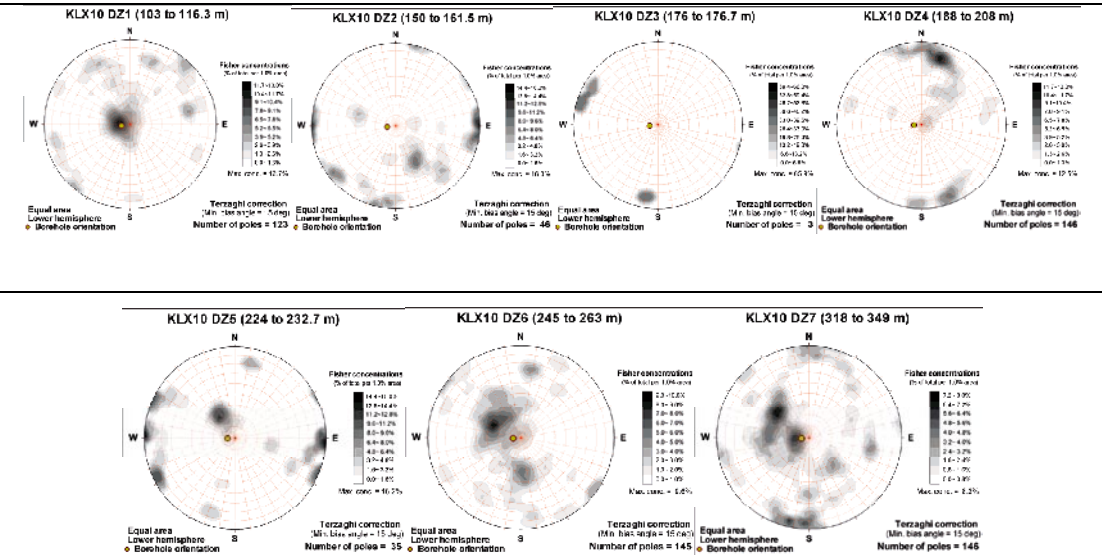
KLX10: 103-349 m (ESHI; DZ1 103-116.3m, DZ2 150-161.5, DZ3 176-176.7m, DZ4 188-208m, DZ5 224-232.7 m, DZ6 245-263 m and DZ7 318-349 m)
 KLX10B: 0-20 m (ESHI DZ1 10.35-20.35m)
 KLX19A: 437-464 m (ESHI DZ4 434-464m)



Deformation style, alteration and geometry

Deformation style: brittle and ductile
Alteration: red staining, chloritisation, epidotisation, argillisation
Strike/dip (right-hand-rule): 246/87
Trace length at ground surface: 2.5 km
Model thickness / model thickness span : 15 m / 10-50 m
Measured thickness (-400 to -600 m elevation): no data
Comment:

Fractures in the deformation zone

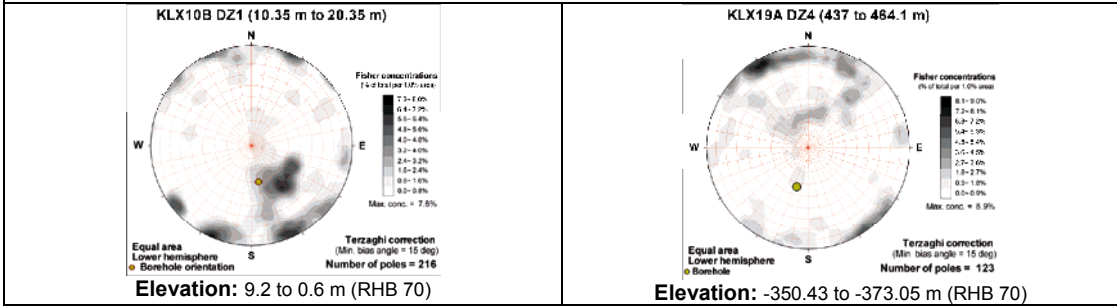


Elevation: -84.0 to 328.0 m (RHB 70)

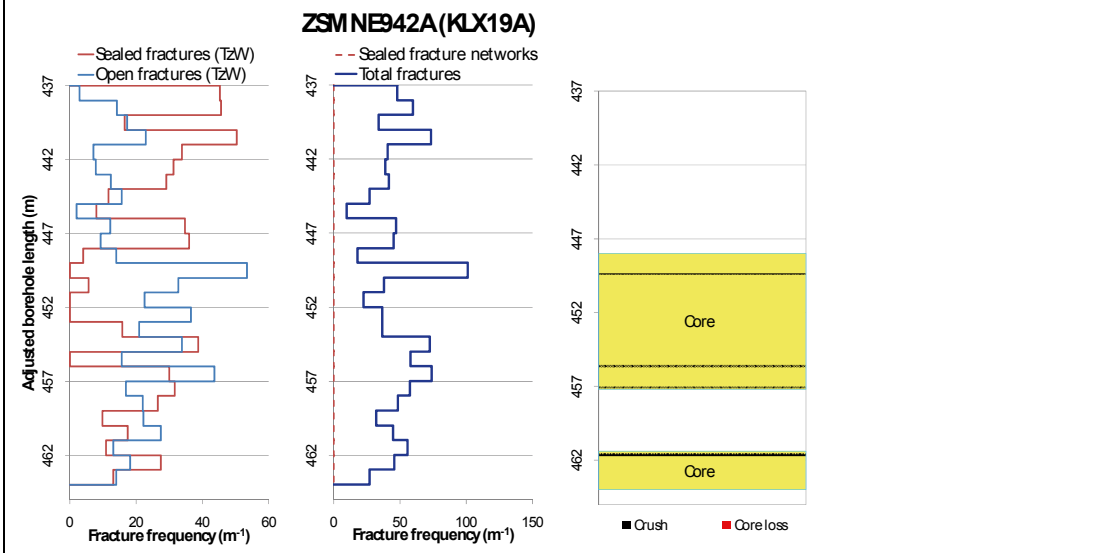
Transmissivity (m²/s)

General dip of PFL-features, elevation -400 to -600m: no data
Measured T (sum T(PFL-f)), elevation -400 to -600m: no data
Number of PFL-features, elevation -400 to -600m: no data
Model T, elevation -400 to -500m: 6.85E-7
Model T, elevation -500 to -600m: 3.94E-7

Deformation zone ZSMNE942A



<p style="text-align: center;">Transmissivity (m²/s)</p> <p>General dip of PFL-features, elevation -400 to -600m: no data</p> <p>Measured T (sum T(PFL-f)), elevation -400 to -600m: no data</p> <p>Number of PFL-features, elevation -400 to -600m: no data</p> <p>Model T, elevation -400 to -500m: 6.85E-7</p> <p>Model T, elevation -500 to -600m: 3.94E-7</p>	<p style="text-align: center;">Transmissivity (m²/s)</p> <p>General dip of PFL-features, elevation -400 to -600m: no data</p> <p>Measured T (sum T(PFL-f)), elevation -400 to -600m: no data</p> <p>Number of PFL-features, elevation -400 to -600m: no data</p> <p>Model T, elevation -400 to -500m: 6.85E-7</p> <p>Model T, elevation -500 to -600m: 3.94E-7</p>
--	--



Deformation zone ZSMNE942A



KLX19A 449-459 m borehole length. Part of DZ4, including part of one (of two) core zone 448.0-457.2 m.

Engineering characteristics

Transition part of zone:

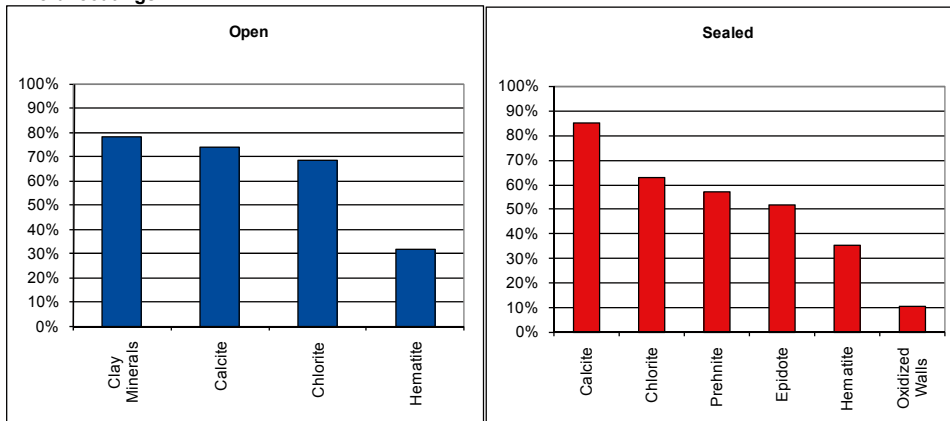
Frequency of open fractures: 7.9 m^{-1}

Std dev: 4.3

Frequency of sealed fractures: 26.8 m^{-1}

Std dev: 17.9

Mineral coatings



Deformation zone ZSMNE942A

Fault core:

Percentage of fault core: 44 %

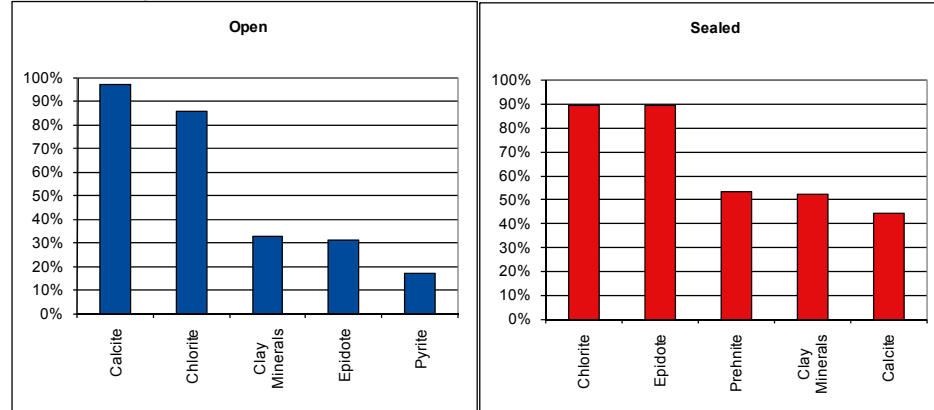
Frequency of open fractures: 12.1 m⁻¹

Std dev: no data

Frequency of sealed fractures: 21.3 m⁻¹

Std dev: no data

Mineral coatings



Deformation zone ZSMNE944A

Borehole intersections (metres along borehole)

KLX18A: 284-292 m (ESHI DZ3 284-292 m)



Deformation style, alteration and geometry

Deformation style: brittle and ductile

Alteration: red staining, chloritisation

Strike/dip (right-hand-rule): 058/75

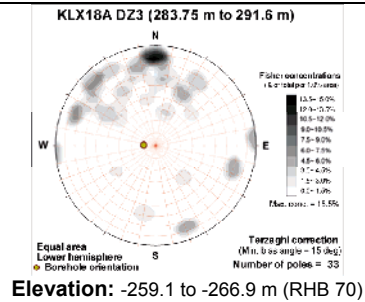
Trace length at ground surface: 1.2 km

Model thickness / model thickness span : 10 m / 5-20 m

Measured thickness (-400 to -600 m elevation): no data

Comment:

Fractures in the deformation zone



Transmissivity (m^2/s)

General dip of PFL-features, elevation -400 to -600m: no data

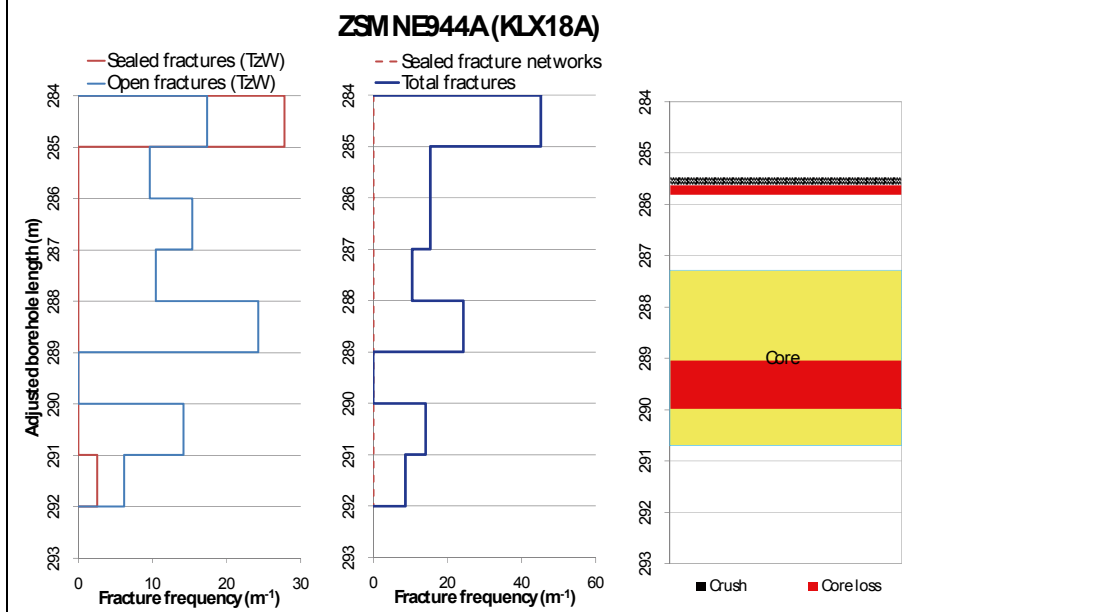
Measured T (sum T(PFL-f)), elevation -400 to -600m: no data

Number of PFL-features, elevation -400 to -600m: no data

Model T, elevation -400 to -500m: 7.54E-8

Model T, elevation -500 to -600m: 4.56E-8

Deformation zone ZSMNE944A



KLX18A 287-293 m borehole length. Part of DZ3, including core zone 287.29-290.70 m.

Engineering characteristics

Transition part of zone:

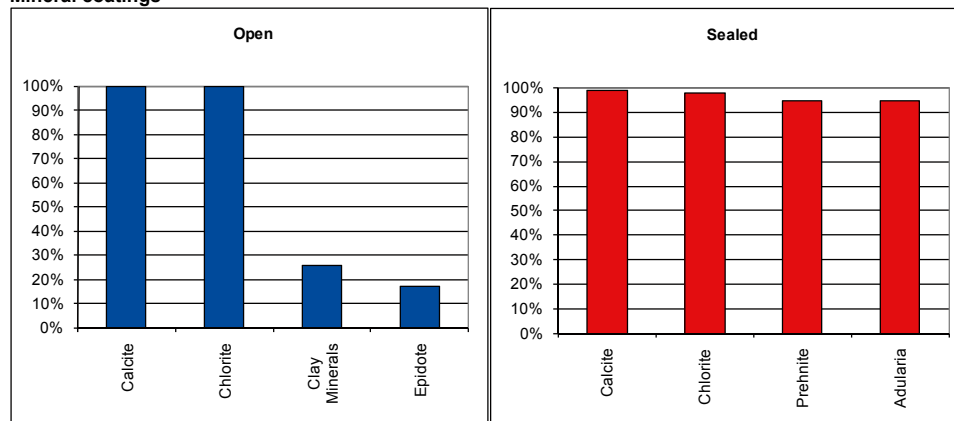
Frequency of open fractures: 7.6 m⁻¹

Std dev: no data

Frequency of sealed fractures: 43.6 m⁻¹

Std dev: no data

Mineral coatings



Fault core: note that core loss, crush and fault rocks define the core

Percentage of fault core: 43 %

Deformation zone ZSMNE944A

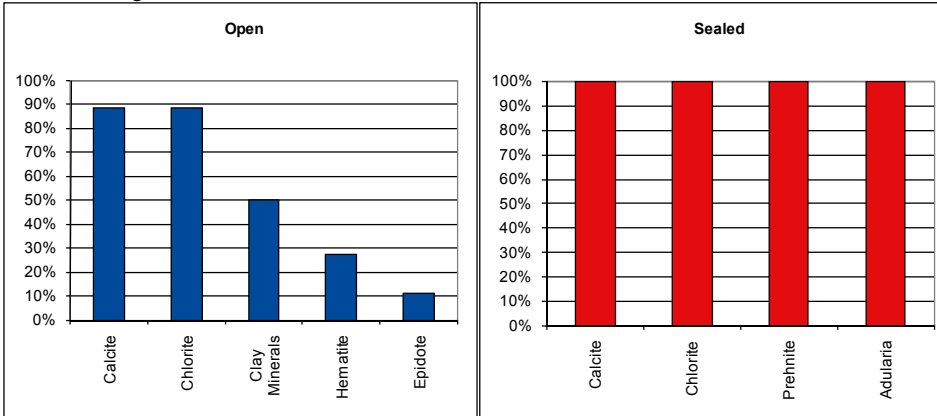
Frequency of open fractures: 5.3 m^{-1}

Std dev: no data


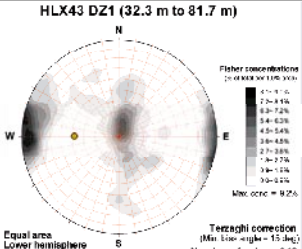
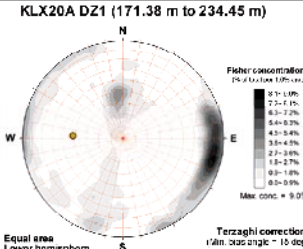
Frequency of sealed fractures: 66.9 m^{-1}

Std dev: no data

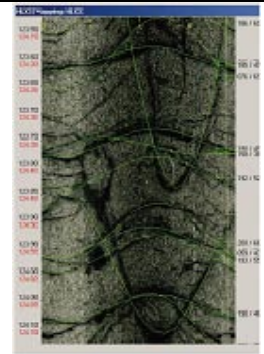
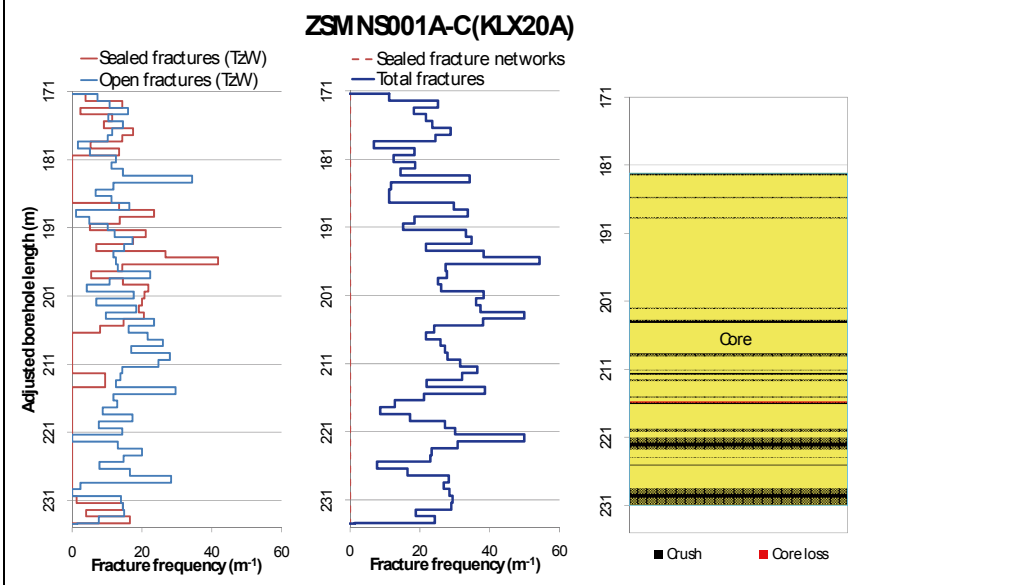
Mineral coatings



N-S Striking deformation zones, steeply dipping

Deformation zone ZSMNS001A-E	
<p>Borehole intersections (metres along borehole)</p> <p>HLX36: 111-191 m (ESHI DZ1 111-191 m) HLX37: 122-147 m (ESHI DZ1 122-147 m) HLX43: 32-82 m (ESHI DZ1 32-82 m) KLX20: 171-234 m (ESHI DZ1 171-234 m)</p>	
<p>Deformation style, alteration and geometry</p>	
<p>Deformation style: brittle and ductile</p> <p>Alteration: Weak red staining, saussuritisation and epidotisation</p> <p>Strike/dip (right-hand-rule): 187/81</p> <p>Trace length at ground surface: 10.9 km</p> <p>Model thickness / model thickness span : 45 m / 20-80 m</p> <p>Measured thickness (-400 to -600 m elevation): no data</p> <p>Comment:</p>	
Fractures in the deformation zone	
<p>HLX43 DZ1 (32.3 m to 81.7 m)</p>  <p>Equal area Lower hemisphere Borehole orientation</p> <p>Terzaghi correction (Min. size-angle = 15 deg) Number of poles = 349</p> <p>Elevation: -0.9 to -39.8 m (RHB 70)</p>	<p>KLX20A DZ1 (171.38 m to 234.45 m)</p>  <p>Equal area Lower hemisphere Borehole orientation</p> <p>Terzaghi correction (Min. size-angle = 15 deg) Number of poles = 459</p> <p>Elevation: -104.4 to -151.7 m (RHB 70)</p>
<p>Transmissivity (m²/s)</p> <p>General dip of PFL-features, elevation -400 to -600m: no data Measured T (sum T(PFL-f)), elevation -400 to -600m: no data Number of PFL-features, elevation -400 to -600m: no data Model T, elevation -400 to -500m: 5.19E-6 Model T, elevation -500 to -600m: 2.98E-6</p>	<p>Transmissivity (m²/s)</p> <p>General dip of PFL-features, elevation -400 to -600m: no data Measured T (sum T(PFL-f)), elevation -400 to -600m: no data Number of PFL-features, elevation -400 to -600m: no data Model T, elevation -400 to -500m: 5.19E-6 Model T, elevation -500 to -600m: 2.98E-6</p>

Deformation zone ZSMNS001A-E



BIPS-image showing the unaltered, fine- to medium-grained, strongly fractured dolerite. Green lines mark the open fractures.



KLX20A 205.71-210.81 m borehole length. Part of DZ1, including part of the dolerite core zone, 182.0-231.0 m.



Slickensided fracture surfaces in the dolerite.

Deformation zone ZSMNS001A-E

Engineering characteristics

Transition part of zone:

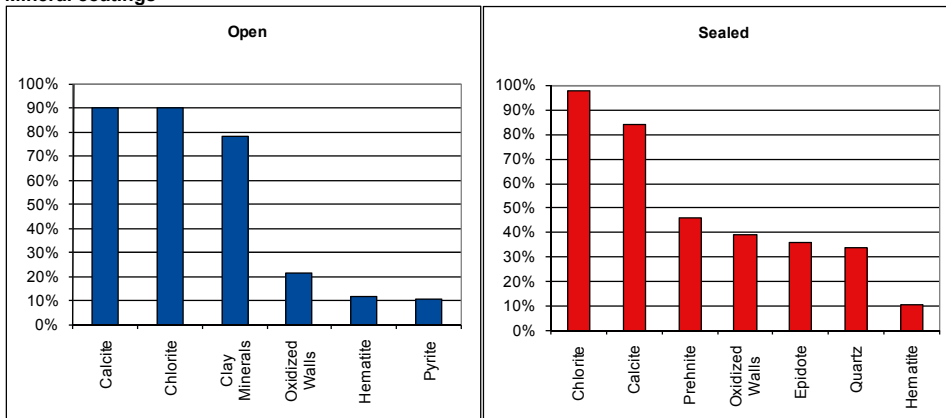
Frequency of open fractures: 5.8 m⁻¹

Std dev: no data

Frequency of sealed fractures: 29.2 m⁻¹

Std dev: no data

Mineral coatings



Fault core:

Percentage of fault core: 77 %

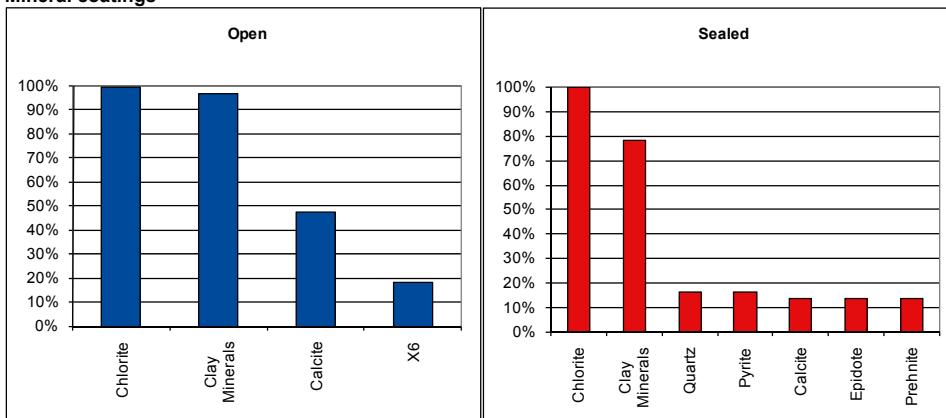
Frequency of open fractures: 14.4 m⁻¹

Std dev: no data

Frequency of sealed fractures: 43.4 m⁻¹

Std dev: no data

Mineral coatings



Deformation zone ZSMNS046A

Borehole intersections (metres along borehole)

KLX09G: 40-68 m (ESHI DZ1 40-68m)

Deformation style, alteration and geometry

Deformation style: ductile and brittle

Alteration: red staining and chloritisation

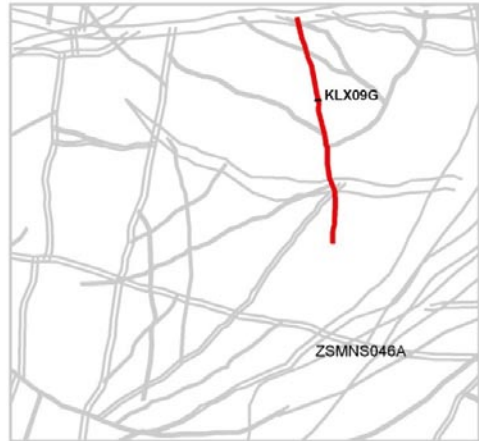
Strike/dip (right-hand-rule): 170/90

Trace length at ground surface: 2.1 km

Model thickness / model thickness span : 20 m / 10-30 m

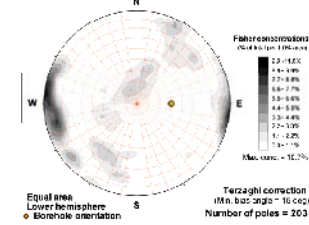
Measured thickness (-400 to -600 m elevation): no data

Comment:



Fractures in the deformation zone

KLX09G DZ1 (40.02 m to 67.52 m)



Transmissivity (m²/s)

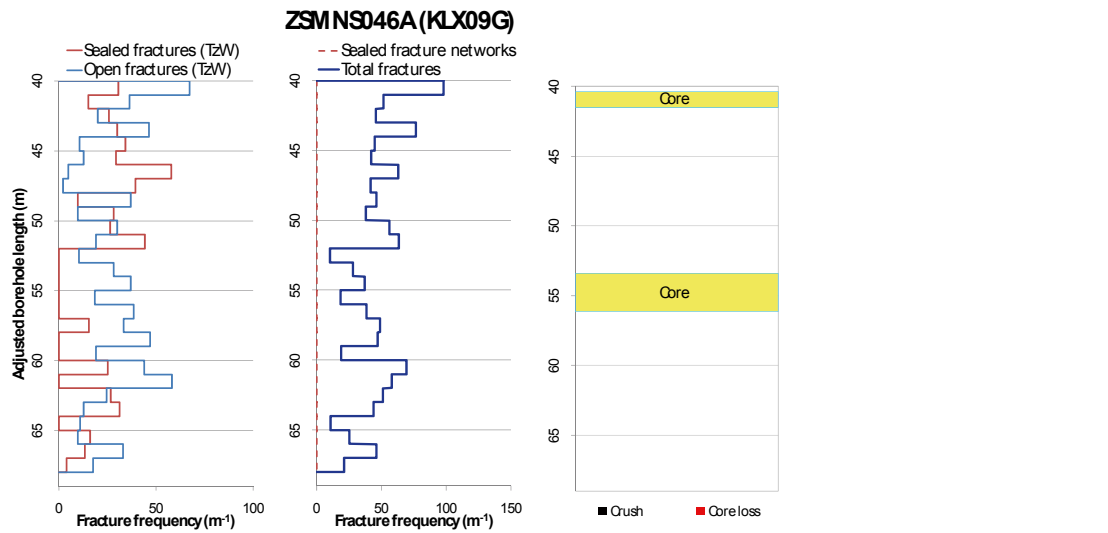
General dip of PFL-features, elevation -400 to -600m: no data

Measured T (sum T(PFL-f)), elevation -400 to -600m: no data

Number of PFL-features, elevation -400 to -600m: no data

Model T, elevation -400 to -500m: 1.49E-6

Model T, elevation -500 to -600m: 8.27E-7



Deformation zone ZSMNS046A



KLX09G 38.95-44.25 m borehole length. Part of DZ1 including one (40.38-41.50 m) of two core zones.

Engineering characteristics

Transition part of zone:

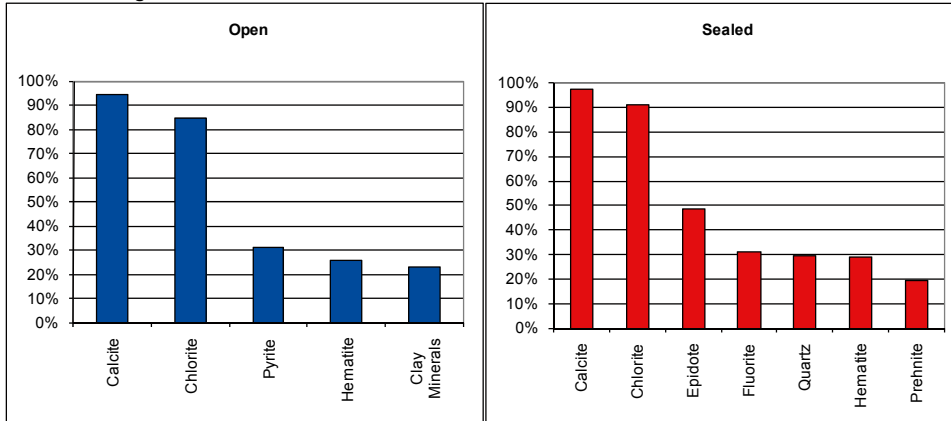
Frequency of open fractures: 6.2 m⁻¹

Std dev: no data

Frequency of sealed fractures: 35.7 m⁻¹

Std dev: no data

Mineral coatings



Fault core:

Percentage of fault core: 14 %

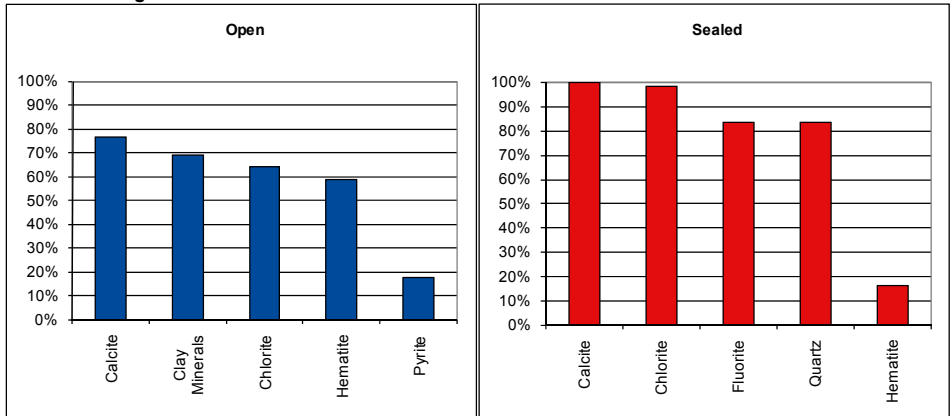
Frequency of open fractures: 10.1 m⁻¹

Std dev: no data

Frequency of sealed fractures: 85.5 m⁻¹

Std dev: no data

Mineral coatings



Deformation zone ZSMNS059A

Borehole intersections (metres along borehole)

HLX34: 33-113 m (ESHI DZ1 33-35m; DZ2 52-55m; DZ3 68-73m; DZ4 85-87m; DZ5 111-113m)
 HLX35: 116-142 m (ESHI DZ1 116-142m)
 HLX38: 23-67 m (ESHI DZ1 23.4-26.5m; DZ2 30.3-32m; DZ3 64.3-66.8m)
 KLX14: 75-125 m (ESHI DZ4 75-125 m)



Deformation style, alteration and geometry

Deformation style: brittle and ductile

Alteration: Weak red staining and epidotisation

Strike/dip (right-hand-rule): 192/88

Trace length at ground surface: 4.8 km

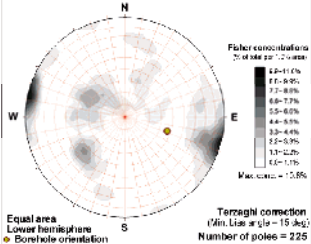
Model thickness / model thickness span : 50 m / 20-80 m

Measured thickness (-400 to -600 m elevation): no data

Comment:

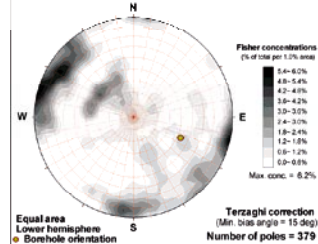
Fractures in the deformation zone

HLX35 DZ1 (116.0783 to 141.7004 m)



Elevation: -83.3 to -104.1 m (RHB 70)

KLX14A DZ4 (74.67 m to 125.35 m)



Elevation: -40 to -77 m (RHB 70)

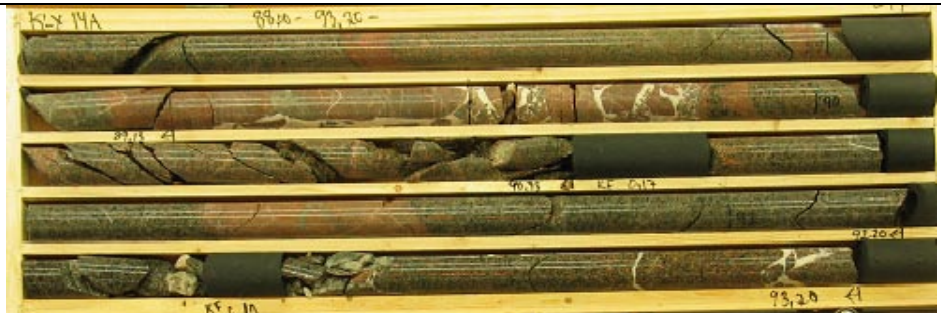
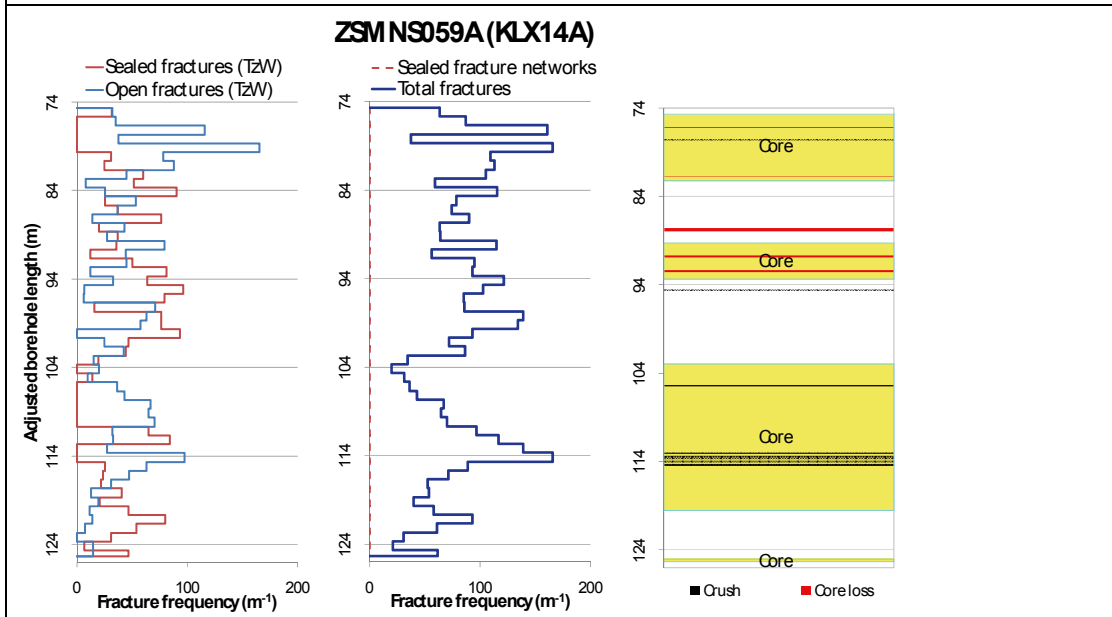
Transmissivity (m²/s)

General dip of PFL-features, elevation -400 to -600m: no data
Measured T (sum T(PFL-f)), elevation -400 to -600m: no data
Number of PFL-features, elevation -400 to -600m: no data
Model T, elevation -400 to -500m: 5.53E-6
Model T, elevation -500 to -600m: 3.18E-6

Transmissivity (m²/s)

General dip of PFL-features, elevation -400 to -600m: no data
Measured T (sum T(PFL-f)), elevation -400 to -600m: no data
Number of PFL-features, elevation -400 to -600m: no data
Model T, elevation -400 to -500m: 5.53E-6
Model T, elevation -500 to -600m: 3.18E-6

Deformation zone ZSMNS059A



KLX14A 88-93.20 m borehole length. Part of DZ4, including one (89.25-93.35 m) of multiple core zones.

Engineering characteristics

Transition part of zone:

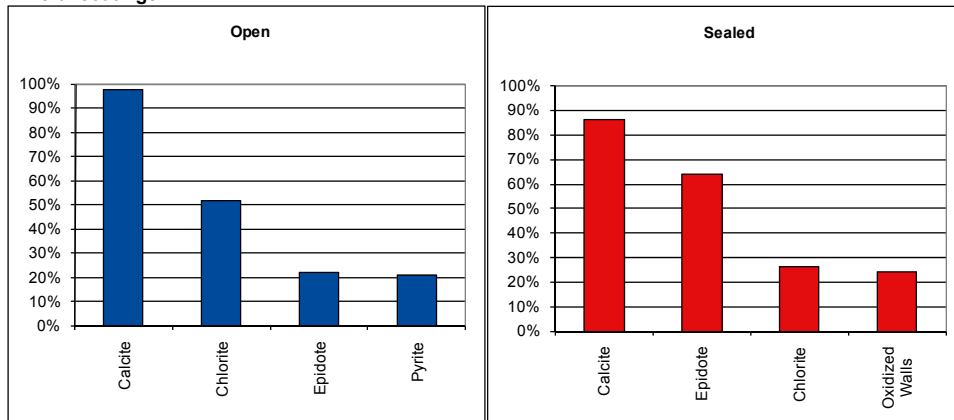
Frequency of open fractures: 4.1 m⁻¹

Std dev: no data

Frequency of sealed fractures: 13.1 m⁻¹

Std dev: no data

Mineral coatings



Deformation zone ZSMNS059A

Fault core:

Percentage of fault core: 56 %

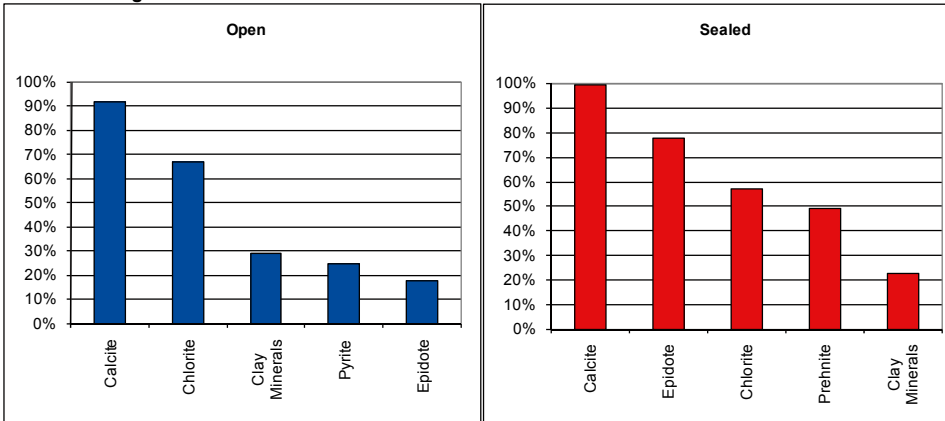
Frequency of open fractures: 10.7 m⁻¹


Std dev: no data


Frequency of sealed fractures: 38.1 m⁻¹

Std dev: no data

Mineral coatings



Deformation zone ZSMNS945A	
<p>Borehole intersections (metres along borehole)</p> <p>None</p>	
<p>Deformation style, alteration and geometry</p> <p>Deformation style: ductile and brittle</p> <p>Alteration: red staining. May not be exclusive to this structure</p> <p>Strike/dip (right-hand-rule): 176/90</p> <p>Trace length at ground surface: 2.0 km</p> <p>Model thickness / model thickness span : 10m / 5-25 m</p> <p>Percentage of fault core: 5 m / +2 m (thickness)</p> <p>Measured thickness (-400 to -600 m elevation): no data</p> <p>Comment: General character based on inferred association with ZSMNS059A and ZSMNS046A</p>	
Fractures in the deformation zone	
<p>(No Borehole intercepts. Inferred similar fracture sets to ZSMNS046A)</p>	
<p>Transmissivity (m²/s)</p> <p>General dip of PFL-features, elevation -400 to -600m: no data</p> <p>Measured T (sum T(PFL-f)), elevation -400 to -600m: no data</p> <p>Number of PFL-features, elevation -400 to -600m: no data</p> <p>Model T, elevation -400 to -500m: 1.49E-6</p> <p>Model T, elevation -500 to -600m: 8.27E-7</p>	
Engineering characteristics	
<p>(No borehole intercepts. Inferred similar characteristics to ZSMNS046A)</p>	

Deformation zone ZSMNS947A	
<p>Borehole intersections (metres along borehole)</p> <p>HLX42: - m (No ESHI interpreted DZ)</p>	
<p>Deformation style, alteration and geometry</p> <p>Deformation style: ductile and brittle</p> <p>Alteration: -</p> <p>Strike/dip (right-hand-rule): 178/90</p> <p>Trace length at ground surface: 1.8 km</p> <p>Model thickness / model thickness span : 20 m / 5-25 m</p> <p>Measured thickness (-400 to -600 m elevation): no data</p> <p>Comment:</p>	
Fractures in the deformation zone	
<p>(No Borehole intercepts. Inferred similar fracture sets to ZSMNS046A)</p>	
Transmissivity (m²/s)	
<p>General dip of PFL-features, elevation -400 to -600m: no data</p> <p>Measured T (sum T(PFL-f)), elevation -400 to -600m: no data</p> <p>Number of PFL-features, elevation -400 to -600m: no data</p> <p>Model T, elevation -400 to -500m: 2.26E-7</p> <p>Model T, elevation -500 to -600m: 1.37E-7</p>	
Engineering characteristics	
<p>(No borehole intercepts. Inferred similar characteristics to ZSMNS046A)</p>	

Deformation zone KLX04_dz6b

Borehole intersections (metres along borehole)

KLX04: 887-914 m – Note this interval differs from: (ESHI DZ6 873-973 m)



Deformation style, alteration and geometry

Deformation style: brittle

Alteration: red staining, epidotisation

Strike/dip (right-hand-rule): 156/67

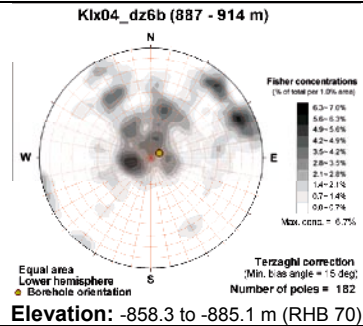
Trace length at ground surface: no data

Model thickness / model thickness span : 14 m / no data

Measured thickness (-400 to -600 m elevation): no data

Comment:

Fractures in the deformation zone



Transmissivity (m²/s)

General dip of PFL-features, elevation -400 to -600m: no data

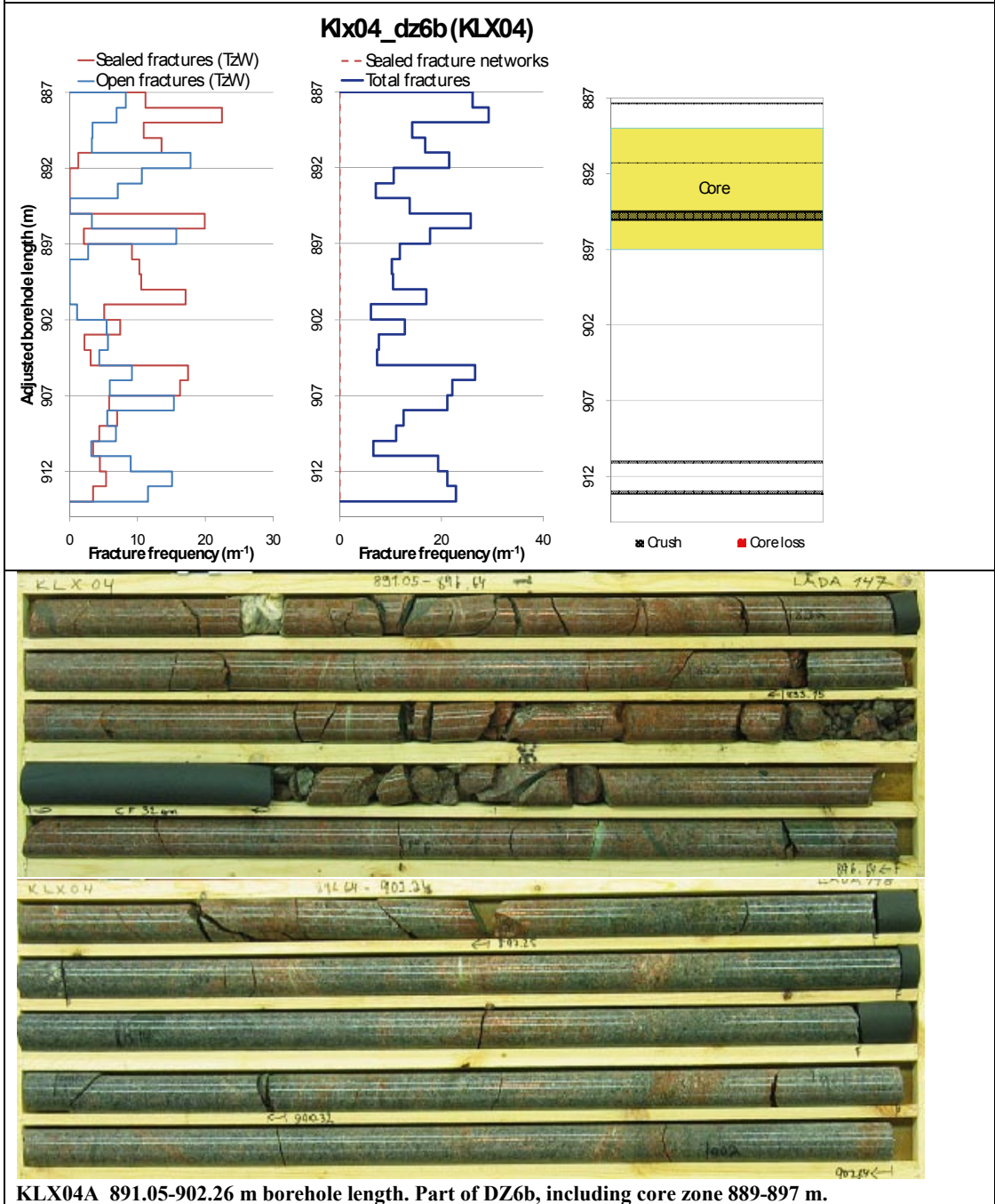
Measured T (sum T(PFL-f)), elevation -400 to -600m: no data

Number of PFL-features, elevation -400 to -600m: no data

Model T, elevation -400 to -500m: 2.26E-7

Model T, elevation -500 to -600m: 1.37E-7

Deformation zone KLX04_dz6b



Deformation zone KLX04_dz6b

Engineering characteristics

Transition part of zone:

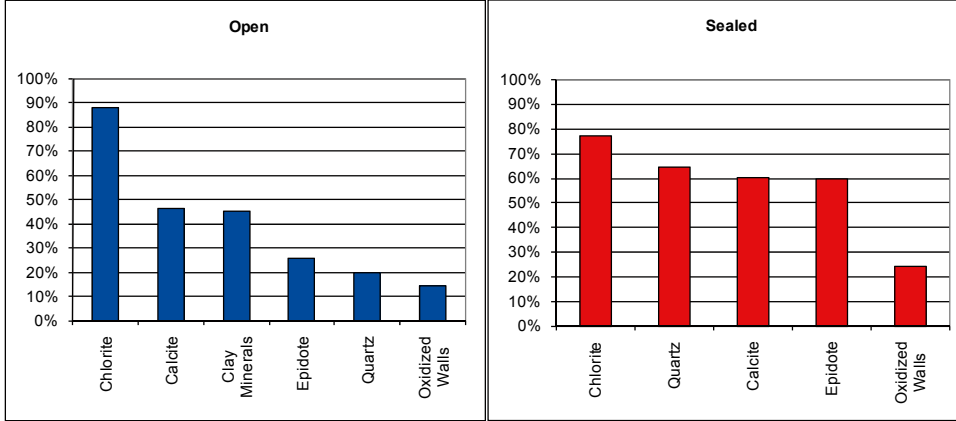
Frequency of open fractures: 5.3 m⁻¹

Std dev: no data

Frequency of sealed fractures: 18.6 m⁻¹

Std dev: no data

Mineral coatings



Fault core:

Percentage of fault core: 30 %

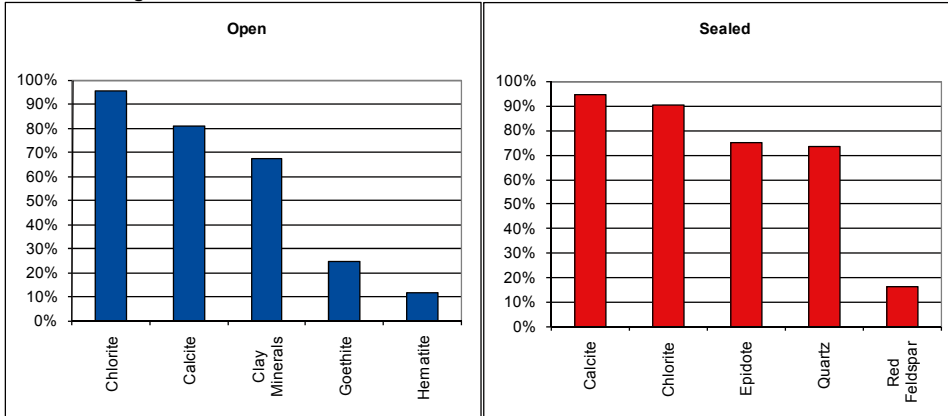
Frequency of open fractures: 8.5 m⁻¹

Std dev: no data

Frequency of sealed fractures: 20.8 m⁻¹

Std dev: no data

Mineral coatings



Deformation zone KLX04_dz6c

Borehole intersections (metres along borehole)

KLX04: 935-972 m (ESHI DZ6 873-973 m)



Deformation style, alteration and geometry

Deformation style: brittle

Alteration: red staining, chloritisation, epidotisation, saussuritisation

Strike/dip (right-hand-rule): 177/42

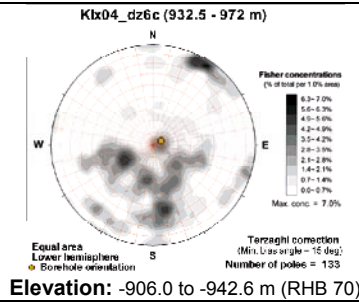
Trace length at ground surface: no data

Model thickness / model thickness span : 30 m / no data

Measured thickness (-400 to -600 m elevation): no data

Comment: Zone orientation based on /Viola et al. 2007a/

Fractures in the deformation zone



Transmissivity (m²/s)

General dip of PFL-features, elevation -400 to -600m: no data

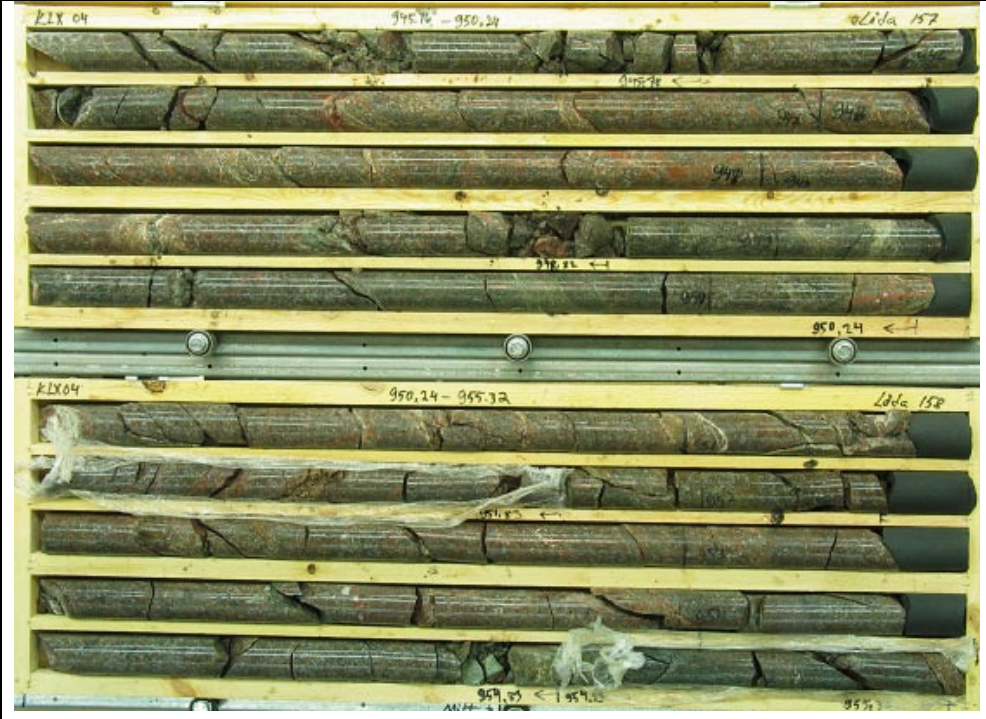
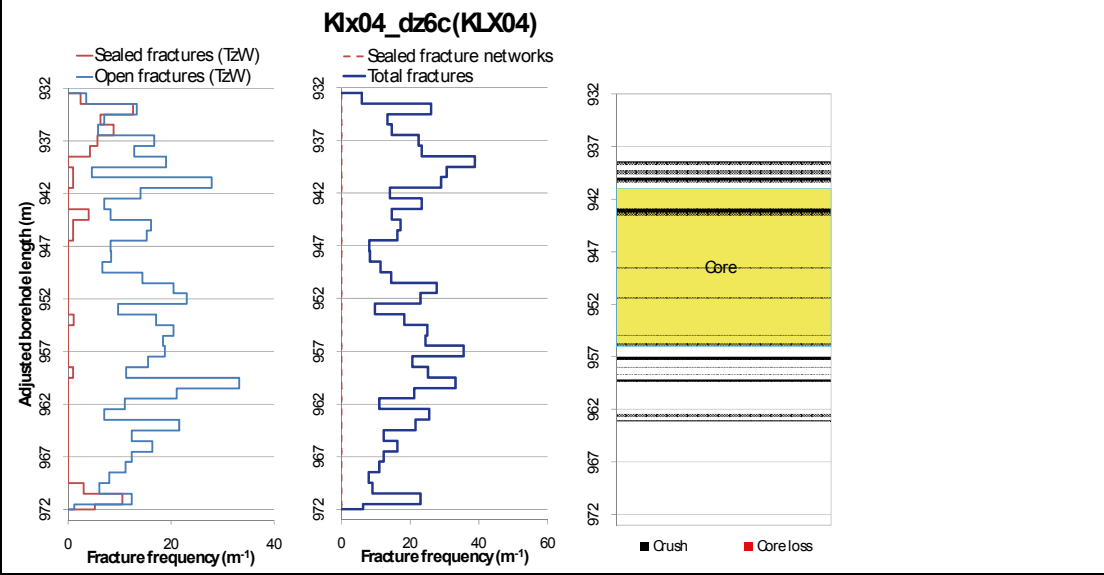
Measured T (sum T(PFL-f)), elevation -400 to -600m: no data

Number of PFL-features, elevation -400 to -600m: no data

Model T, elevation -400 to -500m: 2.26E-7

Model T, elevation -500 to -600m: 1.37E-7

Deformation zone KLX04_dz6c



KLX04A 945.76-955.32 m borehole length. Part of DZ6c including part of core zone 941.0 946.0 m.

Deformation zone KLX04_dz6c

Engineering characteristics

Transition part of zone:

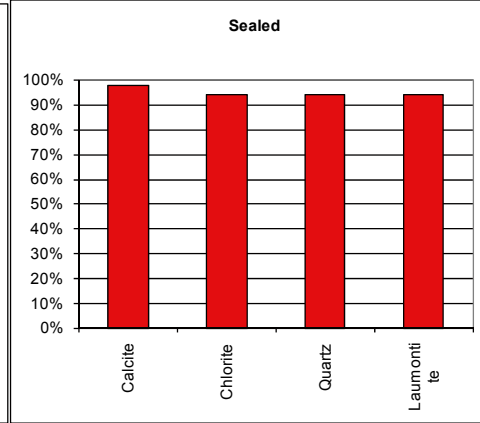
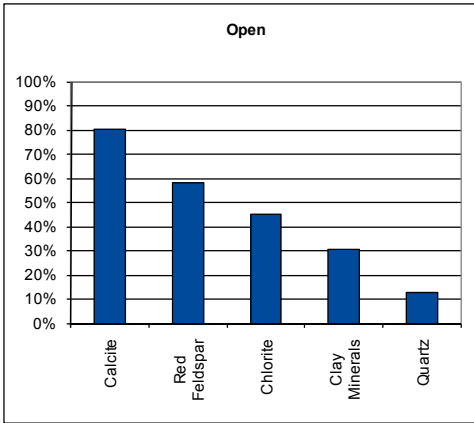
Frequency of open fractures: 14.4 m⁻¹

Std dev: no data

Frequency of sealed fractures: 33.6 m⁻¹

Std dev: no data

Mineral coatings



Fault core:

Percentage of fault core: 38 %

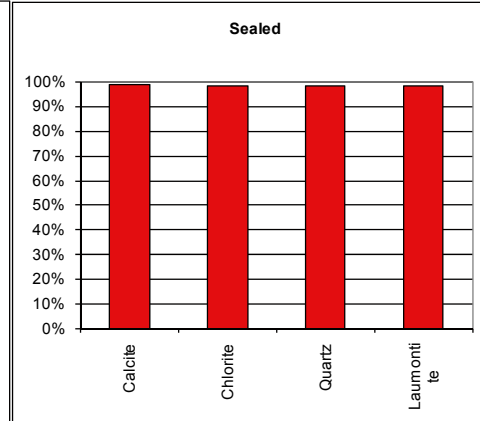
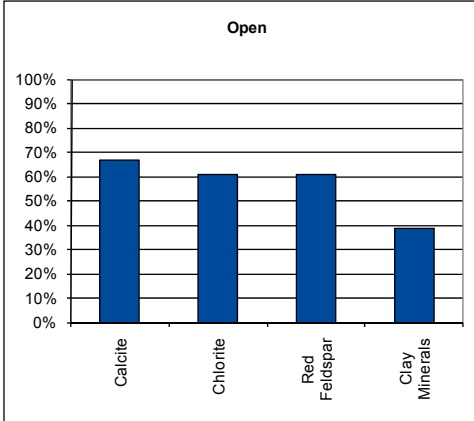
Frequency of open fractures: 13.7 m⁻¹

Std dev: no data

Frequency of sealed fractures: 33.9 m⁻¹

Std dev: no data

Mineral coatings



Deformation zone KLX07_dz13

Borehole intersections (metres along borehole)

KLX07A: 817-836 m (ESHI DZ13 817-836 m)

Deformation style, alteration and geometry

Deformation style: brittle and ductile

Alteration: red staining

Strike/dip (right-hand-rule): 348/65

Trace length at ground surface: 1.0 km

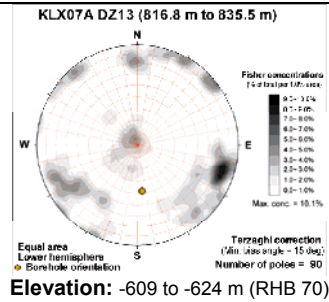
Model thickness / model thickness span : 10 m

Measured thickness (-400 to -600 m elevation): no data

Comment:



Fractures in the deformation zone



Transmissivity (m^2/s)

General dip of PFL-features, elevation -400 to -600m: no data

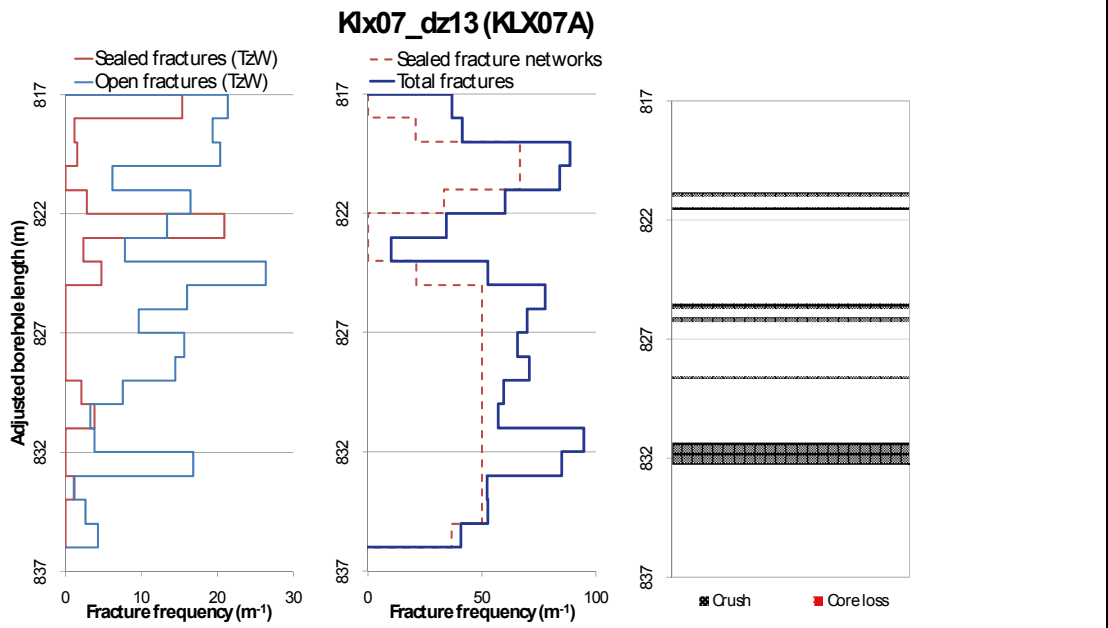
Measured T (sum T(PFL-f)), elevation -400 to -600m: no data

Number of PFL-features, elevation -400 to -600m: no data

Model T, elevation -400 to -500m: 2.26E-7

Model T, elevation -500 to -600m: 1.37E-7

Deformation zone KLX07_dz13



KLX07A, 821.83-832.23 m borehole length. Part of DZ13, no defined core zone.

Deformation zone KLX07_dz13

Engineering characteristics

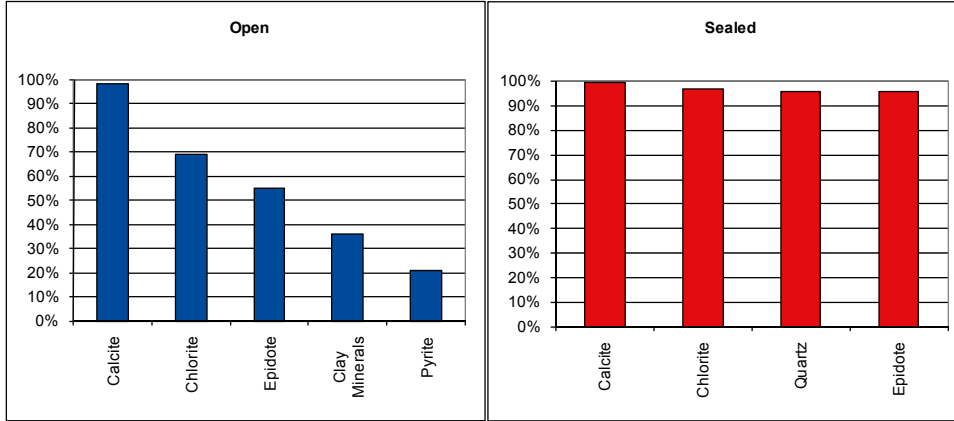
Frequency of open fractures: 12.9 m⁻¹

Std dev: no data

Frequency of sealed fractures: 41.1 m⁻¹

Std dev: no data

Mineral coatings



Deformation zone KLX21B_dz10-12

Borehole intersections (metres along borehole)

KLX21B: 559-707 m (ESHI DZ10 559-572 m, DZ11 577.7- 578 m, DZ12 595-707 m)

Deformation style, alteration and geometry

Deformation style: brittle and ductile

Alteration: red staining, epidotisation

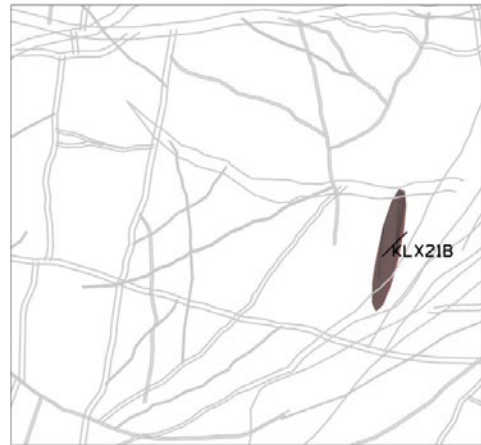
Strike/dip (right-hand-rule): 192/80

Trace length at ground surface: no data

Model thickness / model thickness span : 10 m / no data

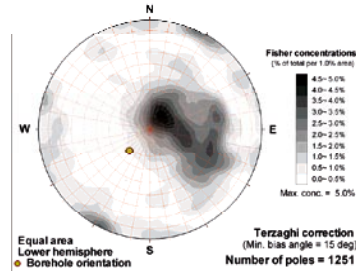
Measured thickness (-400 to -600 m elevation): no data

Comment:



Fractures in the deformation zone

Klx21b_dz10-12 (559 - 707 m)



Elevation: -511.1 to -648.5 m (RHB 70)

Transmissivity (m²/s)

General dip of PFL-features, elevation -400 to -600m: Moderately to sub-horizontally and Steep

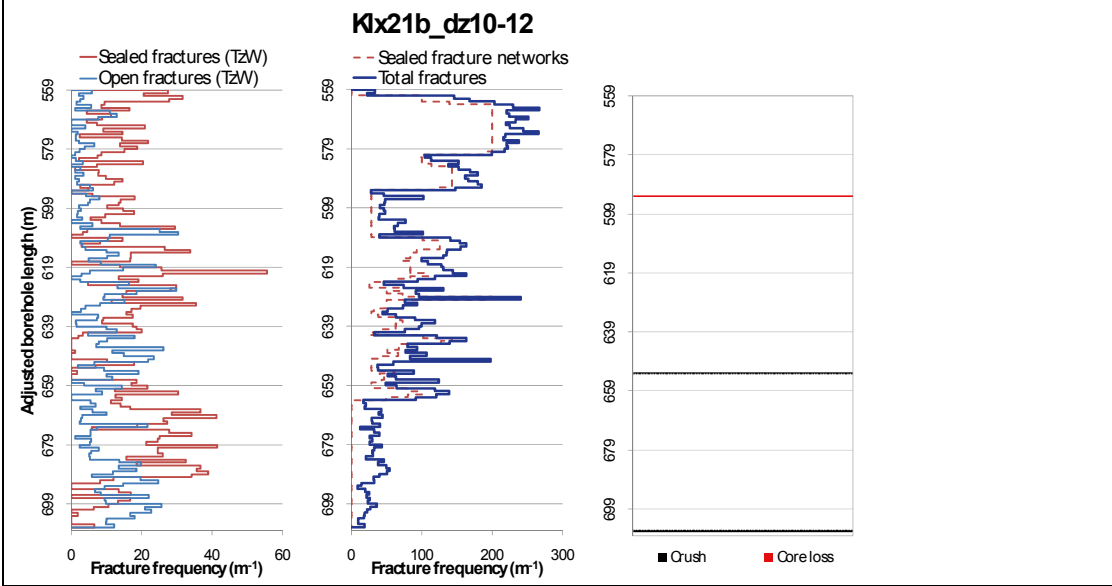
Measured T (sum T(PFL-f)), elevation -400 to -600m: 1.72E-5

Number of PFL-features, elevation -400 to -600m: 21

Model T, elevation -400 to -500m: 2.26E-7

Model T, elevation -500 to -600m: 1.37E-7

Deformation zone KLX21B_dz10-12



KLX21B 641.05-645.65 m Borehole length, part of DZ12 (595-707 m Borehole length). Note the zone is interpreted as have an orientation parallel to the Borehole. No defined core zone.

Deformation zone KLX21B_dz10-12

Engineering characteristics

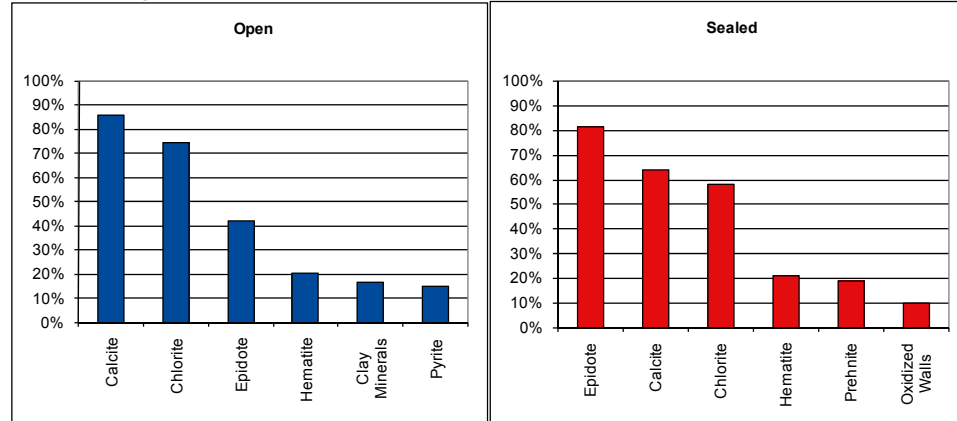
Frequency of open fractures: 4.9 m^{-1}

Std dev: no data

Frequency of sealed fractures: 28.0 m^{-1}

Std dev: no data

Mineral coatings



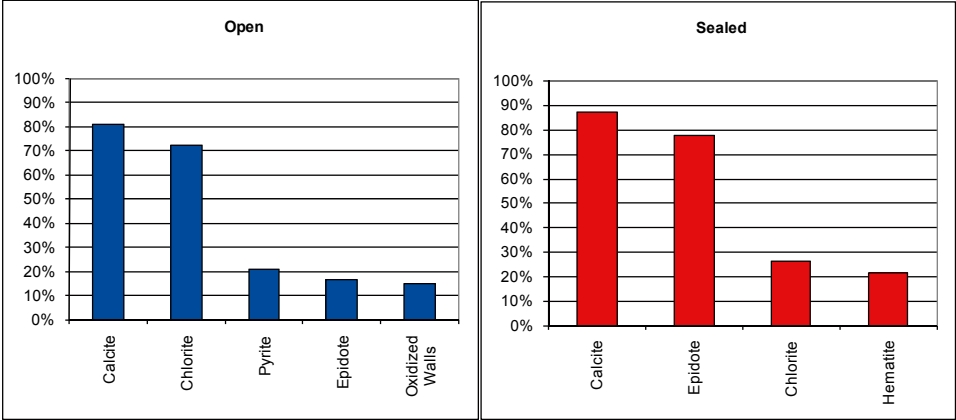
Deformation zone KLX28_dz1



KLX28A 24.62-35.23 m borehole length. Part of DZ1 including core zone (27.7-30.35 m)

Engineering characteristics

Transition part of zone:
 Frequency of open fractures: 2.9 m⁻¹
 Std dev: no data
 Frequency of sealed fractures: 26.7 m⁻¹
 Std dev: no data
Mineral coatings



Deformation zone KLX28_dz1

Fault core:

Percentage of fault core: 14 %

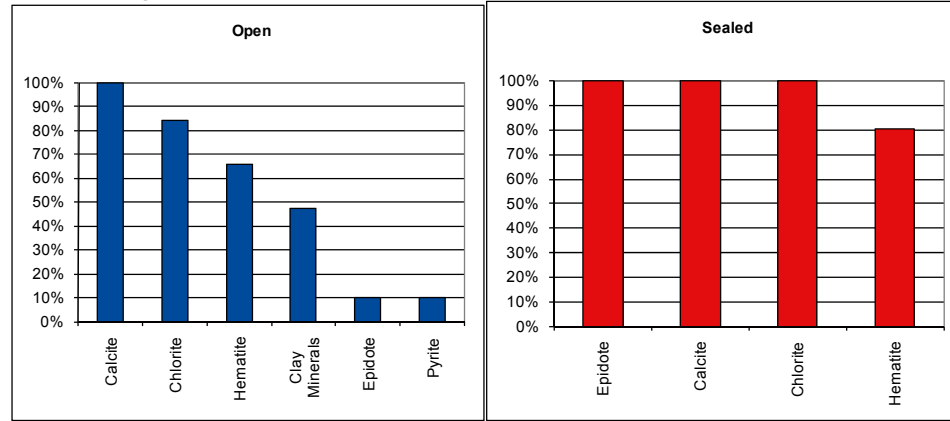
Frequency of open fractures: 14.3 m⁻¹

Std dev: no data

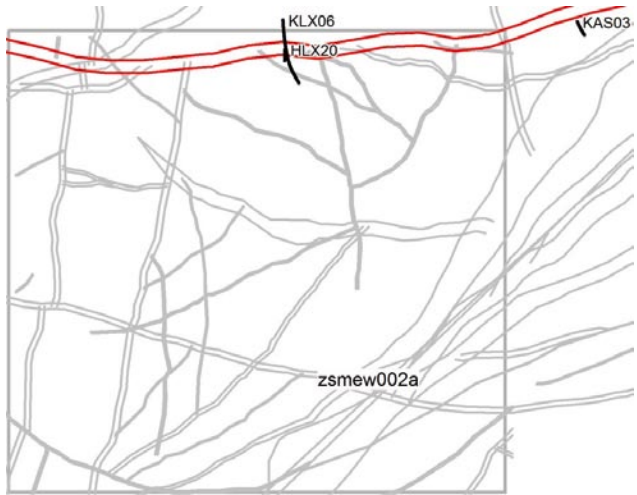
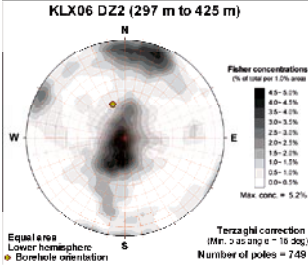
Frequency of sealed fractures: 37.0 m⁻¹

Std dev: no data

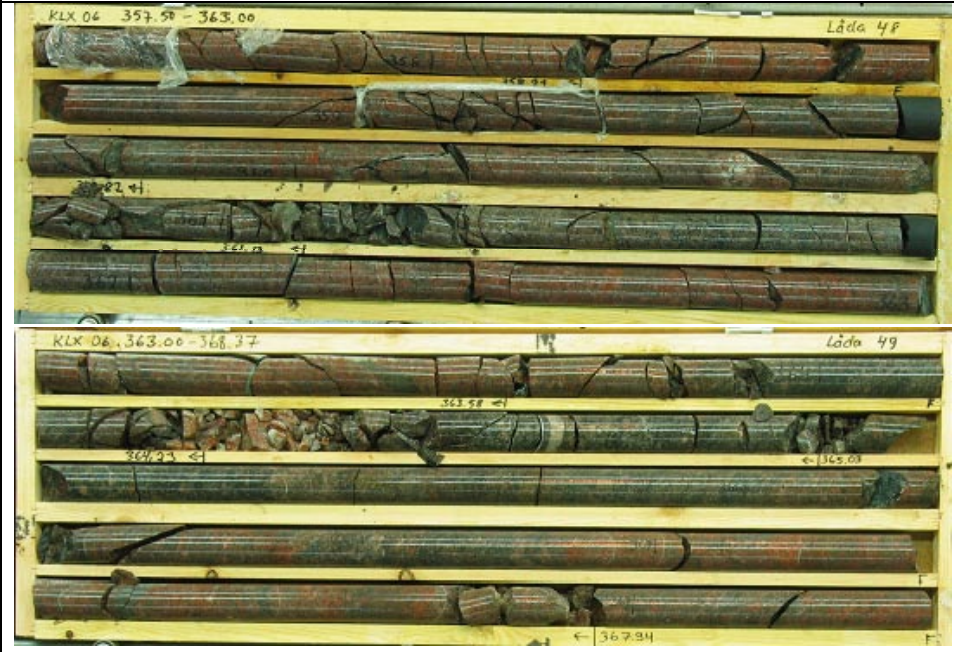
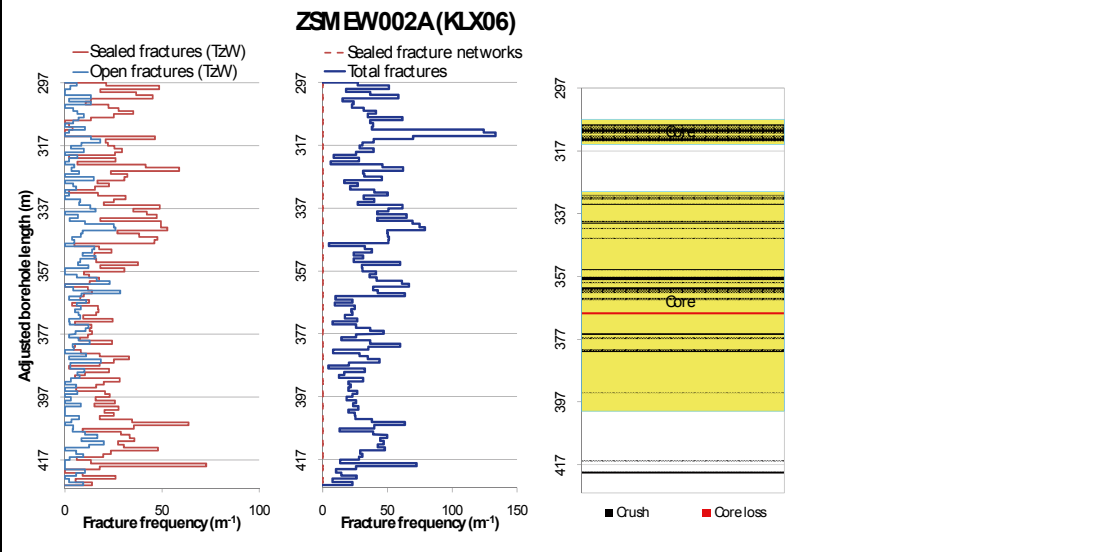
Mineral coatings



E-W to NW-SE striking deformation zones, steep to moderately southward dipping

Deformation zone ZSMEW002A	
<p>Borehole intersections (metres along borehole)</p> <p>HLX20: 90-170m KLX06: 297-425m (ESHI DZ2 297-425m) KAS03: 280-480m</p>	
<p>Deformation style, alteration and geometry</p> <p>Deformation style: brittle and ductile</p> <p>Alteration: red staining, laumontite, saussuritisation and clay alteration,</p> <p>Strike/dip (right-hand-rule): 090/65</p> <p>Trace length at ground surface: 17.9 km</p> <p>Model thickness / model thickness span : 100 m / 20-200 m</p> <p>Measured thickness (-400 to -600 m elevation): no data</p> <p>Comment:</p>	
Fractures in the deformation zone	
 <p>Elevation: -249.1 to -360.5 m (RHB 70)</p>	
Transmissivity (m²/s)	
<p>General dip of PFL-features, elevation -400 to -600m: no data</p> <p>Measured T (sum T(PFL-f)), elevation -400 to -600m: no data</p> <p>Number of PFL-features, elevation -400 to -600m: no data</p> <p>Model T, elevation -400 to -500m: 3.74E-6</p> <p>Model T, elevation -500 to -600m: 2.42E-6</p>	

Deformation zone ZSMEW002A



KLX06 357.5 -368.37 m borehole length. Central part of one core zone.

Deformation zone ZSMEW002A

Engineering characteristics

Transition part of zone:

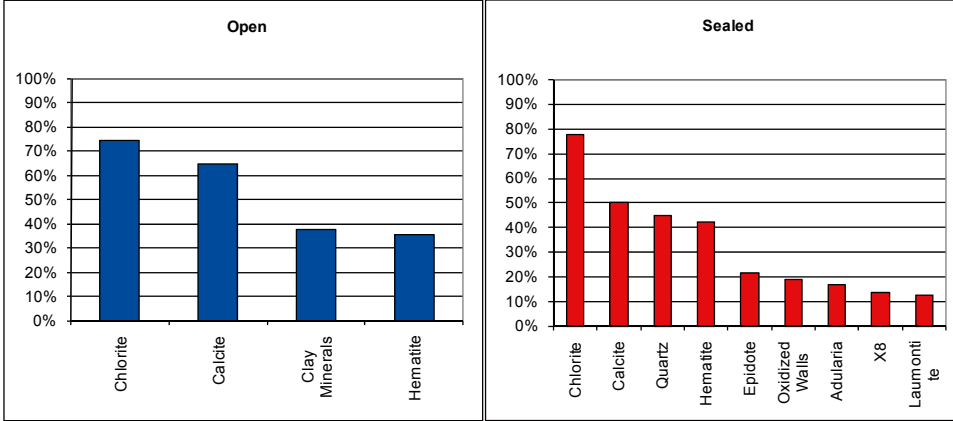
Frequency of open fractures: 2.1 m⁻¹

Std dev: no data

Frequency of sealed fractures: 24.1 m⁻¹

Std dev: no data

Mineral coatings



Fault core:

Percentage of fault core: 61%

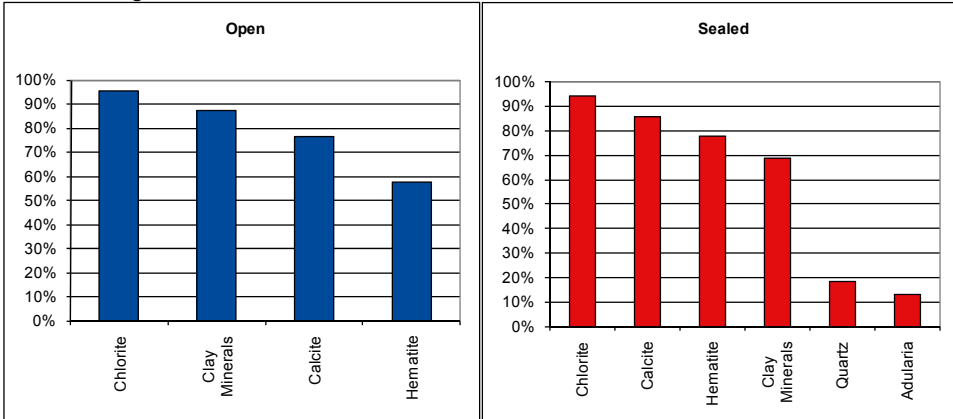
Frequency of open fractures: 8.4 m⁻¹

Std dev: no data

Frequency of sealed fractures: 44.2 m⁻¹

Std dev: no data

Mineral coatings



Deformation zone ZSMEW120A

Borehole intersections (metres along borehole)

KLX13A: 488- 593m (ESHI DZ7 488-593m)



Deformation style, alteration and geometry

Deformation style: brittle and ductile

Alteration: red staining

Strike/dip (right-hand-rule): 080/64

Trace length at ground surface: 1.2 km

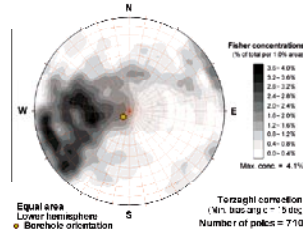
Model thickness / model thickness span : 50 m / 30->60 m

Measured thickness (-400 to -600 m elevation): >50 m

Comment: KLX13A does not penetrate the full thickness of the zone

Fractures in the deformation zone

KLX13A DZ7 (488 m to 593.32 m)



Elevation: -460.0 to -564.2 m (RHB 70)

Transmissivity (m^2/s)

General dip of PFL-features, elevation -400 to -600m: Moderately to sub-horizontally

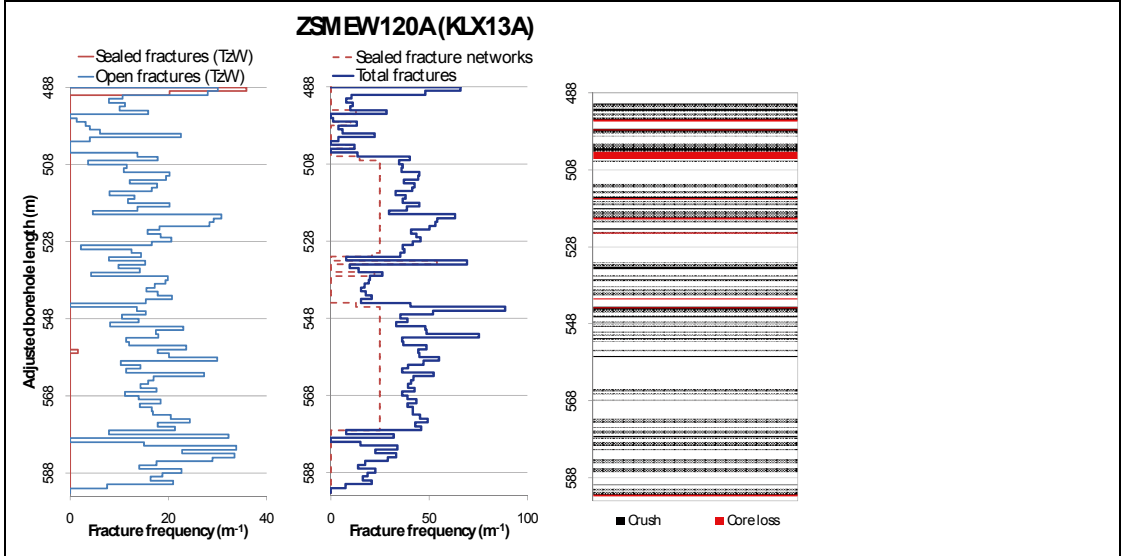
Measured T (sum T(PFL-f)), elevation -400 to -600m: 9.0E-7

Number of PFL-features, elevation -400 to -600m: 39

Model T, elevation -400 to -500m: 4.23E-7

Model T, elevation -500 to -600m: 2.62E-7

Deformation zone ZSMEW120A



KLX13A, 517-528 m borehole length. Part of DZ7.

Deformation zone ZSMEW120A

Engineering characteristics

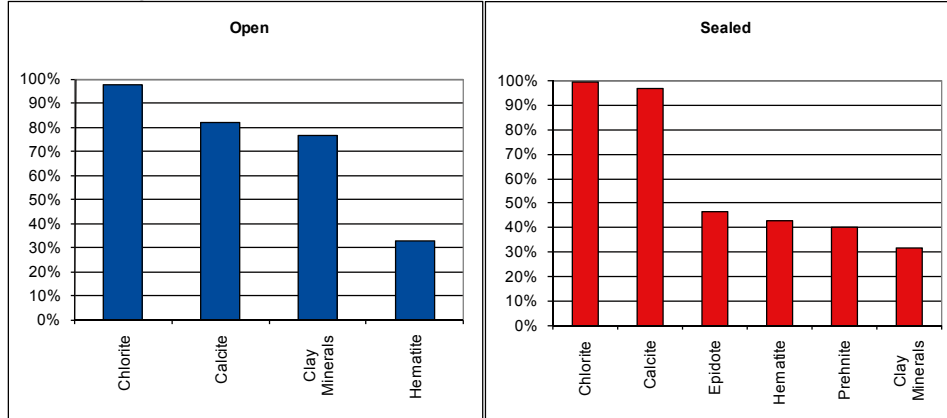
Frequency of open fractures: 22.8 m⁻¹

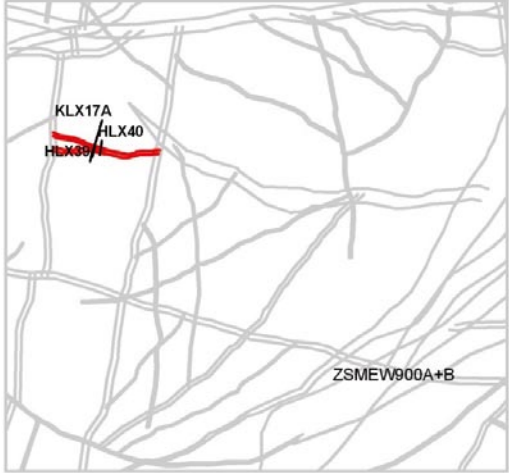
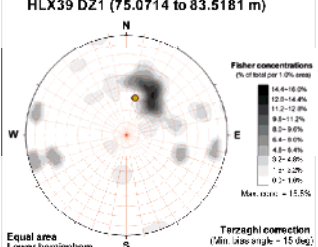
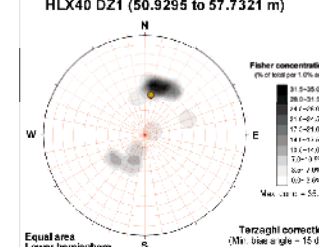
Std dev: no data

Frequency of sealed fractures: 90.4 m⁻¹

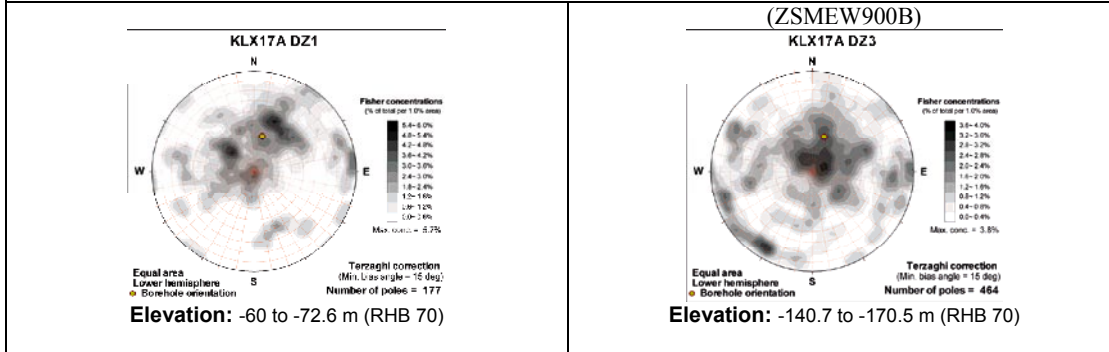
Std dev: no data

Mineral coatings

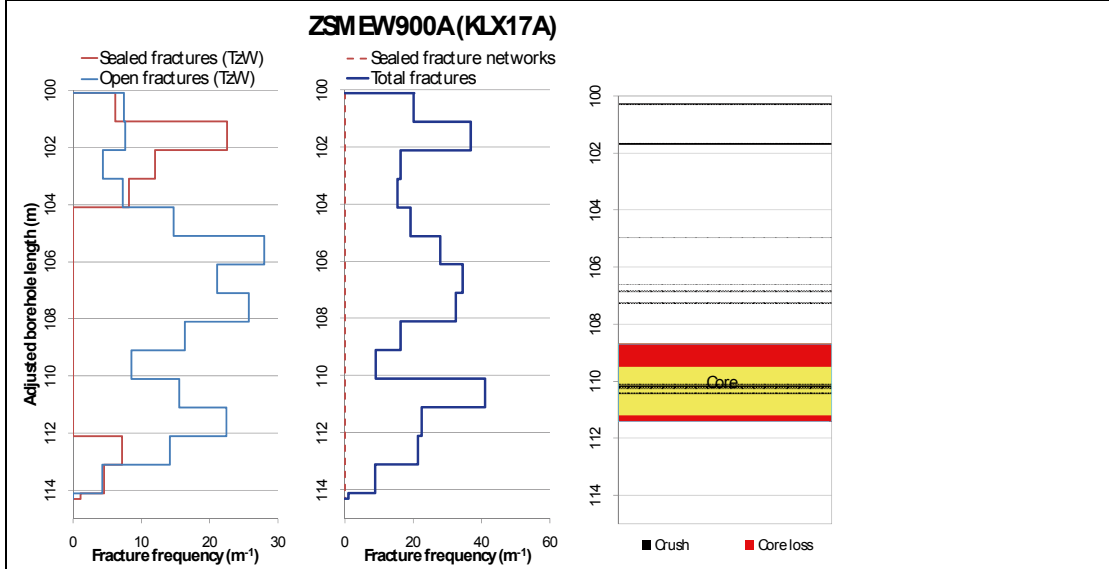


Deformation zone ZSMEW900A-B	
<p>Borehole intersections (metres along borehole)</p> <p>HLX39: 75-85m (ESHI DZ1 75-85m) HLX40: 49.8-59.6m (ESHI DZ1 49.8-59.6m) KLX17: 100.1-114.3m (ESHI DZ1 100.1-114.3m) KLX17: 192.7-227 m (ESHI DZ3 192.7-227m) (ZSMEW900B)</p>	
<p>Deformation style, alteration and geometry</p> <p>Deformation style: brittle and ductile Alteration: red staining, epidotisation and saussuritisation, Strike/dip (right-hand-rule): 092/57 Trace length at ground surface: 0.9 km Model thickness / model thickness span : 25 m / 10-30 m Measured thickness (-400 to -600 m elevation): no data Comment:</p>	
Fractures in the deformation zone	
<p>HLX39 DZ1 (75.0714 to 83.5181 m)</p>  <p>Elevation: -39 to -45.5 m (RHB 70)</p>	<p>HLX40 DZ1 (50.9295 to 57.7321 m)</p>  <p>Elevation: -16.7 to -24.9 m (RHB 70)</p>
<p style="text-align: center;">Transmissivity (m²/s)</p> <p>General dip of PFL-features, elevation -400 to -600m: no data Measured T (sum T(PFL-f)), elevation -400 to -600m: no data Number of PFL-features, elevation -400 to -600m: no data Model T, elevation -400 to -500m: 2.26E-7 Model T, elevation -500 to -600m: 1.37E-7</p>	<p style="text-align: center;">Transmissivity (m²/s)</p> <p>General dip of PFL-features, elevation -400 to -600m: no data Measured T (sum T(PFL-f)), elevation -400 to -600m: no data Number of PFL-features, elevation -400 to -600m: no data Model T, elevation -400 to -500m: 2.26E-7 Model T, elevation -500 to -600m: 1.37E-7</p>

Deformation zone ZSMEW900A-B



<p>Transmissivity (m²/s)</p> <p>General dip of PFL-features, elevation -400 to -600m: no data</p> <p>Measured T (sum T(PFL-f)), elevation -400 to -600m: no data</p> <p>Number of PFL-features, elevation -400 to -600m: no data</p> <p>Model T, elevation -400 to -500m: 2.26E-7</p> <p>Model T, elevation -500 to -600m: 1.37E-7</p>	<p>Transmissivity (m²/s)</p> <p>General dip of PFL-features, elevation -400 to -600m: no data</p> <p>Measured T (sum T(PFL-f)), elevation -400 to -600m: no data</p> <p>Number of PFL-features, elevation -400 to -600m: no data</p> <p>Model T, elevation -400 to -500m: 2.26E-7</p> <p>Model T, elevation -500 to -600m: 1.37E-7</p>
--	--



KLX17A DZ1 100,1-114,3 m Borehole length (ZSMEW900A)
 (core box has been heavily sampled- no suitable photos)

Deformation zone ZSMEW900A-B

Engineering characteristics

Transition part of zone:

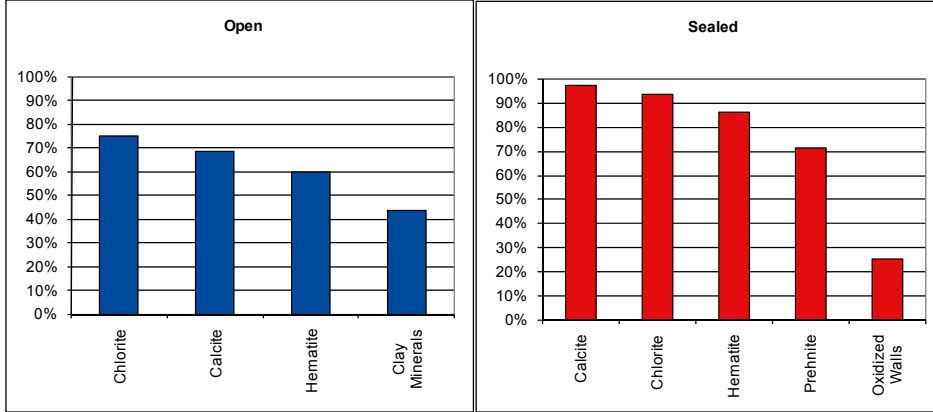
Frequency of open fractures: 14.6 m⁻¹

Std dev: no data

Frequency of sealed fractures: 42.6 m⁻¹

Std dev: no data

Mineral coatings



Fault core:

Percentage of fault core: 15 %

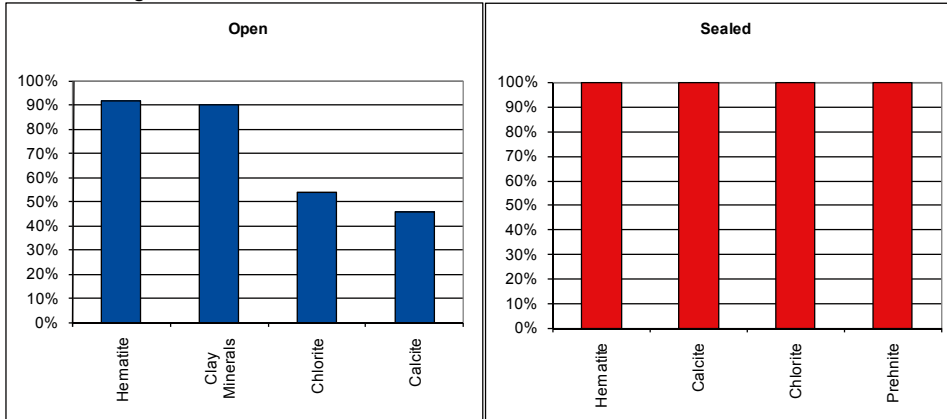
Frequency of open fractures: 18.5 m⁻¹

Std dev: no data

Frequency of sealed fractures: 67.0 m⁻¹

Std dev: no data

Mineral coatings



Deformation zone ZSMNW042A

Borehole intersections (metres along borehole)

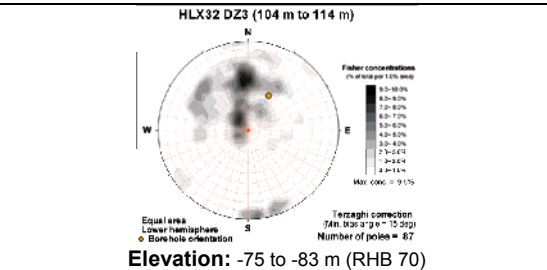
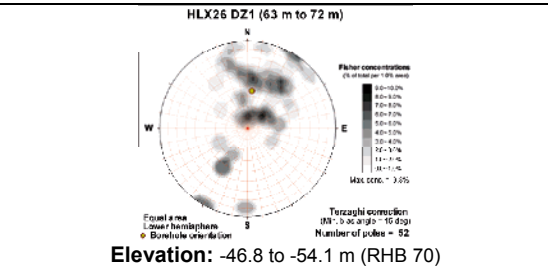
HLX26: 50-80 m (ESHI DZ1 63-72m)
 HLX32: 20-130 m (ESHI DZ3 104-114m)
 KLX15A: 977-1000,4+ m (ESHI 978-1000m)
 KLX27A : 209-255 m (ESHI DZ3 208.5-255.0 m)



Deformation style, alteration and geometry

Deformation style: ductile and brittle
Alteration: oxidation, chloritisation, epidotisation
Strike/dip (right-hand-rule): 105/55
Trace length at ground surface: 8.3 km
Model thickness / model thickness span : 40 m / 20-50 m
Measured thickness (-400 to -600 m elevation): no data
Comment:

Fractures in the deformation zone

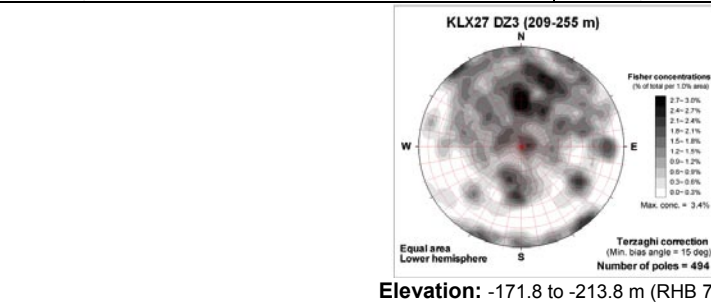


Transmissivity (m²/s)

General dip of PFL-features, elevation -400 to -600m: no data
Measured T (sum T(PFL-f)), elevation -400 to -600m: no data
Number of PFL-features, elevation -400 to -600m: no data
Model T, elevation -400 to -500m: 1.49E-6
Model T, elevation -500 to -600m: 8.27E-7

Transmissivity (m²/s)

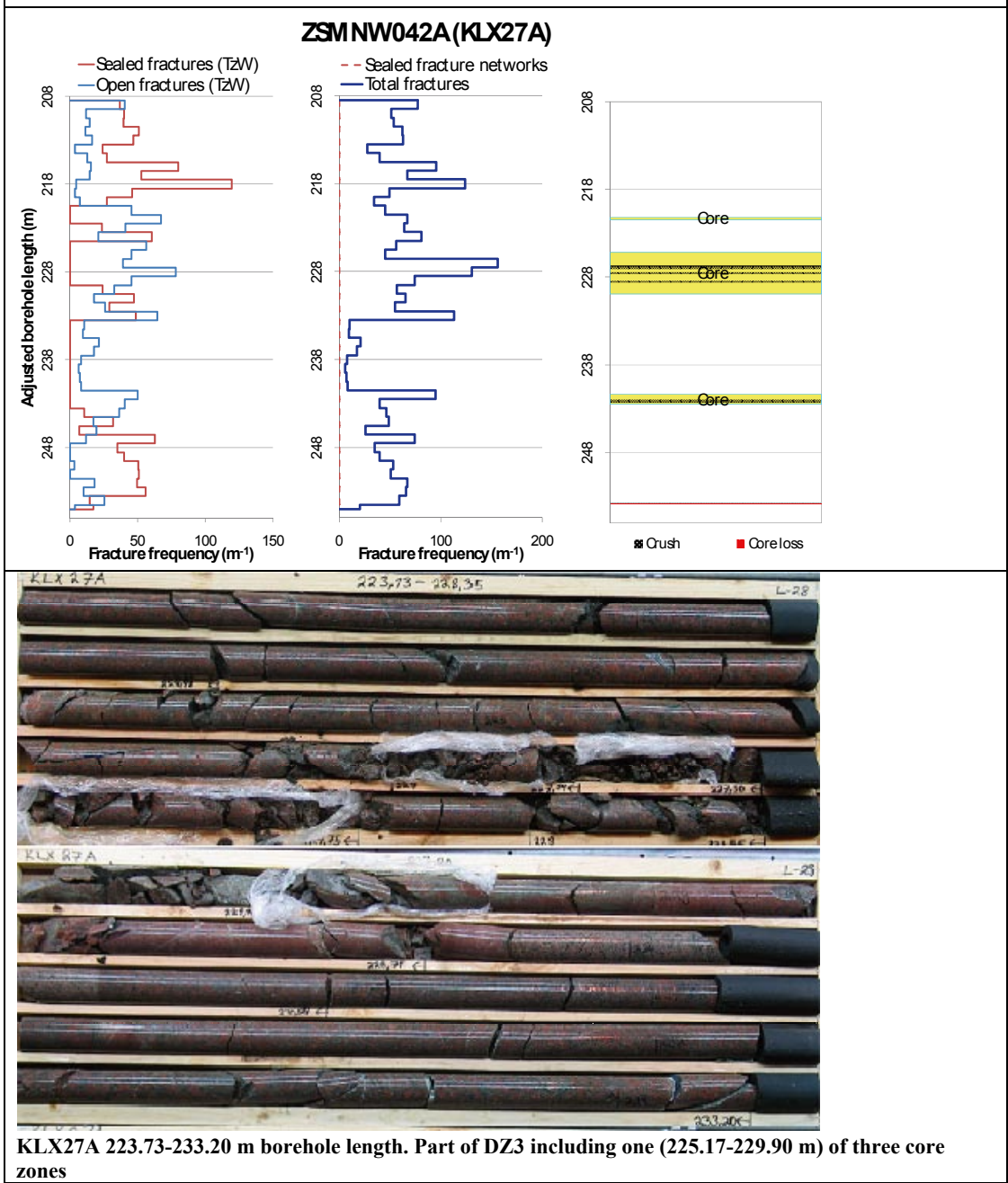
General dip of PFL-features, elevation -400 to -600m: no data
Measured T (sum T(PFL-f)), elevation -400 to -600m: no data
Number of PFL-features, elevation -400 to -600m: no data
Model T, elevation -400 to -500m: 1.49E-6
Model T, elevation -500 to -600m: 8.27E-7



Transmissivity (m²/s)

General dip of PFL-features, elevation -400 to -600m: no data
Measured T (sum T(PFL-f)), elevation -400 to -600m: no data
Number of PFL-features, elevation -400 to -600m: no data
Model T, elevation -400 to -500m: 1.49E-6
Model T, elevation -500 to -600m: 8.27E-7

Deformation zone ZSMNW042A



Deformation zone ZSMNW042A

Engineering characteristics

Transition part of zone:

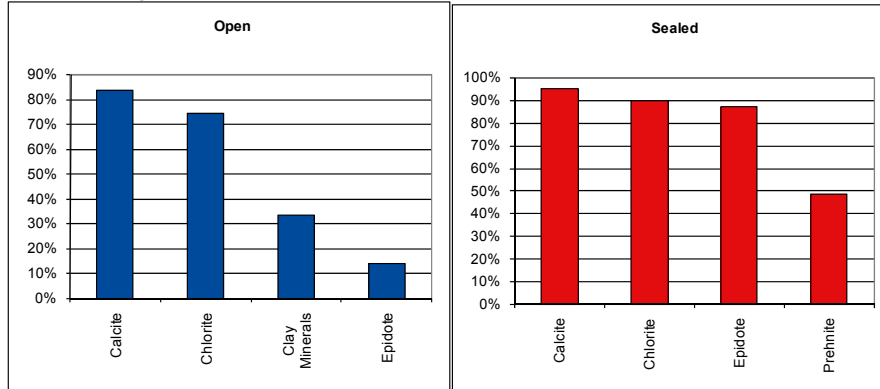
Frequency of open fractures: 4.5 m^{-1}

Std dev: no data

Frequency of sealed fractures: 48.9 m^{-1}

Std dev: no data

Mineral coatings



Fault core:

Percentage of fault core: 13 %

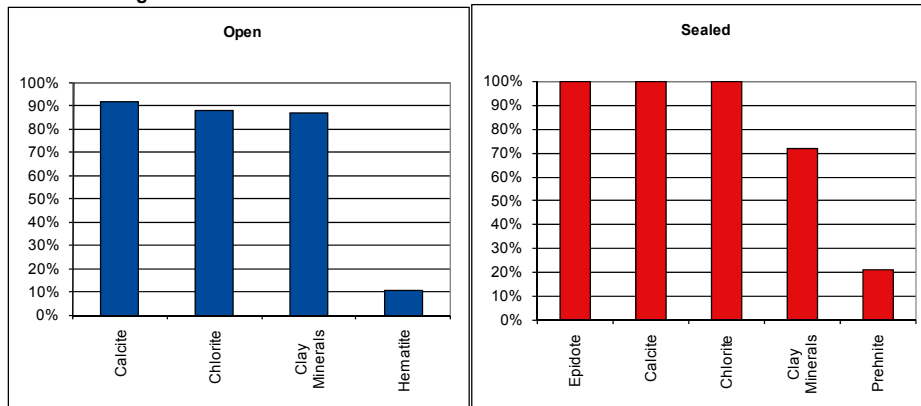
Frequency of open fractures: 24.3 m^{-1}


Std dev: no data

Frequency of sealed fractures: 70.5 m^{-1}

Std dev: no data

Mineral coatings



Deformation zone ZSMNW119A	
<p>Borehole intersections (metres along borehole)</p> <p>no data</p>	
<p>Deformation style, alteration and geometry</p> <p>Deformation style: brittle and ductile</p> <p>Alteration: red staining</p> <p>Strike/dip (right-hand-rule): 130/90</p> <p>Trace length at ground surface: 2.0 km</p> <p>Model thickness / model thickness span : 10 m / 5-20 m</p> <p>Measured thickness (-400 to -600 m elevation): no data</p> <p>Comment:</p>	
Fractures in the deformation zone	
No Borehole intercepts	
Transmissivity (m²/s)	
<p>General dip of PFL-features, elevation -400 to -600m: no data</p> <p>Measured T (sum T(PFL-f)), elevation -400 to -600m: no data</p> <p>Number of PFL-features, elevation -400 to -600m: no data</p> <p>Model T, elevation -400 to -500m: 1.49E-6</p> <p>Model T, elevation -500 to -600m: 8.27E-7</p>	
Engineering characteristics	
No Borehole intercepts	

Deformation zone KLX07_dz7

Borehole intersections (metres along borehole)

KLX07A: 347-388 m (Eshi DZ7 347-388 m)
 HLX21: 20-71 m (Eshi DZ1 18-24m)
 HLX24: 27-40 m (Eshi DZ1 27-40 m)

Deformation style, alteration and geometry

Deformation style: brittle and ductile

Alteration: oxidation, chloritisation, epidotisation

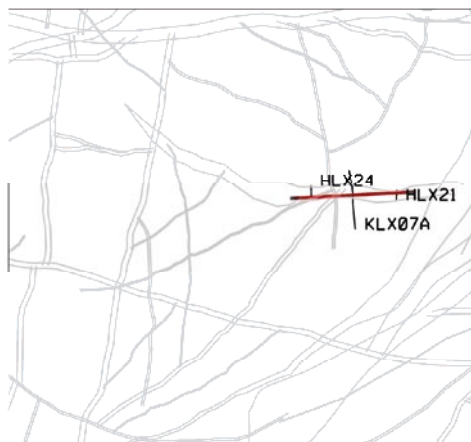
Strike/dip (right-hand-rule): 267/90

Trace length at ground surface: no data

Model thickness / model thickness span : 30 m / no data

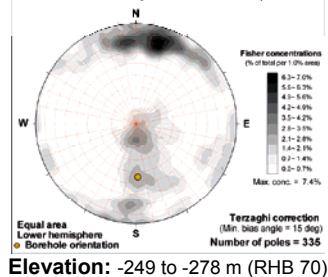
Measured thickness (-400 to -600 m elevation): no data

Comment: The modelled geometry generates theoretical intercepts in HLX21, HLX22, HLX23 and HLX24. While fracture data weakly supports possible correlation with HLX21 and HLX24 no correlation with HLX22 or HLX23 exists. It should be noted that all four hammer holes lie within the complex ZSMEW007A deformation belt.

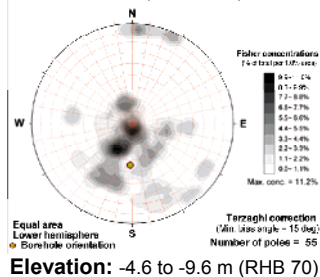


Fractures in the deformation zone

KLX07A DZ7 (347 m to 387.5 m)



HLX21 DZ1 (18 m to 24 m)



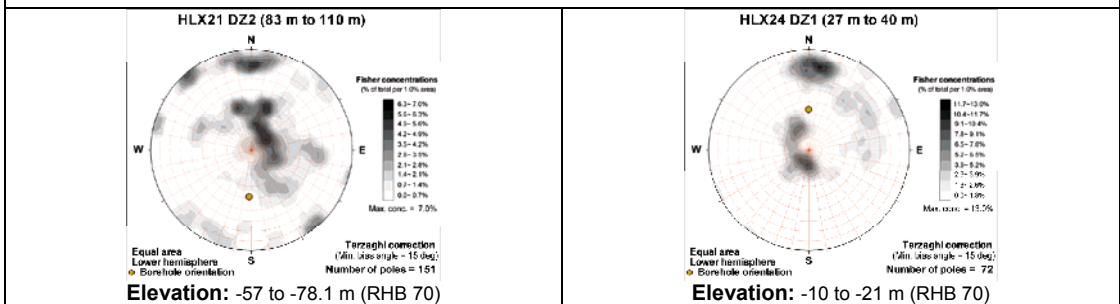
Transmissivity (m^2/s)

General dip of PFL-features, elevation -400 to -600m: no data
Measured T (sum T(PFL-f)), elevation -400 to -600m: no data
Number of PFL-features, elevation -400 to -600m: no data
Model T, elevation -400 to -500m: 2.26E-7
Model T, elevation -500 to -600m: 1.37E-7

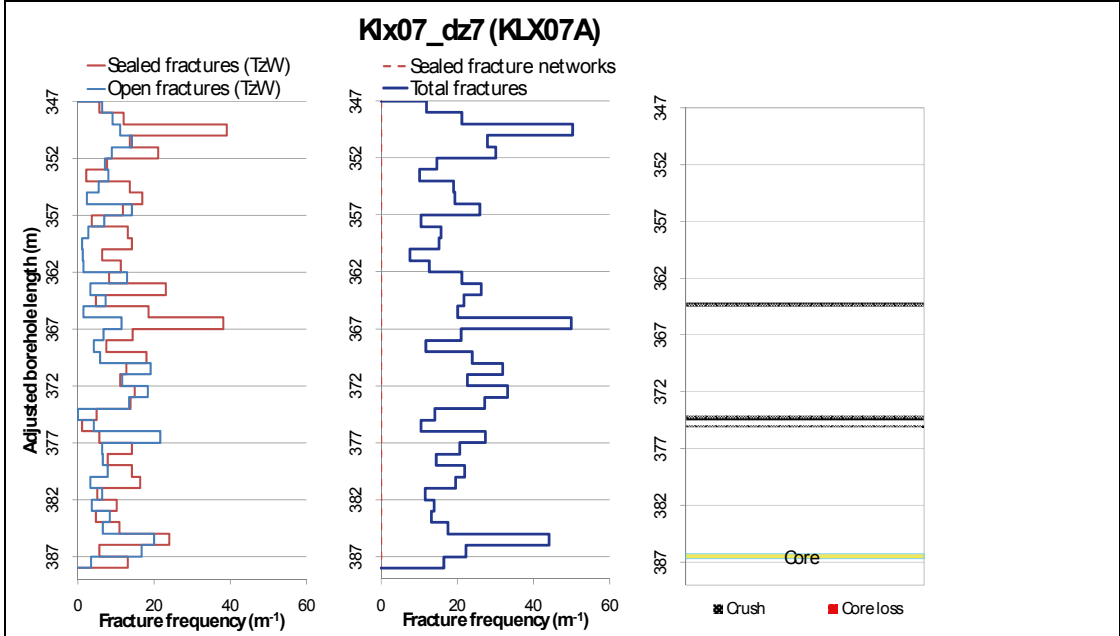
Transmissivity (m^2/s)

General dip of PFL-features, elevation -400 to -600m: no data
Measured T (sum T(PFL-f)), elevation -400 to -600m: no data
Number of PFL-features, elevation -400 to -600m: no data
Model T, elevation -400 to -500m: 2.26E-7
Model T, elevation -500 to -600m: 1.37E-7

Deformation zone KLX07_dz7



<p>Transmissivity (m²/s)</p> <p>General dip of PFL-features, elevation -400 to -600m: no data Measured T (sum T(PFL-f)), elevation -400 to -600m: no data Number of PFL-features, elevation -400 to -600m: no data Model T, elevation -400 to -500m: 2.26E-7 Model T, elevation -500 to -600m: 1.37E-7</p>	<p>Transmissivity (m²/s)</p> <p>General dip of PFL-features, elevation -400 to -600m: no data Measured T (sum T(PFL-f)), elevation -400 to -600m: no data Number of PFL-features, elevation -400 to -600m: no data Model T, elevation -400 to -500m: 2.26E-7 Model T, elevation -500 to -600m: 1.37E-7</p>
--	--



KLX07A 385.03-390.57 m borehole length. Part of DZ7, including core zone 386.3-386.7 m.

Deformation zone KLX07_dz7

Engineering characteristics

Transition part of zone:

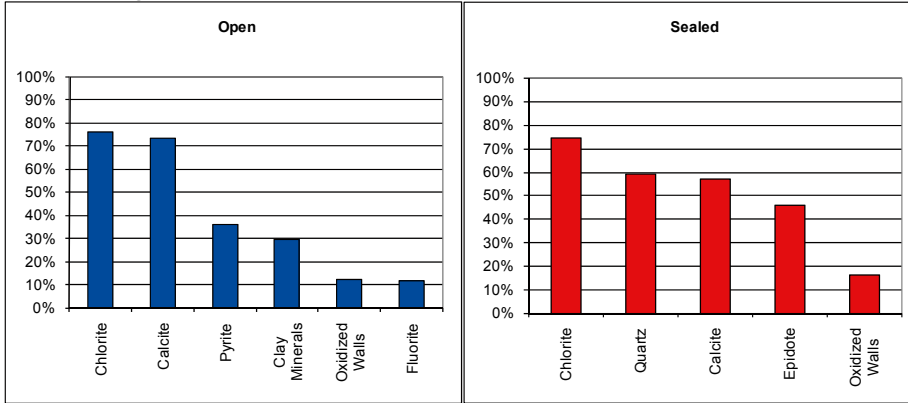
Frequency of open fractures: 5.7 m⁻¹

Std dev: no data

Frequency of sealed fractures: 16.2 m⁻¹

Std dev: no data

Mineral coatings



Fault core:

Percentage of fault core: 1 %

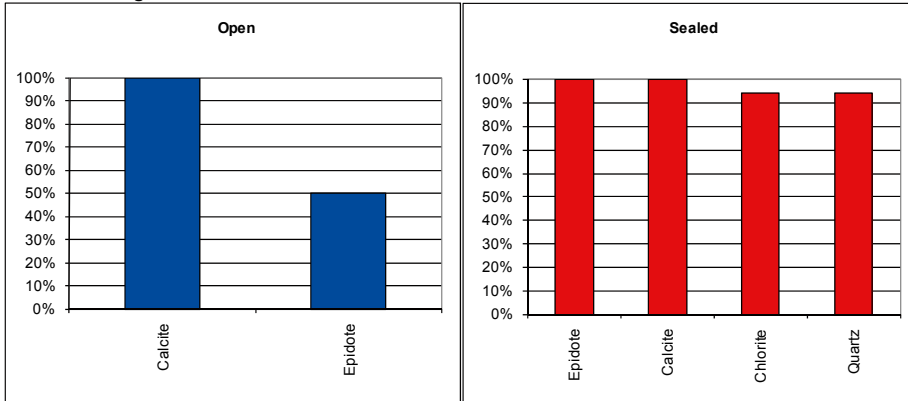
Frequency of open fractures: 10.0 m⁻¹

Std dev: no data

Frequency of sealed fractures: 45.0 m⁻¹

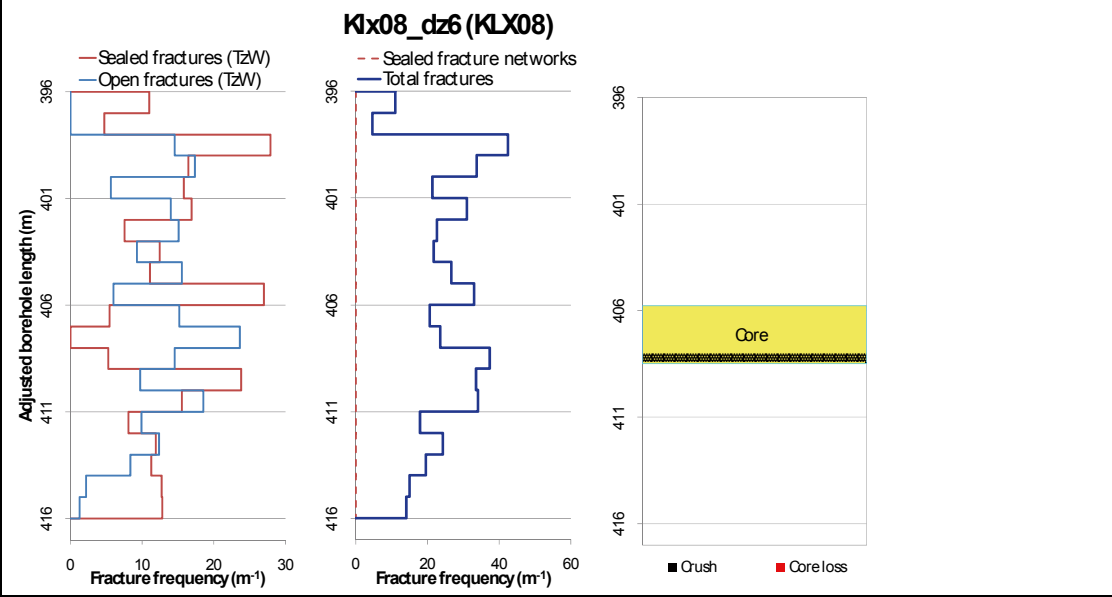
Std dev: no data

Mineral coatings



Deformation zone KLX08_dz6	
<p>Borehole intersections (metres along borehole)</p> <p>KLX08A: 396-416 (Eshi DZ6 396-416 m)</p>	
<p>Deformation style, alteration and geometry</p> <p>Deformation style: brittle</p> <p>Alteration: red staining, epidotisation, saussuritization</p> <p>Strike/dip (right-hand-rule): 296/89</p> <p>Trace length at ground surface: no data</p> <p>Model thickness / model thickness span : 10 m / no data</p> <p>Measured thickness (-400 to -600 m elevation): no data</p> <p>Comment:</p>	
Fractures in the deformation zone	
Transmissivity (m²/s)	
<p>General dip of PFL-features, elevation -400 to -600m: no data</p> <p>Measured T (sum T(PFL-f)), elevation -400 to -600m: no data</p> <p>Number of PFL-features, elevation -400 to -600m: no data</p> <p>Model T, elevation -400 to -500m: 2.26E-7</p> <p>Model T, elevation -500 to -600m: 1.37E-7</p>	

Deformation zone KLX08_dz6



KLX08A 406.24-415.99 m borehole length. Part of DZ6, including core zone (405.77- 408.50 m)

Deformation zone KLX08_dz6

Engineering characteristics

Transition part of zone:

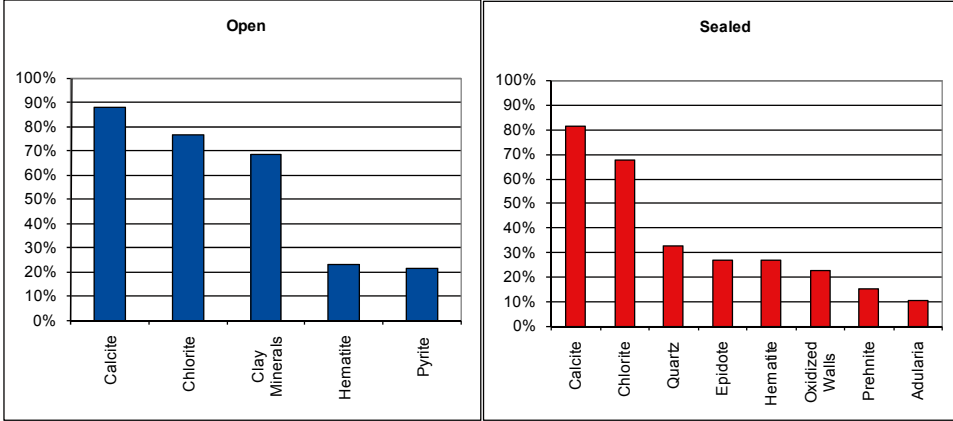
Frequency of open fractures: 6.4 m⁻¹

Std dev: no data

Frequency of sealed fractures: 17.3 m⁻¹

Std dev: no data

Mineral coatings



Fault core:

Percentage of fault core: 14 %

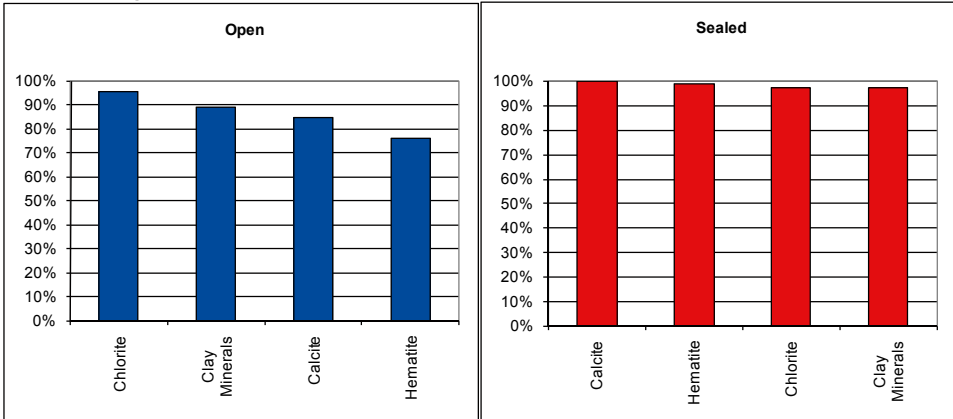
Frequency of open fractures: 16.9 m⁻¹

Std dev: no data

Frequency of sealed fractures: 59.0 m⁻¹

Std dev: no data

Mineral coatings



Deformation zone KLX18_dz9

Borehole intersections (metres along borehole)

KLX18A: 347-388 m (Eshi DZ9 472-489 m)
 HLX30: None (Eshi DZ2 60-68 m)

Deformation style, alteration and geometry

Deformation style: brittle and ductile

Alteration: oxidation, chloritisation, epidotisation

Strike/dip (right-hand-rule): 095/50

Trace length at ground surface: no data

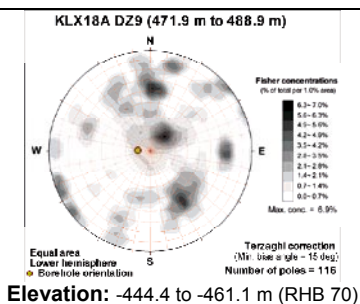
Model thickness / model thickness span : 10 m / no data

Measured thickness (-400 to -600 m elevation): 10m

Comment: orientation is based on detailed mapping of the zone core /Viola et al. 2007a/. An interception at the outer edge of the modelled geometry coincides with Eshi HLX30 DZ2 though no clear correlation is established.



Fractures in the deformation zone



Transmissivity (m^2/s)

General dip of PFL-features, elevation -400 to -600m: Moderately to sub-horizontally

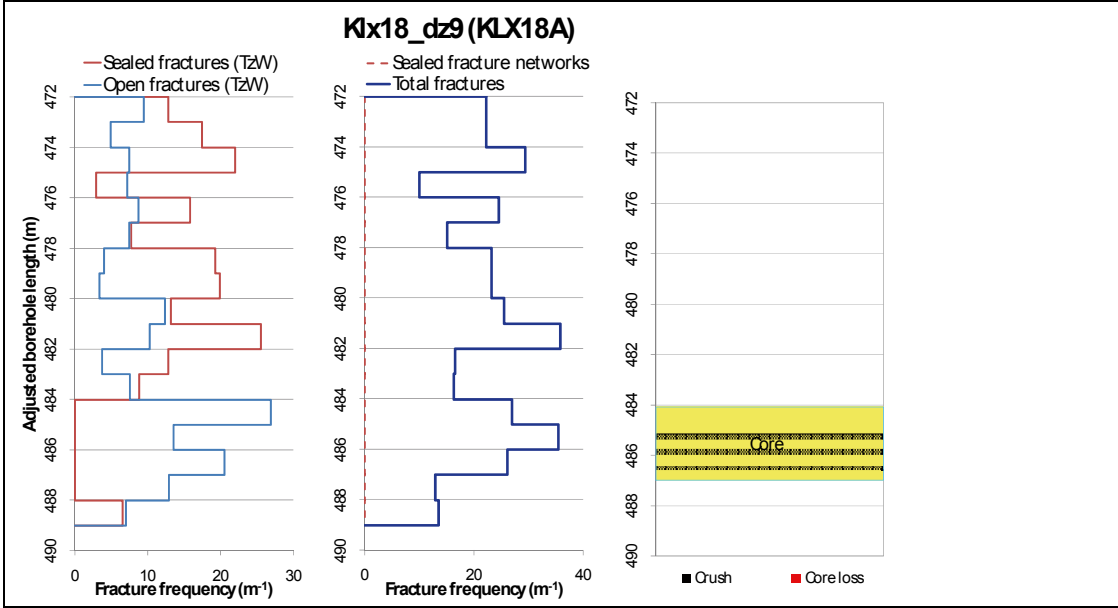
Measured T (sum T(PFL-f)), elevation -400 to -600m: 5.44E-8

Number of PFL-features, elevation -400 to -600m: 9

Model T, elevation -400 to -500m: 2.26E-7

Model T, elevation -500 to -600m: 1.37E-7

Deformation zone KLX18_dz9



KLX18A 478.18-489.10 m borehole length. Part of DZ9, including core zone 484.1-487.0 m.

Deformation zone KLX18_dz9

Engineering characteristics

Transition part of zone:

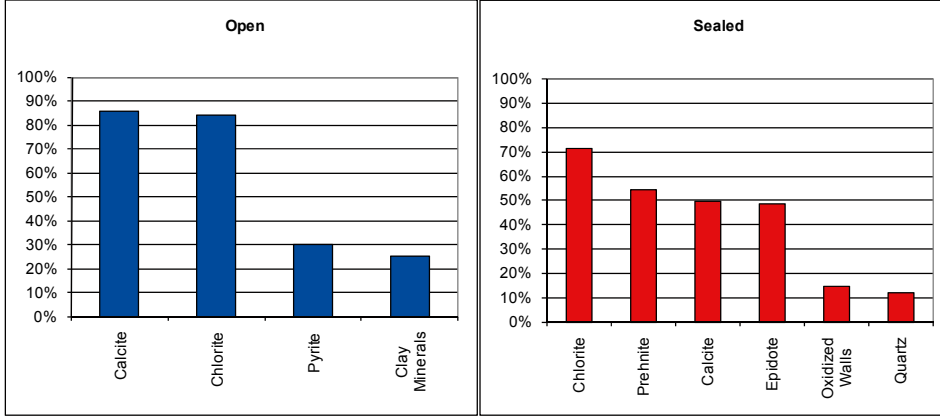
Frequency of open fractures: 4.5 m⁻¹

Std dev: no data

Frequency of sealed fractures: 16.0 m⁻¹

Std dev: no data

Mineral coatings



Fault core:

Percentage of fault core: 17 %

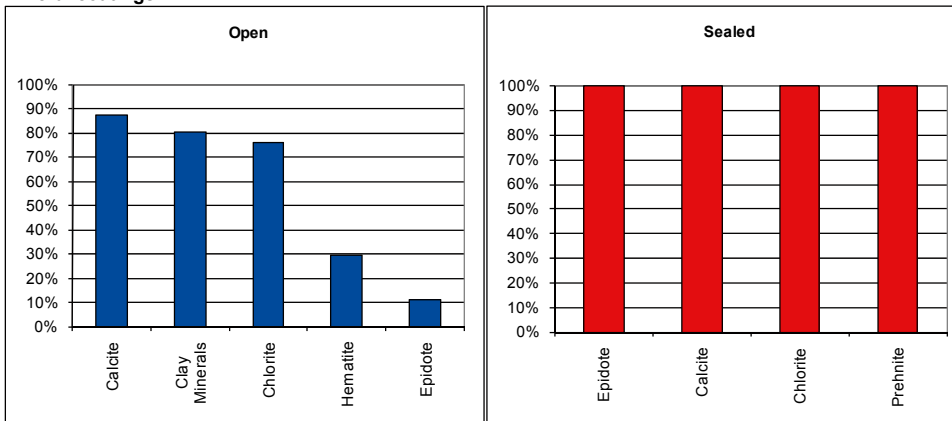
Frequency of open fractures: 24.5 m⁻¹

Std dev: no data

Frequency of sealed fractures: 50.0 m⁻¹

Std dev: no data

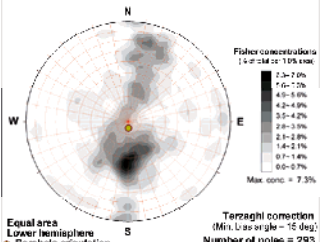
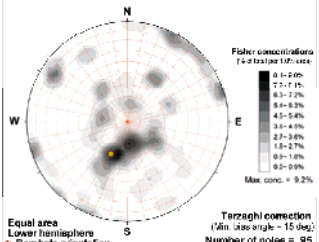
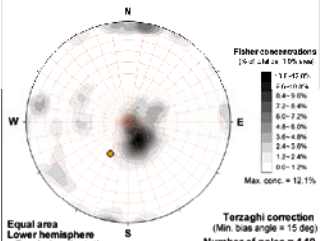
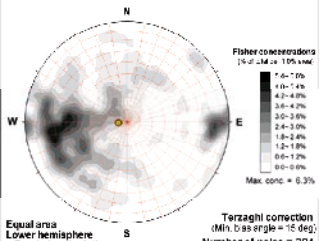
Mineral coatings



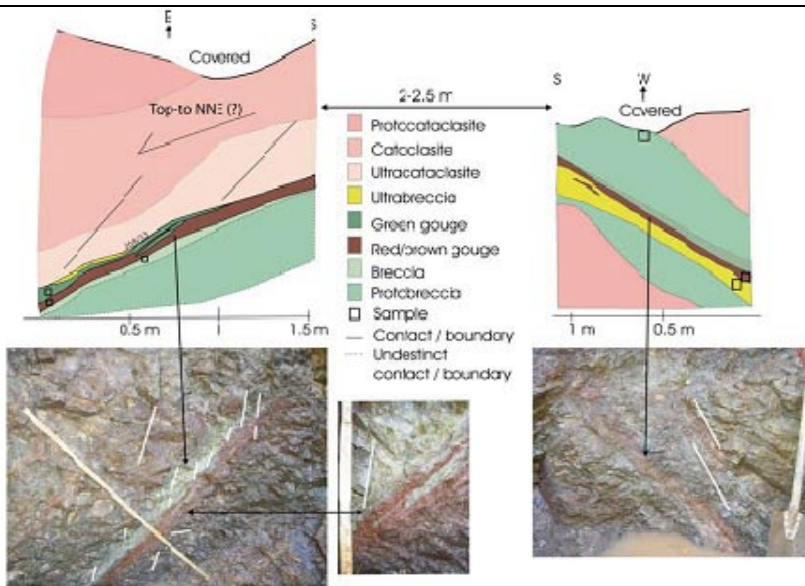
E-W to NW-SE striking deformation zones, steep to moderately northward dipping

Deformation zone ZSMEW007A-C	
<p>Borehole intersections (metres along borehole)</p> <p>HLX10: - m HLX11: - m HLX13: 29-103 m (ESHI DZ1 75-108m) HLX14: - m HLX21: 18-95 m (ESHI DZ1 18-24m) HLX22: 0-163 m (ESHI DZ1 116-119m) HLX23: 0-80 m (ESHI DZ1 47-54m; DZ2 62-67m; DZ3 77-82m) HLX24: 0-150 m (ESHI DZ1 27-40m; DZ2 58-64m, DZ3 137-145m) HLX25: 0-80 m (ESHI DZ1 47-52) HLX30: 0-80 m (ESHI DZ1 10-42m; DZ2 66-74m) HLX31: 50-100 m (ESHI DZ1 60-67m) HLX33: 0-70 m (ESHI DZ1 12-28 m) KLX01: 1000-1020 m (ESHI DZ1 1000-1020m) KLX02: 180-200 m (no ESHI data) KLX04: 310-385 m (ESHI DZ4 325-326m; DZ5 346-355m; DZ11 363.25-363.6m) KLX07A: 105-147 m (ESHI DZ1 105-147m) KLX07B: 124-172 m (ESHI DZ3 124-172m) KLX08: 211-300 m (ESHI DZ3 211,5-220m; DZ4 224,5-242m; DZ5 291-302m) KLX09: 682-722 m (ESHI DZ13 682-722m)</p>	
<p>Deformation style, alteration and geometry</p> <p>Deformation style: brittle</p> <p>Alteration: dominated by red staining, but also sections of epidotisation and saussuritisation,</p> <p>Strike/dip (right-hand-rule): 281/44</p> <p>Trace length at ground surface: 3.3 km</p> <p>Model thickness / model thickness span : 80 m / 20-80 m</p> <p>Measured thickness (-400 to -600 m elevation): no data</p> <p>Comment:</p>	
Fractures in the deformation zone	
<p style="text-align: center;">KLX04 DZ5 (346 m to 355 m)</p> <p style="text-align: center;">Elevation: -320.2 to -329.1 m (RHB 70)</p>	<p style="text-align: center;">KLX07A DZ1 (105 m to 147 m)</p> <p style="text-align: center;">Elevation: -67.4 to -99.3 m (RHB 70)</p>
<p style="text-align: center;">Transmissivity (m²/s)</p> <p>General dip of PFL-features, elevation -400 to -600m: no data</p> <p>Measured T (sum T(PFL-f)), elevation -400 to -600m: no data</p> <p>Number of PFL-features, elevation -400 to -600m: no data</p> <p>Model T, elevation -400 to -500m: A: 1.08E-5, C: 4.23E-7</p> <p>Model T, elevation -500 to -600m: A: 6.56E-6, C: 2.62E-7</p>	<p style="text-align: center;">Transmissivity (m²/s)</p> <p>General dip of PFL-features, elevation -400 to -600m: no data</p> <p>Measured T (sum T(PFL-f)), elevation -400 to -600m: no data</p> <p>Number of PFL-features, elevation -400 to -600m: no data</p> <p>Model T, elevation -400 to -500m: A: 1.08E-5, C: 4.23E-7</p> <p>Model T, elevation -500 to -600m: A: 6.56E-6, C: 2.62E-7</p>

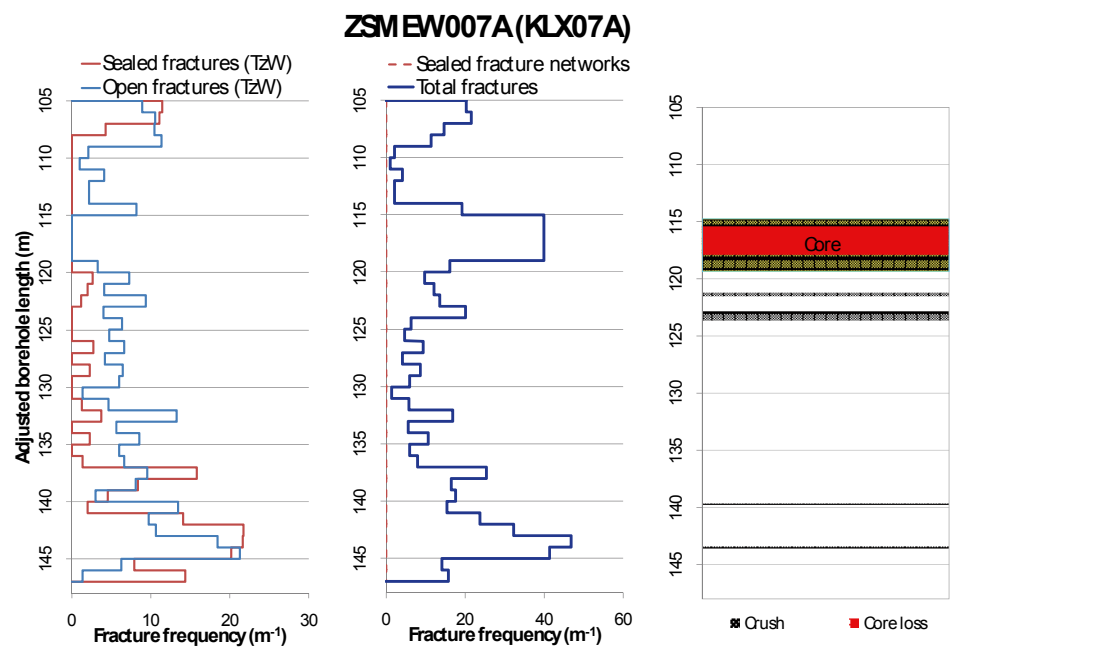
Deformation zone ZSMEW007A-C

<p style="text-align: center;">KLX07B DZ3 (124 m to 172 m)</p>  <p style="text-align: center;">Elevation: -105.2 to -153.0 m (RHB 70)</p>	<p style="text-align: center;">KLX08 DZ3 (211.5 m to 220 m)</p>  <p style="text-align: center;">Elevation: -158.8 to -166.2 m (RHB 70)</p>
<p style="text-align: center;">Transmissivity (m²/s)</p> <p>General dip of PFL-features, elevation -400 to -600m: no data</p> <p>Measured T (sum T(PFL-f)), elevation -400 to -600m: no data</p> <p>Number of PFL-features, elevation -400 to -600m: no data</p> <p>Model T, elevation -400 to -500m: A: 1.08E-5, C: 4.23E-7</p> <p>Model T, elevation -500 to -600m: A: 6.56E-6, C: 2.62E-7</p>	<p style="text-align: center;">Transmissivity (m²/s)</p> <p>General dip of PFL-features, elevation -400 to -600m: no data</p> <p>Measured T (sum T(PFL-f)), elevation -400 to -600m: no data</p> <p>Number of PFL-features, elevation -400 to -600m: no data</p> <p>Model T, elevation -400 to -500m: A: 1.08E-5, C: 4.23E-7</p> <p>Model T, elevation -500 to -600m: A: 6.56E-6, C: 2.62E-7</p>
<p style="text-align: center;">KLX08 DZ4 (224.5 m to 242 m)</p>  <p style="text-align: center;">Elevation: -170.1 to -185.3 m (RHB 70)</p>	<p style="text-align: center;">KLX09 DZ13 (682 m to 722 m)</p>  <p style="text-align: center;">Elevation: -653.6 to -693.4 m (RHB 70)</p>
<p style="text-align: center;">Transmissivity (m²/s)</p> <p>General dip of PFL-features, elevation -400 to -600m: no data</p> <p>Measured T (sum T(PFL-f)), elevation -400 to -600m: no data</p> <p>Number of PFL-features, elevation -400 to -600m: no data</p> <p>Model T, elevation -400 to -500m: A: 1.08E-5, C: 4.23E-7</p> <p>Model T, elevation -500 to -600m: A: 6.56E-6, C: 2.62E-7</p>	<p style="text-align: center;">Transmissivity (m²/s)</p> <p>General dip of PFL-features, elevation -400 to -600m: no data</p> <p>Measured T (sum T(PFL-f)), elevation -400 to -600m: no data</p> <p>Number of PFL-features, elevation -400 to -600m: no data</p> <p>Model T, elevation -400 to -500m: A: 1.08E-5, C: 4.23E-7</p> <p>Model T, elevation -500 to -600m: A: 6.56E-6, C: 2.62E-7</p>

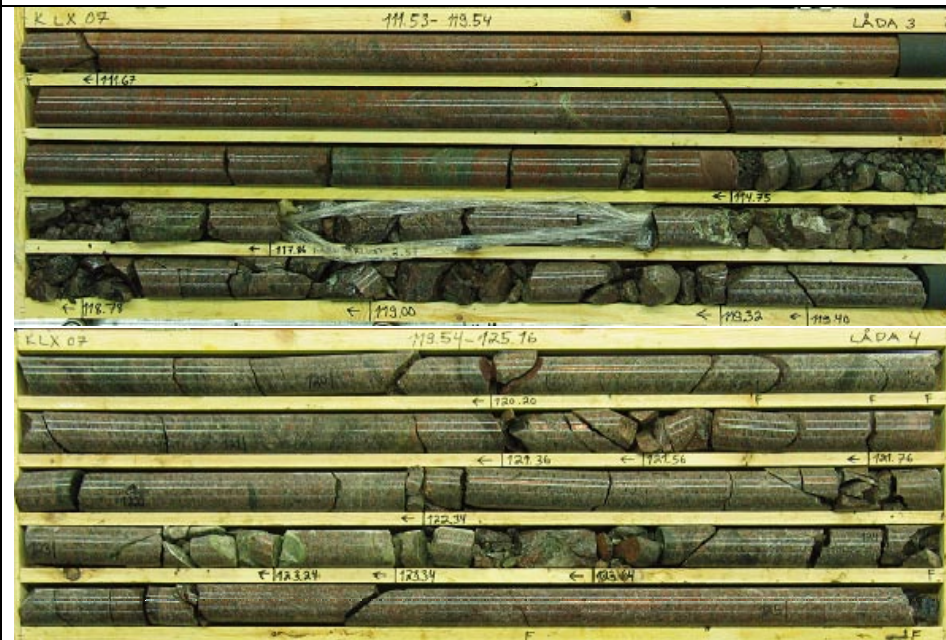
Deformation zone ZSMEW007A-C



Sketch and photographs of trench walls with exposed fault rocks. As exposed in the trench located along profile LSM000280. /Viola and Ganerod, 2006/



Deformation zone ZSMEW007A-C



KLX07A 111,50-125 m borehole length. Part of DZ1 including core zone 114,75-119.40 m.

Engineering characteristics

Transition part of zone:

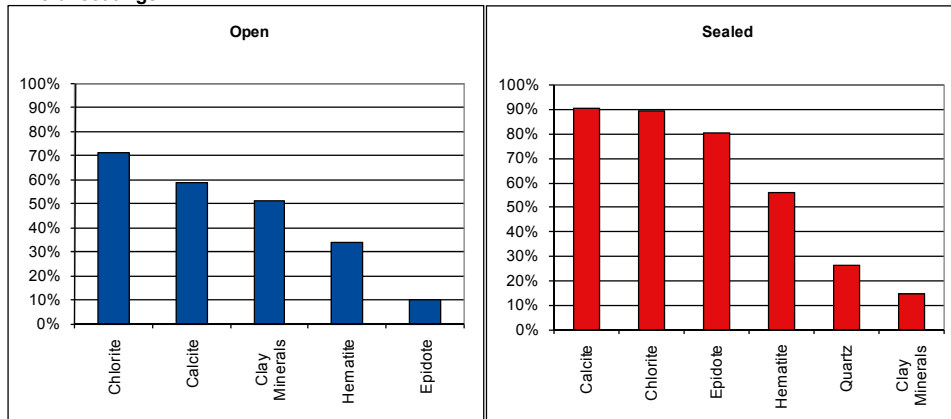
Frequency of open fractures: 5.5 m^{-1}

Std dev: 1.0

Frequency of sealed fractures: 32.5 m^{-1}

Std dev: 13.6

Mineral coatings



Deformation zone ZSMEW007A-C

Fault core:

Percentage of fault core: 10 %

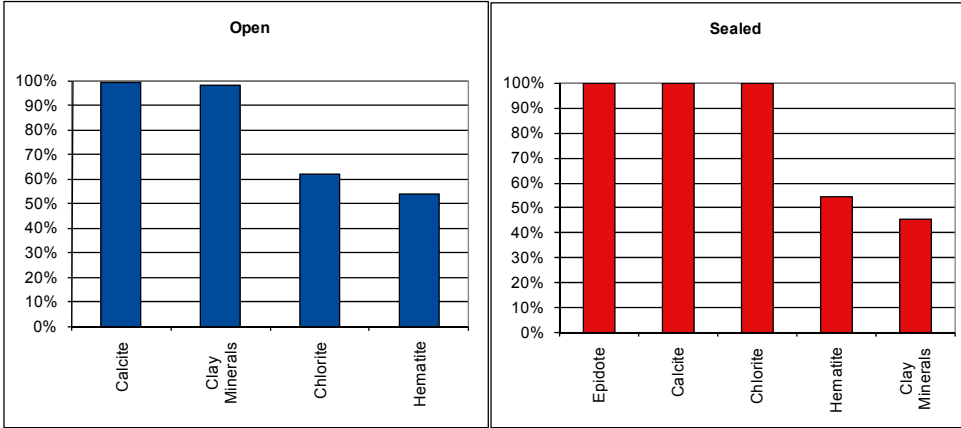
Frequency of open fractures: 40.0 m⁻¹

Std dev: 1.0

Frequency of sealed fractures: 50.2 m⁻¹

Std dev: 0.1

Mineral coatings



Deformation zone KLX07_dz9

Borehole intersections (metres along borehole)

KLX07A: 448-459 m (ESHI DZ9 448-459)

Deformation style, alteration and geometry

Deformation style: brittle and ductile

Alteration: red staining

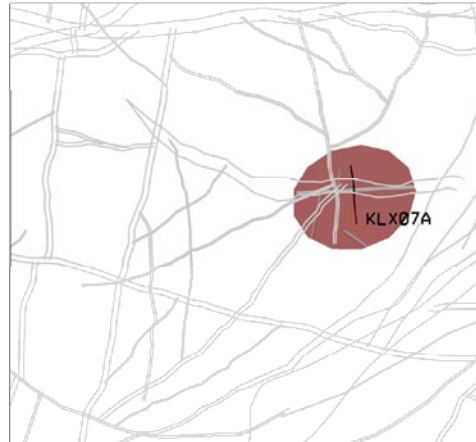
Strike/dip (right-hand-rule): 253/35

Trace length at ground surface: no data

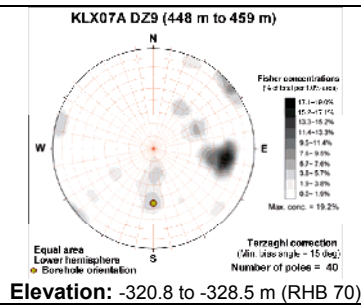
Model thickness / model thickness span : 10 m / no data

Measured thickness (-400 to -600 m elevation): no data

Comment: orientation is based on seismic reflector 'D' /Juhlin 2004/, generally supported by mylonite ca. 250/50; crush 270/45 and fracture orientation concentration. Towards the edge of the modelled geometry there is a theoretical intercept with KLX02 but no evidence of likely correlation.



Fractures in the deformation zone



Transmissivity (m^2/s)

General dip of PFL-features, elevation -400 to -600m: no data

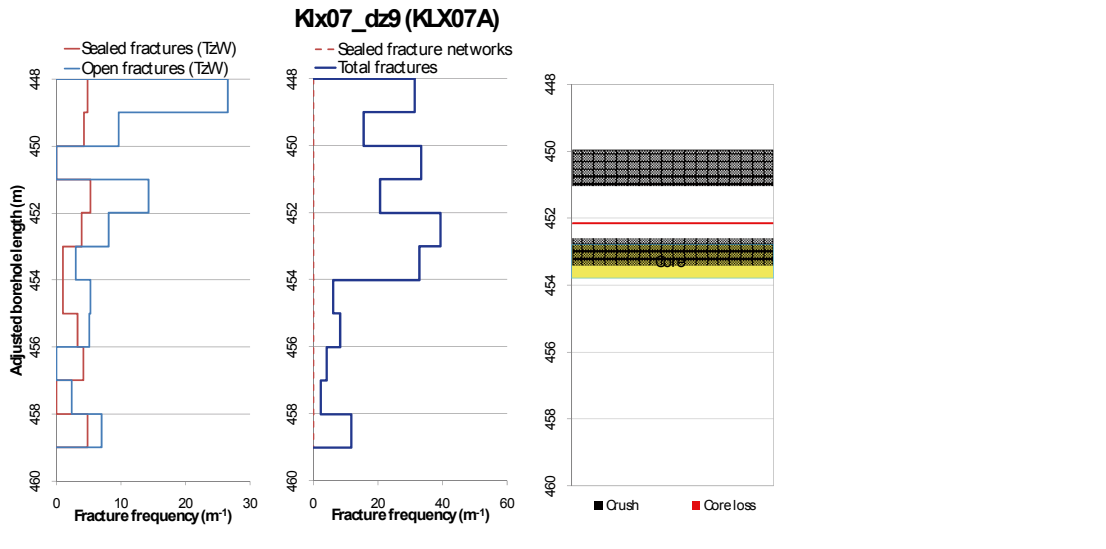
Measured T (sum T(PFL-f)), elevation -400 to -600m: no data

Number of PFL-features, elevation -400 to -600m: no data

Model T, elevation -400 to -500m: 2.26E-7

Model T, elevation -500 to -600m: 1.37E-7

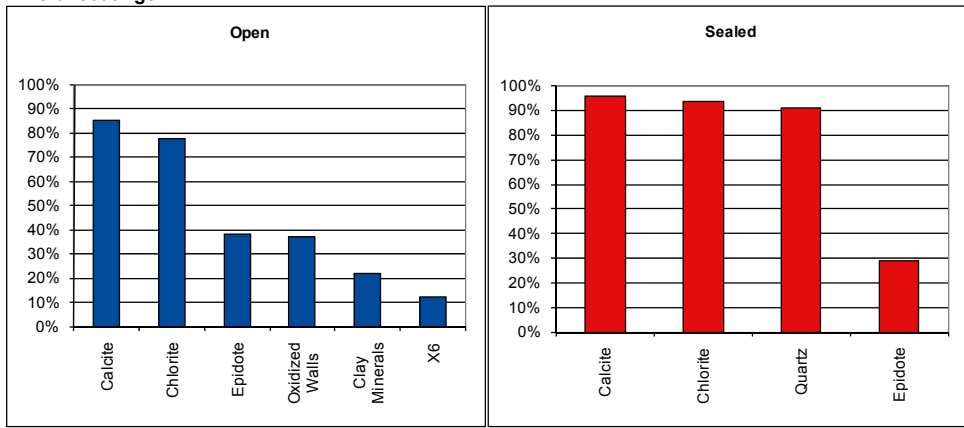
Deformation zone KLX07_dz9



KLX07 451.14- 456.93 m borehole length. Part of DZ9 including core zone 452.80-453.8 m.

Engineering characteristics

Transition part of zone:
 Frequency of open fractures: 10.4 m⁻¹
 Std dev: no data
 Frequency of sealed fractures: 19.1 m⁻¹
 Std dev: no data
Mineral coatings



Deformation zone KLX07_dz9

Fault core:

Percentage of fault core: 9 %

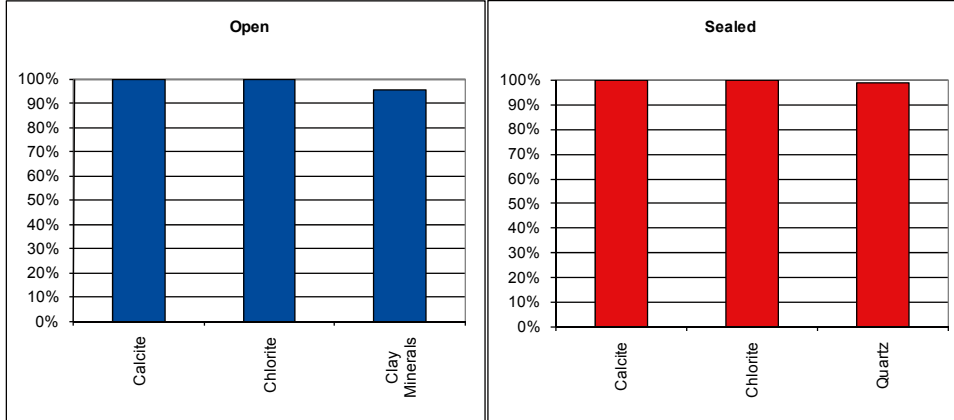
Frequency of open fractures: 45.0 m⁻¹

Std dev: no data

Frequency of sealed fractures: 102.0 m⁻¹

Std dev: no data

Mineral coatings



Deformation zone KLX07_dz11

Borehole intersections (metres along borehole)

KLX07A: 693-724 m (ESHI DZ11 693-724 m)

Deformation style, alteration and geometry

Deformation style: brittle

Alteration: oxidation, chloritisation, epidotisation

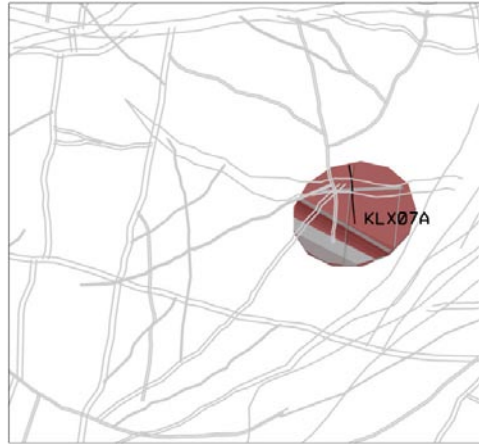
Strike/dip (right-hand-rule): 253/35

Trace length at ground surface: no data

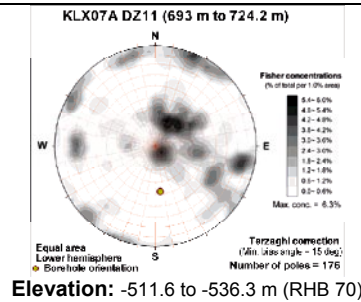
Model thickness / model thickness span : 30 m / no data

Measured thickness (-400 to -600 m elevation): 30 m

Comment:



Fractures in the deformation zone



Transmissivity (m²/s)

General dip of PFL-features, elevation -400 to -600m: Moderately to sub-horizontally and steep

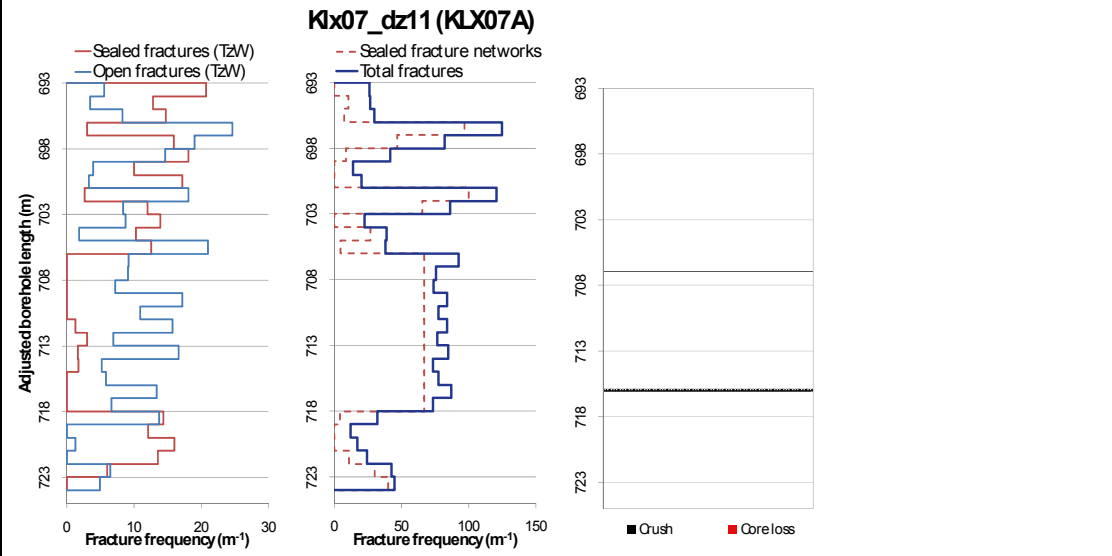
Measured T (sum T(PFL-f)), elevation -400 to -600m: 7.06E-7

Number of PFL-features, elevation -400 to -600m: 8

Model T, elevation -400 to -500m: 2.26E-7

Model T, elevation -500 to -600m: 1.37E-7

Deformation zone KLX07_dz11



KLX07A 702.82-713.53 m borehole length. Part of DZ11 (no defined core zone)

Deformation zone KLX07_dz11

Engineering characteristics

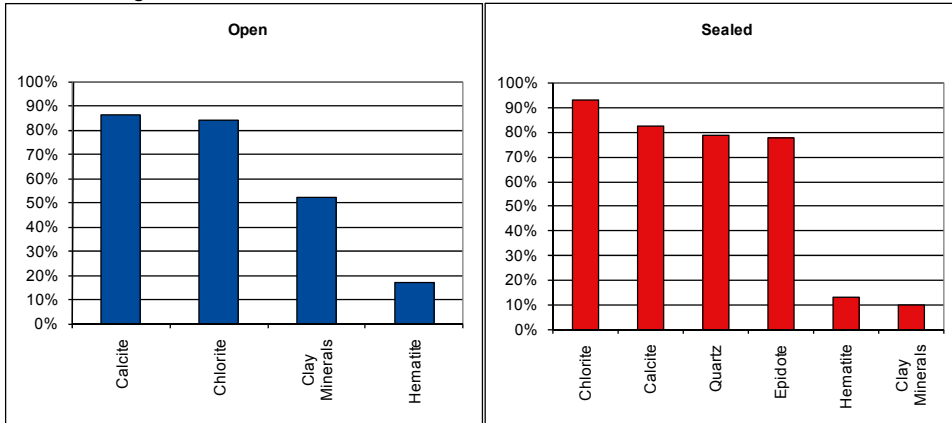
Frequency of open fractures: 6.2 m^{-1}

Std dev: no data

Frequency of sealed fractures: 44.7 m^{-1}

Std dev: no data

Mineral coatings



Deformation zone KLX07_dz12

Borehole intersections (metres along borehole)

KLX07A: 738-785 m (ESHI DZ12 738-785 m)

Deformation style, alteration and geometry

Deformation style: brittle

Alteration: red staining, epidotisation

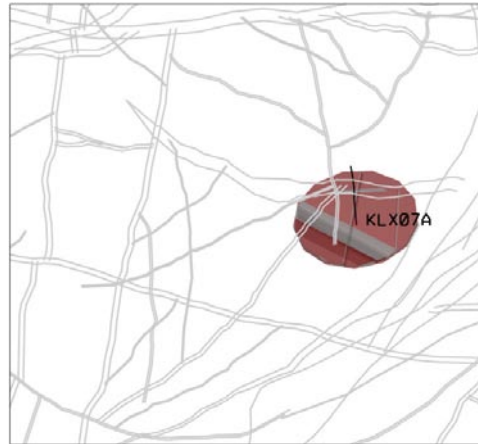
Strike/dip (right-hand-rule): 263/41

Trace length at ground surface: no data

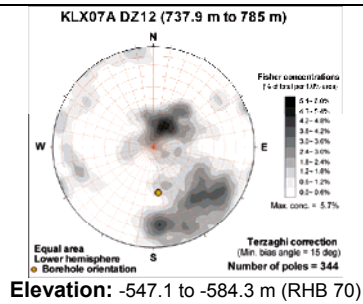
Model thickness / model thickness span : 47 m / no data

Measured thickness (-400 to -600 m elevation): 47 m

Comment:



Fractures in the deformation zone



Transmissivity (m^2/s)

General dip of PFL-features, elevation -400 to -600m: moderately to sub-horizontally and steep

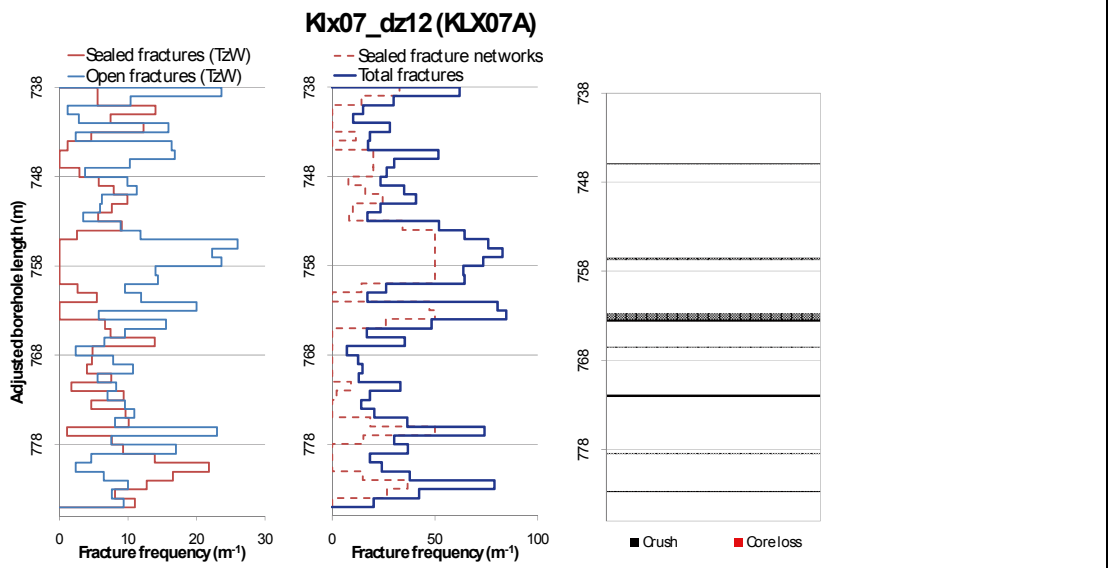
Measured T (sum T(PFL-f)), elevation -400 to -600m: 9.47E-6

Number of PFL-features, elevation -400 to -600m: 21

Model T, elevation -400 to -500m: 2.26E-7

Model T, elevation -500 to -600m: 1.37E-7

Deformation zone KLX07_dz12



KLX07A 745.89-756.90 borehole length. Part of DZ12, no defined core zone.

Deformation zone KLX07_dz12

Engineering characteristics

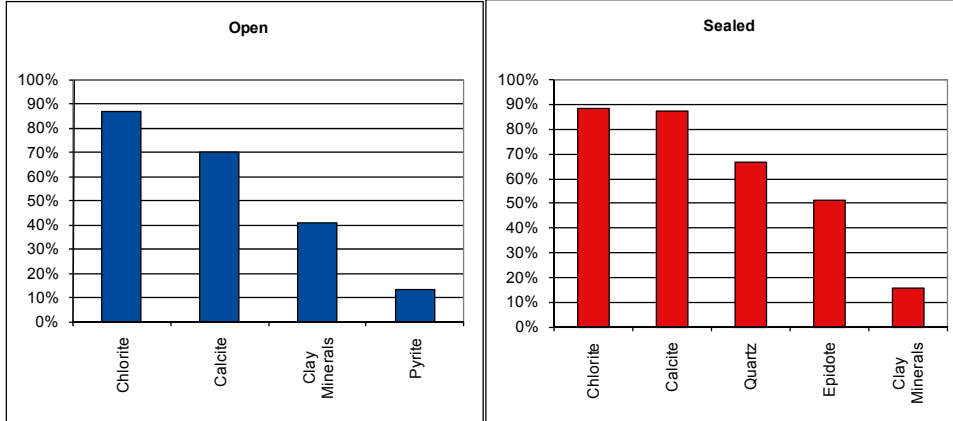
Frequency of open fractures: 10.2 m^{-1}

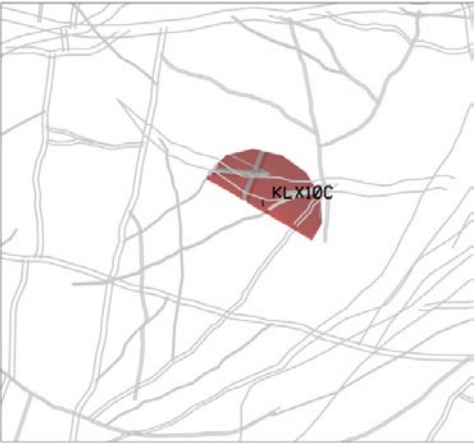
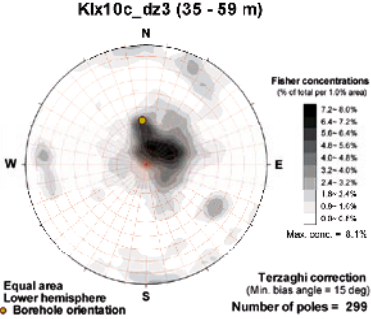
Std dev: no data

Frequency of sealed fractures: 21.4 m^{-1}

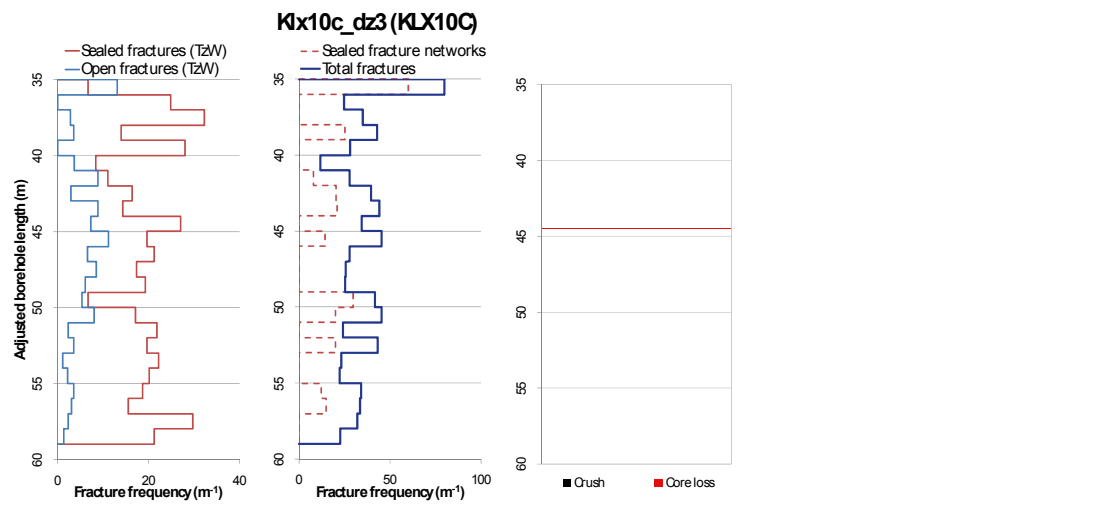
Std dev: no data

Mineral coatings



Deformation zone KLX10C_dz3	
<p>Borehole intersections (metres along borehole)</p> <p>KLX10C: 35-59 m (ESHI DZ3 35-59 m)</p>	
<p>Deformation style, alteration and geometry</p> <p>Deformation style: brittle and ductile</p> <p>Alteration: red staining, epidotisation, saussuritisation.</p> <p>Strike/dip (right-hand-rule): 300/35</p> <p>Trace length at ground surface: no data</p> <p>Model thickness / model thickness span : 10 m / no data</p> <p>Measured thickness (-400 to -600 m elevation): no data</p> <p>Comment: orientation is based on ductile-brittle zones mapped in the drill core. The modelled geometry generates theoretical intercepts in KLX10, KLX10B, HLX31 and HLX33. KLX10 and KLX10B were not cored at this position. HLX31 and HLX33 lack clear correlation but it should be noted both holes lie in the complex ZSMEW007A belt.</p>	
Fractures in the deformation zone	
<p>Klx10c_dz3 (35 - 59 m)</p>  <p>Elevation: -13.3 to -34.3 m (RHB 70)</p>	
Transmissivity (m²/s)	
<p>General dip of PFL-features, elevation -400 to -600m: no data</p> <p>Measured T (sum T(PFL-f)), elevation -400 to -600m: no data</p> <p>Number of PFL-features, elevation -400 to -600m: no data</p> <p>Model T, elevation -400 to -500m: 2.26E-7</p> <p>Model T, elevation -500 to -600m: 1.37E-7</p>	

Deformation zone KLX10C_dz3



KLX10C 39.17-50.46 m borehole length. Part of DZ3

Deformation zone KLX10C_dz3

Engineering characteristics

Transition part of zone:

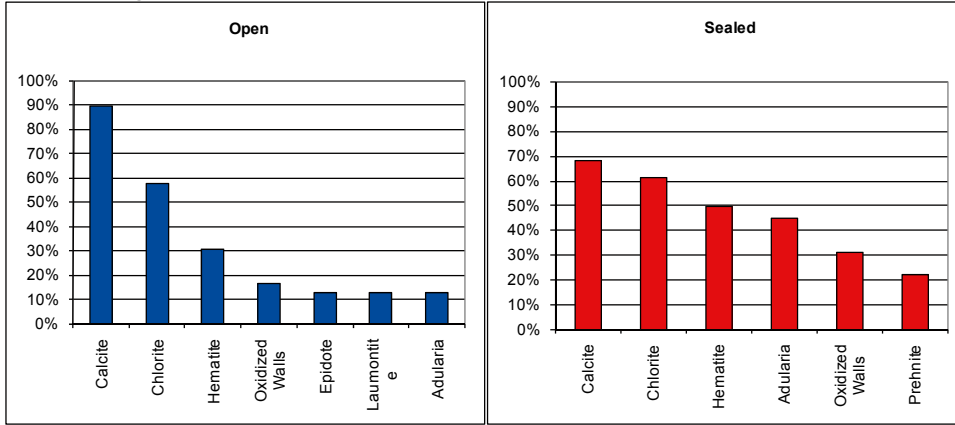
Frequency of open fractures: 3.3 m^{-1}

Std dev: no data

Frequency of sealed fractures: 23.0 m^{-1}

Std dev: no data

Mineral coatings



Deformation zone KLX10C_dz7

Borehole intersections (metres along borehole)

KLX10C: 121-140 m (ESHI DZ7 121-140 m)

Deformation style, alteration and geometry

Deformation style: brittle and ductile

Alteration: red staining

Strike/dip (right-hand-rule): 323/39

Trace length at ground surface: no data

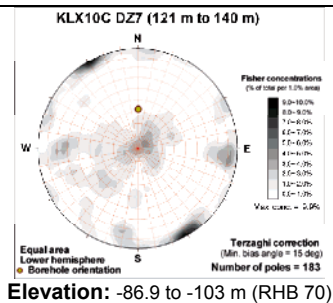
Model thickness / model thickness span : 10 m / no data

Measured thickness (-400 to -600 m elevation): no data

Comment: orientation is based on mapped brittle- ductile indicators in the drill core. The modelled geometry results in theoretical intercepts in KLX10 and HLX31. KLX10 is not cored in this position. No clear correlation with HLX31 has been identified. However, the HLX31 intercept is towards the edge of the modelled zone geometry and this hole lies within the complex ZSMEW007A zone belt.



Fractures in the deformation zone



Transmissivity (m^2/s)

General dip of PFL-features, elevation -400 to -600m: no data

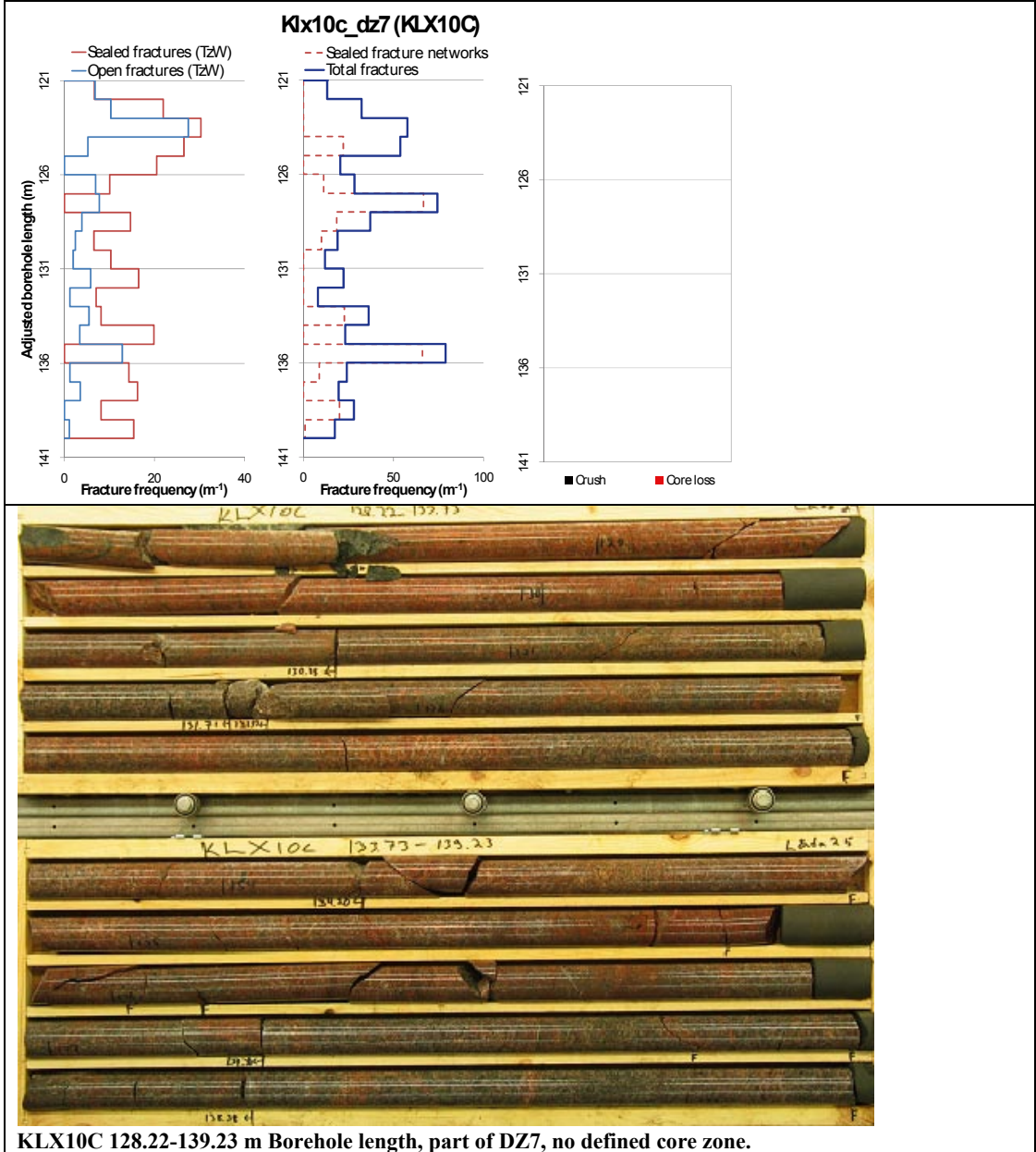
Measured T (sum T(PFL-f)), elevation -400 to -600m: no data

Number of PFL-features, elevation -400 to -600m: no data

Model T, elevation -400 to -500m: 2.26E-7

Model T, elevation -500 to -600m: 1.37E-7

Deformation zone KLX10C_dz7



Deformation zone KLX10C_dz7

Engineering characteristics

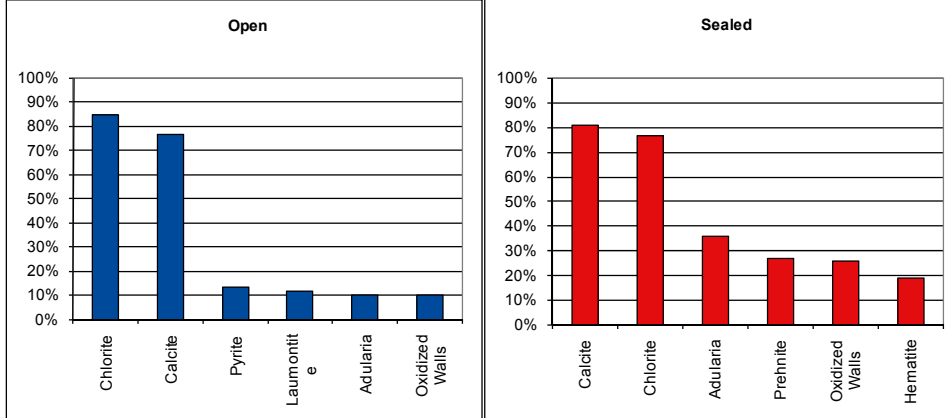
Frequency of open fractures: 3.2 m⁻¹

Std dev: no data


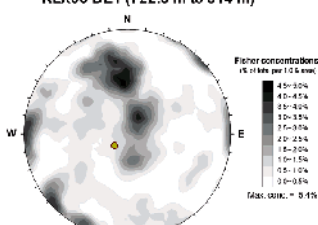
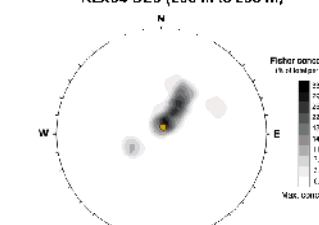
Frequency of sealed fractures: 20.6 m⁻¹

Std dev: no data

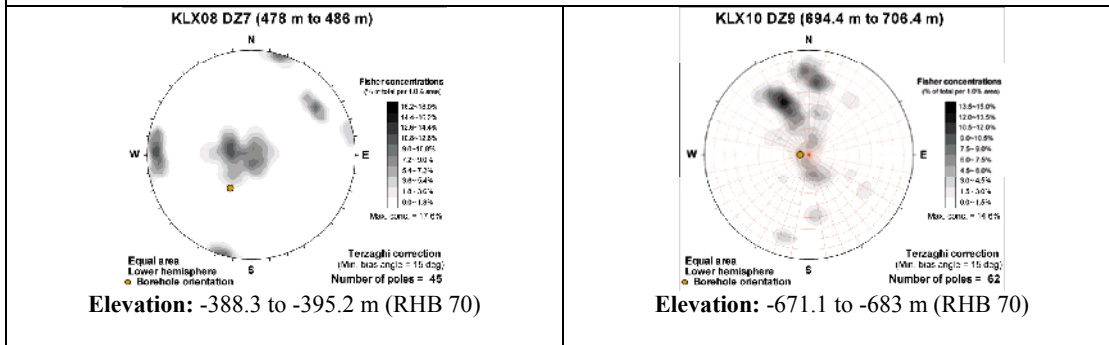
Mineral coatings



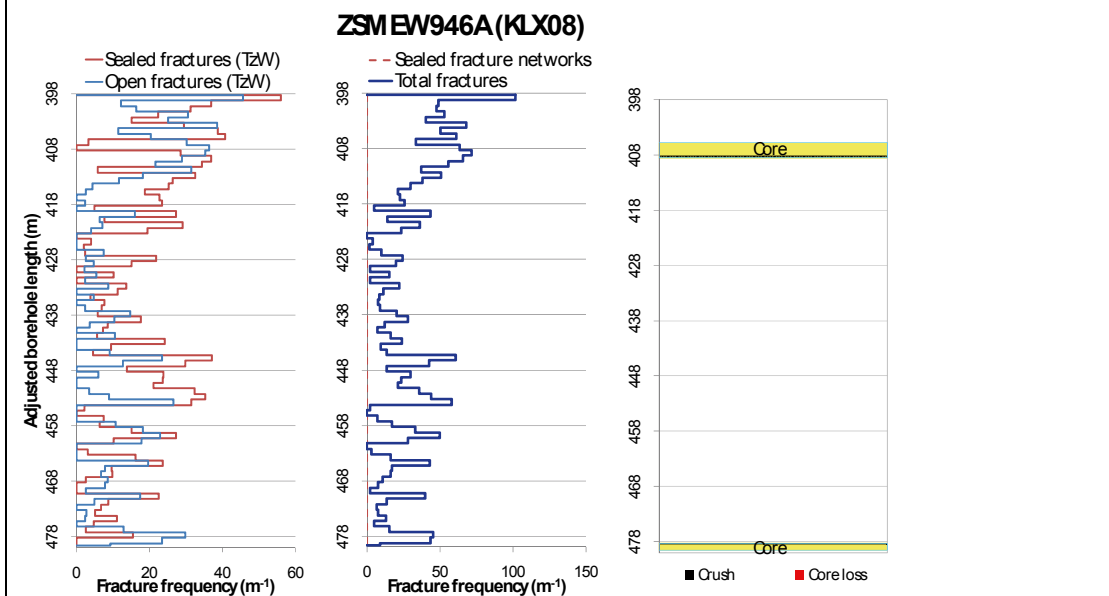
Gently dipping deformation zones

Deformation zone ZSMEW946A	
<p>Borehole intersections (metres along borehole)</p> <p>KLX03: 723-743 m (ESHI DZ1, 722.5-814m) KLX04: 295-298 m (ESHI DZ3 295-298 m). <i>Other potential members of the M1 series are ESHI DZ2 254-258m and ESHI DZ4 325-326m)</i> KLX08: 478-486 m (ESHI DZ7 478-486m). <i>Other potential members of the M1 series: ESHI DZ6 396-416m)</i> KLX10: 698-705 m (ESHI DZ 9 690m to 706m) KLX18: 580 m <i>Other potential members of the M1 series are KLX11 DZ11: 486-513m and DZ13: 577.90-586.16 m)</i></p>	
<p>Deformation style, alteration and geometry</p> <p>Deformation style: ductile and brittle</p> <p>Alteration: red staining and saussuritisation</p> <p>Strike/dip (right-hand-rule): 080/23</p> <p>Trace length at ground surface: no data</p> <p>Model thickness / model thickness span : 10 m / 5-20 m</p> <p>Measured thickness (-400 to -600 m elevation):</p> <p>Comment: ZSMEW946A marks the upper boundary of a much thicker sequence of similarly oriented MDZs and mafic intrusions. The fracture information given here can be taken to be typical of structures in this series.</p>	
Fractures in the deformation zone	
<p style="text-align: center;">KLX03 DZ1 (722.5 m to 814 m)</p>  <p style="text-align: center;">(Borehole length KLX03 723-743 m) Elevation: -682.3 to -701.8 m (RHB 70)</p>	<p style="text-align: center;">KLX04 DZ3 (295 m to 298 m)</p>  <p style="text-align: center;">Elevation: -269.4 to -272.4 m (RHB 70)</p>
<p style="text-align: center;">Transmissivity (m²/s)</p> <p>General dip of PFL-features, elevation -400 to -600m: no data</p> <p>Measured T (sum T(PFL-f)), elevation -400 to -600m: no data</p> <p>Number of PFL-features, elevation -400 to -600m: no data</p> <p>Model T, elevation -400 to -500m: 1.51E-7</p> <p>Model T, elevation -500 to -600m: 5.20E-8</p>	<p style="text-align: center;">Transmissivity (m²/s)</p> <p>General dip of PFL-features, elevation -400 to -600m: no data</p> <p>Measured T (sum T(PFL-f)), elevation -400 to -600m: no data</p> <p>Number of PFL-features, elevation -400 to -600m: no data</p> <p>Model T, elevation -400 to -500m: 1.51E-7</p> <p>Model T, elevation -500 to -600m: 5.20E-8</p>

Deformation zone ZSMEW946A



<p>Transmissivity (m²/s)</p> <p>General dip of PFL-features, elevation -400 to -600m: no data</p> <p>Measured T (sum T(PFL-f)), elevation -400 to -600m: no data</p> <p>Number of PFL-features, elevation -400 to -600m: no data</p> <p>Model T, elevation -400 to -500m: 1.51E-7</p> <p>Model T, elevation -500 to -600m: 5.20E-8</p>	<p>Transmissivity (m²/s)</p> <p>General dip of PFL-features, elevation -400 to -600m: no data</p> <p>Measured T (sum T(PFL-f)), elevation -400 to -600m: no data</p> <p>Number of PFL-features, elevation -400 to -600m: no data</p> <p>Model T, elevation -400 to -500m: 1.51E-7</p> <p>Model T, elevation -500 to -600m: 5.20E-8</p>
--	--



Note ZSMEW946A is interpreted as a sequence of such structures.



KLX08A 476.48-481.84 m borehole length. Part of DZ7 including core zone 478.3-479.5 m. Note ZSMEW946A is interpreted as a sequence of such structures.

Deformation zone ZSMEW946A

Engineering characteristics

Transition part of zone:

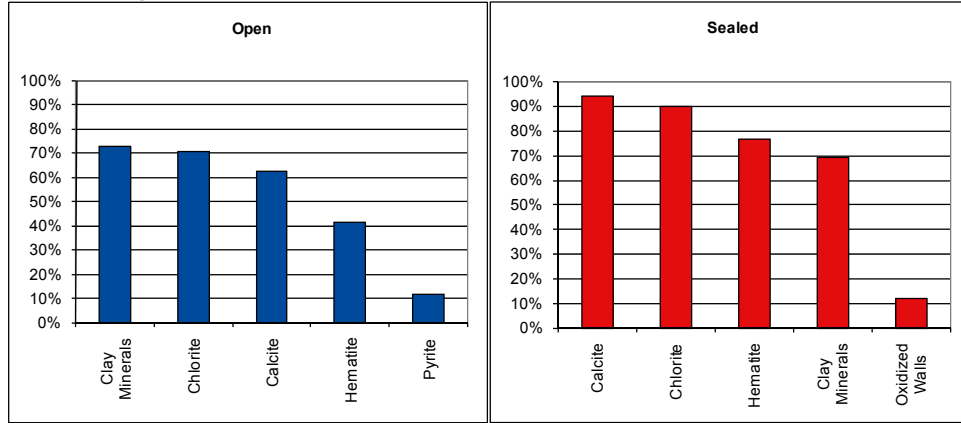
Frequency of open fractures: 9.1 m⁻¹

Std dev: 4.3

Frequency of sealed fractures: 41.7 m⁻¹

Std dev: 51.9

Mineral coatings



Fault core:

Percentage of fault core: 29 %

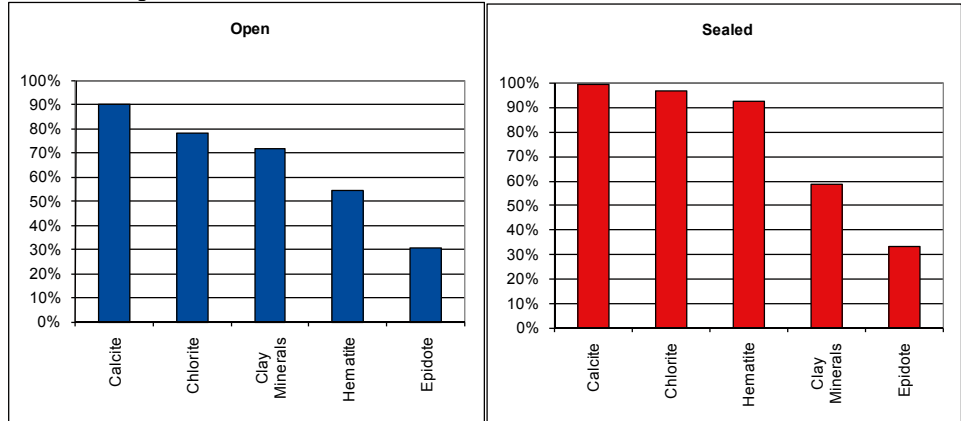
Frequency of open fractures: 19.5 m⁻¹

Std dev: 17.2

Frequency of sealed fractures: 46.5 m⁻¹

Std dev: 31.4

Mineral coatings



Deformation zone KLX03_dz1b

Borehole intersections (metres along borehole)

KLX03: 759-777 m (a part of ESHI DZ1 722-814 m)

Deformation style, alteration and geometry

Deformation style: brittle

Alteration: epidotisation

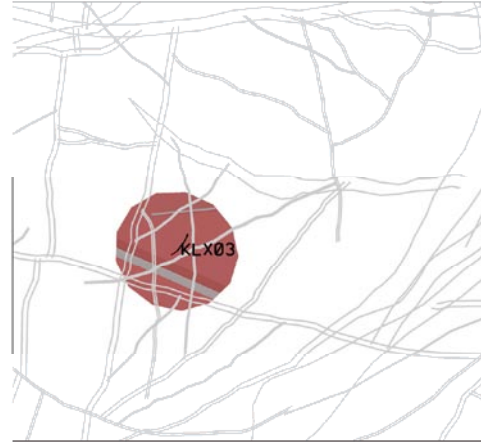
Strike/dip (right-hand-rule): 121/20

Trace length at ground surface: no data

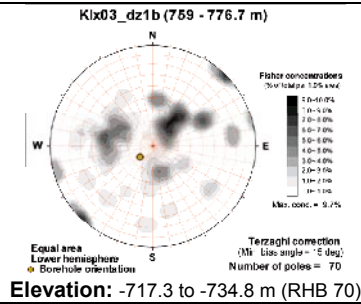
Model thickness / model thickness span : 10 m / no data

Measured thickness (-400 to -600 m elevation): no data

Comment:



Fractures in the deformation zone



Transmissivity (m²/s)

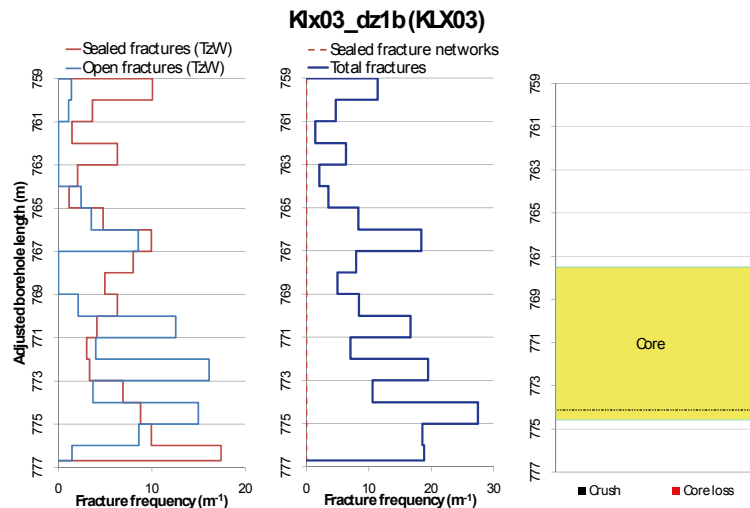
General dip of PFL-features, elevation -400 to -600m: no data

Measured T (sum T(PFL-f)), elevation -400 to -600m: no data

Number of PFL-features, elevation -400 to -600m: no data

Model T, elevation -400 to -500m: 2.26E-7

Model T, elevation -500 to -600m: 1.37E-7



Deformation zone KLX03_dz1b



KLX03A 769.39-774.83 m borehole length. Part of DZ1b including part of core zone 767.50-774.60 m.

Engineering characteristics

Transition part of zone:

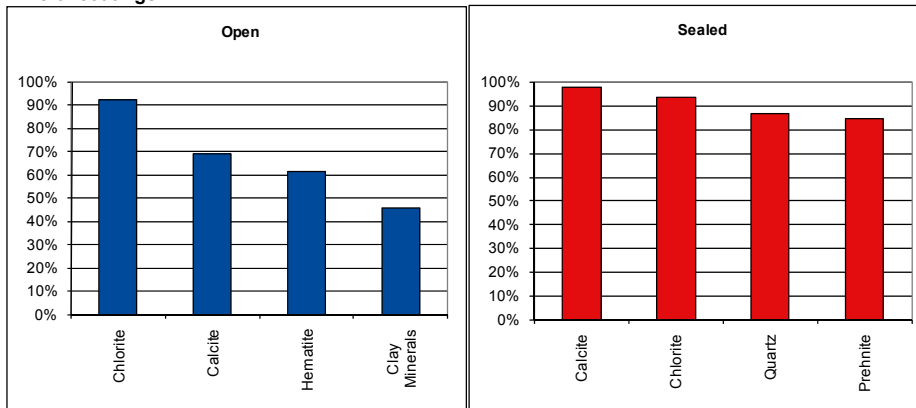
Frequency of open fractures: 2.5 m⁻¹

Std dev: no data

Frequency of sealed fractures: 34.7 m⁻¹

Std dev: no data

Mineral coatings



Fault core:

Percentage of fault core: 40 %

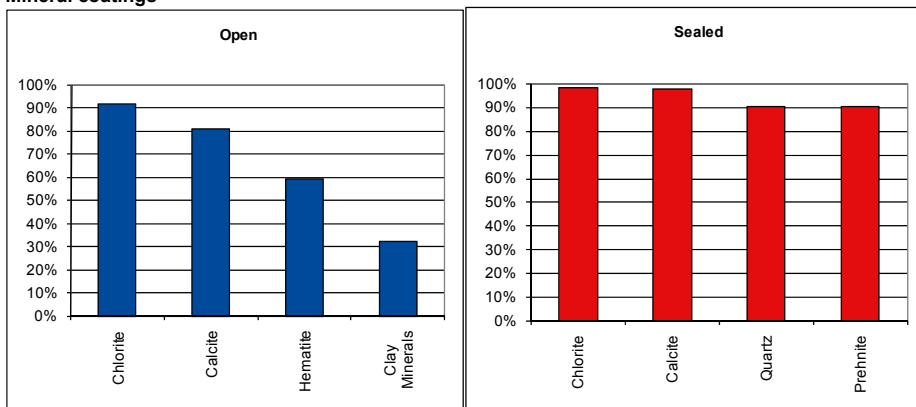
Frequency of open fractures: 5.2 m⁻¹

Std dev: no data

Frequency of sealed fractures: 36.9 m⁻¹

Std dev: no data

Mineral coatings



Deformation zone KLX03_dz1c

Borehole intersections (metres along borehole)

KLX03: 789-801 m (a part of ESHI DZ1 722-814 m)

Deformation style, alteration and geometry

Deformation style: brittle and ductile

Alteration: red staining and saussuritisation

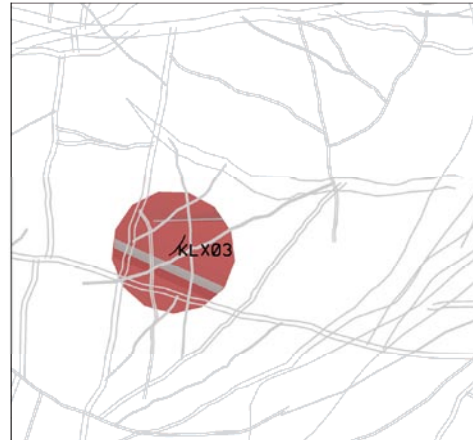
Strike/dip (right-hand-rule): 125/13

Trace length at ground surface: no data

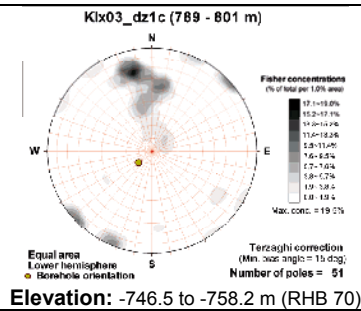
Model thickness / model thickness span : 10 m /no data

Measured thickness (-400 to -600 m elevation): no data

Comment:



Fractures in the deformation zone



Transmissivity (m^2/s)

General dip of PFL-features, elevation -400 to -600m: no data

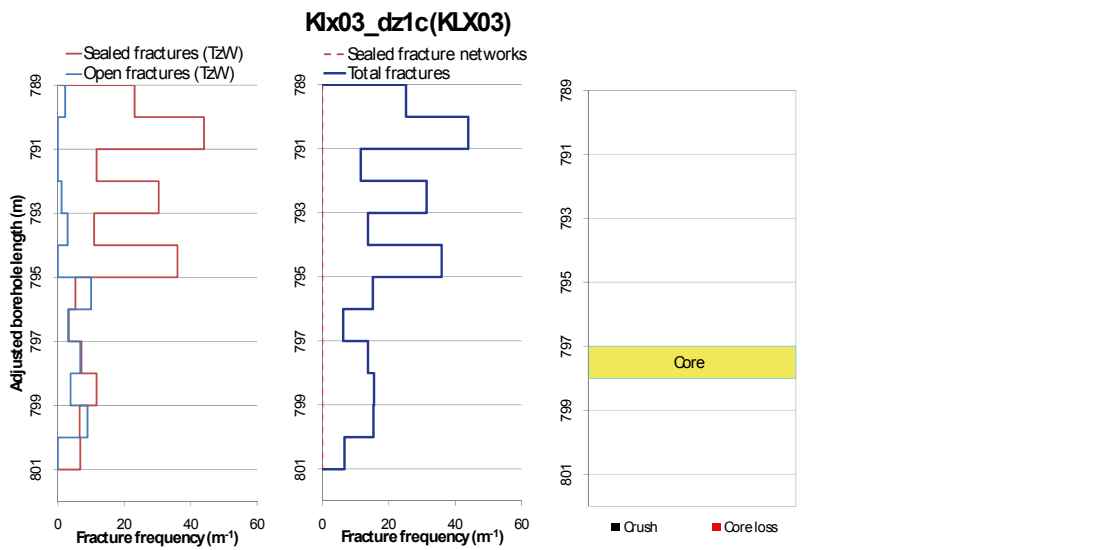
Measured T (sum T(PFL-f)), elevation -400 to -600m: no data

Number of PFL-features, elevation -400 to -600m: no data

Model T, elevation -400 to -500m: 2.26E-7

Model T, elevation -500 to -600m: 1.37E-7

Deformation zone KLX03_dz1c



KLX03A 796.6-801.9 m borehole length. Part of DZ1c, including core zone 797-798 m.

Engineering characteristics

Transition part of zone:

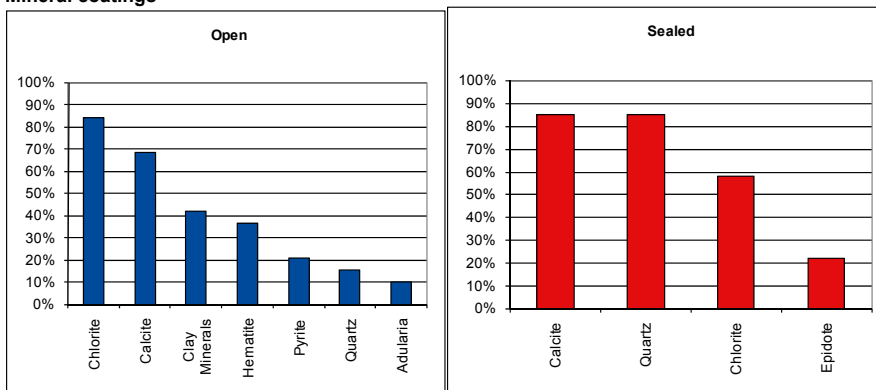
Frequency of open fractures: 1.7 m^{-1}

Std dev: no data

Frequency of sealed fractures: 27.3

Std dev: no data

Mineral coatings



Deformation zone KLX03_dz1c

Fault core:

Percentage of fault core: 8 %

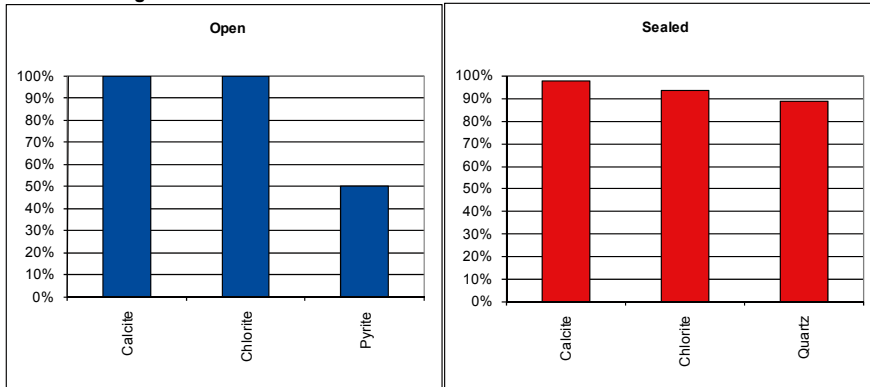
Frequency of open fractures: 4 m⁻¹

Std dev: no data

Frequency of sealed fractures: 46 m⁻¹

Std dev: no data

Mineral coatings



Deformation zone KLX07_dz10

Borehole intersections (metres along borehole)

KLX07A: 645-655 m (part of ESHI DZ10 604-655 m)

Deformation style, alteration and geometry

Deformation style: brittle and ductile

Alteration: red staining

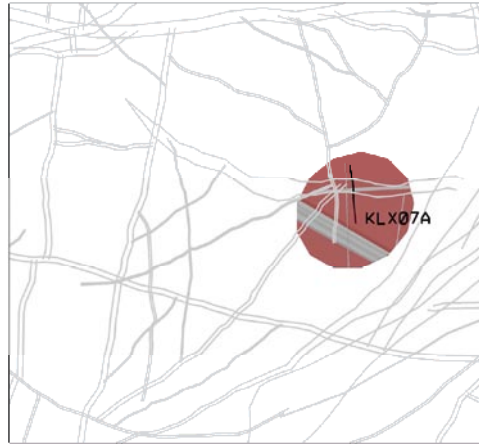
Strike/dip (right-hand-rule): 225/28

Trace length at ground surface: no data

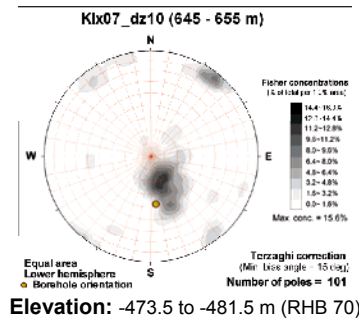
Model thickness / model thickness span : 10 m / no data

Measured thickness (-400 to -600 m elevation): 10 m

Comment: The modelled extent results in intersections at the very outer limits with KLX02 and KLX21B. Neither borehole shows correlation and can superficially be taken to confirm the general limits of the zone.



Fractures in the deformation zone



Transmissivity (m²/s)

General dip of PFL-features, elevation -400 to -600m: Moderately to sub-horizontally

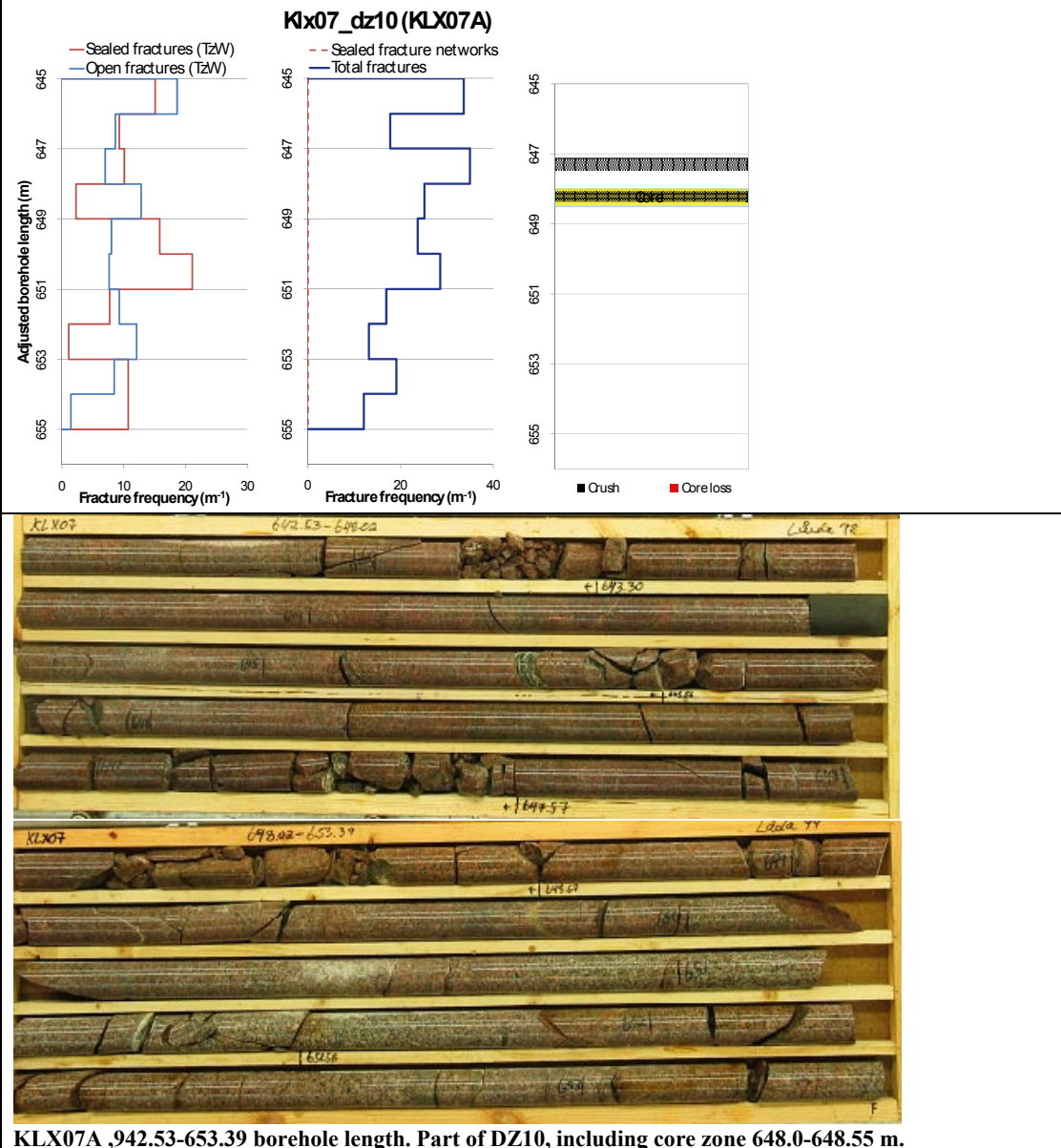
Measured T (sum T(PFL-f)), elevation -400 to -600m: 3.12E-6

Number of PFL-features, elevation -400 to -600m: 11

Model T, elevation -400 to -500m: 2.26E-7

Model T, elevation -500 to -600m: 1.37E-7

Deformation zone KLX07_dz10



Deformation zone KLX07_dz10

Engineering characteristics

Transition part of zone:

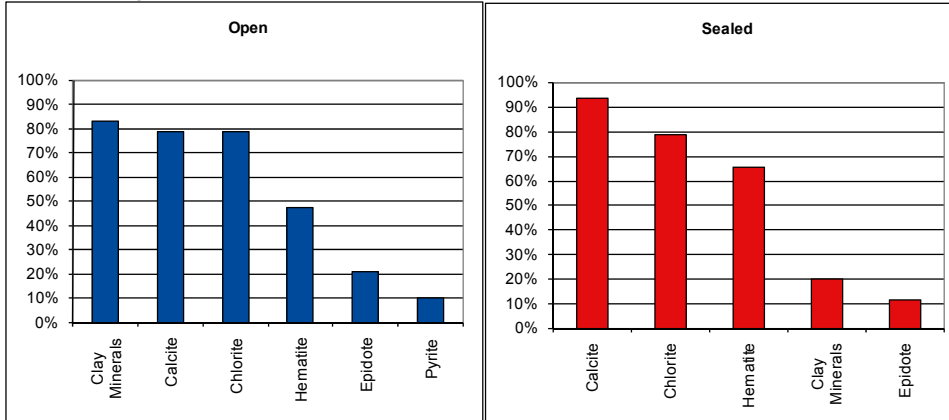
Frequency of open fractures: 9.5 m⁻¹

Std dev: no data

Frequency of sealed fractures: 22.2 m⁻¹

Std dev: no data

Mineral coatings



Fault core:

Percentage of fault core: 5 %

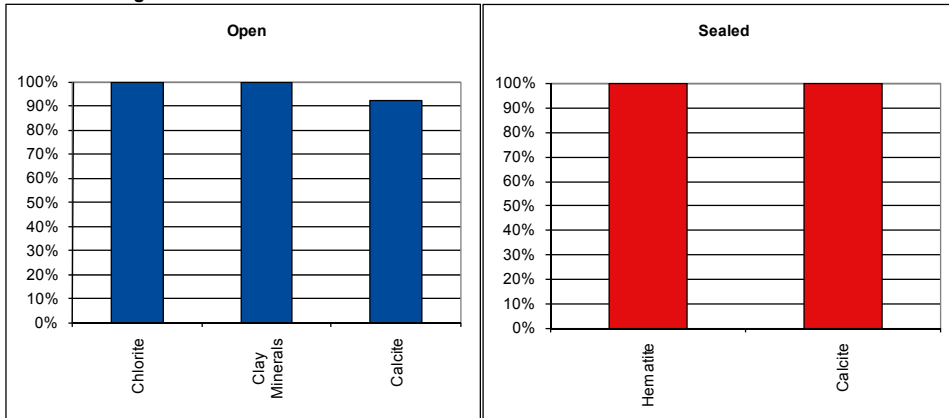
Frequency of open fractures: 26.0 m⁻¹

Std dev: no data

Frequency of sealed fractures: 2.0 m⁻¹

Std dev: no data

Mineral coatings



Deformation zone KLX08_dz10

Borehole intersections (metres along borehole)

KLX08A: 925-940 m (ESHI DZ10 925-940 m)

Deformation style, alteration and geometry

Deformation style: brittle

Alteration: red staining, epidotisation, saussurization

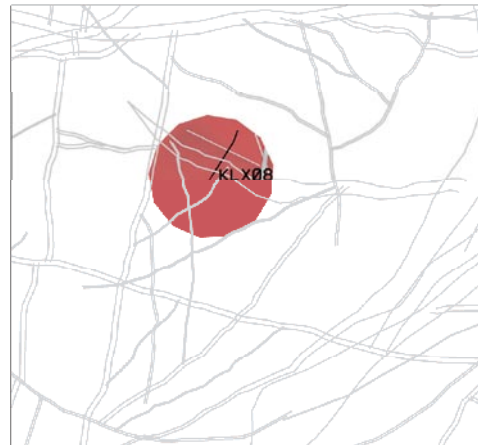
Strike/dip (right-hand-rule): 079/11

Trace length at ground surface: no data

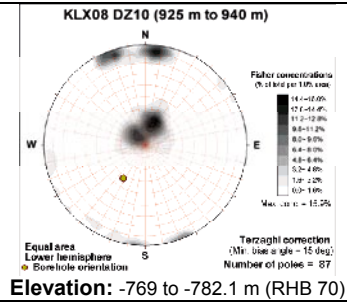
Model thickness / model thickness span : 11 m / no data

Measured thickness (-400 to -600 m elevation): no data

Comment:



Fractures in the deformation zone



Transmissivity (m^2/s)

General dip of PFL-features, elevation -400 to -600m: no data

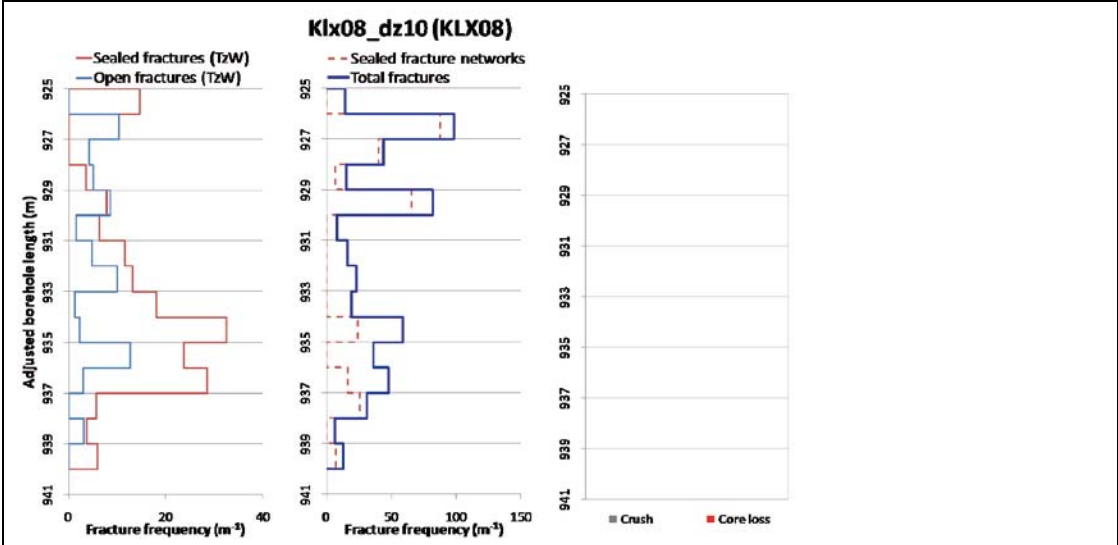
Measured T (sum T(PFL-f)), elevation -400 to -600m: no data

Number of PFL-features, elevation -400 to -600m: no data

Model T, elevation -400 to -500m: 2.26E-7

Model T, elevation -500 to -600m: 1.37E-7

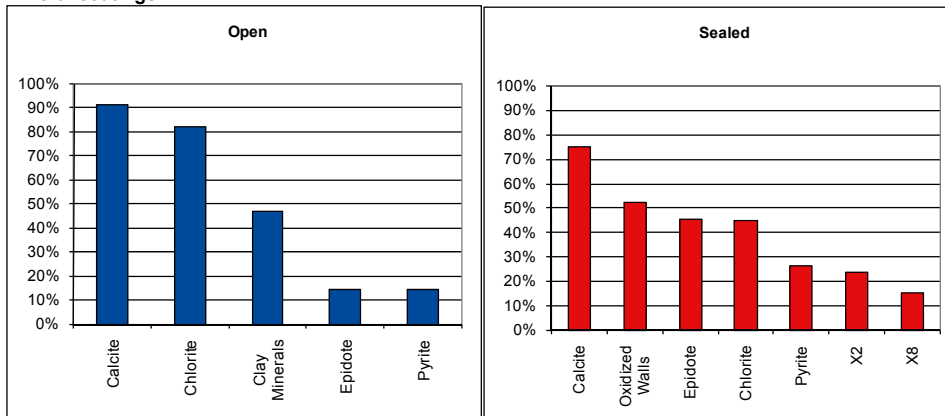
Deformation zone KLX08_dz10



KLX08 925.5-931.91 m Borehole length, part of DZ10, no defined core zone.

Engineering characteristics

Frequency of open fractures: 2.3 m⁻¹
 Std dev: no data
 Frequency of sealed fractures: 25.6 m⁻¹
 Std dev: no data
Mineral coatings



Deformation zone KLX11_dz11

Borehole intersections (metres along borehole)

KLX11A: 486-513 m (ESHI DZ11 486-513 m)

Deformation style, alteration and geometry

Deformation style: brittle

Alteration: red staining, epidotisation

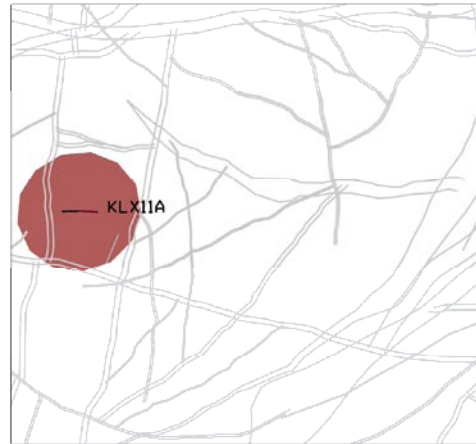
Strike/dip (right-hand-rule): 065/20

Trace length at ground surface: no data

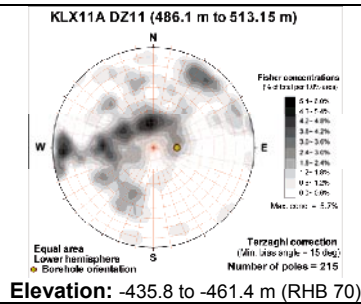
Model thickness / model thickness span : 20 m / no data

Measured thickness (-400 to -600 m elevation): 20 m

Comment: orientation is based on crush and fracture concentration orientations along with kinematic mapping by Viola et al. 2007a. Orientation and elevation makes this zone potentially a western extension of the M1 minor deformation zone series.



Fractures in the deformation zone



Transmissivity (m²/s)

General dip of PFL-features, elevation -400 to -600m: moderately to sub-horizontally

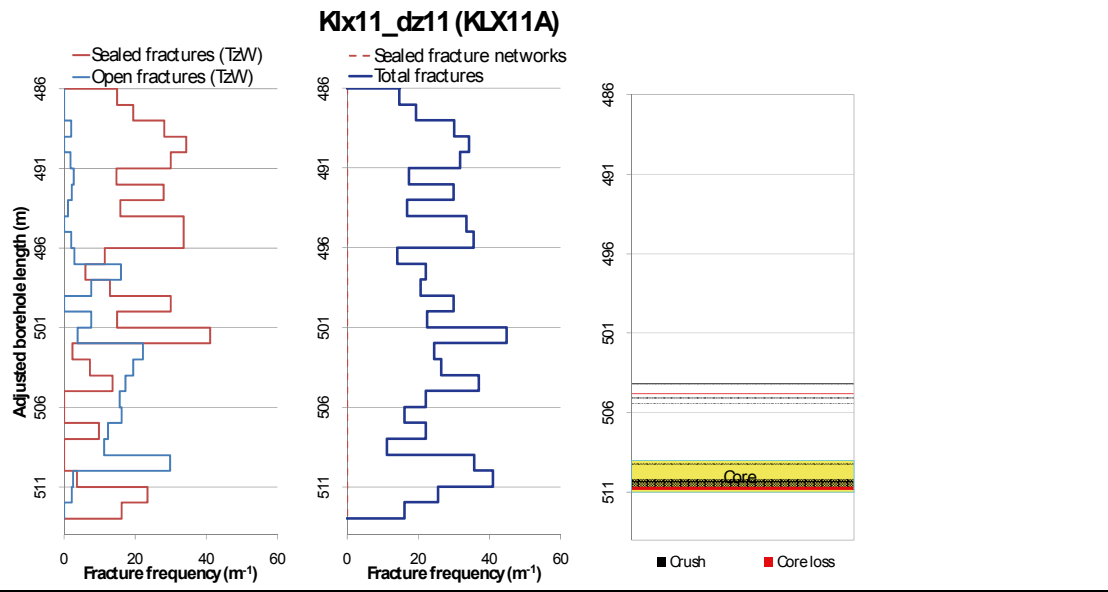
Measured T (sum T(PFL-f)), elevation -400 to -600m: 2.11E-8

Number of PFL-features, elevation -400 to -600m: 6

Model T, elevation -400 to -500m: 2.26E-7

Model T, elevation -500 to -600m: 1.37E-7

Deformation zone KLX11_dz11



KLX11A 501.57-511.90 m borehole length. Part of DZ11 including core zone 509.0-511.0 m.

Deformation zone KLX11_dz11

Engineering characteristics

Transition part of zone:

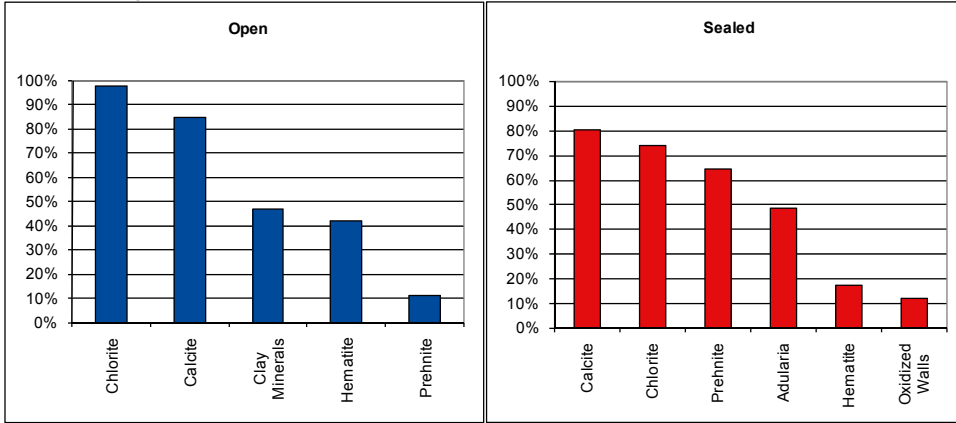
Frequency of open fractures: 6.6 m⁻¹

Std dev: no data

Frequency of sealed fractures: 22.1 m⁻¹

Std dev: no data

Mineral coatings



Fault core:

Percentage of fault core: 7 %

Frequency of open fractures: 30.5 m⁻¹

Std dev: no data

Frequency of sealed fractures: 44.5 m⁻¹

Std dev: no data

Mineral coatings

